

VIM  
(Grossner)

# AJR

cul - H02919-27-P024455

27

American  
Journal of  
Roentgenology

March 1990



# SonoVu US™ — A visible improvement in ultrasound-guided aspiration

The clearly visible bright echoes on the real-time sonogram below mark a breakthrough in accuracy and safety for fine-needle aspiration under ultrasound guidance.

SonoVu US, from E-Z-EM, is the first in a family of procedural needles designed specifically for enhanced ultrasound visualization.

Precisely formed 0.44 mm distal side holes on the cannula closely match the wavelength of ultrasound generated by a 3.5 MHz transducer. Uniform diffraction of the wave at each

hole creates a highly visible echo on the US display.

The side holes also provide a significant increase in needle flow rate, and ensure free flow should the tip become occluded—often the case with spinal or chiba needles.

Developed for use in amniocentesis, the SonoVu design can offer similar benefits in such procedures as US-monitored biopsy and cyst aspiration. For more information on 20- and 22-gauge SonoVu US needles from E-Z-EM, call 1-800-544-4624.

For both the patient and the practitioner, E-Z-EM products set the standards for convenience, safety, and quality in:

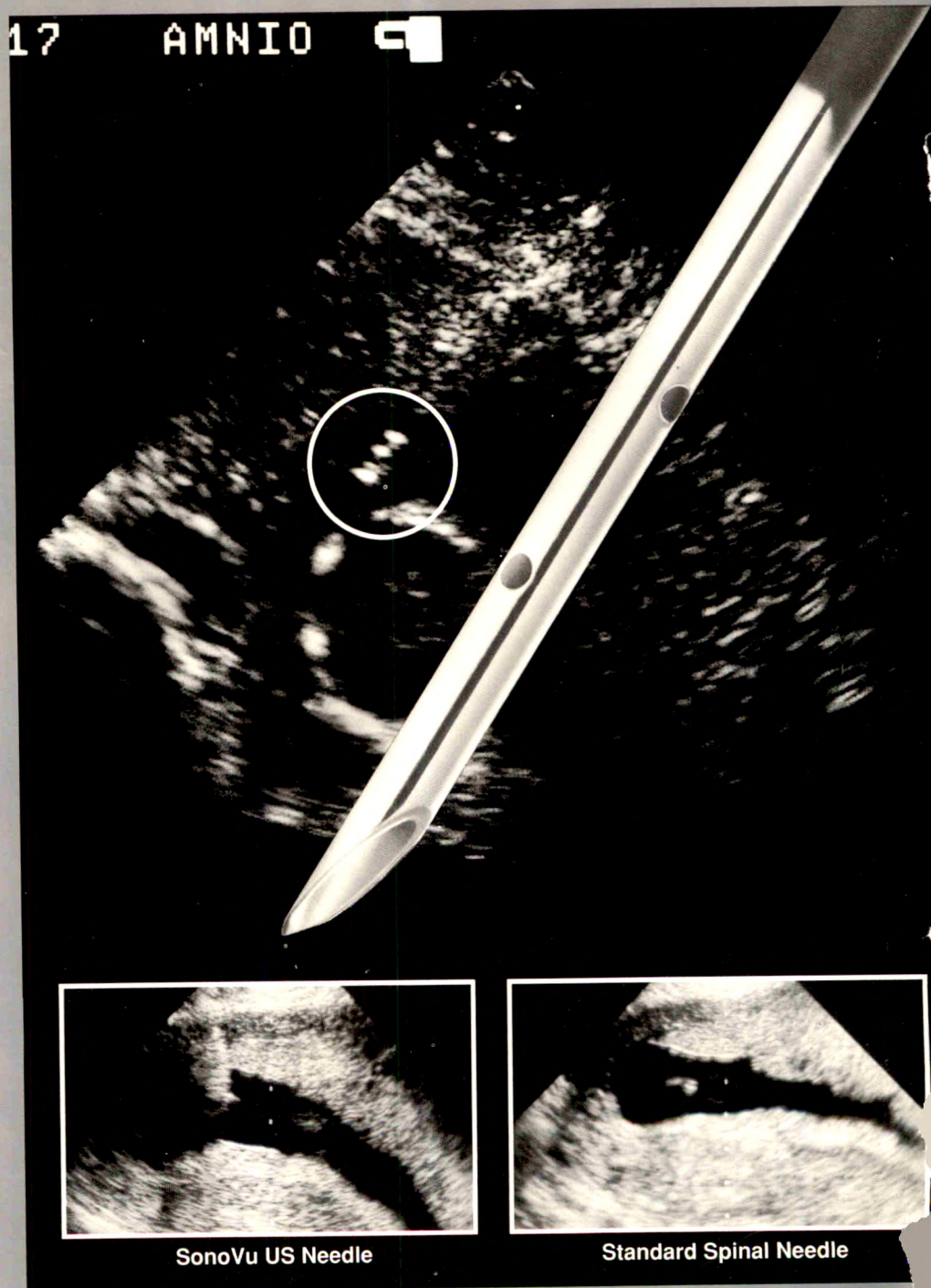
- GI Radiology
- Interventional Radiology
- CT Scanning
- Ultrasound
- Magnetic Resonance Imaging
- Angiography
- CEA Immunostaining
- Radiation Oncology
- Patient Prepping
- Protective Products
- Computerized Information Management Systems



E-Z-EM, Inc.  
Westbury, NY 11590

Circle 5 on the Reader Service Card

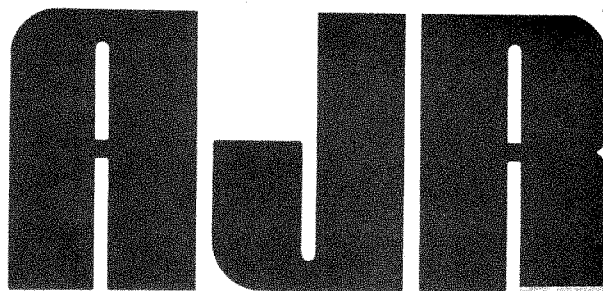
© 1990, E-Z-EM, Inc.



Reference: Amniocentesis Needle with Improved Sonographic Visibility. Radiology 1989; 171: 576 - 577



13.11.90



**American Journal of Roentgenology**  
Diagnostic Imaging and Related Sciences

**Editor-In-Chief** Robert N. Berk, *La Jolla, California*  
*University of California, San Diego*  
*School of Medicine and Medical Center*

**Editor Emeritus** Melvin M. Figley, *Seattle, Washington*

**Associate Editor** Saskia von Waldenburg Hilton, *San Diego, California*

**Consulting Editor** Michael S. Huckman, *Chicago, Illinois*

**Statistician** Charles C. Berry, *San Diego, California*

Ⓟ 24,455

**Editorial Board**

John R. Amberg  
Itamar Aviad  
Mark E. Baker  
Lawrence W. Bassett  
Michael A. Bettmann  
William G. Bradley, Jr.  
N. Reed Dunnick  
David K. Edwards  
Ronald G. Evens  
David S. Feigin  
Sandra K. Fernbach  
Richard H. Gold  
William R. Hendee

John R. Hesselink  
Charles B. Higgins  
Melvyn T. Korobkin  
Faye C. Laing  
Thomas L. Lawson  
Robert G. Levitt  
Bruce L. McClennan  
Richard P. Moser  
Albert A. Moss  
Jeffrey H. Newhouse  
Donald L. Resnick  
Stewart R. Reuter  
Charles A. Rohrmann, Jr.

Peter M. Ronai  
Sjef H. J. Ruijs  
Stuart S. Sagel  
David J. Sartoris  
Stefan C. Schatzki  
William P. Shuman  
Edward A. Sickles  
Barry A. Siegel  
David D. Stark  
Edward T. Stewart  
Murali Sundaram  
Eric vanSonnenberg  
Robert K. Zeman

**Editorial Staff:** Margaret Levene, *managing editor*; Katie L. Spiller, Barbara Rose, Barbara L. Halliburton, and Janine Anderson, *manuscript editors*; Nancy Rydbeck, *office manager*; Sheri Smith, *administrative assistant*; Sandra L. Griffin, *administrative secretary*.

AJR, AMERICAN JOURNAL OF ROENTGENOLOGY (ISSN 0361 803X) is the official journal of the American Roentgen Ray Society and is published monthly by Williams & Wilkins, 428 E. Preston St., Baltimore, MD 21202. Annual dues include \$50 for journal subscription. Second-class postage paid at Baltimore, MD, and at additional mailing offices. Postmaster, send address changes (Form 3579) to AJR, 428 E. Preston St., Baltimore, MD 21202. Subscription rates \$110 (\$155 foreign, \$244 Japan); institutions \$120 (\$165 foreign, \$254 Japan); in training \$25 (\$70 foreign, \$159 Japan); single copy \$16 (\$19 foreign). Japanese rates include airfreight. Japanese yen price is available from our sole agent USACO Corporation, 13-12, Shimbashi 1-Chome, Minato-Ku, Tokyo 105, Japan, telephone 03-502-6471. Airmail rates furnished on request. Indexed by *Current Contents* and *Index Medicus*. Copyright © 1990 by American Roentgen Ray Society.

0361-803X/90\$2.00





# POST GRADUATE COURSE IN NEURORADIOLOGY INCLUDING HEAD AND NECK

**TUESDAY-FRIDAY APRIL 3-6, 1990  
THE GRAND HYATT HOTEL**

A nationally recognized faculty will provide a comprehensive clinically oriented review and update of Neuroradiology and Head and Neck Radiology. Emphasis will be on the increasing application of MRI; however, review of the fundamentals of CT and Myelo-CT will be extensive. Intensive small group workshops will permit participation of all registrants.

**FACULTY:** Drs. Michael M. Ambrosino, Kevin Bannon, Jacqueline A. Bello, Alex Berenstein, R. Thomas Bergeron, Norman E. Chase, In-Sup Choi, Hugh D. Curtin, Michael Deck, Hossein Firooznia, Nancy B. Genieser, Ajax E. George, Sadek K. Hilal, Roy Holliday, Stephen A. Kieffer, Irvin I. Kricheff, Norman E. Leeds, Joseph P. Lin, Andrew W. Litt, Manuel Mourino, Thomas P. Naidich, Richard S. Pinto, Deborah L. Reede, Peter M. Som, Michael Tenner, Jeffrey Weinreb, Robert D. Zimmerman.

**ACCREDITATION:** 28 Category I Credit Hrs.

**FEE:** \$560

**NYU Post-Graduate Medical School  
550 First Avenue, New York NY 10016  
(212) 340-5295**

AJR1/90

## **VASCULAR/INTERVENTIONAL AND NUCLEAR MEDICINE/IMAGING TWO POSITIONS**

The ten member imaging section of the Guthrie Clinic - Robert Packer Hospital desires associates with Fellowship training in the above modalities.

The Guthrie Clinic is a 220 physician multi-specialty clinic serving the Southern Tier of New York and the Northern Tier of Pennsylvania in the beautiful endless mountains.

Outstanding practice opportunities in an environment free of urban hassle.

Please send letter of inquiry with curriculum vitae:

Guthrie Clinic  
Sayre, PA 18840  
717-888-5858  
Attn: G.V. Ippolito  
Vice President

## **CHIEF OF RADIOLOGY DIRECTOR, RESIDENCY PROGRAM**

The University of California, San Francisco and its affiliate, Veterans Administration Medical Center, Fresno are seeking an academically oriented, creative individual with demonstrated strong leadership ability for the position of Chief of Radiology and Director of the Residency Program.

Qualifications include board certification in Radiology and interest, skill, and background in clinical instruction and research.

California location offers delightful living conditions and ready access to both coastal and mountain recreational areas.

Address inquiries and send c.v. to:

David Ira Margolin, M.D., Ph.D.  
Chairman, Search Committee  
2615 E. Clinton Avenue (127)  
Fresno, CA 93703.

UCSF is an AA/EOE, M/F/H/V.



# AJR Guidelines for Authors

Address new and revised manuscripts, correspondence, and classified ads to the Editor:

AJR Editorial Office  
2223 Avenida de la Playa, Suite 200  
La Jolla, CA 92037-3218

Telephone: (619) 459-2229; FAX: (619) 459-8814

Inquiries regarding subscriptions, display advertising, reprints, or permission to republish AJR material should be addressed to the publisher:

The Williams & Wilkins Co.  
428 E. Preston St.

Baltimore, MD 21202 Telephone: 1-800-638-6423

The AJR publishes original contributions to the advancement of medical diagnosis and treatment. Submitted manuscripts should not contain previously published material and should not be under consideration for publication elsewhere. Papers dealing with neuroradiology should be addressed to: American Journal of Neuroradiology, Dept. of Radiology, Massachusetts General Hospital, Boston, MA 02114. At the discretion of the AJR Editor, AJNR articles that are of interest to the general reader may be republished in the AJR. Neuro-radiologic papers sent to the AJR will be forwarded to the Editorial Office of the AJNR.

Manuscript decisions are based on peer review. Reviewers receive manuscripts without title pages to ensure an unbiased review. Statements made in the article, including changes made by the Editor or manuscript editor, are the responsibility of the author and not of the AJR or its publisher. Authors will be sent the edited manuscript, galley proof, and proofs of illustrations. If the corresponding author will be unavailable to review galleys, arrangements should be made for a coauthor or colleague to read and return the proof.

The following guidelines are based on instructions set forth in the **Uniform Requirements for Manuscripts Submitted to Biomedical Journals** (*Ann Intern Med* 1988;108:258-265). Articles will be edited, however, to conform to the individual style of AJR.

## General Guidelines for Major Papers

**Abstract.** Clearly state (in 200 words or less) the purpose, methods, results, and conclusions of the study. Include actual data.

**Introduction.** Briefly describe the purpose of the investigation and explain why it is important.

**Methods.** Describe the research plan, the materials (or subjects), and the methods used, in that order. Explain in detail how disease was confirmed and how subjectivity in observations was controlled.

**Results.** Present results in a clear, logical sequence. If tables are used, do not duplicate tabular data in text, but do describe important trends and points.

**Discussion.** Describe the limitations of the research plan, materials (or subjects), and methods, considering both the

purpose and the outcome of the study. When results differ from those of previous investigators, explain the discrepancy.

## AUTHOR'S CHECKLIST

**For priority handling, complete the following checklist, sign the copyright form on the reverse side of this page, and include both with the manuscript.**

\_\_\_\_\_ Two copies of the manuscript (the original and a photocopy) and two complete sets of figures are submitted. One copy has been retained by the author.

\_\_\_\_\_ If appropriate, AJR Guidelines for case reports, technical notes, pictorial essays, or letters to the Editor have been followed. (See page A5.)

\_\_\_\_\_ The manuscript, including references, figure legends, and tables, is typed double-spaced on 8½ × 11 in. (21.6 × 27.9 cm) *nonerasable* paper. Right-hand margins are not justified.

\_\_\_\_\_ All manuscript pages are numbered consecutively beginning with the abstract. Authors' names do not appear on the manuscript pages.

\_\_\_\_\_ The manuscript is organized as follows: title page, blind title page (title only), abstract, introduction, methods, results, discussion, acknowledgments, references, tables, figure legends, and figures.

\_\_\_\_\_ Informed consent has been obtained from patients who participated in clinical investigations. If experiments were performed on animals, authors complied with NIH guidelines for use of laboratory animals.

\_\_\_\_\_ Use of unfamiliar acronyms and abbreviations is kept to a minimum. When abbreviations are used they are defined at first mention, followed by the abbreviation in parentheses.

\_\_\_\_\_ Metric measurements are used throughout, or the metric equivalent is given in parentheses.

\_\_\_\_\_ Names and locations (city and state only) of manufacturers are given for equipment and nongeneric drugs.

### Title Page

\_\_\_\_\_ The following information is given: title of article; names and complete addresses (including zip code) of all authors; current addresses of authors who have moved since study; acknowledgment of grant or other assistance. The corresponding author is clearly identified, and a current address, phone number, and Fax number are given.

\_\_\_\_\_ Two copies of a blind title page are included giving only the title (without the authors' names) for use in the review process.

### Abstract

\_\_\_\_\_ An abstract of approximately 200 words concisely states the purpose, methods, and results of the study in one paragraph. Actual data are included. Conclusions are stated in a second, summary paragraph.

\_\_\_\_\_ No abbreviations or reference citations are used.



## References

References (not to exceed 35) are typed double-spaced starting on a separate page and are **numbered consecutively in the order in which they appear in the text**.

All references are cited in the text and are enclosed in brackets and typed on line with the text (not superscript).

Unpublished data are not cited in the reference list, but are cited parenthetically in the text, for example, (Smith DJ, personal communication), (Smith DJ, unpublished data). This includes papers submitted, but not yet accepted, for publication.

Inclusive page numbers (e.g., 333–335) are given for all references.

Journal names are abbreviated according to *Index Medicus*.

Style and punctuation of references follow the format illustrated in the following examples (all authors are listed when six or less; when seven or more authors, the first three are listed, followed by “et al.”):

### Journal article

1. Long RS, Roe EW, Wu EU, et al. Membrane oxygenation: radiographic appearance. *AJR* 1986;146:1257–1260

### Book

2. Smith LW, Cohen AR. *Pathology of tumors*, 6th ed. Baltimore: Williams & Wilkins, 1977:100–109

### Chapter in a book

3. Breon AJ. Serum monitors of bone metastasis. In: Clark SA, ed. *Bone metastases*. Baltimore: Williams & Wilkins, 1983:165–180

### Paper presented at a meeting

4. Lau FS, Kirk AN. MR imaging of the spine. Presented at the annual meeting of the American Roentgen Ray Society, Washington, DC, April 1986

## Tables

Each table is typed double-spaced on a separate page without vertical or horizontal rules; each has a short, descriptive title. Tables do not exceed two pages in length and contain at least four lines of data.

Tables are numbered in the order in which they are cited in the text.

Abbreviations are defined in an explanatory note below each table.

Tables are self-explanatory and do not duplicate data given in the text or figures.

All arithmetic (percentages, totals, differences) has been double checked for accuracy, and tabular data agree with data given in the text.

## Figures and Legends

Two complete sets of original figures are submitted unmounted in labeled envelopes.

Figures are clean, unscratched, 5 × 7 in. (13 × 18 cm) glossy prints with **white borders**. A separate print is submitted for each figure *part*.

All figure parts relating to one patient have the same figure number.

Each figure is labeled on the back with the figure number and an arrow indicating “top.” For black-and-white figures, labeling is done on a gummed label, which is then affixed to the back of the print. *Never* use labels on color figures, but write figure number on the back lightly in pencil. *Never* use ink on front or back of any figures.

Author’s names are *not* written on the backs of figures.

Only removable (rub-on) arrows and letters are used on the figures. Symbols are uniform in size and style and are not broken or cracked.

Images are uniform in size and magnification.

Line drawings are done in black ink on a white background. They are professional in quality, and all use the same size type. (Only glossy prints are acceptable.)

Written permission has been obtained for use of all previously published illustrations (and copies of permission letters are included), and an appropriate credit line is given in the legends.

Legends are typed double-spaced, and figure numbers correspond with the order in which the figures are cited in the text.

## Transfer of Copyright Agreement, Conflict of Interest Acknowledgment, Certification of Coauthors, and Exclusive Publication Statement

Complete copyright to the article entitled: \_\_\_\_\_

is hereby transferred to the American Roentgen Ray Society (for United States government employees to the extent transferable), effective if and when the article is accepted for publication in the *American Journal of Roentgenology*. In the case of the authors who are officers or employees of the United States government, the American Roentgen Ray Society recognizes that works prepared by officers or employees of the United States government as part of their official government duties are in the public domain.

Authors reserve all proprietary rights other than copyright, such as patent rights and the right to use all or part of this article in future works of their own. The authors retain the right of replication, subject only to crediting the original source of publication and receiving written permission from the publisher.

Authors guarantee that this manuscript contains no matter that is libelous or otherwise unlawful, invades individual privacy, or infringes any proprietary rights.

Authors understand that they will receive no royalty or other compensation from the American Roentgen Ray Society or the publisher.

Authors guarantee that the editor has been or will be informed of any proprietary or commercial interest or conflicts of interest the authors may have that relate directly or indirectly to the subject of this article.

All authors certify that they have made substantive and specific intellectual contributions to the article and assume public responsibility for its content.

Finally, the authors certify that none of the material in this manuscript has been published previously or is currently under consideration for publication elsewhere.

\_\_\_\_\_  
First author/date

\_\_\_\_\_  
Second author

\_\_\_\_\_  
Third author

\_\_\_\_\_  
Fourth author

\_\_\_\_\_  
Fifth author

\_\_\_\_\_  
Sixth author

**This agreement must be signed by all authors in order for the manuscript to be published.**



### Case Reports

A case report is a brief description of a special case that provides a message that transcends the individual patient.

*Format.* There is no abstract. The introduction should be a short paragraph giving the general background and the specific interest of the case. No more than one case should be described in detail (similar ones can be mentioned briefly in the discussion). Emphasis should be on the radiologic aspects; clinical information must be limited to that necessary to provide a background for the radiology. The discussion should be succinct and should focus on the specific message and relevance of radiologic methods. A review of the literature is not appropriate.

*Length.* Maximum of five double-spaced, typewritten pages, including the references but not the title page or figure legends.

*References.* Maximum of eight.

*Figures.* Maximum of three or four, unless the text is shortened accordingly. Legends must not repeat the text.

*Tables and Acknowledgments.* Not appropriate in case reports.

### Technical Notes

A technical note is a brief description of a specific technique or procedure, modification of a technique, or equipment of interest to radiologists.

*Format.* No abstract, headings, or subheadings are required. If headings are used, they should be a combination of "Case Report," "Materials and Methods," "Results," and "Discussion." A brief one-paragraph introduction should be included to give the general background. Discussion should be limited to the specific message, including the uses of the technique or equipment. Literature reviews and lengthy case reports are not appropriate.

*Length.* Maximum of five double-spaced, typewritten pages, including the references but not the title page or figure legends.

*References.* Maximum of eight.

*Figures.* Maximum of two, unless the text is shortened accordingly.

*Tables and Acknowledgments.* Not appropriate in technical notes.

### Pictorial Essays

A pictorial essay is an article that conveys its message through illustrations and their legends. Unlike other *AJR* articles, which are based on original research, pictorial essays serve primarily as teaching tools, like exhibits at a scientific meeting. They are not encyclopedic book chapters. No abstract is necessary.

*Length.* Maximum of four double-spaced, typewritten pages, including the references but not the title page or figure legends.

*References.* Maximum of four.

*Figures.* Maximum of 30 figure parts. Number should be as few as necessary to convey the message of the paper.

*Tables and Acknowledgments.* Not appropriate in pictorial essays.

### Letters to the Editor and Replies

Letters to the Editor and Replies should offer objective and constructive criticism of published articles. Letters may also discuss matters of general interest to radiologists. Do not end a letter with a hand-written signature.

*Format.* All letters should be typed double-spaced on nonletterhead paper, with no greeting or salutation. Name and affiliation should appear at the end of the letter. Titles for letters should be short and pertinent. The title for a reply is simply "Reply."

*Length.* Maximum of two double-spaced, typewritten pages, including references.

*References.* Maximum of four.

*Figures.* Maximum of two.

*Tables and Acknowledgments.* Not appropriate in Letters to the Editor and Replies.

### Opinions, Commentaries, and Perspectives

Opinions, commentaries, and perspectives are special articles dealing with controversial topics or issues of special concern to radiologists.

*Format.* Include a title page but no abstract. Headings may be used to break up the text.

*Length.* Maximum of five double-spaced, typewritten pages.

*References.* Maximum of five.

*Tables and Figures.* Maximum of four.

### Computer Page Articles

Articles published on the computer page deal with practical computer applications to radiology.

*Format.* Include a title page but no abstract.

*Length.* Maximum of eight double-spaced, typewritten pages.

*References.* Maximum of five.

*Figures and Tables.* Maximum of five. Computer printouts are not acceptable. Figures must be submitted as 5 × 7 in. glossy prints.



# Why Hexabrix has a leg up on the nonionics in peripheral arteriography

## Better patient tolerance.

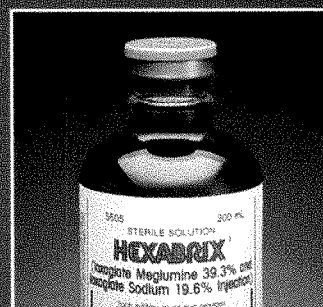
Patient discomfort during femoral arterial run-offs is a well-recognized problem; in some patients, the pain is so severe that it is intolerable. Hexabrix is a well-tolerated choice for peripheral arteriography, particularly femoral arterial run-offs.

## Less heat and pain.

In comparative studies with nonionic media, Hexabrix produced significantly less heat,<sup>1,2</sup> pain,<sup>1,3</sup> and patient discomfort<sup>3</sup> during peripheral arteriography procedures.

## Lower osmolality.

Of the newer low-osmolality agents, Hexabrix offers the lowest osmolality per equivalent iodine concentration.



# HEXABRIX<sup>1</sup>

(ioxaglate meglumine 39.3%/  
ioxaglate sodium 19.6% injection)

F R O M M A L L I N C K R O D T

Please see the following page for references and brief summary of prescribing information.

## Review Article

# Monochorionic Twinning: Sonographic Assessment

Roy A. Filly,<sup>1</sup> Ruth B. Goldstein, and Peter W. Callen

Morbidity and mortality are significantly increased in twin gestations compared with singleton gestations [1]. The relative risk, however, depends on whether each fetus is attached to its own placenta (dichorionic) or must share a placenta (monochorionic). Monochorionic twins have a higher prevalence of growth retardation and death compared with dichorionic twins. Additionally, several unique syndromes occur only in the presence of monochorionicity. Only monochorionic twins can be monoamniotic. If the fetuses must share not only a placenta but an amniotic cavity, they face a very high risk of mortality [2-5].

The identification of a monochorionic twin pregnancy has important obstetric implications, some of which influence pregnancy management and may limit certain treatment options. Therefore, the sonographic examination of all twin pregnancies should include a specific effort to determine chorionicity and amnionicity. Before we describe those sonographic features that are useful in the prediction of chorionicity and amnionicity, it is important to review the embryology of placentation in twin pregnancies.

## Embryology of Twin Placentation

Twin pregnancies result either from fertilization of two ova (dizygotic twins) or from fertilization of a single ovum with subsequent cleavage (monozygotic twins). Dizygotic twins are more common (70%) than monozygotic twins (30%). All dizygotic twins have dichorionic placentation and all dichorionic twins are diamniotic. Monozygotic twins may be either

dichorionic (25%) or monochorionic (75%) depending on the embryologic stage at which cleavage occurs [5].

In order to understand twin placentation, it is necessary to revisit early embryonic structures [6]. The blastocyst is the embryologic stage of development that implants in the uterus. Each blastocyst gives rise to all of the components of the pregnancy, including the placenta and chorionic membrane (from the trophoblast) and the amnion, fetus, umbilical cord, yolk sac, and yolk stalk (from the inner cell mass). Therefore, the number of blastocysts implanting in the uterus determines the number of placentas that develop. Because, for all dizygotic twins, two blastocysts enter the endometrial cavity and implant, this twin type universally manifests dichorionic placentation.

The tissue (chorion) from which the embryonic placenta develops precedes the formation of the amnion. Thus, all dichorionic pregnancies are diamniotic, as well. Unfortunately, two discrete placentas cannot always be identified on gross pathologic inspection after the birth of dichorionic twins. If the blastocysts implant relatively far apart within the endometrial cavity (e.g., anterior and posterior uterine walls), then there will be two discrete placentas at birth. However, if the blastocysts implant relatively close together within the endometrial cavity (e.g., both on the anterior uterine wall), then the developing placental masses will meet and fuse as they grow. Therefore, only a single placental mass will be identified at delivery. Fusion is a relatively common event, occurring in approximately half of dichorionic twin pregnancies.

For monozygotic twins, the stage at which cleavage occurs determines the chorionicity and amnionicity of the pregnancy.

Received October 10, 1989; accepted after revision November 15, 1989.

<sup>1</sup> All authors: Department of Diagnostic Ultrasound (L-374), Box 0628, University of California Medical Center, San Francisco, CA 94143-0628. Address reprint requests to R. A. Filly.

AJR 154:459-469, March 1990 0361-803X/90/1543-0459 © American Roentgen Ray Society



Dichorionicity in monozygotic twins results when cleavage of the zygote occurs at any embryologic stage before blastocyst formation. Thus, two blastocysts will enter the endometrial cavity and implant. Therefore, the placentation will be dichorionic, the same as for dizygotic twins. Again, if the blastocysts implant relatively close together in the endometrial cavity the tendency will be for the placentas to meet and fuse. Dichorionicity occurs in approximately 25% of monozygotic twins.

If cleavage of the embryo occurs at any embryologic stage beyond the formation of the blastocyst, then a single blastocyst enters the endometrial cavity and implants. Where it implants, a single placenta will develop. The embryologic entity that cleaves in this situation is the inner cell mass. In order for monozygotic twins to be dichorionic, the division must occur before the fourth day after fertilization. If the division occurs from the fourth to the eighth days after fertilization (the blastocyst has formed, but the amnion is not yet developed), then monochorionic diamniotic twins will result. The latter is the more common scenario for monozygotic twins, occurring in approximately 75% of cases.

In those unusual circumstances in which cleavage occurs after the eighth day after fertilization, then both the chorion and the amnion already have formed, and thus the twins will share not only a placenta but also a single amniotic cavity. If division occurs after formation of the amnion, the structure that cleaves is the embryonic disk. If division of the embryonic disk is incomplete, various degrees of twin conjoining will result.

Knowing the embryologic sequence is important in understanding the imaging manifestations of twin placentation, amnion formation, and some of the unique syndromes seen in twins. Because all dizygotic twins result from the implantation of two blastocysts, all such twins must be dichorionic. Only monozygotic twins can have monochorionic placentation. Because placental formation precedes amnion formation, all dichorionic twins are also diamniotic. Conversely, all monoamniotic twins must be monochorionic, and all conjoined twins also must be monoamniotic and monochorionic. No other embryologic possibilities can occur.

### Judging Chorionicity and Amnionicity by Sonography

Dizygotic twins are the more common twin type and, as noted, all have dichorionic placentation [1]. Further, 25% of monozygotic twins are also dichorionic. Thus, there is a substantial preponderance of dichorionic twins (approximately 80% of all twins). Unfortunately, approximately half of dichorionic placentas are fused along their border. Therefore, sonographically, it may not be possible to identify two discrete placental masses. The sensitivity of sonographic visualization of two placentas in detecting dichorionicity, as may be anticipated, has been low [7]. However, when two placentas are seen, dichorionicity can be predicted with certainty (Table 1). Similarly, if a membrane is identified separating the twins, diamnionicity can be predicted. In 90% of diamniotic pregnancies, a separating membrane can be identified sonographically

[8]. The visualization of a membrane permits accurate prediction of diamnionicity, but the inability to identify a membrane separating the fetuses of a twin pregnancy is insufficient evidence to diagnose a monoamniotic twin pregnancy. In the unusual situation in which two placentas can be identified but a separating membrane cannot, diamnionicity still may be inferred because it is embryologically impossible to be dichorionic and monoamniotic (Table 1).

If a single placental mass is identified sonographically, it is uncertain whether the placenta is dichorionic (fused) or monochorionic. The next and simplest step to take in this circumstance is to determine fetal sex (Table 1). If the examiner can show confidently that one of the twins is male and the other is female, then dizygosity is confirmed and dichorionicity and diamnionicity may be inferred with certainty. This is one of the most clinically relevant uses of sex determination in fetuses. Unfortunately, if a single placental mass is seen, and the twins are of the same sex, zygosity remains uncertain and chorionicity cannot be predicted.

The membrane separating the twins consists of two layers of amnion in the monochorionic diamniotic twin pregnancy, whereas two layers of amnion plus two layers of chorion separate the twins in the fused, dichorionic diamniotic twin pregnancy. Because of the additional membranous layers, the dichorionic membrane is thicker than the monochorionic membrane. Therefore, it is theoretically and practically possible to determine chorionicity on the basis of the thickness of the visualized membrane. Recent reports of this technique are encouraging [8–10]. A thick membrane usually is seen in dichorionic pregnancies, but some monochorionic diamniotic gestations also have an apparently thick membrane [10]. Similarly, a thin membrane usually is seen in a monochorionic twin pregnancy. When the strengths and weaknesses of the use of membrane visualization for predicting chorionicity are understood, the observation may be used advantageously in the clinical setting.

Among the weaknesses of the membrane thickness approach is the lack of a strict definition regarding what constitutes a thick (Fig. 1) or a thin (Fig. 2) membrane. Although sonographic discrimination of membranes as thin or thick is subjective, Townsend et al. [10] have shown that with experience, a consistent (100% intraobserver concordance, 91% interobserver concordance) interpretation of membrane thickness can be achieved. Unfortunately, with increasing gestational age, thick membranes become progressively thinner in appearance. Therefore, judgment of membrane thickness is always done more accurately earlier in pregnancy than later. In our experience, this judgment can be made with a high degree of accuracy before 22 weeks of gestation (Fig. 1). Especially in the late first trimester and early second trimester, membrane thickness can be judged with ease and virtually 100% accuracy (Fig. 2).

The second problem with using membrane thickness as a predictor of chorionicity is that thin membranes can be made to appear thick artifactually if the beam strikes the membrane directly perpendicularly (i.e., it specularly reflects) (Fig. 3). The artifactual thickening probably is related to the sonographer recording images that would be most convincing to others in

**TABLE 1: Sonographic Prediction of Chorionicity and Amnionicity**

Sonographic Findings		Sex of Twins	Clinicopathologic Findings	
Placental Masses	Membrane		Chorionicity/Amnionicity	Zygoty
2	Yes	Any	DC/DA	Either
2	No <sup>a</sup>	Any	DC/DA	Either
1	Yes	Differ	DC*/DA	DZ
1	No <sup>a</sup>	Differ	DC*/DA	DZ
1	Yes	Same	DC*/DA	Either
			MC/DA	
	Thick <sup>b</sup>		DC*/DA	Either
	Thin <sup>b</sup>		MC/DA	MZ
1	No	Same	Uncertain	Either
	(stuck twin <sup>b</sup> )		MC/DA	MZ
	(entangled cord)		MC/MA	MZ

Note.—DC = dichorionic placentation (nonfused); DA = diamniotic; DC\* = dichorionic placentation (fused); DZ = dizygotic; MC = monochorionic placentation; MZ = monozygotic; MA = monoamniotic.

<sup>a</sup> Membrane must be present but not observed.

<sup>b</sup> Finding predicts clinicopathologic outcome with a high probability but not certainty. For membrane thickness, probability of correct prediction is highest in late first or early second trimester.

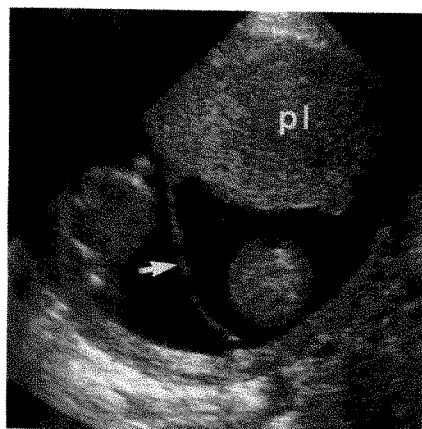


**Fig. 1.**—Dichorionic twin gestation at 18 weeks. Membrane (arrow) is conspicuous during real-time sonography. Thick appearance accurately predicts dichorionicity at this stage of gestation. pl = placenta.

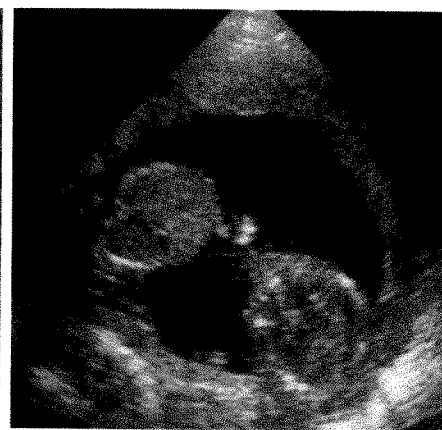


**A**

**Fig. 2.**—Monochorionic diamniotic pregnancy.

**A,** At 11.5 menstrual weeks, no definite membrane is visualized on sonogram. This appearance falsely suggests monoamnioticity.

**B,** 4 weeks later, at 15.6 menstrual weeks, a thin membrane is visible, confirming diamnioticity and monochorionicity.



**B**

proving that a membrane is indeed present and thus photographing images when the membrane is most conspicuous (i.e., appears the thickest). This problem can be avoided by imaging the membrane in a plane not directly perpendicular to the sound beam. This is accomplished best by direct real-time sonographic examination of the membrane whenever uncertainty exists. Artifactual thickening of a thin membrane also may be seen at the attachment site of the membrane to the placenta.

The relatively low sensitivity of the presence of a thin membrane as a predictor of monochorionic diamniotic pregnancies is due to a combination of spurious thickening of the membrane caused by specular reflection and nonvisualization of the membrane. Although in some cases of monochorionic diamniotic pregnancy, a membrane may not be visualized because it is thin and wispy (Fig. 2), in others it is not

visualized because of the close apposition of the membrane to the fetus in that sac. This is caused by a maldistribution of fluid within the twin sacs; in one, a normal to increased amount of amniotic fluid is present, whereas, in the other, a significant diminution occurs in the amount of amniotic fluid. This important phenomenon is discussed in greater detail later.

Potentially, the most sensitive and specific approach for discriminating between monochorionic and dichorionic twin gestations is used early in pregnancy and is an extension of the membrane thickness concept. The structure that radiologists generally refer to as the first trimester "gestation sac," is actually the relatively uniform margin of chorion surrounding the intact embryo before regression of the chorion laeve. Therefore, in dichorionic twin pregnancies, two rings of chorion will be seen, each containing a living embryo (Fig. 4). In monochorionic twin pregnancies, a single ring of chorion will

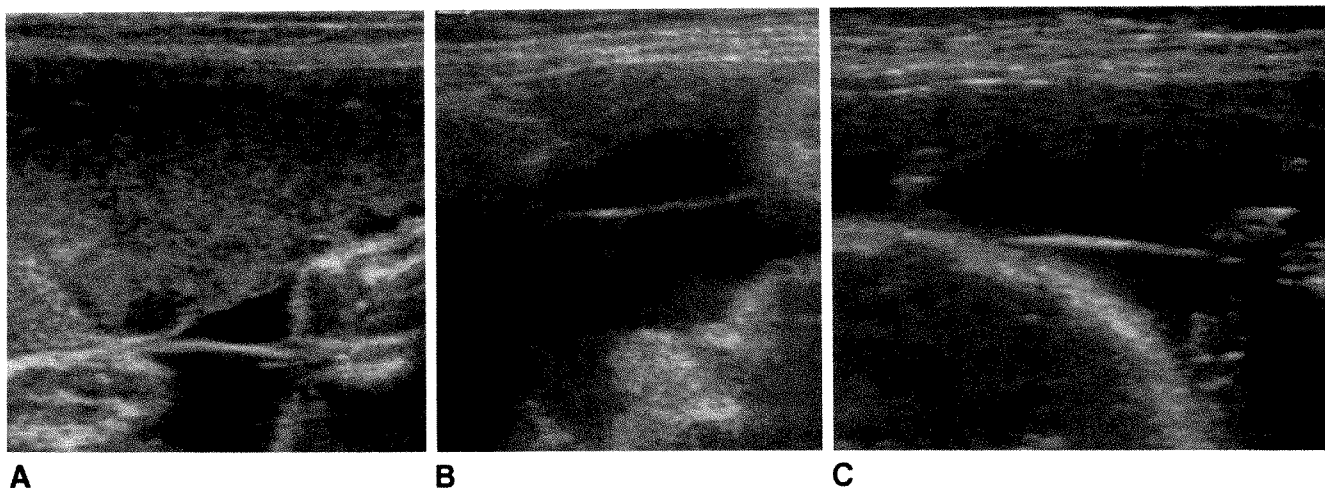


Fig. 3.—A–C, False thick appearance of membrane on sonograms in three different cases of proved monochorionic diamniotic gestations. Membrane is artifactually thickened by specular reflection as beam strikes membrane perpendicularly.

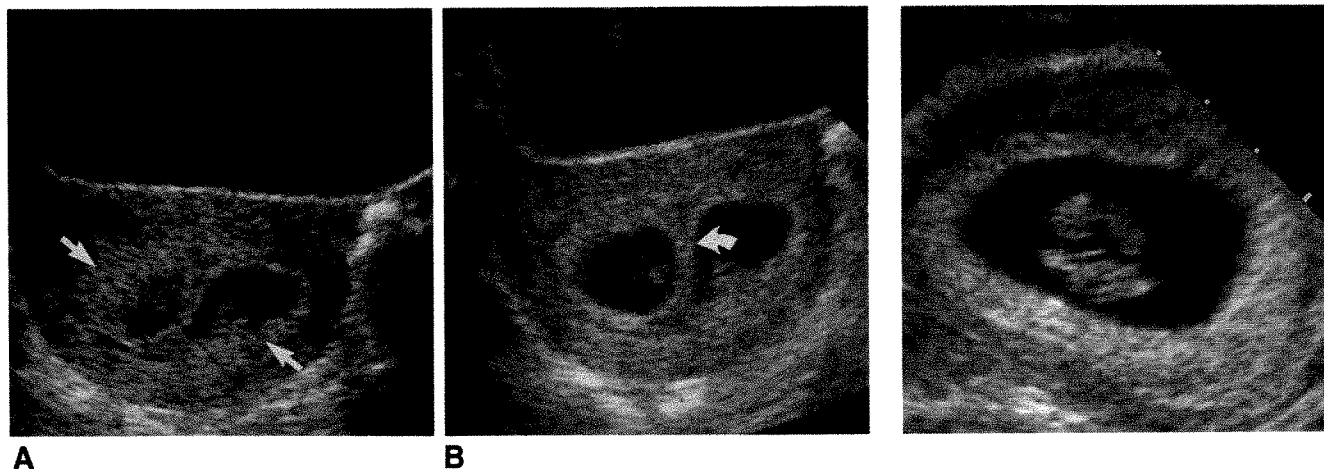


Fig. 4.—A and B, Twin gestations at 8 menstrual weeks. Sonograms show two sacs clearly (straight arrows) separated by a thick membrane (curved arrow). Dichorionicity can be established with 100% certainty at this stage of gestation.

Fig. 5.—Monochorionic pregnancy at 8 menstrual weeks. A single sac on sonogram characterizes pregnancy as monochorionic. Amnionity cannot be determined at this stage. This pregnancy was proved to be diamniotic later in gestation.

be seen that contains both embryos (Fig. 5). Thus, if a woman with a twin pregnancy is examined with sonography early in the first trimester (before 10 weeks), the determination of chorionicity is precise and as easy as counting to two.

Recently, D'Alton and Dudley [11] reported on a new method of determining chorionicity in twin pregnancies, again using observations on the membrane separating the twins. Rather than judging thickness alone, these investigations took advantage of the fact that a dichorionic membrane is composed of four membranous layers (two layers of chorion and two layers of amnion), whereas the monochorionic membrane is composed of two membranous layers only (both amnion). Instead of assessing the effect of the additional layers in the dichorionic twin pregnancy on the membrane thickness, they

counted the membrane layers. If only two layers were sonographically visible, they diagnosed monochorionicity; if three or four layers were visible, they diagnosed dichorionicity. This approach successfully determined the type of placentation in 68 of 69 twin pregnancies. No confirming studies of this method have been published, and we have been unable to confirm this approach in our own experience.

If the methods cited here are used, chorionicity and amnionity (Table 1) can be determined in a high percentage of pregnancies that are less than 22 menstrual weeks old and in a relatively high percentage of later pregnancies. However, an attempt to determine amnionity and chorionicity should be made in any examination of a twin gestation. Determining that twins are monochorionic is important because of the



extraordinary risk that accompanies the situation. When twins are monochorionic, the probability is high (85–100%) that the fetuses will share vascular anastomoses at the placental level [2]. These anastomoses may lead to a number of syndromes that greatly increase twin mortality (twin transfusion syndrome, twin embolization syndrome, acardiac parabiotic twin). Indeed, for monozygotic twins, mortality figures increase with each degree of sharing that the twins encounter. Thus, twins that share a placenta (monochorionic) have a mortality rate that is 2.5 times greater than that of twins that do not share a placenta (dichorionic). The mortality rate in twins that must share an amniotic cavity, as well increases by a factor of five. Similarly, in fetuses that have a significant admixture of blood because of shared circulatory systems at the placental level (twin transfusion syndrome), the mortality rate increases by a factor of approximately five and in extreme cases ("stuck twin" phenomenon) by a factor of nine. Finally, in those unusual fetuses that actually share vital organs of their bodies (most conjoined twins), the relative risk of death increases so greatly that survival is uncommon [1–4, 7].

### **Monochorionic Twin Syndromes**

#### *Twin Transfusion Syndrome*

The twin transfusion syndrome (TTS) results from intra-uterine vascular shunting between the circulations of twins that share a common placenta [2, 12, 13]. The shared circulation usually occurs in a single cotyledon. The sonographic and clinical findings, as well as the outcome, are related to the type and degree of intraplacental vascular connections and the volume of blood that is transfused from the donor to the recipient twin. Sonographically, it is not possible to see the vascular communications at the placental level even with sophisticated instrumentation (color flow Doppler imaging). However, it is possible to identify a number of features that make possible a confident diagnosis of TTS.

It is critically important to be as certain as possible that the twins are monochorionic before the diagnosis of TTS is suggested. Vascular communications between twin circulatory systems is extraordinarily common in monochorionic twin pregnancies and rare, if present at all, in dichorionic twins, whether the placentas are fused or separate [2, 13]. Thus, if sonographic findings (different sexes of the twins, the ability to identify two placental masses, or early confirmation of two gestational sacs or a thick membrane) confirm dichorionicity, then a diagnosis of TTS should not be made regardless of other features that may suggest it. In addition to monochorionicity, a compilation of other findings must be present before TTS can be diagnosed [14]. A significant disparity in the sizes of the twin fetuses is a universal feature of this syndrome. Most often, one twin is normal-sized or nearly so and the other is small and commonly satisfies the established criteria for intrauterine growth retardation. Alternatively, the predicted weight of the smaller twin may not be less than the 10th percentile for gestational age but may be discordantly small (i.e., predicted weight 25% less than that of the larger twin). Unfortunately, earlier in pregnancy, the disparity in size

may not be so striking. In addition to the discrepancy in size, usually a disparity in the amount of amniotic fluid surrounding each twin is visible. The fetus that is growth retarded tends to have diminished amniotic fluid, and the normal sized fetus tends to have increased amniotic fluid. This disparity in the volume of amniotic fluid often progresses to extremes in which one twin is in a markedly polyhydramniotic sac and the other is in a virtually anhydramniotic sac.

The appearance of this extreme disparity has come to be known as the stuck-twin sign (Fig. 6). [7]. The stuck-twin phenomenon originally was described within the context of proving diamnionicity when no membrane was sonographically visible. One fetus of a twin pair moved freely within a normal or increased amount of amniotic fluid, but in each case, the other fetus resided in a position adjacent to the lateral or anterior uterine wall. Further, changes in the position of the mother failed to show an appropriate gravitational response by the "stuck twin," indicating that the fetus was held in place by an inapparent membrane. Other features may be seen with this phenomenon. The membrane that holds the fetus in a fixed position also presses the umbilical cord against the torso of the fetus. This observation is made easily when it is sought specifically. Once the radiologist is convinced that the fetus is being held in place by a membrane, searching the margins of the fetus will often disclose the membrane. Since its original description, it has been noted that the stuck-twin phenomenon occurs most commonly with TTS. However, it would be inappropriate to consider it synonymous with TTS.

Other features commonly are identified in TTS but need not be documented to make the appropriate diagnosis. These features include the development of nonimmune hydrops in one of the twins, most commonly in the normally growing twin in the polyhydramniotic sac (the recipient twin) [15–17]. Similarly, a disparity in the umbilical artery Doppler profiles of the two fetuses is common, although the disparity is not a reliable predictor of which fetus is the donor and which is the recipient, nor can it be used to predict outcome with certainty [18].

The sonographic features of developing TTS may not be sufficiently manifest to permit confident diagnosis in the early second trimester (14–20 weeks). Therefore, it may be difficult to counsel parents regarding the future course and management of their pregnancy. Unfortunately, sequential observation is the only course that can be offered.

The mortality rate from TTS is high, from 40 to 70% [5, 12, 16, 19, 20]. When TTS is fully manifested by the stuck-twin phenomenon, it is a highly lethal entity. Among 25 cases of the stuck-twin phenomenon, the perinatal morbidity was 100% for all twin pairs and prematurity occurred in all cases [17]. Perinatal mortality was 88% for the larger twin and 96% for the smaller (stuck) twin. Simple mathematical calculations with these statistics indicate that both fetuses are commonly lost. If one fetus survives, it is usually the fetus in the polyhydramniotic sac, but occasionally the reverse situation occurs. Thus, it is not possible to predict with certainty which of the fetuses might survive. Despite this inability, these devastatingly high mortality figures have led to aggressive and unusual therapies in recent years [21, 22], including

surgical extraction of one of the twins (usually the oligohydramniotic twin) with continued gestation in an effort to salvage the sibling (surgical selective twin termination).

### *Twin Embolization Syndrome*

A rare complication of TTS follows the death of one twin in utero. Benirschke [2] noted a case of hydranencephaly, splenic infarction, and bilateral renal cortical necrosis in a surviving monozygotic twin in which the co-twin had died in utero. He theorized that the infarcted organs in the surviving twin resulted from transfusion of thromboplastin-rich blood from the dead twin through the vascular anastomoses in the shared placenta. Others [23–26] who have examined similar cases have theorized further that clot or detritus from the dead twin embolizes into the circulation of the surviving twin. The damage to the surviving fetus appears to be related to its gestational age at the time of death of the co-twin. Death of the co-twin early in pregnancy results in atresia and tissue loss; death later in pregnancy results in tissue infarction. Rapidly proliferating organs such as the growing brain, kidneys, and gut appear to be particularly susceptible to the twin embolization syndrome (TES). Brain lesions noted with this syndrome include hydranencephaly, porencephaly, cystic encephalomalacia, and ex vacuo hydrocephalus; all are vascular disruptive lesions.

A recent review of the sonographic findings in six such fetuses showed that the surviving co-twin initially had normal intracranial sonographic anatomy but that subsequently structural brain abnormalities developed after the death of its sibling in utero [24]. Ventriculomegaly was the most commonly identified abnormality, but porencephalic cyst formation, diffuse cerebral atrophy (Fig. 7), and microcephaly were identified also. Gastrointestinal abnormalities were shown prenatally in two fetuses, and in one fetus renal cortical necrosis was sonographically suspected.

The prevalence of TES in the setting of antepartum death of one of a monozygotic twin pair is not firmly established. However, when TES occurs, the prognosis is grim. In the sonographic series under consideration [24], two fetuses were aborted because of sonographic evidence of severe brain damage, and neurologic follow-up on the four live-born twins showed moderate to severe developmental delay.

Prenatal sonographic recognition of TES has important potential therapeutic implications. Theoretically, premature delivery of the affected surviving co-twin may reduce the degree of cerebral damage. However, the theoretical benefit must be balanced with the inherent risks of preterm delivery. It is likely that severe, irreversible damage has occurred by the time the sonographic abnormalities are apparent. Therefore, we and others recommend against premature delivery of the survivor. However, sonographic monitoring of pregnancies with a dead twin, especially twin pregnancies known to be monozygotic, may enable recognition of structural defects in the survivor that are characteristic of TES. Recognition of TES is especially important in order to provide accurate counseling for parents about an anticipated poor outcome. The observations still may alter the timing or mode of delivery, but in the negative sense.

As noted, attempts have been made to terminate one twin selectively in the management of an abnormal twin pregnancy. If selective termination is considered, determination of the chorionicity of the gestation is essential to define fully the risks to the surviving normal sibling. Dichorionic twins are not at risk, whereas monozygotic twins are at risk, for TES. Thus, physicians performing selective feticide in the management of TTS should consider TES as an additional risk to the surviving twin. Indeed, this possibility is what has led researchers to interrupt the umbilical cord surgically and physically extract the smaller of the twins in TTS in order to avoid the possible consequence of TES. Although TES is a rare complication after the death of one of monozygotic twins,

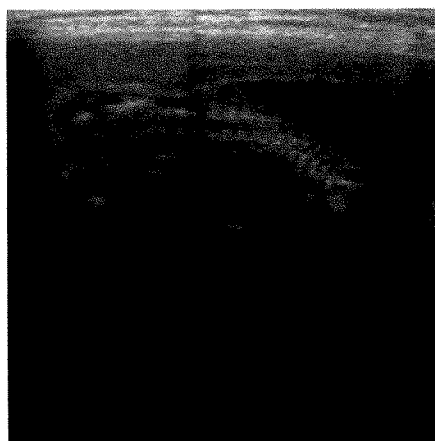


Fig. 6.—Stuck twin. Smaller of twin fetuses was relatively immobile during real-time sonography. Position of this fetus was fixed by a closely apposed amniotic membrane that was difficult to visualize.

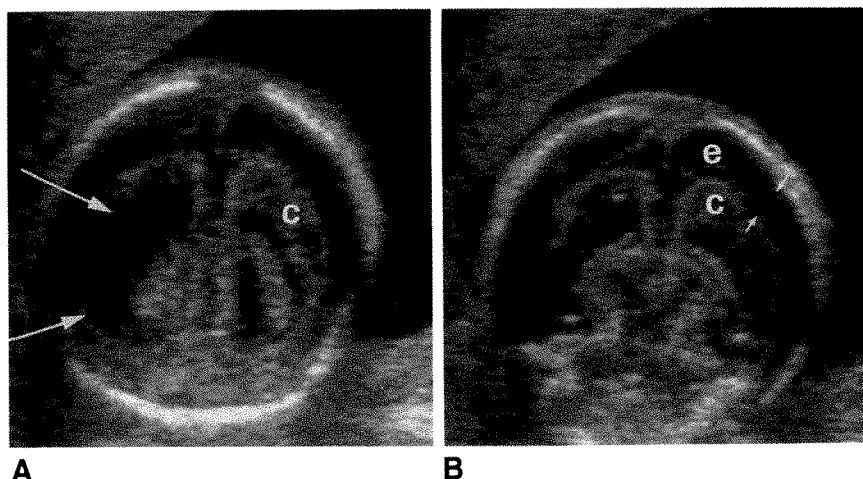


Fig. 7.—A and B, Twin embolization syndrome. Increased echoes in cerebral cortex (c) are noted on sonograms of surviving twin of this monozygotic pregnancy. Ventriculomegaly (long arrows) and marked atrophy are evidenced by enlarged extraaxial space (short arrows, e).

it appears to be a sonographically recognizable syndrome and one that has important prognostic implications for the surviving co-twin.

#### *Acardiac Parabioc Twin*

Acardiac parabioc twin can be seen in monochorionic pregnancies only [27–32]. Although some acardiac twins have an anomalous two-chambered heart, fundamentally what is seen on sonograms is a fetus in utero that, without the aid of a functioning cardiac pump within its own torso, continues to grow progressively, albeit abnormally, throughout gestation. The only conceivable explanation for this bizarre circumstance is that the co-twin is providing the blood supply to its anomalous sibling. Although the vascular communications are highly complex, at the least an arterial-to-arterial and venous-to-venous communication must be present to complete the circuit. Interestingly, in the acardiac fetus, the direction of blood flow in the umbilical cord is reversed. In the umbilical vein, flow is away from the fetus, whereas in the umbilical artery, it is toward the fetus. This is easily understood: the blood entering the body of the anomalous fetus is being pumped directly from the umbilical artery of the co-twin into the umbilical artery of the acardiac twin.

Obviously, the anomalous fetus has no potential for survival. Indeed its "life" depends entirely on the blood supplied by its co-twin through the vascular anastomoses at the placental level. Immediately on delivery, these communications are severed and the "life" of the acardiac fetus halts. Thus, from one perspective, the expected mortality in this twin syndrome must be at least 50% because none of the anomalous co-twins can attain viability. Unfortunately, in our own small experience, there is also substantial risk to the normally developed co-twin that is providing the blood supply to the anomalous fetus. Hemodynamically, this fetus must circulate blood not only for its own body and half of the placenta but also for the body of the co-twin and its half of the placenta. We have seen the sudden death of normal co-twins, presumably because of this stress. Mortality for the normal co-twin has been estimated at 50% [27]. However, if the normal co-twin can be delivered successfully after a point of achieving viability, normal development can be anticipated.

The acardiac parabioc twin may share the same amniotic cavity with the co-twin, which places the pregnancy at the additional risk of cord knotting. It also may be contained within its own amniotic cavity. In our experience, a disparity always exists in the distribution of fluid between the twins; the anomalous twin is in the sac that contains the lesser amount of fluid (usually oligohydramniotic). Indeed, the anomalous twin sac may be anhydramniotic, with the acardiac twin apparently stuck to the uterine wall.

Acardiac fetuses have a relatively characteristic appearance. Usually, the fetus has no head, which leads to one of several synonyms for this entity, acardiac acephaly; however, anencephaly or severe microcephaly may be present. These fetuses tend to have diffuse integumentary edema, and nearly all have cystic hygromas as well (Fig. 8). The upper extremities are either rudimentary or completely absent. However, the

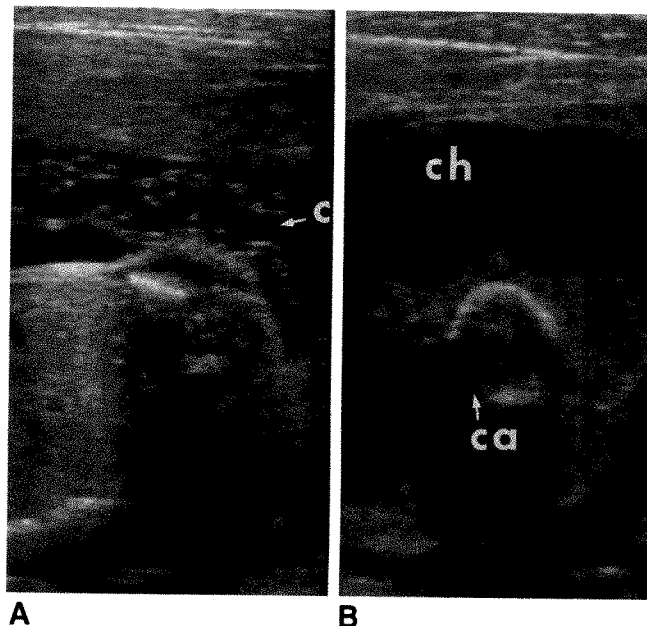


Fig. 8.—Acardiac twin.

A, Sonogram of nonhydropic normal twin shows a prominent umbilical vein in umbilical cord (c).

B, Sonogram of acardiac twin shows diffuse integumentary edema and cystic hygroma (ch). ca = calvaria.

lower extremities are better formed, and the femur, which often appears normal in configuration, can be measured and growth is evident when serial examinations are done. The degree of growth is never as great as the normal co-twin, in our experience. As the name suggests, the thoracic region of the fetuses is characterized by the absence of any visible cardiac pulsation. However, Doppler flow signals can be obtained in the umbilical cord, although the direction of flow is reversed.

Again, identification of this syndrome has potential clinical implications. Extraction of an acardiac parabioc twin has been attempted in utero to prevent the sudden death of the normal co-twin. Similarly, when the twins are monoamniotic, an alteration of the mode of delivery may be undertaken (see section on monoamnioticity). At the least, careful monitoring of this highly anomalous situation is warranted to assess the normal co-twin for growth, development of hydrops fetalis, or deterioration of biophysical profile score or Doppler vascular assessment.

#### *Conjoined Twins*

Conjoined twins are a rare malformation; the estimated prevalence is 1:50,000 to 1:100,000 births [33, 34]. As with all pathologic events associated with monozygosity, conjoined twinning occurs sporadically and does not recur. Conjoined twins develop from incomplete division of the embryonic disk. Division of the embryonic disk after 13 days after fertilization is usually incomplete, resulting in fusion of the twins [6]. Although males are the more common sex among monozygotic twins, 70% of conjoined twins are females



[34]. Most are premature, and the mortality rate is extremely high. Prenatal diagnosis of conjoined twins and characterization of the severity of the malformations is desirable for optimal obstetric management [35, 36]. Severe forms of conjoined twins diagnosed early can be considered for termination via vaginal delivery. In late pregnancy, severity of conjoining influences the decision for vaginal vs cesarean delivery. The latter is reserved for potentially viable and separable fetuses, to minimize fetal morbidity and mortality, and for conjoined twin configurations that obstruct labor.

The site and extent of twin fusion are infinitely variable. Classification systems for conjoined twins are based on the fused anatomic region. The name of the region usually is followed by the suffix *-pagus*, Greek for fastened. For example, *craniopagus* is head-to-head fusion; *thoracopagus* is chest-to-chest fusion; *omphalopagus* is abdomen-to-abdomen fusion [37]. These fusions are usually anterior-anterior and may involve more than one body region. Side-to-side fusions usually begin at the head or buttock end and tend to be quite extensive. It is customary to name these large lateral fusions, which incorporate multiple regions, on the basis of the anatomic part that remains separate. For example, *dicephalus* means two heads but fusion of the thorax and abdomen.

We have examined 12 sets of conjoined twins prenatally, including six thoracoomphalopagus, one thoracopagus, one craniopagus, two dicephalus, and two dipygus conjoined twins (R. Barth, personal communication). Prenatal sonographic findings were used to diagnose conjoined hearts in all cases in which the thorax was joined. One case of conjoined twins was diagnosed on the basis of transabdominal sonography at 11 weeks (Fig. 9). Transvaginal sonography done on the same day better delineated fusion as thoracoomphalopagus and also was used to diagnose a shared heart.

Prenatal diagnosis of conjoined twins was rare in the pre-sonography era. Frequently, the earliest recognition of this malformation occurred during the second stage of labor, with observation of obstruction to delivery. Prenatal sonographic diagnosis of conjoined twins may be straightforward: joining of fetal parts may be obvious (Fig. 10); however, a careful

approach is necessary to avoid misdiagnosis. The diagnosis should be suspected in any twin pregnancy if a single placental site is seen and a separating amniotic membrane cannot be confirmed (no dichorionic or diamniotic twin gestation can be conjoined). Significant sonographic findings include inability to detect separate fetal skin contours (Figs. 9 and 10); both fetal heads persistently at the same level; no change in the relative position of the fetuses; breech and, less commonly, bicephalic presentation; backward flexion of the cervical spine; and a single umbilical cord with more than three vessels. Other findings include shared heart (Fig. 10), liver, brain, or other organs [38–42].

The joining bridge between the fetuses may be relatively small and pliable, allowing rotation of the twins. Thus, it is possible for conjoined twins to have opposite presentations (i.e., cephalic-breech). When the presentation of the twins differs, the diagnosis of conjoined twins may be missed. Alternatively, with severe conjoining, twins may be melded into a conglomerate of tissue, mimicking a singleton pregnancy. Careful search for duplication of any anatomic parts, including the brain, heart, liver, extremities, and spine, will confirm the correct diagnosis of conjoined twins.

Prenatal diagnosis of conjoined twins allows planned obstetric management, including decisions on approach for delivery and minimization of maternal and fetal morbidity and mortality [35, 36]. Early diagnosis is desirable in those cases in which death is highly possible. This will allow parents potentially to select therapeutic termination of the pregnancy before the 24th week of gestation. Precise delineation of the conjoining is important in determining the likelihood of postnatal viability, separability, and mode of delivery. The identification of a shared heart, in particular, carries a poor prognosis with no hope for successful postnatal separation (Fig. 10).

The most common types of conjunction are thoracopagus, omphalopagus, and thoracoomphalopagus twins. These account for more than 70% of conjoined twins [33–35, 43]. Seventy-five percent of conjoined twins are stillborn or die within 24 hr. The remainder survive long enough to be considered for surgical separation. Thoracopagus twins have a high prevalence of congenital heart disease related to the

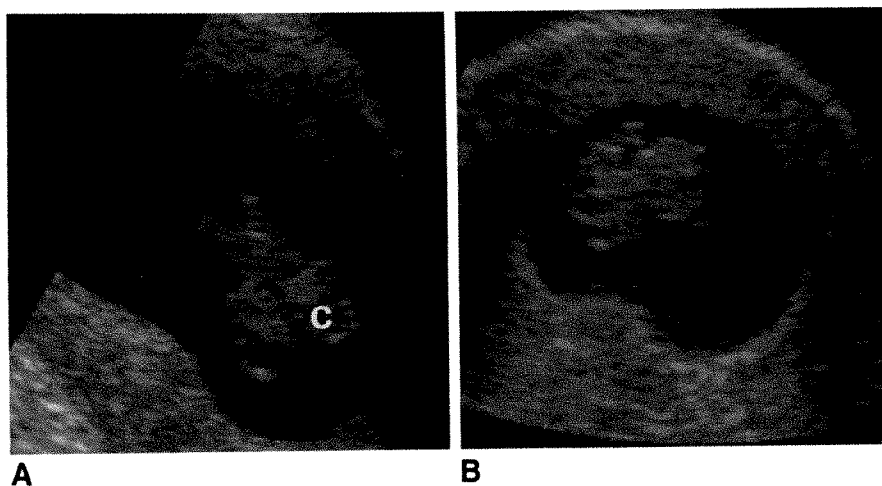
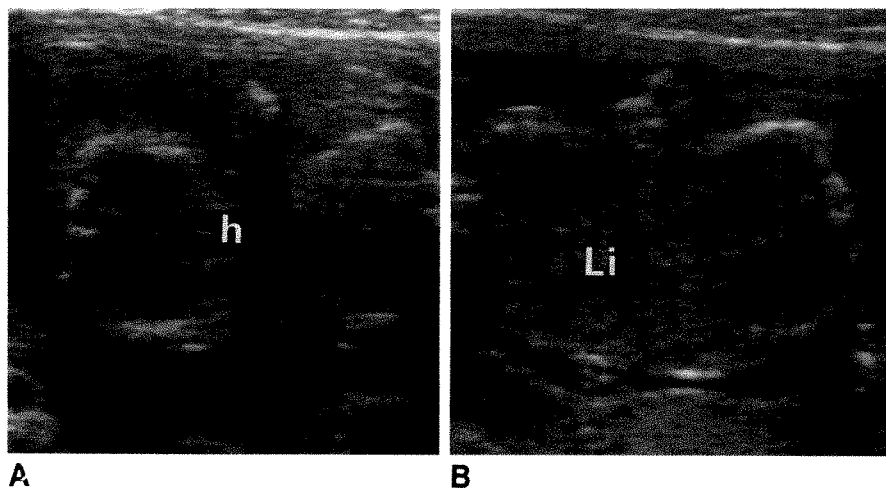


Fig. 9.—A and B, Thoracoomphalopagus twins diagnosed with sonography at 11 menstrual weeks. c = cephalic pole.

Fig. 10.—A and B, Thoracoomphalopagus twinning. Sonograms show fetuses joined at chest (A) and abdomen (B) and sharing a liver. h = heart; Li = liver.



degree of union. The simplest form of conjoining of the hearts is sharing a common pericardium that contains two separate and complete hearts [44]. However, 75% of thoracopagus twins have extensive conjoined hearts precluding successful surgical separation [45]. The most frequent abnormality is two ventricles with various numbers of atria. Ventriculoseptal defect is present in virtually all patients. Omphalopagus twins have a high prevalence of conjoined livers [38]. Associated malformations in omphalopagus include gastrointestinal anomalies, usually omphaloceles, and congenital heart disease. Prenatally, sonography is the most definitive method for diagnosis and characterization of conjoined hearts, thereby predicting chances for postnatal viability. Identification of a common heart indicates a negligible chance for successful surgical separation.

#### *Monoamniotic Nonconjoined Twins*

Sonographic identification of nonconjoined monoamniotic twin pregnancies is important prognostically and can affect obstetric management. Monochorionic monoamniotic twin pregnancies have the highest mortality rate of otherwise uncomplicated twin pregnancies [5]. This is related both to a high frequency of complications present in all twin pregnancies (particularly preterm delivery) and to complications that are unique to these gestations.

The lack of a membrane separating the twin fetuses in monoamniotic pregnancies distinguishes these pregnancies from all other twin pregnancies and may permit prenatal sonographic diagnosis. Several studies [7–10, 46] have shown, however, that lack of sonographic visualization of a membrane is not, on its own, predictive of monoamnicity (Fig. 2). Lack of a separating membrane between the fetuses allows the two umbilical cords to contact each other and become tangled. Because several loops of apparently intertwined umbilical cord may be either the entangled cords of two twins or only the redundant cord of a single twin folded on itself, it is essential to trace both fetal cords to the entangled mass before suggesting the diagnosis of monoam-

nicity (Fig. 11) [47]. Color flow Doppler imaging most likely will be useful in this pursuit.

A complication that accounts for most of the increased mortality in monoamniotic twins is true knotting of the cords [48, 49]. A true knot may cut off circulation, resulting in sudden fetal death, and it undoubtedly accounts for the high fetal loss rate observed in this group. Importantly, the sonographic observation of entanglement of the umbilical cords does not imply impending fetal death [47]. However, this appearance is the basis for the diagnosis of monoamnicity and is the only reliable feature for diagnosing this problem. The cord is a passive structure. Therefore, if the cords of the identical twins are entangled, it can be inferred accurately that no membrane separates the fetuses. Intertwining of twin extremities is not reliable because the extremities can deform a separating membrane. Intertwining of extremities (locking of the twins) is, however, an important observation, also having obstetric implications, but it is not diagnostic of monoamnicity.

Knotted cords may be seen in cases in which the outcome is good for both twins. In our experience, some pregnancies with sonographically visualized entangled cords were monitored for up to 16 weeks without fetal compromise [47]. Doppler sonography of the umbilical vessels may be useful in evaluating which entangled cords have knots with hemodynamic significance, but this has yet to be studied. It is, however, unlikely that any form of monitoring will be useful in predicting the acute cord accident that results in the sudden death of both fetuses. Such accidents tend to occur, however, after the 33rd week of gestation.

The potential for umbilical cord entanglement does not exist in all monoamniotic twin pregnancies. As noted, all conjoined twins are monoamniotic. However, such twins must move in unison. Therefore, they cannot entangle their cords to form true cord knots in the same way that nonconjoined monoamniotic twins do. Further, in many conjoined twins the umbilical cords are fused. This is seen in thoracopagus and omphalopagus twins in which the fused cords may have three, four, five, or even six vessels. Fused cords cannot knot. Therefore, the high mortality rate noted in conjoined twinning is unrelated to cord accidents caused by cord knotting.

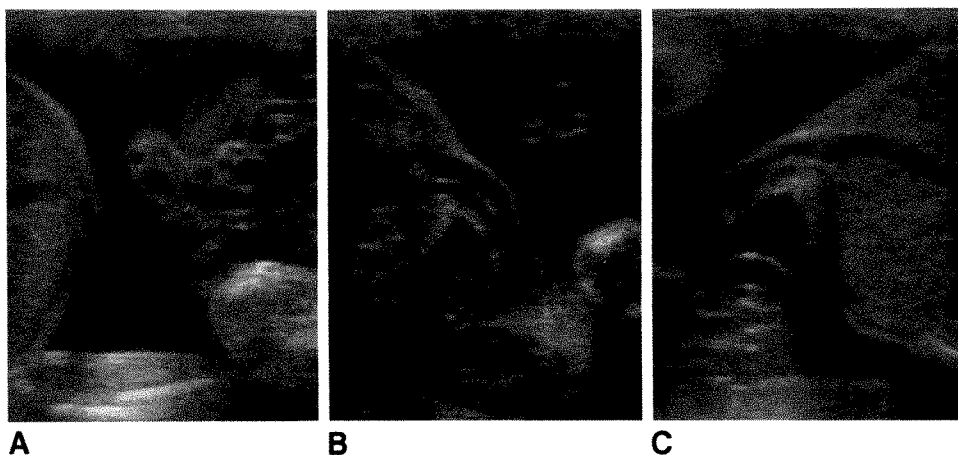


Fig. 11.—A–C, Monoamniotic twins. During real-time sonography, cord of one twin (B) and that of other twin (C) could be followed to an area where they appear to be entangled (A).

Foreknowledge that a twin pregnancy is monoamniotic allows informed obstetric planning. It has been suggested that prenatal recognition of monoamnicity may dictate cesarean delivery. In some of the cases that we have followed, the referring obstetrician chose this approach, with good outcomes [47]. Others chose to follow the pregnancies closely with fetal monitoring for any signs of distress and use surgical delivery as necessary. It seems unlikely that fetal monitoring can be used to predict the acute cord accidents that result in rapid death, but other hemodynamic complications of cord knots (hydrops fetalis) may be detectable. One of the pairs of twins that we monitored was delivered vaginally. An unusual cord complication may occur at the time of vaginal delivery of monoamniotic twins. The cord of the second twin unknowingly may be divided at the time of delivery of the first twin, if it is wrapped around the neck of the first twin. Accurate diagnosis of monoamnicity before delivery could prevent such a mishap.

The observation of entangled umbilical cords in the absence of a membrane separating twin fetuses appears to be a reliable sign for the diagnosis of monoamniotic twin pregnancy. However, the frequency with which this observation will be made is uncertain. Therefore, sonographic visualization of entangled umbilical cords is a specific sign for the diagnosis of monoamniotic twin pregnancies. However, its accuracy remains unknown.

## Conclusions

Sonography has made a dramatic impact on the obstetric management of twin pregnancies. This is based in part on the use of sonography to diagnose prenatally or, more commonly, to exclude the syndromes and complications of twinning that have been described here. In all twin pregnancies, the risk for perinatal morbidity and mortality is high, compared with that in singleton gestations, but when one of the described complications is recognized, the difficulties in management are compounded dramatically. Therefore, despite the relative rarity of some of the entities described, it is vitally important to be familiar with these problems and their sonographic evaluation and diagnosis.

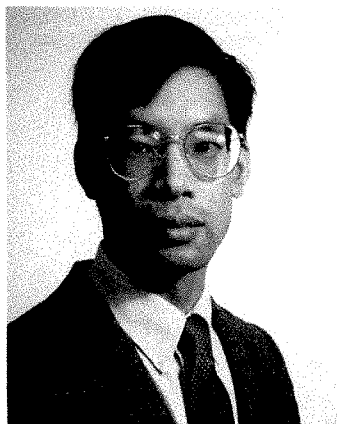
## REFERENCES

1. Berkowitz, RL. Multiple gestations. In: Gabbe SG, Niebyl JR, Simpson JL, eds. *Obstetrics*. New York: Churchill Livingstone, 1986.
2. Benirschke K. Twin placenta in perinatal mortality. *NY J Med* 1961;61:1499–1508.
3. Litschgi M, Stucki D. Course of twin pregnancies after fetal death in utero. *Z Geburtshilfe Perinatol* 1980;184:227–230.
4. D'Alton ME, Newton ER, Cetrulo CL. Intrauterine fetal demise in multiple gestation. *Acta Genet Med Gemellol (Roma)* 1984;33:43–49.
5. Benirschke K, Kim CK. Multiple pregnancy. *N Engl J Med* 1973;288:1276–1329.
6. Moore KL. *The developing human: clinically oriented embryology*, 4th ed. Philadelphia: Saunders, 1988.
7. Mahony BS, Filly RA, Callen PW. Amnionicity and chorionicity in twin pregnancies: prediction using ultrasound. *Radiology* 1985;155:205–209.
8. Hertzberg BS, Kurtz AB, Chor HY. Significance of membrane thickness in the sonographic evaluation of twin gestations. *AJR* 1987;148:151–153.
9. Barss VA, Benacerraf BR, Frigoletto FA. Ultrasonographic determination of chorion type in twin gestation. *Obstet Gynecol* 1985;66:779–783.
10. Townsend RR, Simpson GF, Filly RA. Membrane thickness in ultrasound prediction of chorionicity of twin gestations. *J Ultrasound Med* 1988;7:327–332.
11. D'Alton ME, Dudley DK. The ultrasonographic prediction of chorionicity in twin gestations. *Am J Obstet Gynecol* 1989;160:557–561.
12. Rausen AR, Seki M, Strauss L. Twin transfusion syndrome. *J Pediatr* 1965;66:613–628.
13. Robertson EG, Neer KJ. Placenta injection studies in twin gestation. *Am J Obstet Gynecol* 1983;147:170–174.
14. Danskin FH, Nelson JP. Twin-to-twin transfusion syndrome: what are appropriate diagnostic criteria? *Am J Obstet Gynecol* 1989;161:365–369.
15. Coleman BG, Grumbach K, Arger PH, et al. Twin gestations: monitoring of complications and anomalies with ultrasound. *Radiology* 1987;165:449–453.
16. Brown DL, Benson CB, Driscoll SG, Donbilet PM. Twin-twin transfusion syndrome: sonographic findings. *Radiology* 1989;170:61–63.
17. Patten RM, Mack LA, Harvey D, Cyr DR, Pretorius DH. Disparity of amniotic fluid volume and fetal size: problem of stuck twin—ultrasound studies. *Radiology* 1989;172:153–157.
18. Pretorius DH, Manchester D, Barkin S, Parker S, Nelson TR. Doppler ultrasound of twin transfusion syndrome. *J Ultrasound Med* 1988;7:117–124.
19. Crane JP. Sonographic evaluation of multiple pregnancy. *Semin Ultrasound CT, MR* 1984;5:144–156.
20. De Lia JE, Emery MG, Sheaf SA, Jennison TA. Twin transfusion syndrome: successful in utero treatment with digoxin. *Int J Gynaecol Obstet* 1985;23:197–201.
21. Golbus MS, Cunningham N, Goldberg JD, Anderson R, Filly R, Callen P. Selective termination of multiple gestations. *Am J Med Genetics* 1988;31:339–348.



22. Wittmann BK, Farquharson DF, Thomas WDS, Baldwin VJ, Wadsworth LD. The role of feticide in the management of severe twin transfusion syndrome. *Am J Obstet Gynecol* **1986**;155:1023-1026
23. Schinzel AAGI, Smith DW, Miller JR. Monozygotic twinning and structural defects. *J Pediatr* **1979**;95:921-930
24. Benirschke K, Driscoll SG. *The pathology of the human placenta*. New York: Springer-Verlag, **1967**:91-179
25. Hoyme HE, Higgenbottom MC, Jones KL. Vascular etiology of disruptive structural defects in monozygotic twins. *Pediatrics* **1981**;67:288-291
26. Patten RM, Mack LA, Nyberg DA, Filly RA. Twin embolization syndrome: sonographic detection and significance. *Radiology* **1989**;173:685-689
27. Van Allen MI, Smith DW, Shepart JH. Twin reversed arterial perfusion (TRAP) sequence: a study of 14 twin pregnancies with acardius. *Semin Perinatol* **1993**;7:285-293
28. Kaplan C, Benirschke K. The acardiac anomaly: new case reports and current status. *Acta Genet Med Gemellol* **1979**;28:51-59
29. Bieber FR, Nance WE, Morton CC, et al. Genetic studies of an acardiac monster: evidence of polar body twinning in man. *Science* **1981**;213:775-777
30. Gibson JY, D'Cruz CA, Patel RB, Palmer SM. Acardiac anomaly: review of the subject with case report and emphasis on practical sonography. *J Clin Ultrasound* **1986**;14:541-545
31. Lindahl SA, Baldwin V, Wakeford J. Early diagnosis of an acardiac acephalus twin by ultrasound. *Med Ultrasound* **1984**;8:105-107
32. Benson CB, Bieber FR, Genest DF, Doubilet PM. Doppler demonstration of reversed umbilical blood flow in an acardiac twin. *J Clin Ultrasound* **1989**;17:291-295
33. Edmonds LC, Layde PM. Conjoined twins in the United States 1970-1977. *Teratology* **1982**;25:301-308
34. Potter EL, Craig SM. *Pathology of the fetus and the infant*, 3rd ed. Chicago: Year Book Medical, **1975**:220-236
35. Sakala EP. Obstetric management of conjoined twins. *Obstet Gynecol* **1986**;67:21S-25S
36. Vaughn TC, Powell LC. The obstetrical management of conjoined twins. *Obstet Gynecol* **1979**;53:67
37. Guttmacher AF. Biographical notes on some famous conjoined twins. *Birth Defects* **1967**;3:10
38. Gore RM, Filly RA, Parer JP. Sonographic antepartum diagnosis of conjoined twins—its impact on obstetric management. *JAMA* **1982**;247:3351-3353
39. Chen HY, Hsieh FJ, Huang LH. Prenatal diagnosis of conjoined twins by real-time sonography: a case report. *JCU* **1983**;11:94-96
40. Koontz WL, Herbert WN, Seeds JW, et al. Ultrasonography in the antenatal diagnosis of conjoined twins: a report of two cases. *J Reprod Med* **1983**;28:627
41. Hubinent C, Partola D, Rothschild E, et al. Dicephalus: unusual case of conjoined twins and its prepartum diagnosis. *Am J Obstet Gynecol* **1984**;149:693-695
42. Maggio M, Callen NA, Hamod KA, Sanders RC. The first-trimester ultrasonographic diagnosis of conjoined twins. *Am J Obstet Gynecol* **1985**;152:833-835
43. Abrams SL, Callen PW, Anderson RL, Stephens JD. Anencephaly with encephalocele in craniopagus twins: prenatal diagnosis by ultrasonography and computed tomography. *J Ultrasound Med* **1985**;4:485-488
44. Nichols BL, Blattner RJ, Rudolph AJ. General clinical management of thoracopagus twins. *Birth Defects* **1967**;3:38-51
45. Leachman RD, Latson JR, Kohler CM, McNamara DG. Cardiovascular evaluation of conjoined twins. *Birth Defects, Orig Art Ser* **1967**;3:52-62
46. Blane CE, Di Pietro MA, Johnson M, et al. Sonographic detection of monoamniotic twins. *JCU* **1987**;15:394
47. Townsend RR, Filly RA. Sonography of non conjoined monoamniotic pregnancy. *J Ultrasound Med* **1988**;7:665-670
48. Solerino LJ. Monoamniotic twinning: a survey of the American literature since 1935 with a report of four new cases. *Obstet Gynecol* **1959**;14:205
49. Auckerman H, Berzezinski A. Monoamniotic twin pregnancy. *Gynaecologic* **1960**;150:290

## Felix S. Chew, Recipient of the Melvin M. Figley Fellowship in Radiology Journalism



Out of more than 30 highly qualified candidates, Felix S. Chew was chosen to be the first recipient of the Melvin M. Figley Fellowship in Radiology Journalism sponsored by the American Roentgen Ray Society and the *American Journal of Roentgenology*.

Dr. Chew will serve one month in the La Jolla, CA, editorial office of the *AJR*, during which he will learn the fundamentals of medical writing, manuscript preparation, peer review, manuscript editing, the ethics of medical journalism, and journal publication and printing in personal tutorials given by the *AJR* editors and editorial staff.

Dr. Chew is an assistant professor of radiology at the Massachusetts General Hospital and Harvard Medical School. He received an A.B. from Princeton University, where he was a National Merit Scholar, and an M.D. from the University of Florida. From

1984 until 1987, Dr. Chew was a radiology resident at the SUNY Health Science Center in Syracuse, NY, and in 1987, he joined the faculty at that institution. In 1989, he accepted his present position at the Massachusetts General Hospital.

Author of 20 articles and a book on skeletal radiology, Dr. Chew has shown an interest in medical publication since he was a resident. He has published four articles on radiology journalism in the *AJR* in recent years, including "The scientific literature in diagnostic radiology for American readers: a survey and analysis of journals, papers, and authors," "Coauthorship in radiology journals," and "*AJR*: the 50 most frequently cited papers in the past 50 years." He has served as a manuscript reviewer for the *AJR* since 1987.

## Pictorial Essay

# Identification of Retained Firearm Projectiles on Plain Radiographs

Gerald D. Dodd III<sup>1</sup> and Ronald F. Budzik, Jr.<sup>2</sup>

Firearm projectiles are among the most common metallic foreign bodies seen radiographically. Many different types of such projectiles exist. Their correct identification and classification can have significant impact on medicolegal decisions. Information needed to achieve this has been published primarily in forensic medicine journals; little of these data have been available to radiologists. We present a synopsis of the data that can be used to identify specific types of retained firearm projectiles.

### Handguns

Handguns fire relatively low-velocity (less than 2000 ft/sec [610 m/sec]) projectiles, most commonly solitary bullets [1]. These vary in size, shape, and construction (Fig. 1). The size (caliber) of a bullet equals the internal diameter (bore) of the handgun barrel (most commonly 22 [5.6], 25 [6.4], 32 [8.1], 38 [9.7], and 45 [11.4] hundredths of an inch [mm]). The shape of bullets varies from flat-headed to pointed, and construction varies from bare lead slugs to lead slugs either partially or completely encased in hard metal jackets. The jackets commonly are made of radiodense copper or nickel compounds. However, a few are made of relatively radio-translucent aluminum. Deep circumferential grooves (cannalures) may be present in the shafts of the bare lead slugs, and shallower cannalures may be present in the shafts of jacketed bullets. The size, number, and spacing of the cannalures are specific to the bullet manufacturer.

Occasionally, a small metal BB or explosive firing cap is placed in a hollowed bullet tip to increase the bullet's deformation on impact. Rarely, two bullets may be fired together from the same gun. This usually occurs when one bullet has become lodged in a gun barrel and subsequently is dislodged when a second bullet is fired.

Handguns also are capable of firing multiple small metal pellets similar to those fired from shotguns [2]. This "birdshot" or "ratshot" differs in that the pellets are usually fewer in number (for the same size pellet) than those fired from shotguns.

Determinations about retained handgun projectiles that can be made on the basis of radiographs include approximate caliber, number, jacketing, presence of tip expanders, and the use of ratshot. The calculation of bullet caliber from radiographs reportedly is fraught with error [1]. However, if accurate magnification factors are used the major caliber classes can be separated. The magnification factors are derived from the X-ray tube focal spot-to-film and focal spot-to-bullet distances. The basic formula used to determine true bullet size is true bullet size = (focal spot-to-bullet distance) × (the bullet's image size) ÷ (focal spot-to-film distance). Care must be taken to minimize both geometric magnification (by using a small-focal-spot X-ray tube and large focal spot-to-film distance) and distortion (by positioning the bullet in the center of the X-ray beam).

The number of retained bullets can be counted easily unless fragmentation is excessive. Jacketed bullets can be identified

Received September 5, 1989; accepted after revision October 19, 1989.

<sup>1</sup> Department of Radiology, University Hospital, Cincinnati, OH 45267-0742. Address reprint requests to G. D. Dodd III.

<sup>2</sup> College of Medicine, University of Cincinnati, 231 Bethesda Ave., Cincinnati, OH 45267-0552.

AJR 154:471-475, March 1990 0361-803X/90/1543-0471 © American Roentgen Ray Society



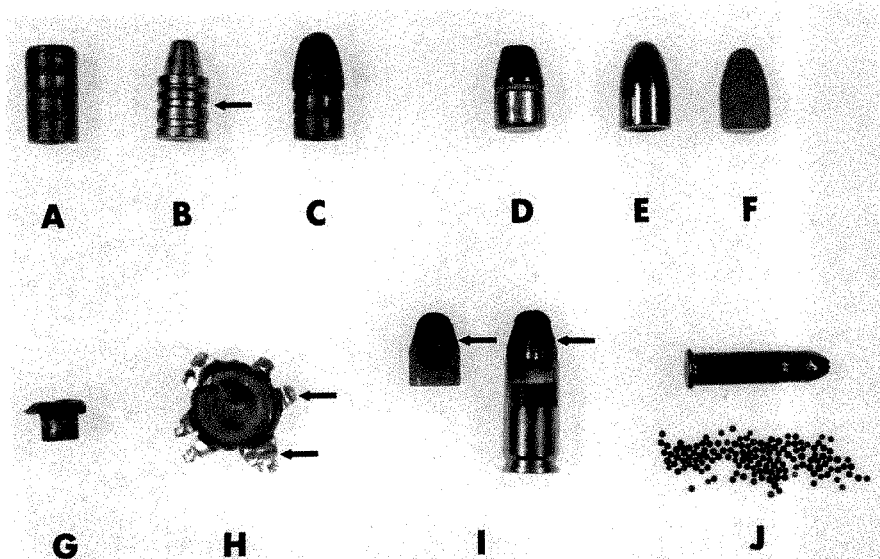


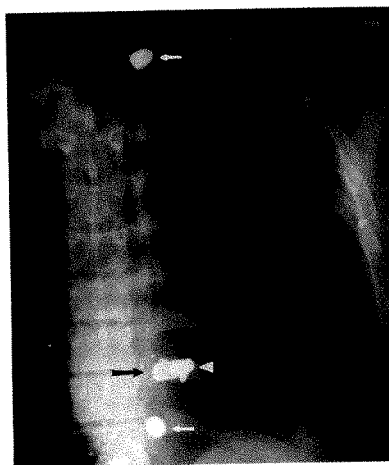
Fig. 1.—Handgun projectiles.

A–D, Nonjacketed “wad-cutter” bullets (A and B), round-tip nonjacketed bullet (C), and partially jacketed bullet (D). Cannalures are present on bullets in A–D but most evident on B (arrow).

E–J, Completely jacketed bullet (E) and cutaway view showing thin jacket-encasing lead core (F), deformed partially jacketed bullet without jacket separation (G), deformed partially jacketed bullet with flaired separating jacket (arrows) evident (H), cutaway views of “expanders” (arrows) embedded in bullet tips (I), and ratshot cartridge and shot (J). Bullets G and H have been fired; all other bullets are unfired.



Fig. 2.—Skull radiograph after handgun injury shows single, jacketed bullet with complete separation of jacket (black arrow) from slug. Note that jacket is more radiolucent than slug. Slug has broken into two major fragments (white arrows). Posterior entrance wound is surrounded by multiple lead fragments.



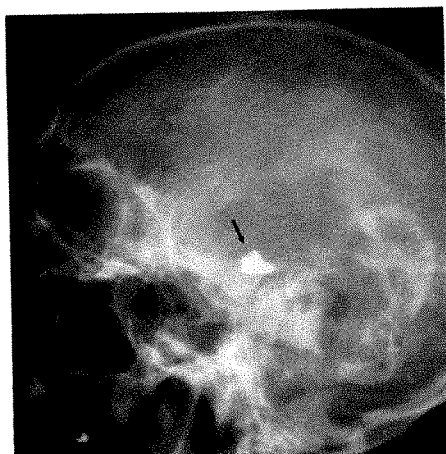
A



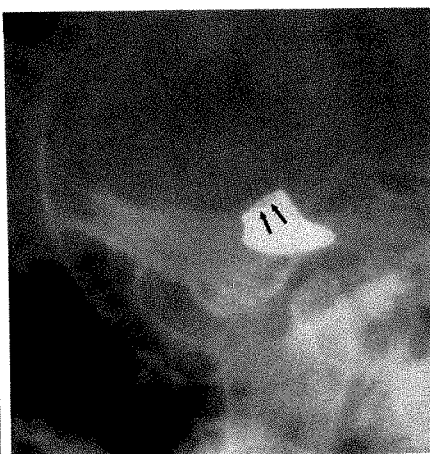
B

Fig. 3.—A, Left hemithorax radiograph after handgun injury shows three jacketed bullets. Two are undeformed (white arrows). One has struck bone and has separated into radiolucent jacket (black arrow) and slug (arrowhead).

B, Enlargement of A shows detail of separation of jacket (arrow) and slug (arrowhead).



A

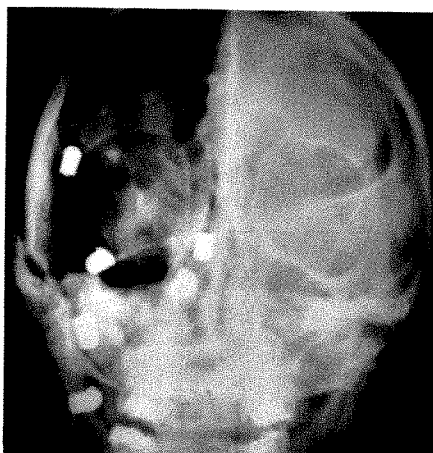


B

Fig. 4.—A, Skull radiograph after handgun injury shows fully jacketed bullet deformed during passage through bone. Subtle radiolucent crescent (arrow) at base of bullet represents loosened jacket. Full jacketing is implied by absence of lead fragments in presence of marked bullet deformity.

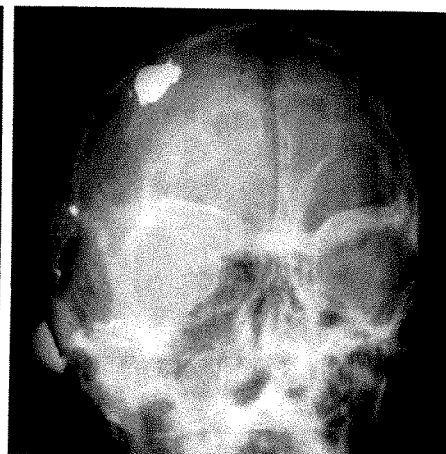
B, Enlargement of A shows detail of loosened radiolucent jacket (arrows).

Fig. 5.—Skull radiograph after handgun injury shows six fully jacketed bullets with minimal deformation even though bone was struck. Full jacketing is implied by absence of lead fragments. Note extensive pneumocephalus, calvarial fractures, and loss of brain parenchyma.



5

Fig. 6.—Skull radiograph after handgun injury shows two nonjacketed lead bullets that failed to penetrate skull. Note marked deformation conforming to convexity of calvaria. This marked deformation with fragmentation and no visible jacket is diagnostic of a nonjacketed bullet.



6

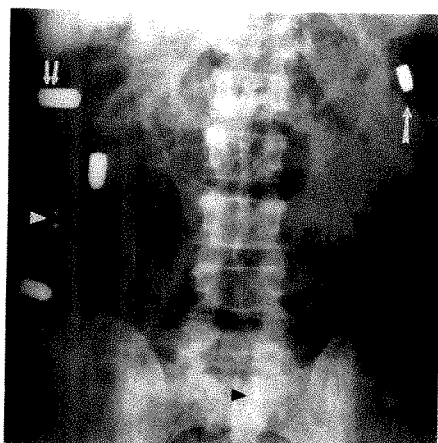


Fig. 7.—Abdominal radiograph after handgun and shotgun injuries shows four undeformed handgun bullets and three shotgun pellets (arrowheads). Three bullets are of same type, with rounded tips and cannalures (small arrows). Fourth bullet has a flat tip (large arrow). Although the two different types of bullets appear to be of different calibers (and thus fired from different guns), no such statement can be made without consideration of the magnification factors. Jacketing cannot be determined because of lack of deformation in soft tissues.

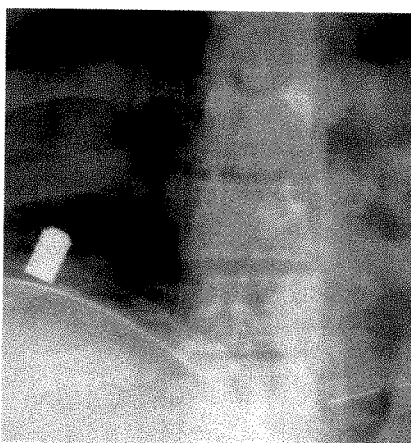


Fig. 8.—Close-up chest radiograph at diaphragm after handgun injury shows undeformed lead bullet with flat head (wad cutter) and multiple circumferential cannalures diagnostic of a nonjacketed bullet.

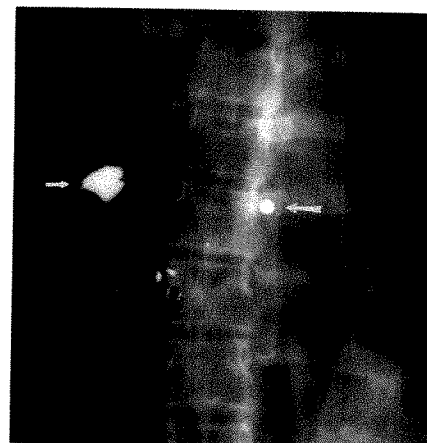
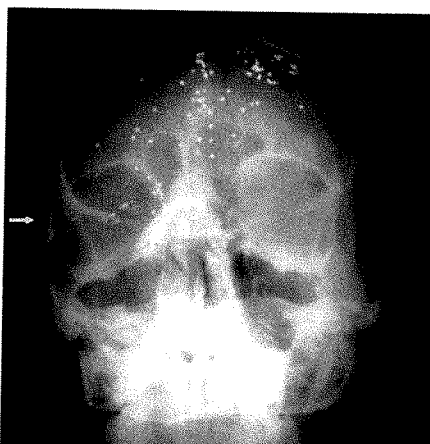


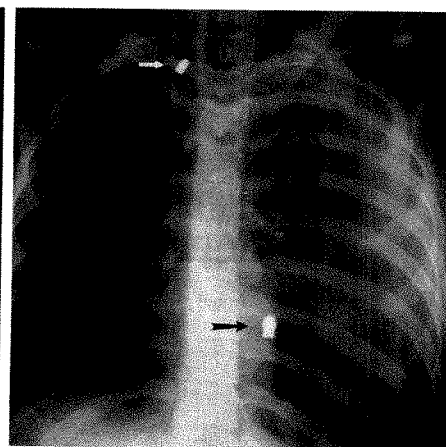
Fig. 9.—Chest radiograph after handgun injury shows two main foreign bodies: a bullet (small arrow) and metal BB (large arrow), which has been dislodged from bullet tip. Bullet was manufactured with a BB in its tip to promote expansion or mushrooming on impact.

Fig. 10.—Skull radiograph after handgun injury shows multiple small pellets in cranium, consistent with ratshot. In this contact injury the gun muzzle was placed against the right temple. The diagnosis of ratshot can be made from the observation of relatively few small pellets with limited penetration of the brain parenchyma and no exit wound. Note lead fragments around entrance wound (arrow).



10

Fig. 11.—Chest radiograph after handgun injury shows two metallic foreign bodies. One is a handgun bullet (white arrow). The other is a zipper (black arrow), which looks like a bullet. Note large left-sided hemothorax caused by real bullet, which entered left lower hemithorax.



11

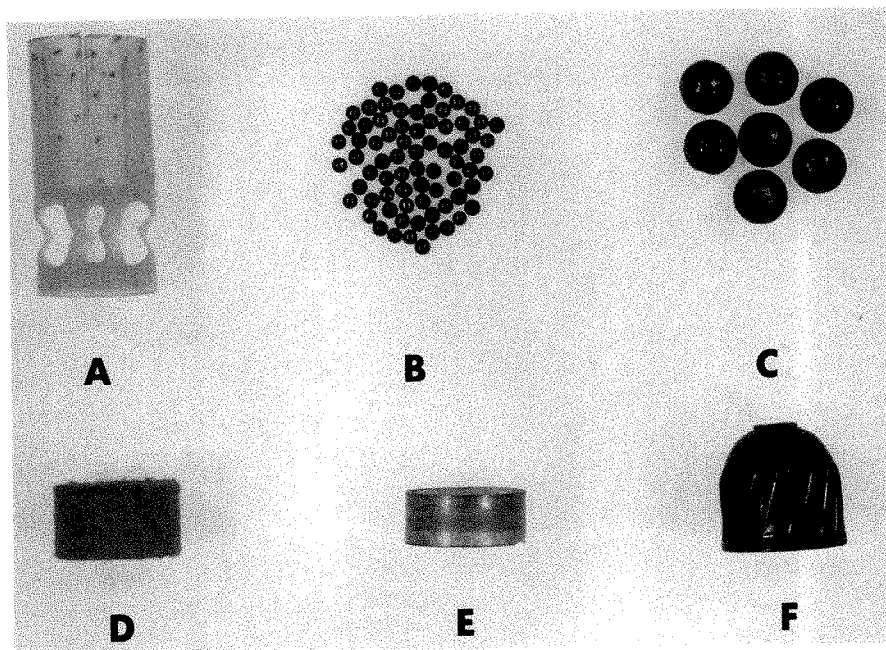


Fig. 12.—Shotgun projectiles. A–F, Plastic packing wads (A and E), birdshot (B), buckshot (C), fiber packing wad (D), and rifled shotgun slug (F). Packing wads are used to separate shot or rifled slugs from gun powder.

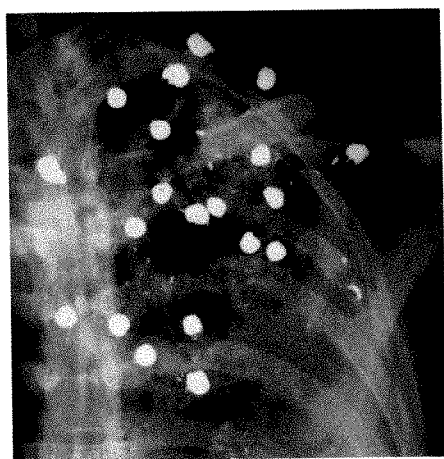


Fig. 13.—Chest radiograph after shotgun injury shows tightly grouped buckshot (multiple large lead balls). The range of fire in this instance was obviously close; however this injury could have been produced with a muzzle-to-target distance of 0–20 ft (6.1 m). Note multiple rib fractures and extensive pulmonary contusion and laceration.



A



B

Fig. 14.—A, Chest radiograph after shotgun injury shows widely dispersed birdshot (multiple small lead BBs) with epicenter located in left upper hemithorax. Faint circular density is present at crossing of left first and second ribs (arrows).

B, Enlargement of A shows detail of circular density representing embedded plastic packing wad made radiodense by lead shot residue (arrows). Identification of wad limits range of fire to 15 ft (4.6 m) or less.

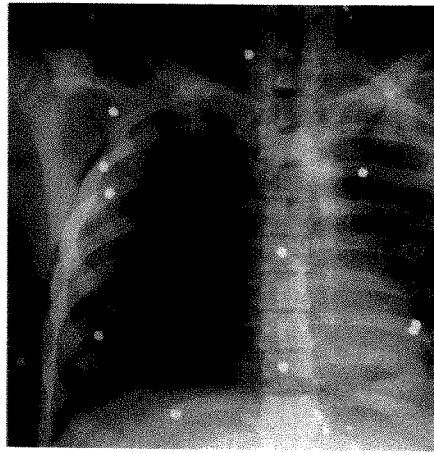
by direct visualization of loosened or separated jackets (Figs. 2–4). Full jacketing can be inferred if a bullet remains intact with little deformation after striking bone (Fig. 5). Marked fragmentation or deformation without visualization of a jacket is consistent with a nonjacketed bullet (Fig. 6). Both jacketed and nonjacketed bullets may remain undeformed if only soft tissue is encountered (Fig. 7). Flat-headed bullets with deep cannalures can be identified as nonjacketed lead bullets (Fig. 8). Bullet-tip expanders can become dislodged on impact and thus appear as a second foreign body (Fig. 9). Ratshot appears as multiple tiny pellets, which are fewer in number than those from shotguns (Fig. 10).

Occasionally, other foreign bodies can simulate bullets (Fig. 11).

### Shotguns

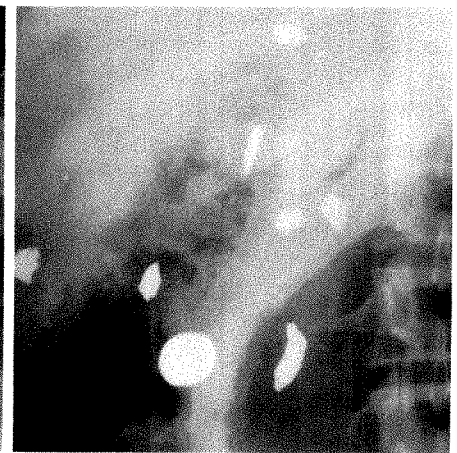
Shotguns [1] typically fire multiple metal pellets (BBs or shot) at one time. The size varies, from the largest buckshot (Fig. 12) to the smallest birdshot. Shotguns come in several sizes; the most common are the 12 and 20 gauges (gauge refers to the number of lead balls fitting the shotgun barrel that adds up to 1 lb [0.45 kg] in weight) and the 0.410-in. (10.4-mm) bore (bore is the internal diameter of the barrel). All shotguns can fire the entire spectrum of lead pellets. A

Fig. 15.—Chest radiograph after shotgun injury shows multiple widely dispersed buckshot without discernible epicenter, consistent with long muzzle-to-target distance. This case represents an exception to the statement that range of fire cannot be determined by distribution of pellets. This degree of dispersion can be accounted for only by a long muzzle-to-target distance. Compare with Fig. 13. Note extensive subcutaneous emphysema and pneumomediastinum.



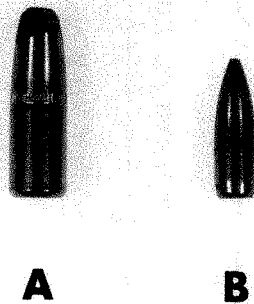
15

Fig. 16.—Right mid abdominal radiograph after rifled shotgun slug injury shows multiple irregular linear fragments that represent walls of rifled slug, with large round density representing the unfragmented leading end of slug. Mottled gas represents stool in ascending colon. Note small pneumoperitoneum outlining medial edge of liver.



16

Fig. 17.—Rifle projectiles.  
A and B, Partially (A) and completely (B) jacketed bullets, both unfired. Both bullets contain a lead core, visible at the tip of bullet A and completely encased within copper alloy jacket in bullet B.



packing wad (plastic or fiber), used to separate gun powder from lead pellets, always is fired simultaneously with the pellets. All shotguns also can fire solitary rifled slugs [3], which are in effect large, hollow, nonjacketed lead bullets. These slugs also are fired with packing wads.

Radiographically, the relative size of the metal spheres can be determined (by using magnification factors) insofar that buckshot (Fig. 13) can be distinguished from birdshot (Fig. 14). However, a more specific distinction between the many sizes is difficult because the differences in size are minimal. Usually, the range of fire (distance from muzzle to target) cannot be determined by the tightness of the shot pattern because of variable in-flight dispersion and ricocheting of the pellets on impact (Figs. 13 and 15). At distances less than 15 ft (4.6 m), the packing wad may enter the victim along with the pellets (Fig. 14). If the wad is seen radiographically, then the maximal range of fire must be less than 15 ft (4.6 m).

Shotgun slugs usually deform and often fragment on impact. The intact slug appears unusually large and fragments are often large and linear (Fig. 16). As with shotgun pellets, the radiographic visualization of a packing wad limits the maximal range of fire to less than 15 ft (4.6 m).

### Rifles

Rifles [1, 2, 4] most commonly fire high-velocity (greater than 2000 ft/sec [610 m/sec]) solitary bullets. The bullets are manufactured in multiple-calibers and are usually completely or partially jacketed (Fig. 17). The bullet tips may be blunt or

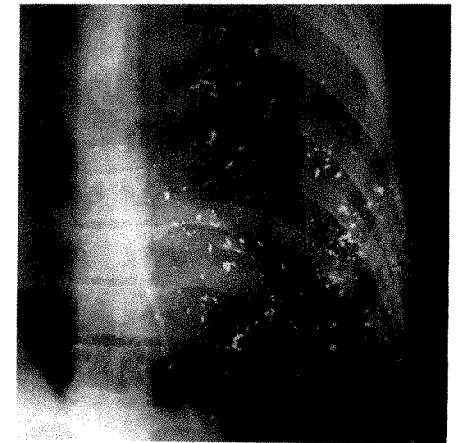


Fig. 18.—Chest radiograph after rifle injury shows typical snowstorm appearance of high-velocity bullet injury with multiple small irregular bullet fragments widely scattered throughout left hemithorax.

pointed. Cannalures are either shallow or absent. Some rifles fire low-velocity small-caliber bullets that are identical to some handgun bullets. These same rifles may also fire ratshot.

Partially jacketed high-velocity bullets produce a typical snowstorm radiographic pattern that consists of multiple, small, irregular, widely scattered metal fragments (Fig. 18). Fully jacketed high-velocity bullets may remain undeformed if soft tissue only is encountered or may appear variably deformed if bone is struck. The low-velocity small-caliber bullets and rifle ratshot cannot be differentiated radiographically from the similar handgun projectiles.

### REFERENCES

- Curran WJ, McGarry AL, Petty CS. *Modern legal medicine, psychiatry, and forensic science*. Philadelphia: Davis, 1980:415-467
- DiMaio VJM, Spitz WU. Injury by birdshot. *J Forensic Sci* 1970;15:396-402
- Petty CS, Hauser JE. Rifled shotgun slugs: wounding and forensic ballistics. *J Forensic Sci* 1968;13:114-123
- Demuth WE Jr. High velocity bullet wounds of the thorax. *Am J Surg* 1968;115:616-625

P24,455



## Book Review

**Basic Medical Techniques and Patient Care for Radiologic Technologists**, 3rd ed. By Lillian S. Torres. Philadelphia: Lippincott, 256 pp., 1989. \$25.95

This new edition is a vast improvement over the first one published in 1979. The book has 12 chapters. Each one begins by stating a goal. This is followed by a number of behavioral objectives to be attained by the reader and a glossary of new terms introduced in the text. The text is laid out in an easy-to-read format with headings that "leap off the page." Each chapter concludes with a test that permits readers to assess their level of comprehension and retention of the material presented.

The subjects covered in the first chapter include legal aspects of radiologic technology, technologist-patient communication, and dealing with the grieving or handicapped patient. The second chapter covers infection control in a logical, practical manner. A chapter on basic patient care in diagnostic imaging is followed by chapters on medical emergencies and on care of patients who have special problems, those who are having barium studies, and those who have drainage tubes. Specific chapters on surgical aseptic technique and catheterization of the urinary bladder are followed by discussions on

assisting with administration of drugs and care of patients during special procedures.

This volume is profusely illustrated with high-quality photographs and a few line drawings. Page 82 has two minor errors. On the basis of the guidelines established by American Heart Association for keeping the patient's airway open, only the head tilt/chin lift or the jaw thrust rather than the neck tilt should be used. The photograph in Figure 52 on the same page shows incorrect hand positioning for external cardiac compression.

This book belongs in every radiology department and should be required reading for the student technologist. It is also useful for graduate technologists who need to refresh their memory on various aspects of patient care.

Herbert F. Gramm  
*Harvard Medical School  
New England Deaconess Hospital  
Boston, MA 02215*

## Perspective

# A Tutorial on Confidence Intervals for Proportions in Diagnostic Radiology

Charles C. Berry<sup>1</sup>

Research in diagnostic radiology often aims to establish the safety and the accuracy of a new procedure or to compare it with other procedures. Frequently, the diagnostic performance of a test can be summarized by proportions such as accuracy, sensitivity, and specificity. Safety may be reflected by the proportion of patients experiencing unpleasant or adverse effects. The confidence interval is useful for summarizing data on proportions. However, the confidence intervals presented in most elementary statistics texts are inappropriate for diagnostic research.

Estimates of proportions can differ considerably from the actual proportions. A proportion based on a large number of subjects is obviously more accurate than one based on a small number, but just how accurate are estimated proportions? News reports of public opinion surveys, which typically include thousands of subjects, frequently cite an accuracy of  $\pm 3\%$  for the percentages that they estimate. Few studies in diagnostic radiology include nearly so many subjects, which suggests an accuracy that is far lower than the  $\pm 3\%$  of the ordinary public opinion survey.

One way to indicate the precision of an estimated proportion is to give a range of values that is consistent with the data. As an example, suppose that a test correctly identified nine of 10 patients with a particular diagnosis, whereas in another series it correctly identified 90 of 100 patients. In each series, 90% of the cases were correctly classified, but it is obvious that the latter data are consistent with a much

smaller range of values. According to one method (described later), the range from 55% to 99.7% is consistent with nine out of 10, and the range from 82% to 95% is consistent with 90 of 100. In many situations, the conclusions drawn from one of these series would differ from those drawn from the other even though 90% of the cases studied were correctly classified in each.

The comparison of two proportions suffers from a related difficulty. When one diagnostic test correctly identifies nine out of 10 cases studied and another also correctly identifies the same nine out of the 10, the observed difference in the proportion correctly identified is exactly zero. At an intuitive level, one might feel that these results demonstrate equal accuracy of the two tests; if one has lower cost or greater convenience, it might be used in preference to the other. However, it is possible that if both tests were applied to a larger series that one test could correctly identify many more patients than the other. It would be useful to know how large a difference between the two tests is consistent with the data. According to one method, the difference of proportions could range from  $-.257$  to  $+.257$ . In other words, the data are consistent with setups in which one test correctly identifies more patients than the other by a margin of 25.7%. Thus, it would generally be inappropriate to consider the two tests as being even approximately equal.

Confidence intervals are simple statistical tools for summarizing data on proportions or differences of proportions

Received August 21, 1989; accepted after revision October 16, 1989.

<sup>1</sup> Department of Community and Family Medicine, University of California, San Diego, School of Medicine, La Jolla, CA 92093-0622. Address reprint requests to C. C. Berry.

AJR 154:477-480, March 1990 0361-803X/90/1543-0477 © American Roentgen Ray Society

that provide an appropriate range of values for the quantity estimated. A tutorial on basic concepts and on several such tools follows.

### Point Estimates vs Interval Estimates

The usual estimate of a proportion is the number of subjects studied with a particular condition divided by the number of subjects under study. This usual estimate is termed a *point estimate*. Although this fraction is a suitable estimate of the proportion, the data could be consistent with a range of values for the proportion. Such a range is termed an *interval estimate*. The most widely used type of interval estimate is the confidence interval.

A confidence interval is a range of values that is consistent with the data in the following sense. The fraction of instances in which a confidence interval contains the correct value is equal to the specified *confidence coefficient*. Thus, the correct value will lie within the range given by an 80% confidence interval in 80% of the instances in which it is used. It is tempting to translate this statement as "the probability that the correct value lies within the computed interval is given by the confidence coefficient," and an informal notion that the confidence coefficient represents the "chance" that the confidence interval contains the correct value is reasonable. However, the translation is not strictly correct, and applying the laws of probability to confidence intervals can yield nonsensical results.

The actual procedure for obtaining a confidence interval depends on the quantity to be estimated (e.g., a proportion or a difference of proportions) and on the study design. Procedures for finding confidence intervals for a proportion and for the difference of two proportions for some simple designs are described below.

### Confidence Interval for Proportions

Tables and graphs of confidence intervals for proportions are widely available in elementary statistics books [1, 2], in the CRC Handbook for Probability and Statistics [3], and elsewhere. The ranges given earlier based on the observation of nine of 10 and for 90 of 100 cases are the 95% confidence intervals from those tables. The tables are based on computations that are rather extensive and are not given here.

If a copy of these tables or graphs is not handy, a formula may be used to approximate the confidence interval for a proportion:

$$\frac{2p + \theta^2 \pm \theta\sqrt{\theta^2 + 4p(1-p)}}{2 + 2\theta^2}$$

where  $p$  is the observed proportion,  $\theta = z_{\alpha/2}/\sqrt{N}$ ,  $\alpha = (1.0 - \text{the confidence coefficient})$ ,  $z_{\alpha/2}$  is the value of the standard normal curve corresponding to the  $(100 - 100\alpha/2)$  percentile (some commonly used values are 1.28 for 80% confidence intervals and 1.96 for 95% confidence intervals), and  $N$  is the number of subjects.

This formula is easy to evaluate by using a computer spreadsheet or a hand calculator. Students and novice users of this approximation are sometimes surprised that the re-

sulting interval is not symmetric about  $p$  and should be warned that this is the case. Readers familiar with a simpler approximation given in many elementary statistics texts (i.e.,  $p \pm z_{\alpha/2}\sqrt{p(1-p)/N}$ ) are warned that it performs poorly compared with the formula given here [4]. This poor performance is marked in the small samples common in research in diagnostic radiology, especially when the underlying proportion is near 1.0, as is often the case for sensitivity or specificity, or near zero, as for proportions of adverse effects. There are actually a number of approximate methods for finding the confidence interval for the binomial proportion. The formula given here was chosen for both accuracy and ease of use.

For values of  $N$  smaller than 20, it is usually recommended that only tables or graphs of the exact confidence intervals be used, but few clinical scientists will find the difference in the exact confidence interval and the recommended approximation to be compelling even for samples as small as  $N = 10$ .

An example is given for the data of Dunnick et al. [5] in which a sensitivity of 100% is reported for renal digital subtraction angiography on the basis of positive studies in 25 of 25 patients. So,  $p = 25/25 = 1.0$  and  $N = 25$ . The 95% confidence limit is found by setting  $\alpha$  to  $1.0 - 0.95 = 0.05$ , finding  $z_{\alpha/2} = 1.96$  from a table of the standard normal curve, finding  $\theta = 1.96/\sqrt{25} = 0.392$ , and substituting these values in the formula provided earlier. The numerator of the result is  $2 + 0.154 \pm 0.392\sqrt{0.154 + 4 \times 1.0 \times 0.0}$ , which simplifies to  $2.154 \pm 0.154$ . The denominator is  $2 + 2 \times 0.154$ . The resulting 95% confidence interval is the range from 0.876 to 1.0, which is written as (0.867, 1.0). When the tables of the exact confidence interval for the binomial proportion are consulted, the result of (0.863, 1.0) agrees closely with the approximation.

Notice that for cases in which the observed proportion is either 0.0 or 1.0, the simplification used in the example worked above can be applied. The confidence interval may be written as (0.0,  $K$ ) if  $p = 0.0$  or as  $(1.0 - K, 1.0)$  if  $p = 1.0$ , where  $K = z_{\alpha/2}^2/(N + z_{\alpha/2}^2)$ . In the case of a 95% confidence interval, this is  $K = 3.84/(N + 3.84)$ . A close approximation to  $K$  is given by the rule "divide 4 by  $N$  plus 4." For the data used in the example above,  $K = 4/(25 + 4) = 0.138$ , which leads to a confidence interval of (0.862, 1.0).

The formula and tables are not applicable to proportions in which the results for some of the units are correlated. One instance in which such intercorrelation occurs is when multiple readers assign diagnoses to each of a set of images; the tendency of readers to agree on diagnoses leads to the correlation. The application of the usual confidence interval for proportions would yield an interval that is too narrow, giving a false sense of precision.

The analysis of studies involving multiple readers and multiple images poses difficulties beyond the scope of this commentary. A tutorial by Hanley [6] on receiver-operating-characteristic (ROC) analysis discusses these difficulties, albeit for data that are different than the simple proportions that we discuss here. The comments and references in that tutorial are appropriate for tests that result in quantitative readings or graded scales. ROC analysis is generally preferred to the analysis of simple proportions for such tests.

### Confidence Interval for the Difference of Proportions from Separate Samples

When proportions are estimated from two different sets of subjects, the difference of the proportions is often of most interest. How large or small a difference of proportions is consistent with the data? The confidence interval for the difference provides an answer to this question. Unfortunately, there are no widely published (and correct) tables of exact confidence intervals for the difference of proportions. Algorithms for finding exact confidence intervals [7] for the difference of proportions are available, but these require extensive computations. An approximate confidence interval can be calculated as follows:

$$p_1 - p_2 \pm \left\{ z_{\alpha/2} \sqrt{\frac{p_1(1-p_1)}{n_1-1} + \frac{p_2(1-p_2)}{n_2-1}} + C \right\}$$

where  $p_1$  and  $p_2$  are the estimated proportions in each group,  $\alpha$  is  $(1 - \text{the confidence coefficient})$ ,  $z_{\alpha/2}$  is the value of the standard normal curve corresponding to the  $(100 - 100\alpha/2)$  percentile,  $n_1$  and  $n_2$  are the numbers of subjects in each group, and  $C$  is  $1/2n_1$ , if  $n_1$  is smaller, or  $1/2n_2$  otherwise.

Again, this is slightly different from the usual formula found in most elementary statistics books, but offers better performance than the usual formula [8]. A further modification to this formula is needed when both observed proportions are zero or one; in that case, the lower confidence limit should be taken as  $-1 + (\alpha/2)^{1/n_1}$  and the upper limit should be taken as  $1 - (\alpha/2)^{1/n_1}$ . With this modification, the approximation appears to be adequate for values of  $n_1$  or  $n_2$  as small as 10.

An example based on the data of Tomlinson et al. [9] compares the proportion of patients experiencing "overall discomfort" when a new preparation for barium enema is used vs the proportion when the standard colon-cleansing method is used. For the new preparation, four of 46 patients experienced discomfort compared with 16 of 43 patients for the standard preparation. The observed proportions are 0.087 and 0.372, and the difference between these is  $-0.285$ . Application of the formula with a confidence coefficient of 80% gives an interval of  $(-0.406, -0.164)$ . The confidence interval for the difference of two proportions is built on an assumption that the observations are made on independent cases. Calculation of this confidence interval by using data from multiple readings of multiple images will tend to produce intervals that are too narrow, giving a false sense of precision.

### Confidence Interval for the Difference of Proportions from the Same Sample

When two proportions are based on the same set of subjects (as when two tests are administered to each of a set of patients), the confidence interval for the difference of proportions may be found as follows. Use  $p_{10}$  to refer to the proportion of subjects in whom the first test is positive and the second is negative and  $p_{01}$  to refer to the proportion of subjects in whom the first test is negative and the second test is positive. The number of subjects is  $N$ . The interval is

given by

$$p_{10} - p_{01} \pm \{ z_{\alpha/2} \sqrt{(p_{10} + p_{01} - (p_{10} - p_{01})^2)/N + 1/2N} \}$$

Again, a further modification may be needed. If both  $p_{10}$  and  $p_{01}$  are zero, find  $k = 1 - (\alpha/2)^{1/N}$  and use  $(-k, k)$  as the confidence interval. If  $p_{10}$  is one, use  $(1-2k, 1)$ , or if  $p_{01}$  is one, use  $(-1, -1+2k)$ . With this modification, the approximation appears to be adequate for samples as small as  $N = 10$ .

As an example, in the data from Gelfand et al. [10], three of 23 cases were correctly detected with oral cholecystography (OCG) but were missed with sonography, leading to  $p_{10} = 0.130$ . One case was detected with sonography but was missed with OCG, leading to  $p_{01} = 0.043$ . Thus, the difference between the observed proportions is 0.087. The 80% confidence interval is  $(-0.044, 0.218)$ .

### Choosing a Confidence Coefficient

Confidence intervals that have very high confidence coefficients will almost always include the correct value, but do so at the expense of covering a wide range of values and therefore being uninformative. Intervals with low confidence coefficients are narrower, but more frequently fail to include the correct value. An 80% confidence interval is usually about half as wide as a 99% confidence interval. The choice is somewhat subjective. Some statisticians suggest reporting several confidence intervals by using different confidence coefficients rather than just one. Common choices for confidence coefficients are 80%, 95%, and 99%.

### Additional References

Confidence intervals for the mean of a series of quantitative measurements and for differences of means may be found in many elementary statistics texts [e.g., 2, 11, and 12]. These intervals are based on an assumed Gaussian distribution for the data. When this assumption is not warranted, a non-parametric confidence interval may be constructed by using the instructions provided by Brown and Hollander [2]. In addition to these texts, the papers reproduced in the edited volume by Bailar and Mosteller [13] and the original chapters therein provide a useful and readable overview of a variety of statistical issues in clinical research.

### Conclusion

In diagnostic research, where sample sizes are often small, the precision of estimates must be communicated effectively. The confidence interval is one way of calculating a range of values consistent with a set of data.

### REFERENCES

1. Ingelfinger JA, Mosteller F, Thibodeau LA, Ware JH. *Biostatistics in clinical medicine*. New York: Macmillan, 1987.
2. Brown BW, Hollander M. *Statistics: a biomedical introduction*. New York: Wiley, 1977.



3. Beyer WH, ed. *CRC handbook of tables for probability and statistics*. Cleveland: Chemical Rubber Company, **1966**
4. Ghosh BK. A comparison of some approximate confidence intervals for the binomial parameters. *JASA* **1979**;74:894-900
5. Dunnick NR, Svetkey LP, Cohan RH, et al. Intravenous digital subtraction renal angiography: use in screening for renovascular hypertension. *Radiology* **1989**;171:219-222
6. Hanley JA. Alternative approaches to receiver operating characteristic analyses. *Radiology* **1988**;168(2):568-570
7. Santner TJ, Snell MK. Small sample confidence intervals for  $p_1-p_2$  and  $p_1/p_2$  in  $2 \times 2$  contingency tables. *JASA* **1980**;75:386-394
8. Hauck WH, Anderson S. A comparison of large sample confidence interval methods for the difference of two binomial proportions. *Amer Stat* **1986**;40:318-322
9. Tomlinson TL, DiPalma JA, Mangano FA. Comparison of a new colon lavage solution (Golytely-RSS) with a standard preparation for barium enema. *AJR* **1988**;151:947-950
10. Gelfand DW, Wolfman NT, Ott DJ, Watson NE Jr, Chen YM, Dale WJ. Oral cholecystography versus gallbladder sonography: a prospective, blinded reappraisal. *AJR* **1988**;151:69-72
11. Daniel WW. *Biostatistics: a foundation for analysis in the health sciences*. New York: Wiley, **1987**
12. Snedecor GW, Cochran WG. *Statistical methods*. Ames: Iowa State Univ. Press, **1980**
13. Bailar JC, Mosteller F, eds. *Medical uses of statistics*. Waltham, MA: *N Engl J Med Books*, **1986**

# Do Chest Radiographic Findings Reflect the Clinical Course of Patients with Sarcoidosis During Corticosteroid Withdrawal?

Michael H. Baumann<sup>1</sup>  
 Charlie Strange  
 Steven A. Sahn

The use of serial chest radiographs to assess disease activity in patients with sarcoidosis is controversial. However, reliance on the symptomatic clinical course to assess disease activity may be misleading. As many patients being treated with corticosteroids have an abrupt clinical deterioration when doses of those medications are decreased, we questioned whether the chest radiograph could depict alterations in disease activity as measured by spirometry in this subset of patients. We retrospectively reviewed the clinical course of all patients with pulmonary sarcoidosis in whom the corticosteroid dose was reduced during a 6-month period. The 15 patients without fever, chills, or purulent sputum during that time were then examined to determine the presence ( $n = 10$ ) or absence ( $n = 5$ ) of a symptomatic relapse. All patients who had a symptomatic relapse also had a fall in forced vital capacity of at least 10%, suggesting an increase in disease activity. Serial chest radiographs were evaluated during and after corticosteroid dose reductions and after clinical recovery on higher steroid doses in the patients who had had a relapse. In eight patients, the disease was in radiographic stage 2 (hilar adenopathy and parenchymal lung disease); in seven patients it was in radiographic stage 3 (parenchymal lung disease alone). The disease did not change stage in any patient during the study. Chest radiographs worsened more frequently in patients who had a clinical relapse (seven of 10) than in those who did not have a relapse (zero of five,  $p < .05$ ). An alveolar chest radiographic pattern ( $n = 4$ ) or reticulonodular pattern ( $n = 3$ ) was noted in the seven patients who had a relapse, with worsening on radiographs often occurring before detection of relapse by symptomatology (four of seven) or spirometry (three of seven). Spirometry and radiographs improved or stabilized after an increase in corticosteroid dose in all 10 patients who had a relapse.

We conclude that serial chest radiographs can reflect clinical relapse in patients with sarcoidosis during corticosteroid dose reduction. Furthermore, worsening seen on chest radiographs may be the first evidence of relapse.

*AJR* 154:481-485, March 1990

Sarcoidosis is a multisystem disorder of unknown cause characterized by the presence of noncaseating epithelioid cell granulomas in the involved organ systems [1]. Worsening disease activity is generally reflected by a worsening clinical course; however, the use of symptomatology alone to guide therapy is extremely unreliable. Despite intrathoracic involvement in 84-99% of patients [2], the use of the chest radiograph to assess disease activity is controversial. Although radiographic staging can determine prognosis [3-5], the value of chest radiography in assessing disease activity remains unproved. Because patients may frequently have a clinical relapse related to corticosteroid withdrawal [6, 7], we evaluated the chest radiograph as a marker of disease activity in such a cohort of sarcoidosis patients with hilar adenopathy and parenchymal lung disease (stage 2) or with parenchymal lung disease alone (stage 3).

Received August 11, 1989; accepted after revision October 16, 1989.

<sup>1</sup> All authors: Division of Pulmonary and Critical Care Medicine, Medical University of South Carolina, 171 Ashley Ave., Charleston, SC 29425. Address reprint requests to M. H. Baumann.

0361-803X/90/1543-0481  
 © American Roentgen Ray Society

## Materials and Methods

By retrospectively reviewing the medical records of all patients with sarcoidosis seen at the Medical University of South Carolina pulmonary clinic within a 6-month period, we identified those patients who were treated with corticosteroids for pulmonary sarcoidosis ( $n = 26$ ). The stage of the disease in patients receiving corticosteroids was stage 2 or stage 3 (stage 0, no radiographic changes; stage 1, bilateral hilar lymphadenopathy; stage 2, bilateral hilar lymphadenopathy and parenchymal infiltration; and stage 3, parenchymal infiltration without bilateral hilar lymphadenopathy [3]). Eleven patients with fever, chills, or purulent sputum were excluded from the study so as not to confuse infection-related decompensation with deterioration due to sarcoidosis. All remaining patients ( $n = 15$ ) had past histologic confirmation of sarcoidosis by either lung or lymph node biopsy. The 15 patients were examined for symptomatic deterioration, defined as the onset or worsening of dyspnea or coughing occurring within 6 months of a decrease in corticosteroid dose (any decrease of at least 5 mg per day or every other day). Furthermore, serial spirometry was used as an objective test of clinical deterioration, serving as an index of disease activity. Breathing capacity was evaluated by using the best of three patient efforts (Collins Model DS-421 Spirometer, Braintree, MA). Spirometric deterioration in the forced vital capacity of 10% or more was considered significant.

At least three standard (144 kVp, 72 in., 8/1 grid) posteroanterior chest radiographs, obtained during corticosteroid withdrawal, were evaluated by two independent observers who were aware only of the patients' diagnosis of sarcoidosis and not of their clinical course. The films were dated and placed in chronological order for viewing. The interpreters were asked to note if any changes occurred in the radiographs. If changes were identified, the interpreters then chose the most abnormal radiograph, noted the radiograph marking the onset of worsening, and graded alveolar filling, reticulonodular infiltrates, pleural abnormalities, and the size of hilar and mediastinal lymph nodes.

Patients who had a clinical relapse were compared with those who did not have a relapse by chi-square analysis; a  $p$  value less than or equal to .05 was considered significant.

## Results

Ten of the 15 patients had a clinical relapse during corticosteroid withdrawal (Table 1). In nine of the 10 patients, the predominant symptom at the time of clinical deterioration was a cough. Dyspnea was the additional or primary complaint in five of the 10 patients. Five of the 15 patients underwent successful corticosteroid withdrawal and composed the "non-relapse" group. All 15 patients had either stage 2 or 3 disease (stage 2, eight patients; stage 3, seven patients); the stages were not different between groups ( $p = \text{NS}$ ).

The forced vital capacity improved  $21.6 \pm 4.7\%$  (mean  $\pm$  standard error) in the five patients who did not have a relapse during corticosteroid withdrawal. By comparison, the 10 patients who had a clinical relapse had a mean forced vital capacity decrement of  $21.0 \pm 3.6\%$  (range,  $-13$  to  $-50\%$ ) during corticosteroid withdrawal; after an increase in corticosteroid dose, the forced vital capacity increased by a mean of  $19.8 \pm 4.5\%$  (range,  $+5$  to  $+56\%$ ).

None of the five patients with a successful corticosteroid withdrawal had deterioration shown on serial radiographs. Conversely, seven of the 10 patients who had a clinical relapse during corticosteroid withdrawal (Table 1) had dete-

rioration shown on at least one or more of the serial radiographs (chi-square = 4.05,  $p < .05$ , Fig. 1). Four of the seven patients with worsening on radiographs had radiographs showing deterioration before clinical relapse; three had a coincident radiographic and clinical deterioration. Three of the four patients who showed deterioration on radiographs before clinical relapse did so before a decline in the forced vital capacity. New alveolar infiltrates were found on radiographs in four of the seven patients; reticulonodular worsening was found in the remaining three patients. Pleural or hilar/mediastinal node changes were not observed. The chest radiograph improved after corticosteroid dose was increased in six of the seven patients who had shown deterioration during corticosteroid withdrawal. In the remaining patient, the interpreters disagreed: one thought the radiographs showed stability and the other, improvement. The sensitivity and specificity of the chest radiograph for detecting a clinical relapse in sarcoidosis in this series were 70% and 100%, respectively.

Agreement between the two independent interpreters was good. The interpreters agreed that radiographs were stable or improved in patients undergoing a successful corticosteroid withdrawal. There was complete agreement regarding the most abnormal radiograph in the seven patients who had a clinical relapse during corticosteroid withdrawal and radiographic deterioration. The interpreters agreed in six of these seven cases about the onset of deterioration shown on radiographs.

## Discussion

The detection of disease activity in pulmonary sarcoidosis is often a difficult clinical problem. Angiotensin-converting enzyme, gallium-67 scanning, bronchoalveolar lavage, spirometry, diffusion capacity, and chest radiography all have been used to assess disease activity in sarcoidosis [8]. An ideal test would be able to detect the lymphocytic alveolitis of sarcoidosis [9] by a sensitive, specific, and noninvasive method; however, no test yet fulfills these criteria.

An elevated serum level of angiotensin-converting enzyme may represent active disease in a patient with sarcoidosis [8]. Levels of angiotensin-converting enzyme may parallel granuloma load, and therefore decreases in the level should reflect pathologic resolution of disease. However, an elevated serum level of angiotensin-converting enzyme is not of diagnostic value and low specificity limits its use. Other diseases associated with an elevation in serum level of angiotensin-converting enzyme include asbestosis, silicosis, berylliosis, diabetes mellitus, and liver cirrhosis.

Pulmonary function testing has been advocated as the best single method to evaluate the activity of sarcoidosis [10]. The forced vital capacity and the diffusion capacity have been shown to be the most useful [10-12]. Furthermore, these tests are thought to be most helpful in detecting changes in disease activity when analyzed serially [10, 11]. Criticism of the use of spirometry is that by the time deterioration is found, irreversible changes may have occurred [13].

Similar criticisms have been leveled against the chest radiograph in monitoring disease activity. Chest radiographic ab-

**TABLE 1: Clinical, Spirometric, and Radiographic Features of Sarcoidosis Patients Who Had a Relapse During Corticosteroid Withdrawal**

Patient	Stage	Symptom	Spirometry		Type	Radiographic Deterioration	
			FVC <sup>a</sup> (%)	FVC <sup>b</sup> (%)		Earliest Time Before Relapse	Improvement After Corticosteroids
1	3	Cough	-13	+22	None		
2	2	Cough/dyspnea	-14	+5	None		
3	3	Dyspnea	-21	+21	None		
4	2	Cough	-16	+21	A	3.0 months <sup>c</sup>	Yes
5	2	Cough/dyspnea	-50	+56	RN	3.9 months	Yes
6	3	Cough/dyspnea	-22	+5	A	4.1 months <sup>c</sup>	Yes
7	2	Cough	-14	+19	A	5.9 months <sup>c</sup>	Yes
8	2	Cough	-29	+20	A	Coincident	Yes
9	2	Cough	-17	+18	RN	Coincident	Yes
10	3	Cough/dyspnea	-14	+11	RN	Coincident	Yes/No <sup>d</sup>
			-21.0 ± 3.6 <sup>e</sup>	+19.8 ± 4.5 <sup>e</sup>			

Note.—FVC = forced vital capacity; Stage 3 = parenchymal infiltration without hilar lymphadenopathy; Stage 2 = bilateral hilar lymphadenopathy plus parenchymal infiltration; A = alveolar; RN = reticulonodular.

<sup>a</sup> FVC during corticosteroid withdrawal.

<sup>b</sup> FVC after corticosteroid increase.

<sup>c</sup> Radiographic decline before FVC decline.

<sup>d</sup> Reader interpretation differs (see text).

<sup>e</sup> Mean ± standard error.

normalities noted in patients with sarcoidosis are thought by some to reflect an irreversible stage of the disease [13]. Other authors suggest that a discerning radiographic evaluation for lung parenchymal changes may be valuable in determining the largely reversible alveolitis of sarcoidosis [14]. The ability to detect the degree of alveolitis present in a patient with sarcoidosis might enable an appropriate therapeutic alteration and reversal of the process.

Because serial chest radiography has never been evaluated as a marker for sarcoidosis disease activity both during and after corticosteroid withdrawal and because of the frequency of clinical relapse related to corticosteroid withdrawal in patients with sarcoidosis [6, 7], we initiated our study to determine the value of serial chest radiographs as an adjunct to spirometry during corticosteroid withdrawal. We found worsening on chest radiographs of seven of 10 patients who had a relapse, compared with none of the five patients who did not have a relapse during corticosteroid withdrawal. Four of these seven patients had evidence of deterioration on radiographs before symptomatic deterioration and three of the four, before spirometric deterioration. Although deterioration on radiographs was often subtle at the earliest time of worsening, serial radiographic assessment allowed us to predict those patients who would subsequently have a relapse.

The new alveolar pattern infiltrates found in four patients most likely reflects a sarcoid alveolitis because other causes of alveolar filling were clinically unlikely. Open-lung biopsy specimens from similar patients have shown a prominence of epithelioid cells, macrophages, and lymphocytes that combine to form the alveolar pattern seen on radiographs [15, 16]. Further, it has been suggested that sarcoid alveolitis tends to resolve without therapy, possibly explaining the resolution in all four patients [16].

Reticulonodular deterioration may represent a primary interstitial inflammatory granulomatous process [15] at different stages of development that later progresses to incite the mononuclear alveolitis seen with bronchoalveolar lavage [17–19]. Hence, these sequentially developing reticulonodular radiographic changes may not represent irreversible fibrosis, but active and potentially reversible disease. Radiographs showing improvement in two patients and stabilization in one patient with reticulonodular deterioration support this contention.

It could be argued that an increased gallium scanning index [8] or bronchoalveolar lavage revealing a mononuclear alveolitis [17–19] might have detected a relapse before the chest radiograph would have detected it. Although alveolitis and reticulonodular changes shown on radiographs may have taken time to evolve, spirometry stabilizing or improving to baseline after reinstitution of therapy argues that delay in corticosteroid intervention was not detrimental. In fact, the 20% frequency of a positive gallium scan in patients without other signs of disease suggests this test may lack specificity [8]. Bronchoalveolar lavage also presents problems in assessing the activity of sarcoidosis because it is an invasive procedure, is variable in the degree of lymphocyte or neutrophil predominance reflective of active disease [9, 17–19], and is controversial as far as the usefulness of unilateral lobar bronchoalveolar lavage as a true reflection of disease activity is concerned [20, 21]. Therefore, the evaluation of the serial chest radiograph may be a judicious means to assess disease activity in sarcoidosis.

In this small series, we found that the chest radiograph was useful clinically because no patient was found with deterioration on radiographs who did not eventually need and respond to corticosteroids. However, we assessed the chest



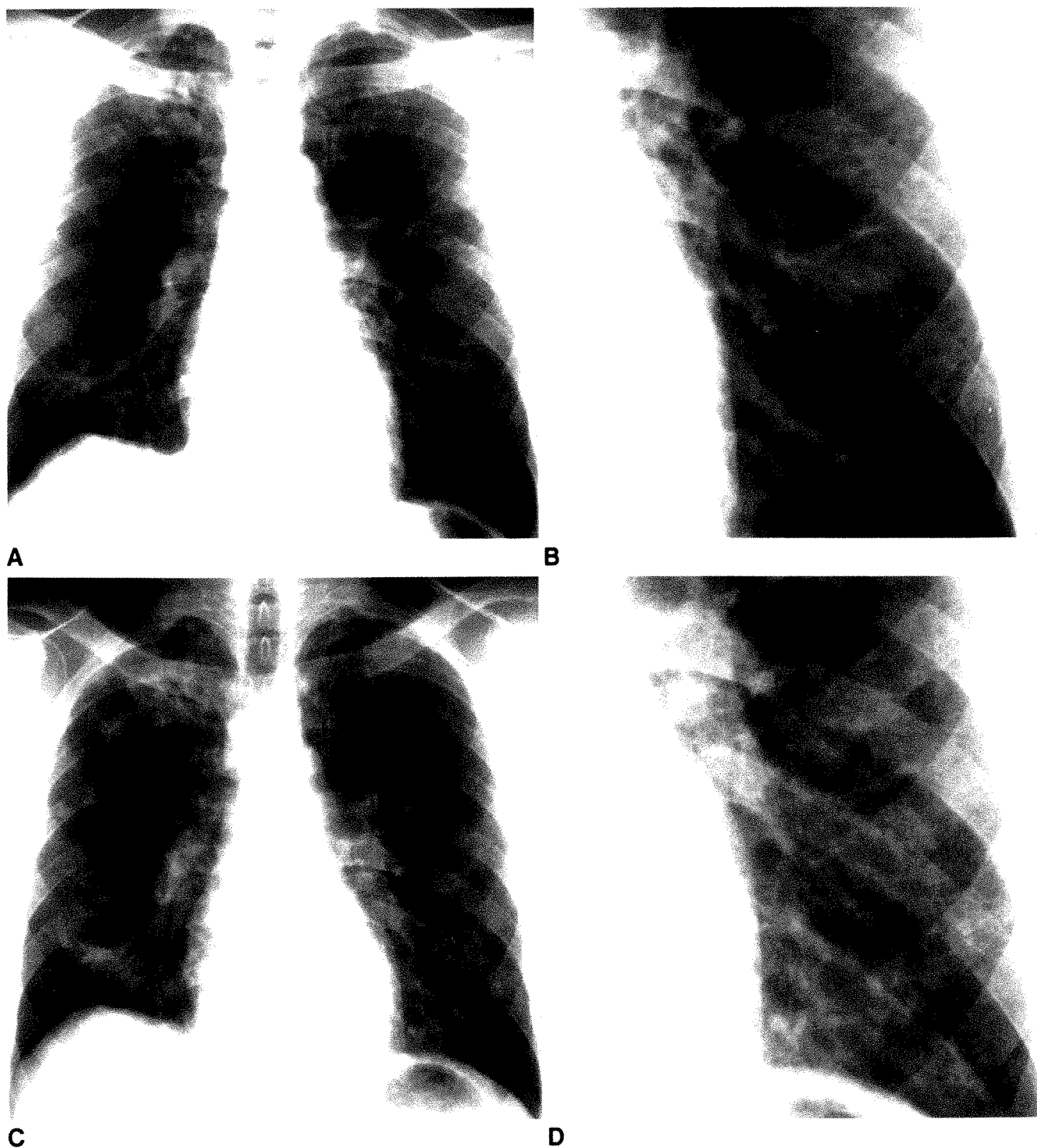


Fig. 1.—A–D, Chest radiographs in a 30-year-old patient with sarcoidosis show development of alveolar infiltrates related to corticosteroid withdrawal. Radiograph (A) and enlargement of part of left lung (B) made before corticosteroid withdrawal show hilar adenopathy and reticulonodular infiltrate consistent with stage 2 sarcoidosis. Subsequent radiograph (C) and enlargement of part of left lung (D) made during corticosteroid withdrawal show development of an alveolar pattern infiltrate.

radiograph in a subset of sarcoidosis patients who underwent corticosteroid withdrawal. The frequency of deterioration shown on radiographs in this group may differ from that in patients not exposed to corticosteroids or on a stable dose

of corticosteroid. Additionally, as in any retrospective study, some factors were uncontrollable. The timing of spirometry and chest radiographs varied from patient to patient, making analysis and recommendations regarding the timing of these

tests during corticosteroid withdrawal difficult. Additionally, the manner in which corticosteroid dose was tapered varied from patient to patient.

In conclusion, despite the chest radiograph being considered by some investigators as an inadequate test to assess the activity of sarcoidosis, we found that the chest radiograph was useful in detecting sarcoidosis deterioration during corticosteroid withdrawal, with a sensitivity of 70% and a specificity of 100%. Further, monitoring of sarcoidosis disease activity with the forced vital capacity was validated by its improvement or stabilization after corticosteroid increase in all 10 patients who had a relapse clinically. However, the chest radiograph may show this deterioration before a decline in forced vital capacity is noted and permit earlier corticosteroid intervention. The clinical importance of earlier discovery of sarcoidosis deterioration during corticosteroid withdrawal by using chest radiography was not assessed and requires further study, both to confirm our observations and to determine the clinical usefulness. We conclude that serial chest radiography can reflect relapse related to corticosteroid withdrawal in patients with sarcoidosis.

#### ACKNOWLEDGMENTS

The authors thank Steven Schabel and Nancy Curry, Department of Radiology, Medical University of South Carolina, for their interpretation of the chest radiographs.

#### REFERENCES

- Mitchell DN, Scadding JG, Heard BE, et al. Sarcoidosis: histopathological definition and clinical diagnosis. *J Clin Pathol* 1977;30:395-408
- James DG, Nevill E, Silzbach LE, et al. A worldwide survey of sarcoid. *Ann NY Acad Sci* 1976;278:321-334
- DeRemee RA. The roentgenographic staging of sarcoidosis: historic and contemporary perspectives. *Chest* 1983;83:128-133
- Flint K, Chir B, Johnson N. Intrathoracic sarcoidosis. *Semin Respir Med* 1985;3:41-51
- Israel H, Karlin P, Menduke H, DeLisser O. Factors affecting outcome of sarcoidosis: influence of race, extrathoracic involvement and initial radiologic lung lesions. *Ann NY Acad Sci* 1986;465:609-617
- Eule H, Weinecke A, Roth I. The possible influence of corticosteroid therapy on the natural course of pulmonary sarcoidosis: late results of a continuing clinical study. *Ann NY Acad Sci* 1986;465:695-701
- Johns CJ, MacGregor MI, Zachary JB, et al. Extended experience in the long-term corticosteroid treatment of pulmonary sarcoidosis. *Ann NY Acad Sci* 1976;278:722-731
- Rizzato G. Markers of activity. *Semin Respir Med* 1986;8:30-41
- Crystal RG. NIH Conference: pulmonary sarcoidosis: a disease characterized and perpetuated by activated lung T-lymphocytes. *Ann Intern Med* 1981;73-94
- Winterbauer RH, Hutchinson JF. Clinical significance of pulmonary function tests: use of pulmonary function tests in the management of sarcoidosis. *Chest* 1980;78:640-647
- Huang CT, Heurich AE, Rosen Y, Moon S, Lyons HA. Pulmonary sarcoidosis. Roentgenographic, functional, and pathologic correlations. *Respiration* 1979;37:337-345
- Marshall R, Karlsh AJ. Lung function in sarcoidosis. *Thorax* 1971;26:402-405
- Baughman RP. Sarcoidosis: usual and unusual manifestations. *Chest* 1988;94:165-170
- Putman CE, Hoeck B. Reassessing the standard chest radiograph for intraparenchymal activity. *Ann NY Acad Sci* 1986;465:595-608
- Sahn SA, Schwarz MI, Lakshminarayan S. Sarcoidosis: the significance of an acinar pattern on chest roentgenogram. *Chest* 1974;65:384-387
- Shigematsu N, Eori K, Matsuba K, Harada S, Takahashi T. Clinicopathologic characteristics of pulmonary acinar sarcoidosis. *Chest* 1978;73:186-187
- Lin YH, Haslam PI, Turner-Warwick M. Chronic pulmonary sarcoidosis: relationship between lung lavage cell counts, chest radiograph, and results of standard lung function tests. *Thorax* 1985;40:501-507
- Hunninghake GW, Gadek JE, Kawanami O, Ferrans VJ, Crystal RG. Inflammatory and immune processes in the human lung in health and disease: evaluation by bronchoalveolar lavage. *Am J Pathol* 1979;97:149-206
- Yeager H, Williams MC, Beekman JF. Sarcoidosis: analysis of cells obtained by bronchial lavage. *Am Rev Respir Dis* 1977;116:951-955
- Staton GW, Check IJ, Fajman WA, Gilman MJ, Pine JR. Analysis of homogeneity of alveolitis in pulmonary sarcoidosis by bilateral bronchoalveolar lavage, gallium-67 lung uptake, and chest radiograph. *Sarcoidosis* 1987;4:8-12
- Cantin A, Raymond B, Rola-Pleszczynski M, Boileau R. Heterogeneity of bronchoalveolar lavage cellularity in stage III pulmonary sarcoidosis. *Chest* 1983;83:485-486

## Book Review

### **Chest Radiographic Analysis.** By Norman Blank. New York: Churchill Livingstone, 673 pp., 1989. \$125

Remember your days as a first-year resident in radiology confronting the vast world of chest radiology and those enormous textbooks? Before my residency, I had obtained a copy of one of Benjamin Felson's earliest efforts, and I can remember sitting in a tent in Vietnam wondering if I ever would understand the simple chest film. For a first- or second-year radiology resident, the choices were indeed sparse. Felson's later work, *Chest Roentgenology*, or Meschan's first edition of *Analysis of Roentgen Signs in General Radiology* were well organized and student oriented, or the neophyte could take on *Diagnosis of Diseases of the Chest* by Fraser and Paré if he or she had enough tenacity. Then came Lucy Squire, who injected humor into an already dynamic text covering the basic fundamentals. But, time has gone by, and advances in chest radiology since the advent of CT and MR require a new approach. Norman Blank fills this need with a book aimed at helping medical students and residents learn the principles of chest-film interpretation. In his work, Blank aspires to teach the student to analyze radiographic data, decide whether findings are normal or abnormal, and integrate radiographic data with clinical findings in order to arrive at a differential diagnosis.

Beyond an introductory section dealing with methods of chest-film analysis, the structure of the book is gleaned easily from the table of contents: the pleura; localizing pulmonary lesions and analyzing pulmonary collapse; pulmonary infection; nodules and neoplasms; the mediastinum; evaluation of the hila and mediastinal tumors, aneurysms, and vascular anomalies; pulmonary edema and edemalike conditions, pulmonary embolism, and infarction; subacute and chronic noninfectious lung disease; and blunt chest trauma. Conspicuously missing are congenital and developmental abnormalities and pulmo-

nary problems of infancy. Bone lesions and cardiac disorders also receive limited space. All images appear in an atlas at the end of the particular chapter in which they are cited. I prefer pictures and diagrams to be inserted in the text rather than lumped at the end. The legends, although useful as a summary, often are lengthy and require extensive page flipping. The radiographs, however, are superb, as are the CT scans and MR images.

Blank's book lacks the breadth of a reference book (try the new edition of *Roentgen Signs in Diagnostic Imaging*). It also could use more diagrams, mnemonics, and humor, but this is only a minor criticism. For its expertise in teaching analysis of chest films and for the excellent images, I heartily recommend it for beginning residents.

Unfortunately, in opting for Blank's text over Felson's, radiology residents will miss Felson's comment on attempts to make a definitive diagnosis on the basis of only one or two films. This feat Felson compared with that of a little boy who, when asked why he always held his thumb in his mouth, replied, "Where else can I put it?" "Although the obvious answer was not supplied in that instance, [Felson continues] it should be emphasized here that one should give conscious consideration to additional studies in every case presenting a diagnostic problem." Blank's work provides yet another additional study worthy of conscious consideration. It serves the professor well as a teaching tool and the resident as a learning device.

Lee B. Milner  
Bluefield Regional Medical Center  
Bluefield, WV 24701

# CT in Differential Diagnosis of Diffuse Pleural Disease

Ann N. Leung<sup>1</sup>  
Nestor L. Müller<sup>1</sup>  
Roberta R. Miller<sup>2</sup>

The CT features of benign and malignant pleural diseases have been described. However, the accuracy of these features in the differential diagnosis of diffuse pleural disease has not been assessed before. Without knowledge of clinical or pathologic data, we reviewed the CT findings in 74 consecutive patients with proved diffuse pleural disease (39 malignant and 35 benign). The patients included 53 men and 21 women 23–78 years old. Features that were helpful in distinguishing malignant from benign pleural disease were (1) circumferential pleural thickening, (2) nodular pleural thickening, (3) parietal pleural thickening greater than 1 cm, and (4) mediastinal pleural involvement. The specificities of these findings were 100%, 94%, 94%, and 88%, respectively. The sensitivities were 41%, 51%, 36%, and 56%, respectively. Twenty-eight of 39 malignant cases (sensitivity, 72%; specificity, 83%) were identified correctly by the presence of one or more of these criteria. Malignant mesothelioma ( $n = 11$ ) could not be reliably differentiated from pleural metastases ( $n = 24$ ).

We conclude that CT is helpful in the differential diagnosis of diffuse pleural disease, particularly in differentiation of malignant from benign conditions.

*AJR* 154:487–492, March 1990

A number of benign and malignant diseases may cause diffuse pleural abnormalities. The most common causes are asbestos-related pleural fibrosis, fibrothorax, empyema, mesothelioma, and metastatic disease. The characteristic CT appearances of these and other diffuse pleural diseases have been described [1–10]. However, no study has analyzed the value of CT in the differential diagnosis of diffuse pleural disease. Because diffuse pleural abnormalities usually consist of various degrees of pleural thickening, calcification, and effusion, an overlap of the CT manifestations of the different benign and malignant pleural diseases would be expected. The aim of our study was to determine the CT features most helpful in the differential diagnosis of diffuse pleural disease.

## Materials and Methods

All patients with diffuse pleural disease seen in our institution between May 1985 and March 1989 who had a definitive diagnosis and in whom CT scans had been obtained were included in this retrospective study. Seventy-four patients were selected by reviewing the medical records and CT reports. Fifty-three were men and 21 were women, with a mean age of 60 years (range, 23–78 years). The hemithorax with the most involvement was the right in 41 cases and the left in 33.

Definitive pathologic diagnosis based on the results of pleural biopsy was available in 38 of 39 cases of malignant pleural disease (11 mesothelioma, 22 metastatic pleural carcinoma, three non-Hodgkin lymphoma, one metastatic melanoma and one liposarcoma), five of eight cases of fibrothorax, and seven of 11 infectious processes. The diagnosis of metastatic adenocarcinoma in one patient was based on cytologic findings in a sample obtained by thoracentesis as well as the concomitant findings of multiple brain and lung metastases. The

Received August 31, 1989; accepted after revision October 16, 1989.

<sup>1</sup> Department of Radiology, University of British Columbia, and Vancouver General Hospital, 855 W. 12th Ave., Vancouver, B.C., Canada V5Z 1M9. Address reprint requests to N. L. Müller.

<sup>2</sup> Department of Pathology, University of British Columbia, and Vancouver General Hospital, 855 W. 12th Ave., Vancouver, B.C., Canada V5Z 1M9.

0361-803X/90/1543-0487

© American Roentgen Ray Society



three patients with fibrothorax who did not have biopsy had known previous history of treated tuberculosis and no change in pleural thickening for 1 year or more.

The 16 patients with asbestos-related pleural disease had documented exposure to asbestos and had been referred either for evaluation of questionable radiographic findings with associated abnormal pulmonary function tests or pleural effusion of unknown cause. All 16 patients had diffuse pleural thickening, defined as blunting of the costophrenic sulcus or localized areas of thickening extending for more than 5 cm in both craniocaudal and transverse diameters. Patients with pleural plaques only were excluded. Six months to 3 years of follow-up in these 16 patients has shown no evidence of malignancy. Infectious pleural disease was diagnosed on the basis of positive cultures of pleural fluid with biopsy confirmation performed in three of four tuberculous empyemas, two of five non-tuberculous empyemas, and both cases of actinomycosis.

The CT scans were obtained on a General Electric 8800 (10 patients) or 9800 (64 patients) scanner (GE Medical Systems, Milwaukee, WI). Contiguous 1-cm collimation scans were obtained from lung apices to the level of the adrenals. All scans were obtained at end-inspiratory lung volumes by using the standard algorithm and were photographed at windows appropriate for lung parenchyma and mediastinum. In 31 cases, additional 1.5-mm collimation scans were obtained at selected levels specific to each case. These thin-section images were reconstructed by using a field of view of 20–25 cm and a high-spatial-resolution algorithm (bone algorithm, high-resolution CT). Except for the asbestos-exposed group, contrast material was administered routinely.

The CT scans were done as part of the initial assessment of these patients at our institution. The CT scans and accompanying chest radiographs were reviewed by two observers who were unaware of the pathologic diagnosis; a conclusion was reached by consensus. The scans were assessed for the presence of pleural effusion; presence, type, and extent of pleural thickening as suggested by previous studies [1–3]; presence or absence of extrapleural invasion; adenopathy; calcified nodes; loss of volume in the involved hemithorax; and coexisting pulmonary parenchymal abnormalities. Mediastinal nodes were considered enlarged if they were greater than 10 mm in long-axis diameter in the transverse plane.

Pleural thickening was classified as either focal plaques or diffuse thickening. Pleural plaques were defined as areas of pleural thickening less than 5 cm in either transverse or craniocaudal extent. The

location of the pleural thickening was classified as parietal, visceral, fissural, or mediastinal. Mediastinal involvement was defined as pleural thickening bordering the mediastinum, and no attempt was made to differentiate parietal from visceral mediastinal pleural involvement. The distinction between visceral and parietal pleural thickening was made only in the presence of pleural effusion. The contour of the pleural thickening was characterized as smooth, irregular, or nodular. Parietal pleural involvement was further characterized by whether it was circumferential (defined as involvement of entire perimeter of hemithorax including mediastinum, or pleural rind), width of thickening, length of craniocaudal extension, and presence or absence of involvement of the lung bases (defined as pleural thickening in the lower third of the hemithorax). Pleural calcification was classified as involving plaques or diffuse thickening. In the cases for which high-resolution CT was available, these additional scans were judged to be of benefit when they enabled a classification change in any of the previously noted characteristics.

All pathologic specimens were reviewed by a pathologist. The histologic assessment of benign vs malignant was determined on the basis of standard architectural and cytologic features. The 11 mesotheliomas included one low-grade papillary epithelial mesothelioma, one desmoplastic mesothelioma, and nine more usual epithelial and mixed patterns. In cases in which the differential diagnosis was between adenocarcinoma and epithelial mesothelioma, the diagnosis of adenocarcinoma was made if neutral mucin and/or carcinoembryonic antigen could be shown [11, 12].

The clinical data were obtained from hospital and office charts. Statistical comparison between selected patient groups was performed by using the chi-square test.

## Results

Seventy-one patients had pleural thickening on CT. In three cases, unilateral pleural effusion was the sole CT manifestation of diffuse pleural malignancy (Table 1).

In patients with pleural thickening, the features most suggestive of a malignant cause were pleural rind (a finding seen only in patients with malignant pleural disease), with a specificity of 100% and a sensitivity of 41%; nodular pleural thickening, with a specificity of 94% and a sensitivity of 51%; parietal pleural thickening greater than 1 cm, with a specificity

TABLE 1: Characteristics of Pleural Disease

Characteristic	Mesothelioma (11)	Metastases (24)	Lymphoma (3)	Asbestos (16)	Empyema (9)	Fibrothorax (8)	Actinomycosis (2)
Nodularity	7	12	1	0	0	2	0
Rind	8	8	0	0	0	0	0
Thickness >1 cm	6	5	2	1	0	1	0
Mediastinal pleural involvement	8	13	1	1	2	1	0
Calcification	0	3	0	11	1	4	0
Invasion	1	2	0	0	0	0	0
Unilateral involvement	9	14	2	0	8	4	2
Extension through entire hemithorax	6	8	0	2	3	2	0
Lung base involvement	8	21	1	15	9	8	2
Visceral pleural involvement	7	11	0	6	9	5	0
Fissural involvement	4	3	0	5	2	2	0
Effusion	11	21	2	6	9	5	0
Plaques	3	3	0	10	0	1	0
Hilar or mediastinal adenopathy	5	10	2	4	2	4	0
Calcified nodes	0	2	0	1	1	3	0
Loss of volume	7	13	1	7	7	3	0

Note.—One case of pleural liposarcoma was not included in this table but was included in the series. Numbers in parentheses are number of patients in each category.

of 94% and a sensitivity of 36%; and mediastinal pleural involvement, with a specificity of 88% and a sensitivity of 56% (Table 1, Figs. 1 and 2). All these features were significantly more common in malignant than in benign pleural thickening ( $p < .01$ , chi-square test). Twenty-eight of 39 cases of malignant pleural disease had one or more of these features as compared with only six of 35 cases of benign pleural disease, representing a sensitivity of 72% and a specificity of 83% for malignancy (Table 1, Fig. 3). The presence of pleural calcification was suggestive of benign cause, with a sensitivity of 46% and a specificity of 92% (Table 1).

In most patients with mesothelioma, the CT findings were identical to those of metastatic pleural disease, including the presence of nodular pleural thickening, pleural rind, mediastinal or chest wall invasion, and loss of volume (Table 1, Fig. 4). Pleural effusion as the only manifestation of pleural malignancy was a feature seen in pleural metastases (two of 24) and not in mesothelioma.

Pleural lymphoma was indistinguishable from other malignant pleural involvement. In this group, adenopathy (hilar and/or mediastinal) was a more consistent finding (two of three); circumferential pleural rind was not seen. The only case of pleural liposarcoma had a virtually pathognomonic appearance: an inhomogeneous pleurally based mass of tissue density intermixed with several areas of fat. Parietal pleural thickening was greater than 1 cm and irregular in contour; invasion into both mediastinum and chest wall was present.

Features distinguishing mesothelioma from benign asbestos-related pleural thickening were essentially the same as those differentiating neoplastic from benign disease (Table 1). The two most useful features in differentiating asbestos-related pleural disease from other benign conditions were the presence of pleural plaques, with a specificity of 95% ( $p < .01$ ) and bilateral pleural involvement, with a specificity of 74% ( $p < .01$ ) for asbestos-related pleural disease (Fig. 5).

All nine cases of empyema were seen on CT as a round or lenticular fluid collection separating slightly thickened visceral and parietal pleural surfaces (Fig. 6). The thickened pleura was usually smooth although sometimes irregular; neither nodularity nor thickening greater than 1 cm was seen (Table 1).

High-resolution CT was helpful in 19 of 31 cases. In 10 cases, better definition of asbestos-related parenchymal changes was obtained; in the remainder, the higher resolution scans confirmed equivocal mediastinal or fissural involvement and nodular pleural thickening (Fig. 2).

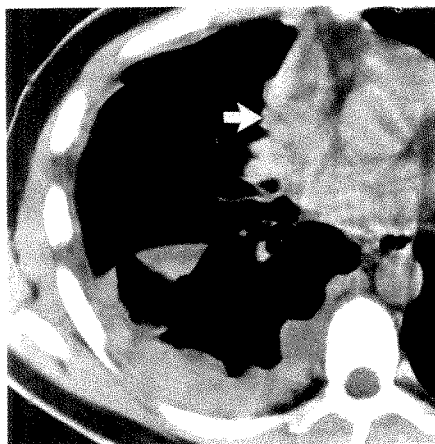


Fig. 1.—1-cm collimation CT scan at level of left atrium in a patient with metastatic melanoma shows right-sided nodular pleural thickening  $>1$  cm. Nodular thickening also involves mediastinal pleura (arrow) and major fissure.

## Discussion

Pleural response to a variety of diseases is limited largely to three radiologically detectable manifestations: effusion, thickening, and calcification.

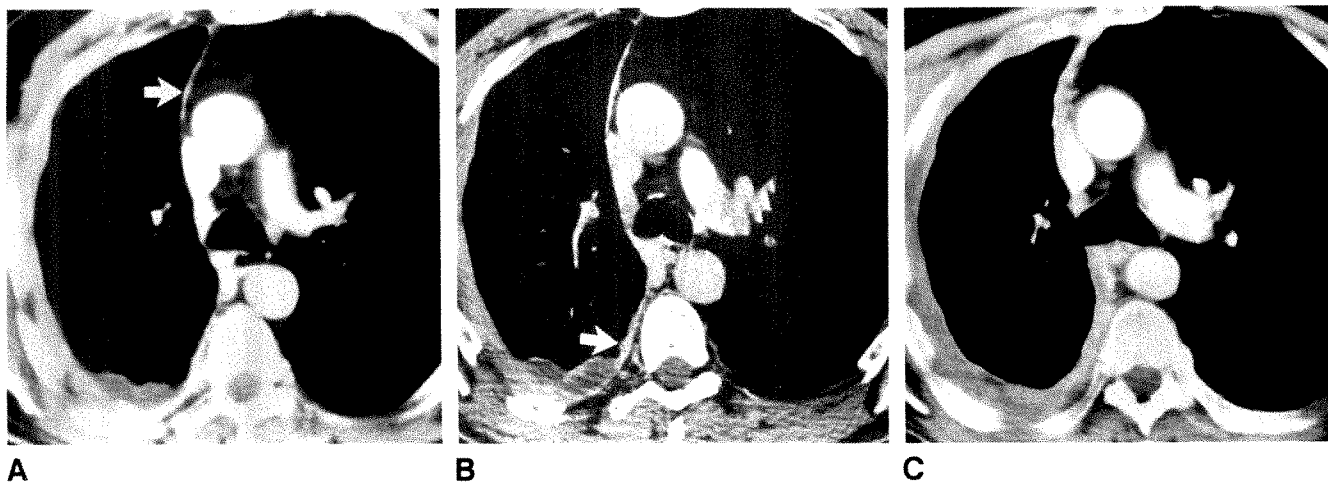
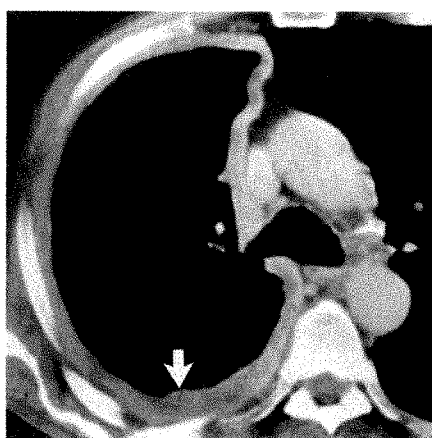


Fig. 2.—CT scans at level of tracheal carina in a 59-year-old man with desmoplastic mesothelioma.  
 A, 1-cm collimation scan at time of presentation shows circumferential right-sided pleural thickening and subtle mediastinal involvement (arrow).  
 B, 1.5-mm collimation scan at time of presentation shows improved definition of the circumferential pleural changes and nodular pleural thickening (arrow).  
 C, 1-cm collimation scan 4 months after presentation shows an increase in width of pleural thickening.



Fig. 3.—1.5-mm collimation CT scan in a patient with fibrothorax caused by *Mycobacterium avium-intracellulare* infection shows nodular pleural thickening with involvement of right major fissure and mediastinal pleura. Anterior surface of parietal pleura was normal. Nodular pleural thickening and mediastinal pleural thickening are usually indicative of malignant pleural disease; they are seen in 14% or less of patients with benign pleural thickening.



A

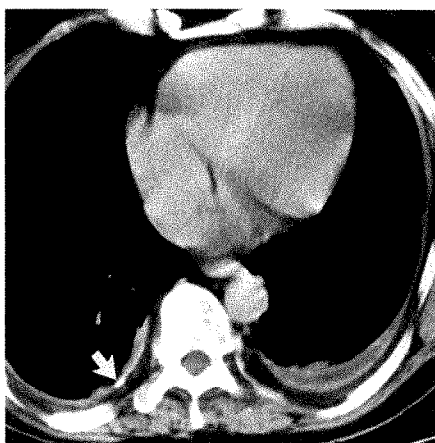


B

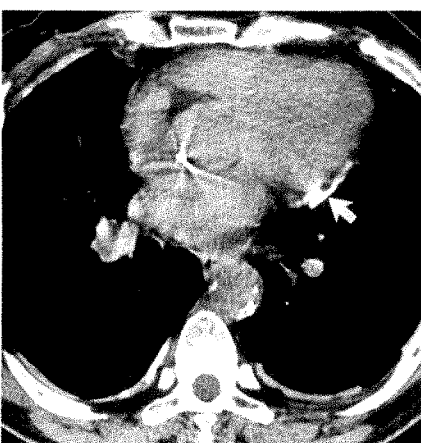
Fig. 4.—Pleural rind.

A, 1-cm collimation CT scan in a 75-year-old man with mesothelioma shows circumferential pleural thickening with mediastinal involvement (pleural rind). Pleural thickening is >1 cm in maximal width (arrow).

B, 1-cm collimation CT scan in a 45-year-old woman with metastatic adenocarcinoma shows a pleural rind with focal areas of nodularity (arrows). CT appearance of metastatic pleural disease cannot be distinguished from malignant pleural mesothelioma.



A



B

Fig. 5.—Asbestos-related pleural disease.

A, 1-cm collimation scan in a 62-year-old man with history of asbestos exposure shows bilateral pleural thickening with a calcified plaque (arrow) and a small left pleural effusion. Parietal pleural thickening extends into anterior third of left hemithorax but does not involve mediastinal pleura.

B, 1.5-mm collimation CT scan in a 61-year-old man with history of asbestos exposure shows bilateral pleural thickening with calcified parietal and mediastinal (arrow) plaques.

Pleural effusion is a common manifestation of diffuse pleural disease. The major objective in CT assessment of unexplained pleural effusion is establishment of benign vs malignant cause. As the main mechanism of pleural fluid formation in malignancy is lymphatic obstruction, the site of blockage may be present at any point between the stomata of parietal pleura and the mediastinal lymph nodes [13]. The resulting effusion is usually an exudate. With the possible exception of hemothorax, measurement of fluid attenuation coefficients has proved unreliable in distinguishing fluid composition [4, 14]. Maffessanti et al. [8] suggested that the absence of pleural thickening does not preclude a neoplastic diagnosis. In that series, seven of 12 patients with normal-appearing pleura had malignant effusions. Our results are similar; in three cases, pleural effusion was the sole manifestation of neoplastic pleural involvement. During thoracotomy in one of

these patients, nodules were seen over the entire surface of the visceral pleura, although pleural thickening could not be seen on CT even in retrospect. Thus, the absence of pleural thickening on CT does not rule out pleural malignancy.

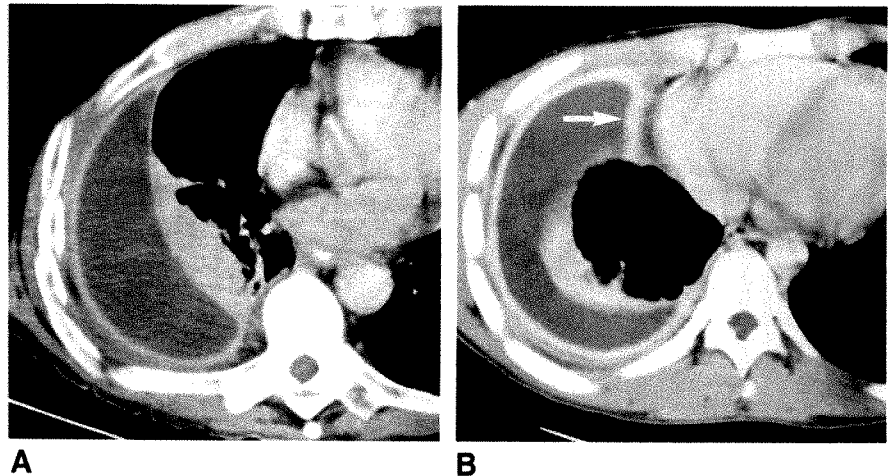
In the presence of pleural thickening, the most useful features in the differentiation of malignant from benign pleural disease are the presence of pleural rind, pleural nodularity, pleural thickening greater than 1 cm, and mediastinal pleural involvement. These features may be seen in mesothelioma and in metastatic pleural disease but are unusual in benign pleural disease. These CT features correlate closely with the pathologic findings. Malignant pleural disease tends to involve the entire pleural surface, whereas reactive pleurisy usually does not affect the mediastinal pleura [15, 16].

The CT differentiation of benign and malignant pleural disease is important because the specific diagnosis is often

Fig. 6.—Empyema.

A, 1-cm collimation CT scan in a patient with a nontuberculous empyema shows a lenticular fluid collection separating smoothly thickened layers of parietal and visceral pleura. Although pleural thickening is extensive, this does not involve mediastinal pleura (i.e., it is not circumferential). Areas of atelectasis are present in right lower lobe.

B, 1-cm collimation CT scan in a patient with a tuberculous empyema shows anterior mediastinal pleural involvement (arrow).



difficult to make by clinical criteria, pleurocentesis, and percutaneous pleural biopsy. Not rarely, a diagnostic thoracotomy is required because of the need to assess the growth pattern of disease and to obtain a relatively large amount of tissue for histologic, immunocytochemical, and ultrastructural studies [11]. Even careful examination and biopsy of the pleura at thoracotomy can fail to establish the diagnosis [17, 18]. Ryan et al. [17] reported 51 patients in whom no cause for a pleura effusion was found at thoracotomy. In 13 of these patients (25%), the diagnosis of malignancy (including lymphoma, carcinoma, and malignant mesothelioma) was established 12 days to 5 years after thoracotomy. The difficulty in pathologically differentiating benign reactive mesothelial cells from mesothelioma is a common and well-known problem, and in many instances, the gross appearance assumes great importance in making this distinction [11]. Insofar as the CT appearance reflects the gross distribution of disease, we believe that the CT findings are helpful in determining whether thoracotomy is recommended and in guiding the surgeon to the sites most likely to yield a positive diagnosis. These sites would include areas with greater than 1 cm pleural thickening, nodular pleural thickening, and thickening of the mediastinal pleura.

The presence of pleural calcification suggests a benign process. In this series, calcification was seen in 16 of 35 patients with benign pleural thickening and in only three of 39 patients with malignant pleural disease. Although calcified plaques may be seen in cases of mesothelioma, they are uncommon [3] and were not seen in any of our 11 mesothelioma patients. The relative absence of pleural calcification in mesothelioma may be due to absorption of calcification by the developing tumor [10] and the fact that a significant number of malignant mesotheliomas (range, 0–87%) are not asbestos-related [19].

Difficulty in distinguishing between mesothelioma and metastatic pleural involvement pathologically [11, 20] and radiologically [3, 5–7] has been recognized. Pathologic diagnosis requires adequate sampling; cytologic examination of pleural fluid and needle biopsy specimens rarely allows a definitive diagnosis of mesothelioma and may provide the misleading interpretation of metastatic carcinoma or benign pleural disease [9, 21, 22]. Discrimination between epithelial types of

mesothelioma and metastatic adenocarcinoma requires histochemical, immunohistochemical, and ultrastructural analysis [11, 12].

Invasion of the chest wall or mediastinum on CT are specific markers for malignancy but have a low sensitivity; they were present in only 8% of patients with malignant pleural involvement in our series. In addition, this sign was not useful in distinguishing mesothelioma from carcinoma. The limitations of CT in assessing the presence or absence of invasion into the chest wall or mediastinum in mesothelioma also have been demonstrated recently by Rusch et al. [23].

Adams et al. [24] have suggested that the presence of hilar adenopathy may be helpful in differentiating metastases from mesothelioma. However, true hilar involvement with no mediastinal involvement is rare in metastatic pleural disease except for bronchogenic carcinoma, lymphoma, and renal cell carcinoma [25]. In our study, hilar adenopathy was identified in only two patients with malignancy. One case was a non-Hodgkin lymphoma and the second case was an adenocarcinoma.

The tendency of mesothelioma to involve the inferior hemithorax has been postulated to be a specific sign [10]. However, in our study basal involvement was present not only in patients with mesothelioma but also in the majority of patients with metastatic pleural disease.

Benign asbestos pleural effusion has been shown by Epler et al. [26] to occur with an approximate prevalence of 3% in the asbestos-exposed population. Effusion is usually unilateral but may be bilateral; other etiologic manifestations of asbestos-related disease may be present or absent. Differentiation between benign asbestos pleural effusion and asbestos-related malignant mesothelioma usually can be made on the basis of the much shorter latency period of benign effusion, which ranges from 10 to 20 years from time of initial exposure [26]. However, close follow-up is necessary as the effusion may be the first manifestation of mesothelioma [3], and routine radiologic studies have been advocated for mesothelioma screening in this high-risk population [22].

Nodularity of pleura has been recognized as a helpful discriminating feature [2, 3, 10]. In our study, nodular pleural thickening was seen in seven (63%) of 11 cases of mesothelioma and in none of the cases of benign asbestos-related

diffuse pleural disease. However, extensive nodular thickening of pleural plaques mimicking mesothelioma has been described [3]. In such cases, open pleural biopsy is the only reliable way to establish the definitive diagnosis of benign disease.

Although loss of volume is a common manifestation in mesothelioma [3], it is also a relatively nonspecific finding seen in a variety of other malignant and benign conditions [6]. In our series, volume loss was seen in approximately 50% of patients, irrespective of the cause of the diffuse pleural disease.

Benign pleural asbestos-related disease generally is acknowledged to be a symmetrical process [27, 28], and in all 16 of our cases, pleural involvement was bilateral. Typically, the changes affect the posterolateral aspect of the pleura [29]. In one of our cases of early malignant mesothelioma, the only sign that suggested possible tumor was the unilaterality of pleural involvement. Although this is not a useful feature in differentiation from other benign diseases, in the select asbestos-exposed subgroup, unilaterality or marked asymmetry of pleural thickening must be considered suggestive of mesothelioma.

Asbestos-related pleural disease was the only benign disease that could be specifically suggested from the CT scan by virtue of the presence of bilateral pleural plaques. Although smooth pleural thickening with associated effusion was suggestive of empyema, such features also were observed in a number of noninfectious processes. No characteristic features of fibrothorax were identified.

Aberle et al. [29, 30] found that high-resolution CT was more sensitive than conventional CT in detection of asbestos-related pleural and parenchymal fibrosis. Our study similarly shows that the scans with higher spatial resolution improved detection of subtle asbestos-related parenchymal changes and allowed confirmation of pleural changes deemed equivocal on conventional CT.

Our study was limited by the relatively small number of cases of some diseases and by the relatively small number of diseases included. However, as all consecutive cases of confirmed diffuse pleural disease studied during a 4-year period were included, this study is a reflection of the incidence and prevalence of the types of diffuse pleural disease posing diagnostic problems in our institution.

We conclude that the CT features most helpful in distinguishing malignant from benign pleural disease are pleural rind, nodular pleural thickening, pleural thickening greater than 1 cm, and mediastinal pleural involvement. Pleural calcification usually implies a benign process. Loss of volume is not a helpful feature. In the majority of patients, mesothelioma cannot be distinguished from metastatic pleural disease on CT. High-resolution CT is superior to conventional CT, particularly in the assessment of asbestos-related pleural disease.

## REFERENCES

1. Krel L. Computed tomography of the lung and pleura. *Semin Roentgenol* 1978;13:213-225

2. Katz D, Krel L. Computed tomography in pulmonary asbestosis. *Clin Radiol* 1979;30:207-213
3. Rabinowitz JG, Efremidis SC, Cohen B, et al. A comparative study of mesothelioma and asbestosis using CT and conventional chest radiography. *Radiology* 1982;144:453-460
4. Williford ME, Hidalgo H, Putman CE, Korobkin M, Ram PC. Computed tomography of pleural disease. *AJR* 1983;140:909-914
5. Grant DC, Seltzer SE, Antman KH, Finberg HJ, Koster K. Computed tomography of malignant pleural mesothelioma. *J Comput Assist Tomogr* 1983;7:626-632
6. Salonen O, Kivisaari L, Standertskjöld-Nordenstam C-G, Somer K, Mattson K, Tammilehto L. Computed tomography of pleural lesions with special reference to the mediastinal pleura. *Acta Radiol [Diagn] (Stockh)* 1986;27:527-531
7. Alexander E, Clark RA, Colley DP, Mitchell SE. CT of malignant pleural mesothelioma. *AJR* 1981;137:287-291
8. Maffessanti M, Tommasi M, Pellegrini P. Computed tomography of free pleural effusions. *Eur J Radiol* 1987;7:87-90
9. Mirvis S, Dutcher JP, Haney PJ, Whitley NO, Aisner J. CT of malignant pleural mesothelioma. *AJR* 1983;140:665-670
10. Krel L. Computed tomography in mesothelioma. *Semin Oncol* 1981;8:302-312
11. Roggli VL, Kolbeck J, Sanfilippo F, Shelburne JD. Pathology of human mesothelioma: etiologic and diagnostic considerations. *Pathol Annu* 1987;2:91-131
12. Ordonez NG. The immunohistochemical diagnosis of mesothelioma: differentiation of mesothelioma and lung adenocarcinoma. *Am J Surg Pathol* 1989;13:276-291
13. Sahn SA. The pleura. *Am Rev Respir Dis* 1988;138:184-234
14. Kollins SA. Computed tomography of the pulmonary parenchyma and chest wall. *Radiol Clin North Am* 1977;15:297-308
15. Herbert A. Pathogenesis of pleurisy, pleural fibrosis, and mesothelial proliferation. *Thorax* 1986;41:176-189
16. Barrett NR. The pleura, with special reference to fibrothorax. *Thorax* 1970;25:515-524
17. Ryan CJ, Rodgers RF, Unni KK, Hepper NGG. The outcome of patients with pleural effusion of indeterminate cause at thoracotomy. *Mayo Clin Proc* 1981;56:145-149
18. Douglass BE, Carr DT, Bernatz PE. Diagnostic thoracotomy in the study of "idiopathic" pleural effusion. *Am Rev Tuberc* 1956;74:954-957
19. Peterson JT, Greenberg SD, Buffler PA. Non-asbestos related malignant mesothelioma: a review. *Cancer* 1984;54:951-960
20. Szpak CA, Johnston WW, Roggli V, et al. The diagnostic distinction between malignant mesothelioma of the pleura and adenocarcinoma of the lung as defined by a monoclonal antibody (B72.3). *Am J Pathol* 1986;122:252-260
21. Shearin JC, Jackson D. Malignant pleural mesothelioma. *J Thorac Cardiovasc Surg* 1976;71:621-627
22. Strankinga WFM, Sperber M, Kaiser MC, Stam J. Accuracy of diagnostic procedures in the initial evaluation and follow-up of mesothelioma patients. *Respiration (Basel)* 1987;51:179-187
23. Rusch VW, Godwin JD, Shuman WP. The role of computed tomography scanning in the initial assessment and the follow-up of malignant pleural mesothelioma. *J Thorac Cardiovasc Surg* 1988;96:171-177
24. Adams VI, Unni KK, Muhm JR, Jett JR, Ilstrup DM, Bernatz PE. Diffuse malignant mesothelioma of pleura. *Cancer* 1986;58:1540-1551
25. Reed JC. *Chest radiology: plain film patterns and differential diagnosis*. Chicago: Year Book Medical Publishers, Inc., 1981
26. Epler GR, McLoud TC, Gaensler EA. Prevalence and incidence of benign asbestos pleural effusion in a working population. *JAMA* 1982;247:617-622
27. Sargent EN, Gordonson J, Jacobson G, Birnbaum W, Shaub M. Bilateral pleural thickening: a manifestation of asbestos dust exposure. *AJR* 1978;131:579-585
28. Preger L. *Asbestos-related disease*. New York: Grune and Stratton, 1978
29. Aberle DR, Gamsu G, Ray CS, Feuerstein IM. Asbestos-related pleural and parenchymal fibrosis: detection with high-resolution CT. *Radiology* 1988;166:729-734
30. Aberle DR, Gamsu G, Ray CS. High-resolution CT of benign asbestos-related diseases: clinical and radiologic correlation. *AJR* 1988;151:883-891



## Case Report

# Cavitary Pulmonary Metastases in Transitional Cell Carcinoma of Urinary Bladder

Priscilla W. Alexander,<sup>1</sup> Colleen Sanders, and Hrudaya Nath

Multiple cavitary nodules are not generally recognized as a manifestation of pulmonary metastases from transitional cell carcinoma of the bladder [1]. We present two cases of cavitary pulmonary nodules proved to be metastases from transitional cell carcinoma of the bladder. We submit that cavitary nodules should be considered as a variant of pulmonary involvement by metastatic transitional cell carcinoma of the bladder. We also recognize the need to prove the cause of cavitary nodules, suspected to be metastases, through biopsy.

## Case Reports

### Case 1

A 52-year-old man with a history of paraplegia who had had an indwelling suprapubic catheter for 9 years developed gross hematuria. A bladder tumor was resected transurethraly, and the diagnosis of grade IV/IV transitional cell carcinoma with squamous differentiation was established. Findings on a chest radiograph at this time were normal. A radical cystoprostatectomy was performed and an ileal conduit was created. Several areas of deep muscular invasion by bladder tumor were present. All lymph nodes sampled in a pelvic dissection were normal. No adjuvant therapy was instituted.

Two and one-half years later the patient presented with a 4-month history of a persistent cough. A chest radiograph revealed multiple nodules, several of which had undergone cavitation. The cavity walls were thick and slightly nodular (Fig. 1). Because cavitated nodules were considered unusual for metastatic transitional cell carcinoma, we considered the possibility of a second primary tumor. Transtho-

racic needle biopsy showed metastatic transitional cell carcinoma with squamous differentiation. The cytologic findings were similar to those seen in the specimen resected from the bladder.

### Case 2

A 56-year-old man developed hematuria and urinary hesitancy. After transurethral resection of a bladder tumor, a grade II/IV poorly differentiated papillary transitional cell carcinoma was diagnosed. Findings on an initial chest radiograph were normal. After radiation therapy, a radical cystectomy and bilateral distal ureterectomy with creation of an ileal conduit were performed. One and one-half years after surgery the patient returned, complaining of a nonproductive cough. A chest radiograph showed numerous pulmonary nodules, several of which were cavitated. The cavities were characterized by thick nodular walls and air/fluid levels (Fig. 2). The appearance of the chest was thought to be consistent with metastatic disease. The need to exclude a second primary tumor led to a transbronchial needle biopsy by which metastatic transitional cell carcinoma was diagnosed. The cytologic findings closely resembled those of the previously resected bladder tumor.

## Discussion

The spread of transitional cell carcinoma of the bladder is primarily due to the regional lymphatics, affecting the gluteal, obturator, and iliac lymph nodes. Distant metastasis typically does not occur in the absence of penetration of the deep muscular layer of the bladder by tumor. The most common sites of distant metastases are liver, lung, mediastinum, bone,

Received September 18, 1989; accepted after revision October 23, 1989.

<sup>1</sup> All authors: Department of Radiology, University of Alabama at Birmingham School of Medicine, 619 S. 19th St., Birmingham, AL 35233. Address reprint requests to H. Nath, Cardiopulmonary Section.

AJR 154:493-494, March 1990 0361-803X/90/1543-0493 © American Roentgen Ray Society



Fig. 1.—Chest radiograph shows a cavitary pulmonary nodule in right lower lobe. An intramural nodule is noted within cavity (arrowheads). Several other cavitary nodules also are present.

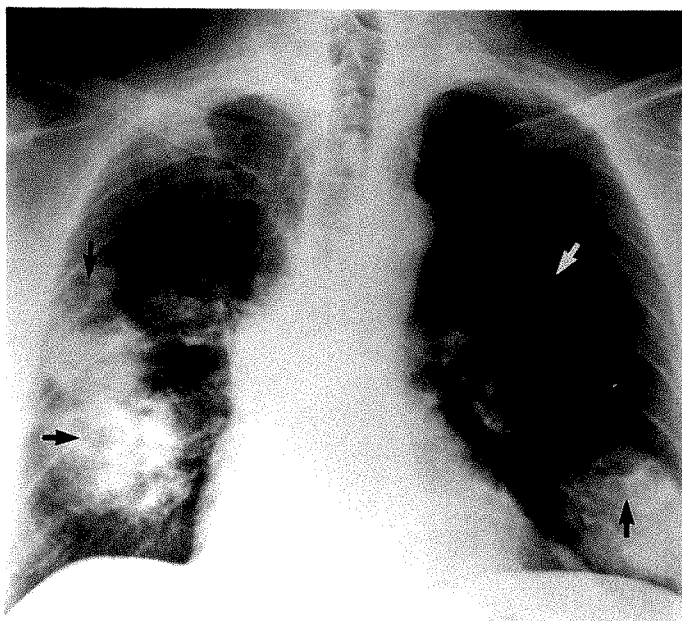


Fig. 2.—Chest radiograph shows multiple cavitary nodules (arrows) in both lungs. Some nodules have become confluent. Cavities have thick nodular walls and several contain air/fluid levels.

and adrenal gland in decreasing order of frequency [1, 2]. Patterns of usual pulmonary involvement include multiple nodules, a solitary mass, or interstitial micronodules. When multiple nodules are present, they are characteristically round and well-circumscribed without calcification or cavitation [1].

The differential diagnosis of multiple pulmonary cavities is not extensive. More common causes include bacterial, fungal, and parasitic infections and immunologic disorders such as Wegener granulomatosis or rheumatoid necrobiotic nodules. Cavitary pulmonary metastases are uncommon. Metastatic squamous cell cancer originating from the larynx, pharynx, esophagus, or uterine cervix accounts for up to two thirds of cavitary metastases. Adenocarcinoma of the colon or rectum is the primary tumor in nearly all of the remaining cavitary metastases. Transitional cell carcinoma of the bladder is rarely cited as a cause of cavitary metastases [3–6]. Ten cases of cavitary pulmonary metastases caused by bladder carcinoma have been reported. Five of those were transitional cell carcinoma, two were squamous cell cancer, and the remainder were not specified. The presence of squamous differentiation in the reported cases of transitional cell carcinoma was not documented.

The mechanism by which squamous cell cancer undergoes cavitation involves central desquamation and cornification allowing accumulation of semiliquid debris. The debris is expelled into the airway, leaving a residual cavity lined with malignant squamous epithelium [3]. As 50–80% of poorly differentiated transitional cell carcinomas show areas of squamous metaplasia, as in case 1, these metastatic tumors may cavitate by central desquamation. Nonsquamous neoplasms may cavitate after growth to several centimeters in diameter, which results in central ischemia and necrosis [3]. In metas-

tases from poorly differentiated transitional cell carcinoma without squamous differentiation, cavitation could be due to central necrosis. Chemotherapy also has been implicated as a cause of cavitation [7]. The mechanism in this situation is probably also tumor necrosis. The liquified contents may be removed by the lymphatics or expectorated. In this instance, the cavity walls are usually thin and virtually imperceptible on plain chest radiographs.

In summary, we present two cases of multiple cavitary pulmonary nodules proved by biopsy to be metastatic transitional cell carcinoma. Cavitary nodules should be considered as an uncommon manifestation of pulmonary involvement by metastatic transitional cell carcinoma. Early biopsy by either transthoracic or transbronchial means will confirm the metastatic nature of excavated pulmonary nodules in a patient with known transitional cell carcinoma of the bladder and will exclude the presence of a second malignant tumor.

#### REFERENCES

1. Goldman SM, Fajardo AA, Naraval RC, Madewell JE. Metastatic transitional cell carcinoma from the bladder: radiographic manifestations. *AJR* 1979;132:419–425
2. Fetter TR, Bogaev JH, McCusky B, Seres JL. Carcinoma of the bladder: sites of metastases. *J Urol* 1959;81:746–748
3. Dodd GD, Boye JJ. Excavating pulmonary metastases. *AJR* 1961;85:277–293
4. Chaudhuri MR. Cavitary pulmonary metastases. *Thorax* 1970;25:375–381
5. Weintraub RA. Roentgenogram of the month. *Dis Chest* 1963;44:633–634
6. Margolis RM, Liss HP. Unusual etiology of cystic lesions in the lung. *Chest* 1986;89:857–858
7. Kier R, Godwin JD. Residual cavities of lung metastases following chemotherapy. *Comput Radiol* 1986;10:293–296

## Case Report

# Reactivation of Tuberculosis in a Donor Lung After Transplantation

Sandra E. Carlsen<sup>1</sup> and Colleen J. Bergin

Recipients of organ transplants are at increased risk of infection not only because of immunosuppression but also because they are susceptible to infection from organisms transferred in the donor organs. Transfer of bacterial [1], viral [2], fungal [3], and protozoal [4] organisms from the donor organ has been well documented in renal and heart transplant recipients, and transfer of cytomegalovirus with clinical reactivation after heart and lung transplantation has been described [5]. Because the lung is a frequent site of chronic infection, transfer of latent pulmonary pathogens in transplanted lungs poses a special problem in heart and lung transplant recipients. We present a case of tuberculosis transmitted to the transplant recipient via the donor lung.

## Case Report

A combined heart and lung transplantation was performed in a 23-year-old woman in whom severe pulmonary arterial hypertension complicated type I truncus arteriosus. Routine immunosuppressive therapy after transplantation included prednisone, cyclosporine, azathioprine, and muromonab-CD3. Postoperatively, she was treated with cefazolin because the cultures from the donor bronchi were positive for *Klebsiella*. During the first 8 weeks after transplantation, she was treated with prednisone and methylprednisolone for one episode of cardiac rejection and with acyclovir and ganciclovir for cytomegalovirus pneumonitis diagnosed by transbronchial biopsy. She was clinically well by week 9, continuing antiviral medications as an outpatient.

Eleven weeks after transplantation, the patient was rehospitalized with fever, chills, and increasing cough. Chest radiographs showed

interval worsening of bilateral opacities in the lower lobes. Histologic specimens obtained at transbronchial biopsy revealed chronic inflammation and evidence of mild pulmonary rejection, but no cytomegalovirus inclusion bodies. She responded clinically and radiographically to treatment for pulmonary rejection with prednisone and methylprednisolone.

Sixteen weeks after transplantation, she was again hospitalized with deteriorating pulmonary status. Chest radiographs showed inhomogeneous bilateral pulmonary opacities with multiple small nodules and a left pleural effusion (Fig. 1A). CT scans also showed multiple, small pulmonary nodules (Fig. 1B) and calcified subcarinal and left hilar lymph nodes (Fig. 1C). Bronchial washings were positive for *Aspergillus*, which was treated with amphotericin B, and an atypical acid-fast bacillus, interpreted as a colonizer. Positive cytomegalovirus shell viral cultures in the oropharynx and urine necessitated retreatment with ganciclovir. After a 3-week course, amphotericin was discontinued because of progressive leukopenia and subsequent negative bronchial washings. Evaluation of the leukopenia by bone-marrow biopsy 21 weeks after transplantation showed a single noncaseating granuloma. After culture of acid-fast bacilli from specimens obtained by a left thoracentesis and bronchial washings, four antituberculous drugs were administered. One week later, the organism that had been identified on bronchoalveolar lavage as an atypical mycobacterium, and thought not to be a pathogen, was definitively identified as *Mycobacterium tuberculosis*. Of note, the preoperative skin test with tuberculin purified protein derivative (PPD) was negative. Histologic sections from transbronchial biopsy 25 weeks after transplantation showed necrotizing granulomatous inflammation. Chest CT at this time showed interval increase in size and number of the bilateral pulmonary nodules, peribronchial thickening, and pleural effusions.

Received August 14, 1989; accepted after revision October 4, 1989.

<sup>1</sup>Both authors: Department of Diagnostic Radiology and Nuclear Medicine, Stanford University School of Medicine, Stanford, CA 94305. Address reprint requests to C. J. Bergin.

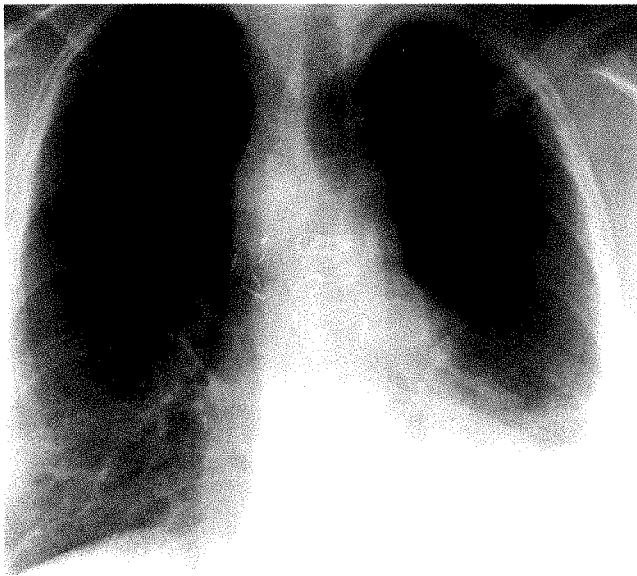
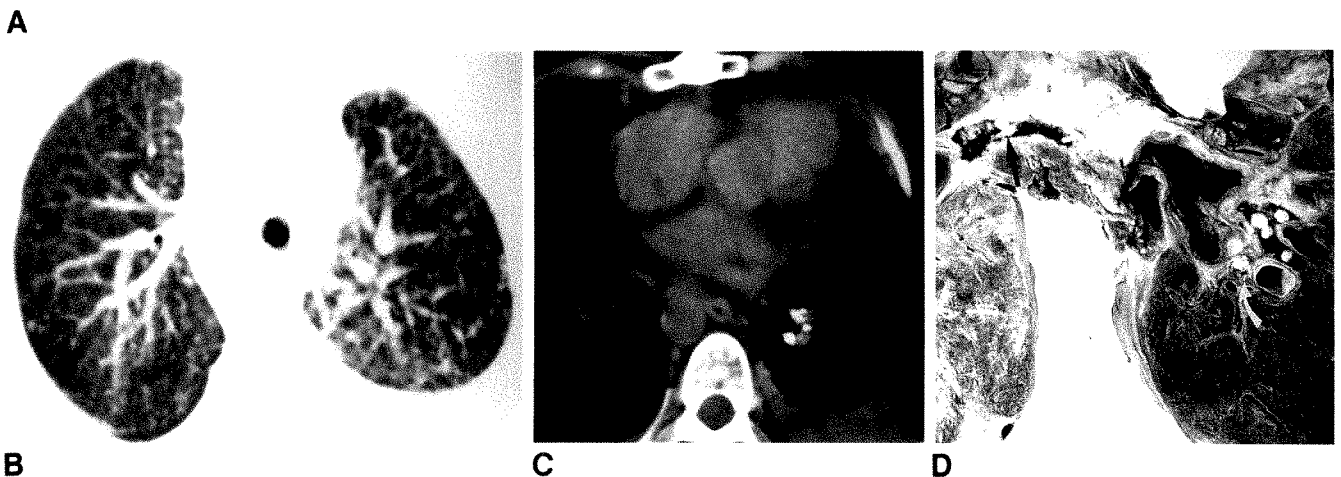


Fig. 1.—Reactivation of tuberculosis in a donor lung used in heart and lung transplantation.

A, Chest radiograph obtained 17 weeks after transplantation shows multiple bilateral pulmonary nodules and a left pleural effusion. Note aortic arch on right side of transplant recipient.

B and C, Axial CT scans show diffuse bilateral pulmonary nodules and calcified left hilar lymph node.

D, Axial gross pathologic section obtained after patient died 31 weeks after transplantation shows calcified subcarinal (black arrow) and left hilar lymph nodes (white arrow) identified on corresponding CT images.



The patient's condition deteriorated progressively despite antituberculous therapy. Lung compliance decreased with ventilatory peak inspiratory pressures up to 70 cm H<sub>2</sub>O. She eventually became hypotensive and anuric and died 31 weeks after transplantation. Autopsy showed disseminated miliary *M. tuberculosis* in the lung, kidney, and bone marrow. Pathologic sections of the donor lungs showed a Ghon complex in the left upper lobe adjacent to the calcified left hilar and subcarinal lymph nodes noted on earlier CT scans (Fig. 1D). Multiple granulomas throughout the lungs contained large numbers of Langhans giant cells, acid-fast bacilli, and surrounding areas of necrosis. Cytomegalic viral pneumonitis also was identified. No evidence was seen of cardiac or pulmonary rejection.

## Discussion

Pulmonary infection is an important complication after organ transplantation. In patients receiving heart and lung transplants, infectious pulmonary organisms can be transmitted within the donor lung. How frequently this occurs is unknown. Although cultures of the donor trachea are often positive for

pathogens or opportunistic organisms, this is of limited use in predicting subsequent infections [5] because lungs are frequently colonized by saprophytes. Indolent pulmonary infection, such as tuberculosis, can be obscured in heart and lung transplant recipients by other pulmonary complications. The chest radiograph may show a confusing picture with combined features of rejection, congestive heart failure, and infection. In our patient, the presence of multiple small nodules on both chest radiographs and CT scans suggested an infectious cause, although no acid-fast bacilli were identified on initial stains. Calcified nodes in the donor lungs, not visible on the chest radiograph, were identified on the first postoperative chest CT scan before microbiologic confirmation of mycobacteria.

Reactivation of *M. tuberculosis* is a concern in any immunocompromised patient, and establishing the diagnosis can be difficult. Radiologic warning signs of previous granulomatous infections therefore may be important in this population. Identification of calcified nodes on chest imaging studies after

heart and lung transplantation should alert the clinician to the likelihood of transfer of tuberculous organisms to the recipient of the donor lung, which may warrant prophylactic treatment with antituberculous drugs. This is particularly important in patients with negative findings on a tuberculin skin test before transplantation. The role of CT in detecting calcified lymph nodes in this population remains to be determined. In our patient, calcified nodes were visible on the CT scans but not on the chest radiographs. The usefulness of posttransplantation chest CT in screening for calcified nodes is unknown and probably depends on the frequency of mycobacterial infection in the donor population. In areas where histoplasmosis or sarcoidosis are endemic, radiologic identification of calcified nodes in the transplanted lung may be of less concern. CT scans have been obtained after transplantation in 20 of 58 heart and lung transplant recipients at Stanford University Medical Center. The patient described in this report is the only one in whom calcified mediastinal or hilar lymph nodes have been identified; importantly, this is the only patient who has developed tuberculosis.

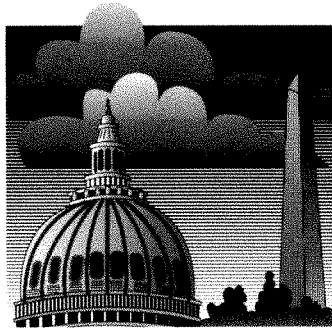
The heart and lung transplant recipient described in this report died of disseminated *M. tuberculosis*. Perhaps earlier diagnosis of the specific organisms would have improved the therapeutic response to antituberculous drugs; furthermore,

prophylactic therapy for tuberculosis when calcified nodes were first identified in the transplanted mediastinum and hilum in this patient might have prevented dissemination of infection. The mediastinum, hilum, and lung should be searched carefully for calcium on chest imaging studies, particularly if signs of respiratory infection develop in the transplant recipient. In geographic areas where histoplasmosis or sarcoidosis are not endemic, detection of calcified mediastinal or hilar nodes within the transplanted lung may warrant prophylactic antituberculous therapy.

#### REFERENCES

1. Doig RL, Boyd PJR, Eykyn S. *Staphylococcus aureus* transmitted in transplanted kidneys. *Lancet* 1975;2:243-245
2. Betts RF, Freeman RB, Douglas RG Jr, Talley TE, Rundell B. Transmission of cytomegalovirus infection with renal allograft. *Kidney Int* 1975;8:385-392
3. Ooi BS, Chen BTM, Lim CH, Khoo OT, Chan KT. Survival of a patient transplanted with a kidney infected with *Cryptococcus neoformans*. *Transplantation* 1971;11:428-429
4. Ryning FW, McLeod R, Maddox JC, Hunt S, Remington JS. Probable transmission of *Toxoplasma gondii* by organ transplantation. *Ann Intern Med* 1979;90:47-49
5. Brooks RG, Hofflin JM, Jamieson SW, Stinson EB, Remington JS. Infectious complications in heart-lung transplant recipients. *Am J Med* 1985;79:412-422





Come to the  
American Roentgen Ray Society

90<sup>th</sup>

---

ANNUAL MEETING

---

Washington, D. C.

---

Sheraton Washington Hotel  
May 13-18, 1990

---

---

Scientific Program (200 papers)

Instructional Courses (60 hours)

Categorical Course on Cardiovascular Imaging

The Caldwell Lecture

Award Papers

Scientific Exhibits

Social, Golf, and Tennis Programs

Guest Programs



# Ileocecal Tuberculosis: CT and Radiologic Evaluation

Emil J. Balthazar<sup>1</sup>  
Richard Gordon<sup>1</sup>  
Donald Hulnick<sup>1,2</sup>

The CT and radiologic findings in 11 patients (five with AIDS and six without AIDS) with ileocecal tuberculosis are described. On CT scans, five cases showed mild circumferential wall thickening of the terminal ileum and cecum, thickening of the ileocecal valve, and a few regional nodes. One case presented as nonspecific small-bowel obstruction. In five patients a more characteristic CT appearance was detected: preferential thickening of the ileocecal valve and medial wall of the cecum, exophytic extension engulfing the terminal ileum, and massive lymphadenopathy with low-density areas consistent with caseation necrosis. Patients with AIDS had a more severe form of involvement than those who did not have AIDS. Barium studies showed ileocecal changes consistent with an inflammatory process.

In conjunction with barium enema, CT is helpful in the initial evaluation of ileocecal tuberculosis, showing the location and extent of intestinal and mesenteric involvement in most cases. Characteristic CT findings are seen when the inflammatory process is severe.

*AJR* 154:499-503, March 1990

The ileocecal region is the most common site of tuberculous involvement in the gastrointestinal tract. The pathophysiology of intestinal involvement as well as its nonspecific clinical and conventional radiographic findings have been documented in the literature [1-5]. Previous reports on CT findings in abdominal tuberculosis have described mainly diffuse forms of peritoneal and mesenteric disease presenting with ascites, peritoneal and mesenteric thickening, and mainly upper abdominal and mesenteric lymphadenopathy [6-8].

It is the purpose of this report to retrospectively review and analyze the CT appearance of 11 patients with ileocecal tuberculosis. Correlation with conventional radiologic examinations and pathologic findings is provided in an attempt to improve diagnostic accuracy and avoid clinical mismanagement, surgical explorations, and unnecessary ileocolic resections.

## Materials and Methods

The abdominal CT scans, barium gastrointestinal studies, and chest films of 11 patients with ileocecal tuberculosis diagnosed and treated in the last 4 years were retrospectively reviewed. The nine male and two female patients were 27-63 years old (average age 40 years). This group contained five human immunodeficiency virus-positive patients with risk factors and clinical histories consistent with AIDS. Among the six non-AIDS patients, three were Native Americans and three were recent emigrants from China and Eastern Europe. The clinical presentation and the reason for radiologic workup included right lower quadrant pain and tenderness, spiking low-grade fever, night sweats, anorexia, weight loss, and normal to slightly elevated WBC count. One patient had clinical and plain film radiologic evidence of small-bowel obstruction.

The diagnosis of intestinal tuberculosis was proved in 10 patients by pathologic and microbiological examinations. Pathologic tissue was obtained by colonoscopy in four patients,

Received September 21, 1989; accepted October 12, 1989.

<sup>1</sup> Department of Radiology, New York University Medical Center, 550 First Ave., New York, NY 10016. Address reprint requests to E. J. Balthazar.

<sup>2</sup> Present address: Department of Radiology, Danbury Hospital, 24 Hospital Ave., Danbury, CT 06810.

0361-803X/90/1543-0499

© American Roentgen Ray Society

colonoscopy and surgical resection in three patients, and surgery alone in three patients. In one patient in whom the colonoscopic biopsy results revealed noncaseating granulomas, the diagnosis of tuberculosis was made on the basis of recent history of tuberculous salpingitis and by the good clinical response to antituberculous chemotherapy. Initial colonoscopic examination and cecal biopsy results revealed only noncaseating granulomas in another patient who was misdiagnosed as having Crohn disease. Corticosteroid therapy was instituted and the patient was readmitted to the hospital 1 month later with miliary tuberculosis. Repeat colonic biopsies at this time were positive for acid-fast bacilli. In all patients in this series, including patients with AIDS, the causative agent was *Mycobacterium tuberculosis* and not *Mycobacterium avium-intracellulare*.

CT examinations were performed on General Electric 8800 and 9800 or Picker 1200 units by using standard techniques. Patients

received IV infusions of contrast material and 750–800 ml of oral, diluted barium solution 50–60 min before scanning. Ten-millimeter collimation at 10- to 15-mm intervals covering the entire abdomen and pelvis was used initially. In addition, in six patients, 5 × 5 mm sections over the region of interest were repeated. Colonoscopy and surgical and pathologic reports were reviewed in each case.

## Results

Chest films were initially normal in seven patients. They showed pulmonary infiltrates in the upper lobes and pleural effusions consistent with tuberculosis in two patients; diffuse interstitial changes were seen in two patients with AIDS. In these last four patients the sputum was positive for tubercu-

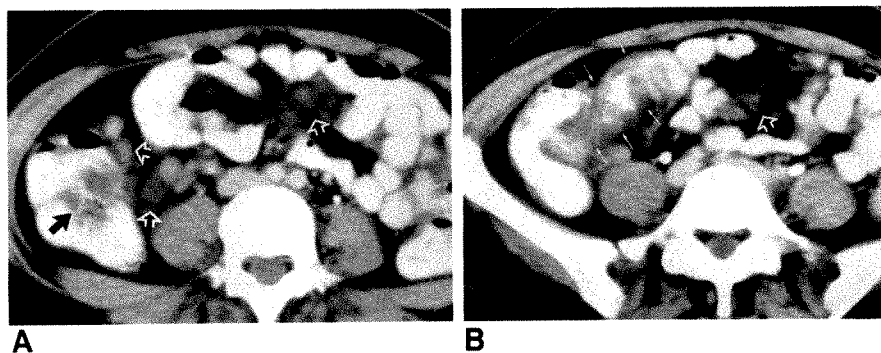
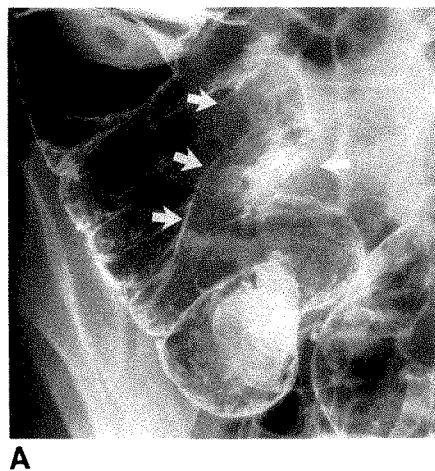


Fig. 1.—Ileocecal tuberculosis mimicking Crohn disease and lymphosarcoma in patient who does not have AIDS.

A, CT scan shows enlargement of ileocecal valve (solid arrow) associated with regional and mesenteric lymphadenopathy (open arrows). Lymph nodes are well seen; they differ in density but have a homogeneous soft-tissue appearance.

B, CT scan shows circumferential thickening of wall of terminal ileum adjacent and proximal to ileocecal valve (solid arrows). Slight streakiness in mesenteric fat and few lymph nodes are present also (open arrow).



A

Fig. 2.—Asymmetric cecal wall thickening in patient with AIDS and ileocecal tuberculosis.

A, Double-contrast barium enema shows wide gaping of ileocecal valve with thickening of valve (arrows). Superficial mucosal erosions in rest of cecum were confirmed with colonoscopy.

B, CT scan shows asymmetric, preferential thickening of medial wall of cecum (black arrows). Thickened wall is slightly heterogeneous in density. A few small mesenteric nodes (small arrows) are between barium-filled loops of small bowel.

C, CT scan shows concentric thickening of terminal ileum and right colon (black arrows). A few regional nodes are seen in mesentery (white arrows).

D, Segmental area of involvement is seen in pelvic ileal loop (arrows). Affected segment has narrowed lumen and circumferential thickened wall. Finding was confirmed with barium small-bowel study.



B



C



D

losis. One patient who presented initially with a normal chest film was misdiagnosed as having Crohn disease. He was treated with corticosteroids and developed miliary pulmonary tuberculosis later.

### CT Scanning

CT findings consisted of two distinct sets of abnormalities. First, enlargement of the ileocecal valve and/or wall thickening of the cecum and terminal ileum, varying in size from 0.5 to 3.0 cm, was detected in 10 cases. In five patients the thickening was mild and symmetric (Fig. 1); in the other five patients the pattern of involvement was more severe and asymmetric (Fig. 2). These patients had excessive thickening along the medial wall of the cecum with a soft-tissue mass centering at the ileocecal valve and engulfing the terminal ileum as well (Figs. 2 and 3). The involved intestinal wall was homogeneous in density in seven cases (Figs. 1 and 3) and showed areas of a slightly heterogeneous appearance in the remaining three cases (Fig. 2). Pericecal or mesenteric fat showed either absence of or only minimal haziness. One

patient had CT findings consistent with distal small-bowel obstruction of unknown cause. In this patient the resected surgical specimen revealed a 1-cm stricture with a focal ulceration obstructing the terminal ileum.

Second, pericecal regional lymphadenopathy was seen in nine patients (Figs. 3 and 4), and more distal mesenteric adenopathy was present in five patients (Figs. 1 and 5). Clusters of small nodes and/or nodal masses varying in size from 0.5 to 5.0 cm were detected (Figs. 1, 3, and 4). They had a homogeneous soft-tissue appearance in five patients (Figs. 1 and 4) or exhibited central areas of low density presumed to correspond to caseous liquefaction in four patients (Figs. 3 and 5). A combination of asymmetric cecal wall thickening and necrotic nodes was present in three patients (Figs. 3 and 5).

There were no radiologic differences between patients with AIDS and those without AIDS except for degree of involvement. As a group, AIDS patients had more severe cecal and ileal wall thickening and larger regional lymphadenopathy. Upper abdominal, retroperitoneal, porta hepatis, or peripancreatic adenopathy as well as ascites or parietal peritoneal thickening were not detected in this group of patients.

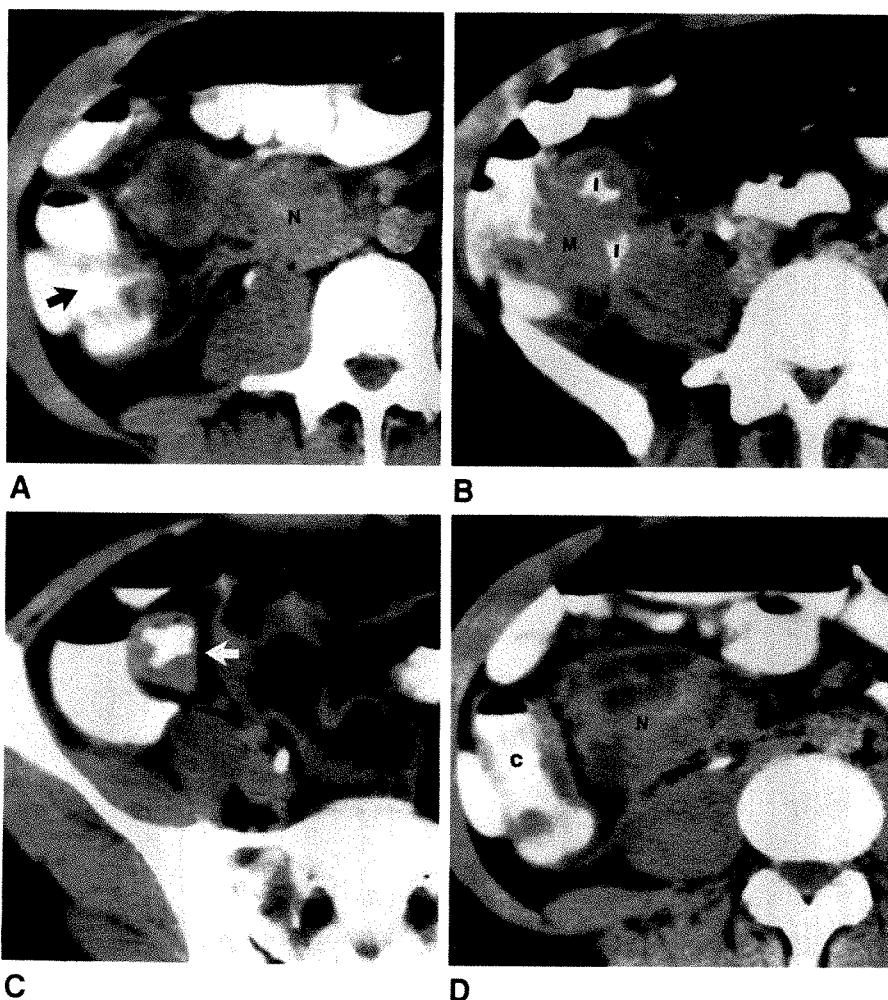


Fig. 3.—Severe ileocecal tuberculosis presenting as large soft-tissue mass and extensive caseation necrosis in patient with AIDS.

A, CT scan shows thickening of ileocecal valve (arrow) and extensive regional lymph nodes presenting as large mesenteric masses (N). Low-density areas consistent with caseation necrosis are present.

B, Large soft-tissue mass (M) is seen mainly on medial CT scan of cecum extending out and engulfing terminal ileum (I). Soft-tissue mass is centered at ileocecal valve.

C, Slightly more proximal CT scan of ileum has circumferential, homogeneous thickened wall (arrow).

D, CT scan shows circumferential thickening of right side of colon (C) with heterogeneous density. Large mesenteric nodal mass contains areas of caseation necrosis (N).

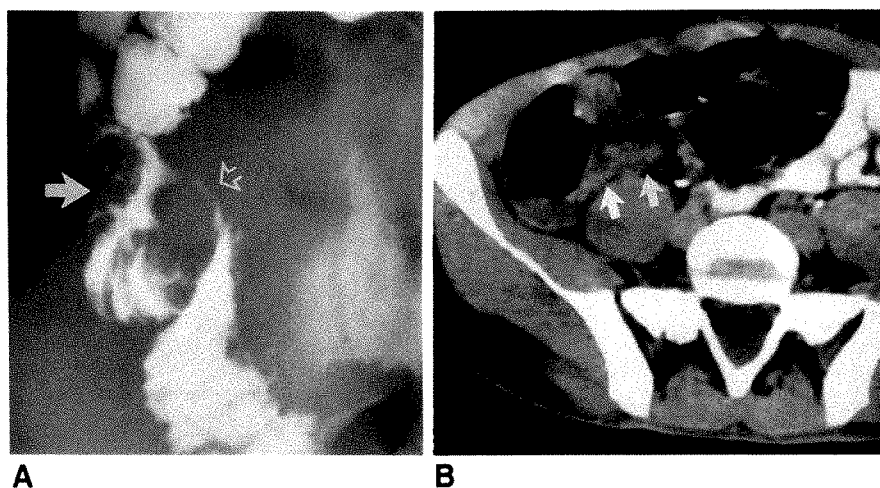


Fig. 4.—CT and barium enema correlation in ileocecal tuberculosis in patient with AIDS.

A, Barium enema shows thickened folds, spasticity, and irregularly contoured cecum (solid arrow). Significant narrowing of short segment of terminal ileum adjacent to ileocecal valve (open arrow) and proximal ileal dilatation are present.

B, CT scan shows heterogeneous soft-tissue density in right lower abdomen produced by cecal wall thickening and adjacent lymphadenopathy (arrows).

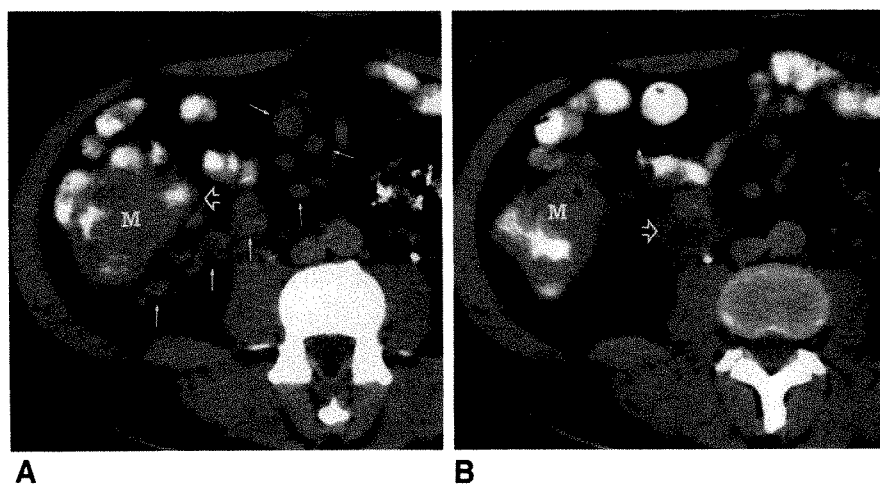


Fig. 5.—CT scans show cecal mass combined with caseation necrosis of mesenteric lymph nodes in patient who does not have AIDS.

A, Homogeneous soft-tissue mass is seen involving cecum (M) and terminal ileum (open arrow). Multiple low-density nodes are seen adjacent to cecum and more distal in mesentery (solid arrows).

B, Cecal thickening is preferentially affecting medial wall (M) and is centered at ileocecal valve. Mesenteric lymph nodes have low density (arrow), and there is haziness in pericecal fat.

### Barium Studies

Barium examinations were performed in 10 patients, including nine barium enemas and six small-bowel examinations. They were done 2–5 days after CT scanning. Barium examinations revealed thickened folds, spasticity, irregular contours, and superficial ulcerations involving the cecum and terminal ileum in 10 patients (Figs. 2 and 4). The terminal ileum was involved over a short segment (3–4 cm) in six patients (Fig. 4) and over a slightly longer segment (10–12 cm) in four patients. A second skip area of more proximal ileal involvement was seen in one patient. No separation of loops or sinus tracts or fistulizations were seen. Small-bowel examination confirmed the presence of distal ileal obstruction in one patient. Follow-up examinations in two symptomatic patients undergoing antituberculous chemotherapy showed partial small-bowel obstructions requiring surgical resections.

### Discussion

Tuberculosis can affect any abdominal organ; it is known to present with protean clinical and radiologic features. The

most common manifestations of intraperitoneal tuberculosis in our population are (1) tuberculous peritonitis, a widespread form of infection involving peritoneal and mesenteric structures and upper abdominal lymph nodes [6–8]; (2) *Mycobacterium avium-intracellulare* enteritis, a diffuse form of intestinal infection seen mainly in AIDS patients [9]; and (3) focal gastrointestinal involvement affecting a relatively short intestinal segment, which is the subject of this report.

Previous pathologic and clinical surveys have shown that although tuberculosis can involve any segment of the gastrointestinal tract, there is a striking preponderance for the ileocecal valve and the adjacent ileum and cecum. This is seen in about 90% of cases [1]. The initial pathologic process, called epithelioid tubercle, is located in the lymphatic tissue of the submucosa. Within 2–4 weeks, it undergoes caseous necrosis, which leads to sloughing of the overlying mucosa and the development of an ulcer. The process continues to extend, ulcerations coalesce, and by lymphatic spread the adjacent mesenteric lymph nodes are involved. Indeed, extensive involvement of the adjacent regional nodes is a well-recognized pathologic feature [1, 10–12]. The cecal wall is thickened and the surrounding nodes are matted and adhere



to the wall of cecum and terminal ileum, forming an inflammatory mass.

Because the major pathologic involvement occurs at the ileocecal valve and adjacent to it, the radiographic appearance of the valve was considered an important indicator of the presence of tuberculous infection. Thickening of the valve lips or wide gaping of the valve, associated with a narrowed terminal ileum (Fleischner sign), has been described as a characteristic sign on barium examination [1, 4]. Although this sign is seen occasionally (Fig. 2), the majority of barium studies show nonspecific inflammatory changes involving the cecum and terminal ileum (Fig. 4). In most patients, the differential diagnosis from Crohn disease cannot be made unless a history of tuberculosis or a positive chest film is present. A normal chest film, however, does not exclude intestinal tuberculosis. In our series, only four of the 11 patients had chest abnormalities. Several other larger series have shown that less than 50% of the patients with intestinal tuberculosis had radiologic evidence of pulmonary disease [1, 2].

The gross morphology of the pathologic process can be evaluated well with CT. A range of CT abnormalities should be expected. When the inflammation is mild, CT shows only slight and symmetric wall thickening and a few small regional nodes (Fig. 1). These changes, seen in five patients in this series, are compatible mainly with Crohn disease, tuberculosis, or ileocecal lymphoma. In these patients, other types of acute inflammatory disease (appendicitis, diverticulitis) usually can be excluded on clinical grounds and because of lack of significant inflammatory changes or fluid collections in the pericecal fat.

When the pathologic process is severe and advanced, as seen in five of our patients, more characteristic abnormalities are evident. The ileocecal valve and the adjacent medial wall of the cecum are thickened. Wall thickening and adjacent lymph nodes form a soft-tissue mass centered at the ileocecal valve, enveloping the terminal ileum (Figs. 2 and 3). The inflammatory mass may have a heterogeneous appearance (Figs. 2 and 4) and large regional nodes are present; some contain low-density centers, consistent with caseation necrosis (Figs. 3 and 5). These findings are incompatible with Crohn disease and unusual for ileocecal lymphoma or cecal carcinoma. In these patients a barium enema study greatly con-

tributes to the correct diagnosis by showing inflammatory ileocecal changes (Fig. 4) and excluding malignancy.

Because of its retrospective nature and the relatively small number of patients in this series, the sensitivity and accuracy of CT in the diagnosis of ileocecal tuberculosis could not be assessed. A definite diagnosis must be established in all cases by means of bacteriologic and/or histologic examination after colonoscopic biopsies. However, in conjunction with barium enema, CT can be used successfully in the initial assessment of patients with ileocecal tuberculosis. The location, as well as the intestinal and mesenteric extent of the inflammatory process, are well demonstrated with CT. Characteristic changes of tuberculous infection may be found, as seen in five of our patients. At the same time, evaluation of distal peritoneal, solid-organ, or retroperitoneal disease can be done. The judicious use of CT in these patients will improve the preoperative diagnosis and, it is hoped, avoid clinical mismanagement or unnecessary exploratory laparotomies.

#### REFERENCES

1. Carrera GF, Young S, Lewicki AM. Intestinal tuberculosis. *Gastrointest Radiol* 1976;1:147-155
2. Werbeloff L, Novis BH, Bank S, Marks I. The radiology of tuberculosis of the gastrointestinal tract. *Br J Radiol* 1973;46:329-336
3. Bentley G, Webster JHH. Gastrointestinal tuberculosis: a 10 year review. *Br J Surg* 1967;54:90-96
4. Gershon-Cohen J, Kremens V. X-ray studies of ileocecal valve in ileocecal tuberculosis. *Radiology* 1954;62:251-254
5. Balthazar EJ, Bryk D. Segmental tuberculosis of the distal colon: radiographic features in 7 cases. *Gastrointest Radiol* 1980;5:75-80
6. Hulnick DH, Megibow AJ, Naidich DP, Hilton S, Cho KC, Balthazar EJ. Abdominal tuberculosis: CT evaluation. *Radiology* 1985;157:199-204
7. Epstein BM, Mann JH. CT of abdominal tuberculosis. *AJR* 1982;139:861-866
8. Dahlene DH Jr, Stanley RJ, Koehler RE, Shin MS, Tishler JMA. Abdominal tuberculosis: CT findings. *J Comput Assist Tomogr* 1984;3:443-445
9. Greene JB, Sidhu GS, Lewin S, et al. *Mycobacterium avium-intracellulare*: a cause of disseminated life-threatening infection in homosexuals and drug abusers. *Ann Intern Med* 1982;97:539-546
10. Paustian FF, Bockus HL. So-called primary ulcerohypertrophic ileocecal tuberculosis. *Am J Med* 1959;27:509-518
11. Tandon HD, Prakash A. Pathology of intestinal tuberculosis and its distinction from Crohn's disease. *Gut* 1972;13:260-269
12. Brombart M, Massion J. Radiologic differences between ileocecal tuberculosis and Crohn's disease. *Dig Dis Sci* 1961;6:589-603

## Book Review

**Sectional Human Anatomy.** Transverse, Sagittal and Coronal Sections Correlated with Computed Tomography and Magnetic Resonance Imaging, 2nd ed. By Man-Chung Han and Chu-Wan Kim. Seoul, Korea: Ilochokak, 199 pp., 1989.

This book is organized as an anatomic atlas. It compares cadaveric sections in various planes with concomitant CT and MR sections of the brain, head, and neck; chest; and abdomen and pelvis. The contents are organized into three parts. Part 1 shows transverse, coronal, and sagittal sections of the brain, head, and neck; part 2 shows transverse and sagittal sections of the chest; and part 3 shows transverse and sagittal sections of the abdomen and pelvis.

The quality of the cadaveric sections and the illustrations thereof are excellent. The quality of the CT and MR sections leaves something to be desired in terms of state-of-the-art imaging. The MR images of CNS anatomy pale when compared with those in an excellent spinal and cranial atlas such as that by Daniels, Haughton, and Naidich, for instance. The CT scans are lacking something in resolution and, in terms of the CNS, it might have been wise to pick a subject with at least some atrophy so that the regions of the cortical sulci and the sylvian fissure might be demonstrated more accurately. Also, the slice thickness is rather large, so that some smaller structures might not be included within the diagrammatic confines of each section.

Points of excellence include the size of the illustrations and the layout. Each two adjacent pages represent one section, a large cadaveric section on the left and split CT and MR sections on the right, with a clearly identifiable diagram showing the exact level. The individual page indexes for each anatomic structure are clearly identifiable and easy to read, being organized in alphabetical order. The cadaveric sections are excellent, and injected dyes allow better visualization of vascular and certain other anatomic structures.

In summary, although other anatomy and anatomy/atlas texts may be superior, especially in terms of thin-section detail and quality of CT and MR images, if detailed information is not desired as might pertain to a radiologic subspecialty (e.g., neuroradiology), this text may suffice. The general radiologist would be more likely than the subspecialist to find this book useful, especially as the clarity and size of the illustrations and the anatomic indexes make it useful as a rapid reference.

Hano A. Siegel  
Mercy Hospital  
San Diego, CA 92103

# Regenerating Nodules of Liver Cirrhosis: MR Imaging with Pathologic Correlation

Kuni Ohtomo<sup>1</sup>  
 Yuji Itai<sup>1</sup>  
 Yumiko Ohtomo<sup>2</sup>  
 Junji Shiga<sup>2</sup>  
 Masahiro Iio<sup>1</sup>

To determine the pathologic basis for low-intensity nodules seen on MR images of the liver in patients with cirrhosis, we obtained spin-echo and gradient-echo MR images in 20 cirrhotic patients in whom partial hepatectomies were subsequently performed for hepatocellular carcinoma. Low-intensity liver nodules were shown on gradient-echo and spin-echo images in eight patients. Pathologic study of the liver in these patients showed that these nodules were regenerating nodules containing hemosiderin. Low-intensity nodules were seen only on T2-weighted spin-echo images in four other patients. Microscopic examination of the liver in these patients showed regenerating nodules without hemosiderin deposits. Broad fibrous septa containing vascular spaces were present in two of these four patients.

These results suggest that regenerating nodules containing hemosiderin or those that are surrounded by vascular fibrous septa are visible on MR images as low-intensity nodules and that gradient-echo images are useful in demonstrating nodules with hemosiderin.

*AJR* 154:505-507, March 1990

In a previous report, we showed that multiple, small, low-intensity nodules in the liver are often observed on MR images of patients with cirrhosis [1]. Some preliminary MR imaging-pathologic correlations with MR images of liver specimens *ex vivo* have disclosed that there is a close relationship between demonstration of low-intensity nodules on MR images and hemosiderin deposits in regenerating nodules of liver cirrhosis [2, 3]. MR imaging-pathologic correlation with *in vivo* MR images is necessary to confirm the results of these reports since changes in the water content and blood flow in specimens might influence the MR demonstration of low-intensity nodules. In this article, we correlated *in vivo* MR images of cirrhotic patients with pathologic specimens obtained after partial hepatectomies were carried out for hepatocellular carcinoma.

## Materials and Methods

Twenty consecutive cirrhotic patients with hepatocellular carcinoma in whom MR images were obtained within 3 months before tumor resections performed between 1986 and 1989 were included in this study. The 20 patients comprised 13 men and seven women 47-73 years old. The cause of liver cirrhosis was viral hepatitis in 19 patients (hepatitis B in six and non-A, non-B in 13) and schistosomiasis in one. MR imaging was performed with a Magnetom unit (Siemens, Erlangen, W. Germany) operated at 1.5 T. Images were constructed with the two-dimensional Fourier transformation technique. The matrix size was 256 × 256 and the scanning diameter was 50 cm, with a zooming factor of 1.2 to 1.5. Spin-echo (SE) 2000/28 (TR/TE) and 2000/75 MR images with a section thickness of 10 mm were obtained at 1.5-cm intervals with two excitations (17.1 min) in 13 patients; SE 2000/22,90 images were obtained in the remaining seven patients. SE 600/17 images were obtained in 12 patients. In addition to SE images, gradient-echo (GRE) images were obtained with fast low-angle shot (FLASH) in all patients. Pulse sequences of GRE images were 19/12 with a flip angle of 90°

Received July 24, 1989; accepted after revision October 23, 1989

<sup>1</sup> Department of Radiology, University of Tokyo, 7-3-1 Hongo, Bunkyo-ku, Tokyo, Japan 113. Address reprint requests to K. Ohtomo.

<sup>2</sup> Department of Pathology, University of Tokyo, Tokyo, Japan 113.

0361-803X/90/1543-0505

© American Roentgen Ray Society

in 19 patients and 25/11/90° in the other patient. With the use of two excitations (12 sec), a single 10-mm sections as obtained during respiratory suspension.

In these 20 patients, tumor resection was carried out within 3 months after MR imaging (in 10 patients, within 2 weeks). The size of resected specimens ranged from 4.5 × 4.5 × 4.0 to 17.0 × 12.0 × 6.0 cm and the size of hepatocellular carcinomas from 1.0 × 1.0 × 0.9 to 5.0 × 4.0 × 3.5 cm. Prussian blue stain was added during routine microscopic examinations to determine whether hemosiderin was present in regenerating nodules and fibrous septa.

## Results

Low-intensity nodules were shown on GRE images and on SE images with a TR of 2000 msec in eight patients (the GRE/SE group) and only on SE images with a TR of 2000 msec in four patients (the SE group). In the other eight patients (the negative group), low-intensity nodules were not revealed on any MR images. In six patients in the GRE/SE group, more low-intensity nodules were seen on GRE images than on SE images and some of the nodules also were bigger on GRE images. Low-intensity nodules were shown more clearly on first-echo SE images (2000/28 or 2000/22) than on second-echo SE images (2000/75 or 2000/90) in four patients in the GRE/SE group and to the same degree in the other four patients. Low-intensity nodules were seen most clearly or only on second-echo SE images in the SE group. On T1-weighted SE images (600/17), low-intensity nodules were shown in three of five patients in the GRE/SE group but in none in the SE group. The size of the low-intensity nodules on MR images ranged from 3 to 15 mm in all patients in the two groups.

Microscopically, the cirrheses in these 20 patients were classified as micronodular (three), micro- and mesonodular (six), mesonodular (10), and macronodular (one). Although there was a wide variety in the size of regenerating nodules, even in single specimens, they almost always ranged from 3 to 20 mm microscopically. Regenerating nodules were sur-

rounded by thin fibrous septa in all patients, and partial thickening of the septa was seen in two of the patients in the SE group. Hemosiderin deposits in regenerating nodules were revealed only in the eight patients in the GRE/SE group; mild hemosiderin deposits also were seen in fibrous septa in two of them. Hemosiderin deposits in regenerating nodules and/or fibrous septa were not seen in the SE and negative groups. Representative MR images and microscopic findings of the GRE/SE and SE groups are shown in Figures 1 and 2, respectively.

## Discussion

Our results suggest that a close relationship exists between MR demonstration of low-intensity nodules and pathologic findings of hemosiderin deposits in regenerating nodules. Low-intensity nodules were revealed more clearly on GRE than on SE images in the GRE/SE group, in which hemosiderin deposits in regenerating nodules were revealed microscopically. This is explained by the fact that the GRE technique including FLASH is more sensitive to the magnetic susceptibility of paramagnetic hemosiderin deposits [4]. In this study, only T1-weighted GRE images were obtained because they were suitable for dynamic MR study of the liver tumors, which was our first concern during this period [5]; T2-weighted GRE images with long TEs and small flip angles must be more useful in demonstrating regenerating nodules with hemosiderin as low-intensity nodules because these images are more sensitive to T2 and T2\* shortening owing to paramagnetic hemosiderin deposits [6]. Hemosiderin deposits in regenerating nodules have been reported to be associated with alcoholic liver injury [7], although the cause of liver cirrhosis in our patients was usually related to viral hepatitis infection.

In the SE group, low-intensity nodules were revealed most clearly on T2-weighted SE images, and regenerating nodules without hemosiderin deposits were surrounded by broad

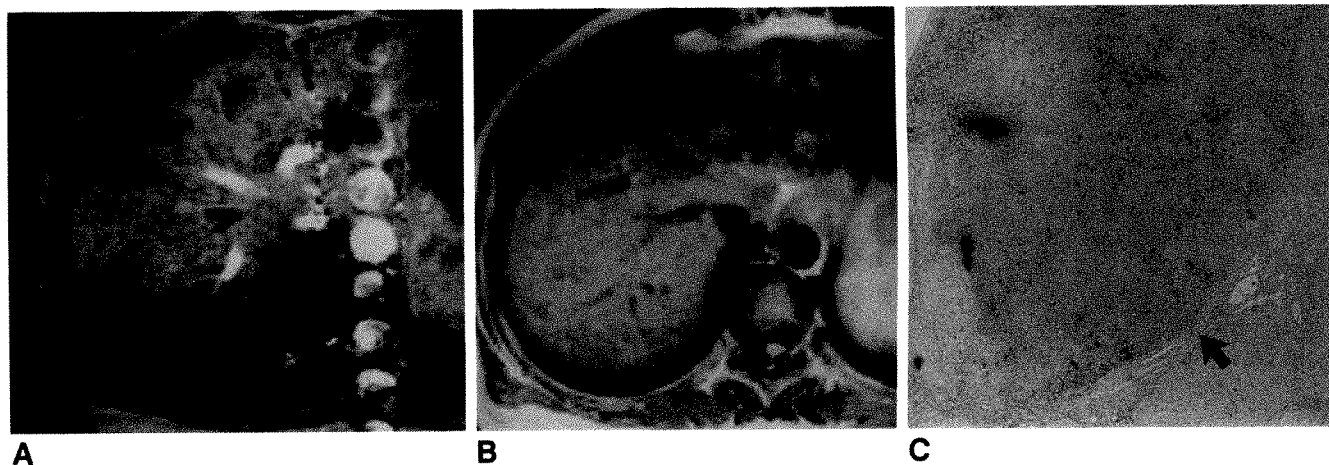


Fig. 1.—Micronodular liver cirrhosis with hemosiderin deposits in regenerating nodules (GRE/SE group). A and B, Low-intensity nodules are shown more clearly on gradient-echo (GRE) image, 19/12/90° (A), than on T2-weighted SE image, 2000/75 (B). C, Hemosiderin deposits, recognized as black dots, are scattered in 3-mm regenerating nodule (arrow). (Prussian blue, original magnification ×10)

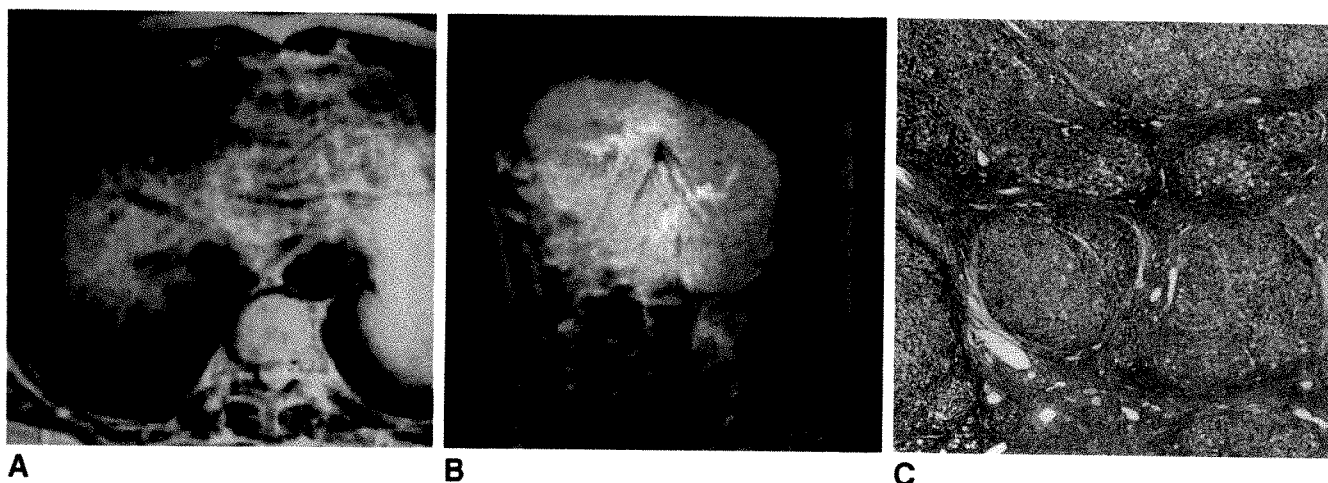


Fig. 2.—Micro- and mesonodular cirrhosis without hemosiderin deposits in regenerating nodules (SE group). A and B, Low intensity nodules are shown on T2-weighted SE image, 2000/90 (A), but not on gradient-echo image, 19/12/90° (B). C, Regenerating nodules are surrounded by broad vascular fibrous septa. (Heidenhain-azan, original magnification  $\times 10$ )

fibrous septa in two patients. Regenerating nodules might be shown as low-intensity nodules in these two patients because broad fibrous septa that contained numerous vascular spaces had relatively high intensities on T2-weighted SE images, just like vascular scars within hepatic tumors [8]. However, in the remaining two patients in the SE group, microscopic examination could not reveal any findings that might have caused low-intensity nodules. The detectability of low-intensity nodules on T1-weighted SE images was quite low in both groups in this study, which agreed with our previous findings [1].

Although the number of patients in this study is limited, our results suggest that regenerating nodules with hemosiderin deposits might be shown as low-intensity nodules on GRE as well as on SE images with long TRs, as is seen with sideroblastic nodules (Gamna) of the spleen [9, 10]. We also suggest that there might be other pathologic entities in which regenerating nodules appearing as low-intensity nodules are shown most clearly on T2-weighted SE images; vascular fibrous septa may be one possibility.

The most important limitation of this study is that direct correlation of MR findings with gross and microscopic findings was not possible because surgical specimens were usually small and ex vivo MR imaging with non-formalin-fixed surgical specimens could not be performed because of the limited availability of the MR unit. Although the size of low-intensity nodules roughly corresponded to that of regenerating nodules in surgical specimens, a more thorough direct MR imaging-pathologic correlation is necessary, and MR images of fresh, whole livers obtained by autopsy or before liver transplantation are needed to confirm our preliminary results. Further

clinical experience is also necessary to determine the sensitivity of MR for demonstrating multiple low-intensity nodules on GRE and/or SE images in cirrhotic patients and to clarify the clinical significance of detecting hemosiderin deposits in regenerating nodules.

#### REFERENCES

1. Itai Y, Ohnishi S, Ohtomo K, et al. Regenerating nodules of liver cirrhosis: MR imaging. *Radiology* 1987;165:419-423
2. Ohtomo K, Itai Y, Ohtomo Y, Shiga J, Minami M, Iio M. MRI demonstration of pseudolobules of liver cirrhosis: particular reference to iron deposits on autopsied specimens (English abstr). *Nippon Igaku Hoshasen Gakkai Zasshi* 1989;49:681-683
3. Kadoya M, Matsui O, Yoshikawa J, et al. MRI of uneven iron deposition in the cirrhotic liver (in Japanese). *Jpn J Magn Reson Med* 1989;9:269
4. Winkler ML, Thoeni RF, Luh N, Kaufman L, Margulis AF. Hepatic neoplasia: breath-holding MR imaging. *Radiology* 1989;170:801-806
5. Yoshida H, Itai Y, Ohtomo K, Kokubo T, Minami M, Yashiro N. Small hepatocellular carcinoma and cavernous hemangioma: differentiation with dynamic FLASH MR imaging with Gd-DTPA. *Radiology* 1989;171:339-342
6. Murakami T, Marukawa T, Sakurai K, et al. Regenerating nodules of liver cirrhosis-evaluation of gradient-echo (FLASH) (in Japanese). *Jpn J Magn Reson Med* 1989;9:270
7. Gal EA. Posthepatic, postnecrotic, and nutritional cirrhosis: a pathological analysis. *Am J Pathol* 1960;36:241-271
8. Rummeny E, Weissleder R, Sironi S, et al. Central scars in primary liver tumors: MR features, specificity, and pathologic correlation. *Radiology* 1989;171:323-326
9. Minami M, Itai Y, Ohtomo K, et al. Sideroblastic nodules of the spleen: MR imaging of portal hypertension. *Radiology* 1989;172:681-684
10. Sagoh T, Itoh K, Togashi K, et al. Gamna-Gandy bodies of the spleen: evaluation with MR imaging. *Radiology* 1989;172:685-687



## **Categorical Course in Cardiovascular and Interventional Radiology**

### **American Roentgen Ray Society 90th Annual Meeting**

**May 13–18, 1990, Sheraton Washington Hotel, Washington, DC**

*Course Director, William J. Casarella, M.D.*

*Course Co-Director, Charles B. Higgins, M.D.*

#### **Sunday, May 13**

10:00–10:30	Basic Physical Principles of MRI in the Cardiovascular System ( <i>Sprawls</i> )
10:30–11:00	MRI of the Great Vessels ( <i>Dinsmore</i> )
11:00–11:30	MRI of Pericardium, Cardiac Masses, and Cardiomyopathy ( <i>Baron</i> )
11:30–12:00	MRI of Congenital Heart Disease ( <i>Gomes</i> )
12:00–12:30	MRI of Ischemic Heart Disease ( <i>Pettigrew</i> )
12:30–2:00	Lunch Break
2:00–2:30	MRI of Valvular Disease ( <i>Higgins</i> )
2:30–3:00	MR Angiography ( <i>Edelman</i> )
3:00–3:30	Coffee Break
3:30–4:30	An Overview of Cardiac Ultrasound: Its Strengths and Weaknesses ( <i>Jaffe</i> )
4:30–5:00	Physical Principles of Doppler Ultrasound ( <i>Kremkau</i> )

#### **Monday, May 14**

1:30–2:30	Doppler Ultrasound in the Carotid and Peripheral Circulation ( <i>Merritt</i> )
2:30–3:15	Ultrasound of Intracranial Circulation ( <i>Ackerman</i> )
3:15–3:45	Coffee Break
3:45–4:30	PET Cardiac Imaging: Radiopharmaceuticals, Technique, and Results ( <i>Schelbert</i> )
4:30–5:15	Doppler Ultrasound Studies of the Abdominal Vessels and Viscera ( <i>Nelson</i> )

#### **Tuesday, May 15**

3:45–4:30	SPECT Cardiac Imaging: Radiopharmaceuticals, Technique, and Results ( <i>DePuey</i> )
4:30–5:15	Ultrasound of Peripheral Venous Disease ( <i>Dorfman</i> )
5:15–5:45	Peripheral Vascular Studies in Nuclear Medicine ( <i>Ziffer</i> )

#### **Wednesday, May 16**

3:45–4:45	Overview of Current Status of Percutaneous Transluminal Angioplasty of Peripheral Vessels ( <i>Schwarten</i> )
4:45–5:30	Renal Angioplasty ( <i>Sos</i> )

#### **Thursday, May 17**

3:45–4:15	Intravascular Stents ( <i>Palmaz</i> )
4:15–5:00	Intravascular Lasers: What's Good and What Isn't ( <i>van Breda</i> )
5:00–5:45	Embolotherapy: Current Trends and Future Prospects ( <i>White</i> )

# Color Doppler Flow Imaging of Liver Tumors

Sachiko Tanaka<sup>1</sup>  
Tsugio Kitamura  
Makoto Fujita  
Katsumi Nakanishi  
Shigeru Okuda

A differential diagnosis of liver tumors was attempted on the basis of the pattern of blood flow within and around tumors on color Doppler flow images. The study comprised 35 patients with liver mass lesions: 20 patients had hepatocellular carcinoma, six had hemangiomas, four had metastatic liver cancers, one had cholangiocellular carcinoma, one had focal fatty liver, and three had liver cysts. A basket pattern (a fine blood-flow network surrounding the tumor nodule) was observed in 15 (75%) of the 20 hepatocellular carcinomas. An image of vessels within the tumor (blood flow that runs into and branches within the tumor) was observed in 13 (65%) of the 20 hepatocellular carcinomas. These two findings were observed only in hepatocellular carcinomas; even when the tumor was smaller than 2 cm in diameter, these findings were observed frequently. In the patients with multiple hepatic metastases, a "detour" pattern (a dilated portal vein meandering around the tumor nodules) was observed. In three of the six hemangiomas, a "spot" pattern (color-stained dots or patches in the central region of the tumor) was seen.

Our experience suggests that hepatocellular carcinomas have a characteristic appearance on color Doppler flow images.

*AJR* 154:509-514, March 1990

The diagnostic accuracy of sonography for hepatocellular carcinoma has been well established [1, 2]. Moreover, a close correlation has been shown between the sonographic image of hepatocellular carcinoma and its microscopic features [3]. Furthermore, sonographically guided percutaneous biopsy permits diagnosis of some small tumors that cannot be visualized by angiography [4]. At present, however, angiography is generally recognized as being second to histologic diagnosis as the method for final diagnosis of hepatocellular carcinoma.

If both the tumor image and blood-flow image could be displayed on a single sonogram by using color Doppler flow imaging, it would be possible simultaneously to obtain information that can be gained with sonography, hepatic arteriography, hepatic venography, and portography. This would be extremely useful in the differential diagnosis of hepatic tumors. However, according to published reports [5, 6], color Doppler flow imaging has not been able to provide information comparable to that obtained by using angiography because the color display of slow blood flow on Doppler imaging is inadequate.

In this study, color Doppler equipment capable of displaying relatively slow blood flow was used, and the differential diagnosis of liver tumors was made on the basis of the color blood-flow pattern within and around the tumor.

## Subjects and Methods

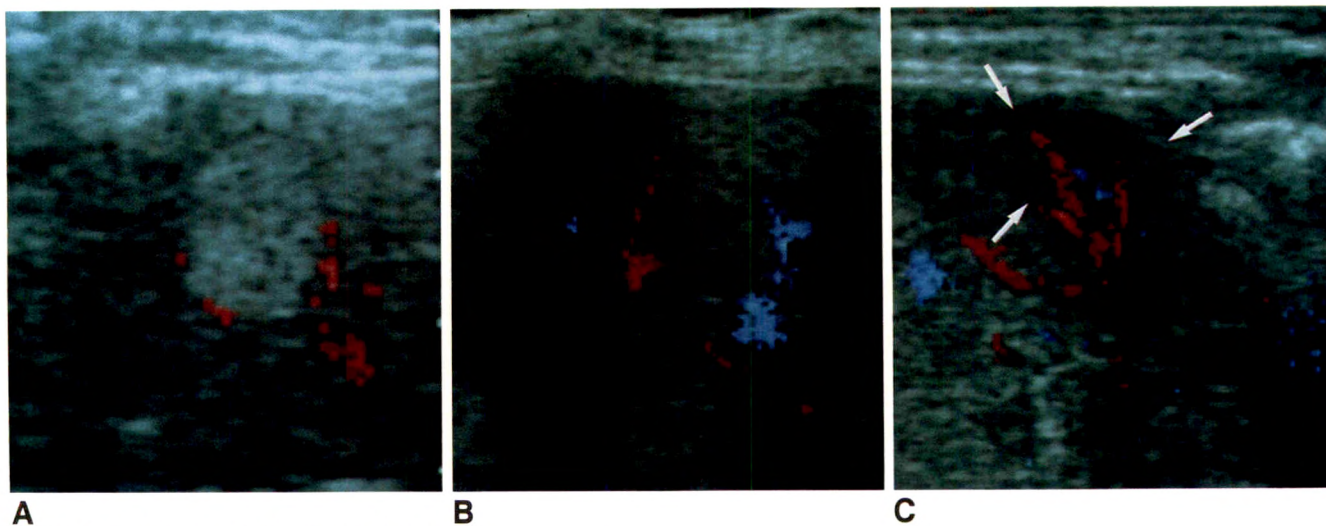
The study comprised 35 patients in whom masses in the liver were confirmed by routine sonography. These included 20 hepatocellular carcinomas (encapsulated type in all cases), six hemangiomas, four metastatic liver cancers (two from the stomach and two from the

Received July 18, 1989; accepted after revision September 19, 1989.

This work was supported in part by a grant-in-aid for Cancer Research (63-1) from the Ministry of Health and Welfare of Japan.

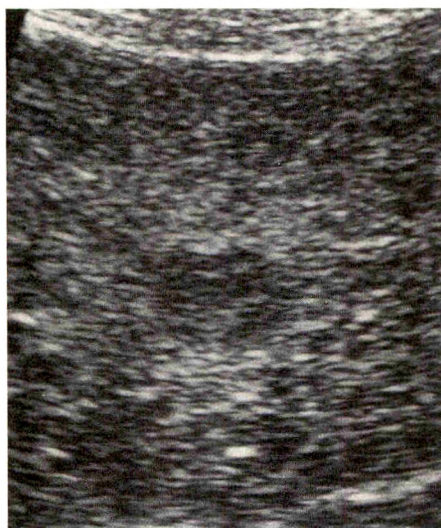
<sup>1</sup> All authors: The Center for Adult Diseases, Osaka, 3-3, Nakamichi, 1-chome, Higashinari-ku, Osaka 537, Japan. Address reprint requests to S. Tanaka.

0361-803X/90/543-0509  
© American Roentgen Ray Society



**Fig. 1.**—Basket pattern in hepatocellular carcinomas.

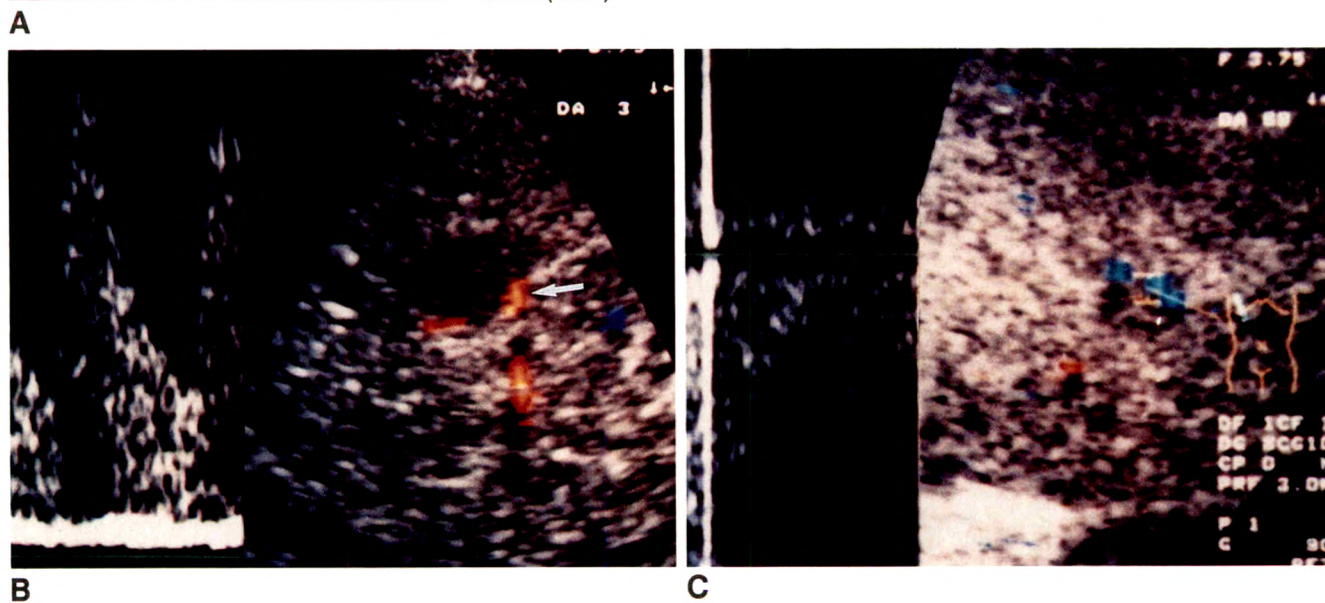
**A–C,** Color Doppler flow images show blood flow surrounding mass (**A** and **B**) and in a prominent net-shaped pattern slightly removed from center of tumor (arrows, **C**).



**Fig. 2.**—Small hepatocellular carcinoma.

**A,** Sonogram shows hypoechoic 1.3-cm lesion.

**B** and **C,** Color Doppler flow images show pulsating blood flow, which approaches lesion from two directions and surrounds tumor nodule (basket pattern). Sampling point of pulsed wave is shown (arrow).





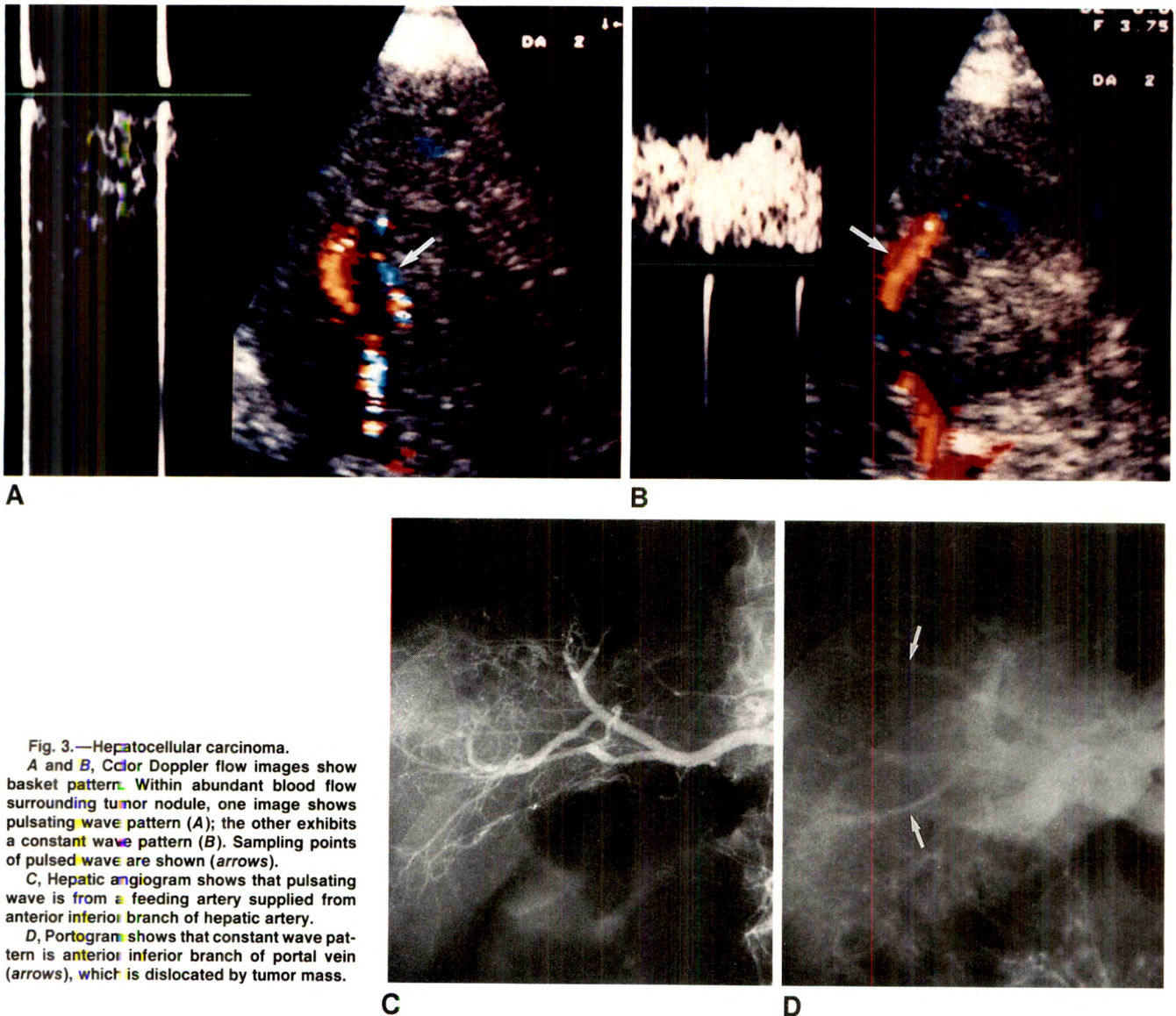


Fig. 3.—Hepatocellular carcinoma.

A and B, Color Doppler flow images show basket pattern. Within abundant blood flow surrounding tumor nodule, one image shows pulsating wave pattern (A); the other exhibits a constant wave pattern (B). Sampling points of pulsed wave are shown (arrows).

C, Hepatic angiogram shows that pulsating wave is from a feeding artery supplied from anterior inferior branch of hepatic artery.

D, Portogram shows that constant wave pattern is anterior inferior branch of portal vein (arrows), which is dislocated by tumor mass.

colon), one cholangiocellular carcinoma, one focal fatty liver, and three liver cysts. Histologic diagnosis was made, after sonographic examination, with tissues obtained by surgery or by sonographically guided fine-needle aspiration biopsy in 10 of the 20 cases of hepatocellular carcinoma, all four cases of metastatic cancer, and the one case of cholangiocellular carcinoma. Angiography was performed in all cases except those of focal fatty liver, liver cyst, and two of the four metastases. The final diagnosis was made with histologic examination and/or angiography in all cases except those of focal fatty liver and liver cyst, which were clinically diagnosed by using sonographic follow-up. The size of the tumor in the 20 hepatocellular carcinoma cases ranged from 1.0 to 7.0 cm in diameter.

The equipment used was a Quantum angiiodiography unit with 7.5- and 5.0-MHz linear-array probes (Quantum Medical Systems, Issaquah, WA) and an SSA-270A unit with 3.75-MHz sector-array probes (Toshiba, Tokyo, Japan). Because the minimal Doppler frequency shift capable of color imaging is 150 Hz with both machines, the slowest blood flow that theoretically can be shown in color is 1.5 cm/sec at 7.5 MHz, 2.3 cm/sec at 5.0 MHz, and 3 cm/sec at 3.75 MHz.

## Results

### Hepatocellular Carcinoma

A basket pattern, that is, a fine blood-flow network surrounding the tumor nodule, was observed in 15 (75%) of the 20 hepatocellular carcinoma cases. At the center of the tumor, blood flow was seen surrounding the periphery of the mass (Fig. 1). In the region slightly removed from the center, abundant blood flow was observed in a net-shaped pattern. In this pattern, vessels cling to the tumor and develop many fine branches around or within the tumor nodule. This basket pattern was observed in all of the five hepatocellular carcinomas smaller than 2 cm in diameter (Fig. 2). When the blood-flow wave pattern was examined, constant waves could be seen in all 15 cases; in 12 (80%), the blood flow also showed pulsating waves. In comparison, angiography showed these waves to be part of the feeding arteries surrounding the tumor and the portal vein running along the periphery of the tumor (Fig. 3).



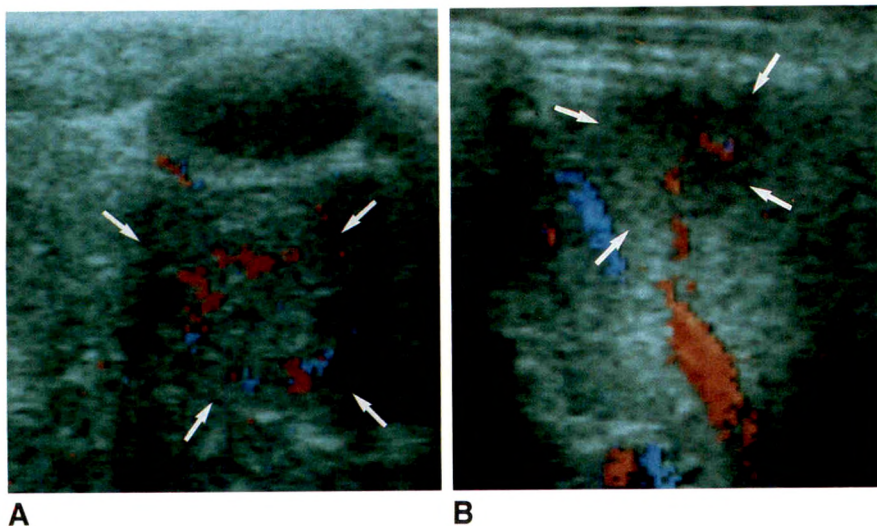


Fig. 4.—Vessels in tumor.

A and B, Color Doppler images show blood flow running and branching within tumor in both relatively large (A) and small (B) hepatocellular carcinomas. Arrows delineate tumor lesions.

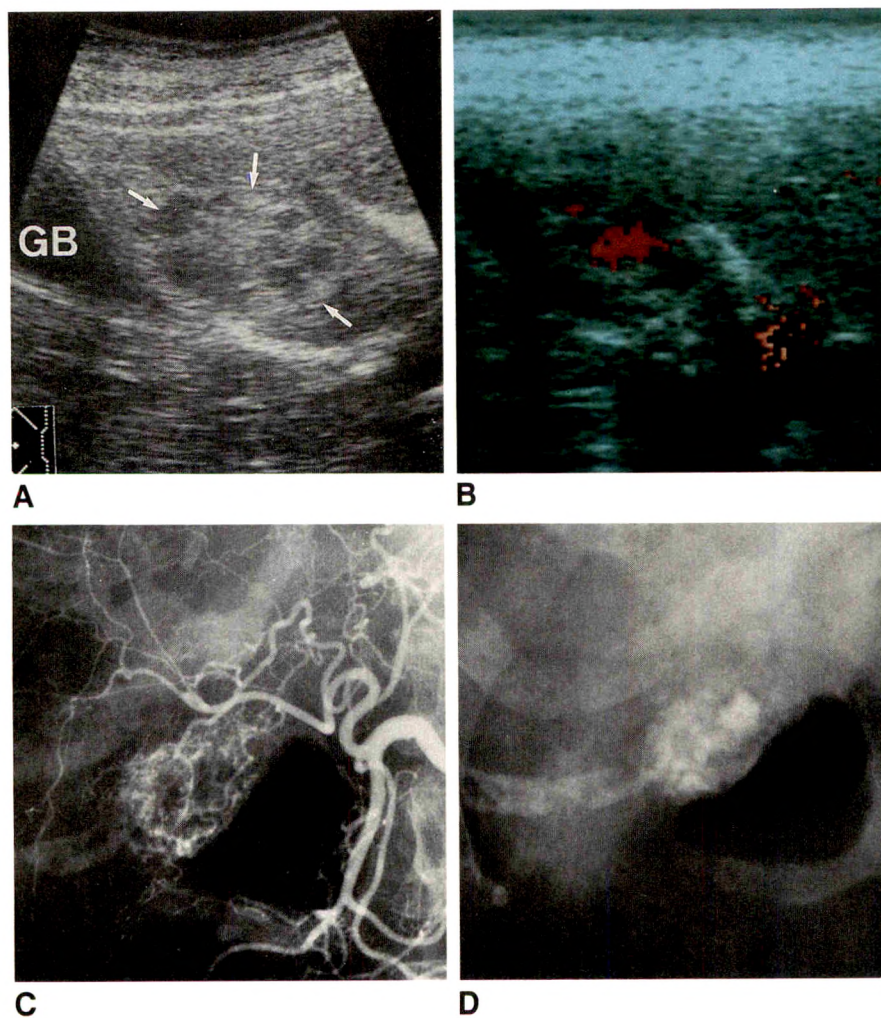


Fig. 5.—Hemangioma.

A, Sonogram shows 3-cm mass (arrows) in liver near gallbladder (GB).

B, Color Doppler flow image shows red spot in center of tumor.

C and D, Hepatic angiograms show characteristic findings of hemangioma with extensive pooling in center of tumor.

An image of vessels within the tumor, that is, blood flow that runs into the tumor mass from the periphery and branches within the tumor, was observed in 13 (65%) of the 20 cases of hepatocellular carcinoma (Fig. 4). In comparison with routine sonography, it was evident with color Doppler

flow sonography that the vessels in the tumor ran along septa within the tumor. The blood flow within the tumor showed a pulsating wave pattern in all cases. Comparison with the angiogram suggested that this pattern represented tumor vessels.



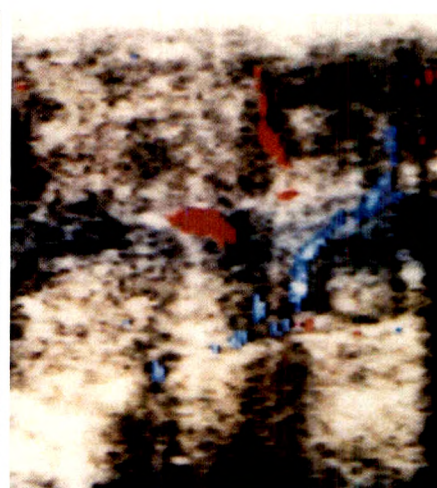
Fig. 6.—Metastases with detour pattern.

A, Sonogram shows multiple metastatic tumors.

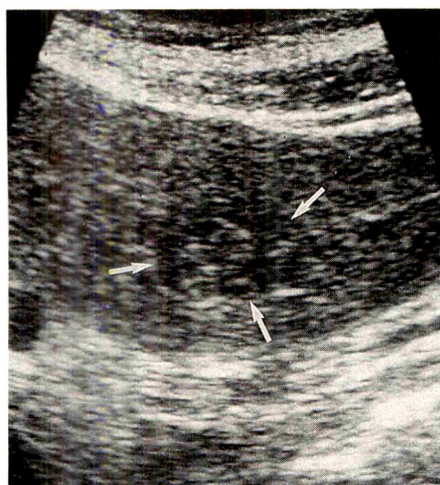
B, Color Doppler color flow image shows dilated intrahepatic portal vein meandering in liver. Unlike basket pattern, blood flow does not cling to tumor but detours.



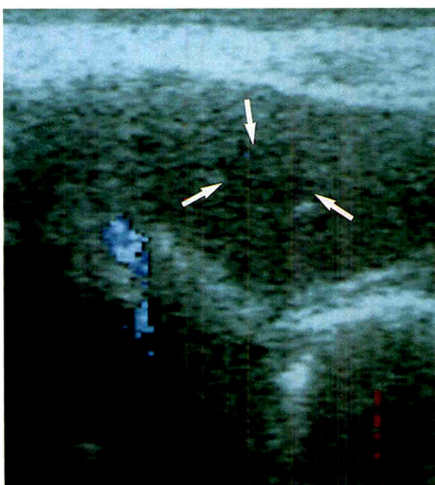
A



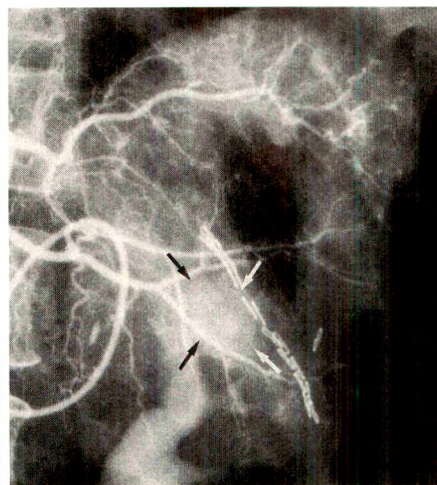
B



A



B



C

Fig. 7.—Solitary small metastatic lesion.

A, Sonogram shows hypoechoic lesion (arrows) in left lobe of liver.

B, Color Doppler flow image shows no blood flow within and around tumor (arrows).

C, Parechymal phase of hepatic arteriogram shows tumor staining (arrows).

In four of the 20 hepatocellular carcinoma cases, no blood flow could be seen near the tumor. Of these four cases, hypovascularity was also observed angiographically in one. In the remaining three cases, adequate color imaging could not be done, probably because the tumor was located too deep within the liver.

#### Hemangioma

In three (50%) of the six cases of hemangioma, the blood-flow image showed a spot pattern, that is, dots or patches, in the central region of the tumor nodule (Fig. 5). In all three of these cases, comparatively extensive pooling was noted in the central region of the tumor on angiography.

#### Metastatic Liver Cancer

Of the four cases of metastatic liver cancer, a detour pattern was observed in two cases (one with a gastric primary and another with a colon primary) with multiple tumor masses in the liver. The portal vein within the liver was dilated and

meandered around the tumor nodules (Fig. 6). Unlike the basket pattern observed in hepatocellular carcinoma, a dilated portal vein did not develop branches to the tumor nodule, but detoured around the nodule and left the nodule without changing the diameter of the vessel.

Each of the two cases in which a detour pattern was not observed had a single mass (1.3 and 2.5 cm in maximal diameter). Both masses were resected. Hepatic angiography in these two cases revealed no tumor vessels or feeding artery, but tumor staining was observed (Fig. 7).

#### Other Cases

In the one case of cholangiocellular carcinoma, color Doppler imaging could not visualize the blood flow within or around the tumor. This tumor was located deep within the liver, and even a routine B-mode image was unclear unless the far gain level was adjusted to a high setting. Hepatic angiography revealed a hypovascular tumor in this case.

No blood flow could be observed in the case of focal fatty liver or the three cases of liver cyst.



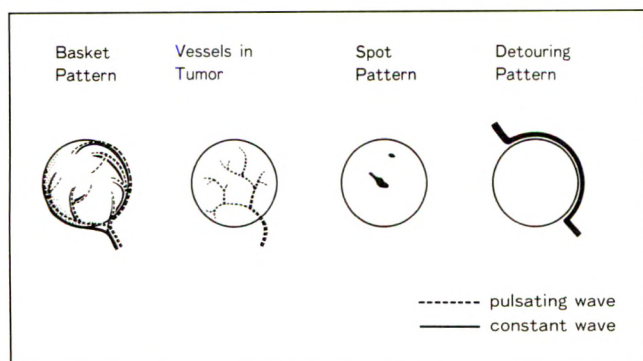


Fig. 8.—Schematic presentation of blood flow in liver tumors as shown by color Doppler flow imaging.

### Hepatic Masses

A schematic presentation of the blood-flow patterns observed in space-occupying lesions of the liver is shown in Figure 8. The basket pattern was observed in 15 (75%) of the 20 cases of hepatocellular carcinoma and the appearance of vessels in the tumor was seen in 13 cases (65%); these findings were not observed in hemangioma, metastatic liver cancer, or other cases. The spot pattern was seen in three (50%) of the six cases of hemangioma, and the detour pattern was seen in metastatic liver cancers in which there were multiple masses.

### Discussion

Color Doppler flow imaging, developed by Namekawa et al. [7], was originally used to evaluate the dynamics of blood flow in the heart and large blood vessels. Its application to liver tumors was initiated in 1985 by Sukigara et al. [5], who reported successful color imaging of the arteries running in the margin of and within the tumor in two cases of advanced hepatocellular carcinoma. Merritt [8] observed increased vascularity in most cases of metastatic liver cancer. However, there have been no reports in the literature on attempts to use color Doppler flow imaging in the differential diagnosis of various types of liver tumors.

The results of our study suggest that the basket pattern and the appearance of vessels in the tumor are characteristic color Doppler flow imaging patterns of hepatocellular carcinoma. These findings were observed in many hepatocellular carcinomas, but not in hemangiomas or metastatic liver cancers.

Ueno et al. [6] reported that visualization of blood flow as a pulsating wave in the margin of or inside a tumor was characteristic of hepatocellular carcinoma. They also reported that hepatocellular carcinomas smaller than 2 cm in diameter showed no color Doppler blood flow. In our study, the basket pattern was observed in all of five hepatocellular carcinoma tumors smaller than 2 cm in diameter, and the vessels were visualized in the tumor in three of the five. The difference in findings presumably is due to the sensitivity of the equipment used for Doppler frequency shifts. Thus, even lower and finer blood flows probably could be visualized in color if adequate instruments are developed.

Taylor et al. [9] reported that high-velocity Doppler signal was detected in hepatocellular carcinoma tumors when pulsed-wave Doppler sonography was used; they suggested that this signal was associated with large pressure gradients

due to arteriovenous shunting. In our study, we also observed a fast pulsating blood flow of 70–90 cm/sec in maximal velocity in feeding arteries entering the tumor, which form part of the basket pattern. Furthermore, in addition to the pulsating wave, a constant wave could be detected in the periphery in hepatocellular carcinoma. Comparing the blood flows shown on the color image with angiographic findings, we found that the blood flow that creates the basket pattern is the portal vein displaced around mass lesions and feeding arteries surrounding tumor nodules. Also, the blood flow within the tumor displayed by color imaging is the pulsating tumor vessel running within the tumor.

In small metastatic lesions in which tumor vessels cannot be observed by angiography and can be identified only by tumor staining at the parenchymal phase, color Doppler imaging of the blood flow was not possible. Merritt [8] reported that abundant blood flow was observed in most liver metastases; in our study, however, abundant portal blood flow was found running along the space between mass lesions only in cases with multiple tumor nodules. Proliferation of pulsating tumor vessels could not be detected in any cases. This is in agreement with the hepatic angiographic finding that most cases of liver metastases from adenocarcinoma are not hypervascular.

In some hemangiomas, a spot pattern was observed in the central region of the tumor. This seems to coincide with the pooling observed in angiography. Ishida et al. [10] also reported that constant wave was recorded in the hypoechoic areas within hemangiomas. However, it is difficult to explain blood flow in the pooling site, and this should be pursued further.

Color Doppler flow imaging provides information on blood flow that supplements the information gained by routine sonography, and thus is useful in the differential diagnosis of liver tumors. However, color imaging of blood flow was insufficient when the tumor was located deep within the liver. We look forward to further improvements in equipment so that we can achieve color imaging of much slower and finer blood flow and also image deep-seated tumors.

### REFERENCES

1. Tanaka S, Kitamura T, Ohshima A, et al. Diagnostic accuracy of ultrasonography for hepatocellular carcinoma. *Cancer* 1986;58:344–347
2. Tanaka S, Kitamura T, Nakanishi K, Okuda S, Kojima J, Fujimoto I. Recent advances in ultrasonographic diagnosis of hepatocellular carcinoma. *Cancer* 1989;63:1313–1317
3. Tanaka S, Kitamura T, Imaoka S, Sasaki Y, Taniguchi H, Ishiguro S. Hepatocellular carcinoma: sonographic and histologic correlation. *AJR* 1983;140:701–707
4. Tanaka S, Kitamura T, Kasugai H, Okano Y, Tatsuta M, Okuda S. Early diagnosis of hepatocellular carcinoma: usefulness of ultrasonically guided fine-needle aspiration biopsy. *JCU* 1986;14:11–16
5. Sukigara M, Takamoto S, Komazaki T, et al. Observation of the hepatoma by the real-time two-dimensional echography: its clinical significance and prospect (English abstr). *Acta Hepatol Jpn* 1985;26:747–752
6. Ueno N, Yamanaka T, Kimura K. Visualization of blood flow in abdominal tumors by the ultrasonic pulsed Doppler method (English abstr). *Nippon Shokakibyo Gakkai Zasshi* 1989;86:1292–1298
7. Namekawa K, Kasai C, Tsukamoto M, Koyano A. Imaging of blood flow using autocorrelation. *Ultrasound Med Biol* 1982;8[suppl 1]:138
8. Merritt CRB. Doppler color flow imaging. *JCU* 1987;15:591–597
9. Taylor KJW, Ramos I, Morse SS, Fortune KL, Hammers L, Taylor CR. Focal liver masses: differential diagnosis with pulsed doppler US. *Radiology* 1987;164:643–647
10. Ishida H, Morikawa P, Nizawa M, Naganuma S, Arakawa H, Masamune O. L'apport du Doppler à émission pulsée dans l'exploration des tumeurs du foie. *JEMU* 1988;178–185

# Dynamic Spin-Echo Imaging with Gd-DTPA: Value in the Differentiation of Hepatic Tumors

Bernard Van Beers<sup>1</sup>  
 Roger Demeure<sup>1</sup>  
 Jacques Pringot<sup>1</sup>  
 Dominique Defalque<sup>1</sup>  
 André Geubel<sup>2</sup>  
 Jean-François Gigot<sup>3</sup>  
 Jacques Jamart<sup>4</sup>

Thirty patients with hemangiomas ( $n = 6$ ), benign liver cell tumors ( $n = 7$ ), and primary or metastatic malignant tumors of the liver ( $n = 17$ ) underwent dynamic MR imaging with Gd-DTPA to determine the value of the procedure in the differentiation of hepatic tumors. The diagnoses were proved by histology or follow-up. Hemangiomas had a significantly greater mean T2 value ( $192.1 \pm 34.8$  msec) than did both benign liver cell tumors ( $71.9 \pm 16.9$  msec;  $p < .01$ ) and primary or metastatic malignant tumors ( $79.7 \pm 21.2$  msec;  $p < .01$ ), but the T2 values of benign liver cell tumors and malignant tumors were not significantly different. Both hemangiomas and benign liver cell tumors had a significantly greater mean signal-intensity ratio ( $1.86 \pm 0.60$  and  $1.77 \pm 0.26$ , respectively) than did malignant tumors ( $1.04 \pm 0.34$ ;  $p < .01$ ) in the early phase after Gd-DTPA administration, and hemangiomas had a significantly greater signal-intensity ratio ( $1.59 \pm 0.21$ ) than did both benign liver cell tumors ( $1.21 \pm 0.08$ ;  $p < .01$ ) and malignant tumors ( $1.06 \pm 0.26$ ;  $p < .01$ ) in the delayed phase.

These results suggest that dynamic MR images obtained after administration of Gd-DTPA are useful in differentiating hepatic hemangiomas, benign liver cell tumors, and malignant liver lesions.

AJR 154:515-519, March 1990

Recent reports have shown that, in most cases, hepatic hemangiomas can be differentiated from malignant hepatic tumors on T2-weighted conventional spin-echo (SE) MR images and dynamic MR imaging with Gd-DTPA [1-8]. This study was undertaken to collect quantitative data to determine the role of dynamic SE imaging with Gd-DTPA relative to that of conventional T2-weighted SE imaging in the differentiation of hepatic tumors.

## Subjects and Methods

During a 6-month period, 30 consecutive patients with hepatic lesions were studied. There were 12 men and 18 women 24-72 years old (mean, 40 years). The tumors included six hemangiomas, seven benign liver cell tumors (six focal nodular hyperplasia and one adenoma), eight metastases (four breast cancers, two colonic cancers, and two pancreatic cancers), six hepatocellular carcinomas, two epithelioid hemangioendotheliomas, and one cholangiocarcinoma. Sixteen patients had a solitary lesion and 14 had multiple lesions. The lesions were 1-15 cm in diameter.

The diagnoses were histologically proved in 13 patients and established with serial imaging studies (intervals of 6 months or more) in 17. The diagnosis of hemangioma was made by arteriography and percutaneous biopsy in one case and by follow-up imaging studies over a 6-month period in five cases. Focal nodular hyperplasia was diagnosed by surgical biopsy in one case; by percutaneous biopsy in two cases; and by <sup>99m</sup>Tc-scintigraphy, dynamic CT, and follow-up imaging studies over a 6-month period in three cases. The diagnosis of adenoma was confirmed by arteriography, dynamic CT, and follow-up imaging studies performed over a 10-month period; these showed reduction in tumor size after contraceptive withdrawal [9]. The diagnosis of metastases was established after partial liver resection in two cases, by

Received September 5, 1989; accepted after revision October 31, 1989.

<sup>1</sup> Department of Radiology, Louvain University, St. Luc University Hospital, Avenue Hippocrate 10, B-1200 Brussels, Belgium. Address reprint requests to B. Van Beers.

<sup>2</sup> Department of Gastroenterology, Louvain University, St. Luc University Hospital, B-1200 Brussels, Belgium.

<sup>3</sup> Department of Surgery, Louvain University, St. Luc University Hospital, B-1200 Brussels, Belgium.

<sup>4</sup> Department of Surgery, Louvain University, ICB, B-1040 Brussels, Belgium.

0361-803X/90/1543-0515

© American Roentgen Ray Society



surgical biopsy of the liver in one case, by the appearance and progressive enlargement of hepatic nodules after surgery of a primary cancer in four cases, and by the discovery of a pancreatic mass and hepatic nodules on dynamic CT scans in a patient with a high tumor marker value (carbohydrate antigenic determinant 19.9, >12,000 U/ml; normal, <60 U/ml). None of the metastases included in this series were hypervascular. Hepatocellular carcinoma was proved after partial resection of the liver in one case, by surgical biopsy in one case, by percutaneous biopsy in one case, and by arteriographic and scintigraphic findings and elevated alpha-fetoprotein levels in three cases. The diagnoses of epithelioid hemangioendothelioma and cholangiocarcinoma were proved after surgical resection.

MR examinations were performed on a 1.5-T imaging system (Gyroscan S 15, Philips, Eindhoven, the Netherlands). SE 295/15 (TR/TE) images of the entire liver with a slice thickness of 10 mm were obtained with a maximum interslice gap of 5 mm and with four excitations. The matrix size was 204 × 256. Multiple T2-weighted images were obtained with 2180/50,100 and two excitations. The dynamic SE sequence consisted of a set of three slices with 235/20, a 10-mm slice thickness, one excitation, a 128 × 256 matrix, and a 36-sec scanning time. The section level containing the main tumor was selected and serial imaging was started before contrast administration and at 30 sec, 1 min 15 sec, and 3 min after the beginning of an IV bolus injection of 0.1 mmol/kg Gd-DTPA (Magnevist, Schering, Berlin, West Germany). In 10 patients, images were obtained up to 15 min after contrast administration. Gd-DTPA was administered within 5 sec in every patient.

The tumor/liver signal-intensity ratio was calculated by dividing the signal intensity of the lesion by that of the liver [10]. The measured signal intensities were sampled from a highly enhanced area with region-of-interest cursors at 30 sec (early phase) and 3 min (delayed phase) after the injection of contrast material. T2 was calculated by fitting experimental signal intensities with the equation,  $I = I_0 \exp(-TE/T2)$ , where  $I$  = signal intensity and  $I_0$  = fitted parameter (mainly a function of proton density, tissue motion, and machine settings). Calculations were performed by using a general nonlinear model, called the Levenberg-Marquardt method [11]. The signal-intensity measurements on conventional T2-weighted images were performed with large operator-defined regions of interest to compound differences of signal intensity in heterogeneous tumors, but the periphery of the tumors was avoided to minimize sampling errors from surrounding liver. Data were reported as means ± standard deviations and compared with the Wilcoxon rank sum test.

## Results

T2 values are shown in Figure 1. The mean T2 values of hemangiomas, benign liver cell tumors, and malignant tumors were  $192.1 \pm 34.8$ ,  $71.9 \pm 16.9$ , and  $79.7 \pm 21.2$  msec, respectively. The differences in T2 values between hemangiomas and benign liver cell tumors, and between hemangiomas and malignant tumors, were statistically significant ( $p < .01$ ), but T2 values of benign liver cell tumor did not differ significantly from values of malignant tumors. When the T2 borderline between hemangiomas and other tumors was set at 130 msec, one metastasis of breast cancer was not classified correctly. However, this lesion was correctly diagnosed as metastasis by its morphologic pattern (target sign) [12]. Histologic study of the tumor after subsegmentectomy showed a myxoid center.

Signal-intensity ratios are shown in Figure 2. Both hemangiomas and benign liver cell tumors had significantly greater

signal-intensity ratios ( $1.86 \pm 0.60$  and  $1.77 \pm 0.26$ , respectively) than did malignant tumors ( $1.04 \pm 0.34$ ;  $p < .01$ ) in the early phase after injection of contrast material (Figs. 3 and 4), and hemangiomas had a significantly greater signal-intensity ratio ( $1.59 \pm 0.21$ ) than did both benign liver cell tumors ( $1.21 \pm 0.08$ ;  $p < .01$ ) and malignant tumors ( $1.06 \pm 0.26$ ;  $p < .01$ ) in the delayed phase. When 1.4 was used as the borderline signal-intensity ratio to differentiate between hemangiomas, benign liver cell tumors, and malignant tumors, the lesions were classified correctly in 28 (93%) of the 30 patients by a two-step analysis. In the first step, tumors with a signal-intensity ratio above 1.4 in the delayed phase were considered as hemangiomas. In the second step, signal-intensity ratios in the early phase were used to distinguish between the other tumors. Tumors with a signal-intensity ratio above 1.4 in the early phase were considered as benign liver cell tumors and tumors with a signal-intensity ratio below 1.4 were considered as malignant tumors. The two lesions not correctly classified by this method were a hepatocellular carcinoma, classified as benign liver cell tumor, and the breast cancer metastasis previously mentioned, again classified as hemangioma (Fig. 5).

## Discussion

T2-weighted conventional SE imaging with T2 measurements is useful for the diagnosis of hemangioma [3, 4], but T2 values cannot be used to discriminate benign liver cell tumor from malignant tumor.

The histology of benign liver cell tumor is often relatively similar to that of normal liver parenchyma, so it is not surprising that relaxation parameters are relatively similar also [13]. A benign liver cell tumor is isointense or slightly hypointense on T1-weighted images and isointense or slightly hyperintense on T2-weighted images [13–15]. The presence of a central scar is inconsistent and cannot be considered a specific feature of benign liver cell tumors [16].

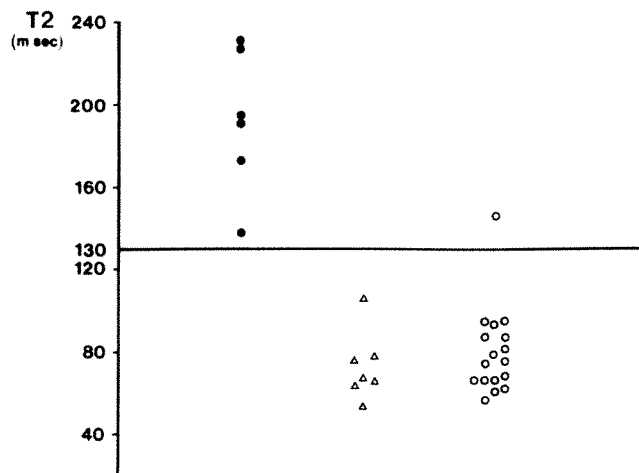


Fig. 1.—T2 values of liver tumors. Benign liver cell tumors (triangles) cannot be distinguished from malignant tumors (open circles). Hemangioma (solid circles).

Fig. 2.—A and B, Signal-intensity ratios (SI) in early phase after Gd-DTPA administration (A) and in delayed phase (B). Hemangioma (solid circles); benign liver cell tumor (triangles); malignant tumor (open circles).

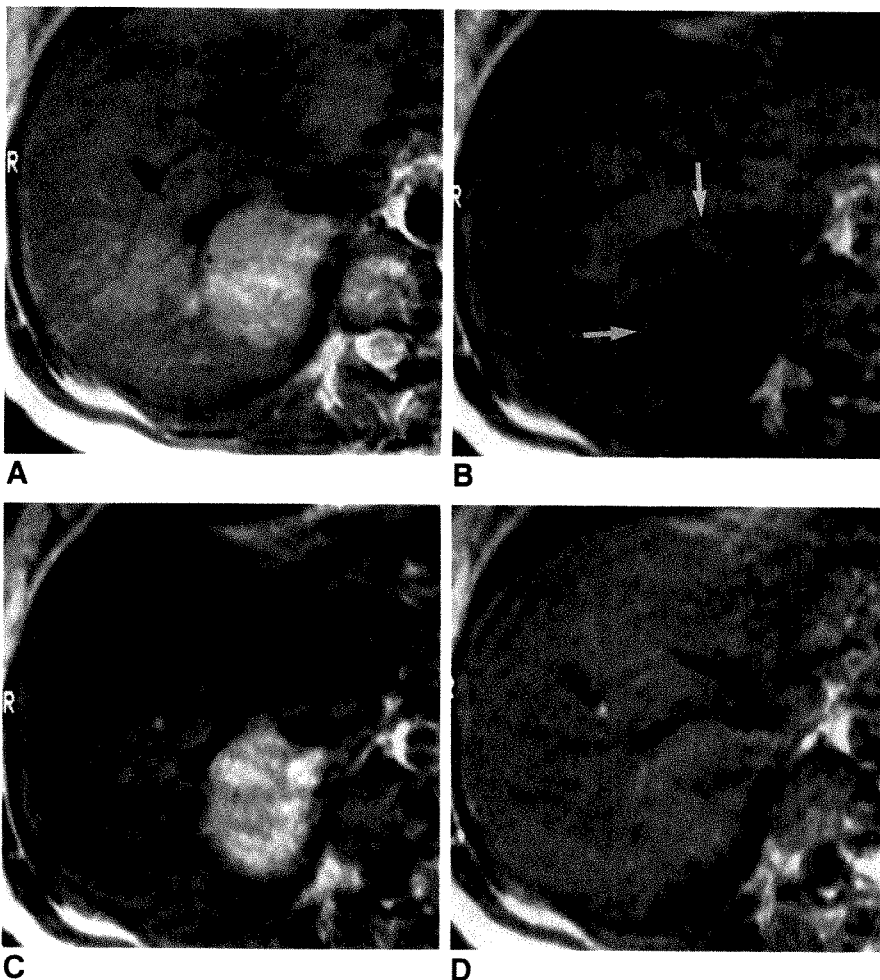
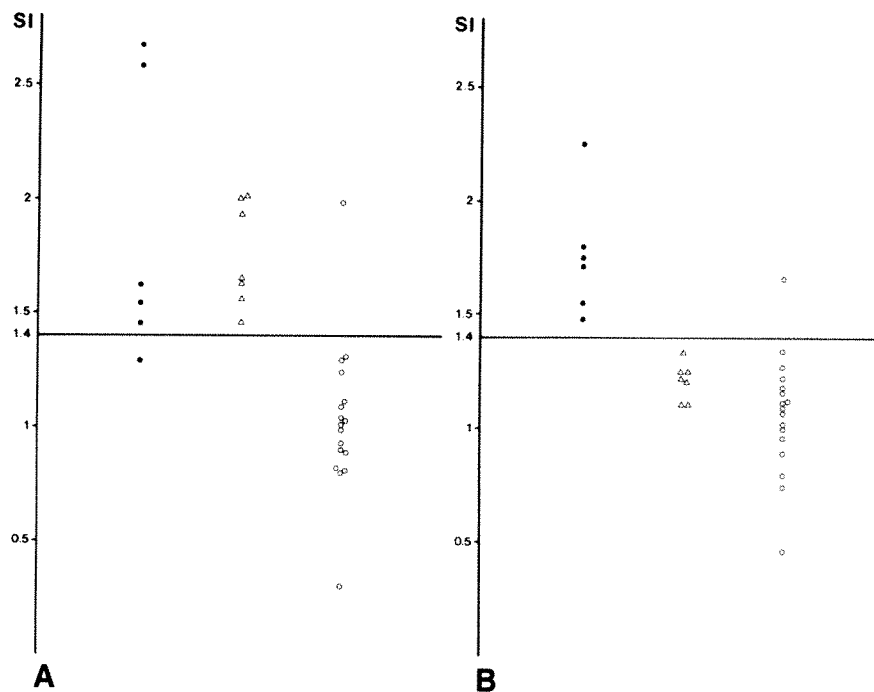


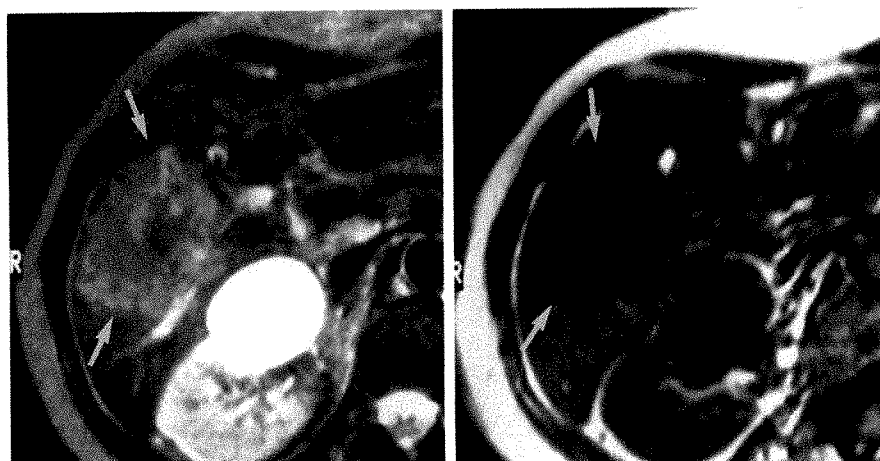
Fig. 3.—Focal nodular hyperplasia.

A, Moderately T2-weighted SE MR image (2180/50) shows slightly hyperintense tumor ( $T_2 = 63$  msec) with smooth borders.

B, Precontrast dynamic SE image (235/20). Tumor is isointense relative to liver and is visible only by its mass effect (arrows).

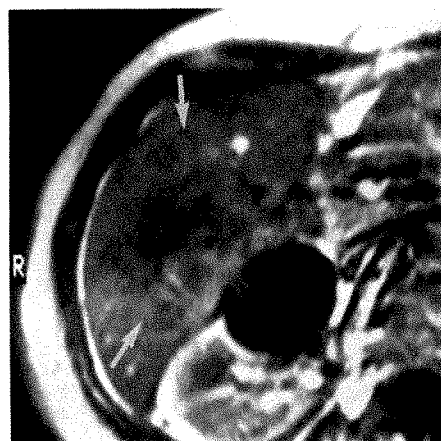
C, Early image after bolus injection of Gd-DTPA. Tumor is completely hyperintense.

D, Delayed image after bolus injection of Gd-DTPA. Tumor is almost isointense.

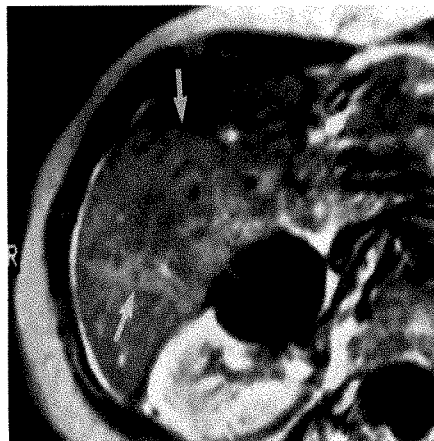


A

B



C



D

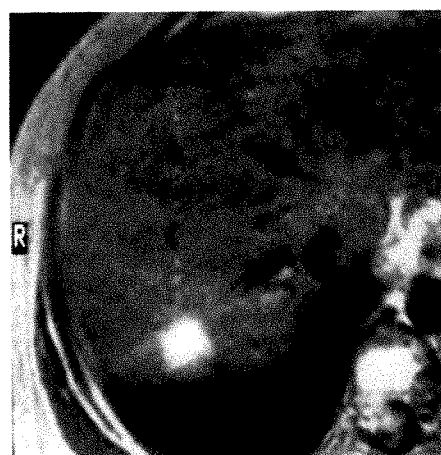
Fig. 4.—Peripheral cholangiocarcinoma.

A, T2-weighted SE MR image (2180/100) shows slightly hyperintense tumor ( $T_2 = 56$  msec) with hypointense center and lobulated contours (arrows).

B, Precontrast dynamic SE image (235/20) shows slightly hypointense lesion (arrows).

C, Early postcontrast image reveals moderate peripheral enhancement (arrows).

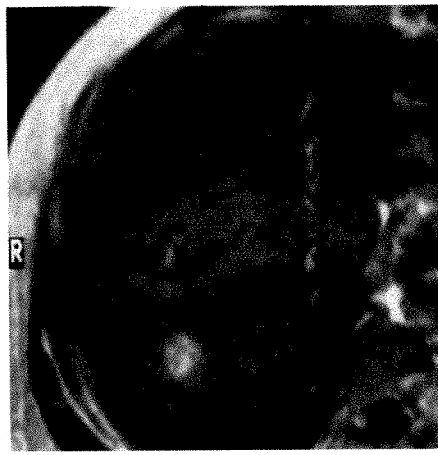
D, Delayed image 3 min after injection shows heterogeneous filling of lesion. Lesion remains moderately hyperintense (arrows).



A



B



C

Fig. 5.—Metastasis from breast cancer.

A and B, T2-weighted SE MR images (2180/50, 100) show marked hyperintense tumor ( $T_2 = 146$  msec). Characteristic target sign is visible.

C, Delayed postcontrast dynamic SE image shows persistent bright enhancement within lesion (signal-intensity ratio = 1.66).

The necrosis and/or hemorrhage prevalent in adenomas account for their greater heterogeneity relative to that seen in focal nodular hyperplasia [13]. However, hemorrhage also can be observed in hepatocellular carcinoma [17]; angio-

sarcoma [18]; and more infrequently in focal nodular hyperplasia [19], hemangioma [20], and metastases [21].

Adenoma [9, 10] and hepatocellular carcinoma [8, 10, 22] may contain fat and appear hyperintense on T1-weighted



images. Other tumors with fatty components include lipomatous tumors (lipoma, angiomyolipoma, myelolipoma) [23] and metastases from clear cell carcinoma of the kidney [22] and dermoid tumor of the ovary [23].

The hemodynamics of benign liver cell tumors are well demonstrated by dynamic MR imaging with contrast material. We observed bright enhancement in the early phase of preferential arterial enhancement and a rapid decrease in intensity. As with CT [24, 25], this enhancement appeared uniform except in areas of necrosis, fibrosis, or hemorrhage.

In this limited series, T2 measurements were useful for differentiating between hemangiomas and other tumors, but signal-intensity ratios on dynamic SE images were useful for differentiating between hemangiomas, benign liver cell tumors, and malignant tumors. However, these data alone do not always allow a correct diagnosis, and the morphologic pattern should be carefully analyzed also [2, 12].

The use of borderline values of T2 and signal-intensity ratios has some pitfalls: First the errors in the measurement of T2 when using multiple-echo techniques are well known [26–28]. Second, diffuse hyperintensity of the tumor in the early phase after contrast administration and rapid washout are not completely specific for benign liver cell tumor. Some hepatocellular carcinomas [25] and hypervascular metastases [29] may demonstrate the same hemodynamic pattern. Third, hemorrhagic or necrotic adenomas may appear hypovascular [30]. Despite these limitations, dynamic MR imaging with contrast material may complement T2-weighted SE sequences and demonstrate the hemodynamic pattern of hypervascular tumors. This may be an aid in the diagnosis of benign liver cell tumor. However, as stated by Welch et al. [24] and Mathieu et al. [25], a single imaging method often will fail to yield the correct diagnosis. The diagnosis of benign liver cell tumor should be based on clinical criteria, scintigraphy, MR imaging, and possibly angiography and histology.

Previous dynamic MR studies used breath-holding. We did not ask our patients to hold their breath because of the length of the sequence (36 sec). This study shows that MR imaging without suspended respiration is feasible. Shorter sequences (gradient-echo sequences) could be preferable for breath-holding. However, with the dynamic SE sequence used in this study, three slices could be obtained. This reduced problems of misregistration of small lesions caused by single-level studies [8]. Presaturation pulses also may be used to eliminate vascular pulsation artifacts at the loss of one slice per multi-section [31].

In conclusion, dynamic MR imaging with Gd-DTPA may help to differentiate liver tumors by assessing their hemodynamics. This may prove useful not only for the diagnosis of hemangiomas but also for the diagnosis of benign liver cell tumors in the proper clinical setting.

## REFERENCES

1. Stark DD, Felder RC, Wittenberg J, et al. Magnetic resonance imaging of cavernous hemangioma of the liver: tissue-specific characterization. *AJR* **1985**;145:213–222
2. Li KC, Glazer GM, Quint LE, et al. Distinction of hepatic cavernous hemangioma from hepatic metastases with MR imaging. *Radiology* **1988**;169:409–415
3. Ohtomo K, Itai Y, Furui S, Yashiro N, Yoshikawa K, Iio M. Hepatic tumors: differentiation by transverse relaxation time (T2) of magnetic resonance imaging. *Radiology* **1985**;155:421–423
4. Ohtomo K, Itai Y, Yoshikawa K, Kokubo T, Iio M. Hepatocellular carcinoma and cavernous hemangioma: differentiation with MR imaging. Efficacy of T2 values at 0.35 and 1.5 T. *Radiology* **1988**;168:621–623
5. Ohtomo K, Itai Y, Yoshikawa K, et al. Hepatic tumors: dynamic MR imaging. *Radiology* **1987**;163:27–31
6. Mano I, Yoshida H, Nakabayashi K, Yashiro N, Iio M. Fast spin echo imaging with suspended respiration: gadolinium enhanced MR imaging of liver tumors. *J Comput Assist Tomogr* **1987**;11:73–80
7. Ohtomo K, Itai Y, Yoshikawa K, Kokubo T, Yashiro N, Iio M. Hepatic haemangioma: dynamic MRI using gadolinium-DTPA. *Eur J Radiol* **1987**;7:257–259
8. Yoshida H, Itai Y, Ohtomo K, Kokubo T, Minami M, Yashiro N. Small hepatocellular carcinoma and cavernous hemangioma: differentiation with dynamic FLASH MR imaging with Gd-DTPA. *Radiology* **1989**;171:339–342
9. Klatskin G. Hepatic tumors: possible relationship to use of oral contraceptives. *Gastroenterology* **1977**;73:386–394
10. Rummeny E, Weissleder R, Stark DD, et al. Primary liver tumors: diagnosis by MR imaging. *AJR* **1989**;152:63–72
11. Press WH, Flannery BP, Teukolsky SA, Vetterling WT. *Numerical recipes. The art of scientific computing*. Cambridge, England: Cambridge University Press, **1986**:523–528
12. Wittenberg J, Stark DD, Forman BH, et al. Differentiation of hepatic metastases from hepatic hemangiomas and cysts by using MR imaging. *AJR* **1988**;151:79–84
13. Menu Y, Arrive L, Grenier P, et al. Imagerie par résonance magnétique de l'adénome hépatique et de l'hyperplasie nodulaire focale. *Ann Radiol (Paris)* **1988**;31:18–24
14. Mattison GR, Glazer GM, Quint LE, Francis IR, Bree RL, Ensminger WD. MR imaging of hepatic focal nodular hyperplasia: characterization and distinction from primary malignant hepatic tumors. *AJR* **1987**;148:711–715
15. Schiebler ML, Kressel HY, Saul SH, Yeager BA, Axel L, Gefter WB. MR imaging of focal nodular hyperplasia of the liver. *J Comput Assist Tomogr* **1987**;11:651–654
16. Rummeny E, Weissleder R, Sironi S, et al. Central scars in primary liver tumors: MR features, specificity, and pathologic correlation. *Radiology* **1989**;171:323–326
17. Hsieh JS, Huang CJ, Huang YS, Sheen PC, Huang TJ. Intraoperative hemorrhage due to spontaneous rupture of hepatocellular carcinoma: treatment by hepatic artery embolization. *AJR* **1987**;149:715–717
18. Mahony B, Jeffrey RB, Federle MP. Spontaneous rupture of hepatic and splenic angiosarcoma demonstrated by CT. *AJR* **1982**;138:965–966
19. Mays ET, Christopherson WM, Barrows GH. Focal nodular hyperplasia of the liver. *Am J Clin Pathol* **1974**;61:735–746
20. Adam YG, Huvos AG, Fortner JG. Giant hemangiomas of the liver. *Ann Surg* **1970**;172:239–245
21. Hamm B. Contrast media—clinical application: liver. In: Runge VM, ed. *Enhanced magnetic resonance imaging*. St. Louis: Mosby, **1989**:244–267
22. Ebara M, Ohto M, Watanabe Y, et al. Diagnosis of small hepatocellular carcinoma: correlation of MR imaging and tumor histologic studies. *Radiology* **1986**;159:371–377
23. Marti-Bonmati L, Menor F, Viczaino I, Vilar J. Lipoma of the liver: US, CT and MRI appearance. *Gastrointest Radiol* **1989**;14:155–157
24. Welch TJ, Sheedy PF, Johnson CM, et al. Focal nodular hyperplasia and hepatic adenoma: comparison of angiography, CT, US, and scintigraphy. *Radiology* **1985**;156:593–595
25. Mathieu D, Bruneton JN, Drouillard J, Caron Pointreau C, Vasile N. Hepatic adenomas and focal nodular hyperplasia: dynamic CT study. *Radiology* **1986**;160:53–58
26. Majumdar S, Orphanoudakis SC, Gmitro A, O'Donnell M, Gore JC. Errors in the measurements of T2 using multiple-echo MRI techniques. I. Effects of radiofrequency pulse imperfections. *Magn Reson Med* **1986**;3:397–417
27. Majumdar S, Orphanoudakis SC, Gmitro A, O'Donnell M, Gore JC. Errors in the measurements of T2 using multiple-echo MRI techniques. II. Effects of static field inhomogeneity. *Magn Reson Med* **1986**;3:562–574
28. Crawley AP, Henkelman RM. Errors in T2 estimation using multislice multiple-echo imaging. *Magn Reson Med* **1987**;4:34–47
29. Bressler EL, Alpern MB, Glazer GM, Francis IR, Ensminger WD. Hypervascular hepatic metastases: CT evaluation. *Radiology* **1987**;162:49–51
30. Casarella WJ, Knowles DM, Wolff M, Johnson PM. Focal nodular hyperplasia and liver cell adenoma: radiologic and pathologic differentiation. *AJR* **1978**;131:393–402
31. Winkler ML, Thoeni RF, Luh N, Kaufman L, Margulis AR. Hepatic neoplasia: breath-hold MR imaging. *Radiology* **1989**;170:801–806

# American Roentgen Ray Society

90th Annual Meeting

May 13–18, Washington, D.C.

## **1990 Caldwell Lecturer**



**Sandra Day O'Connor**

United States Supreme Court Justice

**“The Federal Courts”**

# Gallbladder Contractility in Patients with Spinal Cord Injuries: A Sonographic Investigation

Matilde Nino-Murcia<sup>1</sup>  
Doris Burton<sup>1</sup>  
Paul Chang<sup>1</sup>  
James Stone<sup>2,3</sup>  
Inder Perkash<sup>4</sup>

Approximately 30% of all patients who have spinal cord injuries have gastrointestinal symptoms. One cause is gallstone disease; indeed the literature suggests that gallstones are more common in patients with spinal cord injuries because these patients have impaired contractility of the gallbladder with a reduced ejection fraction. To test this hypothesis, we obtained gallbladder sonograms in 30 patients with spinal cord injuries (16 quadriplegics and 14 paraplegics) and in 32 uninjured age-matched control subjects. Four patients and four asymptomatic control subjects had gallstones and were excluded. The remaining 26 patients and 28 control subjects fasted for 12 hr. Longitudinal and transverse sonograms of the gallbladder were made immediately before the ingestion of 25 g of fat, and at 10, 20, 30, 45, and 60 min thereafter. Gallbladder volumes were measured by using the ellipsoid method. Resting and residual volumes and the emptying times were determined and the ejection fractions were calculated. The ejection fractions were significantly lower ( $p = .003$ ) in the patients than in the control subjects because the resting volumes were lower than in the control subjects ( $p = .013$ ). However, the emptying times and residual volumes were the same in the two groups.

We conclude that gallbladder contractility is normal in patients with spinal cord injuries and that the lower ejection fraction found in such patients is due to a smaller resting volume.

*AJR* 154:521-524, March 1990

Spinal cord injuries are common; there are about 20,000 new cases each year in the United States, and approximately 1,500,000 people in the United States currently are living with some form of spinal cord injury [1]. Gastrointestinal symptoms in these patients also are common; at any one time, approximately 30% of all patients who have spinal cord injuries have gastrointestinal symptoms (Stone JM et al., unpublished data).

One cause of gastrointestinal symptoms in these patients is gallstone disease. Clinicians have been alerted to this possibility, because the prevalence is said to be much higher in these patients than in the general population [2].

One possible explanation for this suggested increased prevalence of gallstones in patients with spinal cord injury is that the gallbladder does not contract and empty as well in these patients as in normal persons [3]. The purpose of this study was to determine if gallbladder contractility is abnormal in patients with spinal cord injuries.

## Subjects and Methods

We performed sonography of the gallbladder in 30 patients with spinal cord injuries and 32 asymptomatic normal age-matched control subjects. Informed consent was obtained after the procedure was explained. Four (13%) of 30 patients with spinal cord injuries and four (13%) of 32 asymptomatic control subjects had gallstones and were excluded from the study.

Received August 31, 1989; accepted after revision October 24, 1989.

<sup>1</sup> Radiology Service, Veterans Administration Medical Center, 3801 Miranda Ave., Palo Alto, CA 94304. Address reprint requests to M. Nino-Murcia, Radiology #114.

<sup>2</sup> Surgical Service, Veterans Administration Medical Center, 3801 Miranda Ave., Palo Alto, CA 94304.

<sup>3</sup> Present address: 3131 Excelsior Blvd., #706, Minneapolis, MN 55416.

<sup>4</sup> Spinal Cord Injury Service, Veterans Administration Medical Center, 3801 Miranda Ave., Palo Alto, CA 94304.

0361-803X/90/1543-0521

© American Roentgen Ray Society



Thus, 26 patients (one woman, 25 men) 24–71 years old (mean, 45 years; standard deviation, 14) with spinal cord injuries but without evidence of gallstones and 28 aged-matched normal volunteers were studied. Ninety-six percent of the patients involved were men because most spinal cord injuries occur in men. All spinal injuries had occurred between 6 months and 39 years earlier. Injury levels ranged from C4 to L3; 14 patients were quadriplegics and 12 were paraplegics (eight T1–T10 and four T11 and below). Patients or control subjects with a history of gastric surgery, vagotomy, or diabetes were not included in the study. Seven patients (27%) had history of either fatty food intolerance or postprandial bloating. These symptoms did not exist before the spinal cord injury; they developed for the first time after the injury.

Each subject fasted at least 12 hr before the sonographic examination. Longitudinal and transverse sonograms were obtained by using a Dasonics unit (Milpitas, CA), with a sector scanner and 3.5- and 5.0-MHz transducers. Images were obtained immediately before a fatty meal was ingested, and at 10, 20, 30, 45, and 60 min after the meal. These times were chosen because within this time frame cholecystokinin will have been released and the gallbladder will have fully contracted [4].

The fatty meal consisted of a commercially available chocolate bar containing 25 g of fat. A fatty meal (rather than cholecystokinin or an analogue) was given because the emptying rate and maximal contraction are the same whether cholecystokinin is injected IV or a fatty meal is ingested [5]. Also it was easier to get the patients and control subjects to volunteer for the study if they were asked to eat a chocolate bar, rather than receive an injection.

Gallbladder volumes were measured by using the ellipsoid method [6] (volume =  $0.52 \text{ [width} \times \text{height} \times \text{length}]}$ ) (Fig. 1). All measurements were made in duplicate, and the averaged values were used in the calculations. Statistical analyses used included *t* tests, chi-square, and analysis of variance. Chi-square analysis showed no significant difference in the age distribution of patients with spinal cord injuries and that of normal control subjects.

The following calculations were performed for each subject: (1) resting volume: the resting volume of the gallbladder after a 12-hr fast, but before the fat was ingested; (2) residual volume: the smallest gallbladder volume observed at any time after ingestion of the fat; (3) ejection fraction:  $1 - (\text{Residual Volume}/\text{Resting Volume}) \times 100$ ; and (4) emptying time: the time from ingesting the first mouthful of the fat to the time at which no further contraction of the gallbladder occurred.

## Results

The mean resting volume in normal control subjects was 28 ml, as compared with 21 ml in patients with spinal cord injuries (Table 1). The two-tailed *t* test showed that this is a statistically significant difference ( $p = .013$ ). On the other hand, the mean residual volume in normal control subjects was 11 ml, as compared with 10 ml in patients with spinal cord injuries. This is not a significant difference ( $p = .688$ ).

The mean ejection fraction in normal subjects was 62%, as compared with 49% in patients with spinal cord injuries. The two-tailed *t* test showed that this was a statistically significant difference ( $p = .003$ ).

Thus the residual volumes were the same as normal, whereas the resting volumes were smaller, in patients with spinal cord injuries; this accounts for the lower ejection fraction in patients with spinal cord injuries. That the residual volumes were the same probably reflects the limits to which the gallbladder can contract. However, because the resting

volume is smaller in patients with spinal cord injuries, their relative residual volume is larger.

The emptying time was 48 min in the normal control subjects and 43 min in patients with spinal cord injuries. The two-tailed *t* test showed that this was not a statistically significant difference ( $p = .175$ ). A plot comparing the change in total ejectable gallbladder volume as a function of time shows that rates of emptying were similar in the two groups (Fig. 2).

## Discussion

This study confirms the results of earlier investigators [3]: the gallbladder ejection fraction decreases in patients with spinal cord injuries. However, in our study, the main variable responsible for the lower ejection fraction was the lower resting volume of the gallbladder, not its contractility. Our evidence supports this conclusion; the two variables that best describe gallbladder contractility are the emptying time and the residual volume. We found no significant difference in the two groups with respect either to the emptying time or the residual volume, so the only possible explanation for the decreased ejection fraction in patients with spinal cord injuries is the lower resting volume we found in those patients.

This lower resting volume may reflect the disturbed function of the sympathetic nerve supply to the gallbladder in patients with spinal cord injuries. The function of the sympathetic nerve supply to the gallbladder is to relax the gallbladder during filling [7–13]. We hypothesize that the reason that the resting volume of the gallbladder was statistically significantly smaller in patients with spinal cord injuries than in normal control subjects was that, in patients with lesions at or above T10, the gallbladder did not fully relax during filling.

To test this hypothesis, we determined if the resting gallbladder volume differed in patients with spinal cord injuries at or above T10 vs those with lesions below T10. Unfortunately, of the 26 patients with spinal cord injuries, only two had lesions below T10. Additional patients with lesions below T10 could not be recruited. The two patients with lesions below T10 did have larger resting volumes than the remaining 24, but the number of patients involved was too small to be of any statistical significance.

That the two variables describing gallbladder contractility, emptying time and residual volume, showed no statistically significant difference in patients with spinal cord injuries as compared with normal control subjects is perhaps best explained by a review of the physiology of gallbladder contraction. The role of the vagus nerve, for example, is not fully understood, although it is known that a vagotomy results in bile stasis in the gallbladder, so that it clearly plays some role [14]. Because the vagus nerve arises in the CNS, however, not in the spinal cord, it is not affected by a spinal cord injury.

The main factor responsible for the initiation of gallbladder contraction is the release of cholecystokinin from the duodenum in the presence of fatty foods [15]. This mechanism also is intact in patients with spinal cord injuries; and the fact that the emptying time was not statistically significantly different in patients with spinal cord injuries vs normal control subjects in our study indicates that cholecystokinin must have

Fig. 1.—A–D. Sonograms of gallbladder before (A, B) and after (C, D) a fatty meal. Length was measured in longitudinal sections (A, C); width and height were measured in transverse sections (B, D).

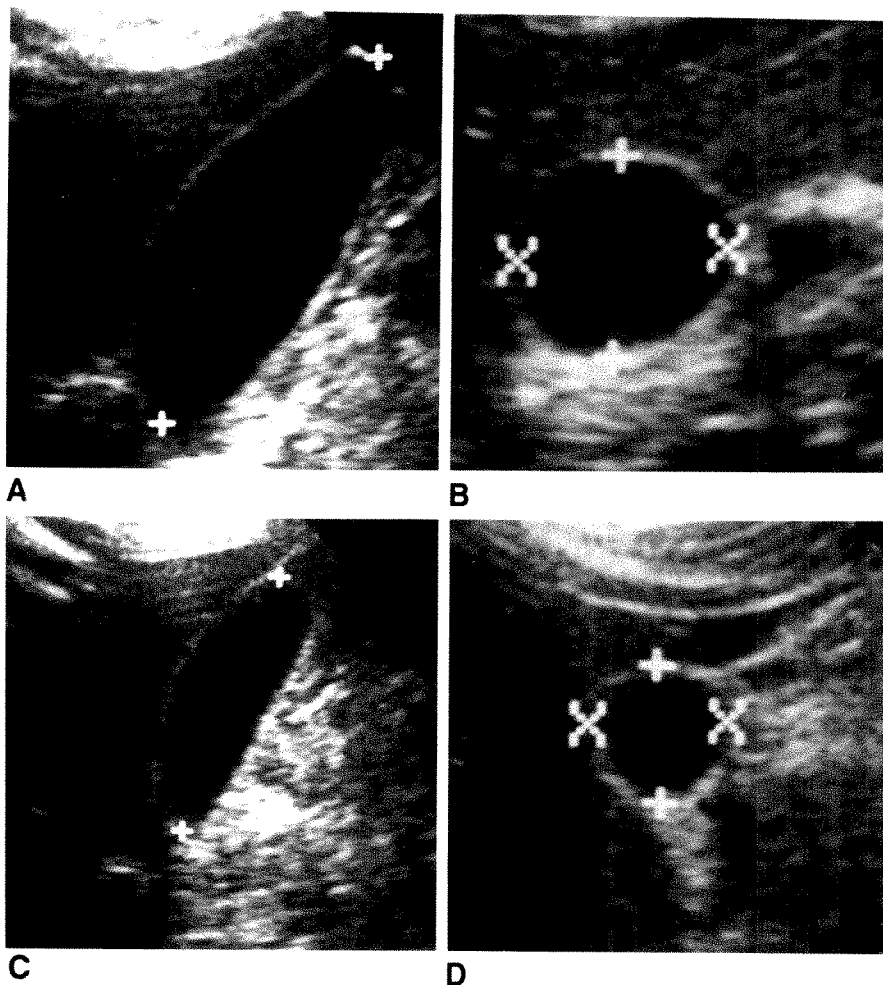


TABLE 1: Comparison of Measurements of Gallbladder Function

Measurement	Normal Subjects	Patients with Spinal Cord Injuries	<i>p</i> Value
Mean resting volume (ml)	28 (2.3)	21 (1.4)	.013*
Mean residual volume (ml)	11 (3.9)	10 (3.8)	.688
Mean ejection fraction (%)	62 (2.1)	49 (3.6)	.003*
Emptying time (min)	48 (2.6)	43 (2.9)	.175

Note.—Numbers in parentheses are standard errors of the mean.

\* Statistically significant.

reached the gallbladder at about the same time in both groups of patients.

It is possible that the lower resting volume found in patients with spinal cord injuries could make their bile more lithogenic. However, as the bile was not chemically analyzed in either patients or control subjects, we could not determine whether its composition is altered in patients with spinal cord injuries.

In conclusion, we find that the two variables that best describe gallbladder contractility, emptying time, and residual volume were not statistically significantly different in patients with spinal cord injuries and in normal control subjects. This

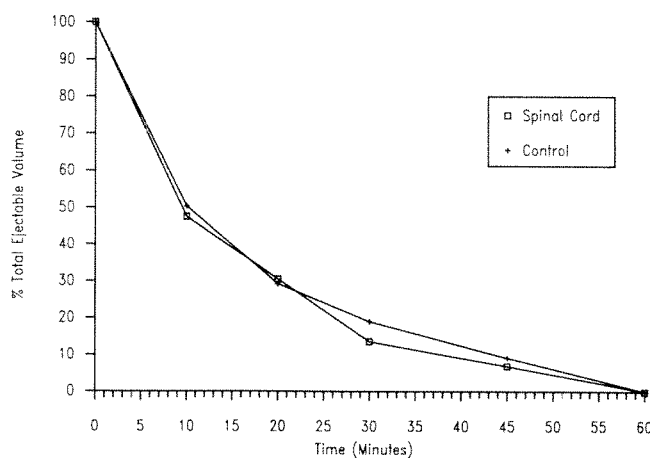


Fig. 2.—Plot showing change in percentage total ejectable gallbladder volume as a function of time in normal control subjects and patients with spinal cord injuries.

is understandable, given that both the vagus nerve and the mechanism regarding the transmission of cholecystokinin to the gallbladder are intact; if the vagus nerve and the cholecystokinin mechanism are unaffected in patients with spinal cord injuries, contractility also should be unaffected.

## ACKNOWLEDGMENT

We thank the Spinal Cord Research Foundation for awarding us the Paul M. Cheremeta Award of the Paralyzed Veterans of America for our research on the physiology of chronic gastrointestinal problems after spinal cord injury. The results presented here are part of that research.

## REFERENCES

1. McKew L. In: U.S. Congress, House. Hearing before the Subcommittee on Hospitals and Health Care of the Committee on Veterans' Affairs, 97th Cong., 2nd sess. 1982;serial 97 (72):25
2. Apstein MD, Dalecki-Chipperfield K. Spinal cord injury is a risk factor for gallstone disease. *Gastroenterology* 1987;92:966-968
3. Chassin-Kaplan SL, Apstein MD, Williams W. Gallbladder dysmotility in spinal cord injury. Presented at the 14th annual meeting of American Spinal Injury Association, San Diego, CA, May 1988
4. Fried M, Mayer EA, Jansen JBM, et al. Temporal relationships of cholecystokinin release, pancreatobiliary secretion, and gastric emptying of a mixed meal. *Gastroenterology* 1988;95:1344-1350
5. Hopman WPM, Rosenbusch G, Jansen JBM, de Jong AJL, Lamers CBHW. Gallbladder contraction: effect of fatty meals and cholecystokinin. *Radiology* 1985;157:37-39
6. Dodds WJ, Grosh WJ, Darweesh RA, Lawson TL, Kishk SA, Kern MK. Sonographic measurement of gallbladder volume. *AJR* 1985;145:1009-1011
7. Goyal RK, Crist JR. Neurology of the gut. In: Sleisenger MH, Fordtran JS, eds. *Gastrointestinal disease*, 4th ed. Philadelphia: Saunders, 1989:21-52
8. Benfield WJ. Physiology of the gallbladder. *Gastroenterology* 1975;69:770-777
9. Crandall LA Jr. Mechanism of contraction and evacuation of the gallbladder. *Arch Intern Med* 1931;48:1217-1224
10. Mack AJ, Todd JK. A study of human gallbladder *in vitro*. *Gut* 1968;9:546-549
11. Persson CGA. Dual effects on the sphincter of Oddi and gallbladder induced by stimulation of the right splanchnic nerves. *Acta Physiol Scand* 1973;87:334-343
12. Whitaker LR. The mechanism of the gallbladder. *Am J Physiol* 1926;78:411-436
13. Winkelstein A, Aschner PW. The mechanism of bile flow from the liver into the intestines. *Am J Med Sci* 1928;171:104-111
14. Johnson FE, Boyden EA. The effect of double vagotomy on the motor activity of the human gallbladder. *Surgery* 1952;32:591-601
15. Ryan JP. Motility of the gallbladder and biliary tree. In: Johnson LR, ed. *Physiology of the gastrointestinal tract*. New York: Raven Press, 1981:473-494



# Hydatid Disease of the Spleen: Imaging Findings in Nine Patients

T. Franquet<sup>1</sup>  
M. Montes<sup>2</sup>  
F. J. Lecumberri<sup>3</sup>  
J. Esparza<sup>4</sup>  
J. M. Bescos<sup>1</sup>

Splenic involvement is uncommon in patients with hydatid disease. The radiologic and clinical findings in nine patients with splenic hydatidosis are described. The three men and six women were 41–76 years old (mean, 58 years). Their histories and physical findings, the results of serologic tests for hydatidosis, and imaging procedures were evaluated. Plain abdominal radiographs were obtained in all nine patients, sonograms in six, and CT scans in seven. Plain films showed calcification of the cyst wall in four of the nine patients. On sonograms, five lesions were anechoic and one was echogenic. On CT scans, all lesions except one were of lower attenuation than the surrounding spleen. None of the lesions enhanced after administration of IV contrast material.

Although rare, splenic hydatidosis should be included in the differential diagnosis when a cystic splenic lesion is identified with sonography or CT.

AJR 154:525–528, March 1990

Splenic involvement in hydatid disease is uncommon, representing less than 2% of all human infestations by *Echinococcus* [1–3]. To our knowledge, previous descriptions of the imaging findings in splenic hydatidosis have been based on sporadic case reports [4–6] and lack pathologic correlation. We studied the imaging findings in nine cases of serologically or surgically proved splenic hydatid disease and correlated the results with clinical and pathologic data.

## Materials and Methods

We retrospectively reviewed the medical records and radiologic findings of nine patients in whom splenic hydatidosis was diagnosed and treated between 1982 and 1988. There were three men and six women 41–76 years old (mean, 58 years). Histories, physical findings, and results of serologic tests (immunoelectrophoresis, latex agglutination, and enzyme-linked immunosorbent assay) for hydatidosis were evaluated.

All patients were examined by conventional radiography. Sonography was performed in six patients; commercially available real-time equipment with 3.5- or 5-MHz transducers was used. The sonographic studies were evaluated with regard to echo texture and definition of the splenic mass. CT examinations were performed in seven patients; pre- and postcontrast images were available in all cases. Each lesion was evaluated for the following CT findings: (1) calcification, (2) precontrast attenuation value, and (3) degree of contrast enhancement.

Abdominal pain was present initially in five patients. Other symptoms included fever in three patients and left chest pain in one patient who also had pulmonary hydatid disease. Intraoperative spread of hydatid disease was observed in two patients.

Capron et al. [7] reported the presence of an antigen specific for *Echinococcus granulosus* that appeared immunoelectrophoretically as a band of characteristic morphology and location when tested against sera from human patients. They named this band arc 5 because of its relative position in the immunoelectrophoretic pattern. The arc 5 of Capron was present in seven patients and absent in two patients who had calcified hydatid cysts. In calcified hydatid cysts it is postulated that the physical status of the hydatid cyst membranes influences the degree of antigen stimulation of the immune system of the host and therefore affects the success of the immunodiagnostic test [7, 8].

Received August 18, 1989; accepted after revision October 11, 1989.

<sup>1</sup> Department of Radiology, Hospital "Virgen del Camino," c/Irunlarrea s/n. 31008 Pamplona, Spain. Address reprint requests to T. Franquet.

<sup>2</sup> Department of Pathology, Hospital "Virgen del Camino," 31008 Pamplona, Spain.

<sup>3</sup> Department of Radiology, Clinica Universitaria de Navarra, Pamplona, Spain.

<sup>4</sup> Department of Radiology, Hospital Provincial de Navarra, Pamplona, Spain.

0361-803X/90/15#3-0525

© American Roentgen Ray Society

Surgical specimens were available in six patients. At surgery, cysts measured 8–16 cm. Macroscopically, the cyst walls were white and smooth in all cases. Most of the cysts (five cases) were fluid-filled; small daughter cysts were observed in one case (Fig. 1B). A dense yellow material was present in one case that also had small peripheral calcifications (Fig. 2C). Microscopically, the cysts comprised three characteristic layers: (1) external layer or adventitia formed by compressed and fibrotic splenic tissue with a diffuse infiltration of lymphocytes, plasma cells, and eosinophils; (2) intermediate layer or cuticula formed by noncellular laminated eosinophilic tissue 1 mm thick; and (3) intimal or germinal layer formed by a discontinuous layer of scoleces and microcysts. At microscopic study, the semisolid filled cyst consisted of a mixture of infolded membranes, fragmented hooklets, and debris, which was part of the hydatid "sand."

## Results

The most common radiographic finding, seen in five of nine cases, was splenomegaly, or a soft-tissue mass, in the left

upper quadrant (with or without calcification). One patient had associated pulmonary involvement. Linear calcification of the spleen was observed on plain radiographs in four of nine patients (Fig. 3). The cysts were partly calcified in two patients and completely calcified in the remaining two. Serologic tests for hydatidosis were negative in patients with intensely calcified cysts.

On sonography (six cases), five masses were anechoic, often with considerable homogeneity. A single cysts was observed in all cases. An intracystic small daughter cysts was seen in one patient (Fig. 1). Only one lesion showed an echogenic (solid) pattern with sonography, corresponding to intracystic infolded membranes and hydatid sand (Fig. 2).

On abdominal CT (seven cases), calcification was evident in four cases. In all cases, the mass or masses were sharply delineated on precontrast and/or postcontrast scans (Fig. 4). All lesions except one were of lower attenuation than the

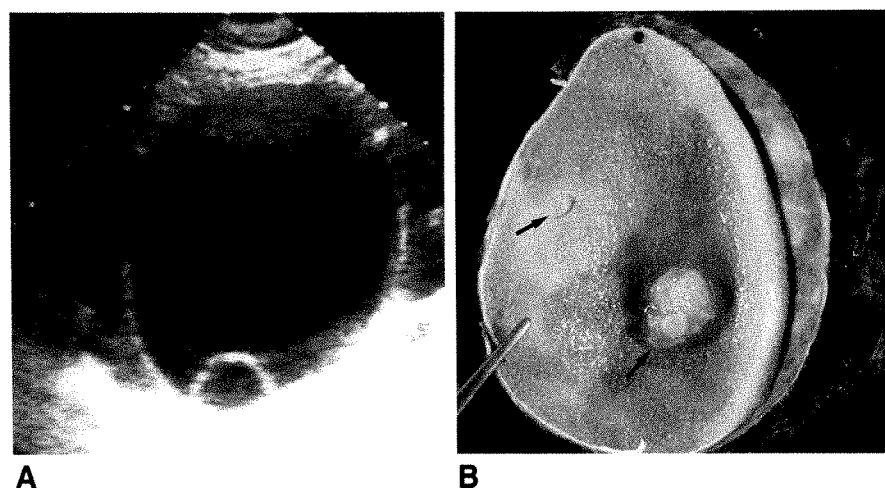


Fig. 1.—48-year-old woman with splenic hydatidosis.

A, Oblique sonogram of left upper quadrant shows spherical anechoic mass containing small cystic lesion.

B, Corresponding gross specimen shows splenic hydatid cyst with whitish cuticular and granular germinal layer. Two small daughter cysts are visible within lesion (arrows).

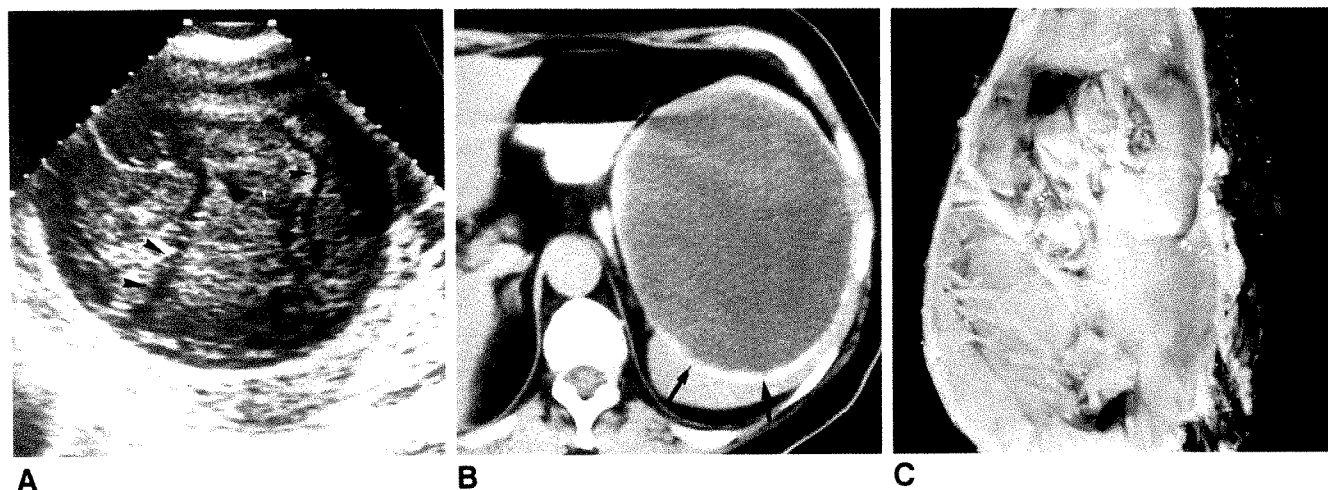


Fig. 2.—Splenic hydatid cyst in 45-year-old woman with abdominal pain.

A, Oblique sonogram shows echogenic (solid) mass corresponding to hydatid cyst. Cyst is filled by echogenic material composed of hydatid sand, infolded membranes (arrowheads), and debris.

B, Unenhanced CT scan shows hypodense splenic mass with discontinuous peripheral rim calcification (arrows).

C, Corresponding gross specimen shows that cyst is occupied by membranes, debris, and fibrin. Calcifications are visible in peripheral layer. Infolding membranes leave clefts occupied by aqueous liquid evident on sonography.

Fig. 3.—63-year-old man with splenic hydatid disease.

A, Plain film shows rounded calcified mass in left upper quadrant.

B, Unenhanced CT scan shows large intra-splenic mass with high CT numbers. Peripheral calcification is also seen clearly on CT. Density of mass is similar to that of liver and spleen.

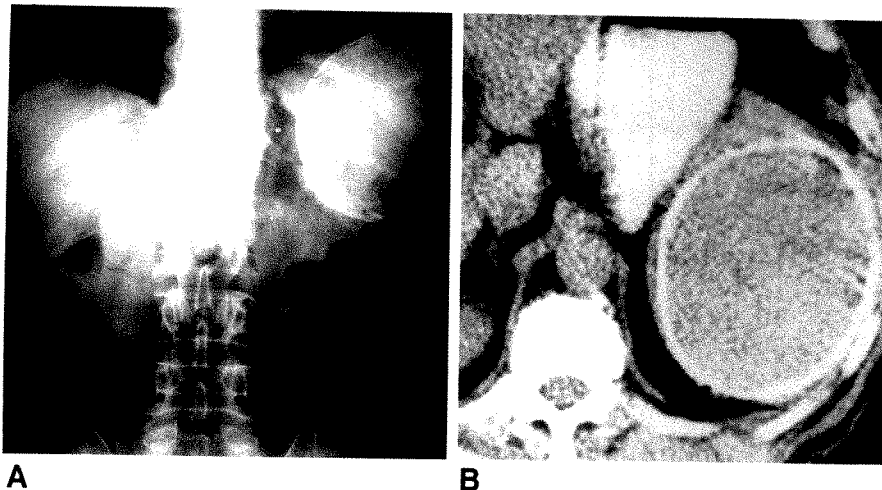
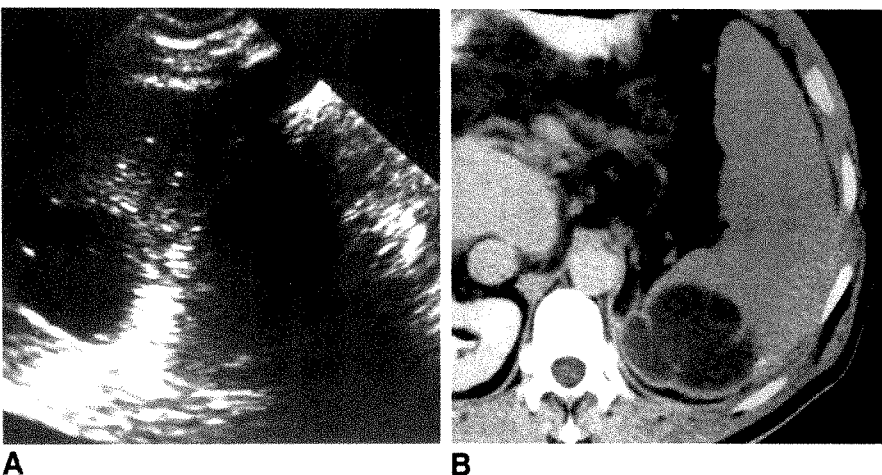


Fig. 4.—Splenic hydatidosis in 57-year-old man with decompensated liver cirrhosis.

A, Longitudinal sonogram of left upper quadrant shows loculated anechoic splenic lesion.

B, Contrast-enhanced CT scan shows multi-loculated hypodense splenic mass, hypertrophied caudate lobe of liver, and ascitic fluid.



surrounding spleen. No lesion enhanced after administration of IV contrast material. Multiple cysts were observed in two patients (Fig. 5). CT provided additional information in three cases: one patient had a small splenic cysts not observed sonographically and another had a calcified hydatid cyst in the liver (Fig. 6); in the third, who had decompensated liver cirrhosis, multiple focal splenic lesions were seen that were highly suggestive of splenic infarcts. In two cases, intraperitoneal hydatid spread was clearly shown on both sonography and CT. The internal cystic content was better delineated by sonography than by CT in one case that showed an echogenic (solid) pattern on sonography.

## Discussion

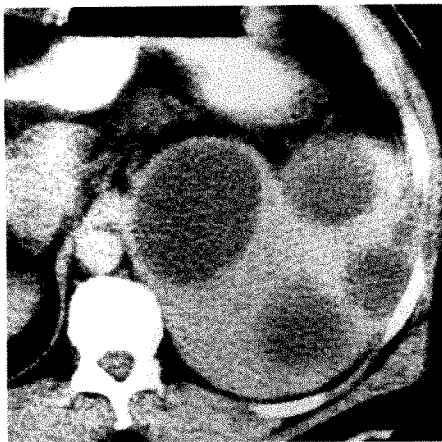
Hydatid disease is caused by the larval form of the genus *Echinococcus*, of which *Echinococcus granulosus* is the most common. The liver and lungs are the most frequently involved organs. Splenic hydatidosis has been found in about 2% of all patients with echinococcosis [1]. Systemic dissemination and intraperitoneal spread from a ruptured liver cyst constitute the two most important sources of splenic infestation.

The clinical manifestations of splenic hydatid disease are nonspecific. Abdominal pain, enlarged spleen, and fever are the most frequently encountered symptoms. However, secondary infection, cyst rupture, and anaphylactic shock may

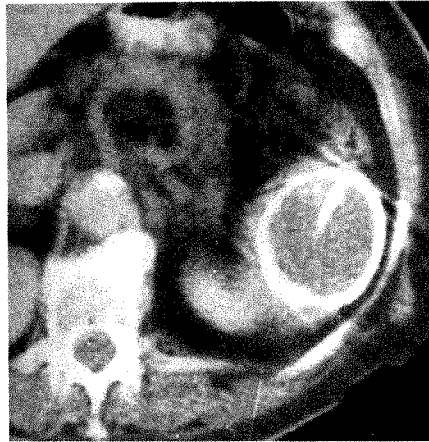
develop [4–6]. Several immunologic tests are highly diagnostic for hydatid disease. The presence of the arc 5 of Capron [7] on immunoelectrophoresis is the most reliable laboratory finding in human hydatidosis [7, 8]. However, in residual or highly calcified hydatidosis, the arc 5 may be absent. False-positive serologic test results have been reported in patients with malignant disease [9].

The radiographic appearance of splenic hydatidosis varies and is influenced mainly by the location of the cyst, age of the cyst, and associated complications, such as secondary infection and rupture [5]. Before the development of cross-sectional imaging, radiographic evaluation of focal splenic lesions was limited to plain abdominal films and isotopic studies. At present, sonography and CT are the most valuable imaging techniques for the diagnosis and evaluation of focal splenic diseases [3]. CT findings of splenic hydatid disease are not specific, although the usefulness of CT in the diagnosis is well established. Our data suggest that CT findings in splenic hydatidosis are similar to those previously described for liver echinococcosis [10–12].

The CT attenuation in hydatidosis depends on the intracystic content. Hydatid cysts usually have a homogeneous fluid content showing water attenuation values on CT. However, hydatid cysts may show high CT values on unenhanced CT scans. The presence of intracystic debris, hydatid sand, and inflammatory cells are presumed to cause the high CT values



5



6

Fig. 5.—Multiple splenic hydatid cysts in asymptomatic 62-year-old man. Unenhanced CT scan shows multiple hypodense lesions corresponding to multiple splenic echinococcal cysts.

Fig. 6.—62-year-old man with residual hepato-splenic hydatidosis. Unenhanced CT scan shows large calcified splenic hydatid cyst.

in these cases [12]. Calcification may occur in the wall of the cyst after the death of the parasite and may be observed on plain abdominal radiographs. However, CT is more sensitive than plain films or sonograms in depicting subtle cyst wall calcification. When there is calcification, it will be shown better on unenhanced CT because IV contrast material may cause the calcification to be masked by the surrounding enhanced splenic parenchyma.

Similarly, the sonographic findings of splenic hydatid cysts are not specific, even if the typical findings of solitary, anechoic lesions are demonstrated. Various sonographic patterns of hydatid cysts have been described [13–17]. In our series, most of the surgically removed splenic cysts were fluid-filled. These pathologic findings support the fact that an anechoic pattern was observed most often. The mixture of infolded membranes, scoleces, and hydatid sand may produce a highly echogenic (solid) pattern on sonography because of the large acoustic impedance differences between the intracystic components. This unusual sonographic pattern was observed in only one case in our series and was demonstrated posteriorly on the corresponding gross specimen.

Recent published reports indicate that MR may be an important imaging technique in the diagnosis and evaluation of hydatid disease [18, 19]. However, we believe that MR should not be used as the first imaging method in the study of patients with proved or suspected hydatid disease.

The main problem in the diagnosis of splenic hydatidosis is in differentiating it from other splenic cystic lesions that have similar appearances on sonography and CT. The differential diagnosis of such lesions includes epidermoid cyst, pseudocyst, large solitary abscess or hematoma, intrasplenic pancreatic pseudocyst, and cystic neoplasm of the spleen [3]. Hydatidosis should be suspected in patients with splenic cystic lesions, particularly in endemic areas. The diagnosis of splenic hydatidosis should be favored if daughter cysts are present within a large cystic lesion or if cystic lesions are observed in other organs such as the liver.

In conclusion, the diagnosis of splenic hydatid disease relies on documentation of the lesion with imaging techniques supported by specific serologic tests. Sonography and CT are the most valuable imaging methods in the evaluation of pa-

tients with clinical, biochemical, or radiologic suspicion for hydatid disease.

#### REFERENCES

1. Bonakdarpour A. Echinococcus disease: report of 112 cases from Iran and a review of 611 cases from the United States. *AJR* 1967;99:660–667
2. Beggs I. The radiology of hydatid disease. *AJR* 1985;145:639–648
3. Dachman AH, Ros PR, Murari PJ, Olmsted WW, Lichtenstein JE. Nonparasitic splenic cysts: a report of 52 cases with radiologic-pathologic correlation. *AJR* 1986;147:537–542
4. Narasimharao KL, Venkateswarlu K, Mitra SK, Metha S. Hydatid disease of the spleen treated by cyst enucleation and splenic salvage. *J Pediatr Surg* 1987;22:138–139
5. Caballero P, Ocon E, Robledo AG, Diaz FJ. Splenic hydatid cysts opening to the colon. *AJR* 1986;147:859–860
6. Varghese C, Balakrishnam V. Hydatid cyst of the spleen—an unusual presentation. *J Assoc Physicians India* 1979;27:1039–1041
7. Capron A, Yarzabal LA, Vernes A, Fruit J. Le diagnostic immunologique de l'échinococcose humaine (bilan personnel a propos de 400 observations). *Pathol Biol (Paris)* 1970;18:357–365
8. Yarzabal LA, Leiton J, Lopez-Lemes H. The diagnosis of human pulmonary hydatidosis by the immunoelectrophoresis test. *Am J Trop Med Hyg* 1974;23:662–666
9. Dar FK, Buhidma MA, Kidwai SA. Hydatid false positive serological test results in malignancy. *Br Med J* 1984;288:1197
10. De Diego JC, Lecumberri FJO, Franquet TC, Ostiz SZ. Computed tomography in hepatic echinococcosis. *AJR* 1982;138:699–702
11. Kalovidouris A, Pissiotis C, Pontifex G, Gouliamos A, Pantea S, Papavasiliou C. CT characterization of multivesicular hydatid cysts. *J Comput Assist Tomogr* 1986;10:428–431
12. Lewall DB, Bailey TM, McCorkell SJ. Echinococcal matrix: computed tomographic, sonographic and pathologic correlation. *J Ultrasound Med* 1987;5:33–35
13. Shulman A, Van Jaarsveld J, Loxton AJ, Grove WH. Pseudosolid appearance of simple and echinococcal cysts in ultrasonography. *S Afr Med J* 1983;63:905–906
14. Niron EA, Ozer H. Ultrasound appearance of hydatid disease. *Br J Radiol* 1981;54:335–338
15. Itzhak Y, Rubinstein Z, Heyman Z, Gerzof S. Role of ultrasound in the diagnosis of abdominal hydatid disease. *JCU* 1980;8:341–345
16. Gharbi HA, Hassine W, Brauner NW, Dupuch K. Ultrasound examination of the hydatid liver. *Radiology* 1981;139:459–463
17. Lewall DB, McCorkell SJ. Hepatic echinococcal cysts: sonographic appearance and classification. *Radiology* 1985;155:773–775
18. Hoff FL, Alsen AM, Walden ME, Glazer GM. MR imaging in hydatid disease of the liver. *Gastrointest Radiol* 1987;12:39–42
19. Lupetin AR, Dash N. Intrahepatic rupture of hydatid cyst: MR findings. *AJR* 1988;151:491–492

## Case Report

# Acute Venous Thrombosis After Pancreas Transplantation: Diagnosis with Duplex Doppler Sonography and Scintigraphy

Ian Boiskin,<sup>1</sup> Martin P. Sandler,<sup>1</sup> Arthur C. Fleischer,<sup>1</sup> and William A. Nylander<sup>2</sup>

The number of pancreas transplantations performed in selected patients with severe diabetes mellitus has increased in recent years. Technical complications after surgery are relatively common and remain a major obstacle to the success of the procedure. According to Hanto and Sutherland [1], acute venous thrombosis is the second most common cause of graft loss and usually occurs in the first week after transplantation. Successful thrombectomy has not been accomplished in any patient; infarction occurs immediately after thrombosis, and the diagnosis is not made early enough to allow revascularization.

Perfusion scintigraphy is a sensitive, albeit nonspecific indicator of abnormal perfusion in the transplanted organ [2]. If the graft is not visualized, arteriography is necessary and is the procedure of choice for further evaluation. The absence of blood flow is thought to signify vascular thrombosis and warrants the removal of the allograft [1].

In a recent case [3] in which duplex Doppler sonography was used in correlation with the radionuclide perfusion study, early diagnosis of allograft renal vein thrombosis was reported. Surgical correction was done immediately, and the transplanted kidney was salvaged.

We describe a case in which, using the same two procedures, we diagnosed an acute venous thrombosis in an allograft pancreas transplant.

## Case Report

A 33-year-old man with severe insulin-dependent diabetes mellitus and recent progressive deterioration in renal function was admitted for pancreas and kidney transplantation. Dialysis had not been started. Onset of diabetes occurred when the patient was 13 years old, and retinopathy and cataracts had developed. Physical examination was unremarkable except for a blood pressure of 210/110 mm Hg and cataracts. Serum creatinine level was 8.0 mg/dl, glucose was 93 mg/dl, amylase was 31 IU/l, and the WBC count was  $4.5 \times 10^3/\mu\text{l}$ .

The patient underwent a whole cadaveric pancreas transplantation and duodenocystostomy. The donor pancreas was placed in the right iliac fossa. The accompanying arterial supply vessels (celiac axis and splenic artery) and venous drainage vessels (splenic and portal veins) were anastomosed to the right common iliac artery and vein, respectively. During the same operation, a cadaveric renal transplantation with ureteroneocystostomy was performed. The donor kidney was placed in the left iliac fossa. No complications developed during surgery.

A few hours postoperatively, an  $^{131}\text{I}$ -orthoiodohippurate ( $^{131}\text{I}$ -Hippuran) renographic study showed normal function in the transplanted kidney. A dynamic radioisotope angiogram with  $^{99\text{m}}\text{Tc}$ -DTPA showed good perfusion to both the kidney and pancreatic transplants (Fig. 1A).

Two days later, the patient's blood pressure increased. Serum glucose levels remained unchanged, and the WBC count was  $7.4 \times 10^3/\mu\text{l}$ . Serum amylase levels, however, increased to 137 IU/l.

Received September 29, 1989; accepted after revision November 6, 1989.

<sup>1</sup> Department of Radiology and Radiological Sciences, Vanderbilt University Medical Center, Nashville, TN 37232-2405. Address reprint requests to M. P. Sandler.

<sup>2</sup> Department of Transplant Surgery, Vanderbilt University Medical Center, Nashville, TN 37232-2405.

AJR 154:529-531, March 1990 0361-803X/90/1543-0529 © American Roentgen Ray Society



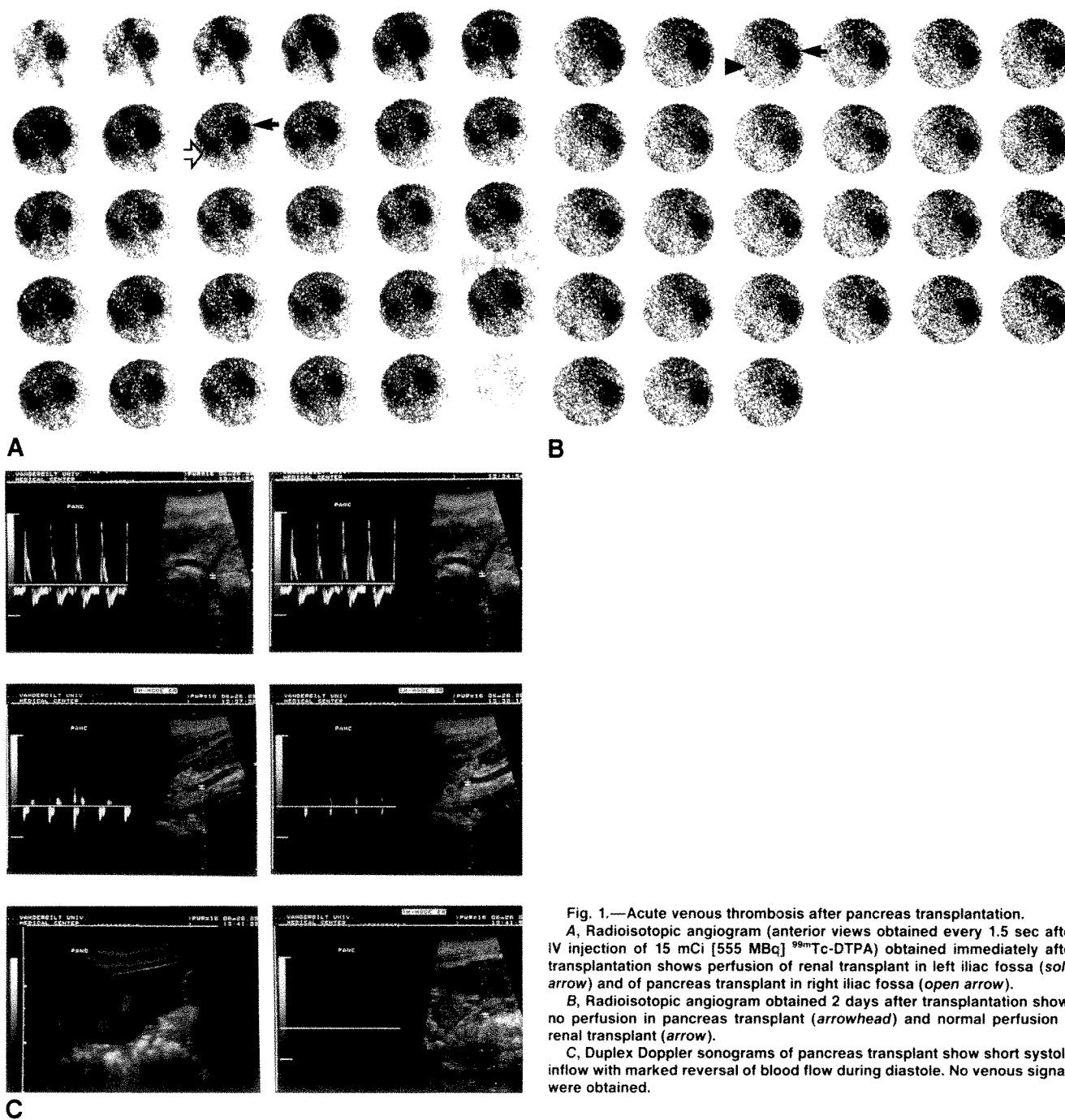


Fig. 1.—Acute venous thrombosis after pancreas transplantation.

A, Radioisotopic angiogram (anterior views) obtained every 1.5 sec after IV injection of 15 mCi [555 MBq]  $^{99m}\text{Tc}$ -DTPA) obtained immediately after transplantation shows perfusion of renal transplant in left iliac fossa (solid arrow) and of pancreas transplant in right iliac fossa (open arrow).

B, Radioisotopic angiogram obtained 2 days after transplantation shows no perfusion in pancreas transplant (arrowhead) and normal perfusion in renal transplant (arrow).

C, Duplex Doppler sonograms of pancreas transplant show short systolic inflow with marked reversal of blood flow during diastole. No venous signals were obtained.

A second  $^{131}\text{I}$ -Hippuran renogram showed normal function in the transplanted kidney. The radioisotope angiogram showed normal perfusion to the kidney transplant. No perfusion to the transplanted pancreas was seen (Fig. 1B).

Duplex Doppler sonographic examination was performed with a 5.0-MHz phased-array transducer (Toshiba 100, Tustin, CA). Doppler arterial flow signals within the main, segmental, and arcuate arteries of the renal transplant were normal. Examination of the pancreas transplant showed flow within the celiac axis and splenic artery. The Doppler waveform of the splenic artery showed short systolic inflow and marked reversal of blood flow during diastole. This was inter-

preted as greatly increased vascular resistance that allowed antegrade flow only. The waveform became progressively more resistive in appearance the closer the examination was to the tail of the pancreas. No venous signals could be obtained from the splenic and portal veins. The right iliac vein and inferior vena cava, however, appeared patent and showed normal flow. The pancreas itself had normal size and morphology (Fig. 1C).

Acute venous thrombosis and obstruction therefore were considered the most likely diagnoses, and the patient underwent emergent surgical exploration. During surgery, the pancreas was found to be discolored and uniformly dark red. Pancreatectomy was performed,

and pathologic examination revealed an acutely infarcted and hemorrhagic organ. Thrombosis was found in the splenic and portal veins.

## Discussion

Approximately 40% of pancreas grafts survive 1 year. Causes of transplant failure include technical surgical problems such as vascular thrombosis and anastomotic leaks, rejection, pancreatitis, and infection [1]. Currently, no definitive test is available for early diagnosis of abnormal function. Alterations in levels of blood glucose and blood and urinary amylase are late, nonspecific markers of pancreas endocrine abnormality [4]. Imaging has an important role in follow-up and can facilitate clinical management by showing vascular complications. A wide variety of techniques have been used, including sonography, CT, and radionuclide scanning [2, 5].

Perfusion scintigraphy is useful for assessing perfusion in the transplanted pancreas.  $^{99m}\text{Tc}$ -DTPA is a convenient radiopharmaceutical because coexisting renal transplants can be imaged simultaneously [6]. The study is a sensitive indicator of normal function. When the results are abnormal, however, it is nonspecific [2]. When the graft cannot be visualized (and thus perfusion is absent), arteriography has been advocated as the next procedure for further evaluation [1]. This is, however, invasive, its specificity has not been determined, and it has the added risk of side effects associated with the use of contrast agents.

Much has been published recently about the use of duplex Doppler sonography in the evaluation of renal allograft arterial flow. Increased vascular impedance that results in decreased diastolic blood flow, and even reversed flow during diastole, most commonly is associated with acute vascular rejection [7]. The findings are not specific. Other conditions, including acute renal vein obstruction, severe acute tubular necrosis, pyelonephritis, and extrarenal compression of the graft, also may be associated with high vascular impedance [3, 8]. The

cause, however, usually can be recognized from the clinical history or other sonographic findings.

Patel et al. [9] have recently shown the measurement of duplex arterial resistive indexes to be highly accurate in the diagnosis of pancreas transplant rejection. The diagnosis of venous thrombosis of the pancreas transplant should be based on the inability to detect venous flow and/or visualization of thrombus within distended splenic or portal veins.

The absence of detectable venous flow on duplex Doppler examination, together with nonvisualization of the pancreas allograft on the radioisotopic angiogram, was thought to indicate acute venous thrombosis in our patient. Although this diagnosis was confirmed surgically, the graft could not be salvaged.

## REFERENCES

1. Hanto DW, Sutherland DER. Pancreas transplantation: clinical considerations. *Radiol Clin North Am* 1987;25:333-343
2. Kuni CC, du Cret RP, Boudneau RJ. Pancreas transplants: evaluation using perfusion scintigraphy. *AJR* 1989;153:57-61
3. Delbeke D, Sacks GA, Sandler MP. Diagnosis of allograft renal vein thrombosis. *Clin Nucl Med* 1989;14:415-420
4. Dafoe DC, Campbell DA, Rocher L, Schwartz R, Turcotte JA. Diagnosis of rejection in simultaneous renal/pancreas (urinary bladder drained) transplantation. *Transplant Proc* 1987;19:2345-2347
5. Patel B, Markivee CR, Mahanta B, Vas W, George E, Garvin P. Pancreas transplantation: scintigraphy, US, and CT. *Radiology* 1988;167:685-687
6. Shulkin BL, Dafoe DC, Wahl RL. Simultaneous pancreas-renal transplant scintigraphy. *AJR* 1986;147:1193-1196
7. Rifkin MD, Needleman L, Pasto ME, et al. Evaluation of renal transplant rejection by duplex Doppler examination: value of the resistive index. *AJR* 1987;148:759-762
8. Warshauer DM, Taylor KJW, Bia MJ, et al. Unusual causes of increased vascular impedance in renal transplants: duplex Doppler evaluation. *Radiology* 1988;169:367-370
9. Patel B, Wolverson MK, Mahanta B. Pancreatic transplant rejection: assessment with duplex US. *Radiology* 1989;173:131-135

## Book Review

**Dysphagia. Diagnosis and Treatment.** Edited by David W. Gelfand and Joel E. Richter. New York: Igaku-Shoin, 382 pp., 1989. \$67.50

Interest in the esophagus is increasing because of the development and acceptance of highly accurate diagnostic procedures and the effectiveness of various treatment strategies. Radiology's contribution is significant and includes the development of double-contrast techniques and videoradiographic studies. This is reflected in the literature and 1988–1989 could be called the year of the esophagus: Two other books, both entitled *Radiology of the Esophagus*, one by Marc S. Levine (Philadelphia: Saunders, 1989) and the other by Dieter N. Hupscher (New York: Thieme, 1988) have been published and have been reviewed recently in the August 1989 issue of *AJR*. *Dysphagia: Diagnosis and Treatment*, however, is different. The two editors, a radiologist and a gastroenterologist, in an attempt to bring "together information from the several principles needed to evaluate and treat patients presenting with swallowing difficulties," produced this handsome multidisciplinary publication written by several authors.

All in all, 20 contributors present in 16 chapters relevant materials from the fields of anatomy, physiology, gastroenterology, radiology and nuclear medicine, surgery, infectious diseases, communication sciences, and biometrics. All contributors appear to be knowledgeable in and authoritative on their fields, and most have made previous significant contributions to the literature.

The book is organized in four parts: "Introduction," "Diagnostic Modalities," "Individual Diseases," and "Conclusion." In the first half, the material is delivered from a technique-oriented approach; in the second half, specific abnormalities are discussed. The introduction contains overviews of the clinical, anatomic, and physiologic complexities of swallowing and dysphagia. The part on diagnostic modalities contains five chapters in which radiography of the oropharyngeal region, radiology of the pharynx and esophagus, esophageal manometry, endoscopy, and radionuclide studies for patients with dysphagia are discussed. It is appropriate for the videoradiographic studies of the oropharyngeal region to be distinguished from the radiographic evaluation of the rest of the pharynx and the esophagus. Aside from an odd sequence in the chapters describing the normal and abnormal videoradiographic findings of oropharyngeal swallowing, the challenge to present a complicated dynamic process (swallowing) is met successfully by providing numerous images and succinct descriptions. Similarly, the chapter on endoscopy, although rather brief in text, is supported with numerous color plates displaying the most common abnormalities.

Individual diseases that produce dysphagia are discussed under

carefully selected topics in the second half of the book. These include esophageal cancer, benign esophageal disease (rings and diverticula, benign tumors, and anatomic vascular conditions that may produce dysphagia), gastroesophageal reflux disease, esophageal motility disorders, infectious esophagitis, and a chapter on miscellaneous traumatic and inflammatory causes of dysphagia (caustic ingestion, foreign bodies in adults and children, pill-induced esophageal injury, radiation, Crohn disease, and skin diseases). The section ends with an informative chapter on surgical therapies for dysphagia. Finally, the volume concludes with a chapter entitled "Multidisciplinary Approach," which unfortunately falls a little short of bringing it all together.

The publication is of high quality, heavily illustrated and well referenced. The book has 373 pages of text with 1017 references, distributed at the end of each chapter, and 192 well-reproduced figures, many with more than one illustration, all with appropriate and useful legends. The book also has 45 well-planned tables. The table of contents is rather scanty, but the index is extensive (nine pages).

*Dysphagia: Diagnosis and Treatment* is a useful volume that, under a catchy title, contains a wealth of information from various disciplines. Unfortunately, in order to fit it all in fewer than 400 short pages, the depth of the presentations is limited. In addition, little, if any, mention is made of CT, MR, endoscopic sonography, and video endoscopy, and a description of the treatment strategies of oropharyngeal swallowing abnormalities is lacking. The multiplicity of the authors and topics and the use of both technique- and abnormality-oriented approaches inherently fragment the information and lead to repetition. Finally, the continuity of the text is based on the selection of topics rather than the context of the subjects, which results in a course-proceedings-like publication. Nonetheless, the breadth of the subjects discussed under one roof makes it a unique publication. The specialists who deal with one aspect of dysphagia will find useful information here from the other experts, and the rest of us who occasionally encounter a patient with dysphagia now have an excellent reference.

Vassilios Raptopoulos  
Jay M. Colby

University of Massachusetts Medical Center  
Worcester, MA 01655

## Technical Note

# Treatment of Acute Esophageal Food Impaction with a Combination of Glucagon, Effervescent Agent, and Water

Donna J. Kaszar-Seibert,<sup>1</sup> William T. Korn, David J. Bindman, and Michael J. Shortsleeve

Esophageal food impaction is a common clinical problem. Various methods of treatment have been described, including the use of glucagon and effervescent agents, either alone or in combination, with various degrees of success [1-8]. Physicians have been reluctant to use the glucagon and effervescent agents since Smith et al. [7] reported a case in which an esophageal perforation occurred after the procedure. We studied the value of combination therapy that uses glucagon, an effervescent agent, and water in the treatment of acute esophageal food impaction in 16 cases. Our results indicate that it is an efficient, safe, and cost-effective form of therapy.

### Subjects and Methods

Between July 1987 and June 1989, 14 patients with 16 episodes of acute ( $\leq 24$  hr) food impaction involving the distal two thirds of the esophagus were examined prospectively with a barium swallow. Subsequently, attempts were made to relieve the obstruction by using a combination of IV glucagon, an effervescent agent (E-Z gas, a product of E-Z-EM), and water. The study included three women and 11 men. Two patients were evaluated and treated on two separate occasions. The patients ranged in age from 25 to 75 years (mean age, 49 years). Meat was the cause of obstruction in 11 episodes, and fruit or vegetable was the cause in five episodes. The mean duration of esophageal obstruction before treatment was 9 hr. Patients were excluded from the study if they had a known (1) sharp foreign body (e.g., plastic eating utensil), (2) rigid fixed obstruction (e.g., esophageal carcinoma or a fixed stricture), (3) esophageal diverticulum, (4) prominent cricopharyngeus muscle, (5) obstruction of greater than 24 hr duration, or (6) obstruction in the proximal third of the esophagus.

The initial examination was performed by giving the patient approximately 5 ml of undiluted barium (E-Z JUG, a product of E-Z-EM) to document fluoroscopically the presence, nature, and location of the foreign body (Fig. 1A). The patient was then placed supine, and 1.0 mg of glucagon was given IV. Immediately afterward, the patient was placed upright and given one packet of E-Z gas in 30 ml of water followed by one cup (240 ml) of water. The E-Z gas consists of sodium bicarbonate, citric acid, and simethicone and will produce not less than 400 ml of CO<sub>2</sub> when added to 30 ml of water. Immediate symptomatic relief was experienced by all in whom the treatment was successful. A second barium esophagogram was obtained to determine if the foreign body had passed. A follow-up barium swallow or endoscopy revealed a lower esophageal ring (Fig. 1B) as the single most common abnormality (60%). The cost of the treatment was \$210, which included the cost of the barium esophagogram, glucagon, and the emergency department fee.

### Results

The administration of the combination of glucagon, E-Z gas, and water resulted in the clearance of food obstruction in 12 of 16 attempts. Patients with lower esophageal rings greater than 15 mm were more likely to respond to treatment. The patients tolerated the procedure well, and no complications occurred. Aspiration, a potential risk, did not occur in any patient.

### Discussion

Impaction of a foreign body in the esophagus is a common clinical problem. Esophagoscopy is often used but is relatively

Received September 19, 1989; accepted after revision November 14, 1989.

<sup>1</sup> All authors: Department of Radiology, Mount Auburn Hospital, Cambridge, MA 02238. Address reprint requests to M. J. Shortsleeve.

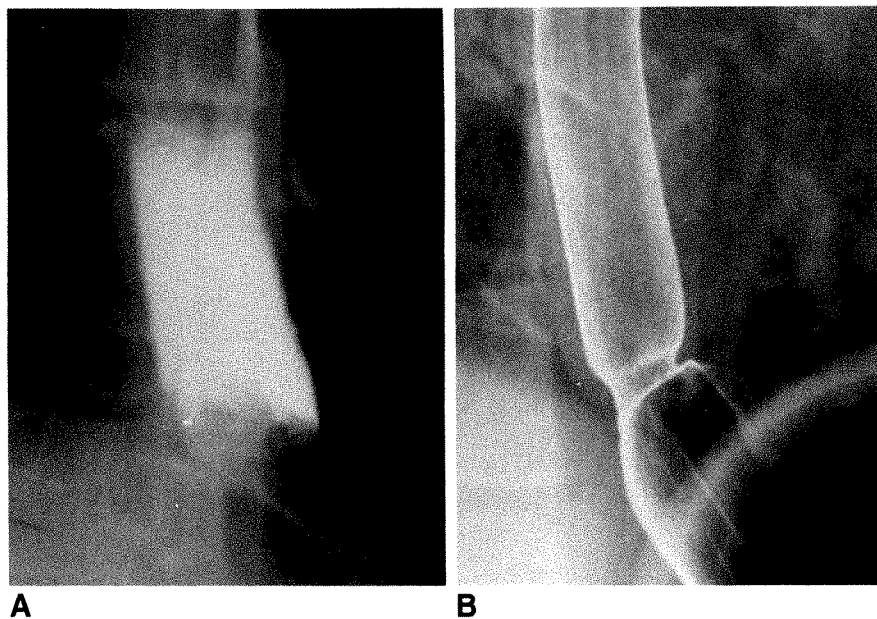


Fig. 1.—A, Pretreatment radiograph shows distal esophageal food impaction causing obstruction in a 46-year-old man who had been eating chicken.

B, Radiograph from follow-up barium esophagogram shows underlying cause of food impaction. A lower esophageal 18-mm ring is now apparent.

expensive, uses invasive equipment, and may require operating room facilities and anesthesia. In addition, perforation can occur. Proteolytic digestion with papain has been successful but can be dangerous, with deaths reported due to perforation and mediastinitis [3, 6]. Glucagon was used to eliminate the impaction in three of six cases reported by Ferrucci and Long [6] and in seven of 19 cases reported by Trenkner et al. [1]. Gas distention of the esophagus led to clearance of the impaction of all eight cases treated by Rice et al. [3]. Zalev [8] reported one case in which he successfully used air insufflation via a nasoesophageal tube coupled with esophageal hypotonia to relieve obstruction.

We reasoned that the combination of glucagon, an effervescent agent, and water would enhance the efficacy of using any one agent alone. Combination therapy capitalizes on (1) the ability of glucagon to decrease lower esophageal tone [4], (2) the capability of the effervescent agent to distend the esophagus, (3) the increased hydrostatic pressure caused by the water, in conjunction with (4) the use of gravity in the upright patient. Smith et al. [7] used glucagon and an effervescent agent with success in three of five cases, but an esophageal perforation occurred in one case. In that case, however, it was not clear if the perforation was a result of the radiologic procedure or of subsequent endoscopy.

In our series, combination therapy relieved the esophageal obstruction in 12 of 16 cases, with immediate symptomatic relief and without complications. The combination therapy was also more cost-effective than esophagoscopy. At our hospital, the cost of radiologic intervention was \$210 (as discussed above), compared with \$2233 when a rigid endoscope was used (includes initial emergency department fee, room charge, pharmacy and medical/surgical supplies, preoperative electrocardiogram, operating room cost, anesthesia, recovery room fee, and barium esophagram) or \$638 when flexible esophagoscopy was used (includes procedure

fee, pharmacy and medical/surgical supplies, electrocardiogram, barium esophagogram, and postprocedure chest radiograph). All costs were calculated from hospital billing records, which did not include physicians' fees. Combination therapy also may benefit patients who would be at high risk for complications with the use of anesthesia or other types of sedation.

Combination therapy is an efficient, safe, and cost-effective form of therapy. However, we advise careful selection of patients to avoid situations that might (1) predispose to esophageal perforation (e.g., presence of esophageal diverticulum, sharp foreign body, or possible mucosal ulceration due to obstruction of greater than 24 hr duration), (2) fail to respond to glucagon (e.g., obstruction in proximal third of esophagus, presence of esophageal carcinoma or fixed stricture), or (3) impede the release of excess gas (e.g., prominent cricopharyngeus muscle).

#### REFERENCES

1. Trenkner SW, Maglinte DDT, Lehman GA, Chernish SM, Miller RE, Johnson CW. Esophageal food impaction: treatment with glucagon. *Radiology* 1983;149:401-403
2. Giordano A, Adams G, Boies L, Meyerhoff W. Current management of esophageal foreign bodies. *Arch Otolaryngol* 1981;107:249-251
3. Rice BT, Spiegel PK, Dombrowski PJ. Acute esophageal food impaction treated by gas-forming agents. *Radiology* 1983;146:299-301
4. Handal KA, Riordan W, Siese J. The lower esophagus and glucagon. *Ann Emerg Med* 1980;9:577-579
5. Friedland GW. The treatment of acute esophageal food impaction. *Radiology* 1983;149:601-602
6. Ferrucci JT, Long JA. Radiologic treatment of esophageal food impaction using intravenous glucagon. *Radiology* 1977;125:25-28
7. Smith JC, Janower ML, Geiger AH. Use of glucagon and gas-forming agents in acute esophageal food impaction (letter). *Radiology* 1986;159:567-568
8. Zalev AH. Radiologic treatment of a patient with the "steakhouse syndrome": case report. *J Can Assoc Radiol* 1988;39:59-61



# Prevalence and Significance of Subchorionic Hemorrhage in Threatened Abortion: A Sonographic Study

Jan Fog Pedersen<sup>1</sup>  
Margit Manton<sup>1, 2</sup>

We performed a prospective study to determine the prevalence and significance of subchorionic hematomas in patients with symptoms of threatened abortion. The study comprised 342 pregnant women who had vaginal bleeding in weeks 9–20 of pregnancy and a live fetus shown with sonography. Sonograms showed a subchorionic hematoma in 62 patients (18%). The average size of the hematoma was 20 ml (range, 2–150 ml). The rate of spontaneous abortion was the same in patients with and without hematoma, seven (11%) of 62 and 28 (10%) of 280, respectively. There was no association between abortion rate and hematoma size. The rate of premature delivery was the same in patients with and without hematoma, seven (11%) of 62 and 32 (11%) of 280, respectively. There was no association between the rate of premature delivery and hematoma size.

Subchorionic hematomas are common and insignificant sonographic findings in patients with vaginal bleeding in weeks 9–20 of pregnancy.

*AJR* 154:535–537, March 1990

Several sonographic studies have shown that a subchorionic hematoma may be seen in patients who have vaginal bleeding during the first half of pregnancy [1–9]. It appears on sonograms as an echo-free or echo-poor intrauterine area outside the membranes, usually elevating part of the placental border from the uterine wall. The hemorrhage may be seen as early as week 9 [2, 9]. Little is known about the frequency of subchorionic hemorrhage, and the reported risk of spontaneous abortion varies considerably [1–9].

In a prospective study, we determined the prevalence and prognostic significance of subchorionic hematoma in women with bleeding in weeks 9–20 of pregnancy and a live fetus shown with sonography.

## Subjects and Methods

Between 1980 and 1987, 358 patients who had vaginal bleeding during the first half of pregnancy were shown to have a live fetus 9–20 weeks of age by using sonography. Nine patients elected to have an abortion; seven patients were lost to follow-up. The remaining 342 patients are included in this study.

The volume of the subchorionic hematoma was calculated by using the formula length  $\times$  width  $\times$  thickness  $\times$  0.5. Patients seen during the first 2 years of the study period were treated with bed rest. Thereafter, no treatment was recommended, but the patients were followed on an outpatient basis. Repeat sonograms were obtained at weekly or biweekly intervals until the hematoma resolved. At each visit, patients were asked if they had had vaginal bleeding. Hematomas smaller than 2 ml were not included in this study.

Gestational age was expressed in completed weeks and was based on sonographic estimation of age (crown–rump length or biparietal diameter) rather than calculated from the last menstrual period. Sonographic examinations in the first 52 months of the study were performed with a static scanner (SonoDIAGNOST B, Philips Industries, Eindhoven, the Netherlands) in combination with a dynamic scanner (SAL 20, Toshiba Medical Systems

Received August 9, 1989; accepted after revision October 12, 1989.

<sup>1</sup> Department of Radiology, Glostrup Hospital, University of Copenhagen, DK-2600 Glostrup, Denmark.

<sup>2</sup> Present address: Department of Radiology, Rigshospitalet, DK-2100 Copenhagen O, Denmark.

0361–803X/90/1543–0535

© American Roentgen Ray Society

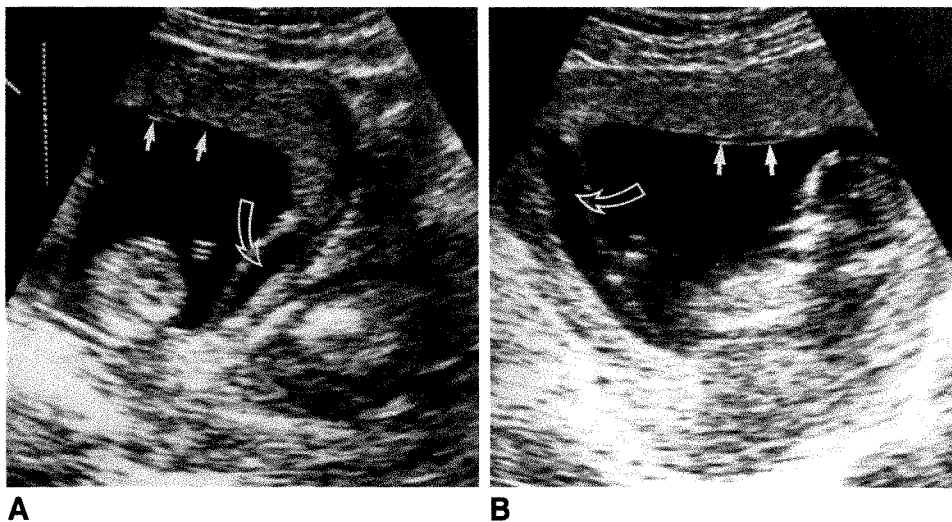


Fig. 1.—A and B, Transverse (A) and longitudinal (B) sonograms at 13 menstrual weeks show membranes and border of placenta to be lifted from uterine wall by subchorionic hemorrhage (open arrows) (estimated volume, 10 ml). Note amniotic membrane over fetal surface of placenta (solid arrows). Pregnancy was successful.

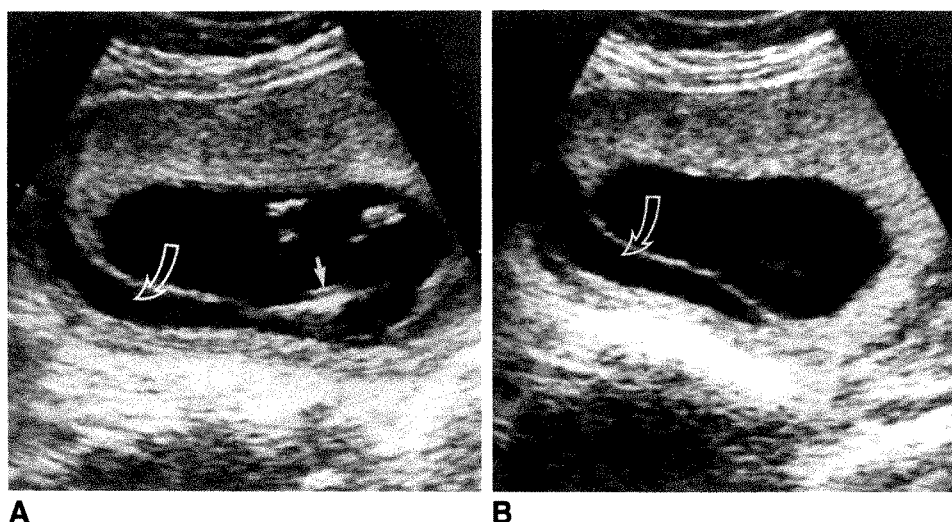


Fig. 2.—A and B, Transverse (A) and longitudinal (B) sonograms at 14 menstrual weeks show subchorionic hemorrhage (open arrows) (estimated volume, 50 ml) elevating membranes and border of placenta. Note short segment of amniotic membrane (solid arrow). Pregnancy was successful.

TABLE 1: Prevalences and Estimated Sizes of Subchorionic Hematomas at Admission in Women with Vaginal Bleeding and Living Fetuses

Gestational Age (wk)	No. of Patients	No. with Hematomas (%)	Mean Volume in ml (range)
9–11	129	22 (17)	9 (2–36)
12–14	123	23 (19)	21 (2–70)
15–20	90	17 (19)	32 (4–150)
Total	342	62 (18)	20 (2–150)

Europe, Den Haag, the Netherlands) and thereafter with a dynamic scanner with a convex-array probe (LSC 7000, Picker International GmbH, München, FRG).

## Results

A subchorionic hematoma (Figs. 1 and 2) was revealed at admission in 62 of 342 patients who had symptoms of threatened abortion in weeks 9–20 (Table 1). This is a prevalence

of 18%. The mean size of the hematomas increased in proportion to gestational age (Table 1). The mean size was 20 ml (range, 2–150 ml). Some of the hematomas showed an initial increase in size during the first weeks of observation, but apart from that the hematomas gradually diminished while the patient experienced intermittent painless vaginal bleeding. By week 24 all hematomas had disappeared.

The overall spontaneous abortion rate was 10%, and the overall rate of premature delivery (delivery at or before day 252) was 11%. Presence of a subchorionic hematoma did not alter these rates. There was no association between the size of the hematoma and the outcome of pregnancy; the mean size of the hematomas was 15 ml (range, 7–50 ml) in seven patients who had a spontaneous abortion and 25 ml (range, 4–70 ml) in seven patients who had a premature delivery.

## Discussion

In our series, 62 of 342 women with vaginal bleeding in weeks 9–20 of pregnancy had a subchorionic hematoma.

Goldstein et al. [2] reported subchorionic hematomas in 10 (20%) of 50 patients between 9 and 16 weeks of gestation with threatened abortion. Stabile et al. [9] found 22 cases (9%) of subchorionic hematoma among 259 patients who had bleeding during the first half of pregnancy. This percentage is unrealistically low, because some of the pregnancies were less than 9 weeks gestation, when a hematoma is not to be expected. These rates thus conform to the 18% hematoma rate found in our study and confirm that subchorionic hemorrhage is a frequent phenomenon in patients with threatened abortion.

The overall spontaneous abortion rate (10%) and premature delivery rate (11%) in patients in our study are similar to those reported by others in patients with threatened abortion and a live fetus [10, 11].

The presence of a subchorionic hematoma did not alter the rate of spontaneous abortion. Other authors have found abortion rates of two of 10 [2], six of 33 [4], three of 29 [6], seven of 16 [7], and none of 22 [9] in patients who had subchorionic hematomas before week 20. This wide variation in abortion rates from 0% [9] to 44% [7] probably is explained in part by the rather small number of patients studied, and in part by different patient populations. Whereas most of these series presumably had an overrepresentation of high-risk pregnancies, as our preliminary report [1] had, the studies by Stabile et al. [9] and our current study include unselected patients with threatened abortion. This may explain why the combined spontaneous abortion rate in these five studies (18 of 110 or 16%) is slightly higher than that found in the present study.

The presence of a subchorionic hematoma did not increase the rate of premature delivery. In other studies, premature delivery rates of none of 10 [2], three of 33 [4], seven of 29 [6], and three of 16 [7] were observed in patients who had

subchorionic hematomas before week 20. Again, the variations in the rates may be due to the small number of patients and to different patient populations. The combined premature delivery rate in these four studies (13 of 88 or 15%) is slightly higher than that in our present study.

## REFERENCES

1. Mantoni M, Pedersen JF. Intrauterine hematoma: an ultrasound study of threatened abortion. *Br J Obstet Gynaecol* 1981;88:47-51
2. Goldstein SR, Subramanyam BR, Raghavendra BN, Horii SC, Hilton S. Subchorionic bleeding in threatened abortion: sonographic findings and significance. *AJR* 1983;141:975-978
3. Ylöstalo P, Ämmälä P, Seppälä M. Intrauterine haematoma and placental protein 5 in patients with uterine bleeding during pregnancy. *Br J Obstet Gynaecol* 1984;91:353-356
4. Jouppila P. Clinical consequences after ultrasonic diagnosis of intrauterine hematoma in threatened abortion. *JCU* 1985;13:107-111
5. Kaufman AJ, Fleischer AC, Thieme GA, Shah DM, James AE. Separated chorioamion and elevated chorion: sonographic features and clinical significance. *J Ultrasound Med* 1985;4:119-125
6. Sauerbrei EE, Pham DH. Placental abruption and subchorionic hemorrhage in the first half of pregnancy: US appearance and clinical outcome. *Radiology* 1986;160:109-112
7. Abu-Yousef MM, Bleicher JJ, Williamson RA, Weiner CP. Subchorionic hemorrhage: sonographic diagnosis and clinical significance. *AJR* 1987;149:737-740
8. Nyberg DA, Mack LA, Benedetti TJ, Cyr DR, Shuman WP. Placental abruption and placental hemorrhage: correlation of sonographic findings with fetal outcome. *Radiology* 1987;164:357-361
9. Stabile I, Campbell S, Grudzinskas JG. Threatened miscarriage and intrauterine hematomas: sonographic and biochemical studies. *J Ultrasound Med* 1989;8:289-292
10. Jouppila P. Clinical and ultrasonic aspects in the diagnosis and follow-up of patients with early pregnancy failure. *Acta Obstet Gynecol Scand* 1980;59:405-409
11. Mantoni M. Ultrasound signs in threatened abortion and their prognostic significance. *Obstet Gynecol* 1985;65:471-475



The Radiology Outreach Foundation (ROF) is a nonprofit corporation whose goal is to help disadvantaged countries improve their health care by providing radiology equipment, books, consultation, education, and training to their practitioners. This assistance is on an application basis that is independent of political, ethnic, or religious orientation of the grantee. It depends on the need of the people and the ability of the ROF to meet that need. The ROF is approved by the U.S. Internal Revenue Service as a tax-exempt organization. It is endorsed by the following radiologic societies:

American Association of Women Radiologists  
 American College of Radiology  
 American Roentgen Ray Society  
 Association of University Radiologists  
 Radiological Society of North America  
 Society of Chairmen of Academic Radiology Departments  
 Society for Pediatric Radiology  
 European Society of Pediatric Radiology

All donations to the ROF are tax deductible. Persons who would like to contribute financially to the ROF, would be interested in being a visiting professor, would like to send books or journals to any of the institutions supported by the ROF, or would like further information about the ROF should write to

Charles A. Gooding, M.D.  
 President  
 Radiology Outreach Foundation  
 3415 Sacramento St.  
 San Francisco, CA 94118 USA

# Differentiation of Seminomatous from Nonseminomatous Testicular Tumors with MR Imaging

John O. Johnson<sup>1</sup>  
Robert F. Mattrey<sup>1,2</sup>  
Julia Phillipson<sup>3</sup>

Distinguishing seminomatous from nonseminomatous testicular neoplasms preoperatively is useful because treatment of these two tumor types is different. We evaluated whether the distinction could be made with MR imaging in six patients with seminomatous and nine patients with nonseminomatous testicular tumors (including teratoma, teratocarcinoma, embryonal cell, and choriocarcinoma). The MR diagnoses, which were obtained from the formal reports of the MR studies done and interpreted before orchiectomy, were compared with the pathologic diagnosis. The distinction between the two tumor types on MR images was based on the signal intensity and heterogeneity of the lesion. We also retrospectively compared the MR findings with tissue histology. MR scans in nonseminomatous tumors showed a marked heterogeneous mix of signals, with some regions less intense and others more intense than normal testicular tissue on both proton-density and T2-weighted images. The typical background signal was nearly equal to normal testicular tissue. The tumors also had a dark band at their periphery that correlated with a fibrous tumor capsule on histologic examination. In contradistinction, seminomatous tumors were isointense with testis on proton-density images and consistently hypointense and relatively homogeneous on T2-weighted images. These tumors typically lacked a capsule on MR images. One lesion, only 3 mm in diameter, could not be characterized on MR images because of limitations in spatial and contrast resolution. In 13 of the 14 lesions that could be characterized, the histologic type was predicted correctly on the basis of the MR appearance. The one error occurred in a patient with pure seminoma. Although the MR appearance of the lesion was otherwise similar to the other seminomas, the lesion had a single focus of bright signal that was due to hemorrhage. This focus was interpreted incorrectly as a nonseminomatous element.

Our findings in this small series of patients suggest that MR imaging can be used to distinguish seminomatous from nonseminomatous testicular tumors.

*AJR* 154:539-543, March 1990

Received July 20, 1989; accepted after revision November 1, 1989.

This work was supported in part by Research Career Development Award NCI-K08-CA01319 to R. F. Mattrey.

<sup>1</sup> Department of Radiology, University of California, San Diego, Medical Center, 410 W. Dickinson St., San Diego, CA 92103.

<sup>2</sup> UCSD/AMI Magnetic Resonance Institute, 410 W. Dickinson St., San Diego, CA 92103. Address reprint requests to R. F. Mattrey.

<sup>3</sup> Department of Pathology, University of California, San Diego, Medical Center, 410 W. Dickinson St., San Diego, CA 92103.

0361-803X/90/1543-0539  
© American Roentgen Ray Society

Recently, MR imaging has emerged as an alternative imaging technique for the diagnosis of scrotal disease [1-5]. MR imaging has been shown to be more sensitive than sonography for the detection of inflammatory [2] and neoplastic [5] conditions of the testicles. The exquisite anatomic detail afforded by MR imaging together with a wide field of view displaying both testicles and inguinal regions on the same image should increase specificity [2, 5], although the exact specificity of the technique has not been defined.

The present study was undertaken to determine if MR imaging can be used to distinguish between the seminomatous and nonseminomatous varieties of testicular tumors, the two tumor types that account for nearly 90-95% of all testicular neoplasms [6].

## Materials and Methods

Fifteen patients with germ cell testicular tumors, six seminomatous and nine nonseminomatous, were imaged at our institution and included in this study. Their ages ranged from 23



to 66 years (mean, 35 years). MR imaging of the scrotum was done in all patients before orchiectomy. The pathology report was used as the basis for the final diagnosis in all 15 patients. The histologic slides of five patients with seminoma and eight with nonseminomatous tumors were reviewed in retrospect and the histology was correlated with the MR findings. The histologic slides of the other two patients could not be located for review.

The MR imaging technique used has been described [1]. A 1.5-T Signa system (GE, Milwaukee, WI) was used. A 12.5-cm, circular, general-purpose surface coil was placed horizontally over the scrotum. Spin-echo pulsing sequence with a TR of 600 msec and TE of 20 msec was performed in the sagittal plane for localization and characterization with a 20-cm field of view. Subsequently, a multiecho sequence with TR of 2000 msec and TE of 20 and 70 msec was performed. By using a  $256 \times 256$  data acquisition matrix, a 16-cm field of view, and two excitations, serial 3-mm coronal images were obtained with 1.5-mm interslice gap. The total scanning time, including positioning of the patient and prescanning calibration for both sequences, was approximately 30 min. The last two patients were studied with the identical protocol except that the matrix was reduced to  $256 \times 192$ , which decreased scanning time by 4 min without degrading diagnostic quality. In one patient, the 7.6-cm surface coil was used in error, which led to rapid degradation of signals and suboptimal signal-to-noise ratio in the far field.

Whether the testicular lesion was a seminomatous or a nonseminomatous tumor was extracted from reports dictated at the time of the MR study. The studies were interpreted by a single reviewer who had access to the clinical data. Given the homogeneous histologic appearance of seminomatous tumors and the heterogeneous histologic mix of nonseminomatous tumors and the tendency of the latter to hemorrhage and necrose, it was hypothesized that the MR signals of these two tumor types should reflect their histologic differences. That is, seminomatous lesions should be homogeneous and nonseminomatous lesions should be heterogeneous in signal. At the time of the review, attention was given to signal-intensity differences between the lesion and the surrounding normal testicular tissue on all sequences, heterogeneity of the signal within the lesion, encapsulation of the lesion, hydrocele formation, and spermatic cord appearance and vascularity. One 3-mm nonseminomatous lesion could not be characterized by MR imaging because of limitations in spatial and contrast resolution.

The images were reviewed postoperatively in conjunction with the pathologic findings to identify other potential differentiating features.

## Results

The correct histologic diagnosis was made on the basis of the MR findings in 13 of the 15 patients. The only interpretive error was made in the patient studied with the 7.6-cm surface coil. This patient, with a pure seminoma on histologic analysis, had a single focus of hemorrhage which had a higher signal than the rest of the lesion on the MR scan. This focus of high signal led to the incorrect interpretation that the tumor, although having the appearance of a seminomatous lesion, had an island of nonseminomatous tissue within it, changing its classification to a nonseminomatous tumor. In another patient in whom the lesion was 3 mm in diameter, the tumor was too small for specific diagnosis with MR. Therefore, of the 14 lesions that could be characterized, one error was made.

An obvious difference between the signal characteristics of seminomatous and nonseminomatous tumors was shown. On proton-density images (2000/20), seminomatous tumors were uniformly equal to or lower in signal intensity than normal testicular tissue. This relationship was accentuated on T2-weighted images as normal testicular tissue increased in signal intensity and tumor remained dark and relatively homogeneous (Figs. 1 and 2). Occasionally, islands of well-defined darker signal intensity were encountered that are presumably regions of dense fibrous stroma.

Conversely, nonseminomatous lesions showed marked heterogeneity with areas of increased and decreased signal intensity on proton-density images that increased in contrast on T2-weighted images (Figs. 3 and 4). These areas pathologically corresponded to tumor hemorrhage and necrosis. The background signal of these lesions was nearly equal to that of normal testicular tissue in seven of the nine cases and darker in two. One of the darker lesions was the 3-mm tumor, which was hemorrhagic on pathologic examination; the other was a 2-cm teratocarcinoma. The latter was distinguished from seminoma because of its heterogeneity on proton-density and T2-weighted images (Fig. 5).

In all patients, regardless of histology, MR imaging showed the presence of a rim of normal testicular tissue, regardless

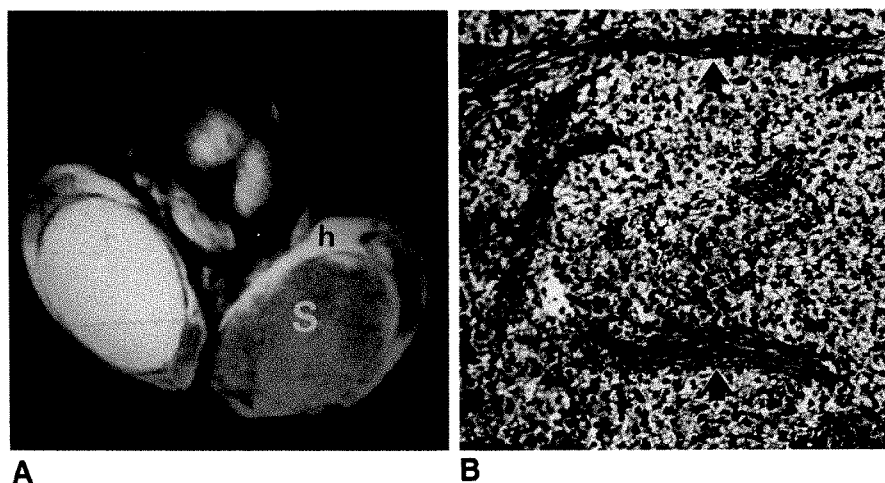


Fig. 1.—Left testicular seminoma (S).

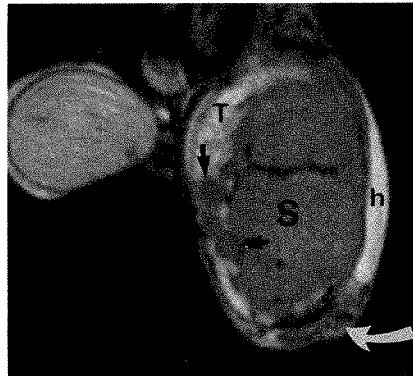
A, T2-weighted MR image, 2000/70. Note that tumor is significantly darker than normal contralateral testis. Also note well-margined small rim of normal testicular tissue near upper pole of testis (arrows) and small ipsilateral hydrocele (h).

B, Histologic section ( $\times 200$ ) shows homogeneous tumor disrupted by short fibrous bands (arrows).

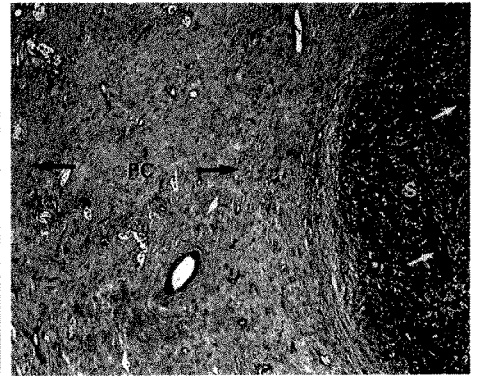
Fig. 2.—Left testicular seminoma (S).

A, T2-weighted MR image, 2000/70. Note that tumor is significantly darker than normal contralateral testis. Well-margined rim of normal testicular tissue (T) along medial surface, multiple nodules seen adjacent to lesion (black arrows), small ipsilateral hydrocele (h), and linear pieces of dark signal are seen surrounding tumor, proved histologically to be a fibrous capsule that was incompletely surrounding tumor. Irregular signal seen outside testis near lower pole did not prove to be tumor as was suspected from MR imaging (white arrow).

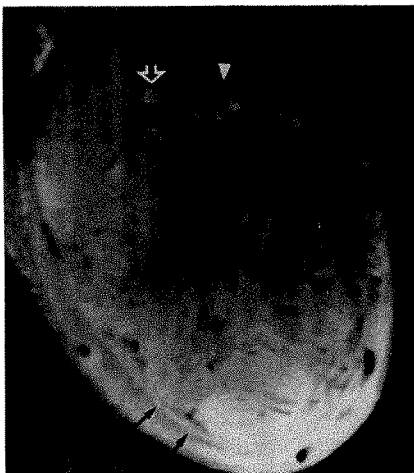
B, Histologic section ( $\times 80$ ) shows homogeneous tumor disrupted by short fibrous bands (white arrows) and separated from normal testis (not shown) by a thick fibrous capsule (FC, black arrows).



A



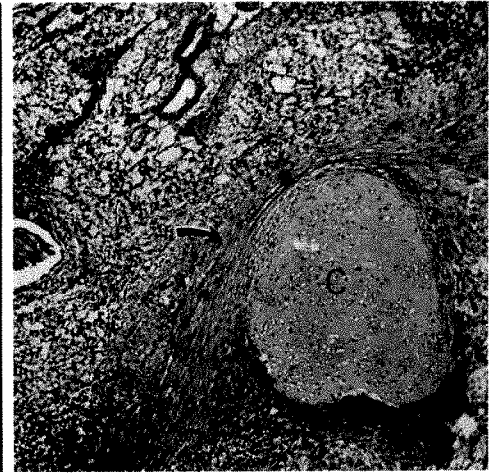
B



A



B



C

Fig. 3.—Embryonal cell with teratomatous elements (nonseminomatous).

A, Coronal proton-density MR image, 2000/20, shows a large ( $7 \times 10$  cm) tumor with heterogeneous signal.

B, T2-weighted MR image, 2000/70, second echo of A, shows a markedly heterogeneous mass with regions of high signal on proton-density image (A) that remain high on T2-weighted image (B, open arrow). Also note areas of intermediate signal on hydrogen-density image (A) that become darker on T2-weighted image (B, arrowhead). These proved to be areas of hemorrhage characteristic of this tumor type. Even with this very large lesion, a rim of normal testicular tissue is still seen (solid arrows) separated from tumor by a thick fibrous tumor capsule that was proved histologically. Note hypervascularity observed along scrotal wall and cord presumably due to the significant tumor burden.

C, Histologic section ( $\times 80$ ) shows heterogeneous tumor containing islands of cartilage (C), fibrous reaction (arrow), and a heterogeneous tumor structure.



A



B

Fig. 4.—Multinodular embryonal cell carcinoma of left testis.

A, Proton-density MR image, 2000/20, shows heterogeneous signals.

B, T2-weighted MR image, 2000/70, second echo of A, shows further increase in signal heterogeneity compared with normal testicular tissue of ipsilateral and contralateral testes.

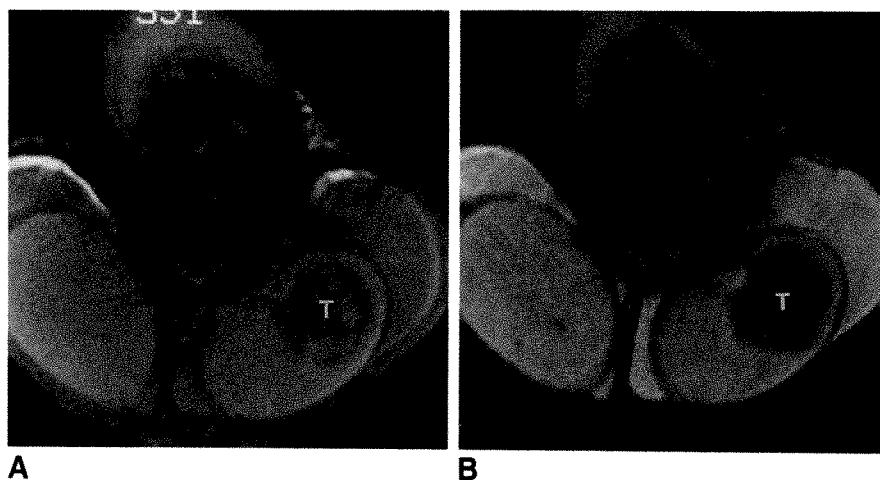


Fig. 5.—Teratocarcinoma (T) of left testis. A, Proton-density MR image, 2000/20, shows heterogeneous signals. B, T2-weighted image, 2000/70, second echo of A, shows further increase in signal heterogeneity compared with normal testicular tissue of ipsilateral and contralateral testes. Although this lesion is predominantly darker than testis on T2-weighted image (B), note that unlike seminomatous lesions, this lesion is darker than testis on proton-density image (A) and heterogeneous on T2-weighted image (B). Note bilateral hydrocele.

of tumor size, which was confirmed pathologically. All lesions had a relatively well-defined margin with the remaining normal testicular tissue. All but two nonseminomatous lesions had a band of dark signal at their perimeter on MR images that on histologic examination was found to be a fibrous tumor capsule. One of the two lesions without a capsule on MR imaging was the 3-mm focus that had a capsule on histology that could not be resolved on MR scans. The histologic slides of the other patient could not be located to ascertain whether the fibrous capsule was absent or whether it could not be resolved from the dark signal of the lesion (Fig. 5). Conversely, only two seminomatous tumors had a dark band at their periphery. One was interrupted and was found to be a fibrous capsule on histologic review. The other completely surrounded the lesion; however, the histologic slide could not be located to confirm the presence of a tumor capsule.

An ipsilateral hydrocele was present in five patients, three with nonseminomatous and two with seminomatous tumors. Only one patient with a very large nonseminomatous lesion had increased cord vascularity (Fig. 3), probably related to the large tumor burden. Finally, the tunica albuginea was thought to be intact on MR imaging in 13 patients and involved by tumor in the other two (Fig. 2). On pathologic examination, the tunica albuginea was found to be intact in all 15 patients.

## Discussion

The differentiation of seminomatous from nonseminomatous lesions is important because patients with pure seminomas are irradiated whereas those with nonseminomatous tumors undergo retroperitoneal dissection and chemotherapy [6]. When seminomatous lesions harbor nonseminomatous elements, patients are classified and treated as if they have a nonseminomatous tumor. At present, definitive therapy is planned after detailed histologic analysis of the resected testes. Although treatment cannot be determined preoperatively in seminomatous lesions because they may harbor nonseminomatous elements, if nonseminomatous tumors are consistently diagnosed preoperatively with 100% specificity,

the information gained may influence care and treatment of patients. Given the emergence of characteristic MR findings of seminomatous and nonseminomatous lesions, it may be possible to provide this specificity with MR imaging. Despite the fact that this study has a small number of cases and that one case with pure seminoma was suspected in error to harbor a nonseminomatous focus, MR imaging may be able to offer this needed specificity. Our only error was partly related to relatively inferior image quality due to the patient's being imaged with the 7.6-cm instead of the 12.5-cm surface coil by mistake. The error was also in the interpretation of the single focus of high signal, which we believe could have been avoided. When nonseminomatous elements coexist with seminomatous elements, the pattern is typically a heterogeneous mix of microscopic islands of nonseminomatous cells rather than a single focus as was seen in this patient.

The differences in the appearance of seminomatous and nonseminomatous tumors on MR images mimic their basic histologic differences. Histologically, the majority of pure seminomas comprise nests of uniform tumor cells separated by fibrous bands containing lymphocytes. Although hemorrhage and necrosis may occur in seminomatous lesions and disrupt their homogeneity as was seen in one of the six cases, these events are unusual and more characteristic for nonseminomatous lesions because of the propensity of the latter to invade blood vessels. The nonseminomatous lesions have a heterogeneous architecture because of either the heterogeneity of their cell type or frequent hemorrhage and/or necrosis. It is not surprising, therefore, that the MR appearance is homogeneous in cases of seminomatous lesions and is markedly heterogeneous in the nonseminomatous variety. This resulted in our ability to distinguish these two lesions preoperatively in 13 of 15 cases. Indeed, when reviewing the published cases [3–5], the appearance of seminomatous and nonseminomatous lesions matched the description outlined in this study, suggesting that MR imaging may indeed be useful for differentiating these two tumor types. However, when lesions are small, the usefulness of MR for characterizing the lesion becomes more difficult because of the limited resolution within the tumor.

The presence of normal-appearing testicular tissue that allows the assessment of tumor margins, although potentially useful in differentiating diffuse inflammatory conditions from neoplasms, does not appear to aid in histologic classification. When a fibrous tumor capsule was seen histologically about the tumor, it was seen on MR images. Even though there was a tumor capsule observed in seven of nine patients with nonseminomatous lesions and in only two of seven with seminomatous tumors, the presence of a capsule did not allow sufficient specificity. It was the heterogeneity followed by the signal characteristics of the lesion that was most helpful.

The presence of an ipsilateral hydrocele and increased cord vascularity did not appear to add specificity. The degree of cord vascularity may help in identifying tumors from inflammatory conditions in the proper clinical setting, because the latter typically present with a hypervascular cord [2].

In summary, our results suggest that MR imaging can be used to provide a preoperative classification of testicular lesions with acceptable specificity. When MR scans show a testicular lesion with lower signal intensity than that of normal testis, and the lesion is relatively homogeneous, the findings are indicative of a seminomatous lesion. On the other hand, when a tumor is markedly heterogeneous, has high signal

nearly equal to that of normal testis, and is surrounded by a tumor capsule, the findings are indicative of a nonseminomatous lesion. Thirteen (87%) of 15 tumors in this study matched these patterns and were classified correctly. Other lesions that do not fit this description or are too small to characterize should be regarded as indeterminate. The percentage of lesions that fall in the indeterminate category is not known. Although this study suggests that it may be 13% (two of 15), a larger series is needed for a more accurate estimate.

#### REFERENCES

1. Baker LL, Hajek PC, Burkhard TK, et al. Magnetic resonance imaging of the scrotum: normal anatomy. *Radiology* **1987**;163:89-92
2. Baker LL, Hajek PC, Burkhard TK, et al. Magnetic resonance imaging of the scrotum: pathologic conditions. *Radiology* **1987**;163:93-98
3. Seidenwurm D, Smathers RL, Lo RK, Carrol CL, Bassett J, Hoffman AR. Testes and scrotum: MR imaging at 1.5 T. *Radiology* **1987**;164:393-398
4. Rholl KS, Lee JKT, Ling D, Heiken JP, Glazer HS. MR imaging of the scrotum with a high resolution surface coil. *Radiology* **1987**;163:99-103
5. Thurnher S, Hricak H, Carroll PR, Pobiel RS, Filly RA. Imaging the testis: comparison between MR imaging and US. *Radiology* **1988**;167:631-636
6. Morse WJ, Whitmore WF. Neoplasms of the testes. In: Walsh PC, Gittes RF, Perlmutter AD, Stamey TA eds. *Campbell's urology*. Philadelphia: Saunders, **1986**:1535-1582

## Book Review

**Ultrasound and Infertility.** By Asim Kurjak. Boca Raton, FL: CRC Press, 213 pp., 1989. \$99.50 (inside U.S.), \$117 (outside U.S.)

Organized into nine chapters, this work is a blend of both the clinical obstetrics and the sonographic imaging involved in diagnosis and treatment of infertility. Subjects covered include basic physics of ultrasound, pathophysiology of infertility, normal sonographic anatomy, ultrasound monitoring of follicular growth and ovulation, transvaginal sonography, in vitro fertilization and embryo transfer, interventional ultrasound in diagnosis and treatment of female infertility, ultrasound Doppler studies of the pelvis, and sonography in male infertility. The editor, an academic obstetrician who has published extensively, is the coauthor of five of these chapters.

It must be said at the outset that the intended audience for this work is, with few exceptions, not the radiologist. Although most of the images presented are of excellent quality, the book is heavily clinically weighted and directed toward those who need at least an overview of the subject of infertility (e.g., obstetric residents). It also could be used as a primer by obstetricians who are considering starting a program of diagnosis and treatment of infertility. For this group, it provides insufficient detail but is a valuable introduction. For all but those few radiologists who are affiliated with an infertility program, the extensive clinical detail is presented in something of a vacuum, and space precludes a complete spectrum of imaging of pelvic pathologic changes. The book may serve the radiologist as an abbreviated reference with respect to clinical matters in infertility, but it presupposes a deeper clinical background than most radiologists have in this field.

Each chapter begins with a table of contents outlining the subjects to be covered, a useful feature, and ends with a bibliography that frequently is quite extensive and relatively current. Twelve-year-old references in ultrasound are, however, with few exceptions, of limited value. The physics chapter is a highly compressed and somewhat confusing treatment of the physics of ultrasound. In an attempt to cover the entire subject in a single chapter, the author regrettably has bypassed basic explanations that the neophyte will require and has gone to levels that will be of limited interest to most practitioners. Although the language in the remainder of the book is relatively clear, the English in this section is frequently awkward and often confusing. The discussion in chapter 2 of the endocrinology of ovulation is an

abbreviated but useful overview; algorithms correlating levels of gonadotropin, prolactin, and sex steroids with causes of primary amenorrhea, for example, are quite useful. Some tables of this nature, although useful, occupy an entire page when one third of the page would be sufficient. This is presumably an editorial miscalculation. Chapters 4, 5, 6, and 7 involve the synthesis of the clinical aspects of infertility and intervention with the use of ultrasound; they are the core of the work and are well done. The practitioner intent on beginning an infertility program would find this a useful guide with a number of pertinent details; it is unlikely to substitute for on-site training at an established facility, however.

The net conclusion of the chapter on Doppler studies of blood flow in the pelvic vessels is that the technique is of limited use now and awaits further development. This probably is accurate, but it negates the value of the chapter, which might best be eliminated. The discussion of sonography in male infertility, although not sufficiently complete or well documented enough for urologic workup of this problem, nevertheless provides the obstetrician with sufficient perspective on the use of ultrasound in the male.

By way of general observation, the quality of reproduction of the scans is excellent; labeling is sometimes sparse, and scattered line drawings are quite helpful. Occasionally, a legend refers to a label that does not appear on the scan. More than the expected number of typographic errors occur throughout the volume. With the exception of the chapter on physics, the language is not a problem. The index, aided by the table of contents preceding each chapter, makes a subject search quite easy.

In summary, the book should be of value in obstetric training programs and, chiefly, for the practicing obstetrician who wants an overview of infertility and a sampling of the ultrasound imaging involved. The price is regrettably somewhat higher than might be wished.

Andrew M. Fried  
*University of Kentucky, Chandler Medical Center*  
Lexington, KY 40536-0084



# Value of Transperineal Sonography in the Assessment of Vaginal Atresia

Kathleen A. Scanlan<sup>1</sup>  
Myron A. Pozniak<sup>1</sup>  
Margaret Fagerholm<sup>1</sup>  
Sander Shapiro<sup>2</sup>

We studied the value of transperineal sonography in the preoperative assessment of seven patients with clinically suspected vaginal atresia. Although transabdominal scanning is useful to determine if hydrocolpos or hydrometrocolpos is present, this method does not allow measurement of the thickness of a caudally placed obstructive septum. This information is useful in planning reconstructive surgery. All seven patients had transabdominal sonography, with five showing a low-lying obstruction. In those five patients, the distance between the perineal surface and the caudal aspect of the distended vagina, measured with electronic calipers on the transperineal sonograms, ranged from 1.0 to 4.0 cm.

We conclude that when vaginal atresia is clinically suspected, transabdominal sonography should be performed to confirm the diagnosis. When a low-lying obstruction is identified, transperineal sonography should be performed to determine the length of the obstructive segment.

*AJR* 154:545-548, March 1990

In the imaging workup of patients with vaginal obstruction, transabdominal sonography is effective for identifying uterine and vaginal fluid collections [1-4]. Associated abnormalities of the fallopian tubes such as hydrosalpinx or hematosalpinx also may be identified. This method, however, does not allow adequate visualization of the entire length of vagina, particularly when a low-lying obstruction is present [5].

To overcome this problem, we performed real-time contact scanning of the perineum to evaluate the obstructive tissue interposed between the perineum and the caudal aspect of the distended vagina. This approach allows direct measurement of the thickness of the obstructing septum.

## Subjects and Methods

Seven patients with clinically suspected vaginal outflow obstruction had transabdominal real-time sonograms. In one case a static B-mode sagittal scan also was obtained. The seven patients ranged in age from 9 to 34 years old, with a mean of 16 years. The five patients who showed hydrocolpos also underwent transperineal scanning. Sonographic findings were correlated with CT images in one case.

Sonograms were obtained on ATL (Bothell, WA) and Acuson (Mountain View, CA) real-time scanners. We obtained 3.5-MHz scans of the pelvis by using a full bladder as a sonic window. Transperineal scanning (5.0 MHz) was performed when the transabdominal scan showed distention of the vagina with fluid and/or debris. Before the transperineal scan, the patient emptied her bladder and the scanning method and its importance were explained. The patient was then placed in a supine lithotomy position, and acoustic gel was applied to the perineum. A Kitecko standoff pad (3M Co., St. Paul, MN) was placed against the perineum (Fig. 1). The pad allows improved imaging of the superficial structures and a more accurate measurement of the distance from the perineum to the caudal margin of the distended vagina. Sagittal real-time scanning was then performed for anatomic orientation and to determine the

Received August 3, 1989; accepted after revision October 26, 1989.

<sup>1</sup> Department of Radiology, University of Wisconsin Clinical Science Center, 600 Highland Ave., Madison, WI 53792. Address reprint requests to K. A. Scanlan.

<sup>2</sup> Department of Obstetrics and Gynecology, University of Wisconsin Clinical Science Center, 600 Highland Ave., Madison, WI 53792.

0361-803X/90/543-0545  
© American Roentgen Ray Society

point of greatest caudal extension of the distended vagina. The transducer was rotated to a coronal position at this level. By using the least pressure possible to obtain an image, the distance from the perineum to the caudal aspect of the distended vagina was measured with electronic calipers. When the differentiation could be made, the more hypoechoic fibromuscular septum was measured separately from subcutaneous fat. The thickness of the septum was confirmed during surgical reconstruction.

Transabdominal scanning showed hydrometrocolpos (Fig. 2) in two patients and hydrocolpos (Fig. 3) in three. Ovaries were identified in all but one of these five patients who had bilateral hydrosalpinx in addition to hydrometrocolpos. She had undergone two previous unsuccessful simple hymenectomies at another institution and developed a clostridial pelvic infection as a result of restenosis after surgery (Fig. 4). During surgery, the ovaries were found to be involved with endometriosis and adhesions.



Fig. 1.—Method of transperineal sonography. Patient is placed in lithotomy position. Acoustic gel is applied and a standoff pad is placed against perineum. A preliminary sagittal scan provides best anatomic orientation.

In one patient with a history of attempted hymenectomy, hydrometros and bilateral hydrosalpinx were identified on transabdominal examination (Fig. 5). Neither cervical or vaginal tissue nor the ovaries could be identified. The findings are compatible with a vaginal-cervical atresia caused by developmental failure of the caudal müllerian ducts. Transperineal scanning was not considered useful in this case because the level of obstruction could be clearly defined transabdominally. The patient underwent successful McEndoe vaginoplasty after abdominal hysterectomy. The ovaries were present, but as in the previous case, were involved with endometriosis and adhesions.

In one patient, neither uterine, cervical, nor vaginal tissue was identified. Both ovaries appeared sonographically normal in this woman with a 46xx karyotype. A short 2-cm caudal segment of vagina was present at the perineum on clinical examination. These findings, like the case above, are compatible with developmental dysplasia of the caudal müllerian ducts. In this syndrome, the distal fallopian tubes and ovaries are usually normally developed. The extreme caudal segment of the vagina may be present, because that portion is derived from the urogenital sinus [6]. As in the case described earlier, a perineal sonogram would not have added information and was not undertaken.

## Results

Transperineal scanning was performed in those patients whose findings included hydrocolpos on transabdominal sonography. In these five cases, a solid tissue septum was seen extending from the caudal aspect of the distended vagina to the perineum. Measurements were obtained in a coronal plane by using a solid gel standoff pad between the transducer and the perineum. Minimal pressure to obtain an image was used to minimize distortion. When identifiable as showing differing echogenicity, the subcutaneous fat was measured separately from the more hypoechoic fibromuscular septum and both measurements were reported. The thickness of this septum (inclusive of all measurable tissue layers) ranged from 1 to 4 cm, with a mean of 2.3 cm. Surgical planning was facilitated by knowledge of the exact tissue thickness as measured by

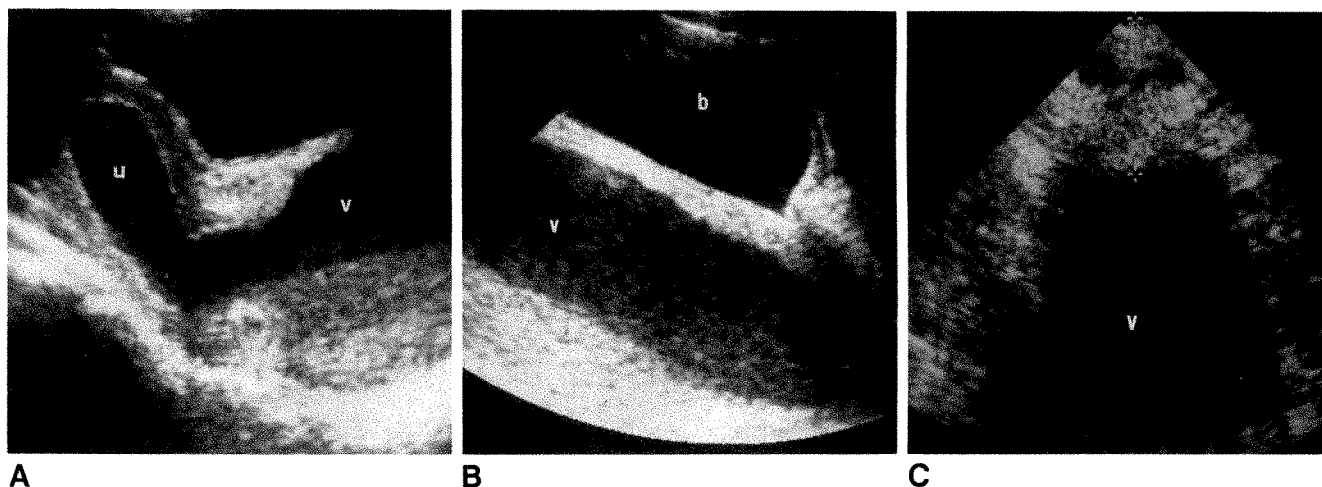


Fig. 2.—9-year-old girl with adrenogenital syndrome and absent vaginal opening.

A, Longitudinal transabdominal sonogram reveals fluid distending uterus (u) and vagina (v). Attempts to image lower vaginal segment transabdominally did not show thickness of obstructing tissue accurately.

B, Longitudinal transabdominal sonogram shows echogenic debris within vagina (v), posterior to bladder (b).

C, Direct-contact coronal perineal sonogram shows a 2.3-cm-thick block of obstructing tissue (calipers). Hypoechoic area at bottom of image is fluid and debris distending vagina (v).

Fig. 3.—12-year-old girl with acute urinary retention.

A, Longitudinal B-mode transabdominal sonogram shows bladder (b), vagina (v), and perineum (p). Note fluid/debris level within hydrocolpos.

B, Coronal transperineal sonogram shows obstructing tissue (arrowheads). Note differences in echogenicity between components, including subcutaneous fat (f) and fibromuscular septum (s). Hypoechoic area is distended vagina (v).

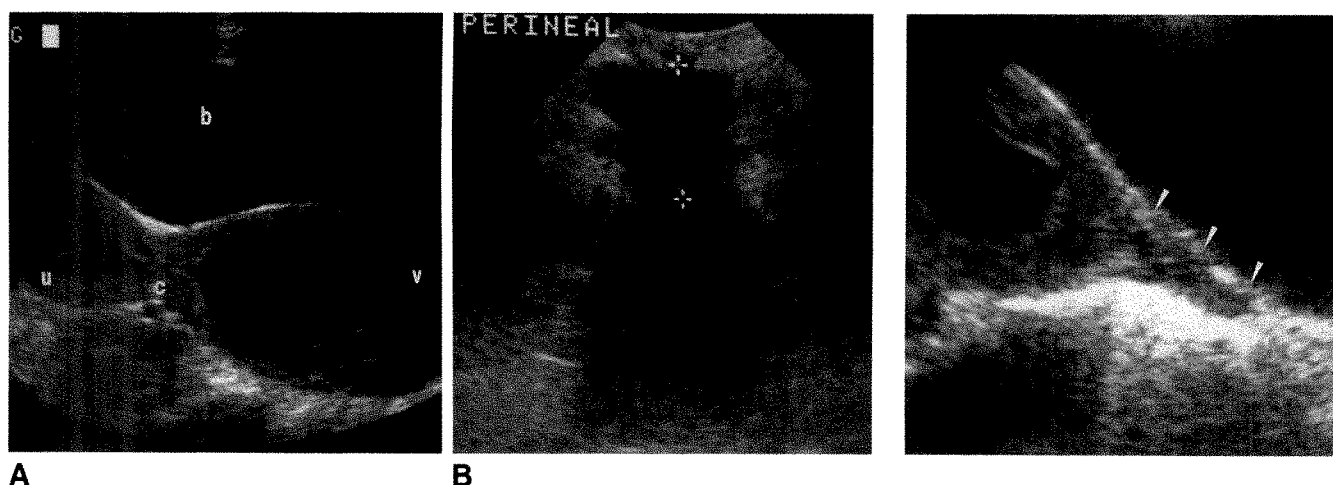
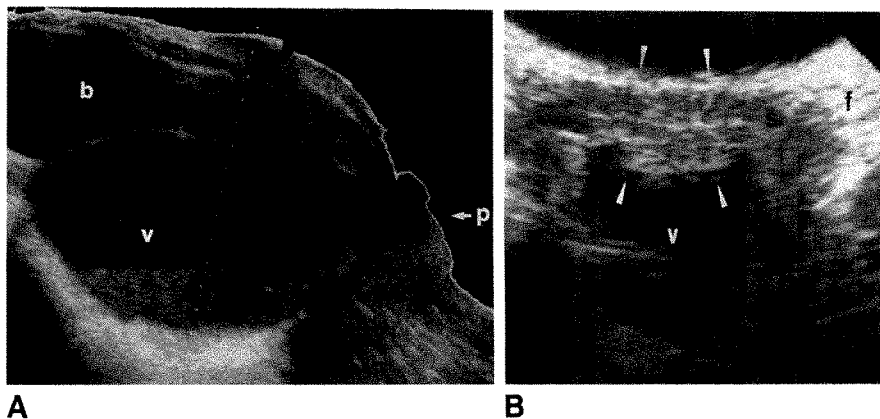


Fig. 4.—14-year-old girl with lower back pain, amenorrhea, and an abdominal mass. Hymenectomy had been attempted twice before.

A, Longitudinal transabdominal sonogram shows hydrometrocolpos with debris. b = bladder; c = cervix; u = uterus; v = vagina.

B, Transperineal sonogram shows differences in echogenicity between various components of tissue. Fibromuscular septum is of lower echogenicity than subcutaneous fat and is measured separately in this case. Total tissue block measured 4.0 cm.

Fig. 5.—13-year-old girl with monthly abdominal cramping. She previously underwent an attempted hymenectomy. Longitudinal transabdominal sonogram shows a tapering of tissue toward lower uterine segment (arrowheads) with no definable cervix or vagina present. Level of obstruction is clear and a transperineal sonogram would not have added information.

perineal scanning. All five patients underwent simple vaginoplasty (excision of the septum and epithelial reapproximation) without the need for skin grafting. Their postoperative courses were unremarkable, and each attained a functional vagina.

## Discussion

When vaginal outflow is obstructed, fluid produced by the cervical glands and vaginal mucosa accumulates proximally. After menarche, blood and endometrial debris accumulates, often causing cyclic pain in the presence of clinical amenorrhea. Urinary obstruction, frequency, or obstipation also may be presenting symptoms. Normally, a remnant of trapped mesenchymal tissue persists at the site where the sinovaginal mass extending cephalad first contacts the caudal aspect of the fused müllerian ducts; this is manifest as the hymen and may on occasion be imperforate [7]. This is the most common cause of hydro/hematocolpos. On clinical examination, a bulg-

ing, thin membrane may be seen as a result of debris and fluid accumulated behind the obstruction. Less commonly, a caudally placed, low vaginal septum resulting from focal vaginal atresia may appear essentially the same. Its greater thickness makes the classic appearance of a bulging purple membrane less likely.

If the vaginal obstruction with substantial tissue thickness is mistakenly treated by simple hymenectomy, recurrent obstruction probably will result [8]. Once the obstructed collection has been contaminated by an attempted and failed drainage procedure, the risk of pelvic infection, abscess formation, sepsis, and infertility is high. These complications can be avoided if the appropriate diagnosis is made and the correct reconstructive procedure is performed initially.

Variations of two major reconstructive techniques are used, depending on the obstructing tissue thickness. For shorter atretic segments, a simple vaginoplasty may be performed with excision of the transverse tissue septum and reapproximation of the vaginal mucosa. For longer obstructions where

such a reapproximation is not possible, a modified McEndoe vaginoplasty may be required. In this procedure, a tunnel is created at the site of the atretic segment and a tube of split-thickness skin is introduced to cover the nonepithelialized segment of vagina [6]. In both instances, dilators are used postoperatively to prevent cicatrization.

Transperineal scanning allowed identification and quantification of the obstructive tissue mass in the five cases in which it was performed. Transperineal scanning was not performed in patients in whom a more proximal site of obstruction could be identified on transabdominal scan. This method would not have contributed significant additional information in these two cases.

Accurate preoperative diagnosis of vaginal atresia/vaginal septum anomalies is important for strategic surgical planning. An atretic vaginal segment or caudal vaginal tissue septum requires quantification of the obstructive segment and differentiation from imperforate hymen, followed by a carefully planned vaginal reconstructive procedure. Transperineal scanning in conjunction with transabdominal scanning pro-

vides valuable anatomic information in the evaluation of and preoperative planning for treating vaginal agenesis.

#### REFERENCES

1. Jolly HF. The use of ultrasonography in elucidating the problem of imperforate vagina. *Aust NZ J Surg* **1983**;53:49-51
2. Valdes C, Malini S, Malinak LR. Sonography in the surgical management of vaginal and cervical atresia. *Fertil Steril* **1983**;40:263-265
3. Malini S, Valdes C, Malinak R. Sonographic diagnosis and classification of anomalies of the female genital tract. *J Ultrasound Med* **1984**;3:397-404
4. Valdes C, Malini S, Malinak LR. Ultrasound evaluation of female genital tract anomalies: a review of 64 cases. *Am J Obstet Gynecol* **1984**;149:285
5. Graham D, Nelson MW. Combined perineal-abdominal sonography in the evaluation of vaginal atresia. *J Clin Ultrasound* **1986**;14:735-738
6. Jones HW, Rock JA. Anomalies of the Mullerian ducts. In: Jones HW, Rock JA, eds. *Reparative and constructive surgery of the female generative tract*. Baltimore: Williams & Wilkins, **1983**
7. Williams PL, Warwick R. Embryology. In: Williams PL, Warwick R, eds. *Gray's anatomy*, 36th Br. ed. Philadelphia: Saunders, **1980**
8. Tindall VR. Malformations and maldevelopments of the genital tract. In: Tindall VR, ed. *Jeffcoates' principles of gynecology*, 5th ed. London: Butterworth, **1987**

## Pictorial Essay

# MR Imaging of the Shoulder: Correlation with Plain Radiography

D. Lawrence Burk, Jr.,<sup>1</sup> David Karasick, Donald G. Mitchell, and Matthew D. Rifkin

Recent advances in surface-coil technology and scanner software have made high-quality MR examinations of the shoulder a practical reality. The high signal-to-noise ratios provided by local coils designed specifically for the shoulder allow imaging with small fields of view and thin sections. New software provides routine oblique imaging with off-center fields of view and no wraparound artifacts. With these state-of-the-art techniques, several studies have shown that MR is as accurate as, if not more accurate than, arthrography in detecting rotator cuff tears [1, 2]. In addition, MR can provide an accurate preoperative assessment of the size of a cuff tear and the condition of the remaining tendon. In the absence of a cuff tear, MR can be useful in evaluating impingement, tendinitis, and bursitis; these cannot be assessed with arthrography. MR also can show other abnormalities such as avascular necrosis, labral tears, tumors, osteomyelitis, and arthritis [3]. Although MR is considerably more expensive than arthrography, it is probable that the additional information obtained in a noninvasive fashion will make MR the procedure of choice for the evaluation of shoulder pain.

For these reasons, MR is frequently the next study performed after conventional radiography. Comparison with the radiographs is essential for a complete evaluation of the MR images. Each of these techniques has distinct advantages and limitations. In this essay we will illustrate examples of these features for a variety of clinical conditions.

## Materials and Methods

The images were selected from over 200 studies of the shoulder obtained on a 1.5-T scanner. Most of the examinations were performed with a loop-gap resonator coil pair (Medical Advances, Milwaukee, WI). The technique has been described in detail [4]. Recent examinations have been performed with an anteriorly positioned, heart-shaped, single-loop coil (Medrad, Pittsburgh, PA, for General Electric Medical Systems, Milwaukee, WI). All studies included coronal oblique spin-echo (SE) 600/25 (TR/TE) and 2000/40,80 sequences as part of the routine protocol. The other imaging parameters were 5-mm slice thickness, 1-mm interslice gap, 128 × 256 matrix, two excitations, and 14-cm field of view. Respiratory compensation and oversampling in the phase- and frequency-encoding axes were used routinely to reduce artifacts.

## MR Imaging–Radiographic Correlation

For routine cases of impingement syndrome and possible rotator cuff tear the radiographic findings are limited mainly to greater tuberosity and acromioclavicular degenerative changes [5]. These findings are nonspecific, and the diagnosis of a rotator cuff tear requires the use of another imaging technique such as MR. However, in rotator cuff arthropathy, the diagnosis usually can be made on plain radiographs because of marked acromiohumeral narrowing, and MR may be useful in assessing the quality of the remaining cuff before

Received August 21, 1989; accepted after revision October 16, 1989.

<sup>1</sup> All authors: Department of Radiology, Jefferson Medical College, Thomas Jefferson University Hospital, 1033 Main Bldg., 10th and Sansom Sts., Philadelphia, PA 19107. Address reprint requests to D. L. Burk, Jr.

AJR 154:549–553, March 1990 0361–803X/90/1543–0549 © American Roentgen Ray Society



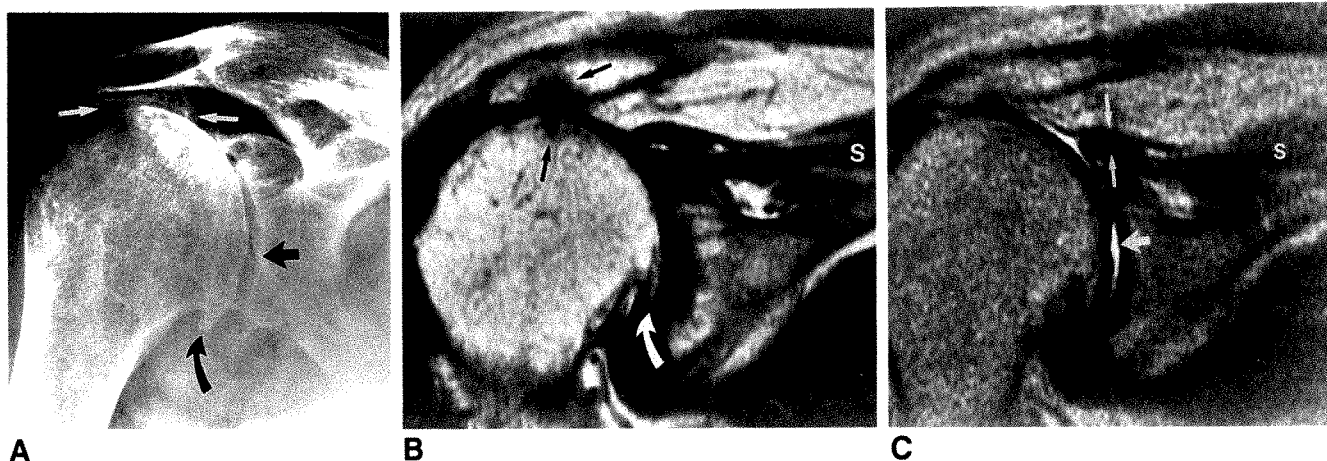


Fig. 1.—Chronic rotator cuff arthropathy.

A, Anteroposterior radiograph shows marked narrowing of acromiohumeral space with subacromial spur (white arrows), osteophyte formation (curved arrow), and slightly irregular glenohumeral articular surfaces (straight black arrow).

B, SE 600/25 coronal oblique MR image also shows acromiohumeral narrowing with better visualization of secondary subchondral marrow changes in acromion and humeral head (black arrows). Humeral osteophyte is filled with fatty marrow (white arrow). Note marked atrophy of supraspinatus muscle (S).

C, SE 2000/80 coronal oblique MR image with arthrogram effect confirms irregularity of glenohumeral articular surfaces (large arrow). Note massive rotator cuff tear with retracted tendon (small arrows) of supraspinatus muscle (S).

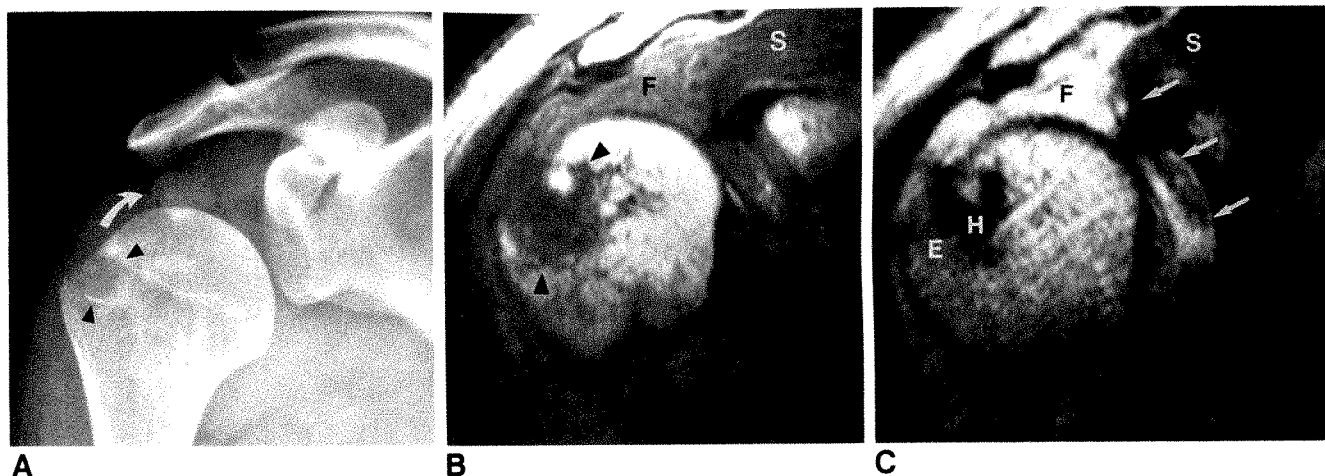


Fig. 2.—Supraspinatus avulsion with greater tuberosity fracture.

A, Anteroposterior radiograph shows defect in lateral aspect of humeral head (arrowheads) with displaced greater tuberosity fragment (arrow). Acromiohumeral space is widened because of humeral traction.

B, SE 600/25 coronal oblique MR image shows slightly larger area of acute hemorrhage and edema at site of avulsion fracture (arrowheads). Acromiohumeral space is narrowed with patient out of traction. Joint fluid (F) is isointense relative to supraspinatus muscle (S).

C, SE 2000/80 coronal oblique MR image shows displaced tendon (arrows) of supraspinatus muscle (S) surrounded by fluid in glenohumeral joint. Joint fluid (F) fills narrowed acromiohumeral space in place of avulsed supraspinatus tendon. Center of fracture site has low signal intensity due to deoxyhemoglobin of acute hemorrhage (H). Peripheral edema (E) has higher signal intensity, similar to that of surrounding marrow.

surgery for total shoulder replacement (Fig. 1). Mild narrowing of the acromiohumeral space also may be present with rotator cuff atrophy, but without cuff tear. In avulsion fractures of the tuberosities, the diagnosis is made with plain radiographs,

but the full extent of injury to the rotator cuff can be determined only on MR, although the fracture fragments themselves may not be visible (Fig. 2). Traumatic avulsion of the cuff also can occur in the absence of a fracture.

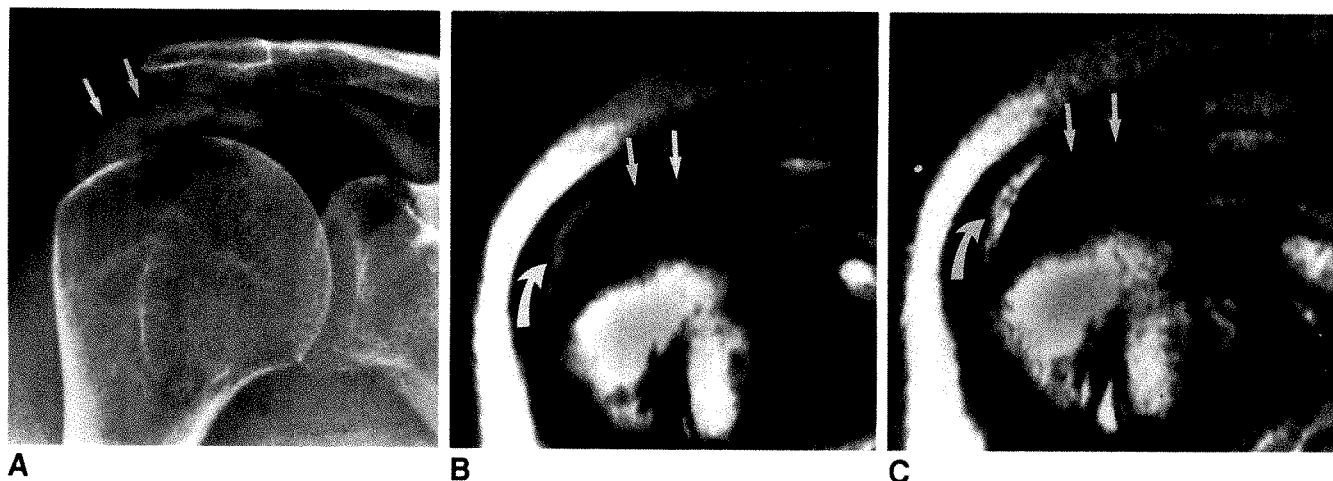


Fig. 3.—Supraspinatus calcific tendinitis.

A, Anteroposterior radiograph shows typical amorphous calcium hydroxyapatite deposit in acromiohumeral space (arrows).

B, SE 600/25 coronal oblique MR image shows areas of signal void (straight arrows) corresponding to intratendinous calcification, which could easily be overlooked and attributed to thickening of fibrocartilaginous tendon. Subdeltoid fat plane has intermediate signal intensity due to inflammation (curved arrow).

C, SE 2000/80 coronal oblique MR image shows thickened supraspinatus tendon (straight arrows) with homogeneous low signal intensity obscuring calcification. Fluid in subdeltoid bursa (curved arrow) has high signal intensity.

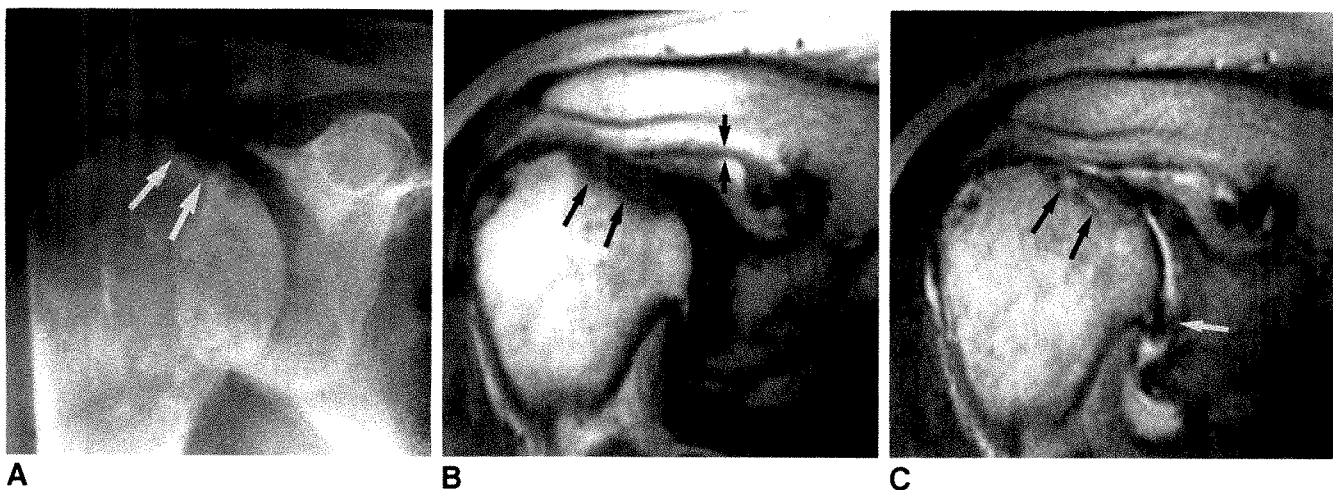


Fig. 4.—Avascular necrosis of humeral head.

A, Anteroposterior radiograph shows subchondral lucency on weight-bearing surface of humeral head (arrows) with vague margin of sclerosis. Since early stages of avascular necrosis are not visible on plain radiographs, these radiographic findings are consistent with later stage of disease.

B, SE 600/25 coronal oblique MR image shows corresponding avascular area in subchondral bone (long arrows). Infraspinatus muscle (short arrows) is markedly atrophic.

C, SE 2000/80 coronal oblique MR image shows high-signal-intensity granulation tissue at reactive margin of avascular zone (black arrows) with adjacent low-signal-intensity rim corresponding to radiographic sclerosis. Fluid outlines small inferior humeral osteophyte (white arrow) that was not well visualized radiographically.

In some situations there are clear advantages of one technique over the other. Calcific tendinitis is easily visualized on plain films, but may be overlooked or only suspected on MR (Fig. 3). The signal void representing calcium hydroxyapatite

within the tendon cannot be easily distinguished from a thickened tendon without calcification. In avascular necrosis, the diagnosis can be made radiographically only when the disease is in the late stages (Fig. 4). As in the hip and other joints,

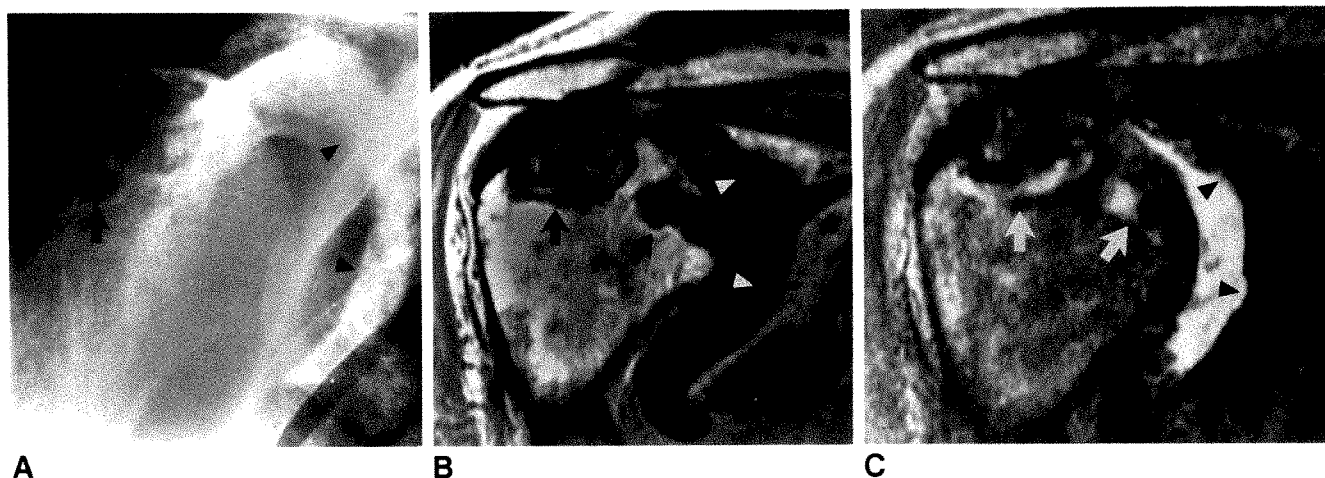


Fig. 5.—Rheumatoid arthritis with large erosions.

A, Anteroposterior radiograph shows large, lucent erosion on lateral aspect of humeral head (arrow) with marked enlargement and deformity of glenoid (arrowheads).

B, SE 600/25 coronal oblique MR image shows corresponding large lateral erosion and additional erosion on humeral articular surface that was not visible radiographically (arrows). Glenoid is markedly remodeled with articular erosions (arrowheads).

C, SE 2000/80 coronal oblique MR image shows humeral erosions filled with heterogeneous material probably representing pannus (arrows). Erosions of glenoid articular surface (arrowheads) are outlined by joint effusion.

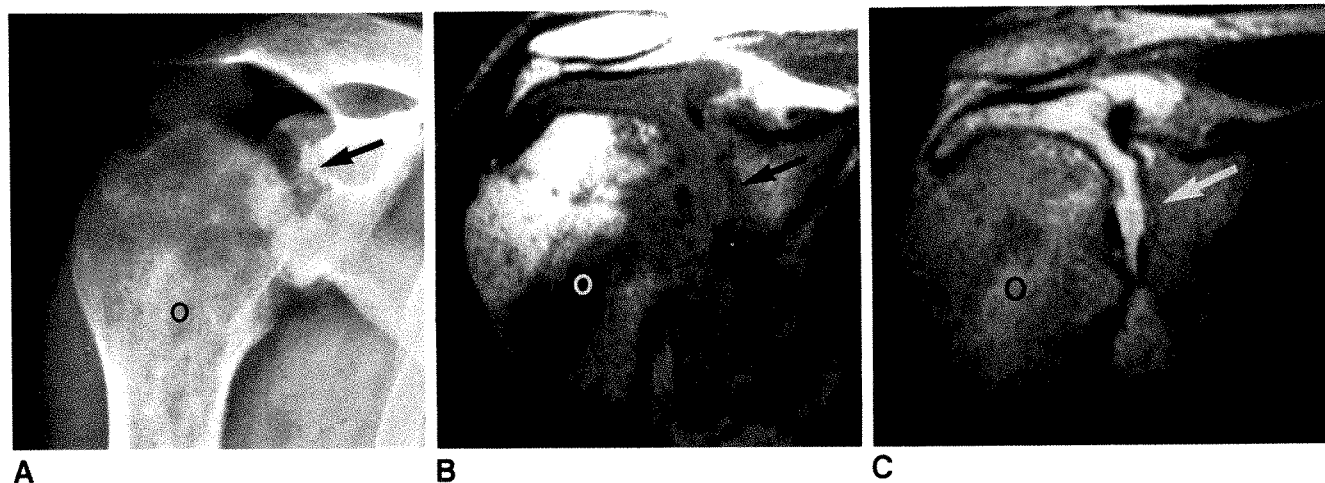


Fig. 6.—Septic arthritis and osteomyelitis.

A, Anteroposterior radiograph shows incongruity of glenohumeral joint with poor definition of articular surfaces (arrow). Humerus has mottled appearance in region involved by osteomyelitis (O).

B, SE 600/25 coronal oblique MR image better shows extensive destruction of subchondral bone of glenoid and humerus (arrow). Extent of abnormal marrow in region of osteomyelitis (O) is better evaluated also.

C, SE 2000/80 coronal oblique MR image shows destruction and collapse of articular surfaces (arrow) outlined by large joint effusion. Humeral osteomyelitis shows some areas of high signal intensity (O).

MR is the most sensitive technique for early detection of avascular necrosis.

For the diagnosis of diseases of the articular surfaces, MR and conventional radiographs frequently are complementary. Erosions and subchondral cysts in rheumatoid arthritis can be evaluated better with MR (Fig. 5), but plain radiographs provide most of the necessary information. Associated rotator cuff tears and synovial cysts can also be detected with MR. In early septic arthritis, no changes are seen on radiographs, whereas MR will show the presence of a joint effusion. In

later stages of joint infection, both techniques will demonstrate destruction of the articular surfaces, but MR is the most sensitive for detecting associated osteomyelitis (Fig. 6).

In some bone lesions such as those filled with fluid, MR images may provide a more specific diagnosis than plain radiographs based on morphologic and signal characteristics (Fig. 7). However, plain radiographs are usually more important for differential diagnosis, and MR is most useful for staging purposes. In some unusual tumors, both studies are nonspecific and a diagnosis may not be made before surgery

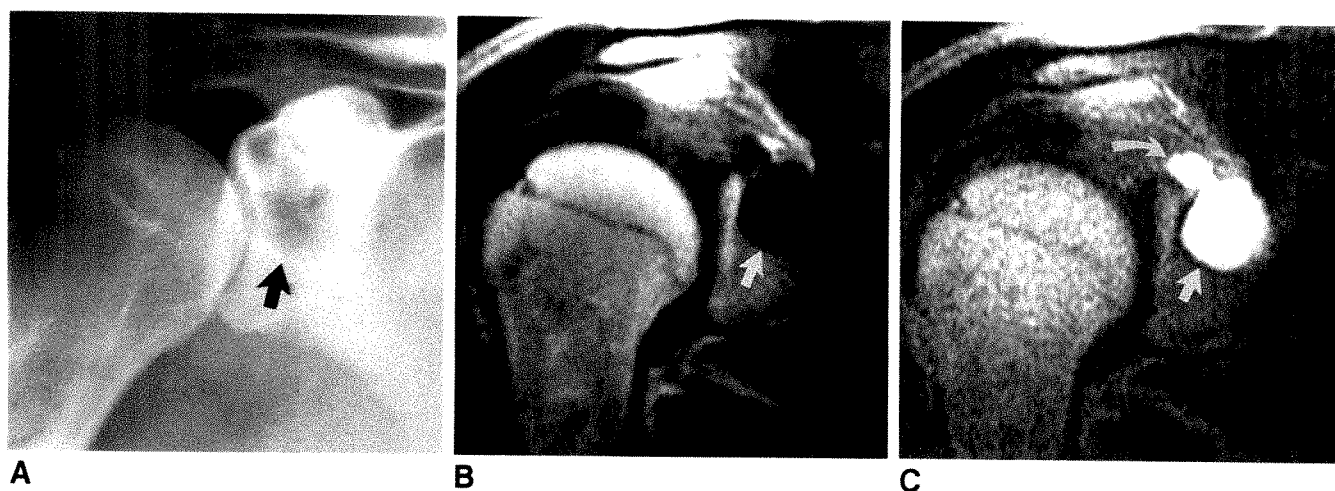


Fig. 7.—Extrasosseous ganglion cyst with glenoid erosion.

A, Anteroposterior radiograph shows nonspecific appearance of radiolucent glenoid lesion (arrow).

B, SE 600/25 coronal oblique MR image shows corresponding extrasosseous lesion eroding into glenoid with well-defined inferolateral margin (arrow).

C, SE 2000/80 coronal oblique MR image shows septation partially separating main cyst (straight arrow) from smaller component, which extends toward point of origin near superior aspect of glenoid (curved arrow). This appearance is highly suggestive of ganglion cyst.

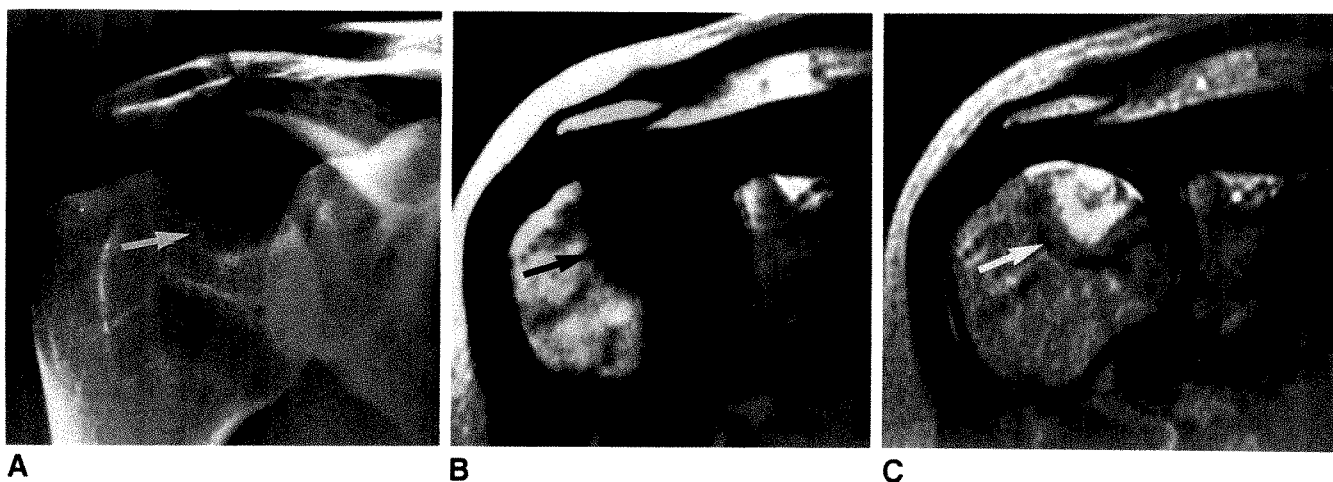


Fig. 8.—Adenocarcinoma metastasis to humeral head.

A, Anteroposterior radiograph shows nonspecific lytic lesion in humeral subchondral bone with incomplete sclerotic margin (arrow).

B, SE 600/25 coronal oblique MR image shows large subchondral marrow lesion (arrow), which is slightly larger than radiographic abnormality because of rapid growth over a period of several weeks.

C, SE 2000/80 coronal oblique MR image shows area of inhomogeneous high signal intensity in center of lesion with rim of low signal intensity (arrow) corresponding to radiographically visible sclerosis. Appearance is nonspecific, and diagnosis was not made before biopsy as patient had no known primary tumor.

(Fig. 8). MR and radiography of the shoulder are complementary studies, and appropriate correlation will be of benefit to both the patient and the radiologist.

#### REFERENCES

1. Burk DL Jr, Karasick D, Kurtz AB, et al. Rotator cuff tears: prospective comparison of MR imaging with arthrography, sonography, and surgery. *AJR* 1989;153:E7-92
2. Zlatkin MB, Iannotti JP, Roberts MC, et al. Rotator cuff tears: diagnostic performance of MR imaging. *Radiology* 1989;172:223-229
3. Zlatkin MB, Dalinka MK, Kressel HY. Magnetic resonance imaging of the shoulder. *Magn Reson Q* 1989;5:3-22
4. Aquilone LF, Burk DL Jr, Blob RD, Brown DL, Rifkin MD, Mitchell DG. Technical optimization of surface coil MRI of the rotator cuff. Presented at the annual meeting of the Society of Magnetic Resonance in Medicine, San Francisco, August, 1988
5. Hardy DC, Vogler JB, White RH. The shoulder impingement syndrome: prevalence of radiographic findings and correlation with response to therapy. *AJR* 1986;147:557-561

## Book Review

**Magnetic Resonance Imaging of Bone and Soft Tissue Tumors and Their Mimics.** A Clinical Atlas. By A. M. A. De Schepper and H. R. M. Degryse. Boston: Kluwer Academic, 130 pp., 1989. \$75

This book was written for radiologists, orthopedic surgeons, and physiotherapists. Its intent is to outline the MR features of primary bone and soft-tissue tumors in atlas form. The material is based on the authors' experience of treating 94 primary bone and soft-tissue tumors and several conditions that may mimic a tumor. The book is divided into five sections. The first is introductory and consists of two chapters on general considerations of bone and soft-tissue tumors and the materials and methods used. This section is brief, but it gives an overview of bone and soft-tissue tumors and emphasizes the need to correlate radiologic and pathologic data. It contains simplified radiologic parameters for the diagnosis of bone tumors based on the tumors' local behavior. In addition, it has several tables giving the MR diagnostic morphologic criteria for nonaggressive (benign) and aggressive (malignant) lesions. Included in this area are several tables listing correlations of signal intensity with various musculoskeletal structures on T1- and T2-weighted images. Furthermore, it has tabular correlation of high and low signal intensities for T1, T2, and proton-density scanning.

The second section of the book, which is the longest, consists of 11 brief chapters on benign bone tumors and mimicking conditions. These include osteoid osteoma, enchondroma, osteochondroma, giant-cell tumor, vertebral hemangioma, solitary and aneurysmal bone cysts, nonossifying fibroma, neoplasticlike eosinophilic granuloma, fibrous dysplasia, and osteomyelitis. The third section is on malignant bone tumors and covers only osteogenic sarcoma and chondrosarcoma. The chapter on osteogenic sarcoma also includes three examples of stress fractures that could be mistaken for the more ominous lesion. The table of contents erroneously gives the same page reference for chondrosarcoma and osteogenic sarcoma.

The fourth section is on benign soft-tissue tumors. It covers lipoma,

neurogenic tumors, soft-tissue hemangioma, and aggressive fibromatosis. The final section covers malignant soft-tissue tumors and includes liposarcoma, malignant fibrous histiocytoma, and rhabdomyosarcoma. The section concludes with two chapters covering the value of gadolinium-DTPA enhanced MR studies and a summary chapter on general conclusions. Each chapter has a graph showing the MR gray scale for each lesion and indicates the changes that may occur with gadolinium enhancement.

The most serious shortcoming of this book is the quality of the illustrations. By and large, they are poor. Although the number is generous, virtually all the illustrations are too dark, and most are muddy. The MR images are extremely grainy. Both the MR images and the CT scans are too small. Illustrations are included of histologic material, which are of little interest to radiologists.

In summary, the authors have provided, within the limitations of a small number of cases, good correlation of radiologic findings with the MR findings and pathologic changes. The authors emphasize the need for conventional radiography. They point out that MR is used to define the intramedullary extent of the lesions and shows the soft-tissue extent of lesions better than CT can. The text is well referenced to 1988. However, the quality of the illustrations is the most severe drawback, and for this reason I cannot recommend this book to American radiologists. Much of the information presented could be obtained from the current radiologic literature. The absence of an index is another shortcoming. Finally, the price for a book with illustrations of this poor quality will serve further to deter many buyers.

Richard H. Daffner  
Allegheny General Hospital  
Pittsburgh, PA 15212



# Value of MR Imaging in Staging Osteochondral Lesions of the Talus (Osteochondritis Dissecans): Results in 14 Patients

Arthur A. De Smet<sup>1</sup>  
David R. Fisher<sup>1</sup>  
Mark I. Burnstein<sup>1</sup>  
Ben K. Graf<sup>2</sup>  
Richard H. Lange<sup>2</sup>

Osteochondral lesions (osteochondritis dissecans) of the talus are common articular lesions that are usually traumatic in origin. Clinical management of these lesions is based on whether or not the fragments are attached. We studied the value of MR imaging in determining the stability of the osteochondral fragments. In 13 of 14 patients who had had correlative surgery, we accurately predicted the presence and extent of attachment of the fragment to the talus by performing preoperative MR imaging. The other patient had a false-positive diagnosis of a chondral fragment. All seven partially attached fragments had an irregular high-signal zone on T2-weighted images at the fragment/talar interface. The four unattached fragments had a complete ring of fluid surrounding the lesion.

On the basis of these findings, we think MR of the ankle can be used to assess accurately talar osteochondral lesion stability and aid in clinical decision making.

*AJR* 154:555-558, March 1990

Osteochondral lesions of the talar dome have been recognized since the first report in 1922 [1]. These lesions have been called osteochondritis dissecans, osteochondral defects, osteochondral fractures, transchondral fractures, and osteochondral lesions [2, 3]. Most are fractures, and a previous episode of trauma has been reported by most patients who have lateral dome lesions and by about 80% of patients who have medial lesions [4, 5]. Because some lesions may not be traumatic in origin, we have elected to use the term "osteochondral lesion" to describe this entity. This terminology allows for alternative causes such as repetitive stress, hereditary ossification defect, abnormal stress due to malalignment, and microemboli with peripheral necrosis of bone [4].

Talar osteochondral lesions normally involve the medial and lateral corners of the talar dome; central lesions occur only occasionally [6]. The medial lesions are usually posterolateral, with a deep craterlike appearance. Lateral lesions are usually thin and shallow and anterolateral [4, 5]. Clinical staging is based on whether the fragment is attached to the talus, partially attached, or completely loose. Partially attached lesions are usually treated with a period of cast immobilization. Unattached fragments must be removed surgically. Because clinically it is difficult to determine lesion stability, we evaluated the usefulness of MR imaging in talar osteochondral lesions.

## Subjects and Methods

We studied the ankles of 22 patients with suspected osteochondral lesions of the talus by using MR imaging. The 14 patients (seven men, seven women) who had correlative ankle arthroscopy or arthrotomy form the group of subjects for this report. Their average age was 22 years (range, 15-42 years). They had had ankle symptoms for various periods: less than 1 year in nine patients, from 1 to 4 years in four patients, and 20 years in the last patient. Eleven patients reported either a specific episode of severe ankle trauma or multiple sprains as preceding their ankle pain.

Received September 5, 1989; accepted after revision October 22, 1989.

<sup>1</sup> Department of Radiology, University of Wisconsin Clinical Science Center, 600 Highland Ave., Madison, WI 53792. Address reprint requests to A. A. De Smet.

<sup>2</sup> Division of Orthopedic Surgery, University of Wisconsin Clinical Science Center, 600 Highland Ave., Madison, WI 53792.

0361-803X/90/1543-0555  
© American Roentgen Ray Society

Nine patients had arthroscopy alone, one had arthrotomy alone, and four had combined arthroscopy and arthrotomy. In the one patient with a misdiagnosis of a chondral fragment, only severe synovitis was found. Two patients had stable osteochondral lesions with mild, overlying cartilage erosion. Seven patients had partially attached lesions, and four had unattached in situ or displaced lesions. The partially attached fragments had soft granulation tissue at their bases. The completely loose fragments were surrounded by joint fluid. Fluid-filled cysts were not found in any patient, but focal areas of loose granulation tissue in the adjacent talus were present in five patients with unstable fragments.

Anteroposterior, mortise, and lateral plain radiographs of the ankle were available for all 14 patients. Thin-section hypocycloidal anteroposterior and lateral tomograms were obtained on 10 patients. Three lesions were lateral. The other 10 proved lesions were in the medial aspect of the talar dome. Two lesions were cartilaginous only, with cysts at the site of the chondral fractures.

All MR examinations were performed on a 1.5-T General Electric (Milwaukee, WI) Sigma MR imaging unit. A transmit-and-receive head coil was used for the first patient, and a dedicated transmit-and-receive extremity coil was used for the next 10. All patients had both coronal and sagittal scans; slices 3- or 5-mm thick and an interslice gap of 1.5 or 2.5 mm were used. The field of view was 12 cm for 13 patients and 16 cm for the patient studied by using the head coil. The following imaging variables were used: 256 × 128 matrix, two excitations, and spin-echo imaging with a TR of 600 msec and a TE of 20 msec for T1-weighted images and a two-echo sequence with a TR of 2000 msec and TEs of 20 msec and 90 msec for proton-density and T2-weighted images, respectively.

All the patients had scans obtained by using both T1- and T2-weighted sequences except the first patient, who had only coronal and sagittal T1-weighted images. The next six patients had coronal and sagittal T1-weighted sections and T2-weighted images in the plane that best visualized the lesion. Our last seven patients had coronal and sagittal T2-weighted images and T1-weighted images in the plane that best visualized the lesion. We settled on this protocol as the T2-weighted sequences best defined fluid or granulation tissue interfaces with the fragments. The examination was completed by using T1-weighted sequences to evaluate T1 characteristics of the lesion and surrounding tissue.

The MR images were evaluated for the following: signal intensity of the fragment, signal intensity or cysts at the fragment/talar interface, and integrity of the subchondral bone plate. Signal intensities were graded by comparing the fragment signal or interface signal with the surrounding talar medullary space: -2 = markedly decreased to absent signal, -1 = moderately decreased signal, 0 = equal intensity to the talus, +1 = moderately increased but less than joint fluid, and +2 = markedly increased and equal to joint fluid.

In an early clinical case, we mistakenly identified a low-signal, thin stripe within the joint space as a chondral fragment. We evaluated each image for the presence or absence of this line to determine whether its appearance varied with imaging plane or imaging variables.

## Results

The two stable osteochondral fragments had fragment signal intensities of -2 on T1-weighted images and -2 and +1 on T2-weighted images (Fig. 1). All 11 partially attached or unattached fragments had -1 or -2 signal intensity on T1-weighted images (Fig. 2). The signal intensity on T2-weighted images of these 11 fragments ranged from -2 to +2, without a definite pattern for the different stages (Fig. 2).

The subchondral bone plate was intact on all imaging sequences in the patient with the false-positive diagnosis of an osteochondral lesion and in one of the two patients with stable lesions. The stable lesion in the other patient (Fig. 1) and the 11 partially attached (Fig. 2) or unattached lesions had disrupted subchondral lines on all imaging sequences (Fig. 2).

The seven partially attached lesions all had irregular +1 or +2 high-signal lines at the fragment/talar interface (Fig. 2). The two stable lesions had no increased signal at the interface (Fig. 1). The four completely detached lesions had high-signal joint fluid encircling the fragment (Fig. 3).

Five of the partially attached or unattached lesions had spherical or oval defects in the talus adjacent to the osteochondral defect. These defects were intermediate signal on T1-weighted images and uniform high signal on T2-weighted images, suggesting cysts (Fig. 3).

A crescentic low-signal intraarticular line was noted in various locations in eight of the 14 patients. This line was seen on coronal scans in the medial corner of the joint (Figs. 1 and 3) in seven patients and in the lateral corner in one. On sagittal images it was present posteriorly (Fig. 4) in five patients and anteriorly in two. The line was seen equally well on T1- and T2-weighted images. This line was not due to intraarticular fluid, which had a characteristic low to intermediate signal on T1-weighted images and high signal on T2-weighted images.

## Discussion

These patients presented with symptoms of persistent ankle pain and histories varying from no trauma to an episode of severe trauma. Similar variable presentations have been reported in other series of patients with osteochondral lesions [7, 8]. The clinical diagnosis of this condition is difficult, and plain film radiographs of the ankle are an important first step in the evaluation.

If an osteochondral lesion is detected on plain films, an important issue in the decision for treatment is whether the fragment is attached. In patients with stable fragments that are fixed firmly with fibrous tissue or fibrocartilage, symptoms may be due to overlying cartilage erosions, as noted in two of our patients. These patients would not need arthroscopy if MR showed that the lesion is stable. The decision on whether to immobilize the ankle or to operate can be made more confidently if the MR studies indicate that the lesion is partially attached or unattached. Conventional and computed arthrotomograms [9, 10] have been used in these situations, but these procedures require injection of the joint and the use of ionizing radiation.

In this study, we have shown that MR of the ankle does allow determination of the status of an osteochondral fragment. The most reliable sign of a partially attached fragment was the presence of a thin, irregular, high-signal line on T2-weighted images at the talar interface with the fragment. All seven partially attached fragments had this sign. It was not present in the two healed fragments. Mesgarzadeh et al. [11] have described a similar high-signal line in osteochondritis dissecans of the femoral condyles and also found it valuable in identifying unstable fragments. At surgery, we found that this line represented loose granulation tissue at the unstable

Fig. 1.—Attached osteochondral fragment at arthroscopy.

A. Anteroposterior ankle tomogram shows medial talar bony fragment without bony union.

B. T1-weighted coronal MR image (600/20) shows fragment has -2 signal. Note low-signal intraarticular line (arrow) and low talar signal centrally (arrowheads) due to sclerotic bone.

C. Spin-density-weighted coronal MR image (2000/20) 2 mm anterior to site in B shows intra-articular low-signal line more clearly. Subchondral bone plate appears disrupted (arrow).

D. T2-weighted coronal MR image (2000/90) still shows intraarticular line and disrupted subchondral bone. Fragment intensity is -2.

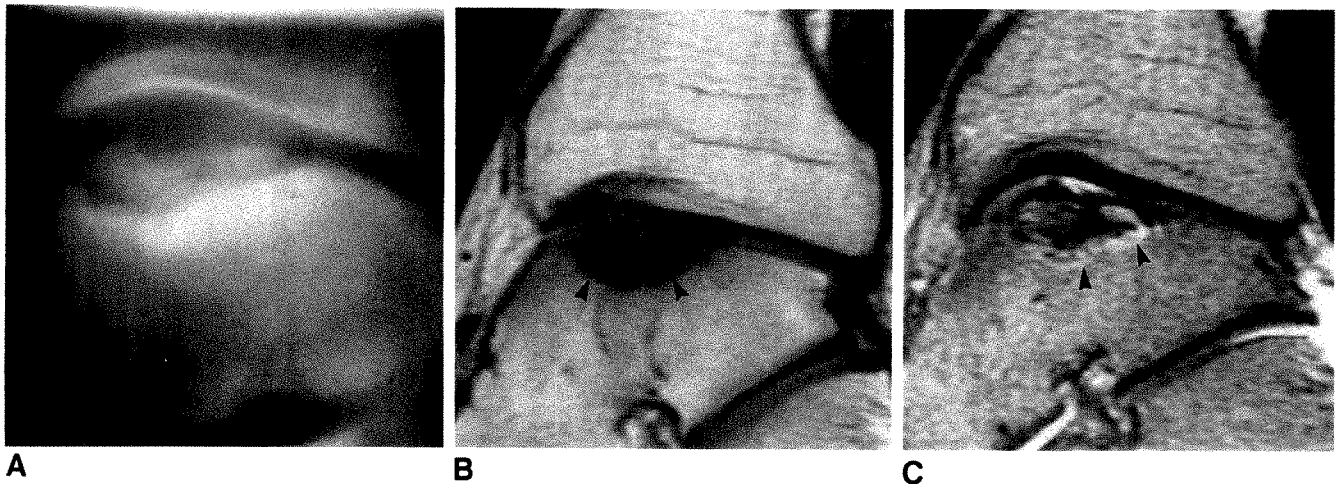
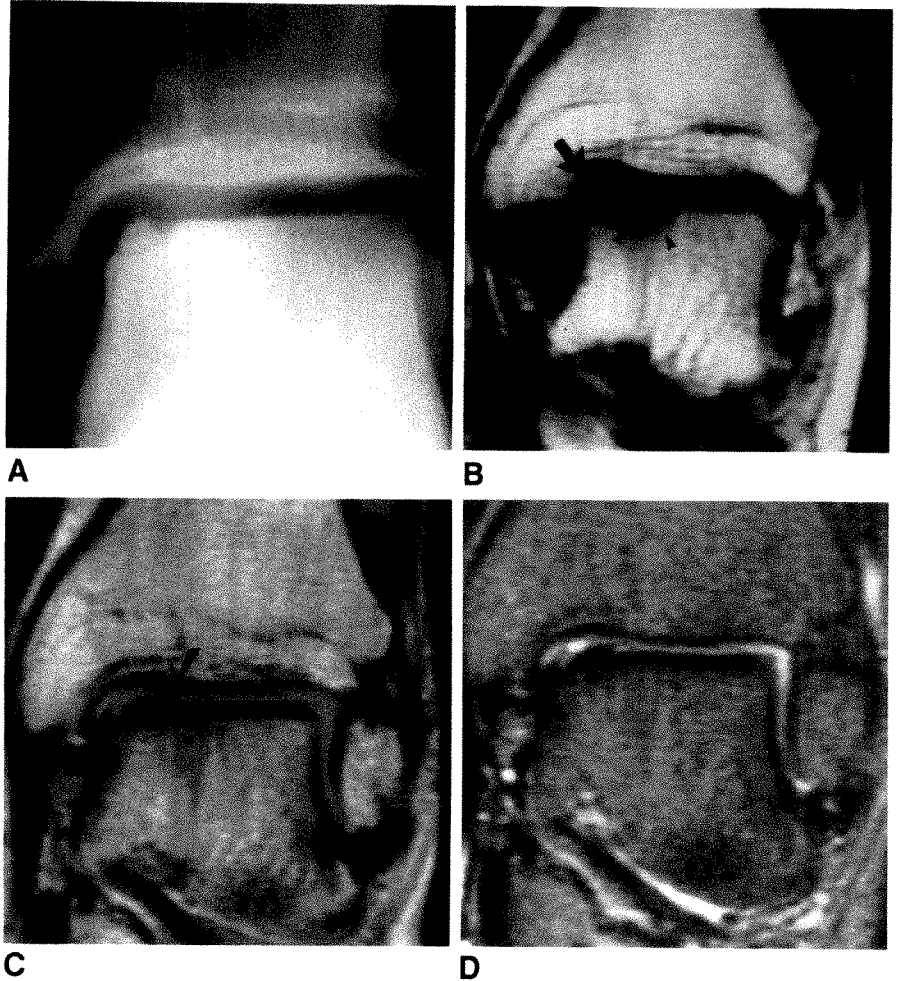


Fig. 2.—Partially attached osteochondral fragment.

A. Lateral hypcycloidal ankle tomogram shows two major fragments with surrounding sclerosis.

B. T1-weighted sagittal MR image (600/20) shows fragments have -1 decreased signal with no signal in sclerotic border (arrowheads). Subchondral bone is disrupted superiorly.

C. T2-weighted-sagittal MR image (2000/90) shows irregular high-signal line at partially attached fragment/talar interface (arrowheads). Signal intensities are 0 in anterior fragment and +2 in posterior fragment. Superior subchondral disruption is seen again.

interface. The four completely unattached fragments were clearly identified on MR images by the presence of a smooth, high-signal fluid line encircling the fragment. Surgery confirmed that these fragments were surrounded by joint fluid.

One report [12] stressed loss of integrity of the cartilage surface as a major finding. We found disruption of the subchondral bone plate in all but one of the loose fragments, but it also occurred with a healed osteochondral lesion.

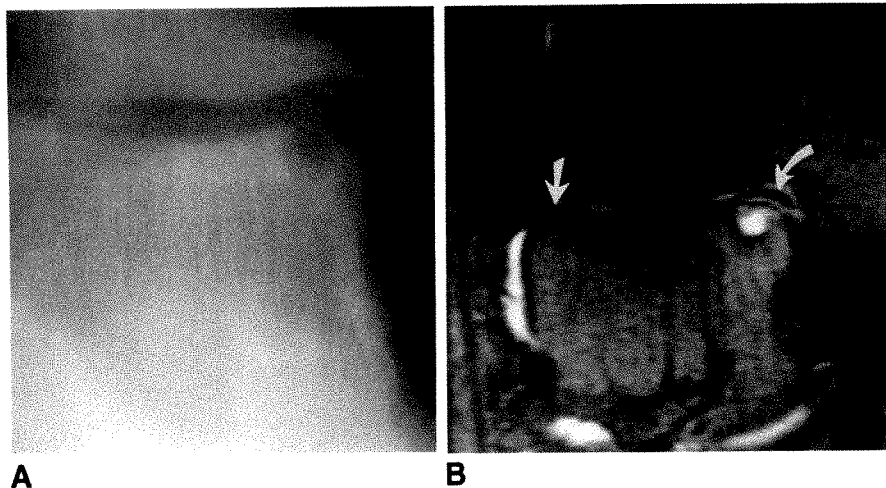


Fig. 3.—Unattached chondral fragment with talar cyst filled with granulation tissue.

A, Anteroposterior ankle tomogram shows medial talar cystic defect.

B, T2-weighted coronal MR image (2000/90) shows high-signal joint fluid outlining thick chondral fragment (curved arrow). Encircling fluid distinguishes fragment from crescentic intraarticular line (straight arrow).

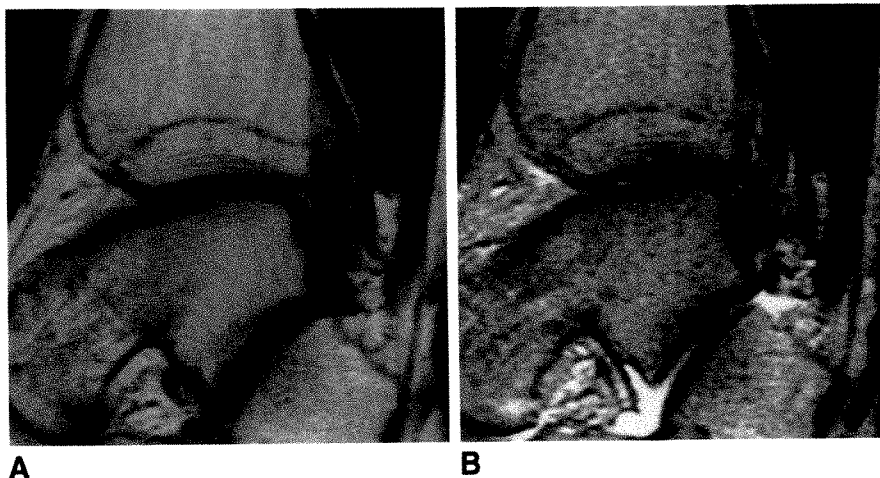


Fig. 4.—False-positive diagnosis of chondral fragment.

A, T1-weighted sagittal MR image (600/20) shows crescentic intraarticular line (arrow).

B, T2-weighted sagittal MR image (2000/90) shows that line persists, mimicking chondral fragment (arrow).

Focal oval or spherical lesions resembling cysts were found at the bases of five of the 11 partially attached or unattached lesions. We had expected that these would be filled with fluid, but at surgery only very loose granulation tissue could be identified. Possibly these defects were traumatic cysts that were filled by the reactive tissue forming at the unstable interface. Alternatively, the granulation tissue may invaginate into weaker areas of trabecular bone. Regardless of the cause, these focal defects were seen only beneath unstable osteochondral lesions in our patients.

Central fragment signal was not useful in distinguishing loose from healed fragments. All fragments had central low signal on T1-weighted images and high, normal, or low signal on T2-weighted images. We could identify no clinical significance of these variable patterns. The low central signal could be due to marrow fibrosis or calcification. The high signal may reflect unabsorbed hemorrhage in the fragments.

The presence of an intraarticular low-signal line has not been reported before. This line was present in both the sagittal and coronal planes and on all imaging sequences. We do not know its cause and could find no surgical explanation such as plica or fibrosis. Because we were unaware of this finding, we made the misdiagnosis of a posterior chondral fragment in one patient (Fig. 4). Physicians who interpret ankle MR images should be aware of this potential source of error.

In summary, MR allows accurate determination of the status of the fragments in chondral and osteochondral lesions of the ankle. With the availability of this new technology, it may

be possible to predict which lesions will heal with conservative therapy and which will require surgical treatment.

#### REFERENCES

1. Kappis M. Weitere Beitrage zur Traumatisc-Mechanischen Entstehung der "Spontanen" Knorpelablosungen. *Deutsche Zertschr Chir* 1922;71: 13-29
2. Newbert AH. Osteochondral fractures of the dome of the talus. *Br J Radiol* 1979;52:105-109
3. Parisien JS. Arthroscopic treatment of osteochondral lesions of the talus. *Am J Sports Med* 1986;14:211-217
4. Flick AB, Gould N. Osteochondritis dissecans of the talus (transchondral fractures of the talus): review of the literature and new surgical approach for medial dome lesions. *Foot Ankle* 1985;5:165-185
5. Canale ST, Belding RH. Osteochondral lesions of the talus. *J Bone Joint Surg [Am]* 1980;62-A:97-102
6. Bauer M, Jonsson K, Linden B. Osteochondritis dissecans of the ankle. *J Bone Joint Surg [Br]* 1987;69-B:93-96
7. Thompson JP, Loomer RL. Osteochondral lesions of the talus in a sports medicine clinic. *Am J Sports Med* 1984;12:460-463
8. Pritsch M, Horosovski H, Farine I. Arthroscopic treatment of osteochondral lesions of the talus. *J Bone Joint Surg [Am]* 1986;68-A:862-864
9. Smith GR, Winquist RA, Allen NK, Northrop CH. Subtle transchondral fractures of the talar dome: a radiological perspective. *Radiology* 1977; 124:667-673
10. Heare MM, Gillespy T, Bittar ES. Direct coronal computed tomography arthrography of osteochondritis dissecans of the talus. *Skeletal Radiol* 1988;17:187-189
11. Mesgarzadeh M, Sapega AA, Bonakdarpour, et al. Osteochondritis dissecans: analysis of mechanical stability with radiography, scintigraphy, and MR imaging. *Radiology* 1987;165:775-780
12. Yulish BS, Mulopulos GP, Goodfellow DB, Bryan PJ, Modic MT, Dollinger BM. MR imaging of osteochondral lesions of talus. *J Comput Assist Tomogr* 1987;11:296-301

## Subtalar Arthrorisis: Evaluation with CT

Douglas K. Smith<sup>1</sup>  
Louis A. Gilula  
William G. Totty

The surgical implantation of a Silastic wedge into the lateral subtalar joint (subtalar arthrorisis) is designed to restrict the osseous malalignment associated with a flexible or neurogenic flatfoot deformity. We used CT to examine patients who had persistent pain after a subtalar arthrorisis and retrospectively reviewed our experience with CT scans of 13 subtalar implants (seven patients) during a 3.5-year period. The CT scans of four asymptomatic subtalar implants showed each implant in the expected position and orientation, and the findings were considered normal. Conversely, the findings on CT scans of all nine painful implants (seven patients) were interpreted as abnormal. The scans showed oblique orientation of four implants (44%), loosening of three implants (33%), extruded methyl methacrylate in the subtalar joint in two implants (22%), and abnormal calcaneal recession in two implants (22%). Five of the nine painful implants were revised with improvement or resolution of symptoms.

Our experience suggests that CT scanning of the subtalar joint can show the position and orientation of a subtalar implant and identify causes of persistent pain after a subtalar arthrorisis.

*AJR* 154:559-562, March 1990

An arthrorisis, or arthroereisis, is the surgical implantation of a bony or Silastic wedge to prop open a joint. A subtalar arthrorisis is performed by implanting a Silastic wedge into the sinus tarsi; this is an increasingly popular surgical treatment for flexible or neurogenic flatfoot deformities. Because these implants are poorly visualized on plain radiographs, we have used CT to examine patients who have persistent subtalar pain after an arthrorisis. As most radiologists are not aware of this procedure and because we were not able to find a single reference to subtalar arthrorises in the radiologic literature, the goals of this paper are (1) to summarize briefly the surgical technique of a subtalar arthrorisis, (2) to describe the normal coronal CT appearance of a subtalar arthrorisis, and (3) to illustrate the normal and selected abnormal CT appearances of the subtalar joint after a subtalar arthrorisis.

### Subjects and Methods

Seven patients were referred during a 3.5-year period for CT evaluation of persistent subtalar pain after a subtalar arthrorisis. All seven patients were referred by podiatrists and had standard radiographs of the ankle showing no radiographic explanation for the patient's persistent pain. The patients were four girls and three boys; their mean age was 11 years (range, 2-16 years). CT scanning was performed by using a previously described technique [1]. Briefly, the patient was placed supine with the hips and knees flexed and the feet flat on the CT table. Serial coronal CT slices were obtained from the posterior extent of the talocalcaneal joint and extending anteriorly through the talonavicular joint with 2-mm collimation and 2-mm intervals. A bone-optimizing algorithm was used, and both bone and soft-tissue windows were obtained.

Received July 31, 1989; accepted after revision October 13, 1989.

<sup>1</sup> All authors: Mallinckrodt Institute of Radiology, Washington University School of Medicine, 510 S. Kingshighway Blvd., St. Louis, MO 63110. Address reprint requests to L. A. Gilula.

0361-803X/90/1543-0559  
© American Roentgen Ray Society



## Results

The CT scans of the four asymptomatic subtalar implants (four patients) were compared with the description of optimal implant position provided by the manufacturer and were interpreted as normal in all four cases (Figs. 1B and 2B). Each implant was oriented vertically with respect to the calcaneus, and the implant articulated normally with the inferior surface of the talus.

The findings on CT scans of all nine painful subtalar implants were interpreted as abnormal. Abnormal lateral orientation was seen with four implants (44%) and was associated with lateral subluxation of the prosthesis with respect to the talus (Figs. 1A and 2A). All four of these abnormally positioned implants were revised with improvement or resolution of symptoms. Continuous lucency of the bone/cement interface consistent with loosening was seen adjacent to three implants (33%) (Fig. 3). In one case, aseptic loosening of the implant was confirmed during surgical revision. The remaining patient (two implants) refused surgical revision. Extruded methyl methacrylate was seen within one subtalar joint of two patients (22%) and was associated with lateral subluxation of the implant in each case (Fig. 2). The extruded methacrylate was confirmed and removed during implant revision. In one

patient, both implants were seated abnormally deep within the calcaneus (22%); this appeared to be the result of excessive resection of the dorsal calcaneus at the time of implantation (Fig. 4). This finding was associated with suboptimal correction of the flatfoot deformity and mild persistent subtalar pain. Surgical revision was not recommended because of the technical difficulty of revising the implants after excessive bone resection and the relatively mild symptoms of the patient.

## Discussion

A flatfoot or pes planus deformity is characterized by excessive talar adduction and subtalar valgus that results in loss of the normal medial plantar arch [2, 3]. Implantation of a Silastic wedge within the sinus tarsi blocks this excessive motion and has been shown to be an effective treatment for flexible flatfoot deformities in selected patients (Fig. 5) [4-8]. The lateral subtalar joint is approached through the sinus tarsi with resection of the anterior 3 mm of the posterior calcaneal facet, decortication of the dorsal calcaneal surface (sulcus calcaneus), and drilling of a vertical fixation hole into the dorsal calcaneus. The fixation stem of the implant is cemented

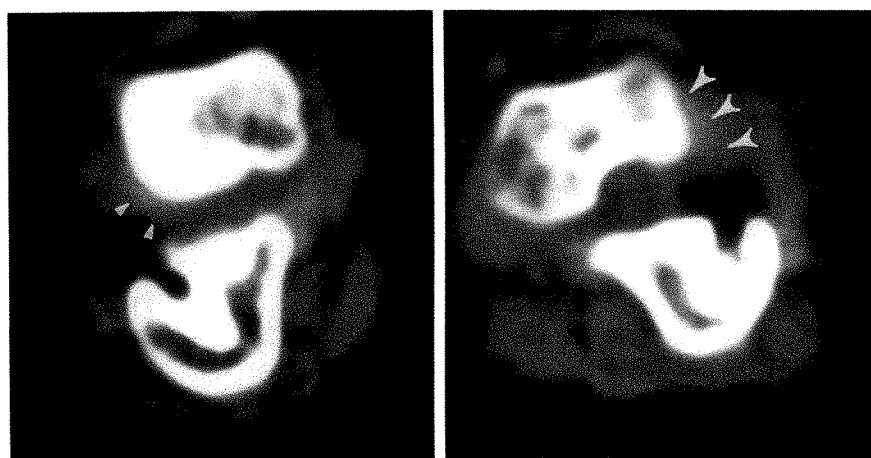


Fig. 1.—Coronal CT scans of bilateral STA-Peg arthroplasties in 4-year-old boy.

A, Oblique orientation of painful right implant with nonossified cartilage of talus (arrowheads) articulating with side of implant.

B, Asymptomatic left implant articulating normally with cartilage of talus (lateral edge outlined by arrowheads).



Fig. 2.—Coronal CT scans of bilateral STA-Peg implants in 15-year-old girl.

A, Abnormal lateral orientation of symptomatic right implant, with talus articulating with side of implant and extruded methyl methacrylate in subtalar joint (arrowhead). Implant was revised with removal of methacrylate.

B, Normal position of asymptomatic left implant.

Fig. 3.—A and B, Coronal CT scans of bilateral STA-Peg implants in 15-year-old girl. Lucencies of bone/cement interfaces are consistent with loosening of prosthesis (arrows). Lucencies are visualized best with bone windows. Patient refused surgery.

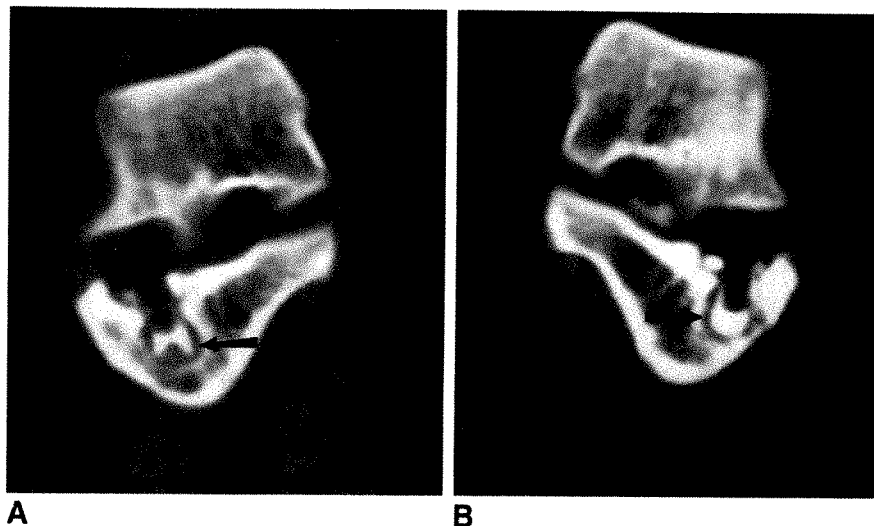
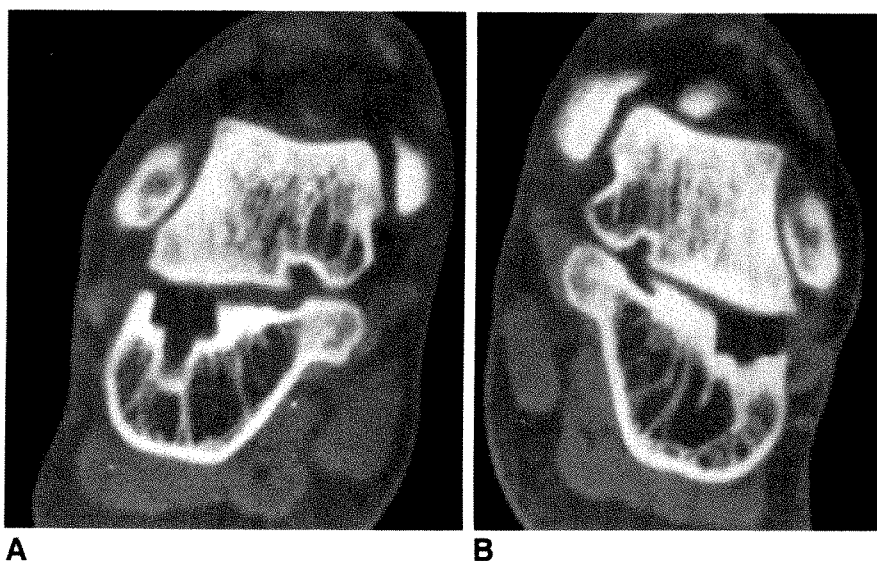


Fig. 4.—A and B, Coronal CT scans of bilateral STA-Peg implants in 11-year-old girl with excessive recession and posterior positioning within calcaneus (left greater than right) associated with suboptimal correction of flatfoot deformities. Abnormal positioning may have resulted from excessive resection of dorsal calcaneus. Surgical revision was not recommended because of technical difficulty of revision and mild symptoms.



into the calcaneal fixation hole with the body of the implant flush against the anterior edge of the posterior facet. The articular surface of the implant articulates with the inferior surface of the talus and props open the posterior subtalar joint. The STA-Peg (Dow Corning Wright, Arlington, TN) is the most commonly used implant and consists of a vertical fixation stem and a horizontal "wedge" or body (Fig. 6) [8]. The implant is available with a flat body (Smith design) or a more popular angled design and with a 9° inclination.

The normal coronal anatomy of the subtalar joint is shown in Figure 7 [1]. The adjacent surfaces of the talus and sulcus calcaneus are gently biconvex, and the talocalcaneal ligament courses obliquely across the sinus tarsi. After a subtalar arthrorrhesis, the fixation stem should be oriented vertically and surrounded by a symmetric sleeve of cement (~0.5 ml) (Fig. 8). The body of the implant should be flush with the resected dorsal surface of the sulcus calcaneus. Oblique orientation of the calcaneal fixation hole may result in the talus articulating with the side rather than the top of the implant (Fig. 9). Oblique orientation of the fixation hole was seen in four (44%) of nine painful implants and tended to be seen in the younger patients (mean age, 8 years). None of the four asymptomatic implants were oriented obliquely. Extruded methyl methacrylate was

seen within the subtalar joint in two cases with oblique orientation of the fixation stem (Fig. 2A). The extruded cement was seen along the medial aspect of the implant and was hidden from the view of the surgeon by the implant. This extruded cement can become a loose body in the subtalar joint.

Continuous lucency of the bone/cement interface was considered highly suggestive of loosening and was seen in the CT scans of three painful implants at an average of 9 months after implantation. Prosthetic loosening may occur in the presence or absence of infection. In one of our cases, aseptic loosening was confirmed during surgical revision [9]. In the remaining patient (two implants), who refused surgical revision for loosening (Fig. 3), no clinical evidence of sepsis (fever or leukocytosis) was seen.

CT may show an abnormally low seating of the implant within the calcaneus. This may be the result of excessive resection of the dorsal calcaneal surface at the time of surgery and in our two cases was associated with suboptimal correction of the flatfoot deformities (Fig. 4).

At our institution, CT scanning has become the preferred imaging technique for the evaluation of painful subtalar arthrorrhesis. MR imaging was used to examine one symptomatic

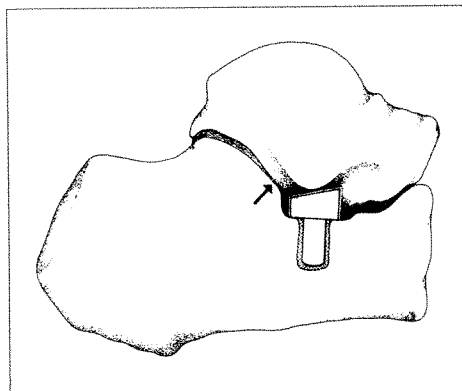


Fig. 5.—Schematic drawing shows normal position of STA-Peg (angled design) implant cemented within sinus tarsi just anterior to posterior subtalar facet (arrow).

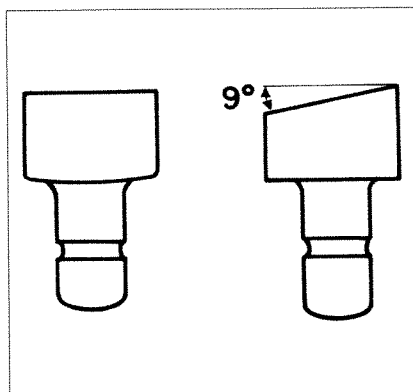


Fig. 6.—Schematic drawing shows Silastic STA-Peg prosthesis as viewed from lateral projection. Original Smith design (left) has a quadrilateral body attached with fixation stem cemented into dorsal calcaneus. More popular angled design (right) is wedge shaped (greater height anteriorly) for further resistance to anterior talar adduction.

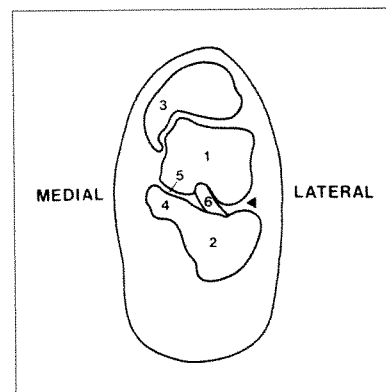
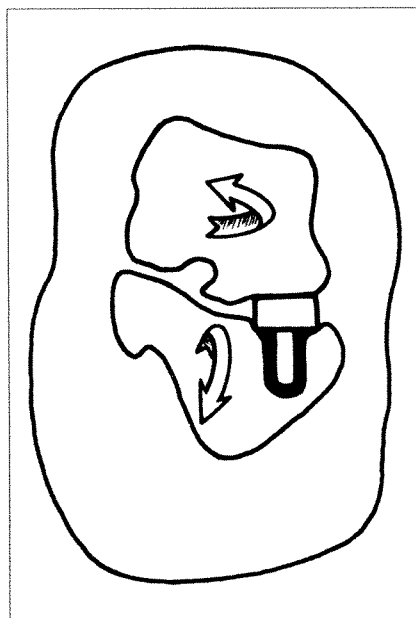
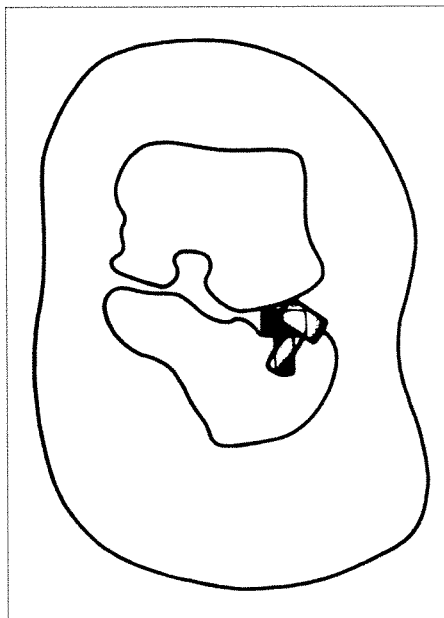


Fig. 7.—Schematic drawing shows coronal slice through sinus tarsi (arrowhead) just anterior to posterior facet. 1 = talus, 2 = calcaneus, 3 = medial malleolus (tibia), 4 = sustentaculum tali, 5 = middle subtalar facet joint, 6 = talocalcaneal interosseous ligament. Surfaces of lateral talus and calcaneus (above and below arrowhead) are gently biconvex in region of STA-Peg insertion.



8



9

Fig. 8.—Schematic drawing shows normal position of STA-Peg implant in coronal plane. Fixation peg is oriented vertically and is surrounded by a symmetric sleeve of cement (shaded area). Flush seating on dorsal calcaneus and talar articulation are normal. Subtalar implant blocks subtalar valgus (calcaneal curved arrow) and maintains talus in an abducted position (talar curved arrow).

Fig. 9.—Schematic drawing shows STA-Peg implant with abnormal lateral direction of fixation hole (white implant) and talus articulating with side of implant. Talus articulates with body of normally oriented implant (black implant).

patient after a subtalar arthrorisis; however, MR did not visualize the bony structures and cement as well as CT scanning did. A subtalar arthrorisis is an uncommon but increasingly popular surgical treatment for pes planus. It is hoped that this paper will familiarize radiologists with the technique of a subtalar arthrorisis, the normal postoperative CT appearance, and some examples of abnormal implant orientation or fixation that may be encountered when evaluating these implants with CT.

## REFERENCES

- Solomon M, Gilula L, Oloff J, Compton T. CT scanning of the foot and ankle: normal anatomy/clinical application and review of the literature. *AJR* 1986;146:1192-1214
- Cowell HR. Pes planus. In: Evans CM, ed. *Surgery of the musculoskeletal system*. New York: Churchill Livingstone, 1983:59-78
- Tachdjian MO. Flexible pes planovalgus (flat foot). In: Tachdjian MO, ed. *The child's foot*. Philadelphia: Saunders, 1985:556-597
- Lanham R. Indication and complications of arthroereisis in hypermobile flatfoot. *J Am Podiatr Med Assoc* 1979;69:178-185
- LeLievre J. Current concepts and correction in the valgus foot. *Clin Orthop* 1970;70:43-55
- Smith S, Millar E. Arthrorisis by means of a subtalar polyethylene peg implant for correction of hindfoot pronation in children. *Clin Orthop* 1983;181:15-23
- Smith S. The STA operation for the pronated foot in childhood. *Clin Podiatr* 1984;1:165-173
- STA-Peg subtalar arthrorisis implant technique manual. Arlington, TN: Dow Corning Wright, 1987
- Stauffer RN. Ten-year followup study of total hip replacement: with particular reference to roentgenographic loosening of the components. *J Bone Joint Surg [Am]* 1982;64-A:983-990

## Pictorial Essay

# Radiologic Appearance of Intramuscular Hemangioma with Emphasis on MR Imaging

Peter C. Buetow,<sup>1</sup> Mark J. Kransdorf,<sup>1,2</sup> Richard P. Moser, Jr.,<sup>2,3</sup> James S. Jelinek,<sup>1,2</sup> and B. Hudson Berrey<sup>4,5</sup>

Intramuscular hemangiomas are a subset of benign vascular lesions of skeletal muscle. Although terminology often is confusing, usually these lesions are classified according to the size of the vessels within the tumor. All hemangiomas contain variable amounts of nonvascular tissue such as fat, smooth muscle, fibrous tissue, myxoid stroma, hemosiderin, thrombus, and even bone [1]. These nonvascular components are most prominent in cavernous or large-vessel hemangiomas; this is especially true of adipose tissue [1]. The MR appearance of intramuscular hemangioma reflects this gross morphology, and in many cases MR may provide a presumptive diagnosis.

The imaging studies of 11 patients with intramuscular hemangiomas were reviewed, and the findings on radiography, angiography, CT, and MR are illustrated. Lesions that mimic intramuscular hemangiomas are also shown and distinguishing features are discussed.

## Materials and Methods

The MR imaging studies of 11 patients with intramuscular hemangioma were reviewed retrospectively in a nonblinded fashion. The group included seven males and four females 3–36 years old (mean, 20). Hemangiomas occurred in the calf (three), thigh (two), arm (two), and foot (one). Two patients had extensive involvement of the upper

extremity, and one had diffuse involvement of the chest wall and back. This group was selected from 135 patients in whom soft-tissue masses of diverse causes were evaluated with MR at Walter Reed Army Medical Center, Washington, DC.

The diagnosis of intramuscular hemangioma was established in accordance with commonly accepted histologic criteria after biopsy in eight cases. In the remaining three cases, the diagnosis was established by characteristic radiographs showing phleboliths in two. In the final case, the diagnosis was established by characteristic MR findings in conjunction with the clinical history of a soft, easily compressed, vascular mass with a bluish tinge that did not change in size or character over time. Two patients had previous surgery and recurrent or residual disease.

All patients had MR imaging, including gradient-recalled acquisition in the steady state (GRASS) sequences in four patients. In addition, nine patients had CT (seven with contrast-enhancement), eight had plain radiography, five had technetium-99m methylene diphosphonate bone scintigraphy with both flow and blood-pool images, four had angiography, and one had venography.

All MR scans were obtained on a GE 1.5-T Signa (General Electric, Milwaukee, WI) or a 1.5-T Teslacon (Technicare, Solon, OH) scanner, except one, which was obtained on a 0.5-T Picker (Picker International, Highland Heights, OH) scanner. Typical scanning sequences included spin-echo (SE) T1-weighted, 300–750/20–34 (TR/TE), and T2-weighted, 1800–2500/80–100, pulse sequences in each plane. At least two orthogonal planes were imaged in every case. The field of view ranged from 12 to 40 cm, the number of signal averages from two to four, and the slice thickness from 5 to 10 mm with a 20–100%

Received August 24, 1989; accepted after revision October 12, 1989.

The opinions or assertions contained herein are the private views of the authors and are not to be construed as official or as reflecting the views of the Department of the Army, the Department of Defense, or the Uniformed Services University of the Health Sciences.

<sup>1</sup> Department of Radiology, Walter Reed Army Medical Center, Washington, DC 20307-5001.

<sup>2</sup> Department of Radiology and Nuclear Medicine, Uniformed Services University of the Health Sciences, Bethesda, MD 20814.

<sup>3</sup> Department of Radiologic Pathology, Armed Forces Institute of Pathology, Washington, DC 20306-6000. Address reprint requests to R. P. Moser, Jr.

<sup>4</sup> Department of Orthopedic Surgery, Walter Reed Army Medical Center, Washington, DC 20307-5001.

<sup>5</sup> Department of Surgery, Uniformed Services University of the Health Sciences, Bethesda, MD 20814.

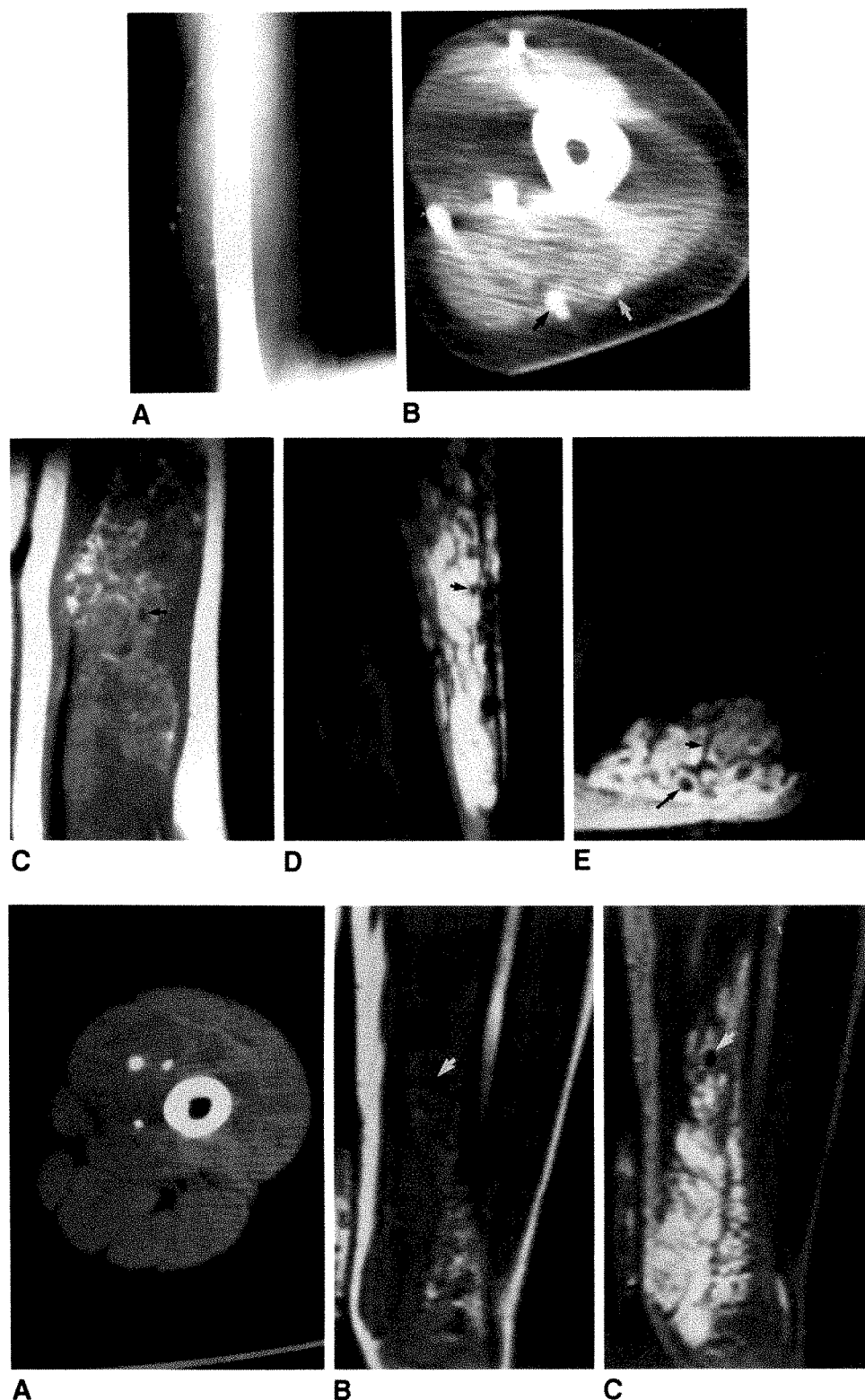


Fig. 1.—Intramuscular hemangioma of triceps in a 23-year-old woman.

A, Radiograph of arm shows multiple phleboliths in soft tissues, suggesting intramuscular hemangioma.

B, Axial contrast-enhanced CT scan confirms presence of phleboliths (arrows) within poorly defined soft-tissue mass. Contrast-enhanced veins could be distinguished from phleboliths on serial axial images.

C, Coronal T1-weighted MR image, 500/20, shows fat distributed in lacelike pattern throughout hemangioma. Subtle signal voids represent phleboliths (arrow).

D, Sagittal gradient-echo MR image, 100/25/10° flip angle, shows high signal intensity compatible with marked vascularity of hemangioma. Within mass are signal voids (arrow) due to phleboliths, also seen on radiograph (A).

E, Axial T2-weighted MR image, 2000/100, shows hemangioma is hyperintense relative to subcutaneous fat. Linear regions isointense relative to skeletal muscle (short arrow) and signal voids representing phleboliths (long arrow) are seen within hemangioma.

Fig. 2.—Intramuscular hemangioma of thigh in a 6-year-old girl.

A, Axial unenhanced CT scan clearly shows phleboliths within soft-tissue mass, although margins of hemangioma are not well defined.

B and C, Corresponding coronal T1-weighted, 600/20, (B) and T2-weighted, 2000/80, (C) MR images show lesion is isointense with regard to skeletal muscle on T1-weighted image, with lacelike areas of increased signal corresponding to fat interposed between vascular elements. Because of lesion's hyperintensity, its extent is clearly visualized on T2-weighted image.

gap depending on the body part imaged. GRASS images (25–100/13–25) were obtained with a 10–30° flip angle.

## Results

On T1-weighted SE images, the hemangiomas were typically isointense relative to skeletal muscle and had poorly

delineated or imperceptible margins. Within the hemangiomas were areas of increased signal approximating that of subcutaneous fat. These were noted in nine cases and varied from fine, delicate, lacelike, or linear strands (Figs. 1C and 2B) to coarse, linear bands (Fig. 3B). Fatty signal predominated in two cases (Fig. 4). On T2-weighted SE images, the heman-



Fig. 3.—Hemangiomatosis of upper extremity in a 3-year-old boy.

A, Radiograph of hand and wrist shows extensive soft-tissue involvement and hypertrophy, with overgrowth of bones.

B and C, Coronal T1-weighted, 600/20, (B) and T2-weighted, 2000/80, (C) MR images of arm show foci of both hyperintense (long arrows) and hypointense (short arrows) signals, corresponding to interlaced fibrous and fatty elements, respectively.

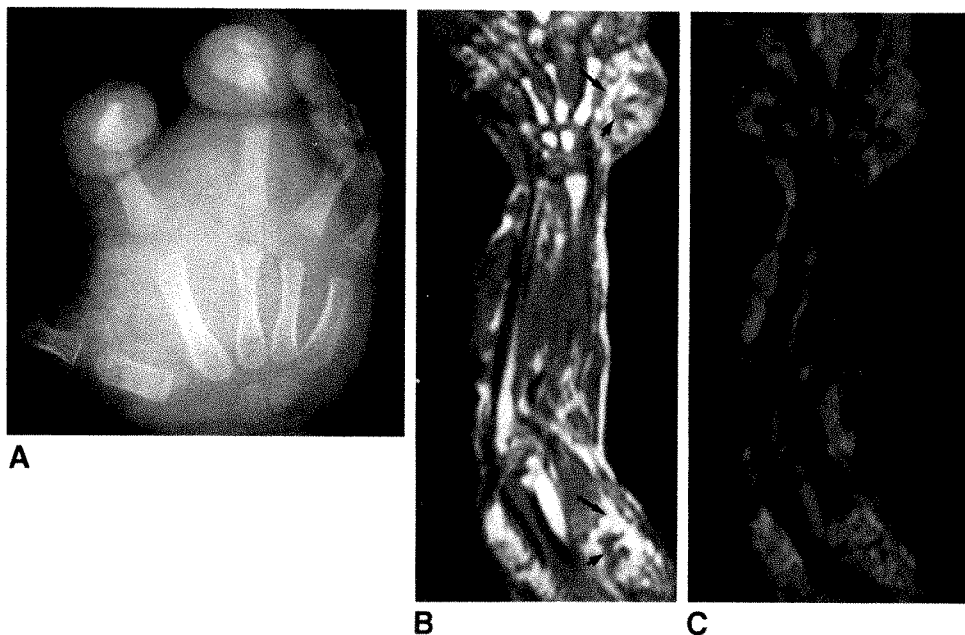


Fig. 4.—Intramuscular hemangioma of thigh in a 24-year-old man.

A, Axial contrast-enhanced CT scan shows mostly fatty mass posterior to femoral neck. Phleboliths (arrow) were not apparent on radiograph (not shown).

B, Axial T1-weighted MR image, 700/32, confirms fatty nature of hemangioma. Within mass are signal voids (arrow) due to phleboliths, corresponding to those noted on CT.

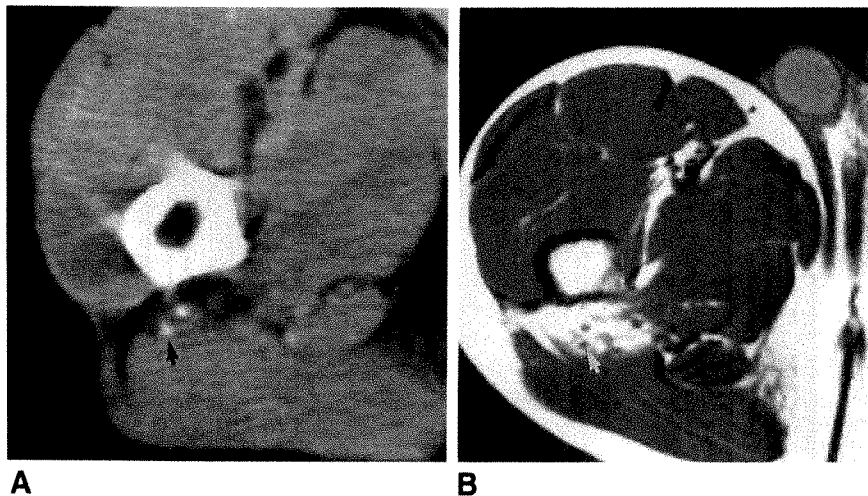
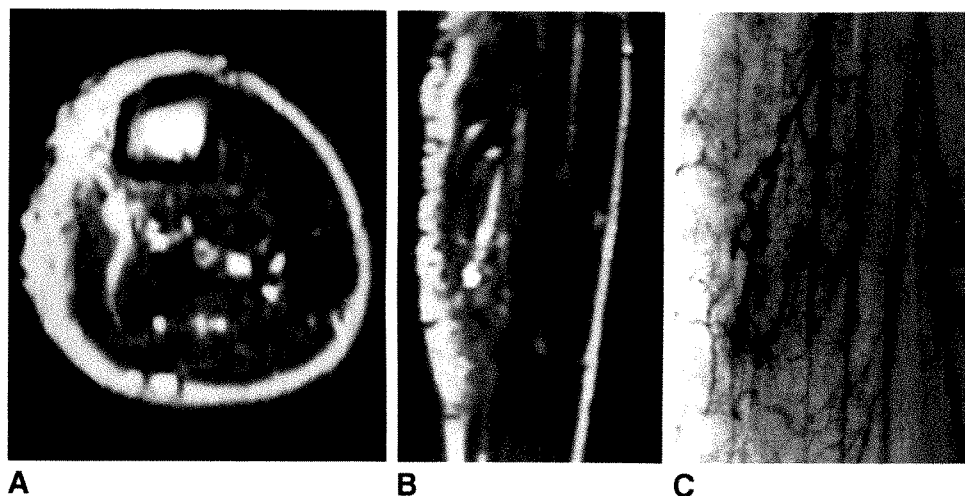
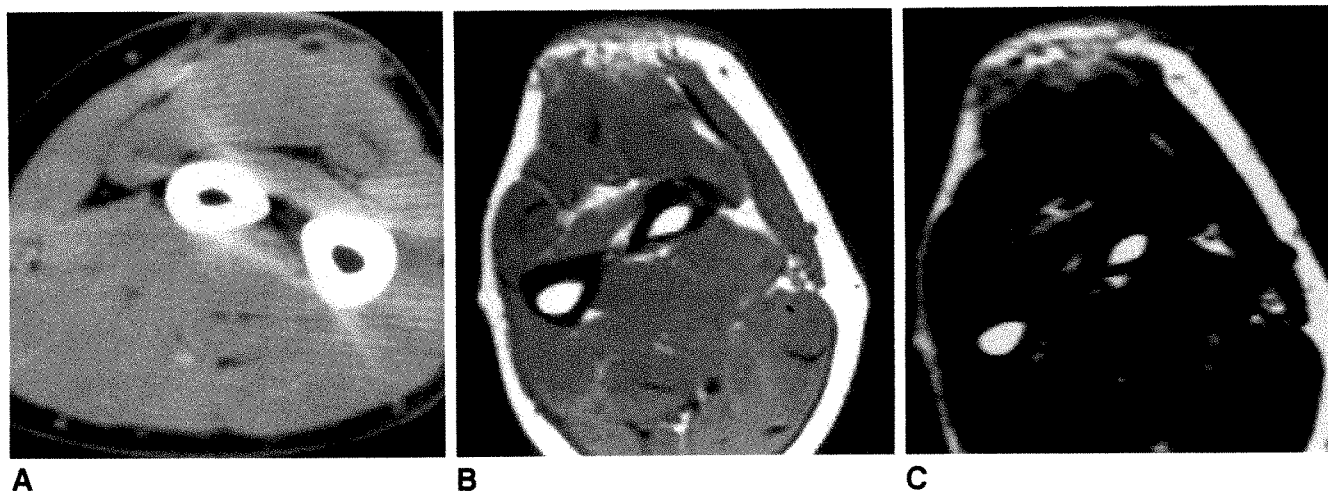


Fig. 5.—Intramuscular hemangioma of left lower leg in a 20-year-old man.

A and B, Axial (A) and coronal (B) T2-weighted MR images, 2000/80, show hemangioma in gastrocnemius muscle, with extension into adjacent subcutaneous fat. More typical pattern seen in Figs. 1–3 is absent. Overgrowth of tibia and soft tissues is readily apparent.

C, Corresponding arteriogram shows nonspecific neovascularity, with “puddling” of contrast material and subtle tumor blush.





**Fig. 6.**—High-grade malignant fibrous histiocytoma of forearm in a 45-year-old man.  
**A**, Axial contrast-enhanced CT scan shows poorly defined soft-tissue mass infiltrating subcutaneous fat.  
**B** and **C**, Corresponding axial T1-weighted, 700/34, (**B**) and T2-weighted, 2000/80, (**C**) MR images show malignant fibrous histiocytoma lacks lacelike fatty pattern typically seen in hemangiomas on T1-weighted images and also lacks typical hyperintense signal seen on T2-weighted images. Lesion infiltrates subcutaneous fat and mimics many findings seen in hemangioma in Fig. 5.

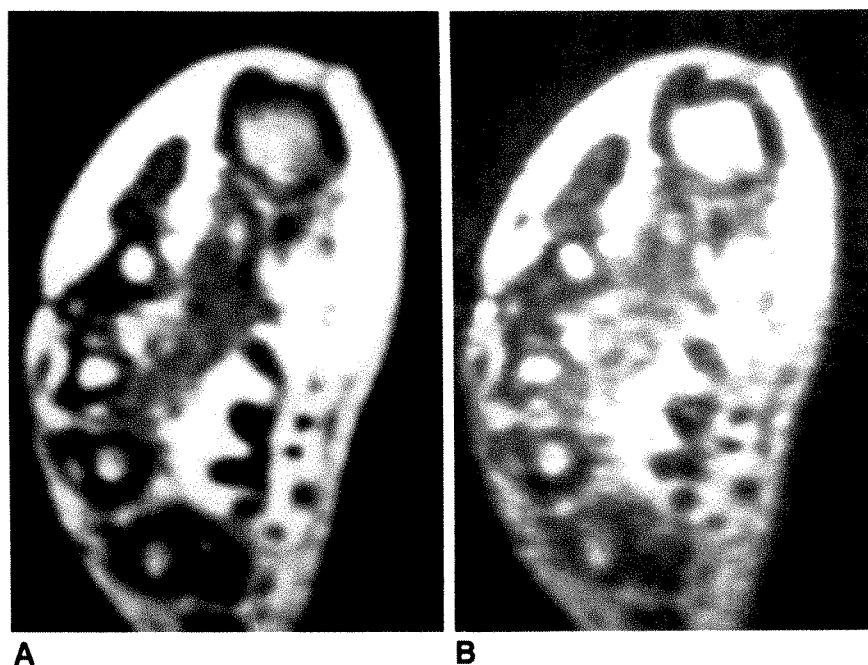


**Fig. 7.**—Lipomatosis of right hand in a 5-month-old boy.

**A** and **B**, Axial T1-weighted, 500/30, (**A**) and T2-weighted, 2500/80, (**B**) MR images show diffuse fatty overgrowth throughout right hand and wrist. Bony overgrowth was better visualized on plain radiographs (*not shown*). Lesion is mostly fatty and mimics those hemangiomas in which fat predominates. Typical features such as hyperintensity on T2-weighted images and lacelike fibrofatty septa are absent.

giomas were typically hyperintense as compared with subcutaneous fat, and the margins were relatively well defined. Within the hemangiomas were areas that were isointense relative to fat and muscle (Figs. 1E and 2C). These were typically linear in configuration. Phleboliths were identified easily in one case (Figs. 2B and 2C) and retrospectively in two additional cases (Figs. 1C–1E and 4B). Phleboliths could not be identified with MR in a fourth case in which they were readily apparent on both plain radiographs and CT scans. Extension of the tumor into the subcutaneous fat was apparent in three cases (Figs. 3 and 5).

On CT, the hemangiomas typically were poorly defined, with tissue attenuation approximating that of skeletal muscle, and contained areas of decreased attenuation, some approaching fat (Figs. 1B and 4A). Phleboliths were identified in four lesions (Figs. 1B, 2A, and 4A); in three of these, they were easily identified on plain radiographs. Two lesions were mostly fatty, thereby allowing confident delineation of their margins (Fig. 4A).

Plain radiographs were available in nine cases. Phleboliths were seen in four (Fig. 1A), and two showed bone overgrowth (Figs. 3 and 5). The patient with extensive chest wall involve-

ment had marked rotatory scoliosis. Three of the five scintigrams showed increased blood-pool activity; two of these also showed increased flow. There was no evidence of increased bone activity.

Three of four hemangiomas assessed angiographically showed small areas of neovascularity and tumor blush (Fig. 5). All showed some small abnormal draining veins. No dominant abnormal feeding vessels could be identified. No arterial abnormality was detected in the final tumor, which was mostly fatty. The single venogram showed an extensive network of dilated draining veins.

## Discussion

The MR appearance of intramuscular hemangiomas reflects the morphology: benign vascular masses containing nonvascular elements such as fat, fibrous and myxoid tissue, smooth muscle, thrombus, and bone [1]. Tumors composed mostly of small vessels (diameter < 20 RBCs) are small-vessel or capillary hemangiomas, whereas those with mostly larger vessels are large-vessel, cavernous, or venous hemangiomas. Mixed-type hemangiomas are composed of large and small vessels in about equal proportions [1]. Cavernous hemangiomas are larger than capillary hemangiomas and usually contain more nonvascular tissue. This is especially true of adipose tissue, so much so that portions of the cavernous hemangioma may be indistinguishable from a lipoma [1]. These nonvascular tissues may be encountered to a lesser extent in mixed-type hemangiomas, and small quantities may be noted in capillary hemangiomas [1]. It is the combination of larger vessels (containing stagnant blood) and nonvascular elements (predominantly fat and fibrous tissue) that produces a characteristic MR appearance (Figs. 1–5).

The marked hyperintensity of these hemangiomas on T2-weighted SE images is related to the increased free water present within the stagnant blood found in the larger vessels of these lesions. Low-signal linear structures throughout the lesion represent the fibrofatty septa between vessels [2]. Lacelike and linear fat signal within the tumor represents fat

between the vascular elements—a feature not emphasized previously as characteristic of hemangioma.

Previous reports [3, 4] have shown the superiority of MR over CT or angiography in delineating the extent of these lesions. Dynamic CT may show contrast enhancement of curvilinear structures with attenuation values similar to those of vessels. CT was more sensitive in detecting phleboliths but did not delineate the extent of the hemangiomas well, except for the two that were mostly fatty (Fig. 4).

The appearance of hemangiomas might be mimicked by rare vascular tumors, such as hemangioendotheliomas or angiosarcomas, but the MR findings in these rare tumors have not been described yet. Tumors that infiltrate the subcutaneous fat (Fig. 6) or are primarily fatty (Fig. 7) may resemble hemangiomas but do not exhibit all of the features encountered in typical hemangiomas, such as lacelike fibrofatty septa, hyperintense T2 signal, and phleboliths. Hemorrhagic lesions might display a similar signal intensity at some point in their evolution, but an accompanying septated pattern would be unusual.

In no instance did angiography establish the diagnosis, but it assisted in planning the surgical approach. Bone scintigraphy could be used confidently to exclude bone involvement, but provided no information not readily derived from MR.

In summary, intramuscular hemangiomas are benign vascular lesions that may contain considerable amounts of nonvascular tissue. This underlying morphology is reflected on MR, which allows a presumptive diagnosis in most cases.

## REFERENCES

1. Allen PB, Enzinger FM. Hemangioma of skeletal muscle: analysis of 89 cases. *Cancer* 1972;29:8–22
2. Livine E, Wetzel LH, Neff JR. MR imaging and CT of extrahepatic cavernous hemangiomas. *AJR* 1986;147:1299–1304
3. Rauch RF, Silverman PM, Korobkin M, et al. Computed tomography of benign angiomatous lesions of the extremities. *J Comput Assist Tomogr* 1984;8:1143–1146
4. Burrows PE, Mulliken JB, Fellows KE, Strand RD. Childhood hemangiomas and vascular malformations: angiographic differentiation. *AJR* 1983;141:483–488

## Book Review

**Handbook of Breast Imaging.** Edited by Mary Ellen Peters, Dawn R. Voegeli, and Kathleen A. Scanlan. New York: Churchill Livingstone, 344 pp., 1989. \$65

The editors of this book, which has several authors, have endeavored to produce a practical introduction to mammography and a study guide for those who are preparing for board examinations. The images are generally of excellent quality and large enough to show the pertinent findings. Arrows are used judiciously. Many variations of the normal and pathologic provide a complete spectrum of mammographic changes.

An excellent chapter on breast anatomy and physiology is clear and concise, with abundant clinical correlation. The detailed and practical chapter on the physics of screen-film mammography is a highlight and contains sections on grids, film processing, phototimers, pitfalls in comparison of mammography equipment, and quality assurance. Criticism might be leveled at the preference for the star method, which tends to underestimate focal spot size in comparison with pinhole and slit measurements.

A timely chapter devoted to fibrocystic changes neatly summarizes the results of the 1985 American College of Pathology Consensus Meeting, noting that only women with a biopsy-proved diagnosis of atypical ductal or lobular hyperplasia are to be considered at moderately increased risk for cancer and that most women with other fibrocystic changes are at no or only slight increased risk. The histologic descriptions would have been enhanced by photomicrographs. A brief chapter on the benign postsurgical breast provides many clues for differentiation of scar from carcinoma and offers the caveat that a prosthesis often precludes a satisfactory mammogram.

The chapter on sonography emphasizes that the chief role of this technique is the differentiation of cystic from solid masses and that it cannot be substituted for mammography as a screening test. The mammography report is treated in a short but pithy chapter that includes suggested phrasings about the limitations of mammography. Other chapters are devoted to benign and malignant disorders, positioning the patient, the postsurgical and irradiated breast, the male breast, galactography, and preoperative localization of nonpalpable lesions. This last chapter fails to mention the usefulness of pneumocystography to rule out an intracystic tumor when an unsuspected cyst is punctured during preoperative needle localization. Instead, follow-up films in 3–6 months are recommended.

The book has a few major disappointments: The chapter on breast

pathology includes misinformation and out-of-date information. For example, the incidence of breast cancer does *not* peak at the menopause; it rises progressively with advancing age except for an abrupt and temporary *dip* at the menopause. A table on TNM classification for staging is obsolete, being derived from 1962 data. The other tabular data and most of the suggested readings in this chapter are 15 to 20 years old. The chapter on clinical diagnosis is disappointing because it lacks application to mammography. For example, it maintains that a correct clinical diagnosis of fibroadenoma can be made in most instances, and no recommendation is made about the need for histologic confirmation or follow-up by mammography or sonography. Fine-needle aspiration biopsy of palpable masses is described cursorily without technical details and without discussing the usefulness of mammographic localization of nonpalpable lesions. It is stated that mammography is superfluous for diagnosing a palpable lesion, and the value of this technique for excluding concomitant nonpalpable malignancy is not mentioned.

In some chapters, few or no statements in the text are referenced even though the lists of suggested readings at the end of the chapters are extensive. A chapter on preoperative localization of nonpalpable lesions mentions several methods to overcome the inability to visualize a lesion in more than one view, but the methods are not described or even referenced by number.

Images of the left breast are placed to the left of the images of the right breast. Although convenient for comparison with xeromammograms, this is the reverse of the traditional placement of images on the view box. Adaptation of a standard policy for image placement might prevent biopsy of the wrong breast because the right breast was mistaken for the left.

In summary, the excellent imaging chapters should prove helpful to radiology residents and other physicians seeking an introductory textbook. Revision of the clinical chapters would make the book even more appealing.

Richard H. Gold  
University of California, Los Angeles, School of Medicine  
Los Angeles, CA 90024-1721

# The Significance of Hematuria in Children After Blunt Abdominal Trauma

H. Philip Stalker<sup>1,2</sup>  
Robert A. Kaufman<sup>1,3,4</sup>  
Kurt Stedje<sup>5</sup>

The clinical significance of hematuria in children who sustain blunt abdominal trauma continues to be debated, as do the criteria for diagnostic imaging in this population. Previous reports have discussed the usefulness of certain clinical predictors of renal injury, such as the amount of hematuria present, the presence of shock or of head injury, and the presence or absence of symptoms or findings on physical examination. To assess the value of such predictors of renal injury in children with posttraumatic hematuria, we reviewed and analyzed the medical records and abdominal CT examinations of 256 children with blunt abdominal trauma. One hundred six children (41%) had hematuria. Thirty-five patients (14%) had renal injury that could be diagnosed by using CT. Nine of these had clinically significant injuries according to our criteria. We found a direct relationship between the amount of hematuria and the severity of renal injury. Hypotension at presentation occurred in 38 patients and was an insensitive predictor of renal injury. The combination of hypotension and hematuria was no more sensitive than hematuria alone in predicting renal injury. Sixty patients had concomitant craniofacial injuries. This subgroup had the same prevalence of hematuria and renal injury as the group that did not have head injuries.

There were no clinically occult renal injuries in the study population. Furthermore, we found that no normotensive child with fewer than 50 RBCs per high-power field had a significant renal injury, and conversely, all children with significant renal injuries had either large amounts of hematuria or shock.

*AJR* 154:569-571, March 1990

Received August 14, 1989; accepted after revision October 24, 1989.

Presented at the 31st annual meeting of the Society for Pediatric Radiology, San Diego, CA, April 1988.

<sup>1</sup> Department of Radiology, University of Cincinnati College of Medicine, and Children's Hospital Medical Center, Cincinnati, OH 45229-2899.

<sup>2</sup> Present address: Radiology Associates of Birmingham, 1920 Huntington Rd., Birmingham, AL 35209.

<sup>3</sup> Department of Pediatrics, University of Cincinnati College of Medicine, Cincinnati, OH 45229-2899.

<sup>4</sup> Present address: Department of Radiology, Le Bonheur Children's Medical Center, 848 Adams Ave., Memphis, TN 38103. Address reprint requests to R. A. Kaufman.

<sup>5</sup> University of Cincinnati College of Medicine, Cincinnati, OH 45267.

0361-803X/90/1543-0569

© American Roentgen Ray Society

Hematuria occurs frequently in children after blunt abdominal trauma, but the clinical significance of this finding and its implication for further diagnostic imaging remain uncertain. This study addresses the following questions that have been raised in the recent medical literature: (1) does the amount of hematuria predict the presence and extent of renal injury [1, 2]; (2) is microhematuria with shock a better predictor of renal injury than microhematuria without shock [3, 4]; (3) would significant renal injuries be missed if imaging evaluation was not performed for asymptomatic patients with small amounts of hematuria [4-7]; (4) are patients with head injury more likely to have hematuria than those without such injuries [2, 6]; and (5) are significant renal injuries ever clinically occult in children [2]?

We reviewed the medical records and abdominal CT scans of 256 children with blunt abdominal trauma and compared the clinical, laboratory, and imaging data of children who had renal injury with the data of those who did not.

## Materials and Methods

Between August 1981 and June 1987, 275 children with blunt abdominal trauma and suspected multiorgan injury were examined by abdominal CT at Children's Hospital Medical Center in Cincinnati. The medical records and CT examinations could be retrieved in 256 of these patients, who are the basis of this report.



Children with blunt abdominal trauma were imaged by CT if single or multiple organ injury was clinically suspected on the basis of physical findings, laboratory evaluation, or the circumstances of injury. All patients who were studied were judged to be hemodynamically stable after appropriate fluid and pharmacologic resuscitation in the emergency department. Examinations were performed either on a GE 8800 or a GE 9800 scanner; oral contrast medium and IV contrast medium given as a bolus were used. Oral contrast medium was omitted when the clinical situation dictated so. CT studies were performed by using dynamic scanning with rapid table incrementation. Details of our criteria for selecting patients and the examination technique have been published [8, 9]. Children with pelvic injuries and fractures were included in the analysis if abdominal injury was suspected clinically.

For each patient, we recorded clinical and laboratory data including the microscopic and dipstick urinalyses, systolic and diastolic blood pressure, hematocrit, symptoms, physical findings, Foley catheter placement and time of placement, and complications of renal injuries. The actual laboratory report of the amount of hematuria was recorded, but only the upper limit of the reported range of RBCs per high-power field (RBC/HPF) was used in data analysis. For this study, hematuria was defined as more than 5 RBC/HPF [10]. The initial systolic and diastolic blood pressures were recorded, whether they were obtained in the emergency department or at the scene of the accident. In some cases, fluid or pharmacologic resuscitation had been performed before the first recording of the blood pressure. For purposes of analysis, hypotension was defined as a systolic or diastolic pressure more than two standard deviations below the mean for that age [11].

Renal injuries were graded I–V according to the scheme of Karp et al. [2]. Grade I injury included a small parenchymal injury without subcapsular or perirenal fluid, an uninjured anomaly. Grade II injury included an incomplete renal laceration, a small amount of subcapsular or perirenal fluid. Grade III injury represented extensive laceration or fracture, large perirenal fluid collection. Grade IV was a shattered kidney, multiple fragments. Grade V represented any vascular injury. For the purpose of this study, significant renal injury was defined as grade III or greater. In addition, we recorded the following: side of trauma, precise location of injury (upper third, middle third, lower third; central or peripheral), percentage volume of injured renal tissue, the presence and volume of perirenal fluid, and the presence of associated intraperitoneal and extraperitoneal injuries including head injuries.

## Results

Of the 275 consecutive patients examined during the study period, medical records and imaging studies were available for 256. There were 170 boys (66%) and 86 girls (34%). The age range was 1–17 years (mean, 7.4 years; standard deviation, 4.1 years).

Thirty-five patients (14%) had renal injury that could be diagnosed by using CT. The distribution of injuries was as follows: 15 patients had grade I injuries, 11 had grade II injuries, five had grade III injuries, one had grade IV injury, and three patients had grade V injuries. Nine patients had injuries of grade III or greater.

One hundred six children (41%) presented with hematuria (Table 1). Of these, 31 (29%) had renal injury on CT. Of the 150 children who presented without hematuria, 146 had normal kidneys, and four had renal injuries (one renal pedicle injury; three small, nondescript, parenchymal hypodensities). Although these hypodensities may have represented small,

TABLE 1: Hematuria vs Renal Injury

Hematuria	Renal Injury (%)	No Renal Injury (%)	Patients (%)
Present	31 (12)	75 (29)	106 (41)
Absent	4 (2)	146 (57)	150 (59)
Totals	35 (14)	221 (86)	256 (100)

preexisting lesions or minor atraumatic abnormalities, we counted them as injuries.

A direct relationship was seen between the amount of hematuria and the severity of renal injury (Fig. 1). The mean number of RBCs on microscopic urinalysis increased as the grade of renal injury increased. In children who had little or no renal injury, RBC/HPF varied from 0 to more than 99. In children with more severe grades of renal injury ( $\geq$  grade III), the amount of hematuria was at least 99 RBC/HPF in all patients but one, a child with a renal pedicle injury who presented in shock but without hematuria.

Thirty-eight patients had either systolic or diastolic hypotension at presentation. Six of these (16%) had imageable renal injuries, two of which were grade III or greater. Sixty patients had craniofacial injury. None of these had renal injuries without significant laboratory or physical abnormalities. This also was true in children whose abdomens were thought to be unassessable because of their depressed state of consciousness or because of previous IV administration of pancuronium bromide. Patients with head injuries had the same prevalence of hematuria (45%) and renal injury (12%) as those without head injuries (41% and 14%, respectively) ( $p > .05$ ).

## Discussion

In our study group, the amount of hematuria predicted both the presence and severity of renal injury. We found that the

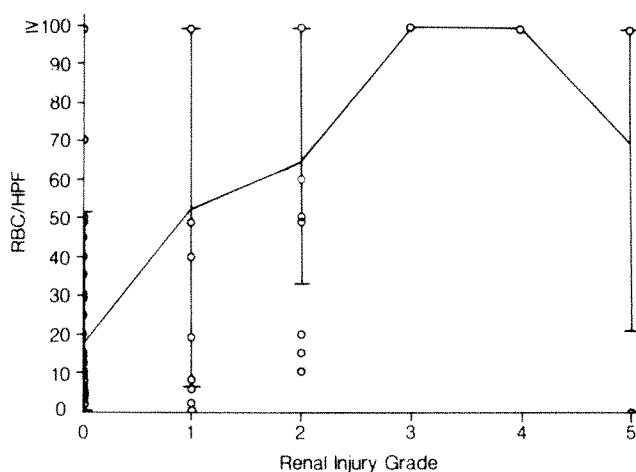


Fig. 1.—Graph shows direct relationship between amount of hematuria and severity of renal injury. Microscopic hematuria increased as grade of renal injury increased. RBC/HPF = RBCs per high-power field.

larger the number of RBCs in the urine, the greater the probability of significant renal injury. This is in contradistinction to the work of Karp et al. [2], who found that hematuria predicted the presence of renal injury but not the severity. As indicated, there was one notable exception in our group: a child with grade V renal injury who presented without hematuria.

These data show that significant renal injuries ( $\geq$  grade III) would not have been missed if CT examinations had not been performed on children whose only physical or laboratory abnormality was a small amount of hematuria. Specifically, in our study, none of the normotensive children with fewer than 50 RBC/HPF had a significant renal injury. This finding is in agreement with studies by Guice et al. [5] and Fortune et al. [6], who found no significant renal injuries in patients with fewer than 30 RBC/HPF. Lieu et al. [12] examined 78 children who had excretory urography for blunt abdominal trauma and found no injuries in patients with less than 20 RBC/HPF and significant renal injury (grade III or greater) only if there was gross hematuria or too many RBCs to count on microscopic analysis. On the basis of this study, the authors recommended that excretory urography (or CT) be performed if the number of RBCs is too numerous to count on microscopic analysis; if it is deemed necessary to diagnose contusion, that investigation be undertaken when hematuria exceeds 20 RBC/HPF; and when there are associated clinical findings that suggest significant injury, urography also may be warranted. All of these studies, and our own, support the thesis that there are insignificant levels of hematuria in children after blunt trauma that do not require further investigation.

In our population, microhematuria with hypotension was not a more sensitive predictor of renal injury than was microhematuria without hypotension. The combination of these findings predicted only one of nine significant renal injuries, whereas hematuria without hypotension correctly predicted seven of nine. Nonetheless, hypotension was an important finding, as the presence of either hematuria or hypotension or both correctly predicted all nine significant renal injuries (Table 2).

An association between head trauma and hematuria has been noted [2, 6] before, and the mere presence of head trauma has been cited as sufficient indication for abdominal CT [13]. We found the same prevalence of hematuria in patients with head injuries as in those without head injuries. Furthermore, as opposed to the data of Beaver et al. [13], none of our patients, whether or not they had a head injury, had clinically occult renal trauma. All had abnormal abdominal physical findings, large amounts of hematuria, shock, or some combination of these.

A recent study [14] performed under similar conditions yielded results almost identical to ours. The study population, age range, and sex distribution were similar. Twenty-six percent of patients who had hematuria had renal injury, compared with 2.5% of patients who did not have hematuria. None of the 41 asymptomatic patients with hematuria had abnormal CT examinations. Both the presence and degree of hematuria were associated with a significantly higher proportion of renal injury, multiple organ injury, and abnormal CT examinations. Both that study and that of Karp et al. [2]

TABLE 2: Renal Injury Predicted by Hematuria or Hypotension

Injury Grade	Hematuria	Hypotension	Both	Either or Both
$\geq$ III ( $n = 9$ )	8	2	1	9
<III ( $n = 247$ ) <sup>a</sup>	98	36	14	120
Total patients ( $n = 256$ )	106	38	15	129

<sup>a</sup> Includes no injury.

concluded that asymptomatic hematuria is a low-yield indication for CT in children with blunt abdominal trauma.

In a large population of children with blunt abdominal trauma, the amount of hematuria was predictive of not only the presence but also the extent of renal injury. The presence of shock was an important copredictor of significant injury. No normotensive child with fewer than 50 RBC/HPF had a significant renal injury, and conversely all children with significant renal injuries had either large amounts of hematuria or shock. No significant renal injuries were clinically occult. We conclude that asymptomatic hematuria with fewer than 50 RBC/HPF in the absence of shock not only is a low-yield indication for abdominal CT in children with blunt abdominal trauma, but that CT in this case is probably unnecessary if the only criterion for investigation is the hematuria itself.

#### ACKNOWLEDGMENT

We thank Patty Felix for her skillful preparation of the manuscript.

#### REFERENCES

- Bright TC, White K, Peters PC. Significance of hematuria after trauma. *J Urol* 1978;120:455-456
- Karp MP, Jewett TC Jr, Kuhn JP, Allen JE, Dokler ML, Cooney DR. The impact of computed tomography scanning on the child with renal trauma. *J Pediatr Surg* 1986;21:617-623
- Hardeman SW, Husmann DA, Chinn HKW, Peters PC. Blunt urinary tract trauma: identifying those patients who require radiological diagnostic studies. *J Urol* 1987;138:99-101
- Nicolaisen GS, McAninch JW, Marshall GA, Bluth RF Jr, Carroll PR. Renal trauma: re-evaluation of the indications for radiographic assessment. *J Urol* 1985;133:183-187
- Guice K, Oldham K, Eide B, Johansen K. Hematuria after blunt trauma: when is pyelography useful? *J Trauma* 1983;23:305-311
- Fortune JB, Brahme J, Mulligan M, Wachtel TL. Emergency intravenous pyelography in the trauma patient. *Arch Surg* 1985;120:1056-1059
- Cass AS, Luxenberg M, Gleich P, Smith CS. Clinical indications for radiographic evaluation of blunt renal trauma. *J Urol* 1986;136:370-371
- Kaufman RA, Towbin R, Babcock DS, et al. Upper abdominal trauma in children: imaging evaluation. *AJR* 1984;142:449-460
- Kaufman RA. Technical aspects of abdominal CT in infants and children. *AJR* 1989;153:549-554
- Norman ME. An office approach to hematuria and proteinuria. *Pediatr Clin North Am* 1987;34:545-560
- Blumenthal S, Epps RP, Heavenrich R, et al. Report of the task force on blood pressure control in children. *Pediatrics* 1977;59(suppl):797-820
- Lieu TA, Fleisher GR, Mahboubi S, Schwartz JS. Hematuria and clinical findings as indications for intravenous pyelography in pediatric blunt renal trauma. *Pediatrics* 1988;82:216-222
- Beaver BL, Colombani PM, Fal A, et al. The efficacy of computed tomography in evaluating abdominal injuries in children with major head trauma. *J Pediatr Surg* 1987;22:1117-1122
- Taylor GA, Eichelberger MR, Potter BM. Hematuria: a marker of abdominal injury in children after blunt trauma. *Ann Surg* 1988;208:688-693

## Book Review

**Breast Imaging.** By Daniel B. Kopans. Philadelphia: Lippincott, 416 pp., 1989. \$65

Over the last decade, breast imaging has emerged as one of the forerunners of current radiology practice. With breast cancer developing in one in 10 American women during their lifetime, and 143,000 new cases of breast cancer being diagnosed annually, awareness of breast cancer has become a major concern for both patients and physicians. Dr. Kopans relies on his vast personal experience as director of breast imaging in the Department of Radiology, Massachusetts General Hospital, in developing a most comprehensive and well-illustrated text dealing with this new imaging subspecialty. The text covers a complete spectrum of the various breast imaging techniques. Most of the book describes the advantages and disadvantages of the gold standard of X-ray mammography in comparison with the other imaging techniques.

The book begins with a brief introduction to the various theories of the development of breast cancer. The efficacy of mass screening is presented, with descriptions of some of the larger studies. This is followed by a chapter reviewing the anatomy, histology, and physiology of the breast.

The bulk of the book is found in the chapter entitled "Mammography," which includes the basic concepts of X-ray mammography, the physics, radiation doses, mammographic positioning, and Dr. Kopans's views on analyzing the normal and abnormal mammogram. The chapter is fairly complete although no mention is made of breast augmentation. In view of the increasing number of breast prostheses being implanted cosmetically and postoperatively, a discussion on this topic would be helpful. A brief, well-illustrated atlas also is included in this chapter with numerous "teaching points," such as one we all seem to overlook occasionally: "Not all upper outer quadrant lesions are benign intramammary lymph nodes." The illustrations throughout the atlas are of good quality and include both X-ray mammograms and xerograms.

The next chapter is devoted entirely to breast sonography, discussing both the myths and appropriate use of this technique for evaluation of breast lesions. The advantages and disadvantages of high-resolution real-time sonography as a complement to mammography is well presented. A sonographic atlas describing 24 different breast masses along with a brief description of the sonographic findings and clinical significance is included. The next chapter correlates the mammographic and sonographic findings with the various pathologic lesions, offering a better understanding of image interpretation and patient management. Another chapter is devoted entirely to needle placement in breast masses, which will be extremely beneficial to physicians who perform fine-needle aspirations. The chapter includes representative mammograms, showing needle placement along with photographs and drawings showing the placement of the needle in the patient's breast in an attempt to familiarize the reader with various ways of positioning and localizing breast masses. A discussion of the advantages of parallax in helping to localize masses and sonographic guidance for aspiration also is included. The final chapter deals with nonmammographic breast imaging techniques, including transillumination and MR imaging, with a brief description of the future of breast imaging with digitalization.

Overall, the book is extremely well written and presents a practical clinical approach for breast imaging. I can recommend this book highly as a welcome addition for the library of any radiologist who deals with breast imaging.

Steven L. Edell  
Riverside Hospital  
Wilmington, DE 19802

# False-negative Duplex Doppler Studies in Children with Hepatic Artery Thrombosis After Liver Transplantation

Theodore R. Hall<sup>1</sup>  
Sue V. Mc Diarmid<sup>2</sup>  
Edward G. Grant<sup>1</sup>  
M. Ines Boechar<sup>1</sup>  
Ronald W. Busuttii<sup>3</sup>

Recent reports describe formation of collateral vessels in children who have hepatic artery thrombosis after liver transplantation. This led us to reevaluate the role of duplex Doppler imaging in this population. Among 135 pediatric liver transplant patients, 20 had arteriography for suspected hepatic artery thrombosis. Duplex and/or color Doppler imaging was performed in 13 of these children. The Doppler examination failed to show hepatic artery signals in five patients. Arteriography showed hepatic artery thrombosis in all five. In three of these, subsequent Doppler examinations showed reappearance of arterial Doppler signals. Arteriography confirmed the interval development of collaterals. Hepatic artery signals were found on the Doppler examinations of the remaining eight patients. Four had normal arteriograms, but the remaining four had hepatic artery thrombosis with collateral formation. Patients with hepatic artery thrombosis and collateral circulation tended to have increased diastolic flow (decreased resistive index). In addition, early scans clearly identified patients with complete thrombosis before collateral formation.

On the basis of our preliminary experience, a child with a liver transplant and a clinical history strongly suggestive of hepatic artery compromise should have arteriography despite an apparently normal Doppler examination.

*AJR* 154:573-575, March 1990

Vascular compromise after liver transplantation may be related to thrombosis of the portal vein, hepatic veins, or hepatic artery [1]. Of the three, thrombosis of the hepatic artery is by far the most common. It typically results in sepsis, infarction, hepatic necrosis, bile duct strictures, and graft failure, requiring retransplantation [2-4]. In reports of large series, the prevalence of thrombosis of the hepatic artery ranged from 11.8% [5] to as high as 42% [6].

Both invasive and noninvasive techniques are available to establish patency of the hepatic artery. The accuracy of duplex sonography in this regard has been well documented [5, 6]. Recent reports [5, 6] have described formation of arterial collaterals in pediatric liver transplant patients who have thrombosis of the hepatic artery. Flint et al. [5] recently examined this problem and reported that Doppler signals were absent in all children who had thrombosis of the hepatic artery (with or without collaterals). Our study was undertaken after we saw arterial Doppler signals in the livers of two children with angiographically proved thrombosis of the hepatic artery and formation of collateral vessels. This prompted us to review the accuracy of duplex Doppler studies in pediatric liver transplant recipients who have thrombosis of the hepatic artery and collateral circulation.

## Materials and Methods

Angiograms or autopsy results were reviewed in all pediatric patients with suspected thrombosis of the hepatic artery after liver transplantation. All studies were performed between December 1, 1984, and November 30, 1988. Among the 135 transplant recipients younger

Received July 7, 1989; accepted after revision October 24, 1989.

<sup>1</sup> Department of Radiological Sciences, University of California, Los Angeles, School of Medicine, 10833 LeConte Ave., Los Angeles, CA 90024-1006. Address reprint requests to T. R. Hall.

<sup>2</sup> Department of Gastroenterology, University of California, Los Angeles, School of Medicine, Los Angeles, CA 90024-1006.

<sup>3</sup> Department of Surgery, University of California, Los Angeles, School of Medicine, Los Angeles, CA 90024-1006.

0361-803X/90/1543-0573  
© American Roentgen Ray Society

than 17 years, 20 were examined with contrast angiography for suspected thrombosis of the hepatic artery. Seventeen duplex Doppler studies were performed in 13 of the 20 patients. The remaining seven patients were seen before the availability of Doppler sonography at our institution and were not included in this study. Duplex Doppler sonography and arteriography were performed within a 48-hr period in all except two patients. In these cases angiography was delayed 4 and 5 days, respectively, until the patient was stable enough for a contrast-enhanced study. All angiograms were obtained via arterial puncture with selective celiac axis and superior mesenteric artery catheterizations.

Our protocol for duplex Doppler in the liver transplant patients includes a real-time survey of the liver and adjacent organs, followed by duplex Doppler sampling of the portal vein, hepatic artery, hepatic veins, and intrahepatic inferior vena cava. Hepatic artery thrombosis was diagnosed on the basis of Doppler sonography when arterial signals were absent in the porta hepatis; both lobes of the liver; and the region of arterial anastomosis from the aorta, celiac axis, or superior mesenteric artery. In all patients in whom the diagnosis was made on the basis of duplex Doppler sonography, an angiogram was obtained for confirmation.

All sonographic evaluations were performed with the ATL Ultramark four or Ultramark 9 (Advanced Technology Laboratories, Bothell, WA) sonographic systems. For real-time and Doppler examinations, 3.0- or 5.0-MHz transducers were used. Frequency selection was based on the size of the patient and the quality of the image and the Doppler signal. Wall filters were set at 50 or 100 Hz. Angle-corrected velocity measurements were used whenever the course of the vessel under investigation was visible by using real-time or color Doppler imaging. Duplex Doppler evaluations (Ultramark four) were performed with mechanical sector scanners. For color Doppler imaging (Ultramark 9), phased-array technology was used. Spectral analysis was performed as part of both duplex and color Doppler examinations. The resistive index ( $[(\text{peak systolic} - \text{end diastolic velocity})/\text{peak systolic velocity}]$ ) was calculated retrospectively in every case. The resistive index in the hepatic artery was also calculated in 70 additional pediatric liver transplant recipients with no clinical signs of hepatic ischemia, graft failure, or bile duct stenoses or radiologic evidence of liver parenchyma damage.

## Results

Five of the 13 patients fulfilled our Doppler criteria for thrombosis of the hepatic artery. The sonographic diagnosis was confirmed by angiography in all five patients. In three of these patients, Doppler sonography identified arterial signals on subsequent examinations. This was thought to be con-

sistent with the interval development of collateral circulation. The times between the initial Doppler examination and the appearance of an arterial Doppler signal were 21, 48, and 62 days, respectively. Collateral circulation was confirmed by repeat angiography in two of these three patients (Fig. 1).

Doppler signals from the hepatic artery were identified in the remaining eight patients. In four of these eight, normal, patent hepatic arteries were seen on angiography. In the other four, thrombosis of the hepatic artery was seen with collateralization. In two of these four patients, color Doppler imaging actually revealed an arterial vessel in the porta hepatis that proved to be a collateral but was indistinguishable from a normal hepatic artery (Figs. 2A and 2B).

A retrospective evaluation of the Doppler spectra of the hepatic arteries in our patients who had angiography revealed a trend toward increased diastolic flow in the seven patients who had thrombosis of the hepatic artery and collateral circulation. The mean resistive index was 0.52 (range, 0.41–0.62). All patients with patent hepatic arteries on Doppler sonography that were confirmed by contrast angiography had a resistive index greater than 0.64 with a calculated mean resistive index of 0.72. In the separate control population of 70 randomly selected pediatric liver transplant recipients with normal Doppler studies, the calculated resistive index ranged from 0.55 to 0.91. The mean resistive index in this population was 0.67 (SD = 0.1). Differences in the mean resistive index of the study population with patent hepatic arteries (0.72) and the control population (0.67) are due to the small number of patients ( $n = 4$ ) in the study group.

The clinical courses of the seven patients with thrombosis of the hepatic artery and collateralization showed abnormalities that could be attributed directly to decreased or absent hepatic arterial flow: relapsing bacteremia and septicemia (7/7), bile duct strictures and segmental biliary dilatation (4/7), and initially technically difficult arterial reconstruction (3/7). Among our patients with thrombosis of the hepatic artery and collateralization, one required retransplantation because of graft failure, four others are awaiting suitable donor organs, and the remaining two are stable on antibiotic therapy.

## Discussion

The liver transplantation program at the University of California, Los Angeles, was started in 1984. Overall survival rate

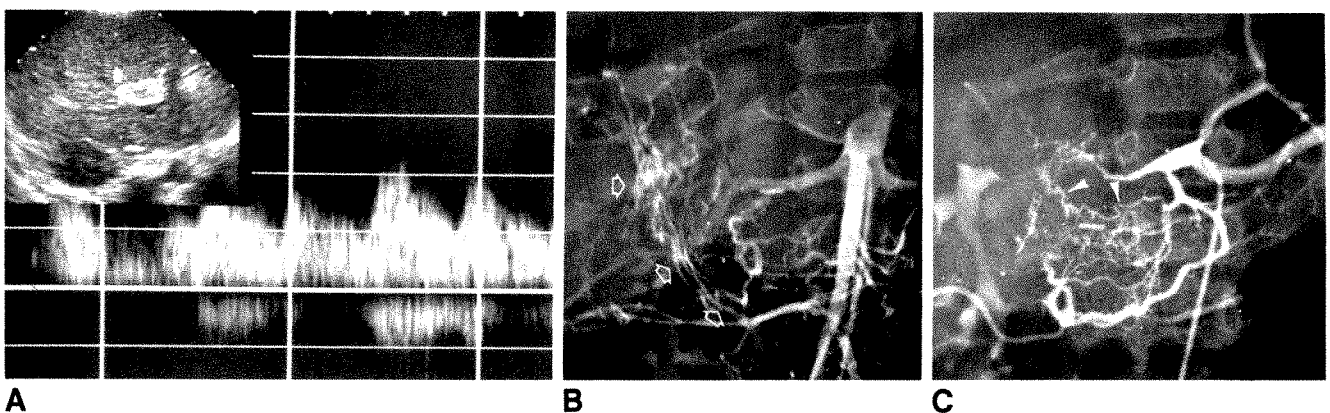


Fig. 1.—Arterial collateral circulation.

A, Duplex sonogram shows typical arterial tracing from right lobe of liver (see inset).

B, Selective superior mesenteric arteriogram clearly shows collateral circulation from branch of superior mesenteric artery (arrows).

C, Selective celiac angiogram in same patient shows hepatic artery thrombosis with several small arterial collaterals (arrowheads).



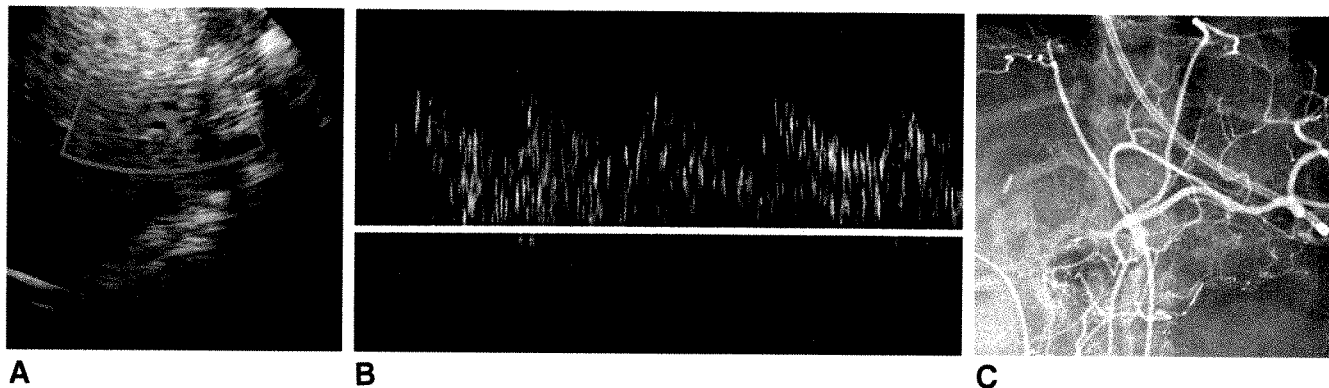


Fig. 2.—Arterial collateral circulation in pediatric liver transplant recipient with thrombosis of hepatic artery.

A, Color-flow Doppler examination of porta hepatis clearly shows flow in transplanted liver.

B, Analysis of spectral display confirms presence of arterial blood flow in porta (calculated resistive index = 0.4).

C, Subsequent arteriogram shows thrombosis of hepatic artery and several tiny collateral vessels. Additional small collaterals were seen when injection of superior mesenteric artery was used (not shown).

in the first 40 pediatric transplant recipients was 80%, with an actuarial survival rate of 78% [7]. Our current survival rate of 82% in pediatric transplant recipients most likely is related to increasing experience in managing posttransplant morbidity and the use of OKT3 monoclonal antibody therapy for the management of rejection [8]. Thrombosis of the hepatic artery, however, continues to be a major problem.

Duplex sonography is the most practical and cost-effective screening method for the evaluation of transplant morphology and vascular integrity. Its usefulness in the evaluation of the hepatic artery is based largely on the assumption that thrombosis will eliminate all arterial flow to the organ. In three of our 11 patients, collateralization was discovered when intrahepatic arterial Doppler signals reappeared after a documented thrombosis. In four others, thrombosis of the hepatic artery was not diagnosed prospectively because arterial Doppler signals within the liver were taken to imply patency of the hepatic artery.

In the native liver, occlusion of the main hepatic artery leads to rapid development of arterial collaterals. Formation of collateral vessels and blood flow in the portal vein decrease the likelihood of hepatic ischemia and infarction in most patients [3, 9]. With liver transplantation, potential collateral pathways are severed; the graft is far more vulnerable to disruption of the central arterial circulation. This pattern is seen in adult transplant recipients; however, collaterals do form in children who receive transplants.

The potential to form collateral circulation may be related to the type of biliary reconstruction performed in pediatric liver transplant recipients. In our pediatric patients, particularly those with a pretransplant diagnosis of biliary atresia, a Roux-en-Y choledochojejunostomy with a straight tube or internal stent is used for biliary anastomoses [7]. This type of reconstruction brings the highly vascular jejunal arterial bed close to the transplanted liver. With arterial occlusion, collateral vessels can be recruited from the jejunal vascular arcade. This hypothesis is supported by the fact that collaterals to the homograft originated from the superior mesenteric artery in all six patients whose collateral circulation was documented by angiography. Adult transplant recipients undergo a different type of biliary reconstruction (choledochocholedochostomy), which leads to more complete dearterialization and less opportunity for collateral formation.

Our findings are contrary to those recently reported by Flint et al. [5]. In their series, 34 (92%) of 37 cases of thrombosis of the hepatic artery were diagnosed correctly by duplex Doppler imaging. A Doppler signal was not identified in any child in their study population who had arterial collaterals. Clearly, however, arterial flow is present in the liver if collateralization has occurred. The reason for the disparity in the two studies is uncertain. Technical factors such as system sensitivity, wall-filter settings, or transducer frequency may have played a role.

When our experience is analyzed, a number of ways of differentiating between patients with a patent hepatic artery and those with thrombosis and collateralization may exist. Thus far, the most promising possibility is the finding of increased diastolic flow (decreased resistive index) in children who have formation of collateral vessels. Serial scanning potentially can identify the first, possibly subclinical, episode of complete thrombosis before formation of collateral vessels occurs. Both hypotheses, however, require further investigation. On the basis of our experience, children with a strongly suggestive clinical history of thrombosis require arteriography even if the duplex Doppler study shows arterial patency.

## REFERENCES

1. Busuttil RW, Goldstein LI, Danovitch GM, et al. Liver transplantation today. *Ann Intern Med* 1986;104:377-389
2. Shaw BW, Gordon RD, Iwatsuki S, et al. Hepatic retransplantation. *Transplant Proc* 1985;17:264-271
3. Starzel TE, Groth CG, Brettschneider L, et al. Orthotopic homotransplantation of the human liver. *Ann Surg* 1968;168:3:392-415
4. Tzakis AG, Gordon RD, Shaw BW, et al. Clinical presentation of hepatic artery thrombosis after liver transplantation in the cyclosporine era. *Transplantation* 1985;40:667-671
5. Flint EW, Sumkin JH, Zajko AB, et al. Duplex sonography of hepatic artery thrombosis after liver transplantation. *AJR* 1988;151:481-483
6. Wozney P, Zajko AB, Bron KM, et al. Vascular complications after liver transplantation: a 5-year experience. *AJR* 1986;147:657-663
7. Busuttil RW, Colonna JO, Hiah JR, et al. The first 100 liver transplants at UCLA. *Ann Surg* 1987;206:4:387-402
8. Goldstein G, Kremer AB, Barnes L, Hirsch RL. OKT3 monoclonal antibody reversal of renal and hepatic rejection in pediatric patients. *J Pediatr* 1987;111:6(2):1046-1050
9. Groth CG, Porter KA, Otte JB, et al. Studies of blood flow and ultrastructural changes in rejecting and non-rejecting canine orthotopic liver homografts. *Surgery* 1968;63(4):658-668

## Book Review

**Brain Imaging. An Introduction.** By John R. Bradshaw. Stoneham, MA: Butterworths, 249 pp., 1989. \$70, softcover

This softcover, well-produced book attempts to use different neuroradiologic diagnostic techniques to illustrate a variety of pathologic conditions. It is divided into two parts. Part 1 describes diagnostic techniques. Part 2, in a rather innovative way, uses clinical neurologic information as an introduction to 100 case presentations.

Part 1 is disappointing. The author does not develop areas in neuroanatomy, pediatric disease, and plain film pathology but touches on them incompletely. Nuclear and sonographic studies are shown without examples or indications of where they specifically apply. With regard to angiography, the author advocates giving injections by hand, cerebral catheters with side holes, and the ability of angiograms to differentiate infarcts from low-grade gliomas, all of which have less than universal acceptance.

Part 2, which makes up 70% of the book, is a delight. The cases flow easily and quickly, with many pearls and good differential diagnostic points developed. The cases range from the mundane subdural hemotoma to the CT appearance of a bifrontal leukotomy. Case discussions are mostly well crafted and succinct in a uniquely British

way. The cases are heavily weighted to CT scans; only 11 MR images are used.

The print is easy to read, and the photographs appear to be accurate reproductions of the original studies. The index is a helpful aid to all radiographic and clinical information. However, the bibliography is a woeful listing of only three sources; all are texts of English publishers. A more complete section of references, including journal selections, after each section and, in some cases, after each clinical discussion would have added significantly to the depth of all topics.

Ordinarily I would recommend this book for section 2 alone to radiology and neuroscience house staff as well as the nursing staff in neurologic intensive care units if the cost were \$30 to \$40. At \$70, you might want to wait for the library or departmental copy to arrive.

Edward V. Grayson  
Memorial Hospital  
Hollywood, FL 33021

# MR Imaging in Patients with Intractable Complex Partial Epileptic Seizures

Betty Sue Brooks<sup>1</sup>  
 Don W. King<sup>2</sup>  
 Taher El Gammal<sup>1</sup>  
 Kimford Meador<sup>2</sup>  
 Farivar Yaghmai<sup>3</sup>  
 Jack N. Gay<sup>4</sup>  
 Joseph R. Smith<sup>5</sup>  
 Herman F. Flanigin<sup>5</sup>

Detailed neurologic studies, high-field-strength MR imaging, and CT scanning were performed preoperatively in 53 patients with intractable complex partial seizures who underwent surgical treatment for epilepsy. Macroscopic structural (tumoral or vascular) lesions were found in 28% of patients. The remainder had pathologic findings consistent with mesial temporal gliosis. Tumors were found in 22% of the patients and were benign or of low-grade malignancy in every case. MR was accurate in the preoperative diagnosis of structural lesions, including very small occult tumors and cryptic vascular malformations. In patients with mesial temporal gliosis, there was correlation between the MR observation of a unilaterally dilated anterior temporal horn and the EEG-identified seizure focus and side of temporal lobectomy. However, MR demonstrated T2-weighted signal abnormalities correlating with the epileptogenic focus in only 8% of cases of mesial temporal gliosis.

MR provided useful information in 28% of patients who underwent surgery for refractory complex partial epilepsy. MR obviated invasive EEG monitoring in 93% of the patients with structural lesions. MR was useful in only 8% of the patients with pathologic changes of mesial temporal gliosis.

*AJNR* 11:93-99, January/February 1990; *AJR* 154:577-583, March 1990

Previous reports have evaluated the contributions of low- and mid-field-strength MR imaging in patients with partial epilepsy and have compared the diagnostic efficacy of MR and CT [1-6] or of MR, CT, and positron emission tomography [7-9] in these patients. The efficacy of MR performed at a high field strength vs CT in a group of epilepsy patients, including a subgroup of 26 surgical cases of complex partial seizures, was reported recently [10]. We report the results of preoperative high-field-strength MR examinations in 53 patients who underwent surgery for intractable complex partial seizures; surgical and pathologic correlations were available for each case.

## Materials and Methods

Fifty-three patients with complex partial seizures refractory to medical management underwent surgery during the period between October 1985 and October 1988. The patients were 7-54 years old (average,  $26 \pm 12$ ) and included 23 males and 30 females. The average duration of seizure disorder was 18 years (range, 1-52 years). Pertinent medical history in the subgroup of 38 patients with mesial temporal gliosis included seizure disorders that began with a clinically documented episode of high fever and febrile seizures in two patients and a history of meningoencephalitis in three other patients whose seizures began within the first decade. There was a history of perinatal intracranial hemorrhage in one patient in whom seizures began at age 16. Finally, there was a history of severe head trauma in four other patients. Seizures began in late childhood in one of these four patients, in whom a subdural hematoma had been evacuated at age 18 months. This was the only patient in this series in whom cranial surgery had been performed previously. In two patients, seizures began 2 and 12 months after closed head injury, at ages 7 and 16 years, respectively. In the fourth patient,

Received February 7, 1989; revision requested April 19, 1989; revision received May 26, 1989; accepted June 5, 1989.

Presented in part at the annual meeting of the Southeastern Neuroradiological Society, Boca Raton, FL, September 1988.

<sup>1</sup> Department of Radiology, Neuroradiology Section, The University of Alabama at Birmingham, 619 S. 19th St., Birmingham, AL 35233. Address reprint requests to B. S. Brooks.

<sup>2</sup> Department of Neurology, The Medical College of Georgia, 1120 15th St., Augusta, GA 30912.

<sup>3</sup> Department of Pathology, The Medical College of Georgia, Augusta, GA 30912.

<sup>4</sup> The Medical College of Georgia, Augusta, GA 30912.

<sup>5</sup> Department of Surgery, Section of Neurosurgery, The Medical College of Georgia, Augusta, GA 30912.

0361-803X/90/1543-0577

© American Roentgen Ray Society

a head injury with associated loss of consciousness and no other sequelae occurred at age 5; complex partial seizures began at 37 years of age.

Preoperative evaluation in all patients included history and physical examination, neuropsychological testing, continuous video and EEG monitoring with scalp and sphenoidal electrodes, and angiography with intracarotid amobarbital sodium (Wada) testing. Invasive EEG monitoring was required for definitive localization of the seizure focus in 41 of the patients; this was achieved with depth electrodes in 39 patients and with multicontact subdural grid electrodes in two children. Invasive EEG monitoring was omitted when obvious structural lesions were seen on neuroimaging studies or the noninvasive presurgical assessment was already definitive for a unilateral ictal focus.

Patients with a seizure focus in the vicinity of a functional area underwent craniotomy under local anesthesia with awake stimulation mapping of local functioning areas. The surgical technique in all cases consisted of the subpial method of resection. En bloc resection of several centimeters of the anterior hippocampus was also included in all anterior temporal lobectomies whenever either presurgical or intraoperative testing confirmed that the opposite mesial temporal structures would support recent memory function. The extent of resection was guided by intraoperative electrocorticography in all patients.

Cranial CT without and with IV contrast enhancement was performed on a General Electric 9800 scanner in 48 patients. Standard transaxial nonenhanced scans were obtained with contiguous 10-mm sections. Contrast-enhanced CT was performed by using a modified technique with gantry angulation to obtain optimal temporal-lobe views [11]. Section planes parallel to the long axis of the temporal lobe were obtained with 10 contiguous 3-mm slices; the remainder of the brain was scanned with 10-mm-thick sections at 10-mm intervals.

MR studies were performed in all patients on a 1.5-T superconducting magnet (Signa, General Electric Medical Systems, Milwaukee, WI). Sagittal T1-weighted images, 800/20/4 (TR/TE/excitations), were acquired with a 24-cm field of view, 3-mm slice thickness with 0.6-mm interslice gap, and 256 × 256 acquisition matrix. Intermediate and T2-weighted cardiac-gated coronal and transaxial images, 2000/20/70/1, were acquired by using a 5-mm slice thickness with 2.5-mm interslice gap and 256 × 256 acquisition matrix. The field of view was 24 cm for the transaxial and 20 cm for the coronal images. Approximately one half of the MR studies performed before August 1987 did not have cardiac gating; in these cases the number of excitations used was two. In obtaining the transaxial images, an attempt was made to position the patient with the chin up so as to correspond as closely as possible to the transaxial temporal-lobe CT images. The imaging parameters provided pixel dimensions of approximately 1 × 1 mm in the imaging plane.

MR interpretation was performed without knowledge of the EEG findings; in the majority of patients, MR was performed before admission for electrophysiological monitoring. CT also was performed either on an outpatient basis shortly before admission or on the day of admission before beginning the EEG studies. All patients had surgery after definitive identification of a unilateral seizure focus; pathologic correlation was available in every case.

## Results

The resected tissue showed important pathologic changes in all patients. Fifteen of the 53 patients had tumors or vascular malformations (Table 1). Thirty-eight patients had pathologic changes consistent with mesial temporal gliosis

(neuronal degeneration and loss, neuronal heterotopia, and fibrillary astrocytic proliferation).

Tumor histology is summarized in Table 2. Benign or low-grade malignant tumors were present in all 12 cases. Tumors were located in the temporal lobe in eight of 12 cases (Figs. 1–3). One patient had a ganglioglioma in the right posterior frontal operculum. One patient with tuberous sclerosis had a giant cell astrocytoma in the right posterior frontal region (Fig. 4). One patient had a juvenile fibrillary astrocytoma predominantly in the occipital lobe (Fig. 5) and one patient had a grade II astrocytoma in the right putamen and insula (Fig. 6). Vascular malformations were found in three patients. One patient had a left temporal thrombosed arteriovenous malformation (Fig. 7) and one a left temporal and another a right hippocampal cavernous hemangioma.

Preoperative MR was correct in the diagnosis of tumor in 11 of 12 cases and suggested either posterior cerebral infarct or low-grade tumor in the remaining patient with occipital juvenile fibrillary astrocytoma (Fig. 5). MR correctly diagnosed the three patients with vascular malformations. Thus, MR diagnosis was specific for diagnoses of tumor or vascular malformation in 14 (93%) of 15 patients with structural lesions and showed abnormal signal changes in all 15.

CT scans without and with contrast enhancement were available in 10 of the 15 patients with tumors and vascular malformations. CT correctly diagnosed low-grade glioma in two of four patients with gangliogliomas and was unavailable in the other two cases with this diagnosis. In the patient with a right putaminal and insular astrocytoma, the CT scan was interpreted as tumor or vascular malformation. CT missed the diagnosis of tumor in one patient each with oligodendroglioma, giant cell astrocytoma, and benign fibrillary astrocytoma. In the patient with occipital juvenile fibrillary astrocytoma, CT favored the diagnosis of infarct. In the three patients with vascular malformations, CT diagnosis of a calcified vascular

**TABLE 1: Surgical Findings in 53 Patients with Intractable Complex Partial Seizures**

Finding	No. (%)
Tumors	12 (22)
Vascular malformations	3 (6)
Pathologic changes of gliosis	38 (72)
Total	53 (100)

**TABLE 2: Tumors in 12 Patients with Intractable Complex Partial Seizures**

Tumor	No.
Ganglioglioma	4
Benign fibrillary astrocytoma	3
Fibrillary astrocytoma grade II/IV	2
Oligodendroglioma	1
Juvenile fibrillary astrocytoma	1
Giant cell astrocytoma	1
Total	12

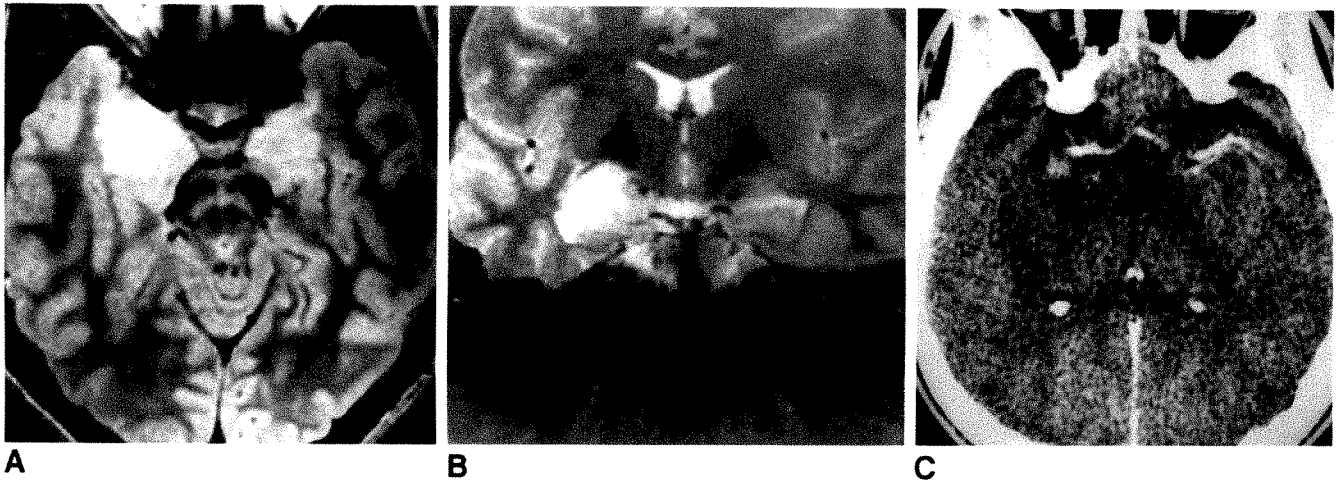


Fig. 1.—Right temporal ganglioglioma in a 19-year-old woman.  
 A and B, Intermediate-weighted transaxial (A) and T2-weighted coronal (B) MR images show abnormal high signal of tumor anterior and superior to temporal horn.  
 C, Focal small abnormal tumoral enhancement on transaxial CT might not have been apparent without use of angled temporal-lobe CT technique.

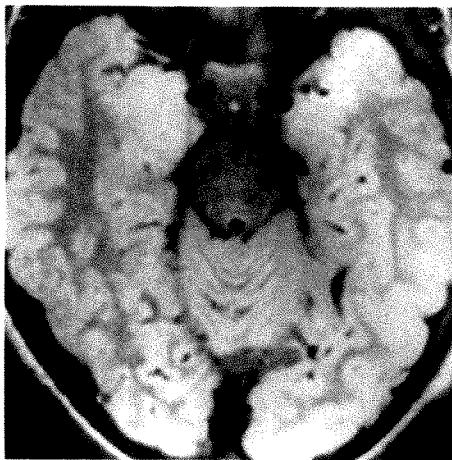


Fig. 2.—Oligodendroglioma in an 11-year-old boy. Intermediate-weighted transaxial MR image shows right mesial temporal abnormal high signal involving gray and white matter diffusely. Pathologically, tumor was cellular without calcification and involved all of the amygdala and uncus with extension into hippocampus.

malformation was made in one case (Fig. 7) and the diagnosis of vascular malformation or vascular tumor was suggested in the other two cases. CT was therefore “positive” for a structural lesion in seven of 10 cases, providing a specific diagnosis of tumor or vascular malformation in three of these and a false-negative interpretation in three patients with tumors.

Pertinent CT and MR findings in patients with mesial temporal gliosis are summarized in Table 3. CT studies in 32 (89%) of 36 patients were either normal or showed nonspecific findings such as generalized or cerebellar atrophy. Two patients had a CT diagnosis of unilateral dilatation of a temporal horn that was contralateral to the side of epileptogenic

focus and surgery in both. In one other patient CT was thought to show dilatation of both temporal horns. In a single patient with left mesial temporal gliosis, CT revealed an area of low attenuation in the anteromesial left temporal lobe in the same location that MR demonstrated a high-signal abnormality on T2-weighted images.

Major MR findings in the 38 patients with pathologically proved mesial temporal gliosis are also summarized in Table 3. Thirty (79%) of 38 patients had either normal studies or nonspecific findings such as cerebral or cerebellar atrophy. In contradistinction to CT, MR detection of unilateral dilatation of the temporal horn was ipsilateral to the side of seizure focus and surgery in each of six cases. Only three (8%) of 38 patients had MR signal changes in the mesial temporal region (Fig. 8). Pathology in these cases showed moderate gliosis in one case and severe gliosis in the other two.

Clinical follow-up information at intervals ranging from 6 months to 1 year was available for 35 of the 53 surgical patients. Twenty-six patients (74%) were seizure-free; another four patients (11%) had rare seizures, defined as no more than one or two seizures per year. Five patients (14%) had less than a 90% reduction in seizure frequency.

## Discussion

Partial seizures begin in a localized area of cerebral cortex, most often the temporal lobe, and are considered complex if there is associated alteration of consciousness. A significant number of patients in this subcategory of seizure diagnosis are refractory to medical management [12, 13]. Since the early 1950s, temporal lobectomy has provided a cure or a substantial improvement for many of these patients. Mesial temporal sclerosis or gliosis is the most common pathologic abnormality found [13]. Theories as to its cause include hypoxic damage to the hippocampus and parahippocampal



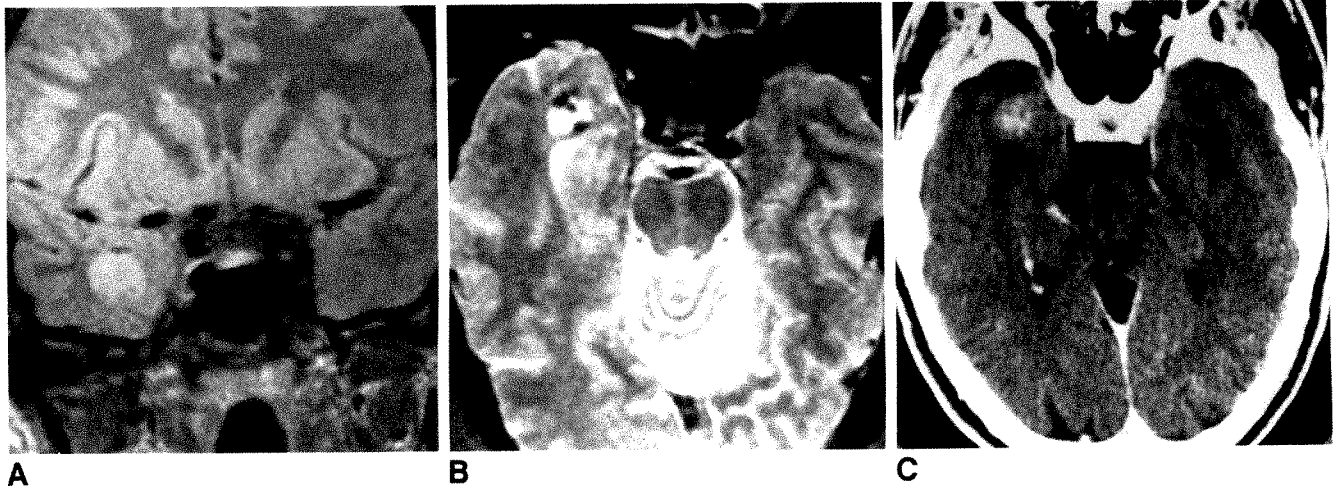


Fig. 3.—Benign fibrillary astrocytoma.

A-C, Intermediate-weighted coronal (A) and T2-weighted transaxial (B) MR images show well-defined round tumor containing calcifications (B). Mass effect produces deformity with posterior displacement of right temporal horn evident on both transaxial MR (B) and contrast-enhanced CT (C).

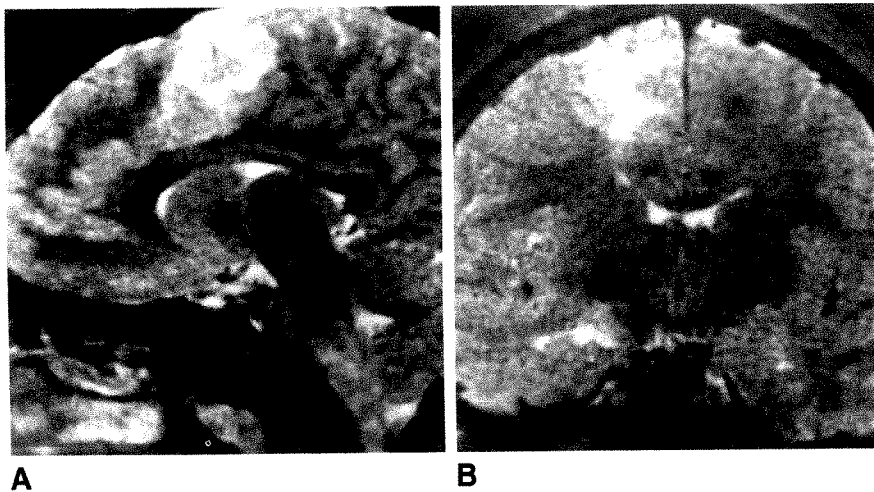


Fig. 4.—Giant cell astrocytoma in a 10-year-old girl with tuberous sclerosis.

A and B, T2-weighted sagittal (A) and coronal (B) MR images show posterior frontal parasagittal mass extending to level of corpus callosum. Tumor was composed of dysplastic cerebral tissue containing many giant astrocytes and a few giant neurons. CT without and with contrast enhancement was completely negative.

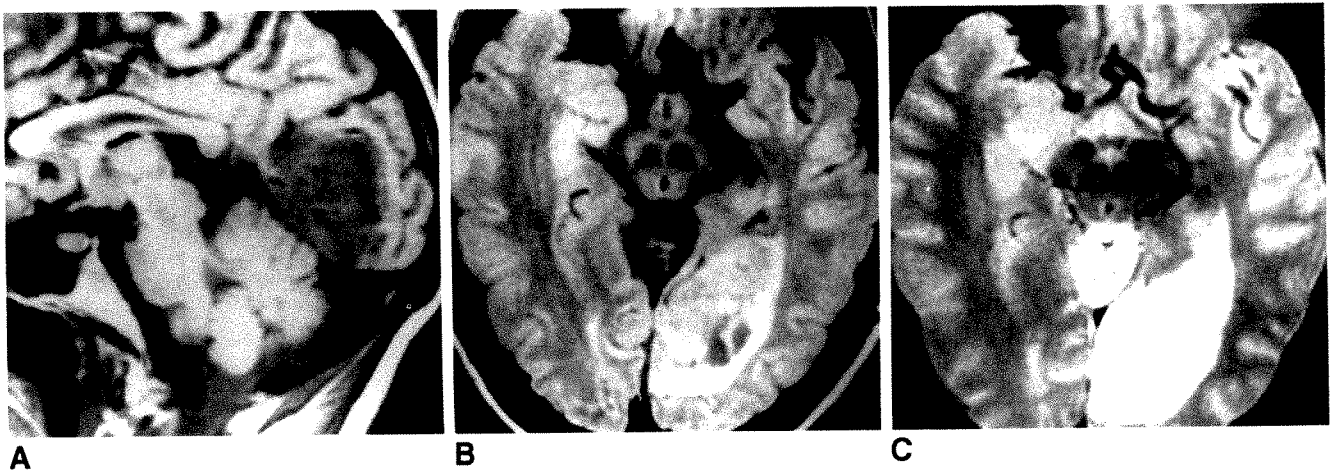


Fig. 5.—Juvenile cystic fibrillary astrocytoma in a 25-year-old woman.

A-C, Sagittal T1-weighted (A) and transaxial intermediate- (B) and T2- (C) weighted images reveal occipital tumor with posterior temporal extension that has very high signal on T2-weighted series (C). Microcysts were found to be a major component pathologically.

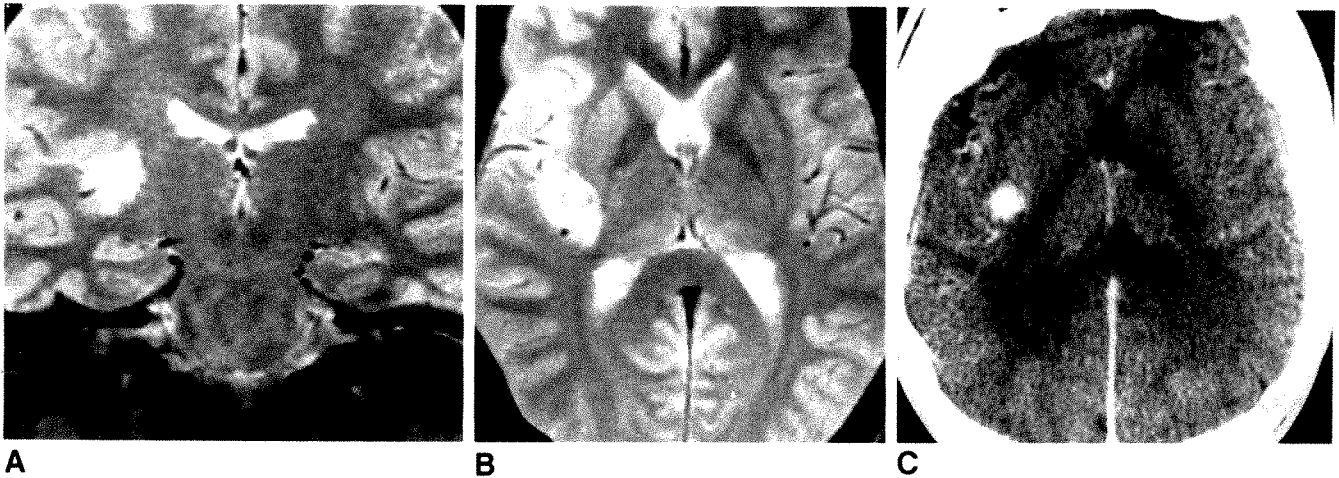


Fig. 6.—Right putaminal and insular astrocytoma, grade II/IV.

A–C, T2-weighted coronal (A) and transaxial (B) MR images and contrast-enhanced transaxial CT scan (C). Tumor with surrounding edema is best delineated on transaxial MR.

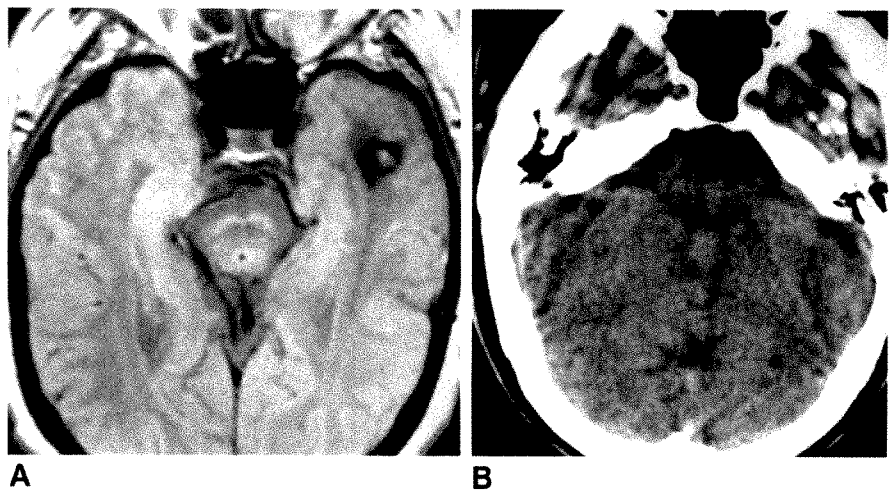


Fig. 7.—Thrombosed arteriovenous malformation in a 52-year-old man.

A, Intermediate-weighted transaxial MR image reveals lesion adjacent and anterolateral to left temporal horn.

B, Unenhanced CT scan shows popcorn calcifications.

Calcifications and old hemorrhage of surrounding tissue were noted at pathologic examination.

regions and pathologic change that occurs in response to repeated seizures [14, 15].

In our series, mesial temporal gliosis was present in 38 (72%) of 53 patients. Macroscopic structural lesions were present in the remaining 28% of cases. Tumors constituted 22% of cases and included four cases of ganglioglioma, a relatively rare tumor; ganglioglioma, therefore, represented 33% of the tumors in this series. It is of interest that gangliocytoma, a closely related tumor, was reported recently in three patients with childhood epilepsy [16]. In addition, several patients with benign fibrillary astrocytomas were noted to have scattered mature ganglion cells within what was predominantly a fibrillary astrocytic tumor. Neuronal heterotopia is a pathologic change associated with mesial temporal sclerosis, and the concurrence of tumor and changes of mesial temporal gliosis in seizure patients has been noted previously [13].

MR was successful in detecting the structural lesions, and provided a diagnosis of tumor in three patients that was missed by CT. However, the insensitivity of MR in patients with complex partial seizures and mesial temporal gliosis is also clearly demonstrated in this series. MR failed to demonstrate signal abnormalities in 35 of 38 patients with subsequent pathologically proved mesial temporal gliosis. The literature has been inconsistent in regard to the correlation of mesial temporal gliosis and the prevalence of abnormal high-intensity signal changes on T2-weighted MR images. In MR studies at low and mid field strengths, temporal-lobe T2 signal abnormalities were reported in several isolated cases [17, 18] and in 11 of 14 patients with mesial temporal gliosis in one previous series [19]. However, a similar study by Sperling et al. [8] found no MR abnormalities in 18 patients with mesial temporal gliosis and intractable complex partial seizures. One previous study with high-field-strength MR [20] found tem-

poral mediobasal high-signal-intensity areas on T2-weighted images in three of 12 patients with mesial temporal gliosis, but pathologic studies revealed no differences between the findings in these three cases and in the remaining nine patients. In another series of 31 patients with temporal-lobe epilepsy who were examined at 1.5 T [21], only one of 14 cases with mesial temporal gliosis showed a high-intensity

T2-weighted signal abnormality in the corresponding temporal lobe. MR was also negative in eight of 12 patients in the series of Heinz et al. [10] who were operated on for complex partial seizures and did not have tumors. A diagnosis of mesial temporal sclerosis was proved in three of these, while the surgical technique of subpial aspiration did not permit a definitive diagnosis in two; in the other three no diseased tissue was found. Surgical and pathologic correlation was not mentioned for the four cases in which MR was positive. The unilateral temporal-lobe T2 high-signal focus of mesial temporal gliosis may be a small and relatively subtle abnormality. It is possible that previous studies performed at low and mid field strengths, where the ratio of image contrast to noise is lower compared with high-field-strength examinations, were relatively more susceptible to interpretation error from "shading" artifacts and from carotid pulsation artifacts, especially on the coronal projection. In these previous studies, motion suppression techniques were not yet available or were not used.

Previous attempts with pneumoencephalography, and more recently with nonionic contrast CT cisternography [22], to define an atrophic temporal lobe or uncus herniation have met with varied success. Although the number of cases in our current series is small, the data suggest that MR may accurately detect a unilateral, focally dilated anterior temporal horn in patients with a unilateral seizure focus in the same temporal lobe. This may be a subtle or "soft" sign but can provide ancillary evidence that may be helpful in the surgical decision-making process in some borderline cases. Further correlation of this particular finding in a larger number of temporal lobectomy patients should prove of interest.

In summary, MR provided an important contribution in the preoperative diagnosis of tumor or vascular malformation in 28% of 53 patients operated on for refractory complex partial epilepsy. MR afforded a surgical decision without the need for invasive EEG monitoring in 14 of 15 patients with structural lesions. MR was found to be contributory in only a small number of patients (8%) with pathologic changes of mesial temporal gliosis.

**TABLE 3: CT and MR Findings in 38 Intractable Complex Partial Seizure Patients with Mesial Temporal Gliosis**

Study/Finding	No.
<b>CT</b>	
Negative	25
Generalized cerebral and/or cerebellar atrophy	6
Dilatation of one or both temporal horns	3
Unilateral low-attenuation anteromesial temporal lobe	1
Posterior cranial hemiatrophy	1
Not available	2
Total	38
<b>MR</b>	
Negative	19
Cerebellar atrophy	4
Generalized cerebral atrophy	2
Posterior cranial hemiatrophy	1
Frontal bone flap <sup>a</sup> ; occipital focal atrophy	1
Chiari I malformation with hydrocephalus	1
Lacunar infarcts/white-matter ischemic foci	2
Unilateral dilatation of temporal horn	2
Unilateral dilatation of temporal horn; cerebellar atrophy	2
Unilateral dilatation of temporal horn; generalized cerebellar atrophy	1
Abnormal mesial temporal high signal on T2	1
Abnormal mesial temporal high signal on T2; diffuse cerebral and cerebellar atrophy	1
Abnormal mesial temporal high signal on T2; unilateral dilatation of temporal horn; cerebellar atrophy	1
Total	38

<sup>a</sup> Caused by evacuation of a traumatic subdural hematoma during infancy.

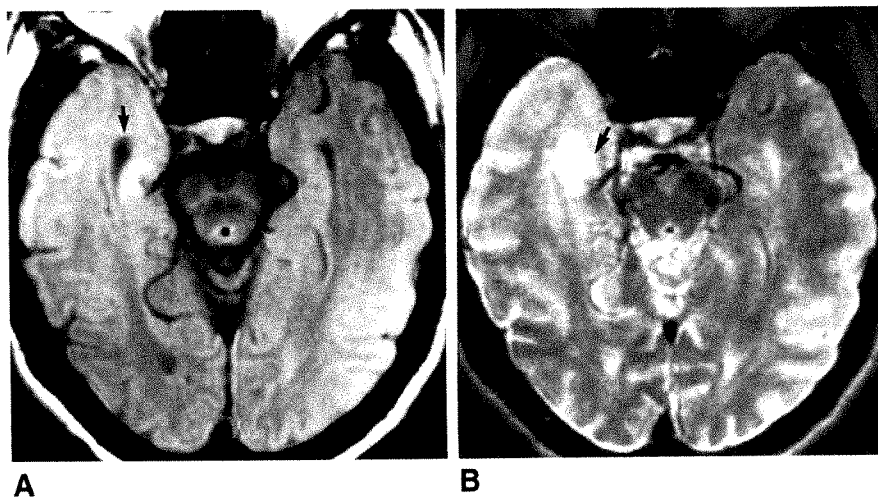


**Fig. 8.—Mesial temporal gliosis in a 47-year-old woman.**

**A,** Intermediate-weighted transaxial MR image shows focal dilatation of right anterior temporal horn (arrow) and mild increased signal intensity of right uncus.

**B,** T2-weighted transaxial image shows abnormal high-intensity signal (arrow) medial to dilated temporal horn.

## REFERENCES

1. Laster DW, Perry JK, Moody DM, Ball MR, Witcofski RL, Riela AR. Chronic seizure disorders: contribution of MR when CT is normal. *AJNR* **1985**; 6:177-180
2. McLachlan RS, Nicholson RL, Black S, Carr T, Blume WT. Nuclear magnetic resonance imaging: a new approach to the investigation of refractory temporal lobe epilepsy. *Epilepsia* **1985**;26(6):555-562
3. Ormson MJ, Kispert DB, Sharbrough FW, et al. Cryptic structural lesions in refractory partial epilepsy: MR imaging and CT studies. *Radiology* **1986**;160:215-219
4. Jabbari B, Gunderson CH, Frantz W, et al. Magnetic resonance imaging in partial complex epilepsy. *Arch Neurol* **1986**;43:869-872
5. Schorner W, Meencke H-J, Felix R. Temporal lobe epilepsy: comparison of CT and MR imaging. *AJR* **1987**;149:1231-1239
6. Avrahami E, Cohn DF, Neufeld M, et al. Magnetic resonance imaging (MRI) in patients with complex partial seizures and normal computerized tomography (CT) scan. *Clin Neurol Neurosurg* **1987**;89(4):231-235
7. Latack JT, Abou-Khalil BW, Siegel GJ, Sackellares JC, Gabrielsen TO, Aiser AM. Patients with partial seizures: evaluation by MR, CT, and PET imaging. *Radiology* **1986**;159:159-163
8. Sperling MR, Wilson G, Engel J, Babb TL, Phelps M, Bradley W. Magnetic resonance imaging in intractable partial epilepsy: correlative studies. *Ann Neurol* **1986**;20:57-62
9. Theodore WH, Dorwart R, Holmes M, Porter RJ, Di Chiro G. Neuroimaging in refractory partial seizures: comparison of PET, CT and MRI. *Neurology* **1986**;36:750-759
10. Heinz ER, Heinz TR, Radtke R, et al. Efficacy of MR vs CT in epilepsy. *AJNR* **1988**;9:1123-1128
11. El Gammal T, Adams RJ, King DW, So EI, Gallagher BB. Modified CT techniques in the evaluation of temporal lobe epilepsy prior to lobectomy. *AJNR* **1987**;8:131-134
12. Feldman RG. Complex partial seizures (psychomotor or temporal lobe seizures). In: Browne TR, Feldman RG, eds. *Epilepsy: diagnosis and management*. Boston: Little, Brown, **1983**:39-50
13. Glaser GH. Treatment of intractable temporal lobe-limbic epilepsy (complex partial seizures) by temporal lobectomy. *Ann Neurol* **1980**;8:455-459
14. Falconer MA. Mesial temporal (Ammon's horn) sclerosis as a common cause of epilepsy. Etiology, treatment and prevention. *Lancet* **1974**;1:767-770
15. Scheibel ME, Crandall PH, Scheibel AB. The hippocampal-dentate complex in temporal lobe epilepsy. *Epilepsia* **1974**;15:55-80
16. Altman NR. MR and CT characteristics of gangliocytoma: a rare cause of epilepsy in children. *AJNR* **1988**;9:917-921
17. Grant R, Hadley DM, Condon B, et al. Magnetic resonance imaging in the management of resistant focal epilepsy: pathological case report and experience of 12 cases. *J Neurol Neurosurg Psychiatry* **1987**;50:1529-1532
18. Maertens PM, Machen BC, Williams P, et al. Magnetic resonance imaging of mesial temporal sclerosis: case reports. *J Comput Tomogr* **1987**;11:136-139
19. Kuzniecky R, de la Sayette V, Ethier R, et al. Magnetic resonance imaging in temporal lobe epilepsy: pathological correlations. *Ann Neurol* **1987**;22:341-347
20. Lesser RP, Modic MT, Weinstein MA, et al. Magnetic resonance imaging (1.5 Tesla) in patients with intractable focal seizures. *Arch Neurol* **1986**;43:367-371
21. Fobben ES, Zimmerman RA, Sperling MR, et al. MR imaging in temporal lobe epilepsy. Presented at the annual meeting of the Radiological Society of North America, Chicago, November **1988**
22. Wyler AR, Bolender NF. Preoperative CT diagnosis of mesial temporal sclerosis for surgical treatment of epilepsy. *Ann Neurol* **1983**;13:59-64



## Book Review

**Dento Maxillo Facial Radiology.** Edited by Peter N. Hirschmann. Stoneham, MA: Butterworths, May 1989;18(2):49-96 and August 1989;18(3):97-149. By subscription, 4 issues annually for £55

This is the official journal of the International Association of Dentalmaxillofacial Radiology (IADMFR), as the name implies. The vast majority of the articles are from dental schools throughout the United States and Europe. The topics are quite varied and range from education and training programs to clinical issues and computerized diagnosis.

All of the papers are refereed; however, the scientific quality of the articles seems to fluctuate. Those that are related specifically to dental problems have high-quality illustrations and are well organized. Those on other regions, such as paranasal sinuses, salivary glands, or larynx, are not based on state-of-the-art technology, and the articles do not seem to be as well documented by top-quality illustrations. An abstract section is included, which is quite brief but well thought out in the choice of first-rate articles.

The subscription rate for the journal is £55 annually, but the rate is reduced for members of the IADMFR. This journal is recommended for dental radiologists, radiology dental technologists, and radiologists who devote a significant percentage of their time to dental problems. Radiologists and surgeons who manage mandibular lesions would do well to stay abreast of this journal. General radiologists, technologists, or residents in radiology would do better to keep a standard textbook of dental radiology for handy reference rather than a clinical journal with inevitable gaps of knowledge.

William Hanafee  
*University of California, Los Angeles*  
*Los Angeles, CA 90024-1721*



# Tumors of the Nasopharynx and Adjacent Areas: MR Imaging with Gd-DTPA

T. Vogl<sup>1</sup>  
S. Dresel<sup>1</sup>  
L. T. Bilaniuk<sup>2</sup>  
G. Grevers<sup>3</sup>  
K. Kang<sup>1</sup>  
J. Lissner<sup>1</sup>

The purpose of this study was to describe our experience with Gd-DTPA-enhanced MR imaging in the evaluation of the most common nasopharyngeal tumors. Forty-two patients with tumors of the nasopharynx and adjacent spaces had MR imaging before and after IV injection of Gd-DTPA. Images were obtained with a 1.0-T superconducting magnet imaging system in transverse, coronal, and sagittal planes with T1- and T2-weighted sequences. MR images were compared with CT scans and tumor histology. The studies were categorized by using a grading system with grades ranging from unsatisfactory (grade 0) to optimal (grade 3). Contrast-enhanced MR enables better identification of small anatomic details such as both palatini muscles and the pharyngobasilar fascia. MR after Gd-DTPA was superior to CT in all cases except for tumors of the maxillary sinuses.

MR with Gd-DTPA is recommended for tumors that are small and difficult to detect on the initial nonenhanced MR examination or that show subtle infiltrations. Because of the increased cost and longer examination time, MR with Gd-DTPA does not need to be done when large tumors are well delineated.

*AJNR* 11:187-194, January/February 1990; *AJR* 154:585-592, March 1990

The complex patterns created by spread of nasopharyngeal tumors with involvement of soft tissue and bony structures require an imaging method that distinguishes both soft tissue and bone. MR imaging has shown that its superior soft-tissue contrast resolution depicts tumor margins in the nasopharynx and related spaces more accurately than CT does [1-3]. Thus, MR has remarkably improved the diagnosis of lesions of this area. With the introduction of the contrast medium Gd-DTPA, MR might become even more advantageous. The purpose of this study was to describe our experience with Gd-DTPA in the evaluation of lesions of the nasopharyngeal region.

## Materials and Methods

Over a 3-year period 42 patients with primary and secondary tumors of the nasopharynx and adjacent spaces were examined with MR before and after IV injection of the contrast medium Gd-DTPA. Secondary tumors were defined as processes primarily located in adjacent structures but extending into the nasopharynx. The 42 cases comprised 16 primary tumors (11 squamous cell carcinomas, three lymphoepithelial, and two adenoid-cystic carcinomas) and 26 secondary tumors (10 maxillary sinus squamous cell carcinomas, four oropharyngeal tumors, and 12 miscellaneous tumors such as lymphomas, lymphoid hyperplasia, and cysts). The MR findings were compared with the results of contrast-enhanced CT and histologic examinations.

Nine MR examinations were performed at a field strength of 0.35 T and 33 examinations at 1.0 T on a Siemens Magnetom unit. Images were acquired by using a 30-cm head coil. Five- or eight-millimeter-thick sections were made in two or three planes (axial, coronal, sagittal), depending on the extent of the tumor.

Received March 24, 1989; revision requested April 24, 1989; revision received June 2, 1989; accepted June 13, 1989.

<sup>1</sup> Department of Radiology, University of Munich, Marchioninstr. 15, 8000 München 70, West Germany. Address reprint requests to T. Vogl.

<sup>2</sup> Department of Radiology, Neuroradiological Section, Hospital of the University of Pennsylvania, 3400 Spruce St., Philadelphia, PA 19104.

<sup>3</sup> Department of Otorhinolaryngology and Head and Neck Surgery, University of Munich, 8000 München 70, West Germany.

0361-803X/90/1543-0585

© American Roentgen Ray Society

**TABLE 1: Plain vs Gd-DTPA-Enhanced MR and Gd-DTPA-Enhanced MR vs Contrast-Enhanced CT in the Evaluation of Tumors of the Nasopharynx**

Type of Nasopharyngeal Tumor	No.	MR Grade <sup>a</sup>		Gd-DTPA MR vs CT <sup>b</sup>
		Plain	Gd-DTPA	
Primary				
Squamous cell carcinoma	11	2	3	MR+
Lymphoepithelial and adenoid-cystic carcinoma	5	2	3	MR+
Secondary				
Squamous cell carcinoma of maxillary sinus	10	2	2	MR = CT
Tumor of the oropharynx	4	2	3	MR+
Other (e.g., lymphoma, lymphoid hyperplasia, cyst)	12	2	3	MR+
Total	42			

<sup>a</sup> T1-weighted MR, 500/25, was graded on a scale of 0–3. 0 = unsatisfactory; 1 = satisfactory; 2 = good; 3 = optimal. Gd-DTPA was injected in a dose of 0.2 ml or 0.1 mmol/l per kg body weight.

<sup>b</sup> MR+ = MR superior to CT; MR = CT means MR and CT were of equal value.

After a sagittal survey image was obtained for the purpose of craniocaudal orientation, images were obtained in the axial orientation with a long, 1600/25,90 (TR/TE), and a short, 500/25, spin-echo (SE) sequence and in the coronal orientation with a short sequence with the same parameters. After injection of contrast medium, images were obtained in the axial plane with a short SE sequence; 28 cases were also studied in the coronal plane. In seven cases during and after injection of Gd-DTPA, a very short sequence, 30/13, with a flip angle of 30° was performed every minute over a period of at least 8 min in order to measure the change in signal intensity over time. Gd-DTPA was administered in a dose of 0.2 ml or 0.1 mmol/l per kg body weight.

CT scans were obtained on a Siemens Somatom 2 or DRH unit. Four-millimeter-thick sections were obtained after injection of contrast material.

The results of nonenhanced MR, MR with Gd-DTPA, and contrast-enhanced CT were evaluated subjectively. The diagnostically important structures of the nasopharynx were analyzed on T1-weighted (plain and Gd-DTPA), T2-weighted, and proton-density images. The studies were assessed in three separate categories. The first and second categories dealt with the quality of MR images; grades ranging from unsatisfactory (grade 0) to optimal (grade 3) were assigned (Table 1). Grade 0 was defined as unsatisfactory because of motion or metallic artifacts. Grade 1 was defined as allowing recognition of tumor masses at least 5 mm in diameter. Designation of grade 2 meant clear delineation of tumor masses from the most important surrounding structures (such as pterygoid muscles). Studies were given a grade of 3 if, in addition to demarcation of masses, it was possible to identify the smaller anatomic structures (tensor and levator veli palatini muscles), appreciate their relationship to the tumor, and also characterize the tumor tissue (i.e., necrosis, vascularity). The same grading system was used for comparing the value of different pulse sequences (Table 2). In the third category, MR and CT were compared (Table 1).

The actual T1 and T2 relaxation times were determined with the help of the software program of the MR imager. For T1 evaluation two pulse sequences were necessary with different TRs and the same TE; for T2 evaluation a sequence with two echoes was needed. With the scanner operating at 1.0 T, moderate T1 relaxation times were defined as those within a range between 800 and 1300 msec moderate T2 relaxation times as those within a range between 50 and 100 msec. Values below these ranges were defined as low and values above these ranges as high relaxation times. The ratio of

**TABLE 2: Comparison of Different MR Pulse Sequences and Gd-DTPA in Evaluating Tumor Infiltration**

Location	Grade by MR Pulse Sequence and with Enhancement			
	T1-Weighted	Proton-Density	T2-Weighted	Gd-DTPA
Superficial structures				
Pharyngeal recess	2	3	2	3
Torus tubarius	2	3	2	3
Muscles				
Levator veli palatini muscle	2	2	1	3
Tensor veli palatini muscle	2	2	1	3
Medial/lateral pterygoid muscle	2	3	2	3
Longus colli muscle	2	3	2	3
Deep structures				
Parapharyngeal space	2	3	2	3
Infratemporal fossa	2	2	2	3
Sphenoid bone, skull base	2	2	2	2
Carotid artery	2	2	2	3
Cavernous sinus	2	2	2	3
Eustachian tube	1	2	1	2
Pharyngobasilar fascia	1	1	1	2
Walls of maxillary sinuses	1	2	1	2

Note.—Visualization was graded on a 0–3 scale: 0 = unsatisfactory; 1 = satisfactory; 2 = good; 3 = optimal. MR pulse sequences: T1-weighted, 500/25; proton-density, 1600/25; T2-weighted, 1600/90. Gd-DTPA was administered in a dose of 0.2 ml or 0.1 mmol/l per kg body weight.

signal intensities before and after administration of Gd-DTPA was measured by dividing the signal intensity of the enhanced tumor by the signal intensity of the nonenhanced tumor. A low enhancement factor was defined as one with a ratio of 1.3 or lower. Between 1.3 and 1.8 the enhancement factor was considered medium; above 1.8 the enhancement factor was considered high.

## Results

The diagnostically important structures of the nasopharynx were analyzed on T1-weighted (plain and Gd-DTPA), T2-weighted, and proton-density images. The normal superficial

Fig. 1.—Normal anatomy of nasopharyngeal structures on axial MR images, 500/17, before and after Gd-DTPA administration.

A, Plain image. Differentiation of specific nasopharyngeal structures is difficult.

B, After Gd-DTPA enhancement. Enhancement of mucosa, fat, and muscle fasciae provides better anatomic detail. 1 = longus colli muscle; 2 = pharyngeal recess; 3 = torus tubarius; 4 = levator veli palatini muscle; 5 = tensor veli palatini muscle; 6 = medial pterygoid muscle; 7 = lateral pterygoid muscle; 8 = carotid artery; 9 = nasal turbinate; 10 = maxillary sinus.

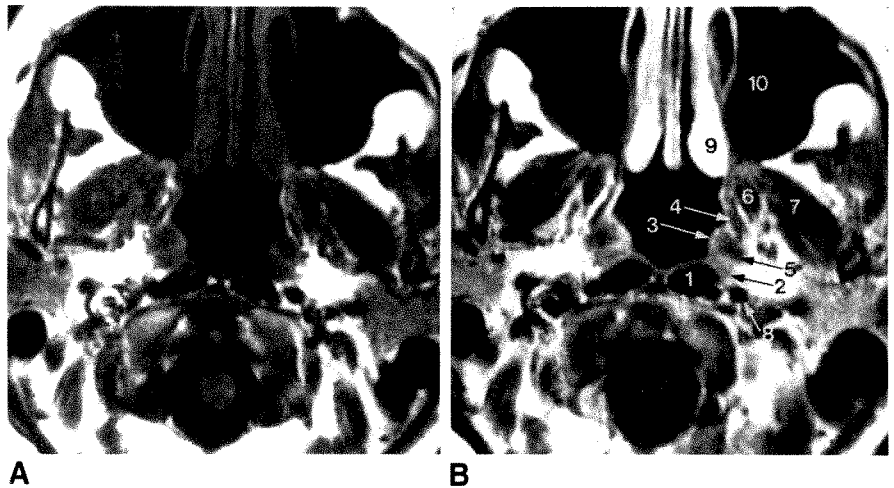


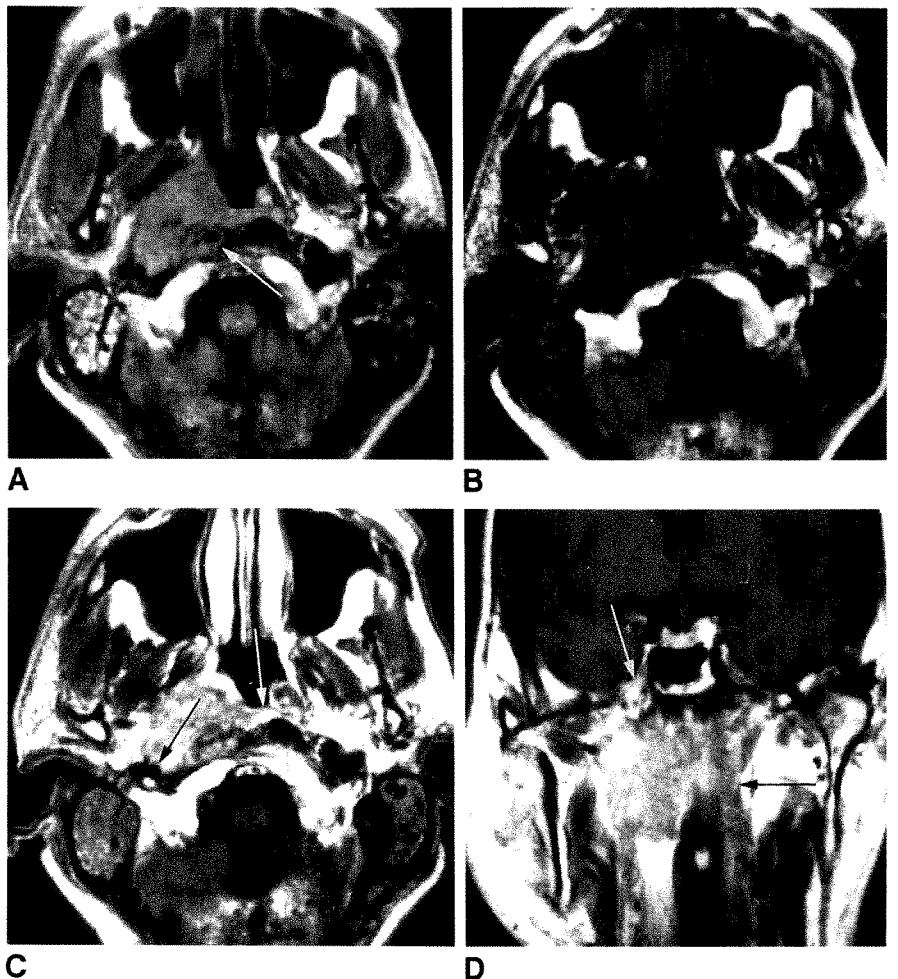
Fig. 2.—Primary squamous cell carcinoma of the nasopharynx.

A, Axial SE 1600/25 image, unenhanced. Right nasopharyngeal tumor of moderate signal intensity infiltrates parapharyngeal space and longus colli muscle (arrow). There is destruction of anteroinferior portion of right temporal bone and fluid in mastoid cells.

B, Axial SE 900/25 image, unenhanced. Tumor is of same signal intensity as muscle. It can only be speculated whether or not tumor crosses midline.

C, Axial SE 500/25 image, Gd-DTPA-enhanced. Tumor enhances inhomogeneously and less than mucosa. There is infiltration and displacement of sheath of right carotid artery (black arrow), longus colli muscle, torus tubarius, levator and tensor veli palatini muscles, and pharyngobasilar fascia. There is also extension of tumor to right parapharyngeal space with displacement of pterygoid muscle. Midline has been crossed (white arrow), and there is infiltration of left pharyngeal recess.

D, Coronal SE 500/25 image, Gd-DTPA-enhanced. Inhomogeneous tumor infiltrates and destroys wall of right sphenoid sinus, infiltrates cavernous sinus (white arrow), and crosses midline (black arrow).



structures like the torus tubarius and the pharyngeal recess were best delineated on proton-density and Gd-DTPA-enhanced T1-weighted images. The levator and tensor veli palatini muscles, the pterygoid muscles, and the pharyngobasilar fascia were better identified after Gd-DTPA because

sharper contrast was achieved between these structures and adjacent tissues. This was due to a slight increase in signal intensity after Gd-DTPA of the normal lymphoepithelial mucosa as well as of fascial planes that surround the muscles (Fig. 1 and Table 2). Arteries usually show a flow void, but at

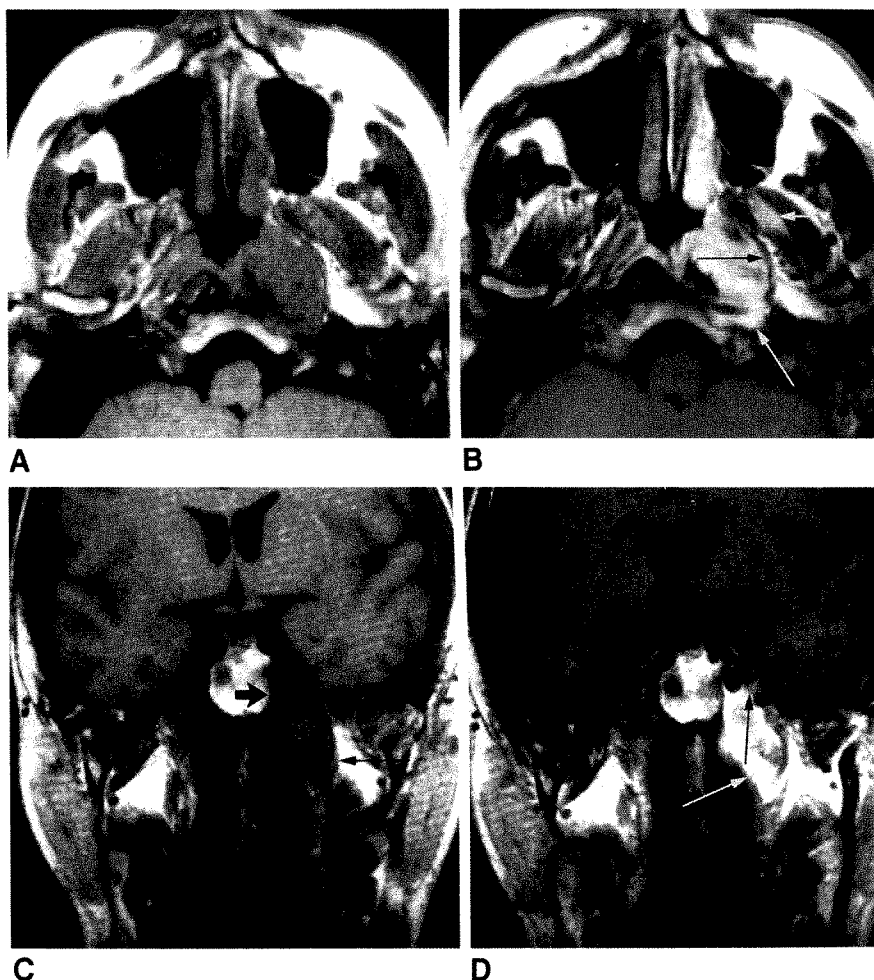


Fig. 3.—Adenoid-cystic carcinoma of nasopharynx.

A, Axial SE 500/25 image, unenhanced. Exact delineation of left nasopharyngeal tumor is not possible because it has the same signal intensity as muscles and mucosa.

B, Axial SE 500/25 image, Gd-DTPA-enhanced. There is marked enhancement of tumor, which destroys skull base (long white arrow) and infiltrates levator veli palatini and longus colli muscles on left side. There is also infiltration of left pterygoid muscles (short white arrow). Differentiation of tumor from enhanced left turbinate is difficult. Left margin of tumor is well demarcated by muscles it has displaced, thus indicating expansion and not infiltration of parapharyngeal space (black arrow).

C, Coronal SE 500/25 image, unenhanced. There is good delineation of tumor from fat (long arrow), but not from adjacent muscles. There is destruction of cranial base with extension into clivus (short arrow).

D, Coronal SE 500/25 image, Gd-DTPA-enhanced. Skull-base infiltration and involvement of cavernous sinus (black arrow) are seen better after tumor enhancement. Also, enhancement provides a sharp interface between tumor and longus colli muscle (white arrow). However, tumor and fat are of similar intensities.

TABLE 3: Characterization of Common Tumors of the Nasopharynx

Type of Tumor	Tumor Extent	Margins	Homogeneity	Signal Intensity	Enhancement Factor
Primary squamous cell carcinoma	Nasopharyngeal mucosa, nasal cavity, infiltration of skull base	Unsharp	Necrotic areas, inhomogeneous	Moderate T1, moderate T2	1.6
Lymphoepithelial and adenoid-cystic carcinomas	Aggressive growth with skull-base infiltration	Sharp	Some necrosis	Moderate T1, moderate to high T2	2.0
Secondary squamous cell carcinomas	Infiltration and destruction of maxillary sinuses	Unsharp	Necrosis, inhomogeneous	Low to moderate T1, moderate T2	1.8
Lymphoma	Rarely, bony infiltration	Sharp	Homogeneous	Moderate T1, moderate T2	1.6

Note.—Enhancement factor is a ratio of signal intensities before and after Gd-DTPA. Moderate T1 values were 800–1300 msec; moderate T2 values were 50–100 msec. Values below these ranges were defined as low and values above these ranges as high relaxation times. Pulse sequences: T1-weighted, 500/25; T2-weighted, 1600/90; proton-density, 1600/25.

the skull base veins with slowly flowing blood can be identified before and after Gd-DTPA as structures of high signal intensity. For demonstrating bony structures of the skull base, such as the clivus, the value of the contrast-medium-enhanced T1-weighted sequence depends on the increase in the signal intensity of the tumor. If the tumor showed a great

increase it was sometimes difficult to delineate it from fat and bone marrow, which also enhanced prominently. In the case of minimally or moderately enhancing tumors, the bone marrow after Gd-DTPA was brighter than the tumor, and infiltration of the tumor into bony structures was seen very well. The nasal mucosa and turbinates often get very bright on

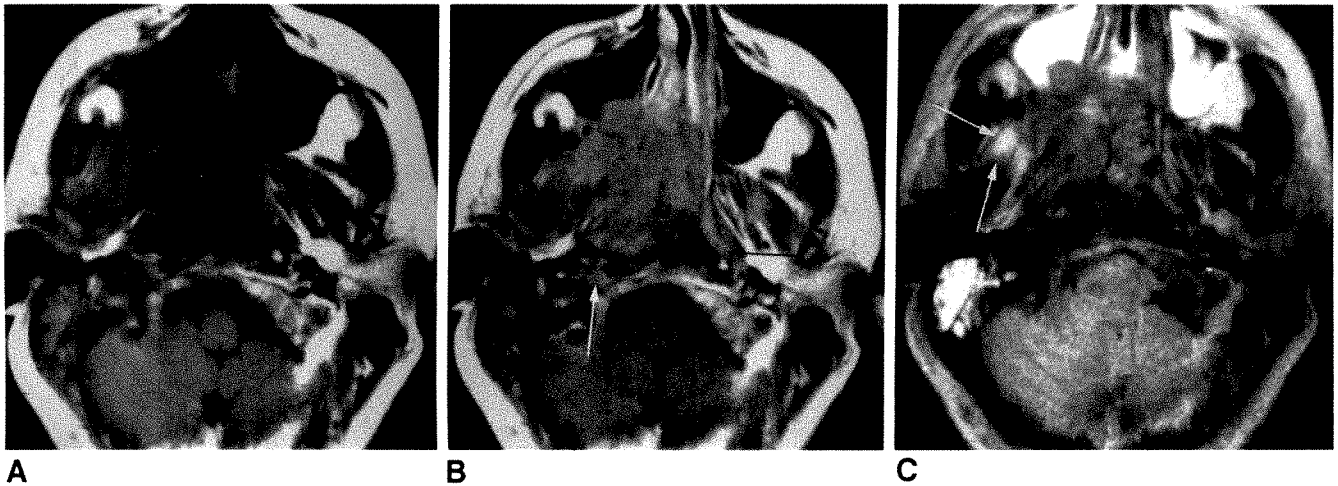


Fig. 4.—Maxillary sinus carcinoma involving nasopharynx.

A, Axial SE 500/25 image, unenhanced. Large tumor has produced destruction of posterior wall of right maxillary sinus and has infiltrated nasopharynx, parapharyngeal space, and infratemporal fossa. Right pterygoid muscle appears infiltrated by tumor. Tumor shows low signal intensity and homogeneous pattern.

B, Axial 500/25 image, Gd-DTPA-enhanced. After administration of Gd-DTPA, tumor shows an increase in signal intensity in comparison with fluid in maxillary sinuses. Intact enhanced mucosa is identified in anterior part of nasal cavity. Tumor has destroyed posterior part of right maxillary sinus, posterior part of nasal cavity, and inferior aspect of temporal bone (white arrow) and has infiltrated prevertebral muscles. Middle third of right lateral pterygoid muscle does not enhance as much as tumor (compare with C). Left parapharyngeal space and left pharyngeal recess appear uninvolved (black arrow).

C, Axial SE 1000/90 image, unenhanced. T2-weighted image allows good differentiation between tumor tissue and hyperintense fluid in maxillary sinus. Middle third of right pterygoid muscle is of high signal intensity (arrows), thought to represent edema at edge of tumor. Fluid is in mastoid sinus.

enhanced MR. Therefore, it may be difficult to completely delineate an enhancing tumor if it is contiguous with the nasal cavity.

In 16 patients with primary nasopharyngeal tumors 11 patients had squamous cell carcinomas. All these tumors showed an infiltration of the levator and tensor veli palatini muscles and of the pharyngobasilar fascia. Because of eustachian tube obstruction, fluid was seen in the mastoid cells in 10 of these patients. Seven squamous cell carcinomas invaded the sphenoid and cavernous sinuses and three extended to the nasal cavity. Unsharp margins and necrotic areas were characteristic of these tumors (Fig. 2). Low-

intensity nonenhancing regions within the tumor mass were considered to represent necrosis; this was confirmed at surgery. A discrete crossing of the midline by the tumor could be seen only on the contrast-enhanced images, but was suspected on the preenhancement images (Fig. 2). Gross infiltration of the longus colli muscle was well demonstrated on enhanced MR but was also well shown on the proton-density images. However, subtle extension of these tumors to the pterygoid muscles could be judged best on images with Gd-DTPA enhancement, because the signal intensity of squamous cell carcinomas on the plain image was about the same as that of muscles. The squamous cell carcinomas

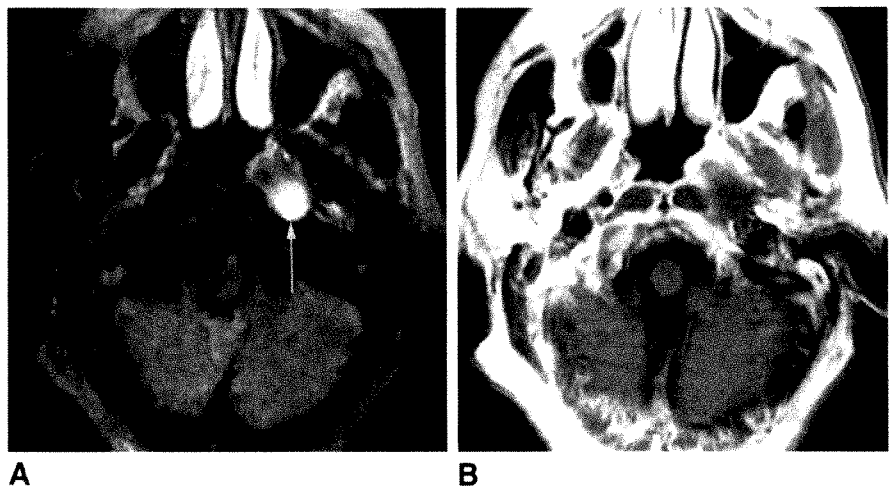


Fig. 5.—Cyst of naso- and oropharynx (surgically proved).

A, Axial SE 1600/90 image, unenhanced. Sharply delineated lesion of high signal intensity (arrow) is located in left nasopharynx.

B, Axial SE 500/25 image, Gd-DTPA-enhanced. There is no enhancement of cyst, which displaces normal nasopharyngeal structures anteromedially. A lower section (not shown) demonstrated contrast enhancement of cyst wall.



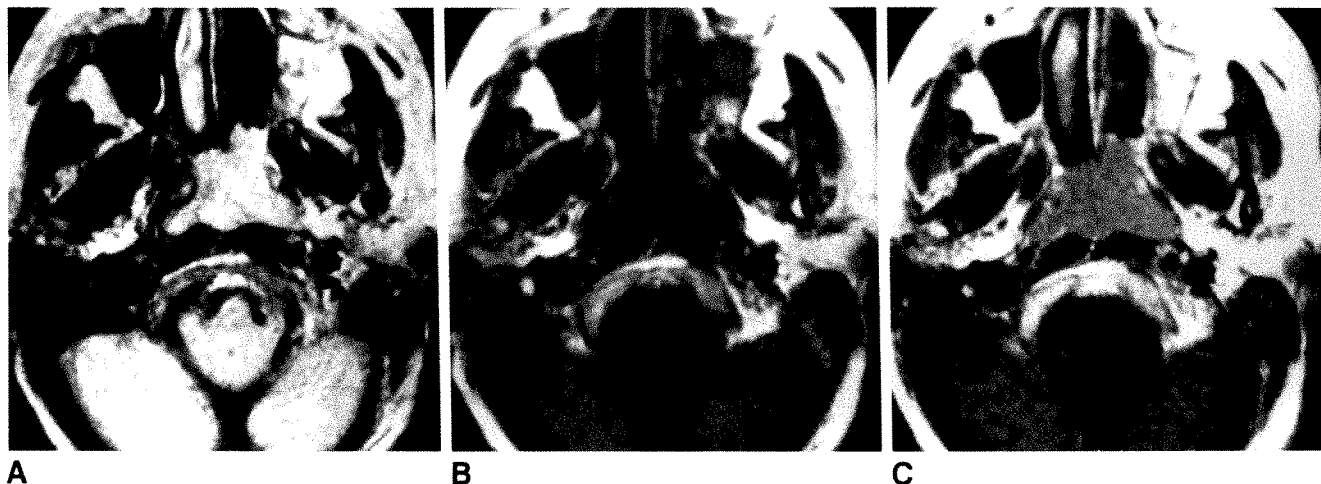


Fig. 6.—Lymphoma of nasopharynx.

A, Axial SE 1600/90 image, unenhanced. Nasopharynx is completely filled with homogeneous tissue. Proton-density image (not shown) showed slightly higher signal intensity in mass when compared with signal intensity of muscles. Fluid is in left maxillary sinus.

B, Axial SE 500/25 image, unenhanced. Tumor on T1-weighted images has signal intensity similar to that of brain.

C, Axial SE 500/25 image, Gd-DTPA-enhanced. Tumor shows homogeneous pattern of enhancement. There is no infiltration, but slight compression of veli palatini muscles bilaterally.

showed a medium increase after Gd-DTPA administration. The calculation of relaxation times showed moderate T1 and moderate T2 values. We examined three patients with lymphoepithelial and two patients with adenoid-cystic carcinomas. These tumors showed an aggressive growth pattern with early skull-base infiltration (Fig. 3). In some cases, it was difficult even after Gd-DTPA to judge whether the tumor crossed the midline or not. In our experience, the normal mucosa generally showed a greater increase in signal intensity after administration of Gd-DTPA than tumor masses did. On the contrast-enhanced image these tumors had sharp margins with small necrotic areas. Adenoid cystic and lymphoepithelial carcinomas had a high enhancement factor of about 2, moderate T1, and moderate to high T2 values (Table 3).

The most frequent secondary nasopharyngeal tumors were squamous cell carcinomas of the maxillary sinuses. In 10 patients these tumors showed characteristics similar to the primary nasopharyngeal carcinomas. As in the primary carcinomas, we found a moderate increase in signal intensity after administration of Gd-DTPA and moderate T1 and T2 values. On plain T1-weighted and on proton-density images it was difficult or impossible to differentiate tumor masses in the maxillary sinus from inflammatory changes and fluid. These could be distinguished on enhanced MR, but the distinction was clear on T2-weighted images, on which fluid was very bright and tumor was of low intensity. If the posterior part of the tumor infiltrated the longus colli muscle, it could be judged best on enhanced MR images. Also, discrimination between inflammation and tumor in the anterior part was possible on these images (Fig. 4). Infiltration of the bony walls of the maxillary sinuses was seen better on CT, but the exact extension of the tumor was seen better on MR.

A further advantage of contrast-enhanced MR was the discrimination between solid tumor and fluid-containing cystic processes. In our patient group one patient had a cyst of the

nasopharynx and oropharynx (Fig. 5). A solid tumor was excluded and the likelihood of a cystic process was supported after Gd-DTPA.

Another important differential diagnosis, especially in young patients, is the discrimination between lymphoid hyperplasia and any kind of lymphoma. In two patients with lymphoma and in three patients with lymphoid hyperplasia, we saw no difference in the tumor pattern on T1-weighted plain images and T2-weighted images. Only small asymmetry was noted in the nasopharyngeal mass due to a lymphoma. After injection of the contrast medium Gd-DTPA, the lymphoid hyperplasia showed septations in its internal pattern (Fig. 6). The lymphoma did not enhance as much as lymphoid hyperplasia did and its inner structure was homogeneous (Fig. 7).

The fast imaging technique was used in four cases of primary squamous cell carcinomas, two cases of secondary squamous cell carcinomas, and one case of lymphoepithelial carcinoma. Lymphoepithelial carcinoma reached an optimal increase in signal intensity after 180 sec and squamous cell carcinomas after 240 sec, with a slight decrease after that time. Three examinations were unsatisfactory because of motion or metallic artifacts.

## Discussion

With both CT and MR, it is necessary to carry out the examination using at least two orientations, axial and coronal; however, coronal scanning is often difficult to perform in CT, particularly in older patients. In our study, sagittal views did not support the diagnostic management; only two or three midline slices were useful. No additional information was provided over that obtained with axial and coronal slices. CT provides better resolution of cortical bone detail [4–8]. However, even with contrast enhancement, CT delineation of muscles and mucosa from tumor is often unsatisfactory. The

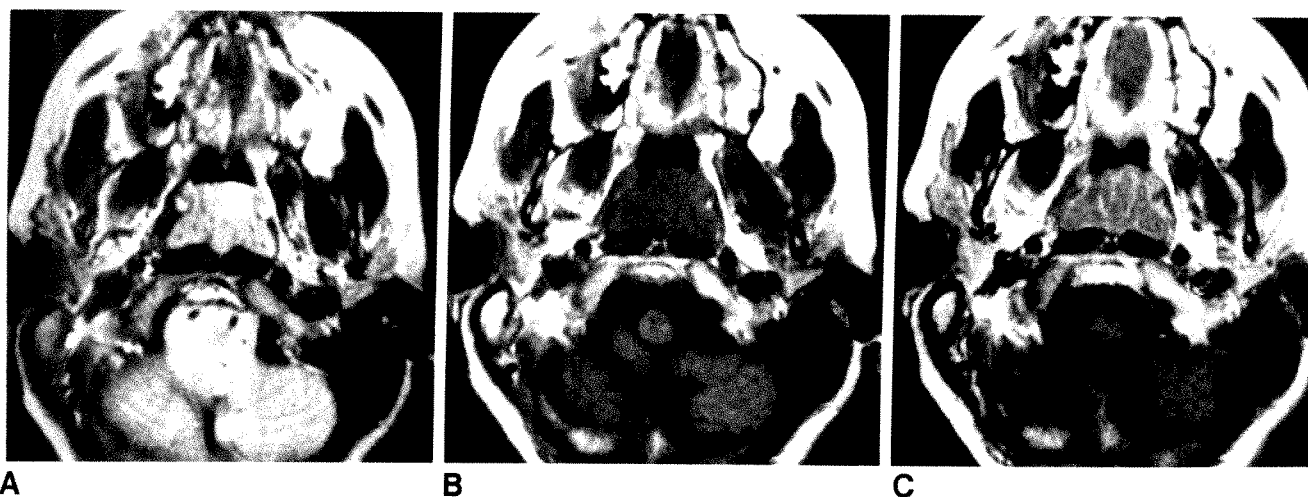


Fig. 7.—Lymphoid hyperplasia in nasopharynx.

A, Axial SE 1600/90 image, unenhanced. On T2-weighted image, nasopharyngeal tissue is bright and shows slight inhomogeneity and scattered internal patterns.

B, Axial SE 500/25 image, unenhanced. Mass is sharply margined, symmetrical, and of homogeneous low signal intensity. It has appearance similar to that of lymphoma in Fig. 6.

C, Axial SE 500/25 image, Gd-DTPA-enhanced. After Gd-DTPA administration, tumor shows moderate increase in signal intensity with inhomogeneous internal pattern mainly consisting of septations. As in lymphoma, there is compression of veli palatini muscles on both sides.

accurate relationship to vessels and nerves often cannot be demonstrated [9]. With MR, multiplanar imaging can show tumor extension in all three orientations, especially extension along cranial nerves V, VII, IX, and X [10–12]. MR with Gd-DTPA allows recognition of infiltration or involvement of the sheath of the carotid artery and the jugular vein. Also, contrast-medium-enhanced MR, with its better soft-tissue contrast, allows exact differentiation among small anatomic details, such as demonstration of both palatini muscles and the pharyngobasilar fascia [12, 13]. This fascia, as an essential structure for the evaluation of diseases of the nasopharynx, is not seen on CT scans. It separates the two most important compartments, the parapharyngeal space and the intrapharyngeal structures. Infiltration of this fascia is a sure sign of an aggressive tumor [4, 10, 11, 14].

In the differential diagnosis between tumor and inflammation, MR with T1- and T2-weighted sequences is superior to CT. Information regarding inflammation was best seen on T2-weighted images, but discrimination was also possible on contrast-enhanced T1-weighted sequences because the tumor usually did not enhance as much as the inflamed tissues.

Cystic processes with high signal intensities on T2-weighted images show no significant enhancement after contrast medium, but the walls of the cysts do enhance [15]. Contrast-enhanced MR allows appreciation of the internal patterns of the neoplasm, as for example necrosis or vascularity, but with both MR and CT mucosal spreading tumors were difficult to detect because the mucosa shows a high signal intensity on plain MR that increases after injection of Gd-DTPA. If tumor infiltrates bone marrow it is sometimes difficult to distinguish bone marrow from tumor. Both marrow and tumor enhance after administration of Gd-DTPA; the type of tumor determines which one becomes brighter. If the tumor shows an area of hemorrhage at a stage when it is very bright

on the T1-weighted nonenhanced image, after Gd-DTPA the tumor will enhance but the hemorrhage will not; thus, it may be difficult to differentiate between solid tumor and hemorrhage after Gd-DTPA administration. There is only limited experience concerning the fast imaging technique with Gd-DTPA for nasopharyngeal tumors. We have yet to find a significant difference; the different patterns of Gd-DTPA enhancement do not enable correlation between findings and histologic features. But different enhancement factors might be a criterion for discrimination.

It appears that Gd-DTPA is helpful in delineating nasopharyngeal tumors and their extension [16], but unenhanced T1 and T2 images are still needed. In addition, CT scans should be obtained if there is any question about infiltration of cortical bone.

The advantages of Gd-DTPA are better delineation of early infiltration by tumors and the possibility of improving differential diagnostic considerations. In diagnosing diseases of the nasopharynx and surrounding tissues, MR with Gd-DTPA is recommended as the method of choice in the evaluation of small tumors with infiltrating growth patterns, which are difficult to detect on the initial nonenhanced MR examination. Gd-DTPA is not needed in tumors that are well demarcated on plain T1- and T2-weighted sequences. In the follow-up to determine tumor recurrence, contrast medium is helpful when visualization of tumor areas is poor on T1- and T2-weighted nonenhanced images. The improved tumor delineation and identification of spread are helpful in planning radiation therapy.

#### REFERENCES

1. Dillon WP, Mills CM, Kjos B, Degroot J, Brant-Zawadzki M. Magnetic resonance imaging of the nasopharynx. *Radiology* 1984;152:731–738

2. Lloyd G, Land V, Phelps P, Howard D. MRI in evaluation of nose and paranasal sinus disease. *Br J Radiol* **1987**;60:957-968
3. Modder U, Lenz M, Steinbrich W. MRI of facial skeleton and parapharyngeal space. *Eur J Radiol* **1987**;7:6-10
4. Mancuso AA, Hanafee WN. Nasopharynx and parapharyngeal space. In: *Computed tomography and magnetic resonance imaging of head and neck*. Baltimore: Williams & Wilkins, **1985**:428-443
5. Zinreich SJ, Kennedy DW, Rosenbaum AE, Gayler BW, Kumar AJ, Stammberger W. Paranasal sinuses: CT imaging requirements for endoscopic surgery. *Radiology* **1987**;163:769-775
6. Bohman RN, Mancuso AA, Thompson J, Hanafee W. CT approach to benign nasopharyngeal masses. *AJR* **1981**;136:173-180
7. Silver JA, Mawad ME, Hilal SK, et al. Computed tomography of the nasopharynx and related spaces. Part I: Anatomy. *Radiology* **1983**;147:725-731
8. Silver JA, Mawad ME, Hilal SK, et al. Computed tomography of the nasopharynx and related spaces. Part II: Pathology. *Radiology* **1983**;147:733-738
9. Hagemann J, Witt CP, Jend-Rossmann T, Hörmann L, Jend HH, Bucheler E. Wertigkeit der Computertomographie bei Tumoren des Epi- und Oropharynx. *ROFO* **1983**;139:373-378
10. Teresi LM, Lufkin RB, Hanafee WN, et al. MR imaging of the nasopharynx and floor of the middle cranial fossa. Part I: Normal anatomy. *Radiology* **1987**;164:811-816
11. Teresi LM, Lufkin RB, Hanafee WN, et al. MR imaging of the nasopharynx and floor of the middle cranial fossa. Part II: Malignant tumors. *Radiology* **1987**;164:817-821
12. Vogl T. Kernspintomographie des Gesichtsschädels. In: Lissner J, Seiderer M, eds. *Klinische Kernspintomographie*. Stuttgart: Enke, **1986**:210-220
13. Mees K, Vogl T, Bauer M. MRI in diseases of head and neck—diagnostic possibilities. *Laryngo Rhinol-Otol (Stuttg)* **1987**;66:543-546
14. Mancuso AA, Bohman L, Hanafee W, Maxwell D. Computed tomography of the nasopharynx: normal and variants of normal. *Radiology* **1980**;137:113-121
15. Römer T, Tausch-Tremel R, Hamm B, Felix R, Wolf K-J. KST der Nasennebenhöhlen unter Verwendung von Gd-DTPA und Multiecho-Sequenzen. *ROFO* **1988**;149:171-177
16. Vogl T, Brüning R, Grevers G, Mees K, Bauer M, Lissner J. MRI of the oropharynx and tongue: comparison of plain and Gd-DTPA studies. *J Comput Assist Tomogr* **1988**;12:3-12

## The Cerebellum: 3. Anatomic-MR Correlation in the Coronal Plane

Gary A. Press<sup>1</sup>  
James W. Murakami<sup>2</sup>  
Eric Courchesne<sup>2</sup>  
Marjorie Grafe<sup>3</sup>  
John R. Hesselink<sup>1</sup>

Thin (5-mm) coronal high-field (1.5-T) MR images of four human brain specimens and 14 normal volunteers were correlated with myelin-stained microtomic sections of the specimen cerebella. The primary white-matter tracts innervating several hemispheric (posterior quadrangular, superior, and inferior semilunar, gracile, biventer, tonsil) and vermian (declive, folium, tuber) lobules are oriented perpendicularly to the coronal plane of section and are shown well on proton-density-weighted (long TR/short TE) and T2-weighted (long TR/long TE) spin-echo images, which provide excellent contrast between gray and white matter. Several of the surface sulci and fissures of the cerebellar hemispheres (including the superior posterior, horizontal, secondary, and posterolateral fissures) also course perpendicular to the coronal plane and are depicted well on T1-weighted (short TR/short TE) and T2-weighted images, which maximize contrast between CSF and parenchyma. The opportunity for side-to-side comparison of the hemispheres is a distinct advantage of the coronal view. Nevertheless, more obliquely oriented surfaces (preculminate, primary, inferior posterior, inferior anterior, and intraventricular fissures) and deep hemispheric structures (primary white-matter tracts to central, anterior quadrangular, and floccular lobules) may be obscured by volume-averaging in the coronal plane; moreover, much of the finer anatomy of the vermis is depicted poorly. The constant surface and deep anatomy of the cerebellum revealed on coronal images in normal volunteers encourages detailed mapping.

MR imaging in the coronal plane should be especially useful in identifying, localizing, and quantifying normal and abnormal morphologic differences between the cerebellar hemispheres.

*AJNR* 11:41–50, January/February 1990; *AJR* 154:593–602, March 1990

Received May 11, 1989; accepted July 18, 1989.

This work was supported by National Institute of Neurological Diseases and Stroke grant 5-RO1-NS19855 awarded to E. Courchesne.

<sup>1</sup> Department of Radiology and Magnetic Resonance Institute, University of California, San Diego, School of Medicine, 225 Dickinson St., San Diego, CA 92103-1990. Address reprint requests to G. A. Press.

<sup>2</sup> The Neuropsychology Research Laboratory, Children's Hospital Research Center, San Diego, CA 92123.

<sup>3</sup> Department of Pathology, University of California, San Diego, School of Medicine, San Diego, CA 92103-1990.

0361-803X/90/1543-0593  
© American Roentgen Ray Society

The cerebellum may be conceptualized as a stack of multiple transverse lobules, each of which is crescent-shaped with a wedge-like cross section that widens toward the periphery [1]. The spaces between the crescents are analogous to the cerebellar fissures. Transverse folds or sheets of white matter ("primary tracts" [1]) extend from central white-matter bodies (corpora medullaria) into the lobules. Because of this anatomic arrangement, it is most difficult to identify individual cerebellar lobules on axial MR images, which section parallel or nearly parallel to the courses of several important fissures and primary white-matter tracts. The sagittal plane of section (perpendicular to the courses of the fissures and white-matter tracts) proved ideal for the depiction of the anatomy of the lobules of the vermis and hemispheres, as described previously [1–3] (see Parts 1 and 2 of this report). The coronal plane of section (also perpendicular to the courses of many of the cerebellar fissures and white-matter tracts) offers an additional advantage by affording a side-to-side comparison on the same image.

This communication (Part 3) addresses specifically the topographic relationships of the cerebellar vermis and hemispheres in the coronal plane, and identifies detailed anatomy on coronal microtome and MR sections.

## Materials, Subjects, and Methods

MR studies of four formalin-fixed cadaver brains and 14 normal, healthy volunteers (13 male and one female 13–38 years old; mean age, 24.5 years) were performed in the coronal plane using a 1.5-T superconducting magnet (Signa, General Electric, Milwaukee). All volunteers and specimens were imaged with the use of a standard head coil. In all instances, 5-mm-thick slices with a matrix size of 256 × 256 were acquired using spin-echo sequences. A field of view (FOV) of 16–18 cm was used in volunteers; in specimen studies, an FOV of 12 cm was selected. T1-weighted sequences had the pulse parameters 600/20/4–6 (TR/TE/excitations). All volunteers received long TR examinations that were cardiac-gated to every other or every third heart beat, achieving an effective TR of approximately 2400–3800 msec, depending on the heart rate of each subject. Either two or four excitations per slice were used on long TR examinations of volunteers. A presaturation RF pulse for eliminating blood-flow artifacts along the Z axis (flow-void 1) was also used. Nongated long TR sequences performed on specimen brains had a TR of 2800 msec. TE values in long TR examinations were 20 and 70 msec, corresponding to proton-density-weighted and T2-weighted images, respectively. Slices obtained in volunteers were separated by a 3-mm gap. Specimen brains were imaged without interslice gaps (interleaved sections). A 28-sec scout sequence, 200/20/1 (24-cm FOV, 256 × 128 matrix), in the axial and sagittal planes was used to verify precise positioning of the subject or specimen brain before performing the protocol sequences. In every MR study, the coronal slices to be examined were selected by using this routine: On a midline sagittal scout image a line was drawn connecting the anterior aspect of the lingula and the nodulus [1]. Coronal sections through the entire cerebellum were then obtained parallel to the resulting line. The superior colliculus marked the anterior margin of the imaged region, whereas the inner table of the occipital bone at the level of the torcular Herophili marked the posterior margin in each instance.

Before MR, the specimen brains were fixed for 2–4 weeks in 10% neutral-buffered formalin. After MR, the cerebellum and brainstem were separated from the cerebral hemispheres and sectioned in the coronal plane at a thickness of 5 mm. The tissue blocks were dehydrated in a graded series of alcohols, cleared in xylene, and embedded in paraffin. Coronal sections of the cerebellum and brainstem were cut at a thickness of 15 µm using a Multirange Microtome (LKB, Stockholm). Adjacent anatomic sections corresponding closely to the MR images obtained by our normal volunteer protocol were stained with H and E and Luxol fast blue–cresyl violet.

The normal anatomic features of the cerebellar vermis and hemispheres visualized on the MR images and on the corresponding anatomic sections were determined by comparison with standard

references of neuroanatomy [4, 5], myelin-stained cerebellar sections [6, 7], and cerebellar embryogenesis and development [8–11].

Many systems of nomenclature have been used to describe the normal anatomy of mammalian and human cerebella [6, 9, 10]. In this report we follow closely the terminologies chosen by Ito [9] and Larsell [10].

## Results

### Gross Anatomic Features of the Cerebellum

Prior reports have discussed in detail the gross anatomy of the vermis [2, 3] and the hemispheres [1] of the cerebellum. A brief review of key anatomic elements will help in understanding the appearance of the cerebellum on successive coronal sections and MR images shown in this article.

The two large lateral masses (hemispheres) and wormlike median segment (vermis) of the cerebellum are traversed by a series of fissures. The whole of the cerebellum is thereby divided into three lobes, each containing a number of transverse-oriented lobules (see Table 1). The arrangement of the fissures, lobes, and lobules of the cerebellum is shown diagrammatically in Figure 1. The deep primary fissure is an important landmark separating the anterior and posterior lobes of the cerebellum. The posterolateral fissure separates the flocculonodular lobe from the posterior lobe. Additional, shallower fissures subdivide the anterior and posterior lobes into lobules (I–IX of the vermis and HII–HIX of the hemispheres). No hemispheric counterpart of vermician lobule I exists in humans [6, 9]. The flocculonodular lobe of the cerebellum contains only one vermician lobule (nodulus [X]) and one hemispheric lobule (flocculus [HX]). With the exceptions of the prepyramidal fissure (confined to the vermis) and the inferior posterior and inferior anterior fissures (confined to the hemispheres), the remainder of the fissures extends across the entire cerebellum.

From a central confluence of white matter known as the corpus medullare, three paired cerebellar peduncles extend proximally into the brainstem, whereas smaller primary white-matter tracts radiate distally into the lobules of the vermis and hemispheres. The central body of white matter is much larger within the hemispheres than within the vermis [1, 6].

Situated within the medial aspect of the corpus medullare posterolateral to the fourth ventricle are the paired deep nuclei

**TABLE 1: Components of the Human Cerebellum**

Cerebellar Lobe	Vermian Lobule Nomenclature		Hemispheric Lobule Nomenclature	
	Ito [9]	Larsell [10]	Ito [9]	Larsell [10]
Anterior	Lingula	I	—	HI <sup>a</sup>
	Centralis	II, III	Central lobule	HII, HIII
	Culmen	IV, V	Quadrangular lobule, anterior portion	HIV, HV
Posterior	Declive	VI	Quadrangular lobule, posterior portion	HVI
	Folium vermis	Superior VIIA	Semilunar lobule, superior portion	HVIIA
	Tuber vermis	Inferior VIIA	Semilunar lobule, inferior portion	HVIIA
		VIIIB	Gracile lobule	HVIIIB
	Pyramis	VIIIA, VIIIB	Biventer	HVIII
	Uvula	IX	Tonsil	HIX
Flocculonodular	Nodulus	X	Flocculus	HX

Note.—This table is reprinted from Courchesne et al. [3].

<sup>a</sup> Hemispheric counterpart of vermician lobule I is usually absent in humans [6, 9].



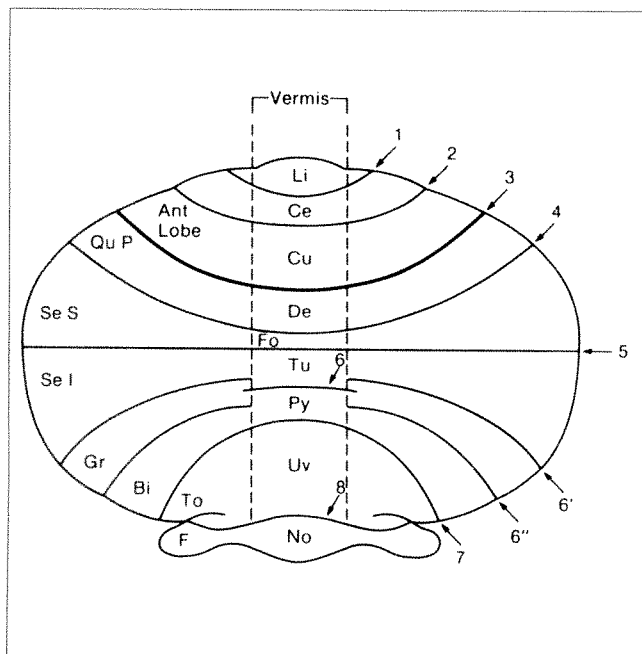


Fig. 1.—Diagram of lobar and lobular structure of cerebellum. This anatomic diagram of human cerebellum permits rapid identification of locus of any given term used in this article. Abbreviations used to designate the anterior lobe of the hemisphere as a whole, and each of the individual lobules of the posterior lobe of the hemisphere and flocculus, are positioned on the left side of the diagram. Arranged on the right side of the diagram are the numerals used to designate the major fissures subdividing the cerebellum. Confined by the central pair of broken lines are abbreviations used to designate the lobules of the vermis. Drawn in bold fashion is the primary fissure (3), which forms the boundary between the anterior and posterior lobes of the cerebellum. See key for abbreviations. (Reprinted from Press et al. [1].)

of the cerebellum. From medial to lateral they are the fastigial, globose, emboliform, and dentate nuclei. The largest and most familiar of the cerebellar nuclei, the dentate, has characteristic undulating outwardly convex margins [1].

#### Anatomic Features of the Cerebellum on Coronal Microtome and MR Sections

Analysis of the anatomic features of the cerebellum in six coronal sections showed sequential and reproducible changes in the contours and relationships of the individual lobules, corpora medullaria and smaller white-matter branches, brainstem, adjacent cisterns, and cerebellar fissures.

The individual lobules of the cerebellar *hemispheres* could be identified confidently and consistently by recognizing (1) the intrinsic order of branching and configuration of their primary white-matter tracts (evident on proton-density- and T2-weighted images) and (2) the sequence of fissures that divides the cerebellar parenchyma into discrete lobules (evident on T1- and T2-weighted images). The positions and configurations of the surrounding noncerebellar structures often provided helpful secondary clues. Within the *vermis*, however, identification of individual lobules on coronal sections was difficult because of volume-averaging of the more delicate fiber pathways and gray-matter structures, combined with variability of the precise angle of branching (and sectioning) of the primary tracts.

#### Key to Abbreviations Used in Figures

A	artifact of sectioning
Ant Lobe	anterior lobe of cerebellar hemisphere
ao	atlantooccipital joint
A Ve	lobules of anterior lobe of vermis
Bi	biventer
C	central lobule
Ce	centralis
Cm	corpus medullare
Cu	culmen
C1	posterior arch of C1 vertebra
D	dentate nucleus
De	declive
dm	digastric muscle
F	flocculus
fm	foramen magnum
Fo	folium vermis
Gr	gracile lobule
ibf	intrabiventral fissure
icp	inferior cerebellar peduncle
jb	jugular bulb
jt	jugular tubercle
Li	lingula
M	medulla
ma	rectus capitis posterior major muscle
mcp	middle cerebellar peduncle
Mi	midbrain
mi	rectus capitis posterior minor muscle
mv	medullary velum
No	nodulus
P	pons
pl	posterior cortical lip of foramen magnum
pt	primary white-matter tract
P Ve	lobules of posterior lobe of vermis
Py	pyramis
Qu A	quadrangular lobule, anterior portion
Qu P	quadrangular lobule, posterior portion
scp	superior cerebellar peduncle
Se I	semilunar lobule, inferior portion
Se S	semilunar lobule, superior portion
so	superior oblique muscle
tf	transverse fossa
To	tonsil
Tu	tuber vermis
Uv	uvula
V	fourth ventricle
1	precentral fissure
2	preculminate fissure
3	primary fissure
4	superior posterior fissure
5	horizontal fissure
6	prepyramidal fissure (vermis only)
6'	inferior posterior fissure (hemisphere only)
6''	inferior anterior fissure (hemisphere only)
7	secondary fissure
8	posterolateral fissure
9	vallecule
10	paramedian sulcus

Several observations can be made if the coronal anatomic or MR sections are considered in sequence from the most anterior plane (1) toward the most posterior plane (6).

*Surface features:*

1. In each coronal plane of section, the overall appearance of the brainstem and cerebellum is similar to a bird or butterfly with wings outstretched. In planes 1 and 2 (Figs. 2 and 3), the dorsal aspect of the midbrain, pons and/or fourth ventricle, and medulla constitute the "body" from which extend the "wings" formed by the middle cerebellar peduncles, corpora medullaria, and anterior portion of the hemispheric parenchyma. In planes 3–6 (Figs. 4–7), the body (now consisting of varying lobules of the vermis only) appears much smaller, whereas the wings (now consisting of the posterior portion of the hemispheric parenchyma and corpora medullaria or primary white-matter tracts) at first increase (plane 3, Fig. 4) and then decrease (planes 4–6, Figs. 5–7) in size.

2. The crescent-shaped lobules of the cerebellum have varying radii of curvature [1]; consequently, all are not present in every coronal section. For example, the group of anterior lobules (HII–HV) of the hemispheres and those of the vermis (I–V) have small radii relative to the posterior lobules (e.g., HVIIA and HVII B); accordingly, the bulk of the anterior lobules is seen on the anterior-most three sections obtained by our MR protocol, whereas several posterior lobules are seen in five or six sections.

3. Unlike the crescent-shaped lobules forming the greater portion of the cerebellum, the flocculus and tonsil are smaller, ovoid lobules that protrude from the anterior and inferomedial surfaces of the hemispheres, respectively [1]. The flocculus is one of three bands of parenchyma adjacent to the middle cerebellar peduncle on coronal plane 1 (Fig. 2). The flocculus is sandwiched between a band of parenchyma above the peduncle (containing the anterior aspect of the central and

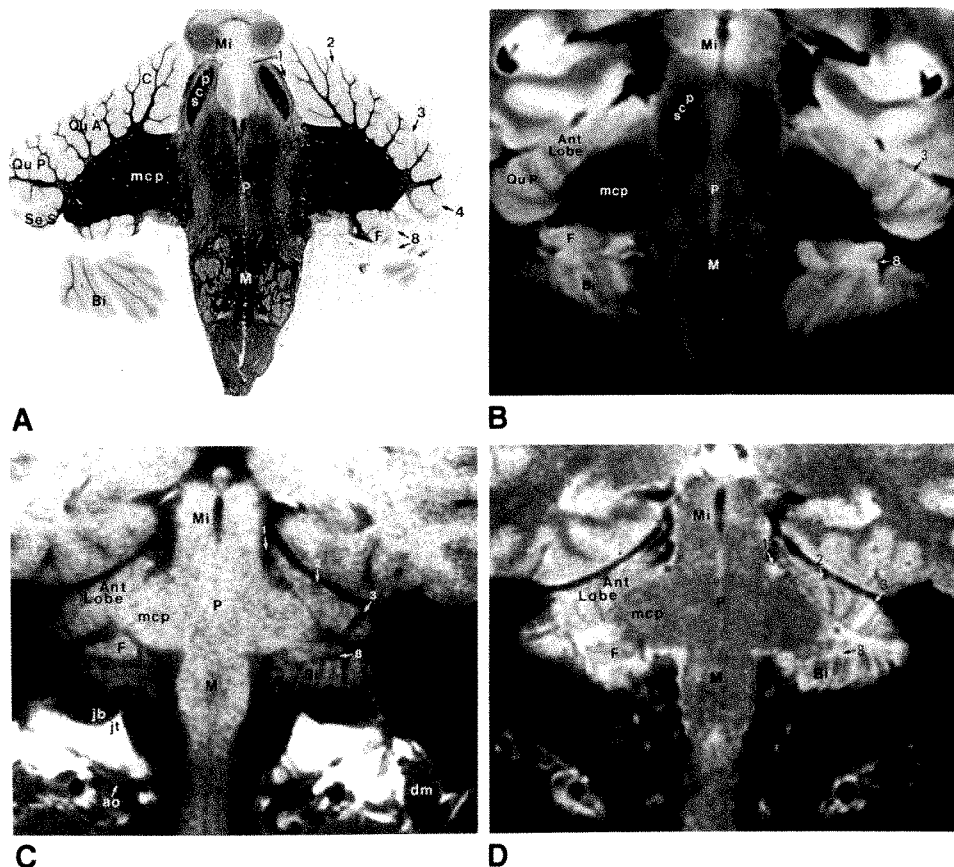


Fig. 2.—Plane 1, through brainstem, middle cerebellar peduncles, flocculus, and anterior-most portions of cerebellar hemispheres. See key for abbreviations.

A, Coronal microtome section of specimen brain. (Luxol fast blue–cresyl violet myelin stain)

B, Corresponding coronal proton-density-weighted image, 2800/20/4, of the same specimen brain before sectioning.

C and D, Coronal T1-weighted, 600/20/4 (C), and cardiac-gated T2-weighted, 3642/70/2 (D), images of 38-year-old normal male volunteer.

Midbrain, pons, and medulla are continuous; middle cerebellar peduncles join pons to cerebellar hemispheres. Superior cerebellar peduncles diverge within midbrain just beneath their decussation. Three distinct symmetric bands of cerebellar parenchyma arranged above and below middle cerebellar peduncles appear to converge laterally in plane 1. Single band above peduncle represents anterior aspect of central and anterior quadrangular lobules on each side. Depending on precise angle of section and size of lobules, small portions of posterior quadrangular lobule and superior semilunar lobule may be sectioned at lateral-most aspect of this band. Middle band of tissue situated immediately beneath middle cerebellar peduncle represents flocculus of cerebellar hemisphere. Posterolateral fissure separates flocculus from third band of hemispheric tissue situated most inferiorly. This third band is the anterior aspect of the biventer. Primary white-matter tracts to anterior lobules of hemispheres, although shown well on thin (15- $\mu$ m) microtome section (A), remain poorly resolved on thicker (5-mm) MR images (B and D) owing to volume-averaging. Extracerebral landmarks in this plane are best demonstrated on T1-weighted image (C) and include posterior aspect of jugular tubercle (jt), jugular bulb (jb), atlantooccipital joint (ao), and insertion of posterior belly of digastric muscle (dm) medial to mastoid tip.

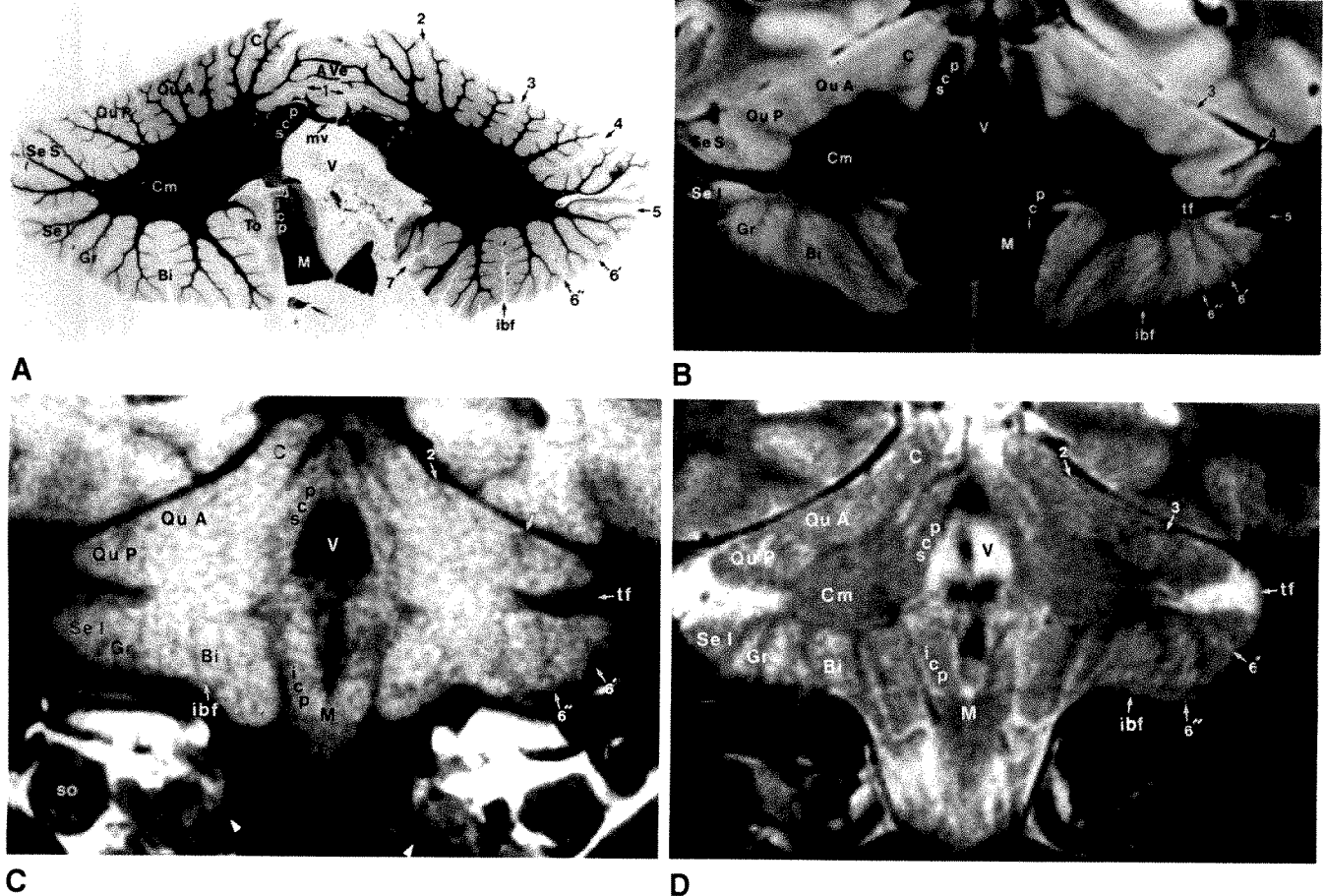


Fig. 3.—Plane 2, through fourth ventricle, superior and inferior cerebellar peduncles, medulla, corpora medullaria, and anterior and posterior lobes of cerebellum. See key for abbreviations.

A, Coronal microtome section of specimen brain. (Luxol fast blue-cresyl violet myelin stain)  
 B, Corresponding coronal proton-density-weighted image, 2800/20, of same specimen brain before sectioning.  
 C and D, Coronal T1-weighted, 600/20 (C), and cardiac-gated T2-weighted, 3642/70 (D), images of 38-year-old normal male volunteer.  
 Flocculus is no longer present. Fourth ventricle is most prominent in this section. Its superolateral margins are formed by superior cerebellar peduncles; inferior cerebellar peduncles are separated from inferolateral margins of fourth ventricle by vestibular nuclei. In this section a laterally directed space, the transverse fossa (tf, B-D), is formed by converging folia of superior, lateral, and inferior hemispheric surfaces; this space may be distinguished from a true cerebellar fissure by its relatively large size and "nonanatomic" separation of lobules (e.g., posterior quadrangular and inferior semilunar lobules on C and D). Depending on precise plane of section, quadrigeminal plate or anterior extreme of anterior lobe of vermis may be sectioned above fourth ventricle. Primary white-matter tracts to larger lobules of posterior lobe of cerebellar hemispheres (e.g., inferior semilunar, gracile, biventer) are better resolved than those to smaller lobules of anterior lobe (B and D). This is true also of more posterior coronal MR images (compare with Figs. 4B, 4D, 5B, and 5D). On T1-weighted image (C), gray and white matter have similar signal intensity. Nevertheless, borders of parenchyma with surrounding CSF are better defined on T1-weighted image than on T2-weighted image (D), owing to persistent CSF flow artifacts adjacent to medulla, which resemble parenchyma on latter image. In this plane, note that biventer forms inferomedial border of each hemisphere, where it abuts medulla (B and C). Extraparenchymal landmarks identified in this plane in vivo include vertebral arteries (arrowheads) entering subarachnoid space above sulcus anterior and superior oblique muscles (so) sectioned transversely beneath occipital bone (C).

anterior quadrangular lobules) and an additional band below the peduncle (containing the anterior aspect of the biventer).

On coronal planes 3 and 4 (Figs. 4 and 5) (posterior to the medulla), the tonsils are seen in an immediately paramedian location, indenting the lateral aspects of the inferior vermis. The tonsils lie medial to the medial segment of the biventer on each side.

4. The superior posterior, horizontal, secondary, and posterolateral fissures, which form the boundaries of many of the cerebellar lobules, are reliably sectioned perpendicular to their course, and visible on coronal T1-weighted images (Figs. 2C, 3C, 4C, 5C, 6C, and 7C) or T2-weighted images (Figs. 2D, 3D, 4D, 5D, 6D, and 7D). The intracural sulcus 1, which divides the superior semilunar lobule into superior and inferior

portions [1, 6, 12], is also seen consistently on several of these images (Figs. 4C, 5C, 6C, and 7C). The lateral portion of the precentral fissure, which separates the central lobule from the junction of the midbrain and pons [1], is reliably seen on both the anatomic section (Fig. 2A) and MR images (Figs. 2C and 2D) through plane 1.

In normal volunteers, only the approximate locations of the more obliquely sectioned primary, inferior posterior, inferior anterior, and intrabiventral fissures may be identified on T2-weighted images (Figs. 3D, 4D, 5D, and 6D) as radially oriented peripheral zones of mild hyperintensity relative to parenchyma. The primary fissure lies in the zone of hyperintensity just medial and superior to the primary tract innervating the posterior quadrangular lobule; the inferior posterior

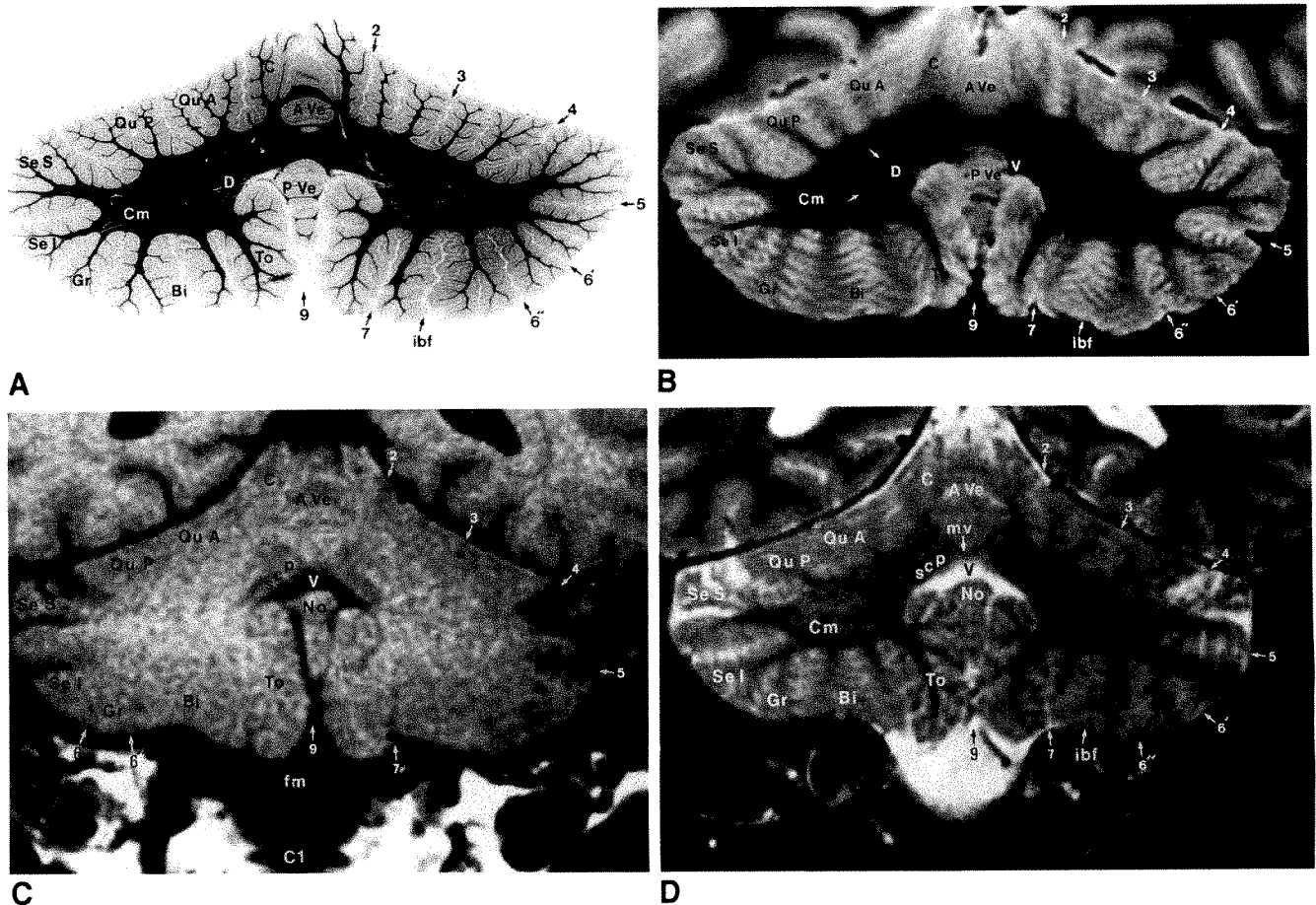


Fig. 4.—Plane 3, through anterior and posterior lobes of cerebellar hemispheres and vermis. See key for abbreviations.

A, Coronal microtome section of specimen brain. (Luxol fast blue-cresyl violet myelin stain)

B, Corresponding coronal proton-density-weighted image, 2800/20, of same specimen brain before sectioning.

C and D, Coronal T1-weighted, 600/20 (C), and cardiac-gated T2-weighted, 3642/70 (D), images of 38-year-old normal male volunteer.

This is the initial section posterior to the medulla; only the posterolateral recesses of the fourth ventricle are included. The inferomedial aspect of each hemisphere is now formed by tonsils, which abut inferior aspect of vermis superiorly, and may abut each other inferiorly in midline. This is the final section to include a small portion of the central lobule. Corpus medullare attains its greatest size on this image. Dentate nucleus is seen clearly within medial aspect of each corpus medullare on proton-density-weighted image (B). White matter immediately peripheral to nucleus (B, arrows) has lower signal intensity than remainder of white matter, most likely because of iron deposition. Transverse fossa is no longer present. Horizontal fissure (5) separates superior and inferior semilunar lobules, whereas intracural sulcus 1 (unlabeled) divides superior semilunar lobule into superior and inferior portions. Detailed anatomy of vermis is not well defined in coronal plane. Nevertheless, fourth ventricle, and overlying medullary velum and central confluence of vermian white matter, provide landmarks for dividing lobules of anterior lobe of vermis from those of posterior lobe and nodulus. Extraparenchymal landmarks in this plane include CSF within foramen magnum (fm, C) and vallecule posterior to brainstem, and posterior arch of C1 (C1, C).

fissure lies between the primary tracts innervating the inferior semilunar and gracile lobules; and the inferior anterior fissure lies between the primary tracts innervating the gracile lobule and the lateral segment of the biventer.

The preculminate fissure separating the central and anterior quadrangular lobules of the anterior lobe tends to be obscured completely on coronal MR images (Figs. 2B–2D, 3B–3D, and 4B–4D) relative to microtome sections (Figs. 2A, 3A, and 4A). The reasons for this are (1) its vertical orientation and small radius of curvature, which causes it to be sectioned most obliquely on coronal images, combined with (2) volume averaging inherent in 5-mm-thick MR sections. Thinner (15- $\mu$ m) microtome sections minimize these difficulties and depict the finest anatomic details. The expected location of the preculminate fissure is indicated on the MR images (Figs. 2C, 2D, 3C, 3D, and 4B–4D).

*Deep features:*

1. In plane 1 (Fig. 2), the middle cerebellar peduncles join the pons to the corpora medullaria of the cerebellar hemispheres; the multiple slender primary tracts emanating directly from the periphery of the hemispheric corpora medullaria help to distinguish them from the middle cerebellar peduncles, which have no subordinate branches.

2. Unlike the larger middle cerebellar peduncles, which originate from the ventrolateral surface of each hemisphere and course nearly horizontally to reach the pons, the smaller superior and inferior cerebellar peduncles originate more medially and course nearly vertically to reach the brainstem. For this reason, the superior and inferior peduncles are sectioned longitudinally in the coronal plane, whereas the middle peduncles are sectioned more transversely. The fourth ventricle is the key to localizing the superior and inferior cerebellar peduncles in planes 2 and 3 (Figs. 3 and 4). The superior peduncles on each side and superior medullary velum in the

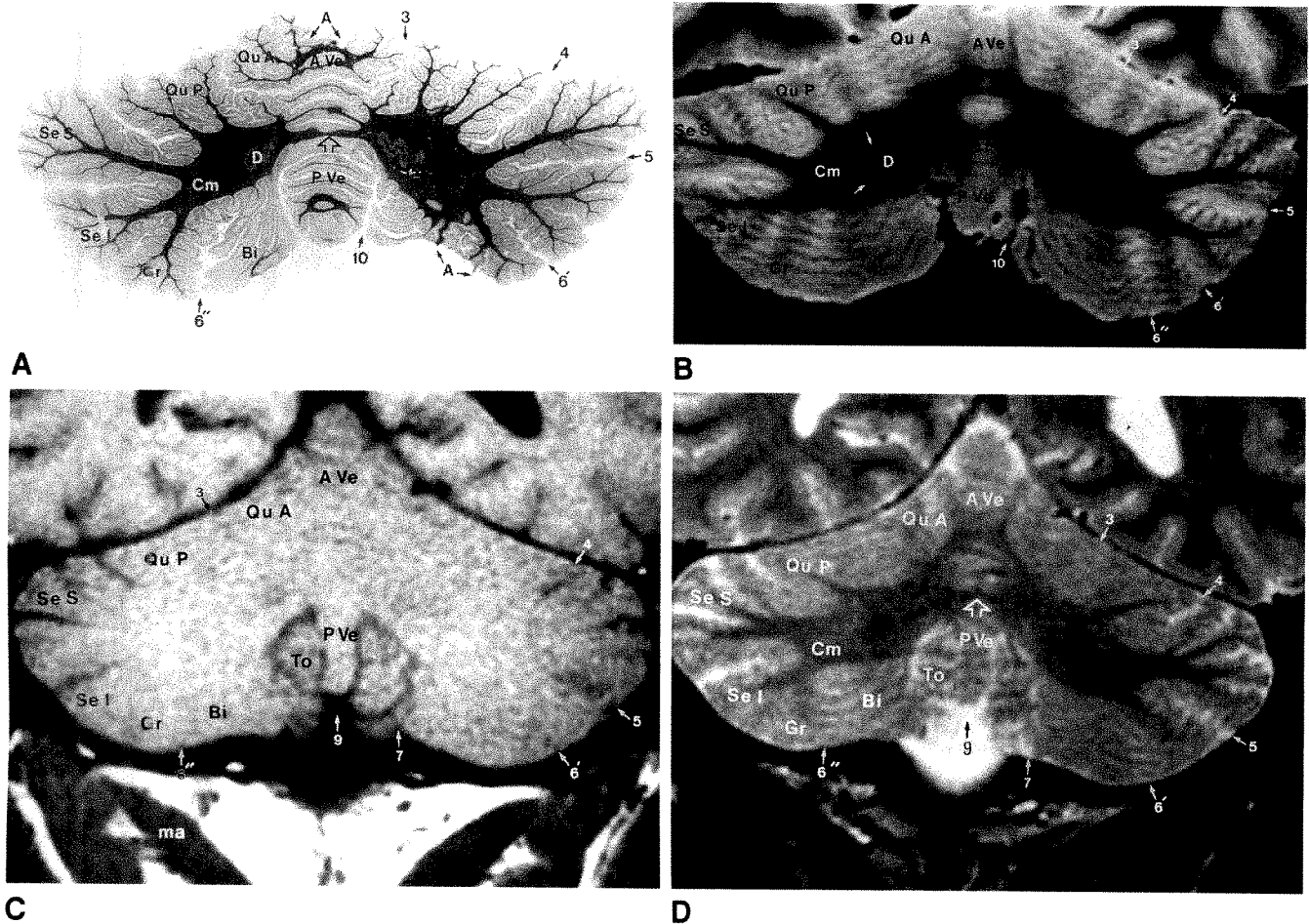


Fig. 5.—Plane 4, through anterior and posterior lobes of cerebellar hemispheres and vermis. See key for abbreviations.

A, Coronal microtome section of specimen brain. (Luxol fast blue-cresyl violet myelin stain)

B, Corresponding coronal proton-density-weighted image, 2800/20, of same specimen brain before sectioning.

C and D, Coronal T1-weighted, 600/20 (C), and cardiac-gated T2-weighted, 3642/70 (D), images of 38-year-old normal male volunteer.

Corpora medullaria begin to decrease in size in this section. This is the last section to include a small portion of the tonsils (C and D). Two major bands of white matter crossing vermis are resolved on MR (B and D): superior band (unlabeled) is a portion of the primary tract to culmen that ascends in a nearly vertical course; inferior band (open arrows, A, B, and D) is horizontally oriented primary tract connecting to declive, folium, and tuber. These white-matter bands help distinguish anterior lobe of vermis (above upper band) from posterior lobe of vermis (below lower band) (B and D). Portion of vermis between two bands represents region of overlap between anterior and posterior lobes of vermis. Solid arrows indicate iron deposition in region of dentate. Distinctive V-shaped configuration of rectus capitus posterior major (ma) muscles is an extraparenchymal landmark identified in this plane (C).

midline form an arch over the top of the fourth ventricle (Figs. 3A and 4D); the inferior peduncles, on the other hand, lie medial to the corpora medullaria, separated from the fourth ventricle by the vestibular nuclei, and course inferiorly to form the greater part of the dorsal portion of the medulla (Fig. 3).

3. The branching pattern of the primary white-matter tracts to the hemispheres is constant [1], and many of the tracts may be identified in successive coronal sections. Above the primary fissure, only the single tract innervating the central lobule is frequently visualized on coronal MR planes 2 and 3 (Figs. 3B, 3D, 4B, and 4D). The tracts connecting to the anterior quadrangular lobule are sectioned more obliquely on coronal MR images and usually remain unresolved (Figs. 3B, 3D, 4B, 4D, 5B, and 5D). Nevertheless, they are well visualized on the anatomic sections (Fig. 3A, 4A, and 5A). The next clearly identifiable primary tracts on coronal MR connect the corpus medullare with the posterior quadrangular lobule. These tracts lie inferior to the primary fissure on planes 2–6

(Figs. 3–7). Situated immediately above and below the horizontal fissure are the primary tracts to the superior and inferior semilunar lobules, respectively; these tracts were seen in T2-weighted coronal MR planes 3–6 (Figs. 4–7) in all specimens and normal volunteers. The tract innervating the gracile lobule is resolved on three planes (Figs. 3–5) only, situated medial to the tract to the inferior semilunar lobule. The biventer receives two primary tracts, one directed inferolaterally and the other inferomedially to innervate the two segments of the lobule (planes 2 and 3, Figs. 3 and 4). The primary tract innervating the tonsil originates most medially from the inferior aspect of the corpus medullare. The tract may be identified only on coronal plane 3 (Fig. 4) immediately posterior to the brainstem.

4. Although, in our experience, the vermician white-matter branching pattern is constant also [3], only the horizontally oriented primary tract connecting with the declive, folium, and tuber [3] is sectioned reliably perpendicular to its course in



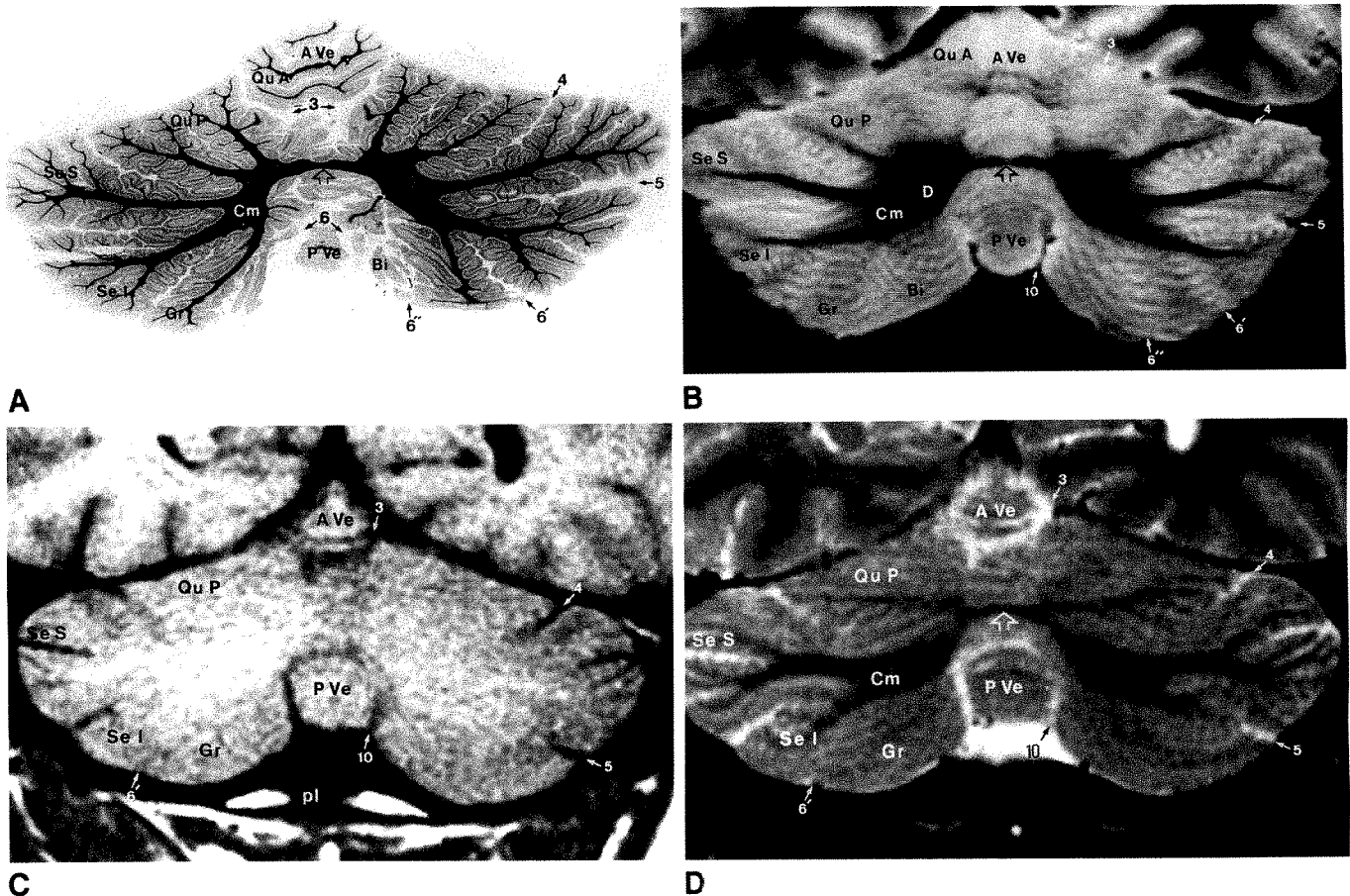


Fig. 6.—Plane 5, through posterior lobules of cerebellar hemispheres and anterior and posterior lobes of vermis. See key for abbreviations.

A, Coronal microtome section of specimen brain. (Luxol fast blue-cresyl violet myelin stain)

B, Corresponding coronal proton-density-weighted image, 2800/20, of same specimen brain before sectioning.

C and D, Coronal T1-weighted, 600/20 (C), and cardiac-gated T2-weighted, 3642/70 (D), images of 38-year-old normal male volunteer.

This section includes mainly (if not exclusively) lobules of posterior lobe of hemispheres. Only a small portion of the anterior quadrangular lobule may be seen (A and B). Primary fissure (3, A, C, and D) traverses vermis above white-matter tract to declive, folium, and tuber (open arrows, A, B, and D), whereas prepyramidal fissure (6) may be identified beneath this tract and is especially well seen on anatomic section (A). Because this plane lies posterior to tonsils, it is the biventer or gracile lobule (depending on precise point of section) that forms inferomedial margin of cerebellar hemispheres. This is the final section to include a portion of the corpora medullaria. An extraparenchymal landmark identified in this plane in vivo is posterior lip (pl) of foramen magnum (C).

the coronal plane; this tract provides a helpful landmark for the localization of these three lobules as a group in MR planes 4–6 (Figs. 5–7). Less reliably visualized is the thicker, nearly vertically oriented primary tract innervating the culmen [3]; portions of this tract may be visualized in MR planes 4 and 5 (Figs. 5B, 5D, and 6B). The individual tracts to the lingula, centralis, pyramis, uvula, and nodule of the vermis are indistinct on MR. The reasons for this include their oblique course relative to the coronal plane of section combined with their more delicate caliber, which permits volume-averaging with overlying gray matter on MR sections.

5. The dentate nucleus is visualized within the medial portion of each corpus medullare on planes 3 and 4 (Figs. 4 and 5); it appears as an oval curvilinear structure with an undulating margin. The dentate is seen best on proton-density-weighted images of specimen brains (Figs. 4B and 5B); its signal intensity is intermediate between that of white and gray matter. The white matter situated immediately peripheral to the nucleus is more hypointense than the remainder of the

corpora medullaria (Figs. 4B and 5B). Deposition of iron within the region of the dentate nucleus and surrounding white matter [13] may account for these unique signal-intensity characteristics. The remaining deep nuclei (fastigial, globose, and emboliform) of the cerebellum, which lie within the corpora medullaria medial to the dentate, are not resolved on MR, likely owing to their small size (<1 cm) [1].

#### Imaging landmarks in coronal MR:

By using the slice-selection routine outlined in Materials, Subjects, and Methods, we obtained reproducible coronal sections through the cerebellum, posterior fossa, and posterior cervicocranial junction region in our normal volunteers. Nonparenchymal landmarks consistently identified in each of the six imaging planes in our volunteers included (1) plane 1 (Fig. 2C): posterior aspect of jugular tubercle, jugular bulb, atlantooccipital joint, and insertion of posterior belly of digastric muscle medial to mastoid tip; (2) plane 2 (Fig. 3C): vertical portion of sigmoid sinus, vertebral arteries entering subarachnoid space above sulcus arteriosus, and transverse section

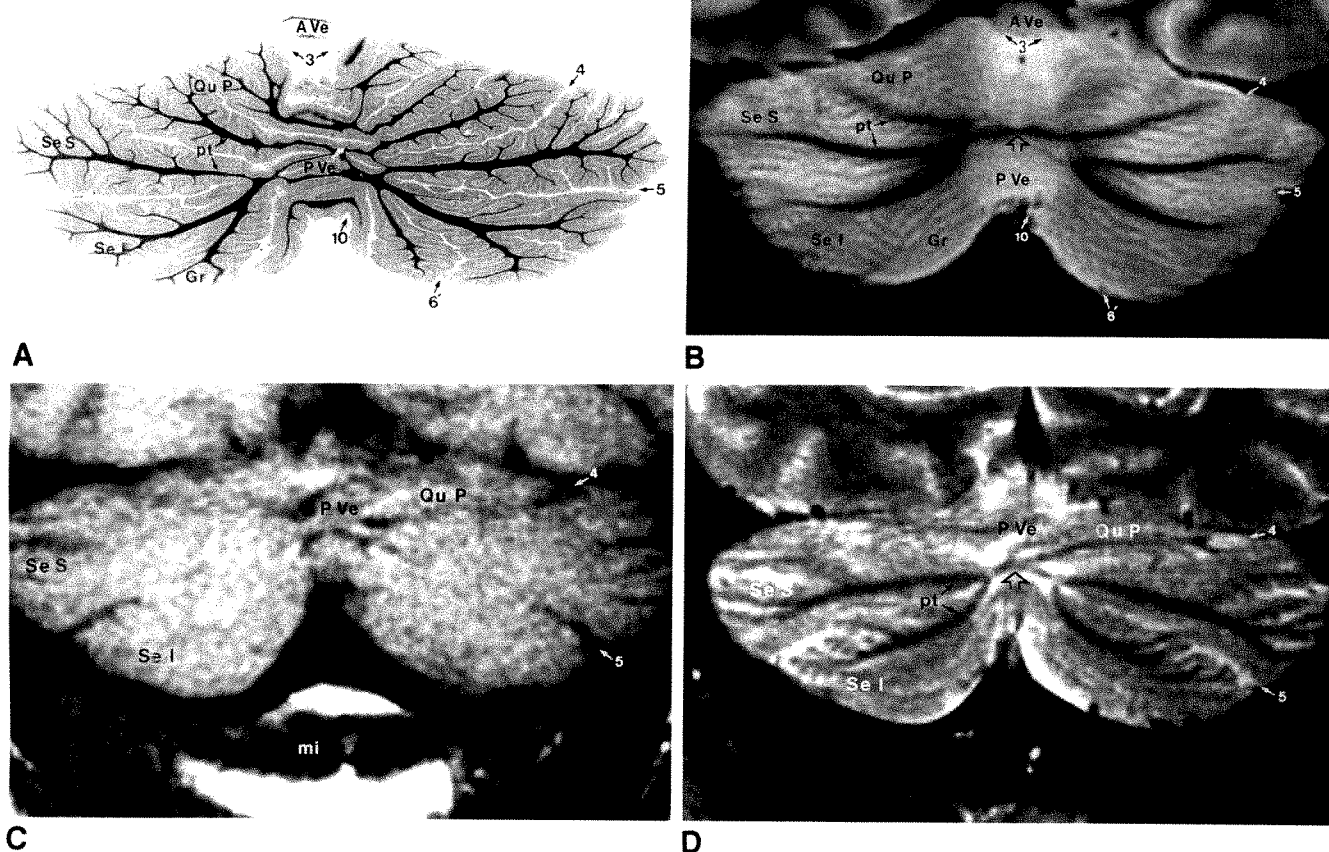


**Fig. 7.**—Plane 6, through posterior lobe of cerebellar hemispheres and vermis. See key for abbreviations.  
**A,** Coronal microtome section of specimen brain. (Luxol fast blue-cresyl violet myelin stain)  
**B,** Corresponding coronal proton-density-weighted image, 2800/20, of same specimen brain before sectioning.  
**C and D,** Coronal T1-weighted, 600/20 (**C**), and cardiac-gated T2-weighted, 3642/70 (**D**), images of a 38-year-old normal male volunteer.  
 Primary white-matter tracts innervating posterior quadrangular, superior, and inferior semilunar lobules on either side diverge laterally (**B** and **D**). Posterior extreme of vermis is sectioned in vicinity of termination of primary tract to declive, folium, and tuber (open arrows, **B** and **D**). Extraparenchymal landmark consistently identified in this plane in vivo is horizontally oriented junction of rectus capitis posterior minor (**mi**) muscles in midline immediately beneath occipital bone (**C**).

of superior oblique muscles beneath the occipital bone; (3) plane 3 (Fig. 4C): CSF within foramen magnum posterior to brainstem, and posterior arch of C1; (4) plane 4 (Fig. 5C): distinctive curve of the rectus capitis posterior major muscles diverging on either side of a triangular-shaped space filled with suboccipital fat; (5) plane 5 (Fig. 6C): posterior lip of foramen magnum; and (6) plane 6 (Fig. 7C): horizontal junction of the rectus capitis posterior minor muscles in the midline immediately beneath the occipital bone. The posterior aspect of the straight sinus at its junction with the torcular Herophili appears on the coronal section just posterior to the vermis (not shown).

## Discussion

The surface features and deeper anatomy of the cerebellar vermis and hemispheres in normal individuals are highly standardized, encouraging detailed mapping and quantification.

The overall transverse orientation of most of the lobules of the cerebellum explains why the sagittal and coronal planes of section are ideal for systematically depicting its physiologically significant parts. Excellent resolution of the horizontally oriented white-matter tracts, overlying cortex, surface sulci, and fissures of the bulk of the cerebellar hemispheres may be obtained by thin-section coronal MR. Moreover, the opportunity for side-to-side comparison is a distinct advantage provided by the coronal view. Nevertheless, those delicate primary tracts and surface features within the vermis and hemispheres that are oriented obliquely to the horizontal plane remain undisclosed by coronal MR owing to volume averaging. In particular, most of the detailed anatomy of the anterior lobe of the vermis and hemispheres and the inferior portion of the posterior lobe of the vermis (i.e., the pyramis, uvula, and nodulus) is poorly resolved on coronal images. Fortunately, the sagittal plane shows well the detailed anatomy of the entire vermis [2, 3] and the bulk of the hemispheres [1]. However, several primary tracts to the smaller lobules of the

anterior lobe of the cerebellar hemispheres remain unresolved even on 5-mm-thick sagittal MR images [1].

We speculated that the serpentine configuration of the dentate nuclei combined with iron deposition within their substance hampered their visualization on long TR sequences performed in the sagittal plane [1]. To our surprise, the dentate nuclei were visualized reliably in similarly fixed specimen brains studied in the coronal plane using the same sequences. Perhaps owing to their intrinsic shape, volume averaging of surrounding low-intensity white matter is decreased when the dentate nuclei are sectioned in the coronal plane. This result requires further investigation.

Knowledge of the detailed anatomy of the cerebellum as revealed by MR has proved useful in the comparison of various patient groups. For example, decreased size of the declive, folium, and tuber of the vermis was measured in a subpopulation of adult patients with autism [14]. A similar observation was made in patients with fragile X, a chromosomal abnormality associated with mental retardation and autisticlike symptoms [15], and in patients with schizophrenia associated with perinatal brain insult [16]. Recently, when the cumulative area of the cerebellar hemispheres of autistic individuals was measured on sagittal MR images, decreased cerebellar hemisphere size was demonstrated also [17].

Certain sensory, motor, and cognitive functions are known to be influenced predominantly by one or the other cerebellar hemisphere. For example, dysarthria is more common after injury to the left superior paravermian cerebellar hemisphere [18]; on the other hand, the inferolateral portion of the right hemisphere is important in semantic association, as shown by increased metabolic activity on positron emission tomographic scans [19]. In addition, naturally occurring asymmetries in cerebral-hemisphere (frontal-lobe) metabolism are correlated with asymmetry in the opposite direction in cerebellar-hemisphere metabolism in normal subjects [20]. Likewise, lesions of one cerebral hemisphere (frontal [21] or parietal [22] lobe) are associated with decreased glucose and oxygen metabolism and diminished blood flow in the contralateral cerebellar hemisphere (crossed cerebellar diaschisis). Most recently, evidence for a "reverse cerebellar diaschisis" (reduction in glucose metabolism within certain portions of the cerebral hemispheres owing to a reduction in specific cerebellar efferents to thalamus and forebrain structures) was found in patients with paraneoplastic cerebellar degeneration [23]. We speculate that MR imaging in the coronal plane will facilitate identification and quantification of normal and abnormal morphologic differences between the cerebellar hemispheres by allowing a side-to-side comparison in the same image. The detailed map of the cerebellum presented herein may enhance the specificity of studies correlating the anatomy of the cerebellum with its functions and metabolism.

Finally, we emphasize that the coronal and sagittal planes of section are ideal for visualizing intrinsic cerebellar anatomy. Accurate assessment of the normal anatomy of the brainstem [24], as well as localization and characterization of lesions of the posterior fossa extrinsic to the cerebellum (e.g., internal

auditory canal neurinomas, meningiomas), may require axial images [25].

## REFERENCES

1. Press GA, Murakami JW, Courchesne E, et al. The cerebellum in sagittal plane—anatomic-MR correlation: 2. The cerebellar hemispheres. *AJNR* 1989;10:667-676, *AJR* 1989;153:837-846
2. Press GA, Courchesne E, Murakami JW, Hesselink JR. The vermis in sagittal plane. Presented at the annual meeting of the American Society of Neuroradiology, Chicago, May 1988
3. Courchesne E, Press GA, Murakami JW, et al. The cerebellum in sagittal plane—anatomic-MR correlation: 1. The vermis. *AJNR* 1989;10:659-665, *AJR* 1989;153:829-835
4. Nieuwenhuys R, Voogd J, Huijzen C. *The human central nervous system: a synopsis and atlas*, 2d ed. New York: Springer-Verlag, 1981
5. Carpenter MB. *Human neuroanatomy*, 7th ed. Baltimore: Williams & Wilkins, 1976
6. Angevine JB Jr, Mancall EL, Yakovlev PI. *The human cerebellum. An atlas of gross topography in serial sections*. Boston: Little, Brown, 1961
7. DeArmond SJ, Fusco MM, Dewey MM. *Structure of the human brain: a photographic atlas*. New York: Oxford University, 1976
8. Fox CA, Snider RS, eds. *The cerebellum*. Amsterdam: Elsevier, 1967
9. Ito M. *The cerebellum and neural control*. New York: Raven, 1984
10. Larsell O. The development of the cerebellum in man in relation to its comparative anatomy. *J Comp Neurol* 1947;87:85-129
11. Lemire RJ, Loeser JD, Leech RW, Alvord EC Jr. *Normal and abnormal development of the human nervous system*. Hagerstown, MD: Harper & Row, 1975
12. Larsell O, Jansen J. *The comparative anatomy and histology of the cerebellum*, vol. 3. *The human cerebellum, cerebellar connections and cerebellar cortex*. Minneapolis: University of Minnesota, 1972
13. Drayer BP, Burger P, Darwin R, Riederer S, Herfkens R, Johnson GA. Magnetic resonance imaging of brain iron. *AJNR* 1986;7:373-380
14. Courchesne E, Yeung-Courchesne R, Press GA, Hesselink JR, Jernigan TL. Hypoplasia of cerebellar vermal lobules VI and VII in infantile autism. *N Engl J Med* 1988;318:1349-1354
15. Reiss AL, Patel S, Kumar AJ, Freund L. Preliminary communication: neuroanatomical variations of the posterior fossa in men with the fragile X (Martin-Bell) syndrome. *Am J Med Genet* 1988;31:407-414
16. Nasrallah HA, Schwartzkopf SB, Coffman JA, Olson SC. Hypoplasia of the cerebellar vermal lobules VI and VII on MRI scans in schizophrenia is associated with perinatal brain insult (abstr). Presented at the International Congress of Schizophrenia Research, San Diego, April 1989
17. Murakami JW, Courchesne E, Press GA, Yeung-Courchesne R, Hesselink JR. Reduced cerebellar hemisphere size and its relationship to vermal hypoplasia in autism. *Ann Neurol* 1989;46:689-694
18. Lechtenberg R, Gilman S. Speech disorders in cerebellar disease. *Ann Neurol* 1978;3:285-290
19. Petersen SE, Fox PT, Posner MI, Mintun MA, Raichle ME. Positron emission tomographic studies of the processing of single words. *Neuroscience* 1989;1:153-170
20. Junck L, Gilman S, Rothley JR, Betley AT, Koeppe RA, Hichwa RD. A relationship between metabolism in frontal lobes and cerebellum in normal subjects studied with PET. *J Cognitive Neuropsychol* 1988;8:774-782
21. Martin WR, Raichle ME. Cerebellar blood flow and metabolism in cerebral hemisphere infarction. *Ann Neurol* 1983;14:168-176
22. Lenzi GL, Frackowiak SJ, Jones T. Cerebral oxygen metabolism and blood flow in human cerebral ischemic infarction. *J Cereb Blood Flow Metab* 1982;2:321-335
23. Anderson NE, Posner JB, Sidtis JJ, et al. The metabolic anatomy of paraneoplastic cerebellar degeneration. *Ann Neurol* 1988;23:533-540
24. Han JS, Bonstelle CT, Kaufman B, et al. Magnetic resonance imaging in the evaluation of the brainstem. *Radiology* 1984;150:705-712
25. Press GA, Hesselink JR. MR imaging of cerebellopontine angle and internal auditory canal lesions at 1.5 T. *AJNR* 1988;9:241-251

# CT of Intracranial Cryptococcosis

Mark J. Popovich<sup>1</sup>  
Robert H. Arthur  
Edward Helmer

CT scans of 35 patients with intracranial cryptococcal infection were reviewed retrospectively. Studies were normal in 43% of the patients. Positive findings in others included diffuse atrophy in 34%, mass lesions (cryptococcoma) in 11%, hydrocephalus in 9%, and diffuse cerebral edema in 3%. Two unusual types of cryptococcoma were encountered, namely gelatinous pseudocysts and an intraventricular cryptococcal cyst. All findings were nonspecific for CNS cryptococcosis.

The results suggest that CNS cryptococcosis should be considered in all patients at risk for the disease who have these abnormal CT findings, no matter what their initial clinical presentation. In addition, MR demonstration of gelatinous pseudocysts in one patient indicates that this technique may be helpful in locating cryptococcal mass lesions not visualized on CT.

*AJNR* 11:139-142, January/February 1990; *AJR* 154:603-606, March 1990

Infection with *Cryptococcus neoformans* is the most common fungal disease of the central nervous system. Rarely seen in otherwise healthy individuals, it more commonly occurs as an opportunistic infection in immunosuppressed patients, debilitated patients with cancer or diabetes, those treated with steroids or chemotherapy, and, most commonly, AIDS patients. The increase in AIDS cases over the past several years has resulted in an increase in CNS cryptococcal infections, with approximately 5% of AIDS patients developing CNS involvement [1, 2]. Among the infectious agents causing CNS disease in AIDS, *Cryptococcus* ranks third in frequency behind the human immunodeficiency virus (HIV) and *Toxoplasma gondii* [3]. Because many AIDS patients do not exhibit specific symptoms of CNS infection, routine evaluation of these patients with cranial CT has been suggested, regardless of their presenting symptoms.

Intracranial infection with *Cryptococcus* may assume a variety of CT appearances, none of which are specific for the disease. Previous reports have documented the various CNS manifestations, including hydrocephalus, gyral enhancement, and multiple nodules (both enhancing and nonenhancing) [4, 5]. Prior to this study, the largest series involved 20 patients from Malaysia, none of whom were reported to have AIDS [6].

This study examines the cranial CT findings of 35 patients with proved cryptococcosis of the CNS. Two unusual CT manifestations of CNS cryptococcosis were encountered, each of which has been described only once previously in the English-language radiologic literature. In addition, an unusual manifestation of cryptococcal meningoencephalitis demonstrated on MR is reviewed.

## Materials and Methods

We undertook a retrospective study of 35 diagnosed cases of cryptococcal infection of the CNS occurring at our institution during the period August 1984 through August 1988.

Received April 4, 1989; revision requested May 16, 1989; revision received June 22, 1989; accepted July 3, 1989.

<sup>1</sup> All authors: Department of Diagnostic Imaging, Kaiser Foundation Hospital, 1505 N. Edgemont St., Los Angeles, CA 90027. Address reprint requests to M. J. Popovich.

0361-803X/90/1543-0603  
© American Roentgen Ray Society

Patients' ages ranged from 26 to 84 years, with a mean age of 43.2 years. Thirty-one patients were men and four were women. Of the total, 28 patients (80%) had AIDS. Twenty-six of the AIDS patients were homosexual males, one was female with a bisexual husband, and one patient had contracted the disease through a blood transfusion. Of the seven non-AIDS patients, two were on high-dose steroid therapy (one for sarcoidosis and another for immune thrombocytopenic purpura), one was diabetic, one had systemic lupus erythematosus, one was an alcoholic, and two had lymphoma (one of whom was on concurrent chemotherapy for the disease). The overall mortality from cryptococcal infection was 31%. In all cases, CNS cryptococcosis was diagnosed by positive CSF cultures, and in one patient an open brain biopsy was also confirmatory.

A cranial CT study done with a fourth-generation scanner was obtained for each patient at the time of initial presentation and before the diagnosis of cryptococcosis was known. Five-millimeter-thick axial images were obtained through the posterior fossa, and 10-mm-thick axial images were obtained through the remainder of the brain. Twenty-eight patients received IV contrast infusion, 26 patients (74%) at the time of the initial study and two (6%) on subsequent follow-up studies. Seven patients (20%) did not receive IV contrast medium because of a history of contrast allergy or renal insufficiency. An MR imaging study of one patient was obtained on a 0.35-T superconductive system. Spin-echo images at 10-mm intervals were obtained through the brain, including single-echo T1-weighted coronal images and double-echo T2-weighted axial images.

## Results

The initial clinical presentations of the patients studied are listed in Table 1. Several patients had more than one significant presenting symptom. One AIDS patient had no symptoms referable to the CNS, but a cranial CT was ordered prior to lumbar puncture. There was no correlation between presenting symptoms and the presence of intracranial mass lesions on CT, and, in addition, no correlation between CT findings and the severity of the disease or its eventual outcome.

The cranial CT findings are listed in Table 2. No abnormalities were seen in 43% of the patients. Significant atrophy was seen in about a third (12/35) of the patients. Nine of these 12 patients were generally much younger and had AIDS; the atrophy was probably due to direct HIV infection. One of these patients was 74 years old and not an AIDS patient; the atrophy was probably related to age. Age was possibly a factor in a second patient who was 84 and had contracted AIDS from a blood transfusion. Hydrocephalus was present in three patients (9%). Generalized cerebral edema was the only finding in one patient with AIDS. Two patients had nonspecific findings that could not definitely be

attributed to cryptococcal infection, even though they subsequently had positive CSF cultures. These included a non-enhancing low-density lesion in the genu of the corpus callosum and several nonenhancing low densities in the occipital lobes that may have represented infarcts. These two patients were not included in the group of cases of cryptococcal mass lesions.

Cryptococcal mass lesions were present in four patients (11%). The CT appearances of these lesions are listed in Table 3. Following are abbreviated case histories on these four patients.

### Case 1

A 52-year-old man with AIDS-related complex was in relatively good health until the night prior to admission when he awoke with a headache and altered mental status, associated with photophobia, nausea, and vomiting. Upon admission his vital signs were normal and he was afebrile. Blood studies and electrolytes were normal.

A CT scan was obtained prior to a lumbar puncture and revealed multiple ring-enhancing lesions with surrounding edema (Fig. 1). CSF analysis resulted in a positive India ink stain for *Cryptococcus*. The patient was started on amphotericin B. Subsequent CSF cultures grew *Cryptococcus*. During the hospitalization the patient's mental status returned to normal and his headaches resolved. Follow-up CT studies showed gradual resolution of the intracerebral lesions.

### Case 2

A 47-year-old woman presented with a 3-day history of acute onset of worsening headache, nausea, vomiting, and somnolence. Upon admission, she could not give a coherent history. Physical examination demonstrated a left pronator drift, bilaterally upgoing toes, left-sided sensory extinction, and a left hemianopsia. CT showed a large cystic mass within the temporal horn of the right lateral ventricle, with significant mass effect and midline shift to the left (Fig. 2).

Because the patient did not respond to medical management, a craniotomy was performed. An incision into the right temporal lobe allowed entry into the dilated temporal horn and revealed a viscous yellow-green material surrounding the choroid plexus (cultures of this material confirmed the diagnosis of cryptococcosis). Multiple loculated areas of CSF separated by fibrous septations were also noted

**TABLE 1: Major Presenting Symptoms in 35 Patients with CNS Cryptococcal Infection**

Symptom	No. of Cases	(%)
Headache	23	(66)
Altered mental status	10	(29)
Fever	9	(26)
Generalized weakness	4	(11)
Visual disturbances	3	(9)
Seizures	2	(6)
Nuchal rigidity	2	(6)
No CNS symptoms	1	(3)

**TABLE 2: Cranial CT Findings in 35 Patients with CNS Cryptococcal Infection**

Finding	No. of Cases	(%)
Normal	15	(43)
Diffuse atrophy	12	(34)
Mass lesions	4	(11)
Hydrocephalus	3	(9)
Diffuse cerebral edema	1	(3)

**TABLE 3: Appearance of Intracranial Cryptococcal Mass Lesions on CT Scans in Four Patients**

Finding	No. of Cases	(%)
Multiple gelatinous pseudocysts	2	(6)
Intraventricular cryptococcoma	1	(3)
Multiple ring-enhancing lesions	1	(3)



within the temporal horn. A ventriculojugular shunt was placed. The patient was treated with amphotericin B and 5-fluorocytosine. She was eventually relieved of her symptoms and discharged in improved condition with a normal cryptococcal titer.

### Case 3

A 30-year-old homosexual man with AIDS had a history of previous hospitalization for cryptococcal meningitis, which was treated with amphotericin B. CT scans several months prior to this admission were normal. For the 4 weeks prior to this admission he had experienced increasingly severe headaches, with nausea and vomiting.

His vital signs and physical examination were normal, as were routine laboratory studies. CT revealed multiple nonenhancing cystic lesions in the basal ganglia bilaterally (Fig. 3). CSF showed positive India ink stain, growth of *Cryptococcus*, and a cryptococcal antigen titer of 1:16,384. Because of previous lack of response to amphotericin B, he was started on 5-fluorocytosine. During the hospital course his headaches slowly resolved, as did his nausea and vomiting. A repeat lumbar puncture prior to discharge showed an antigen titer of 1:512 and CSF cultures were negative. A CT scan several months

after discharge showed a decrease in size and number of the presumed gelatinous pseudocysts.

### Case 4

A 50-year-old homosexual man with AIDS had been hospitalized 2 months previously, at which time a diagnosis of cryptococcal meningitis was made from positive CSF cultures. He was initially treated with IV amphotericin B. CT at that time was normal. CT several weeks after discharge showed multiple new cystic lesions in the basal ganglia and thalamus bilaterally, very similar in appearance to the lesions described in Fig. 3. These lesions were initially considered to be infarcts, possibly related to vasculitis complicating his cryptococcal meningitis. CSF culture remained positive for *Cryptococcus*. Because of a poor response to IV amphotericin B, he was started on intrathecal amphotericin B. Subsequently, the patient experienced lower extremity weakness as a result of arachnoiditis caused by the intrathecal medication. The treatments were terminated, his lower extremity weakness slowly resolved, and he was discharged. One month later he returned to the hospital with *Pneumocystis carinii* pneumonia and died despite medical treatment.

Fig. 1.—Case 1: Ring-enhancing cryptococcoma. Contrast-enhanced axial CT scan shows a ring-enhancing low-density lesion with surrounding edema. Additional lesions were seen in cerebral hemispheres bilaterally.

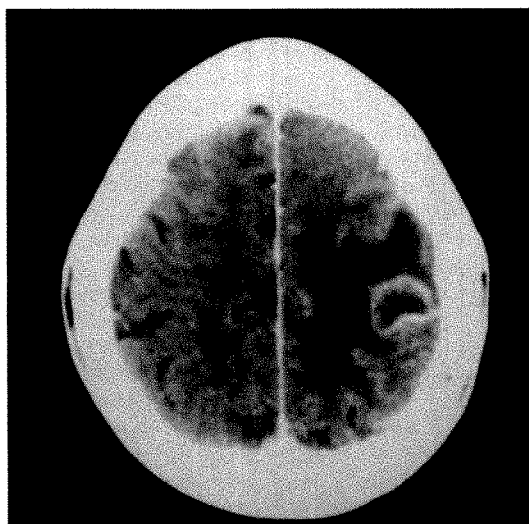


Fig. 2.—Case 2: Intraventricular cryptococcoma. Contrast-enhanced CT scan shows expansion of right temporal horn by a cystic intraventricular mass. Surrounding edema is causing midline shift.

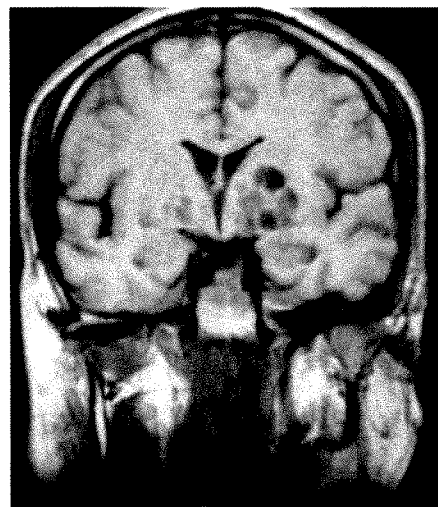
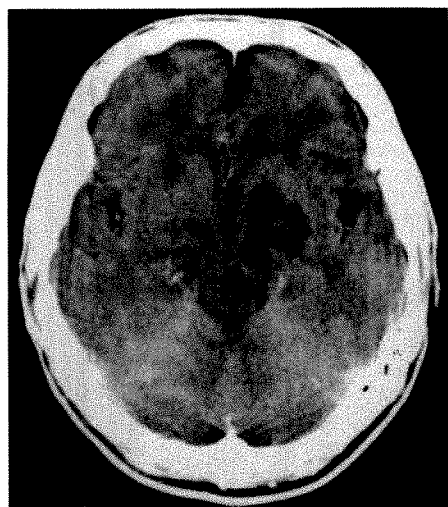


Fig. 3.—Case 3: Gelatinous pseudocysts.  
A, Contrast-enhanced axial CT scan shows multiple nonenhancing cystic nodules in basal ganglia bilaterally, more extensively involving the left.  
B, T2-weighted axial MR image (1500/80) reveals multiple high-intensity basal ganglia lesions. Additional areas of involvement, not appreciated on CT, are present on right.  
C, T1-weighted coronal MR image (500/30) shows cryptococcal cysts in basal ganglia.

## Discussion

*Cryptococcus neoformans* is an encapsulated yeastlike fungal organism that is ubiquitous in our environment. The organism gains entrance to the human body through the respiratory tract. From this initial focus of infection in the lung, the organism may be disseminated hematogenously to other organs, with a special predilection for the CNS. Meningitis is the most frequent clinical manifestation.

In normal hosts, these fungi usually induce a chronic granulomatous reaction. Immunosuppressed patients may display virtually no inflammatory reaction, and gelatinous masses of fungi may develop. Infection may extend from the basal cisterns into the brain substance via the perivascular spaces (Virchow-Robin spaces), producing multiple small cysts filled with the organism. These lesions have been termed "soap bubble" lesions [7] or "gelatinous pseudocysts" [8] and may precede the formation of granulomas.

A study of the CT manifestations of CNS cryptococcal infection in 35 patients over a 4-year period is presented. Of the 35 cases, 80% were AIDS patients. The most common presenting symptom was headache, seen in 66% of our patients. This is similar to that noted in previous studies [5, 6]. Besides the nine patients presenting with fever, all but one patient had symptoms referable to the CNS. As has been reported previously [4, 6], we found no direct relationship between the patients' presenting symptoms and CT findings, nor was CT an indicator of eventual outcome. Of the patients with mass lesions on CT, two had headaches and two had altered mental status as well as headaches. These symptoms were no different than those in the majority of patients without mass lesions.

In 43% of our patients there was no demonstrable CNS pathology on CT, thus these were presumed to represent cases of uncomplicated cryptococcal meningitis. Generalized cerebral atrophy was the most common abnormality, seen in 34% of cases; it was probably caused by HIV infection in several cases. Hydrocephalus was present in 9% of patients; it is thought to result from chronic meningeal inflammation causing CSF obstruction. Cryptococcal mass lesions were seen in 11% of patients. This is lower than in any study published to date, with the reported incidence of cryptococcoma ranging from a low of 15% [6] to a high of 25% [9].

Biopsy proof was available in only one of our four cases of mass lesions (case 2). Both cases 1 and 3 were similar in their clinical and radiographic courses, although the appearances of the cryptococcomas were different. In each instance, the workup revealed positive cryptococcal cultures and was negative for all other infectious etiologies, including toxoplasmosis, cytomegalovirus, tuberculosis, and pyogenic causes. While other differential possibilities such as lymphoma and progressive multifocal leukoencephalopathy could not be entirely excluded, the clinical and radiographic response to anticytotoxic therapy indicates that these mass lesions were caused by *Cryptococcus*. Case 4 is included because of the presence of presumed gelatinous pseudocysts almost identical to the lesions seen in case 3. This patient also had positive cryptococcal cultures and no evidence of other infectious etiologies. The patient died before follow-up CT or CSF analysis could be done. An autopsy was not performed.

Most of the parenchymal masses in the literature have been described as multiple enhancing nodules, either solid or ring-

like in appearance [1, 4-6, 10]. One study described multiple nonenhancing low-density lesions thought to represent gelatinous pseudocysts in the basal ganglia and thalamus [8], and a single case report described an intraventricular cystic cryptococcoma [11]. Each of these unusual mass lesions was found in our group of patients, and each presented specific problems in differential diagnosis. None is specific for *Cryptococcus*, with the differential possibilities including infectious causes such as toxoplasmosis, cytomegalovirus, progressive multifocal leukoencephalopathy, tuberculous granulomas, or pyogenic abscesses, as well as noninfectious etiologies including lymphoma and metastatic disease. The ring-enhancing lesions in case 1 were first interpreted as metastatic disease and the intraventricular cryptococcoma (case 2) was diagnosed as a trapped temporal horn of unknown origin. Our two cases of gelatinous pseudocysts (cases 3 and 4) were originally interpreted as deep infarcts due to vasculitis resulting from basal meningitis. MR imaging in one of these patients was more sensitive than CT, demonstrating additional cystic lesions not evident on the prior CT scans. MR was also useful in confirming the cystic nature of these basal ganglia lesions and in differentiating them from infarcts.

In summary, a wide variety of CT findings may be seen in CNS cryptococcosis, though none is specific for the disease. While the most common finding was a normal appearance on CT, the spectrum of abnormalities demonstrated included diffuse atrophy, hydrocephalus, diffuse edema, and mass lesions. Several forms of cryptococcoma have been described in the literature and each of these variations was seen in our study. These results also emphasize the importance of considering cryptococcosis in any patient with AIDS who displays intracranial masses on CT, regardless of symptoms. In addition, MR may be more sensitive than CT in detecting these lesions, perhaps even demonstrating parenchymal involvement not apparent on CT.

## REFERENCES

1. Zuger A, Louie E, Holzman RS, Simberloff MS, Rahal JJ. Cryptococcal disease in patients with the acquired immunodeficiency syndrome. Diagnostic features and outcome of treatment. *Ann Intern Med* 1986;104:234-240
2. Eng RHK, Bishburg E, Smith SM, Kapilo R. Cryptococcal infections in patients with acquired immune deficiency syndrome. *Am J Med* 1986;81:19-23
3. Gabuzda DH, Hirsh MS. Neurologic manifestations of infection with human immunodeficiency virus. Clinical features and pathogenesis. *Ann Intern Med* 1987;107:383-391
4. Cornell SH, Jacoby CG. The varied computed tomographic appearance of intracranial cryptococcosis. *Radiology* 1982;143:703-707
5. Waterston JA, Gilligan BS. Cryptococcal infections of the central nervous system: a ten year experience. *Clin Exp Neurol* 1987;23:127-137
6. Tan CT, Kuan BB. Cryptococcus meningitis, clinical-CT scan considerations. *Neuroradiology* 1987;29:43-46
7. Robbins SL, Cotran RS, Kumar V. *Pathologic basis of disease*. Philadelphia: Saunders, 1984:355-356
8. Garcia CA, Weisberg LA, Lacorte WSJ. Cryptococcal intracerebral mass lesions: CT pathologic considerations. *Neurology* 1985;35:731-734
9. Long JA, Herdt JR, Di Chiro G, Cramer HR. Cerebral mass lesions in torulosis demonstrated by computed tomography. *J Comput Assist Tomogr* 1980;4:766-769
10. Arrington JA, Murtagh FR, Martinez CR, Schitzlein HN. CT of multiple intracranial cryptococcoma. *AJNR* 1984;5:472-473
11. Ofori-Kwakye SK, Wang AM, Morris JH, O'Reilly GV, Fischer EG, Rumbaugh CL. Septation and focal dilatation of ventricles associated with cryptococcal meningoencephalitis. *Surg Neurol* 1986;25:253-260

# Intracranial Ganglioglioma: MR, CT, and Clinical Findings in 18 Patients

Mauricio Castillo<sup>1</sup>  
 Patricia C. Davis<sup>1</sup>  
 Yoshii Takei<sup>2</sup>  
 James C. Hoffman, Jr.<sup>1</sup>

**Eighteen cases of pathologically proved intracranial gangliogliomas were reviewed to determine their MR, CT, and clinical characteristics. Seventeen patients were evaluated with contrast-enhanced CT and 14 were studied by MR imaging. Eight tumors were predominantly cystic; half of these demonstrated some contrast enhancement, and five contained calcifications. These cystic gangliogliomas were located, in order of decreasing frequency, in the cerebellum, temporal, frontal, and parietal lobes. Ten tumors were solid; eight of these showed contrast enhancement, and only one contained calcifications. Small cysts were present in one solid mass. Solid gangliogliomas occurred preferentially in the temporal lobes. On MR, the findings were nonspecific and reflected the CT findings. In one patient who received gadolinium-DTPA the lesion did not enhance. Clinically, all patients presented with nonfocal long-standing symptoms and all but three were alive an average of 18 months after the initial diagnosis.**

**Pathologists are recognizing ganglioglioma with increasing frequency, and although its radiographic characteristics vary, it should be included in the differential diagnosis when the above-described findings are encountered.**

*AJNR* 11:109-114, January/February 1990; *AJR* 154:607-612, March 1990

Ganglioglioma is thought to be a rare primary lesion that accounts for only 0.4 to 0.9% of all intracranial tumors [1, 2]. These tumors differ from the most common gliomas in that they contain both glial elements and differentiated nerve cells [3]. These relatively low-grade neoplasms generally behave in a benign fashion and have a favorable prognosis. We present the CT and MR findings correlated with the clinical, surgical, and histological characteristics in 18 patients with proved intracranial gangliogliomas.

## Materials and Methods

From 1984 to 1988, 18 patients with intracranial gangliogliomas were evaluated at our institution. The patients were 1 to 70 years old; 13 were male, 5 were female. All cases were histologically proved. All radiographic studies and medical records were reviewed retrospectively. In 16 cases, preoperative CT studies were obtained before and after the IV administration of contrast medium (100 ml of 60% iohalamate meglumine). The CT studies were obtained on a variety of late-generation scanners by means of our routine protocol; that is, axial 5-mm sections through the posterior fossa were followed by 10-mm sections through the remainder of the brain. One patient had only a contrast-enhanced CT study.

MR studies were obtained before surgery in 14 patients by using both spin-echo T1-weighted, 500-800/20-50 (TR/TE), and T2-weighted, 1500-2000/50-100, sequences. Transverse 10-mm images were obtained in all patients, and coronal 10-mm images were acquired in three cases. The MR studies were done on either a 0.5-T (six studies) or a 1.5-T (eight studies) Philips unit. Gadolinium-DTPA (0.1 mmol/kg) was administered intravenously to one patient. One patient was preoperatively evaluated by MR only.

Three patients had selective cerebral angiography with cut film.

The CT and MR studies were reviewed with special attention given to the following

Received April 4, 1989; revision requested May 30, 1989; revision received June 16, 1989; accepted June 16, 1989.

<sup>1</sup>Department of Radiology, Emory University Hospital, 1364 Clifton Rd., N.E., Atlanta, GA 30322. Address reprint requests to P. C. Davis.

<sup>2</sup>Department of Pathology, Emory University Hospital, Atlanta, GA 30322.

0361-803X/90/1543-0607  
 © American Roentgen Ray Society

parameters: location, size, and internal characteristics (solid, cystic, and presence of calcifications) of the lesion; its pattern of enhancement; and the presence of associated abnormalities.

Thirteen patients had postoperative follow-up contrast-enhanced CT studies. Three patients who had recent surgery were followed only with MR. No follow-up studies were available in two instances. The postoperative studies were evaluated for the presence of recurrent tumor (local or disseminated) and the effects of treatment.

The histological diagnosis of ganglioglioma was made in accordance with the following criteria: (1) lesions were composed of neoplastic astrocytes, and (2) lesions demonstrated the presence of neoplastic ganglion cells, which often exhibited Nissl substance or gave origin to neuronal processes as demonstrated by silver impregnation methods (six cases).

## Results

The clinical findings at presentation for the 18 patients studied, the postoperative diagnoses, location of tumors, method of treatment, and follow up are summarized in Table 1.

On CT, eight tumors were primarily cystic (Fig. 1). Four cystic lesions demonstrated laminar (two cases) or nodular (two cases) areas of contrast enhancement along their margins (Fig. 2). Four cystic neoplasms did not enhance. Calcifications were present in five cases. On MR, the cystic components of these lesions appeared heterogeneous and mainly of low signal intensity with respect to the normal CSF on the T1-weighted images. On T2-weighted images, these tumors were of increased signal intensity (Fig. 3). The eight cystic lesions were located in the cerebellum (three cases) temporal lobes (two cases), frontal lobes (two cases), and parietal lobe (one case) (Table 2).

CT showed 10 tumors to be predominantly solid. These tumors were either hypodense (two tumors), isodense (four tumors), or slightly hyperdense (four tumors) with respect to the adjacent normal parenchyma (Fig. 4) (Table 3). All but two

of the masses showed some degree of contrast enhancement (Fig. 5). Calcification was detected in one solid tumor (Fig. 6). Small cysts were present in one lesion. On MR, the appearance of these solid tumors varied widely on the T1-weighted images: three were slightly hypointense, three were isointense, and three were slightly hyperintense relative to normal gray matter (Fig. 7) (Table 4). On the T2-weighted images, all but one of these lesions were of increased signal intensity. The solid tumors were found in the cerebellum (one lesion), temporal lobes (five lesions), suprasellar region (one lesion), and basal ganglia (three lesions). In one patient who received gadolinium-DTPA (0.1 mmol/kg), the lesion did not enhance (Fig. 8).

All gangliogliomas (cystic and solid) measured between 2 and 10 cm in their greatest dimension.

One patient with a proved ganglioglioma had no recognizable neoplasm by either CT or MR. This patient had undergone partial resection of the right temporal lobe for an astrocytoma, but because of recurrent seizures the patient was reoperated and further resection of the right temporal lobe showed the presence of ganglioglioma.

Histological examination of all lesions was confirmatory for ganglioglioma. In three patients (cases, 2, 3, and 8) anaplastic components were present.

Postoperative studies were available in 16 patients. Thirteen patients had follow-up contrast-enhanced CT studies and three patients were followed only with MR. No follow-up studies were available in two patients who died. All patients were followed an average of 18 months (range, 8–42 months) after their initial surgery, and all follow-up studies demonstrated postsurgical changes (encephalomalacia) or other treatment-related changes (diffuse atrophy, periventricular white matter disease) but no evidence of recurrent tumor or growth of the residual neoplasm. Although one patient died of unrelated causes, the last available follow-up study showed no change in the size and configuration of the tumor.

**TABLE 1: Clinical Features of Patients with Ganglioglioma**

Case No.	Age (years)	Sex	Clinical Presentation	Preop. Diagnosis	Treatment	Follow up (months)	Outcome
1	21	F	Headaches	Glioma	TR	30	Alive
2	70	M	Confusion	Glioma	PR, CT*	15	Dead
3	17	M	Seizures	Oligodendroglioma	PR, RT*	42	Alive
4	51	M	Headaches	Glioma	PR	24	Alive
5	16	M	Seizures	Glioma	TR, RT	8	Alive
6	62	M	Memory loss	Glioma	PR	—	Dead
7	59	F	Headaches	Glioma	PR	—	Dead
8	24	F	Weakness	Glioma	PR, RT*	24	Alive
9	26	M	Seizures	Glioma	PR, RT	4	Alive
10	8	F	Headaches	Glioma	PR, RT	2	Alive
11	17	M	Seizures	Glioma	PR, RT	6	Alive
12	15	M	Headaches	Glioma	PR, RT	24	Alive
13	34	M	Seizures	Oligodendroglioma	PR, RT	12	Alive
14	7	M	Headaches	Craniopharyngioma	PR, RT	36	Alive
15	36	M	Seizures	Oligodendroglioma	PR, RT	14	Alive
16	55	M	Seizures	Glioma	PR, RT	12	Alive
17	1	F	Headaches	Glioma	PR	24	Alive
18	1	M	Headaches	Neuroblastoma	PR, RT	24	Alive

Note.—TR = total resection, PR = partial resection, RT = radiation therapy, CT = chemotherapy, \* = tumor with anaplastic component.

Fig. 1.—Case 1.

A, Contrast-enhanced CT scan shows area of low attenuation in left temporal lobe. Note subtle enhancement of posterior margins of lesion (arrows).

B, On this coronal MR image (500/30) through mid temporal lobes, lesion appears hypointense and of similar signal intensity to that of CSF. Note well-defined margins. On T2-weighted image (not shown), lesion was of increased signal intensity.

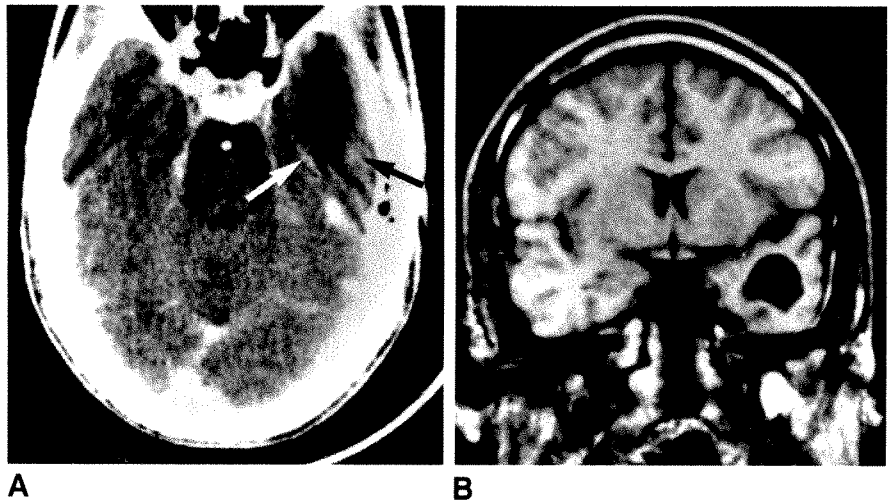


Fig. 2.—Case 17.

A, Contrast-enhanced CT scan shows cystic ganglioglioma with minimal enhancement of posterior margin of cyst present within cerebellum. On the basis of radiographic findings, this lesion cannot be differentiated from a cystic astrocytoma.

B, Axial MR section (2000/80) at same level shows lesion to be of increased signal intensity with well-defined margins. A shunt catheter is present in region of frontal horn of right lateral ventricle.

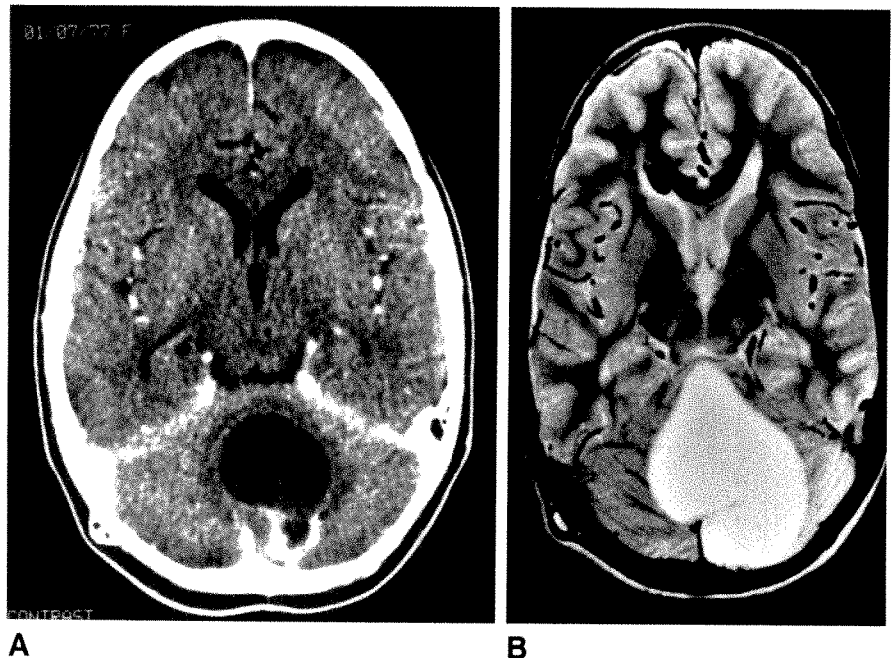


TABLE 2: Location of Cystic and Solid Lesions in 18 Patients with Ganglioglioma\*

	Cystic	Solid	Total
Temporal	2	5	7
Frontal	2	—	2
Parietal	1	—	1
Suprasellar	—	1	1
Basal ganglia	—	3	3
Cerebellum	3	1	4
Total	8	10	18

\* One lesion was not identified by either MR or CT.

## Discussion

The term ganglioglioma was initially proposed to describe CNS tumors containing both glial and neuronal elements [4, 5]. Gangliogliomas differ from gangliocytomas in that the latter

TABLE 3: CT Findings in 17 Patients with Ganglioglioma\*

	Hypodense	Isodense	Hyperdense	+Enhancement	Ca <sup>++</sup>
Cystic	8	—	—	4	5
Solid	2	4	4	8	1

\* One lesion was not identified by either MR or CT.

are composed purely of neuronal elements and contain no glial components [6, 7]. Ganglion neoplasms are classified according to their stages of differentiation and to the relative proportion of neuronal to glial elements, as follows: gangliocytoma, ganglioglioma, ganglioneuroblastoma, anaplastic ganglioglioma, and neuroblastoma [8, 9].

Gangliogliomas can occur at any age, and the pediatric and adult populations are believed to be equally affected [1, 3, 10, 11]. Clinically, both the age and gender distribution of our patients reflect that reported in the literature.



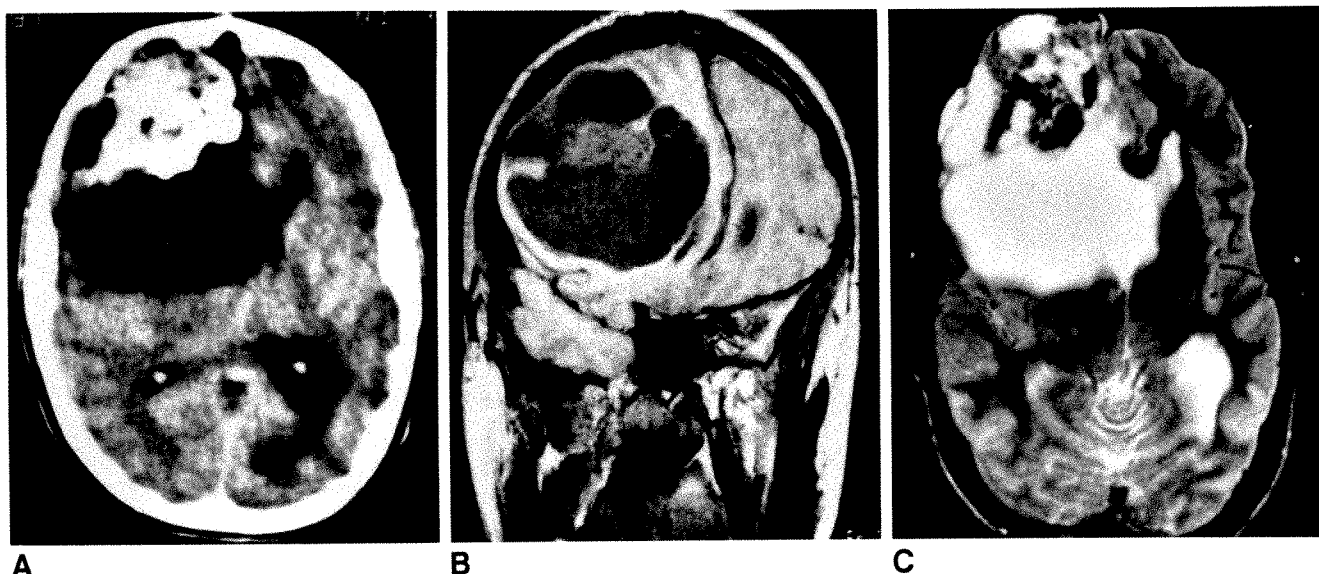


Fig. 3.—Case 3.

A, Contrast-enhanced CT scan shows large cystic ganglioglioma occupying right frontal lobe. Note large areas of calcification and absence of definite enhancement. There is dilatation of left lateral ventricle.

B, Coronal MR image (500/30) shows contents of cystic lesion to be heterogeneous. A rim of slightly increased signal intensity surrounds lesion.

C, Axial MR image (2000/80) at same level as A shows fluid within lesion to be hyperintense. Calcifications are seen in areas of signal void in anterior aspect of tumor. Margins of lesion are relatively well defined and no associated edema is present.

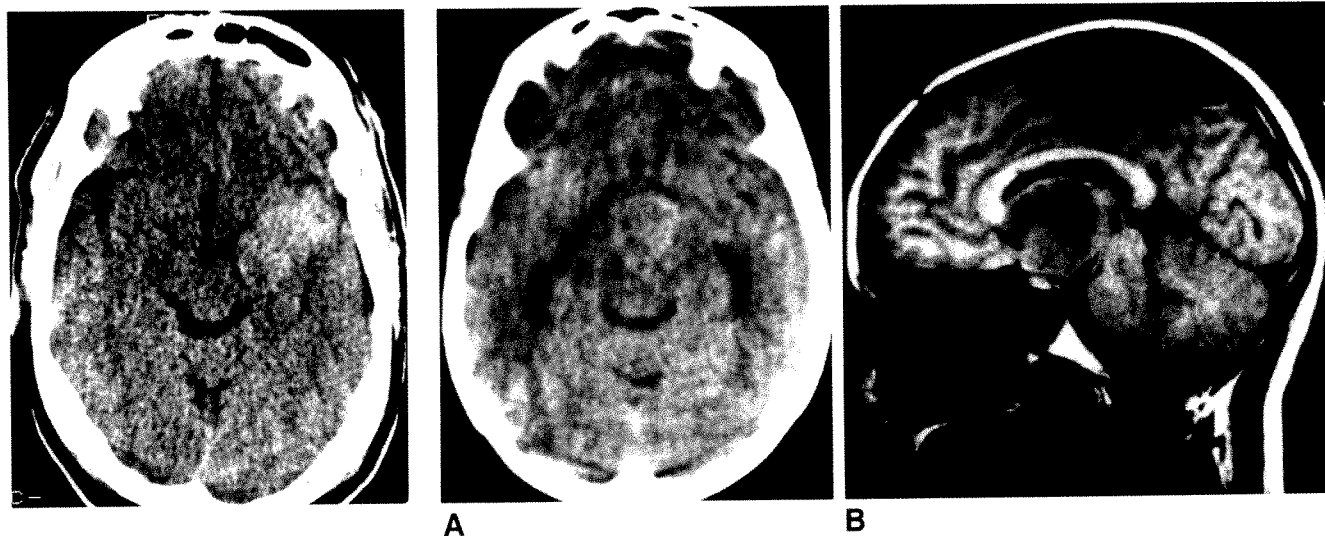


Fig. 4.—Case 4. Noncontrast CT scan shows hyperdense, ill-defined mass in left temporal lobe. There is mass effect upon ipsilateral sylvian fissure. Tumor did not enhance after IV administration of contrast medium.

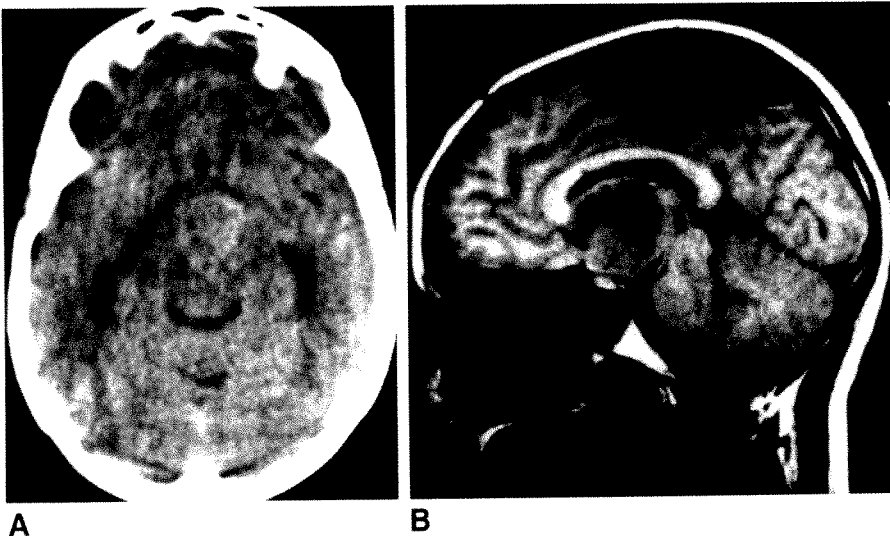


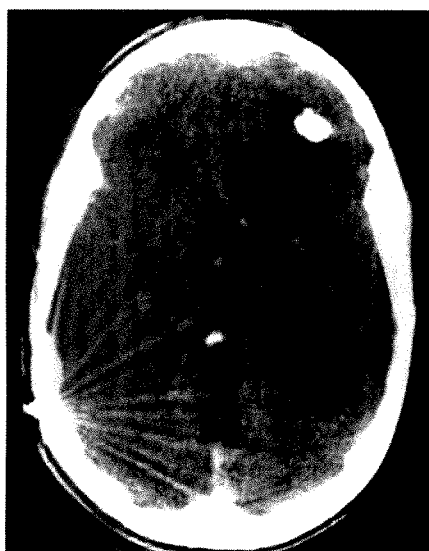
Fig. 5.—Case 14.

A, Noncontrast CT scan shows round, slightly hyperdense mass in suprasellar region. There is dilatation of temporal horns of lateral ventricles.

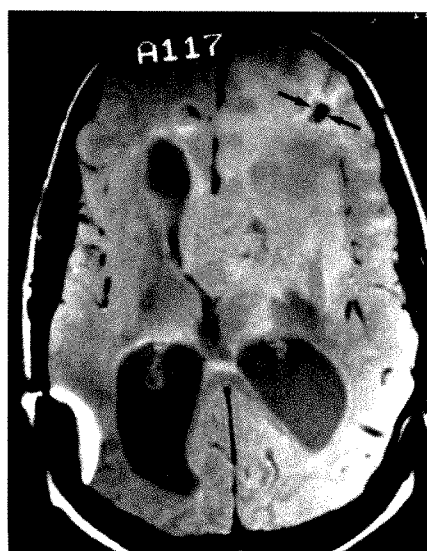
B, Midline sagittal MR image (550/30) shows suprasellar mass to be heterogeneous but predominantly of intermediate signal intensity. Pituitary gland is seen caudad to mass.

Previously published series agree that the most common location is the temporal lobes [1–3, 11]. However, gangliogliomas can also occur in other parts of the cerebrum as well as in the cerebellum, brainstem, spinal cord, and optic nerves [8, 10, 12–14]. In our series, seven of 16 lesions were found in the temporal lobes. The remainder of the tumors were randomly distributed throughout other parts of the brain. As expected, the clinical presentation of all our cases was related

to the presence of nonspecific long-standing symptoms, which probably reflect the slow-growing nature of the lesion (Table 1). Despite the benign nature of the neoplasms, complete resection was accomplished in only two cases, because of the location and size of these lesions. Anaplastic components were found in three of our patients. Of these, one patient died as a result of tumor recurrence; the others were alive without recurrence at 24 and 36 months after diagnosis.



A



B

Fig. 6.—Case 15.

A, Contrast-enhanced CT scan shows low-attenuation lesion in left frontal lobe that contains a large calcification in its anterior aspect. There is no definite enhancement.

B, MR image (1800/30) obtained 6 weeks after CT study (A) shows large tumor to be isointense with gray matter. Areas of calcification are well seen (arrows). In the interval, hydrocephalus has developed as a result of shunt malfunction.

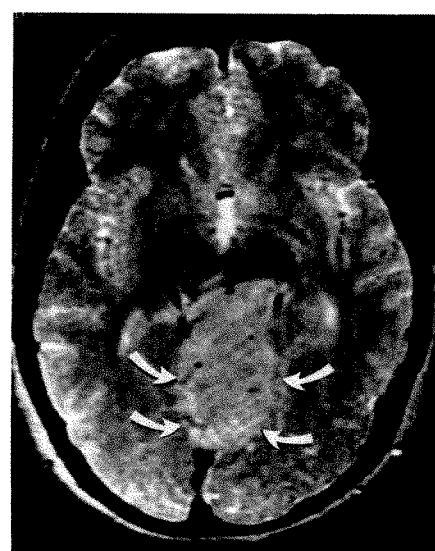


Fig. 7.—Case 10. Axial MR image (2000/80) shows large ganglioglioma arising in cerebellar vermis (arrows). Lesion is slightly hyperintense relative to normal brain parenchyma. On T1-weighted MR study (not shown), the lesion was also slightly hyperintense. Radiographically, the lesion is indistinguishable from Lhermitte-Duclos disease.

TABLE 4: MR Findings in 14 Patients with Ganglioglioma\*

	T1-Weighted			T2-Weighted		
	Low	Intermediate	High	Low	Intermediate	High
Cystic	7	—	—	—	—	7
Solid	3	3	1	—	1	4

\* One lesion was not identified by either MR or CT.

In a review of 48 cases of pathologically proved ganglioglioma compiled from the literature, Dorne et al. [1] found that 38% of the lesions were cystic in nature, the remainder of the patients harbored solid tumors. The solid tumors in that review had a wide variety of appearances on noncontrast CT studies (38% were low density, 15% were isodense, 15% were high density, 32% were mixed density, and 17% were indeterminate density). After contrast administration, enhancement was noted in half the lesions. Although our findings agree with the above, we are uncertain as to the meaning of the term *indeterminate density* used in that article.

The MR characteristics of ganglioglioma have not been well established. In one series, Denierre et al. [2] described four cases. Two solid masses were of increased signal intensity on the T1-weighted images and of low signal intensity on the T2-weighted images. The short T1 relaxation characteristics of these solid masses are hard to explain, as the presence of hemorrhage, cholesterol, or proteins was not mentioned. Two patients had cystic tumors with long relaxation times on both the T1- and T2-weighted images. Our results differ somewhat

from those mentioned above. The solid masses in our cases showed a variable and nonspecific appearance on T1-weighted images. On T2-weighted images, all solid lesions showed some degree of increased signal intensity. Four cystic lesions were heterogeneous and slightly hyperintense relative to normal CSF on the T1-weighted images. On the T2-weighted images, these cystic lesions showed increased signal intensity. In their series, Denierre et al. [2] observed that "there was good contrast between the lesion and the normal brain tissue." Although we believe that this observation might be valid for the cystic tumors, we were unable to distinguish well-defined tumor margins from the adjacent brain parenchyma in six cases of solid gangliogliomas examined by MR. It is conceivable that gadolinium-DTPA-enhanced MR studies may be helpful in better delineating the margins in some tumors. In our series only one patient received gadolinium-DTPA; the tumor in this patient did not enhance (Fig. 8).

Calcifications occurred in five (28%) of our 18 patients. It is not surprising that calcifications within gangliogliomas have not previously been detected by MR. We were able to visualize nonspecific areas of signal void by MR in all patients in whom CT showed calcifications. The areas of calcifications in our cases were fairly large, and on MR, with only spin-echo techniques used, they could not be differentiated from vessels with high flow or areas of old hemorrhage without previous knowledge of the CT findings.

Cerebral angiography showed three lesions to be avascular, a radiographic finding that has previously been reported [15].

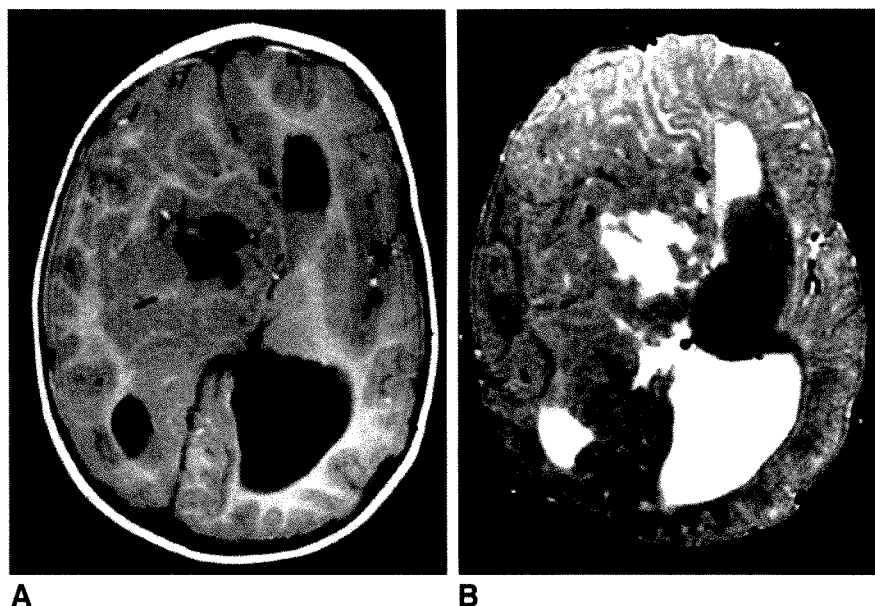


Fig. 8.—Case 18.

**A**, Axial MR image after Gd-DTPA administration shows large, nonenhancing ganglioglioma in region of right basal ganglia. Mass is isointense with gray matter and contains two central cystic components. Hydrocephalus is present.

**B**, Axial MR section (2000/80) at same level shows cystic components of lesion to be of increased signal intensity. Solid portion of mass remains isointense with normal gray matter.

From the radiographic and histological viewpoint, an important differential diagnosis when considering ganglioglioma of the cerebellum is that of Lhermitte-Duclos diseases [16, 17]. This lesion contains neuronal elements, and pathologically it is thought to represent a hamartoma. Clinically, this lesion behaves as a true neoplasm: it distorts the normal cerebellar architecture and causes thickening of the overlying folia, a pattern similar to that seen in one of our patients (Fig. 7).

Follow-up studies of our patients occurred 2 to 42 months after initial treatment. Fifteen patients were known to be alive at the completion of this study, and CT or MR studies showed no recurrence of the tumor in those patients in whom total resection was accomplished and no significant change in the size of those tumors that were only partially resected. The latter observation could be related to the relatively short follow-up period.

Ganglioglioma was not considered in the preoperative differential diagnosis in any of our patients. However, ganglioglioma is being recognized with increasing frequency by pathologists. In our series, nonenhanced MR images did not provide additional useful information to that obtained from the contrast-enhanced CT scans. Because of its relatively better prognosis as compared with the more usual types of brain neoplasms, radiologists should include ganglioglioma in the differential diagnosis of intracranial masses when (1) a relatively large cystic mass is present (preferentially located in the temporal lobes or the cerebellum) that has little or no discernible solid components, has margins that enhance only slightly, and that at times contains dense and large calcifications; or (2) a solid, poorly defined mass is found in the temporal lobes that is generally hypodense by CT or of increased signal intensity on T2-weighted MR images.

#### REFERENCES

1. Dorne HL, O'Gorman AM, Melanson D. Computed tomography of intracranial gangliogliomas. *AJNR* 1986;7:281-285
2. Denierre B, Stinchnoth FA, Hori A, Spoerri O. Intracerebral gangliogliomas. *J Neurosurg* 1986;65:177-182
3. Johanson JH, Rekate HL, Roesmann U. Gangliogliomas: pathological and clinical correlation. *J Neurosurg* 1981;54:58-63
4. Perkins OC. Ganglioglioma. *Arch Pathol Lab Med* 1926;2:11
5. Courville CB. Ganglioglioma: tumors of the central nervous system: review of the literature and report of two cases. *Arch Neurol Psychiatry* 1930;24:439-491
6. Altman NR. MR and CT characteristics of gangliocytoma: a rare cause of epilepsy in children. *AJNR* 1988;9:917-921
7. Rommel T, Hamer J. Development of ganglioglioma in computed tomography. *Neuroradiology* 1983; 24:237-239
8. Mizuno J, Nishio S, Barrow DL, et al. Ganglioglioma of the cerebellum: case report. *Neurosurgery* 1987;21:584-588
9. Russell DS, Rubinstein LJ. *Pathology of the tumors of the nervous system*, 4th ed. Baltimore: Williams & Wilkins, 1977:261-282
10. Nass R, Whelan MA. Gangliogliomas. *Neuroradiology* 1988;22:67-71
11. Zimmerman RA, Bilaniuk LT. Computed tomography of intracerebral gangliogliomas. *J Comput Tomogr* 1979;3:24-30
12. Garcia CA, McGarry PA, Collada M. Ganglioglioma of the brainstem. *J Neurosurg* 1984;60:431-434
13. Henry JM, Heffner RR, Earle KM. Gangliogliomas of the central nervous system: clinicopathological study of fifty cases (abstr). *J Neuropathol Exp Neurol* 1978;37:626
14. Gritzman MC, Snyckers FD, Proctor NS. Ganglioglioma of the optic nerve. *S Afr Med J* 1983;63:863-865
15. Katz MC, Kier EL, Schechter M. The radiology of gangliogliomas and ganglioneuromas of the central nervous system. *Neuroradiology* 1972;4:69-73
16. Ambler M, Pagacer S, Sidman R. Lhermitte-Duclos disease (granule cell hypertrophy of the cerebellum): pathological analysis of the first familial cases. *J Neuropathol Exp Neurol* 1969;28:622-647
17. Oppenheimer DR. A benign "tumor" of the cerebellum: report on two cases of diffuse hypertrophy of the cerebellar cortex with review of nine previously published cases. *J Neurol Neurosurg Psychiatry* 1955;18:199-203

# Treatment of Iliac Artery Stenoses with the Wallstent Endoprosthesis

C. Raillat<sup>1</sup>  
H. Rousseau<sup>1</sup>  
F. Joffre<sup>1</sup>  
D. Roux<sup>2</sup>

Sixteen symptomatic iliac artery stenoses and three occlusions in 16 patients were treated by the percutaneous implantation of Wallstent endoprostheses (Medinvent SA, Lausanne, Switzerland). The endoprosthesis consists of stainless steel monofilaments braided into a self-expanding cylinder. The indications for placement were restenosis after angioplasty (10 cases), failed arterial dilatations (eight cases), and restenosis after endarterectomy (one case). The prostheses used had a mean diameter of 8 mm (range, 6–10 mm) and were placed in the external iliac (14 cases) and common iliac (five cases) arteries. The 16 stenoses were greater than 80%, and the three occlusions were longer than 7 cm. Mean length of the lesions treated was 7 cm (range, 4–14 cm). Three of the arteries thrombosed after treatment, one 2 days later and two in the month after implantation of the stent. On clinical and angiographic follow-up (mean, 15 months; range, 1–24 months) no symptoms or stenoses reappeared in the remaining 16 cases.

Our experience in these cases suggests that implantation of a Wallstent endovascular prosthesis is a valuable technique for the treatment of external and common iliac artery stenoses.

*AJR* 154:613–616, March 1990

Among the new techniques that have emerged in recent years as potential complements to percutaneous transluminal angioplasty is percutaneous endoprosthesis implantation. Experimental studies performed in animals [1, 2] have shown that the procedure is useful for restoring patency of occluded arteries. We report our experience with the Wallstent endoprosthesis in 19 stenotic lesions of the iliac artery.

## Subjects and Methods

The Wallstent endoprosthesis, designed and developed by Medinvent SA (Lausanne, Switzerland), is composed of stainless steel monofilaments woven into a braided cylindrical structure (Fig. 1). Its self-expanding properties are due to the spring qualities of the metal alloy and the fact that the filament crossing points are not fixed but are free to slide or pivot over each other. This renders the device highly flexible, both constrained on its delivery catheter, which thus can be introduced via even tortuous vessels, and in situations where curvatures and luminal irregularities are encountered. The 77% macroporosity of the device permits rapid endothelialization and good patency of collateral vessels bridged by its structure.

The endoprosthesis is ready-mounted on a delivery catheter, which is equipped with a central lumen for insertion of a guidewire or injection of contrast material. The external shaft of the coaxial catheter terminates in an invaginated rolling membrane that contains the prosthesis on the catheter tip. Progressive retraction of the membrane, rather in the manner of the peeling back of a stocking, leads to controlled deployment, the prosthesis elastically seeking its unconstrained diameter. The diameter of the unconstrained prosthesis used is 15–20% larger than the diameter of the treated vessel, so that the prosthesis is held against the vessel by radial force.

The implantation technique used was similar to that of conventional angioplasty, generally

Received April 10, 1989; accepted after revision October 26, 1989.

<sup>1</sup> Service de Radiologie, C.H.U. Rangueil, 1 avenue J. Poulhes, 31054 Toulouse Cedex, France. Address reprint requests to C. Raillat.

<sup>2</sup> Service de Chirurgie Cardiovasculaire, C.H.U. Rangueil, 31054 Toulouse Cedex, France.

0361-803X/90/1543-0613  
© American Roentgen Ray Society

following the same procedure and using the same guidewire. Under local anesthesia the catheter was introduced via the ipsilateral common femoral artery in 16 cases and the contralateral artery in three cases. Endoprostheses were selected so that the length was sufficient to cover the entire diseased region even if this required several prostheses. The mean diameter of the prostheses was 8 mm (range, 6–10 mm) and, in most cases, a single prosthesis sufficed. The length of the arterial segments covered by the prostheses ranged from 4 to 14 cm (mean, 7 cm).

All patients gave informed consent, the protocol having been approved by the hospital ethics committee. The study group consisted of 16 men with a mean age of 50 years (range, 38–65 years). Stenosis or occlusion had occurred in the internal iliac artery in 14 patients and in the common iliac artery in five patients. Twenty-three endoprostheses were inserted. All vessels treated were more than 80% obstructed.

Patients were given 100 mg/day aspirin (Aspegic, Synthelabo, Le Plessis Robinson, France) and 225 mg/day dipyridamole (Cleridium 150, Marcofina, Paris, France) from 48 hr before treatment to 6 months afterward. Heparin was given during the procedure and for 24 hr after treatment. Clinical examination, Doppler studies, and angiography were performed at 1 month, 6 months, and 1 year after placement of the endoprostheses.

## Results

Immediate results of placement of Wallstent endoprostheses were excellent in all cases. Angiography showed

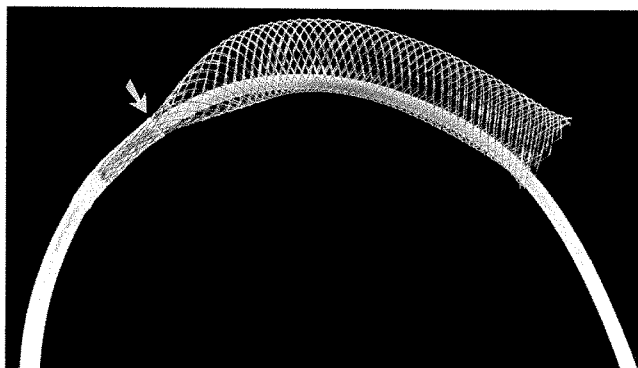


Fig. 1.—Photograph of Wallstent endoprosthesis; withdrawal of sheath (arrow) allows progressive release of endoprosthesis.

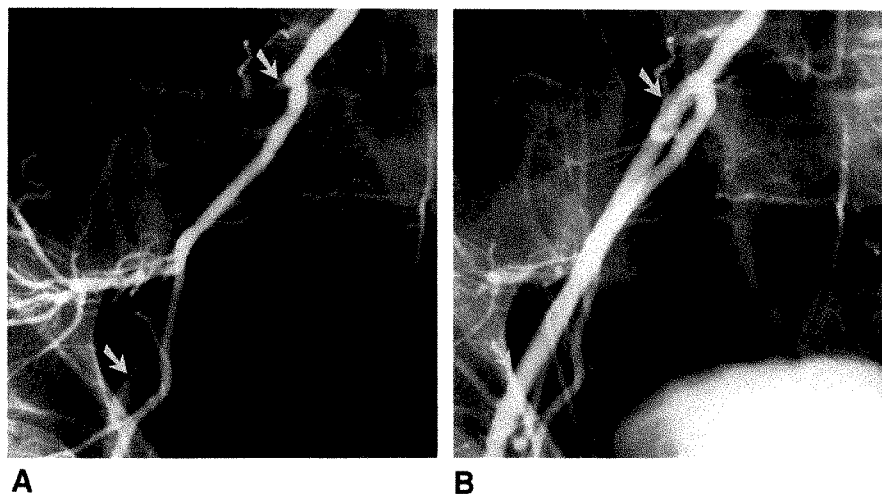


Fig. 2.—A, Angiogram shows obstruction of right external iliac artery (between arrows). B, Angiogram after insertion of two endoprostheses shows normal blood flow (between arrows).

the vessel diameter to be identical to that of the healthy vessel (Fig. 2). At the same time, there was a clear improvement in downstream pressures after endoprosthesis placement, as compared with the result after angioplasty alone.

Acute thrombosis of the treated vessel developed in one patient and did not respond to fibrinolytic therapy. Thromboses occurred in two vessels within the month after the prosthesis was implanted. One was treated by surgery. In both cases, the postimplantation angiogram showed a subintimal dissection at the proximal extremity of the prosthesis, probably the result of a balloon angioplasty (Fig. 3).

No case of restenosis occurred in the areas with endoprostheses. Conversely in two cases, stenoses occurred distal to the prosthesis in areas where angioplasty had been performed. These lesions were treated by repeated angioplasty and endoprosthesis implantation with excellent results (Fig. 4).

In a follow-up period ranging from 6 months to 2 years, good results were noted in 16 (84%) of 19 lesions. These results included the absence of symptoms, recovering of pulses, and correction of Doppler indexes. Angiography showed regular arterial walls (Fig. 5).

## Discussion

After 20 years of use, angioplasty is now an accepted procedure. A recurrence rate of 10–30% in iliac angioplasty [3, 4] occurs in the first 6 months after the procedure and always has been the major drawback [3, 5].

A variety of new approaches to overcome the inadequacies of angioplasty have emerged during the last few years. In 1969, Dotter [6] published his pioneering work on spiral and tubelike endoprostheses. New endoprosthesis designs that have been developed and evaluated in animals in the last 7 years show good patency, tissue compatibility, and rapid intimalization within a few weeks.

Experiments in our laboratory with Wallstent endoprostheses [1, 2] show excellent tolerance of the device within the vessel. Studies show presence of a fine fibrin deposit, localized thrombus on the surface of the endoprosthesis, and rapid endothelial covering. Intimal hyperplasia occurs, but is limited, stabilizes in a few weeks, and contracts by 3–6



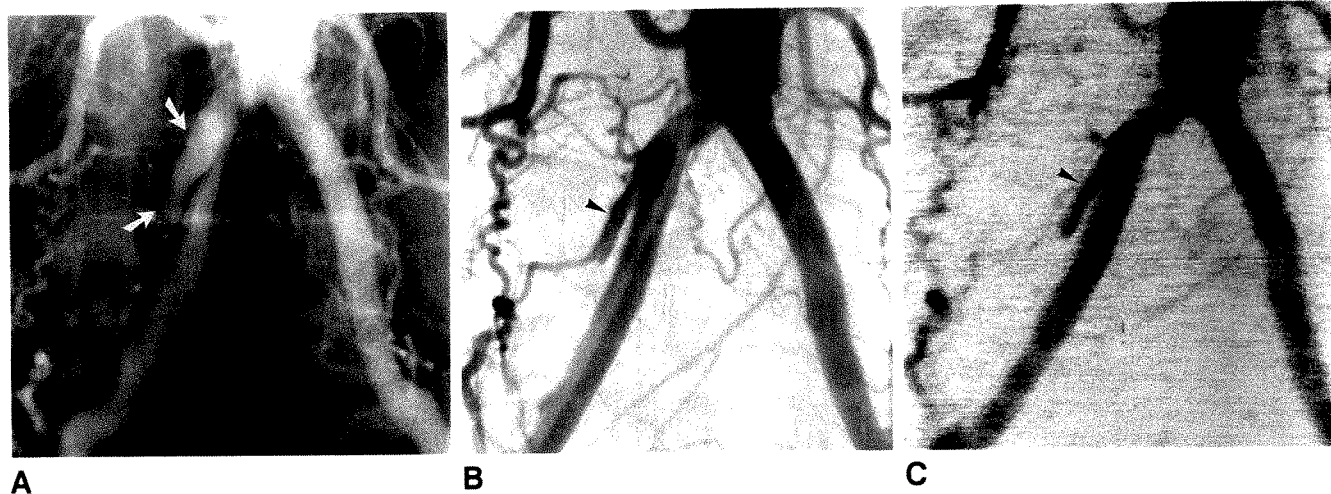


Fig. 3.—A, Angiogram shows irregular stenosis with intimal dissection of iliac artery (arrows).  
 B, Angiogram shows endoprosthesis placed after angioplasty (between arrows). Superior extremity of stent (upper arrow) does not cover dissection totally (arrowhead).  
 C, Angiogram obtained 15 days after angioplasty shows a persisting channel (arrowhead). Iliac artery thrombosed 20 days after angioplasty.

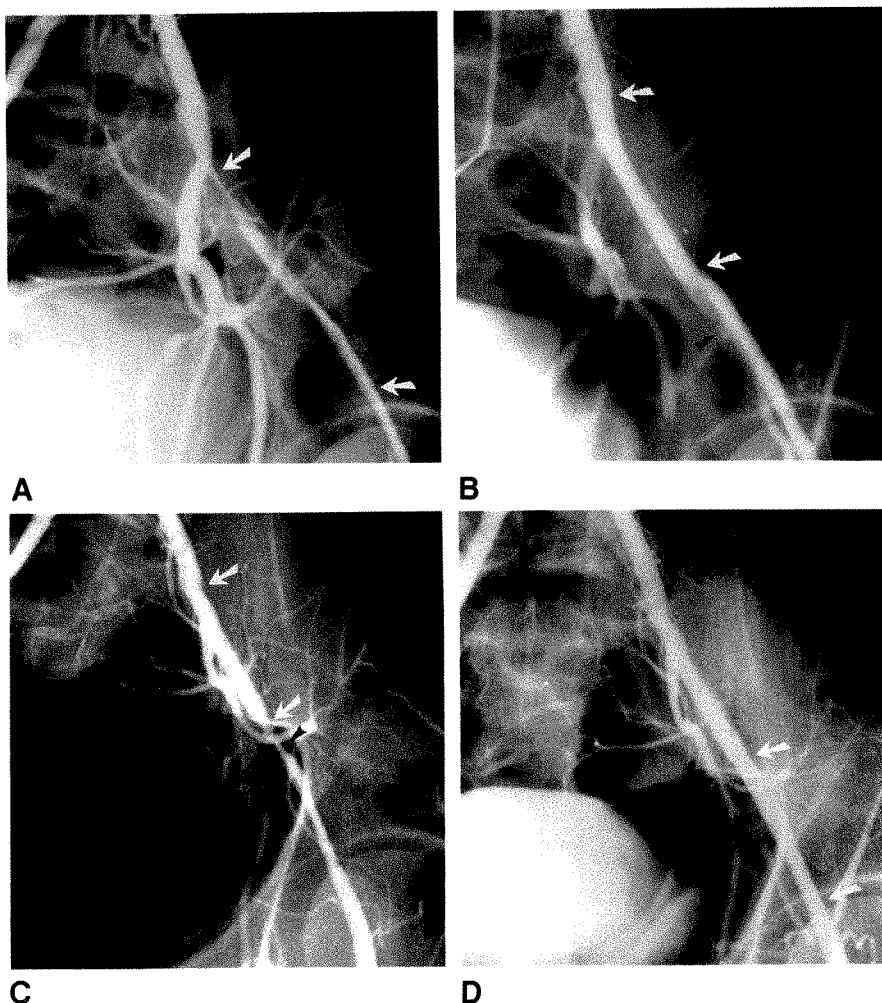


Fig. 4.—A, Angiogram shows marked stenosis of external iliac artery (between arrows).  
 B, Angiogram after extensive angioplasty of external iliac artery. A stent (between arrows) was placed then on proximal lesion. Below stent, a subintimal dissection (arrowhead) persists.  
 C, Angiogram 1 year later shows restenosis at dilated and nonstented lesion (arrowhead). Proximal stenosis that is covered by stent (between arrows) remains perfectly patent.  
 D, Angiogram after angioplasty shows second endoprosthesis (between arrows) that was placed on distal lesion.

months. We found that the Wallstent endoprosthesis not only did not stimulate atheromatous proliferations in the vessels of a rabbit model, but had a protective effect related to the device and the creation of a superficial fibrotic covering [2].

Even though our results have shown the Wallstent endoprosthesis to be only mildly thrombogenic in normal canine arteries, other authors [7–9] have shown that stents in normal arteries or arteries that have been treated with balloon dila-

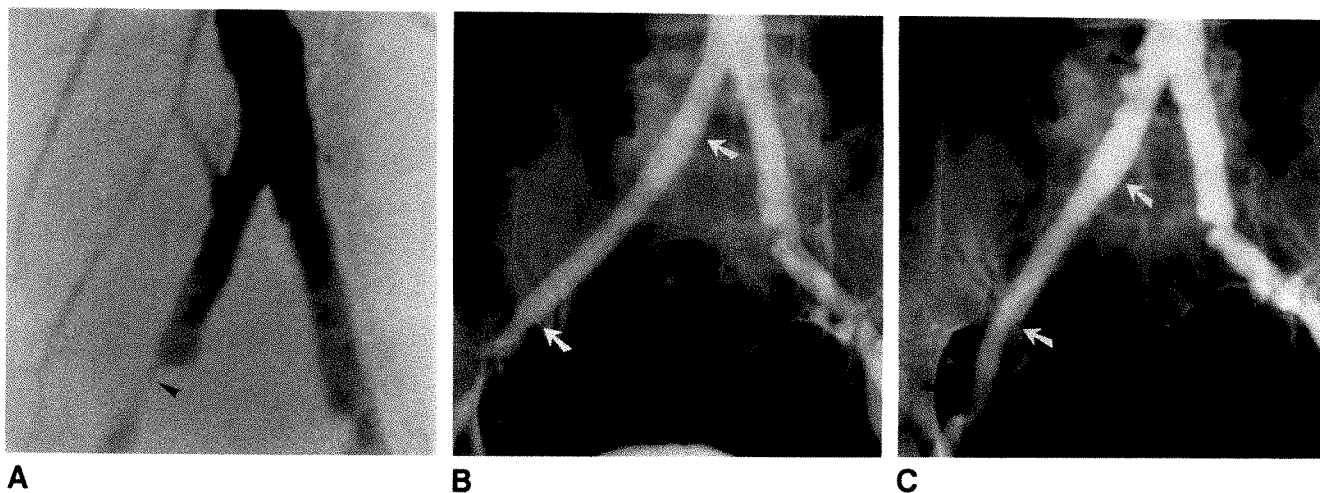


Fig. 5.—A, Angiogram shows iliac restenosis 18 months after angioplasty (arrowhead). B, Angiogram shows Wallstent endoprosthesis immediately after implantation (between arrows). C, Angiogram obtained 2 years after implantation of Wallstent shows a low degree of intimal proliferation inside stent (between arrows) whereas new lesions appear upstream and downstream from prosthesis (arrowheads).

tation require only mild anticoagulation. Nonetheless, the first clinical results emphasize the difference between normal animal vasculature and diffusely diseased vessels in patients. Thus, the first few weeks after implantation represent a critical period in which thrombotic complications can occur. We noted three cases, one in the acute phase that was partially due to prolonged femoral compression. In both cases of thrombosis that occurred in the first 4 weeks, angiography showed extensive subintimal dissection. It appears that in vessels previously treated by angioplasty, the prosthesis should cover the entire segment, removing all wall irregularities and dissection.

These thromboses occurred only in patients who were not given oral anticoagulants. The results of our work in femoropopliteal stenoses [10] show that administration of oral anticoagulants is preferable and that they should be administered for 2 months until intimalization has occurred.

In the first 6 months of the follow-up period, two stenoses occurred in the vascular segment that was not covered by the prosthesis, further indicating the necessity of covering the entire segment treated by angioplasty. Apart from the three thromboses, no restenoses occurred in the vessels with endoprostheses during the follow-up period from 6 months to 2 years.

Palmaz [11] showed satisfactory short- and medium-term results in his patients with common and external iliac artery stenosis treated by a stent. Initially only those patients who had stenoses that reoccurred after balloon dilatation were selected for prosthesis placement. Subsequently, we enlarged the indications to include acute-phase failures of primary dilatation (residual pressure gradient, residual stenosis >30%, and significant intimal dissections) and long iliac recanalizations, that is, high-risk lesions, which are known to have poor patency rates at short and medium term after classic angioplasty.

Systematic implantation of endoprostheses after all angioplasties appears to be uncalled for, given the reasonable results with angioplasty in treating most but not all iliac stenoses. On the other hand, restricting its use to restenosis alone is equally untenable, given the clear value of the endo-

prosthesis in acute-phase angioplasty failures. Thus, we favor an intermediate position, implanting an endoprosthesis each time we see a high risk or strong probability of restenosis or occlusion. We include in that group occlusions, complex stenoses, and long stenoses, which have a poor prognosis after angioplasty.

The use of percutaneously implantable endoprostheses is already a significant advancement in the treatment of iliac atheromatous lesions. Considering that the acute complications can be ascribed to the development phase of a radically new technique, the medium-term results appear excellent, and use of the endoprosthesis is valuable for those cases in which the results of conventional angioplasty are unsatisfactory.

#### REFERENCES

1. Rousseau H, Puel J, Joffre F, et al. Self-expanding endovascular prosthesis: an experimental study. *Radiology* 1987;164:709-714
2. Rousseau H, Joffre F, Raillat C, et al. A self-expanding endovascular stent in experimental atherosclerosis. *Radiology* 1989;170:773-778
3. Colapinto RF, Harries-Jones P, Johnston KW. Percutaneous transluminal dilatation and recanalization in the treatment of peripheral vascular disease. *Radiology* 1980;135:583-587
4. Van Andel GJ, Van Erp WF, Krepel VM, Breslau PJ. Percutaneous transluminal dilatation of the iliac artery: long-term results. *Radiology* 1985;156:321-323
5. Samson RH, Sprayregen S, Veith FJ, Scher LA, Gupta SK, Acer E. Management of angioplasty complications, unsuccessful procedures and early and late failures. *Ann Surg* 1984;199:234-239
6. Dotter CT. Transluminally placed coilspring endarterial tube grafts: long term patency in canine popliteal artery. *Invest Radiol* 1969;4:329-332
7. Palmaz JC, Windeler SA, Garcia F, Tio FO, Sibbit RR, Reuter SR. Atherosclerotic rabbit aortas: expandable intraluminal grafting. *Radiology* 1986;160:723-726
8. Duprat G, Wright KC, Charsangavej C, Wallace S, Gianturco C. Self-expanding metallic stents for small vessels: an experimental evaluation. *Radiology* 1987;162:469-472
9. Palmaz JC. Balloon-expandable intravascular stent. *AJR* 1988;150:1263-1269
10. Rousseau H, Raillat C, Joffre F, Knight CJ, Ginestet MC. Treatment of femoropopliteal stenoses by means of self-expandable endoprostheses: mid-term results. *Radiology* 1989;172:961-964
11. Palmaz JC, Richter GM, Noeldge G, et al. Intraluminal stents in atherosclerotic iliac artery stenosis: preliminary report of a multicenter study. *Radiology* 1988;168:727-731

## Technical Note

# Removal of Intimal Hyperplasia in Vascular Endoprostheses by Atherectomy and Balloon Dilatation

Dierk Vorwerk<sup>1</sup> and Rolf W. Guenther

Different types of vascular endoprostheses have been described as supplementary techniques to percutaneous transluminal dilatation [1, 2]. However, obstruction of the stent by hyperplastic intima may occur [3]. Attempts to recanalize obstructed endoprostheses by balloon dilatation are not as satisfactory as balloon dilatation of nonstented vessels because the stent is unable to expand like a native vessel. For this reason, the Simpson atherectomy catheter [4] was used in seven cases for the management of restenosis within endovascular stents.

### Materials and Methods

Eight of 92 patients with Wallstent implants (Medinvent Inc., Lausanne, Switzerland) presented with reobstruction due to intimal hyperplasia within the stent [2]. The endoprosthesis used is a flexible device woven from metallic filaments; it expands actively to its predetermined size and attaches itself to the vessel wall.

Simple balloon dilatation was performed in two patients (one hemodialysis shunt, one superficial femoral artery) because atherectomy was not available, but the procedure failed to restore the stent lumen completely. One of these patients underwent atherectomy 10 months later.

In another patient with an implant, shunt balloon dilatation alone reduced stent restenosis to about 20%, but occlusion occurred 24 hr later, necessitating thrombectomy. Control angiography showed a recoiled high-grade stenosis.

Consequently, the Simpson atherectomy catheter was used in that case and another six patients (two women, five men) as a primary technique for removal of the hyperplastic intima. In two patients the

stents were located in the superficial femoral artery, in three in the draining vein of polytetrafluorethylene implant hemodialysis fistulas, in one in a Brescia-Cimino shunt, and in one in the common iliac artery. In all cases, 7-French atherectomy devices were used, which were inserted through an introducer sheath with a 7-French inner diameter. The follow-up period after stent placement varied from 3 (implant shunt) to 12 (iliac artery) months. In two implant shunts, thrombosis occurred before atherectomy, necessitating lysis therapy.

### Results

Insertion of the Simpson device was no problem in the implant shunts and the iliac artery, but it required careful manipulation after antegrade puncture of the femoral artery to introduce the stiff housing. Because only an older type of the instrument without extended housing was available, several removals and reinsertions of the system were necessary to remove the tissue segments from the housing. Because the guidewire at the housing tip tends to twist after a few insertions, it had to be cut off in three cases. Generally, the soft lesions inside the stents were passed easily by the housing. Within the middle portion of all stents in implant shunts or the superficial femoral artery, the hyperplastic intima was removed easily (Fig. 1). In all cases, hyperplastic intima at both the proximal and distal ends of the stent could not be totally atherectomized; residual stenoses were left in that location and were successfully treated by subsequent balloon dilatation (6–7 mm). In the iliac artery, the 7-French atherectomy device was unable to resect all stenosing material, even

Received August 11, 1989; accepted after revision October 11, 1989.

<sup>1</sup> Both authors: Department of Diagnostic Radiology, Technical University of Aachen, Pauwelsstrasse, D-5100 Aachen, West Germany. Address reprint requests to D. Vorwerk.

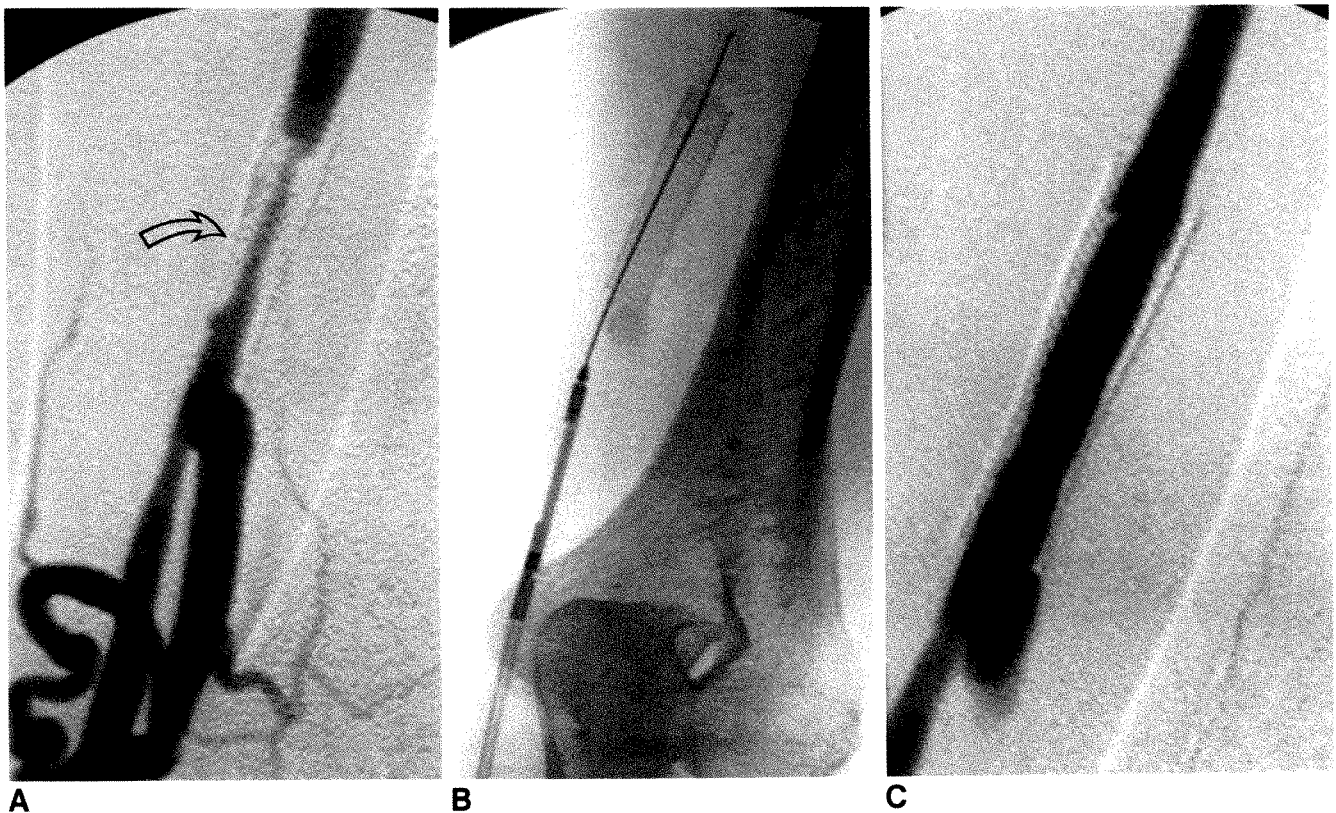


Fig. 1.—Percutaneous atherectomy inside vascular endoprosthesis.

A, Filiform stenosis (arrow) due to intimal hyperplasia within Wallstent of draining vein of brachial implant shunt.

B, Simpson atherectomy catheter within shunt.

C, After atherectomy and balloon dilatation, lumen is fully restored, showing smooth cuts and regular wall.

inside the stent: the rigid housing could not be completely adapted to the stent wall in the slightly curved vessel.

No perforation or embolization occurred after atherectomy. A bolus of 5000 IU of heparin was administered during the procedure and was followed by IV heparin infusion (1000 IU/hr for 24 hr) in all patients; 100 mg of aspirin per day was prescribed for arterial stents. All patients were discharged the next day; the arteriovenous shunts were used for hemodialysis immediately after the procedure. The follow-up period varied from 1 to 10 months after atherectomy; a restenosis of a superficial femoral artery was detected 9 months after and a restenosis of a shunt was detected 3 months after atherectomy. Repeat atherectomy was performed in the femoral artery; no revision of the shunt has been necessary.

## Discussion

Endovascular stents appear to be useful adjuncts to balloon angioplasty [1, 2]. Several types of stents have been described that become covered by a neointima within several weeks [1]. Early and midterm results in the iliac arteries have been encouraging [5]; the restenosis rate is low. In our series of 70 patients it was less than 10% [6]. The development of flexible devices such as the self-expanding Wallstent and small-sized insertion systems allows implantation in more

peripheral vessels such as the femoral arteries or hemodialysis fistulas [3, 7]. The restenosis rate in those vessels, however, is much higher compared with that of iliac stents [3, 5]. Consequently, the problem of neointimal hyperplasia may restrict the use of stent placement in complicated femoral or shunt lesions, such as occluding intimal dissection. In any event, reliable percutaneous techniques are required to control the long-term side effects of stent placement.

The most important components of balloon angioplasty are irreversible stretching of the media and disruption of the lesion [8]. Neither concept is easily applicable to stenoses within stents, because plastic deformation of the vascular lumen by media stretching is prevented by the circular stent wall. This is particularly true for the Wallstent, which cannot be expanded to more than its predetermined diameter, once incorporated into the vascular wall. Compression or dislodgment of the obstructing material through the interspaces of the stent would be alternative effects of balloon dilatation, although, because of the elasticity of the hyperplastic intima, those mechanisms are unlikely to provide an irreversible effect. The Simpson device, however, permits excision of vascular material percutaneously, introducing an alternative means for restoration of the vascular lumen [4].

The atherectomy catheter also is well suited for use in obstructed stents. The irregularly shaped hyperplastic intima

can be cut parallel to the stent wall by the rotating cutter while the eccentric balloon is securely supported by the opposite stent wall. In addition, perforation of the vessel is prevented by the stent itself. Instead of remodeling the vessel, one can remove and analyze the occluding material. The efficiency of the device is limited if a stenosis is located at the end of a stent that is incorporated into the wall. As the housing remains fixed within the stent lumen, the preserved elasticity of the nonstented wall may allow parts of the lesion to escape while being pressed into the catheter housing. Thus, for lesions positioned at both ends of a stent, it seems useful to combine atherectomy and balloon dilatation. The Simpson catheter was not convincing in our case of iliac restenosis, because the effective diameter of the available 7-French catheter was certainly not large enough for that location. The problem may be overcome by the use of larger instruments. The immediate effect of percutaneous excision of intimal hyperplasia is satisfying; long-term effects are not yet available.

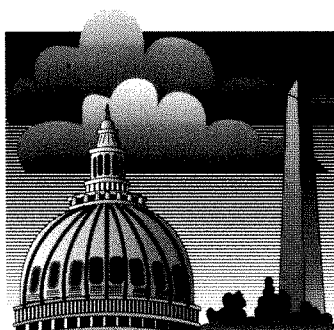
In conclusion, percutaneous removal of hyperplastic intima by using the Simpson catheter is a technically effective means of recanalizing self-expanding endovascular stents in periph-

eral vessels, but it may need to be combined with balloon dilatation for lesions located at the ends of a stent.

#### REFERENCES

1. Palmaz JC, Sibbitt RR, Reuter SR, Tio FO, Rice WJ. Expandable intraluminal graft: a preliminary study. *Radiology* **1985**;156:73-77
2. Sigwart U, Puel J, Mirkovitch V, Joffre F, Kappenberg L. Intravascular stents to prevent occlusion and restenosis after transluminal angioplasty. *N Engl J Med* **1987**;316:701-706
3. Triller J, Mahler F, Do D, Thalmann R. Die vaskuläre Endoprothese bei femoro-poplitealer Verschlusskrankheit. *ROFO* **1989**;150:328-334
4. Simpson JB, Johnson DE, Thapliyal HV, Marks DS, Braden LJ. Transluminal atherectomy: a new approach to the treatment of atherosclerotic vascular disease. *Circulation* **1985**;72[suppl 3]:146
5. Palmaz JC, Richter GM, Noeldge G, et al. Intraluminal stents in atherosclerotic iliac artery stenosis: preliminary report of a multicenter study. *Radiology* **1988**;168:727-731
6. Guenther RW, Vorwerk D, Bohndorf K, Peters I, El-Din A. Intravascular stents for the treatment of iliac and femoral artery stenoses and occlusions. *Radiology* **1989**;172:725-730
7. Guenther RW, Vorwerk D, Bohndorf K, et al. Venous stenoses in dialysis shunts: treatment with self-expanding metallic stents. *Radiology* **1989**;170:401-405
8. Wolf G, LeVein R, Ring E. Potential mechanisms of angioplasty. *Cardio-vasc Intervent Radiol* **1984**;7:11-17





Come to the  
American Roentgen Ray Society

90<sup>th</sup>

---

ANNUAL MEETING

---

Washington, D. C.

---

Sheraton Washington Hotel  
May 13-18, 1990

---

---

Scientific Program (200 papers)

Instructional Courses (60 hours)

Categorical Course on Cardiovascular Imaging

The Caldwell Lecture

Award Papers

Scientific Exhibits

Social, Golf, and Tennis Programs

Guest Programs



## Technical Note

# A Simple Device to Facilitate Percutaneous Insertion of the Kimray-Greenfield Filter

Ronald J. Zagoria,<sup>1</sup> Michael D. Scott, Vincent J. D'Souza, and Raymond B. Dyer

Percutaneous placement of Kimray-Greenfield filters (KGF) (Medi-tech Inc, Watertown, MA) has been described [1, 2]. Advantages include (1) ability to perform KGF placement at the time of inferior vena cavography or pulmonary angiography, (2) ability to place the KGF via either the jugular or femoral vein without the need for a surgical cutdown, (3) superior fluoroscopic capabilities in the angiography suite compared with operating room fluoroscopy, and (4) shortened procedure time compared with surgical KGF placement. A disadvantage of percutaneous placement of KGFs is that flow through the vein cannot be controlled by the angiographer. During surgical placement, the vein is mobilized and cross-clamped above the venotomy, minimizing blood loss and risk of air embolus. With percutaneous placement, a 24-French filter holder is advanced over an angiographic guidewire through a 24-French sheath and into the vein. The carrier catheter for the filter is 11-French in diameter. Once the filter holder is advanced beyond the sheath, bleeding and air intake may occur through the lumen of the sheath if it is left in place. These complications can be minimized by using a modified 24-French Amplatz dilator (Cook Inc., Bloomington, IN) to occlude the lumen of the sheath while allowing unimpeded advancement of the carrier catheter. This modified dilator can be used with either an Amplatz sheath (Cook Inc., Bloomington, IN) or a Coons-Amplatz sheath (Medi-tech Inc., Watertown, MA).

### Materials and Methods

The 24-French Amplatz dilator is tapered at its end to fit snugly over an 8-French catheter. The first step in modifying this dilator to

fit over the 11-French KGF carrier catheter is to shorten the tapered end by 6 mm with a sharp scalpel blade (Fig. 1). The dilator is then incised along its long axis so that it can be fitted over the 11-French catheter (Fig. 1). The tapered end of the modified dilator should fit snugly around the catheter, but the catheter should slide easily through its lumen. The modified dilator should resume its cylindrical shape with close apposition of its edges, indicating that the end diameter is at least 11-French. These dilator modifications can be completed during the procedure by using a sterile scalpel blade or a dilator can be modified in advance, sterilized, and packaged for use when needed. We have found the latter method to be more convenient.

At the time of KGF placement, the modified dilator is backloaded on the carrier catheter (Fig. 2) and advanced until its tip abuts the filter holder. A single piece of sterile tape is then wrapped around the nontapered end of the modified dilator to prevent accidental advancement of this device into the vein and also to appose its edges better. The percutaneous tract is then dilated to 24-French, and an unmodified dilator and sheath are advanced into the vein. After the dilator is removed from the sheath, the KGF delivery system is advanced over a guidewire into the sheath. The modified dilator can be advanced as far as the edge of the sterile tape. Then the carrier catheter is advanced further by pushing it through the lumen of this modified dilator.

### Results and Discussion

We have used this device in two patients without complications, and we have found that this easily created modified dilator facilitates the percutaneous placement of KGFs. Before the use of this device, we found that hemorrhage and introduction of air were difficult to control while the filter holder was in the vein beyond the sheath lumen. This reusable device

Received September 18, 1989; accepted after revision November 3, 1989.

<sup>1</sup> All authors: Department of Radiology, Bowman Gray School of Medicine, 300 S. Hawthorne Rd., Winston-Salem, NC 27103. Address reprint requests to R. J. Zagoria.

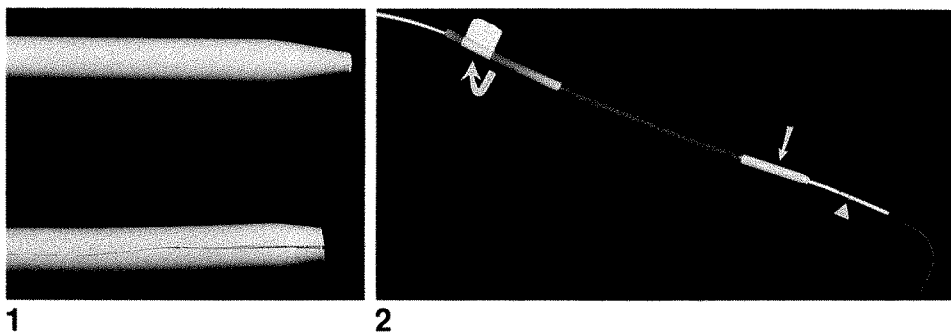


Fig. 1.—Standard Amplatz 24-French dilator (top) is modified by trimming 6 mm off tapered end and making a longitudinal incision through dilator to permit backloading onto Kimray-Greenfield filter carrier catheter.

Fig. 2.—Modified dilator (straight arrow) is backloaded on Kimray-Greenfield filter carrier catheter behind filter holder (arrowhead). Tape has been wrapped around nontapered end of dilator (curved arrow).

fits snugly over the carrier catheter and minimizes bleeding and venous air intake with the sheath left in place. We recommend its use in conjunction with the Coons-Amplatz sheath, which has a flexible proximal end with apposable edges, so that bleeding is greatly decreased during the interval between dilator removal and advancement of the filter holder into the sheath [3]. In this interval, the KGF delivery system must be loaded onto the guidewire and advanced to the sheath. Before use of this modified dilator, partial hemostasis was achieved during KGF positioning by compressing the flexible edges of this sheath around the 11-French carrier catheter. However, this technique requires continuous manual compression, and the seal around the catheter is imperfect. The same problems exist with the alternative method of removing the sheath once the KGF is within the vein. These limitations may lead the operator to rush KGF placement. Our

device, which provides near complete hemostasis without requiring continuous manual pressure, allows easy and unhurried manipulation of the carrier catheter for ideal KGF positioning with continued venous access through the sheath during placement.

#### REFERENCES

1. Denny DF, Cronan JJ, Dorfman GS, Esplin C. Percutaneous Kimray-Greenfield filter placement by femoral vein puncture. *AJR* 1985;145:827-829
2. Tadavarthy SM, Castaneda-Zuniga W, Salomonowitz E, et al. Kimray-Greenfield vena cava filter: percutaneous introduction. *Radiology* 1984;151:525-526
3. Pais SO, Mirvis SE, De Orchis DF. Percutaneous insertion of the Kimray-Greenfield filter: technical considerations and problems. *Radiology* 1987;165:377-381

## Pictorial Essay

# Artifacts in Maximum-Intensity-Projection Display of MR Angiograms

Charles M. Anderson,<sup>1,2</sup> David Saloner,<sup>1,2</sup> Jay S. Tsuruda,<sup>2</sup> Lorraine G. Shapeero,<sup>2,3</sup> and Ralph E. Lee<sup>1</sup>

Recently, MR angiograms of the carotid and intracranial arteries have shown excellent depiction of these vessels [1, 2]. The angiograms are typically derived by acquiring a three-dimensional Fourier transform (3DFT) volumetric data set and then projecting the sections to calculate an angiogramlike image from a given viewing angle. Projections are easier to interpret than are the original multiple sections because tortuous vessels can be traced more readily. In addition, the projection is similar in appearance to that of conventional angiography. When forming projection images, the maximum-intensity-projection (MIP) algorithm [3] is used most often, rather than a simple summation of the sections (Fig. 1). The MIP provides superior contrast between high-intensity blood and surrounding low-intensity stationary tissue because it does not sum up the background across the entire projected volume, but rather picks out the maximum intensity voxel encountered in the projected ray.

Despite the advantages of MIPs, our preliminary experience with MR angiography is that vascular anatomy is systematically distorted by the unusual contrast behavior of MIPs when many sections are projected. The purpose of this essay is to illustrate these artifacts.

### Materials and Methods

Images were acquired on a 1.5-T Siemens Magnetom unit (Siemens AG, Erlangen, West Germany) with a linearly polarized head

coil. MR angiograms and MIPs were derived by using software provided by Gerhard Laub of Siemens Medical Systems. For carotid angiography, 3DFT fast low-angle shot (FLASH) or fast imaging with steady precession (FISP) was used with velocity compensation in the slice and frequency-encoding directions, 30–40/8 (TR/TE),  $\theta = 25$ – $30^\circ$ ,  $256 \times 256 \times 64$  matrix, and voxel size of  $1 \times 1 \times 1.25$  mm. For intracranial angiography, 3DFT FLASH or FISP was used with velocity compensation in the slice and frequency-encoding directions, 30–50/8, 10 (TR/TE),  $\theta = 20$ – $30^\circ$ , and  $256 \times 256 \times 32$ – $64$  matrix. Slab thickness was chosen to provide a voxel size of  $1 \times 1 \times 1$ – $1.25$  mm. MIPs were calculated on a  $256 \times 256$  grid. For viewing angles that were nearly  $0^\circ$ , no interpolation was used. For steep viewing angles, an eight-point linear interpolation was used.

### Discussion

The contrast behavior of summation projections and MIPs differs as more sections are included in the projection calculation (Fig. 2). In the summation projection, contrast is quickly lost as more sections are included, even when there is moderately effective suppression of signal from background tissue. However, in the MIP, excellent contrast is maintained even when many sections are included, so long as the vessel intensity is about 2 SD above the mean background noise. If contrast is less strong, so that vessel intensity is only about 0.5 SD above background, fluctuations in the background exceed the vessel as more sections are included in the

Received September 11, 1989; accepted after revision October 16, 1989.

Presented at the annual meeting of the Society of Magnetic Resonance in Medicine, Amsterdam, the Netherlands, August 1989.

<sup>1</sup> Department of Radiology (114), San Francisco Veterans Administration Center, 4150 Clement St., San Francisco, CA 94121. Address reprint requests to C. M. Anderson.

<sup>2</sup> Department of Radiology, University of California, San Francisco, School of Medicine, Third and Parnassus, San Francisco, CA 94143.

<sup>3</sup> Department of Radiology, Letterman Army Medical Center, Presidio, San Francisco, CA 94129.

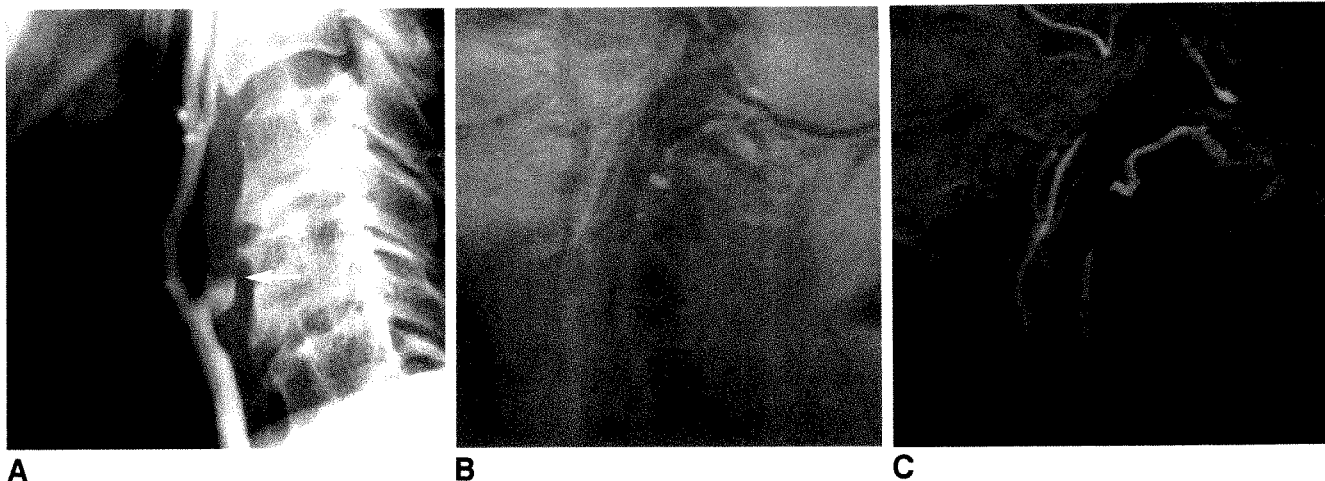


Fig. 1.—Comparison of summation-projection and maximum-intensity-projection (MIP) displays of MR angiograms of carotid arteries. A, Conventional lateral angiogram of carotid bifurcation in patient with occlusion of internal carotid artery (arrow). B, Summation projection of 32 sagittal sections of MR angiogram. C, MIP of same 32 sagittal sections shows superior contrast and background suppression. In summation projection, background value is sum of background in all 32 sections, whereas in MIP, background is highest feature on one of the sections.

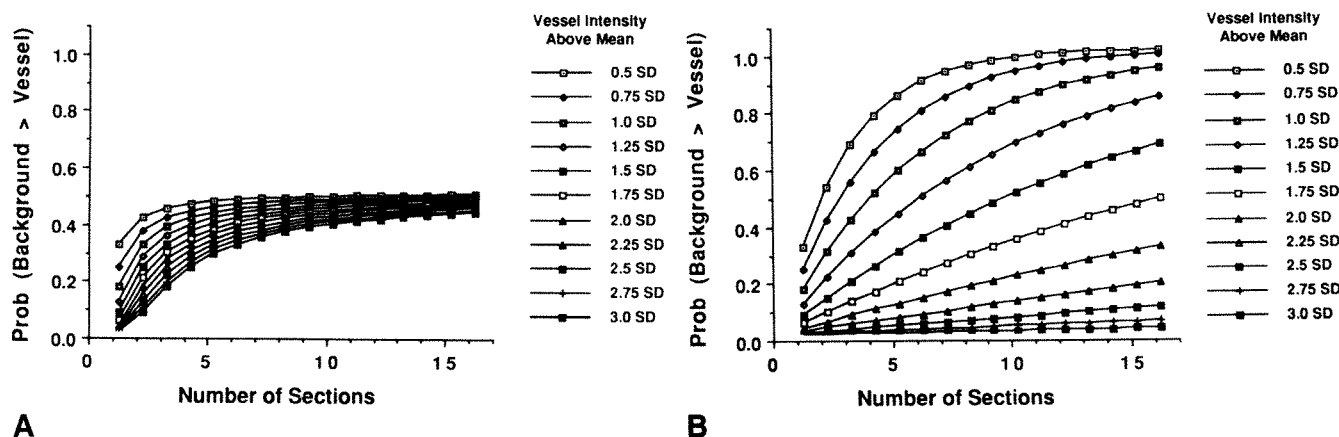


Fig. 2.—Probability (Prob) that intensity of a pixel in background will exceed intensity of a pixel in vessel, plotted as a function of number of sections in projection. Each line corresponds to a given vessel intensity expressed as standard deviations (SD) above background, assuming a normal distribution of background intensities.

A, Summation-intensity projection, calculated with formula,  $P(n, l_v) = 1 - (F(l_v/n))$ , where  $P$  is probability that vessel intensity is exceeded,  $l_v$  is intensity of a pixel-containing vessel expressed as standard deviations above mean background on a single section,  $F(l)$  is area under normal curve from  $-\infty$  to  $l$ , and  $n$  is number of sections projected. Contrast is quickly lost in summation projections as number of sections increases, even when contrast on individual sections is strong.

B, Maximum-intensity projection (MIP), calculated with formula,  $P(n, l_v) = 1 - F(l_v)^n$ . When many sections have been projected, preservation of contrast on MIP depends on ratio of vessel intensity to highest background intensities rather than to mean background. From this graph, it can be seen that if vessel intensity is at least 2 SD above background, the probability that the vessel will be obscured does not increase appreciably when up to 16 sections are included in the projection.

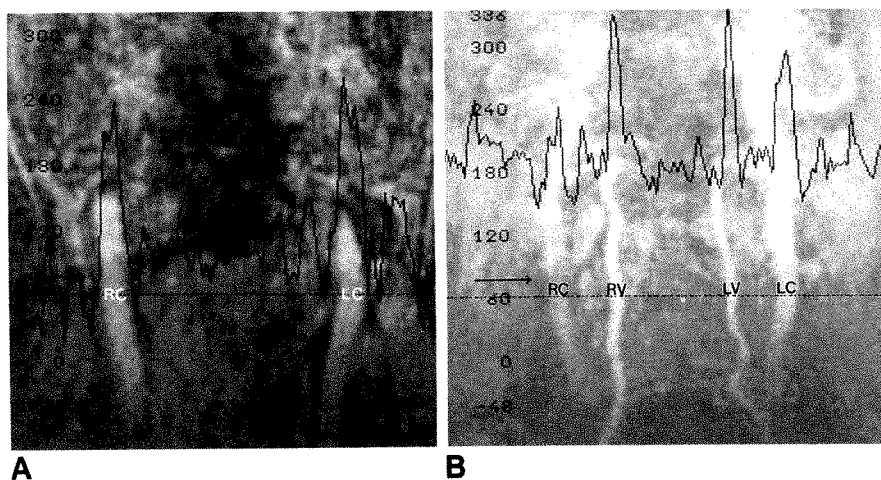


Fig. 3.—Artifactual narrowing of vessels on MIP display of MR angiograms.

A, Single coronal section of 3-D MR acquisition through both common carotid arteries (RC = right; LC = left). Contrast is poor because of inadequate inflow, but on this section, vessel contours are clearly distinguishable. Intensity profile is overlaid on image, taken at level of dotted line. Edges of vessels are less intense than centers. Widths are 10.0 mm (RC) and 9.5 mm (LC). Note large fluctuation in background pixel intensities. Highest background values are greater than some pixels within vessels. Mean background intensity is 85.

B, MIP of 32-section acquisition in A. Both common carotid arteries appear narrower. Mean background has increased to 165, resulting in brighter background and obscuring all but central portion of vessels, which results in apparent widths of 6.8 mm (RC) and 7.4 mm (LC). Highest intensity features are right (RV) and left (LV) vertebral arteries.



Fig. 4.—Artifactual narrowing of basilar and carotid arteries on maximum-intensity-projection (MIP) display of MR angiograms.

A, Single coronal section that passes through basilar artery (solid arrow) and intrapetrous portions of internal carotid arteries (open arrows).

B, MIP of entire 32-section data set. Note apparent reduction in caliber of vessels.

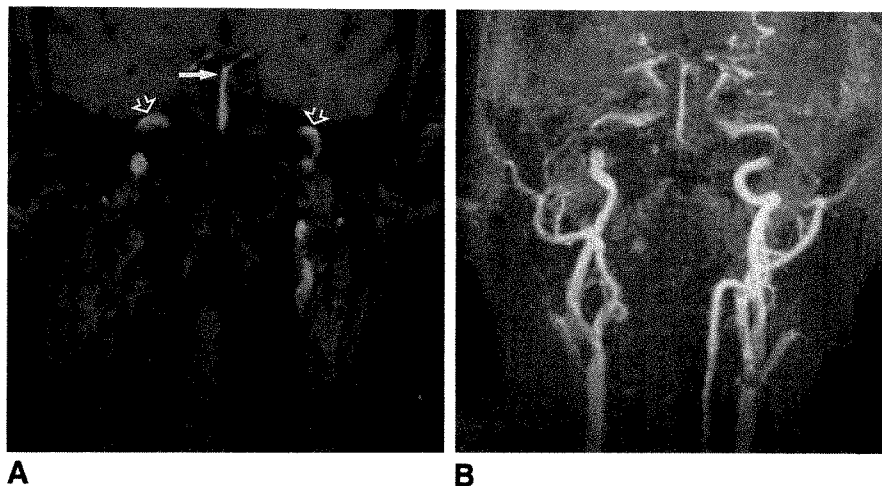
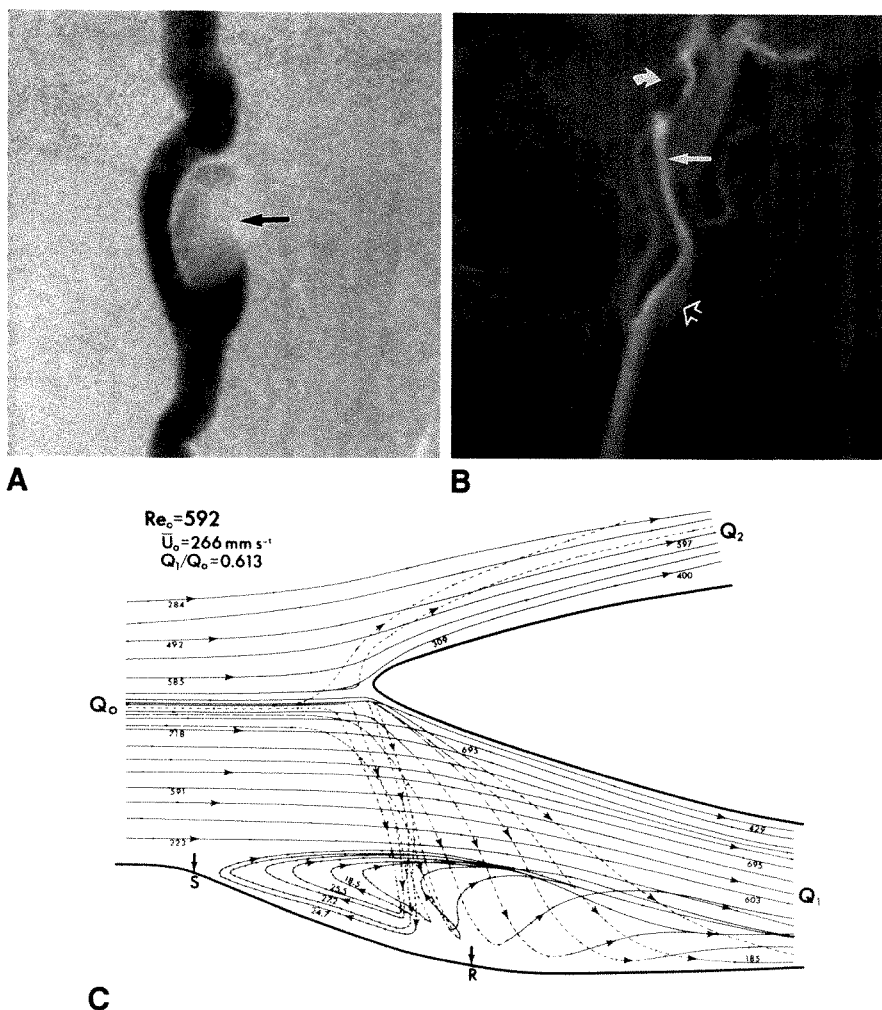


Fig. 5.—Example of artifactual narrowing of internal carotid artery (ICA) on maximum-intensity projection (MIP) display of MR angiograms and loss of signal due to commonly observed flow separation phenomena.

A, Conventional lateral angiogram of patient with balloon embolization of distal ICA aneurysm (arrow). Note true caliber of artery. Carotid bulb was normal.

B, Sagittal MIP of same patient shows site of balloon embolization (curved arrow), artifactual reduction in caliber of ICA (straight solid arrow), and low intensity of carotid bulb (open arrow).

C, Fluid-flow pattern observed in flow separation phenomena. Low intensity in bulb and marked reduction in apparent caliber of postbulb ICA can be explained by stagnant eddies resulting from separation of main laminar streamline from vessel wall. This effect is exaggerated by MIP.  $Re_0$  = Reynolds number;  $\bar{U}_0$  = mean velocity of common carotid artery;  $Q_0$ ,  $Q_1$ ,  $Q_2$  = flow rates of common, internal, and external carotid arteries, respectively; S = point of flow separation; R = region of stagnant flow. (Reprinted from Motomiya and Karino [4], by permission of the American Heart Association, Inc.)



projection. This leads to a nonlinear contrast response; vascular features with intensities only as great as the maximum background variation vanish completely, whereas signal from that portion of the vessel that is well above background variation is maintained.

The most consistent distortion introduced by MIP is the apparent reduction in vessel width. Because the edges of vessels are less intense than the center, these regions are the first to be obscured by background fluctuations, and vessels appear narrower on MIPs than on individual sections

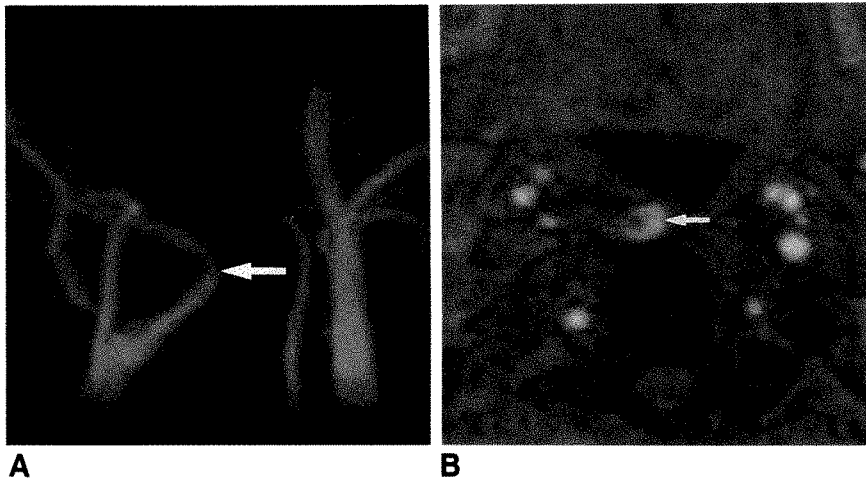


Fig. 6.—Example of signal loss due to turbulence at bend in artery leading to apparent vessel narrowing on maximum-intensity-projection display of MR angiograms. Correct vessel caliber can be seen on single, unprojected image.

A. Coronal maximum-intensity projection of neck shows tortuous right carotid artery (arrow) passing posterior to pharynx. Vessel is artifactually narrowed.

B. Single axial MR image shows laminar stream at medial margin of lumen (arrow) and along vessel wall circumferentially, whereas central portion of vessel is dark owing to turbulence.

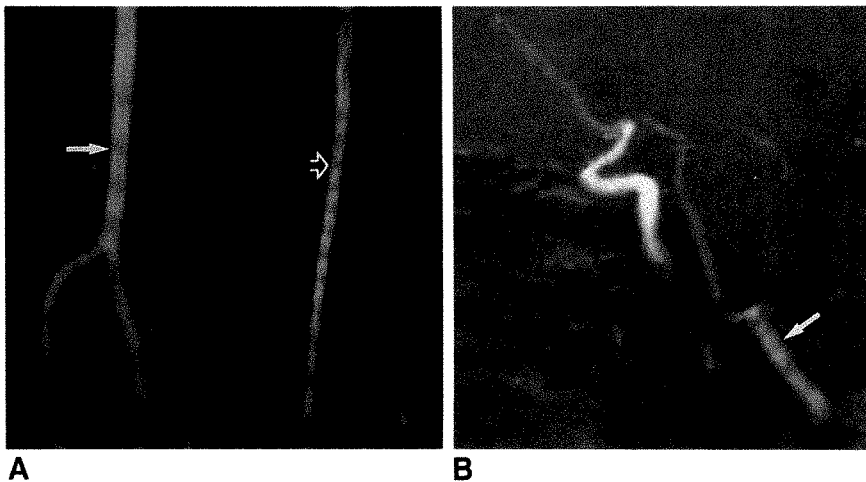


Fig. 7.—Stripe artifact encountered when vessels pass obliquely between projected sections on maximum-intensity-projection (MIP) display of MR angiograms.

A. Coronal MIP of trifurcation vessels of knee. Popliteal artery (solid arrow) and saphenous vein (open arrow) display periodic dark stripes.

B. Stripes in vertebral artery (arrow) in sagittal MIP of head. This effect is seen when vessels run obliquely between sections, causing maximum intensity to be shared between sections. In MIPs, but not in summation projections, this reduction in absolute intensity results in pronounced reduction in intensity relative to maximum background. Stripes may be eliminated by use of narrower slices.

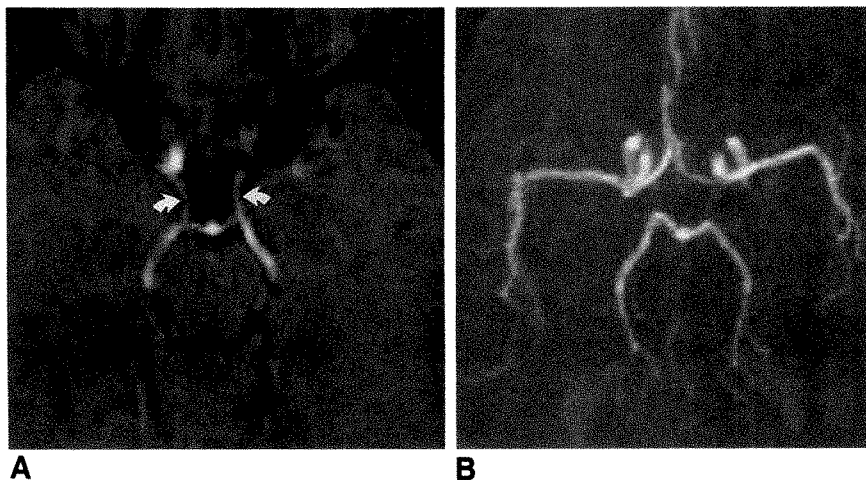


Fig. 8.—Small vessels, apparent on individual sections, are often not appreciated on maximum-intensity-projection (MIP) display of MR angiograms.

A. Single section through circle of Willis. Posterior communicating branches are well seen (arrows). In part this is due to excellent contrast with saturated CSF in cisterns.

B. Maximum-intensity projection of entire three-dimensional data set. Background is more intense. Posterior communicators are barely visible.

(Figs. 3 and 4). This phenomenon could be compared with an island that becomes smaller as the sea level rises around it. The pixel intensities are smaller at the edge of the vessels owing to both slower laminar inflow along the vessel walls

and partial voluming of the marginal pixels with a lower intensity background.

An even greater reduction in apparent vessel diameter may result from local "streamline" blood-flow patterns. These oc-

Fig. 9.—Stenosis in carotid siphon is exaggerated on maximum-intensity-projection (MIP) display of MR angiograms.

A, Sagittal MIP through carotid siphon shows apparent critical stenosis of cavernous carotid artery (*arrow*).

B, Reference to single section through this vessel shows degree of stenosis has been greatly overestimated, probably because of turbulent signal loss, which is amplified by nonlinear contrast behavior of MIP.

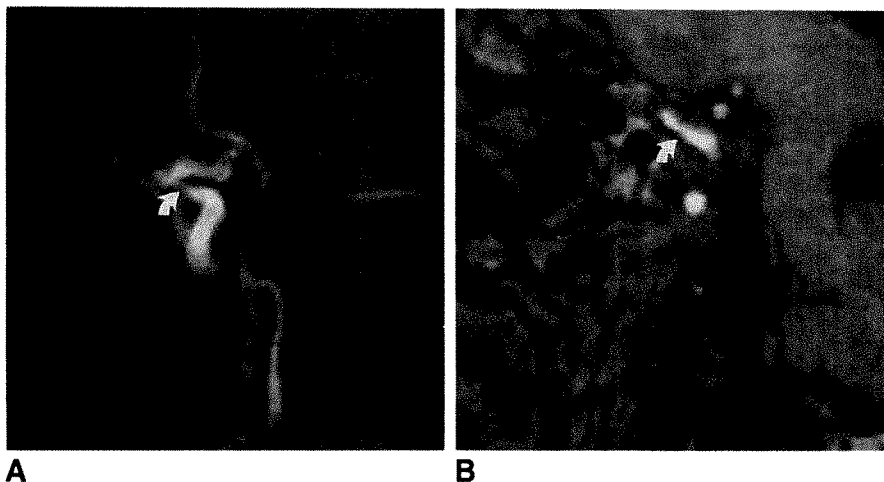


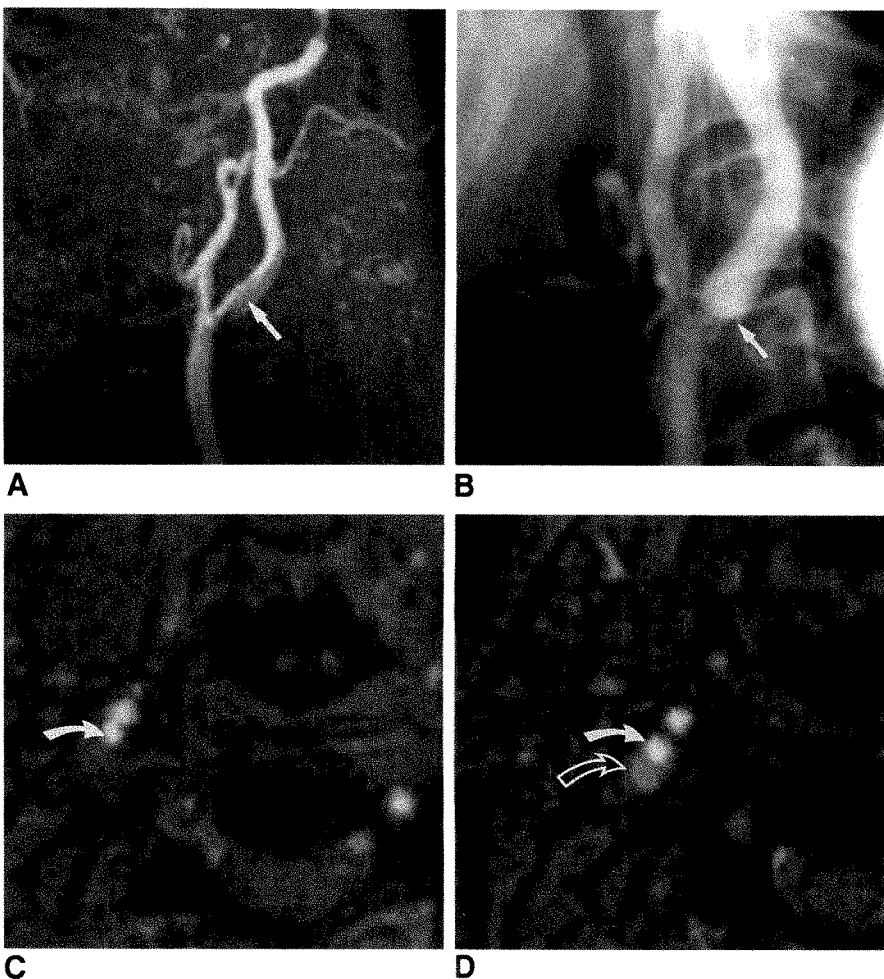
Fig. 10.—Exaggeration of stenosis on maximum-intensity-projection (MIP) display of MR angiograms; stenosis is assessed more accurately on individual slice.

A, Sagittal MIP of carotid bifurcation shows long-segment signal loss in bulb (*arrow*). One cannot distinguish between plaque, turbulence, and flow separation as causes of signal loss.

B, Conventional angiogram reveals that length of stenosis is overestimated on MIP. Short-segment stenosis at internal carotid artery (ICA) origin quickly broadens out in bulb to form overhanging edge (*arrow*).

C, Individual axial section through stenosis shows diameter of proximal ICA (*arrow*).

D, Above stenosis one can distinguish an intense streamline (*solid arrow*) anteromedially in ICA and less intense stagnant blood laterally (*open arrow*). Less intense portion of artery is not visible on MIP, thus exaggerating apparent length of stenosis. This illustrates importance of viewing individual sections in addition to projection when interpreting MR angiography.



cur when laminar streams of blood flow on one edge of the vessel, while blood along the other edge is stagnant or countercurrent. Blood in the stream is quickly replenished with unsaturated spins and appears bright, while stagnant blood becomes saturated and appears dark. In the carotid bifurcation, this is often the result of "flow separation" [4]. Only the bright streamline may be apparent on the projected

image (Fig. 5). Laminar streams may flow adjacent to more turbulent blood in vessels that follow a tortuous course (Fig. 6).

Partial voluming of pixels is also responsible for a striping artifact (Fig. 7). As a small vessel passes obliquely between sections, the vessel intensity is shared between the pixels of two adjacent sections. The maximum intensity therefore is

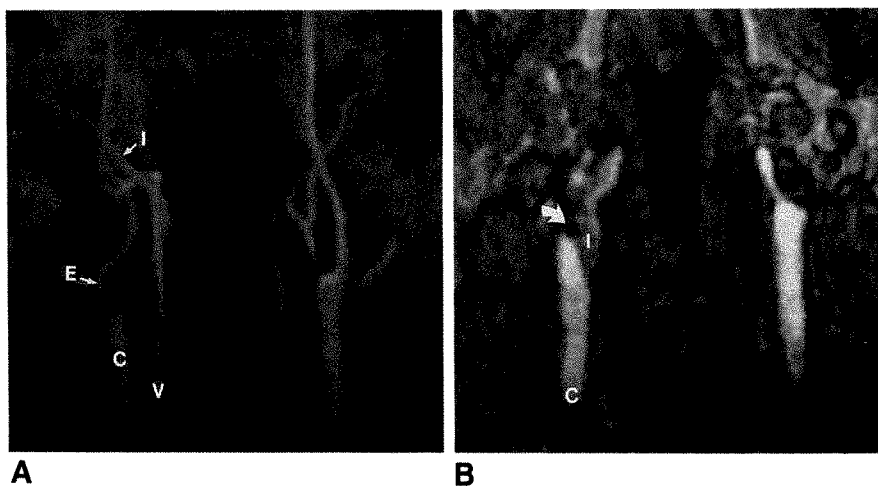


Fig. 11.—When blood flow is highly compromised, vessel intensity is too weak for successful maximum-intensity-projection (MIP) display of MR angiograms, but vessel may be seen on individual section.

A, Coronal MIP of carotid vessels. Proximal right internal carotid artery appears absent. C = right common carotid artery; E = external carotid artery; I = distal internal carotid artery; V = vertebral artery.

B, Single section through right carotid bifurcation. Despite very poor inflow, one can visualize critical stenosis with turbulent jet (small dark dot at tip of arrow) communicating between common (C) and faintly seen patent internal (I) carotid arteries. Jet was confirmed by Doppler sonography.

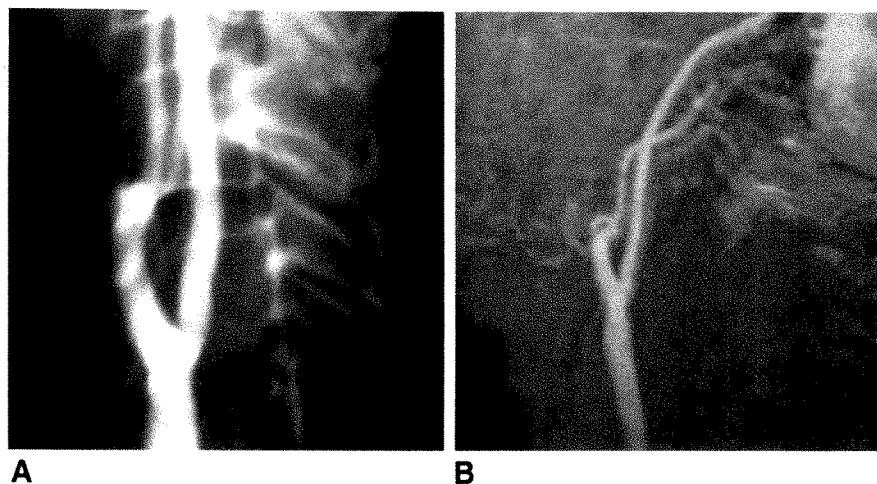


Fig. 12.—Successful maximum-intensity-projection (MIP) display of MR angiograms, owing to strong contrast on individual sections.

A, Conventional lateral angiogram of carotid bifurcation.

B, Sagittal MIP of same vessels. Excellent results may be obtained in MIP when inflow is adequate and acquisition parameters can be optimized. This may include reducing presaturation of blood entering region of interest, limiting  $\theta$  and acquisition volume so as to prevent saturation of blood, applying cushions to side of head to eliminate motion, minimizing TE, minimizing voxel size, and using RF coils tailored to region of interest.

cut in half, leading to periodic dark stripes across the vessel. Because of the nonlinear behavior of MIP, which emphasizes small differences in intensity, these stripes can be very evident when pixel size is large compared with vessel diameter.

When the vessel is even smaller with respect to pixel size, as is the case in the posterior communicating branch of the internal carotid artery, the vessel may disappear altogether on the projection, even when it is quite apparent on an individual section (Fig. 8).

Typically, arterial stenoses are accompanied by local turbulence, which leads to decreased signal. This relative signal loss is amplified by MIP and can result in possible overestimation of vascular stenosis (Fig. 9) or nonvisualization of the patent poststenotic vessel.

Turbulence and other flow phenomena are a constant obstacle in MR angiography of vascular disease. When an apparent contour deformity of the vessel is noted, a distinction must be made between mural plaque; turbulence, which may exist in the absence of underlying disease; and flow separation. Occasionally, these are better differentiated by referring to the individual sections (Fig. 10). When a vessel appears absent, one must distinguish between occlusion, slow inflow,

and turbulence. Again, reference to the individual sections may be useful (Fig. 11).

## Conclusions

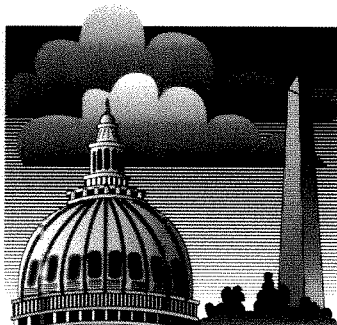
Although MIP provides angiogramlike images with contrast superior to that of summation projection, lower-intensity features of the vessels may be lost. This in turn leads to an apparent reduction in vessel diameter, an overestimation of blood turbulence or stenosis, and a loss of visualization of small or slow-flowing vessels. Therefore, it is essential to refer to the individual slices when interpreting an MR angiogram, by using the projection image as a road map.

Some investigators have advocated the use of display techniques other than MIP, such as volume and surface rendering, to avoid these artifacts [5, 6]. Alternatively, MIP could be improved by projecting together only a small number of sections at a time or by clipping the three-dimensional data set outside of the volume of the vessels of interest before projection in order to minimize background. Further reduction in background could be achieved by applying a filter to the

sections to decrease variance. The best strategy, however, is to optimize the acquisition variables in order to increase vascular signal and resolution and minimize background noise. Under the best inflow conditions, excellent results may be obtained (Fig. 12).

## REFERENCES

1. Masaryk TJ, Modic MT, Ross JS, et al. Intra-cranial circulation: preliminary clinical results with three-dimensional (volume) MR angiography. *Radiology* **1989**;171:793-799
2. Masaryk TJ, Modic MT, Ruggieri PM, et al. Three-dimensional (volume) gradient-echo imaging of the carotid bifurcation: preliminary clinical experience. *Radiology* **1989**;171:801-806
3. Rosnick S, Laub G, Braeckle R, et al. Three dimensional display of blood vessels in MRI. In: *Proceedings of the IEEE Computers in Cardiology Conference*. New York: Institute of Electrical and Electronic Engineers, **1986**:193-196
4. Motomiya M, Karino T. Flow patterns in human carotid artery bifurcation. *Stroke* **1984**;15:50-56
5. Vandermeulen D, Bosmans H, Van Henke P, Suetens P, Marchal G. 3-D angiography of the brain: postprocessing for improved blood vessel visualization (abstr). In: *Book of abstracts for SMRM 8th annual meeting*. San Diego: Society of Magnetic Resonance in Medicine, **1986**:867
6. Hu X, Tan K, Alperin N, Levin D, Mengeot M. An integrated 3-D display of intracranial vasculature and the brain surface created by volume rendering MR data (abstr). In: *Book of abstracts for SMRM 8th annual meeting*. San Diego: Society of Magnetic Resonance in Medicine, **1989**:869



Scientific Program (200 papers)

Instructional Courses (60 hours)

Categorical Course on  
Cardiovascular Imaging

The Caldwell Lecture

Award Papers

Scientific Exhibits

Social, Golf, and Tennis Programs

Guest Programs



Come to the  
American Roentgen Ray Society

90<sup>th</sup>

ANNUAL MEETING

Washington, D. C.

Sheraton Washington Hotel

May 13-18, 1990

## Book Review

**Pocket Atlas of Head and Neck MRI Anatomy.** By Robert B. Lufkin and William N. Hanafée. New York: Raven, 76 pp., 1989. \$13.95

This brief but succinct guide to basic MR anatomy of the head and neck is designed to serve as a portable atlas and is formatted to fit easily into the pocket of a lab coat. It should be made clear what this book *is*, that is, a multiplanar atlas of extracranial head and neck anatomy. It is *not* a gross anatomy atlas, nor does it consider the brain.

Sections are organized into neck (both supra- and infrahyoid) and larynx; oropharynx and tongue; nasopharynx, skull base, and sinuses; and temporal bone. All three major imaging planes are represented in each section. Only the major structures are labeled in each image, but this is acceptable as the book seems intended primarily for trainees and medical students. It also could be a nice introduction for practicing radiologists who are new to MR of the no-man's land

between the skull base and thoracic inlet. Imaging of the head and neck is a growing segment of many radiology practices, and familiarity with this type of normal anatomy is necessary.

The basic anatomy is depicted satisfactorily. However, the images are from a low-field scanner and consequently do not have the fine detail that many higher-field-strength systems display routinely. Nevertheless, this is a nice and inexpensive guide to keep at hand in film-viewing areas.

Anne G. Osborn  
University of Utah, School of Medicine  
Salt Lake City, UT 84132



## Technical Note

# Halo Vest for Cervical Spine Fixation During MR Imaging

Frank G. Shellock<sup>1</sup> and Gina Slimp

The potential risks and problems associated with performing MR imaging in patients with metallic implants or metallic materials are related to movement or dislodgement, induction of electrical current, heating, and the misinterpretation of an artifact as an abnormality [1–3]. Therefore, use of MR imaging to assess cervical spine trauma in patients who require stabilization of the spine with a halo vest is frequently impossible because these devices are composed of metallic materials that produce mild to severe artifacts [4]. In addition, there is a theoretical hazard of inducing electrical current in the ring portion of the halo vest as a result of Faraday's law of electromagnetic induction, whereby a current can be induced in a closed-loop conductor as it moves through a magnetic field [1, 4].

In consideration of these factors, patients with halo vests are typically not regarded as suitable candidates for MR imaging. This is unfortunate because MR imaging frequently may provide a useful diagnostic evaluation of the spinal cord and associated soft-tissue structures that is unobtainable by other imaging techniques.

Recently, a specially designed halo vest was developed from materials that have little or no interaction with the electromagnetic fields used for MR imaging. We evaluated artifacts and safety-related aspects of using this halo vest during MR imaging of the cervical spine.

## Materials, Methods, and Results

The halo vest (Ambulatory Halo System, All Orthopedic Appliances Co., Division of Kirschner Medical, Greenwood,

SC) is predominantly composed of nonferromagnetic, non-conductive materials (Fig. 1). The halo ring, two connector blocks, and hinge plates that fit on the front and back of the vest are made from Lexan 3413 resin (high-performance polycarbonate resin reinforced with 30% glass fiber, General Electric Co.). The two upright connectors are made from high-pressure laminate (National Electrical Manufacturers Association, NEMA G-10 grade epoxy/glass cloth). The only metallic parts of this device are the pins used for fixation of the halo ring to the skull, which are composed of titanium (American Society Testing Materials, ASTM F67-83 grade unalloyed titanium).

An evaluation of deflection forces was performed as previously described [2] to determine the ferromagnetic qualities of the various parts of this halo vest. None of the components of the halo vest interacted with the 1.5-T static magnetic field. Heating was evaluated by using a noncontact infrared thermometer to measure surface temperatures immediately before and after MR imaging, which simulated a routine examination of the cervical spine. No significant heating (i.e., less than 0.5°C maximal temperature change) of any portion of the halo vest resulted from this procedure. As the materials used in the construction of this halo vest are essentially nonconductive and nonferromagnetic, heating or inducing current in this device during MR imaging is unlikely.

In order to assess potential artifacts produced by the halo vest, MR imaging was performed with the device placed around a standard quality control Plexiglas phantom. We used a 1.5-T, 64-MHz MR scanner (General Electric Company, Milwaukee, WI) and a 5-in (12.7 cm) circular receive-only

Received September 13, 1989; accepted after revision October 26, 1989.

<sup>1</sup> Both authors: Section of Magnetic Resonance Imaging, Department of Diagnostic Radiology, Cedars-Sinai Medical Center and UCLA School of Medicine, 8700 Beverly Blvd., Los Angeles, CA 90048. Address reprint requests to F. G. Shellock.

AJR 154:631–632, March 1990 0361–803X/90/1543–0631 © American Roentgen Ray Society

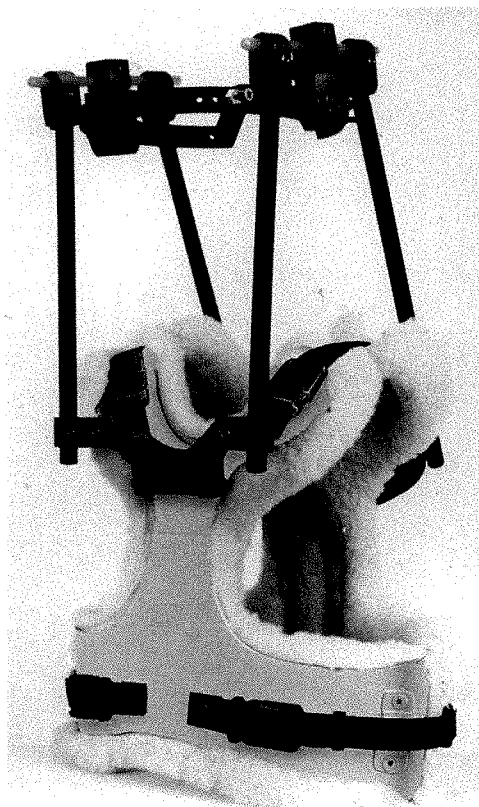


Fig. 1.—Halo vest composed of nonferromagnetic, nonconductive materials can be used during MR imaging.

surface coil as follows: spin-echo, sagittal plane, 600/20 (TR/TE), 256 × 192 matrix, four excitations, 4.0-mm slice thickness, no slice gap, 24-cm field of view; and gradient-recalled acquisition in the steady state (GRASS), axial plane, 24/13, 15° flip angle, 256 × 128 matrix, four excitations, 5.0-mm slice thickness, no slice gap, 24-cm field of view.

As the images of the phantom were deemed to be acceptable (the titanium skull pins produced only minor artifacts that did not appear to affect the area of interest), the halo vest was then placed on a normal subject and MR imaging was performed on the cervical spine by using the aforementioned

pulse sequences. Although the titanium screws were not inserted into the skull, they were positioned on the perimeter of the ring and placed close to the skull of the subject. The obtained images were considered of sufficient quality to be diagnostic, with no degradation or distortion of the anatomy of the spinal cord, soft-tissue structures, or bony anatomy of the cervical spine.

## Discussion

In a previous evaluation of the effect of various halo vests on image quality, these devices were reported to cause image distortion that depended on the type of material used to construct the halo rings and uprights [4]. Halo vests made from stainless steel produced the poorest image quality, followed by those made from aluminum, titanium, and graphite [4]. This prior study did not assess deflection forces, heating, or induced currents [4], all of which could present hazards to the patient if the halo vest is primarily composed of ferromagnetic and/or conductive materials.

Our results indicate that high-field-strength MR imaging can be used to evaluate the cervical spine of patients wearing a halo vest made mostly from nonferromagnetic, nonconductive materials. Advantages of using this particular type of halo vest include the following: (1) there are no associated deflection forces, (2) heating is minimal, (3) there are no artifacts that distort the imaging area of interest, and (4) induced currents are unlikely. Therefore, MR imaging may be used safely and effectively to evaluate patients with cervical spine trauma who require immobilization by means of a halo vest, if the vest is made of nonferromagnetic, nonconductive materials.

## REFERENCES

1. Shellock FG. Biological effects and safety aspects of magnetic resonance imaging. *Magn Reson Q* 1990 (in press)
2. Shellock FG. MR imaging of the metallic implants and materials: a compilation of the literature. *AJR* 1988;151:811-814
3. Pusey E, Lufkin RB, Brown RKJ, et al. Magnetic resonance imaging artifacts: mechanisms and clinical significance. *RadioGraphics* 1986;6:891-911
4. Ballock RT, Hajek PC, Byrne TP, Garfin SR. The quality of magnetic resonance imaging, as affected by the composition of the halo orthosis. *J Bone Joint Surg [Am]* 1989;71-A:431-434

## Ghost Artifact on Gradient-Echo Imaging: A Potential Pitfall in Hepatic Imaging

Paul M. Silverman,<sup>1</sup> Richard H. Patt, Phillip A. Baum, and George P. Teitelbaum

Standard evaluation of the liver with MR uses spin-echo imaging with T1- and T2-weighted pulse sequences [1]. A short inversion-time inversion recovery (STIR) sequence has been used as an adjunct to standard pulse sequences because it provides certain advantages, including fat suppression, additive effects of T1 and T2 relaxation on tissue brightening, and a high signal-difference-to-noise ratio in the detection of liver metastases [2, 3]. All of these sequences require a long acquisition time and thus are compromised by motion and respiratory artifacts. The recent use of gradient-echo imaging to scan the liver allows acquisition of data within a single breath-hold [4]. In using this technique to examine patients with various types of hepatic disease, we noticed a disturbing artifact that mimicked a space-occupying lesion. Appreciation of this artifact is important in interpreting scans acquired with a gradient-echo pulse sequence.

### Materials and Methods

MR imaging was performed on an asymptomatic subject by using a 1.5-T superconducting magnet (Siemens, Magnetom, Iselin, NJ). Single breath-hold (25 sec) gradient-echo, fast imaging with steady-state precession (FISP) scans were obtained with a single average and a  $256 \times 256$  matrix. Parameters included a flip angle of  $45^\circ$ , repetition time (TR) of 50 msec, and an echo time (TE) of 12 msec. On scans through the liver, a "pseudolesion" was detected in the left lobe. The artifactual nature of this lesion was confirmed by real-time sonography directed to the left hepatic lobe. Additionally, gradient-echo imaging was performed with the phase-encoding direction shifted  $90^\circ$  and with the flip angle varied at  $25^\circ$  and  $80^\circ$ .

### Results

The initial gradient-echo MR image showed a 1.5-cm hyperintense area in the left lobe of the liver (Fig. 1A). No clear trail of signal was defined in the phase-encoding direction connecting the hyperintense area with the major abdominal vessels. Directed sonography showed normal hepatic parenchyma in this area, suggesting that this was a pseudolesion.

Repeated MR imaging with the phase-encoded direction shifted  $90^\circ$  confirmed a normal left hepatic lobe (Fig. 1B). A trail of high-intensity signal in the horizontal phase-encoded direction coursed through the aorta and inferior vena cava, representing periodic phase-related ghost artifact. Gradient-echo scanning at flip angles of  $25^\circ$  and  $80^\circ$  (Fig. 2) in addition to  $45^\circ$  showed that the periodic phase-related artifact was accentuated at the higher flip angles.

### Discussion

Gradient-echo imaging has become more widely used in MR with the quest for more rapid scanning techniques, especially with the introduction of paramagnetic contrast agents [1, 4]. Techniques such as FISP allow a scan to be completed within the time span of a patient's single breath-hold. This improves image quality by decreasing motion-associated artifacts. Unlike its appearance in spin-echo images, flowing blood appears bright. Because of this, gradient-echo images are valuable for visualizing flowing blood in vessels to confirm patency and for showing intravascular thrombosis. The artifacts from the intensely bright flowing blood are displayed in the phase-encoded direction, usually through the left lobe of the liver, and thus are more obvious on gradient-echo images than on standard spin-echo imaging sequences in which flowing blood shows a relative signal void.

In the present case, a bright, well-defined, round ghost artifact was superimposed over the left lobe, mimicking a space-occupying lesion (Fig. 1A). If an associated periodic phase-related ghost artifact traced to vascular structures such as the inferior vena cava, aorta, or major hepatic veins can be identified, this is recognized readily as a common MR artifact. When such an association is not clear, as in this case, a true lesion should be excluded. Flipping the phase-encoded gradient  $90^\circ$  is a simple method of confirming this finding as an artifact (Fig. 1B) and is often used for optimal assessment of the left lobe of the liver when segmental hepatic resection is contemplated. Alternatively, one can apply a presaturation

Received August 25, 1989; accepted after revision October 10, 1989.

<sup>1</sup> All authors: Department of Radiology, Georgetown University Hospital, 3800 Reservoir Rd., N.W., Washington DC 20007. Address reprint requests to P. M. Silverman.

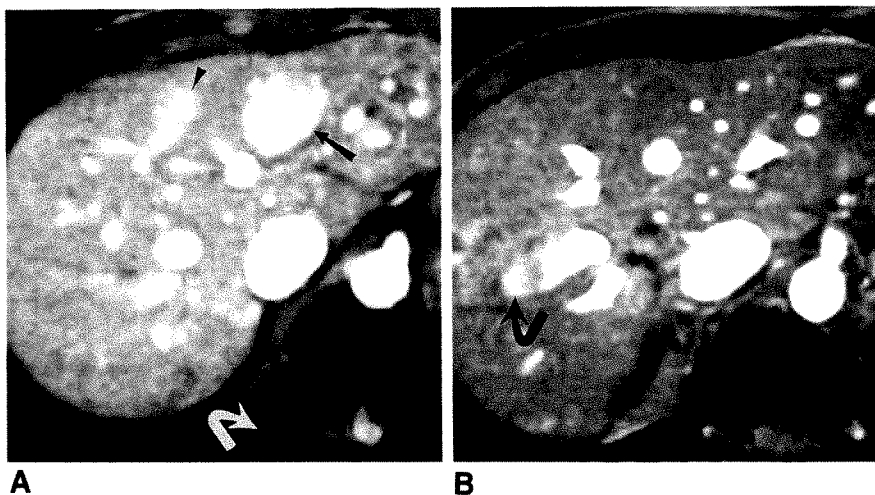


Fig. 1.—A, Fast imaging with steady-state precession (FISP), 45°-flip-angle MR image of upper liver. Phase-encoded direction in y-axis. A focal bright pseudolesion (straight arrow) is noted in left lobe. Extremely subtle phase artifact is difficult to see (curved arrow). A smaller pseudolesion that is harder to see is noted (arrow-head) anterior to right hepatic vein.

B, FISP, 45°-flip-angle MR image with phase-encoding direction shifted 90°. No lesions are present. Phase-related artifact is clearly evident (curved arrow); artifacts from aorta and inferior vena cava are superimposed.

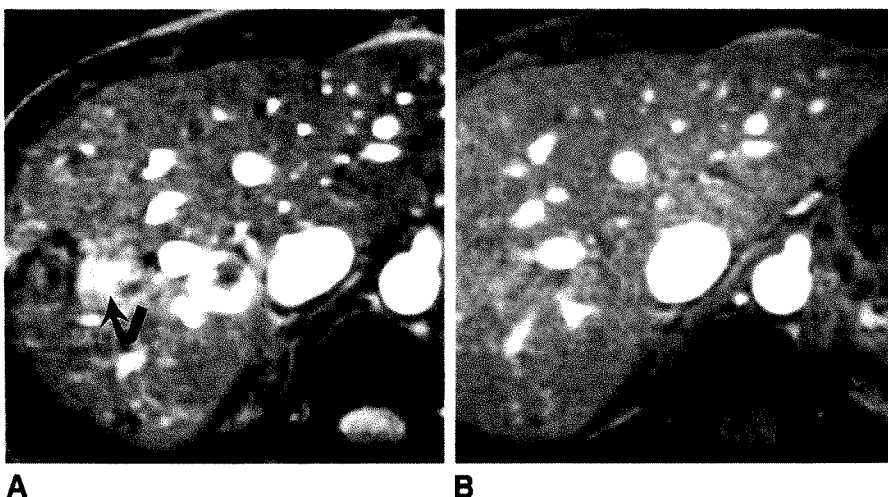


Fig. 2.—A, Fast imaging with steady-state precession (FISP), 80°-flip-angle MR image. Phase-related artifact (arrow) is accentuated at largest flip angle.

B, FISP, 25°-flip-angle MR image. Phase-related artifact is minimized compared with that at flip angles of 45° and 80°.

slab to either side of the slice of interest to cause flowing blood to appear dark. The presaturation technique is advantageous because it eliminates the artifact rather than shifting it in another direction. Sonography also is helpful for evaluating the hepatic parenchyma.

Also, we assessed the effect of the flip angle on the conspicuity of this phase-related artifact. The best flip angle for maximal contrast between normal hepatic tissue and lesions is predicted to be approximately 40°–55° for FISP imaging [4]. In FISP, T2\* has a relatively dominant effect in distinguishing tumor from normal liver, with tumor being bright. We observed that the greater the flip angle, the more conspicuous the artifact in the phase-encoded direction (Fig. 2). The increased artifact is related to increased flow-related enhancement as the flip angle approaches 90°. This has been shown with flip angles greater than 60° in in-vitro flow phantom studies [5].

Gradient-echo imaging sequences including FISP provide high-contrast images of the liver with excellent delineation of the hepatic vasculature and are being used more frequently in abdominal imaging. The high-signal-intensity phase artifact associated with blood vessels may be superimposed on parenchymal organs. An appreciation of flow-related artifacts and their relation to different pulse-sequence parameters in

gradient-echo imaging is important in interpretation of these scans. When a focal lesion is noted directly anterior or posterior to a vascular structure in the phase-encoded direction on gradient-echo imaging, the images should be evaluated carefully to detect the most subtle periodic ghost artifacts (Fig. 1A). Even if this is not clearly defined, a change in the phase-encoded direction or use of a presaturation technique can be performed simply and rapidly to confirm the artifact and avoid potential misdiagnosis.

#### REFERENCES

1. Stark DD. Liver. In: Stark DD, Bradley WG, eds. *Magnetic resonance imaging*. St. Louis: Mosby, 1988:934–1059.
2. Shuman WP, Baron RL, Peters MJ, Tazioli PK. Comparison of STIR and spin-echo MR imaging at 1.5 T in 90 lesions of the chest, liver, and pelvis. *AJR* 1989;152:853–859.
3. Paling MR, Abbitt PL, Mugler JP, Brookeman JR. Liver metastases: optimization of MR imaging pulse sequences at 1.0 T. *Radiology* 1988;167:695–699.
4. Unger EC, Cohen MS, Gatenby RA, et al. Single breath-holding scans of the abdomen using FISP and FLASH at 1.5 T. *J Comput Assist Tomogr* 1988;12:575–583.
5. Teitelbaum GP, Ortega HV, Vinitski S, et al. Optimizing gradient echo imaging parameters for intracaval filters and trapped thromboemboli. *Radiology* (in press).

## Perspective

# Planning a Totally Digital Radiology Department

H. K. Huang,<sup>1</sup> Hooshang Kangarloo, Paul S. Cho, Ricky K. Taira, Bruce K. T. Ho, and K. K. Chan

A recent survey in July 1989 [1] indicates that there are approximately 50 picture archiving and communication systems (PACS) installed in Japan and about 30 installed or to be delivered in the United States and Europe. These systems are of various degrees of complexity and each tries to address a small portion of the management and processing requirements of a given radiology subspecialty. Because of the complexity of a total PACS, there is yet to be described in the literature a comprehensive plan for an entire radiology department. Two hospitals have plans for a total PACS project: the Madigan Army Hospital in Washington and Hokkaido University Hospital in Japan. At UCLA, we still believe that PACS should be implemented in a modular fashion. At a recent departmental retreat meeting on the topic of "Future Practice of Radiology," our department endorsed a plan for total PACS implementation during the next 5 years. This paper presents the perspective of this plan.

## Background

During the past 3 years we have developed two PACS modules, one in the pediatric radiology section and the other in the coronary care unit. The pediatric PACS module has six  $512 \times 512$  pixel display monitors and is used for case review and daily conferences. The PACS module in the coronary care unit consists of three  $512 \times 512$  pixel display monitors and uses an analog broadband communication system to

send images from the pediatric radiology host computer to the coronary care unit. Both systems have been in clinical use for over 2 years. Our 2 years of clinical experience show that clinicians are extremely pleased with the display stations and are enthusiastic about using them. The disadvantage of these two systems are the low-resolution display monitors, both of which are  $512 \times 512$  pixels. The detailed clinical results for these two systems are documented elsewhere [2, 3]. In April 1989, we upgraded both display stations to  $1K \times 1K$  pixel resolution. In the pediatric radiology section, six  $1K \times 1K$  pixel noninterlaced display monitors are used, and in the coronary care unit, two  $1K \times 1K$  pixel noninterlaced display monitors are used.

There are two other PACS modules being implemented in our department, an image network consisting of MR, CT, and sonographic images, and a PACS module for the thoracic radiology section. Descriptions of these two modules are given in the PACS Handbook '89 [4]. This paper describes the future development of PACS in our department.

## The Center for Health Sciences and the Medical Plaza

A new UCLA Medical Plaza across the street from the present hospital (the Center for Health Sciences) will be opened in the third quarter of 1990. The purpose of the Medical Plaza is to provide ambulatory care. When it is fully occupied, the radiology department will perform approxi-

Received September 13, 1989; accepted after revision November 1, 1989.

Presented at the Eighth Symposium on Japanese Medical Imaging and Technology (JAMIT)/Sixth International Symposium on Picture Archiving and Communication Systems (JPACS), Osaka, Japan, July 1989.

This work was supported in part by U.S. Public Health Service grant numbers R01 CA 39063 and R01 CA 404565 awarded by the National Cancer Institute, Department of Health and Human Services. Konica Photo Ltd., Philips Medical Systems of North America, Mitsubishi Electric Corp., Kodak, and Hitachi Maxell, Ltd. are also providing support for this research.

<sup>1</sup> All authors: Department of Radiological Sciences, UCLA School of Medicine, Los Angeles, CA 90024. Address reprint requests to H. K. Huang.

mately 80,000 procedures per year. Currently the department of radiology in the Center for Health Sciences performs approximately 190,000 procedures per year. These include both inpatients and outpatients. When the ambulatory care center opens in the Medical Plaza, all the outpatient services will be conducted in the new facility. The radiology department will occupy approximately 30,000 square feet spanning two levels. The new facility will have two CT scanners, two MR scanners, three gamma cameras, three sonography units, three mammography units, and about 10 radiographic and fluorographic rooms. In addition, one computed radiography system will be installed in the pediatric radiology area. An additional two new computed radiography units may be installed, depending on the available image quality for general chest and bone radiographic studies. The radiology department in the Medical Plaza and the current radiology department in the Center for Health Sciences will be under a single administration.

The question was raised whether or not to plan the implementation of a totally digital radiology department for both the Medical Plaza and the Center for Health Sciences. Our current thought is that implementing a totally digital radiology operation is easier in the Medical Plaza than in the current radiology department in the Center for Health Sciences for two reasons. First, it is easier to design a totally digital department when the building floor plan is still flexible. Second, the current radiology department is organized according to radiology subspecialties which makes the department fragmented and therefore difficult for PACS implementation. After careful consideration we devised the following plan. In the Center for Health Sciences, we will implement a  $2K \times 2K$  pixel display station in pediatric radiology for primary diagnosis. In addition, we will complete the integration of the CT, MR, and sonography subsystems and implement the thoracic chest PACS module. In the Medical Plaza, we will implement a CT/MR network and a pediatric PACS module that are similar to the network and the module in the Center for Health Sciences. We will develop a central archiving station and review stations for CT, MR, bone, chest, and other specialties. An image-communication network will be established between the Center for Health Sciences and the Medical Plaza.

#### **Communication Between the Center for Health Sciences and the Medical Plaza**

The distance between the Center for Health Sciences and the Medical Plaza is less than 2000 feet. However, if we lay a fiber-optic cable between a PACS host computer in the Department of Radiological Sciences in the Center for Health Sciences and a host computer in the Medical Plaza, the actual cable requirement is 4700 feet, or a little less than 1.5 km. We have installed 64 optical fibers with specifications satisfying the FDDI (Fiber Distributed Data Interface) requirement. The fiber is run through a tunnel under the street separating the two buildings. The fiber's outer diameter is  $125.0 \pm 2.0$   $\mu\text{m}$ , and the inner diameter is  $62.5 \pm 3.0$   $\mu\text{m}$ . The price of the fiber is approximately 40 cents per fiber per foot. One end of the cable at the Center for Health Sciences will be connected

to a second fiber-optic-cable system dedicated to the medical school by the UCLA campus network authority. This cable will run throughout the radiology department. The other end of the cable will be connected to a third fiber-cable system in the Medical Plaza. This cable system will span the entire radiology department. The method of connecting these three sets of cable system has not been finalized.

We are contemplating three possible network connections between the two buildings. The first is a 1 gigabit per second network (UltraNetwork, San Jose, CA). The second is a 100 megabit per second rooted-tree network (Canstar, Toronto, Canada). The concentrator (or the hub) of the Canstar network can connect to various acquisition nodes through an EIU (Ethernet Interface Unit) with a maximum speed of 10 megabits per second, or to a display station through a HIU (host interface unit) with a maximum speed of 100 megabits per second. The third is a standard FDDI network with a maximum speed of 100 megabits per second. All three types of network are now in our department for testing. Within the next 6 months, we will derive an efficient architecture to link these three networks [5].

Within the Center for Health Sciences, and within the Medical Plaza, we will use Ethernet for transmitting images between the image acquisition devices and the computer of a PACS module and from the computer to one of several optical storage devices. For image transmission between the computer and a display station, we will use the FDDI and the Ultranet. We think that it is not necessary to use FDDI for connecting the image acquisition devices and the optical storage devices because they have relatively slower transfer rates. On the other hand, image transmission between the host computer and display stations requires a high transfer rate because workstation usage is demanding during clinical hours. In this case, FDDI or the faster network is necessary.

#### **PACS Clusters and Image Data Base**

As we are implementing the PACS in a modular fashion, we have decided to adopt a hierarchical file directory system [6]. In this architecture, a master directory contains image descriptive data of all inpatients registered in the Center for Health Sciences and all outpatients registered in the Medical Plaza. The PACS module (or modules) forms a cluster and each cluster maintains a cluster directory (Fig. 1). The cluster directory contains only image descriptive data of patients belonging to the cluster. The optical storage device in a cluster contains images of patients belonging to the cluster. The master directory will be connected to the radiology information system to obtain demographic data and report information on patients. A cluster directory as well as the master directory is updated when a new patient's image is acquired. Each cluster maintains a data management system responsible for image management of that particular cluster and can communicate with other clusters.

Of the PACS modules, earlier modules will consist of older components and newer modules will use the latest technology. For economic reasons, we cannot upgrade older modules whenever a new module is implemented. However, a



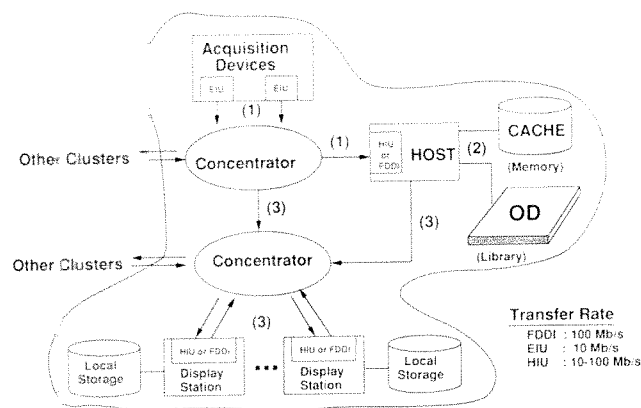


Fig. 1.—Architecture of a cluster. (1) Acquisition devices transmit images to concentrator (hub) and host computer. (2) Images are reformatted to American College of Radiology/National Electrical Manufacturers Association logical standard, stored temporarily in cache memory and archived onto optical disk library. (3) Reformatted images are selectively sent to proper display stations where they are stored in local storage for up to 2 weeks. FDDI = Fiber Distributed Data Interface; EIU = Ethernet interface unit; HIU = host interface unit.

component in a module will be replaced when it becomes incompatible with other modules.

#### Clusters in the Center for Health Sciences

In the Center for Health Sciences, the pediatric radiology module and the coronary care unit module form a cluster, using the VAX-11/750 computer (Digital Equipment Corporation, Maynard, MA) as the host (an older technology). This cluster acquires images from a computed radiography system, MR, CT, and sonography. Images are sent to a file server, which is composed of both magnetic and optical storage devices. The optical storage consists of a 64-platter Filenet (Costa Mesa, CA) optical library with two Hitachi 301 (Tokyo, Japan) optical disk drives. Each platter can store 2.6 gigabytes of data. The file server is connected to a display station with six 1K × 1K pixel monitors and a display station with two 2K × 2K pixel monitors in pediatric radiology and a two-monitor 1K display station in the coronary care unit. The magnetic disks in the file server also can store images transferred from other clusters on a temporary basis. This cluster remains unchanged operationally regardless of any other future PACS development except that hardware and software will be upgraded periodically. This upgrading should not affect the operation of other clusters.

The second cluster in the Center for Health Sciences is the CT, MR, and sonography network. Images are sent from acquisition devices to a hub of the network (equivalent to a telephone switch circuit) connected to a file server consisting of a Kodak 6800 optical library (Rochester, NY) and a set of magnetic disk drives. The library contains 100 platters with 6.8 gigabytes storage capacity per platter. The server is connected to a second hub, which in turn is connected to different display stations through a network with a 100 megabits per second transfer rate. The cluster also has its own

cluster directory and is updated immediately upon acquisition of images.

#### Clusters in the Medical Plaza

The PACS operation in the Medical Plaza will initially consist of two clusters: one handles all the MR, CT, and sonographic images and the second, all pediatric radiology images. Other new clusters will be added when it becomes necessary. The operation of this cluster is similar to that of any cluster in the Center for Health Sciences. The optical disk library in this cluster will store images of patients originating from the Medical Plaza.

#### Communication Between Clusters in the Center for Health Sciences and the Medical Plaza

The cluster directories in the Center for Health Sciences and the cluster directories in the Medical Plaza will be linked by the master directory (Fig. 2). As an example, when a pediatric patient is transferred from outpatient to inpatient, a patient status change will trigger transfer of this patient's images from the optical storage in the Medical Plaza to the pediatric radiology cluster in the Center for Health Sciences. Both cluster directories and the master directory will be updated and show that this particular patient has been transferred to the pediatric radiology cluster in the Center for Health Sciences as an inpatient. Images of this patient originally stored in the Medical Plaza optical library will be transferred through the fiber-optic link and stored in the pediatric radiology file server in the Center for Health Sciences. The images are then transmitted from the file server to the pediatric viewing station's local storage. However, this set of images will not be stored in the optical library in the Center for Health Sciences because permanent records are already in the Medical Plaza optical library. This patient's images will remain in

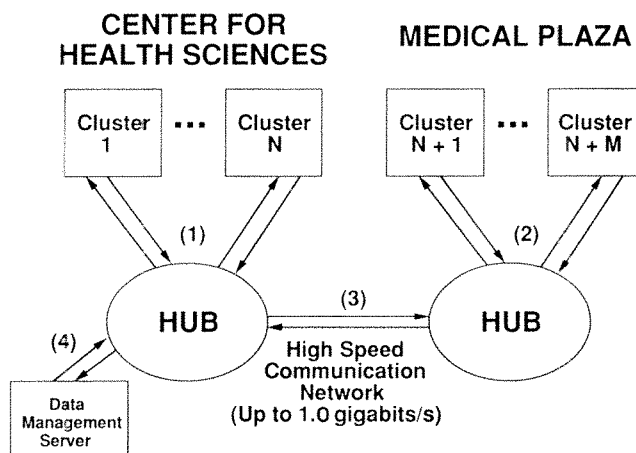


Fig. 2.—Architecture of a total picture archiving and communication system with many clusters. (1) Many clusters in Center for Health Sciences are connected to a hub. (2) Many clusters in Medical Plaza are connected to a second hub. (3) Two hubs are connected with a high-speed communication network. (4) Data management server controls data and image flow through network.

the temporary magnetic storage assigned to the display station until the patient is discharged. All new images of this patient acquired in the Center for Health Sciences as an inpatient will be appended to the same patient's file in the local storage. These newly acquired images also will be transmitted to the Medical Plaza optical library for long-term archiving.

Similar operational procedures can be derived if an inpatient from the Center for Health Sciences is transferred to the Medical Plaza as an outpatient. Thus, it does not matter whether the patient is originally registered as an outpatient in the Medical Plaza or as an inpatient in the Center for Health Sciences, because both locations can access images via the master directory of the data management system and the PACS network. The only difference is that if the patient is originally registered as an outpatient, the patient's images will be permanently stored in the optical library of the Medical Plaza. On the other hand, if the patient is originally registered in the Center for Health Sciences as an inpatient then the images of this patient will be stored permanently in the optical library of the pediatric cluster in the Center for Health Sciences. As far as system operations are concerned, this permanent storage arrangement is transparent to the user. From a departmental point of view, only one image management system exists; the master directory keeps track of where the images are stored. This method of management will allow functional unity in a physically divided department. We anticipate that about 20% of the images will be transferred between the Center for Health Sciences and the Medical Plaza. As the data management system is independent of the hardware configuration, a change in any piece of hardware will not affect the operation of the file directory system.

Currently, the two working PACS modules in pediatric radiology and in the coronary care unit in the Center for Health Sciences use custom-built data-base-management software. Images of different format and sources are first converted to a UCLA standard image format [7], which has description headers that are logically compatible with the American College of Radiology/National Electrical Manufacturers Association standard [8] before they are stored in the data bases. However, when we integrate many PACS modules throughout the department, we will use a commercial data-base-management system because of the complexity in the data-management requirements. For this reason we have installed the SYBASE (SYBASE, Emeryville, CA) data-base-management system. This data-base system is a true relational data-base system and can perform all the functions described previously. We will gradually convert the current data bases in pediatric radiology and in the coronary care unit to this new data-base system. Once it is implemented, the manufacturer will continue upgrading the data-base-management system. However, regardless of the upgrading, the image data will remain intact. The approach we are taking will minimize the chances of our hardware and software becoming obsolete. In dealing with the hardware, we can upgrade any piece of equipment within a cluster without affecting the total PACS operation, and the manufacturer will maintain and upgrade the data-base functionality of the software. At the same time,

the integrity of the image data will remain intact in the data base. We also can replace any cluster in the PACS with a commercial module when it becomes apparent that the commercial system outperforms the laboratory module.

### Pitfalls in Implementation of PACS Modules

During our past 3 years of experience with the PACS systems, we have identified a few operational difficulties that should be circumvented in a successful PACS implementation. To begin with, a prototype PACS system is difficult to upgrade in a clinical environment. Although we have implemented two PACS modules and they have been in operation for 2 years, we find that the day-to-day operation, service maintenance, and maintaining the integrity of the system can be very tedious and time consuming. There are two reasons for this. First, once a system is released for clinical operation it is difficult to service the system because it is used 24 hr a day and 7 days a week. As it is a prototype system, it is one of a kind. It is difficult for a research team to upgrade a system and test it in clinical environment unless a second similar system is also available in the research laboratory. As a result, the research team always plays a catch-up game once the system is in clinical use.

Second, a successful operation of PACS relies on consistent uptime of image acquisition devices including CT, MR, and computed radiography. An image acquisition device does go down from time to time because of preventive maintenance, operator errors, and so forth. If one imaging acquisition device is not functioning properly, images from this device will not be transmitted to the PACS host computer during the time of image generation. As a result, the image data base is not up to date and requires an operator to retrieve images from other stations or digitize a piece of film. This will cause the arrival of images at a workstation to be delayed. In the worst case, the communication protocol in the network, if not supervised properly, can even fail to transmit the images. Another difficulty is that when a major component upgrade is performed in a cluster it will affect the clinical perspective. For example, in pediatric radiology, we upgraded the system from  $512 \times 512$  pixel monitors to  $1K \times 1K$  pixel monitors. As a result, image quality improves but the display time increases from 2 sec to 5 sec. Many explanations have to be made to the clinicians for them to accept this compromise. This psychological factor was not anticipated when we upgraded the pediatric system from  $512 \times 512$  pixel to  $1K \times 1K$  pixel monitors. Operating the PACS smoothly requires a special operator's attention to the system. We had to train a person with some knowledge of digital image processing, image acquisition, and display stations, as well as X-ray technology for maintaining the operational integrity of the system. This requirement was not anticipated when we implemented the system. We now have a new category of profession in our department called the PACS coordinator. We plan to continue to recruit from the existing technologist pool in the department. Along with these difficulties, we also have made the following observations.

First, we believe that PACS should be implemented in a modular fashion. There are many aspects in a given operating condition and environment that make one module quite different from another. Each module should have its own specifications and the module will require a period of refinement before it is clinically useful. As the learning process improves, the acceptance of the newer modules by clinical users will become faster and easier.

Second, we believe all technologies required to implement PACS are available. The only two exceptions might be digital image acquisition of conventional radiographs and image communication. As of today, we are still not convinced that computed radiography images can completely replace conventional analog films for all types of procedures because of various requirements. However, we do expect that computed radiography manufacturers can improve the image quality to equal that of conventional analog images in the near future. In image transmission, faster hardware and smarter protocols still need to be developed for efficient communication.

Lastly, we do not recommend that every radiology department or hospital implement its own PACS system in-house, as it does require substantial financial and manpower commitment. With clinical data of PACS generated by other research centers and our department, we hope the manufacturers will be able to adapt and use this information, and come up with turnkey PACS systems with specifications suitable for different hospitals or departments.

In summary, we believe that the implementation of PACS in a radiology department or a hospital is inevitable. All the

technology is available. The question concerning PACS implementation is not why, but when. With cooperation from the radiology community and the manufacturers, we believe PACS can be implemented successfully [9]. PACS will serve as a powerful tool for better health care delivery and for facilitating research and teaching.

#### REFERENCES

1. Huang HK, Cho PS, Taira RK, Ho BK, Chan KK. Picture archiving and communication systems in Japan—three years later. *AJR* 1990;154:415–417
2. Taira RK, Mankovich NJ, Boechat MI, Kangaroo H, Huang HK. Design and implementation of a picture archiving and communication system for pediatric radiology. *AJR* 1988;150:1117–1121
3. Cho PS, Huang HK, Tillisch J, Kangaroo H. Clinical evaluation of a radiologic picture archiving and communication system for a coronary care unit. *AJR* 1988;151:823–827
4. Huang HK. Experience in the use of PACS: present problems and future plans. In: Tsujiuchi J. *PACS handbook '89*. Tokyo: Japanese PACS Society, 1989:33–43
5. Templeton AW, Cox GG, Dwyer SJ III. Digital image management networks: current status. *Radiology* 1988;169:193–199
6. Chu WW. Performance of the file directory system for data bases in star and distributed network. *AFIPS Conf Proc* 1976;45:3–13
7. Ratib O. *Image file structure and data communication format*, IPL Note 23.01. Los Angeles: UCLA, 1988
8. *ACR-NEMA digital imaging and communication standard*, Publication 300-85. Washington, D.C.: NEMA, 1985
9. Mezrich RS. The implication of PACS for radiology practice. *AJR* 1988;151:828

# FORTHCOMING ARTICLES

## SPECIAL ARTICLES

**Progress in radiology. State of the art: endorectal sonography of the prostate gland.** Rifkin MD, Dahnert W, Kurtz AB

**Radiographic evaluation of the solitary pulmonary nodule.** Webb WR

## PULMONARY RADIOLOGY

**Does knowledge of the clinical history affect the accuracy of chest radiograph interpretation?** Good BC, Cooperstein LA, DeMarino GB, et al.

## BREAST RADIOLOGY

**New mammography screen-film combinations: imaging characteristics and doses.** Kimme-Smith C, Bassett LW, Gold RH, Zheutlin J, Gornbein JA

## GASTROINTESTINAL RADIOLOGY

**Doppler sonography: a noninvasive method for evaluation of hepatic venoocclusive disease.** Brown BP, Abu-Yousef M, Farner R, LaBrecque D, Gingrich R

**Fluoroscopically guided percutaneous gastrostomy and gastroenterostomy: analysis of 158 consecutive cases.** Hicks ME, Surratt RS, Picus D, Marx MV, Lang EV

**Pictorial essay. Imaging and intervention of biliary complications after hepatic transplantation.** Letourneau JG, Hunter D, Payne WD, Day DL

## GENITOURINARY RADIOLOGY

**Selective osteal salpingography and transvaginal catheter dilation in diagnosis, classification, and treatment of fallopian tube obstruction.** Lang EK, Dunaway HE Jr, Roniger WE

**Case report. Uterine perforation simulating urachal carcinoma: CT diagnosis.** Kronthal AJ, Fishman EK, Sanders RC, Epstein JJ, Brendler CB

## MUSCULOSKELETAL RADIOLOGY

**Early and late bone marrow changes after radiation: MR evaluation.** Stevens SK, Moore SG, Kaplan ID

**Cervical spondylolysis: imaging findings in 12 patients.** Forsberg DA, Vogler JB III, Wiener MD, Martinez S

**Traumatic lumbar hernia: CT diagnosis.** Faro SH, Racette CD, Lally JF, Wills JS, Mansoor A

**Case report. CT diagnosis of posterior perineal hernia.** Lubat E, Gordon RB, Birnbaum BA, Megibow AJ

**The value of MR imaging to monitor the effect of chemotherapy on bone sarcomas.** Holscher HC, Bloem JL, Nooy MA, Taminiau AHM, Eulderink F, Hermans J

**Pictorial essay. MR imaging of sacral and presacral lesions.** Wetzel LH, Levine E

**Technical note. MR of the shoulder with 0.2-T permanent magnet unit.** Sasaki M, Ehara S, Nakasato T, et al.

## PEDIATRIC RADIOLOGY

**Digitized portable abdominal radiographs in neonates with necrotizing enterocolitis: diagnostic quality compared with nondigitized images.** Gross GW, Ehrlich SM, Wang Y

**Doppler evaluation of renal transplants in children: a prospective analysis with histopathologic correlation.** Drake DG, Day DL, Letourneau JG, et al.

**Coronary angiographic abnormalities in infants and children with pulmonary atresia, hypoplastic right ventricle, and ventriculo-coronary communications.** Burrows PE, Freedom RM, Benson LN, et al.

**Pictorial essay. Current evaluation of patients with abnormal viscerotrial situs.** Hernanz-Schulman M, Genieser NB, Ambrosino MM, et al.

**Case report. Bowel obstruction in an infant with AIDS.** Sivit CJ, Taylor GA, Patterson K, Thompson R, Josephs SH

**Case report. Cervical and basicranial diastematomyelia.** Herman TE, Siegel MJ

## NEURORADIOLOGY

**Gd-DTPA-enhanced MR imaging of the brain in patients with meningitis: comparison with CT.** Chang KH, Han MH, Roh JK, Kim IO, Han MC, Kim C-W

**Age-related changes in the cervical facet joints: studies with cryomicrotomy, MR, and CT.** Fletcher G, Haughton VM, Ho K-C, Yu S

**Lumbar disk herniation and canal stenosis: value of intraoperative sonography in diagnosis and surgical management.** Montalvo BM, Quencer RM, Brown MD, et al.

**Primary cerebral neuroblastoma: CT and MR findings in 12 cases.** Davis PC, Wichman RD, Takei Y, Hoffman JC Jr

**Intracranial ependymoma and subependymoma: MR manifestations.** Spoto GP, Press GA, Hesselink JR, Solomon M

## INTERVENTIONAL RADIOLOGY

**Technical note. A simple phantom for learning needle placement for sonographically guided biopsy.** Silver B, Metzger TS, Matalon TAS

**Technical note. Endovaginal sonography for guidance in draining pelvic fluid collections.** Abbitt PL, Goldwag S, Urbanski S

## VASCULAR RADIOLOGY

**Lower extremity venous thrombosis in patients with acute hip fractures: determination of anatomic location and time of onset with compression sonography.** Dorfman GS, Froehlich JA, Cronan JJ, Urbanek PJ, Herndon JH

**Early detection of saphenous vein arterial bypass graft stenosis by color-assisted duplex sonography: a prospective study.** Polak JF, Donaldson MC, Dobkin GR, Mannick JA, O'Leary DH

## RADIATION PHYSICS

**Performing JCAHO dose calculations with the aid of a microcomputer spreadsheet program.** David G, Price SC

## PERSPECTIVE

**Attitudes of American radiologists toward practice: present and future.** Brogdon BG, Heveron ED, Diamond JJ

## ARRS ANNUAL MEETING CASE OF THE DAY QUESTIONS

**Chest case of the day.** Stull MA, Clark LR, Reagan K, et al.

**Musculoskeletal case of the day.** Stull MA, Glass-Royal M

**Abdominal case of the day.** Silverman PM, Hayes WS, Cooper CJ, et al.

**Neuroradiology case of the day.** Deveikis JP, Cammarata CA, Reid WM, et al.

## Computer-Aided Management of Residents' On-Call and Vacation Schedules

Charles E. Kahn, Jr.<sup>1</sup>

The task of compiling residents' schedules is time-consuming and is often complicated by unforeseen events and changes in personnel. Many academic radiology departments delegate this responsibility to the chief resident. This report describes two modules of a radiology information system that assist in managing residency schedules, particularly residents' on-call and vacation schedules.

The programs were written in the ANSI-standard MUMPS programming language and run on a PDP 11/44 (Digital Equipment Corporation, Boston, MA) with the M/11+ operating system (Intersystems, Boston, MA). They operate as modules of the MARS radiology information system [1], which is available to all department personnel on approximately 100 terminals located at workstations in our clinical facility and department offices.

### On-Call Schedule

The system displays the on-call schedule as a monthly calendar (Fig. 1). The current month is displayed by default. Users may view the schedule for any past or future month. The calendar indicates the current date with hyphens and the user's days on call with asterisks. All department physicians, technologists, and clerical workers can view this schedule. Only residents can modify the information.

The chief resident establishes the initial schedule and can alter it if necessary. Programs allow the chief resident to assign individual dates and to schedule a group of residents over a period of time in a specified rotation order. The system

can print the schedule for any range of dates and tally the number of days for each resident by day of the week. The chief resident can assign days individually and can adjust the schedule to ensure equitable assignments.

Because the schedule is compiled without consideration of individual vacations and other conflicts, residents frequently trade their assigned days on call. This exchange now is recorded on the computer system. After two residents have agreed to a suitable trade, one of them enters the information on the computer system. The resident enters the date he or she would like to take; the system verifies the date and indicates the currently assigned resident. The resident may either take the other's date without trade, or may make a one-for-one exchange with the other resident. Residents cannot trade away another's assignments. The system alerts the user if the trade involves different days of the week. The trade becomes effective after one of the two parties enters the information on the computer.

The system ensures accountability for all dates traded. The resident must confirm the trade, acknowledge the other party's assent, and enter his or her password. The trade is recorded immediately and the schedule is updated accordingly. An audit trail records the initial assignment, the dates traded, the parties to the trade, and the date of the transaction. Residents may view this audit trail at any time (Fig. 2).

In addition to on-call responsibilities, the same programs maintain other schedules, such as the residents' conference schedule and the schedule for Saturday morning coverage. As with the on-call schedule, residents may view the current schedule and trade their assignments from any terminal in the

Received September 15, 1989; accepted after revision October 31, 1989.

<sup>1</sup> Department of Radiology, University of Chicago, 5841 S. Maryland Ave., Box 429, Chicago, IL 60637. Address reprint requests to C. E. Kahn, Jr.

Resident On Call						
June 88						
Sun	Mon	Tue	Wed	Thu	Fri	Sat
			1 Rosenblum	2 Wong	3 Melliere	4 Sennett
5 Kurland	6 Kim	7- Wong	8 Jokich	9 Kurland	10 Stillman	11 Wong
12 Sennett	13 ** Kahn	14 Wong	15 Kim	16 Jokich	17 ** Kahn	18 Stillman
19 Kurland	20 Wong	21 Kim	22 ** Kahn	23 Sennett	24 Wong	25 Jokich
26 Wong	27 Sennett	28 ** Kahn	29 Diamond	30 Stillman		

>>> Month (Trade, Check, Print): █

Fig. 1.—On-call schedule for June 1988. System indicates current date with hyphens and user's assignments with asterisks.

Resident On Call			
Check date:	9-2 Friday, September 2, 1988		
Resident	Comments	Entered by	
Rosenblum	assigned	CK	03/27/88
Wong	traded 11/12/88 with Rosenblum	EW	04/02/88
M Diamond	traded 05/27/88 with Wong	MD	04/29/88
Kahn	traded 08/12/88 with M Diamond	CK	05/06/88

: █

Fig. 2.—For any specified date, residents can view audit trail, which records initial assignment and all subsequent trades.

department. The chief resident can print listings of each resident's assignments; these listings are printed periodically, usually as bimonthly updates, and are distributed to the residents.

### Vacation Schedule

Another module of the MARS computer system manages the residents' vacation schedules. For each academic year, the chief resident enters the residents' names and their allotted number of vacation and meeting days. Residents may schedule vacation days singly or in blocks as long as the schedule is open on those days. Our residents have established a policy that allows no more than five residents to be absent from the department each working day. Absences include vacation, meetings, elective time, and participation in the six-week-long Armed Forces Institute of Pathology course.

The computer system performs the necessary bookkeeping functions, such as calculating each resident's number of vacation days remaining, and will not allow residents to schedule more than their allotted number of days. In addition, it will not allow more than five residents to be scheduled to be out of the department on any single day. The chief resident can override these limits for emergencies and special circumstances.

A resident may view the vacation schedule for a month or a week at a time. The monthly schedule (Fig. 3) displays department holidays, the resident's days off, and days available for additional days off. The weekly listing (Fig. 4) provides greater detail: for the specified week, it displays the names of the residents who are scheduled to be absent and the nature of their absence. A resident also can review a listing of his or her scheduled absences for the entire academic year.

VACATION						
November 88						
Sun	Mon	Tue	Wed	Thu	Fri	Sat
		1 ...	2 ...	3 ...	4 ...	5
6	7 ...	8 ...	9 -Meeting-	10 -Meeting-	11 -Meeting-	12
13	14 -Meeting-	15 -Meeting-	16 ...	17 ...	18 .	19
20	21 .	22 ..	23 ..	24 HOLIDAY	25 -Vacation-	26
27	28 .....	29 .....	30 .....			

Fig. 3.—Vacation schedule for November 1988. Holidays and user's vacation days are indicated. Number of "dots" beneath each date indicates number of residents who may schedule vacation on that date.

VACATION				
Monday 21 Nov 88	Tuesday 22 Nov 88	Wednesday 23 Nov 88	Thursday 24 Nov 88	Friday 25 Nov 88
open	open	open	HOLIDAY	CLOSED
1 Wong(V)	Wong(V)	Wong(V)	*****	Kahn(V)
2 Brack(V)	Brack(V)	Brack(V)	*****	Wong(V)
3 Kim(V)	Kim(V)	Kim(V)	*****	Stillman(V)
4 Backus(V)	.	.	*****	M Diamond(V)
5 .	.	.	*****	Rosenblum(V)
PC Goethe	Hegarty	Kahn	Goethe	Hegarty
A=AFIP C=Cardiac E=Elective M=Meeting V=Vacation X=Out				
Week of: █				

Fig. 4.—Weekly vacation calendar indicates who will be absent during specified week. Reason for absence is described by letter codes in parentheses next to residents' names; codes are explained at bottom of screen. Up to five residents may be out of department on any workday. AFIP = Armed Forces Institute of Pathology course; PC = postcall resident.



## Discussion

The computerized on-call schedule has replaced a manually generated "master list," which was available for use only in our physician lounge. On this paper form, one date was often traded by several residents, with the result that it was sometimes difficult to determine who was truly responsible for coverage on that date. The official schedule on the radiology information system now clearly indicates the coverage responsibilities and is available to all residents at widely separated sites throughout our department. Residents may access the schedule at any time from their work area and can update it instantly. The audit trail ensures accuracy and accountability of the information. The list of each resident's assignments can be printed and distributed on demand.

The system greatly simplifies the chief resident's task of compiling the academic year's on-call and conference schedules and relieves secretaries of typing the schedules. The residents have expressed a high degree of satisfaction with the system and have found it to be accurate and easy to use. In addition, our technical and film-room staff have been greatly pleased that they can quickly identify the on-call resident. The system has been in use for 1½ years.

The vacation schedule, previously recorded in a weekly calendar kept and updated by the chief resident, is now open to all residents so that they can plan their vacations. Residents no longer need to consult the chief resident to plan or select vacation days. The bookkeeping functions, such as counting the number of vacation days remaining, are performed automatically by the system.

Several articles have described computer programs that assist in formulating and updating schedules for radiology departments [2-4]. Unlike these scheduling packages, which run on microcomputer systems, our scheduling system is integrated with the mainframe computer system that provides clinical and administrative functions to our entire radiology department. The advantage of integration with a radiology information system is that all radiology personnel can view the schedules, and residents can make changes without leaving their work areas. Rather than a possibly outdated

paper copy of the schedule, the current schedule is always available for viewing. Also, unlike the centralized approach to scheduling adopted by these other systems, our system allows all residents to participate in formulating the schedule. After the chief resident compiles the initial schedule, any resident can change the schedule to suit his or her needs by trading with other residents.

The programs are easily modified and adapted. A new schedule calendar for resident coverage of an affiliated hospital was added in less than 5 min of programming time. Attending radiologists now have computer-maintained schedules of their weekend, holiday, and noon-hour coverage; these programs were developed with minor modification of the residents' scheduling programs.

Although the scheduling programs have been incorporated into a particular information system, they can be modified for use with other MUMPS-based systems. Programs written in the MUMPS programming language are very portable. Several radiology information systems, such as MARS II (ADAC Incorporated, Boston, MA) and DECrad (Digital Equipment Corporation, Boston, MA), and hospital information systems, such as the Veterans Administration's COSTAR system, are based on MUMPS. A public-domain MUMPS interpreter is available for the IBM PC and compatible microcomputers [5]. A copy of the programs' source code can be obtained from the author for a nominal charge.

## REFERENCES

1. Lehr JL. Installation of MARS II at the University of Chicago. In: *Proceedings of the eighth conference on computer applications in radiology*. Chicago: American College of Radiology, 1984:35-46.
2. Reinus WR, Totty WG. Computer-assisted scheduling of radiologists. *AJR* 1986;147:203-204.
3. Larson TC III, Larson SL, Harle TS. Computer-assisted scheduling of radiology resident call. *Invest Radiol* 1986;21:424-426.
4. Charletta DA. Microcomputer-assisted residency data management. *Invest Radiol* 1988;23:224-226.
5. Yaksick W, Walters RF. microMUMPS. Davis, CA: Division of Computer Science, University of California, Davis, 1986.

## Book Review

**Radiology Administration.** A Business Guide. By Wayne T. Stockburger. Philadelphia: Lippincott, 228 pp., 1989. \$29.95

Changing patterns and complexity of medical practice have resulted in the increasing use of business techniques in radiology administration. Some of the factors that have led to these changes include a more competitive environment, multiple types of patient payment plans, a need for quality assurance, marketing of radiology, and use of computers for radiology information systems. In order to manage these problems, a number of innovative business techniques have been developed that facilitate sound radiology management. In today's competitive medical marketplace, a working knowledge of these business practices as applied to radiology is essential for the success or even survival of a medical practice.

*Radiology Administration* is an easily understood introductory text that describes business techniques as applied to radiology. The book can be read in about 2 hr, although a thorough understanding and working knowledge obviously require further study. It is worthwhile reading for radiologists who want to become familiar with radiology management even though they may not be involved in it directly. Although readers with no background in business or economics should be able to understand the book, the material will be more meaningful to those who have a basic knowledge of these subjects.

Chapter 1 has a good discussion of the unique relationships of patient and physician consumers to a radiology practice. Stockburger discusses the different expectations of these two consumer groups. Subsequent chapters cover analysis of patient payment mix, work load and staffing, costs and revenue, and inventory management. The book has an excellent chapter that describes the increasingly important subject of quality assurance programs in radiology. Mar-

keting methods as applied to radiology are covered thoroughly, although this section mentions only briefly the ethical concerns that must be considered when marketing medical practice; perhaps this issue could have been given more emphasis. For those interested in the use of computers in radiology, the book has an excellent introduction to radiology information systems and picture archiving and communication systems. The final chapter explains the differences that exist in the administration of teaching hospitals. The discussion contrasts differences in fiscal matters, equipment acquisition, and marketing. A limited discussion is presented of the problems that arise in administration of a department that has both academic and service goals.

In the past, several books have described planning and organization of radiology departments, and some have included limited discussion of business practices. This publication is the first to provide an overview of many business techniques applied to radiology. In addition, it includes comments about future directions of radiology management, including radiology information systems and picture archiving and communication systems. I recommend *Radiology Administration* to those who are contemplating or beginning a career in radiology administration, and to radiologists and others who have an interest in how business techniques are applied to radiology.

C. John Rosenquist  
University of California, Davis, Medical Center  
Sacramento, CA 95817

## Meeting News

### American College of Radiology Summit Meeting, August 1989

Bruce L. McClennan<sup>1</sup> and Glen W. Hartman<sup>2</sup>

This year's summit meeting of the American College of Radiology (ACR) in Park City, Utah, August 3–5, 1989, marked the 10th anniversary of the ACR Intersociety Commission. This, the last summit meeting of the entrepreneurial 1980s, was successful and productive, bringing together the leaders of 38 radiologic societies. All radiologic societies in the United States with more than 50 members were invited to send representatives to this year's summit meeting, which was one of the largest ever held. The mission of the Intersociety Commission, carried out through its summit meeting, is to promote communication among the leaders of national radiologic societies, providing them with access to all resources of the American College of Radiology, with the chairman of the Intersociety Commission serving as the ombudsman for all radiologic organizations. The meeting was focused on professional relationships; the title of the conference was "Professional Relationships: Cooperative or Competitive?" The discussions were divided into hospital-based practice issues, non-hospital-based practice issues, and human-resources development, moderated by Kay Vydareny, John Tampas, and J. Frank Wilson, respectively.

In 1923, Dr. Russell Carman pointed out in his presidential address to the Radiological Society of North America that "radiologists have consistently objected to the haphazard work of inadequately trained physicians and laymen. . . . their objections have often been misconstrued as arising from personal and pecuniary motives, but, as a sober matter of fact, the conscientious radiologist has thought more of his art than of himself" [1]. "Turf" issues are not new to diagnostic

radiology and radiation oncology, and turf battles are played out in different arenas daily.

Members of the summit addressed a variety of issues related to professional relationships in different practice environments. They explored strategies for fostering cooperation, minimizing competition or conflict of interest between specialties, promoting good care of patients, and encouraging quality imaging training and research. Many recurring subjects permeated the three discussion groups. These included patients' access, care of and contact with patients, self-referral, quality assurance and quality control, subspecialization and residency training, research in radiology, the need for data and data analysis, credentialing, marketing, and public relations.

The preliminary sessions included addresses by leaders of the ACR and Paul Ginsberg, head of the Physicians Payment Review Commission (PPRC, a commission that is responsible for Medicare reimbursement to physicians). Jerome Shapiro, head of the ACR Task Force on Standards defined competence as being equal to standards plus continuing medical education (CME). He further noted that the CME of a radiologist should be validated, with evidence that it is related to clinical outcomes, and that standards do not guarantee quality. Dr. Shapiro detailed the progress of his commission on the issues of standards setting in radiology and stressed the need for uniformity, creditability, and minimalism. High standards are admirable, but often elusive, and minimal or very basic standards are the best beginning. Lee Rogers, chairman of the ACR Board of Chancellors, noted the ACR's strong

Received October 10, 1989; accepted after revision November 14, 1989.

<sup>1</sup> Chairman, Intersociety Commission; Mallinckrodt Institute of Radiology, Washington University Medical Center, 510 S. Kingshighway Blvd., St. Louis, MO 63110. Address reprint requests to B. L. McClennan.

<sup>2</sup> Past Chairman, Intersociety Commission; Diagnostic Radiology, Mayo Clinic, 200 First St. S.W., Rochester, MN 55901.

AJR 154:645–646, March 1990 0361–803X/90/1543–0645 © American Roentgen Ray Society

commitment to standards development, practice models, and guidelines. He noted that credentialing seems to be the byword of late and that recertification is not currently an active issue. A brief synopsis of the Stark Bill (HR 939) on imaging centers and the relative value scale (RVS) was given, stressing that the critical concerns of the resource-based RVS are the fairness of geographic variation in interspecialty-income distribution, conversion factors, and data-base errors.

The status of the congressional initiatives on health care financing was detailed by Donald Lavanty, legislative consultant to the ACR. Dr. Ginsberg's address focused on fee schedules and the Hsiao RB-RVS. He explained that the Hsiao study was deemed to be likable and friendly by the members of his commission and that they favored its adoption. He spoke of the efforts being made toward establishing expenditure targets (total cost targets) as ceilings on total Medicare expenditures, but noted that the PPRC favors smaller subtargets as a first approach strategy. He also discussed practice guidelines and standards-setting and noted that the government should in some way fund studies to develop standards but certainly should not develop the standards themselves—that is the role of radiologists. Spirited discussion with Dr. Ginsberg on the issue of self-referral took place in an attempt to make him aware of the scope of the problem of nonradiologists performing and being reimbursed for radiologic procedures.

### Work Groups

The three work groups developed white papers in their respective areas. Hospital-based professional relationships were the focus of Kay Vydareny's group. She noted the growing competition and attractiveness of the new technologies, which fosters competition among specialties for acquisition, control, use, and reimbursement. Areas where ground has been lost or gained by radiology were explored. The role of subspecialty societies was stressed in terms of training and credentialing of radiologists and development of standards. An "if you can't beat 'em, join 'em" approach to the spirit of cooperation was espoused and the need for more and better research and joint research and treatment of patients was emphasized. The subjects of marketing and public relations were ever present in these discussions, which focused on radiologists' interactions with patients and direct care of patients. Recommendations were made to the college for (1) more and better data to support "radiology by radiologists," that is, numbers to substantiate the amount of radiology done by nonradiologists; (2) changes and strengthening of residency training programs, and (3) radiologic research.

During discussions of interprofessional relationships in non-hospital-based practices, emphasis was placed on ownership and self-referral. Outpatient imaging and radiation therapy centers and the effects of various types of ownership of these centers were carefully explored, with indications that an expanded role for ownership by radiologists may occur soon. Strong sentiment for ACR resolution 39 (1988), opposing ownership of imaging centers by referring physicians, was espoused. The resolution states:

The position of the American College of Radiology is that the practice of self-referral of patients for a diagnostic or therapeutic medical procedure may not be in the best interest of the patient.

Accordingly, referring physicians should not have a direct or indirect financial interest in diagnostic or therapeutic facilities to which they refer patients. . . . The American College of Radiology supports legislative efforts prohibiting reimbursement for any diagnostic or therapeutic procedure carried out in a facility in which the referring physician has a direct or indirect financial interest.

The self-referral issue, its inherent potential conflict of interest, and the moral and ethical dilemmas therein were all discussed in depth. The necessity for more and better data about nonphysician ownership and the conflicts of interest that lead to self-referral were noted. Strategies exploring the principles of quality assurance, quality control, and risk management were examined as possible ways of fostering cooperation and eliminating some of the competitive situations. Once again, marketing and public relations were discussed with the underlying theme that self-referral was not in the interest of the best care of patients and the best radiologic service. The summit position on the extent of the problems of self-referral is contrary to the American Medical Association's (AMA) position, which is that self-referral is a focal (local) and uncommon problem.

The work group on human-resources development carefully explored the current crises in availability of health care technologists, nurses, and other allied health professionals. Existing data from the April 1989 Summit on Manpower held under the auspices of the American Healthcare Radiology Administrators (AHRA, Loretta L. Hanwell, chair) was discussed in depth. The need for more and better data to document the need for more technologists and other qualified personnel and radiologists was raised. This meeting of representatives of 17 organizations, including the ACR, held a follow-up conference in November 1988 at which extensive data documented a shortage of radiology and nuclear medicine technologists. The work group on human-resources development urged the ACR to work with subspecialty societies and other radiologic organizations to focus their ideas and resources on the shortage of paraprofessionals as well as clinical-medical physics personnel throughout the country.

Recommendations by these work groups concerning professional relationships (turf issues), the impact of self-referral on these relationships, standards of practice, and personnel shortages were delivered to the ACR, its Board of Chancellors and its Council, various commissions and committees, and task forces. The ACR Council and Board of Chancellors may then direct their opinions or their policies formulated from Summit recommendations to Congress, federal agencies, third-party payers, national health organizations, individual societies (e.g., AMA, National Institutes of Health), and other interested parties—most notably, the public at large. The impact of the summit meeting will ultimately be felt at many levels as we seek to increase public and private awareness of our concerns that appropriate and cost-effective diagnostic radiology, radiation oncology, and medical physics services for care of patients be available and of high quality, delivered by trained and competent radiologists, radiation oncologists, and nuclear medicine physicians.

### REFERENCE

1. Carman RD. The future of radiology. *Radiology* 1924;2:41-45

## Review Article

# Technology Assessment: The Contribution of Professional Organizations

William R. Hendee<sup>1</sup>

Assessment and accountability are becoming the watchwords of medical practice and reimbursement. Medical technologies, especially "big ticket" technologies such as those used in radiology, are obvious targets for increased attention. Providing enhanced accountability while preserving access to technologies for patients who need them requires expert knowledge and medical judgment. No more important role can be envisioned for professional medical organizations and technically expert physicians in practice.

### Historical Perspective

The past 40 years have witnessed momentous improvements in the quality of health care. They also have seen major shifts in the ways that the delivery of health care is evaluated and reimbursed. This period has been divided by Relman [1] into three eras: expansion, cost containment, and assessment and accountability.

### *Era of Expansion*

High enthusiasm for biomedical research and its clinical benefits, including advances in diagnostic imaging, was exhibited in the 1950s and 1960s. It also was a time for recognizing the rights of all persons to access to quality health care. Employer-subsidized health benefits, private health insurance, Medicare, and Medicaid increased the demand for health services. Hospitals, medical schools, and research institutes grew in size and number to meet the

demand. For the first time in history, delivery of health care became a profitable enterprise rather than a charitable service. In the exuberance over research advances, new medical technologies, and expansion of health care services, one question lurked unanswered: How were these changes to be paid for?

### *Era of Cost Containment*

Partly because of trends introduced during the era of expansion, health care costs rose inexorably in the 1970s and 1980s. In response, health care payers (principally businesses, third-party carriers, and the government) introduced measures to slow the rising costs. Two decades after introduction of Medicare, health care costs had risen from less than 4% to more than 11% of the United States gross national product. The rise continues today.

Enhanced intensity and improved access were not the only factors contributing to rising costs of health care [2]. Other factors included population growth; population aging; inflation, especially labor costs; and liability coverage against malpractice claims. These factors all increased the costs of health care services in the United States.

Early in the cost-containment era, front-end controls (e.g., health systems agencies and technology review commissions) were introduced to control the expansion of medical facilities and technologies. When these measures proved ineffective, back-end controls (e.g., diagnosis-related groups [DRGs], preferred provider services [PPSs], and health maintenance

Received August 25, 1989; accepted after revision October 12, 1989.

<sup>1</sup> Vice President for Science and Technology, American Medical Association, 535 N. Dearborn St., Chicago, IL 60610. Address reprint requests to W. R. Hendee.

organizations [HMOs]) were developed to constrain expenditures by controlling the reimbursement process for medical services. Reimbursement for physicians' services was included in these efforts through measures such as the resource-based relative value system (RBRVS) and expenditure targets (ETs).

Cost control measures of the era of cost containment had little effect on the rising costs of health care. As with many other societal problems, rising health care costs cannot be addressed successfully by trying to constrain the supply of services. The rise in costs is driven principally by the increasing demand for more health services by more people.

The only sure way to reduce costs in a demand-dominated situation is to deny services to some who need them (i.e., rationing of health care) and to limit the intensity of services (i.e., the use of technology) when they are provided. Today that is precisely the course of action being pursued by payers of health services, including governmental agencies. This course creates a conflict between government and social policy on the one hand and the expectations and rights of individuals on the other.

Efforts to avoid visible conflict are largely responsible for the failure of front-end and back-end efforts to control health care expenditures. Now a major new initiative is evolving to move American medicine into a different era of health care delivery. This initiative offers major opportunities for involvement of health care providers in its planning and implementation.

#### *Era of Assessment and Accountability*

The basic challenge to any medical procedure is, does it contribute positively to the health and well-being of the patient? This challenge is the foundation of concepts such as "outcome measures" [3], "outcomes management" [4], the "assessment of medical practice" [5], and "quality assurance." It underlies efforts of the Health Care Financing Administration (HCFA) to characterize the effectiveness of health care by examining morbidity and mortality statistics from the Medicare data base. It explains the current interest in data about adverse reactions, problems during patients' recoveries, durations of the recovery period, and rates of readmission. It also explains present concerns over geographic, institutional, and practitioner variations in health care delivery. And it enhances interest in medical technology assessment, where technology is defined by the Office of Technology Assessment (OTA) of the U.S. Congress as "techniques, drugs, equipment and procedures used by health care professionals in delivering medical care to individuals, and the systems within which such care is delivered" [6].

No medical discipline is spared from facing this challenge. But some, such as radiology, must confront it more directly than others because of their dependence on "big-ticket" technologies. Radiology is one of the principal targets of the era of assessment and accountability.

#### **Methods of Technology Assessment**

Various approaches are available for evaluating the usefulness of medical technologies, including imaging procedures.

Each approach has certain strengths and weaknesses in its explicitness, universality, and clinical meaningfulness.

#### *Randomized Controlled Clinical Trials*

Randomized controlled clinical trials (RCCTs) are the most rigorous approach to evaluation of medical technologies. When properly designed and executed, an RCCT applies the full power of statistical analysis to determination of the clinical usefulness of a technology. In some applications, such as evaluation of a new pharmaceutical that competes with existing drugs for treatment of conditions that are not life-threatening, an RCCT can be designed and implemented in a relatively straightforward manner. But when a drug provides hope to patients who have a life-threatening or untreatable disease, profound ethical concerns are raised by insistence on an RCCT with patients assigned randomly to treatment and control groups. These concerns have caused a relaxation of the insistence on RCCTs in several instances, including the recent introduction of the "Modified Treatment Investigational New Drug" application process of the U.S. Food and Drug Administration (FDA) for drugs intended for patients with terminal and untreatable diseases such as human immunodeficiency virus infection and certain forms of cancer.

In the evaluation of imaging technologies, RCCTs are particularly difficult to implement. They depend on well-defined protocols, large numbers of patients, and random assignment of patients to study and control groups. They are expensive and time-consuming and usually require multiple institutions and investigators to eliminate bias introduced by specific groups of patients, equipment capabilities, and diagnostic skills. An institution with a new imaging technology is understandably inclined to encourage its use for all eligible patients, especially when the costs of the technology are recaptured from patient fees. Physicians face an ethical dilemma in depriving patients of a technology that could influence treatment of a particular disease or injury.

Few imaging technologies have been evaluated by RCCTs. Exceptions include investigations of the usefulness of imaging procedures to detect occult disease in asymptomatic patients. Examples are attempts to identify lung cancer in asymptomatic male smokers [7, 8] and breast cancer in asymptomatic women without risk factors for the disease [9, 10].

#### *Decision Modeling*

An essential first step in evaluating an imaging procedure is to determine its technical performance. Characteristics that define performance include precision (reproducibility), safety, and reliability. Often reliability is expressed in terms of sensitivity and specificity, where sensitivity connotes the ability of a procedure to detect disease when it is present, and specificity describes the ability of a test to correctly exclude disease when it is absent. Graphical presentation of the sensitivity and specificity of a diagnostic test yields a receiver-operating-characteristics (ROC) curve for the test [11].



### Case Series

A case series is a collection of studies in which a technology is used for a specific condition of a patient. Studies can be compiled into a case series if they are conducted longitudinally over time and if all eligible patients are admitted to the studies. The series may be prospective or retrospective; the former is considered more reliable because of greater assurance that all eligible patients have entered the series. The value of a case series is enhanced by comparison with a control group, even though patients are not assigned randomly to control or study populations. Often a case series reflects the experience of a single institution and may be biased by the skill of the investigators, particular model of the technology used, procedures followed in application of the technology, and population of patients drawn to the institution. Many case series are presented as technology assessments in the radiologic literature, and some exemplify the biases intrinsic in this evaluative method. The presence of such biases in clinical series recently has attracted attention in the radiologic literature [12, 13].

### Case Studies

A case study is a comprehensive review of several features of a particular technology, such as its clinical applications, economic and ethical implications, and potential for future research and development. Examples include the reports of the Congressional Office of Technology Assessment (OTA) [14] and the guideline reports of the hospital technology series of the American Hospital Association. The AMA/Trends reports of the American Medical Association are another example, as represented by a case study report on sonography currently in preparation. Recent reports of the AMA's Council on Scientific Affairs concerning imaging technologies such as mammography, MR imaging, and positron emission tomography are further examples of case studies. These reports have been published in the *Journal of the American Medical Association (JAMA)* in the past couple of years.

Case studies are designed as wide-ranging "snapshots in time" of the state of development and clinical applications of a particular medical technology. They tend to draw heavily on the literature, with discretion exercised by authors chosen for their expertise and objectivity. If carefully conducted and extensively documented, case series are useful "state-of-the-art" references to particular technologies, especially for those contemplating the purchase and use of the technologies.

### Metanalysis

Metanalysis is a statistical technique for extracting answers to well-defined questions about a subject through analysis of the scientific literature concerning the subject. Review of the scientific literature is an essential feature of all approaches to technology assessment. Published studies often reflect limited experience, however, and may not provide definitive answers to questions about efficacy, effectiveness, and safety of a particular technology. Metanalysis permits the results of several studies to be combined in an effort to

address questions that may not be answerable with any one study [15].

Extraction of definitive answers by combining several equivocal studies is appealing. The methods of metanalysis are still rather primitive, however, and many challenges remain. Combined studies must be comparable enough to permit "pooling" of data, and the literature search must be sufficiently comprehensive to capture an adequate number of representative and relevant studies so that selection bias is eliminated. Negative studies are often not published but may be important to evaluation of a particular technology.

Metanalysis is a developing field with considerable promise not only for technology assessment, but also for many applications in scientific research and clinical medicine [16]. Metanalysis has been used only rarely for technology assessments in diagnostic imaging. One example is its recent use to determine the clinical usefulness of mammographic screening in younger asymptomatic women [10].

### Consensus Development

Achievement of a collective opinion about the value of a particular technology through interaction of a group of experts is termed *consensus development*. The process is often informal, such as that used in the consensus development conferences of the National Institutes of Health (NIH). In this approach, a small panel of experts is assembled to hear testimony about the clinical usefulness and potential of a particular technology. Then the panel drafts responses to specific questions about the technology, and these responses are discussed with those offering testimony and with others in the audience. Through repeated exchanges, a final document is prepared that purportedly reflects the consensus of the assembly. Although useful, this approach is vulnerable to subjective influence by the small number of experts on the panel and by forceful persons in the audience. Several NIH consensus conferences have addressed imaging technologies, including mammographic screening, sonography in pregnancy, CT, and MR imaging.

One approach to reduction of potential bias in the group-judgment approach is use of the DELPHI technique [17]. In this method, expert panelists are isolated and unknown to each other. Initial opinions about a technology are obtained from each panelist, and a summary is prepared and distributed to the panel. Each panelist is then asked to respond to the original questions with knowledge of the collective opinion of the panel. This process is repeated several times until a final report can be prepared that reflects a panel consensus.

### Opinion Surveys

A straightforward approach to assessing the value of a particular technology is solicitation of opinions from experts and the compilation of these opinions into a report of collective opinion. The experts do not interact with each other, and they are unable to modify their opinions, once stated, except possibly through review of the final report. The most widely known opinion surveys related to medical technologies are performed by the Diagnostic and Therapeutic Technology

Assessment (DATTA) program, functioning under the Council of Scientific Affairs of the AMA. These surveys use highly structured questions and a choice of specific answers to arrive at a group decision about the safety and efficacy of a particular technology. Answers to questions of safety and efficacy are categorized as established, investigational, promising, doubtful, and unacceptable. The process permits expression of dissenting viewpoints from a majority decision and provides a rapid method for assessment of the clinical value of a particular technology. Several DATTA opinions have examined imaging technologies, including mammographic screening and transrectal sonography for examinations of the prostate.

The panel of potential contributors to a DATTA opinion currently consists of more than 1700 physicians nominated by medical specialty organizations (44%), medical schools (36%), state medical societies (12%), and others (8%). When representatives of this panel are selected for a particular DATTA opinion, physicians are chosen who are expert in the technology or who refer patients to it. Typically, 30–100 physicians contribute to a DATTA opinion. As with any technology assessment effect, the opinion survey suffers from certain limitations, including presentation of a point of view that reflects the clinical use of a technology rather than the "cutting edge" of the technology's development. The point of view also may, at times, reflect the opinions principally of advocates of a technology, despite efforts to eliminate bias through involvement of many contributors.

### Organizations Performing Technology Assessment

Several organizations are involved in medical technology assessment, and more are becoming interested as the topic gains visibility in government, business, and medical circles. The OTA was established by the U.S. Congress to study the ways that technology affects people's lives. The Division of Health and Life Sciences of OTA conducts case studies of technologies under the guidance of an advisory board of experts and with counsel from institutions and organizations within the private sector. The time for completion of a study and preparation of a report averages 18 months.

Questions about coverage of new technologies under Medicare are addressed by the federal Office of Health Technology Assessment (OHTA). This office is under the jurisdiction of the National Center for Health Services Research and Technology Assessment which also has responsibility for health services research studies on concerns such as geographic variations in practice patterns. Technology assessments are performed by OHTA for HCFA, the federal agency responsible for Medicare reimbursement policies. A panel of physicians and members of the OHTA staff determine priorities for assessments, often in response to queries from Medicare contractors (fiscal intermediaries), manufacturers, and insurers. Notices of pending assessments are listed in the *Federal Register*, and input is requested from interested organizations and individuals. The process is time-consuming, with assessments often requiring 2–3 years from the time a request is made to HCFA to culmination in an OHTA report.

Several factors influence a decision by HCFA and OHTA to consider a particular technology for a coverage decision to guide Medicare contractors [18]. These factors include the following: the service is a significant medical advance; the service is a "new product," and Medicare currently covers no similar technology; the service is likely to be used in more than one region of the country; the service is likely to be a significant expense for Medicare; the service has potential for rapid diffusion and application; experts disagree about the safety, efficacy, and appropriateness of the service; fiscal intermediaries have treated the service inconsistently; and the service is outmoded and it is possible that coverage should be withdrawn. Any one of these factors is considered by HCFA and OHTA as sufficient to initiate review of a technology. This position is a contentious issue within the medical community.

In deciding about coverage and reimbursement, private-sector third-party carriers frequently must evaluate the clinical usefulness of particular technologies. Criteria for these decisions are illustrated by those of the National Blue Cross and Blue Shield Association [19]. A recommendation for coverage by this agency usually requires that a technology satisfy five criteria: (1) the technology must have final approval from appropriate governmental regulatory bodies, (2) the scientific evidence must permit conclusions concerning the effect of the technology on health outcome, (3) the technology must improve the net health outcome, (4) the technology must be at least as beneficial as all established alternatives, and (5) the benefit must be attainable outside an investigational setting. Application of these criteria, and acquisition of the requisite data to satisfy them, can significantly delay coverage and reimbursement of a technology after it is approved by the FDA for commercial release [20].

At the Institute of Medicine of the National Academy of Sciences, The Council on Health Care Technology was established in 1986 to promote technology assessment in health care. The council consists of 16 members and serves as a clearinghouse for information related to medical technologies and their assessment. It also intends to improve the procedures of technology assessment; identify needs in technology assessment; stimulate the assessment of medical technologies; and promote education, training, and assistance related to technology assessment.

In 1981, the American College of Physicians established the Clinical Efficacy and Assessment Project (CEAP) for evaluation of medical technologies [21]. Technologies are selected for assessment on the basis of the degree of interest to internists, potential for widespread application, and anticipation of significant benefit or risk. From 10 to 12 topics are selected each year; the time for completion ranges from 9 to 15 months. The reports are reviewed extensively by expert advisers and ultimately become official positions of the college.

A task force on assessment of diagnostic and therapeutic cardiovascular procedures develops guidelines on diagnosis and management of cardiovascular disease under the aegis of the American College of Cardiology and the American Heart Association [22]. Topics are selected by the task force from suggestions of members of both organizations, and reports

examine several features of a technology, including sensitivity and specificity, indications and contraindications, and cost-effectiveness. Reports also consider the training, credentialing, and facilities recommended for use of the technology. The average time from selection of a topic to release of a report is 18 months.

The AMA has several activities related to technology assessment. The text *Drug Evaluations* [23], now nearing its seventh edition, is the most comprehensive sourcebook available worldwide on the comparative use of pharmaceuticals in medical practice. The AMA's Council on Scientific Affairs publishes several reports on medical technologies each year in *JAMA*. In 1982, the AMA formed the DATTA program described earlier. Ten to 12 assessments are performed each year, and the reports are published in *JAMA*. The average time from selection of a DATTA topic to submission of a report to *JAMA* for publication is about 3 months.

Recently the American College of Radiology started a multi-institutional study with certain features of technology assessment. This effort, termed the Radiologic Diagnostic Oncology Group (RDOG) study and supported with funds from the National Cancer Institute, is directed first at comparison of the effectiveness of CT with that of MR imaging for staging lung cancer. A parallel study focuses on a comparison of MR imaging and transrectal sonography for staging prostatic cancer. Additional studies are being designed for identification of preferred methods for staging colorectal and pancreatic cancer. These studies are coordinated by the Department of Health Policy Analysis at Harvard University.

## Conclusions

The importance of technology assessments by professional organizations such as the American College of Radiology, American College of Cardiology, American College of Physicians, and AMA cannot be overemphasized. Organizations such as these have access to the practice environment and the clinical judgment required to evaluate the effectiveness and appropriateness of particular technologies in a clinical setting. This judgment is crucial to continued development and use of medical technologies in an efficacious and cost-conscious manner for improvement of care and well-being of patients.

As Kent and Larson [24] have emphasized, the effectiveness of technology assessment efforts often can be enhanced through multidisciplinary efforts involving physicians from several specialties. If an effective counterbalance to efforts to control costs through restrictions on coverage and reimbursement of medical technologies is not developed, further limitations on the access of patients to quality health care can be anticipated. In providing this counterbalance, medical organizations can help physicians advocate the rights of patients to continued access to the quality of health care that they need and deserve. No purpose is closer than that of

advocacy of patients to the true role of professional medical organizations.

## REFERENCES

1. Reiman AS. Assessment and accountability: the third revolution in medical care. *N Engl J Med* **1989**;319:1220-1222
2. Schwartz WB. The inevitable failure of current cost-containment strategies. *JAMA* **1987**;257:220-224
3. Fineberg HV. Effects of clinical evaluation on the diffusion of medical technology. In: Institute of Medicine. *Assessing medical technologies*. Washington, DC: National Academy Press, **1985**:176-210
4. Ellwood PM. Outcomes management: a technology of patient experience. *N Engl J Med* **1980**;318:1549-1556
5. Roper WG, Winkenwerder W, Hackbarth GM, Krakauer H. Effectiveness in health care: an initiative to evaluate and improve medical practice. *N Engl J Med* **1988**;319:1197-1202
6. Institute of Medicine. *Assessing medical technologies*. Washington, DC: National Academy Press, **1985**:1
7. Melamed MR, Flehinger BJ, Zaman MB, Heelan RT, Hallerman ET, Martin N. Detection of true pathologic stage 1 lung cancer in the screening program and the effect on survival. *Cancer* **1981**;47[suppl.]:1182-1187
8. Wooner LB, Fontana RS, Sanderson DR, et al. Mayo lung project: evaluation of lung cancer screening through December 1979. *Mayo Clin Proc* **1981**;56:544-555
9. Shapiro S. Evidence on screening for breast cancer from a randomized trial. *Cancer* **1977**;39:2722-2782
10. Eddy DM, Hasselblad V, McGivney WT, Hendee WR. The value of mammography screening in women under 50 years. *JAMA* **1988**;259:1512-1519
11. Metz CE. Basic principles of ROC analysis. *Semin Nucl Med* **1978**;7:283-298
12. Wolf GL. Poor quality of clinical research in radiology: another indictment. *Radiology* **1989**;170:311-312
13. Cooper LS, Chalmers TC, McCatty M, Berrier J, Sacks HS. The poor quality of early evaluations of magnetic resonance imaging. *JAMA* **1988**;259:3277-3280
14. Office of Technology Assessment. *Strategies for medical technology assessment*. Washington, DC: U.S. Government Printing Office, **1982**
15. Louis TA, Fineberg H, Mosteller F. Findings for public health from meta-analysis. In: *Annual review: public health, 1985*. Palo Alto, CA: Annual Reviews Inc., **1986**
16. Goodman C. Quantitative synthesis methods. In: Institute of Medicine. *Assessing medical technologies*. Washington, DC: National Academy Press, **1985**:125-126
17. Dalkey NC. *The DELPHI method: An experimental study of group opinion*. Santa Monica, CA: Rand Corp., **1969**
18. Glenn KJ. Assessing medical technology. *Medicine and Health Perspectives*. Washington, DC: Medicine and Health, June 5, **1989**
19. Blue Cross/Blue Shield. *Technology evaluation criteria*. Chicago: Blue Cross and Blue Shield Association, **1987**
20. McGivney WT, Hendee WR. Regulation, coverage and reimbursement of medical technologies. *Int J Radiat Oncol Biol Phys* (in press)
21. American College of Physicians. *Clinical Efficacy Assessment Project [CEAP]: Fact sheet, procedural manual and final report*. Philadelphia: American College of Physicians, **1983**
22. American College of Cardiology. *Statements of charge: Joint ACC/AHA Task Force on Assessment of Cardiovascular Procedures (and Subcommittees), Cardiovascular Procedures Committee, and Cardiovascular Norms Committee*. Bethesda, MD: American College of Cardiology, **1985**
23. American Medical Association. *Drug evaluations*, 6th ed. Chicago: AMA, **1988**
24. Kent DL, Larson EP. Magnetic resonance imaging of the brain and spine. Is clinical efficacy established after the first decade? *Ann Intern Med* **1988**;108:402-424

## Implications of Technology Assessment for the Radiologist

C. John Rosenquist<sup>1</sup>

In this issue of the *AJR*, Hendee has written a timely and perceptive article about the increasing importance of technology assessment in radiology [1]. He explains why technology assessment has become important, describes the various methods for evaluating new technology, and discusses the government and private organizations that are involved in this process. Hendee makes the important point that radiologists, either directly or through professional organizations such as the American College of Radiology, should take an active role in technology assessment.

Why has technology assessment become such an active area of investigation? Probably the most compelling reason is the effort being made to curb the continuing increase in costs of medical care in this country. Because of these increasing costs, many knowledgeable experts in health policy and health economics believe that rationing and resource allocation are inevitable [2]. As new technology is one of the major factors increasing medical costs, it is obviously important to know whether a new test or procedure has a beneficial effect on a patient's outcome.

Radiologists may be involved with the issues of technology assessment in several different ways. They should be well informed about the type of evaluations described by Hendee and may be involved in research activities that address these issues. It also is important to understand the steps in evaluation of technology described by Hillman [3]. The five-stage progression of technology assessment includes evaluation of image efficacy, diagnostic and therapeutic efficacy, patient's outcome, and cost-effectiveness. Every radiologist should be aware of the various levels of acceptance of new technology

as applied to radiology. The first level compromises those procedures of proved usefulness and cost-effectiveness. An example is the use of chest radiographic examination for patients suspected of having pneumonia. The second consists of technology of proved usefulness but of questionable cost-effectiveness. An example in this category is the use of nonionic contrast agents for all contrast injections. The third level comprises procedures of unproved usefulness and cost-effectiveness. An example in this category is the use of sonography for prostate cancer screening.

The radiologist should be aware of several ethical and legal issues that may arise as a result of technology assessment and subsequent health policy decisions. The physician may find himself in an ethical dilemma because of his responsibility for an individual patient vs the health needs of society [4]. On the one hand, the physician should serve an individual patient as the patient's advocate. On the other, the well-informed physician may be aware of the limits of medical resources and realize the need to establish policies concerning the best use of these resources. If, as expected, the future will bring a greater limitation of medical resources, this ethical dilemma will become more pervasive.

There are two legal concerns that have arisen because of technology assessment. The first is the potential for antitrust litigation based on alleged attempts to restrain medical practice [5]. For example, if a large medical insurance company decided against reimbursement for a new procedure, could this be regarded as restraint of trade? Challenges to reimbursement decisions based on antitrust probably would be based on Section 1 of the Sherman Act, which "prohibits

This article is a commentary on the preceding article by Hendee.

<sup>1</sup> Department of Radiology, University of California, Davis, School of Medicine, Rm. 1009R, Professional Bldg., 4301 X St., Sacramento, CA 95817. Address reprint requests to C. J. Rosenquist.

contracts, combination, and conspiracy in restraint of trade or commerce." Those who have studied this problem recommend that care be taken to base technology assessment decisions on careful review of all evidence and that legal counsel be obtained if decisions extend beyond opinions to recommendations regarding reimbursement or use of new procedures.

The second legal issue relates to the potential for liability should a patient's outcome be affected adversely by a decision based on technology assessment. For example, if the government, a health maintenance organization, or an insurance company decides that a procedure is not indicated or not cost-effective, there is the potential for liability if a patient suffers as a result of this decision. Thus far, the courts have been reluctant to take this position and have generally followed the "standard of care" policy. Again, the best defense against this possibility is a thorough, meticulous, and well-documented study of the technology in question.

In his paper, Hendee makes the point that radiologists should be involved in technology assessment in order to balance needs of patients, which are the concern of the practicing physician, against the direction of health policy decisions, which are more concerned with aggregate health care. He makes this recommendation because of the possibility that health policy may place inappropriate emphasis on the goal of limiting new technology in order to curb health care costs. While I agree completely with Hendee's recommendation, there are several additional reasons why radiologists and other physicians should be involved in this process. First, the physician is best able to identify what new technol-

ogies should be assessed. Second, the physician who is trained in methods of technology assessment may be helpful in deciding what type of assessment, as described by Hendee, is likely to be successful. Is a controlled clinical trial possible or ethical, or would a less-expensive case trial be adequate? In some cases, a new technology is of such obvious benefit that perhaps no trial is needed. These types of questions are best answered by the physician who is knowledgeable in this field. Finally, radiologists and other physicians should be instrumental in encouraging federal and private support for clinical studies of technology assessment.

Despite their different perspectives, health policy analysts and physicians share a common goal. Both are interested in determining if a new technology will improve the patient's outcome. By working together, it should be possible to establish a system in which the government, industry, and medical organizations cooperate in the evaluation of new technology before its introduction into general medical practice.

#### REFERENCES

1. Hendee WR. Technology assessment: the contribution of professional organizations. *AJR* **1990**;154:647-651
2. Evans RW. Health care technology and the inevitability of resource allocation and rationing decisions. *JAMA* **1983**;249:2047-2053
3. Hillman BJ. The value of imaging technology to patients' health. *AJR* **1988**;150:1191-1192
4. Weale A. *Cost and choice in health care: the ethical dimension*. London: King Edward's Hospital Fund, **1988**
5. Rose M, Leibenluft RF. Antitrust implications of medical technology assessment. *N Engl J Med* **1986**;314:1490-1493

### Castleman Disease of the Greater Omentum

Castleman disease is an uncommon disorder of lymphoid tissue that results in a benign hypervascular mass, usually in the mediastinum [1]. To our knowledge, no case of Castleman disease involving the greater omentum has been reported [2].

A homogeneous, hypoechoic mass in the greater omentum was found incidentally on sonography in a 56-year-old asymptomatic woman. CT showed a well-margined mass that enhanced after the administration of IV contrast medium (Fig. 1). Angiography showed a hypervascular lesion with large feeding vessels. The mass had a low signal, isointense with abdominal muscles, on T1-weighted (SE 300/30) MR images and a high signal on T2-weighted images. At surgery, an omental mass  $4 \times 4 \times 5$  cm was removed, and histologic examination indicated Castleman disease of the hyaline-vascular type.

According to Keller et al. [1], Castleman disease has two histologic varieties: the hyaline-vascular type, which is more common (90%) and usually asymptomatic, and the plasma-cell type, which may be associated with fever, anemia, and hypergammaglobulinemia. Castleman disease usually involves the mediastinum, but it may occur in any region of the body in which lymph nodes are found. The greater omentum has no lymph nodes; however, it does have small collections of lymphocytes, histiocytes, and plasma cells throughout. The sonographic, angiographic, CT, and MR findings in Castleman disease have been described [3, 4] and are considered nonspecific. On contrast-enhanced CT, the masses caused by the plasma-cell type

enhance less than those associated with the hyaline-vascular type, reflecting the plasma-cell type's lesser vascularity [3]. Castleman disease should be considered in the differential diagnosis of vascular omental masses.

Santi Volta  
Ilario Carella  
Michele Gaeta  
Giuseppe Mantineo  
Alfredo Blandino  
Ospedale Piemonte  
98100 Mesina, Italy

### REFERENCES

1. Keller AR, Hochholzer L, Castleman B. Hyaline vascular and plasma cell types of giant lymph node hyperplasia of the mediastinum and other locations. *Cancer* 1972;29:670-683
2. Gloor F, Torhorst J. Tumors. In: Liebermann-Meffert D, White H, eds. *The greater omentum*. New York: Springer-Verlag, 1983:147-154
3. Joseph N, Vogelzang RL, Hidvegi D, Neiman HL. Computed tomography of retroperitoneal Castleman disease (plasma cell type) with sonographic and angiographic correlation. *J Comput Assist Tomogr* 1985;9:570-572
4. de Geer G, Webb WR, Scilitto R, Golden J. MR characteristics of benign lymph node enlargement in sarcoidosis and Castleman's disease. *Eur J Radiol* 1986;6:145-148

### Hydronephrosis Caused by Carcinoma of the Vermiform Appendix

The diagnosis of carcinoma of the appendix rarely is established preoperatively because the most common signs and symptoms are the same as those of acute appendicitis, periappendiceal abscess, or ovarian and cecal tumor. We describe a case in which the symptoms were caused by obstruction of the right ureter.

A 72-year-old man was admitted because of persistent pain in the right flank. Sonography and retrograde pyelography showed hydronephrosis and hydroureter caused by obstruction of the ureter (Fig. 1). CT showed that the right ureter was obstructed by a mass between the right common iliac artery and the cecum at the level of the pelvic brim. Barium enema did not show evidence of any colonic involvement, but no filling of the vermiform appendix occurred. Laparotomy revealed a 2- to 3-cm mass fixed to the cecum; the vermiform appendix could not be identified. Examination of a biopsy specimen showed poorly differentiated, partly mucinous adenocarcinoma of the vermiform appendix with infiltration of the ureter. A right hemicolectomy and local resection of the ureter were performed.

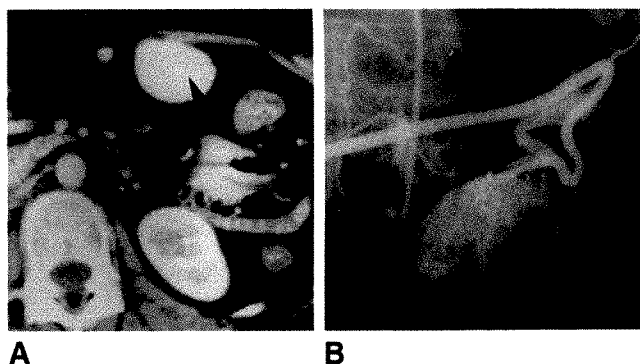


Fig. 1.—Contrast-enhanced CT scan (A) and selective arteriogram of right gastroepiploic artery (B) show a vascular mass in greater omentum (arrow) in a woman with Castleman disease.



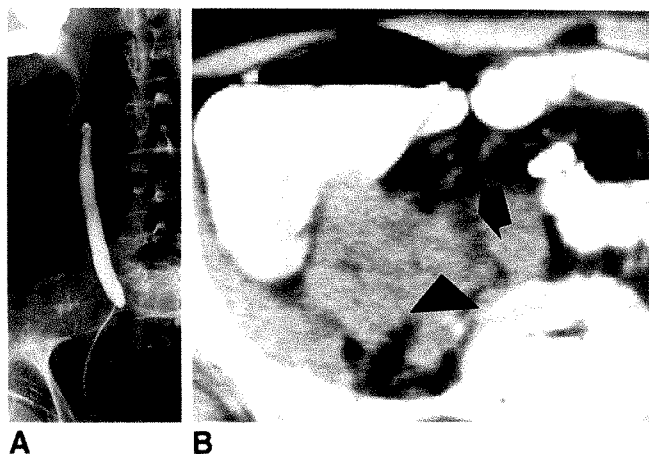


Fig. 1.—Hydronephrosis caused by carcinoma of vermiform appendix.  
A, Retrograde pyelogram shows hydronephrosis and hydroureter due to obstruction of ureter at pelvic brim.  
B, Contrast-enhanced CT scan shows right ureter (arrow) encased in a mass adjacent to cecum (arrowhead).

The signs and symptoms of adenocarcinoma of the vermiform appendix are not specific for this entity. Consequently, all removed appendixes should be examined histologically. Other pathologic conditions of the vermiform appendix that may lead to hydronephrosis are primary or secondary retroperitoneal fibrosis, severe appendicitis [1, 2], and carcinoid tumor. Hepatic, pulmonary, peritoneal, and omental implantation frequently are present. Ovarian metastases are quite rare, however. Infiltration of cecum, terminal ileum, urinary bladder, and retroperitoneum with ureteral obstruction may occur [3], as seen in our case. An important, though rare, complication of mucus-secreting papillary adenocarcinoma is peritoneal pseudomyxoma. Various investigators recommend right hemicolectomy with regional lymphadenectomy in all cases of adenocarcinoma. Others prefer appendectomy alone if the infiltration is limited to mucosa.

A. K. Wakhloo  
University of Freiburg  
Freiburg, FRG  
W. Remmele  
G. Gamstaetter  
M. Weidenfeld  
Horst-Schmidt Kliniken  
Wiesbaden, FRG

## REFERENCES

1. Feldberg MAM, van Waas PFG, ten Haken GB. CT diagnosis of periaortic fibrotic reactions in aortic aneurysms. *J Comput Assist Tomogr* 1982;6:465-471
2. Moncada R, Raffensperger J, Wasserman D, Freeark R. Hydronephrosis secondary to acute appendicitis in children. *Pediatr Radiol* 1974;2:121-124
3. Andersson A, Egerdahl L, Boquist L. Primary carcinoma of the appendix. *Ann Surg* 1976;183:53-57

## Subcutaneous Splenosis

A 57-year-old asymptomatic man who had had a right nephrectomy for renal cell carcinoma 4 years previously had CT of the abdomen to exclude recurrence. Pertinent past history included splenectomy after a shrapnel injury to the spleen in the 1950s.

CT showed a mass in the right renal fossa encircling the colon.

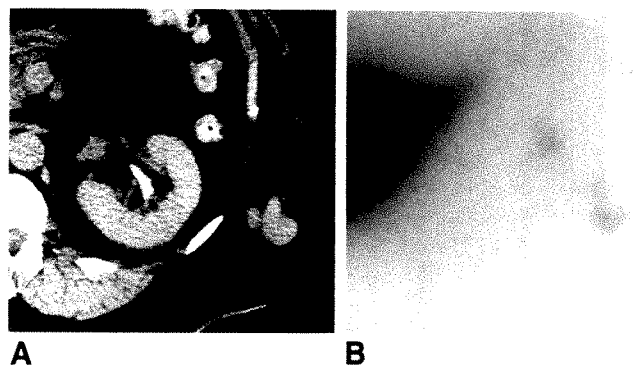


Fig. 1.—Subcutaneous splenosis in a 57-year-old man.  
A, CT scan shows nodules in subcutaneous tissue of left flank.  
B, Left anterior oblique scintigram shows uptake of radionuclide in liver and in nodules of splenic bed and subcutaneous tissue on left side.

Native spleen was not present. Soft-tissue masses of 1–3 cm were seen in the splenic bed, and similar nodules were seen in the subcutaneous tissue of the left side of the abdomen near a scar (Fig. 1A). Splenosis in the splenic bed was presumed. The subcutaneous nodules suggested the differential diagnosis of metastases from recurrent renal cell carcinoma vs splenosis (Fig. 1B). <sup>99m</sup>Tc-sulfur colloid scintigraphy showed uptake of radionuclide in the splenic bed and in the subcutaneous nodules, suggesting splenosis. CT-guided percutaneous needle biopsy was performed by using an 18-gauge ABC needle (Monoject, St. Louis, MO). Examination of the specimen showed the characteristic findings of splenic tissue. The patient was taken to the operating room, and recurrent renal cell carcinoma was resected from the right renal fossa.

To our knowledge, this is only the fourth reported case of splenosis outside the abdominal or thoracic cavities and the first case reported in the radiologic literature [1–3]. Splenosis is a well-known finding after splenic trauma. Characteristically, splenic nodules are found in the region of the spleen or splenic bed if the patient has had a splenectomy. Occasionally, splenosis occurs elsewhere in the abdominal cavity or in the left thorax [4] if the left hemidiaphragm has been disrupted. A separate condition, splenic heterotopia, probably accounts for splenic tissue found in the heart, liver, kidney, or scrotum.

In this case of splenosis, we can suggest a mechanism for the development of the subcutaneous splenules. When this patient's ruptured spleen was removed through a flank incision, small pieces of splenic tissue probably were implanted in the wound. These ultimately proliferated and developed a vascular supply and became functioning splenic nodules.

Subcutaneous splenosis is certain to remain a rare finding. However, when a patient has the appropriate clinical history and CT findings, this diagnosis should be considered.

James R. Grantham  
Forrest C. Clore  
Gainesville Veterans Affairs Medical Center  
Gainesville, FL 32602

## REFERENCES

1. Gill AJ. Traumatic autograft of splenic tissue in the body wall. *J Lab Clin Med* 1944;29:247-253
2. Raper AB. Splenosis: a sequel of rupture of the spleen. *E Afr Med J* 1951;28:265-269
3. Cohen EA. Splenosis: review and report of subcutaneous splenic implant. *Arch Surg* 1954;69:777-784
4. Hart CM, Clore FC, Hood CI. Chest mass in a paraplegic. *Chest* 1989;95:1121-1122

### Left Intercostal Approach for Percutaneous Biliary Drainage After Right Trisegmentectomy

We present a case of an unusual approach for percutaneous transhepatic biliary drainage.

A 67-year-old woman with carcinoma of the sigmoid colon had resection of the colon. Three years later, right trisegmentectomy was performed to remove a large solitary hepatic metastasis. Six months after the trisegmentectomy, jaundice occurred because of the recurrence of tumor at the site of resection.

Two previous attempts to perform percutaneous biliary drainage via the anterior approach failed because of the mostly subcostal position of the remaining liver. On the basis of the CT scan (Fig. 1), a left intercostal route was chosen, and percutaneous transhepatic biliary drainage was performed. An endoprosthesis was placed 2 days later without difficulty. No pleural complications were observed. Outpatient follow-up was continued until the patient died of underlying disease.

After right trisegmentectomy, the lateral segment of the left lobe of the liver remains attached to both the diaphragm (triangular ligament) and the inferior vena cava. Therefore, after compensatory hypertrophy, the liver extends into the left upper quadrant rather than filling the right subphrenic space. As the pleural deflection crosses the midclavicular line at the eighth rib [1], percutaneous access through the seventh interspace in our patient carried the risk of pleural transgression [2].

Reinhard M. Walter  
Stanford University, Medical Center  
Stanford, CA 94305  
Axel Gebauer  
Gerhard Mostbeck  
I. Medizinische Universitätsklinik  
Vienna, Austria

### REFERENCES

1. Last RJ. *Anatomy: regional and applied*, 6th ed. New York: Churchill Livingstone, 1978:242
2. Neff CC, Mueller PR, Ferrucci JT Jr, et al. Serious complications following transgression of the pleural space in drainage procedures. *Radiology* 1984;152:335-341

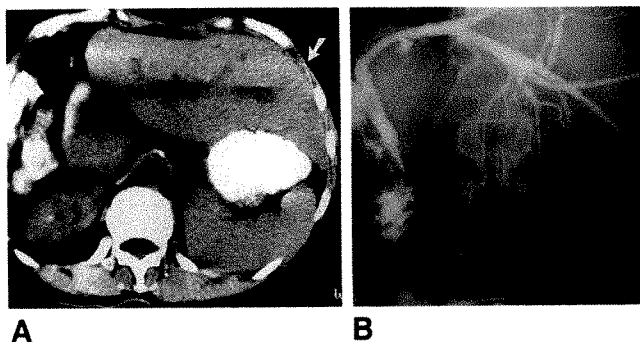


Fig. 1.—Left intercostal approach for percutaneous biliary drainage.  
A, CT scan at level of liver shows optimal access route is via left seventh interspace (arrow) 11 cm lateral to midline and 7 cm anterior to midaxillary line.  
B, Cholangiogram obtained after placement of endoprosthesis (catheter still in place) shows access route.

### Transvaginal Sonography in Early Pregnancy

We read with great interest the article by Bree et al. [1] on transvaginal sonography and early pregnancy. Shortly thereafter, we examined a pregnant woman 41 days after her last menstrual period (quantitative  $\beta$ -human chorionic gonadotropin [ $\beta$ -HCG], 9000 mIU/ml). A gestational sac with a mean diameter of 14 mm was identified. Although a 2- to 3-mm embryo was visible, no fetal pulsations could be detected. Six days later, the level of  $\beta$ -HCG had increased to 25,000 mIU/ml, and on the seventh day, 1 week after the first sonogram, the mean diameter of the sac had increased to 19 mm, and the fetal pole, with clearly visible cardiac pulsations, had increased to 6 mm.

Although the data of Bree et al. are a useful frame of reference, we think that they should beware of trying to establish absolutes where perhaps no absolutes exist. Although the level of  $\beta$ -HCG in our initial study did not satisfy the discriminatory level (10,800 mIU/ml) of Bree et al., the other two criteria, menstrual age (more than 40 days) and size of the gestational sac (greater than 9 mm), clearly were satisfied. Practicing radiologists and sonographers therefore should be cautious in defining viability and fetal demise on the basis of nonfulfillment of one or even two of the criteria suggested by Bree et al.

Michael A. Weiss  
Dennis J. McCabe  
Radiology Associates, P.C.  
Vienna, VA 22180

### REFERENCE

1. Bree RL, Edwards M, Böhm-Vélez M, Beyler S, Roberts J, Mendelson EB. Transvaginal sonography in the evaluation of normal early pregnancy: correlation with HCG level. *AJR* 1989;153:75-79

### Reply

I thank Drs. Weiss and McCabe for their interest in our article [1]. The data presented were meant to be used as a guideline for establishing discriminatory levels for gestational sac, yolk sac, and, particularly, embryo and heartbeat relative to gestational age, level of  $\beta$ -human chorionic gonadotropin ( $\beta$ -HCG), and sac size. I agree that the quantitative data should not be used absolutely for each laboratory and that differences may exist, depending on the equipment, transducer frequency, and the method of determination of levels of  $\beta$ -HCG by the individual laboratory. On the other hand, the few other similar studies [2-4] have reported data much like that presented in our article. Each department probably should test the criteria we reported and determine if any deviation occurs that can be explained by individual differences in equipment and technique. I agree that it is best to be cautious in defining embryonic viability and embryonic demise and that it is always best to give the embryo the benefit of the doubt and perform a repeat examination.

Weiss and McCabe's example of a 2- to 3-mm embryo without cardiac pulsations is surprising. Our experience and the experience of others suggests that this is extremely rare. In fact, it is common to be able to see the embryonic cardiac pulsation before the embryo actually is identified. Again, this discrepancy may be related to the type of sonographic equipment and the frequency of the transducer.

I welcome further studies that may support or contradict the data that we presented. Our clinical experience, however, since the collection of the data and publication of the article has supported the quantitative data, and we have not had many disappointing experiences.

Robert L. Bree  
University of Michigan  
Ann Arbor, MI 48109-0030

## REFERENCES

1. Bree RL, Edwards M, Böhm-Vélez M, Beyler S, Roberts J, Mendelson EB. Transvaginal sonography in the evaluation of normal early pregnancy: correlation with HCG level. *AJR* 1989;153:75-79
2. Bernashek GM, Rudelstorfer R, Csaicsich P. Vaginal sonography versus serum human chorionic gonadotropin in early detection of pregnancy. *Am J Obstet Gynecol* 1988;158:608-612
3. Goldstein SR, Snyder JR, Watson C, Danon M. Very early pregnancy detection with endovaginal ultrasound. *Obstet Gynecol* 1988;72:200-204
4. Fossum GT, Davajan V, Kletzky DA. Early detection of pregnancy with transvaginal ultrasound. *Fertil Steril* 1988;49:788-791

### Sonographic Findings in Crossed Renal Ectopia Without Fusion

Anomalies of renal migration can take many forms, including crossed ectopia, in which both kidneys are found on the same side but the ureter of the ectopic kidney crosses the midline to insert in the bladder normally. When this occurs, some degree of renal fusion usually occurs also. Crossed ectopia without fusion is rare, and to my knowledge, sonographic findings in this condition have not been reported.

An 18-year-old woman was referred for pelvic sonography in lieu of pelvic examination as part of her physical evaluation. Sonograms showed a normal nulliparous uterus and ovaries. Incidental scans revealed absence of the left kidney and an apparently normal right kidney. Follow-up excretory urography showed crossed renal ectopia without fusion; the left kidney was just below and medial to the normal right kidney (Fig. 1). Review of the earlier sonograms showed that the right lower pole was visualized incompletely and that structures below that level were obscured by gas. Sonograms obtained after the excretory urograms showed an intrinsically normal-appearing ectopic kidney. Real-time sonography clearly showed the upper kidney moving separately from the lower kidney during respiration, thus verifying lack of fusion.

This case illustrates both a limitation and an advantage of sonographic evaluation of kidneys. The earlier study did not locate the ectopic kidney because of gas, but real-time identification of separate motion of adjacent kidneys verified the specific diagnosis of ectopia without fusion at the time of follow-up.

Detection of renal anomalies is important because they may be associated with other genitourinary abnormalities and with diseases of other organ systems. Also, the more severe the renal anomaly, the more susceptible that abnormal kidney is to trauma, infection, obstruction, and stone formation, each of which may be atypical in clinical presentation. Determining the presence and degree of fusion

can be difficult with excretory urography because upper and lower poles of the kidneys often overlap (not a problem in the present case because they were clearly separate). In such a circumstance, real-time sonography can be used to make the diagnosis of nonfusion by showing separate motion during respiration.

Roderick Saxey  
Woodland Park Hospital  
Portland, OR 97220

### Bone Scans and Ballet Dancers

Dr. Nussbaum and colleagues' clever use of bone scanning to preserve ballet careers [1] raises a problem related to the exquisite capacity of skeletal scintigraphy for the detection of radiographically occult stress injuries. Of the 23 dancers in their series, 18 had focal uptake of radionuclide in asymptomatic areas. Do such scintigraphic findings call for rest or immobilization? If so, many athletic individuals with clinically insignificant stress-remodeling reactions [2-4] will be subjected to the trauma of avoiding physical activity. Alternatively, if abnormalities in asymptomatic areas can be disregarded, how can healthy bone repair in symptomatic regions be distinguished from radiographically occult fractures? Our approach is to include an early blood-pool image to compare with the skeletal phase. We and others [3-5] have observed that acute fractures are associated with impressively increased vascularity. Both healthy reactions to stress and minor stress injuries show less intense blood-pool activity. Careful clinical correlation, attention to precise technique for optimal anatomic localization, and close rapport with referring physicians are additional prerequisites to optimal use of skeletal scintigraphy in sports medicine.

C. Richard Goldfarb  
Fukiat Ongseng  
Howard Finestone  
Beth Israel Medical Center  
New York, NY 10003

## REFERENCES

1. Nussbaum AR, Treves ST, and Micheli L. Bone stress lesions in ballet dancers. *AJR* 1988;150:851-855
2. Matheson GO, Clement DB, McKenzie DC, et al. Scintigraphic uptake of  $^{99m}\text{Tc}$  at non-painful sites in athletes. *Sports Med* 1987;4:65-75
3. Rupani HD, Holder LE, Espinola DA, Engin SI. Three-phase radionuclide bone imaging in sports medicine. *Radiology* 1985;156:187-196
4. Mauer AH. Radionuclide studies in sports medicine (Continuing education lecture 42). Society of Nuclear Medicine, New York, 1985
5. Matin P. Nuclear medicine: trauma and sports medicine. *Semin Nucl Med* 1988;18:90-111

### Reply

We thank Dr. Goldfarb et al. for their interest and comments on our study [1]. As they indicate, our analysis of the bone scans of 23 ballet dancers showed the marked ability of skeletal scintigraphy to detect stress lesions of bone. These lesions included stress fractures as well as the less severe and less significant stress reactions (stress-induced remodeling of bone). We agree that the three-phase bone scan is a useful adjunct in differentiating between these two abnormalities [2]. Its application to the analysis of injuries sustained by ballet dancers should be beneficial. However, our study was done retrospectively, and three-phase bone scans were not performed at our institution during the study period (1980-1983). Nevertheless, several studies [2-4] have shown that delayed images are helpful in the analysis of bone injury: Stress fractures exhibit a more focal, intense uptake compared with the more diffuse, less intense uptake

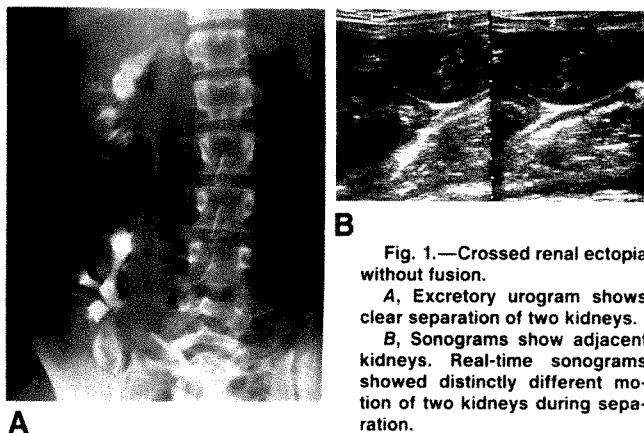


**Fig. 1.—Crossed renal ectopia without fusion.**  
A, Excretory urogram shows clear separation of two kidneys.  
B, Sonograms show adjacent kidneys. Real-time sonograms showed distinctly different motion of two kidneys during separation.

of stress reaction. We agree with Goldfarb et al. that all patients who have abnormal bone scans do not require immobilization, and we did not imply otherwise in our study. Of the 18 dancers who had areas of increased uptake that was asymptomatic, many had scintigraphic findings more consistent with stress reactions. And of course, we agree that close clinical correlation is essential in maximizing the information obtained from skeletal scintigraphy.

Anna Nussbaum Blask  
Children's Hospital National Medical Center  
Washington, DC 20010  
S. Ted Treves  
Lyle Micheli  
The Children's Hospital, Harvard Medical School  
Boston, MA 02115

## REFERENCES

1. Nussbaum AR, Treves ST, Micheli L. Bone stress lesions in ballet dancers: scintigraphic assessment. *AJR* 1988;150:851-855
2. Rupani HD, Holder LE, Espinola DA, Engin SI. Three-phase radionuclide bone imaging in sports medicine. *Radiology* 1985;156:187-196
3. Roub LW, Gumerman LW, Hanley EN Jr, Clark MW, Goodman M, Herbert DL. Bone stress: a radionuclide imaging perspective. *Radiology* 1979;132:431-438
4. Holder LE, Michael RH. The specific scintigraphic pattern of "shin splints in the lower leg": concise communication. *J Nucl Med* 1984;25:865-869

## Muscles of Mastication

The article by Schellhas [1] has an inaccurate statement. The motor supply to the anterior belly of the digastric muscle is by V-3 and not by the seventh cranial nerve [2-4].

Richard E. Rosenthal  
University of Pittsburgh  
Pittsburgh NMR Institute  
Pittsburgh, PA 15213

## REFERENCES

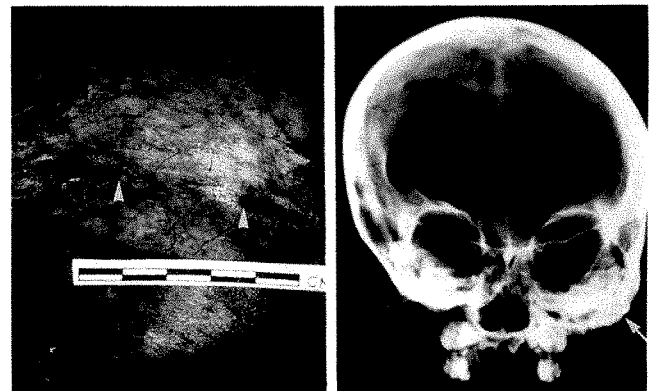
1. Schellhas KP. MR imaging of muscles of mastication. *AJR* 1989;153:847-855
2. Snell RS. *Clinical anatomy for medical students*. 1973:630
3. Grant JCB. *Grant's atlas of anatomy*. 1972:654-655
4. Pansky B, House EL. *Review of gross anatomy*. 1975:40

## Enlarged Parietal Foramina and Craniosynostosis in an American Indian Child

In 1913, the complete cranium and mandible of a 3- to 5-year-old American Indian child were excavated from a 2000-year-old burial mound near Palo Alto, California. The cranium has enlarged parietal foramina (Fig. 1A) 2.5 × 0.4 cm (left foramen, maximal length and maximal breadth) and 2 × 0.2 cm (right foramen). The defects are open slits with smooth, beveled borders (endo- and ectocranially) that increase in thickness as they approach the sagittal suture. Each defect has a tiny projection of bone near the midline, indicating the position of the normal foramen for passage of the emissary vein.

The cranium also has complete craniosynostosis of the sagittal suture and partial obliteration of the coronal and right lambdoidal sutures. Premature closure of the sutures has resulted in a skewing of the right temporal bone and distortion of the inferior right parietal and occipital bones (Fig. 1B). The sutures of the face and hard palate are unremarkable.

Normal parietal foramina are small, circular perforations 1 to 2 mm in diameter in the median posterior portion of the parietal bones. Enlarged parietal foramina, an autosomal dominant trait [1] resulting



A

B

**Fig. 1.—Enlarged parietal foramina and craniosynostosis in bones of a 3- to 5-year-old excavated from a 2000-year-old burial mound.**

**A, Photograph shows slitlike enlarged parietal foramina (arrowheads denote normal position of foramina).**

**B, Radiograph shows marked deformity of right temporal bone (arrow).**

in faulty ossification of the parietal bones, vary greatly in size and shape. Rarely, defects may be 5 cm in diameter. The anomaly was described first by Welcker in 1862 [2], and Goldsmith [3] later reported 16 cases in five generations of the Catlin family.

The present case is of interest both because of its marked deformity due to craniosynostosis and because of the unusual slitlike enlarged foramina. This case is of radiologic importance in differentiating a congenital skeletal anomaly from surgical intervention, trauma, and pathologic conditions, including infection, multiple myeloma, meningocoele, epidermoidoma, and cleidocranial dysostosis.

Robert W. Mann  
Smithsonian Institution  
Washington, DC 20560

## REFERENCES

1. McKusick VA. *Mendelian inheritance in man*, 4th ed. Baltimore: Johns Hopkins Press, 1975
2. Welcker H. *Untersuchungen ueber Wachstum und Bau des menschlichen Schädels*. Leipzig: W. Engelmann, 1862
3. Goldsmith WM. The Catlin mark: the inheritance of an unusual opening in the parietal bones. *J Hered* 1922;13:69-71

## Incipient Lingual Cortical Mandibular Defect in a 10- to 12-Year-Old American Indian Child

The archeological remains of a 10- to 12-year-old American Indian child excavated from New Jersey has an incipient lingual cortical mandibular defect. Because of the ambiguity of skeletal sex indicators in children, sex could not be estimated reliably. Cultural artifacts found in association with other nearby burials suggest that the child died before A.D. 1740.

The left mandible has a small ovoid defect 4 × 2 mm with a depth of less than 1 mm (Fig. 1). The defect is near the angle of the mandible, 2 mm above the inferior border and just posterior to the groove for the facial artery (antegonion). Grossly, the defect has a well-defined margin and an irregularly surfaced central island of bone. Radiographically, the defect has a central lucency partially surrounded by a wide sclerotic "halo." The inferior margin of the defect abuts the dense inferior border of the mandible. The right ramus is unremarkable.

Lingual cortical defects of the mandible have been reported fre-

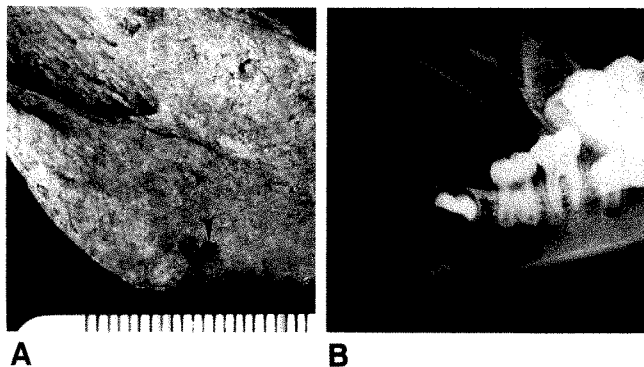


Fig. 1.—Incipient lingual cortical mandibular defect.

A, Photograph shows a small lingual defect (arrowhead) near angle of mandible.

B, Radiograph shows a defect with a central area of rarefaction surrounded in part by a wide band of sclerotic bone.

quently in both the clinical [1, 2] and anthropologic [3] literature. Although the cause of lingual defects, often referred to as Stafne idiopathic defects, remains obscure, clinical findings strongly support a developmental, not congenital or traumatic, origin, resulting from pressure erosion by the submandibular salivary gland.

Lingual cortical defects are found mostly in men more than 35 years old. The three youngest persons on record with lingual defects are males: an 11-year-old from Sweden and a 17-year-old and an 18-year-old from Japan. The present example, therefore, is important for several reasons: (1) This child is the youngest person with a lingual defect reported from an archaeological site. (2) The child is one of the two youngest persons with a lingual defect reported in the clinical and anthropologic literature. (3) This case is a premortem lingual defect in the early stage of development. (4) Radiographs show that a sclerotic border may be an early indicator of a developing defect (examination of more than 5000 dry mandibles has revealed similar incipient defects in adults only).

Robert W. Mann  
Smithsonian Institution  
Washington, DC 20560

#### REFERENCES

1. Stafne EC. Bone cavities situated near the angle of the mandible. *J Am Dent Assoc* 1942;29:1969-1972
2. Karmiol M, Walsh RF. Incidence of static bone defect of the mandible. *Oral Surg* 1968;26:225-228
3. Finnegan M, Marcsik A. Anomaly or pathology: the Stafne defect as seen in archaeological material and modern clinical practice. *J Hum Evol* 1980;9:19-31

#### Automated Filing of "Teaching" Radiographs Under the ACR Index of Roentgen Diagnosis

An article [1] recently published in *M.D. Computing* describes a computerized system for filing radiographs with educational value according to the *Index for Roentgen Diagnosis* [2] published by the American College of Radiology. The software described is unique because it includes the entire *Index for Roentgen Diagnosis* and formulates the final code numbers from the anatomic and pathologic diagnostic terms entered from the keyboard. This eliminates the need to find code numbers. The software also provides an easy method for adding new terms and associated code numbers to the anatomy and pathology files. Added terms become part of the standard files,

and nearly unlimited comments about each radiograph can be included by automatically adding records. Each user establishes an individual identification code that is appended to each record for a given radiograph along with the date of the entry.

The hardware requirements are minimal. A PC- or AT-compatible microcomputer with a 20-megabyte hard disk and 512 kilobytes of random access memory is adequate to store more than 70,000 teaching radiograph entries.

The software is available for \$10 from C. R. Markivee, M.D., Department of Radiology, St. Louis University Medical Center, St. Louis, MO 63104. Both source code and executable files are available in printed form and on either 5¼- or 3½-in. disk. A small instruction manual is included.

C. R. Markivee  
St. Louis University, Medical Center  
St. Louis, MO 63104

#### REFERENCES

1. Markivee CR, Chenoweth JL, Abbas SA, Patel BK, Sauci SF. X-File: a program for maintaining a radiographic teaching file. *MD Computing* 1989;6(3):167-180
2. *Index for roentgen diagnosis*, 3rd ed. Washington, DC: American College of Radiology, 1986

#### Hypertension and Radiation

Many years have been invested in studying the effects of radiation on the body, and still there are surprises. In our survey of 300 radiologists who have been practicing their specialty for at least 25 years, 210 responded to the question about the presence or absence of hypertension. The prevalence of hypertension in this select group was 25%. Stamler et al. [1] and Dyer et al. [2] found a prevalence of 35% in white men 55 to 74 years old.

It is surprising that among those who have had chronic exposure to radiation for 25 years or more, prevalence of hypertension is lower than in those who have had little or only background radiation in their life span. We wonder, how can this be explained?

We would like to believe that being a radiologist has some side benefits, like a protective effect of radiation that has not been known heretofore. Our fellow physicians would like to believe that radiologists lead such a low-pressure life that the decreased prevalence is due to the serenity of our working surroundings. The United States government would like to believe that every bit of radiation is a danger to our health. The people of Europe would like to believe that a radioactive cloud did not pass over them. The Palestine Liberation Organization would like to believe that they have a radioactive device. And environmentalists believe that 5% of our basements are radioactive.

With such highly variable attitudes on radiation, it is time to spend some effort searching for the beneficial effects of radiation. How much better it would be to tell our patients that "just a little dab (of X-rays) will do you," rather than have them so fearful of radiation that they will not have examinations even when it is in their own best interest.

Before the advent of antibiotics, low-dose radiation therapy was used for treatment of pneumonia and parotitis. It also was used for supraspinatus tendonitis, asthma, ulcers, pain, tonsillitis, mastitis, lymphadenitis, thrombophlebitis, and sinusitis [3]. It is only because of the fear of radiation and the availability of safer treatment that X-rays were dropped as a method of treatment. Did we throw out the baby with the bath water?

We suggest that *if* long-term radiation has a protective effect, we should proceed to find what other benefits may be derived from our years of radiology practice. For instance, we do not know how long-term radiation has affected cardiovascular disease, emphysema, brain atrophy, or hammer toes.

At least 4320 radiologists have been working with ionizing radiation for 25 years or more [4]. They provide a fertile field of information as to the possible beneficial effects of X-rays on the body. And they are just sitting out there in front of their view boxes waiting to contribute their history, time, and tissues to the benefit of their fellow humans. Maybe a study of this select group would dispel some of the fears of X-rays.

It should be our duty as radiologists to pursue such a study. If we were adequately to investigate the possibilities of the beneficial effects of low-dose radiation, we undoubtedly would find additional benefits and show our public why we as a group are younger at heart, have fewer acute diseases, are more good-looking, are more brilliant, have more beautiful spouses, have more entertaining children, and knew all along that it was due to X-rays.

So, step right up and get your daily dose of X-rays with a smile on your face.

William J. Bean  
David M. Mullin  
Ronald M. Porter  
Jupiter, FL 33458

#### REFERENCES

1. Stamler J, Stamler R, Pullman TN. *The epidemiology of hypertension: proceedings of an international symposium*. New York: Grune & Stratton, 1967
2. Dyer AR, Stamler J, Shekelle RB, et al. Hypertension in the elderly. *Med Clin North Am* 1977;61:513-515
3. Scherer E. The significance of radiation therapy with low doses. *Rontgen-blatter* 1965;18:400-406
4. *American College of Radiology Membership Directory 1986*. Reston, VA: American College of Radiology, 1986

Letters are published at the discretion of the Editor and are subject to editing.

Letters to the Editor must not be more than two *double-spaced*, typewritten pages. One or two figures may be included. Abbreviations should not be used. See Author Guidelines, page A5.

Material being submitted or published elsewhere should not be duplicated in letters, and authors of letters must disclose financial associations or other possible conflicts of interest.

Letters concerning a paper published in the *AJR* will be sent to the authors of the paper for a reply to be published in the same issue. Opinions expressed in the Letters to the Editor do not necessarily reflect the opinions of the Editor.



## Review of Current Literature

Initials and addresses of corresponding authors are provided in parentheses for each article so that the reader can obtain reprints directly. Abstracts are printed verbatim from each journal.

### The New England Journal of Medicine

**The effect of cigarette smoking on neutrophil kinetics in human lungs.** MacNee W, Wiggs B, Belzberg AS, Hogg JC (JCH, University of British Columbia Pulmonary Research Laboratory, St. Paul's Hospital, 1081 Burrard St., Vancouver, B.C. V6Z 1Y6, Canada). *N Engl J Med* 321:924-928, Oct. 1989

Neutrophils may play a part in the pathogenesis of the centrilobular emphysema associated with cigarette smoking. The capillary bed of the lungs concentrates neutrophils approximately 100-fold with respect to erythrocytes, producing a large pool of marginated cells. We examined the effect of cigarette smoking on the kinetics of this pool of cells, using  $^{99m}\text{Tc}$ -labeled erythrocytes to measure regional blood velocity and  $^{111}\text{In}$ -labeled neutrophils to measure the removal of neutrophils during the first passage through the pulmonary circulation, their subsequent washout from the lungs, and the effect of local blood velocity on the number of neutrophils retained in each lung region.

We observed no difference in these measurements between subjects who had never smoked ( $n = 6$ ) and smokers who did not smoke during the study ( $n = 12$ ). However, subjects who did smoke during the study ( $n = 12$ ) had a significantly slower rate of washout of radiolabeled neutrophils from the lung ( $0.08 \pm 0.04$  of the total per minute, as compared with  $0.13 \pm 0.06$  in smokers who did not smoke during the experiment and  $0.14 \pm 0.08$  in nonsmokers) ( $P = 0.02$ ). We also observed an increase in the regional retention of labeled neutrophils with respect to blood velocity in 5 of the 12 subjects who smoked during the study, but in none of the other subjects.

We conclude that the presence of cigarette smoke in the lungs of some subjects increases the local concentration of neutrophils, and suggest that the lesions that characterize emphysema may be a result of the destruction of lung tissue by neutrophils that remain within pulmonary microvessels.

**Prognosis of abdominal aortic aneurysms: a population-based study.** Nevitt MP, Ballard DJ, Hallett JW Jr. (DJB, Mayo Clinic, 200 1st St., S. W., Rochester, MN 55905). *N Engl J Med* 321:1009-1014, Oct. 1989

Information is incomplete about the rate of expansion of abdominal aortic aneurysms and the risk of rupture in relation to their size. To address these questions, we conducted a population-based study. Of the 370 residents of Rochester, Minn., with an aneurysm initially diagnosed from 1951 through 1984, 181 had the aneurysm docu-

mented by ultrasound examination. Among the 103 patients who underwent more than one ultrasound study, the diameter of the aneurysm increased by a median of 0.21 cm per year. Only 24 percent had a rate of expansion of 0.4 cm or more per year.

Among the 176 patients who had an unruptured aneurysm at the time of the initial ultrasound study, the cumulative incidence of rupture was 6 percent after 5 years and 8 percent after 10 years. However, the risk of rupture over five years was 0 percent for the 130 patients with an aneurysm less than 5 cm in diameter and 25 percent for the 46 patients with an aneurysm 5 cm or more in diameter. All 16 patients who had ruptures had aneurysms that were 5 cm or more in diameter at the time of the rupture.

These population-based data challenge the clinical perception that aneurysms typically expand at a rate of 0.4 to 0.5 cm per year. Our data also suggest that for aneurysms less than 5 cm in diameter the risk of rupture is considerably lower than has been reported previously. However, the risk of rupture is substantial for aneurysms 5 cm or more in diameter.

**Asbestos-associated diseases in a cohort of cigarette-filter workers.** Taicott JA, Thurber WA, Kantor AF, et al. (JAT, Dana-Farber Cancer Institute, 44 Binney St., Boston, MA 02115). *N Engl J Med* 321:1220-1223, Nov. 1989

To estimate the effects on health of occupational exposure to crocidolite, a highly toxic form of asbestos, we studied a cohort of 33 men who worked in 1953 in a Massachusetts factory that manufactured cigarette filters containing crocidolite fibers from 1951 to 1957.

Twenty-eight of the men have died, as compared with 8.3 deaths expected. This increased mortality was attributable to asbestos-associated diseases. Fifteen deaths were caused by cancer, as compared with 1.8 expected (relative risk, 8.2; 95 percent confidence interval, 4.6 to 13.4), including eight from lung cancer, five from malignant mesothelioma, and two from other types of cancer.

There were seven deaths from nonmalignant respiratory disease, as compared with 0.5 expected (relative risk, 14.7; 95 percent confidence interval, 5.9 to 30.3), of which five were due primarily to asbestosis. In contrast, the mortality rates from cardiovascular diseases and all other causes were not increased. Four of the five living workers have pulmonary asbestosis; three of them have recently diagnosed cancers, including two additional lung cancers.

We conclude that the extremely high morbidity and mortality in these workers were caused by intense exposure to crocidolite asbestos fibers.

### Cancer

**Nodular form of bleomycin-related pulmonary injury in patients with osteogenic sarcoma.** Santrach PJ, Askin FB, Wells RJ, Aziz-

khan RG, Merten DF (FBA, Surgical Pathology, North Carolina Memorial Hospital, Chapel Hill, NC 27514). *Cancer* 64:806-811, 1989

Bleomycin (BLEO), an antitumor antibiotic effective against a variety of malignancies, has been associated classically with a pulmonary toxic reaction producing diffuse interstitial fibrosis. However, BLEO-related pulmonary nodules have been reported recently, mostly in children and young adults treated for germ cell tumors. A different, apparent hypersensitivity reaction with prominent eosinophilic infiltrates has been seen in other patients. This report details the clinical history, radiographic features, and histopathologic condition of three patients with osteogenic sarcoma in whom pulmonary nodules developed during the course of their multiagent, BLEO-containing chemotherapy. The predominant histopathologic lesion was bronchiolitis obliterans-organizing pneumonia (BOOP); one patient had a significant eosinophilic infiltrate also. Pulmonary lesions developed in all of these patients after relatively low doses of BLEO (<200 mg). All of these patients underwent open lung biopsy to establish the diagnosis. Reported cases of BLEO-induced pulmonary injury other than diffuse fibrosis are reviewed and comparisons are made with those in the current report. Also, suggestions are made for the management of these patients.

Reprinted by permission from the American Cancer Society.

**Small bore catheter drainage and sclerotherapy for malignant pleural effusions.** Parker LA, Charnock GC, Delany DJ (LAP, Dept. of Radiology, University of North Carolina School of Medicine, Campus box #7510, Chapel Hill, NC 27599-7510). *Cancer* 64:1218-1221, 1989

The accumulation of large amounts of fluid in the pleural space is a common sequela of disseminated carcinomatosis. Traditional management has included therapeutic thoracentesis or the placement of a large bore chest tube for drainage with the subsequent installation of a sclerosing agent in an attempt to achieve pleural symphysis. An evaluation of all patients treated in this manner during a 4-year period was undertaken to assess the degree of success obtained with a large bore standard chest tube versus a small pigtail catheter. A study group consisting of 20 patients with a total of 24 pleural effusions was treated with drainage and sclerotherapy. In this group, eight of 13 effusions were adequately treated with pigtail catheter drainage and sclerotherapy, compared with four of 11 effusions adequately treated with standard chest tube drainage and sclerotherapy. Although the numbers are small, it appears that pigtail catheter drainage and sclerosis is at least as successful as the more traditional drainage with the standard chest tube.

Reprinted by permission from the American Cancer Society.

**Hepatocellular carcinoma presenting as bone metastasis.** Liaw CC, Ng TK, Chen TJ, Liaw YF (YFL, Liver Unit, Chang Gung Memorial Hospital, 199 Tung Hwa N. Rd., Taipei, Taiwan 10591, Republic of China). *Cancer* 64:1753-1757, 1989

In a consecutive series of 395 patients with pathologically verified hepatocellular carcinoma, 20 patients (5%) had bone metastasis at initial presentation. Of these, 16 were men and four women ranging from 26 to 64 years of age (median, 50 years). The age, sex, hepatitis B surface antigen seropositivity, alpha-fetoprotein level, and frequency of associated cirrhosis were not statistically different from those in patients without initial bone metastasis. Initial presentation was usually the result of spinal lesion with neurologic compression, and chest wall or scalp mass. Metastasis most commonly involved spine and ribs, and occurred as osteolytic lesions or extrapleural mass. Computed tomography proved best for demonstrating an expansile soft tissue mass with bony destruction. Angiography showed hypervascular appearance over the destructive bone area. Treatment results were poor. The follow-up period ranged from 3 weeks to 14 months with a median survival of 5 months. The data suggested that hepatocellular carcinoma be ruled out in patients with osteolytic lesions.

Reprinted by permission from the American Cancer Society.

**Secondary acute myelocytic leukemia after adjuvant therapy for early-stage breast carcinoma: a new complication of cyclophosphamide, methotrexate, and 5-fluorouracil therapy.** Geller RB, Boone LB, Karp JE, et al. (RBG, The Johns Hopkins Oncology Center, Rm. 3-109, 600 N. Wolfe St., Baltimore, MD 21205). *Cancer* 64:629-634, 1989

The occurrence of treatment-related hematologic malignancies after adjuvant therapy with alkylating agents for gastrointestinal cancers, ovarian carcinoma, and breast cancer and after treatment for Hodgkin's disease, non-Hodgkin's lymphoma, germ-cell tumors, and multiple myeloma has been well documented. Adjuvant chemotherapy is frequently used for the treatment of early stage breast cancer, and to date there has been no increase in the incidence of secondary myelodysplastic syndromes or acute leukemia after cyclophosphamide-based regimens when compared with surgical controls. This report describes two patients who developed acute myelocytic leukemia only after exposure to cyclophosphamide, methotrexate, and 5-fluorouracil adjuvant therapy. These two cases of acute leukemia, which developed 3 years after diagnosis of breast cancer and initiation of chemotherapy, were characterized by trilineage dysplasia and pancytopenia, and had abnormalities of chromosomes 5 and 7: characteristics consistent with treatment-related leukemia. Many women are diagnosed with early stage breast cancer each year who are potential candidates for adjuvant therapy. Although certain subgroups of patients have been shown to benefit from adjuvant therapy, continued efforts must be directed at identifying responders so that others will not be exposed to the additional risks of chemotherapy.

Reprinted by permission from the American Cancer Society.

**Intraarterial infusion chemotherapy for metastatic liver tumors using multiple anti-cancer agents suspended in a lipid contrast medium.** Taniguchi H, Takahashi T, Yamaguchi T, Sawai K (HT, 1st Dept. of Surgery, Kyoto Prefectural University of Medicine, Kawaramachi-Hirokohji, Kamigyo-ku, Kyoto, 602, Japan). *Cancer* 64:2001-2006, 1989

An ethiodized oil, Lipiodol (Lipiodol Ultra-Fluid, Laboratoire Guerbet, Paris, France), when injected into the hepatic artery, is selectively retained by liver tumors. Thus, anti-cancer agents suspended in Lipiodol can be delivered specifically to liver tumors. Before clinical trials of this new drug delivery system were begun, the movements of drugs suspended in Lipiodol were examined *in vitro*. It was found that 5-fluorouracil, doxorubicin, and mitomycin C were continuously released from oil phase to water phase, and when these three drugs were collectively suspended in Lipiodol, each was related independently. During clinical investigations, 42 patients with unresectable metastatic liver tumors were treated with intraarterial infusions of anti-cancer drugs in Lipiodol. As a result, the administration of a combination of anti-cancer agents suspended in Lipiodol was shown to be effective in controlling metastatic liver tumors. It was concluded that such a method could be applied to a variety of metastatic liver tumors with different drug sensitivities.

Reprinted by permission from the American Cancer Society.

**Hepatic arterial injection chemotherapy with cisplatin suspended in an oily lymphographic agent for hepatocellular carcinoma.** Shibata J, Fujiyama S, Sato T, Kishimoto S, Fukushima S, Nakano M (JS, 3rd Dept. of Internal Medicine, Kumamoto University Medical School, 1-1, Honjo 1-chome, Kumamoto 860, Japan). *Cancer* 64:1586-1594, 1989

A method to prepare cisplatin suspended in an oily lymphographic agent, Lipiodol (LPS), has been established to deliver cisplatin to hepatocellular carcinoma (HCC) by the hepatic artery. Seventy-one patients, one Stage I, 16 Stage II, 16 Stage III, and 38 Stage IV, were treated with LPS therapy. A partial response was obtained in 33 cases (46.5%), a minor response in 20 cases (28.2%), and no change in 18 cases (25.3%). In 34 patients whose serum alpha-fetoprotein (AFP) levels were greater than 400 ng/ml, the serum AFP levels

decreased in 31 patients (91.2%). The AFP decreased by more than 50% in 25 cases (73.5%) and more than 75% in 19 cases (55.9%). The plasma des- $\gamma$ -carboxy prothrombin (DCP) levels decreased in all of the 26 DCP-positive patients. The survival rate was 77% at 6 months and the 1-year survival rate was estimated to be 55%. The patients treated with LPS therapy survived longer compared with patients given Lipiodol containing neocarcinostatin by the hepatic artery. Complications such as acute gastroduodenal mucosal lesions (24%), cholecystitis (2.8%), pancreatitis (7%), delayed jaundice (7%), and hepatic encephalopathy (4.2%) were observed after therapy. The peak plasma platinum (Pt) concentrations determined as ultrafilterable Pt occurred 5 to 20 minutes, and 5 to 60 minutes as total Pt after the end of LPS injection. The Pt concentrations in the tumor tissues were 42 times higher in four operated cases and 7.1 times higher in six autopsy cases than those in the nontumorous tissue. These results suggest that LPS selectively accumulates in the HCC, is long-lasting and gradually releases the drug. In addition it is effective as a new anti-cancer therapy for hepatocellular carcinoma.

Reprinted by permission from the American Cancer Society.

**Urinary tract cancers found by homescreening with hematuria dipsticks in healthy men over 50 years of age.** Messing EM, Young TB, Hunt VB, Wehbie JM, Rust P (EMM, G5/347, 600 Highland Ave., Madison, WI 53792). *Cancer* 64:2361-2367, 1989

In a homescreening study of 235 asymptomatic men, 50 years of age and older without known causes of hematuria, tested their urine each week with a chemical reagent strip for the presence of blood for 1 year. Forty-four men had hematuria at least once, and 31 had a full urologic evaluation. Of these, eight were found to have urinary cancers and seven had nonmalignant diseases warranting immediate treatment. In six of these 15 men (only two with cancer) hematuria occurred in over 1/3 of the testings, and in four hematuria was found on microscopic urinalysis at the time of urologic evaluation. The degree of hematuria was unrelated to the seriousness of its cause. We conclude that in this population hematuria occurs intermittently and when found, regardless of quantity or symptoms, serious underlying pathology must be ruled out. Furthermore, regular hematuria home testing offers a promising means of detecting urinary cancers and other diseases that warrant therapy in asymptomatic men 50 years of age and older.

Reprinted by permission from the American Cancer Society.

## Chest

**Nodular pulmonary opacities in patients with rheumatoid arthritis: a diagnostic dilemma.** Jolles H, Moseley PL, Peterson MW (HJ, Radiology, Virginia Commonwealth University, Box 471 MCV Sta., Richmond, VA 23298-0470). *Chest* 96:1022-1025, 1989

Nodular opacities are a well-known pulmonary manifestation of rheumatoid arthritis (RA), occurring most often in seropositive men who smoke and have subcutaneous nodules. In the past 15 years two cases of lung carcinoma presenting as pulmonary nodules have been reported in patients with rheumatoid disease. We present seven patients with seropositive RA and subcutaneous nodules who had new pulmonary nodule(s) noted on chest roentgenograms. All but one were current smokers. Carcinoma was found in all patients at bronchoscopy or thoracotomy. Four patients had solitary nodules (one was cavitory); the remaining three patients had multiple bilateral nodules that cavitated in one case. All patients had interstitial abnormality (peribronchial/vascular thickening) with basal predominance in three, and there was evidence of pleural thickening/fluid in three patients. These results strongly suggest that histologic proof of presumed rheumatoid pulmonary nodules be obtained.

## Circulation

**Recurrent ischemia without warning: analysis of risk factors for in-hospital ischemic events following successful thrombolysis with intravenous tissue plasminogen activator.** Ellis SG, Topol EJ, George BS, et al. (SGE, University of Michigan Medical Center, Cardiology, B1F245, 1500 E. Medical Center Dr., Ann Arbor, MI 48109). *Circulation* 80:1159-1165, 1989

Ischemic events after successful thrombolysis have been reported to occur in 18-32% of patients treated for acute myocardial infarction with thrombolytic therapy, and previous studies in which patients received streptokinase suggest that risk of early recurrent ischemia is closely related to the presence of a high-grade residual stenosis. If these events are predictable after intravenous recombinant tissue plasminogen activator (rt-PA) thrombolytic therapy, then further intervention after its use could be targeted at selected patients. One-hundred ninety-two patients from the Thrombolysis and Angioplasty in Myocardial Infarction (TAMI) I and TAMI III trials had successful rt-PA-mediated thrombolysis without immediate coronary angioplasty (PTCA). One-hundred seventy-four of these patients (92%) had pre-hospital discharge angiography. The mean age was  $56 \pm 11$  years; 81% were men; the infarct-related artery was the left anterior descending in 76 (39.8%), the left circumflex in 24 (12.6%), and the right coronary artery in 91 (47.6%). Thrombolysis with rt-PA resulted in a residual  $73 \pm 13\%$  diameter and  $0.95 \pm 0.51$  mm stenosis by quantitative coronary arteriography, and Thrombolysis in Myocardial Infarction (TIMI) flow grade 2 in 59.2% and 3 in 40.8% of stenoses as assessed on angiograms obtained 90 minutes after the initiation of rt-PA therapy. Recurrent ischemic events (ischemia requiring emergency percutaneous transluminal coronary angioplasty or urgent bypass surgery, reocclusion of the infarct-related artery, or cardiac death) occurred in 41 patients (21.3%). The recurrent ischemic events were not related to any of eight prospectively defined variables: the infarct-related artery, TIMI flow grade, percent diameter stenosis, absolute luminal diameter, angiographically-defined thrombus, diffuse disease or ectasia in the infarct-related artery, or Ambrose morphology of the infarct-related stenosis. Thus, 1) recurrent ischemic events are frequent after rt-PA and 2) such events are not predictable by findings available by in-depth quantitative and morphologic assessment at the time of angiography performed 90 minutes after rt-PA administration. It follows with the inability to stratify a patient's risk of recurrent ischemia that the decision for triage to coronary revascularization procedures after successful thrombolysis with rt-PA remains an especially difficult one.

## Gastroenterology

**Upper esophageal sphincter opening and modulation during swallowing.** Jacob P, Kahrilas J, Logemann JA, Shah V, Ha T (PJ, Dept. of Medicine, Northwestern University, Chicago, IL). *Gastroenterology* 97:1469-1478, 1989

Studies were done on 8 normal subjects with synchronized video-fluoroscopy and manometry to facilitate a biomechanical analysis of upper esophageal sphincter opening and volume-dependent modulation during swallowing. Movements of the hyoid and larynx, dimensions of sphincter opening, and intraluminal sphincter pressure were determined at 1/30th-s intervals during swallows of 1, 5, 10, and 20 ml of liquid barium. Our analysis subdivided upper esophageal sphincter activity during swallowing into five phases: (a) relaxation, (b) opening, (c) distention, (d) collapse, and (e) closure. Sphincter relaxation occurred during laryngeal elevation and preceded opening by a mean period of 0.1 s. Opening occurred as the sphincter was pulled apart via muscular attachments to the hyoid such that the hyoid coordinates at which sphincter opening and closing occurred were constant among bolus volumes. Sphincter distention after opening was modulated by intrabolus pressures rather than graded hyoid movement. The generation of intrabolus pressure coincided with the posterior thrust of the tongue that culminated in pharyngeal wall

contact and the initiation of pharyngeal peristalsis. Larger volume swallows were associated with greater intrabolus pressure and increased bolus head velocity. The duration of sphincter opening increased in conjunction with a prolongation of the anterior-superior excursion of the hyoid and a delay in the onset of pharyngeal peristalsis (the event that determined the timing of sphincter closure). We conclude that transsphincteric transport of increasing swallow bolus volumes is accomplished by modulating sphincter diameter, opening interval, and flow rate (reflected by bolus head velocity). Furthermore, upper esophageal sphincter opening is an active mechanical event rather than simply a consequence of cricopharyngeal relaxation.

Reprinted with permission by the American Gastroenterological Association.

**Ultrasonic Doppler studies of hepatocellular carcinoma and comparison with other hepatic focal lesions.** Ohnishi K, Nomura F (KO, 1st Dept. of Medicine, Chiba University School of Medicine, Chiba, Japan). *Gastroenterology* 97:1489-1497, 1989

One hundred fifty-four liver lesions, including 63 hepatocellular carcinomas, were studied to determine the value of duplex ultrasound in the diagnosis of small hepatocellular carcinomas. Arterial Doppler signals were obtained either within the body of the tumor, at its periphery, or in both locations, from 28 of 37 hepatocellular carcinomas  $\leq 3$  cm in diameter and from all 26 hepatocellular carcinomas with a diameter  $> 3$  cm. Arterial Doppler signals were obtained at the periphery of 5 of 7 cholangiocarcinomas, 4 of 11 liver metastatic tumors, and 5 of 23 hemangiomas. No such signals were obtained from 29 regenerative nodules, 10 hepatic pseudotumors, and 11 liver cysts. The mean peak systolic frequency seen in hepatocellular carcinoma (1.2 kHz) was significantly greater than in cholangiocarcinoma (0.6 kHz), metastatic tumors (0.5 kHz), or hemangiomas (0.3 kHz). A peak systolic frequency of  $> 3$  kHz was found in 6 of 8 hepatocellular carcinomas  $\geq 4$  cm in diameter with angiographically proven arteriportal shunting, whereas the value in other hepatocellular carcinomas or other hepatic focal lesions was  $< 2.6$  kHz. This study showed that the peak systolic shift was related to the degree of arteriportal shunting. Because shunting is either minor or non-existent in small hepatocellular carcinomas, the value of duplex Doppler ultrasound in the diagnosis of these lesions appears to be limited.

Reprinted with permission by the American Gastroenterological Association.

**Changes in bile duct diameter after cholecystectomy: a 5-year prospective study.** Hunt DR, Scott AJ (DRH, University Dept. of Surgery, The St. George Hospital, Kogarah, Australia). *Gastroenterology* 97:1485-1488, 1989

In this prospective study, we have measured with ultrasound the diameter of the common hepatic duct and the common bile duct in a series of 24 patients having elective cholecystectomy. Preoperative measurements by ultrasound were compared with measurements taken directly from operative cholangiograms and excellent correlation was observed ( $r = 0.938$ ). Studies were repeated 1 mo, 12 mo, and 5 yr after operation. Of 21 patients returning for study at 5 yr, there were 4 patients with 1-mm ducts before surgery who showed an increase in the size of the common hepatic duct but in none was the final measurement  $> 4$  mm. Mean common hepatic duct diameter ( $n = 21$ ) increased from 3.95 mm before to 4.48 mm 5 yr after surgery ( $p = 0.24$ , paired  $t$ -test). Common bile duct was more easily seen after cholecystectomy and of 13 ducts satisfactorily measured 1 and 5 yr after surgery, 7 showed an increase in size (mean common hepatic duct 1 yr = 4.77 mm, 5 yr = 5.92 mm,  $p = 0.059$ , paired  $t$ -test). Significant dilatation of the common hepatic duct was seen in only 2 of 21 patients, but a strong trend to minor dilatation was observed in the common bile duct after cholecystectomy.

Reprinted with permission by the American Gastroenterological Association.

## Digestive Diseases and Sciences

**Diagnostic accuracy of fine-needle aspiration biopsy in patients with hepatocellular carcinoma.** Bru C, Maroto A, Bruix J, et al. (JB, Liver Unit, Hospital Clínic i Provincial, C/Villarreal 170, Barcelona 08036, Spain). *Dig Dis Sci* 34(11):1765-1769, Nov. 1989

The present study was undertaken to investigate the diagnostic usefulness of fine-needle aspiration biopsy (FNAB) in a large series of patients with hepatocellular carcinoma (HCC) seen over a 1-year period. During 1986, ultrasonographically guided percutaneous FNAB was performed in 72 patients with suspected HCC. A final diagnosis of HCC was made in 58 patients. The presence or absence of HCC was ascertained by histological examination and/or by other diagnostic procedures ( $\alpha_1$ -fetoprotein, computed tomography, arteriography) and by clinical follow-up (repeated ultrasonographic controls) and/or by surgery or necropsy. A total of 61 FNABs were carried out in these 58 patients. Only 42 (69%) of the 61 FNABs allowed the diagnosis of HCC. This moderate diagnostic sensitivity was not related to tumor size. Only one false positive result was observed in the non-HCC group. Therefore, the diagnostic specificity of FNAB for HCC was 93%, with a positive predictive value of 97% and a negative predictive value of 40%. These results show that FNAB is a useful diagnostic technique in patients with HCC. However, these data also show that there is a large proportion (31%) of subjects with false negative results. Therefore, we suggest that further efforts should be made to improve the diagnostic accuracy of this procedure.

**Motility disorders and stress.** Camilleri M, Neri M (MC, Gastroenterology Research Unit, Mayo Clinic, Rochester, MN 55905). *Dig Dis Sci* 34(11):1777-1786, Nov. 1989

The association between emotion and gastrointestinal dysfunction has been postulated for centuries, and all practicing clinicians have anecdotal experience of the association between stress and irritable bowel syndrome (IBS). However, definite proof of an etiologic link between stress and gut motor dysfunction remains elusive, despite the large number of publications on this topic.

A critical appraisal of methodology, use of controls, data interpretation, and significance of findings in the published literature is necessary to assess the present state of knowledge and to develop more meaningful studies in the future. This review attempts to summarize these perspectives.

## Clinical Orthopaedics and Related Research

**Roentgenographic findings in pigmented villonodular synovitis of the knee.** Flandry F, McCann SB, Hughston JC, Kurtz DM (FF, Hughston Orthopaedic Clinic, 6262 Hamilton Rd., Columbus, GA 31995). *Clin Orthop* 247:208-219, Oct. 1989

Twenty-nine cases of pigmented villonodular synovitis (PVS) of the knee in 27 patients were reviewed to determine characteristic roentgenographic findings. All cases met strict histologic criteria for diagnosis. Four cases were localized PVS (LPVS), and 25 cases were diffuse PVS (DPVS). Roentgenographic findings were largely in the soft tissues. Cystic invasion of bone or degenerative changes were rare, although present in some cases. When present in DPVS, these changes were most pronounced in the patellofemoral articular surface. In the cases of DPVS, large posterior tumefactions did not correlate with extraarticular extension. Clinical behavior of PVS was governed more by anatomic site and form of disease than by the severity of histologic or roentgenographic findings.

**Familial expansile osteolysis.** Wallace RGH, Barr J, Osterberg PH, Mollan RAB (RGHW, The Queen's University of Belfast, Dept. of Orthopaedic Surgery, Musgrave Park Hospital, Belfast BT9 7JB, Northern Ireland). *Clin Orthop* 248:265-277, Nov. 1989.

Familial expansile osteolysis (FEO) is a unique bone dysplasia, which has, over five generations, affected 42 members of a Northern Ireland family. The disease follows a classic autosomal dominant pattern of inheritance. The condition is distinct enough in its clinical features and natural history to be recognized as a new and unique disease. There are both general and focal skeletal changes, the latter having a predominantly peripheral distribution and an onset from the second decade. Progressive osteoclastic resorption accompanied by medullary expansion leads to severe and painful disabling deformities with a tendency to pathologic fracture. Most affected members of the family have an associated early-onset deafness and loss of dentition as a result of unique middle ear and dental abnormalities. The serum alkaline phosphatase and urinary hydroxyproline are elevated to a variable degree, whereas other biochemical indices are normal. The response of the disease to a therapeutic trial using parenteral dichloro-methylene-diphosphonate (dichloro-MDP) produced an initial rapid biochemical response, which was not sustained.

## The Journal of Urology

**Has ultrasound influenced the therapy concept of blunt scrotal trauma?** Kratzik CH, Hainz A, Kuber W, et al. (CK, Dept. of Urology, University of Vienna Medical School, Vienna, Austria). *J Urol* 142:1243-1246, Nov. 1989

We present the ultrasonic diagnoses and treatment of 44 patients with blunt scrotal trauma (rupture of the testis, hematocele, intratesticular hematoma and hematoma of the scrotal layers). Purely intratesticular hematoma without any other accompanying injury also can be detected sonographically. When massive scrotal swelling is present ultrasound is valuable to determine the status of the underlying testis even if discrete fracture planes of the tunica cannot always be detected. To achieve best long-term results early surgical intervention should be performed in cases of rupture of the testicle and hematocele, while hematoma of the scrotal layers and purely intratesticular hematoma can be treated conservatively.

## Pediatrics

**Intraventricular hemorrhage in preterm infants: declining incidence in the 1980s.** Philip AGS, Allan WC, Tito AM, Wheeler LR (AGSP, Division of Neonatology, Maine Medical Center, 22 Bramhall St., Portland, ME 04102). *Pediatrics* 84(5):797-801, Nov. 1989

Ultrasound has been routinely used since late 1979 to diagnose periventricular-intraventricular hemorrhage in infants whose gestational age was 34 weeks or less. During the years 1980 to 1987 the ultrasound scans were interpreted by one person, and a steady decline in incidence of periventricular-intraventricular hemorrhage was observed. Both for infants of 34 weeks or less and for very low birth weight (<1500 g) infants, periventricular-intraventricular hemorrhage incidence decreased, respectively, from 34% and 39% in 1980 to 1981 to 19% and 25% in 1986 to 1987. This decrease was confined to true intraventricular hemorrhages, which decreased from 22% in 1980 to 1981 to 7% in 1986 to 1987 for infants of  $\leq 34$  weeks' gestation. These results were not influenced by a change in the distribution of birth weights or gestational ages of the infants evaluated nor by a change in the inborn to outborn ratio. The incidence of periventricular-intraventricular hemorrhage was lower in infants born by cesarean section than those delivered vaginally, but the decrease could not be attributed to an increased number of deliveries by cesarean section. Although there were undoubtedly changes in neonatal care during this time period, no planned intervention occurred. It was concluded that pharmacologic intervention studies must be interpreted with caution.

Reprinted by permission of PEDIATRICS © 1989.

## The Journal of Nuclear Medicine

**Human pharmacokinetics of samarium-153 EDTMP in metastatic cancer.** Singh A, Holmes RA, Farhangi M, et al. (RAH, Section of Nuclear Medicine, 2N-19, 1 Hospital Dr., University of Missouri Hospital and Clinics, Columbia, MO 65212). *J Nucl Med* 30:1814-1818, 1989

Samarium-153 ethylenediaminetetramethylene phosphonic acid ( $[^{153}\text{Sm}]\text{EDTMP}$ ) has been proposed to palliate pain resulting from osteoblastic metastatic bone cancer. Encouraging results in dogs with primary malignant bone cancer provided the catalysis for human biodistribution studies in five patients with metastatic skeletal carcinoma. The objective was to assess the preferential localization of  $[^{153}\text{Sm}]\text{EDTMP}$  in bony lesions and compare it to the  $^{99\text{m}}\text{Tc}$ -labeled phosphonates. Blood clearance of  $[^{153}\text{Sm}]\text{EDTMP}$  was rapid with minimal accumulation in nonosseous tissues. Both radiopharmaceuticals showed identical lesion uptake in 23 paired lesions ( $p > 0.05$ ). This indicates that the two radiopharmaceuticals concentrate in metastatic skeletal lesions by the same mechanism and since  $[^{153}\text{Sm}]\text{EDTMP}$  emits beta radiation it may be therapeutically useful in ameliorating metastatic bony cancer pain.

## Journal of Ultrasound in Medicine

**Fetal femur length to detect trisomy 21: a reappraisal.** LaFollette L, Filly RA, Anderson R, Golbus MS (RAF, Dept. of Diagnostic Radiology, L374, University of California, San Francisco, School of Medicine, San Francisco, CA 94143). *J Ultrasound Med* 8:657-660, Dec. 1989

An association between short femur length (FL) relative to the biparietal diameter (BPD) measured in the second trimester and the Down syndrome recently has been reported by Benacerraf et al (1987). Fetuses meeting an easily calculated criterion were stated to have a high probability for trisomy 21. We compared the biometric data from a selected group of 229 normal second trimester fetuses with 30 fetuses of similar gestational age with karyotype-proven trisomy 21. We found a substantial difference in femur lengths of normal fetuses in our population compared to that reported by Benacerraf et al. The reason for the difference is unclear. Further, we were unable to demonstrate a statistically discernible deviation of measured versus predicted femur lengths in the Down syndrome cohort employing either the formula recommended by Benacerraf et al or a formula calculated from our normal cohort.

Reprinted with permission by the American Institute of Ultrasound in Medicine.

## Journal of Computer Assisted Tomography

**Pulmonary infarction: CT appearance with pathologic correlation.** Balakrishnan J, Meziane MA, Siegelman SS, Fishman EK (SSS, Dept. of Radiology, Johns Hopkins Hospital, 600 N. Wolfe St., Baltimore, MD 21205). *J Comput Assist Tomogr* 13(6):941-945, Nov./Dec. 1989

The CT appearance of 12 proven pulmonary infarcts in 10 patients was analyzed and correlated with pathologic appearance. The diagnosis of pulmonary infarction was clinically suspected in only 2 of the 10 patients. A pleural based parenchymal density with convex, bulging borders and linear strands directed from the apex of the density toward the hilum was noted in each case ( $n = 12$ ). Other features were a truncated apex ( $n = 10$ ), a broad pleural base ( $n = 10$ ), and scattered areas of reduced attenuation within the lesions ( $n = 7$ ). This distinctive complex of findings on CT should raise a strong suspicion of pulmonary infarction.

**Gadolinium-DTPA enhancement of lung radiation fibrosis.** Werthmuller WC, Schiebler ML, Whaley RA, Mauro MA, McCartney WH (MLS, Dept. of Radiology, MRI CB 7515, University of North Carolina at Chapel Hill, Chapel Hill, NC 27599-7515). *J Comput Assist Tomogr* 13(6):946-948, Nov./Dec. 1989

Gadolinium-diethylenetriamine pentaacetic acid (DTPA) enhancement of radiation-induced apical pulmonary fibrosis was observed in two patients previously treated for breast cancer. In one case the fibrosis was biopsied twice, with no change in its CT appearance over 3 years. Gadolinium-DTPA may enhance benign apical fibrosis after radiation therapy and should not, in and of itself, be used as evidence of recurrent malignancy.

**Comparison of conventional and computed arthrotomography with MR imaging in the evaluation of the shoulder.** Habibian A, Stauffer A, Resnick D, et al. (DR, Dept. of Radiology, Veterans Administration Medical Center, 3350 La Jolla Village Dr., San Diego, CA 92161). *J Comput Assist Tomogr* 13(6):968-975, Nov./Dec. 1989

To compare conventional arthrography and computed arthrotomography (CAT) with magnetic resonance (MR) imaging in the evaluation of the shoulder, we studied 18 patients who underwent conventional double contrast arthrography and CAT, and T1-, balanced, and T2-weighted MR imaging. The arthrograms were independently reviewed by two of the authors and the MR images were independently reviewed by three other authors in a systematic fashion with the aid of a prewritten evaluation form. The findings were compared among reviewers and between imaging methods. We found MR comparable to conventional arthrography in the evaluation of the rotator cuff; however, MR also enabled evaluation of tendonitis, which could not be accomplished with conventional arthrography. Because of MR's superior soft tissue imaging capability, we were able to stage the impingement syndrome. Magnetic resonance also allowed evaluation of the glenoid labrum and capsuloligamentous structures and assessment of instability in a fashion similar to CAT. In most cases, information obtained from MR equaled or exceeded that obtained from conventional arthrography and CAT. With refinement in technique and increased experience, we believe that MR may replace arthrography in the evaluation of the shoulder.



## News

### Clinical Seminar in Diagnostic Ultrasound

The Western Pennsylvania Hospital is sponsoring the 4th annual Clinical Seminar in Diagnostic Ultrasound, March 23–25, at the Pittsburgh Hyatt Hotel, Pittsburgh. The focus of this year's seminar is obstetric and vascular sonography. Topics to be considered are Doppler physics, applications of color flow Doppler imaging, carotid and vertebral duplex sonography, deep abdominal and peripheral venous Doppler studies, use of Doppler sonography in the obstetric patient, abdominal and prostatic imaging, neurosonography, transvaginal ultrasound, gynecologic sonography, fetal imaging, and obstetric reporting and quality assurance. Course directors: Ellen B. Mendelson and Marcela Bohm-Velez. Guest faculty: P. N. Burns, Elias Kazam, B. S. Mahony, Laurence Needleman, B. A. Spirt, and D. A. Willard. Category 1 credit: 20 hr. Fee: physicians, \$425; technicians, residents, and fellows, \$225. Information: Dept. of Continuing Medical Education, The Western Pennsylvania Hospital, 4800 Friendship Ave., Pittsburgh, PA 15224; (412) 578-6926.

### Intervention Radiology Annual Meeting

The Society of Cardiovascular & Interventional Radiology (SCVIR) will hold its 15th annual meeting on interventional radiology at the Fontainebleau Hilton, Miami Beach, FL, March 26–29. Established and emerging procedures in interventional radiology will be reviewed. The course will include refresher courses, workshops, scientific sessions, works in progress, and live case demonstrations. Fee: SCVIR members, none; nonmembers, \$595; residents, \$250. Information: (703) 648-8953.

### Mammography for the General Radiologist

The Dept. of Radiology, Tufts–New England Medical Center, will sponsor the 1990 tutorials, Mammography for the General Radiologist, March 26–29, May 21–24, Sept. 10–13, and Oct. 22–25, in Boston. The course is designed to teach a practical approach to mammographic interpretation and needle localization. Enrollment in each session is limited to 25 participants. Category 1 credit: 28 hr. Fee: \$700. Information: Marc J. Homer, M.D., Box 388, Dept. of Radiology, New England Medical Center, 750 Washington St., Boston, MA 02111; (617) 956-0045.

### Diagnosis and Treatment of Neoplastic Disorders

The Oncology Center, the Johns Hopkins Medical Institutions, is sponsoring Diagnosis and Treatment of Neoplastic Disorders: Medi-

cal, Surgical, and Radiotherapeutic Aspects, March 29–30, at the Johns Hopkins Medical Institutions, Baltimore. Category 1 credit: 14.5 hr. Fee: physicians, \$250; non-Maryland physicians in training, \$100. Information: Francette Boling, Program Coordinator, The Johns Hopkins Medical Institutions, Office of Continuing Education, Turner Bldg., 720 Rutland Ave., Baltimore, MD 21205; (301) 955-2959.

### University of North Carolina Annual Radiology Symposium

The Dept. of Radiology and the Office of Continuing Medical Education, University of North Carolina, are sponsoring the 14th annual University of North Carolina Radiology Symposium, March 30–April 1, at the Mariner's Inn, Hilton Head, SC. The course will emphasize new techniques and state-of-the-art concepts and will concentrate on the role of contrast agents in MR imaging of the brain and body. Special focus sessions on AIDS and child abuse will be included. Enrollment will be limited to 60 participants. Course director: Mark L. Schiebler. Guest faculty: H. Goldstein, M. Nelson, D. D. Stark, J. Steidley, and R. A. Zimmerman. Category 1 credit: 14 hr (includes 2 hr credit on AIDS for Florida physicians). Fee: physicians, \$425; residents and fellows (letter required), \$200. Information: Office of Continuing Education, School of Medicine, CB# 7000, 231 MacNider Bldg., University of North Carolina, Chapel Hill, NC 27599-7000; (919) 962-1128.

### Postgraduate Course in Neuroradiology

The Post-Graduate Medical School, NYU Medical Center, is offering a postgraduate course on neuroradiology, including the head and neck, April 3–6, at the Grand Hyatt Hotel, New York City. The course will provide a comprehensive clinically oriented review and update of neuroradiology and head and neck radiology. Emphasis will be on the increasing application of MR imaging; however, review of the fundamentals of CT and CT myelography will be extensive. Intensive small group workshops will be included. Category 1 credit: 28 hr. Fee: \$560. Information: NYU Medical Center, Post-Graduate Medical School, 550 1st Ave., New York, NY 10016; (212) 340-5295.

### Annual Spring Roentgen Conference

The New Orleans Radiology Society will hold its 12th annual Spring Roentgen Conference—Diagnostic and Interventional Radiology: State-of-the-Art, 1990—at the Omni Royal Orleans Hotel, New Orleans, April 4–8. Practical discussion of all aspects of diagnostic and interventional radiology will be featured. In addition, the American

College of Radiology will provide updates on the business and legal aspects of practicing radiology in 1990. Program chairmen: Joseph J. Darlak and Abner M. Landry, Jr. Category 1 credit: 20 hr. Fee: physicians, \$450; residents (letter required), \$275. Information: Marty Landry, M.D., P.O. Box 19991, New Orleans, LA 70119.

### **Bone and Joint Radiology**

The Post-Graduate Medical School, NYU Medical Center, is offering a postgraduate course on bone and joint radiology, April 6–8, at the Grand Hyatt Hotel, New York City. The course will provide a comprehensive and practical review and update of recent developments in CT and MR imaging of the spine and extremities. Small group workshops will focus on problems encountered in everyday practice. Category 1 credit: 16 hr. Fee: \$320. Information: NYU Medical Center, Post-Graduate Medical School, 550 1st Ave., New York, NY 10016; (212) 340-5295.

### **MRI Workshop in Hawaii, 1990**

MRI Workshop in Hawaii, 1990 will be held April 8–13 at the Hyatt Waikoloa, Big Island, HI. Lecturers will review clinical disorders and discuss new and future developments in MR imaging in the mornings. Small focus groups will provide time for extended discussion in the late afternoons. Category 1 credit: 30 hr. Fee: \$550. Information: Susan Block, Dept. of Nuclear Medicine, Queen's Medical Center, 1301 Punchbowl St., Honolulu, HI 96813; (808) 547-4544.

### **OB/GYN Ultrasound for the 90's—The Next Generation**

Dartmouth-Hitchcock Medical Center, Hanover, NH, will host OB/GYN Ultrasound for the 90's—The Next Generation, April 28. The course is designed primarily for practicing sonographers and physicians involved in diagnostic ultrasound. The emphasis will be on state-of-the-art obstetric and gynecologic ultrasound. Topics will include complex fetal morphologic analysis, transvaginal examination, and interventional obstetrics. Category 1 credit: 7 hr. Fee: SDMS members, \$50; nonmembers, \$80. Information: Dennis Seguin, Dept. of Ultrasound, Dartmouth-Hitchcock Medical Center, Hanover, NH 03756; (603) 646-7434.

### **Blood Vessel Imaging Using Ultrasound Techniques**

Blood Vessel Imaging Using Ultrasound Techniques: Residential Course/Workshop will be held May 16–18 at the Dolphin Hotel, Southampton, Hampshire, United Kingdom. The course is designed to cover the basic principles of ultrasound techniques and provide a review of the current state of ultrasound arteriography and venography. The format will include lectures, demonstrations, and workshops. Specialists will discuss the application of ultrasound techniques in the assessment of cerebral, peripheral, abdominal, obstetric, and neonatal vasculature. Information: Mr. K. N. Humphries, Blood Vessel Imaging Course, 10 Swale Dr., Chandlers Ford, Hampshire SO5 3QY, United Kingdom; telephone: 0703 260003.

### **Clinical Magnetic Resonance Imaging**

The Dept. of Radiology, Yale University, School of Medicine, will offer Clinical Magnetic Resonance Imaging, May 21–23, at the Yale–

New Haven Hospital MRI Center. Topics will include neurologic, musculoskeletal, and abdominal applications of MR imaging. Enrollment is limited to 20 participants. Course director: Ruben Kier. Category 1 credit: 21.5 hr. Fee: physicians, \$550; residents, fellows, and technologists, \$400. Information: Office of Post-Graduate and Continuing Medical Education, Yale University, School of Medicine, 333 Cedar St., P. O. Box 3333, New Haven, CT 06510; (203) 785-4578.

### **Clinical MRI: 1990 Update**

Massachusetts General Hospital, Boston, is sponsoring Clinical MRI: 1990 Update, May 23–26. Category 1 credit: 28 hr. Fee: physicians, \$525; residents and fellows, \$425. Information: Dept. of Continuing Medical Education, Harvard Medical School, Boston, MA 02115; (617) 732-1525.

### **Emergency Radiology 1990**

Massachusetts General Hospital, Boston, is sponsoring the annual Harvard Medical School postgraduate course Emergency Radiology 1990: Introduction to Emergency Imaging, CT and MR of Trauma, Three-Dimensional Trauma Imaging, May 29–June 1. Fee: physicians, \$500; residents and fellows, \$400. Information: Dept. of Continuing Medical Education, Harvard Medical School, Boston, MA 02115; (617) 732-1525.

### **Advanced Techniques in MRI**

The Dept. of Radiology, Duke University, Medical Center, Durham, NC, will present Advanced Techniques in MRI, June 16–22, at Kiawah Island, SC. The course, which is supported in part by General Electric Medical Systems, Milwaukee, WI, is intended for physicians, physicists, engineers, and technologists who are seeking a fundamental understanding of the technology of MR. The course begins with the basic principles of MR and continues to descriptions of high-speed imaging techniques, cardiac imaging, and spectroscopy. Particular attention will be given to a description of the physical basis of MR and the mechanisms by which it is exploited. Clinical examples will be included when appropriate. Course coordinator: G. Allan Johnson. Information: G. Allan Johnson, Ph.D., Dept. of Radiology, Box 3302, Duke University, Medical Center, Durham, NC 27710; (919) 660-2711, ext. 4354.

### **Diagnostic Radiology**

The Dept. of Radiology, Bowman Gray School of Medicine, will hold its 7th annual summer continuing education meeting at the Kingston Plantation, Myrtle Beach, NC, June 17–22. A variety of topics in diagnostic radiology will be covered. Category 1 credit: 20 hr. Information: Pat Rice, Dept. of Radiology, Bowman Gray School of Medicine, Winston-Salem, NC 27103; (919) 748-2470.

### **Pediatric Nuclear Medicine Categorical Seminar**

The Pediatric Nuclear Medicine Club of the Society of Nuclear Medicine is sponsoring a 1-day course at the Washington Convention Center, Washington, DC, June 18. The course is designed to familiarize the practicing radiologist with the technical aspects of pediatric nuclear medicine procedures and their indications and interpretation. Course director: Aslam R. Siddiqui. Fee: through May 17, \$80; after May 17, \$100. Information: Society of Nuclear Medicine, 136 Madison Ave., New York, NY 10016-6760; (212) 889-0717.

## Liver Imaging

Massachusetts General Hospital and Harvard Medical School will present **Liver Imaging: Present and Future Trends in MRI, CT, US**, June 25–27, at the Westin Hotel, Copley Place, Boston. This international, interdisciplinary symposium will address advances in imaging technology that affect clinical management of liver disease. The main focus will be on noninvasive techniques, such as MR, CT, and sonography. The faculty will present up-to-date results of new clinical imaging techniques. Emphasis will be on efficacy for detection of lesions, comparative results with the various techniques, ultrafast MR imaging and CT scanning, new contrast agents, MR spectroscopy, and vascular flow imaging. Course directors: Joseph T. Ferrucci and David D. Stark. Category 1 credit: 21 hr. Fee: physicians, \$450; residents and fellows, \$350. Information: Dept. of Continuing Medical Education, Harvard Medical School, Boston, MA 02115; (617) 732-1525.

## Advances in Radiation Oncology Physics

The American Association of Physicists in Medicine (AAPM) Summer School Meeting, **Advances in Radiation Oncology Physics: Dosimetry, Treatment Planning, Brachytherapy**, will be held at the University of Kansas, Lawrence, KS, July 16–20. This intermediate-level course will present the state of the art and will include such subjects as equipment evaluation, calibration and dosimetry protocols, computerized treatment planning, quality assurance, teletherapy, and brachytherapy. Special emphasis will be given to advances in three-dimensional treatment planning, on-line imaging, and remote afterloaders in brachytherapy and to the various AAPM task groups for radiation oncology physics. Program directors: James A. Purdy and Larry D. Simpson. Information: American Association of Physicists in Medicine, 335 E. 45th St., New York, NY 10017; (212) 661-9404.

## Musculoskeletal Imaging

The Dept. of Radiology, Hoag Memorial Hospital-Presbyterian, will present **Musculoskeletal Imaging**, July 23–25, at the Ritz Carlton Resort Hotel, Laguna Niguel, CA. The course will concentrate on current whole-body musculoskeletal applications and clinical correlation. Program director: Joel Lipman. Category 1 credit: 14.75 hr. Fee: physicians, \$350; residents, fellows, and technologists, \$200. Information: Dawne Ryals, Ryals & Associates, P. O. Box 1925, Roswell, GA 30077-1925; telephone: (404) 641-9773; fax: (404) 552-9859.

## Symposium on Magnetic Resonance Imaging

The Dept. of Radiology, Hoag Memorial Hospital-Presbyterian, will present the 4th annual Symposium on Magnetic Resonance Imaging, July 26–29, at the Ritz Carlton Resort Hotel, Laguna Niguel, CA. The course is designed to provide clinicians and radiologists with an update on the current use of MR and an introduction to newer applications. Program director: Michael Brant-Zawadzki. Category 1 credit: 22 hr. Fee: physicians, \$425; residents, fellows, and technologists, \$300. Information: Dawne Ryals, Ryals & Associates, P. O. Box 1925, Roswell, GA 30077-1925; telephone: (404) 641-9773; fax: (404) 552-9859.

## Annual Northern Imaging Meeting

The 3rd annual Northern Imaging Meeting will be held Aug. 4–8 at Molson Lake Lodge, which is 300 miles north of Winnipeg, Manitoba.

The course will review topics in sonography, CT, and interventional radiology. Four lectures will be given each day. Registration is limited to 30 participants. Registration deadline is April 15. Faculty: George Leopold, R. B. Jeffrey, J. W. Charboneau, and E. A. Lyons. Category 1 credit: 12 hr. information: (701) 282-7154.

## Interventional Radiology/2nd Marmara Medical Days

Interventional Radiology/2nd Marmara Medical Days will be held Sept. 19–21 at Marmara University, Medical School, Haydarpaşa-Istanbul, Turkey. Guest speakers: Y. S. Erozan, L. Forsberg, H. H. Holm, K. Ivancev, M. Y. Kellett, F. K. Mostofi, and G. Vallancien. Free communications will be highly appreciated; for details apply before April 1. Information: Atif Akdas, M.D., Marmara University, Medical School, Haydarpaşa-Istanbul, Turkey; fax: (1) 3380277.

## American Lithotripsy Society Annual Meeting

The American Lithotripsy Society will hold its 4th annual meeting at the Sheraton Harbor Island Hotel, San Diego, CA, Oct. 11–14. The meeting will include presentations of abstracts, poster sessions, and a trade exhibition. Deadline for receipt of abstracts is March 30. Information: American Lithotripsy Society, 13 Elm St., Manchester, MA 09144; telephone: (508) 526-8330; fax: (508) 526-4018.

## The American Board of Radiology Examinations

Written examinations for the American Board of Radiology (ABR) are scheduled for Sept. 27–28. Oral examinations will be held at the Executive West Hotel in Louisville, KY, June 4–8. The ABR will accept applications for admission to the examinations after July 1, but not later than Sept. 30, in the year *preceding* the year in which the examination is to be taken. For application forms and further information: Office of the Secretary, The American Board of Radiology, 300 Park, Ste. 440, Birmingham, MI 48009.

## Meeting and Course Review

For the reader's convenience, a summary of upcoming meetings and courses is provided. Detailed listings are given in the *AJR* issue given in parentheses.

**Visiting Fellowships in Radiology at MGH**, times arranged, Boston (April 1989)

**Biliary Lithotripsy Visiting Fellowships**, times arranged, Philadelphia (April 1989)

**Visiting Fellowship in Interventional Radiology**, times arranged, Baltimore (Sept 1989)

**Visiting Fellowships at UCSF**, times arranged, San Francisco (Sept 1989)

**Preceptorships in Transrectal Ultrasound of the Prostate**, Ann Arbor, MI (Sept 1989)

**Sun Valley Imaging**, Feb. 24–March 4, Sun Valley, ID (Nov 1989)

**LSU Seminar at Aspen**, Feb. 25–March 2, Aspen, CO (Dec 1989)

**Neuroradiology and Body Imaging**, Feb. 26–March 2, Acapulco, Mexico (Nov 1989)

**Neuroradiology at Snowbird**, Feb. 26–March 2, Snowbird, UT (Feb)

**Interventional Radiology in Cardiovascular Pathology**, Feb. 28–March 2, Toulouse, France (Aug 1989)

**Philadelphia Symposium on Biliary Lithotripsy**, March 1–3, Philadelphia (Nov 1989)

**Fellowships in Biliary Lithotripsy**, March 1-3, May 3-5, and June 7-9, Baltimore, MD (Dec 1989)  
**Advanced Seminar in Diagnostic Imaging**, March 2-4, Laguna Niguel, CA (Feb)  
**Skeletal Symposium**, March 5-9, Sun Valley, ID (Dec 1989)  
**Postgraduate MR Imaging**, March 5-9, Coronado (San Diego), CA (Feb)  
**Differential Diagnosis in Radiology**, March 9-11, Ann Arbor, MI (Jan)  
**Current Topics in Diagnostic Imaging**, March 12-16, Cerromar Beach, Puerto Rico (Nov 1989)  
**Obstetrics and Gynecology**, March 12-16 and April 16-20, Philadelphia (Jan)  
**MR Imaging: Principles, Methodology, and Applications**, March 12-16, Grindelwald, Switzerland (Feb)  
**Ultrasound 1990**, March 13-16, Boston (Nov 1989)  
**Doppler Velocimetry in Clinical Obstetrics**, March 14 and April 25, Baltimore (Nov 1989)  
**Pediatric Radiology 1990**, March 15-17, Philadelphia (Dec 1989)  
**Drugs, Behavior, and the Brain: Advances in PET and SPECT Imaging of the Brain**, March 15-17, Baltimore (Feb)  
**Basic Concepts of Swallowing and Swallowing Disorders**, March 21, Baltimore (Nov 1989)  
**Symposium on Dysphagia III**, March 22-23, Baltimore (Nov 1989)  
**Yale Symposium on Duplex and Doppler Ultrasound**, March 22-23, New Haven, CT (Dec 1989)  
**Abdominal Ultrasound**, March 26-29 and June 11-14, Philadelphia, (Jan)  
**Prostate Ultrasound**, March 30 and June 15, Philadelphia (Jan)  
**Skeletal Radiology 1990**, March 31-April 5, Scottsdale, AZ (Nov 1989)  
**Joint American-European Course in Davos, Switzerland**, April 1-7, Davos (Jan)  
**Society of Computed Body Tomography Annual Course**, April 2-6, Palm Springs, CA (Nov 1989)  
**Prenatal Diagnosis of Congenital Anomalies**, April 2-6, Sonora Bay, Mexico (Feb)  
**National Council on Radiation Protection and Measurements Annual Meeting**, April 4-5, Washington, DC (Nov 1989)  
**Automated Percutaneous Discectomy Workshops**, April 7-8, Washington, DC (Sept 1989)  
**Radiation Research Society Annual Meeting**, April 7-12, New Orleans (Nov 1989)  
**Ultrasound in Obstetrics and Gynecology**, April 8-10, Ann Arbor, MI (Jan)  
**Advanced Imaging of the Musculoskeletal System**, April 14-15, Coronado (San Diego), CA (Feb)  
**San Diego Residents Radiology Review Course**, April 15-20, Coronado (San Diego), CA (Feb)  
**Introduction to Interventional Radiology**, April 21, Coronado (San Diego), CA (Feb)  
**Clinical Nuclear Medicine 1990**, April 23-26, Cambridge, MA (Nov 1989)  
**International Symposium on Diagnostic Imaging**, April 23-27, Barcelona, Spain (Dec 1989)  
**Radiation Oncology Clinical Research Seminar**, April 26-28, Gainesville, FL (Jan)

**American Association of Physicists in Medicine Spring Seminar**, April 27-29, San Diego, CA (Dec 1989)  
**Spring Diagnostic Ultrasound Conference**, April 27-29, Los Angeles (Feb)  
**Radiology Review Course**, April 29-May 4, Miami, FL (Feb)  
**Mid-Pacific Diagnostic Ultrasound Conference**, May 1-5, Kaula, HI (Feb)  
**Advances in CT and MRI**, May 2-4, Ann Arbor, MI (Feb)  
**Symposium in Diagnostic Ultrasound**, May 4-6, New York City (Feb)  
**Congress of the European Federation of Societies for Ultrasound in Medicine and Biology**, May 6-11, Jerusalem, Israel (May 1989)  
**Biliary Calculus Disease**, May 7-9, Boston (Nov 1989)  
**Diagnostic Imaging in Musculo-Skeletal Radiology**, May 10-11, Glasgow, Scotland (Dec 1989)  
**Cardiovascular and Interventional Radiology**, May 13-18, Brussels, Belgium (Dec 1989)  
**27th Congress of the European Society of Paediatric Radiology**, May 14-18, Munich, West Germany (Jan)  
**Musculoskeletal MRI for Orthopedists and Radiologists**, May 28-June 1, Sonesta Beach Hotel (Dec 1989)  
**Italian Society of Radiology and Nuclear Medicine**, May 30-June 3, 1990, Turin, Italy (Nov 1989)  
**American Society of Emergency Radiology Annual Meeting**, June 2, Boston (Feb)  
**American College of Medical Physics Annual Meeting**, June 7-10, Austin, TX (Dec 1989)  
**Radiology in Scandinavia and the Soviet Union**, June 16-30, Copenhagen, Malmö, Stockholm, Helsinki, and Leningrad (Feb)  
**Nuclear Medicine Technology Certification Examinations**, June 23 and Sept. 22; application deadlines, April 21 and July 21, respectively (Nov 1989)  
**International Course in Cardiovascular Interventional Radiology**, July 11-13, Leeds, United Kingdom (Dec 1989)  
**American Association of Physicists in Medicine Annual Meeting**, July 22-26, St. Louis (Feb)  
**Copenhagen Symposium on Uroradiology**, Aug. 27-30, Herlev, Denmark (Feb)  
**European Society of Head and Neck Radiology Annual Meeting**, Sept. 12-15, Brescia (Lake of Garda), Italy (Feb)  
**International Conference on Ultrasound Angiography**, Sept. 25-28, London, United Kingdom (Feb)

*AJR* carries announcements of courses, symposia, and meetings of interest to its readers if received a minimum of 5 months before the event. There is no charge; receipt of items by the *AJR* Editorial Office is not acknowledged. Submit items for publication typed double-spaced. Provide title, date, location, brief description, sponsor, course directors, fees, category I credit, and address and telephone number for additional information. Faculty from the host institution will not be listed. Guest faculty names will appear only if initials are provided. Mail news items to *AJR* Editorial Office, 2223 Avenida de la Playa, Suite 200, La Jolla, CA 92037-3218.

# **33RD Annual Meeting of The Society for Pediatric Radiology, The Westin Hotel, Fountain Square, Cincinnati, Ohio, April 19-22, 1990**

The members, officers, and program committee of The Society for Pediatric Radiology (SPR) proudly announce the 33rd annual meeting of The SPR in Cincinnati, OH, April 19-22, 1990. The meeting schedule is listed below. Meeting registration and hotel reservation request forms are printed on the reverse page. The meeting registration form should be mailed directly to Lynne Tiras, International Meeting Managers, 4550 Post Oak Place, Suite 248, Houston, Texas 77027. The hotel reservation request form should be sent directly to The Westin Hotel, Fountain Square, Cincinnati, OH 45202. Further information about the meeting and registration can be obtained from Carol M. Rumack, M.D., Secretary, The Society for Pediatric Radiology, Department of Radiology, University of Colorado Health Sciences Center, 4200 East Ninth Avenue, Box A030, Denver, CO 80262; (303) 270-4512.

## **Wednesday, April 18, 1990**

6:00-9:00 p.m. Registration

## **Thursday, April 19, 1990**

7:00 a.m. Continental Breakfast  
Registration  
8:00-12:30 p.m. Symposium: Congenital Heart Disease: Present and Future Considerations  
12:30 p.m. Lunch  
2:00-5:00 p.m. Scientific Papers  
5:00 p.m. Adjourn  
6:30 p.m. Welcome Reception  
Cincinnati Art Museum

## **Friday, April 20, 1990**

7:30 a.m. Continental Breakfast  
8:00 a.m. Pioneer's Session  
8:15-9:50 a.m. Scientific Papers of Pioneer's Session  
9:50-11:00 a.m. Business Meeting  
11:00-12:30 p.m. Short Papers  
12:30 p.m. Adjourn

## **Saturday, April 21, 1990**

7:30 a.m. Continental Breakfast  
8:00-12:00 Noon Scientific Papers  
12:00 Noon Lunch  
1:00-4:00 p.m. Scientific Papers  
4:00 p.m. Neuhauser Lecture  
5:00 p.m. Presentation of 1990 Awards of The Society for Pediatric Radiology  
6:00 p.m. Adjourn  
6:30 p.m. Reception and Annual Dinner  
The Westin Hotel Ballroom

## **Sunday, April 22, 1990**

7:30 a.m. Continental Breakfast  
8:00-9:30 a.m. Film Reading Panel  
9:30-10:30 a.m. Funded Research in Pediatric Radiology: Why and How?  
10:30-1:00 p.m. Short Papers  
1:00 p.m. Adjourn

# MEETING REGISTRATION FORM

Name \_\_\_\_\_  
Last First M.I.

City \_\_\_\_\_ State \_\_\_\_\_ Zip \_\_\_\_\_

SPR Member \_\_\_\_\_

Yes No Guest's Name \_\_\_\_\_

\$100.00	SPR Member (active, associate, emeritus), ESPR, ASPI
\$ 50.00	Society Member Guest
\$250.00	Physicians (Non-Members SPR)
No Fee	Radiologist-In-Training, Resident or Fellow (with verification), and Accompanying Person
\$250.00	Non-Society Member
\$ 75.00	Non-Society Member Accompanying Person

# Hotel Reservation Form

Name \_\_\_\_\_ Single \_\_\_\_\_  
Last First M.I.

City, State, Zip \_\_\_\_\_ Phone \_\_\_\_\_

Arrive \_\_\_\_\_ Depart \_\_\_\_\_ Sharing Room With \_\_\_\_\_

Credit Card (Circle One)      AMEX      VISA      M/C      DINER

Card # \_\_\_\_\_ Expiration Date \_\_\_\_\_

Name on Card \_\_\_\_\_

Signature\_\_\_\_\_

Please fill out and mail this form to The Westin Hotel, Fountain Square, Cincinnati, Ohio 45202  
To guarantee your reservation we require: First and Last Nights Deposit by Credit Card, Check or Money Order  
Deposit refundable if reservation is cancelled 48 hours prior to arrival.



# Invitation to the 1990 American Roentgen Ray Society Meeting in Washington, DC, May 13-18, 1990

I am pleased to extend an invitation to all radiologists to attend the 90th annual meeting of the American Roentgen Ray Society in Washington, DC, May 13-18, 1990. In keeping with the ARRS tradition, outstanding scientific and social programs will be provided.

The excitement of a meeting set in Washington, DC, requires no further description. The opportunity for busy radiologists to attend a major national meeting while enjoying all that Washington, DC, has to offer is ideal.

The scientific program, instructional courses, and categorical course are certain to be interesting and informative (see schedule below).

## Scientific Program

Two hundred scientific papers have been selected from more than 400 abstracts. Scientific sessions will be devoted to all major body systems, angiography, interventional techniques, sonography, and mammography, as well as technologies. Special emphasis has been placed on discussion of new developments.

The innovative and extremely well-received Friday morning minisymposium is entitled "Musculoskeletal Radiology Update 1990." An outstanding faculty has been assembled for what I am sure will be a very stimulating program.

## Instructional Courses

Joseph T. Ferrucci, Chairman of the Instructional Course Committee, has put together 60 instructional courses. Faculty members have been drawn from across the entire country. A superlative educational experience is anticipated, and advance registration is recommended.

## Categorical Course

An extraordinary categorical course on cardiovascular-interventional radiology has been fashioned. The course covers all aspects of the field, including equipment and principles of diagnosis. This course is certain to be popular, and advance registration is advised.

## Summary of 1990 American Roentgen Ray Society Meeting

Sunday May 13	Monday May 14	Tuesday May 15	Wednesday May 16	Thursday May 17	Friday May 18
	8-9:30 Instructional courses	8-9:30 Instructional courses	8-9:30 Instructional courses	8-9:30 Instructional courses	8-10 Symposium: musculoskeletal imaging update
10-12:30 Categorical course: cardiovascular- interventional radiology	10-10:30 Opening cere- monies				
	10:30-12:30 Scientific programs	10-12:30 Scientific programs	10-12:30 Scientific programs	10-12:30 Scientific programs	10:30-12:30 Symposium: musculoskeletal imaging update
2-3 Categorical course: cardiovascular- interventional radiology	1:30-3:15 Categorical course: cardiovascular- interventional radiology	1:30-3:30 Scientific programs	1:30-3:30 Caldwell lecture and award session	1:30-3:30 Scientific programs	
3:30-5 Categorical course: cardiovascular- interventional radiology	3:45-5:15 Instructional courses and cate- gorical course: cardiovascular- interventional radiology	4-5:45 Instructional courses and cate- gorical course: cardiovascular interventional radiology	4-5:30 Instructional courses and cate- gorical course: cardiovascular- interventional radiology	4-5:45 Instructional courses and cate- gorical course: cardiovascular- interventional radiology	

**Scientific Exhibits**

The 220 scientific exhibits coordinated by John Madewell will cover the entire breadth of the field of diagnostic radiology. The technical exhibits will be integrated among the scientific exhibits to enhance the interaction of the attendees with our technical exhibitors.

**Caldwell Lecture**

U.S. Supreme Court Justice Sandra Day O'Connor has agreed to present the Caldwell Lecture at the 1989 meeting. The title of Justice O'Connor's presentation will be "Our Federal Courts." This promises to be one of the highlights of the meeting.

**Social Events**

Washington, DC, offers an unlimited number of diversions, and Abner M. Landry, Jr., Chairman of the Annual Meeting Committee, has engaged a Washington DC-based tour consultant to plan a variety of outstanding tours. The annual golf and tennis tournaments for attendees and their companions are scheduled for Monday. The traditional cocktail party given by the society in the exhibit area for all registrants will be Tuesday evening and will provide a convenient meeting place before an evening on the town.

This promises to be a truly outstanding event in exceptional surroundings. I hope you will be able to accept our invitation. Plan now to attend.

M. Paul Capp  
President-Elect, ARRS

# 1990 ARRS Meeting Summary, May 13–18, 1990 Washington, DC

A comprehensive description of the meeting, including the instructional courses, categorical course, and the Friday symposium, appears in this issue of the *AJR*. Meeting and registration forms can be found in the February and March issues. These may be photocopied.

## Accreditation

All courses and scientific sessions carry AMA Category 1 credit on an hour-for-hour basis.

## Meeting Format

**Scientific Program.** Sessions will be grouped in parallel sessions so that registrants may choose topics related to their interests. A total of 189 scientific papers will be presented, Monday–Thursday, May 14–17. In addition, on Wednesday, May 16, the afternoon session will feature award papers and the Caldwell Lecture, which will be delivered by U.S. Supreme Court Justice Sandra Day O'Connor. (Special Note: Companions and spouses of registered meeting attendees are welcome to attend the Caldwell Lecture presented by Justice O'Connor.) On Friday, May 18, there will be a special 4-hr symposium, Current Topics in Musculoskeletal Imaging.

**Categorical Course in Cardiovascular-Interventional Radiology.** This 15.5-hr course will be Sunday–Thursday.

**Luncheon Sessions.** Registrants may enroll in special luncheon sessions, Monday–Thursday. A box lunch will be provided.

## Exhibits

**Scientific and Technical Exhibits and Case of the Day Presentations** will be presented in the exhibit hall of the Sheraton Washington Hotel, Monday–Thursday, May 14–17. The Case of the Day will be presented by Margaret Stull of Georgetown University Hospital, Washington, DC.

## Local Activities

**General Reception.** Tuesday evening, May 15, for all registrants.

**Golf Tournament.** Monday, May 14, Kenwood Country Club. Transportation leaves the hotel at 11 a.m.; shotgun start is at 12:30 p.m.

**Men's and Women's Tennis Tournaments.** Monday, May 14, at the Kenwood Country Club.

**Local Tours.** See February issue of the *AJR* for a description of the activities and registration forms.

## Meeting Registration

Preregistration will be accepted until April 27. There will be on-site registration. Official badges and program books will be available at the registration desk, Sheraton Washington Hotel. No confirmations will be mailed.

## Course Registration

Register early—enrollment is limited. List first, second, and third choices for each period. Also, indicate whether you wish to take the categorical course. Deadline for registration by mail is April 27. All ticket orders will be filled according to postmarked date. Course tickets will *not* be mailed. Tickets will be available on and after Sunday, May 13 (after 1 p.m.), at the ARRS registration desk in the Sheraton Washington Hotel. There will be on-site registration for courses not already filled.

## Hotel Registration

Reservations are handled by the ARRS Housing Bureau, Sheraton Washington Hotel, Attn: Reservations Office, 2660 Woodley Rd., Washington, DC 20008. These must be received by April 13. Make check payable to Sheraton Washington Hotel. See reservation form in February or March *AJR* for prices and complete instructions.

## Fees

Meeting:

ARRS members and resident members	No fee
Nonmembers	\$250
Nonmember physicians in training (with verification)	25
Categorical course (all who attend)	75
Luncheon sessions/each	12
Golf tournament	75
Tennis tournaments	50
Local tours	20–75

## Cancellations and Fee Refunds (Excluding Hotel Fees)

Fees will be refunded only if cancellation is received by April 27. Send to American Roentgen Ray Society, 1891 Preston White Drive, Reston, VA 22091.

## Transportation Discounts

United Airlines is offering discounts, up to 40%, on airfares. Call (800) 521-4041 and mention ARRS account number 0053D.

Hertz Rent A Car is offering special rates on car rentals. Call (800) 772-3773 and mention that you are attending the American Roentgen Ray Society annual meeting.

# 1990 American Roentgen Ray Society Instructional Courses and Symposium

Joseph T. Ferrucci, Director

Sixty Instructional Courses will be presented during the 90th annual meeting of the American Roentgen Ray Society (ARRS) beginning Monday, May 14, and continuing through Thursday, May 17. Each of the Instructional Courses listed on the next page will be 90 min long. In addition, there will be a week-long Categorical Course in Cardiovascular-Interventional Radiology and a half-day Symposium, Current Topics in Musculoskeletal Imaging.

The Categorical Course in Cardiovascular-Interventional Radiology will have 15.5 hr of instruction and will begin on Sunday, May 13, and conclude on Thursday, May 17. The Symposium, Current Topics in Musculoskeletal Imaging, will be on Friday, May 18, from 8 a.m. to 12 noon. All courses carry Category 1 credit on an hour-to-hour basis.

## Registration Information

To register for courses, complete the meeting registration form in this section and mail promptly. Tickets also will be available at the Instruction Course Registration Desk, Sheraton Washington Hotel for courses that have not been sold out. All courses will take place in the headquarters' hotel.

After reviewing the course list, select three for each morning and afternoon session. Write the course number and name of the first instructor on the registration form. Please note that the -01 residents'-masters' tutorials are intended primarily for residents and that attendance will be limited.

All who register for the Categorical Course in Cardiovascular-Interventional Radiology (including ARRS members) must pay a fee of \$75 and must take the entire series of classes. The Categorical Course totals 15.5 hr of instruction and includes a syllabus.

## Course Schedule

### Sunday, May 13, through Thursday, May 17

The Categorical Course in Cardiovascular-Interventional Radiology will have 15.5 hr of instruction over 5 days. Topics and instructors are listed on p. 678.

### Monday, May 14, through Friday, May 18

A total of 60 courses will be offered (see next page) plus a Symposium, Current Topics in Musculoskeletal Radiology.

### Symposium: Current Topics in Musculoskeletal Imaging Friday, May 18, 1990, 8:00 a.m. to 12:00 p.m.

Time	Topic (Presenter)
8:00 a.m.	Controversies in the evaluation of osteoporosis ( <i>Rosenthal D</i> )
8:30 a.m.	The role of MRI in the evaluation of musculoskeletal neoplasms ( <i>Braunstein E</i> )
9:00 a.m.	Imaging of spinal trauma ( <i>Daffner R</i> )
9:30 a.m.	The role of MRI in shoulder imaging ( <i>Brahme S</i> )
10:00 a.m.	The elbow ( <i>Pitt MJ</i> )
10:30 a.m.	MRI of the knee ( <i>Dalinka M</i> )
11:00 a.m.	The role of MRI in hip imaging ( <i>Bassett L</i> )
11:30 a.m.	Imaging of the foot and ankle with emphasis on MRI ( <i>Forrester DM</i> )

Note.—There is no fee for this symposium. However, to facilitate planning, please register on the meeting registration form.

## ACR Luncheon Presentations on Socioeconomics of Radiology

A series of luncheon presentations on the socioeconomic of radiology will be arranged by the American College of Radiology (ACR). A box lunch will be provided. The presentations do not conflict with other elements of the program. Advance registration is required. Cost per session is \$12.

### Date, Topic, Speaker

Monday, May 14: Status and Update on RVS, James M. Moorefield, M.D.  
 Tuesday, May 15: Standard Setting Update, Jerome H. Shapiro, M.D.  
 Wednesday, May 16: Contrast Media, Mark M. Mishkin, M.D.  
 Thursday, May 17: Governmental Issues, Otha W. Linton

## American Roentgen Ray Society Instructional Courses: May 14–May 17, 1990

Topic	Monday	Tuesday	Wednesday	Thursday
Morning (all sessions being at 8:00 a.m.)				
Residents'-masters' tutorial: update & personal Obstetrics/gynecology	101. GI radiology: simplify, multiply. <i>Carlson HC</i> 102. Update on the placenta. <i>Sanders R</i>	201. Perspectives on obstetrical sonography. <i>Leopold G</i> 202. Fetal measurements for estimating age and growth. <i>Hadlock FP</i>	301. Neuroradiology: Present status of MR vs CT. <i>Taveras JM</i> 302. Transvaginal sonography in obstetrics and gynecology. <i>Fleischer AC, Rao B, Kepple DM</i>	401. The hip as a mirror of pediatric bone disease. <i>Poznanski AK</i> 402. Second and third trimester fetal anomalies. <i>Kurtz A</i>
Chest	103. Practical approach to intensive care radiology. <i>Spinn PW, Goodman L</i>	203. Lung tumor staging. <i>Pugatch R</i>	303. Pulmonary infections and their complications. <i>Choplin RH</i>	403. Advances in thoracic radiology: high resolution CT and MRI. <i>McLoud TC</i>
Gastrointestinal	104. CT-pathologic correlations: pancreatitis, liver tumors. <i>Gedgaudas-McCles RK, Ros PR</i>	204. Colon cancer detection. <i>Gelfand D, Laufer I</i>	304. Radiologic pathologic correlations: gallbladder, intestinal tumors. <i>Lichtenstein J, Olmsted W</i>	404. Current approaches to biliary tract disease. <i>Zeman R</i>
Radiologic practice/miscellaneous	105. Pointers on scientific manuscript preparation. <i>Berk RN, Levene M, Hilton S, Spiller KL</i>	205. The battle over "turf": who has it and how to get it. <i>Hillman B</i>	305. Functional aspects of the radiology department. <i>Janower ML</i>	405. The future of digital radiology: technical & clinical considerations. <i>Ovitt TW, Hunter T</i>
Neuroradiology	106. Gadolinium enhanced MRI of the brain and spine. <i>Hassan AN</i>	206. AIDS related CNS disease. <i>Davis DO</i>	306. Craniocerebral trauma. <i>Kieffer SA, Cacayorin ED</i>	406. CT of the spine. <i>Helms CA</i>
Pediatrics/nuclear medicine	107. Nuclear cardiology in clinical practice. <i>Thrall JH</i>	207. Imaging of childhood infection. <i>Woods BP</i>	307. Brain SPECT imaging. <i>Holman L</i>	407. Pediatric abdominal trauma: current concepts. <i>Kushner DC, Kuhn J, Taylor G</i>
Genitourinary	108. Imaging renal infections. <i>McCannan BL</i>	208. CT and MRI of the kidney and adrenal. <i>Newhouse J, Amis S</i>	308. Low osmolar contrast agents. <i>Mishkin MM, Wolf G</i>	408. CT/MRI of the retroperitoneum. <i>Lee JKT, Heiken J</i>
Thorax/abdomen I	109. Duplex and color flow Doppler of the abdomen, pelvis, and extremities. <i>Merritt CB</i>	209. CT and US guided biopsies: practical approaches, pitfalls, and new techniques. <i>Charboneau JW, Reading C</i>	309. CT of the acute abdomen. <i>Stanley RJ, Wittenberg J</i>	409. Imaging in thoracoabdominal trauma. <i>Mirvis SE, Foley WD</i>
Musculoskeletal	110. The analytic approach to the film (an imaging discipline). <i>Edeiken J, Jacobson HG</i>	210. Imaging the acutely injured cervical spine. <i>Harris JH, Swischuk LE</i>	310. Criteria for diagnosis of bone tumors. <i>Norman A</i>	410. Arthropathies: radiologic pathologic correlations. <i>Madewell JE</i>
Afternoon (all sessions begin at 4:00 p.m.)				
Head and neck	111. MR of the head and neck. <i>Lufkin RB, Jabour B</i>	211. Endocrine imaging—update. <i>Doppman J</i>	311. Imaging of the sinonasal cavities. <i>Som P</i>	411. MR of the joints, including temporomandibular. <i>Harms S</i>
New technology	112. Biliary lithotripsy. <i>Ferrucci JT, Burhenne HJ</i>	212. Percutaneous laser angioplasty. <i>McCowan T, Cragg A, Ferris EJ</i>	312. Computer assisted 3-D imaging: state of the art. <i>Fishman EK, Ney FG</i>	412. PET scanning. <i>Hubner KF, Besozzi MC, Buonocore E</i>
Breast	113. How to evaluate the success of a mammography practice. <i>Sickles EA</i>	213. Screening mammography. <i>McLelland R</i>	313. Screen-film mammography: equipment, technique and interpretation. <i>Feig SA</i>	413. Analyzing the mammogram. <i>Kopans DB</i>
Magnetic resonance imaging	114. MRI of the spine. <i>Ramsey RG</i>	214. MRI of the male and female pelvis. <i>Fritzsche PJ, McCarthy S</i>	314. MRI contrast agents. <i>Saini S, Hahn PF</i>	414. Practical aspects of MR image interpretation. <i>Stark DD, Bradley WG</i>
Thorax/abdomen II	115. Ultrafast CT scanning. <i>Sheedy P</i>	215. Interventional thoracic radiology. <i>Barth KH, Westcott JL</i>	315. Biliary calculus disease: interventional management. <i>Mueller PR, Teplick SL</i>	415. Imaging of swallowing disorders. <i>Jones B</i>

## **Categorical Course in Cardiovascular and Interventional Radiology**

### **American Roentgen Ray Society 90th Annual Meeting**

**May 13–18, 1990, Sheraton Washington Hotel, Washington, DC**

*Course Director, William J. Casarella, M.D.  
Course Co-Director, Charles B. Higgins, M.D.*

#### **Sunday, May 13**

10:00–10:30	Basic Physical Principles of MRI in the Cardiovascular System ( <i>Sprawls</i> )
10:30–11:00	MRI of the Great Vessels ( <i>Dinsmore</i> )
11:00–11:30	MRI of Pericardium, Cardiac Masses, and Cardiomyopathy ( <i>Baron</i> )
11:30–12:00	MRI of Congenital Heart Disease ( <i>Gomes</i> )
12:00–12:30	MRI of Ischemic Heart Disease ( <i>Pettigrew</i> )
12:30–2:00	Lunch Break
2:00–2:30	MRI of Valvular Disease ( <i>Higgins</i> )
2:30–3:00	MR Angiography ( <i>Edelman</i> )
3:00–3:30	Coffee Break
3:30–4:30	An Overview of Cardiac Ultrasound: Its Strengths and Weaknesses ( <i>Jaffe</i> )
4:30–5:00	Physical Principles of Doppler Ultrasound ( <i>Kremkau</i> )

#### **Monday, May 14**

1:30–2:30	Doppler Ultrasound in the Carotid and Peripheral Circulation ( <i>Merritt</i> )
2:30–3:15	Ultrasound of Intracranial Circulation ( <i>Ackerman</i> )
3:15–3:45	Coffee Break
3:45–4:30	PET Cardiac Imaging: Radiopharmaceuticals, Technique, and Results ( <i>Schelbert</i> )
4:30–5:15	Doppler Ultrasound Studies of the Abdominal Vessels and Viscera ( <i>Nelson</i> )

#### **Tuesday, May 15**

3:45–4:30	SPECT Cardiac Imaging: Radiopharmaceuticals, Technique, and Results ( <i>DePuey</i> )
4:30–5:15	Ultrasound of Peripheral Venous Disease ( <i>Dorfman</i> )
5:15–5:45	Peripheral Vascular Studies in Nuclear Medicine ( <i>Ziffer</i> )

#### **Wednesday, May 16**

3:45–4:45	Overview of Current Status of Percutaneous Transluminal Angioplasty of Peripheral Vessels ( <i>Schwarten</i> )
4:45–5:30	Renal Angioplasty ( <i>Sos</i> )

#### **Thursday, May 17**

3:45–4:15	Intravascular Stents ( <i>Palmaz</i> )
4:15–5:00	Intravascular Lasers: What's Good and What Isn't ( <i>van Breda</i> )
5:00–5:45	Embolotherapy: Current Trends and Future Prospects ( <i>White</i> )



# Meeting and Local Activities Registration Form: ARRS 90th Annual Meeting May 13-18, 1990, Washington, DC

If you plan to attend, please complete this form. Official badges and program booklets will be available at the ARRS Registration Desk, Sheraton Washington Hotel. **There will be no confirmations before the meeting.** Preregistration by mail will be accepted until April 27. On-site registration will be available.

**Make all checks payable to: American Roentgen Ray Society**

Mail to: American Roentgen Ray Society  
1891 Preston White Drive  
Reston, VA 22091

**Please type or print:**  
Registrant

\_\_\_\_\_  
Last Name First Name or Initials

\_\_\_\_\_  
Street

\_\_\_\_\_  
City State ZIP Code

Accompanying Guest

\_\_\_\_\_  
Name (Accompanying person's name to be printed on badge)

\_\_\_\_\_  
Street

\_\_\_\_\_  
City State ZIP Code

**Check those desired:**      Registration fee:

☐ Member ARRS ..... None

☐ Nonmember ..... \$250

☐ Physician in training  
(please fill where indicated below) ..... \$25

☐ Course faculty, presenter of  
scientific paper, scientific  
exhibitor (circle one) ..... None

☐ ACR luncheon course,  
Monday, May 14 ..... \$12

☐ ACR luncheon course,  
Tuesday, May 15 ..... \$12

☐ ACR luncheon course,  
Wednesday, May 16 ..... \$12

☐ ACR luncheon course,  
Thursday, May 17 ..... \$12

☐ Categorical course on cardio-  
vascular-interventional  
radiology ..... \$75

☐ Social program (see next  
page) ..... \_\_\_\_\_

**Total enclosed** ..... \_\_\_\_\_

## Section on Instruction

Please register early for Instructional Courses. Attendance is limited. List first, second, and third choices for each day by course number. Ticket orders are filled according to postmark. ARRS members, nonmembers, and those in radiology training may take all courses without charge except the categorical course. **For the categorical course, all must pay \$75. All who wish to attend courses must complete this section. Residents and nonmembers must pay the meeting registration fee also.**

Course tickets will be available at the ARRS Registration Desk at the Sheraton Washington Hotel on and after Saturday, May 12, at 1 p.m.

Complete section at right for courses other than the categorical course. Be sure to fill out second and third choices for each day.

Course Choices	Morning			Afternoon		
	1st	2nd	3rd	1st	2nd	3rd
Monday						
Tuesday						
Wednesday						
Thursday						

Friday \_\_\_\_\_. Check if you wish to attend the musculoskeletal symposium (only course offered this day).

### For Physicians in Training:

\_\_\_\_\_ is in training in my department.

Training Program Director \_\_\_\_\_

Institution \_\_\_\_\_ Date \_\_\_\_\_

(OVER)

## Local Activities

No refunds after April 27

Sunday, May 13, 1-5 p.m., A National Tribute	_____ tickets @ \$22	\$ _____
Sunday, May 13, 8-10:30 p.m., Monuments by Moonlight Champagne Tour	_____ tickets @ \$32	\$ _____
Monday, May 14, 9:30 a.m.-4 p.m., Capitol Hill Tour	_____ tickets @ \$49	\$ _____
* Monday, May 14, 9:30 a.m.-4 p.m., The Nation's Capitol	_____ tickets @ \$42	\$ _____
Monday, May 14, 9 a.m.-2:30 p.m., Shopping Safari	_____ tickets @ \$28	\$ _____
Tuesday, May 15, 8:30 a.m.-5:30 p.m., George Washington's Washington	_____ tickets @ \$50	\$ _____
Tuesday, May 15, 1:30-4:30 p.m., Orient Express	_____ tickets @ \$22	\$ _____
* Tuesday, May 15, 5:30-10 p.m., Evening at a Dinner Theatre	_____ tickets @ \$48	\$ _____
Wednesday, May 16, 10-11:30 a.m., Secrets of a White House Chef	_____ tickets @ \$25	\$ _____
Thursday, May 17, 10 a.m.-3:30 p.m., Georgetown Homes and Gardens	_____ tickets @ \$50	\$ _____
Friday, May 18, 10 a.m.-2:30 p.m., Doll Museum, DAR Museum, National Press Club	_____ tickets @ \$45	\$ _____
Friday, May 18, 9 a.m.-5 p.m., Colonial Annapolis	_____ tickets @ \$60	\$ _____

Preregistration is required.

\* Tour designed for children 12 years old and older.

## Annual ARRS Golf Tournament, Monday, May 14

The tournament will be at the Kenwood Country Club, Washington, DC. Transportation, luncheon, greens fee, cart, and prizes are included in the \$75 fee. Preregistration is important.

Name: \_\_\_\_\_ Telephone: \_\_\_\_\_  
Address: \_\_\_\_\_  
Hotel: \_\_\_\_\_ Handicap (if any) \_\_\_\_\_  
My foursome includes (list handicaps): \_\_\_\_\_  
\_\_\_\_\_ tickets @ \$75 \$ \_\_\_\_\_

## Men's and Women's Tennis Tournaments, Monday, May 14

The tournaments will be at the Kenwood Country Club, Washington, DC. Tennis attire is required. Fee of \$50 includes transportation, luncheon, court fees, and balls.

Name: \_\_\_\_\_ Telephone: \_\_\_\_\_  
Address: \_\_\_\_\_  
\_\_\_\_\_ tickets @ \$50 \$ \_\_\_\_\_

# Hotel Registration Form: ARRS 90th Annual Meeting May 13–18, 1990, Sheraton Washington Hotel Washington, DC

**Mail to:****ARRS Housing Bureau**

Sheraton Washington Hotel

Attention: Reservations Office

2660 Woodley Rd. at Connecticut Ave., N.W.

Washington, DC 20008

**(PLEASE MAKE CHECKS PAYABLE TO THE SHERATON WASHINGTON HOTEL—NOT TO THE ARRS)**

Individual guest name \_\_\_\_\_

Address \_\_\_\_\_

City &amp; State \_\_\_\_\_ ZIP \_\_\_\_\_

Arrival date/time \_\_\_\_\_ Departure date/time \_\_\_\_\_

Individual requesting reservation \_\_\_\_\_

Address \_\_\_\_\_

City &amp; State \_\_\_\_\_ ZIP \_\_\_\_\_

**Please forward with your reservation a deposit** of one night's room rate to be applied to the last night of your scheduled stay, or provide credit card information to guarantee your reservation. The hotel accepts American Express, Diners Club, Carte Blanche, Visa, and Master Card credit cards. The deposit will hold your room until 6 a.m. of the morning following your scheduled arrival date. In the event of an early departure, the deposit is nonrefundable unless the hotel is notified prior to or at the time of check-in. Cancellation notice of 14 days is required for a deposit refund.

**Check accommodations desired**

Room Category	Rate
<b>Singles</b>	
Standard .....	— \$135
Deluxe .....	— \$148
Concierge .....	— \$156–176
<b>Doubles</b>	
Standard .....	— \$160
Deluxe .....	— \$172
Concierge .....	— \$180–201
1-bedroom suite .....	— \$260–360
2-bedroom suite .....	— \$320–450

**Important Information:**

1. Reservations must be received by the Sheraton Washington Hotel/ARRS Housing Bureau no later than April 13 to be assured of written confirmed accommodation. Reservations after that time are subject to availability. We urge you to make your reservations promptly.
2. Written confirmation of your reservation will be sent to you by the hotel.
3. To change or cancel reservations, please call the hotel directly at (202) 328-2000.
4. If you plan to share a room, please send in only one housing form. Be sure to list all names of occupants of rooms. Assignment is delayed until complete information is received.
5. Check-in is after 3 p.m., or earlier if the room is available. Check-out time is 1 p.m.
6. Parking is available at the hotel.

Deposit amount (1 night's rate) \$ \_\_\_\_\_

☐ Check enclose☐ Credit card: \_\_\_\_\_

Type of card

Exp. date

Card number

Signature

# American Roentgen Ray Society: Officers, Committees, and Membership Information

## Officers

**President:** Ronald G. Evens

**President-elect:** M. Paul Capp

**1st Vice-president:** John A. Kirkpatrick, Jr.

**2nd Vice-president:** A. Everette James, Jr.

**Secretary:** Glen W. Hartman

**Treasurer:** Beverly P. Wood

**Executive Council:** R. J. Alfidi, R. N. Berk, B. G. Brogdon, M. P. Capp, W. J. Casarella, R. G. Evens, J. T. Ferrucci, Jr., R. A. Gagliardi, G. W. Hartman, J. A. Kirkpatrick, Jr., A. Landry, Jr., G. R. Leopold, J. E. Madewell, A. A. Moss, L. F. Rogers, J. H. Thrall, K. H. Vydareny, B. P. Wood, A. K. Poznanski, chairman

## Committees

**Editorial Policy:** R. N. Berk, M. M. Figley, S. V. Hilton, M. S. Huckman, C. A. Rohrmann, Jr., S. S. Sagel, R. J. Stanley, N. O. Whitley, W. J. Casarella, chairman

**Education and Research:** C. B. Higgins, B. J. Hillman, R. A. McLeod, W. M. Thompson, B. G. Brogdon, chairman

**Finance and Budget:** R. J. Alfidi, R. C. Gedgaudas-McClees, G. R. Leopold, J. R. Thornbury, J. Thrall, chairman

**Nominating:** R. A. Gagliardi, N. O. Whitley, R. J. Alfidi, chairman

**Publications:** C. A. Rohrmann, Jr., S. S. Sagel, R. J. Stanley, N. O. Whitley, W. J. Casarella, chairman

**Membership:** R. J. Alfidi, A. A. Moss, K. H. Vydareny, G. R. Leopold, chairman

## Representatives to Other Organizations

**American Board of Radiology:** J. A. Kirkpatrick, Jr., E. C. Klatte, L. F. Rogers

**American College of Radiology:** R. A. Gagliardi, G. A. Kling, J. E. Madewell, L. F. Rogers

**American Medical Association House of Delegates:** S. F. Ochsner, K. L. Krabbenhoft, alternate

**American National Standards Institute:** M. Haskin

**National Council on Radiation Protection and Measurements:** H. L. Friedell, E. L. Saenger

## Meeting Arrangements

**Annual Meetings:** May 13–18, 1990, Sheraton Washington, Washington, DC; May 5–10, 1991, Sheraton Boston, Boston

**Annual Meeting Committee:** H. C. Carlson, J. K. Crowe, G. P. Janetos, R. R. Lukin, A. Landry, Jr., chairman

**Instruction Courses:** R. J. Stanley, associate chairman, J. T. Ferrucci, Jr., chairman

**Scientific Program:** R. J. Alfidi, E. Buonocore, D. O. Davis, K. B. Hunter, T. C. McCloud, W. A. Murphy, Jr., A. E. Robinson, L. B. Talner, J. H. Thrall, M. P. Capp, chairman

**Scientific Exhibits:** R. J. Churchill, A. A. Moss, R. G. Ramsey, J. E. Madewell, chairman

## ARRS Membership

An application form is printed in the February issue of the Journal. For consideration at the 1991 ARRS meeting, send completed forms before February 1, 1991, to American Roentgen Ray Society, 1891 Preston White Dr., Reston, VA 22091. Active members are graduates of an approved medical or osteopathic school or hold an advanced degree in an allied science. They must practice radiology or work in an associated science in the United States or Canada and be certified by the American Board of Radiology, American Osteopathic Board of Radiology, or Royal College of Physicians of Canada or otherwise adequately document training and credentials. Corresponding members are foreign radiologists or scientists who are active in radiology or an allied science. Members-in-training are residents or fellows in radiology or postgraduate students in an allied science. Additional application forms can be obtained from the ARRS offices in Reston, VA.

## Business Office

Paul Fullagar, Executive Director, American Roentgen Ray Society, 1891 Preston White Dr., Reston, VA 22091; (703) 648-8900

# Classified Advertisements

## Positions Available

**OPPORTUNITY FOR YOUNG, WELL-TRAINED, AGGRESSIVE RADIOLOGIST** to join 5-person group in a small, midwestern city near St. Louis. Excellent equipment including mobile MRI. Competitive salary leading to early partnership. Reply to Box U40, AJR (see address this section). 3xa

**FACULTY NEURORADIOLOGIST, THOMAS JEFFERSON UNIVERSITY HOSPITAL**—The Dept. of Radiology at Thomas Jefferson University Hospital and Jefferson Medical College, Philadelphia, will have a new faculty neuroradiology position available July 1, 1990. This is due to rapid growth in our neuro/ENT division and the opening of 3 additional MRI units by that date. Jefferson has very large and active neurology, neurosurgery, and ENT clinical services, as well as strong commitments to research and teaching. Our Neurosciences Imaging Center includes angio, myelography, CT, and MRI units together in a discrete area of the dept. The current neuro/ENT division includes 5 full-time faculty and 4 fellows. Candidates can be either at the junior or senior level; rank and compensation will be determined by previous experience. Excellent salary and benefits are provided. Contact David C. Levin, M.D., Chairman, Dept. of Radiology, Thomas Jefferson University Hospital, Philadelphia, PA 19107. Jefferson is an equal opportunity/affirmative action employer. 3xa

**ISRAEL, DIAGNOSTIC RADIOLOGY.** Opportunities for 3-4 week or longer working vacations in a number of Israeli medical centers, on a volunteer basis. Positions varied, arrangements flexible. For information contact: Jonathan H. Fish, M.D., 1844 San Miguel Dr. #302, Walnut Creek, CA 94596; (415) 947-0560 2-4xa

**NEURORADIOLOGIST**—The University of Texas Health Science Center at San Antonio is seeking a qualified academic neuroradiologist to fill an immediate opening. Send cover letter and CV to John R. Jenkins, M.D., Director of Neuroradiology, The University of Texas Health Science Center, 7703 Floyd Curl Dr., San Antonio, TX 78247-7800. 3-8ap

**PRACTICE IN THE COASTAL PLAIN OF NORTH CAROLINA** at a well-established 100-bed hospital seeks third radiologist. 23,000/24,000 procedures/yr. General radiology including mammography, CT, ultrasound, and nuclear medicine. No angio, interventional, or MRI. Compensation and benefits competitive. Available immediately. Contact Roanoke-Chowan Radiology Associates, Inc., P.O. Box 459, Ahoskie, NC 27910; (919) 332-0111. 3-6ap

**BREAST IMAGING RADIOLOGIST, THOMAS JEFFERSON UNIVERSITY HOSPITAL**—The Dept. of Radiology at Thomas Jefferson University Hospital in Pennsylvania is recruiting a faculty-level, breast imaging radiologist to help staff our new Breast Imaging Center. The Center is spacious and state-of-the-art and currently performs approximately 85 studies/day, including ultrasound, cyst aspirations, and needle localizations. Further growth is anticipated. The position can be tailored to the interests of the candidate; it can either involve full-time breast imaging work or can focus on breast imaging part-time with additional time allocated to our ultrasound and general diagnostic divisions. Dedicated research time is available. Faculty incomes and fringe benefits are generous. Interested individuals should contact either Stephen Feig, M.D., Director of Breast Imaging, or David Levin, M.D., (Dept. Chairman), at the Dept. of Radiology, Thomas Jefferson University Hospital, Philadelphia, PA 19107; (215) 955-7264. Jefferson is an equal opportunity/affirmative action employer. 3a

**NEURORADIOLOGIST/MRI**—Two positions available; Fellowship training a necessity. Group of 7 radiologists seek BC colleague in multihospital practice. Must be capable as general diagnostic radiologist as well. Position available July 1990. Send letter and CV to Neel E. Bennett, M.D., Medical Director and Chairman, Dept. of Radiology, Holy Cross Hospital, 1050 E. South Temple, Salt Lake City, UT 84102; (801) 350-4636. 3xa

**HOSPITAL-BASED DIAGNOSTIC RADIOLOGISTS** seek sixth partner for 375-bed, tertiary-care center in Spokane, WA. We seek a partner with skills or experience in all modalities including MR. Current partners rotate through all areas except MR. GE 1.5-T magnet, GE 9800, Imatron Fasttrak, Acuson ultrasound equipment. Opening June 1990. Send CV to Spokane Radiology Consultants, W. 801 Fifth Ave., Ste. 205, Spokane, WA 99204. 3ap

**DARTMOUTH-HITCHCOCK MEDICAL CENTER, DEPT. OF RADIOLOGY** is offering a permanent position for a BC/BE, GI radiologist to be part of the abdominal imaging section at the Mary Hitchcock Memorial Hospital. This is a 400-bed hospital with 80 radiology personnel who perform 55,000 inpatient and 45,000 outpatient exams/yr. The dept. consists of 13 staff and 9 residents covering the full range of modern radiologic practice. Become a member of the 200-physician, academic, multispecialty group that forms the clinical faculty of Dartmouth Medical School. Position has responsibility for a full scope of general diagnostic procedures with emphasis on GI fluoroscopy. Interest in teaching and research essential. Interested candidates should write to P. K. Spiegel, M.D., Dartmouth-Hitchcock Medical Center, Dept. of Radiology, 2 Maynard St., Hanover, NH 03756. AA/EOE. 3-5a

**ACADEMIC RADIOLOGY: POSITIONS AVAILABLE AT ALL APPOINTMENT LEVELS**—Opportunities exist in general radiology, neuro-radiology, and other subspecialty areas. Salary levels commensurate with experience and highly competitive for the greater New York area. Contact Joshua A. Becker, M.D., Professor and Chairman, SUNY Health Science Center at Brooklyn, 450 Clarkson Ave., Brooklyn, NY 11203; (718) 270-1603. EO/AA employer. DMC#CO315. 3a

**LOCUM TENENS POSITIONS** throughout the country. Work for a wk to a yr, at your convenience. Malpractice insurance, housing, and travel paid. Excellent compensation and interesting jobs. LOCUM Medical Group, 30100 Chagrin Blvd., Cleveland, OH 44124; call toll-free (800) 752-5515. 3-8ap

**PHOENIX, AZ**—Maricopa Medical Center has opportunities for additional BC/BE staff radiologists. Write or call P. T. LeRona, M.D., Dept. of Radiology, Maricopa Medical Center, P.O. Box 5099, Phoenix, AZ 85010; (602) 267-5361. 3ap

**ABDOMINAL RADIOLOGIST**—The Dept. of Radiology at the Albany Medical College has an immediate opening for a faculty position in abdominal imaging. The candidate should have fellowship training or demonstrated experience in cross-sectional imaging. Clinical duties will be in ultrasound, body CT, body MR, and GI/GU. The candidate also will participate in medical student and postgraduate education and be able to pursue clinical and basic research interests. Academic rank and salary are commensurate with experience. The dept. has 23 attending staff, 3 fellows, and 16 residents. Please contact James C. Peters, M.D., Interim Chairman, Dept. of Radiology, Albany Medical College, 43 New Scotland Ave., Albany, NY 12208; (518) 445-3277. Albany Medical College is an equal opportunity/affirmative action employer. 3-5ap

**ORTHOPEDIC RADIOLOGIST**—A position is available at the University of Rochester Medical Center, Strong Memorial Hospital, Dept. of Radiology, a 750-bed, tertiary-care facility. An appointment as assistant professor or higher is available at a level appropriate to experience. Research and teaching opportunities are available in a strong academic dept. with state-of-the-art radiologic equipment. Send CV to Robert E. O'Mara, M.D., Professor and Chair, Diagnostic Radiology, Box 648, University of Rochester Medical Center, Rochester, NY 14642. EO/AA/M-F employer. 3-6ap

**VASCULAR/INTERVENTIONAL RADIOLOGIST**—Large radiology group in western Massachusetts is seeking a BC vascular/interventional radiologist to join existing 5-person vascular/interventional team. Fellowship or equivalent experience required. Must also have expertise in CT and general diagnostic radiology. Primary assignment at 868-bed, tertiary-care hospital with radiology residency program. Practice also includes 3 community hospitals and 6 private offices. Full partnership after 1 yr. Available by July 1990. Send CV to W. Max Cloud, M.D., Radiology and Imaging, Inc., 130 Maple St., Springfield, MA 01103. 3-5ap

**RADIOLOGIST(S)**—Multihospital, private-group practice seeking board-certified radiologists. Special procedure capability desirable. One position exists in Orange County, one in Westchester County, and one in Bergen County. Respond to Kenneth S. Schwartz, M.D., Northern Metropolitan Radiology Associates, P.C., 3630 Hill Blvd., Jefferson Valley, NY 10535. (914) 245-8935. 3ap

**PEDIATRIC RADIOLOGIST**—Full-time faculty position, Dept. of Radiology, Children's Hospital Medical Center, Cincinnati, OH, with academic rank of assistant professor to professor in Dept. of Radiology and Pediatrics, University of Cincinnati College of Medicine, available July 1, 1990. Salary and fringe benefits are highly competitive; salary is based on academic rank and experience. Candidates must be certified in diagnostic radiology by the ABR or its equivalent, must have completed a fellowship in pediatric radiology, must have a demonstrated interest and qualifications in basic and/or clinical pediatric imaging research, and must be eligible for active membership in the Society for Pediatric Radiology. Duties include clinical service, teaching, and research. Professional coverage includes conventional radiography, ultrasonography, CT, MRI, nuclear medicine, and digital radiography. The faculty radiologist must have demonstrated expertise in pediatric nuclear medicine, abdominal imaging, and Doppler sonography. Children's Hospital Medical Center and University of Cincinnati are affirmative action/equal opportunity employers. Address inquiry and CV to Donald R. Kirks, M.D., Director, Dept. of Radiology, Children's Hospital Medical Center, Cincinnati, OH 45229-2699; (513) 559-8058. 3ap

**VASCULAR/INTERVENTIONAL RADIOLOGIST**—The University of Maryland is seeking an additional faculty member, with fellowship training, for its Section of Vascular and Interventional Radiology. The medical center is an 800-bed, acute-care hospital and tertiary referral center with an active and varied interventional practice. A new 324-bed VA hospital is now under construction and will be adjacent to and connected to the university. The duties of the new faculty member will be limited to vascular and interventional radiology. Interested persons should contact Gerald S. Johnston, M.D., Dept. of Diagnostic Radiology, 22 S. Greene St., Baltimore, MD 21201; (800) 866-8667, ext. 3477. Affirmative action/equal opportunity employer. 3&5ap

**NUCLEAR MEDICINE/MRI IN HAWAII**—Position available for 500-bed, private, in-hospital practice combining both specialties. Board-certification required. Top-notch equipment in large dept. Honolulu and Oahu combine to form a cosmopolitan urban and suburban tropical paradise. Stimulating work, relaxing lifestyle. Marc Coel, M.D., Queen's Medical Center, 1301 Punchbowl St., Honolulu, HI 96813; (808) 547-4544. 3ap

**POSITION OPEN IMMEDIATELY**—Board-certified radiologist needed to join busy, 3-member radiology group with practice in central and southwestern Pennsylvania. Central Pennsylvania practice involves imaging (all modalities) and southwestern Pennsylvania practice involves an outpatient imaging facility consisting of radiography, fluoroscopy, ultrasound, CT, nuclear medicine, mammography, and MR. Job leading to full partnership with competitive salary and benefits. Send letters of inquiry with CV to R & R Consultants, Box 160, Adamsburg, PA 15611; (412) 483-6564. 3-4a

**RADIOLOGIST**—This 52-physician, multispecialty clinic is seeking a second radiologist for general radiologic procedures excluding CT and MRI. Experience or formal training in mammography required. Located in western Montana, abundant 4-season recreational opportunities. Offered salary and benefits generous. Send CV to Ethan Russo, M.D., Western Montana Clinic, P. O. Box 7609, Missoula, MT 59807. 3ap

**BC/BE RADIOLOGIST**, preferably with training and experience in neuroradiology, to join 5-member radiology group in Savannah, GA. Practice includes coverage of 300-bed, acute-care hospital and new private office. Excellent facilities with state-of-the-art CT, nuclear medicine with SPECT, general and vascular ultrasonography, mammography, fluoroscopy, neuro/angio/interventional, and MRI. Generous salary and benefits with early partnership. Savannah is an attractive coastal community with expanding economy and outstanding year-round recreational resources. Send CV with letter of inquiry to Thomas H. Philbrick, M.D., Savannah Radiologists, P. O. Box 14444, Savannah, GA 31499. 3-5ap

**IMMEDIATE OPENING**—BC/BE radiologist to join medium-sized group in Austin, TX. Special interest, expertise, or fellowship training in body imaging and/or interventional radiology is necessary. Practice covers major trauma center and outpatient radiology facility. In addition to general diagnostic services, outpatient facility also provides CT and MRI services on 2 GE 9800 scanners and on GE 1.5-T and 0.5-T MR units. Applicants are requested to contact Drs. Gray, Lava, or Boyd at 711 W. 38th St., Ste. B-8, Austin, TX 78705; (512) 454-8718. 3-5ap

**UPSTATE NEW YORK**—Progressive group seeks a board-certified diagnostic radiologist and a neuroradiologist willing to do some general radiology. Full range of services (MRI, ultrasound, Doppler, angiography) provided at 2 acute-care hospitals with state-of-the-art equipment. Excellent salary and benefits with early partnership. Reply to Box Y58, *AJR* (see address this section). 3-4ap

**DIAGNOSTIC RADIOLOGIST**—Immediate opening for board-eligible/board-certified radiologist to join private practice serving 2 100-bed hospitals in southwestern Arkansas. Generous compensation package with 12-24 wk off for personal or professional development. Must be proficient in general, CT, ultrasound, mammography, and nuclear medicine. Shareholder status available. Send letter and CV to Joseph W. Baxter, Jr., M.D., Box 1318, Hope, AR 71801. 3ap

**DIAGNOSTIC RADIOLOGIST**—BC radiologist for practice in central Maine. Strong skills in R/F, CT, ultrasound, and mammography required. The 52-bed hospital is located in a beautiful, rural community 35 mi. from Bangor. Radiologist will be employed and supported by 15-member, Bangor-based group. Partnership is offered after 3 yr. Liberal vacation, CME leave, and fringe benefits included. Contact Peter Holman, Administrator, Andrews, Lynch & Field, Radiologists, 276 State St., Bangor, ME 04401; (207) 945-6877. 3ap

**FULL-TIME BC RADIOLOGIST** needed to staff outpatient women's diagnostic center in suburban Dallas. Experience in mammography and OB/GYN sonography preferred. No call responsibilities. Attractive compensation package. Send CV to Box Y56, *AJR* (see address this section). 3xap

**ANGIOGRAPHY/INTERVENTIONAL RADIOLOGIST**—Position available at the New Jersey Medical School, Newark, NJ, July 1, 1990. Academic position will include resident supervision, scholarly activity, and clinical practice. Excellent equipment. Rapidly developing institution and dept. Recent completion of fellowship in angio/interventional and board-certification, or current faculty member in current academic section in angio/interventional would be considered. Compensation starting at \$150,000 for entry level. Please contact Gail Eliot, M.D., Acting Chairperson, Dept. of Radiology, NJMS, University Hospital, C-320, 150 Bergen St., Newark, NJ 07103; (201) 456-5188 or 5189. 3-5ap

**UCSD SCHOOL OF MEDICINE**—The Dept. of Radiology is seeking an ultrasonologist to participate in clinical service, medical student and resident teaching, and research projects. Participation in other diagnostic subspecialties is available. Qualifications required: board-eligibility/certification, California medical license, and 1-yr fellowship in ultrasound. Title Series: Assistant professor (in-residence or clinical series, not currently a tenure-track position); level based on years experience; salary commensurate with rank and step of appointment based on the established salary schedule of the UCSD School of Medicine Faculty Compensation Plan. The University of California, San Diego, is an equal opportunity/affirmative action employer. All CVs received before March 31, 1990, will be given full consideration. Send to George R. Leopold, M.D., Professor and Chairman, Dept. of Radiology, UCSD Medical Center, 225 Dickinson St., San Diego, CA 92103-1990. 3a

**BE/BC GENERAL DIAGNOSTIC RADIOLOGIST**, experienced in CT, ultrasound, mammography, and nuclear medicine, wanted for established 2-person practice at 150-bed community hospital in rural southeastern Virginia. Opening July 1990. Competitive salary, benefits. Send CV to Box Y70, *AJR* (see address this section). 3-5ap

**INTERVENTIONAL/ANGIOGRAPHER**—The Dept. of Diagnostic Imaging of Temple University Hospital and School of Medicine is recruiting a section head of vascular/interventional radiology. The dept. has an active practice in angiography, angioplasty, and interventional radiology. A research vascular suite is available in the School of Medicine to support the research interests of diagnostic imaging faculty. Candidates should be board-certified and have fellowship training in angiography/interventional radiology. Teaching, research, and administrative skills are also desirable. Contact Francis J. Shea, M.D., Professor and Acting Chairman, Dept. of Diagnostic Imaging, Temple University Hospital, Broad and Ontario Sts., Philadelphia, PA 19140. Temple University is an affirmative action/equal opportunity educator and employer. 3a

**RADIOLOGIST**—Full-time; nice, small, well-located North Carolina town. Join active, hospital-based, service-oriented practice. General diagnostic, nuclear medicine, ultrasound, CT, and mobile MRI. No arteriography. Reply with CV to Box Y50, *AJR* (see address this section). 3-5ap

**RADIOLOGIST**—Associate diagnostic radiologist to join a 4-radiologist group in Massachusetts. Hospital and private practice. All diagnostic modalities. Interest in angiography and interventional radiology preferred. Reply Box Y54, *AJR* (see address this section). 3-5ap

**PART-TIME RADIOLOGIST** wanted to do routine diagnostic work in central western Pennsylvania, near Pittsburgh. No specials. Apply to Box R14, *AJR* (see address this section). 3ap

**PEDIATRIC RADIOLOGIST**—William Beaumont Hospital is a modern, tertiary-care medical center with a strong residency and fellowship program in diagnostic radiology. We are seeking a pediatric radiologist to join the full-time pediatric radiologist on our staff. The position would involve 50% pediatric radiology at this time, with a future option of progressive increased involvement in pediatric radiology as our children's center continues to expand. The medical center is located in southeastern Michigan, with nearby desirable living areas and summer and winter resort activities. Compensation and benefits are generous and very competitive. Send CV to Jalil Farah, M.D., Chairman, Diagnostic Radiology, William Beaumont Hospital, 3601 W. 13 Mile Rd., Royal Oak, MI 48072. 3-5a

**DIAGNOSTIC RADIOLOGIST WANTED JULY 1990**—Progressive, expanding, 320-bed, acute-care hospital with all imaging modalities. Ability in diagnostic, vascular, and sectional imaging, obstetric and vascular ultrasound. Competitive salary and benefits leading to partnership. Growing community. Good schools and cultural facilities. Easy access to Pacific Coast, Sierra Nevada mountains, national parks, San Francisco, and Los Angeles. Address inquiries to D. N. Shuster, M.D., St. Agnes Hospital, 1303 E. Herndon, Fresno, CA 93710. 2-3ap

**NEURORADIOLOGIST**—UMDNJ, NJ Medical School, is seeking a full-time neuroradiologist. The service function will be combined ¾ time at University Hospital (518 beds) and ¼ time at the East Orange VA Hospital (700 beds). Two GE CT scanners, 1.5-T GE Signa MRI, and Philips digital angiography at University Hospital. Two other neuroradiologists in the section. Teaching and resident (16 residents) review required. Future will include medical office complex. Respond to Gail Eliot, M.D., Acting Chairperson, Dept. of Radiology, University of Medicine and Dentistry, 150 Bergen St., Newark, NJ 07103; (201) 456-5188. An equal opportunity employer. 2-4ap

**NYU MEDICAL CENTER, RADIOLOGY DEPT.**—Faculty position available for a Director of Ultrasound, and junior faculty positions available in ultrasound and in bone and joint radiology. Contact Norman E. Chase, M.D., Professor and Chairman, Dept. of Radiology, NYU Medical Center, 550 First Ave., New York, NY 10016. An equal opportunity affirmative action employer. 2-4ap

**ATLANTA, GA**—Rare opportunity to join 3-member group based in small, rapidly growing, 5-yr-old hospital and new outpatient facility. This tremendously exciting practice is located in the most affluent and family oriented suburb of Atlanta, within 30 min. of both downtown and beautiful lake resort area. All members of the group are proficient in all modalities, including MRI. Competitive salary and benefits leading to partnership. Send CV to Stephen Bruno, M.D., 2215 Roxburgh Dr., Roswell, GA 30076. 2-3ap



**POSITION AVAILABLE IMMEDIATELY FOR A GENERAL DIAGNOSTIC RADIOLOGIST**, with training or experience in vascular/interventional radiology, to complete staffing for the new VA Medical Center in Minneapolis, MN. Dept. includes MRI, CT, cyclotron with PET scanner, interventional vascular suite, neuroradiology suite, mammography, color-flow Doppler ultrasonography, plus more. Affiliated with the University of Minnesota with non-tenure-track appointment available at appropriate level. Research and teaching opportunities available. Board certification mandatory. One yr fellowship training or equivalent experience in interventional radiology desirable. Send letters of inquiry with CV to Donovan B. Reinke, M.D., Chief of Diagnostic Radiology Service — 114, VA Medical Center, One Veterans Dr., Minneapolis, MN 55417; (612) 725-2038. EOE. 2a

**BC RADIOLOGIST**—General radiology, ultrasound, CT, nuclear medicine, and angiography. Affluent community. Percentage of revenue, plus \$150,000 and benefits, first yr. Good personality and desire to build practice essential. Reply to D. Fischer, M.D., 1301 McCallie Ave., Chattanooga, TN 37404; (615) 622-7512. 2-3ap

**GENERAL RADIOLOGIST**—221-bed, affiliated, GM&S VA Medical Center in the Black Hills is searching for a board-certified or eligible radiologist to join our staff. Located in the southwestern Black Hills with excellent schools, both summer and winter recreational activities, no crime, and no state income tax. An excellent benefit package includes liberal vacation and sick leave, federal retirement/social security, health and life insurance programs, and malpractice insurance. Call or write Chief of Staff, VA Medical Center, Hot Springs, SD 57747; (605) 745-2049. 2-4a

**THE UNIVERSITY OF LOUISVILLE, DEPT. OF DIAGNOSTIC RADIOLOGY** is seeking applications from BC/BE diagnostic radiologists to fill full-time faculty positions in the following areas in its 400-bed teaching hospital: (1) cross-sectional body imaging, (2) general radiology (GI, GU, bone, chest). Candidates must be willing to participate in undergraduate and graduate teaching, and in research activities in their respective areas. These are fine opportunities in a growing and busy dept. with excellent equipment. Both tenure and non-tenure track appointments are available, and academic rank will be commensurate with training and experience. Compensation negotiable and competitive. Louisville continues to be ranked as one of the top 10 places to live in America by Rand McNally. Send inquiries with CV and three references to: Hollis A. Thomas, M.D., Professor and Chairman, Dept. of Diagnostic Radiology, Humana Hospital-University of Louisville, 530 S. Jackson St. Louisville, KY 40202. An equal opportunity/affirmative action employer. 2-3a

**UNIVERSITY OF MEDICINE & DENTISTRY OF NJ, NJ MEDICAL SCHOOL** is seeking 2 section chiefs. Section chief in GI radiology requires fellowship training in GI radiology or current experience in GI section or an academic radiology dept. Section chief in Chest radiology requires fellowship training in Chest radiology or current experience in Chest section of an academic radiology dept. Section chiefs will have full clinical responsibility for all imaging modalities relating to the subspecialty, training of residents in the section, and development of research goals for the section. Salaries are excellent. Supportive dept. with opportunity to explore and develop own interests. Excellent equipment. Send resume to Gail Eliot, M.D., Acting Chairman, NJMS Dept. of Radiology, University Hospital, 150 Bergen St., Newark, NJ 07103; (201) 456-5188. 2-4ap

**DIAGNOSTIC RADIOLOGIST**—Opening for board-certified radiologist to join a young, dynamic, 6-person radiology group near Gettysburg, PA, approximately 90 min from downtown Washington, DC. Modalities include special procedures, CT, MRI, nuclear medicine with SPECT, and mammography. Two community-based hospitals with several outpatient imaging facilities. Hospital campus also includes close affiliation with a Johns Hopkins University-sponsored cancer treatment center. Competitive salary and benefits leading to partnership opportunity. Rapidly growing community, ideally situated not far from the Baltimore-Washington area, between Pittsburgh and Philadelphia. Outstanding skiing, fishing, hunting, and boating in the region including the Chesapeake Bay. Position available July 1, 1990. Please submit CV along with names and addresses of 3 references to Robert S. Pyatt, M.D., Dept. of Radiology and Diagnostic Imaging, The Chambersburg Hospital, 112 N. Seventh St., Chambersburg, PA 17201; (717) 267-7181. 2-4ap

**S.E. GEORGIA**—Immediate position available for a board-certified/eligible diagnostic radiologist to join a 2-person staff covering 4 hospitals and a diagnostic imaging center located in Vidalia, GA. Excellent benefits package, opportunity for partnership, as well as starting salary of \$100,000+. Skills must include general diagnostics, ultrasound, nuclear medicine, mammography, CT, and special procedures. Send letters of inquiry along with CV and letters of reference to Director, Regional Diagnostics, P. O. Box 147, Vidalia, GA 30474. 2xa

**MAINE**—General radiologist to join busy practice affiliated with modern, 92-bed, acute-care hospital. Diagnostic modalities include ultrasound, mammography, angiography, nuclear medicine, and mobile CT. Beautiful 4-season recreation area close to skiing, hunting, and fishing. Excellent school system. Competitive first yr salary with partnership available by the second yr. Send CV to New England Health Search, 63 Forest Ave., Orono, ME 04473; (207) 866-5680 or (207) 866-5685. 1-3ap

**DIAGNOSTIC RADIOLOGIST WITH SPECIAL INTEREST IN ANGIOGRAPHY AND INTERVENTIONAL RADIOLOGY**—The Dept. of Radiology at the University of Texas Medical School at Houston has an immediate opening at the Hermann Hospital, and an opening for July 1, 1990, at the Lyndon Baines Johnson General Hospital, for an experienced interventionist/angiographer with strong interest in patient care and teaching. Research interest and experience are important, but not essential. Although the principal responsibilities will be in intervention/angiography, there will be an opportunity to be involved in other clinical areas of the candidate's interest. The position will include teaching at the medical student and resident levels. Candidate must be a diplomate of the ABR and have completed at least a 1-yr interventional/angiography fellowship, have a Texas state medical license, and have had at least 1 yr postfellowship experience. Candidates with the qualifications for a senior assistant professor or associate professor appointment are preferred. Academic rank will be commensurate with qualifications. Compensation will be based on the most recent AAMC survey and the candidate's qualifications and experience. Please submit CV, along with the names and addresses of 3 references, to John H. Harris, Jr., M.D., D.Sc., Professor and Chairman, Dept. of Radiology, The University of Texas Medical School at Houston, 6431 Fannin, Ste. 2.132, Houston, TX 77030. The University of Texas Health Science Center at Houston is an equal opportunity employer. Women and minorities are encouraged to apply. 1-6a

**THE MALLINCKRODT INSTITUTE OF RADIOLOGY AT THE WASHINGTON UNIVERSITY SCHOOL OF MEDICINE** announces a faculty position in the section of vascular and interventional radiology. The Mallinckrodt Institute of Radiology provides radiology services to Barnes Hospital and St. Louis Children's Hospital, comprising approximately 1300 beds. The vascular and interventional section is involved in all aspects of vascular and nonvascular interventional radiology. We currently perform approximately 5700 procedures/yr. A major remodeling effort is under way at the Institute. This includes 4 new special procedure rooms. Excellent facilities are available for clinical and animal research. If you are interested in an academic position in a rapidly developing interventional section, please contact Daniel Picus, M.D., Chief, Vascular and Interventional Radiology, Mallinckrodt Institute of Radiology, 510 S. Kingshighway Blvd., St. Louis, MO 63110; (314) 362-2900. 2-4a

**DIRECTOR OF CLINICAL MAGNETIC RESONANCE**—The Dept. of Radiology at the University of Texas Medical School at Houston has an opening for a radiologist at the assistant, associate, or full professor level, who will direct clinical activities, medical student and resident teaching, and clinical research in the university MRI center at Hermann Hospital. Candidate will be expected to conduct or direct clinical or basic research in MR leading to grant support. Candidates must have demonstrated experience in direction of a clinical MRI unit, teaching, research, writing, and obtaining grant support, and have a strong publication background. Candidate must be board-certified by the ABR and must have a Texas medical license. Compensation will be based on the most recent AAMC survey and candidate's qualifications. Please forward a CV, and the names and addresses of 3 references, to John H. Harris, Jr., M.D., D.Sc., Professor and Chairman, Dept. of Radiology, The University of Texas Medical School at Houston, 6431 Fannin, Ste. 2.132, Houston, TX 77030. The University of Texas Health Science Center at Houston is an equal opportunity employer and encourages women and minority candidates to apply. 1-6a

**ASSISTANT OR ASSOCIATE PROFESSOR OF NEURORADIOLOGY**—The University of Texas Medical School at Houston has openings for neuroradiologists at the Lyndon Baines Johnson General Hospital and the Hermann Hospital to perform clinical neuroradiology and participate in resident and medical student teaching. Candidates must have completed an approved residency in diagnostic radiology and a 2-yr neuroradiology fellowship. Candidates must be board-certified by the ABR, or equivalent, and must have a Texas medical license. Compensation will be based on the most recent AAMC survey and the candidate's qualifications. Applicants should send a CV, along with the names and addresses of 3 references, to John H. Harris, Jr., M.D., D.Sc., Professor and Chairman, Dept. of Radiology, The University of Texas Medical School at Houston, 6431 Fannin St., Ste. 2.132, Houston, TX 77030. The University of Texas Health Science Center at Houston is an equal opportunity employer and encourages women and minority candidates to apply. 1-6a

**AMMOGRAPHER**—Second mammographer sought to join busy, rapidly growing, private-practice breast center and faculty of Cedars-Sinai Medical Center Radiology Dept. Additional duties include noninterventional, general radiology, and hospital teaching responsibilities for residents. Superb opportunity for board-certified radiologist. Please respond to R. James Brenner, M.D., Cedars-Sinai Radiology Dept., Ste. 5416, 8700 Beverly Blvd., Los Angeles, CA 90048; (213) 855-3701. 1-3ap

**DIAGNOSTIC RADIOLOGY**—Progressive 4-member group in Sacramento, CA, seeks BC/BE radiologist. Should be familiar with all imaging modalities. Practice includes 220-bed hospital and outpatient office. Competitive salary leading to early partnership. Generous benefit package. Send CV to Fred L. Stargardt, M.D., American River Radiology Medical Group, Inc., 3837 Mission Ave., #5, Carmichael, CA 95608. 2-4ap

**RADIOLOGIST**—Immediate opening for a qualified, board-certified/eligible radiologist to work in an outpatient imaging center located 40 mi. north of El Paso, TX. Must have knowledge of general radiology and experience with ultrasound, CT, and nuclear medicine. Interested doctors should send CV to Sun View Imaging Services, P.O. Box 8624, Las Cruces, NM 88006. 1-3ap

**IMMEDIATE OPENING**—Excellent opportunity to join 6-member radiology group in Johnstown, PA, located approximately 75 mi. from Pittsburgh in the Allegheny Mountains. Practice covers 2 hospitals and does approximately 100,000 procedures/yr. Johnstown, recently selected as Pennsylvania's "community of the year," is noted for its low crime rate, scenic beauty, and high quality of life. Applicant should be competent in all phases of diagnostic radiology including MR, CT, ultrasound, nuclear medicine, and angio. Well-established group with good clinical staff interaction. Excellent starting salary and benefits, with equal partnership to follow. If interested, please call and/or forward CV to Jon Abrahams, M.D., Conemaugh Valley Memorial Hospital, Dept. of Radiology, 1088 Franklin St., Johnstown, PA 15905; (814) 533-9188. 1-3a

**FACULTY POSITIONS AVAILABLE IN DIAGNOSTIC RADIOLOGY**—On July 1, 1990, the faculty of the University of Texas Medical School at Houston (UTMSH) will assume clinical practice, teaching, and research at the Lyndon Baines Johnson (LBJ) General Hospital, newly constructed by the Harris County Hospital District, in Houston, TX. LBJ General will be a principal medical student teaching affiliation of the UTMSH, is certified for 300 beds (with expansion capabilities to approximately 500 beds) and is projected to perform approximately 130,000 imaging procedures the first yr. The Dept. of Radiology at LBJ is fully equipped with new, state-of-the-art GE equipment, including a 9800 Quick CT scanner with 3-D software and an LU angiographic unit, and comparable routine, R&F, ultrasound, and nuclear equipment. Full-time UTMSH faculty positions exist for 5 associate professors and 10 assistant professors with clinical, teaching, and research interests in all aspects of diagnostic imaging. Residents who have just completed training and are board-certified will be offered the rank of assistant professor at an annual salary of \$90,000. Fellows who have completed training and are board-certified will be offered the rank of assistant professor at an annual salary of \$100,000. These salaries may be increased depending on the candidate's education and experience beyond either residency or fellowship, and in addition to base salary, total fringe benefits of approximately 20% of the base salary will be provided. Associate professor compensation will be based on the most recent AAMC survey and the candidate's qualifications. Candidates must be diplomates of the ABR, or its equivalent, and must have a Texas medical license. Applicants are requested to send their CV to John H. Harris, Jr., M.D., D.Sc., Professor and Chairman, Dept. of Radiology, The University of Texas Medical School at Houston, 6431 Fannin St., Ste. 2.132, Houston, TX 77030. The University of Texas Health Science Center at Houston is an equal opportunity employer. Women and minorities are encouraged to apply. 1-6a

**ASSISTANT, ASSOCIATE, OR FULL PROFESSOR OF THORACIC RADIOLOGY**—The University of Texas Medical School at Houston has an opening for a thoracic radiologist to perform clinical thoracic radiology exams and procedures and participate in resident and medical student teaching. Candidates should have completed an approved residency in diagnostic radiology and must have postresidency experience or training in thoracic radiology. Candidates must be board-certified by the ABR, or equivalent, and must have a Texas medical license. Compensation will be based on the most recent AAMC survey and the candidate's qualifications. Applicants should send a CV, along with the names and addresses of 3 references, to John H. Harris, Jr., M.D., D.Sc., Professor and Chairman, Dept. of Radiology, The University of Texas Medical School at Houston, 6431 Fannin St., Ste. 2.132, Houston, TX 77030. The University of Texas Health Science Center at Houston is an equal opportunity employer and encourages women and minority candidates to apply. 1-6a

**ASSISTANT, ASSOCIATE, OR FULL PROFESSOR OF DIAGNOSTIC RADIOLOGY**—The University of Texas Medical School at Houston has an opening for a general diagnostic radiologist to perform clinical radiologic exams and procedures and to participate in resident and medical student teaching. Candidates should have completed an approved residency in diagnostic radiology. Postresidency experience or training would be preferable, but not mandatory, at the assistant professor level. Candidates must be board-certified by the ABR, or equivalent, and must have a Texas medical license. Compensation will be based on the most recent AAMC survey and the candidate's qualifications. Applicants should send a CV, along with the names and addresses of 3 references, to John H. Harris, Jr., M.D., D.Sc., Professor and Chairman, Dept. of Radiology, The University of Texas Medical School at Houston, 6431 Fannin St., Ste. 2.132, Houston, TX 77030. The University of Texas Health Science Center at Houston is an equal opportunity employer and encourages women and minority candidates to apply. 1-6a

**SEATTLE AREA**—Opening for a BC general diagnostic radiologist with basic angio and interventional skills. Washington license not required. Teaching hospital, regular hours, limited call, and 5-yr contract. Call G. Bernstein, M.D.; (206) 840-9652. 1-3xa

**DIAGNOSTIC RADIOLOGY, PACIFIC NORTHWEST, MRI, CT, AND ULTRASOUND**—Progressive group of 4 radiologists seeks board-certified radiologist with subspecialty interest and expertise in MRI, CT, and ultrasound. Busy, dynamic practice in regional medical center hospital, privately owned MRI center (presently mobile unit—planning for fixed site in spring 1990), plus private outpatient office. Located in beautiful recreation area in the Inland Northwest. World-class lakes for boating and sailing. Excellent skiing, hunting, and fishing. Family-oriented environment 30 min from Spokane. Competitive starting salary with full partnership in 1 yr. Send CV to Richard Hehn, M.D., Radiology Associates of North Idaho, 1104 Ironwood Dr., Coeur d'Alene, ID 83814; (208) 667-0886. 1-3ap

**SITKA, ALASKA**—Challenging diagnostic radiology practice, JCAHO-accredited Alaska Native Indian Health Service Hospital. Includes ultrasound and mammography. Close professional association with primary-care physicians. Requires acceptance in USPHS Commissioned Corps. Send inquiries, CV, and references to S. Carlson, M.D., Clinical Director, Mt. Edgecumbe Hospital, 222 Tongass Dr., Sitka, AK 99835; (907) 966-8310. 1-5ap

**DIAGNOSTIC RADIOLOGIST**—BC/BE to join 2 radiologists in 50-physician, multispecialty clinic. Fellowship in body imaging preferred. Practice includes general radiography, CT, ultrasound, MRI, and film-screen mammography. Excellent first yr salary leading to partnership. Send CV to Michael D. Lavine, M.D., 333 Dixie Hwy., Chicago Heights, IL 60411. 1-3ap

**DIAGNOSTIC RADIOLOGIST**—The University of Tennessee, Memphis/University Physicians Foundation has an opening for a radiologist at the instructor or assistant professor level. Applicant must be board-certified/eligible in diagnostic radiology. Subspecialty interests are encouraged but not required. Blacks, women, handicapped, and other minorities are encouraged to apply. University of Tennessee, Memphis/University Physicians Foundation is an equal employment opportunity/affirmative action/Title IX/Section 504 employer. Send CV to Barry Gerald, M.D., Chairman, Dept. of Radiology, University of Tennessee, Memphis, 800 Madison Ave., Memphis, TN 38163. 3xa

**ULTRASOUND RADIOLOGIST**—The University of Tennessee, Memphis/University Physicians Foundation has an opening for a radiologist in ultrasound at the instructor or assistant professor level. Applicant must be board-certified/eligible in diagnostic radiology. Additional training in ultrasound is highly desirable and the applicant should be particularly conversant with obstetric ultrasonography. Blacks, women, handicapped, and other minorities are encouraged to apply. The University of Tennessee, Memphis/University Physicians Foundation is an equal employment opportunity/affirmative action/Title IX/Section 504 employer. Send CV to Barry Gerald, M.D., Chairman, Dept. of Radiology, University of Tennessee, Memphis, 800 Madison Ave., Memphis, TN 38163. 3xa

**PEDIATRIC RADIOLOGIST**—The University of Tennessee, Memphis/University Physicians Foundation has an opening for a pediatric radiologist. Faculty rank of assistant or associate professor based on experience. Applicant must be board-certified/eligible in diagnostic radiology. At least 1 yr of postgraduate training in a recognized program in pediatric radiology is required. Primary work sites will be LeBonheur Children's Medical Center and St. Jude Children's Research Hospital. Blacks, women, handicapped, and other minorities are encouraged to apply. The University of Tennessee, Memphis/University Physicians Foundation is an equal employment opportunity/affirmative action/Title IX/Section 504 employer. Address inquiries to Barry Fletcher, M.D., Chairman, Diagnostic Imaging Dept., St. Jude Children's Research Hospital, 332 N. Lauderdale, Memphis, TN 38101, or Robert A. Kaufman, M.D., Director, Dept. of Radiology, The University of Tennessee, Memphis/LeBonheur Children's Medical Center, 800 Madison Ave., Memphis, TN 38163. 3xa

**MRI RADIOLOGIST NEEDED**—A position will be available July 1, 1990, at Good Samaritan Regional Medical Center in Phoenix, AZ. The hospital is a 750-bed, tertiary-care facility offering the most up-to-date radiology services. The radiology group is seeking to add a new associate who is board-certified and has at least 1 yr of MR fellowship training. Responsibilities primarily include body MR interpretation. The hospital will have 2 high-strength magnets and there also will be a midstrength magnet at a satellite office. The position offers an academic-style practice with the benefits of a private radiology group. A competitive salary and benefits are offered leading to partnership. Please contact Ted Ditchek, M.D., or Aubrey Palestrant, M.D.; (602) 239-4601. 1-4ap

**RADIOLOGIST, TYLER, TX**—The University of Texas Health Center at Tyler, Dept. of Radiology, Tyler, TX, invites applications for a faculty position at the level of assistant or associate professor, to open July 1, 1990. Interest in teaching and/or research is desired but not required. Progressive, 4-person dept. practices general radiology including interventional, with a total of 27,000 exams/yr. The University of Texas Health Center at Tyler, the state's designated chest disease hospital, is located just outside of Tyler on a beautiful, 600-acre campus amid the forests and lakes of East Texas. The dept. also supports a rapidly growing, dynamic research group located on campus in a new, state-of-the-art research facility. Year-round tennis, golf, and boating are available in addition to excellent schools. Competitive first-yr salary and an unsurpassed benefits package are offered. Send CV to J. R. Shepherd, M.D., University of Texas Health Center at Tyler, P. O. Box 2003, Tyler, TX 75710; (214) 877-7100. The University of Texas Health Center at Tyler is an affirmative action, equal opportunity employer. Minorities are encouraged to apply. 12-5a

**DIAGNOSTIC RADIOLOGIST FOR FLORIDA GULF COAST**—The University of South Florida (USF) Dept. of Radiology, is recruiting a board-certified general diagnostic radiologist. Previous subspecialty training or special interest in musculoskeletal radiology preferred. This is a combined appointment with the Tampa Veterans Hospital and the Dept. of Radiology, USF, at the assistant or associate professor level, dependent on prior credentials. Competitive salary and generous fringe benefits are derived from both institutions. The location is the beautiful west coast of Florida with ideal climate. The position involves clinical service, teaching of radiology residents, and research. Send letters of inquiry with CV to Michael Vermess, M.D., Professor of Radiology, Chief, Radiology Service, James A. Haley Veterans' Hospital, 13000 Bruce B. Downs Blvd., Tampa, FL 33612. 3ap

**GENERAL RADIOLOGIST** needed July 1, 1990, or sooner to replace retiring member of 3-person group servicing a small but busy hospital in scenic area of western Pennsylvania; also own private outpatient office. Necessary skills: general, CT, ultrasound, mammography, and nuclear medicine. Generous salary with early advancement to partnership available. Contact Alan Stankiewicz, M.D., 623 Lang Ave., Patton, PA 16668; (814) 674-8508. 12-5ap

**DIAGNOSTIC RADIOLOGIST**—Progressive, 4-member group in eastern North Carolina seeks BC/BE radiologist with multimodality interests and fellowship training in MR or interventional radiology to join a 10-person group serving a 337-bed acute-care hospital and 2 outpatient clinics. Teaching opportunities are available with residents of subspecialty services on rotation from Stanford University Hospital and our own medical residents. We are currently siting a GE 1.5-T MRI system and installing a new LU arm. Competitive salary and excellent benefits. Please send inquiries and CV to Bruce Baker, M.D., Chief, Dept. of Radiology, Kaiser-Permanente Medical Center, 900 Kiely Blvd., Santa Clara, CA 95051; (408) 236-4444. EOE 2-4a

**NORTHERN CALIFORNIA/SAN FRANCISCO BAY AREA**—The Permanente Medical Group is seeking a BC radiologist with multimodality interests and fellowship training in MR or interventional radiology to join a 10-person group serving a 337-bed acute-care hospital and 2 outpatient clinics. Teaching opportunities are available with residents of subspecialty services on rotation from Stanford University Hospital and our own medical residents. We are currently siting a GE 1.5-T MRI system and installing a new LU arm. Competitive salary and excellent benefits. Please send inquiries and CV to Bruce Baker, M.D., Chief, Dept. of Radiology, Kaiser-Permanente Medical Center, 900 Kiely Blvd., Santa Clara, CA 95051; (408) 236-4444. EOE 2-4a

**THE OREGON HEALTH SCIENCES UNIVERSITY**, Dept. of Radiology, Portland, OR, invites applications for faculty positions in MRI, neuro-radiology, general radiology, skeletal radiology, vascular and interventional radiology, GU radiology, pediatric radiology, computed body tomography, and ultrasound. A second Ph.D. NMR scientist also is being sought. The Oregon Health Sciences University is an affirmative action, equal opportunity employer. Send CV to Richard W. Katzberg, M.D., Chairman of Diagnostic Radiology, L340, The Oregon Health Sciences University, 3181 S.W. Sam Jackson Park Rd., Portland, OR 97201-3098. 5-4ap

**DIAGNOSTIC RADIOLOGIST**—Immediate opening for a board-certified/eligible general diagnostic radiologist at the VA Medical Center, Atlanta, GA. Must be proficient in body CT, ultrasound, and related interventional procedures. We offer a full range of federal employee benefits. Qualified applicants will receive a clinical faculty appointment at the Emory University Medical School. For further information, call Jeanie McCleary at (404) 728-7637 or write VA Medical Center, 1670 Clairmont Rd., Atlanta (Decatur), GA 30033. EOE. 1-4a

**IMMEDIATE UNEXPECTED OPENING FOR BE/BC DIAGNOSTIC RADIOLOGIST** to join 5-man group in Missoula, MT, a university city of 50,000, located in mountainous, western Montana. Looking for a general radiologist with proficiency in MRI, ultrasound, CT, angiography, etc. Administrative skills preferable. Our group of 6 full-time radiologists covers both of Missoula's hospitals (210 and 130 beds). Progressive medical environment with 100+ physicians. One yr to full partner income and 2 yr to partnership. Abundant, nearby recreational opportunities including skiing, fishing, backpacking, hunting, etc. Send CV to Missoula Radiology, Inc., P. O. Box 2039, Missoula, MT 59806. 3-4ap

**VASCULAR/INTERVENTIONAL RADIOLOGIST**—Board-certified radiologist with fellowship training in vascular/interventional radiology wanted to share already established vascular/interventional practice by expanding 7-person, fee-for-service radiology group (corporation) serving a medical center composed of a 235-bed community hospital and a 100-bed cancer center, with a large outpatient practice, residency affiliation, and ongoing research program. We are looking for an individual who also wants to be actively involved in MRI/CT and the other imaging modalities of the practice. Please submit CV to William H. Hartz, M.D., Dept. of Radiology, Jeanes Hospital and Fox Chase Cancer Center, Philadelphia, PA 19111; (215) 728-2158. 3ap

**THE RADIOLOGY DEPT.**, University of Massachusetts Medical Center, is seeking a full-time radiologist with interest in trauma, emergency room, and musculoskeletal radiology. The Medical Center is a 370-bed university hospital and medical school located in Worcester, MA, approximately 40 mi. west of Boston. The dept. consists of 19 clinical staff, 12 residents, and 3 fellows and sees approximately 120,000 exams/yr. The dept. is well-equipped with 2 fourth-generation CT scanners, two 1.5-T GE MR scanners, and a 2.0-T small-bore unit for animal research. The hospital is a major trauma center and is serviced by 2 Life Flight helicopters. The candidate must be board-eligible/certified and have a clinical background in skeletal radiology. Please send CV/requests to Dr. Edward H. Smith, Chair, Dept. of Radiology, University of Massachusetts Medical Center, 55 Lake Ave. N., Worcester, MA 01655. The University of Massachusetts Medical Center is an equal opportunity employer. 3-5a

## Positions Desired

**GENERAL DIAGNOSTIC RADIOLOGIST**—Board-certified, MRI fellowship. Four yr angio/interventional experience in busy practice. Prefer general diagnostic with some subspecialization. Competent in nuclear medicine and ultrasound. Desire partnership opportunity. Impeccable references. Available July 1990. Reply Box Y52, AJR (see address this section). 3-6bp

## Fellowships and Residencies

**NEURORADIOLOGY FELLOWSHIP, THOMAS JEFFERSON UNIVERSITY HOSPITAL**—An unexpected opening for a neuroradiology fellow is available in the Dept. of Radiology at Thomas Jefferson University Hospital, beginning July 1990. The Division of Neuroradiology has close clinical and research relationships with Jefferson's very active neurology, neurosurgery, orthopedic surgery, and otolaryngology depts. Complete training in ENT radiology is part of this program. Five full-time faculty members currently staff this division. Clinical facilities include 2 dedicated CT scanners, a myelography room, a biplane angiography room with DSA, and a GE 1.5-T MRI unit. Two more MRI units will be operational by the summer of 1990. Contact Carlos Gonzalez, M.D., Director of Neuroradiology, 1009 Main Bldg., Thomas Jefferson University Hospital, Philadelphia, PA 19107; (215) 928-5447. Jefferson is an affirmative action/equal opportunity employer. 3xc

**FELLOWSHIPS AT THOMAS JEFFERSON UNIVERSITY HOSPITAL**—The Dept. of Radiology at Thomas Jefferson University Hospital in Philadelphia offers 6 different fellowship programs each yr: ultrasound/CT/MRI - contact Barry Goldberg, M.D.; cardiovascular/interventional - contact Geoffrey Gardiner, Jr., M.D.; neuroradiology/ENT - contact Carlos Gonzalez, M.D.; chest/breast imaging - contact Robert Steiner, M.D. or Stephen Feig, M.D.; MRI - contact Matthew Rifkin, M.D.; and musculoskeletal (including MRI) - contact David Karasick, M.D. We have a large and well-equipped dept. performing 180,000 exams/yr. Our ultrasound division occupies a spacious new facility and provides training in all phases of ultrasound, including obstetrical, vascular, lithotripsy, and endoluminal. The dept. has 3 modern CT scanners and operates 3 GE 1.5-T MRI units also. The interventional radiology division recently has opened an entirely new angio suite housing state-of-the-art Philips units with DSA. This division performs the full range of both vascular and nonvascular interventional procedures. The neuroradiology division is housed in a neurosciences imaging center containing all imaging modalities in a single comprehensive facility. A large new breast imaging center now operates 5 mammography units and performs breast ultrasound studies also. All program directors listed above can be contacted at the Dept. of Radiology, Thomas Jefferson University Hospital, Philadelphia, PA 19107. Jefferson is an equal opportunity/affirmative action employer. 3xc

**FELLOWSHIP IN MRI/CT/ULTRASOUND**—Starting July 1, 1990, a 1-yr fellowship is available at the Medical Center of Delaware, an 1100-bed, tertiary-care, teaching hospital performing over 2100 body and spine MR, 3600 body and spine CT, and 10,000 ultrasound studies/yr. The fellowship program offers training in body MRI, CT, and ultrasound. MRI and CT of the spine are included, and experience in cranial MRI is available as an elective. For further information, contact John S. Wills, M.D., Dept. of Radiology, Medical Center of Delaware, Newark, DE 19718. 2-3cp

**FELLOWSHIP IN PEDIATRIC RADIOLOGY—**

LeBonheur Children's Medical Center/St. Jude Children's Research Hospital/The University of Tennessee, Memphis/University Physicians Foundation, Inc. combined program in pediatric radiology offers a 1- or 2-yr fellowship in pediatric radiology. There are approximately 75,000 pediatric exams performed annually by 10 full-time radiologists. Two fellowship positions are available annually. Training includes all aspects of pediatric imaging, including neonatal, neuro, nuclear, oncologic, cardiovascular, special and interventional procedures, ultrasound, CT, and MRI. Facilities include Doppler ultrasound, CT, and MRI. Opportunity to participate in MRI and other imaging research. Blacks, women, handicapped, and other minorities are encouraged to apply. The University of Tennessee, Memphis/University Physicians Foundation, Inc. is an equal employment opportunity/affirmative action/Title IX/Section 504 employer. Address inquiries to Barry D. Fletcher, M.D., Chairman, Diagnostic Imaging Dept., St. Jude Children's Research Hospital, 332 N. Lauderdale, Memphis, TN 38101 or Robert A. Kaufman, M.D., Director, Dept. of Radiology, LeBonheur Children's Medical Center/The University of Tennessee, Memphis, 800 Madison Ave., Rm. 114C Chandler, Memphis, TN 38163. 3xc

**THE UNIVERSITY OF PITTSBURGH** offers fellowships in angiography/interventional radiology, abdominal imaging (CT/ultrasound/MRI), neuroradiology, pediatric radiology, and MRI. Positions in all of these areas are available to begin July 1991. A fellowship position in pediatric radiology and 1 in abdominal imaging are also available to begin July 1990. Interested applicants should send letters of inquiry and CV to Lawrence A. Cooperstein, M.D., Dept. of Radiology, Presbyterian-University Hospital, DeSoto at O'Hara Sts., Pittsburgh, PA 15213. 3-7cp

**FELLOWSHIP IN PEDIATRIC RADIOLOGY AT CHILDRENS HOSPITAL LOS ANGELES—CHLA**

is offering fellowships starting July 1991 in general pediatric radiology, pediatric neuroradiology, and pediatric nuclear radiology. This 300-bed hospital has 8 full-time radiology faculty and extensive pediatric specialty services. The dept. is equipped with MRI, color Doppler ultrasound, CT, SPECT, special procedures suite, and PET scanning (at USC campus). Research programs are in place. Active transplant, oncology, neurology, neonatal, and trauma services are features of the hospital. Send inquiries to Beverly P. Wood, M.D., Dept. of Radiology, 4650 Sunset Blvd., Los Angeles, CA 90027; (213) 669-5686. Childrens Hospital Los Angeles is an affirmative action/equal opportunity employer. 2-3cp

**ANGIOGRAPHY/INTERVENTIONAL RADIOLOGY FELLOWSHIP—**

New York Medical College will offer a 1-yr fellowship to begin July 1, 1991. The program includes training in all phases of diagnostic angiography and interventional radiologic techniques. Training is based at Westchester County Medical Center, a 650-bed, tertiary-care center located on the medical college campus in a prestigious suburban setting only about 1/2 hr from New York City. Active participation in clinical management of patients is emphasized. Approximately 900 procedures were performed in 1989. Current research interests include transmesenteric sclerosis of portal varices and hepatic arterial chemoembolization. A new digital interventional suite will open in February 1990. A digital biplane imaging suite is anticipated before July 1991. For additional information and application, contact Stuart Katz, M.D., Dept. of Radiology, New York Medical College, Valhalla, NY 10595; (914) 285-8388. 2-4c

**PEDIATRIC RADIOLOGY FELLOWSHIP, IMMEDIATE OPENING—**

Position available for fellowship in pediatric radiology, 1 or 2 yr, beginning on July 1, 1990, or July 1, 1991. Full training with abundant hands-on experience with all imaging modalities. Supported by strong Dept. of Pediatrics with a good mixture of patient material. Excellent teaching on a 1-to-1 basis and ample opportunity for pursuing academic interests. Apply to Leonard E. Swischuk, M.D., Dept. of Radiology, The University of Texas Medical Branch, Child Health Center, C-65, Galveston, TX 77550; (409) 761-2096. UTMB is an equal opportunity M/F/H/V affirmative action employer. UTMB hires only individuals authorized to work in the United States. 2-4c

**PEDIATRIC RADIOLOGY FELLOWSHIP—**

The Dept. of Radiology at Children's Hospital of Philadelphia (CHOP) offers a 1- or 2-yr pediatric radiology fellowship beginning July 1, 1990. CHOP is a 294-bed pediatric hospital. Radiology has an attending faculty of 11 and performs 80,000 cases/yr (plain films, fluoroscopy, ultrasound, CT, nuclear medicine, neuroradiology, angiography/interventional radiology, and MRI). Our equipment is state-of-the-art and new since 1988, including ATL ultrasound equipment, with duplex and color-flow Doppler, gamma camera with SPECT, and a high-resolution fast Siemens Somatom Plus CT scanner. A 1.5-T Siemens Magnetom MRI installation devoted to children has recently opened. We have an active teaching program for radiology residents and fellows. The patient population is large and varied, from routine emergencies to complicated tertiary-care problems. The fellowship provides not only a broad clinical experience with subspecialty training but offers opportunities for clinical and basic research and scholarship. Applicants must have completed a diagnostic radiology residency, be board-certified or eligible, and must obtain a Pennsylvania medical license. Special (1-yr) cross-sectional imaging (CT, ultrasound, and MRI) fellowships negotiable also. Salary and fringe benefits are highly competitive. Address inquiries to Sandra S. Kramer, M.D., Dept. of Radiology, The Children's Hospital of Philadelphia, 34th St. and Civic Center Blvd., Philadelphia, PA 19104; (215) 590-2575. The Children's Hospital of Philadelphia and the University of Pennsylvania are equal opportunity/affirmative action employers. 2-4cp

**FELLOWSHIPS IN ABDOMINAL IMAGING—**

The Dept. of Radiology at the University of Texas Medical School at Houston has openings for 2 abdominal imaging fellowships to begin July 1991. Under faculty direction and supervision, candidates will further their training in the specialty of abdominal imaging including CT, ultrasound, and MRI through 4-mo rotations in each service. Candidate will participate in teaching in each section at the medical student and resident levels, will have the opportunity to conduct basic or clinical research, and will be expected to prepare and submit at least 1 scientific article to an appropriate refereed journal. Candidate must be a graduate of an approved U.S. medical school or its equivalent, must have completed an approved residency in diagnostic radiology, must be a diplomate of the ABR, and must have a Texas medical license. Please submit CV, along with the names and addresses of 3 references, to John H. Harris, Jr., M.D., D.Sc., Professor and Chairman, Dept. of Radiology, The University of Texas Medical School at Houston, 6431 Fannin St., Ste. 2.132, Houston, TX 77030. The University of Texas Health Science Center at Houston is an equal opportunity employer. Women and minorities are encouraged to apply. 1-6c

**FELLOWSHIPS IN NEURORADIOLOGY—**

The Dept. of Radiology at the University of Texas Medical School at Houston has openings for 1- and 2-yr neuroradiology fellowships to begin July 1990 and July 1991. Under faculty supervision, candidates will be responsible for neuroradiologic exams and procedures (i.e., angiograms, myelograms, CT, MR imaging, and in vivo spectroscopy). The candidate will participate in teaching at the medical student and resident levels and will conduct basic or clinical research. Candidate must be a graduate of an approved U.S. medical school or its equivalent, must have completed an approved residency in diagnostic radiology, must be a diplomate of the ABR, and must have a Texas medical license. Please submit CV, along with the names and addresses of 3 references, to John H. Harris, Jr., M.D., D.Sc., Professor and Chairman, Dept. of Radiology, The University of Texas Medical School at Houston, 6431 Fannin St., Ste. 2.132, Houston, TX 77030. The University of Texas Health Science Center at Houston is an equal opportunity employer. Women and minorities are encouraged to apply. 1-6c

**FELLOWSHIPS IN PEDIATRIC RADIOLOGY, JULY 1991—**

The Dept. of Radiology, Children's Hospital Medical Center, Cincinnati, OH, offers 1- or 2-yr fellowships in pediatric radiology beginning July 1991. Children's Hospital Medical Center is a 355-bed institution where approximately 100,000 radiological exams are performed annually by 13 full-time faculty radiologists. Four fellowship positions are available annually. Training includes all aspects of pediatric imaging: neonatal radiology, neuroimaging, musculoskeletal radiology, cardiovascular and thoracic imaging, abdominal imaging, oncologic imaging, ultrasonography, nuclear medicine, CT, MRI, and vascular/interventional techniques. Facilities include digital fluoroscopy, Acuson and ATL ultrasound units with Doppler and color-flow Doppler capabilities, Gamma and SPECT tomographic nuclear cameras, GE 9800 Quick CT scanner, 1.5-T GE MRI, and cardiac catheterization/angiographic suite with digital vascular imaging. Numerous opportunities to participate in both clinical and basic research. Salary and fringe benefits are highly competitive. Candidates must be board-certified or board-qualified in diagnostic radiology and must be able to obtain an Ohio medical license. Children's Hospital Medical Center and the University of Cincinnati College of Medicine are affirmative action/equal opportunity employers. Address inquiry and CV to Donald R. Kirks, M.D., Director, Dept. of Radiology, Children's Hospital Medical Center, Elland and Bethesda Aves., Cincinnati, OH 45229-2899; (513) 559-8058. 1-12cp

**FELLOWSHIP POSITIONS—**

Applications are invited now for July 1991. Positions are available in neuroradiology, vascular/interventional radiology, and body imaging (CT/ultrasound/MRI). For information, contact James R. Schmidgall, M.D. or Richard W. Katzberg, M.D., Chairman, Dept. of Radiology, L-340, Oregon Health Sciences University, 3181 S. W. Sam Jackson Park Rd., Portland, OR 97201. 7-6c

**FELLOWSHIP IN ULTRASOUND AND BODY**

**CT/MRI—**July 1, 1991 to June 30, 1992, at the New York Hospital/Cornell Medical Center. Dept. provides state-of-the-art equipment, including Acuson ultrasound, GE 9800 CT, and GE Signa 1.5-T MR. Wide variety of ultrasound exams include abdominal, OB-GYN, color Doppler, small parts, neonatal head, transvaginal, and transrectal. Applicants should be ABR eligible or certified. Send CV to Elias Kazam, M.D., Dept. of Radiology, The New York Hospital/Cornell Medical Center, 525 E. 68th St., New York, NY 10021. 1-3cp

**MRI FELLOWSHIP AT THOMAS JEFFERSON UNIVERSITY HOSPITAL**—A new MRI fellowship position has been created in the Dept. of Radiology of Thomas Jefferson University Hospital, Philadelphia. This 1-yr position encompasses a full range of clinical and research activities. The MRI division includes 6 staff physicians, 2 MRI physicists, and 3 Signa systems (1.5T). The position is available as of Jan. 1990, but applications will also be taken for the academic year beginning in July 1990. Send inquiries to Matthew Rifkin, M.D., Dept. of Radiology, Thomas Jefferson University Hospital, Philadelphia, PA 19107. Jefferson is an equal opportunity/affirmative action employer. 9-6c

**CARDIOVASCULAR-INTERVENTIONAL RADIOLOGY FELLOWSHIP**—Available July 19, 1989. One-year fellowship program at a 750-bed teaching hospital. Extensive clinical experience involving all aspects of cardiovascular imaging, interventional vascular and nonvascular procedures, and availability for clinical or animal research. Send CV and Inquiries to Oscar H. Gutierrez, M.D., Dept. of Radiology, Box 648, University of Rochester Medical Center, Rochester, NY 14642. An equal opportunity employer (M/F). 1-6c

### Tutorials/Courses

**SIXTH ANNUAL LONDON-PARIS ULTRASOUND CONGRESS, SEPTEMBER 15-22, 1990**—Category I accreditation followed by OPTONAL LOIRE VALLEY BICYCLE TOUR. For information contact Medical Seminars International, Inc., 9800 D Topanga Canyon Blvd., Ste. 232, Chatsworth, CA 91311; (818) 700-9821. 3-8d

**ALASKA 90—CRUISE THE INLAND PASSAGE**, July 6-13, 1990. Patrick Collett, M.D., University of Southern California, MRI tutorial and course. Category I CME credits. For information, contact Medical Seminars International, Inc., 9800 D Topanga Canyon Blvd., Ste. 232, Chatsworth, CA 91311; (818) 700-9821. 1-6d

### Other

**LOIRE VALLEY BICYCLE ULTRASOUND CONGRESS**, Sept. 22-29, 1990. Optional, following Sixth London-Paris Fall Ultrasound Congress. For information, contact Medical Seminars International, Inc., 9800 D Topanga Canyon Blvd., Ste. 232, Chatsworth, CA 91311; (818) 700-9821. 1-3e

**VISITING PROFESSORSHIP, THOMAS JEFFERSON UNIVERSITY HOSPITAL**—The Dept. of Radiology at Thomas Jefferson University Hospital in Philadelphia offers a visiting professorship in our Division of General Diagnostic Radiology. The position commences July 1990 and will be available for 2 yr, while several of our faculty members are on sabbatical leave. Funding for the position is appropriate for a senior faculty member from another institution on sabbatical with partial funding or for a junior faculty member. In addition to working in the General Diagnostic Division, the visiting radiologist will have access, for research or educational purposes, to state-of-the-art MRI, CT, and ultrasound units, and to well-equipped physics and physiology research laboratories. Liberal research time will be available. Interested individuals should contact David C. Levin, M.D., Chairman, Dept. of Radiology, Thomas Jefferson University Hospital, Philadelphia, PA 19107. Jefferson is an equal opportunity/affirmative action employer. 11-10e

## AJR Classified Advertisements Information

### Box Responses and Address for Ad Placement

Write Box \_\_\_\_\_, AJR, 2223 Avenida de la Playa, Suite 200, La Jolla, CA 92037-3218; (619) 459-2229; FAX: (619) 459-8814.

### How to Place an Ad

AJR accepts classified advertising for Positions Available, Positions Desired, Fellowships and Residencies, and Tutorials/Courses. Ads are accepted by mail or FAX.

**Rates:** \$6.00/line with a \$30 minimum charge. Box service is \$10 additional for each month the ad appears. There are discounts for multiple insertions: 10% for 2-3 insertions; 20% for 4 or more. To estimate lines, count all words and divide by 7.

**Billing:** Ads must be prepaid, or advertisers will be billed after the ad appears providing a purchase order number is submitted with the advertising copy. Terms are net 30 days.

**Deadlines:** 6 weeks prior to issue date. For specific deadlines, telephone the AJR editorial office.

### Estimating Ad Charges

Line charge: divide total words by 7 and multiply by \$6.00	.....	\$
Multiple insertions? If so, multiply by number	.....	x
Subtotal	.....	\$
Discount applies to two or more insertions. Subtract 10% if ad appears 2-3 months, 20% if 4 months or more	.....	-
Subtotal	.....	\$
Box response requested? If so, multiply number of months by \$10.00	.....	+
Approximate advertising charge	.....	\$

# GET THE MOST OUT OF IMAGING PROCEDURES

NEW!

## Fetal Sectional Anatomy and Ultrasonography

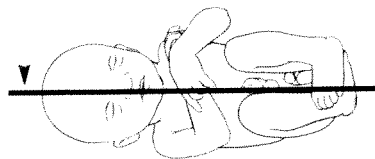
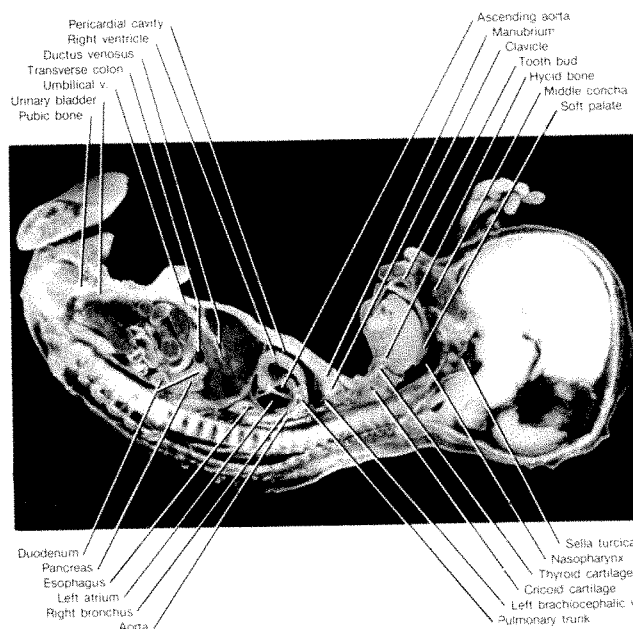
Lewis H. Nelson III, MD and  
Walter J. Bo., PhD

Enhance your interpretive skills with the one text that helps you translate the two-dimensional images on paper to the three-dimensional image you actually see.

Combining images and drawings, this text-free atlas provides the facts you need to get the most out of ultrasonographic procedures. Anatomical sections that feature both sagittal and transverse orientation make this book easy to use during scanning, while the clearly-labeled illustrations eliminate the need for cross-referencing to tables.

Drs. Nelson and Bo have created an atlas which employs not only ultrasonography, but also magnetic resonance imaging and computer tomography as imaging modalities to present a complete reference of fetal anatomy. Serial transverse sections of a mid-pregnancy male fetus and sagittal sections of a term, anencephalic female fetus are labeled on the actual image for easy identification at a glance.

1988/224 pages/365 illustrations/6400-2/\$65.00/\$78.00 outside the US and Canada



*Ordering is as easy as picking up your phone:*

In the US just dial, toll-free  
1-800-638-0672.

30 day FREE trial for all books! (US only)

NEW!

## Computed Cranial and Spinal Imaging

### A Practical Introduction

John M. Stevens

Superb illustrations and eminent authors distinguish this new work on optimal imaging of neurological disorders.

From initial choice of imaging modality through interpretation of results, this text spells out exactly how to approach investigation and management decisions, with the strengths, limitations, and uses of CT and MRI examined clearly and in detail. Both normal and pathological appearances of the brain, spine, paranasal sinuses, and orbits are examined with extensive accompanying illustrations. You'll also find essential information on when to administer intravenous or intrathecal contrast enhancement.

1988/224 pages/illustrated/  
7931-X/\$44.95 (available only in  
North America)



**Williams & Wilkins**

428 East Preston Street  
Baltimore, Maryland 21202

Broadway House  
2-6 Fulham Broadway  
London SW6 1AA England





## Fuji sets the standard

### Super HR Series Films, The Ultimate in Sharpness.

Fuji's quest for the ultimate sharpness in medical imaging films has produced yet another breakthrough in emulsion technology and set a new standard for image quality.

### Fuji's Sharpest X-ray Film Ever

$\Sigma$ (Sigma) Localized Latent Image Centers ( $\Sigma$ LIC) grain technology and Crossover Control Technology (CCT) increase the efficiency of the film emulsion and significantly reduce the adverse effects of crossover exposure, resulting in Fuji's sharpest x-ray film ever.

### Superior Processing Stability

Specific Localized Latent Image speck formation with high development potential ( $\Sigma$ LIC Grain) results in increased tolerance to changes in developer temperature. This means Fuji Super HR Series Films provide exceptional processing stability for more consistent results.

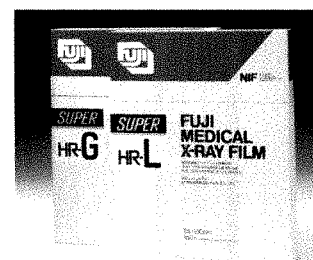
Ask your local Fuji representative or call (800)431-1850 [in CT (203) 353-0300].

CIRCLE 7 ON READER SERVICE CARD



### The Reason for Change!

Burbank - Chicago - Stamford, CT.



## PROGRESS IN RADIOLOGY

- 459 Review article. Monochorionic twinning: sonographic assessment. Filly RA, Goldstein RB, Callen PW

## SPECIAL ARTICLES

- 471 Pictorial essay. Identification of retained firearm projectiles on plain radiographs. Dodd GD III, Budzik RF Jr  
477 Perspective. A tutorial on confidence intervals for proportions in diagnostic radiology. Berry CC

## PULMONARY RADIOLOGY

- 481 Do chest radiographic findings reflect the clinical course of patients with sarcoidosis during corticosteroid withdrawal? Baumann MH, Strange C, Sahn SA  
487 CT in differential diagnosis of diffuse pleural disease. Leung AN, Müller NL, Miller RR  
493 Case report. Cavitary pulmonary metastases in transitional cell carcinoma of urinary bladder. Alexander PW, Sanders C, Nath H  
495 Case report. Reactivation of tuberculosis in a donor lung after transplantation. Carlsen SE, Bergin CJ

## GASTROINTESTINAL RADIOLOGY

- 499 Ileocecal tuberculosis: CT and radiologic evaluation. Balthazar EJ, Gordon R, Hulnick D  
505 Regenerating nodules of liver cirrhosis: MR imaging with pathologic correlation. Ohtomo K, Itai Y, Ohtomo Y, Shiga J, Iio M  
509 Color Doppler flow imaging of liver tumors. Tanaka S, Kitamura T, Fujita M, Nakanishi K, Okuda S  
515 Dynamic spin-echo imaging with Gd-DTPA: value in the differentiation of hepatic tumors. Van Beers B, Demeure R, Pringot J, et al.  
521 Gallbladder contractility in patients with spinal cord injuries: a sonographic investigation. Nino-Murcia M, Burton D, Chang P, Stone J, Perkash I  
525 Hydatid disease of the spleen: imaging findings in nine patients. Franquet T, Montes M, Lecumberri FJ, Eparza J, Bescos JM  
529 Case report. Acute venous thrombosis after pancreas transplantation: diagnosis with duplex Doppler sonography and scintigraphy. Boiskin I, Sandler MP, Fleischer AC, Nylander WA  
533 Technical note. Treatment of acute esophageal food impaction with a combination of glucagon, effervescent agent, and water. Kaszar-Seibert DJ, Korn WT, Bindman DJ, Shortsleeve MJ

## GENITOURINARY RADIOLOGY

- 535 Prevalence and significance of subchorionic hemorrhage in threatened abortion: a sonographic study. Pedersen JF, Mantoni M  
539 Differentiation of seminomatous from nonseminomatous testicular tumors with MR imaging. Johnson JO, Mattrey RF, Phillipson J  
545 Value of transperineal sonography in the assessment of vaginal atresia. Scanlan KA, Pozniak MA, Fagerholm M, Shapiro S

## MUSCULOSKELETAL RADIOLOGY

- 549 Pictorial essay. MR imaging of the shoulder: correlation with plain radiography. Burk DL Jr, Karasick D, Mitchell DG, Rifkin MD  
555 Value of MR imaging in staging osteochondral lesions of the talus (osteochondritis dissecans): results in 14 patients. De Smet AA, Fisher DR, Burnstein MI, Graf BK, Lange RH  
559 Subtalar arthrosis: evaluation with CT. Smith DK, Gilula LA, Totty WG  
563 Pictorial essay. Radiologic appearance of intramuscular hemangioma with emphasis on MR imaging. Buetow PC, Kransdorf MJ, Moser RP Jr, Jelinek JS, Berrey BH

## PEDIATRIC RADIOLOGY

- 569 The significance of hematuria in children after blunt abdominal trauma. Stalker HP, Kaufman RA, Stedje K  
573 False-negative duplex Doppler studies in children with hepatic artery thrombosis after liver transplantation. Hall TR, Mc Diarmid SV, Grant EG, Boechat MI, Busuttil RW

## NEURORADIOLOGY

- 577 MR imaging in patients with intractable complex partial epileptic seizures. Brooks BS, King DW, El Gamal T, et al.  
585 Tumors of the nasopharynx and adjacent areas: MR imaging with Gd-DTPA. Vogl T, Dresel S, Bilaniuk LT, Grevers G, Kang K, Lissner J  
593 The cerebellum: 3. Anatomic-MR correlation in the coronal plane. Press GA, Murakami JW, Courchesne E, Grafe M, Hesselink JR  
603 CT of intracranial cryptococcosis. Popovich MJ, Arthur RH, Helmer E  
607 Intracranial ganglioglioma: MR, CT, and clinical findings in 18 patients. Castillo M, Davis PC, Takei Y, Hoffman JC Jr

## VASCULAR RADIOLOGY

- 613 Treatment of iliac artery stenoses with the Wallstent endoprosthesis. Raillat C, Rousseau H, Joffre F, Roux D  
617 Technical note. Removal of intimal hyperplasia in vascular endoprostheses by atherectomy and balloon dilatation. Vorwerk D, Guenther RW  
621 Technical note. A simple device to facilitate percutaneous insertion of the Kimray-Greenfield filter. Zagoria RJ, Scott MD, D'Souza VJ, Dyer RB

## MR IMAGING

- 623 Pictorial essay. Artifacts in maximum-intensity-projection display of MR angiograms. Anderson CM, Saloner D, Tsuruda JS, Shapeero LG, Lee RE  
631 Technical note. Halo vest for cervical spine fixation during MR imaging. Shellock FG, Slimp G  
633 Technical note. Ghost artifact on gradient-echo imaging: a potential pitfall in hepatic imaging. Silverman PM, Patt RH, Baum PA, Teitelbaum GP

## COMPUTER PAGE

- 635 Planning a totally digital radiology department. Huang HK, Kangaroo H, Cho PS, Taira RK, Ho BKT, Chan KK  
641 Computer-aided management of residents' on-call and vacation schedules. Kahn CE Jr

## MEETING NEWS

- 645 Summary of the 1989 American College of Radiology summit meeting. McClennan BL, Hartman GW

## COMMENTARIES

- 647 Review article. Technology assessment: The contribution of professional organizations. Hendee WR  
652 Implications of technology assessment for the radiologist. Rosenquist CJ

## OTHER CONTENT

- 470 Melvin M. Figley Fellowship recipient  
Book reviews 476, 486, 504, 532, 544, 554, 568, 572, 576, 584, 630, 644  
640 Forthcoming articles  
654 Letters  
661 Review of current literature  
667 News  
671 SPR Scientific Program: 33rd annual meeting, April 19-22  
673 Invitation to 1990 ARRS meeting  
675 ARRS 1990 meeting summary  
676 ARRS 1990 meeting courses and symposium  
679 1990 ARRS meeting registration forms  
682 American Roentgen Ray Society information  
683 Classified advertisements  
A3 Guidelines for authors  
A16 AJR business and subscriber information

# AJR

American  
Journal of  
Roentgenology



April 1990

# SonoVu US™ — a visible improvement in ultrasound-guided aspiration.

The clearly visible bright echoes on the real-time sonogram below mark a breakthrough in accuracy and safety for fine-needle aspiration under ultrasound guidance.

SonoVu US, from E-Z-EM, is the first in a family of procedural needles designed specifically for enhanced ultrasound visualization.

Precisely formed 0.44 mm distal side holes on the cannula closely match the wavelength of ultrasound generated by a 3.5 MHz transducer. Uniform diffraction of the wave at each

hole creates a highly visible echo on the US display.

The side holes also provide a significant increase in needle flow rate, and ensure free flow should the tip become occluded—often the case with spinal or chiba needles.

Developed for use in amniocentesis, the SonoVu design can offer similar benefits in such procedures as US-monitored biopsy and cyst aspiration. For more information on 20- and 22-gauge SonoVu US needles from E-Z-EM, call 1-800-544-4624.

For both the patient and the practitioner, E-Z-EM products set the standards for convenience, safety, and quality in:

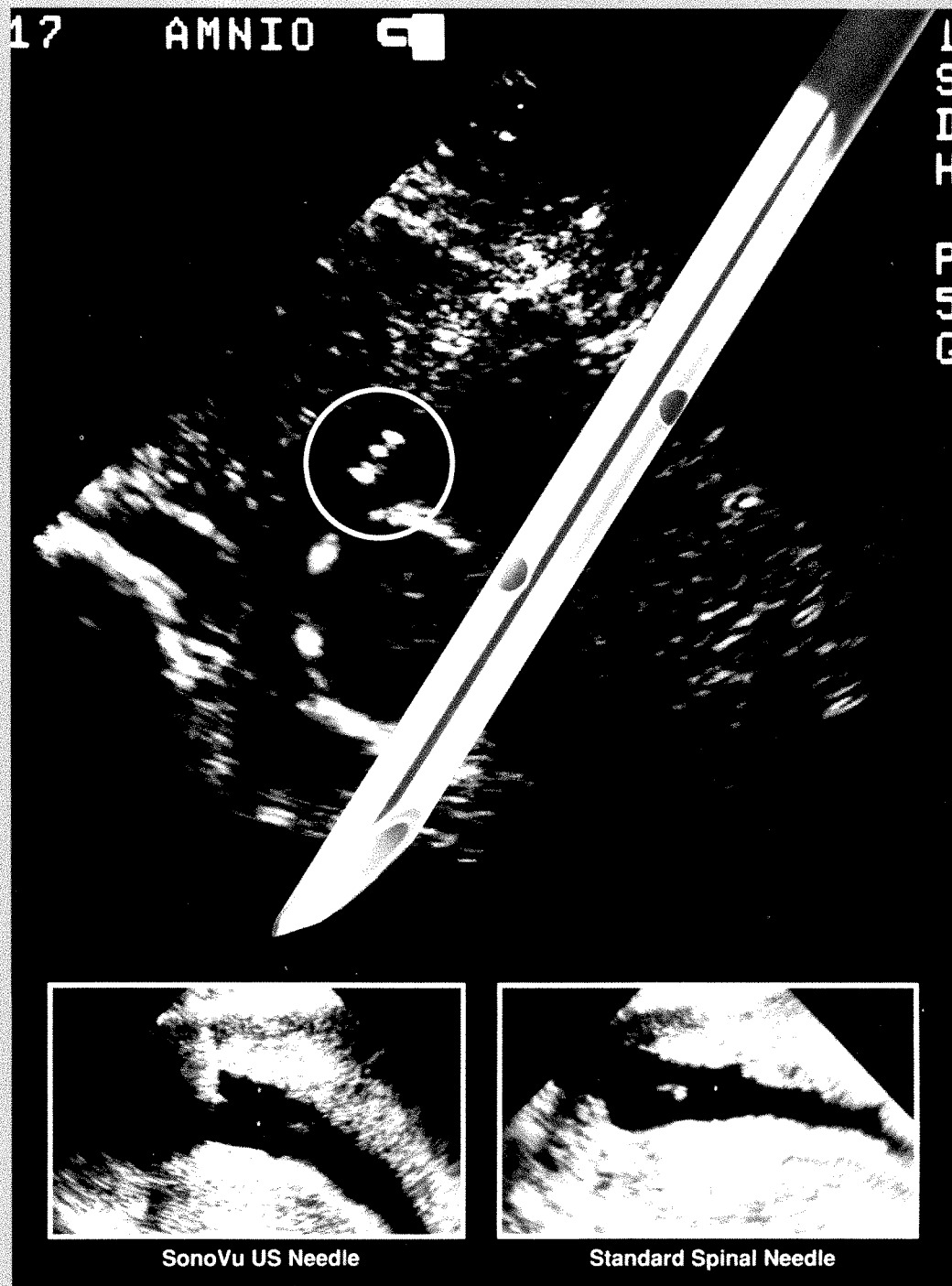
- GI Radiology
- Interventional Radiology
- CT Scanning
- Ultrasound
- Magnetic Resonance Imaging
- Angiography
- CEA Immunostaining
- Radiation Oncology
- Patient Prepping
- Protective Products
- Computerized Information Management Systems



E-Z-EM, Inc.  
Westbury, NY 11590

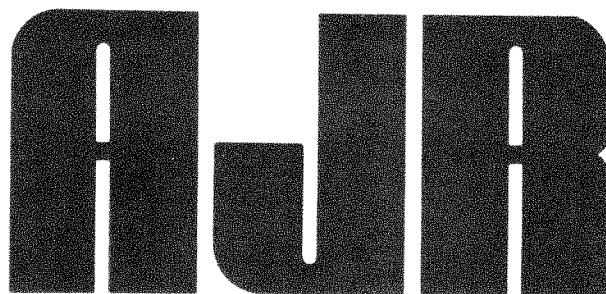
Circle 5 on the Reader Service Card

© 1990, E-Z-EM, Inc.



Reference: *Amniocentesis Needle with Improved Sonoaraphic Visibility*. Radiology 1989; 171: 576 - 577.

Official Journal of the American Roentgen Ray Society



**American Journal of Roentgenology**  
Diagnostic Imaging and Related Sciences

- Editor-In-Chief** Robert N. Berk, *La Jolla, California*  
*University of California, San Diego*  
*School of Medicine and Medical Center*
- Editor Emeritus** Melvin M. Figley, *Seattle, Washington*
- Associate Editor** Saskia von Waldenburg Hilton, *San Diego, California*
- Consulting Editor** Michael S. Huckman, *Chicago, Illinois*
- Statistician** Charles C. Berry, *San Diego, California*

**Editorial Board**

- |                         |                          |                    |
|-------------------------|--------------------------|--------------------|
| John R. Amberg          | John R. Hesselink        | Peter M. Ronai     |
| Eliamar Aviad           | Charles B. Higgins       | Sjef H. J. Ruijs   |
| Mark E. Baker           | Melvyn T. Korobkin       | Stuart S. Sagel    |
| Lawrence W. Bassett     | Faye C. Laing            | David J. Sartoris  |
| Michael A. Bettmann     | Thomas L. Lawson         | Stefan C. Schatzki |
| William G. Bradley, Jr. | Robert G. Levitt         | William P. Shuman  |
| N. Reed Dunnick         | Bruce L. McClennan       | Edward A. Sickles  |
| David K. Edwards        | Richard P. Moser         | Barry A. Siegel    |
| Ronald G. Evens         | Albert A. Moss           | David D. Stark     |
| David S. Feigin         | Jeffrey H. Newhouse      | Edward T. Stewart  |
| Sandra K. Fernbach      | Donald L. Resnick        | Murali Sundaram    |
| Richard H. Gold         | Stewart R. Reuter        | Eric vanSonnenberg |
| William R. Hendee       | Charles A. Rohrmann, Jr. | Robert K. Zeman    |

**Editorial Staff:** Margaret Levene, *managing editor*; Katie L. Spiller, Barbara Rose, Barbara L. Halliburton, and Janine Anderson, *manuscript editors*; Nancy Rydbeck, *office manager*; Sheri Smith, *administrative assistant*; Sandra L. Griffin, *administrative secretary*.

AJR, AMERICAN JOURNAL OF ROENTGENOLOGY (ISSN 0361-803X) is the official journal of the American Roentgen Ray Society and is published monthly by Williams & Wilkins, 428 E. Preston St., Baltimore, MD 21202. Annual dues include \$50 for journal subscription. Second-class postage paid at Baltimore, MD, and at additional mailing offices. Postmaster, send address changes (Form 3579) to AJR, 428 E. Preston St., Baltimore, MD 21202. Subscription rates \$110 (\$155 foreign, \$244 Japan); institutions \$120 (\$165 foreign, \$254 Japan); in training \$25 (\$70 foreign, \$159 Japan); single copy \$16 (\$19 foreign). Japanese rates include airfreight. Japanese yen price is available from our sole agent USACO Corporation, 13-12, Shimbashi 1-Chome, Minato-Ku, Tokyo 105, Japan, telephone 03-502-6471. Airmail rates furnished on request. Indexed by *Current Contents* and *Index Medicus*. Copyright © 1990 by American Roentgen Ray Society.

0361-803X/90\$2.00



# Radiologist MRI Fellowship

The Saudi Arabian Oil Company (SAUDI ARAMCO) Medical Services Organization in Saudi Arabia requires a Radiologist with MRI and neuroradiology experience. American Board Certification and two years' experience after residency is required.

Saudi Aramco's medical facilities provide comprehensive medical care to our employees and their dependents. The patient population is approximately 200,000. The Dhahran Health Center, recently expanded to 483-beds, has all major specialty services as well as most sub-specialties and functions as a referral center. The district clinics each have out-patient and emergency facilities including one clinic with a new 80-bed hospital.

Employment with Saudi Aramco will provide you with interesting lifestyle in a multicultural environment, including comfortable living arrangements, free medical care while in Saudi Arabia, fine schools and a broad spectrum of recreational opportunities, plus 36 calendar days of vacation annually, allowing for extensive travel. We provide an attractive compensation package which includes an expatriate premium.

For immediate consideration, send resume to: **ASC, Employment Dept. 06G-020-0, P.O. Box 4530, Houston, Texas 77210-4530** or call **Velma Guy** at **1-800-827-5700 ext. 8060** or **713-432-8060**.

## SAUDI ARAMCO

World Class Opportunities.



# AJR Guidelines for Authors

Address new and revised manuscripts, correspondence, and classified ads to the Editor:

AJR Editorial Office

2223 Avenida de la Playa, Suite 200

La Jolla, CA 92037-3218

Telephone: (619) 459-2229; FAX: (619) 459-8814

Inquiries regarding subscriptions, display advertising, reprints, or permission to republish *AJR* material should be addressed to the publisher:

The Williams & Wilkins Co.

428 E. Preston St.

Baltimore, MD 21202 Telephone: 1-800-638-6423

The *AJR* publishes original contributions to the advancement of medical diagnosis and treatment. Submitted manuscripts should not contain previously published material and should not be under consideration for publication elsewhere. Papers dealing with neuroradiology should be addressed to: American Journal of Neuroradiology, Dept. of Radiology, Massachusetts General Hospital, Boston, MA 02114. At the discretion of the *AJR* Editor, *AJNR* articles that are of interest to the general reader may be republished in the *AJR*. Neuro-radiologic papers sent to the *AJR* will be forwarded to the Editorial Office of the *AJNR*.

Manuscript decisions are based on peer review. Reviewers receive manuscripts without title pages to ensure an unbiased review. Statements made in the article, including changes made by the Editor or manuscript editor, are the responsibility of the author and not of the *AJR* or its publisher. Authors will be sent the edited manuscript, galley proof, and proofs of illustrations. If the corresponding author will be unavailable to review galleys, arrangements should be made for a coauthor or colleague to read and return the proof.

The following guidelines are based on instructions set forth in the **Uniform Requirements for Manuscripts Submitted to Biomedical Journals** (*Ann Intern Med* 1988;108:258-265). Articles will be edited, however, to conform to the individual style of *AJR*.

## General Guidelines for Major Papers

**Abstract.** Clearly state (in 200 words or less) the purpose, methods, results, and conclusions of the study. Include actual data.

**Introduction.** Briefly describe the purpose of the investigation and explain why it is important.

**Methods.** Describe the research plan, the materials (or subjects), and the methods used, in that order. Explain in detail how disease was confirmed and how subjectivity in observations was controlled.

**Results.** Present results in a clear, logical sequence. If tables are used, do not duplicate tabular data in text, but do describe important trends and points.

**Discussion.** Describe the limitations of the research plan, materials (or subjects), and methods, considering both the

purpose and the outcome of the study. When results differ from those of previous investigators, explain the discrepancy.

## AUTHOR'S CHECKLIST

**For priority handling, complete the following checklist, sign the copyright form on the reverse side of this page, and include both with the manuscript.**

\_\_\_\_\_ Two copies of the manuscript (the original and a photocopy) and two complete sets of figures are submitted. One copy has been retained by the author.

\_\_\_\_\_ If appropriate, *AJR* Guidelines for case reports, technical notes, pictorial essays, or letters to the Editor have been followed. (See page A5.)

\_\_\_\_\_ The manuscript, including references, figure legends, and tables, is typed double-spaced on 8½ × 11 in. (21.6 × 27.9 cm) *nonerasable* paper. Right-hand margins are not justified.

\_\_\_\_\_ All manuscript pages are numbered consecutively beginning with the abstract. Authors' names do not appear on the manuscript pages.

\_\_\_\_\_ The manuscript is organized as follows: title page, blind title page (title only), abstract, introduction, methods, results, discussion, acknowledgments, references, tables, figure legends, and figures.

\_\_\_\_\_ Informed consent has been obtained from patients who participated in clinical investigations. If experiments were performed on animals, authors complied with NIH guidelines for use of laboratory animals.

\_\_\_\_\_ Use of unfamiliar acronyms and abbreviations is kept to a minimum. When abbreviations are used they are defined at first mention, followed by the abbreviation in parentheses.

\_\_\_\_\_ Metric measurements are used throughout, or the metric equivalent is given in parentheses.

\_\_\_\_\_ Names and locations (city and state only) of manufacturers are given for equipment and nongeneric drugs.

## Title Page

\_\_\_\_\_ The following information is given: title of article; names and complete addresses (including zip code) of all authors; current addresses of authors who have moved since study; acknowledgment of grant or other assistance. The corresponding author is clearly identified, and a current address, phone number, and Fax number are given.

\_\_\_\_\_ Two copies of a blind title page are included giving only the title (without the authors' names) for use in the review process.

## Abstract

\_\_\_\_\_ An abstract of approximately 200 words concisely states the purpose, methods, and results of the study in one paragraph. Actual data are included. Conclusions are stated in a second, summary paragraph.

\_\_\_\_\_ No abbreviations or reference citations are used.

## References

References (not to exceed 35) are typed double-spaced starting on a separate page and are **numbered consecutively in the order in which they appear in the text**.

All references are cited in the text and are enclosed in brackets and typed on line with the text (not superscript).

Unpublished data are not cited in the reference list, but are cited parenthetically in the text, for example, (Smith DJ, personal communication), (Smith DJ, unpublished data). This includes papers submitted, but not yet accepted, for publication.

Inclusive page numbers (e.g., 333–335) are given for all references.

Journal names are abbreviated according to *Index Medicus*.

Style and punctuation of references follow the format illustrated in the following examples (all authors are listed when six or less; when seven or more authors, the first three are listed, followed by “et al.”):

### Journal article

1. Long RS, Roe EW, Wu EU, et al. Membrane oxygenation: radiographic appearance. *AJR* 1986;146:1257–1260

### Book

2. Smith LW, Cohen AR. *Pathology of tumors*, 6th ed. Baltimore: Williams & Wilkins, 1977:100–109

### Chapter in a book

3. Breon AJ. Serum monitors of bone metastasis. In: Clark SA, ed. *Bone metastases*. Baltimore: Williams & Wilkins, 1983:165–180

### Paper presented at a meeting

4. Lau FS, Kirk AN. MR imaging of the spine. Presented at the annual meeting of the American Roentgen Ray Society, Washington, DC, April 1986

## Tables

Each table is typed double-spaced on a separate page without vertical or horizontal rules; each has a short, descriptive title. Tables do not exceed two pages in length and contain at least four lines of data.

Tables are numbered in the order in which they are cited in the text.

Abbreviations are defined in an explanatory note below each table.

Tables are self-explanatory and do not duplicate data given in the text or figures.

All arithmetic (percentages, totals, differences) has been double checked for accuracy, and tabular data agree with data given in the text.

## Figures and Legends

Two complete sets of original figures are submitted unmounted in labeled envelopes.

Figures are clean, unscratched, 5 × 7 in. (13 × 18 cm) glossy prints with **white borders**. A separate print is submitted for each figure part.

All figure parts relating to one patient have the same figure number.

Each figure is labeled on the back with the figure number and an arrow indicating “top.” For black-and-white figures, labeling is done on a gummed label, which is then affixed to the back of the print. *Never* use labels on color figures, but write figure number on the back lightly in pencil. *Never* use ink on front or back of any figures.

Author’s names are *not* written on the backs of figures.

Only removable (rub-on) arrows and letters are used on the figures. Symbols are uniform in size and style and are not broken or cracked.

Images are uniform in size and magnification.

Line drawings are done in black ink on a white background. They are professional in quality, and all use the same size type. (Only glossy prints are acceptable.)

Written permission has been obtained for use of all previously published illustrations (and copies of permission letters are included), and an appropriate credit line is given in the legends.

Legends are typed double-spaced, and figure numbers correspond with the order in which the figures are cited in the text.

## Transfer of Copyright Agreement, Conflict of Interest Acknowledgment, Certification of Coauthors, and Exclusive Publication Statement

Complete copyright to the article entitled: \_\_\_\_\_

is hereby transferred to the American Roentgen Ray Society (for United States government employees to the extent transferable), effective if and when the article is accepted for publication in the *American Journal of Roentgenology*. In the case of the authors who are officers or employees of the United States government, the American Roentgen Ray Society recognizes that works prepared by officers or employees of the United States government as part of their official government duties are in the public domain.

Authors reserve all proprietary rights other than copyright, such as patent rights and the right to use all or part of this article in future works of their own. The authors retain the right of replication, subject only to crediting the original source of publication and receiving written permission from the publisher.

Authors guarantee that this manuscript contains no matter that is libelous or otherwise unlawful, invades individual privacy, or infringes any proprietary rights.

Authors understand that they will receive no royalty or other compensation from the American Roentgen Ray Society or the publisher.

Authors guarantee that the editor has been or will be informed of any proprietary or commercial interest or conflicts of interest the authors may have that relate directly or indirectly to the subject of this article.

All authors certify that they have made substantive and specific intellectual contributions to the article and assume public responsibility for its content.

Finally, the authors certify that none of the material in this manuscript has been published previously or is currently under consideration for publication elsewhere.

\_\_\_\_\_  
First author/date

\_\_\_\_\_  
Second author

\_\_\_\_\_  
Third author

\_\_\_\_\_  
Fourth author

\_\_\_\_\_  
Fifth author

\_\_\_\_\_  
Sixth author

**This agreement must be signed by all authors in order for the manuscript to be published.**

### Case Reports

A case report is a brief description of a special case that provides a message that transcends the individual patient.

*Format.* There is no abstract. The introduction should be a short paragraph giving the general background and the specific interest of the case. No more than one case should be described in detail (similar ones can be mentioned briefly in the discussion). Emphasis should be on the radiologic aspects; clinical information must be limited to that necessary to provide a background for the radiology. The discussion should be succinct and should focus on the specific message and relevance of radiologic methods. A review of the literature is not appropriate.

*Length.* Maximum of five double-spaced, typewritten pages, including the references but not the title page or figure legends.

*References.* Maximum of eight.

*Figures.* Maximum of three or four, unless the text is shortened accordingly. Legends must not repeat the text.

*Tables and Acknowledgments.* Not appropriate in case reports.

### Technical Notes

A technical note is a brief description of a specific technique or procedure, modification of a technique, or equipment of interest to radiologists.

*Format.* No abstract, headings, or subheadings are required. If headings are used, they should be a combination of "Case Report," "Materials and Methods," "Results," and "Discussion." A brief one-paragraph introduction should be included to give the general background. Discussion should be limited to the specific message, including the uses of the technique or equipment. Literature reviews and lengthy case reports are not appropriate.

*Length.* Maximum of five double-spaced, typewritten pages, including the references but not the title page or figure legends.

*References.* Maximum of eight.

*Figures.* Maximum of two, unless the text is shortened accordingly.

*Tables and Acknowledgments.* Not appropriate in technical notes.

### Pictorial Essays

A pictorial essay is an article that conveys its message through illustrations and their legends. Unlike other *AJR* articles, which are based on original research, pictorial essays serve primarily as teaching tools, like exhibits at a scientific meeting. They are not encyclopedic book chapters. No abstract is necessary.

*Length.* Maximum of four double-spaced, typewritten pages, including the references but not the title page or figure legends.

*References.* Maximum of four.

*Figures.* Maximum of 30 figure parts. Number should be as few as necessary to convey the message of the paper.

*Tables and Acknowledgments.* Not appropriate in pictorial essays.

### Letters to the Editor and Replies

Letters to the Editor and Replies should offer objective and constructive criticism of published articles. Letters may also discuss matters of general interest to radiologists. Do not end a letter with a hand-written signature.

*Format.* All letters should be typed double-spaced on nonletterhead paper, with no greeting or salutation. Name and affiliation should appear at the end of the letter. Titles for letters should be short and pertinent. The title for a reply is simply "Reply."

*Length.* Maximum of two double-spaced, typewritten pages, including references.

*References.* Maximum of four.

*Figures.* Maximum of two.

*Tables and Acknowledgments.* Not appropriate in Letters to the Editor and Replies.

### Opinions, Commentaries, and Perspectives

Opinions, commentaries, and perspectives are special articles dealing with controversial topics or issues of special concern to radiologists.

*Format.* Include a title page but no abstract. Headings may be used to break up the text.

*Length.* Maximum of five double-spaced, typewritten pages.

*References.* Maximum of five.

*Tables and Figures.* Maximum of four.

### Computer Page Articles

Articles published on the computer page deal with practical computer applications to radiology.

*Format.* Include a title page but no abstract.

*Length.* Maximum of eight double-spaced, typewritten pages.

*References.* Maximum of five.

*Figures and Tables.* Maximum of five. Computer printouts are not acceptable. Figures must be submitted as 5 × 7 in. glossy prints.

**All submissions to the *AJR* must be accompanied by a completed copy of the Author's Checklist and the signed Copyright Agreement.**



MR

## Progress in Radiology

# State of the Art: Endorectal Sonography of the Prostate Gland

Matthew D. Rifkin,<sup>1</sup> Wolfgang Dähnert, and Alfred B. Kurtz

The development of cross-sectional imaging techniques has enabled direct visualization of the prostate. Because sonography is noninvasive, it is a valuable technique for use in detecting prostate disease, particularly cancer. By placing a transducer in the rectum close to the prostate, it is possible to use high-resolution transducers with sharply focused near fields. Endorectal (transrectal) sonography was first used in the 1960s and 1970s [1, 2] and has since become an important clinical tool. The purpose of this article is to (1) review the anatomy of the prostate as it relates to endorectal sonography and cancer of the prostate, (2) review the clinical indications for endorectal sonography, (3) review the technique of performing the procedure, and (4) illustrate the sonographic features of the normal and abnormal prostate gland.

### Anatomy of the Prostate Gland

The understanding of the gross and microscopic anatomy of the prostate has changed during the past few decades. The classic understanding of prostate anatomy was the division of the gland into five lobes, termed Lowsley's lobar concept of anatomy. This method has been used to identify the prostate and prostatic disease for close to 100 years [3]. However, Lowsley's concept of anatomy did not consider the different histologic components of the prostate but was based purely on anatomic position as defined in the embryonic and fetal gland [3]. In this description, the prostate was divided into five major lobes (Fig. 1). The first, the anterior lobe, was

in the anterior portion of the prostate. It was situated from the anterior margin of the gland to the level of the prostatic (also termed the posterior) urethra posteriorly. The middle or median lobe was a smaller area between the proximal prostatic urethra (as its anterior margin) and the ejaculatory ducts (as the median lobe's posterior margin). This lobe extended from the base (the cephalic margin of the prostate) caudad to the level of the verumontanum (where the ejaculatory ducts insert into the prostatic urethra) in the midportion of the prostate. The posterior lobe encompassed the posterior portion of the prostate and was situated posterior to the ejaculatory ducts (in the superior half of the prostate) and the prostatic urethra (in the caudal portion of the gland). The posterior lobe extended to the posterior margins of the gland. The fourth and fifth lobes were the two large lateral lobes that extended from the lateral margin of the prostate bilaterally toward the middle part of the gland. None of the lobes had clearly defined medial margins.

Since the 1960s, a zonal concept of anatomy has evolved, initially developed by McNeal [4] and then modified over the past 25 years [5–7]. This anatomic orientation defines the prostate in terms of its cellular components and is divided into three major areas (Fig. 2): the anterior portion of the prostate, the central gland, and the peripheral gland. We have modified this terminology slightly to coincide with cross-sectional imaging.

1. *Anterior prostate.*—The anterior portion of the gland is actually nonprostatic tissue. It is fibromuscular stroma, which is quite thick anteriorly. The thin, fibrous prostate capsule,

Received August 17, 1989; accepted after revision November 16, 1989.

<sup>1</sup> All authors: Department of Radiology, Thomas Jefferson University Hospital, 1033 Main Bldg., 10th and Sansom Sts., Philadelphia, PA 19107. Address reprint requests to M. D. Rifkin.



laterally and posteriorly, is an extension of the thick anterior fibromuscular stroma.

2. *Central gland.*—The central gland is the central portion of the prostate. It includes the thin lining of the proximal urethra (the periurethral glandular tissue) and extends from the base (the superior portion of the prostate) caudad to the level of the verumontanum. The central gland also comprises smooth muscle fibers of the internal sphincter and the transition zone, a small bilobed structure situated just cephalad to the verumontanum. The transition zone is a portion of the

central gland (by cross-sectional anatomy), but is acinar tissue—the only acinar tissue not part of the peripheral gland.

3. *Peripheral gland.*—The peripheral gland is composed of the acinar tissue of the prostate and is divided into central and peripheral zones. The central zone is situated posterior to (and is distinctly separate from and should not be confused with) the central gland. It extends posteriorly to surround the bilaterally paired ejaculatory ducts. Similar to the central gland, the central zone extends caudad to the level of the verumontanum. The peripheral zone comprises the posterior portion of the prostate; the apical (inferior) area of the gland; and the lateral, posterolateral, and anterolateral portions of the prostate. It is the largest portion of the prostate, approximately 75% of the volume of the normal postpubescent prostate.

A comparison of the Lowley lobar and McNeal zonal concepts of anatomy is both possible and important because of the need to compare clinical findings and terminology (clinicians may still refer to lobar anatomy) with imaging studies (which should use zonal anatomy). For example, the anterior lobe correlates with the anterior fibromuscular stroma. The median lobe and central zone are similar, but the latter is larger, extending slightly more posteriorly. The sum of the posterior and two lateral lobes correlates to a large extent with the peripheral zone.

Initially, McNeal's concept of zonal anatomy had little utility in the clinical sphere or in diagnostic imaging. However, with the development of cross-sectional imaging studies, endorectal prostate sonography and MR imaging, the zonal concept of anatomy became a useful technique to apply to imaging because the different areas can be defined. Both sonography and MR imaging can differentiate the normal central gland from the normal peripheral gland. In the hyperplastic prostate, they differentiate benign hyperplastic areas from normal tissues.

The zonal concept of anatomy is also useful because it incorporated a clearer understanding of the development of

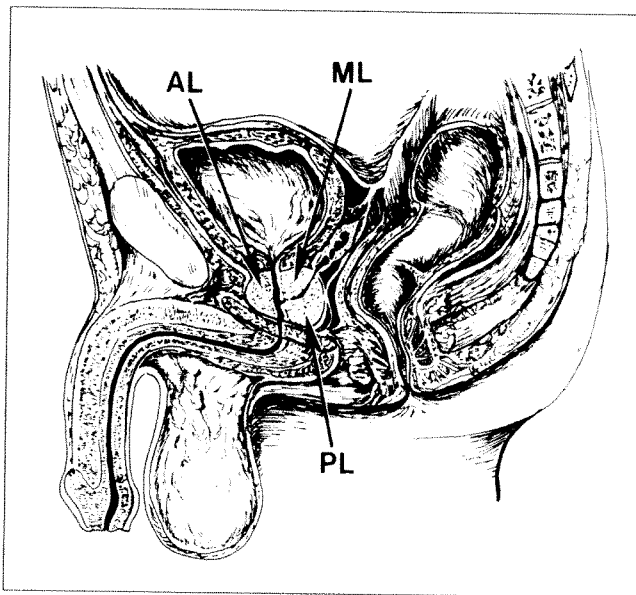


Fig. 1.—Lobar anatomy. Sagittal line diagram of male pelvis in midline shows prostate, situated between bladder, rectum, pubic bones, and urogenital diaphragm. Anterior lobe (AL) is anterior to prostatic urethra, middle lobe (ML) is in superior midportion of prostate between urethra and ejaculatory ducts, and posterior lobe (PL) is posterior to ejaculatory ducts.

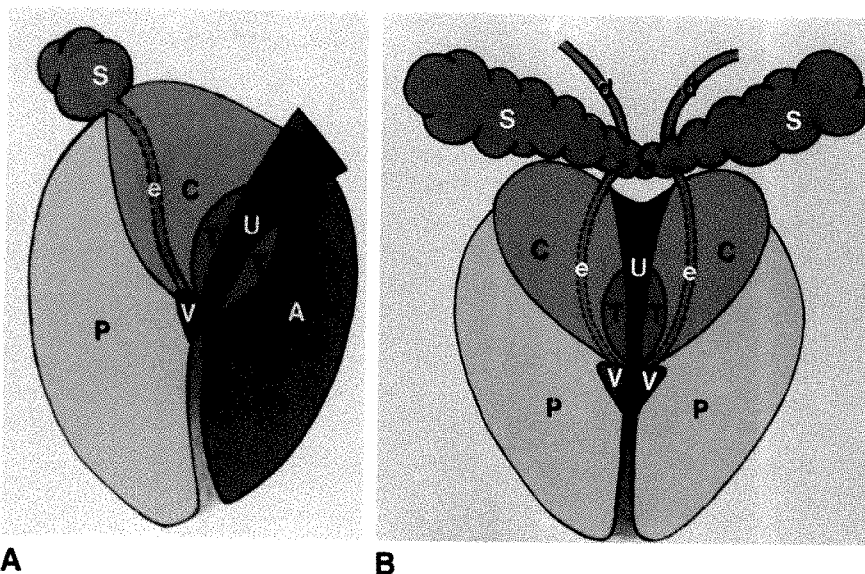


Fig. 2.—Zonal anatomy.

A and B, Diagrams of prostate in coronal (A) and midline sagittal (B) orientations show prostate and its zones. A = anterior fibromuscular stroma; C = central zone; d = vas deferens; e = ejaculatory ducts; P = peripheral zone; S = seminal vesicle; T = transition zone; V = verumontanum; U = periurethral glandular area.



disease. The origin of prostatic disease within the gland was poorly understood under Lowsley's concepts of lobar anatomy. It was previously thought, for example, that cancers only arise in the posterior lobe and benign prostatic hyperplasia develops predominantly in the lateral and, to a lesser degree, median lobes. These concepts were based on the clinical presentation of disease, not on actual positioning of the tumors or on a cellular basis, and were inaccurate. Lobar anatomy was found to be particularly confusing when imaging techniques were developed that could image the internal areas of the prostate. The concept of zonal anatomy has clarified much of this misunderstanding.

It is now understood that prostate cancer develops in the acinar tissue predominantly the peripheral prostate [4-9]. Although the peripheral zone is three times larger in volume than the central zone (in the normal-sized gland), prostate cancer develops seven times more often in the peripheral zone [7-9]. Approximately 70% of all cancers develop in the peripheral zone and 10% in the central zone. An additional 20% develop from the transition zone of the central gland [9]. Portions of the peripheral gland are situated in the anterior half of the prostate. Stated a different way, it has been shown that about 50% of cancers arise in the anterior half of the prostate, including all those cancers from the transition zone (20% of the total), central zone (10%), and anteriorly situated portions of the peripheral zone [9].

In contrast benign prostatic hyperplasia develops exclusively from the central gland, approximately 95% from the transition zone, and 5% from the periurethral glandular tissue. Prostatitis develops (when not due to surgical manipulation) exclusively in the acinar prostate. This distribution is similar to that of prostatic cancer, predominantly in the peripheral zone.

### Technique of Endorectal Sonography

The initial development of endorectal transducers permitted imaging in only a single orientation [1, 2]. However, with the advancement of technology, multiorientation imaging is now possible and has been found to be essential in the evaluation of the prostate [10]. The use of at least two imaging planes allows visualization in three dimensions, thus permitting more accurate localization of abnormalities and extent of disease. Multiple images can be obtained by a variety of techniques and instruments including multiple single-plane transducers, incorporation of two fixed transducers into a single probe (biplane probes), multi- or omnidirectional imaging in which a single transducer rotates within the probe, or a single oblique or end-fire transducer that can be rotated to allow omnidirectional imaging.

Regardless of the type or types of transducers used, three major planes are imaged: the axial, sagittal, and oblique coronal-axial. All orientations view the cross-sectional anatomy in slightly different presentations, although axial and oblique coronal-axial planes may appear similar. The true axial plane permits rapid assessment of the size, shape, and symmetry of the prostate. Scans obtained in the most cephalic position visualize the seminal vesicles as symmetrically paired

structures. As the transducer is withdrawn, sequential visualization of the prostate occurs from the base (which images the central zone and central gland predominantly), to the midportion (which identifies the peripheral zone predominantly and the transition zone and anterior fibromuscular stroma), to the apex (Fig. 3).

Sagittal midline images show the periurethral tissues (the central gland), the prostatic urethra, the anterior fibromuscular stroma, and the peripheral gland. Parasagittal images can be obtained by gently rotating the transducer clockwise or counterclockwise from the midline sagittal plane. The seminal vesicles are seen as more rounded structures situated at the posterior superior portion of the prostate between the urinary bladder and the rectum. As the transducer is rotated slightly to either side, the central gland and urethra (both midline structures) are not identified, and, depending on the degree of rotation, only the peripheral and central zones are seen (Fig. 4).

When using an oblique or end-firing transducer, both longitudinal and oblique axial scans can be obtained by rotating the transducer a full 180°. Although the conventional sagittal images will still be produced, the axial scans will be oriented more obliquely. For those axial images obtained toward the base of the gland, the obliquity is oriented more coronally; for those images obtained more toward the apex of the prostate, the images assume a truer axial orientation. Images of the prostate appear more elongated in these views than when obtained in a true axial orientation (Fig. 5).

### Sonographic Features of Prostatic Disease

#### *Benign Prostatic Hyperplasia*

In normal young men without benign prostatic hyperplasia, there may be no clear differentiation between the sonographic appearances of the central and peripheral glands. When benign prostatic hyperplasia develops, the two areas are clearly defined. As benign prostatic hyperplasia develops from the central gland, the peripheral gland becomes compressed and distorted, and may be identified on all the imaging planes (Fig. 6). This results in marked sonographic differences between the central and peripheral portions of the prostate. Benign prostatic hyperplasia is generally clearly defined as a well-demarcated, well-differentiated enlargement of the central gland. A single, relatively well-demarcated focus may be identified, or multiple benign hyperplastic nodules (termed adenomas) may be noted. The area separating the hyperplastic tissue from the compressed peripheral zone is the "surgical capsule." This region at the surgical capsule may be demarcated by (1) a well-defined change in echogenicity, (2) a hypoechoic rim (termed halo), and/or (3) calcifications (Fig. 6).

#### *Prostatitis*

Prostatitis, when due to hematogenous spread of infection, involves the peripheral gland. When due to postsurgical instrumentation, the central gland can be affected. Acutely, there are no specific features on sonography unless an abscess develops, in which case an anechoic to hyperechoic

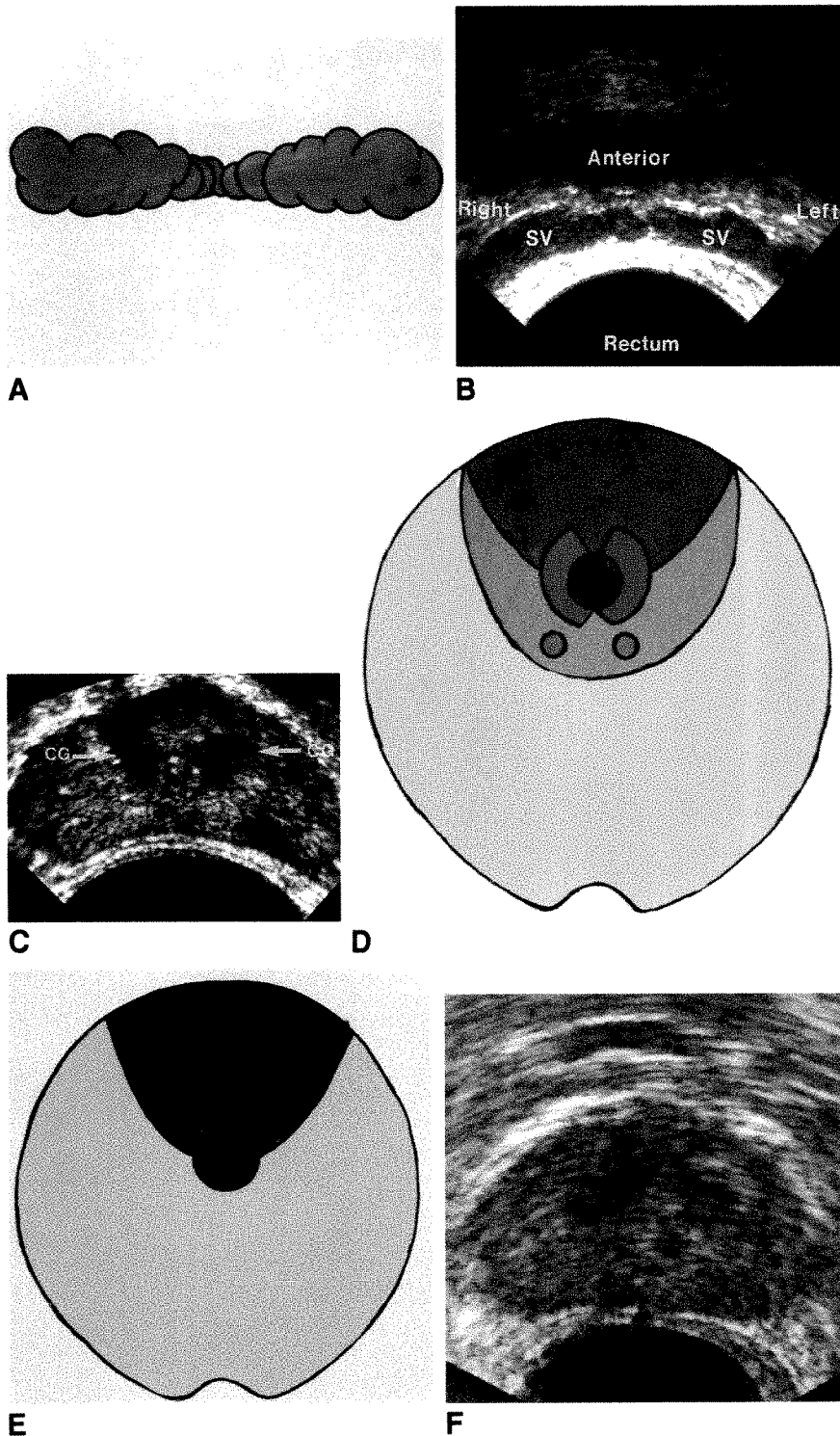


Fig. 3.—Axial imaging. When imaging in axial orientation, transducer is placed within rectum and withdrawn sequentially to obtain axial (transverse) images of prostate.

A and B, Diagram (A) and sonogram (B) show seminal vesicles (SV).

C and D, sonogram (C) at level of bilobed transition zone (in red) of prostate and diagram (D) show central gland (CG) as slightly hypoechoic structure.

E and F, Diagram (E) and sonogram (F) below level of verumontanum show relatively homogeneous prostate.

area with a thin or thick wall may be seen. The sonographic findings are not diagnostic, but, in conjunction with the clinical findings, are highly suggestive of the diagnosis. Dystrophic calcifications in the peripheral gland due to chronic inflammation may be identified, but often cannot be differentiated from prostatic calculi developing from other causes.

#### Cancer

Although prostate cancer may have a variety of appearances, classically it presents in the peripheral zone as a relatively poorly margined hypoechoic area. These lesions

are often obvious on the sonographic examination because of the considerable differences in echogenicity between tumor and normal-appearing glandular tissue (Fig. 7). Although these lesions may be obvious at first glance, on closer inspection, the margins are generally poorly defined with areas of cancer blending into normal-appearing tissue. However, not all large lesions (defined as greater than 5 mm in size) have this typical sonographic appearance. Studies have shown that up to 40% of tumors greater than 5 mm in size, when evaluated by radical prostatectomy specimens, cannot be identified by the endorectal sonogram [11]. These are not seen directly because they are of the same echogenicity as the remainder of

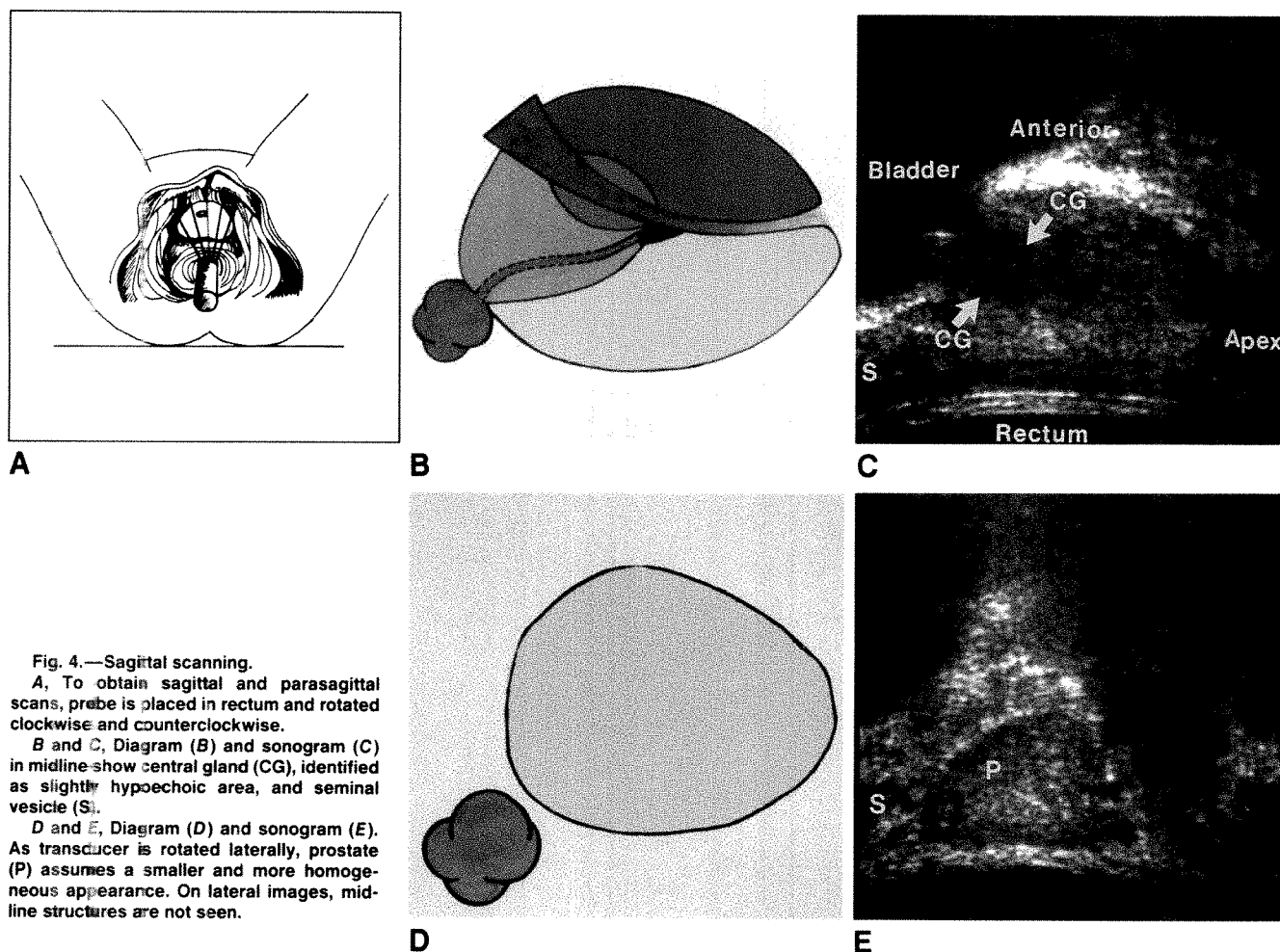
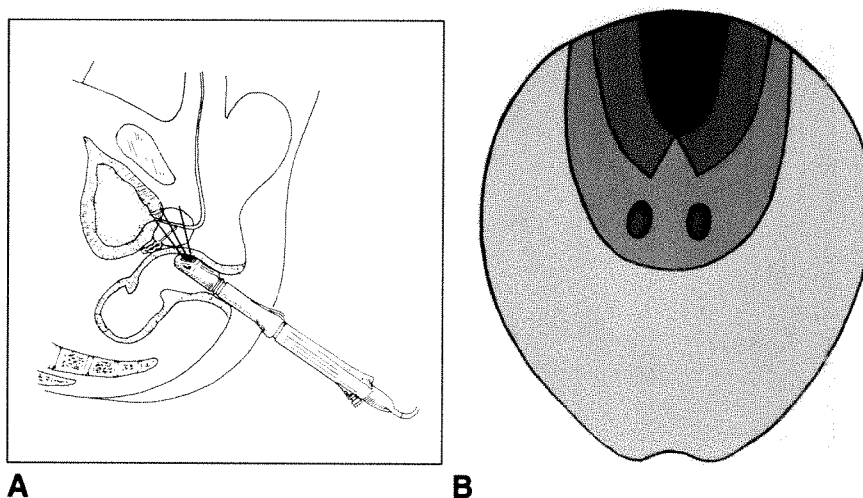


**Fig. 5.—Coronal imaging.**  
**A,** With an oblique or end-fire transducer in rectum, rotation of transducer will permit oblique coronal images.

**B,** Diagram shows angle of obliquity to be obtained toward base of gland (at level of transition zone) and oblique axial scans to be obtained toward apex of prostate.



the prostate, but some may still be identified by their secondary characteristics (i.e., capsular bulge or erosion) (Fig. 8). Capsular bulge is not a specific sign of tumor infiltration, although irregularity of the pericapsular fat (the hyperechoic margins surrounding the prostate) is highly suggestive of

tumor infiltration. Additionally, lesions with mixed echogenic appearances, with subtle scattered areas of increased echogenicity mixed with areas of decreased echogenicity, also may be defined (Fig. 9). The exact reason for these differences in the echogenic appearance of prostate cancer is uncertain

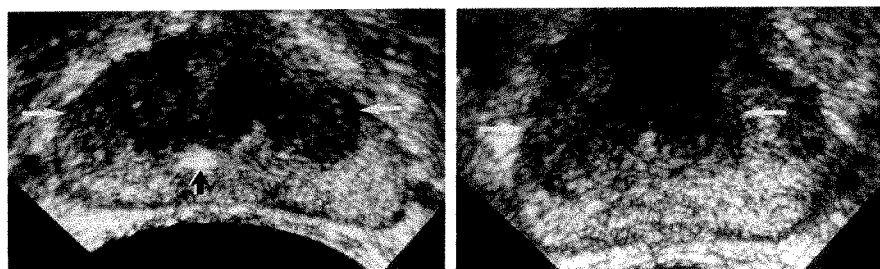


Fig. 6.—Benign prostatic hyperplasia.

A and B, Axial (A) and oblique coronal (B) images show typical benign prostatic hyperplasia with hypoechoic relatively well-margined enlarged central gland. Hyperplastic tissue is separated from compressed peripheral zone by surgical capsule. A bright echogenic focus, a calculus (short arrow), and significant differences in contrast of central (long arrows) and peripheral glands denote surgical capsule. Note elongated appearance of oblique coronal image (B) as compared with true axial scan (A).

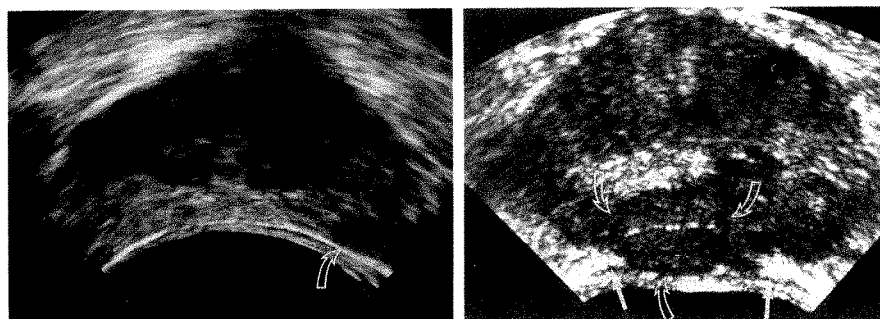


Fig. 7.—Prostate carcinoma. Axial scan shows small hypoechoic focus, a carcinoma, in left posterolateral aspect (arrow).



Fig. 8.—Isoechoic cancer. Axial image shows isoechoic, poorly defined cancer (curved arrows), which causes disruption of normally present periprostatic fat. Normal fat (straight arrows) is seen on both sides of area infiltrated by tumor. Carcinoma has sonographic characteristics that make direct identification of cancer difficult, but secondary sonographic characteristics (i.e., capsular invasion) are clearly evident.

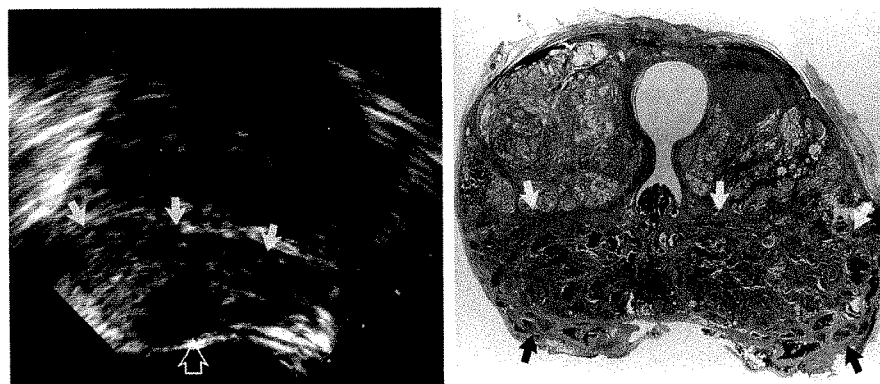


Fig. 9.—Invasive cancer.

A and B, Axial sonogram (A) compared with whole-mount pathology section of radical prostatectomy specimen (B) shows clearly defined, small hypoechoic focus (open arrow). However, careful inspection of sonogram shows more hyperechoic elements distorting entire posterior portion of prostate (solid arrows). This large abnormal area on sonogram corresponds to carcinoma (B, arrows), which is infiltrating entire posterior portion of prostate.

but may be related to a number of factors: (1) Gleason grade of the tumor (an index of the cellular differentiation), (2) fibrotic change, (3) intermixing of benign prostatic tissue with cancer, (4) increased number of interfaces, (5) tumor size, and (6) undefined causes [12–14].

The hypoechoic, peripherally oriented lesion is not pathognomonic for prostate cancer. Other lesions (all benign) may mimic the appearance of cancer. These include inflammation, fibrosis, infarction, smooth muscle surrounding the ejaculatory duct, and benign prostatic hyperplasia, among others.

A number of studies have shown that the positive predictive value (the percentage of lesions that are suspicious on sonography and are cancer) ranges from 0% to 52% (Table 1) [15, 18–21]. The overall average suggests that the positive predictive value of a hypoechoic, peripherally oriented lesion is approximately 25–30%. For lesions that are palpable or

when the level of prostate-specific antigen is elevated, the positive predictive value may be higher. For these reasons, if a suspicious lesion—including (1) the hypoechoic peripherally oriented lesion, (2) the echogenically asymmetric peripheral zone, (3) a focal bulge within the prostate, and (4) a capsular or pericapsular irregularity—is identified on endorectal sonography, it requires further evaluation by biopsy.

### Prostate Biopsy Under Sonographic Guidance

Sonographically guided prostate biopsies were first described in the early 1980s [22–25]. This technique initially used a transperineal biopsy approach with endorectal sonographic guidance. Although it was initially described using an axially oriented scanner, greater accuracy and simplicity were obtained by using the longitudinally oriented sonogram for

guidance [23, 24]. More recently, sonographically guided transrectal biopsy has become an accepted tool [26, 27].

Both approaches for biopsy of the prostate are accurate and relatively safe, although certain technical considerations and precautions must be taken, depending on the approach, to ensure a safe, painless, and diagnostic procedure. For the transrectal biopsy, there is a risk of contamination of the prostate with fecal material. A cleansing enema should be administered immediately before biopsy. Appropriate antibiotics also should be given to minimize the risk of sepsis. A number of broad-spectrum oral antibiotics can be used, and should be administered at least 1 hr before biopsy (to reach therapeutic blood serum levels) and for 2 days thereafter. The transperineal approach requires neither cleansing enema nor antibiotic coverage. However, unlike the transrectal approach, it does require cleansing of the perineum with an antimicrobial solution just before puncture and extensive use of a local anesthetic.

**TABLE 1: Positive Predictive Value (PPV) of Sonography when a Hypoechoic Peripheral Lesion Is Identified in the Prostate**

Reference	No. of Lesions	No. of Cancers	PPV (%)
Rifkin and Choi [18]	80	17	21
Rifkin <sup>a</sup>	353	89	25
MacIntyre et al. [21]	109	20	18
Lee et al. [16]	149	77	52
Chancellor et al. [15]	43	0	0
Ragde et al. [38]	138	50	36
Total	872	255	29

Note.—Positive predictive value = percentage of patients with a positive test who actually have disease. All cases of cancer were diagnosed by sonographically guided biopsy.

<sup>a</sup> Unpublished data.

In order to ensure that the transrectal prostate biopsy is painless, the needle should not pass through the anal sphincter (Fig. 10). When performed correctly, the transrectal biopsy does not require anesthesia or sedation.

The transperineal approach requires local anesthesia to reduce pain, and it should be administered superficially into the skin and subcutaneous tissues. The pericapsular area should be infiltrated with anesthesia (Fig. 11). Approximately 15 ml of 1% Xylocaine will eliminate almost all patient discomfort. If local anesthesia is not administered appropriately, the transperineal biopsy may be quite uncomfortable for the patient.

When performing a prostate biopsy, either aspiration cytology or core biopsy can be performed. Frequently both are used. The core biopsies have been simplified by the use of automatic trigger devices that permit a safe, rapid (<0.1-sec) biopsy. A number have been developed and are commercially available. They have improved patient acceptance. It has allowed safer procedures to be performed on an outpatient basis, without need for hospitalization, catheterization, or expensive recovery room costs. It is important to realize that when using the automatic trigger devices for biopsy, the needle will extend forward about 2 cm. Thus, the tip of the needle should be placed just proximal to the lesion to ensure that the appropriate material is sampled.

The use of core or aspiration cytology biopsy depends on the experience of the cytopathologist. The accuracy for diagnosis of cancer is about the same with both [18]. However, grading of the tumor (evaluation of cellular anaplasia) is often easier with a core of tissue.

There has been some controversy in regard to the best approach (i.e., transrectal vs transperineal) for biopsy. Both are equally accurate [26] and, except for the minimally increased risk of bleeding and sepsis for the transrectal approach, equally safe. The proponents who have stated that

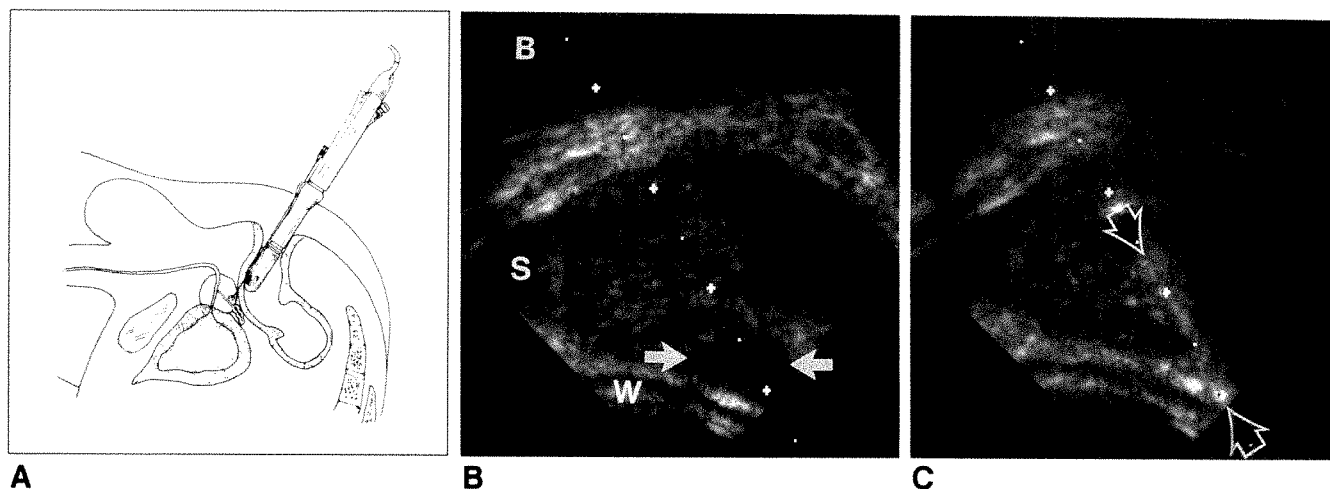


**Fig. 10.—Transrectal biopsy.**

A, Diagram shows transrectal biopsy with transducer placed in rectum and attached biopsy needle placed into lesion within prostate.

B, Endorectal sonogram shows lesion (arrows) and that line of needle placement (alternating dots and crosses) will be properly positioned. B = bladder; W = rectal wall; S = seminal vesicle.

C, Needle (arrows) is identified during biopsy.

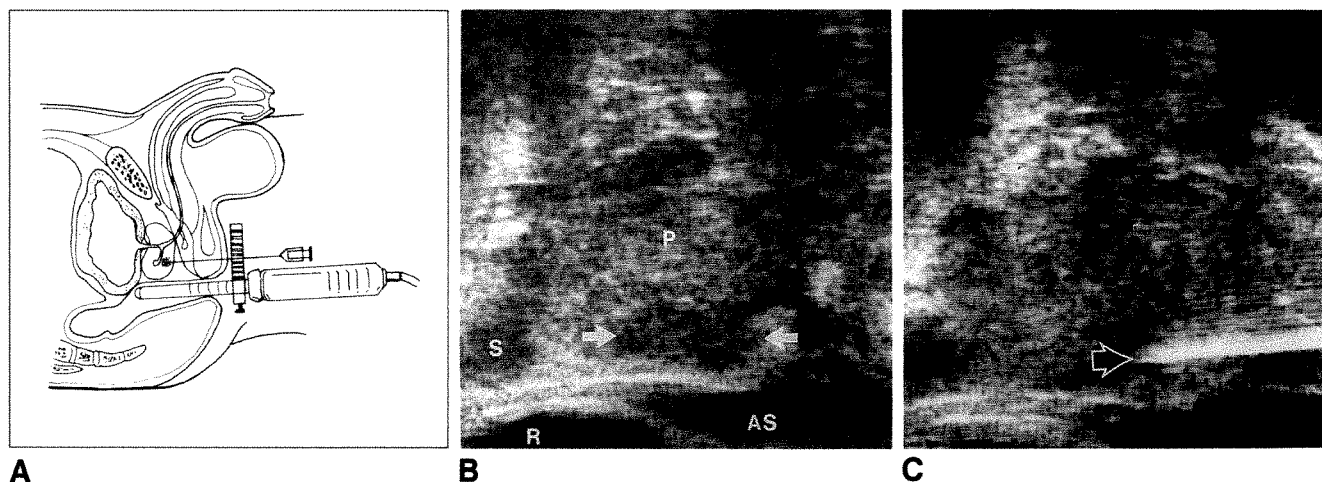


**Fig. 11.—Transperineal biopsy.**  
**A,** Diagram shows transperineal biopsy with longitudinally oriented transducer within rectum with a biopsy guide placed on transducer and needle positioned through perineum into prostate.  
**B,** Longitudinally oriented sonogram shows lesion (arrows). AS = anal sphincter; P = prostate; R = rectum; S = seminal vesicle.  
**C,** Sonogram shows needle (arrow) being positioned directly into lesion.

the transrectal biopsy is less uncomfortable than the transperineal approach have generally not used equivalent techniques. Our experience in over 2000 biopsies has shown that when appropriate local anesthesia (15 ml of 1% Xylocaine) is administered into the subcutaneous and deeper tissues to the level of the prostate capsule and the automatic trigger devices are used, the approaches are equally comfortable for the patient.

The transrectal approach is appropriate for almost all lesions. However, if an abscess is suspected, then it may be appropriate to use the transperineal approach initially for diagnostic drainage so that there is no risk of infection with fecal material.

Regardless of the technique used, sonographically guided biopsies are far more accurate than conventional digitally guided biopsies, even for most palpable lesions. Our experience and other studies have demonstrated that up to 30–35% of digitally guided biopsies of palpable lesions, which on initial digitally guided biopsy show no evidence of malignancy, show positive findings for cancer on repeat biopsy under sonographic guidance [28, 29]. Thus, although a conventional biopsy may be indicated for some palpable lesions (particularly for lesions in which sonography is inconclusive), if a conventional biopsy shows no evidence of cancer, a repeat biopsy with sonographic guidance is still indicated. Obviously, for the nonpalpable lesion or for the subtly abnormal digital rectal examination, sonographically guided biopsies are necessary. An abnormality on the sonogram, however, should be present to ensure an accurate sonographically guided biopsy.

#### Calculation of Tumor Size

Sonography cannot always clearly identify tumor size and volume (Fig. 9). Prostate cancer may be multifocal and/or irregular, infiltrating throughout the prostate. Because of the variable appearance of tumor, upward of 50% of cancers will be under- or overestimated by volume on endorectal sonog-

raphy [11]. Studies have suggested that sonography can be used to assess volumes, and some researchers have developed a sonographic staging system that evaluates the size of the lesion as a criterion for stage. These sonographic stages, which may affect treatment options, may have no validity.

#### Clinical Indications For Prostate Sonography

There has been much discussion and resulting controversy concerning the clinical indications and uses of prostate sonography (Fig. 12). The following are our recommended indications.

##### *Evaluation of Patients with an Abnormal Digital Rectal Examination*

Sonography should be performed when the digital rectal examination is abnormal. Sonography can differentiate a benign process (e.g., cyst or calculus), from a more suspicious process. It can be used to determine the significance of an asymmetric or indurated gland and help determine which lesions or areas of the prostate require further evaluation (i.e., biopsy). Not every palpable lesion, however, can be identified by using sonography. Subtle changes in the capsule and/or shape of the prostate allow visualization of more lesions than do echogenic changes alone. The exact accuracy of sonography or the ability to identify all lesions has not been determined, but a large study has shown that sonography fails to detect 40% of cancers (not all palpable) larger than 5 mm in diameter [11].

##### *Biopsy Guidance*

This is one of the most important uses of sonography of the prostate. Sonography is an accurate, safe approach to



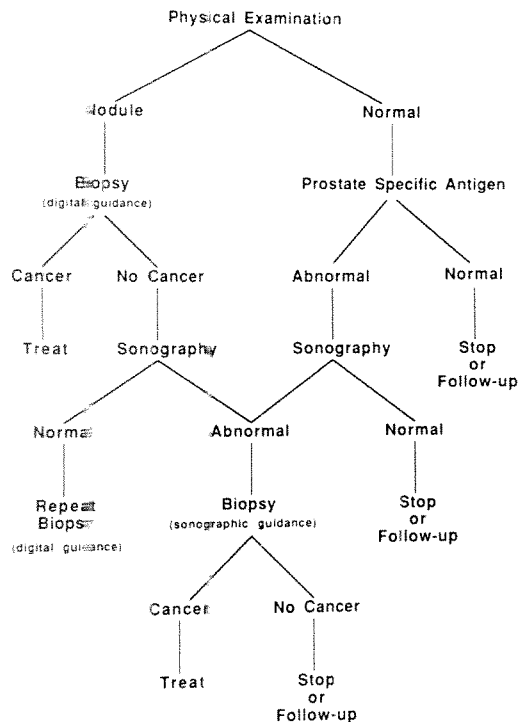


Fig. 12.—Algorithm for patient workup used at Thomas Jefferson University Hospital.

obtain tissue from a focal area of the gland. Not all biopsies need to be performed under sonographic guidance, but subtle or nonpalpable lesions cannot be sampled accurately with biopsy under conventional digital guidance.

#### Abnormal Laboratory Studies

Men who have a normal digital rectal examination may still harbor unsuspected prostate cancer. Nonimaging tests have been developed to suggest the presence of prostate cancer. For example, prostatic acid phosphatase, when elevated above normal levels, suggests not only the presence of prostate cancer, but also that the tumor has extended beyond the confines of the gland. Prostate-specific antigen, when elevated, suggests the presence of prostate cancer. The higher the value, the more likely that malignancy exists. Both tests do have false-positive studies, and thus sonography can help delineate the presence of a nonpalpable cancer and guide for biopsy.

#### Prostatic Inflammation

Sonography is generally not warranted in patients with acute prostatitis. However, in patients who do not respond to antibiotics, sonography may delineate a fluid collection indicative of an abscess.

#### Infertility

Occasionally, male infertility may be due to agenesis or atresia of the seminal vesicles or ejaculatory duct obstruction.

Endorectal sonography can be used to identify these anatomic abnormalities.

#### Staging of Prostate Cancer

Endorectal sonography can only detect local extension of disease. Although preliminary studies have suggested a high accuracy for staging of cancer [30–32], a large-scale study correlating 219 radical prostatectomy specimens with the sonographic findings has shown an accuracy of about 60% [11]. Once cancer is diagnosed, staging is best performed by MR imaging [11].

#### Screening

Should screening be used to detect prostate cancer earlier than is now possible by the digital rectal examination, and if so, should sonography be the technique used? The statistics of prostate cancer—it is the most prevalent cancer, the most frequently diagnosed (over 100,000 new cases per year), and the second most lethal tumor in the American male population (over 28,000 deaths per year [33])—suggest that earlier diagnosis would be beneficial. However, despite these numbers, we must realize that more men will die with clinically unsuspected cancer than of the disease. For example, autopsy studies have shown that over 30% (and up to 50%) of men over 50 years of age who have died of a cause other than prostate cancer have cancer on serially sectioned prostates. Whereas many of the tumors are microscopic, and probably insignificant, many may be large [34]. An additional study of men undergoing cystoprostatectomy for bladder (but no suspected prostate) cancer has shown that 47% harbor prostate cancer, confirming the autopsy studies [35].

An important consideration, yet to be fully evaluated, is what constitutes a clinically significant cancer. McNeal et al. [8] have suggested that prostate cancer becomes more anaplastic and invasive as it enlarges. It also has been shown that cancer becomes aggressive (on a cellular basis) when it attains an estimated size of only 0.2–1.0 cm in diameter [36]. It has also been shown that the metastatic potential of the tumor is essentially nil before it reaches 1 cm<sup>3</sup> in volume and increases dramatically when it is above that size [8]. Although treatment options have been defined (but not universally accepted) for prostate cancer (e.g., that confined malignancy be treated by radical surgery and invasive disease by palliative therapy), new approaches may have to be defined [17, 37]. For example, should all nonpalpable cancers (many being detected with sonographic screening) be treated? If so, what type of therapy should be used? Will the morbidity of treatment be more significant than the potential morbidity of an untreated small cancer?

If we assume that screening is necessary, another important consideration is the efficacy and comparative accuracy of screening with sonography compared with conventional techniques such as the digital rectal examination. Preliminary studies have suggested that sonography is more accurate and sensitive in detecting prostate cancer than the digital rectal examination is [19, 38]. However, these studies were

constructed to prove the benefit of sonography. Either the results of the physical examination were ignored or the expertise of the examiner was not necessarily as great as that of those performing and interpreting the sonography. Additionally, these studies were statistically biased to show great accuracy of sonography. Both assumed (surely incorrectly) that if the sonogram did not show an abnormality, no cancer existed. This is obviously fallacious. A prospective study of 219 men with prostate cancer, all of whom underwent radical prostatectomies because of clinical stage A or B disease, has shown that endorectal sonography with state-of-the-art equipment could not detect 40% of cancers greater than 5 mm in size [11]. These large tumors (not the microscopic lesions) are those that need to be detected if a technique is to be used appropriately for screening. There is no question that sonography can identify nonpalpable tumors, but what should be done with them and when?

Prostate sonography is not a screening tool now, although it may be in the future. Cancer can be detected, but the data are not available to show (1) the sensitivity and specificity of the technique applied to the appropriate patient population, (2) the accuracy of sonography compared with that of other techniques, or (3) improvement in prognosis by detecting and treating cancers that would be identified with an early screening program.

## REFERENCES

1. Takahashi H, Ouchi T. The ultrasonic diagnosis in the field of urology. In: *Proceedings of the 4th meeting of the Japanese Society of Ultrasonics in Medicine, Tokyo*, no. 2. **1984**;35-37
2. Watanabe H, Kaiho H, Tanaka M, Terasawa Y. Diagnostic application of ultrasonotomography to the prostate. *Invest Urol* **1971**;8:548-559
3. Goss CM, ed. *Gray's anatomy*, 28th ed. Philadelphia: Lea & Febiger, **1966**
4. McNeal JE. Morphogenesis of prostatic carcinoma. *Cancer* **1965**;18:1659-1666
5. McNeal JE. Regional morphology and pathology of the prostate. *Am J Clin Pathol* **1968**;49:347-357
6. Blacklock NJ, Boushill K. The zonal anatomy of the prostate in men and the rhesus monkey (*Macaca mulatta*). *Urol Res* **1977**;5:163-167
7. McNeal JE. The prostate gland. *Monogr Urol* **1988**;9:36-54
8. McNeal JE, Kindrachuk RA, Freiha FS, Bostwick DG, Redwine EA, Stamey TA. Patterns of progression in prostate cancer. *Lancet* **1986**;1:60-63
9. McNeal JE. Normal anatomy of the prostate and changes in benign prostatic hypertrophy and carcinoma. *Semin US CT MRI* **1988**;9:329-334
10. Rifkin MD. Transrectal prostatic ultrasonography: comparison of linear array and radial scanners. *J Ultrasound Med* **1985**;4:1-5
11. Rifkin MD, Gatsonis C, Zerhouni E, et al. Endorectal US and MR imaging: accuracy for staging prostate cancer. Presented at the annual meeting of the Radiological Society of North America, Chicago, November **1989**
12. Rifkin MD, Friedland GW, Shortliffe L. Prostatic evaluation by transrectal endosonography: detection of carcinoma. *Radiology* **1986**;158:85-90
13. Rifkin MD, McGlynn ET, Choi H. Echogenicity of prostate cancer correlated with histologic grade and stromal fibrosis: endorectal US studies. *Radiology* **1989**;170:549-552
14. Salo JO, Rannikko S, Makinen J, Lehtonen T. Echogenic structure of prostatic cancer imaged on radical prostatectomy specimens. *Prostate* **1987**;10:1-9
15. Chancellor MB, McHugh TA, Dorr RP, VanAppledorn CA. Transrectal prostate ultrasonography before transurethral prostatectomy, its value in screening for stage A cancer. *J Urol* **1987**;137 (4, part 2):241A
16. Lee F, Littrup PJ, Kumasaka G, Borlaza GS, McLeary RD. Use of transrectal ultrasound in the diagnosis, guided biopsy, staging and screening of prostate cancer. *RadioGraphics* **1987**;7:627
17. Adolfsson J, Fahraeus B. The natural course of prostatic carcinoma in relation to initial cytological grade. *J Urol* **1988**;140:1452-1454
18. Rifkin MD, Choi H. Endorectal prostate ultrasound: implications of the small peripherally placed hypoechoic lesion. *Radiology* **1988**;166:619-622
19. Lee F, Littrup PJ, Torp-Pedersen ST, et al. Prostate cancer: comparison of transrectal US and digital rectal examination for screening. *Radiology* **1988**;168:389-394
20. Bree R, Roberts J, Jafri S. Transrectal ultrasound guided biopsy of the prostate: techniques and results. *J Ultrasound Med* **1988**;7(suppl 10):S79
21. MacIntyre RC, Peron SE, Madrazo B, Cerny JC. Ultrasound guided needle biopsy of the prostate gland. *J Urol* **1987**;137(4, part 2):242A
22. Rifkin MD, Kurtz AB, Goldberg BB. Prostate biopsy utilizing transrectal ultrasound guidance: diagnosis of nonpalpable cancers. *J Ultrasound Med* **1983**;2:165-167
23. Rifkin MD, Kurtz AB, Goldberg BB. Sonographically guided transperineal prostatic biopsy: preliminary experience with a longitudinal linear array transducer. *AJR* **1983**;139:745-747
24. Fornage BD, Touche DH, Deglaire M, Faroux MJC, Simatos A. Real-time ultrasound-guided prostatic biopsy using a new transrectal linear-array probe. *Radiology* **1983**;146:547-548
25. Holm HH, Gammelgaard J. Ultrasonically guided precise needle placement in the prostate and the seminal vesicles. *J Urol* **1981**;125:385-387
26. Rifkin MD. *Ultrasound of the prostate*. New York: Raven, **1987**
27. Torp-Pedersen ST, Lee F, Littrup PJ, et al. Transrectal biopsy of the prostate guided by transrectal ultrasound: experience with longitudinal and multiplanar scanning. *Radiology* **1988**;170:23-27
28. Ajzen SA, Goldenberg SL, Allen GJ, Cooperberg PL, Chan NH, Jones EC. Palpable prostatic nodules: comparison of US and digital guidance for fine-needle aspiration biopsy. *Radiology* **1989**;171:521-523
29. Resnick MI. Transrectal ultrasound guided versus digitally directed prostatic biopsy: a comparative study. *J Urol* **1988**;139:754-757
30. Pontes JE, Eisenkraft F, Watanabe O, Ohe H, Saitoh M, Murphy GP. Preoperative evaluation of localized prostatic carcinoma by transrectal ultrasonography. *J Urol* **1985**;134:289-291
31. Andriole GL, Kavoussi LR, Torrence RJ, Lepor H, Catalona WJ. Transrectal ultrasonography in the diagnosis and staging of carcinoma of the prostate. *J Urol* **1988**;140:758-760
32. Perrapato SD, Carothers GG, Maatman TJ, Soechtig CE. Comparing clinical staging plus transrectal ultrasound with surgical-pathologic staging of prostate cancer. *Urology* **1989**;33:103-105
33. Silverberg E, Lubera JA. Cancer statistics, 1989. *CA* **1989**;39:3-20
34. Montie JE, Wood DP Jr, Pontes JE, Levin HS. Adenocarcinoma of the prostate identified by serial sectioning of the prostate after cystoprostatectomy for carcinoma of the bladder. *J Urol* **1988**;139(4, part 2):315A
35. Franks LM. Latent carcinoma of the prostate. *J Pathol* **1954**;68:603-616
36. Akazaki K, Stemmermann GN. Comparative study of latent carcinoma of the prostate among Japanese in Japan and Hawaii. *JNCI* **1973**;50:1137-1144
37. McNeal JE, Price HM, Redwine EA, Freiha FS, Stamey TA. Stage A versus stage B adenocarcinoma of the prostate: morphological comparison and biological significance. *J Urol* **1988**;139:61-65
38. Ragde H, Bagley CM Jr, Aldape HC, Blasko JC. Prostate cancer screening with high resolution transrectal ultrasound. *J Endourol* **1989**;3(2):115-123

## Review Article

# Radiologic Evaluation of the Solitary Pulmonary Nodule

W. Richard Webb<sup>1</sup>

The diagnostic evaluation of a patient with a solitary pulmonary nodule is a common problem in radiologic practice. Although there is no universally accepted definition of a solitary pulmonary nodule, this term is usually used to refer to a lung lesion that is reasonably well defined, round or oval, and less than 5 or 6 cm in diameter.

The differential diagnosis of a solitary nodule is extensive, but its radiologic evaluation is primarily directed at distinguishing nodules that are benign, and thus inconsequential, from nodules that are malignant or potentially malignant, and require treatment. The large majority of solitary nodules detected radiographically are benign [1-3].

A variety of radiologic procedures have been used for the examination of patients with a solitary pulmonary nodule. Currently, plain chest radiographs and CT are of most value. Simply stated, the goals of imaging in patients with an undiagnosed lung nodule are (1) to make a specific diagnosis; or (2) if a specific diagnosis cannot be made, to distinguish benign nodules from those that are indeterminate and thus potentially malignant; or (3) if benign and malignant cannot be distinguished, to help determine what should be done next.

### Clinical Considerations

Clinical and historical data, such as dwelling and travel history, risk factors for carcinoma (e.g., smoking), and skin test results should be considered in the evaluation of any patient with a solitary pulmonary nodule, but these data are not generally specific enough to alter the patient's diagnostic evaluation or eventual treatment. However, before imaging

studies are performed or interpreted, several very important clinical factors should be considered.

First, in patients less than 30 years of age, the prevalence of bronchogenic carcinoma is so low that a solitary pulmonary nodule generally should be followed-up radiologically without any further evaluation, unless the patient has a known extrathoracic primary malignancy [4]. In some patients in this age group, needle biopsy is performed before follow-up; biopsy may be requested if the patient is very concerned about the possibility of carcinoma, or has a significant risk factor for carcinoma.

Although a history of an extrathoracic primary malignancy suggests that a solitary nodule is a metastasis rather than a lung cancer, this is not always the case [5]. In a patient over 35 with an extrathoracic malignancy and a solitary nodule, the likelihood that the nodule represents a bronchogenic carcinoma depends on the cell type of the extrathoracic tumor. If the extrathoracic malignancy is of squamous cell origin, the nodule is most likely a lung cancer. If the extrathoracic primary is a melanoma or sarcoma, the nodule is probably a metastasis. An extrathoracic adenocarcinoma indicates that the lung nodule has about 50% chance of being lung cancer.

Sputum cytology should be obtained in all patients with a solitary pulmonary nodule in whom cancer is considered a possibility. False-positive sputum cytology is rare (0.7-3%) and a positive sputum cytology is the most reliable preoperative method (except biopsy) for diagnosing a pulmonary malignancy. False-negative cytology is far more common, occurring in 10-30% of all patients with lung cancer and in

Received August 14, 1989; accepted after revision November 14, 1989.

<sup>1</sup> Department of Radiology, University of California, San Francisco, San Francisco, CA 94143-0628.

up to 60% of those with peripheral malignancies. Thus, negative cytology does not preclude the presence of a malignant lesion.

### Chest Radiographs

A number of plain film criteria have been reported to be of some value in diagnosing a lung nodule as benign. These include smallness, regular or round shape, smooth contour, sharp edge definition, the presence of satellite lesions, a slow or very fast doubling time, and absence of cavitation. However, these plain film criteria rarely allow a specific diagnosis of benignity to be made. Even attempts to use computers to aid in diagnosis have not resulted in more than 90% accuracy in distinguishing benign and malignant lesions [6]. The individual patient with a solitary pulmonary nodule cannot be properly managed with this degree of uncertainty as to whether or not a nodule is benign.

However, two radiologic features—dense or central calcification and absence of growth—can be used to indicate that a solitary pulmonary nodule is benign, for all practical purposes. In patients with either finding, a solitary pulmonary nodule can be followed with sequential chest radiographs at progressively increasing intervals (2 months at first, increasing to 1 year if the nodule is unchanging), but no other examination is usually necessary.

### Calcification

Dense central, laminated, or diffuse calcification virtually excludes malignancy (Fig. 1). Although bronchogenic carcinomas (scar carcinomas) may incorporate an adjacent calcified granuloma, resulting in a mass with calcification, the

calcification is usually eccentric rather than central (Figs. 1 and 2). In addition, bronchogenic carcinomas may themselves calcify; this calcification is often stippled and is frequently not detectable radiologically (Fig. 1). In a study of 72 patients with malignant solitary pulmonary nodules, calcification was visible on radiographs of the resected specimen in 10, but in only one was calcification detectable on standard chest radiographs [7]. In the same study, 67 of 135 benign lesions (mostly granulomas and hamartomas) contained calcifications on specimen radiographs; in 46, these calcifications also were visible on standard chest radiographs. Metastatic malignant tumors (particularly osteogenic sarcoma, chondrosarcoma, and thyroid carcinoma) can show stippled or homogeneous calcification, but the nodules are usually multiple.

Calcification in a solitary pulmonary nodule is usually best appreciated on low-kilovoltage radiographs, but these are of limited value except in obvious examples. Fluoroscopy can also be of value in projecting a nodule away from overlying densities, therefore allowing calcification to be seen more clearly, but this technique is not routinely used because of relatively poor resolution.

### Growth Rate

The growth rate of a solitary pulmonary nodule (usually quantitated by using doubling time—the time required for a doubling of volume) has been used to determine its likelihood of being malignant [8]. A pulmonary nodule that doubles in volume in less than 1 month or more than 18 months is usually benign.

However, the overlapping growth rates of benign and malignant lesions, particularly among rapidly growing nodules, makes the use of doubling time hazardous as an absolute indicator of benignity. Nevertheless, it is generally agreed that a solitary pulmonary nodule that does not grow over a 2-year period is benign and does not require resection. Only rare exceptions to this rule have been reported. Therefore, a vigorous search for old films must be the first step in the evaluation of a noncalcified solitary pulmonary nodule. If films 2 years or older show the pulmonary nodule to be unchanged, follow-up radiographs at intervals are all that is usually necessary.

If no old films are available, or if prior films are not old enough, the diagnostic approach may be based on the patient's age and the plain radiographic appearance of a lesion. If the patient is less than 30 years of age and the pulmonary nodule appears benign (small, round, sharply defined), follow-up with standard chest radiographs generally is sufficient. However, if the patient is older, has a history of an extrathoracic tumor, or if the lesion does not appear benign (i.e., it is large, irregular, poorly defined, or spiculated), further diagnostic procedures must be performed.

Also, occasionally a patient with an acute process, such as pulmonary embolism or focal pneumonia, can present with a nodular density on chest radiographs. In a patient with acute symptoms, a follow-up radiograph in 1–2 weeks can sometimes show a decrease in the size of a nodule, indicating its benign nature. In some patients without symptoms, repeat

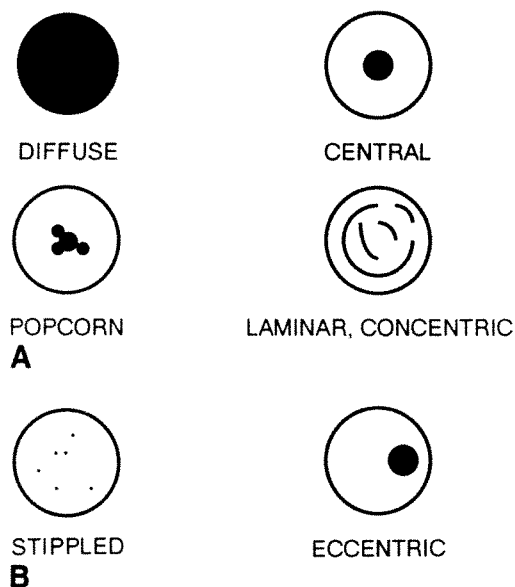
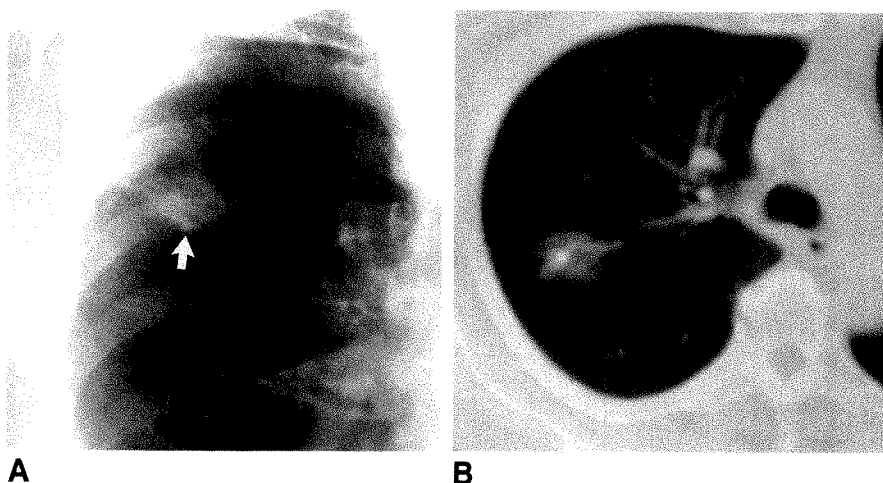


Fig. 1.—A and B, Some patterns of benign (A) and "malignant" (B) calcification seen on plain radiographs or CT scans can be helpful in predicting that a lung nodule is benign. Malignant patterns can be seen with either benign or malignant lesions.

Fig. 2.—A, Plain radiograph in patient with a nodule in right upper lobe shows eccentric calcification (arrow). Mass is poorly defined and spiculated, suggesting malignancy.

B, Conventional CT scan at this level shows nodule and focus of calcification. At surgery, this was a carcinoma engulfing a granuloma. Thus, this tumor may represent a scar carcinoma arising in relation to the inflammatory lesion.



radiographs will show a similar decrease in size, indicating that the lesion is benign. Because of this, one or two follow-up radiographs at 1- to 2-week intervals are often obtained in a patient with a solitary nodule, usually during examination, to assess the stability of the lesion. However, it is not advisable in most subjects to obtain follow-up radiographs, *hoping* that a nodule will decrease in size. Furthermore, in some patients with cancer, nodules become less well defined as they grow and can appear smaller.

## CT

CT is performed in most patients with a solitary pulmonary nodule to define the morphology of the lesion, detect calcification, and help in biopsy planning. It has largely replaced conventional tomography for these indications. Although conventional CT with 1-cm collimation can provide this information in some cases, CT with thin collimation, and particularly high-resolution CT, is superior to conventional CT in delineating nodule morphology and allowing the detection of calcification. When studying a patient with a solitary nodule by using CT, we typically obtain contiguous high-resolution CT scans through the nodule, monitored by the radiologist, followed by a conventional CT study aimed at evaluating the remainder of the lung parenchyma, mediastinum, and hila.

### Confirmation of a Nodule and Delineation of Morphology

When a solitary nodule is suspected on plain radiographs, CT is often used to confirm that a nodule is present and to define its morphologic characteristics. In addition to conventional CT (contiguous 1-cm collimation), thin-slice, high-resolution CT scans can be quite variable in evaluating focal pulmonary parenchymal lesions [9]. We commonly obtain several contiguous high-resolution scans through the abnormal area in a patient with a lung nodule. A few types of nodular lung lesions have morphologic characteristics typical enough to allow a diagnosis to be made on CT (Fig. 3). These include arteriovenous fistulas, rounded atelectasis, focal consolidation, pleural plaques, fungus balls (Fig. 4), and mucous plugs. Pulmonary malignancies (particularly adenocarcino-

mas) often appear irregular and spiculated on high-resolution CT, and this appearance strongly suggests malignancy (Fig. 5) [10].

Identification with CT of multiple lung nodules in a patient in whom a single nodule is visible on plain films suggests metastases as the likely diagnosis, but lung cancer in association with other causes of lung nodules (e.g., granulomas) must also be considered, particularly if one nodule is dominant. Furthermore, any patient with lung cancer has an increased risk (compared with the general population) of having a second lung cancer synchronous with the first. Thus, if two nodules are visible, both may be primary lung cancers, and both may be resectable. However, this is rare and occurs in less than 1% of patients [11, 12].

### CT Nodule Densitometry

In 1980, Siegelman et al. [13] suggested the use of quantitative CT densitometry for the detection of calcium in lung nodules, thus indicating their benignity. They indicated that calcification invisible on plain radiographs or tomograms could be detected by high CT numbers by using CT with thin collimation. In their initial report [13], 91 solitary pulmonary nodules with an uncalcified appearance on conventional tomography were studied with CT. Averaging the highest CT numbers for each nodule, all 45 primary tumors and 13 metastatic nodules were found to have values of less than 164 H, whereas 20 of 33 benign nodules were identified as such by a representative CT number of over 164 H. Other investigators had difficulty in duplicating their results [14, 15], largely because of differences between scanners and image reconstruction algorithms. In general, most benign nodules were found to have representative CT values much less than the 164 H cutoff that has been reported. However, other authors confirmed the potential usefulness of this technique, and the results of Siegelman et al. were subsequently confirmed in a larger series [16–18]. From 22% to 36% of lung nodules that cannot be shown to contain calcium by using conventional tomograms are found to contain calcium by using CT [16–18].

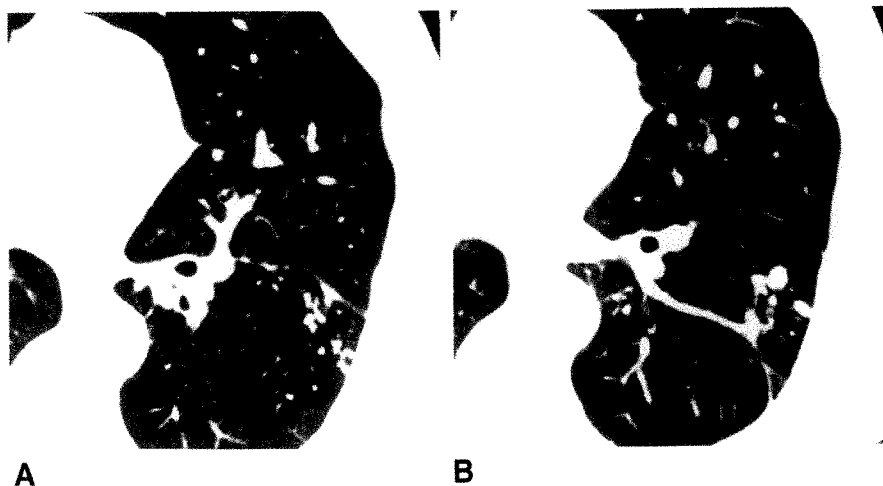


Fig. 3.—A and B, High-resolution CT scans at two levels in patient with a poorly defined 1-cm nodule visible on chest radiographs. On high-resolution CT, nodule is seen to consist of a number of smaller, well-defined nodular densities. This appearance suggests a granulomatous disease, and CT-guided needle aspiration biopsy results showed an atypical *Mycobacterium*.

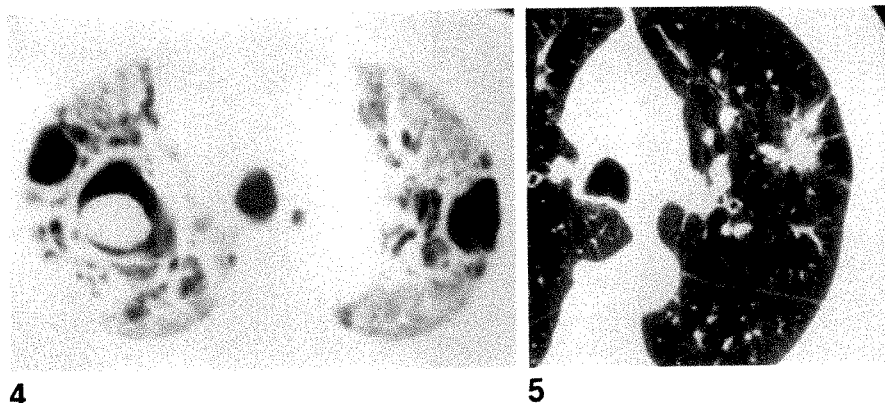


Fig. 4.—CT scan in patient with usual interstitial pneumonitis and a nodule in right upper lobe. Intracavitary mass strongly suggests the presence of a fungus ball.

Fig. 5.—High-resolution CT scan in patient with a nodule in upper lobe. Spiculated mass is very suspicious for carcinoma. Nodule densitometry is not appropriate with nodules having this appearance on plain films or CT scans, because many represent tumors. An adenocarcinoma was found at surgery.

Further study of individual scanners, scanner geometry, and reconstruction algorithms emphasized the rather considerable variation in nodule density measurements obtained with different scanners, for nodules of different sizes, in different locations, and in patients of different size and chest wall thickness [19]. These variables made the use of CT number criteria applicable to one machine difficult or impossible to use on another. It was a difficult problem.

One approach to solving this problem was the development of an anthropomorphic phantom for use in chest CT [20]. This phantom can simulate the shape, dimensions, and density of thoracic structures in most patients. Cylinders of various diameters, made of plastic to correspond to the density of a calcified nodule (described as having a density of 164, 190, and 264 H in different publications [20–22]), serve as the reference density for a solitary pulmonary nodule. In this technique, after a patient with a solitary nodule is studied with thin collimation, the phantom is put together to simulate the same slice level, chest wall thickness, nodule location, and size, and then the phantom is scanned with the identical CT technique that was used in scanning the patient (Fig. 6). Then, the densities of pixels in the patient's nodule and the phantom nodule are compared. If pixels in the lung nodule are denser than those in the phantom nodule, calcium is considered to be present [21–23]. Thus, this phantom is

assumed to provide a measurement of density independent of equipment-related or patient-related variations.

However, as stated above, because lung carcinomas can contain some calcium, not all nodules shown to contain calcium on CT scans can be diagnosed as benign. It has been recommended that in order to call a nodule benign, dense pixels must be diffuse or central within the nodule, account for 10% or more of the cross-sectional area, and be visible on more than one scan; in other words, the detectable calcification must be of substantial size and central within the nodule (what would be expected for a benign lesion). Thus, CT nodule densitometry with this phantom is not only quantitative, but is qualitative as well. It can be thought of as being used in a way similar to, but in a more objective fashion than, conventional tomography.

Also, in order to reduce the risk of calling a calcified carcinoma benign, it has been recommended that a nodule be lobulated or smooth rather than spiculated if it is to be diagnosed as benign, and less than 2 cm in size [16, 21–23]. Large or spiculated nodules are much more likely to be carcinomas than smaller, better defined lesions. Because of this, patients who have nodules that are larger than 2 cm or appear spiculated on plain radiographs should not undergo CT nodule densitometry; with such nodules, densitometry would be of no value.



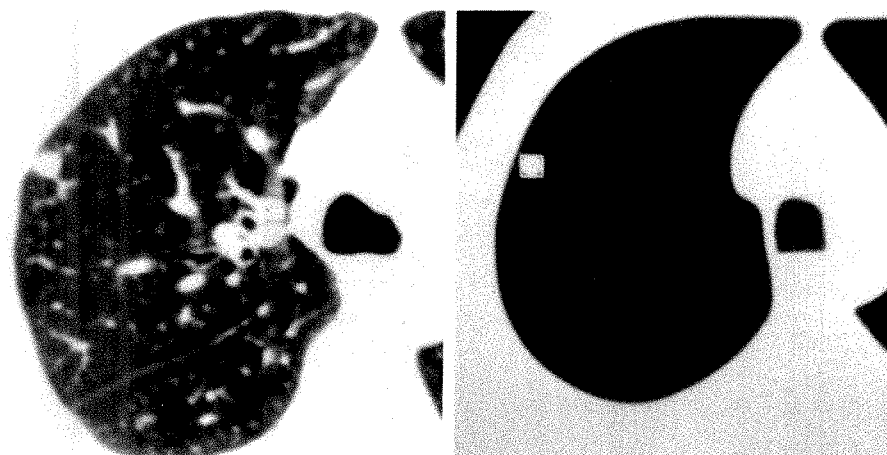


Fig. 6.—A, Thin, collimated CT scan reconstructed with standard algorithm in patient with a small nodule in right lung.

B, CT phantom has been constructed to simulate same slice level, nodule size, and location, and phantom has been scanned by using identical technical factors.

C, CT numbers recorded from nodule include many pixels exceeding 100 H and some exceeding 200 H.

D, Numbers recorded from phantom nodule are considerably lower. Thus, lung nodule is calcified.

A

	X	126	127	128	129	130	131	132	133	134
Y	283	-738	-640	-491	-401	-386	-347	-300	-370	-555
284	-648	-489	-294	-177	-126	-64	-24	-147	-430	202
285	-426	-269	-117	-35	18	82	94	-24	-319	203
286	-192	-81	5	38	87	141	118	2	-279	204
287	-118	-23	41	85	161	206	135	-25	-326	205
288	-187	-77	2	85	184	227	136	-88	-419	206
289	-354	-183	-55	52	146	186	72	-221	-554	207
290	-579	-396	-228	-103	3	42	-92	-405	-696	208
291	-737	-654	-538	-433	-337	-301	-375	-563	-751	209

B

	X	117	118	119	120	121	122	123	124	125
Y	202	-839	-618	-383	-241	-206	-283	-477	-742	-919
203	-627	-279	-61	12	30	-13	-146	-446	-782	204
204	-399	-64	32	36	38	27	-1	-196	-613	205
205	-265	13	35	33	31	19	23	-74	-482	206
206	-241	24	33	33	31	21	36	-52	-461	207
207	-339	-9	50	42	26	28	43	-113	-549	208
208	-533	-163	-2	34	37	26	-40	-316	-722	209
209	-765	-464	-226	-109	-86	-152	-323	-622	-890	210
210	-921	-799	-623	-499	-473	-562	-714	-880	-972	

C

D

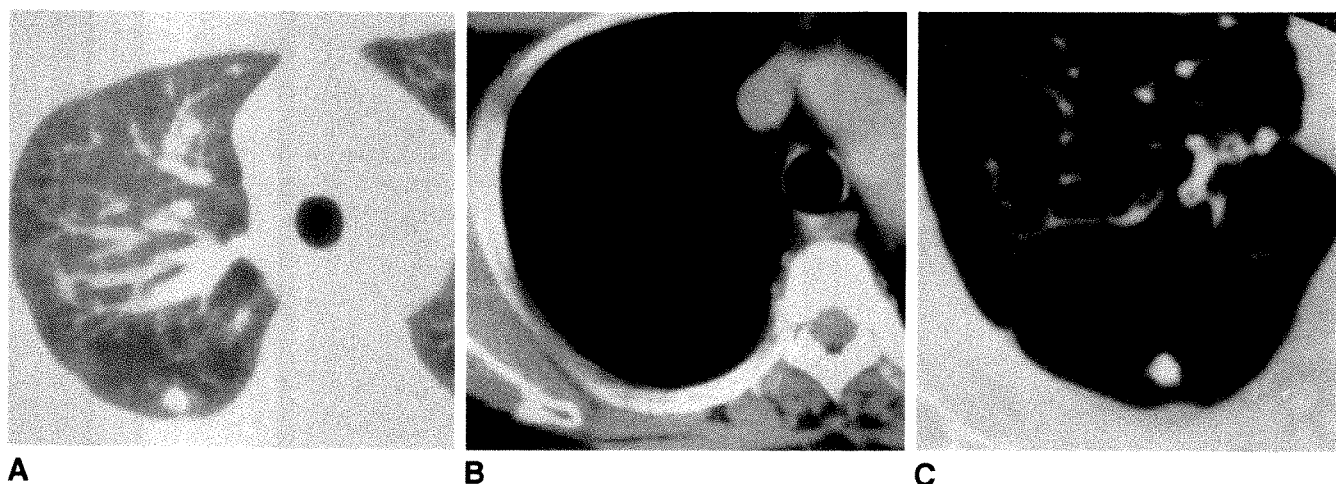


Fig. 7.—A, Conventional CT scan with 1-cm collimation at level of a nodule in right lung.

B, With mediastinal window for this slice, nodule is invisible and no evidence of calcification is shown.

C, Thin, collimated scan shows nodule is densely calcified. Measured CT numbers exceeded 400 H.

In a cooperative study [21] of this phantom, 298 pulmonary nodules were evaluated. Of 69 nodules determined to contain substantial calcification, 68 were benign and one was malignant. Of the 229 remaining patients who had nodules that did not contain substantial calcification (indeterminate nodules), 176 had malignant nodules.

It must be emphasized that the thin-section (1.5-mm) technique is necessary when using CT for the diagnosis of nodule calcification. Calcium easily diagnosable on thin-section CT is sometimes invisible with 1-cm collimation (Fig. 7). Also, in regard to the study reporting the use of the chest phantom for nodule densitometry [21], in approximately half of the

cases in which a nodule could be called benign, calcium was easily visible within the lesion on the thin-section scans, and the phantom itself was unnecessary. Furthermore, concurrent improvements in scanner technology allow more accurate density measurements with CT, obviating a phantom in many cases. Some current scanners appear to be better densitometers, and less susceptible to variations in CT number measurement, than the scanners that prompted the invention of this phantom [24]. In our institution we routinely perform nodule densitometry using a GE 9800 machine, without using a nodule phantom. Although varying technical factors (kVp, mA, reconstruction algorithm) can be used in performing nodule densitometry with adequate results, we prefer using relatively high-kVp settings (because of decreased image noise and a more linear relationship between CT number and calcium content) and a high-spatial-frequency algorithm (GE bone), which improves spatial resolution and may be slightly more sensitive than the standard algorithm for detecting small amounts of calcium [24]. Nodules with visible calcification on the thin-section scans will generally have CT number values of about 400 H on the GE 9800 (Fig. 7). We regard nodules with CT numbers of more than 200 to contain calcium (Fig. 6) [24].

CT with thin collimation can also be valuable in diagnosing pulmonary hamartomas. In one study [25], 30 of 47 patients with a hamartoma were correctly diagnosed with CT because of visible fat, either focal or diffuse (CT numbers ranging from -40 to -120 H); fat and calcification; or diffuse calcification (Fig. 8).

### Dual-Energy Techniques

It has been suggested that the amount of calcium present in a lung nodule can be quantified by using a dual-energy CT scanning technique [26]. Elements with high atomic numbers (calcium) exhibit different degrees of X-ray absorption at different energies. By noting the attenuation of the X-ray beam at different energies, one can accurately quantify the amount of calcium in an area of interest. However, because

of technical difficulties, this technique has not yet been used clinically in a large series. Replicating the exact same level on the two different scans obtained with different energies is the primary difficulty with this technique.

Preliminary experiments with dual-energy digital radiography with the two energy measurements obtained simultaneously have been reported recently [27]. Because there is exact correspondence of the dual-energy images, the problems of misregistration occurring with CT have been avoided. With this technique, measurements of calcium in simulated lung nodules in a phantom have been quite accurate. However, as with dual-energy CT, digital radiography techniques remain experimental.

### Use of Imaging to Guide Biopsies

If plain radiography and CT do not allow a specific diagnosis to be made, and no calcification is visible within the nodule, a biopsy may be necessary. Depending on the clinical situation, and the prejudices of the patient's physician, several options are available. These may include needle lung biopsy, bronchoscopy, mediastinoscopy, or thoracotomy. To some degree, imaging studies can be valuable in making this choice.

### Aspiration Lung Biopsy or Bronchoscopy?

Aspiration needle biopsy has become firmly established in the investigation of peripheral solitary pulmonary nodules suspected of being neoplastic [28, 29]. Biopsies can be performed on lesions as small as 1 cm, although the minimum size varies with the skill of the operator. Confirmation of the tip of the needle within the lesion must be obtained. Biplane fluoroscopy is the most conventional method, but single-plane fluoroscopy and CT may also be used.

Needle biopsy of the lung is a safe procedure. Although pneumothorax occurs in about 20% of patients, intercostal tube evacuation is required in only a few percent. In patients with carcinoma, hemorrhage and death are uncommon; dis-

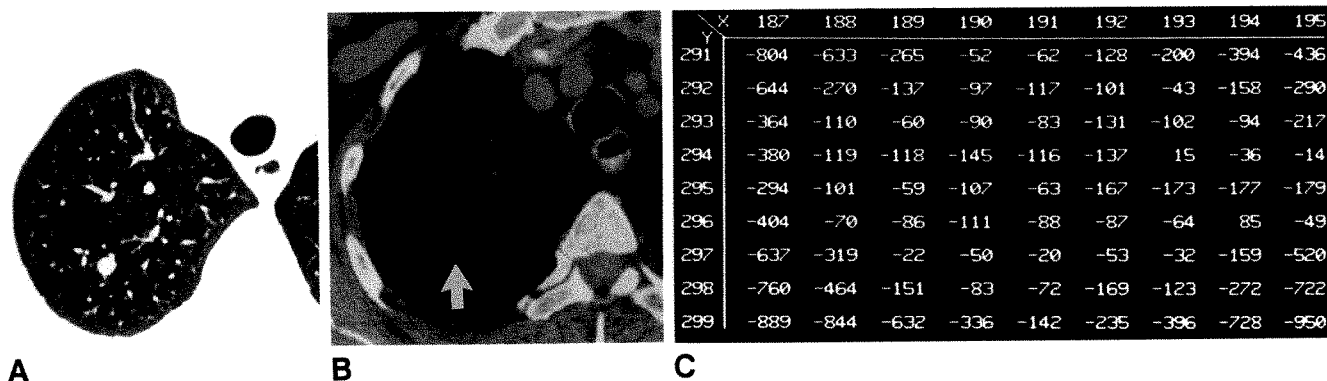


Fig. 8.—A, High-resolution CT scans with lung window settings in patient with a small nodule detected on plain films. B, With mediastinal window settings, nodule (arrow) appears to be of a density similar to that of subcutaneous fat. C, CT numbers measured from this nodule indicate it is entirely or almost entirely fat. Hamartomas can have this appearance. This lesion was followed up with plain radiographs and remained unchanged in size.

semination of malignant cells from an aspiration biopsy may occur rarely.

Needle aspiration will yield malignant cells in more than 90% of neoplastic nodules. This percentage can be optimized by having a cytologist on hand at the time of the biopsy, and repeating the biopsy if specimens are negative. Cytologic determination of cell type is good for squamous cell carcinomas and adenocarcinomas, but poor for undifferentiated tumors. A bacterial diagnosis can be made in almost 70% of infectious nodules. The diagnosis of a benign nodule (e.g., hamartoma) can also be made, though this usually requires a larger aspirate than for the diagnosis of malignancy.

The indications for needle aspiration biopsy vary between institutions, often determined at least in part by the preference of the surgeon. I think an argument can be made for reserving needle biopsy for those patients with solitary pulmonary nodules who are not candidates for thoracotomy because of age, complicating illness, or because the lesion is suspected of being a metastatic deposit. Because of the relatively high false-negative rate (up to 10%) in patients with carcinoma, a negative biopsy cannot be taken to mean that no tumor is present. If a patient can tolerate surgery, a solitary pulmonary nodule that could represent a malignancy is often resected without a preliminary needle biopsy. In patients suspected of having a benign nodule because of its appearance or growth rate or the patient's age, needle biopsy can be used to make a specific diagnosis of a benign lesion or to increase the likelihood of a benign process prior to radiologic follow-up. It is important to note that the role of needle biopsy in patients with a solitary nodule can vary considerably from one institution to the next.

CT can be helpful in planning a needle aspiration biopsy [30], even if CT is not used for the biopsy itself. First, CT can indicate the depth of the lesion, and the needle can be marked for the appropriate depth. Second, CT can help in planning the biopsy approach. If bullae lie in the path of the needle, or the needle must cross a fissure to reach the lesion, the risk

of pneumothorax is increased, and a different approach might be used.

Bronchoscopy is most accurate in diagnosing central masses with an endobronchial component, whereas needle biopsy is best for peripheral lesions. Thus, the location of the lesion can be important in choosing the biopsy procedure. CT can be quite valuable in this regard. If an endobronchial lesion is detected with CT, or bronchial narrowing at the site of a hilar mass is visible, bronchoscopy directed to the proper level is most appropriate (Fig. 9) [31]. In some patients, CT will show an endobronchial lesion beyond the visibility of the bronchoscope, and thus guide the biopsy attempt.

### CT for Staging Cancer in Patients with a Solitary Nodule

If a patient with a lung nodule is known to have a carcinoma from needle aspiration biopsy or cytology, or is strongly suspected of having a malignant lesion, then the radiologic examination, particularly with CT, has an additional goal—specifically to determine the resectability of the tumor.

However, the use of CT for staging cancer in patients with solitary nodules is controversial. Because of the relatively low likelihood of mediastinal node metastases in patients with solitary lung nodules who do not have evidence of hilar or mediastinal mass on plain radiographs, a number of surgeons perform thoracotomy on patients with a potentially malignant nodule without further biopsy or staging procedures (including CT). For example, in a recent survey of thoracic surgeons [32], only 15% of surgeons would obtain a CT scan preoperatively to evaluate the extent of the disease in a patient with a peripheral nodule. Furthermore, the value of CT in staging cancer in patients with T1 lesions (peripheral nodules  $\leq 3$  cm in diameter) has not been clearly established, and some investigators believe it may provide misleading information regarding the status of mediastinal nodes [33–35]. In patients with a solitary nodule, if mediastinal node metastases are found at surgery, they may be resectable with a reasonable chance of cure if they are ipsilateral [36], and particularly if they are low in the mediastinum and the primary tumor is squamous cell.

Some thoracic surgeons believe that positive lymph nodes found at mediastinoscopy rule out effective surgery treatment of lung cancer [37, 38]; in several studies, patients with positive findings on mediastinoscopy had a relatively poor survival rate after surgical resection, compared with patients in whom mediastinoscopy showed negative results but positive nodes were found at surgery. Because of this, these surgeons perform mediastinoscopy in all lung cancer patients, including those with a solitary nodule. Recently, two studies [37, 38] found mediastinoscopy and CT to have the same reasonably high sensitivity for detecting mediastinal node metastases. However, as would be expected, mediastinoscopy was 100% specific (no normal cases were called abnormal), whereas CT had a specificity of 50–65%. Despite this, these authors recommend that CT (in addition to mediastinoscopy) be performed in evaluating patients with solitary nodules. In their opinion, if CT shows abnormal lymph nodes, it should be used to guide mediastinoscopy and

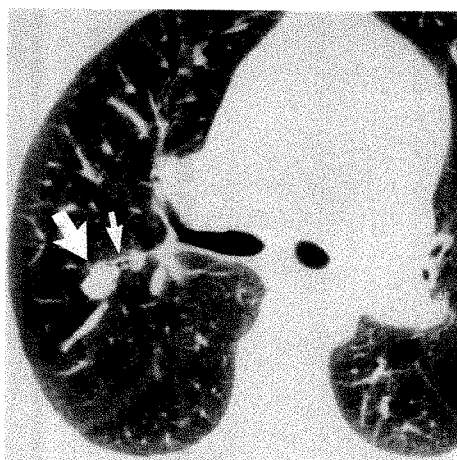


Fig. 9.—CT scan in patient with a small nodule in right lung shows nodule (large arrow) is closely related to posterior segmental bronchus of right upper lobe (small arrow). Because of this, it was approached bronchoscopically rather than with a percutaneous biopsy; brush cytology findings were positive.

biopsy. However, it is also pointed out that biopsy should not be limited to nodes that appear abnormal on CT; other nodes may be the ones involved by tumor.

## REFERENCES

1. Bateson EM. An analysis of 155 solitary lung lesions illustrating the differential diagnosis of mixed tumors of the lung. *Clin Radiol* **1965**;16: 51-65
2. Edwards WM, Cox RS Jr, Garland LH. The solitary nodule (coin lesion) of the lung: an analysis of 52 consecutive cases treated by thoracotomy and a study of preoperative diagnostic accuracy. *AJR* **1962**;88:1020-1042
3. Ray JF, Lawton BR, Magnin GE, et al. The coin lesion story: update 1976. Twenty years experience with early thoracotomy for 179 suspected malignant coin lesions. *Chest* **1976**;70:332-336
4. Trunk G, Gracey DR, Byrd RB. The management and evaluation of the solitary pulmonary nodule. *Chest* **1974**;66:236-239
5. Cahan WG, Castro EB, Hadju SI, et al. The significance of a solitary lung shadow in patients with colon carcinoma. *Cancer* **1974**;33:414-421
6. Rotte KH, Meiske W. Results of computer-aided diagnosis of peripheral bronchial carcinoma. *Radiology* **1977**;125:583-586
7. O'Keefe ME Jr, Good CA, McDonald JR. Calcification in solitary nodules of the lung. *AJR* **1957**;77:1023-1033
8. Nathan MH. Management of solitary pulmonary nodules: an organized approach based on growth rate and statistics. *JAMA* **1974**;227: 1141-1144
9. Mayo JR, Webb WR, Gould R, et al. High-resolution CT of the lungs: an optimal approach. *Radiology* **1987**;163:507-510
10. Kuriyama K, Tateishi R, Doi O, et al. CT-pathologic correlation in small peripheral lung cancers. *AJR* **1987**;149:1139-1143
11. Stark P. Multiple independent bronchogenic carcinomas. *Radiology* **1982**; 145:599-601
12. Bower SL, Choplin RH, Muss HB. Multiple primary bronchogenic carcinomas of the lung. *AJR* **1983**;140:253-258
13. Siegelman SS, Zerhouni EA, Leo FP, et al. CT of the solitary pulmonary nodule. *AJR* **1980**;135:1-13
14. Godwin JD, Speckman JM, Fram EK, et al. Distinguishing benign from malignant pulmonary nodules by computed tomography. *Radiology* **1982**;144:349-351
15. Godwin JD. The solitary pulmonary nodule. *Radiol Clin North Am* **1983**; 21:709-720
16. Siegelman SS, Khouri NF, Leo FP, Fishman EK, Braverman RM, Zerhouni EA. Solitary pulmonary nodules: CT assessment. *Radiology* **1986**; 160:307-312
17. Proto AV, Thomas SR. Pulmonary nodules studied by computed tomography. *Radiology* **1985**;153:149-153
18. Huston J, Muhm JR. Solitary pulmonary nodules: evaluation with a CT reference phantom. *Radiology* **1989**;170:653-656
19. Zerhouni EA, Spivey JF, Morgan RH, et al. Factors influencing quantitative CT measurements of solitary pulmonary nodules. *J Comput Assist Tomogr* **1982**;6:1075-1087
20. Zerhouni EA, Boukadoum M, Siddiky MA, et al. A standard phantom for quantitative analysis of pulmonary nodules by computed tomography. *Radiology* **1983**;149:767-773
21. Zerhouni EA, Stitik FP, Siegelman SS, et al. CT of the pulmonary nodule: a cooperative study. *Radiology* **1986**;160:319-327
22. Khouri NF, Meziane MA, Zerhouni EA, Fishman EK, Siegelman SS. The solitary pulmonary nodule; assessment, diagnosis, and management. *Chest* **1987**;91:128-133
23. Zerhouni EA, Stitik FP. Controversies in computed tomography of the thorax: the pulmonary nodule-lung cancer staging. *Radiol Clin North Am* **1985**;23:407-426
24. Im J-G, Gamsu G, Gordon D, et al. CT densitometry of pulmonary nodules in a frozen human thorax. *AJR* **1988**;150:61-66
25. Siegelman SS, Khouri NF, Scott WW Jr, et al. Pulmonary hamartoma: CT findings. *Radiology* **1986**;160:313-317
26. Cann CE, Gamsu G, Birnberg FA, et al. Quantification of calcium in solitary pulmonary nodules using single- and dual-energy CT. *Radiology* **1982**; 145:493-496
27. Hickey NM, Niklason LT, Sabbagh E, Fraser RG, Barnes GT. Dual-energy digital radiographic quantification of calcium in simulated pulmonary nodules. *AJR* **1987**;148:19-24
28. Herman PG, Hessel SJ. The diagnostic accuracy and complications of closed lung biopsies. *Radiology* **1977**;125:11-14
29. Khouri NF, Stitik FP, Erozan YS, et al. Transthoracic needle aspiration biopsy of benign and malignant lung lesions. *AJR* **1985**;144:281-288
30. vanSonnenberg E, Casola G, Ho M, et al. Difficult thoracic lesions: CT-guided biopsy experience in 150 cases. *Radiology* **1988**;167:457-461
31. Naidich DP, Sussman R, Kutcher WL, Aranda CP, Garay SM, Ettenger NA. Solitary pulmonary nodules: CT-bronchoscopic correlation. *Chest* **1988**;93:595-598
32. Epstein DM, Stephenson LW, Geffer WB, et al. Value of CT in the preoperative assessment of lung cancer: a survey of thoracic surgeons. *Radiology* **1986**;161:423-427
33. Pearlberg JL, Sandler MA, Beute GH, et al. T1 NO MO bronchogenic carcinoma: assessment by CT. *Radiology* **1985**;157:187-190
34. Heavey LR, Glazer GM, Gross BH, et al. The role of CT in staging radiographic T1 NO MO lung cancer. *AJR* **1982**;146:285-290
35. Conces DJ Jr, Klink JF, Tarver RD, Moak GD. T1 NO MO lung cancer: evaluation with CT. *Radiology* **1989**;170:643-646
36. Martini N, Flehinger BJ, Zaman MB, et al. Results of resection in non-oat cell carcinoma of the lung with mediastinal lymph node metastases. *Ann Surg* **1983**;198:386-396
37. Ratto GB, Mereu C, Motta G. The prognostic significance of preoperative assessment of mediastinal lymph nodes in patients with lung cancer. *Chest* **1988**;93:807-813
38. Staples CA, Muller NL, Miller RR, Evans KG, Nelems B. Mediastinal nodes in bronchogenic carcinoma: comparison between CT and mediastinoscopy. *Radiology* **1988**;167:367-372

# Does Knowledge of the Clinical History Affect the Accuracy of Chest Radiograph Interpretation?

Barbara C. Good<sup>1</sup>  
Lawrence A. Cooperstein<sup>1</sup>  
Georgine B. DeMarino<sup>1</sup>  
Linda M. Miketic<sup>1</sup>  
Rose C. Gennari<sup>1</sup>  
Howard E. Rockette<sup>2</sup>  
David Gur<sup>1</sup>

To examine the effect that a concise, objective, and potentially computer-extractable history would have on diagnostic accuracy in the interpretation of chest radiographs, we designed and tested a computerized patient-history form that could be integrated realistically into the clinical environment. We performed a series of studies in which 247 posteroanterior normal (79) and abnormal (168) chest radiographs were interpreted by four board-certified radiologists, both with and without accompanying clinical histories. The radiologists recorded their confidence rating of the presence or absence of one or more of the following abnormalities: interstitial disease, nodule, and pneumothorax. Analysis of receiver operating characteristics showed that, with the exception of interpretation of one abnormality by one radiologist, there were no statistically significant differences ( $p < .05$ ) between cases interpreted with and without the history form for any of the radiologists.

The results of our study suggest that knowledge of clinical history does not affect the accuracy of chest radiograph interpretations for the detection of interstitial disease, nodules, and pneumothoraces. These results may not be applicable to other clinical situations.

*AJR* 154:709-712, April 1990

In 1962, Tuddenham [1] stated that "our perception of ambiguous stimulus patterns in film reading may be strongly influenced by such external forces as our index of suspicion or knowledge of the clinical history." Although it has not been proved definitively, many radiologists think that the availability of a patient's medical history during interpretation of radiographs influences the interpretation in a positive way and helps increase diagnostic accuracy [2-4]. On the other hand, a number think that information that augments film interpretation may be a distraction [5, 6]. Others have claimed that it is not clear if any effect, either positive or negative, occurs [7]. In reality, the extent to which the amount and type of available clinical information affects diagnosis has not been documented extensively. Clouding the issue are the facts that (1) many variables remain uncontrolled in the studies that have been carried out and (2) large, multiabnormality studies on the effect of clinical information on accuracy levels are rare. In addition, most of the pertinent studies have been conducted by using chest radiographs ([6] and [8] are exceptions to this), and the possibility that the history may be more valuable for some procedures or abnormalities than others has been recognized, yet rarely investigated comprehensively.

In a previous study [9], we assessed radiologists' perceptions of preferences for a concise computerized history form. Our study indicated that all 20 board-certified radiologists tested would use a brief (fewer than 100 words), rapidly accessible (<5 sec) clinical history if it were provided along with the radiographs. Specific preferences existed about what information should appear and the order in which it should appear. In the randomized, multireader, multiabnormality study described here, we investigated what effect, if any, such a history would have on observer performance in the interpretation of a series of posteroanterior chest films.

Received August 28, 1989; accepted after revision November 20, 1989.

This work was supported in part by National Institutes of Health grant P01 CA43684.

<sup>1</sup> Department of Diagnostic Radiology, RC509 Scaife Hall, University of Pittsburgh, Pittsburgh, PA 15261. Address reprint requests to B. C. Good.

<sup>2</sup> Department of Biostatistics, University of Pittsburgh, Pittsburgh, PA 15261.

0361-803X/90/1544-0709  
© American Roentgen Ray Society.

## Materials and Methods

### Selection of Cases and Controls for the Study

Cases and controls for this study (Table 1) were selected sequentially from among patients undergoing posteroanterior chest imaging at our inpatient and outpatient facilities. All the films used in the study (79 normal and 168 abnormal cases) were acquired over a period of approximately 1 year. Three abnormalities—nodule, interstitial disease, and pneumothorax—were examined.

Each image was interpreted by a chest radiologist. Abnormal images were classified as subtle, typical, or gross (very easily detected) disease. The radiologist also rated the image quality of the film as excellent, good, acceptable, poor, or unacceptable. Extremely easy cases and those images rated unacceptable were eliminated. The remaining images were then interpreted independently by another chest radiologist. Radiographs on which the first and second ratings of difficulty were agreed on were then accepted as potential cases for that diagnosis. A ratio of approximately 1:1 of subtle to typical examples of each abnormality was attained. The radiologists who helped select cases did not serve in the subsequent study of receiver operating characteristics (ROCs). Information on cases admitted to the study was then entered into a computerized data base.

### Verification of Diagnoses: Cases and Controls

As all the studies were retrospective, abnormal cases were confirmed by surgical reports (i.e., nodule biopsy) or by follow-up with other procedures (e.g., CT) or clinical status and a previous or later radiograph that was interpreted independently as showing the abnormality in question. To verify controls, a disease-free interval of 1 year was confirmed from source documents such as normal follow-up radiologic and physical examinations. If source documents were not sufficient to meet the study requirements, we contacted the referring physician to confirm the duration of the disease-free state.

### Preparation of Clinical Histories for the Study

The histories used information that could be entered into a computerized data base as a part of the record for a patient or could be extracted from existing computerized data bases with minimal or no involvement of professional personnel. The form is designed to be used on an IBM PC and is modular in structure. Figure 1 is a sample from among the computerized histories used in the study.

Four nonphysician staff members were trained in case review and compiled and wrote the concise patient histories used in the study

from information available in the patient chart up to the date and time of the radiograph in question. All histories were reviewed by a physician for content and accuracy. An attempt was made to keep each history within a format of 100 words or less.

All completed histories were entered into the computer data base in which each was accessible by social security number, case number, and date of the radiologic examination to be used in the ROC study.

In order to ensure uniformity and consistency in the information provided, all cases (radiographs and clinical histories) were reviewed by a team of a radiologist and imaging division staff members; minor editing was performed during this final review. In approximately 5% of the cases, information was omitted that clearly would enable the diagnosis to be made. For example, in a case in which the reason for performing an imaging procedure was "prelung biopsy of subtle nodule, right upper lobe," these words were replaced with "none available." Such changes were made only for cases in which the image we selected to use in the study could be substituted for a previous image on which the same abnormality was first diagnosed.

<b>SS#:</b> 000-00-000	<b>Sex:</b> F	<b>Age:</b> 36
<b>PROCEDURE:</b> Chest / 1-6-88		
<b>CHIEF COMPLAINT/REASON FOR STUDY:</b>		
Cold symptoms; cervical nodes		
<b>HPI</b>		
Previous mycoplasmal pneumonia (12/87)		
<b>IMPRESSIONS OF ORDERING PHYSICIAN</b>		
? pneumonia		
<b>RESULTS FROM PREVIOUS RADIOGRAPHIC STUDIES</b>		
LLL pneumonia (12/87)		
<b>PHYSICAL EXAM RESULTS</b>		
Negative		
<b>PAST MEDICAL HISTORY</b>		
Acute lymphocytic leukemia; in remission		

Fig. 1.—Format for computerized histories of patients in this study. SS = Social Security; HPI = history of present illness; LLL = left lower lobe.

TABLE 1: Cases and Controls by Disease Category and Degree of Subtlety

Type of Disease	No. of Cases	No. of Abnormalities		
		Subtle	Typical	Total
Single abnormality				
Interstitial	60	37	23	60
Nodule	34	21	13	34
Pneumothorax	34	18	16	34
Multiple abnormalities				
Interstitial/nodule	16	9/4	7/12	32
Nodule/pneumothorax	1	0/1	1/0	2
Interstitial/pneumothorax	14	7/8	7/6	28
Interstitial/nodule/pneumothorax	9	8/1/4	1/8/5	27
<b>Total</b>	<b>247<sup>a</sup></b>	<b>118</b>	<b>99</b>	<b>217</b>

<sup>a</sup> Includes the 79 patients with no chest abnormalities (controls).



### Conduct of the Study

Four board-certified radiologists blindly interpreted the 247 chest films in a series of 10 sessions. When the patient history was included in the interpretation, it appeared on the screen of the computer, which was placed next to the view box. All readers were instructed to read the clinical history, when it was available, at least once. After reading the history, the radiologist completed a computerized scoring form. Questions on this form were organized by disease (interstitial disease, nodule, pneumothorax), and the reader was asked to rate on an ordinal scale the likelihood of the presence or absence of each (1 = definitely absent, 2 = probably absent, 3 = possibly present, 4 = probably present, 5 = definitely present). All films were interpreted twice, once with and once without the clinical history. To avoid reader order effects, the sessions with and without histories were interchanged for each reader. The order of case interpretation was randomized throughout the series, and the time to interpret any given case was not restricted. The time required to diagnose (review, interpret, and rate) each case, with or without history, was recorded by the computer.

In sessions in which the history was used, the radiologists sometimes viewed the image first in a cursory manner and then read the history; in other cases they viewed the image intently and then read the history. One radiologist often appeared to read the history before studying the image, and one read many of the histories rapidly and appeared to concentrate mainly on the image.

### Results

Results from the four readers were analyzed by using the computer program CORROC2 developed by Metz [10]. The area under the ROC curve, which can be used as an index of diagnostic accuracy; standard deviations; and *p* values were determined for the readings both with and without history, as shown in Table 2. With the exception of the interpretation of one abnormality from one radiologist, no significant differences in diagnostic accuracy occurred for any of the radiologists at the *p* < .05 level (two-tailed *t* test). Furthermore, six of the 12 disease-specific comparisons (four interpreters and

three disease categories) showed a decrease in accuracy when clinical history was provided; only four showed an improvement. The results for all radiologists by using both the paired *t* test [10] and the method described by Swets and Pickett [11] were not significant for any of the abnormalities (*p* ≥ .49).

It was only in interpreting nodule cases that one radiologist showed a significantly higher accuracy rate when the history was *not* present. The reason for this one notable deviation from the others is unclear, but we speculate that it could be because some radiologists do not perform as well when taken out of their "natural" environment. Histories of some of the cases misdiagnosed by this radiologist included information on other abnormalities (e.g., coronary heart disease with bypass) that had been followed routinely. In these cases, the history may have steered the radiologist away from a correct diagnosis.

When our data were analyzed according to the subgroups "typical" and "subtle," the availability of the clinical history yielded no improvement for either category, and in particular for the subtle case category, in which improvement, if any, would be expected (Table 2). Our results were not affected when the cases with modified histories were excluded from the analysis. Although our findings were negative, the sample size estimates in our study did not result in a high probability of detecting small changes in performance. However, for a moderate-sized difference of 0.10 in the area under the ROC curve, we estimate that the probability of an individual radiologist for detecting a difference for each of the three specific diseases was 0.99, 0.80, and 0.54 for interstitial disease, nodules, and pneumothoraces, respectively. The lower probability for pneumothoraces occurred because the readers tended to polarize their scores for this disease. We have assumed an  $\alpha$  level of .05, two-tailed test, and have used estimates of correlation from our data set. In our comparison of the average performances of the radiologists with and

**TABLE 2: Area Under Receiver Operating Characteristic (ROC) Curve for Overall Film Readings and Subtle Cases**

Abnormality/Reader No.	Overall Film Readings			Subtle Cases		
	Mean Area Under ROC Curve (SD)		<i>p</i>	Mean Area Under ROC Curve (SD)		<i>p</i>
	With History	Without History		With History	Without History	
Interstitial disease						
1	0.90 (0.02)	0.86 (0.02)	.15	0.88 (0.03)	0.84 (0.03)	.23
2	0.87 (0.02)	0.90 (0.02)	.29	0.85 (0.03)	0.88 (0.03)	.30
3	0.89 (0.02)	0.89 (0.02)	.82	0.85 (0.03)	0.85 (0.03)	.88
4	0.93 (0.02)	0.93 (0.02)	.52	0.90 (0.02)	0.92 (0.02)	.36
Nodule						
1	0.85 (0.04)	0.87 (0.03)	.69	0.74 (0.08)	0.75 (0.06)	.93
2	0.78 (0.06)	0.92 (0.02)	.006 <sup>a</sup>	0.68 (0.09)	0.84 (0.05)	.08
3	0.85 (0.04)	0.82 (0.05)	.58	0.72 (0.08)	0.79 (0.07)	.41
4	0.94 (0.02)	0.88 (0.04)	.10	0.88 (0.04)	0.86 (0.04)	.61
Pneumothorax						
1	0.92 (0.04)	0.93 (0.04)	.94	0.86 (0.08)	0.89 (0.06)	.76
2	0.91 (0.04)	0.94 (0.03)	.40	0.84 (0.07)	0.88 (0.06)	.56
3	0.91 (0.05)	0.97 (0.02)	.14	0.84 (0.08)	0.94 (0.04)	.20
4	0.98 (0.02)	0.95 (0.04)	.30	0.98 (0.01)	0.93 (0.01)	.24

<sup>a</sup> Significant at *p* < .05 (two-tailed *t* test).

without clinical histories, we have estimated the 95%, two-tailed, upper confidence bounds on performance with clinical history to be 0.04, 0.12, and 0.05 for interstitial disease, nodules, and pneumothoraces, respectively. Overall, despite inter- and intrareader variability, no significant difference occurred between the amount of time taken to interpret cases with history ( $66 \pm 22$  sec) and the amount of time for those without history ( $64 \pm 23$  sec). We attribute this finding to the concise and well-structured format of the clinical histories used in this study.

## Discussion

The impact that knowledge of a patient's history has on observer performance in radiology has been studied and debated for many years. In 1963, Schreiber [3] reported a statistically significant increase in the true-positive rate when a clinical history was provided; it had no impact on the false-positive rate. In another study, Potchen et al. [5] found a statistically significant increase in the detection of abnormalities with a suggestive as opposed to an irrelevant patient history. They found no differences in the interpretation of normal radiographs. When Doubilet and Herman [12] inserted test chest radiographs into the daily workload of radiologists who were unaware that a study was being carried out, they found a statistically significant increase in the rate of true-positive interpretations in the presence of a suggestive as compared with a nonsuggestive history, along with a concomitant increase in false positives.

In one of the few studies performed that did not use chest radiographs to examine this question, Eldevik et al. [6] concluded from an investigation using spinal CT scans and myelograms that (1) a significant number of interpretations were changed when the clinical history was known and (2) more studies were interpreted correctly without the clinical history than with it.

Berbaum et al. [4, 7, 8] have carried out a number of studies on this topic. In a study [4] using chest radiographs, they found that an appropriate clinical history results not just in improved decision making but in improved perceptual performance. In other studies, they showed that, except in cases of nodules, categorical prompts correct for specific abnormalities in the chest led to better detection rates [7]; in a bone study [8] they noted that "clues regarding location of trauma facilitate detection of fractures."

It would be desirable, in a study like the one we have conducted, to use a non-disease-specific format that provides for the evaluation of any abnormality. However, in such a case, currently available tools for analysis of observer performance allow only the evaluation of an interpreter's ability to discriminate between normal and abnormal images, without regard for the type of abnormality in question. In addition, multiabnormality cases cannot be incorporated easily into such a study.

Our findings on the impact of a patient history on radiograph interpretation are contrary to those obtained by several other investigators who noted improvement in diagnostic accuracy with the inclusion of a history [7, 8]. We think this may be because many of the previous studies used "cuing"-type histories, that is, histories that were constructed to relate

directly to the abnormality being tested and thus led a priori to better performance.

A difficulty common to all studies of the use of the history in radiologic interpretation is the lack of an agreed-on definition of what constitutes a history. In addition, there is the question of whether the history should be a prompting one, even though in some cases it may steer the radiologist on an incorrect course. We have interpreted the term *history* to mean a concise, objective, and potentially computer-extractable version of what exists in the patient's chart, accompanied by the referring physician's comments, when available.

## Conclusions

The results of our study suggest that knowledge of clinical history does not affect the accuracy of chest radiograph interpretations for the detection of interstitial disease, nodules, and pneumothoraces. However, findings for one type of procedure or, in fact, for a set of predefined abnormalities may not be applicable to the process when different imaging procedures (e.g., mammography) or other abnormalities are involved. Even if history is not important for detection, it may have an important role in determining the specific nature and significance of detected abnormalities.

## ACKNOWLEDGMENTS

We thank Marc Felice, Jill King, Nancy Obuchowski, and Kathleen Sidorovich for supervising and performing many of the tasks associated with this project. The efforts, discussions, and ongoing contributions of Charles E. Metz, University of Chicago, to our project are greatly appreciated.

## REFERENCES

1. Tuddenham WJ. Visual search, image organization, and reader error in Roentgen diagnosis. *Radiology* **1962**;78:694-704
2. Bundy AL. Re: The legal importance of the medical history (letter). *Radiology* **1984**;153:264
3. Schreiber MH. The clinical history as a factor in roentgenogram interpretation. *JAMA* **1963**;185:137-139
4. Berbaum KS, Franken EA, Dorfman DD, et al. Tentative diagnoses facilitate the detection of diverse lesions in chest radiographs. *Invest Radiol* **1986**;21:532-539
5. Potchen EJ, Gard JW, Lazar P, Lahaie P, Andary M. The effect of clinical history data on chest film interpretation: direction or distraction (abstr). *Invest Radiol* **1979**;14:404
6. Eldevik OP, Dugstad G, Orrison WW, Haughton VM. The effect of clinical bias on the interpretation of myelography and spinal computed tomography. *Radiology* **1982**;145:85-89
7. Berbaum KS, Franken EA, Dorfman DD, Barloon TJ. Influence of clinical history upon detection of nodules and other lesions. *Invest Radiol* **1988**;23:48-55
8. Berbaum KS, El-Khoury GY, Franken EA, Kathol M, Montgomery WJ, Hesson W. Impact of clinical history on fracture detection with radiography. *Radiology* **1988**;168:507-511
9. Good BC, Cooperstein LA, Gur D. Radiologists' perceptions of and preferences for a concise computerized history form during radiologic interpretations. *Proc SPIE* **1988**;914(B):970-975
10. Metz CE. Some practical issues of experimental design and data analysis in radiological ROC studies. *Invest Radiol* **1989**;24:234-245
11. Swets JA, Pickett RM. Fundamentals of accuracy analysis. In: Evaluation of diagnostic systems: methods from signal detection theory. New York: Academic Press, **1982**:15-45
12. Doubilet P, Herman PG. Interpretation of radiographs: effect of clinical history. *AJR* **1981**;137:1055-1058

# New Mammography Screen/Film Combinations: Imaging Characteristics and Radiation Dose

Carolyn Kimme-Smith<sup>1</sup>  
Lawrence W. Bassett<sup>1</sup>  
Richard H. Gold<sup>1</sup>  
Joanne Zheutlin<sup>1</sup>  
Jeffrey A. Gornbein<sup>2</sup>

Five types of film (Kodak OM, Kodak OM-SO177, Konica CM, Dupont Microvision, and Fuji MiMa) exposed in combination with seven different intensifying screens (Min R, Min R Medium, Siemens Orthox MA, Kyokka HR Mammo Fine, Agfa Gevaert Detail S (old and new), and Konica Monarch) were processed for either 90 sec (at 33.3°C) or 3 min (at 35.0°C). The films imaged a Computerized Imaging Reference System phantom with additional detail test objects placed on its surface to produce four groups of objects with which to evaluate resolution and contrast. For objects that tested resolution, the Kyokka HR Mammo Fine (Fuji) screen was statistically significantly superior; for objects that tested contrast, the Konica Monarch screen was statistically significantly superior. Extended processing did not affect Dupont and Kodak OM film as much as it affected the other films. It did affect contrast for the other films tested. The mean glandular doses from gridless exposures ranged from 32 to 80 mrad (0.32–0.80 mGy) over all film/screen/processing combinations for a 4.5-cm-thick test object. Several new film/screen combinations can provide images superior to the Kodak Min R/OM combination at a reduced radiation dose.

The Kyokka HR Mammo Fine (Fuji) screen was found statistically superior in radiographic resolution of mammographic test objects and the Konica Monarch screen was found to be superior in defining contrast.

*AJR* 154:713–719, April 1990

During the past 2 years, all of the major film manufacturers have introduced new films, and some also have introduced new screens, for mammography. Although extended development has become an acceptable method to increase the speed of some single-emulsion films [1, 2], Kodak recently changed their OM film to make it less dependent on processing parameters. The earlier version of OM film is now designated OM-SO177. Mammographers now have a wide variety of film/screen/processing combinations that reduce radiation dose. Because some of these combinations may affect image quality, we evaluated a large number of them, basing our tests on the visibility of simulated calcifications and low-contrast masses. Evaluation of the first version of Kodak's T-Mat M double emulsion film combined with two Min R Fast screens uncovered a problem in depicting tiny microcalcifications [3, 4]. Earlier film/screen combinations were tested [5, 6] with images obtained of a mammography test object constructed of breast-equivalent material and containing 78 fixed details on which to judge image quality [7]. These studies did not test radiographic contrast and resolution separately, but grouped them together when scoring the number of details present in a film image. The more recent study [6] tested a variety of processors and processing chemicals, which did not significantly affect the scores, and used extended processing (2.5 min) exclusively.

Although more rigorous methods of analysis are available for studies of this kind [8, 9], the large number of screens, films, and processor parameters tested precluded analyses of Wiener spectra, Detective Quantum Efficiency, and Modulation Transfer Function for each combination. Instead, this work follows the

Received July 25, 1989; accepted after revision November 13, 1989.

<sup>1</sup> Iris Cantor Center for Breast Imaging, UCLA School of Medicine, Los Angeles, CA 90024. Address reprint requests to C. Kimme-Smith.

<sup>2</sup> Department of Biomathematics, UCLA School of Medicine, Los Angeles, CA 90024.

0361-803X/90/1544-0713

© American Roentgen Ray Society

**TABLE 1: Film/Processor Time, Technique, Optical Density, and Dose for Gridless Exposures of a 4.5-cm Test Object**

Screen	Film	Development Time	mAs	Optical Density	Mean Glandular Dose <sup>a</sup> in mrad (mGy)	No. of Films	No. of Times Tested <sup>b</sup>
Min R	OM SO177	3 min	50	1.20	64.8 (0.648)	2	3
		90 sec	63	1.02	80.0 (0.800)	5	5
	OM (new)	3 min	50	1.22	64.8 (0.648)	1	1
		90 sec	63	1.05	80.0 (0.800)	1	3
	Dupont	3 min	40	1.25	51.1 (0.511)	1	2
		90 sec	50	1.33	64.8 (0.648)	1	2
	Fuji	3 min	50	1.23	64.8 (0.648)	1	2
		90 sec	63	1.09	80.0 (0.800)	1	3
	Konica	3 min	40	1.25	51.1 (0.511)	1	2
		90 sec	50	1.14	64.8 (0.648)	1	2
Min R (med)	OM SO177	3 min	32	1.18	40.3 (0.403)	1	1
		90 sec	40	1.07	51.1 (0.511)	5	6
	OM (new)	3 min	32	1.12	40.3 (0.403)	1	1
		90 sec	40	1.07	51.1 (0.511)	2	3
	Dupont	3 min	25	1.16	32.0 (0.320)	6	6
		90 sec	32	1.15	40.3 (0.403)	1	3
	Fuji	3 min	32	1.28	40.3 (0.403)	6	6
		90 sec	40	1.10	51.1 (0.511)	1	2
	Konica	3 min	28	1.26	35.5 (0.355)	2	2
		90 sec	32	1.22	40.3 (0.403)	2	4
Siemens	OM SO177	3 min	40	1.10	51.1 (0.511)	1	2
		90 sec	50	1.09	64.8 (0.648)	1	2
	Dupont	3 min	32	1.15	40.3 (0.403)	1	2
		90 sec	40	1.25	51.1 (0.511)	1	3
	Fuji	3 min	40	1.12	51.1 (0.511)	1	3
		90 sec	50	1.13	64.8 (0.648)	1	3
	Konica	3 min	32	1.25	40.3 (0.403)	1	2
		90 sec	40	1.14	51.1 (0.511)	1	1
	OM SO177	3 min	50	1.26	64.8 (0.648)	1	3
		90 sec	63	1.27	80.0 (0.800)	1	1
Fuji	Dupont	3 min	40	1.30	51.1 (0.511)	1	1
		90 sec	50	1.34	64.8 (0.648)	1	3
	Fuji	3 min	40	1.14	51.1 (0.511)	1	2
		90 sec	63	1.22	80.0 (0.800)	1	2
	Konica	3 min	40	1.36	51.1 (0.511)	1	2
		90 sec	50	1.35	64.8 (0.648)	1	2
	OM SO177	3 min	25	1.15	32.0 (0.320)	2	2
		90 sec	32	1.14	40.3 (0.403)	2	2
	OM (new)	3 min	25	1.09	32.0 (0.320)	1	1
		90 sec	40	1.19	51.1 (0.511)	1	1
Afga-S (old)	Dupont	3 min	25	1.16	32.0 (0.320)	2	2
		90 sec	32	1.23	40.3 (0.403)	2	2
	Fuji	3 min	25	1.15	32.0 (0.320)	2	2
		90 sec	32	1.15	40.3 (0.403)	1	2
	Konica	3 min	25	1.30	32.0 (0.320)	2	3
		90 sec	32	1.24	40.3 (0.403)	2	2
	OM SO177	3 min	25	1.11	32.0 (0.320)	1	2
		90 sec	32	1.08	40.3 (0.403)	1	2
	OM (new)	3 min	32	1.31	40.3 (0.403)	1	2
		90 sec	40	1.13	51.1 (0.511)	1	2
Afga-S (new)	Dupont	3 min	25	1.16	32.0 (0.320)	1	2
		90 sec	32	1.27	40.3 (0.403)	1	2
	Fuji	3 min	25	1.18	32.0 (0.320)	1	2
		90 sec	32	1.11	40.3 (0.403)	1	2
	Konica	3 min	25	1.19	32.0 (0.320)	1	3
		90 sec	32	1.26	40.3 (0.403)	1	2
	OM SO177	3 min	40	1.08	51.1 (0.511)	2	4
		90 sec	50	1.08	64.8 (0.648)	1	2
	OM (new)	3 min	50	1.34	64.8 (0.648)	1	1
		90 sec	63	1.23	80.0 (0.800)	3	3
Konica	Dupont	3 min	40	1.09	51.1 (0.511)	1	3
		90 sec	50	1.32	64.8 (0.648)	3	3
	Fuji	3 min	40	1.27	51.1 (0.511)	2	4
		90 sec	50	1.13	64.8 (0.648)	1	3
	Konica	3 min	40	1.28	51.1 (0.511)	2	4
		90 sec	50	1.23	64.8 (0.648)	2	3

<sup>a</sup> According to Tables 1 and 3 from Rosenstein et al. [10].

<sup>b</sup> For each radiologist.

example of earlier studies [5, 6] by being primarily concerned with the radiologists' assessments of each combination's imaging characteristics. However, in order to ensure that the results of these tests would be useful clinically, rigorous statistical methods were used to analyze the results.

## Materials and Methods

Five films (Kodak OM, Kodak OM-SO177, Dupont Microvision, Fuji MiMa, and Konica CM) and seven screens (Min R, Min R Medium, Siemens Orthox MA, Kyokka HR Mammo Fine, Agfa Gevaert Detail S (old and new), and Konica Monarch) were tested. After these tests were made, Dupont Microvision significantly improved their film, and Kodak is still revising the new OM film introduced in August 1988. For each screen/film combination, two processing methods were used: 90 sec at 33.3°C (92°F) and 3 min at 35°C (95°F) (Table 1). Kodak M63 processors with Kodak RP chemicals were used for both processing methods. Sensitometer strips were run on each of the 9 days when these images were processed. Average gradient was  $3.00 \pm 0.08$  and relative speed varied less than 6% on these days.

Because the Siemens and Fuji screens were tested before the new Kodak OM film was available, they were not tested with that film. As a result, 36 rather than 70 ( $5 \times 7 \times 2$ ) film/screen/processing combinations were tested. The 66 combinations were used to image a Computerized Imaging Reference System (CIRS, Norfolk, VA) 4.5-cm-thick epoxy mammography phantom consisting of a 3.5-cm thickness composed of 30% glandular-equivalent, 70% adipose-equivalent material surrounded by a 0.5-cm shell of adipose-equivalent material. Embedded in the phantom were groups of calcium carbonate specks (0.35, 0.27, 0.23, 0.20, 0.16, and 0.12 mm in diameter) and round, glandular-equivalent masses (6, 5, 4, 3, 2, and 1 mm in diameter). Half of these masses had fibrils radiating from them. In addition, eight plastic-coated ring binders (anuli 1.3 cm in diameter with 0.6-cm centers) were arbitrarily distributed on top of the phantom, near the skin line where contrast would be least. These anuli have been used successfully in other film studies to evaluate low contrast differences [4]. Three clusters of irregularly shaped simulated calcifications (crushed clam shells ranging in size from 0.25 to 1.00 mm) were placed between the phantom and the film/screen combination. Their position near the image plane eliminated the effect of focal spot size (Fig. 1).

The images were made with a General Electric 500-T dedicated mammography unit operated at 65-cm source-to-image distance, without a grid, and at 26 kVp. The kilovoltage setting, which was checked twice during the study by a Machlett Dynalyzer (Eimac, San Carlos, CA), varied less than 4%. The GE unit has a molybdenum anode and 0.03-mm molybdenum filtration, requires a three-phase power supply, and has a 0.3-mm half-value layer at 26 kVp (including the compression plate). The large focal spot, measured with a 0.03-mm pinhole, is  $0.32 \times 0.25$  mm at the chest wall.

Each combination was exposed by using a manual technique to achieve an optical density (OD) at the chest wall between 1.02 and 1.36 (mean over all films = 1.20, standard deviation = 0.08). Table 1 records the milliamperage seconds, OD, and computed mean glandular dose for each combination. The dose was calculated by using the same manual technique as required for the phantom exposure. A Victoreen 660-4A chamber (correction factor 1.14 at 30 kVp), calibrated in 1987 at the Center for Diseases and Radiological Health, measured the exposure in air for each technique. Then the mean glandular dose was calculated by multiplying it by 0.175 (from Table 1 or 3 of Rosenstein et al. [10]).

Optical density was not always the same for exposures of the same screen/film combinations. Where multiple images were obtained

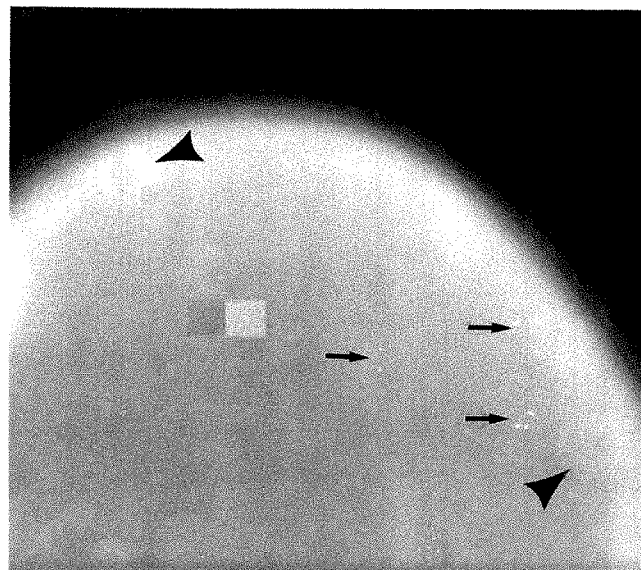


Fig. 1.—Computerized Imaging Reference System epoxy mammography test object with added low-contrast anuli on periphery (arrowheads), added calcifications (arrows), and calibrated clusters of six calcifications on right chest wall extending toward nipple and graduated masses with fibrils on left chest wall extending diagonally left.

for one screen/film combination, the OD for the first exposure is reported in Table 1. For no reimaged combination did the exposure differ from the previous exposure by more than 0.08 OD. Except for the Fuji, Siemens, and new Agfa screens, which were available to us for only a limited time, the other screens were combined with all five films and were reimaged and tested from two to six times to increase the reliability of the results. The images of those film/screen combinations for which only one image was obtained were usually retested several times (see Table 1). All the screens were tested in the cassettes supplied by the manufacturers. The cassettes were not tested for film/screen contact, because poor contact would be part of the screen/cassette system and is included in these experiments under the designation "screens."

The images were interpreted by three board-certified radiologists specializing in mammography. Two of the radiologists have been interpreting mammograms for over 10 years, and the third radiologist had been interpreting mammograms exclusively for the preceding year. Each film was masked at the edges to prevent identification of film type. All films were randomly coded with a two-character code for identification by the physicist, who presented the images to the radiologists. Five sets of films were interpreted in five viewing sessions during a 9-month period. Sets contained 32, 32, 38, 30, and 30 films each. Each set of images was interpreted on a mammography viewbox, with an opaque shield around each image, and with a magnifying hood-type viewer available.

Four scores were recorded for each film: two for resolution (the simulated embedded calcifications and the crushed clam shells) and two for radiographic contrast (the embedded masses and the anuli). The embedded calcifications were tested for visibility by recording the number of clusters that were visible, while the crushed-clam-shell simulated calcifications (placed next to the film plane) were ranked for sharpness by assigning one of three values depending on their "sharpness" compared with the sharpness in other films. The number of embedded masses visible and the number of added anuli imaged on the film were recorded, with the two scores serving as a test for image contrast. The test data consisted of four scores for each of 163 films with three radiologists interpreting independently.

A repeated measures analysis of variance (ANOVA) was done to compare scores by using screen brand, film brand, and processing method as design factors and each particular radiologist as a random repeated measure factor to account for each of the three radiologists evaluating the same 163 films. After this analysis, the significant design factors were examined to identify which types of film, screen, and/or processing were significantly different from other films, screens, or processing. To accomplish this, pairwise comparisons of means for all the films made with the same design factors were made by using the Tukey studentized range procedure [11] to correct for multiple comparisons.

The effects of differences between the same brand of film, for those 21 film combinations that were reimaged, and radiologist variations when rereading the same film, for those 57 film combinations that were retested, were treated as random effects and were pooled together as the noise in the analysis. This is a conservative treatment of the experimental data.

After the statistical analysis of the data, one screen/film/processor combination, which was found to be statistically superior, was tested clinically on 22 patients by imaging the right breast with the "superior" combination and the left breast with our usual combination: Min R Medium/OM-SO177 developed for 44 sec at 35°C.

## Results

As a result of reimaging and retesting so many of the film/screen/processing combinations, the noise statistics were low and mainly due to film variations rather than radiologists' variations. For three of the four tests, embedded calcifications, crushed-clam-shell sharpness, and the contrast of anuli on the surface of the test object, 75–80% of the noise variance was due to film variations. Only for the test that involved counting the embedded masses was the noise mainly due to variations among the three radiologists. The results of counting the masses embedded in the phantom were submerged in the noise of the experiment so that no statistically significant results were found for this test. Tables 2 and 3 report those film/screen/processor combinations with average scores higher than the other combinations. Not all the scores in Tables 2 and 3 were statistically significant. The scores for Min R/OM-SO177, the industry standard, are also reported at the bottom of each column in Tables 2 and 3. For the third test, the eight added anuli, only 10 film/screen combinations were significantly better than the bottom three combinations when the Tukey test was applied (Table 4).

For the groups of calcium carbonate specks embedded in the CIRS phantom, only the type of screen significantly affected score outcome ( $p = .01$ ). In particular, the old Agfa screen was significantly poorer than the Kyoka (Fuji) screen. However, if one looks at what this implies in radiographic terms, the size of the smallest specks imaged by both the old Agfa screen and the Kyoka screen ranged between 0.23 and 0.20 mm. The mean number of calcification clusters seen on images made by Fuji screens was 3.65 (i.e., calcifications with diameters of 0.35, 0.27, 0.23, and some 0.20 mm were seen), and for Agfa screens the mean was 3.33. Thus, more of the Fuji combinations imaged the 0.20 mm specks than the Agfa combinations. Whether this small difference is diagnostically significant depends on many factors independent of the film/screen combination, such as viewing distance, power of the magnifier used, radiologist vision, ambient and viewing-box light, and fatigue. For the crushed-clam-shell test, statistically significant differences between film processing methods were found for some screen/film combinations ( $p = .03$ ). When film exposed in an old Agfa cassette was processed for 90 sec, it did significantly poorer in this test than films exposed in a new Agfa cassette or a Fuji cassette and processed for 3 min. Screens alone also showed significant differences in this test ( $p = .0004$ ), particularly between the old and new Agfa screens and between the old Agfa screen and the Fuji screen, with the new Agfa screen and the Fuji screen significantly superior.

The crushed-clam-shell test had three possible values: unsharp (1), sharp (2), and very sharp (3). The mean scores for the old Agfa, Siemens, and Min R Medium screens were below 2, but the mean for the Fuji screen was 2.3, implying that the Fuji screen was usually judged "sharp" or "very sharp," whereas the old Agfa, Siemens, and Min R Medium screens were more likely to be judged "unsharp" or "sharp."

Both the tests described earlier showed that screens alone were important for resolution discrimination. The combination of film and screen was found to be important for good contrast discrimination ( $p = .0001$ ). Screens ( $p = .046$ ) and screen/processing ( $p = .041$ ) were of borderline significance, but the Tukey test showed that the screens that did well in the contrast test were not the same screens that did well in the resolution tests; the Konica screen was significantly better than the Siemens screen for identifying the added anuli. When

**TABLE 2: Film/Screen/Processing Combinations Scoring Highest on Resolution**

Phantom Calcification				Crushed Clam Shells			
Screen	Film	Processing <sup>a</sup>	Mean Score	Screen	Film	Processing <sup>a</sup>	Mean Score
Fuji	OM-SO177	90	4.0	New Agfa	Fuji	3	2.7
Siemens	OM-SO177	3	4.0	Konica	OM	3	2.7
Fuji	Konica	3	3.8	New Agfa	OM-SO177	3	2.7
Fuji	Fuji	90	3.8	Fuji	Fuji	3	2.5
New Agfa	OM	90	3.8	Konica	Fuji	3	2.5
Min R	OM-SO177	90	3.7	Fuji	Konica	3	2.5
Konica	Konica	90	3.7	Min R	Konica	90	2.5
Min R	Fuji	90	3.7	Min R <sup>b</sup>	OM-SO177	90	2.2
Min R <sup>b</sup>	OM-SO177	3	3.3	Min R <sup>b</sup>	OM-SO177	3	1.9

<sup>a</sup> 90-sec processing at 33.3°C or 3-min processing at 35°C.

<sup>b</sup> Not among top-scoring combinations, but included for comparison.



**TABLE 3: Film/Screen/Processing Combinations Scoring Highest on Contrast**

Ring Binders Anuli				Phantom Masses <sup>a</sup>			
Screen	Film	Processing <sup>b</sup>	Mean Score	Screen	Film	Processing <sup>b</sup>	Mean Score
Konica	Dupont	90	8.0	Min R	Fuji	90	3.3
Min R	Dupont	90	8.0	Konica	OM	3	3.0
New Agfa	Fuji	3	7.8	Fuji	OM-SO177	3	2.9
Min R	Fuji	3	7.8	Min R	OM-SO177	3	2.8
New Agfa	OM	3	7.8	Konica	OM	90	2.8
Fuji	OM-SO177	3	7.8	Min R (med)	OM-SO177	90	2.7 <sup>c</sup>
Konica	Dupont	3	7.7	Min R <sup>d</sup>	OM-SO177	90	2.6
Min R <sup>d</sup>	OM-SO177	90	7.5				
Min R <sup>d</sup>	OM-SO177	3	7.4				

<sup>a</sup> None of the combinations for this test showed significant differences.<sup>b</sup> 90-sec processing at 33.3°C or 3-min processing at 35°C.<sup>c</sup> 20 combinations scored 2.67, a further indication that this test lacked significance.<sup>d</sup> Not among top-scoring combinations, but included for comparison.**TABLE 4: Significantly Better Screen/Film Combinations for Contrast Discriminations**

Superior Screen/Film Combinations	Average No. of Anuli out of 8	Compared with Screen/Film	Average No. of Anuli
Konica/Dupont	7.89	Fuji/Dupont	6.44
New Agfa/OM	7.75		
Min R/Dupont	7.75		
Fuji (Kyokka)/OM-SO177	7.73		
Konica/Fuji	7.67		
Agfa/Fuji	7.67	New Agfa/Konica <sup>a</sup>	6.40
Min R/OM	7.58		
Min R/OM-SO177	7.50		
Konica/OM	7.50	Agfa/OM <sup>a</sup>	6.17
Konica/Konica	7.43		

<sup>a</sup> The screen/film combinations in the first column that appear on the same line or above the same line as this entry are significantly better for contrast discrimination than is this screen/film combination.

the processing method was included as a variable, film exposed in the Siemens cassette and processed for 90 sec had significantly lower scores than film processed for 3 min and exposed to either Fuji, Kodak Min R, or even old Agfa cassettes. Table 4 lists the screen/film combinations with the highest average scores. The fourth column lists screen/film combinations that are statistically significantly poorer for contrast discrimination than the combinations listed in the first column. This table shows that if Dupont film is used, it should be used with the Konica rather than Fuji screens to obtain good contrast. However, the Fuji screen combined with OM-SO177 film is superior to the old Agfa screen operating with the new OM film or the new Agfa screen operating with Konica film.

The Hurter and Driffield (H and D) curves for four of the five films are shown in Figure 2. The sensitometer strips (exposed to calibrated green light) were developed in the 3-min processor; the new OM film was not included, because it is less affected by extended processing. When H and D curves were drawn for both processing methods, the effects of 3-min processing was greatest for Kodak OM-SO177 film (Fig. 3A) and least for Dupont Microvision film (Fig. 3B). Dupont Microvision film has been redesigned since these tests, but is still less sensitive to extended processing.

For the clinical study of 22 patients performed at the

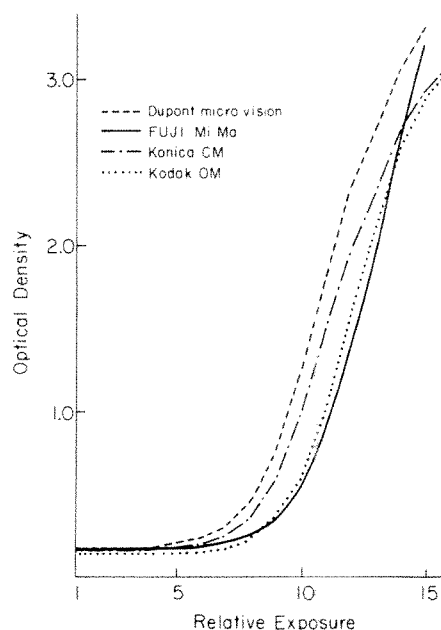


Fig. 2.—Hurter and Driffield curve, obtained from a sensitometer emitting green light, comparing four of five films tested in this study when developed for 3 min at 35°C. Kodak OM is OM-SO177 film.

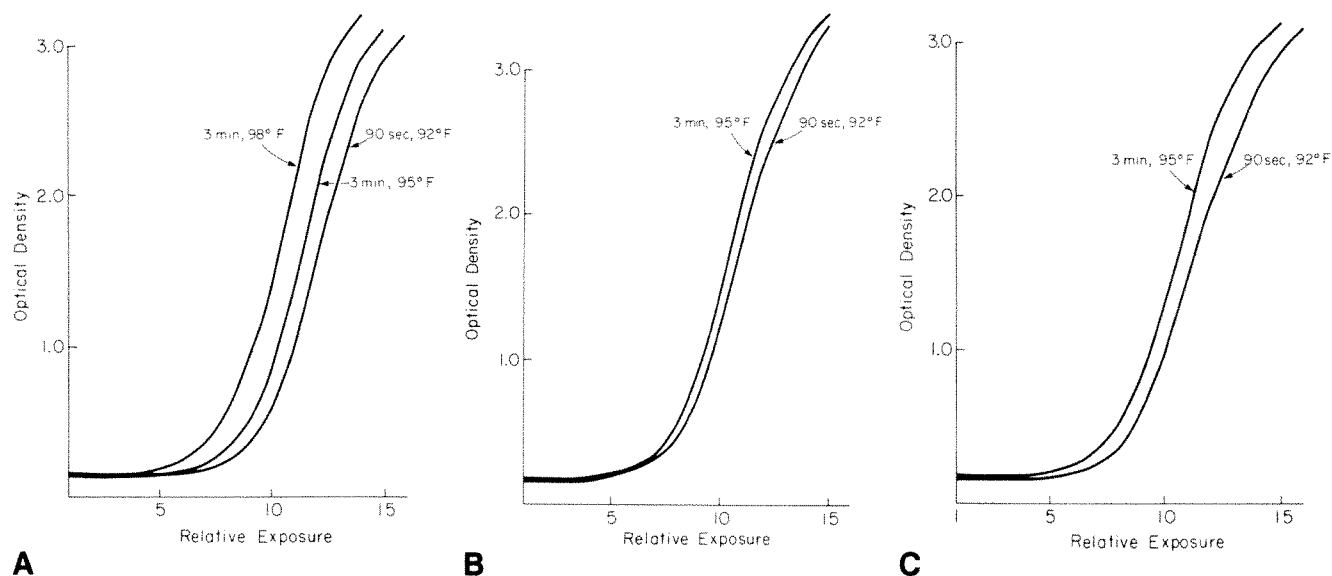


Fig. 3.—Effects of processing parameters on Kodak OM-SO177 (A), Dupont Microvision (B), and Konica CM (C) as shown by Hurter and Driffield curves exposed to calibrated step wedges of green light.

conclusion of the test object study, Kyoka (Fuji) screens were combined with OM-SO177 film and processed for 3 min. All right breasts were imaged with this combination at 20% more radiation and compared with images of the left breast that had been made with Min R Medium screens, OM-SO177 film and 3-min processing. Three radiologists graded the films as either "the same," "slightly better," "better," or "significantly better." Five of the 22 cases had OD differences sufficiently large to exclude them from the comparison. Of the remaining 17 cases (with two views each), the two more experienced radiologists did not see much difference between the two screens, while the less experienced radiologist found the Fuji screen "slightly better" in 14 comparisons and the Min R Medium screen "slightly better" in nine comparisons. All the cases studied were screening mammograms, and none had microcalcifications or masses.

## Discussion

The ANOVA results show that screens alone are of primary importance for good resolution. This is the result of good test scores for all the films imaged with a particular screen, no matter what film is combined with it. Screens that are superior at representing resolution targets are not always superior, when combined with specific films, for good contrast discrimination. When screens and processing are combined and tested for significance with respect to contrast, three of the four best combinations were processed for 3 min. This corresponds with the anuli test results in Table 3, in which five of the seven entries include 3-min processing. Processing also was important for the crushed-clam-shell test, because both top scorers, the Fuji and new Agfa screens, were best when combined with 3-min processing. This also corresponds to the Table 2 entries and may indicate that calcification

sharpness is also a function of contrast, because extended processing increases contrast [2].

In order to state that the results of these tests are valid for all radiologists whose training in mammography is similar to the three radiologists in this study, the combined variance between radiologists and between the same radiologist re-reading the same film was calculated as the "noise variance" of these experiments. Thus, if the mean of the test results for all the films made from one type of film, or screen, or development method, or combinations of these, subtracted from the mean for a different film, screen, etc. was not much greater than the combined noise variance, then the test result was not statistically significant. If differences between radiologists had been one of the tests evaluated by these experiments, instead of being considered a random effect, noise variance would have been reduced and more differences between individual screens would have been found to be significant. But then, results could not be applied to all radiologists, but only the specific ones in this study. However, because of the low noise variance of the radiologists when their differences are taken as a random effect, the results reported in this paper can be applied to all radiologists with training similar to that of the three radiologists in this study.

Mean glandular doses listed for the various combinations (Table 1, column 6), would double if grids supplied by GE-CGR or Philips were used. Breasts with more glandular tissue would require from 30% to 50% higher exposures. Thus, the new combinations will produce doses from 74 to 208 mrad (0.74–2.08 mGy) in a clinical environment where grids are usually needed. Many radiologists prefer to read dark films, ranging from 1.3 to 1.6 OD. This practice also will increase the exposure required clinically. Another difficulty when converting Table 1 doses to clinical doses is the difference in reciprocity failure between the films. These films require from

20% to 35% more exposure when exposure time increases from 0.6 sec to 2.4 sec (C. Kimme-Smith, L. W. Bassett, R. H. Gold, unpublished data). If a facility has an underpowered mammography unit and cannot image a patient in less than a second, differences in reciprocity failure will change the radiation doses required clinically from those in Table 1. The GE 500-T unit that was used in the experiments was able to expose these films in less than 0.63 sec, so reciprocity failure was minimized. Any unit that cannot deliver 100 mA in a second (assuming 8 mR/mAs, 0.08 mGy/mAs) may not conform to the radiation dose estimates of Table 1.

The inconclusive results of the clinical test of one of the screens judged superior in the test-object studies illustrates the difficulties inherent in selecting a new screen on the basis of clinical comparisons alone. The small differences between many of these new screen/film combinations implies that radiologists now have a large selection of almost equivalent combinations to select from. Among the superior screens and screen/film combinations, certain combinations of screen/film/processor development time can reduce doses to 40% of those expected from a Kodak Min R/OM-SO177 combination developed for 22 sec. When these combinations are examined for resolution and contrast capabilities, several of them are superior to the standard Min R/OM-SO177 combination processed conventionally. Specifically, Kyokka screens (distributed by Fuji) are superior for resolution discrimination when combined with any of the films in this study. When combined with OM-SO177, they are also among the better screens for contrast discrimination. The Konica screen combined with four of the five films also was superior to Kodak Min R/OM-SO177 for contrast discrimination. Three-minute processing improved the perception of sharpness in microcalcifications

as well as contrast discrimination. The most widely used new screen, Kodak's Min R Medium, was not among the significantly superior screens for either contrast or resolution discrimination. Radiologists specializing in mammography now have a wide choice of screen/film/processing options available and can reduce radiation dose to their patients by a variety of methods without decreasing image quality.

## REFERENCES

1. Law J, Kirkpatrick A. Film processing for mammography. *Br J Radiol* **1988**;61:939-942
2. Kimme-Smith C, Rothschild PA, Bassett LW, Gold RH, Moier C. Mammography film processor temperature, development time and chemistry: effect on dose, contrast, and noise. *AJR* **1989**;152:35-40
3. Hall DA, McCarthy KA, White G, et al. Comparison of two screen-film combinations in contact and magnification mammography: detectability of microcalcifications. *Radiology* **1988**;168:657-659
4. Kimme-Smith C, Bassett LW, Gold RH, Roe D, Orr J. Mammographic dual screen-dual emulsion film combinations: visibility of simulated microcalcifications and effect on image contrast. *Radiology* **1987**;165:313-318
5. Kirkpatrick AE, Law J. A comparative study of films and screens for mammography. *Br J Radiol* **1987**;60:73-78
6. Law J, Kirkpatrick AE. Films, screens, and cassettes for mammography. *Br J Radiol* **1989**;62:163-167
7. White DR, Tucker AK. A test object for assessing image quality in mammography. *Br J Radiol* **1980**;53:331-335
8. Nishikawa RM, Yaffe MJ. Signal-to-noise properties of mammographic film-screen systems. *Med Phys* **1985**;12:32-39
9. Arnold BA, Webster EW, Kalisher L. Evaluation of mammographic screen-film systems. *Radiology* **1978**;129:179-185
10. Rosenstein M, Anderson LW, Warner GG. *Handbook of glandular tissue doses in mammography*. Washington DC: Health & Human Services Publication FDA 85-8239, **1985**
11. Miller RG. *Simultaneous statistical inference*. New York: Springer Verlag, **1981**:37-47

We regret to announce that Glen W. Hartman, secretary of the ARRS, died February 18, 1990, in Rochester, MN. A memorial service was held on February 22 at the Gloria Day Lutheran Church in Rochester. Memorial contributions can be made to the Radiology Centennial, Inc., % ARRS, 1891 Preston White Dr., Reston, VA 22091. Dr. Hartman will be missed deeply by members of the society, his family, and friends.

# Doppler Sonography: A Noninvasive Method for Evaluation of Hepatic Venocclusive Disease

Bruce P. Brown<sup>1</sup>  
 Monzer Abu-Yousef<sup>1</sup>  
 Robert Farner<sup>1</sup>  
 Douglas LaBrecque<sup>2</sup>  
 Roger Gingrich<sup>2</sup>

Hepatic venocclusive disease is a serious complication associated with chemotherapy and radiation used in bone marrow transplantation patients. In the past, liver biopsy has been the only reliable means of diagnosing venocclusive disease. Biopsy in such patients may be dangerous or impossible because of severe coagulopathies. The purpose of our study was to evaluate duplex Doppler sonography in diagnosing hepatic venocclusive disease. We measured the blood velocity and flow in the portal vein, hepatic vein, and inferior vena cava of six patients who were histologically proved to have developed hepatic venocclusive disease after bone marrow transplantation. There were three men and three women with a mean age of 32 years (range, 21–44 years). Examination with Doppler sonography suggested the diagnosis a mean of 41 days (range, 11–62 days) after transplantation. In three patients, the diagnosis was suggested by reversed or “to and fro” flow in the portal vein. In the other three patients, the diagnosis was suggested by a decreased flow in the portal vein. One of these patients with decreased flow had subclinical hepatic venocclusive disease. In this patient, it was not the absolute level of flow but the decrease from a baseline established before ablative therapy that suggested the diagnosis. The amplitude of pulsatility in the hepatic veins appeared to decrease with the onset of venocclusive disease. In the hepatic veins and inferior vena cava, flow toward the heart was maintained.

Our findings suggest that duplex Doppler sonography may be useful in detection of hepatic venocclusive disease. We speculate that, with wider experience, Doppler sonographic detection of decreased or reversed flow in the portal vein, in the proper clinical setting, may provide a noninvasive means of reliably diagnosing hepatic venocclusive disease in patients too ill to undergo liver biopsy.

*AJR* 154:721–724, April 1990

Venocclusive disease of the liver is a progressive, concentric, nonthrombotic occlusion of small intrahepatic veins, which is produced by inflammation of the endothelium. In the United States, it is most commonly associated with the use of chemotherapeutic agents and radiation therapy used before bone marrow transplantation [1–4].

Although liver biopsy is usually diagnostic of venocclusive disease, biopsy cannot be performed because of coagulopathy in a significant number of patients. To date, no noninvasive liver tests that can accurately diagnose this disorder have been developed. Recently, Doppler sonography showed reversal of blood flow in the portal vein of a patient with hepatic venocclusive disease [5].

We used duplex Doppler sonography to examine hepatic blood flow in six patients who were documented histologically to have hepatic venocclusive disease after undergoing bone marrow transplantation. In addition, we correlated the sonographic results with concurrent clinical, laboratory, and pathologic findings.

Received March 20, 1989; accepted after revision November 20, 1989

Presented in part at the annual meeting of the American Roentgen Ray Society, New Orleans, LA, May 1989.

<sup>1</sup> Department of Radiology, University of Iowa College of Medicine, Iowa City, IA 52242. Address reprint requests to B. P. Brown.

<sup>2</sup> Department of Internal Medicine, University of Iowa College of Medicine, Iowa City, IA 52242.

0361-803X/90/1544-0721

© American Roentgen Ray Society

## Subjects and Methods

From March of 1987 through July 1988, we examined the blood-velocity profile in the hepatic vessels of 31 patients who received chemotherapy and radiation before undergoing bone marrow transplantation. One patient (Table 1, patient 5) was followed up with a fixed protocol of Doppler examinations before and after radiation and chemotherapy without reference to her clinical status. The remaining patients were referred for Doppler sonography after clinical and biochemical abnormalities suggested liver disease.

The study group (Table 1) included three men and three women with a mean age of 32 years (range, 21–44 years). All transplants were allogeneic and HLA matched. Two were from unrelated and four were from related donors. All patients underwent ablative chemotherapy before transplantation. Six patients underwent total body radiation therapy before transplantation. All patients received antilymphocyte globulin as prophylaxis against development of graft-versus-host disease. Two patients had histories of significant drinking, but none had known clinical liver disease. Before ablation therapy and transplantation, no patient had significant symptoms or signs referable to the abdomen or liver. Three patients had minor elevations in aspartate aminotransferase level before transplantation, but no other abnormalities were seen in the biochemical tests of liver function.

Venocclusive disease was confirmed by transjugular liver biopsy in one patient, open liver biopsy in three patients, and autopsy in two patients. Histologic confirmation was made within 1–3 days of the clinical diagnosis in five patients and at 32 days in the remaining patient.

Examinations were interpreted without knowledge of biochemical tests or the clinical status of the patients. Clinical and biochemical data were gathered from the patients' charts after all the Doppler examinations had been performed. Doppler measurement of maximum blood velocity and vessel diameter were made in the same cross section of the portal vein. The volume of flow through the portal vein was calculated according to the method of Moriyasu et al. [6]. Care was taken to select Doppler measurements with small angles of interrogation to minimize sampling error in measurement of Doppler

shift. We excluded Doppler measurements that were obtained while patients were taking drugs to support blood pressure and when arterial blood pressure determined on admission had changed significantly from the baseline level. Patients with signs of right ventricular failure were not included in the study. Because of the difficulties in standardizing the quantitative measurement of velocity, diameter, and flow in the hepatic veins and inferior vena cava, only qualitative judgments of direction and configuration of velocity profile were attempted in these vessels.

All Doppler examinations were done with an Acuson 128 scanner with a 3-MHz linear array transducer. Patients were examined in the supine or left posterior oblique position after at least 6 hr fasting.

## Results

Doppler findings suggested hepatic venocclusive disease a mean of 41 days after transplantation (range, 11–62 days). Three patients had obvious abnormalities of flow in the portal vein on Doppler studies: two had reversed flow (Fig. 1A) and one had to-and-fro flow.

In the other three patients, the diagnosis of hepatic venocclusive disease was suggested by the presence of less dramatic decreases of flow in their portal veins on Doppler studies. In two of these patients, the portal vein velocities and/or flows were below the normal values established for our laboratory. The other patient was followed up with serial Doppler examinations before and after bone marrow ablation and transplantation. In this patient, it was not the absolute value of velocity in the portal vein but the decline from baseline that suggested the diagnosis. This patient was asymptomatic but had abnormal liver biochemical tests that were thought to be due to graft-versus-host disease. However, because her posttransplantation Doppler studies showed a trend toward decreased velocity and flow in the portal vein compared

TABLE 1: Patient and Doppler Data

Patient No.	Age (yr)	Sex	Diagnosis	Days from Transplantation <sup>a</sup>	Portal Vein		
					Diameter (cm)	Velocity <sup>b</sup> (cm/sec)	Flow <sup>b</sup> (ml/min)
1	35	M	Acute nonlymphocytic leukemia	62 <sup>c</sup>	1.2	-11	-746
2	21	M	Acute lymphocytic leukemia	60 <sup>c</sup>	0.8	8	241
				69	0.7	-26	-600
				77	0.8	-18	-543
				40 <sup>c</sup>	0.7	8	185
3	24	M	Acute lymphocytic leukemia	53 <sup>c</sup>	1.0	-11	-518
4	36	F	Granulocytic sarcoma	61	1.2	-21	-1425
				84	0.9	14	534
				-9	0.7	30	693
				7	0.8	28	844
5	44	F	Acute nonlymphocytic leukemia	14	1.0	16	754
				22 <sup>c</sup>	1.0	12	565
				28	1.0	15	707
				41	0.9	18	687
				74	0.7	26	600
				11 <sup>c</sup>	1.1	19/-13	1083/-741
				36	1.4	16	1478
6	30	F	Chronic myelogenous leukemia				

<sup>a</sup> Negative numbers signify the number of days before transplantation; positive numbers signify the number of days after transplantation.

<sup>b</sup> Negative numbers indicate hepatofugal velocity or flow.

<sup>c</sup> The day after transplantation when sonographic examination suggested the diagnosis of venocclusive disease.



with baseline studies, the possibility of hepatic venocclusive disease was raised. This diagnosis was subsequently confirmed by open liver biopsy 3 days later.

The macroscopic hepatic veins were examined with Doppler sonography in five patients at the time of diagnosis (Fig. 1B). All were patent, with flow toward the heart. In one patient, the hepatic veins were judged to be reduced in diameter. In three patients, the flow velocity pattern was triphasic. In two, this pattern was biphasic, and in one it was monophasic. Except for a decrease in the amplitude of phases, no significant change was noted in the flow-velocity pattern with the onset of hepatic venocclusive disease.

The inferior vena cava was patent with flow toward the heart in all patients in whom hepatic venocclusive disease developed (Fig. 1C). One patient had narrowing of the intrahepatic portions of the inferior vena cava by extrinsic compression from a swollen liver. In one patient, the vena cava was judged to be dilated, but there was no identifiable outflow obstruction and no sign of right ventricular failure.

In general, when the sonogram first suggested the diagnosis, patients with the most obvious reductions of flow in the portal vein had the most severe abdominal pain, the worst liver tenderness, and the most severely deranged liver biochemical studies.

In the four patients with abdominal pain (Table 1, patients 1–4), the aspartate aminotransferase and total bilirubin levels had risen a mean of 35 and 16 times their respective baseline values established before transplantation. In the two patients (5 and 6) without abdominal pain, the aspartate aminotransferase level had fallen 0.32 times baseline in one and had risen 0.12 times baseline in the other. The total bilirubin level in these two patients had risen a mean of eight times from baseline values.

In all specimens of liver tissue, the central veins were narrowed or occluded by subintimal fibrin deposition and intimal proliferation. In addition, centrilobular sinusoidal congestion occurred with various degrees of hepatocyte necrosis and hemorrhage.

Five of the six patients died. Death occurred a mean of 70 days after transplantation (range, 43–96 days) and a mean of 8 days (range, 1–19 days) after the diagnosis of hepatic venocclusive disease was suggested by using sonography. All died of overwhelming infection. The one living patient remains without abdominal complaints 173 days after transplantation and 151 days after the diagnosis of hepatic venocclusive disease was suggested with Doppler sonography and later confirmed with liver biopsy. Her follow-up Doppler sonograms have shown slight improvement, with increasing portal flow velocity. Her alkaline phosphatase and aspartate aminotransferase levels have continued to be elevated. We suspect she has residual subclinical liver disease.

## Discussion

Our studies suggest that noninvasive measurements of velocity and flow in the portal vein can confirm the clinical suspicion of hepatic venocclusive disease. In addition, Doppler imaging may be useful in detecting early or subclinical venocclusive disease if patients are examined serially after establishing baseline flows before chemotherapy and transplantation.

Our correlations of sonographic, clinical, and biochemical data showed a spectrum of findings. At one end were patients with significant abdominal pain, liver tenderness, and rapidly worsening liver function. These patients were thought, after clinical evaluation, to have some type of acute liver disease. In this group, Doppler studies showing diminished or reversed portal flow allowed us to narrow the differential diagnosis and help confirm the clinical suspicion of venocclusive disease of the liver. At the other end of the spectrum were those patients with only slight abnormalities in liver function and few clinical signs or symptoms. In these patients, the finding of decreased portal blood flow on Doppler studies suggested the diagnosis of hepatic venocclusive disease, which had not been suspected.

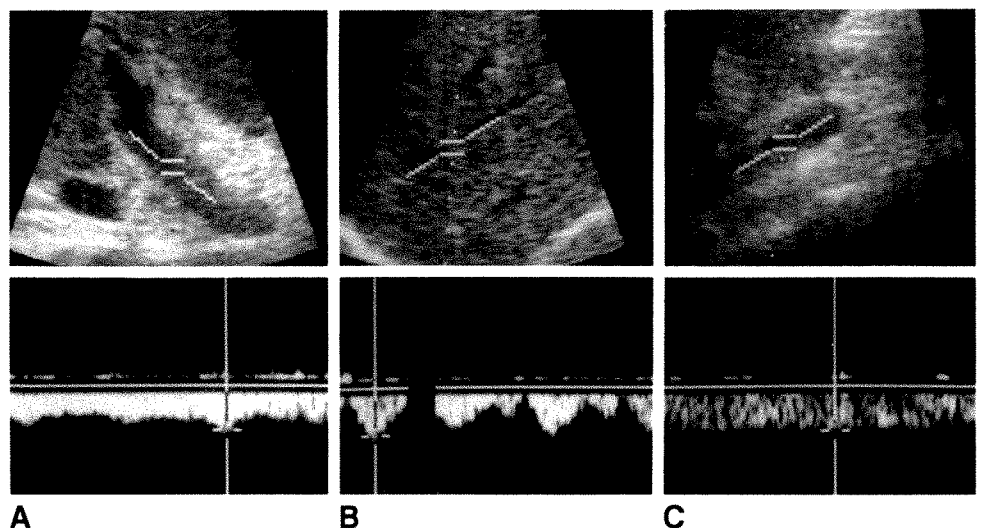


Fig. 1.—Velocity profile of portal vein (A), hepatic veins (B), and inferior vena cava (C) 61 days after transplantation. Note that flow in portal vein is hepatofugal. In hepatic vein and inferior vena cava, flow continues toward heart.

Quantitative measurement of portal vein flow has many pitfalls [7, 8]. It has generally been accepted that normal values in portal blood flow show a wide range from patient to patient. However, when the same patient is studied serially, Doppler studies have been shown to be reproducible [6, 9]. In preliminary studies, we measured flow in the portal vein with Doppler methods in 17 normal fasting patients. From patient to patient, we saw a wide range of variation in volume of blood flow in the normal portal vein ( $971 \pm 572$  ml/min, mean  $\pm$  S.D.) with a coefficient of variation of  $\pm 59\%$ . However, in these same patients, the coefficient of variation was only  $\pm 12\%$  when we measured three serial flows in the same patient in one 10-min session. Likewise, measurement of blood velocities in the portal vein varied somewhat between patients ( $21.8 \pm 4.3$  cm/sec, mean  $\pm$  S.D.) with a coefficient of variation of  $\pm 20\%$ . However, serial measurements in the same patient showed a coefficient of variation of only 9%.

On one hand, these findings suggest that it may be difficult to make quantitative comparisons of flow in one patient vs that in another. On the other hand, they suggest that serial Doppler flow and velocity measurements in the same patient should be reliable in detecting changes from an established baseline. The usefulness of serial examinations after bone marrow transplantation is shown by the suggestion of subclinical venoocclusive disease in a patient who was followed up with Doppler studies after establishing baseline values before ablative therapy.

Our data suggest that Doppler evaluation of liver blood flow is useful in detecting hepatic venoocclusive disease and may prove valuable in confirming the diagnosis of venoocclusive disease in patients where clinical suspicion is high. Serial Doppler studies may allow detection of the less dramatic changes in portal flow in early or subclinical disease, where there is little suspicion of hepatic venoocclusive disease. With

wider experience, we speculate that hepatic Doppler imaging may provide a reliable, noninvasive means of diagnosing hepatic venoocclusive disease in patients too ill to undergo liver biopsy. Further prospective studies of Doppler evaluation of blood flow in the portal vein will be required to confirm these preliminary data.

#### ACKNOWLEDGMENTS

We acknowledge the expert technical assistance of Carol Chenoweth and Mysti Grant.

#### REFERENCES

1. Schulman HM, McDonald GB, Matthews DE, et al. An analysis of hepatic venoocclusive disease and centrilobular hepatic degeneration following bone marrow transplantation. *Gastroenterology* **1980**;79:1178-1191
2. McDonald GB, Sharma P, Matthews DE, Schulman HM, Thomas ED. Venoocclusive disease of the liver after bone marrow transplantation: diagnosis, incidence and predisposing factors. *Hepatology* **1984**;4:116-122
3. Dulley FL, Kanfer EJ, Applebaum FR, et al. Venoocclusive disease of the liver after chemoradiotherapy and autologous bone marrow transplantation. *Transplantation* **1987**;43:870-873
4. Rollins BJ. Hepatic venoocclusive disease. *Am J Med* **1986**;81:297-306
5. Kriegshauser SJ, Charboneau JW, Letendre L. Hepatic venoocclusive disease after bone marrow transplantation: diagnosis with duplex sonography. *Am J Radiol* **1988**;150:289-290
6. Moriyasu F, Nishida D, Ban N, Nakamura T, et al. Measurement of portal vascular resistance in patients with portal hypertension. *Gastroenterology* **1986**;90:710-717
7. Gilli RW. Pulsed Doppler with B-mode imaging for quantitative blood flow measurement. *Ultrasound Med Biol* **1979**;5:223-235
8. Burns PN, Taylor KJW, Blei AT. Doppler flowmetry and portal hypertension. *Gastroenterology* **1987**;92:824-826
9. Ohnishi K, Masyuki S, Koen H, Nakayama T, Nomura F, Okuda K. Pulsed Doppler flow as a criterion of portal venous velocity: comparison with cineangiographic measurements. *Radiology* **1985**;154:495-498

# Fluoroscopically Guided Percutaneous Gastrostomy and Gastroenterostomy: Analysis of 158 Consecutive Cases

Marshall E. Hicks<sup>1</sup>  
R. Stephen Surratt<sup>1</sup>  
Daniel Picus<sup>1</sup>  
M. Victoria Marx<sup>1,2</sup>  
Elvira V. Lang<sup>1,3</sup>

We reviewed our experience with 158 consecutive patients who underwent either percutaneous gastrostomy or percutaneous gastroenterostomy during a 2-year period. The catheters used included Foley catheters (36), Cope-type gastric catheters (86), or Carey-Alzate-Coons gastrojejunostomy catheters (36). Gastrojejunostomy tubes were placed in patients with gastroesophageal reflux or aspiration, gastric atony, or partial gastric obstruction. Ninety percent of the tubes were placed for feeding purposes. The technical success rate was 100%. Thirty-day follow-up was obtained in 89%. Thirty-day mortality was 26%, reflecting the substantial number of debilitated patients. No deaths were directly related to tube placement. Major morbidity was 6% and included hemorrhage, peritonitis, tube migration, and sepsis. Minor morbidity was 12%. There was no difference in 30-day mortality or feeding tolerance between the tube types ( $p < .05$ ). Patients with Foley catheters had more complications necessitating surgical intervention and an increased incidence of tube changes required within 30 days. These were the only statistically significant differences between the tubes ( $p < .05$ ).

Our results show that percutaneous gastrostomy is a safe and effective means of gastroenteric feeding or decompression. Because of the fewer complications and ease of insertion, the Cope type of gastrostomy tube has become our preferred catheter for percutaneous feeding or decompression.

*AJR* 154:725-728, April 1990

For over 100 years, surgical gastrostomy and gastrojejunostomy were the standard methods of direct enteral access. This began to change, however, with the development of percutaneous endoscopic gastrostomy in 1979 [1-3]. Despite the lower morbidity and mortality with endoscopic placement, the search for a simpler, safer means of gastroenteric access has continued, resulting in the recent development of fluoroscopically guided percutaneous gastrostomy.

Early series of fluoroscopically guided percutaneous gastrostomies contained small numbers of patients, but favorable morbidity and mortality rates were reported when comparisons were made with endoscopic placement [4-7]. Recently, larger series have begun to emerge, substantiating the results of the initial reports [8-12]. We report our experience with percutaneous gastrostomy and gastroenterostomy in 158 consecutive patients, comparing three different types of tubes used during a 2-year period.

## Materials and Methods

We reviewed the medical records of the first 161 consecutive patients referred for percutaneous gastrostomy or gastrojejunostomy. One hundred fifty-eight procedures were performed. The procedure was not attempted in three cases (two patients with overlying colon and one with massive gastroesophageal reflux in whom we were unable to maintain adequate inflation of the stomach for safe percutaneous puncture). The study group of 158 patients included 95 women (60%) and 63 men (40%). The mean age was 67 years; the

Received July 24, 1989; accepted after revision November 20, 1989.

Presented at the annual meeting of the American Roentgen Ray Society, New Orleans, May 1989.

<sup>1</sup> Mallinckrodt Institute of Radiology, Washington University School of Medicine, 510 S. Kingshighway Blvd., St. Louis, MO 63110. Address reprint requests to M. E. Hicks.

<sup>2</sup> Present address: Department of Radiology, University of Michigan, 1500 E. Medical Center Dr., Ann Arbor, MI 48109-0030.

<sup>3</sup> Present address: Department of Radiology, Stanford University School of Medicine, Stanford, CA 94305-5105.

0361-803X/90/1544-0725  
© American Roentgen Ray Society

median age was 71 years. Four patients (2.5%) had ascites. Three patients (1.9%) had histories of prior gastric surgery; this included two patients who had gastrojejunostomies for palliative treatment of pancreatic carcinoma and one patient who had a Billroth I operation for peptic ulcer disease. T fasteners (Meditech, Watertown, MA) were used in seven patients (4.4%), including one patient on peritoneal dialysis, one uncooperative patient, and one patient with ascites [13]. At the time of tube placement, 72 patients (46%) or their families had requested that no resuscitative measures be undertaken in the event of cardiopulmonary arrest.

Of the 90% of tubes placed for feeding purposes, the majority were for patients with neurologically impaired swallowing mechanisms (104 patients). Other feeding indications included patients with tumors of the ears, nose, or throat (10 patients), esophageal obstruction (nine patients), and miscellaneous indications (19 patients). Only 10% of the tubes were for decompression of the stomach or small bowel in patients with bowel obstruction.

In the first 36 patients who underwent gastrostomy, 16- or 18-French Foley catheters were placed (Bard, Covington, GA). In the remaining 86 patients undergoing gastrostomy, 12- or 14-French Cope-type catheters were placed (Cook, Bloomington, IN). Gastrojejunostomy catheters were placed in 36 patients. All 36 had the Carey-Alzate-Coons gastrojejunostomy catheter (Cook). Candidates for these gastroenteric feeding tubes included patients with documented aspiration, gastric atony, or partial gastric obstruction.

Local anesthetic was used in all cases. IV sedation with midazolam and morphine sulfate was used routinely. No patient received general anesthesia. Procedures were performed under fluoroscopic guidance, with the exception of one case in which CT was used because the patient had extensive bowel gas in the vicinity of the stomach. No additional imaging techniques were used to identify liver or colon. Antibiotics were not given routinely. Glucagon (1 mg, Lilly, Indianapolis, IN) was given IV to inhibit gastric motility.

All catheters were placed by using the Seldinger technique with air insufflation of the stomach via an indwelling nasogastric tube. After puncture with an 18-gauge Teflon-sheathed needle (Cook), an 0.038-in. (1-mm) Amplatz extra-stiff guidewire (Cook) was passed into the stomach. We used a method for puncture described and refined by Wills and Oglesby [14]. Cope catheters were placed after serial dilatation of the tract. Foley catheters and gastrojejunostomy catheters were placed through a peel-away sheath of the appropriate size. When T fasteners were used, they were placed before catheter insertion. Catheters were secured to the skin with 0-prolene (Ethicon, Inc., Somerville, NJ).

Tube feedings were initiated on the day after placement for gastrostomy tubes, unless a complication precluding feeding developed. Gastrojejunostomy patients routinely began receiving feedings on the same day as tube placement. The nasogastric tube usually was removed the day after the procedure.

The chi square and Van der Waerden one-way tests were used to compare the tube types for differences in patient age, sex, code status, morbidity, mortality, feeding tolerance, and required tube changes and to identify risk factors with respect to increased morbidity and mortality ( $p < .05$ ).

## Results

The technical success rate was 100% in all 158 cases in which the procedure was attempted. More than one puncture was required in 10 cases (6%). This was usually because the stomach deflated during placement of the catheter. In all instances the additional puncture was successful.

Thirty-day follow-up was obtained in 141 patients (89%). The 30-day mortality rate calculated from these 141 patients was 26%. Twenty-seven of the 36 patients who were dead at 30 days died of unrelated causes. Although there were no cases where tube placement was definitely related to the death of a patient, there were three cases (2%) in which a complication occurred from tube placement that negatively altered the clinical course of the patient and may have contributed to the patient's death. In an additional six patients (4%), no obvious precipitating cause of death was recorded in the physician's record note section of the chart; however, in all, multiorgan failure was believed to be the cause of death. All six of these patients were assigned the status of "no code." Three of these patients died less than 48 hr after uncomplicated placement of a gastrostomy tube. The other three also had uncomplicated procedures and were tolerating tube feedings before they died.

Morbidity was divided into major and minor. Major morbidity was defined as a complication that (1) required an additional interventional procedure, (2) prolonged the hospital stay, (3) required a transfusion, or (4) required IV antibiotics.

Major morbidity consisted of five cases of hemorrhage (3%), two cases of peritonitis (1%), two cases of tube migration (1%), and one case of sepsis (1%). Three of the five patients with hemorrhage recovered uneventfully. One of these patients was on steroids for lupus cerebritis at the time of tube placement and experienced gastrointestinal bleeding after the procedure. Diffuse gastritis was found with endoscopy after tube placement. The patient was transfused with 3 units of packed RBCs and the bleeding resolved. The gastritis healed with tapering the administration of the steroids. In another patient, there was a small amount of bleeding with the initial puncture at the time of catheter placement. This was probably from perforation of a vein in the posterior wall of the stomach. The hemoglobin dropped 2 g/dl over a 2-day period, and the nasogastric tube aspirate was positive for occult blood, indicating a small amount of persistent hemorrhage. This patient was transfused with 2 units of packed RBCs and the bleeding ceased. In a third patient, another slow gastrointestinal hemorrhage was manifested by a melanotic stool and a decrease in hematocrit from 39% to 27% over a 3-day period. No difficulties were noted in tube placement. This patient experienced no further bleeding after transfusion with 2 units of packed RBCs.

The remaining two patients with bleeding complications were classified as having possible tube-related deaths, although both had ongoing multisystem failure. One of these two patients was on Coumadin for atrial fibrillation with a prothrombin time greater than 40 sec at the time of gastrojejunostomy tube placement. Gastrointestinal hemorrhage ensued after catheter placement. Although the bleeding subsided within 12 hr after the procedure with correction of the prothrombin time by transfusion of 10 units of fresh frozen plasma and 6 units of packed RBCs, the patient died 5 days after tube placement. She had chronic renal failure and congestive heart failure; the acute cause of death was respiratory failure. The other patient had an occult hemorrhage; the hematocrit dropped from 34% to 20% in the 2 weeks

after tube placement. The patient had a prolonged ileus, which may have been caused by the occult hemorrhage or ongoing urosepsis. The family requested that no supportive measures be given and the patient died 16 days after catheter placement.

One of the two patients included in the peritonitis complication group was a patient in acute renal failure with altered mental status. This made clinical evaluation of this complication difficult, although peritonitis was suspected. This was the only case in which an additional puncture at the time of placement was associated with morbidity. The patient's family requested that no further supportive therapy be given and the patient died 6 days after tube placement. The other case of peritonitis was proved and occurred after deflation of the balloon on the Foley gastrostomy catheter 1 day after tube placement. This patient required a Stamm gastrostomy and lavage and recovered uneventfully.

Of the two cases of tube migration, one also had a Foley catheter that eroded into the lesser sac 12 days after tube placement. A resultant abscess required surgical evacuation with a jejunostomy tube placement. The other tube migration complication was caused by a Cope catheter that was partially outside the stomach. An additional percutaneous gastrostomy tube was placed and the patient recovered uneventfully. The final major morbidity complication was in a patient with *Proteus* sepsis from a wound infection. This patient recovered with IV antibiotics.

Minor morbidity included skin infection (seven patients), transient increase in fever or WBCs (seven patients), transient ascitic leak (two patients), minor skin bleeding (two patients), and catheter migration (one patient). All minor complications were either self-limiting or required minimal wound care.

Of the patients in whom tubes were placed for feeding indications, 88% tolerated the feeding without difficulty. Aspiration or significant reflux was seen in only 5% of patients. Diarrhea resulting in termination of feedings or morbidity was observed in only 3% of patients. Other feeding difficulties included prolonged ileus and large gastric residuals (4%).

Tube changes within 30 days involved 15% of the tubes. When exchange for a like tube was necessitated, the reason was either a defective hub on the tube, a deflated balloon (on Foley catheters), or a tube clogged because of improper flushing or feeding. This occurred with five Foley catheters, three Cope catheters, and four gastrojejunostomy catheters. Five successful and two unsuccessful conversions of gastrostomy catheters to gastrojejunostomy catheters were performed. Two gastrojejunostomy catheters were converted to gastrostomy tubes, both in patients who became less at risk for aspiration because of improvement in clinical status. Both patients tolerated gastrostomy feedings.

No statistically significant difference was demonstrable between the three tube types with regard to patient age, sex, code status, major or minor morbidity, 30-day mortality, or feeding tolerance. There were two statistically significant differences between the tube types. Foley catheters were used in the two cases in which complications resulted in surgery, and a higher rate of tube changes was required for the Foley catheters in the 30-day follow-up period.

Patients who were classified as no code at the time of tube placement were at risk for death within the 30-day follow-up period ( $p < .05$ ); however, the no-code status did not entail a higher incidence of morbidity. Other risk factors found not to be statistically significant for an increase in morbidity or mortality included sex, age, difficulty with placement, or anatomic considerations such as ascites or prior gastric surgery.

## Discussion

The reported procedure-related mortality for surgical gastrostomy ranges from 1.8% to 6.0% [15, 16]. Mortality related to percutaneous endoscopic gastrostomy placement generally is reported as less than 2% [17, 18]. Procedure-related morbidity ranges from 13% to 23% with surgically placed tubes and from 10% to 20% with endoscopic placement [3, 15, 19]. The largest published fluoroscopically guided percutaneous gastrostomy series reported a procedure-related mortality of 0.8% and overall morbidity of 6.0% [12].

In an attempt to define our population of patients more clearly, the patients were classified by code status. The large number of no-code patients reflects the significant number of debilitated and terminally ill patients included in our study group. To our knowledge, no other study has used this gross indicator of health to discern differences in outcome from the procedure.

Even though the patients were not randomized, our study provides data to compare three different types of tubes. The only statistically significant differences between the tube types were an increased incidence of morbidity requiring surgery in the Foley catheter group and more frequent tube changes required in the Foley catheter group in the 30-day follow-up period. Although Foley catheters were the initial type of gastrostomy tube placed fluoroscopically at this institution, the two complications requiring surgery in the Foley catheter group (deflation of the balloon with peritonitis and erosion of the tube through the posterior stomach) appear more related to the nature of the tube than to inexperience with placement. For these reasons, we have abandoned the Foley catheter for use as a gastrostomy tube.

At least three of the major morbidity complications in our series were probably preventable. The association of corticosteroid use and ulcer disease is a subject of debate. The patient in this study on steroids for lupus cerebritis with a gastrointestinal hemorrhage from gastritis should nevertheless serve as a reminder to anticipate this as a possible complication of gastrostomy in patients at risk for ulcer disease or gastritis. The patient on Coumadin with an elevated prothrombin time also had gastrointestinal hemorrhage, which was an avoidable and unfortunate complication of gastrostomy. The third preventable complication represents the only case where a Cope catheter migrated. This resulted either from improper securing of the fixation string or improper placement during formation of the loop. "Twirling" the catheter after formation of the loop during fluoroscopic observation ensures that the catheter is intraluminal and not intraperitoneal or partially formed in the wall of the stomach. In addition,

the two complications requiring surgery may have been preventable if Cope catheters had been used instead of Foley catheters.

As we found no difference in feeding tolerance or requirement for tube change within 30 days (between Cope catheters and gastrojejunostomy catheters), we have not altered our practice of placing a gastrostomy tube rather than gastrojejunostomy tube for routine feeding access. We reserve gastrojejunostomy tubes for patients with known gastroesophageal reflux or documented aspiration, gastric atony, or partial gastric obstruction.

The orientations of the muscular layers in the stomach wall are advantageous to percutaneous gastrostomy placement. Three distinct layers run in different directions: an inner oblique layer, a middle circular layer, and an outer longitudinal layer. This arrangement is probably the reason we were able to puncture and dilate the stomach wall without peritoneal leakage even if the access route was lost at the time of initial tube placement. This occurred in 10 cases; an additional puncture proved adequate for access in all cases. In only one case was additional puncture and tube placement associated with morbidity; as mentioned previously, this was not a statistically significant factor in morbidity.

The muscular coat of the stomach is also probably responsible for the fact that it has proved unnecessary to appose the gastric wall and the anterior abdominal wall. Our series serves as further evidence that routine use of T fasteners for this purpose is not required. We have used T fasteners only in selected instances. We have found them useful for uncooperative patients when it is feared that the tube might be removed inadvertently. They are also helpful for conversion of a gastrostomy tube to a gastrojejunostomy tube within 7 days after placement. Because gastrocutaneous tracts are usually mature at 7 days, we do not use T tacks for conversion of gastrostomy tubes to gastrojejunostomy tubes more than 1 week after placement [18, 20]. Finally, we have used them in patients with ascites or those on peritoneal dialysis.

The indications for gastrostomy or gastrojejunostomy and the classification of complications vary among institutions and make comparisons between reported series difficult. In addition, there are differences in patient populations and referral patterns. Our definition of major morbidity included some complications that would have been classified as minor complications in other studies, such as tube migration or infection requiring antibiotics or tube removal [12, 17, 21, 22]. However, we believe that our classification reflects a definite distinction between levels of care necessary for patient support in the morbidity phase of the complication. The method of classification of complications must be a consideration when comparing results of different series of gastrostomy placement, whatever the means of insertion.

In summary, our results compare favorably with surgical and percutaneous endoscopic gastrostomy as a safe and effective means of gastroenteric feeding or decompression.

We compared Foley catheters, Cope catheters, and gastrojejunostomy catheters for differences in morbidity, mortality, feeding tolerance, and tubal patency. Foley catheters had a higher frequency of morbidity requiring surgery and required more tube changes in the 30-day follow-up period. Therefore, we prefer the Cope type of gastrostomy tube for initial gastrostomy tube placement unless a gastrojejunostomy tube is indicated.

## REFERENCES

1. Preshaw RM. A percutaneous method for inserting a feeding gastrostomy tube. *Surg Gynecol Obstet* **1981**;152:658-660
2. Gauderer MW, Ponsky JL, Izant RJ. Gastrostomy without laparotomy: a percutaneous endoscopic technique. *J Pediatr Surg* **1980**;15:872-875
3. Ponsky JL, Gauderer MW, Stellato TA. Percutaneous endoscopic gastrostomy: review of 150 cases. *Arch Surg* **1983**;118:913-914
4. Tao HH, Gillies RR. Percutaneous feeding gastrostomy. *AJR* **1983**;141:793-794
5. Wills JS, Oglesby JT. Percutaneous gastrostomy. *Radiology* **1983**;149:449-453
6. Wills JS, Oglesby JT. Percutaneous gastrostomy: further experience. *Radiology* **1985**;154:71-74
7. Ho CS, Gray RR, Goldfinger M, Rosen IE, McPherson R. Percutaneous gastrostomy for enteral feeding. *Radiology* **1985**;156:349-351
8. vanSonnenberg E, Wittich GR, Cabrera OA, et al. Percutaneous gastrostomy and gastrojejunostomy. 2. Clinical experience. *AJR* **1986**;146:581-586
9. Alzate GD, Coons HG, Elliott J, Carey PH. Percutaneous gastrostomy for jejunal feeding: a new technique. *AJR* **1986**;147:822-825
10. Gray RR, St. Louis EL, Grosman H. Percutaneous gastrostomy and gastrojejunostomy. *Br J Radiol* **1987**;60:1067-1070
11. Ho CS, Yee ACN, McPherson R. Complications of surgical and percutaneous nonendoscopic gastrostomy: review of 233 patients. *Gastroenterology* **1988**;95:1206-1210
12. Halkier BK, Ho CS, Yee ACN. Percutaneous feeding gastrostomy with the Seldinger technique: review of 252 patients. *Radiology* **1989**;171:359-362
13. Brown AS, Mueller PR, Ferucci JT. Controlled percutaneous gastrostomy: nylon T-fastener for fixation of the anterior gastric wall. *Radiology* **1986**;158:543-545
14. Wills JS, Oglesby JT. Percutaneous gastrostomy. *Radiology* **1988**;167:41-43
15. Ruge J, Vazquez RM. An analysis of the advantages of Stamm and percutaneous endoscopic gastrostomy. *Surg Gynecol Obstet* **1986**;162:13-16
16. Wasiljew BK, Vjiki GT, Beal JM. Feeding gastrostomy: complications and mortality. *Am J Surg* **1982**;143:194-195
17. Larson DE, Burton DD, Schroeder KW, DiMaggio EP. Percutaneous endoscopic gastrostomy: indications, success, complications, and mortality in 314 consecutive patients. *Gastroenterology* **1987**;93:48-52
18. Ponsky JL, Gauderer MW, Stellato TA, Aszodi A. Percutaneous approaches to enteral alimentation. *Am J Surg* **1985**;149:102-105
19. Stiegmann G, Goff J, VanWay C, Perino L, Pearlman N, Norton L. Operative versus endoscopic gastrostomy. Preliminary results of a prospective randomized trial. *Am J Surg* **1988**;155:88-92
20. vanSonnenberg E, Wittich GR, Brown LK, et al. Percutaneous gastrostomy and gastroenterostomy. 1. Techniques derived from laboratory evaluation. *AJR* **1986**;146:577-580
21. Grant JP. Comparison of percutaneous endoscopic gastrostomy with Stamm gastrostomy. *Ann Surg* **1988**;207:598-603
22. Sangster W, Cuddington GD, Bachulis BL. Percutaneous endoscopic gastrostomy. *Am J Surg* **1988**;155:677-679



## Pictorial Essay

# Imaging of and Intervention for Biliary Complications After Hepatic Transplantation

Janis Gissel Letourneau,<sup>1</sup> David W. Hunter,<sup>1</sup> William D. Payne,<sup>2</sup> and Deborah L. Day<sup>1</sup>

Biliary complications are common after hepatic transplantation and the clinical presentation often is nonspecific; consequently, radiologic studies are usually pivotal for diagnosis [1]. In addition, interventional radiologic biliary techniques can be applied to these complications and are therapeutic in

selected patients [1]. In this essay we illustrate the valuable role of radiologic imaging and intervention in such biliary complications, presenting representative examples of imaging studies for their diagnosis and interventional biliary procedures for their treatment.

**Fig. 1.**—Diagram of choledochojejunostomy. Straight surgical catheter is placed across anastomosis and externalized through Roux-en-Y loop to stent anastomosis and permits monitoring of bile production in early posttransplantation period. Roux-en-Y loop is tacked to anterior abdominal wall and can be percutaneously punctured for retrograde opacification of biliary system after surgical catheter has been removed. Arterialization is provided by celiac axis to hepatic artery (arrow) or hepatic artery to hepatic artery reconstruction.

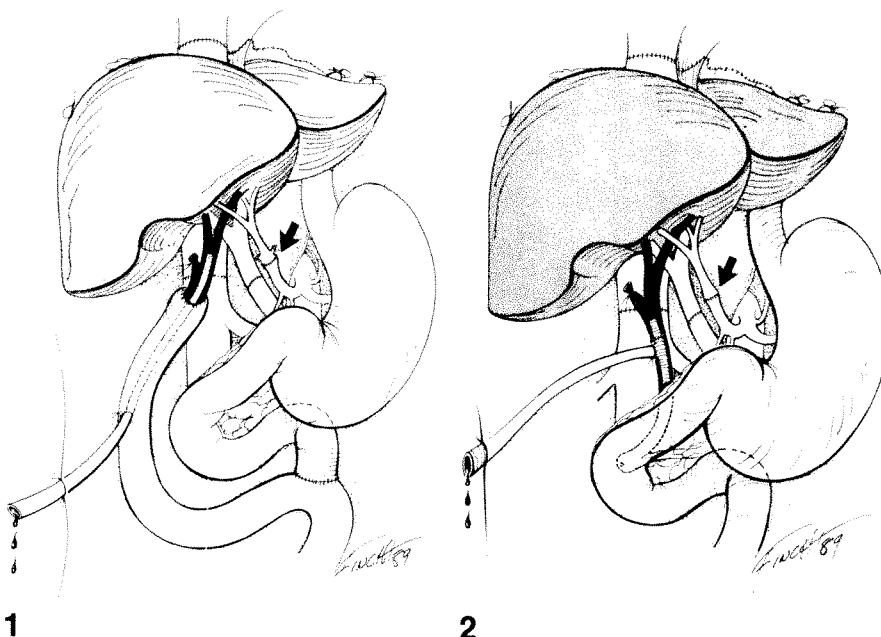


**Fig. 2.**—Diagram of choledochocholedochostomy. Externalized T-tube catheter stents this type of biliary reconstruction. Graft arterialization is usually a hepatic artery to hepatic artery reconstruction (arrow) when size of vessels permits.

Received September 21, 1989; accepted after revision November 6, 1989.

<sup>1</sup> Department of Diagnostic Radiology, University of Minnesota, Box 292, UMHC, Harvard St. and E. River Rd., Minneapolis, MN 55455. Address reprint requests to J. G. Letourneau.

<sup>2</sup> Department of Surgery, University of Minnesota, Minneapolis, MN 55455.

AJR 154:729-733, April 1990 0361-803X/90/1544-0729 © American Roentgen Ray Society

## Materials and Methods

During the past 5 years, 151 hepatic transplants have been done at our institution in 77 children and 64 adults, with 10 of these patients undergoing retransplantation. Three types of biliary reconstruction have been used: cholecystojejunostomy (a procedure no longer commonly performed because of the high rate of associated biliary complications), choledochojejunostomy (Fig. 1), and choledochocholedochostomy (Fig. 2). At transplantation, a catheter is placed across the anastomosis and is externalized with choledochojejunostomy and choledochocholedochostomy reconstructions;

these catheters are left in place for 4–8 weeks if the postoperative course is uncomplicated.

Cholangiography can be done through the surgically placed catheters; if the catheter tip has been dislodged or if a stricture identified, percutaneous transhepatic cholangiography is done, providing potential access for biliary drainage and pressure-flow studies. After a transhepatic tract has been established, balloon dilatation of strictures and basketing and flushing of intraluminal material are possible. Scintigraphy, sonography, and CT also can be used in screening for biliary complications (Fig. 3 and 4); false-negative studies occur occasionally in the setting of biliary obstruction [2, 3].

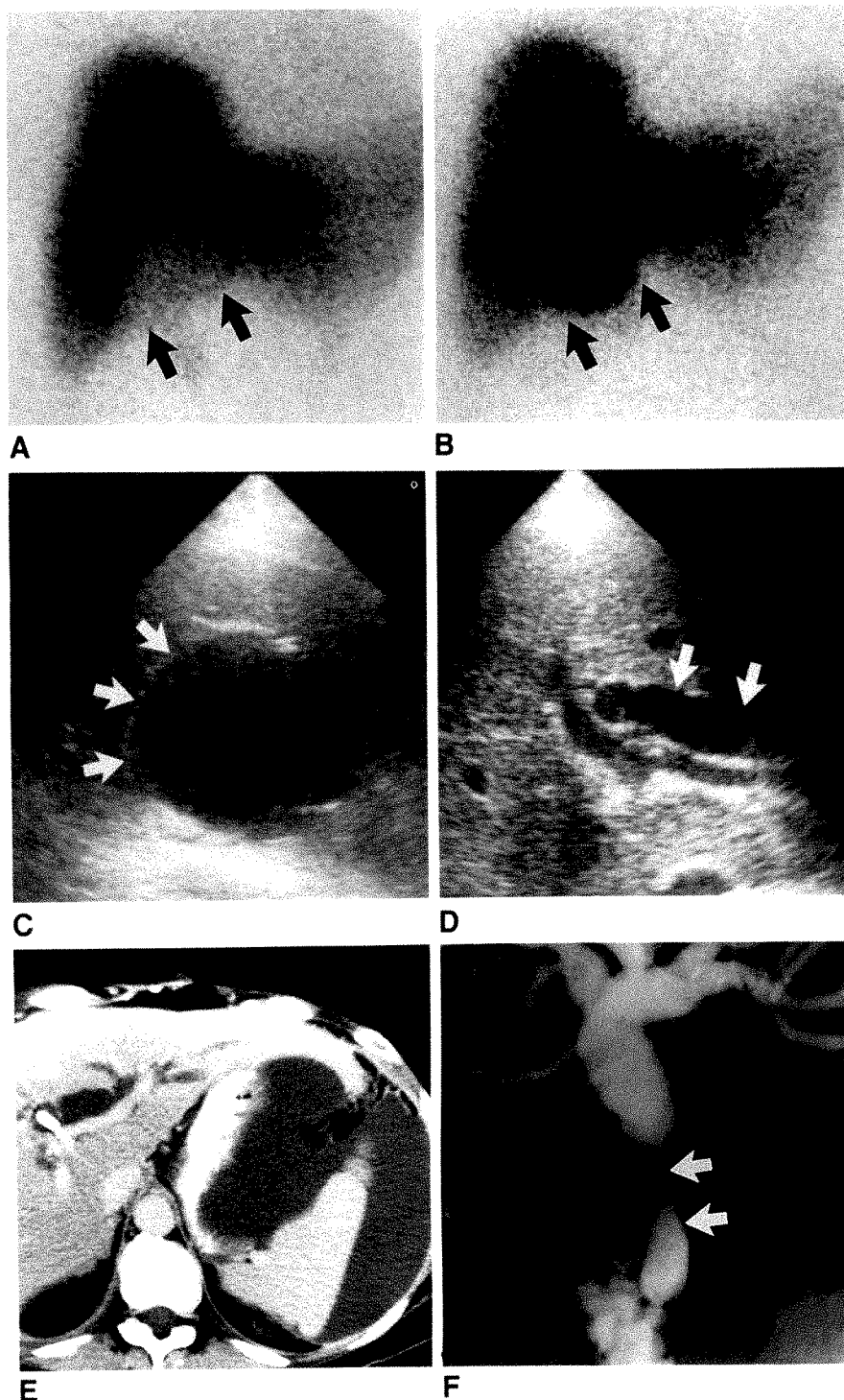


Fig. 3.—Recurrent cholangiocarcinoma in a 43-year-old woman after choledochocholedochostomy reconstruction. Because of inadvertent T-tube dislodgment, biliary leakage and obstruction exist concomitantly. Signs and symptoms were nonspecific; consequently, hepatobiliary scintigraphy and sonography were performed on same day as screening examinations. However, when there is high suspicion of biliary leak, and when biliary catheter is in place, cholangiography is first diagnostic examination.

A, Hepatobiliary scintigram 45 min after injection of radionuclide shows photopenic area (arrows).

B, Delayed (4-hr) scintigram shows intense radiotracer activity in subhepatic space (arrows), indicating biloma.

C, Transverse sonogram confirms subhepatic fluid collection (arrows); dislodged T tube is present in posterior aspect of collection. Biloma was drained percutaneously.

D, Transverse sonogram of porta hepatis shows bile leak is associated with common ductal dilatation (arrows).

E, CT scan 6 weeks later shows persistent biliary dilatation despite percutaneous transhepatic biliary drainage. A large amount of ascites is also present.

F, Cholangiogram shows partial obstruction to flow and proximal ductal dilatation due to irregular narrowing near common ductal anastomosis (arrows). Biopsy findings were recurrent cholangiocarcinoma.

## Results

### *Comparison of Complications in Pediatric and Adult Recipients*

Biliary complications have been identified in 31% of pediatric and 22% of adult recipients, with complications being seen between 1 day and 4 years after transplantation [1]. In both pediatric and adult liver recipients, biliary obstruction is twice as common as leakage [1]. In children, the small size of the ducts probably predisposes to biliary obstruction; in adults, preexisting sclerosing cholangitis and reconstruction with a choledochojejunostomy appear to be the major factors predisposing to biliary obstruction [1]. Biliary obstruction and leakage can, however, occur concomitantly, particularly with cholecystojejunostomy and choledochojejunostomy reconstructions.

Complications occur in one-fourth of children with a choledochojejunostomy; typically, anastomotic obstruction is seen and is amenable to radiologic management alone (Fig. 5).

Leakage after choledochojejunostomy is half as likely as obstruction (Fig. 6). Whether or not leakage is associated with obstruction, radiologic management is based on percutaneous biliary diversion coupled with percutaneous drainage of complicating fluid collections.

All adults at our institution who undergo reconstruction with a choledochojejunostomy have preexisting sclerosing cholangitis; half of such patients have biliary complications, with anastomotic strictures (Fig. 7) seen twice as often as anastomotic leaks [1]. Intrahepatic biliary strictures are also seen (Fig. 8). As is true for children with choledochojejunostomy reconstructions, radiologic intervention, consisting of biliary drainage, stricture dilatation, and percutaneous biloma drainage, has been effective treatment in these patients [2].

Complications are seen in one-third of children and 10% of adults who undergo choledochocholedochostomy, with obstruction only slightly more common than leakage [1]. These complications are diverse and include benign and malignant anastomotic strictures (Fig. 9), anastomotic leakage, T-tube

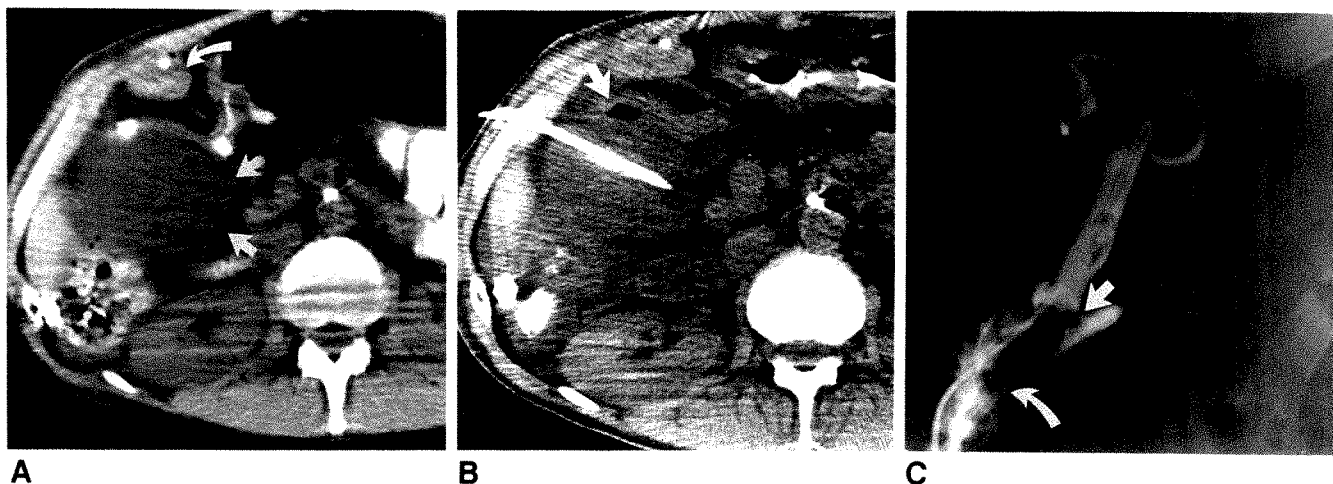


Fig. 4.—Anastomotic leak of choledochojejunostomy in a 52-year-old man with preexisting sclerosing cholangitis.

A, CT scan shows subhepatic fluid collection (straight arrows) deep relative to Roux-en-Y loop (curved arrow); Roux-en-Y loop is tacked to anterior abdominal wall.

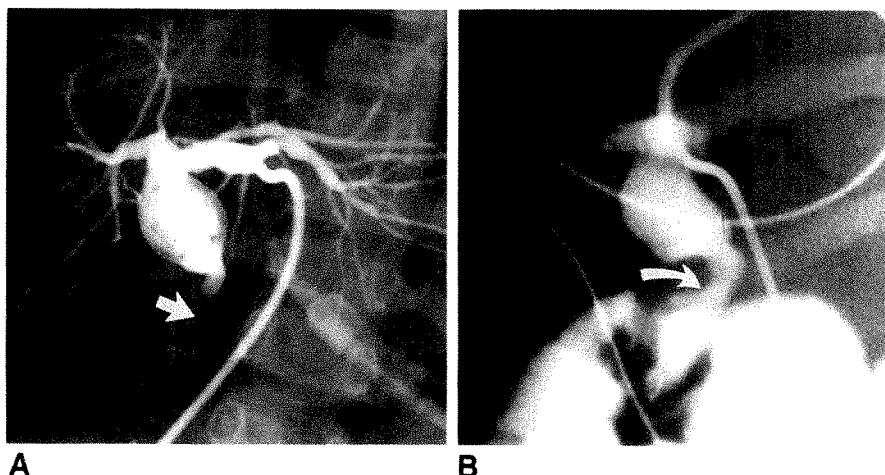
B, CT scan shows biloma drained percutaneously. A small amount of air has been introduced into fluid collection (arrow).

C, Cholangiography performed through surgically placed catheter shows anastomotic leak (straight arrow). Tip of percutaneous drainage catheter (curved arrow) is seen near extravasated contrast material.

Fig. 5.—Complete obstruction of a choledochojejunostomy in a 4-year-old girl who underwent liver transplantation for extrahepatic biliary atresia.

A, Cholangiography through percutaneous biliary drainage catheter reveals complete obstruction to flow at anastomosis (arrow). Balloon dilatation of stricture was performed.

B, Follow-up cholangiogram shows widely patent anastomosis (arrow), although proximal biliary dilatation persists. Pressure-flow studies indicated no significant obstruction, despite biliary dilatation. No further radiologic or operative intervention was necessary.



dislodgment, and postbiopsy bile leak (Fig. 10). Despite successful use of interventional techniques in some of these patients, retransplantation and reoperation have been required in others because of suboptimal positioning of the surgical catheter, massive biliary leakage, or other unrelated problems, such as portal vein thrombosis or chronic rejection.

#### *Arterial Thrombosis and Biliary Complications*

Loss of graft arterialization predisposes the patient to biliary complications [4]; almost half of patients with arterial thrombosis have biliary obstruction, leakage, or both (Figs. 6 and

11). Although nonsurgical management can be successful, graft and patient survival are severely compromised and retransplantation sometimes is required.

#### *Diffuse Biliary Abnormalities*

Diffuse biliary abnormalities are often identified by cholangiography in the absence of obstruction or leakage; findings include diffuse narrowing, stretching, and separation of intrahepatic ductal branches (Fig. 12). These findings are nonspecific, being seen with acute rejection, preservation injury, infarction, and hepatitis.

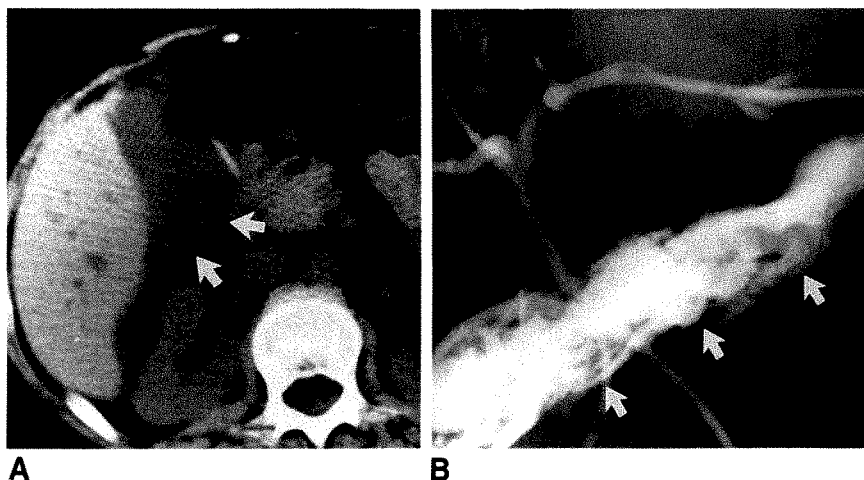


Fig. 6.—Anastomotic leak in a 12-year-old boy with hepatic artery thrombosis after liver transplantation with a choledochojejunostomy.

A, CT scan shows moderate-sized subhepatic fluid collection (arrows).

B, After percutaneous biliary diversion and percutaneous catheter drainage of biloma, cholangiography reveals extravasation of contrast material into subhepatic collection (arrows).

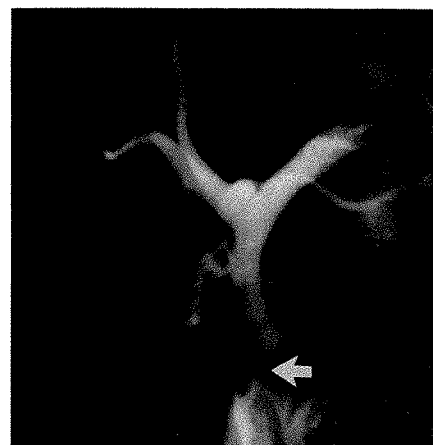


Fig. 7.—Cholangiogram shows partial obstruction with tight anastomotic stricture (arrow) in a 53-year-old man with preexisting sclerosing cholangitis, which was treated successfully with balloon dilatation.

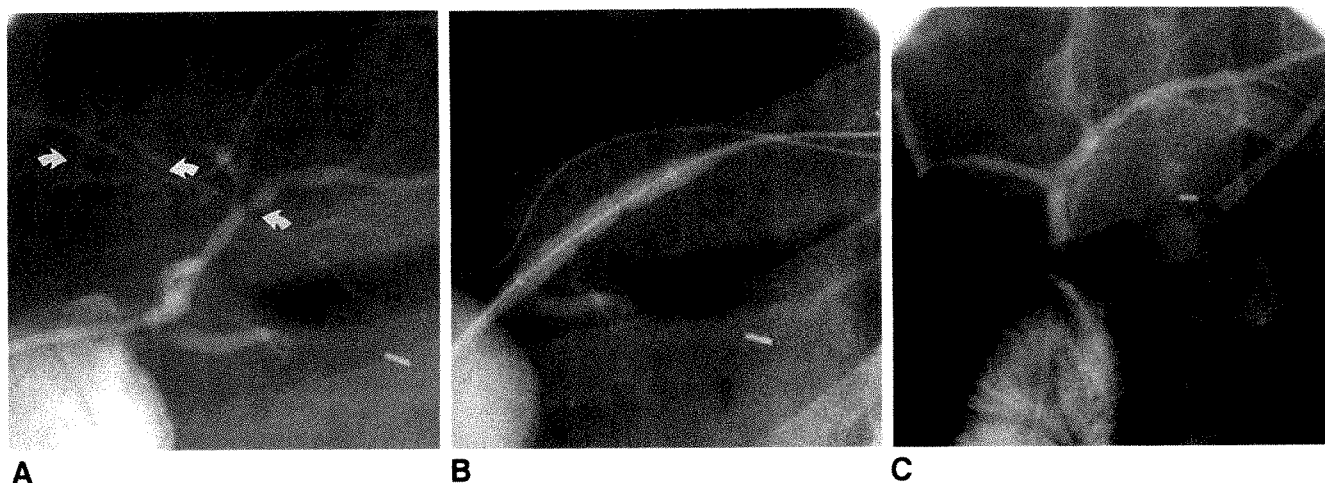


Fig. 8.—Intrahepatic strictures after liver transplantation for sclerosing cholangitis in a 32-year-old woman.

A, Transjejunal cholangiogram reveals multiple intrahepatic biliary strictures (arrows).

B, Balloon dilatation of strictures in left hepatic lobe is done at a later date with a 4-mm-diameter angioplasty catheter.

C, Good technical results are obtained from balloon dilatation. Nonetheless, repeat dilatation was required in the same biliary segment 2 months later; however, no further radiologic or surgical intervention was necessary after that.

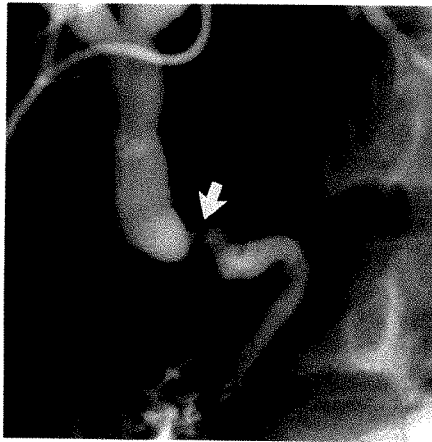
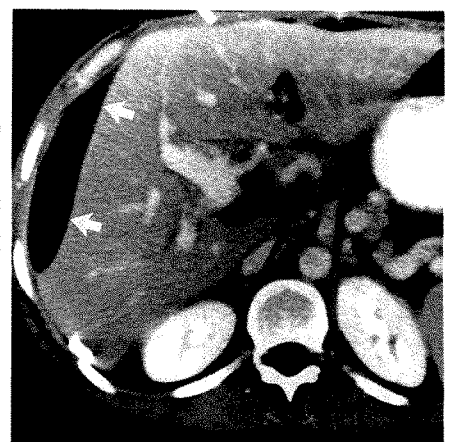


Fig. 9.—Partial obstruction of choledochocholedochostomy reconstruction in a 14-year-old girl with Wilson disease. Cholangiogram shows mild proximal dilatation with kinking and partial obstruction at anastomosis (arrow). Partial obstruction resolved with percutaneous biliary decompression alone, probably because of resolution of postoperative anastomotic edema.



A

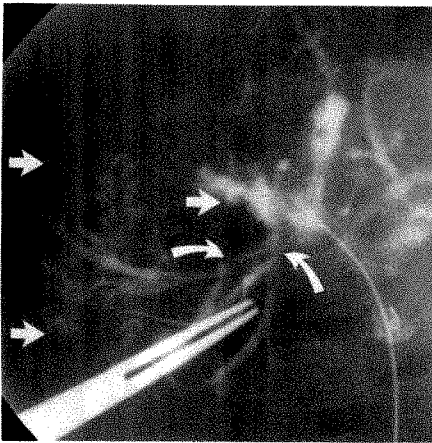


B

Fig. 10.—Postbiopsy leak in a 38-year-old woman with a choledochocholedochostomy.

A, Cholangiography through a T-tube catheter reveals a bile leak from a peripheral duct in right lobe (straight arrow). Contrast material extravasates into perihepatic space (curved arrows), where large surgical drain is present.

B, CT scan through same area shows that some perihepatic fluid (arrows) is not being evacuated by surgical drain. Some periportal fluid is seen also.



A



B

Fig. 11.—Hepatic artery thrombosis and diffuse biliary abnormalities in an 18-month-old girl who underwent liver transplantation for extrahepatic biliary atresia.

A, Percutaneous transhepatic cholangiogram reveals multiple bile leaks (straight arrows) and strictures (curved arrows) [5].

B, Corresponding CT scan shows numerous areas of parenchymal low density, compatible with infarct and bile leak.

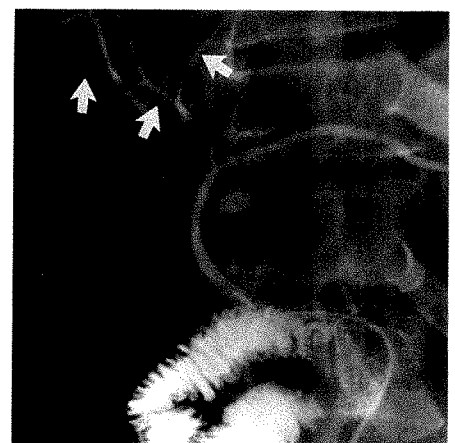


Fig. 12.—Diffuse, nonspecific cholangiographic findings in the early postoperative period in a 46-year-old man with preexisting sclerosing cholangitis. Cholangiography performed through straight surgical catheter shows ductal narrowing, stretching, and separation of right lobar biliary radicals (arrows).

## Conclusions

Diagnosis of biliary complications after hepatic transplantation is problematic; definitive characterization requires cholangiography. Interventional biliary procedures can be used successfully to treat these complications; however, surgical revision and retransplantation are sometimes required.

## REFERENCES

1. Letourneau JG, Castañeda-Zúñiga WR. The role of radiology in the diagnosis and treatment of biliary complications after liver transplantation. *Cardiovasc Intervent Radiol* (in press)
2. Letourneau JG, Day DL, Hunter DW, et al. Biliary complications after liver transplantation in patients with preexisting sclerosing cholangitis. *Radiology* 1988;167:349-351
3. Zemel G, Zajko AB, Skolnick ML, et al. The role of sonography and transhepatic cholangiography in the diagnosis of biliary complications after liver transplantation. *AJR* 1988;151:943-946
4. Zajko AB, Campbell WL, Logsdon GA, et al. Cholangiographic findings in hepatic artery occlusion after liver transplantation. *AJR* 1987;149:485-489
5. Dalen K, Day DL, Ascher NL, et al. Imaging of vascular complications after hepatic transplantation. *AJR* 1988;150:1285-1290

# American Roentgen Ray Society

90th Annual Meeting

May 13–18, Washington, D.C.

## **1990 Caldwell Lecturer**



**Sandra Day O'Connor**

United States Supreme Court Justice

**“The Federal Courts”**



# Selective Osteal Salpingography and Transvaginal Catheter Dilatation in the Diagnosis and Treatment of Fallopian Tube Obstruction

Erich K. Lang<sup>1</sup>  
Heber E. Dunaway, Jr.<sup>2</sup>  
William E. Roniger<sup>2</sup>

Selective salpingography and transvaginal catheter dilatation were performed in 157 women with infertility to diagnose, localize, and classify obstructive diseases of the fallopian tubes and to correct obstruction of the proximal (uterine-end) tube. In 61 (39%) of the patients, the selective salpingograms showed patent tubes despite the fact that two previous hysterosalpingograms showed obstruction of the proximal (uterine-end) tube. Transvaginal catheter dilatation successfully recanalized the proximal portion of the tubes in 79 (82%) of 96 patients with obstructed tubes. In 18 of 25 with successful transvaginal catheter dilatation and 6-month follow-up salpingography, the tubes remained patent. Coexisting disease of the distal (ovarian-end) tubes was diagnosed in 29 (18%) of the patients. Pregnancy was achieved in 11 of the 157 patients (six in whom obstructions were corrected by transvaginal catheter dilatation and five in whom selective salpingograms showed patent tubes). There were no complications due to the procedure.

The excellent diagnostic and therapeutic yield, lack of complications, and low cost justify the use of these percutaneous techniques to investigate female infertility and to treat obstruction of the uterine end of the fallopian tube.

*AJR* 154:735-740, April 1990

Transvaginal fallopian tube catheterization and dilatation to recanalize the proximal (uterine-end) fallopian tube are rapidly gaining acceptance for the diagnosis and treatment of tubal obstruction [1-5]. The procedures are advocated both to improve diagnosis of the precise site or sites of obstruction and to recanalize proximal obstructions of the tube. Management of obstructions involving the distal tubes (ovarian end) remains in the domain of microsurgery [6-8]. Isolated obstruction of the proximal fallopian tube amenable to transvaginal dilatation and recanalization is thought to be the cause of infertility in about 20% of the patients [9]. Obstruction of the distal tubes causes infertility in about 30% of such patients; endocrine abnormalities or pathologic conditions of the uterus cause abnormalities in the remainder [9-11].

## Subjects and Methods

The study comprised 157 women 23-46 years old (average age, 34 years) with primary or secondary infertility of an average duration of 4.6 years. Hysterosalpingograms showed bilateral (141 patients) or unilateral (16 patients) nonfilling of the fallopian tubes. The preliminary workup in all of the patients consisted of a hysterosalpingogram and an endocrine profile (estradiol, follicle-stimulating hormone, luteinizing hormone, prolactin, and dehydroepiandrosterone sulfate). In patients with nonfilling of the fallopian tubes, a second hysterosalpingogram was obtained to verify the observation before proceeding to selective salpingography.

Prior or subsequent laparoscopy and/or exploration for tubal microsurgery or fimbrioplasty were performed in 142 patients. For the first 100 patients, laparoscopy was performed to verify the findings of selective osteal salpingography. In others, laparoscopy was used for assessment of disease of the distal (ovarian-end) tubes and harvesting of ova. Transvaginal

Received August 22, 1989; accepted after revision November 9, 1989.

Presented at the annual meeting of the American Roentgen Ray Society, New Orleans, May 1989.

<sup>1</sup> Department of Radiology, Louisiana State University Medical Center, 1542 Tulane Ave., New Orleans, LA 70112. Address reprint requests to E. K. Lang.

<sup>2</sup> The Fertility Center of Louisiana, 200 W. Esplanade, Suite 210, Kenner, LA 70065.

0361-803X/90/1544-0735

© American Roentgen Ray Society

gamete transfer or GIFT (gamete intrafallopian transfer) procedures were carried out in nine of the patients.

Success of the procedure (i.e., pregnancy) was established by phone follow-up either directly to the patient or to her referring physician. Contact was retained with all but one of the patients for periods of 6 months to 2½ years. We attempted to obtain a follow-up hysterosalpingogram 6 months after the procedure in all patients who were not pregnant at that time; 25 patients returned for this examination.

Patients were considered for selective osteal salpingography, transvaginal catheter tubal recanalization, and selective catheter (2-French) salpingography after obstruction of the proximal (uterine-end) tubes had been shown on two consecutive hysterosalpingograms [1–3]. The procedure was usually performed immediately after the second hysterosalpingogram.

The procedures were performed in the follicular phase of the patient's menstrual cycle, most often after administration of 325 mg of aspirin. In five patients, IV glucagon or terbutaline was given [5]. All patients received doxycycline hyclate (Warner Chilcott, Morris Plains, NY), 100 mg twice a day for 2 days before and 3 days after the procedures.

#### Technique

Hysterosalpingograms were obtained by using a balloon catheter placed in the endocervical canal. If the tubes failed to opacify after two successive injections of Conray 60 (Mallinckrodt, St. Louis, MO), selective osteal salpingography was performed. For this procedure, patients were premedicated with 25 mg of Demoral (Winthrop Pharmaceuticals, New York, NY) intramuscularly. If the patient still had discomfort, fentanyl (Elkins-Sin, Cherryhill, NJ) was given IV.

A fluoroscopic table equipped with a spot-film device and a 105-mm camera was used. Once the cervix was visualized, a tenaculum was applied at the 12 o'clock position. The cervical canal was then probed with a uterine probe. A 9-French Teflon sheath and 5.5-French torque-controlled polyethylene catheter (Cook, Spencer, IN) and a 0.035-in. (0.89-mm) (Cook, Bloomington, IN) guidewire, flush

with the end of a 9-French Teflon sheath, were introduced into the lower uterine segment.

Simultaneous traction on the tenaculum and advancement of the relatively stiff 9-French Teflon sheath straightened the uterus and corrected retroflexion and anteflexion. Moreover, the tenaculum could be used to rotate the uterus slightly, thus facilitating advancement of the 5.5-French torque-controlled catheter into the uterine cornu. This, however, is carried out under fluoroscopic control with a 0.035-in. (0.89-mm) J guidewire leading by 1.5 cm. After exchanging the guidewire for a soft-tipped 0.035-in. (0.89-mm) straight guidewire and leading with the soft-tipped guidewire, the 5.5-French catheter is wedged into the tubal ostium and selective salpingography is attempted with injection of 1.5–2.0 ml of Conray 60. An additional 2.5 ml of contrast medium may be deployed to document spillage from the fimbriated end and identify adhesions and attendant loculation of contrast medium around the fimbriated end of the tubes. Custom reshaping of the tip of the 5.5-French catheter in steam was carried out if attempts to engage the cornua failed.

Tubal recanalization was attempted in all patients in whom efforts, so far, had failed to opacify the tubes. A tapered guidewire, 0.016–0.013 in. (0.41–0.34 mm), with a floppy platinum tip (Target Therapeutics, Graz, Austria) was advanced into the interstitial and isthmic segments of the tubes through the 5.5-French catheter seated in the cornu (Fig. 1).

If resistance was encountered, the tapered guidewire was reinforced by a tapered catheter, 2.2–1.5 French (Cook, Spencer, IN), or the Tracker catheter, 3.0–2.2 French (Target Therapeutics). The guidewire leading by ½–1 cm and the catheter were used in combination as a bougie dilator. With a controlled to-and-fro probing motion, the guidewire and catheter were gradually advanced and the stenotic and obstructed segment was dilated (Fig. 2). This was continued until the catheter had been passed through the entire isthmic segment. The tapered ultrasoft-tipped guidewire may be advanced for another 2.5 cm to probe this segment of the tube. At this point, a tapered 2-French catheter is advanced over the guidewire, the guidewire is removed, and the selective salpingogram obtained with the injection of 1.5–2.5 ml of Conray 60. Both early filling and, if present, spillage were recorded on spot films. Disease of the distal tubes (fimbriated end) was carefully documented in anteroposterior and oblique projec-

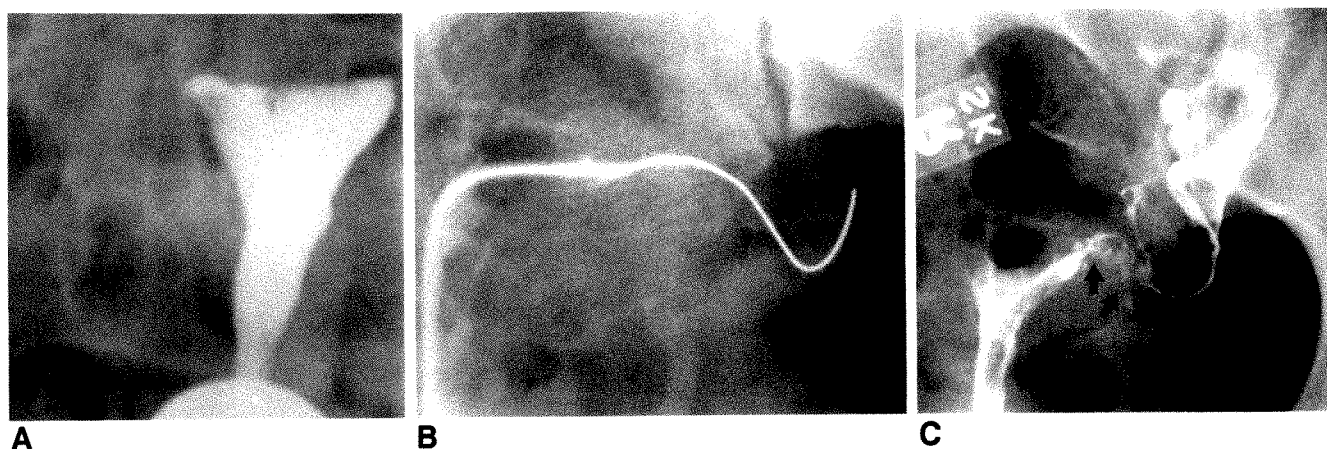


Fig. 1.—Patient with bilateral obstruction of proximal portion of fallopian tubes caused by salpingitis isthmica nodosa treated by transvaginal catheter dilatation of the tubes.

A, Hysterosalpingogram shows nonfilling of both tubes.

B, Spot radiograph shows left uterine cornu engaged with precurved 5.5-French catheter. A 0.015-in. (0.39-mm) ultrasoft platinum-tipped guidewire has been advanced into midportion of left tube; interstitial and isthmic segments are dilated with a 2-French catheter tapered to 1.6 French.

C, Follow-up osteal salpingogram shows filling of left tube in its entirety with spillage of contrast medium from fimbriated end (arrow). Collections of contrast medium (arrow) surrounding isthmic segment indicate salpingitis isthmica nodosa; irregular lumina of interstitial and isthmic segments suggest endosalpingitis.

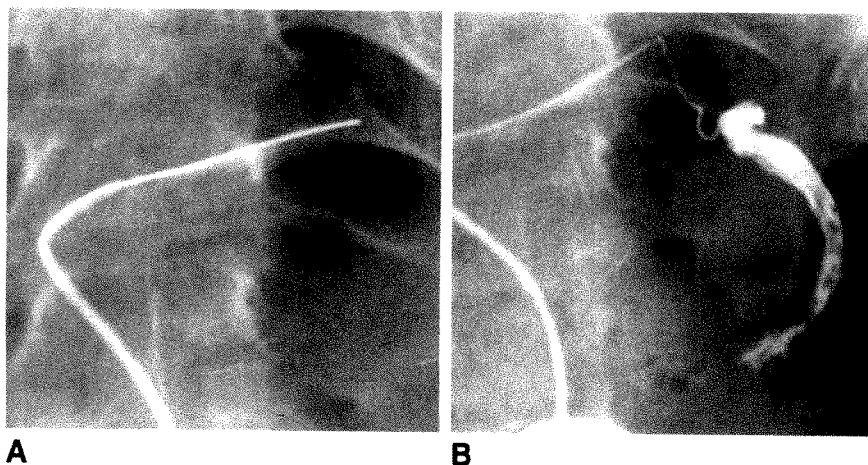


Fig. 2.—Patient with successful recanalization of strictured segments of proximal tubes.

A, Spot film shows left cornu engaged by pre-curved 5.5-French catheter and ultrasoft 7.5-cm platinum-tipped 0.015-in. (0.39-mm) guidewire advanced through interstitial and isthmic segments of fallopian tubes. A 2-French catheter tapered to 1.6 French has been passed over guidewire to dilate obstructed segment.

B, Spot radiograph after injection through tapered 2-French catheter shows patency and normal appearance of distal tube.

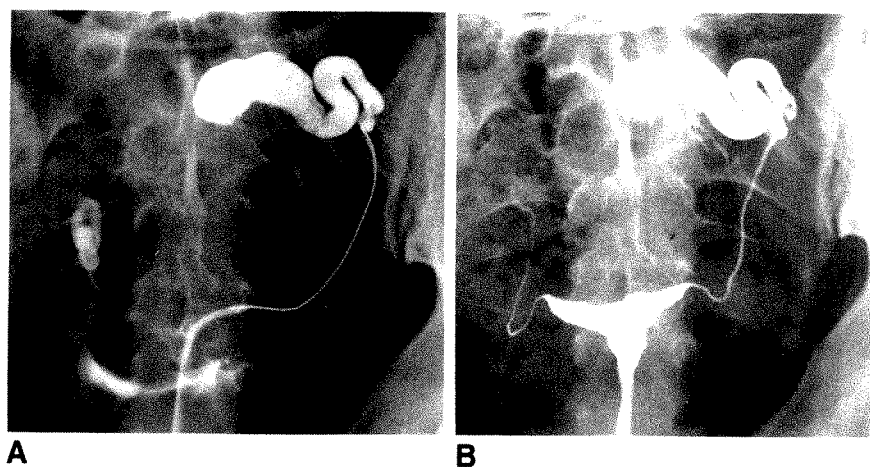


Fig. 3.—Patient with coexisting disease of proximal and distal tubes.

A, Spot film shows obstruction of proximal (uterine-end) tube. Guidewire is advanced to interstitial and isthmic segments of left tube.

B, Subsequent hysterosalpingogram confirms patency of interstitial, isthmic, and mid segment of tube, but shows large pyosalpinx with occlusion of distal tube.

tions for consideration for surgical correction such as fimbrioplasty or laparoscopic lysis of adhesions (Fig. 3).

After completion of this phase of the study, the tapered catheter was withdrawn and another selective ostial salpingogram was obtained through the 5.5-French catheter to assess the effect of transluminal bougie dilatation on the proximal tube.

Balloon dilatation was used only if synechiae in the cornual ostium impeded access to the tubes. For purpose of disrupting the synechiae and establishing access to the tubes, a tapered 0.014-in. (0.36-mm) platinum-tipped guidewire was advanced into the midportion of the tubes. A coronary balloon catheter (US Catheter, Billerica, MA) with a 2-mm balloon was then seated in the cornu and the balloon inflated until rupture of the synechiae. Migration of the balloon into the uterine fundus was prevented by forcing the curved 7-French introducing catheter against the balloon.

Postprocedural hysterosalpingograms were obtained in a fashion identical to the initial hysterosalpingogram. Fluoroscopic time for selective salpingography ranged from 30 sec to 2 min. Depending on the complexity of the abnormality encountered, recanalization procedures per tube ranged from 45 sec to 11 min.

## Results

In 61 of the 157 patients, patency of the tubes was shown by selective ostial salpingography. In four of these patients, one tube appeared obstructed on the hysterosalpingogram; in 57, both tubes were obstructed (Table 1).

Submucosal leiomyomas prevented filling on hysterosalpingography in nine patients (Fig. 4). In three patients, nonfilling of one tube appeared to be due to a bicornuate uterus. In 14 patients, nonfilling of the tubes was caused by a sharp angulation between the interstitial and isthmic segments of the tubes. The spasm causing the angulation was modified by subsequent passage of the guidewire and the tubes filled readily thereafter (Fig. 5). A mild form of salpingitis isthmica nodosa was the probable cause for initial nonfilling in five other patients. In 26 patients the precise cause for the initial nonfilling remains unknown.

In 78 patients, tubal obstruction was successfully treated by dilatation (Table 1). Among these patients, salpingitis isthmica nodosa was the most common cause of the obstruction, occurring in 41 patients. In nine of our patients, stenosis at the tubocornual reimplantation site was found to be responsible for the obstruction; in six, obstruction was due to a stenosis at the site of reversal surgery for tubal ligation. In seven patients, the interstitial segments of the tubes were obstructed; in two, the mid tube region had an obstruction of undetermined cause. In three patients, debris appeared to be the cause; in nine other patients, the cause for the initial obstruction of the tube remained obscure.

Selective catheter salpingograms after correction of the proximal obstruction documented distal disease of the tubes

**TABLE 1: Results of Selective Salpingography and Transvaginal Catheter Dilatation of the Fallopian Tubes**

Finding	No. of Patients
Obstruction of the proximal (uterine-end) fallopian tubes	
Unilateral	16
Bilateral	141
Total	157
Patent on selective salpingography	
Unilateral	4
Bilateral	57
Total	61
Successful recanalization by catheter dilatation	
Unilateral	9
Bilateral	69
Total	78
Successful balloon dilatation of cornual region	1
Failure to respond to catheter recanalization attempts	
Unilateral	2
Bilateral	15
Total	17

or extensive peritubal adhesions around the fimbriated end in 24 patients; this was unilateral in 10 and bilateral in 14.

In one patient with extensive synechiae in the cornu, balloon dilatation of the cornual segment was carried out with resultant restoration of patency and opacification of the tube.

In 17 patients, we were neither able to fill the tubes by selective injection nor recanalize them by bougie dilatation. During exploratory surgery, all patients had variable degrees of inflammatory proximal disease; one-third were found to have massive associated distal disease of the tubes.

Pregnancies were achieved in 11 patients. In five of these patients, the tubes were patent on selective osteal salpingography. In six, proximal obstruction had been corrected by transvaginal tube dilatation. Two of these six also had been subjected to fimbrioplasty or laparoscopic fimbriolysis. Two patients delivered healthy infants, five were ongoing pregnant, two had spontaneous abortions in the first trimester, and two had blighted ova. On average, pregnancies occurred within 4 months after the procedure (range, 1.5–13 months). No ectopic pregnancies were found.

In 54 patients without disease of the distal tubes in whom recanalization of the proximal tubes by catheter dilatation was

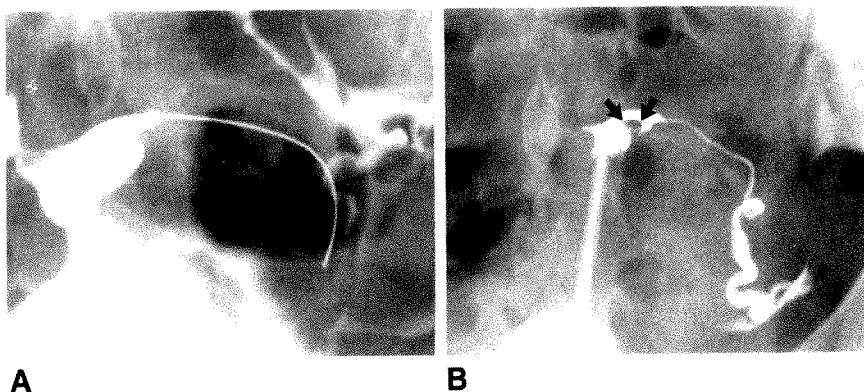


**Fig. 4.**—Patient with ball-valve obstruction of cornu caused by submucosal fibroid.

**A.** Spot radiograph shows guidewire passed over submucosal fibroid in left uterine cornu and advanced into midportion of tube.

**B.** Injection of contrast medium through 2-French catheter barely advanced into interstitial segment of left tube shows normal tube. Precurved 5.5-French catheter depresses submucosal fibroid (arrows).

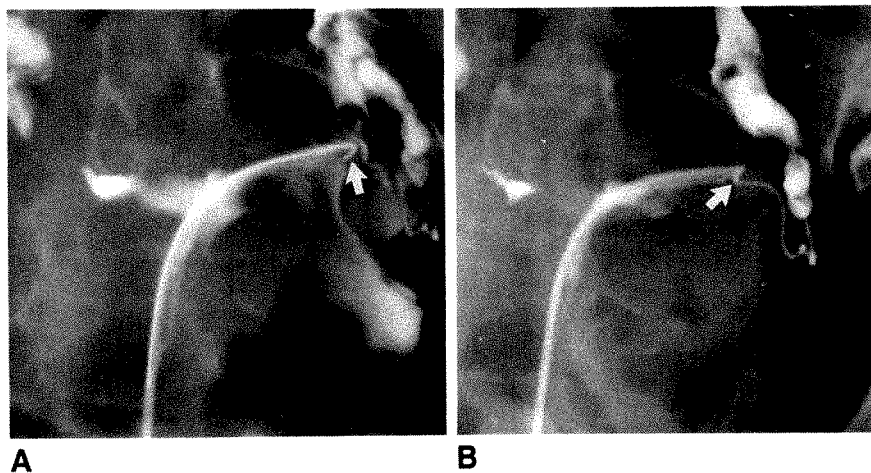


**Fig. 5.**—Patient with obstruction attributable to muscle spasm.

**A.** Spot radiograph shows sharp angle indicated by ultra-soft-tipped guidewire (arrow) in interstitial segment.

**B.** Subsequent osteal salpingogram shows sharp angle of interstitial segment of tube (arrow). Passage of guidewire or use of prostaglandin antagonists often corrects this appearance, apparently by moderating muscle spasm.

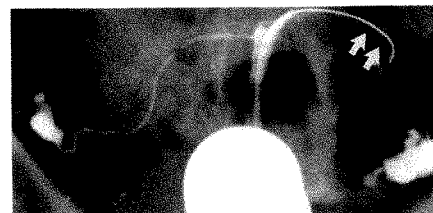


**Fig. 6.**—Patient with adhesions around fimbriated end of tube. Spot film after catheter dilatation of interstitial and isthmic segments shows tube patent to fimbriated end. Puddling of contrast medium around fimbriated end indicates adhesions and need for fimbriolysis. Small collections of contrast medium around isthmic segment indicate salpingitis isthmica nodosa (arrows).

successful, four pregnancies occurred. In 14 patients in whom the proximal tubes had been recanalized by catheter bougie dilatation and disease of the distal tubes corrected by fimbrioplasty or laparoscopic lysis, two pregnancies occurred (Table 2).

The status of patency of the tubes was assessed 6 months after the primary procedure in 25 patients who had yet to achieve pregnancy. The tubes were found to be patent in 18 patients: in 16 of 21 patients in whom disease was limited to the proximal tubes and treated by transvaginal catheter dilatation and in two of four in whom proximal disease was managed identically and distal disease was treated by fimbrioplasty or laparoscopic lysis (Table 2).

We observed no complications such as perforation of the tubes or extravasation or leakage of contrast medium after transvaginal catheter dilatation of obstructed proximal tubes.

## Discussion

Selective osteal salpingography is an effective tool to differentiate functional from organic obstruction of the fallopian tubes; this is often not possible by hysterosalpingography. Persistent spasm at the cornua causing a nearly 90° angle between the interstitial and isthmic segments of the tubes may have been responsible for nonfilling of the tubes on hysterosalpingograms in almost one-fourth of our patients. Although IV administration of glucagon has been used successfully to reverse apparent cornual obstruction in about one-third of such patients, there remains a substantial group refractory to this type of management [12]. Aspirin and oral prostaglandin antagonist have shown a similar salutary response in our patients [13]. Repeat hysterosalpingograms after premedication of patients with prostaglandin antagonist demonstrated unabated filling of some tubes that appeared obstructed on preceding studies. There remained, however, a substantial segment of patients who did not respond to prostaglandin antagonist but showed patent tubes after trans-

vaginal catheterization with a soft-nose platinum-tipped guidewire had been carried out. It is presumed that persistent spasm or debris in the tubes may have been responsible for the nonfilling and that this condition was corrected by mere passage of the guidewire.

Undetected submucosal fibroids causing a ball-valve obstruction at the level of the cornua were another common cause (about 15% of our patients) for nonfilling of the tubes on hysterosalpingograms. Undetected congenital anomalies such as a bicornuate uterus at times led to the erroneous misdiagnosis of nonfilling of one tube. Organic disease such as synechiae in the uterus likewise caused nonfilling.

Selective osteal salpingography alone or after transvaginal catheter dilatation was capable of showing the status of the tubes in 89% (140 to 157) of our patients. Most importantly, the technique characterized obstructive lesions by location, proximal or distal tubes or both, and by probable cause. After recanalization of the proximal segment of the tubes, selective salpingography or osteal salpingography made possible detailed assessment of the distal end of the tube. Obstruction of the distal tubes mandates surgical intervention, fimbriolysis, fimbrioplasty, or similar procedures (Fig. 6). The need for such microsurgical procedures on the fimbriated tube was identified in 24 of our 79 patients in whom we were first able to recanalize the obstructed proximal tube by transvaginal catheter dilatation and in five patients in whom proximal tubes were shown to be patent on selective salpingography.

Transvaginal catheter (bougie) dilatation proved successful for recanalizing obstructed segments of the tubes in 82% (79 of 96) of our patients. This success rate is considerably higher than for microsurgical procedures such as tubocornual or ampullar interstitial anastomosis [14]. The 6-month follow-up hysterosalpingogram showed the tubes to remain patent in 72% (18 of 25) of our patients; again, an acceptable long-term result. The success rate for transvaginal catheter dilatation of proximal tube obstruction, however, varied greatly for different underlying causes. Cicatricial changes attendant to inflammatory disease, salpingitis isthmica nodosa, appeared to respond best, particularly if not complicated by

**TABLE 2: Prevalence of Pregnancy and Documented Patency of Tubes on 6-Month Follow-ups in Patients with Successful Balloon Recanalization of Obstructed Tubes**

Underlying Cause	No. of Patients	No. of Pregnancies	No. Not Pregnant at 6-Month Follow-up	
			Total	Tubes Patent on Follow-up Hysterosalpingogram
Without distal disease				
Unilateral tube obstruction	6	1	2	1
Bilateral tube obstruction	48	3	19	15
With uncorrected distal disease				
Unilateral	2	0	0	0
Bilateral	8	0	0	0
With distal disease corrected by fimbrioplasty, laparoscopic lysis				
Unilateral	1	0	0	0
Bilateral	13	2	4	2

extensive peritubal disease. In the presence of peritubal disease, we sometimes elected to perform a tubocornual anastomosis despite ability to recanalize the obstructed segment by transvaginal catheter dilatation because of the known propensity for later cicatricial obstruction. Stenosis complicating prior tubocornual or ampullar interstitial anastomoses or microanastomoses reversing prior tuboligations proved to be more refractory to transvaginal catheter dilatation; nonetheless, an attempt at recanalization by this percutaneous method appears justified.

The ultimate test for this procedure, the rate of pregnancy attained, was 7% in our series, less than reported for similar transvaginal procedures by other investigators [2, 3, 5]. The cause for this is not known at present.

On the basis of our experience, we recommend selective salpingography first, and if necessary, transvaginal catheter dilatation to recanalize an obstructed proximal tube. This approach will identify a large number of patients with normal tubes who need no further laparoscopic investigation and can be expected to attain pregnancy provided other conditions such as ovulation, hormonal status, and partner fertility are met. For most patients with organic disease involving only the proximal tubes, transvaginal catheter dilatation and recanalization suffice to correct the condition and permit passage of the ovum through the tubes. Moreover, the ability of this technique to identify other causes of infertility such as disease of the distal tubes, submucosal fibroids, leiomyomas, or synechiae of the uterus facilitates appropriate surgical or endoscopic correction.

## REFERENCES

1. Platia MP, Krudy AG. Transvaginal fluoroscopic recanalization of proximally occluded oviduct. *Fertil Steril* **1985**;44:704-706
2. Thurmond AS, Novy M, Uchida BT, Rosch J. Fallopian tube obstruction: selective salpingography and recanalization. *Radiology* **1987**;163:511-514
3. Thurmond AS, Rosch J, Patton PE, Burry KA, Novy M. Fluoroscopic transcervical fallopian tube catheterization for diagnosis and treatment of female infertility caused by tubal obstruction. *RadioGraphics* **1988**;8:621-640
4. Confino E, Friberg J, Gleicher N. Preliminary experience with transcervical balloon tuboplasty. *Am J Obstet Gynecol* **1988**;159:370-375
5. Thurmond AS, Novy M, Rosch J. Terbutaline: in diagnosis of interstitial fallopian tube obstruction. *Invest Radiol* **1988**;23:209-210
6. McComb P, Gomel D. Cornual occlusion and its microsurgical reconstruction. *Clin Obstet Gynecol* **1980**;23:1229-1241
7. Musich JR, Behrman SJ. Surgical management of tubal obstruction at the utero tubal junction. *Fertil Steril* **1983**;40:423-441
8. Trimbos-Kemper TCM, Trimboos JB, Van Hall EV. Adhesion formation after tubule surgery: results of the eight day laparoscopy in 188 patients. *Fertil Steril* **1985**;43:395-400
9. Nordenskjold F, Ahlgren M. Laparoscopy in female infertility. *Acta Obstet Gynecol Scand* **1983**;62:609-615
10. Snowden EU, Jarrett JC, Dawood MY. Comparison of diagnostic accuracy of laparoscopy, hysteroscopy and hysterosalpingography in evaluation of female infertility. *Fertil Steril* **1984**;41:709-713
11. Sulak PJ, Letterie GS, Coddington CC, Hayslip CC, Woodward JE, Klein TA. Cystology of proximal tubal occlusion. *Fertil Steril* **1987**;48:437-440
12. Winfield AC, Pittaway D, Maxson W, Daniell J, Wentz AC. Apparent cornual occlusion in hysterosalpingography: reversal by glucagon. *AJR* **1982**;139:525-527
13. Lang EK. Prostaglandin antagonists reversable cornual spasm. *Obstet Gynecol* (in press)
14. Patton PE, Williams TJ, Coulam CB. Results of microsurgical reconstruction in patients with combined proximal and distal tubal occlusion: double obstruction. *Fertil Steril* **1987**;48(4):670-674



## Case Report

# Uterine Perforation Simulating Urachal Carcinoma: CT Diagnosis

Alan J. Kronthal,<sup>1</sup> Elliot K. Fishman,<sup>1</sup> Roger C. Sanders,<sup>1</sup> Jonathan I. Epstein,<sup>2</sup> Janet E. Kuhlman,<sup>1</sup> and Charles B. Brendler<sup>3</sup>

Urachal neoplasms are characterized by their typical location in the midline position within the space of Retzius and their predominant extravesical extension. Prognosis is poor and differentiation from other neoplasms and nonneoplastic processes is important for determining both prognosis and treatment. Entities such as infected urachal cysts and primary bladder carcinomas arising in the apex occasionally have a similar appearance. In addition, ovarian and gastrointestinal neoplasms, as well as inflammatory gastrointestinal masses from Crohn disease or diverticulitis, can rarely occur in this location. This case illustrates how an inflammatory mass resulting from uterine perforation can simulate a urachal neoplasm and, in patients with known uterine manipulation, must be included in the differential diagnosis of vesical dome masses.

## Case Report

This 32-year-old woman, 0-0-2-0 (term-premature-aborted-living), underwent pelvic sonography 6 months after her second spontaneous abortion. It revealed an enlarged uterus, multiple fibroids, and a mass in the dome of the bladder (Figs. 1A-1C). CT (Fig. 1D) confirmed a mass in the bladder dome extending anteriorly toward the rectus muscle, compatible with a urachal carcinoma. Cystoscopy revealed a 2-cm mass, apparently extrinsic, eroding into the bladder dome with normal overlying mucosa. During surgery, the umbilicus and urachus were found to be unremarkable. A mass, however, was encountered between the dome of the bladder and the uterus. This

extended submucosally into the bladder. Further dissection revealed a 3 × 2 × 2 cm necrotic mass within the myometrium that was thought to be the primary site of carcinoma. Pathologic examination of the resected area revealed marked acute and chronic inflammation with prominent xanthomatous reaction. The uterus and dome of the bladder had areas of necrobiosis, often seen in traumatic injury [1]. There was no evidence of tumor. On further questioning, the patient confirmed that a dilatation and curettage had been performed 6 months earlier, after her second spontaneous abortion. The patient complained of severe dysuria after that procedure, during which perforation of the uterus and bladder is presumed to have occurred.

## Discussion

The differential diagnosis for vesical dome masses has included urachal neoplasms, urachal cysts, vesical and ovarian tumors, and gastrointestinal malignant neoplasms and inflammatory masses. Urachal cancer is a rare malignancy, accounting for less than 0.34% of all bladder cancers [2]. Ninety-five percent are mucin-producing adenocarcinomas, and the remaining 5% include transitional, squamous, and anaplastic cell carcinomas [3]. The sites of origin are juxtavesical or intravesical (90%), at the middle (6%), and near the umbilicus (4%) [4]. They typically involve the anterior bladder dome and exhibit predominantly extravesical growth along the urachus. Fifty to seventy percent have calcifications [2, 5]. They invariably lie exactly midline or slightly off midline. Densities vary between solid, cystic, and mixed. Urachal

Received August 25, 1989; accepted after revision November 21, 1989.

<sup>1</sup> The Russell H. Morgan Department of Radiology and Radiological Science, The Johns Hopkins Medical Institutions, 600 N. Wolfe St., Baltimore, MD 21205. Address reprint requests to E. K. Fishman.

<sup>2</sup> Department of Pathology, The Johns Hopkins Medical Institutions, Baltimore, MD 21205.

<sup>3</sup> Department of Urology, The Johns Hopkins Medical Institutions, Baltimore, MD 21205.

AJR 154:741-743, April 1990 0361-803X/90/1544-0741 © American Roentgen Ray Society

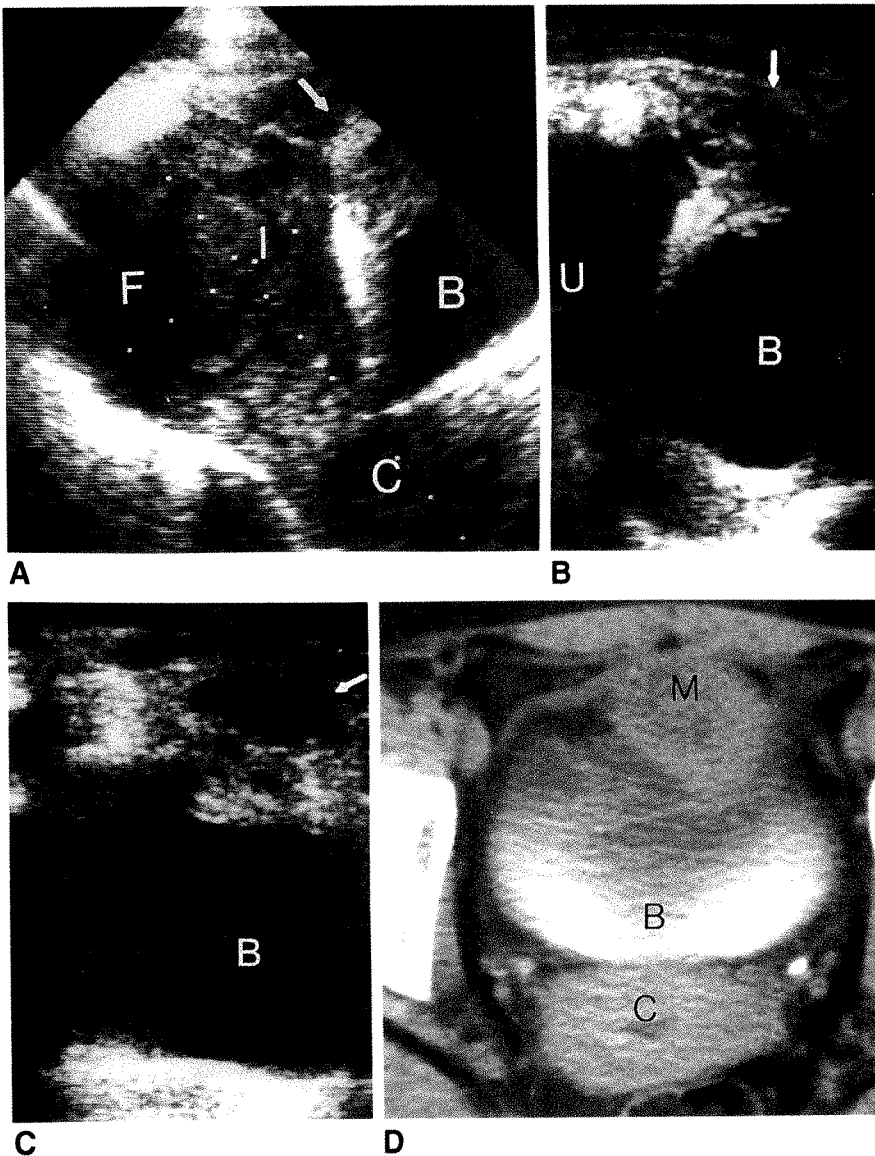


Fig. 1.—A, Sagittal sonogram reveals a mass (arrow) in dome of bladder (B). Fibroids and a component of inflammatory infiltrate (I) are noted in anterior portion of uterus. Bright echoes posterior to mass were thought to represent bowel gas. C = cervix, F = uterine fundus.

B and C, Sagittal (B) and transverse (C) images obtained with a linear-array transducer show mass (arrow) in dome of bladder (B). U = uterus.

D, CT scan shows a 2.5 × 2 × 3 cm mass (M) extending anteriorly from dome of bladder (B). C = cervix.

neoplasms usually occur between the ages of 40 and 70, and hematuria is the most common symptom, followed by a palpable suprapubic mass, abdominal pain, dysuria, and umbilical discharge [5]. Treatment is usually an en-bloc partial or total cystectomy with pelvic lymphadenectomy and umbilectomy [6].

Urachal cysts result from incomplete obliteration of the urachal lumen during gestation. They typically occur in the portion of the remnant adjacent to the bladder and are usually asymptomatic unless they become infected. Infected cysts usually occur in children and young adults. Fever, suprapubic pain, and dysuria are the common symptoms. CT usually shows a mass involving the dome of the bladder with a fluid-filled center [7]. The younger age of onset, the lack of hematuria or calcifications, and the presence of inflammatory changes in surrounding tissues favor the diagnosis of infected urachal cyst over carcinoma [4]. Treatment consists of primary drainage of the abscess cavity, followed by interval excision of the remnant.

Vesical dome carcinoma accounts for 6% of all vesical tumors. Transitional cell carcinoma predominates, but adenocarcinoma, squamous, and mixed-type carcinomas may occur. Vesical dome tumors typically show predominantly intravesical growth and are less likely to be midline. There are usually no associated calcifications [2]. These findings aid in differentiating this tumor from a urachal neoplasm. Treatment for transitional cell carcinoma is either transurethral resection or total cystectomy, depending on the stage.

Local invasion or metastatic involvement of the bladder dome may result from adenocarcinoma of the ovary, prostate, cervix, or gastrointestinal tract. However, usually this occurs late in the course of the disease, and the primary site has often been determined by other means [8].

Perforation of the uterus is a rare complication of dilatation and curettage. In this case, the resulting inflammatory mass simulated a urachal carcinoma. It exhibited primarily extravascular extension along the midline, within the space of Retzius (bounded by the transversalis fascia ventrally and the perito-

neum dorsally). The lack of calcifications and the patient's age, although not typical for urachal carcinoma, were not sufficient reasons to exclude the diagnosis. A history of recent uterine surgical manipulation is therefore important in suggesting an alternative diagnosis. The patient was treated with urachal resection, partial cystectomy, and partial uterine resection. The surgical approach and extent of resection would have been altered had the correct preoperative diagnosis been made.

The differential diagnosis for vesical dome masses has included urachal carcinoma and cysts, primary bladder cancer, ovarian tumors, and occasionally gastrointestinal malignant neoplasms and inflammatory masses. This case illustrates how a perforated uterus after dilatation and curettage can result in an inflammatory mass that presents in a similar location and exhibits features compatible with a urachal neoplasm. For both prognostic and treatment purposes, the

question of recent uterine manipulation must be raised in the evaluation of vesical dome masses.

#### REFERENCES

1. Herbold DR, Frable WJ, Kraus FT. Isolated noninfectious granulomas of the ovary. *Int J Gynecol Pathol* **1984**;2:380-391
2. Narumi Y, Sato T, Kuriyama K, et al. Vesical dome tumor: significance of extravesical extension on CT. *Radiology* **1988**;169:383-385
3. Baumgartner B, Frederick M, Austin M. Adenocarcinoma of the urachus with vesicocenteric fistula. *Urol Radiol* **1984**;6:55-57
4. Rao B, Scanlon K, Hinke M. Abdominal case of the day. *AJR* **1986**;146:1074-1079
5. Brick S, Friedman A, Pollack H, et al. Urachal carcinoma: CT findings. *Radiology* **1988**;169:377-381
6. Korobkin M, Cambier L, Drake J. Computed tomography of urachal carcinoma. *J Comput Assist Tomogr* **1988**;12:981-987
7. Goldman I, Caldamone A, Gauderer M, Hampel N, Wesselhoeft C, Elder J. Infected urachal cysts: a review of 10 cases. *J Urol* **1988**;140:375-378
8. Sheldon C, Clayman R, Gonzalez R, Williams R, Fraley E. Malignant urachal lesions. *J Urol* **1984**;131:1-8

## Book Review

**Radiographic Measurements.** By Robert D. Rosenberg. Philadelphia: Lippincott, 125 pp., 1989. \$14.95, softcover

This small, compact, spiral-bound, softcover book is intended as a pocket-sized manual of practical radiographic measurements. Its author has tried to produce a concise source of useful clinical information. The book fulfills these goals.

The manual has 10 chapters, a bibliography, and an index. The first chapter provides brief overviews of Bayes' theorem and the definitions of standard deviations and then lists various radiation doses from diagnostic radiology and nuclear medicine examinations. This chapter also includes concise enumerations of occupational and nonoccupational radiation dose limits, as well as a useful conversion table of dose units (curies, rems, sieverts, grays, and so forth). Chapters 2 through 10 provide values for radiographic measurements, tables, and diagrams specific to the areas of obstetric and gynecologic sonography, neuroradiology, cardiovascular system, mammography, gastrointestinal system, genitourinary system, musculoskeletal system, endocrine organs, and nuclear medicine. The largest parts of the book are devoted to measurements used in obstetrics and gynecology (44 pages) and in examinations of the musculoskeletal system (22 pages). Minimal emphasis is placed on mammography and the genitourinary system (two pages each).

The main strength of this book is its concise, compact nature. It is extremely easy to find a measurement and extract it for use. Because of its structure, the book is not encyclopedic or all-inclusive. Most departments still will require a standard reference, such as *Atlas of Roentgenographic Measurements*, by Keats and Lusted, to find more uncommonly used measurements or to understand the actual techniques of acquiring the measurements. Because of its brevity, this manual omits descriptions of standardized techniques used to acquire the radiographs for measurement and detailed descriptions of the techniques or pitfalls of measurements. The manual fulfills its goals of providing a concise and portable book of useful, practical measurements. The bibliography is extensive and current. It is perhaps most useful to have this manual available at the viewbox; it will be used most frequently by radiology residents and other clinical house staff. The price, in today's expensive book marketplace, is relatively modest.

Robert A. Clark  
H. Lee Moffitt Cancer Center and Research Institute  
Tampa, FL 33682-0179

# Early and Late Bone-Marrow Changes After Irradiation: MR Evaluation

Susan K. Stevens<sup>1,2</sup>  
 Sheila G. Moore<sup>1</sup>  
 Irving D. Kaplan<sup>3</sup>

Knowledge of the chronologic evolution of bone-marrow changes during and after radiation therapy is essential in differentiating normal postradiation changes from other marrow abnormalities. The appearance of the lumbar vertebral bone marrow was studied on 55 serial spin-echo and short-T1 inversion-recovery (STIR) MR images obtained in 14 patients receiving radiation therapy for Hodgkin disease, seminoma, or prostate carcinoma. Images were obtained before, at weekly intervals during, and at various monthly intervals up to 14 months after a 3- to 6-week course of fractionated paravertebral lymph-node irradiation of 1500–5000 rad (15–50 Gy). During the first 2 weeks of therapy, there was no definite change in the appearance of the marrow on spin-echo images; however, there was an increase in signal intensity on the STIR images, apparently reflecting early marrow edema and necrosis. Between weeks 3 and 6, the marrow showed an increasingly heterogeneous signal and prominence of the signal from central marrow fat, shown best on T1-weighted images. Late marrow patterns (6 weeks to 14 months after therapy) varied and consisted of either homogeneous fatty replacement or a band pattern of peripheral intermediate signal intensity, possibly representing hematopoietic marrow surrounding the central marrow fat. No focal marrow lesions or soft-tissue edema were identified during the course of radiation therapy; their presence should raise the possibility of the presence of a pathologic process other than radiation change.

These data suggest that MR can detect radiation-induced marrow changes as early as 2 weeks after starting therapy, and that there are at least two distinct types of late marrow MR patterns.

*AJR* 154:745–750, April 1990

MR imaging has been shown to be a useful technique in the evaluation of bone marrow. Studies using both spin-echo and chemical-shift imaging techniques to show marrow changes in response to radiation therapy have reported bright signal intensity within vertebral marrow on T1-weighted and out-of-phase images. This bright marrow signal is thought to represent fatty infiltration after radiation therapy [1–4]. Marrow changes correspond to the boundaries of the radiation portals and have been detected as early as 9 days after completion of a month-long course of radiation therapy [1].

Although the appearance of acute radiation changes in marrow on MR images has been described in patients receiving fractionated total body irradiation [5, 6], these findings are complicated by simultaneous bone-marrow transplantation and do not necessarily represent changes that will be seen in patients not receiving transplants. No current knowledge of the chronologic evolution of the MR appearance of early marrow changes after fractionated localized radiation therapy exists. In order to determine the spectrum of appearances of normal marrow on MR imaging in the first days and weeks as well as several months after institution of radiation therapy, we conducted a prospective study evaluating the lumbar vertebral marrow of 14 patients receiving incidental radiation to otherwise normal vertebral bodies.

Received August 14, 1989; accepted after revision November 7, 1989.

Presented at the annual meeting of the American Roentgen Ray Society, New Orleans, May 1989.

<sup>1</sup> Department of Diagnostic Radiology, Felix Bloch Laboratory, Stanford University Medical Center, Room S-052, Stanford, CA 94305-5105. Address reprint requests to S. G. Moore.

<sup>2</sup> Present address: Department of Radiology, University of California School of Medicine, University of California at San Francisco, San Francisco, CA 94143.

<sup>3</sup> Department of Radiation/Oncology, Stanford University Medical Center, Stanford, CA 94305.

0361-803X/90/1544-0745

© American Roentgen Ray Society

**TABLE 1: Summary of Patients Undergoing Radiation Therapy**

Diagnosis/Case No.	Age	Radiation Therapy		Days of MR <sup>b</sup>
		Dose <sup>a</sup> (rad)	Duration (weeks)	
Hodgkin disease				
1	45	3990	5	−25, 1, 21, 28, 35
2	26	4020	5	0, 8, 16, 22, 390
3	26	4020	5	9, 17, 24, 379
4	17	4050	5	0, 8, 23, 36, 420
5	41	4380	6	79, 136, 199, 339
6	38	4400	5	190
7	73	3600	6	180, 281
8	49	4385	5	−1, 24, 31, 141
9	13	1500	6	0, 9, 15, 84
10	33	4400	5	−10, 3, 35
Seminoma				
11	34	3000	3	0, 10, 17, 24, 73
12	39	3090	3	0, 8, 15, 22, 53
Prostate cancer				
13	70	5000	6	20, 24, 34, 46
14	68	5000	6	10, 23, 36, 42

Note.—Chemotherapy had been administered previously in three cases: Adriamycin, bleomycin, vinblastine, and dacarbazine in cases 8–10 and, in addition, nitrogen mustard, Oncovin, procarbazine, and prednisone in cases 9 and 10.

<sup>a</sup> 180–200 rad (1.8–2 Gy)/day when administered.

<sup>b</sup> Days after starting radiation therapy.

## Subjects and Methods

Fifty-five MR examinations of the lumbar spine in 14 patients 13–73 years old were performed with a 0.38-T resistive magnet (RX 4000, Resonex, Sunnyvale, CA). Patients were imaged before and during a 3- to 6-week course of fractionated paravertebral lymph-node irradiation for either Hodgkin disease, seminoma, or prostate carcinoma. Patients were screened with either bone scans, bone-marrow biopsies, or CT prior to receiving radiation and were found to have no evidence of marrow disease. Three patients received a 4-week course of chemotherapy 2–4 weeks before starting their course of radiation therapy, at which time peripheral blood counts were normal. These patients had not had MR scans before receiving chemotherapy. Clinical data are summarized in Table 1.

Sagittal spin-echo T1-weighted, 300/30,75 (TR/TE), and T2-weighted, 2000/30,75, images were obtained by using 10-mm-thick slices with a 20% gap between consecutive sections. Ten and two acquisitions were obtained for T1- and T2-weighted images, respectively, with a 256 × 256 image matrix. In addition to spin-echo imaging, short-T1 inversion-recovery (STIR) images, 1500/100/30 (TR/TI/TE), were obtained. Two averages were acquired with a 256 × 256 image matrix. Patients were imaged before the onset of radiation therapy, weekly for 4–6 weeks, and at various monthly intervals up to 14 months thereafter. Not every patient was imaged during every time interval, however, and in three patients the first MR scan was obtained 6 or more weeks after starting irradiation (Table 1).

Data were analyzed by using an intensity grading system. For spin-echo images, a grade 1 signal intensity was given to the marrow if the marrow signal intensity was equal to that of muscle, a grade 2 signal intensity was given to the marrow if the signal intensity of the marrow was greater than that of muscle but less than that of fat, and a grade 3 signal intensity was given to the marrow if the marrow signal intensity was equal to that of fat (fatty marrow). In addition to a signal-intensity grade, homogeneity or heterogeneity of the marrow, as well as the presence or absence of surrounding soft tissue or disk edema, were noted. Edema of the soft tissues or intervertebral disk was considered present if increased signal intensity on T2-weighted spin-echo images with corresponding intermediate to low signal

intensity on T1-weighted images and/or increased signal intensity on STIR images were seen.

T1 and T2 relaxation times of vertebral marrow were calculated from the spin-echo images. T1 relaxation time was calculated by using successive approximation to fit the acquired data to an exponential curve based on the signal strength acquired for two different values of TR. T2 relaxation time was calculated by using the signal-intensity measurements for two different TEs and the assumption that hydrogen, TR, and T1 are constant. Signal strength is therefore proportional to  $\exp(-TE/T2)$  [7]. The regions of interest used in calculating the relaxation times included all vertebral marrow from L1 through L5 shown on any particular image, provided the vertebral body was not near the edge of the coil. Discrete central areas of marrow were measured for each vertebral body; care was taken not to include disk or posterior spinous ligaments. In each case the individual regions of interest consisted of more than 40 pixels, with an average standard deviation of calculated relaxation times of less than 10%. Statistical analysis of the calculated T1 and T2 relaxation times as a function of time after institution of radiation therapy was performed by using the sign test.

Pathologic specimens for correlation with the MR findings were not obtained from any of our patients during the course of radiation therapy, as none of our patients had evidence of tumor involvement of the marrow when irradiation was initiated. Patients were monitored with serial blood chemistries, complete blood counts, and chest and plain abdominal radiographs. No patient showed evidence of clinical disease immediately after the course of irradiation, and the four patients imaged 1 year or more after receiving radiation therapy were all disease-free at the time of their last MR scan.

## Results

### Spin-Echo Imaging

The appearance of the bone marrow on T1-weighted spin-echo images essentially did not change during days 1–10 after the institution of radiation therapy in six of seven patients



imaged. The marrow signal intensity remained either equal to or greater than that of muscle but less than that of fat, depending on the signal intensity of the marrow before therapy. Between days 11 and 24, there was either no change in the appearance of the marrow (five of 11 patients) or there was a slight increase in the amount of central fat (six of 11 patients). Between weeks 3 and 6, the most consistent changes were either increasing heterogeneity of the marrow (four of 10 patients) or an increase in the central marrow fat (six of 10 patients). The earliest detectable increase in signal intensity on T1-weighted images occurred on day 8; by 6 weeks after the initiation of radiation therapy, increased signal intensity and evidence of early fatty infiltration were seen in all but one of the 11 patients imaged (Fig. 1). From week 6 onward this heterogeneous marrow pattern evolved in one of two ways: either it became progressively homogeneous with fairly diffuse bright signal intensity or it developed into a band pattern with a peripheral region of intermediate signal intensity

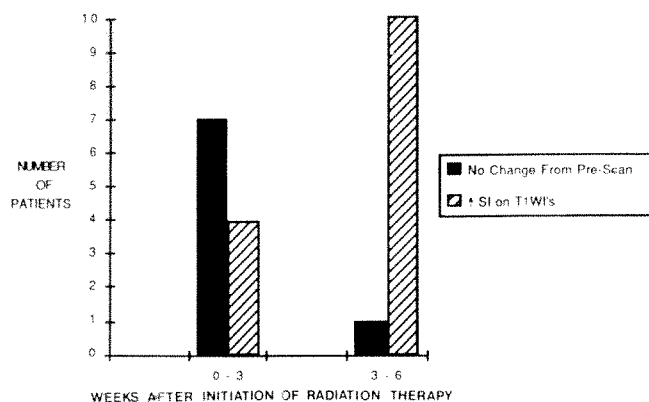


Fig. 1.—Time of initial appearance of increased signal intensity (SI) on T1-weighted images (T1WI's), indicating replacement by fatty marrow. Pre-scan = scan obtained before irradiation.

surrounding a central zone of bright signal intensity. In half of our patients imaged more than 6 weeks after radiation therapy was started, the homogeneous pattern of diffusely increased signal intensity developed (Fig. 2); in the other half, the band pattern developed (Fig. 3). Those who manifested the late marrow band pattern were slightly younger (age range, 13–39 vs 34–73) than those exhibiting the homogeneous pattern. Of those who developed the late band pattern, two-thirds (four of six) had homogeneous marrow before receiving radiation; the other third had a heterogeneous or a bandlike pattern. Of those who developed the late homogeneous marrow pattern, four of six initially had homogeneous marrow; the other two had heterogeneous preradiation marrow. Both marrow patterns were seen at all radiation doses with two exceptions: the homogeneous pattern only was identified in the two patients receiving 5000 rad (50 Gy) for prostate carcinoma, and the band pattern only was noted in the single child receiving 1500 rad (15 Gy) (Fig. 4).

Prior chemotherapy appeared to have no effect on determining which marrow pattern ultimately developed. Of the three patients who had received chemotherapy (all of whom had Hodgkin disease), marrow patterns before and after irradiation changed from heterogeneous to homogeneous, homogeneous to heterogeneous, and remained heterogeneous in patients aged 49, 33, and 13 years, respectively.

T2-weighted images during the first 21 days of radiation therapy showed either no change (six of 11 patients) or a subtle increase in signal intensity in the marrow suggesting edema and/or necrosis (five of 11 patients). During weeks 3–6, there was either no change in the marrow (six of 10 patients) or the emergence of a mottled pattern of intermediate signal intensity greater than that of muscle but less than that of fat (four of 10 patients); this appearance either remained unchanged or became more homogeneous at time points more than 6 weeks after starting radiation therapy.

No focal marrow lesions were seen at any time during or after the course of radiation therapy. There was no evidence

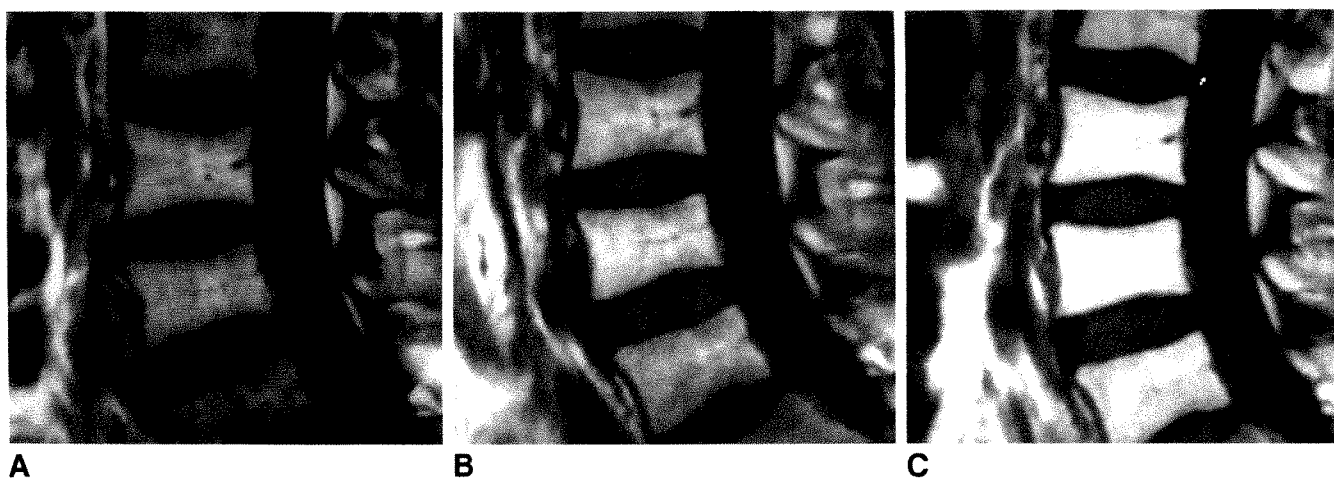


Fig. 2.—Sagittal T1-weighted spin-echo images (300/30) of lumbar spine in 34-year-old patient with seminoma.

A, Before radiation therapy.

B and C, 24 (B) and 73 (C) days after initiation of radiation therapy. Note evolution of homogeneous marrow pattern with increased signal intensity.

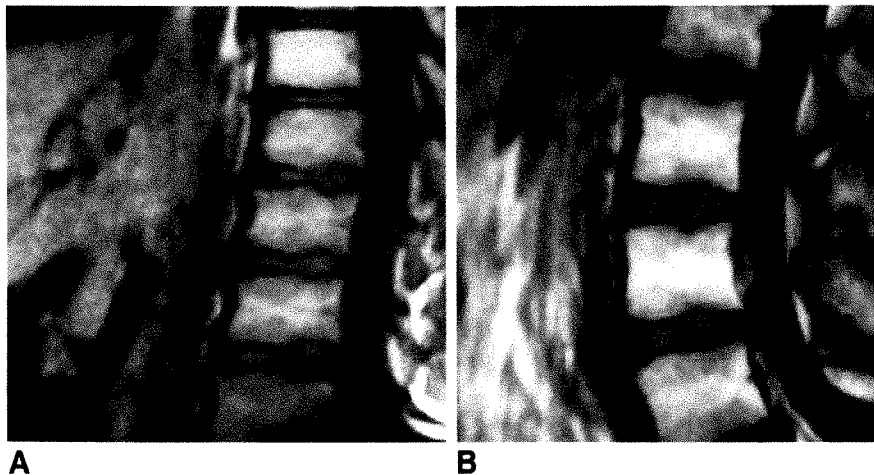


Fig. 3.—A and B, T1-weighted images (300/30) of 17-year-old patient with Hodgkin disease before (A) and 14 months after (B) 4050 rad (41 Gy) to lumbar spine. Peripheral zone of intermediate/low signal intensity surrounds central marrow fat.

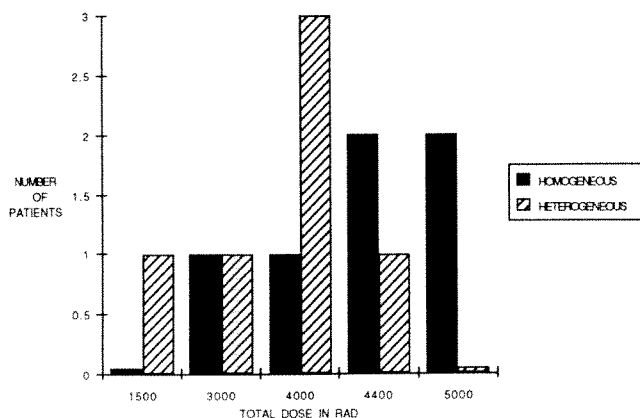


Fig. 4.—Type of late (6 weeks after initiation of radiation therapy) marrow pattern observed according to total dose of radiation received.

of edema in the soft tissues or intervertebral disks on T2-weighted images in any of the patients.

#### STIR Imaging

On the STIR images there was an increase in signal intensity of the vertebral marrow (greater than fat, less than or equal to fluid) appearing at various times between days 7 and 24, with a peak incidence 9 days after initiation of radiation therapy. This increase in signal intensity was seen in nine of the 10 patients who underwent STIR imaging in the first 3 weeks after starting radiation therapy. From weeks 3 through 6, there was a progressive decrease in signal intensity of the vertebral marrow in all patients, and heterogeneity was noted in five of nine. After 6 weeks, two marrow patterns evolved: patients who manifested the late fatty homogeneous marrow pattern on T1-weighted images exhibited diffusely decreased signal intensity on the STIR images; those whose marrow demonstrated the late band pattern of peripheral intermediate signal intensity and central increased signal intensity on T1-weighted images showed reciprocal changes on STIR images consisting of a peripheral zone of bright signal intensity alternating with a central region of low signal intensity (Figs. 5 and 6). In all but two patients, postradiation fatty infiltration of the

marrow was detectable on the STIR images at the same time that it was noted on the T1-weighted images. In the two exceptions, increased-signal-intensity fatty infiltration on T1-weighted images was seen approximately 2 weeks sooner than the decrease in signal intensity on the STIR images.

#### Relaxation Times

T1 and T2 relaxation times were calculated and plotted as a function of time after institution of radiation therapy. There was a trend toward an increase in T1 relaxation time within the first 3 weeks after radiation therapy, but this was not statistically significant. No discernible pattern in T2 relaxation time was seen (Fig. 7).

#### Discussion

Several studies describing the initial effects of localized irradiation on both the histologic structure and hematopoietic function of bone marrow have already been reported [8]. Although Lehar et al. [9] described dramatic reductions in cellularity in the first 16 days after 2000 rad (20 Gy) of localized radiation therapy for breast, lung, and esophageal carcinoma, their study did not evaluate marrow changes beyond this time. Knospe et al. [10] described the histologic effects of a single dose of 2000–10,000 rad (20–100 Gy) of localized radiation therapy to rat bone marrow observed from 24 hr to 1 year after treatment. At 2000 rad (20 Gy) they reported an initial uniform depression of marrow cellularity with disruption of the sinusoids, edema, and hemorrhage within the first week. There was a subsequent increase in hematopoietic activity as well as an increase in marrow cellularity during the second week, postulated to represent an influx of cells from remote unirradiated areas. A concomitant increase in fatlike material was seen. At 1–3 months, marrow cellularity as well as the number of marrow sinusoids were decreased. Endosteal fibrosis was also noted. At 6 months, evidence was present of both hematopoietic and sinusoidal regeneration.

We found characteristic MR changes in lumbar vertebral marrow following localized radiation therapy; this may reflect some of the findings noted on pathologic examination. Little change was seen in signal intensity of the vertebral marrow

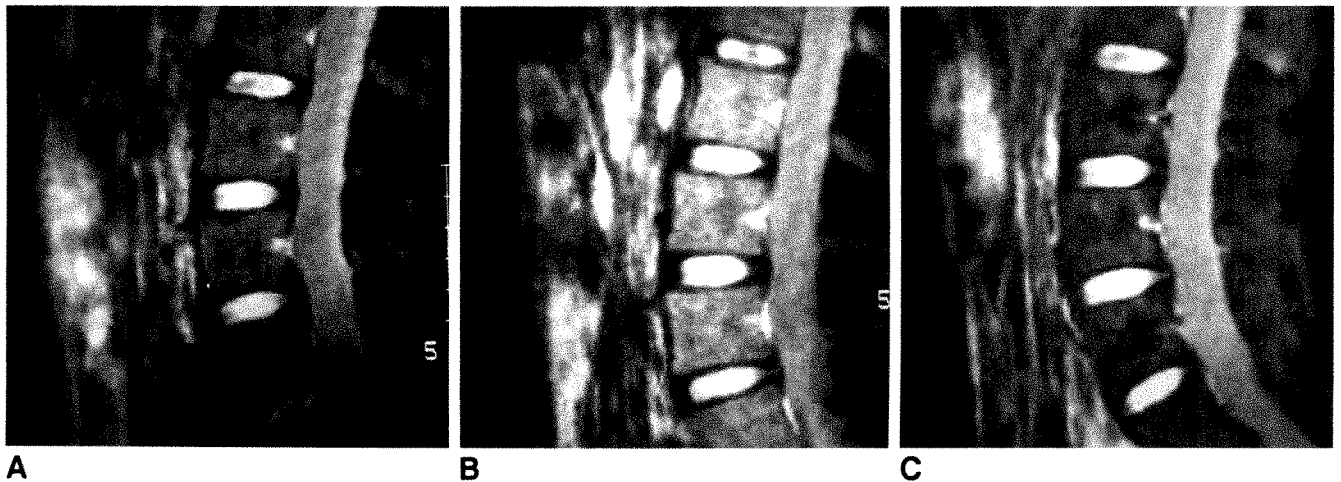


Fig. 5.—A–C, STIR images (1500/100/30) of 33-year-old Hodgkin disease patient before irradiation (A) and at 3 (B) and 35 (C) days after initiation of 4400 rad (44 Gy) paravertebral lymph-node irradiation. Diffusely increased signal intensity represents edema on day 4 compared with pretherapy scan. By day 36 (C), decreased signal from central marrow fat is seen.

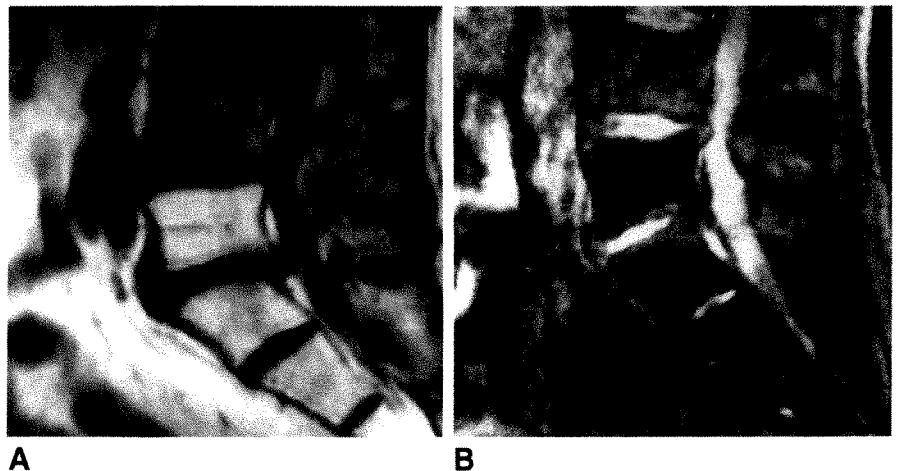


Fig. 6.—A and B, T1-weighted, 300/30 (A), and STIR, 1500/100/30 (B), images of lower lumbar spine in 70-year-old patient with prostate carcinoma 46 days after initiating a 6-week course of 5000 rad (50 Gy). Diffusely homogeneous bright signal intensity on T1-weighted image corresponds to identical region of decreased signal intensity on STIR image.

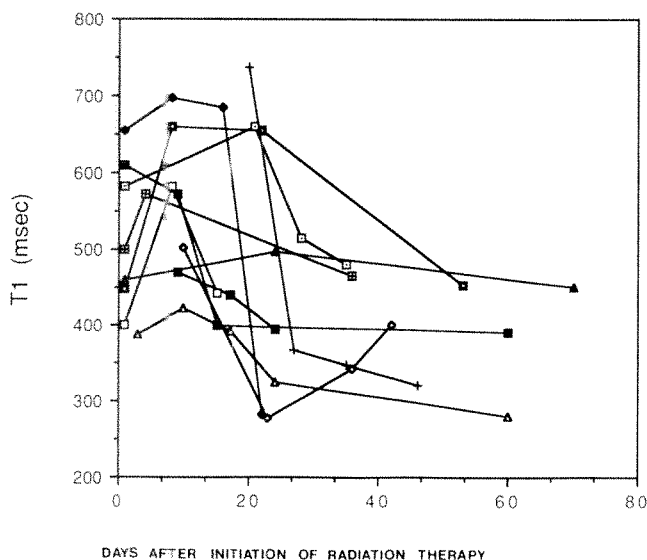


Fig. 7.—Calculated T1 relaxation time as a function of time after institution of radiation therapy for individual patients.

on the spin-echo images within the first 3 weeks after radiation therapy in most of the patients; however, on STIR images, an increase in signal intensity was noted during this time, which may reflect early cellular edema and hemorrhage as well as the early influx of unirradiated cells suggested in the report of Knospe et al. [10]. T2-weighted images were less useful in evaluating marrow changes than either T1-weighted or STIR images because of a loss of appreciable contrast between the increased-signal-intensity red marrow and decreased-signal-intensity fatty marrow on the second echo of the T2-weighted sequence.

In most patients, a heterogeneous pattern of mottled marrow developed by week 3. The heterogeneous pattern of the vertebral marrow in some cases was dominated by a predominance of central fat surrounding the basivertebral vein. Between weeks 3 and 6 the pattern of either diffusely heterogeneous vertebral marrow or marrow with a predominance of central fat persisted and often became more pronounced. Three to six weeks also corresponds to the time when pathologic changes consisting of decreased marrow cellularity, marrow healing, and regeneration of fatty marrow are

seen. The MR findings of heterogeneous low and high signal intensity would therefore appear to correspond with fibrosis and fat infiltration, although direct pathologic correlation is needed for confirmation.

Half of our patients developed a late (6-week after therapy) homogeneous pattern of diffusely increased signal intensity representing diffuse fatty infiltration. This is a pattern that has been described previously [1, 2]. However, the other half of our patients developed a band pattern of peripheral intermediate signal intensity with central increased-signal-intensity marrow surrounding the basivertebral vein, which may represent peripheral hematopoietic marrow with central marrow fat. This pattern has not been reported previously. We saw the band pattern in our younger patients, suggesting the possibility that the ability of marrow to regenerate after radiation therapy may be age-dependent [11]. The appearance of a late band pattern in our younger patients that was identical to that noted in regenerating vertebral marrow of bone-marrow-transplant patients suggests the possibility of a similar pattern of hematopoietic regeneration in these two populations, possibly related to vertebral blood flow after reconstitution of the marrow sinusoids [6, 8, 12–15]. Histopathologic evaluation of the lumbar vertebral bodies in our patient population would be necessary for definitive correlation.

The effect of radiation dose on late marrow pattern was not elucidated in our study. Patients developed homogeneous and band marrow patterns at all doses of radiation therapy administered, with the exceptions that the youngest patient (a 13-year-old who received a total radiation dose of 1500 rad [15 Gy]) developed a band pattern and the prostate carcinoma patients exhibited homogeneous patterns only. Whether the findings seen in the patients with prostate carcinoma are due to the fact that these patients were older (mean age, 69), received a higher dose of radiation therapy (5000 rad [50 Gy]), or received pelvic irradiation remains unknown. Knospe et al. [16] found similar results: In four of five patients with Hodgkin disease who were imaged with  $^{52}\text{Fe}$  bone-marrow scanning 24 months after radiation therapy to both mantle and pelvis, there was greater residual inhibition of erythropoiesis in the pelvic field than in the mantle field.

The patients who had undergone chemotherapy before irradiation did not show early or late marrow patterns different from those who had not received chemotherapy. It should be noted that our population size is small (three patients), and further studies are necessary to evaluate fully the effects of chemotherapy prior to radiation therapy in determining the marrow pattern after irradiation.

Finally, we saw no evidence of focal marrow lesions in any of our patients, nor was there any soft-tissue or intervertebral-disk edema. The presence of focal spinal lesions or soft-tissue edema should raise the possibility of a metastatic lesion or other abnormality after radiation therapy including radiation necrosis.

#### ACKNOWLEDGMENTS

We thank Lincoln Moses for statistical analysis, Michelle Gaudette and Neal Duenas for valuable contributions, and Mark Riesenberger and Ann McGrath for assistance in manuscript preparation.

#### REFERENCES

1. Remedios PA, Colletti PM, Raval JK, et al. Magnetic resonance imaging of bone after radiation. *Magn Reson Imaging* **1988**;6:301–304
2. Ramsey RG, Zacharias CE. MR imaging of the spine after radiation therapy: easily recognizable effects. *AJR* **1985**;144:1131–1135
3. Wismer GL, Rosen BR, Buxton R, Stark DD, Brady TJ. Chemical shift imaging of bone marrow: preliminary experience. *AJR* **1985**;145:1031–1037
4. Nyman R, Rehn S, Glimelius B, et al. Magnetic resonance imaging in diffuse malignant bone marrow diseases. *Acta Radiol [Diagn] (Stockh)* **1987**;28(2):199–205
5. McKinstry CS, Steiner RE, Young AT, Jones L, Swirsky D, Aber V. Bone marrow in leukemia and aplastic anemia: MR imaging before, during, and after treatment. *Radiology* **1987**;162:701–707
6. Stevens SK, Moore SG. MR imaging of marrow after transplantation. *Radiology* **1988**;169(P):192
7. Dooms GC, Hricak H, Mosely ME, Bottles K, Fisher M, Higgins CB. Characterization of lymphadenopathy by magnetic resonance relaxation times: preliminary results. *Radiology* **1985**;155:691–697
8. Rubin P. Hematopoietic tissues and blood. In: Rubin P, Casarett GW, eds. *Clinical radiation pathology*, vol. 2. Philadelphia: Saunders, **1968**:778–849
9. Lehar TJ, Kiely JM, Pease GL, Scanlon PW. Effect of focal irradiation on human bone marrow. *AJR* **1966**;96:183–190
10. Knospe WH, Blom J, Crosby WH. Regeneration of locally irradiated bone marrow. I. Dose dependent, long-term changes in the rat, with particular emphasis upon vascular and stromal reaction. *Blood* **1966**;28:398–415
11. Sacks EL, Goris ML, Glatstein E, Gilbert E, Kaplan HS. Bone marrow regeneration following large field radiation. *Cancer* **1978**;42:1057–1065
12. Sabin FR. Bone marrow. *Physiol Rev* **1928**;8:191–244
13. DeBruyn PPH, Breen PC, Thomas TB. The microcirculation of the bone marrow. *Anat Rec* **1970**;168:55–68
14. Crock HV, Yoshizawa H. The blood supply of the lumbar vertebral column. *Clin Orthop* **1976**;115:6–21
15. VanDyke D. Similarity in distribution of skeletal blood flow and erythropoietic marrow. *Clin Orthop* **1967**;52:37–51
16. Knospe WH, Rayudu VMS, Cardello M, Friedman AM, Fordham EW. Bone marrow scanning with  $^{52}\text{Fe}$  ( $^{52}\text{Fe}$ ). *Cancer* **1976**;37:1432–1442

## Cervical Spondylolysis: Imaging Findings in 12 Patients

David A. Forsberg<sup>1</sup>  
Salutario Martinez<sup>1</sup>  
James B. Vogler III<sup>2</sup>  
M. David Wiener<sup>1</sup>

Cervical spondylolysis is defined as a corticated cleft between the superior and inferior articular facets of the articular pillar, the cervical equivalent of the pars interarticularis in the lumbar spine. Associated dysplastic changes and spina bifida suggest that the lesion is congenital. It is a rare condition; only 70 cases have been previously reported in the world literature. Recognition of this disorder and differentiation from traumatic articular pillar fracture or dislocation is of paramount importance in patients who have had cervical spine trauma. The present study details radiologic features in 12 patients 20–80 years old with cervical spondylolysis. Plain film radiologic findings were correlated with hypocycloidal high-resolution tomography (nine patients), CT (six patients), and MR imaging (one patient). Seven patients had spondylolysis at C6 (three bilateral) and five had the abnormality at C4 (all unilateral). Nine of 12 patients were initially misdiagnosed. Characteristic radiologic features include (1) a well-marginated cleft between the facets, (2) a triangular configuration of the pillar fragments on either side of the spondylolytic defect, (3) posterior displacement of the dorsal triangular pillar fragment, (4) hypoplasia of the ipsilateral pedicle, (5) spina bifida at the involved level, and (6) compensatory hyper- or hypoplasia of the ipsilateral articular pillars at the level above and/or below the defect. A multistudy approach was often necessary to demonstrate these findings.

Heightened awareness of the radiologic features of cervical spondylolysis should allow one to differentiate it from articular pillar fracture or dislocation.

*AJR* 154:751–755, April 1990

Only 33 cases of cervical spondylolysis have been reported in the English language literature [1–21] since Perlman and Hawes [1] first described a case in 1951. Because of the rarity of this lesion, radiologic recognition can be difficult. Cervical spondylolysis is a corticated defect of the cervical articular masses between the facet joints. Associated findings have not been clearly defined, as the literature on the subject includes mostly case reports. The present study was undertaken to assess the characteristic radiologic findings of cervical spondylolysis. Multiple imaging techniques were evaluated.

### Materials and Methods

We reviewed the medical records and diagnostic imaging studies of 12 patients with cervical spondylolysis who were admitted to our institution between 1957 and 1989. Two of these patients have been reported previously [4]. Records were reviewed with attention to patient's age, sex, duration of symptoms, previous history of trauma, clinical diagnosis, and treatment. Cervical spine radiographs were available in all 12. Polytomograms were obtained in nine cases, CT scans in six cases, and MR images in one case. CT examinations were performed on GE 8800 or 9800 scanners. MR images were obtained on a 1.5-T Signa system (GE, Milwaukee, WI) with spin-echo pulse sequences. These images were reviewed retrospectively with attention to the following features: presence of a smoothly corticated cleft of the articular masses, configuration of the involved articular pillar, spinal alignment, pedicle

Received October 19, 1989; accepted after revision December 1, 1989.

Presented at the annual meeting of the American Roentgen Ray Society, New Orleans, May 1989.

<sup>1</sup> Department of Radiology, Box 3169, Duke University Medical Center, Durham, NC 27710. Address reprint requests to S. Martinez.

<sup>2</sup> Department of Radiology, Mayo Clinic Jacksonville, 4500 San Pablo Rd., Jacksonville, FL 32224.

0361-803X/90/1544-0751  
© American Roentgen Ray Society

morphology, configuration of the articular masses above and/or below the involved level, and presence of spina bifida.

Nine men and three women 20–80 years old composed the study group. Nine of the 12 presented after trauma (eight after motor vehicle accidents, one after left shoulder trauma). Three had nontraumatic neck pain of 1–5 years in duration. Nine cases were initially misdiagnosed, seven as fracture or dislocation, one as degenerative joint disease, and another as normal. All patients had normal physical examinations, with the exceptions of a 44-year-old man who had mildly decreased sensation to pinprick bilaterally in the C7 dermatomes and a 20-year-old man who had mild left shoulder weakness.

## Results

In each patient, only one cervical spine level displayed a spondylolytic defect. Half of our 12 patients had left unilateral spondylolysis, and three each had either right unilateral or bilateral cervical spondylolysis. The sixth cervical vertebra was affected most often (seven patients). Of these, three had bilateral cervical spondylolysis. The other cervical segment affected in this series was the fourth vertebra. All five of these patients displayed unilateral defects, four on the left and one on the right. Posterior displacement of a dorsal triangular fragment was observed in 10 patients. Hypoplastic ipsilateral pedicles and dysplasia of the ipsilateral articular processes above and/or below the level of the defects were found in all 12 patients. In seven patients spina bifida was observed. Only five had anterolisthesis, all less than 3 mm.

### Conventional Radiographic and Tomographic Findings

Lateral radiographs showed a deformed articular mass posterior to the rest of the cervical pillars in 10 of the 12 patients (Fig. 1). Of the remaining two patients, the abnormality could not be visualized. One had a shoulder artifact; in the other, no significant posterior displacement was noted.

Anterolisthesis of less than 3 mm was observed in five patients, three of whom had bilateral spondylolysis.

Oblique views showed deformed articular masses in all patients. A poorly defined, well-corticated vertical defect divided the articular masses into two irregular triangular fragments. The ventral fragment articulated with the facet above;

the dorsal fragment articulated with the subjacent facet (Fig. 2). Hypoplasia of the ipsilateral pedicle was evident in all cases (Fig. 2). Similarly, all patients had dysplastic changes of the ipsilateral articular pillar above and/or below the affected level. These changes were either hyperplastic or hypoplastic with irregular facet joints (Fig. 1). Hyperplastic pedicles above the spondylolytic level were observed in four instances. Enlargement of the ipsilateral vertebral foramen was seen in most of our patients.

Anteroposterior radiographs revealed spina bifida of the involved level in seven patients; however, this view was limited in showing other features (Fig. 3). The abnormal facet joints caused by the spondylolytic defect were visualized partially in only two patients. Similarly, the ipsilateral hypoplastic pedicle was difficult to identify (Fig. 3).

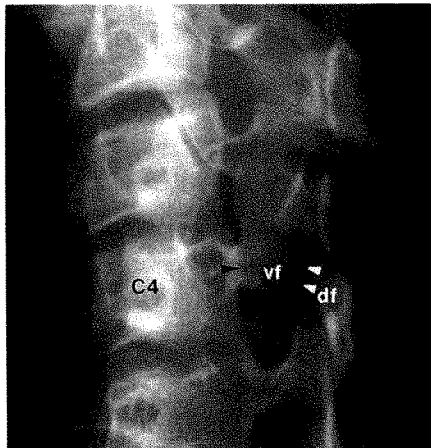
Tomographic evaluation of the cervical spine in both coronal and sagittal planes was performed in nine patients. In four patients, the coronal tomograms suggested the diagnosis of cervical spondylolysis. The inferior facet joint of the dysplastic articular mass was seen in a characteristic horizontal orientation (Fig. 4) because of the orientation of the two triangular fragments. Sagittal tomograms in all nine patients clearly showed apposition of two triangular fragments across a well-margined vertical defect creating the shape of a cleft bow tie (Fig. 5). Furthermore, posterior displacement of the dorsal triangular fragment and alignment changes in the adjacent facet articulations were well demonstrated. Although the cleft-bow-tie appearance was suggested on oblique radiographs in three patients (Fig. 2), the sagittal tomograms were conclusive and diagnostic in all nine.

## CT

Axial CT images provided useful anatomic information at the affected level in all six patients studied with this technique. CT showed a well-corticated, smoothly margined spondylolytic defect in the mid articular mass in all patients. The defect ran in the coronal plane, dividing the articular pillar into uneven ventral and dorsal fragments (Fig. 6). The dorsal fragment was more posterior than the contralateral normal



1



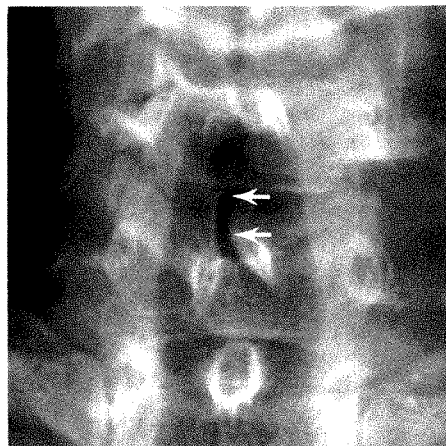
2

Fig. 1.—Bilateral C6 spondylolysis in a 32-year-old woman injured in a motor vehicle accident. Lateral cervical radiograph shows grade I anterolisthesis and posteriorly positioned, deformed articular mass (arrow). In this projection, similar features may be observed with a traumatic lesion.

Fig. 2.—Left C4 spondylolysis in a 20-year-old man injured in a motor vehicle accident. Oblique cervical radiograph shows well-margined cleft (white arrowheads) and ventral (vf) and dorsal (df) fragments forming characteristic cleft bow tie. Posteriorly positioned dorsal fragment articulates with subjacent articular process. Also shown is ipsilateral hypoplastic pedicle (black arrowhead). These features are diagnostic of spondylolysis.

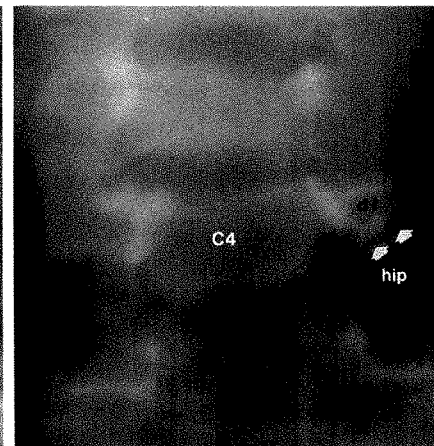


Fig. 3.—Right C6 spondylolysis in a 27-year-old man injured in a motor vehicle accident. Anteroposterior cervical radiograph shows spina bifida occulta at involved level (arrows), which should raise index of suspicion for cervical spondylolysis.

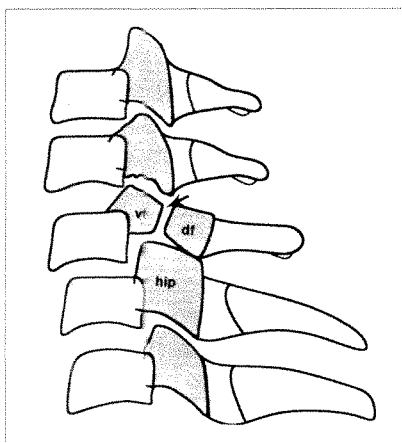


3

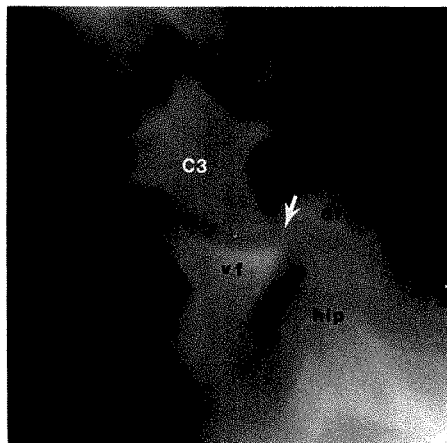
Fig. 4.—Left C4 spondylolysis in a 44-year-old man with a 5-year history of chronic neck pain. Coronal tomogram shows inferior facet joints (arrows) of dorsal spondylolytic fragment (df) articulating with hyperplastic inferior pillar (hip). Compare with contralateral normal articular pillar.



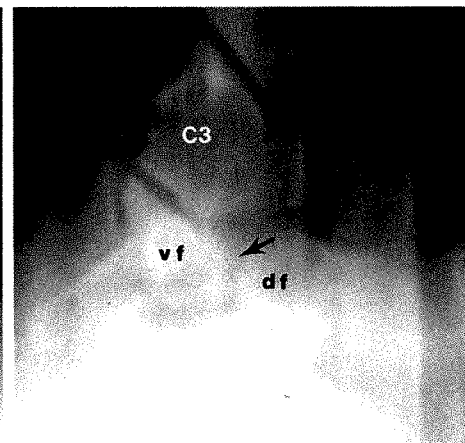
4



A



B



C

Fig. 5.—Diagram and sagittal tomograms show typical cleft-bow-tie configuration.

A, Drawing shows characteristic features of cervical spondylolysis in the sagittal plane: (1) articular mass cleft (arrow); (2) triangular configuration of ventral (vf) and dorsal (df) fragments, similar to a cleft bow tie; (3) posterior displacement of dorsal fragment, which articulates with compensatory hyperplastic inferior pillar (hip); and (4) anterior fragment, which articulates with superior dysplastic articular mass.

B, Left C4 spondylolysis in a 21-year-old man injured in a motor vehicle accident.

C, Left C4 spondylolysis in a 20-year-old man injured in a motor vehicle accident.

articular pillar. Hypoplasia of the ipsilateral pedicle also was seen in all patients. Similarly, four patients had a dysplastic ipsilateral lamina that was more horizontal than, posterior to, and smaller than the normal contralateral lamina (Fig. 6). Spina bifida was seen in three patients.

#### MR

One patient with cervical spondylolysis was studied with MR. The examination was nondiagnostic because of poor definition of the osseous anatomy. In another case of suspected cervical spondylolysis, MR was helpful in excluding this diagnosis. In this instance, the patient had neck pain after a motor vehicle accident. Conventional radiographs showed anterolisthesis, deformity of the articular processes, and posterior displacement of an apparent dorsal fragment. On to-

mography, a deformed articular mass simulated the configuration seen in cervical spondylolysis; however, no pillar cleft could be demonstrated (Fig. 7A). CT showed a deformed articular mass also without a cleft. The rest of the arch, including the pedicle, lamina, and spinous process, was normal (Fig. 7B). MR also showed a similar configuration but demonstrated contiguous marrow signal extending the length of the deformed articular mass, indicating a healed fracture (Fig. 7C) rather than a spondylolytic defect. On further questioning, this patient admitted to a previous neck fracture from a motor vehicle accident years before this admission.

#### Discussion

Seventy cases of cervical spondylolysis have been reported to date in the world literature [22–26]. The lesion occurs most

often at the C6 level (52 cases). Thirteen cases have been reported at C2, two at C3, seven at C4, and five at C5. Some patients had more than one level of involvement. To date, a case of C7 spondylolysis has not been reported. The majority of the patients affected are men (42 males, 20 females; in seven the sex was not reported). Ages have ranged from 5 to 57 years. Most patients presented after an episode of minor trauma [2–4] or with chronic neck and shoulder pain [5–12]. With rare exceptions, the patients did not have short- or long-term neurologic deficits. These features coincide with the findings of the current series. In our group, most of the patients were men (nine) who presented after minor trauma and had no neurologic deficits. Similarly, the C6 level and the left side of the neck were affected most often. Contrary to previous reports, in our series nine of the 12 defects were unilateral; only three patients had bilateral lesions.

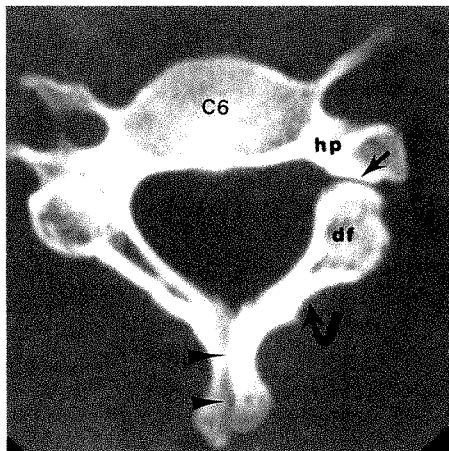


Fig. 6.—Left C6 spondylolysis in a 34-year-old man injured in a motor vehicle accident. CT scan shows smoothly margined cleft (*straight arrow*), posteriorly positioned dorsal fragment (*df*), hypoplastic ipsilateral pedicle (*hp*), and spina bifida occulta (*arrowheads*). Dysplastic ipsilateral lamina is also seen (*curved arrow*). These findings are diagnostic.

Radiologically, cervical spondylolysis is characterized by a vertical spondylolytic defect in the involved articular mass creating two triangular fragments, each having smooth cortical margins. These fragments are often apposed at the defect, producing a cleft-bow-tie configuration in the sagittal plane (Fig. 5). The dorsal triangular component typically is displaced posteriorly. The ipsilateral pedicle, being hypoplastic, also shows dysplastic changes in all instances. Similarly, dysplastic changes consisting of hypoplasia or hyperplasia generally are found in the ipsilateral articular pillar above and/or below the involved site. Secondary osteoarthritis due to abnormal spine mechanics may occur, particularly in older patients. Spina bifida occulta is another common finding. Widening of the vertebral foramen at the affected level has been reported [3] and was present in the majority of our cases. The deformed articular masses and associated findings observed in our analysis of oblique radiographs were the most valuable features on conventional films for radiologic diagnosis of cervical spondylolysis. Tomography allowed better anatomic definition of the spondylolytic defect and associated dysplastic and degenerative changes of the affected articular mass than conventional radiographs did. In addition, it established whether unilateral or bilateral defects were present. The sagittal plane proved to be most helpful. CT in the axial plane provided good detail of the posterior arch. The spondylolytic defect was well shown in all cases studied with this technique. MR was not helpful in the one case of cervical spondylolysis we studied. It was, however, helpful in excluding the diagnosis in another (Fig. 7C). A combined multistudy approach was necessary to reach a definitive diagnosis in most cases.

The CT findings of cervical spondylolysis differ from those described for lumbar spondylolysis [27]. In the lumbar region, the defect involves the pars interarticularis (portion of the arch lying between the superior and inferior articular processes). However, in the cervical spine the cleft is localized in the articular mass at the junction of the superior and inferior facets, which could be considered the cervical equivalent to the pars interarticularis [4]. In addition, there is greater dysplasia of the cervical vertebrae, which may reflect a congenital

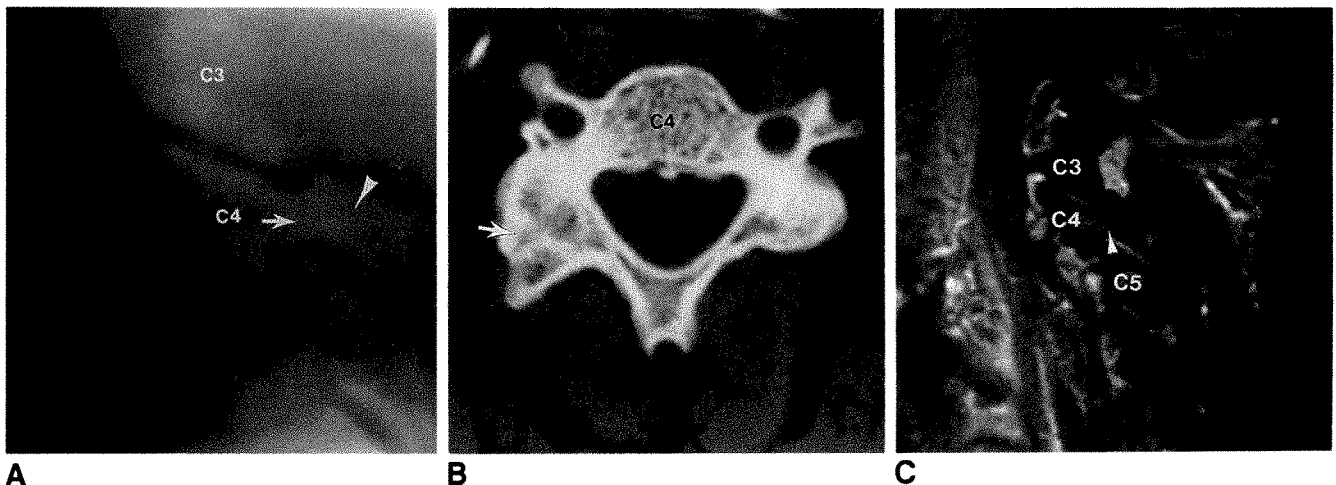


Fig. 7.—Healed C4 articular mass fracture in a 41-year-old man injured in a motor vehicle accident, thought to have cervical spondylolysis. A, Sagittal tomogram shows posttraumatic deformity of articular mass (*arrow*) and posterior displacement of apparent dorsal fragment (*arrowhead*), which is fused to rest of articular mass, mimicking cervical spondylolysis. No cleft is seen. B, CT scan shows deformed articular pillar without cleft (*arrow*) (compare with Fig. 6.). Pedicle, lamina, and spinous process are normal. C, T2-weighted parasagittal MR image, 2000/40 (TR/TE), shows contiguous marrow signal extending length of healed C4 articular mass fracture (*arrowhead*). Importantly, no cleft is demonstrated, showing this is not cervical spondylolysis.

cause of the process. The MR features of lumbar spondylolysis have been described recently [28, 29]; however, to date, the MR appearance of cervical spondylolysis has not been reported. As cervical spondylolysis is a condition affecting the osseous structures of the vertebral arch, it may be shown better by other techniques.

The cause of spondylolytic defects is unknown. Several theories have been proposed [4, 12]. Failure of chondrification and ossification centers to unite is one such theory. This may account for the spectrum of posterior arch defects, which includes cervical spondylolysis as well as an absent pedicle. It may be the result of an error in formation of the blastema or cartilage in the region of the articular pillar. The presence of associated anomalies argues for a congenital cause, yet postmortem examinations of neonates have never revealed a spondylolytic defect [4]. It may be that a dysplastic spine is simply more predisposed to develop spondylolytic defects from whatever cause. Although posttraumatic nonunion and pseudoarthrosis have been presumed, no definitive evidence exists to support this theory.

Cervical spondylolysis is most likely to be confused with traumatic unilateral interfacet dislocation, articular mass fracture, or congenitally absent pedicle. Several features enable their differentiation. In contrast to cervical spondylolysis, unilateral interfacet dislocation is characterized by spondylolisthesis greater than 3 mm, rotation with a lack of superimposition of the articular masses, and malalignment of the spinous processes. Sagittal tomography or reformatted CT should show an anteriorly displaced articular mass with a normal configuration. Soft-tissue swelling may be present in unilateral interfacet dislocation but is notably absent in cervical spondylolysis that is uncomplicated by other injuries. Acute articular mass fractures will not be smoothly corticated, as the spondylolytic defect is in cervical spondylolysis. The presence of soft-tissue swelling or neurologic symptoms also would favor a diagnosis of acute fracture. Differentiation of a chronic nonunited articular mass fracture from cervical spondylolysis may be difficult; however, the presence of associated dysplastic changes of the ipsilateral pedicle and laminae would favor cervical spondylolysis. An initial misdiagnosis of facet dislocation or articular mass fracture occurred in seven of our cases.

As in cervical spondylolysis, a posteriorly displaced dysplastic articular mass is typical of the absent cervical pedicle, and spina bifida is often present. Conversely, a dysplastic transverse process and enlargement of the adjacent neural foramen are always components of absent pedicle. Furthermore, vertebral body fusion is occasionally seen in this condition but was not observed in our cases of cervical spondylolysis.

In summary, the radiologic features of cervical spondylolysis are distinctive, and diagnosis often can be strongly suspected from plain films. Tomograms and CT can help confirm the diagnosis in equivocal cases. The role of MR in evaluation of this condition has not been established. A multi-study approach is helpful.

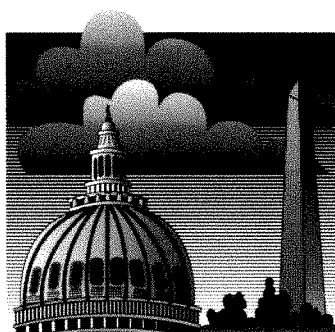
Awareness of the radiologic features of cervical spondylolysis will decrease the potential for misdiagnosis and inappropriate therapy.

## ACKNOWLEDGMENT

We gratefully acknowledge the clerical assistance of Juanita Cates.

## REFERENCES

1. Perlman R, Hawes LE. Cervical spondylolisthesis. *J Bone Joint Surg [Am]* 1951;33-A:1012-1013
2. Azouz EM, Chan JD, Wee R. Spondylolysis of the cervical vertebrae. *Radiology* 1974;111:315-318
3. Op Den Orth JO, Penning AL, Kluft O. Unilateral spondylolysis of the sixth cervical vertebra. *J Bone Joint Surg [Am]* 1969;51-A:1379-1382
4. Charlton OP, Gehweiler JA, Morgan CL, Martinez S, Daffner RH. Spondylolysis and spondylolisthesis of the cervical spine. *Skeletal Radiol* 1978;3:79-84
5. Kosnik EJ, Johnson J, Scoles PV, Rossel CW. Cervical spondylolisthesis. *Spine* 1979;4:203-205
6. Gehweiler JA, Martinez S, Clark WM, Miller MD, Stewart GC. Spondylolisthesis of the axis vertebra. *AJR* 1977;128:682-684
7. Sheikholeslamzadeh S, Aalami-Harandi B, Fateh H. Spondylolisthesis of the cervical spine. *J Bone Joint Surg [Br]* 1977;59-B:95-96
8. Hanai K, Miyashita T, Saburi H. Cervical spondylolisthesis. *Acta Orthop Scand* 1976;47:63-66
9. Guillaume J, Rouleau J, Fardou H, Treil J, Manelfe C. Congenital spondylolysis of the cervical vertebrae with spondylolisthesis and frontal narrowing of the spinal canal. *Neuroradiology* 1976;11:159-163
10. Prioleau GR, Wilson CB. Cervical spondylolysis with spondylolisthesis. *J Neurosurg* 1975;43:750-753
11. Hasue M, Kikuchi S, Matsui T, Machida H, Kurokawa T, Kataoka O. Spondylolysis of the axis. *Spine* 1983;8:901-906
12. Schwartz AM, Wechsler RJ, Landy MD, Wetzner SM, Goldstein SA. Posterior arch defects of the cervical spine. *Skeletal Radiol* 1982;8:135-139
13. Durbin FC. Spondylolisthesis of the cervical spine. *J Bone Joint Surg [Br]* 1956;38-B:734-735
14. Niemeyer T, Peming L. Functional roentgenographic examination in a case of cervical spondylolisthesis. *J Bone Joint Surg [Br]* 1963;45-A:1671-1678
15. Dawley JA. Spondylolisthesis of the cervical spine. Case report. *J Neurosurg* 1971;34:99-101
16. Moseley I. Neural arch dysplasia of the sixth cervical vertebra: "congenital cervical spondylolisthesis." *Br J Radiol* 1976;49:81-83
17. Fardon DF, Fielding JW. Defects of the pedicle and spondylolisthesis of the second cervical vertebra. *J Bone Joint Surg [Br]* 1981;63-B:526-528
18. Kish KK, Wilner HI. Spondylolysis of C2: CT and plain film findings. *J Comput Assist Tomogr* 1983;7:517-518
19. Barnes DA, Borns P, Pizzutillo PD. Cervical spondylolisthesis associated with the multiple nevoid basal cell carcinoma syndrome. *Clin Orthop* 1982;162:26-30
20. Karasick S, Karasick D, Wechsler RJ. Unilateral spondylolysis of the cervical spine. *Skeletal Radiol* 1983;9:259-261
21. Nordstrom REA, Lahdenranta TV, Kaitila II, Laasonen EMI. Familial spondylolisthesis of the axis vertebra. *J Bone Joint Surg [Br]* 1986;68-B:704-706
22. Hanakita J, Kondo A, Suzuki T. Nontraumatic spondylolysis of the axis vertebra. *No Shinkei Geka* 1985;13:1097-1101
23. Collignan JC, Flandray P. Cervical spondylolisthesis. *J Belge Radiol* 1981;64:495-499
24. Villette L, Lesoin F, Mathevon H, Psuivo JP, Clarisse J, Jomin M. Les spondylolyses isthmiques de l'axis. *Ann Chir* 1986;40:211-214
25. Labbe A, Campagne D, Merle P. Spondylolisthesis congenital de la sixième vertebra cervicale. *Ann Radiol (Paris)* 1983;26:692-694
26. Morvan G, Busson J, Frot B, Nahum H. Cervical spondylolysis—seven cases. Review of the literature. *J Radiol* 1984;65:259-266
27. Grogan JP, Hemminghytt S, Williams AL, Carrera GF, Haughton VM. Spondylolysis studied with computed tomography. *Radiology* 1982;145:735-742
28. Grenier N, Kressel HY, Schiebler ML, Grossman R. Isthmic spondylolysis of the lumbar spine: MR imaging at 1.5T. *Radiology* 1989;170:489-493
29. Johnson DW, Farnum GN, Latchaw RE, Erba SM. MR imaging of the pars interarticularis. *AJR* 1989;152:327-332



Come to the  
American Roentgen Ray Society

90<sup>th</sup>

---

ANNUAL MEETING

---

Washington, D. C.

---

Sheraton Washington Hotel

May 13-18, 1990

---

---

Scientific Program (200 papers)

Instructional Courses (60 hours)

Categorical Course on Cardiovascular Imaging

The Caldwell Lecture

Award Papers

Scientific Exhibits

Social, Golf, and Tennis Programs

Guest Programs



# Traumatic Lumbar Hernia: CT Diagnosis

Scott H. Faro<sup>1</sup>  
C. Dyeanne Racette<sup>2</sup>  
James F. Lally<sup>1</sup>  
John S. Wills<sup>1</sup>  
Amir Mansoor<sup>2</sup>

A lumbar hernia usually involves protrusion of extraperitoneal fat or bowel through an area of weakness in the posterolateral abdominal wall bounded superiorly by the 12th rib, inferiorly by the iliac crest, posteriorly by the erector spinae muscle, and anteriorly by the posterior border of the external oblique muscle. Most are due to an acquired nontraumatic or congenital cause. Acute blunt abdominal trauma is a rare cause of lumbar hernia; to our knowledge, the CT diagnosis of this variety has not been reported. Since 1985, approximately 850 patients have undergone emergent abdominal CT for evaluation of acute abdominal trauma at our hospital; in seven of these patients, a traumatic lumbar hernia was diagnosed prospectively. In three patients, CT showed a flank hematoma with herniation of bowel through the lumbar triangle. CT showed pelvic fractures in three other patients, accompanied by herniation of bowel in one patient, herniation of extraperitoneal fat in another, and herniation of extraperitoneal fat and blood in the third. One patient had both a flank hematoma and a pelvic fracture with herniation of bowel.

Acute traumatic lumbar hernia is a rare but significant abnormality that should be considered in patients with blunt abdominal trauma, especially in those with large flank hematomas and pelvic fractures. The hernia contents, associated injuries, and disrupted muscle layers are all well demonstrated on CT.

*AJR* 154:757-759, April 1990

Lumbar hernias occur within the superior or inferior lumbar triangle. Both triangles are areas of relative weakness in the posterolateral abdominal wall. The superior lumbar (Grynfeltt-Lesshaft) triangle is an inverted triangle that is bound by the 12th rib superiorly, the internal oblique muscle anteriorly, and the erector spinae muscle posteriorly. The latissimus dorsi muscle forms the roof of the triangle, and the aponeurosis of the transversalis muscle forms the floor. The inferior lumbar (Petit's) triangle is an upright triangle bordered inferiorly by the iliac crest, anteriorly by the external oblique muscle, and posteriorly by the latissimus dorsi muscle. Superficial fascia and skin constitute the roof of the triangle, and the lumbar fascia, internal oblique muscle, and aponeurosis of the transversalis muscle form the floor [1]. Lumbar hernias occur most often in the superior lumbar triangle; most are due to an acquired nontraumatic or congenital cause and less commonly are due to trauma.

CT diagnosis of traumatic lumbar hernias associated with surgical flank incisions or iliac bone graft donor sites has been described; to our knowledge, however, there have been no reports of the CT diagnosis of lumbar hernia due to acute blunt abdominal trauma. We present our experience with the CT diagnosis of acute traumatic lumbar hernia in seven patients and describe the role of CT in the initial examination and follow-up of these patients.

## Materials and Methods

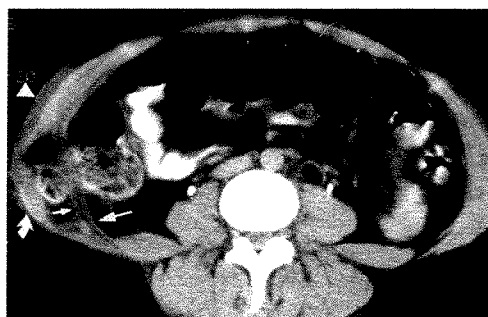
Since 1985, approximately 850 patients have undergone emergent abdominal CT at The Medical Center of Delaware for evaluation of acute abdominal trauma. In seven of these

Received June 23, 1989; accepted after revision October 19, 1989.

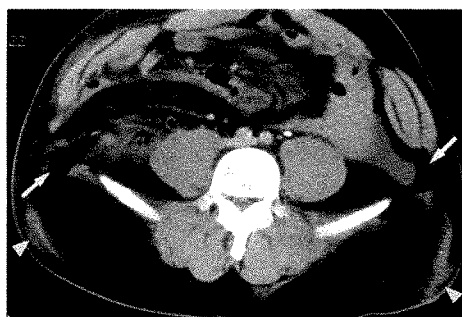
<sup>1</sup> Department of Radiology, The Medical Center of Delaware, 4755 Stanton-Ogletown Rd., Newark, DE 19718. Address reprint requests to S. H. Faro.

<sup>2</sup> Department of Surgery, Ste. 125, Medical Arts Pavilion, 4745 Stanton-Ogletown Rd., Newark, DE 19713.

0361-803X/90/1544-0757  
© American Roentgen Ray Society



1



2

Fig. 1.—CT scan in a 32-year-old woman involved in an automobile accident reveals herniation of bowel through thinned transversus abdominis muscle (*long straight arrow*) and internal oblique muscle (*short straight arrow*). Hernia is covered by external oblique muscle (*curved arrow*). Arrowhead = right flank hematoma.

Fig. 2.—CT scan in a 46-year-old man who was an unrestrained driver in a motor vehicle accident shows bilateral lumbar hernias (*arrows*) and bilateral flank hematomas (*arrowheads*).

patients, an inferior lumbar hernia was diagnosed prospectively. The patients included two women and five men, whose ages ranged from 21 to 78 years. The hospital charts of the seven patients were reviewed, with specific attention to mechanism of injury, history of lumbar hernia, associated injuries, and surgical treatments. All seven patients were involved in motor vehicle accidents. Three patients were unrestrained during the accident, two were restrained, and whether the remaining two patients used seat belts is unknown. No history of lumbar hernia was present in this group of patients. Large flank hematomas were the major clinical findings in three patients. Three other patients suffered pelvic fractures, one with pubic symphysis diastasis, one with sacral fractures and bilateral pubic bone fractures, and the third with multiple comminuted pelvic fractures. The last patient had both a large flank hematoma and an avulsion fracture of the right iliac crest.

CT scans were obtained with either a Picker 600SX or Picker 1200SX CT scanner (Picker, Highland Heights, OH) with 1-cm-thick slices at intervals of 1 cm through the abdomen and 2 cm through the pelvis. All patients received 450 ml of barium sulfate 1.2% w/w (Readi-CAT, E-Z-Em, Inc., Westbury, NY) via nasogastric tube 30 min before the CT scan. IV contrast material was given to all patients by a rapid bolus infusion of 75 ml of iohalamate meglumine 60% (Conray, Mallinckrodt, St. Louis, MO), followed by approximately 50 ml by slow drip infusion during scanning.

Three patients had palpable, symptomatic lumbar hernias. Two of these patients underwent emergent exploratory laparotomy and surgical repair of the hernias after CT. The third patient had an elective repair of the lumbar hernia. The remaining four patients had nonpalpable, asymptomatic lumbar hernias. Two of these patients were treated conservatively (observation). A third patient initially was treated conservatively, and 6 weeks after the trauma a large abscess developed in the region of the lumbar hernia. This abscess was drained surgically. Enterointeric and enterocutaneous fistulas that required small-bowel resection developed subsequently. The fourth patient had emergent exploratory laparotomy after CT, but the small lumbar hernia was not repaired.

## Results

In all seven patients, CT clearly showed a lumbar hernia(s), all of which involved the inferior lumbar triangle. Three of the seven patients with a traumatic lumbar hernia on CT had large flank hematomas as the major associated finding. The hematoma was on the same side as the lumbar hernia. In one patient, the CT scan showed a right lumbar hernia with bowel herniation through thinned transversus abdominis and internal oblique muscles (Fig. 1). A second patient had a small left lumbar hernia on CT, with bowel herniation. The third patient

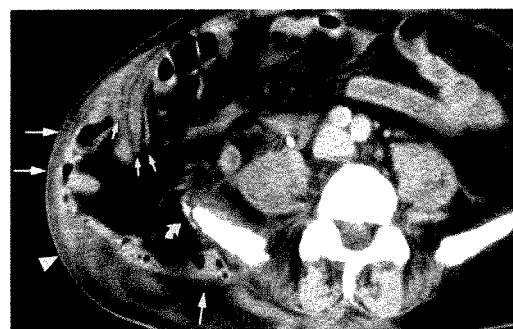


Fig. 3.—CT scan in a 78-year-old man who was a restrained driver in a motor vehicle accident reveals herniation of bowel (*long straight arrows*) through torn layers (medial to lateral) of transversus abdominis, internal oblique, and external oblique muscles (*short straight arrows*). A right flank hematoma (*arrowhead*) and an avulsion fracture of right iliac crest (*curved arrow*) are also present.

had extensive bilateral flank hematomas and bilateral lumbar hernias with bowel herniation on CT (Fig. 2). The CT scan of a fourth patient showed both a right flank hematoma and an avulsion fracture of the right iliac crest, with herniation of bowel through a right lumbar hernia (Fig. 3).

Pelvic fractures were the major associated injuries in the remaining three patients with lumbar hernias. One had herniation of extraperitoneal fat through a right lumbar hernia on CT. Another had free intraperitoneal fluid on CT (proved surgically to be hemoperitoneum) and a left lumbar hernia containing extraperitoneal fat and a similar fluid density, presumably blood. The CT scan obtained in the third patient at the time of admission showed a right lumbar hernia with herniation of bowel, probably colon (Fig. 4A). This patient was discharged in satisfactory condition but returned to the emergency room 2 weeks later with a fever and a palpable, fluctuant right flank mass. A CT scan at this time (6 weeks after the initial trauma) showed a large heterogeneous fluid collection with associated gas, representing an abscess in the region of the right lumbar hernia (Fig. 4B).

## Discussion

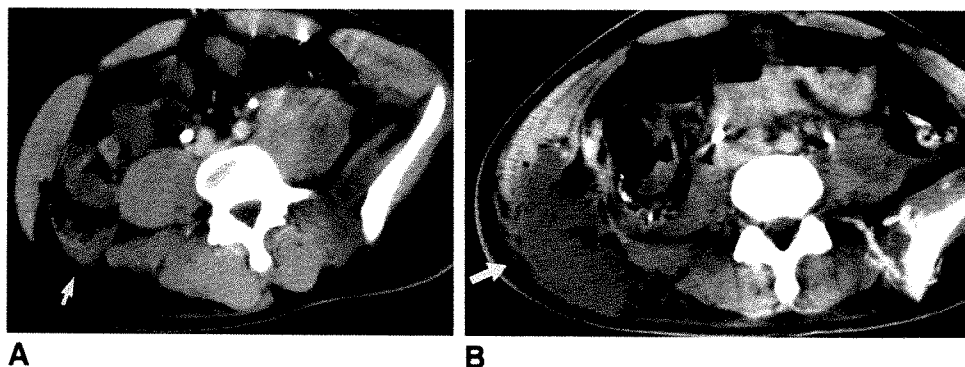
Less than 300 cases of lumbar hernia have been described in the literature [1]. Most of these hernias are due to an acquired nontraumatic or congenital cause [1]. The remaining lumbar hernias are due to trauma [1, 2]. Recent studies have



Fig. 4.—CT scans in a 21-year-old man involved in a motor vehicle accident. It was not known if he was wearing a seat belt.

A, CT scan just above right iliac crest after trauma reveals herniation of bowel in posterolateral abdominal wall (arrow).

B, Second CT scan 6 weeks after trauma shows a large heterogeneous fluid collection with associated gas (arrow), representing an abscess, in right posterolateral flank.



reported lumbar hernias resulting from direct surgical trauma and occurring postoperatively at the sites of flank incisions and iliac crest bone graft donor sites [2–4]. Acute blunt abdominal trauma is a rare but significant cause of lumbar hernia. To our knowledge, the CT diagnosis has not been described before.

The major clinical findings in our patients were large flank hematomas and pelvic fractures. These associated injuries were diagnosed accurately with CT. Three of the seven patients had palpable, symptomatic flank masses resulting from trauma. The differential diagnoses included flank hematoma and/or lumbar hernia. CT was able to show the presence of these abnormalities as well as show the anatomy of the adjacent muscle layers; furthermore, the contents of the hernia were well shown by this imaging technique.

Lumbar hernias, which have a natural history of a gradual increase in size over time [1], can result in significant morbidity, ranging from chronic lower back pain to bowel strangulation [5]. Bowel incarceration occurs in approximately 25% of these hernias, and strangulation may occur in 10%. Two of our seven patients had significant morbidity related to the hernia. One patient continued to have a palpable, symptomatic lumbar hernia and underwent elective surgical repair. A second patient developed a large flank abscess in the region of the lumbar hernia that required surgical drainage. This abscess presumably was due to microperforation of herniated

bowel. The CT diagnosis of lumbar hernia was of value in the management of these patients.

The majority of lumbar hernias have been diagnosed on physical examination; only recently has CT become a major diagnostic technique. CT allows the diagnosis of asymptomatic, nonpalpable lumbar hernias. We believe that these hernias can be monitored clinically until symptoms develop and that all symptomatic lumbar hernias should undergo repair. CT is also beneficial in the follow-up of asymptomatic patients who develop flank pain or a palpable flank mass after the initial trauma.

#### ACKNOWLEDGMENTS

We thank Karen McFadden and Suzie McCormick for their help with the preparation of this paper and Douglas Bugel for the photography.

#### REFERENCES

1. Swartz WT. Lumbar hernia. In: Nyhus LM, Condon RE, eds. *Hernia*, 2nd ed. Philadelphia: Lippincott, 1978:409–426.
2. Baker ME, Weinerth JL, Andriani RT, Cohan RH, Dunnick NR. Lumbar hernia: diagnosis by CT. *AJR* 1987;148:565–567.
3. Kane VG, Silverstein GS. CT demonstration of hernia through an iliac crest defect. *J Comput Assist Tomogr* 1986;10:432–434.
4. Lawdahl RB, Moss CN, Van Dyke JA. Inferior lumbar (Petit's) hernia. *AJR* 1986;147:744–745.
5. Florer RE, Kiriluk L. Petit's triangle hernia, incarcerated: two case reports. *Am Surg* 1971;37:527–530.



The Radiology Outreach Foundation (ROF) is a nonprofit corporation whose goal is to help disadvantaged countries improve their health care by providing radiology equipment, books, consultation, education, and training to their practitioners. This assistance is on an application basis that is independent of political, ethnic, or religious orientation of the grantee. It depends on the need of the people and the ability of the ROF to meet that need. The ROF is approved by the U.S. Internal Revenue Service as a tax-exempt organization. It is endorsed by the following radiologic societies:

American Association of Women Radiologists  
American College of Radiology  
American Roentgen Ray Society  
Association of University Radiologists  
Radiological Society of North America  
Society of Chairmen of Academic Radiology Departments  
Society for Pediatric Radiology  
European Society of Pediatric Radiology

All donations to the ROF are tax deductible. Persons who would like to contribute financially to the ROF, would be interested in being a visiting professor, would like to send books or journals to any of the institutions supported by the ROF, or would like further information about the ROF should write to

Charles A. Gooding, M.D.  
President  
Radiology Outreach Foundation  
3415 Sacramento St.  
San Francisco, CA 94118 USA

## Case Report

### CT Diagnosis of Posterior Perineal Hernia

Edward Lubat,<sup>1</sup> Richard B. Gordon, Bernard A. Birnbaum, and Alec J. Megibow

Perineal hernias are rare hernias occurring through defects in the pelvic floor musculature. To our knowledge, CT demonstration of these hernias has not been reported in the literature. We describe CT findings in two such cases.

#### Case Report

A 68-year-old man had had a mass in the right buttock for 1 year. He had had no previous surgery. Physical examination showed a large soft mass in the medial and inferior aspect of the right buttock

(Fig. 1A). CT scans (Figs. 1B and C) showed distended loops of sigmoid colon and small bowel in the right ischioirectal fossa in the area of the palpable mass. The normal right levator ani muscle could not be identified. During surgery, the entire sigmoid colon and a small segment of ileum were found to have herniated into the right ischioirectal fossa through a defect in the levator ani muscle.

#### Discussion

The perineal hernia is one of the least common types of hernias [1]. It was first described in the 18th century [2], and

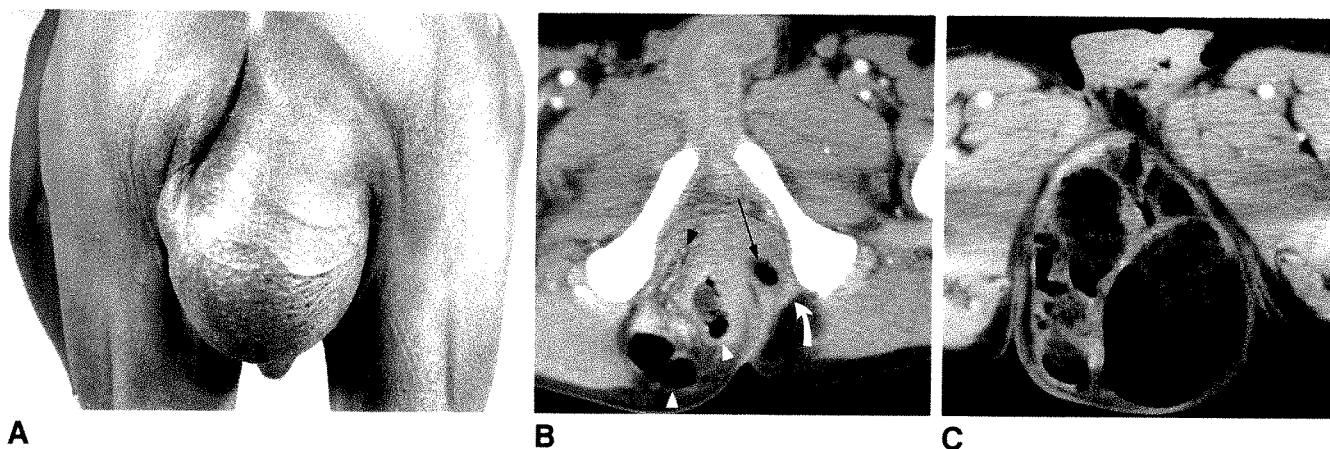


Fig. 1.—Perineal hernia in a 68-year-old man.

A, Posterior view of patient shows a large mass involving inferomedial aspect of right buttock and right perineal region.

B, CT scan of lower pelvis shows right ischioirectal fossa containing herniated loops of sigmoid colon (white arrowheads). Vessels are identified coursing in sigmoid mesocolon (black arrowhead). Rectum (black arrow) is deviated to left. Levator ani muscle (white arrow) is seen on left but not on right.

C, CT scan 2 cm inferior to B shows multiple loops of sigmoid colon filling entire clinically evident mass.

Received October 23, 1989; accepted after revision December 4, 1989.

<sup>1</sup> All authors: Department of Radiology, NYU Medical Center, 560 First Ave., New York, NY 10016. Address reprint requests to E. Lubat.

AJR 154:761-762, April 1990 0361-803X/90/1544-0761 © American Roentgen Ray Society

fewer than 100 cases have been reported to date. It is five times more common in women, presumably because of weakening of the pelvic floor as a result of pregnancy and childbirth. The peak age at the time of occurrence is between 40 and 60 years.

Anatomically, these hernias are classified as anterior or posterior, depending on the relationship to the transverse perineal muscle (Fig. 2). The posterior is the less common variety and occurs through a defect in the levator ani muscle or between the levator ani and the coccygeus muscles. The anterior perineal hernia occurs through the urogenital diaphragm and is said to occur only in females. The perineal hernia sac may contain bowel, bladder, or omentum.

These hernias are classified further into primary and secondary types. Most of the primary types are acquired and may be related to states associated with increased abdominal pressure (e.g., pregnancy, obesity, or chronic ascites) or chronic infection of the pelvic floor. Congenital defects are extremely rare causes of primary hernias. Secondary perineal hernias are incisional hernias related to previous surgery,

particularly pelvic exenteration, abdominal perineal resection, and perineal prostatectomies. Perineal hernias are said to occur after 3% of pelvic exenterations and 1% of abdominal perineal resections.

Clinical diagnosis may be difficult. Signs usually consist of a perineal, labial, or gluteal mass, which may cause discomfort upon sitting. Physical examination reveals a soft mass, and the hernia is usually reducible. Strangulation is uncommon because the hernia neck tends to be wide and the muscular defect elastic. Surgical reduction and repair usually are accomplished via an abdominal approach.

Radiographic demonstration of these hernias by plain film or barium enema has been reported twice [3, 4], both before the CT era. In the second of our two cases, barium enema showed posterior and inferior herniation of the sigmoid colon adjacent to the rectum and into the left buttock with almost complete obstruction to retrograde flow of barium beyond the herniated loop of sigmoid. A CT scan (Fig. 3) showed sigmoid colon adjacent to the distal rectum and anal canal. The loop and hernia sac could be followed into the ischiorectal fossa. The left levator ani muscle could not be identified.

In the normal pelvis, CT is able to show the muscular anatomy of the pelvic floor. The coccygeus muscle is seen coursing between the coccyx and ischium, and the levator ani sling encircles the distal rectum (Fig. 3A). As our cases of posterior perineal hernias demonstrate, CT directly depicts the location of herniated bowel loops within the ischiorectal fossa adjacent to the anal canal. The loops extend below the expected level of the levator ani muscle, which in our cases, was not identified on the side of the hernia.

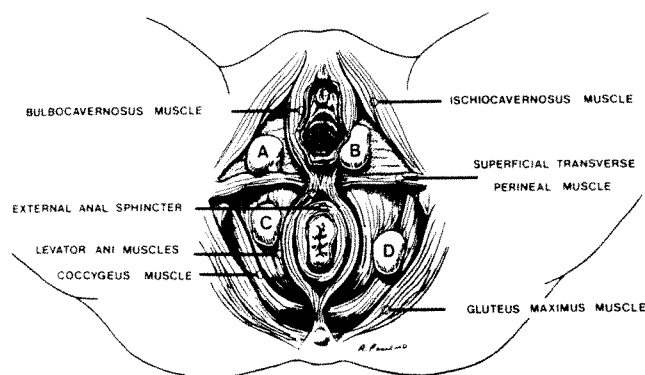


Fig. 2.—Drawing shows anatomy of perineal musculature. Perineal hernias may be anterior (A, B) or posterior (C, D), depending on relationship to transverse perineal muscle. Posterior variety may occur through levator ani muscle (C) or between levator ani and coccygeus muscles (D). (Reprinted with permission from Pearl [1].)

#### REFERENCES

1. Pearl RK. Perineal hernia. In: Nyhus LM, Condon RE, eds. *Hernia*, 3rd ed. Philadelphia: Lippincott, 1989:442-446.
2. De Garengeot RJC. Sur plusieurs hernies singulières. *Mem Acad R Chir (Paris)* 1743;1:699.
3. Trackler RT, Koehler PR. The radiographic findings in posterior perineal hernia. *Radiology* 1968;91:950-955.
4. Steiner A. Hernie périméale postéro-latérale. *J Chir (Paris)* 1965;90:87-90.

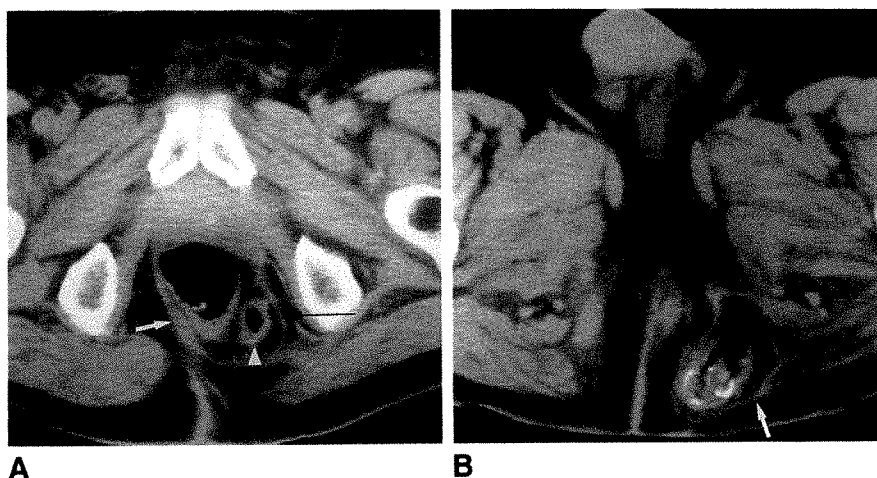


Fig. 3.—Perineal hernia in a 62-year-old man. A, CT scan of lower pelvis shows loop of sigmoid colon (arrowhead), surrounded by fat and hernia sac (black arrow), in left ischiorectal fossa, adjacent to rectum. Normal levator ani muscle is seen on right (white arrow) but not on left side.

B, More inferior CT scan shows bowel and hernia sac (arrow) extending into subcutaneous tissues of left buttock.

# The Value of MR Imaging in Monitoring the Effect of Chemotherapy on Bone Sarcomas

Herma C. Holscher<sup>1</sup>  
 Johan L. Bloem<sup>1</sup>  
 Marianne A. Nooy<sup>2</sup>  
 Anton H. M. Taminiau<sup>3</sup>  
 Frits Eulerink<sup>4</sup>  
 Jo Hermans<sup>5</sup>

We studied the value of MR imaging in monitoring the response of Ewing sarcoma and osteosarcoma to chemotherapy. Relative signal-intensity changes on MR images in the course of chemotherapy were compared with changes in tumor volume and histopathologic findings. MR scans (T1- and T2-weighted spin-echo images) were obtained in 20 patients with bone sarcoma. The first MR scan was obtained before the administration of chemotherapy in all patients. The follow-up scan was obtained in the course of treatment, before surgery. Tumor-volume and signal-intensity measurements of the intra- and extraosseous components of the tumor were analyzed. In 17 patients, histopathologic findings of the resected tumor were available for comparison with the MR images. In 12 of 17 patients there was complete agreement between changes in tumor volume, changes in the signal intensity of the extraosseous tumor component on T2-weighted images, and histopathology. In another four cases, changes in signal intensity correlated either with histopathology or with changes in tumor volume. In one patient with a pathologic fracture, no such correlation existed. A significant correlation was found between changes in signal intensities and pathologic response ( $r = .57$ ,  $p = .02$ ), as well as between changes in tumor volume and pathologic response ( $r = .53$ ,  $p = .03$ ). No correlation could be found between changes in signal intensity of the intraosseous tumor component and changes in tumor volume or histopathology.

We conclude that the signal intensity of the extraosseous component of bone sarcomas on T2-weighted MR images in addition to changes in tumor volume may be useful in evaluating response to chemotherapy.

*AJR* 154:763-769, April 1990

Developments in preoperative local tumor staging and (neo)adjuvant chemotherapy have accelerated the use of limited or limb-saving surgery in patients with bone sarcoma. In clinical trials, patients with Ewing sarcoma and osteosarcoma are treated pre- and postoperatively with chemotherapy in an attempt to decrease tumor viability and to attack early microscopic spread of tumor [1-3]. Imaging studies, especially angiography and CT, have been used in the preoperative evaluation of chemotherapy [4-9]. However, a reliable, noninvasive test to quantify the (early) response of the primary tumor to chemotherapy is not yet available. MR spectroscopy is being used in experiments to evaluate its potential in monitoring chemotherapy [10-12].

In this study we evaluated MR imaging of characteristics before and after preoperative chemotherapy to assess the ability of the technique to show local response to treatment. Because bone sarcoma often has a heterogeneous appearance on MR images, especially when the intra- and extraosseous components are considered together, the signal intensities of the intra- and extraosseous tumor components were measured separately.

## Materials and Methods

Between May 1986 and July 1988, 21 patients (15 with osteosarcomas and six with Ewing sarcomas) were monitored preoperatively with MR imaging, both once before and once after

Received August 23, 1989; accepted after revision November 10, 1989.

Presented in part at the annual meeting of the American Roentgen Ray Society, New Orleans, May 1989.

<sup>1</sup> Department of Diagnostic Radiology, Bldg. I, C2-S, University Hospital Leiden, Rijnsburgerweg 10, 2333 AA Leiden, the Netherlands. Address reprint requests to H. C. Holscher.

<sup>2</sup> Department of Clinical Oncology, University Hospital Leiden, 2333 AA Leiden, the Netherlands.

<sup>3</sup> Department of Orthopedic Surgery, University Hospital Leiden, 2333 AA Leiden, the Netherlands.

<sup>4</sup> Department of Pathology, University Hospital Leiden, 2333 AA Leiden, the Netherlands.

<sup>5</sup> Department of Medical Statistics, University Hospital Leiden, 2333 AA Leiden, the Netherlands.

0361-803X/90/1544-0763

© American Roentgen Ray Society

preoperative chemotherapy. In one patient with a Ewing sarcoma, no macroscopic tumor was discernible with MR imaging after treatment. The patient was not treated surgically. This patient was excluded from the study because no volume or signal-intensity measurements could be made on the images after chemotherapy treatment. The mean age of the 20 patients included in the study was 18 years (range, 6–36 years). Tumors were located in the femur (12 patients); proximal tibia (five patients); and rib, lumbar vertebral body, and clavicle (one patient each). Chemotherapy was administered according to protocols of the European Organisation for Research and Treatment of Cancer and the Cooperative Ewing Sarcoma Study; combinations of several chemotherapeutic agents (Adriamycin, l-phosphamide, methotrexate, cisplatin, vincristine, cyclophosphamide, and dactinomycin) were used. None of the patients received adjuvant preoperative radiation therapy. MR imaging was performed before and after the complete preoperative chemotherapy schedule in all patients. The interval during which patients were monitored varied from 2 to 3 months in 19 patients; it was 7 months in one patient.

MR imaging was performed with a 0.5-T imager (Philips, Shelton, CT). Large tumors were imaged with a head coil (eight patients) or body coil (seven patients); six smaller tumors were imaged with paired flexible surface coils with a homogeneous field sensitivity [13]. Spin-echo images, 550/30 (TR/TE), were used for T1-weighting; T2-weighting was obtained with 2000/100 images. The T1-weighted sequences were usually made in the sagittal plane with four measurements per data line and an acquisition matrix of  $256 \times 256$ . The T2-weighted images were made in the transverse plane throughout the entire tumor with two measurements per data line and an acquisition matrix of  $180 \times 256$ .

Quantitative region of interest (ROI) measurements of signal intensities were obtained in the intra- and extraosseous tumor components, and in normal fat. The ROI was chosen to be as large as possible, but was at least  $1 \text{ cm}^2$ . When surface-coil images were analyzed, the distance of the various sample volumes to the coil was kept constant. The ROIs were selected with a cursor. No measurements were obtained if the imaging technique was insufficient, that is, if there was a nondefined pulse sequence or various artifacts (motion, susceptibility). Each tissue sample was measured three times. The mean signal intensity of these three measurements was used in the analysis to dilute the influence of heterogeneity of the tumor component. The relative signal intensity of the tumor was calculated as the ratio of the signal intensity of the tumor to the signal intensity of subcutaneous fat. The quotient of the relative signal intensity of the tumor measured after chemotherapy to that measured before chemotherapy was calculated and expressed as a signal-intensity ratio. These signal-intensity ratios were compared with tumor volumes measured on MR images before and after chemotherapy. The volume of the entire tumor was calculated with the formula for elliptical masses;  $\text{volume} = \pi/6 \times \text{height} \times \text{width} \times \text{depth}$ . The maximum height was measured on sagittal images; the maximum width and depth were measured on the transverse images. The quotient of the tumor volume after chemotherapy to the tumor volume before treatment was expressed as a tumor-volume ratio. The signal-intensity and tumor-volume measurements were performed in concert by two radiologists without knowledge of clinical and histopathologic data.

In addition to this comparison between signal-intensity ratio and tumor-volume ratio, both ratios were correlated with the histopathologic response based on the resected specimen in 17 patients (13 with osteosarcomas and four with Ewing sarcomas). The tumor was not resected in three patients because of metastases (two patients) or irresectability (one patient). The pathologic response was graded as good (++) when the tumor specimen removed after chemotherapy showed (sub)total necrosis; probably good (+) when, in comparison

with the biopsy material, the histopathologic picture of the removed tumor suggested important destruction of tumor tissue judged by the presence of low cellularity in large areas, major necrosis, or fibrosing clearing reaction; or poor (–) when the tumor was still cellular without (or with limited) necrosis or fibrosis, especially when compared with the biopsy specimen. This grading was based on evaluation of the intra- and extraosseous tumor components combined and was done without knowledge of the MR results.

Signal-intensity ratios, tumor-volume ratios, and pathologic response were correlated with each other, and expressed as correlation coefficients.

## Results

The data for tumor-volume ratios, signal-intensity ratios, and pathologic response are summarized in Table 1 and Figure 1. We considered a difference in tumor volume or signal intensity of less than 5% not to represent substantial change. Accordingly, tumor-volume ratios and signal-intensity ratios between 0.95 and 1.05 were interpreted as stable.

### *Signal Intensity and Histopathology*

The histopathologic findings of 17 resected tumors were compared with signal-intensity ratios. A good response (six of which were certain and four of which were probable) was assumed in 10 patients. A poor response was seen in seven patients.

*Signal intensity of the intraosseous component of the tumor on T1-weighted sequences.*—In 14 patients, the signal intensity of the intraosseous component of the tumor on T1-weighted images could be compared with histopathology. No correlation was found between changes in signal intensity and pathologic response ( $r = .10$ ,  $p = .73$ ).

*Signal intensity of the extraosseous component of the tumor on T1-weighted sequences.*—In 14 patients, the signal intensity of the extraosseous component of the tumor on T1-weighted images could be compared with histopathology. No correlation was found between changes in signal intensity and pathologic response ( $r = .15$ ,  $p = .62$ ).

*Signal intensity of the intraosseous component of the tumor on T2-weighted sequences.*—In 16 patients, the signal intensity of the intraosseous component of the tumor on T2-weighted images could be compared with histopathology. No correlation was found between changes in signal intensity and pathologic response ( $r = .09$ ,  $p = .75$ ).

*Signal intensity of the extraosseous component of the tumor on T2-weighted sequences.*—In 17 patients, the signal intensity of the extraosseous component of the tumor on T2-weighted images could be compared with histopathology (Fig. 1A). A correlation was found between a decrease in signal intensity and good pathologic response and between an increase of signal intensity and poor pathologic response ( $r = .57$ ,  $p = .02$ ). In 14 of 17 patients, a relation was seen with pathologic response, in that a decrease in the signal-intensity ratio of the extraosseous component of the tumor indicated a good response (Fig. 2) and an increase or stable signal intensity indicated a poor response (Fig. 3). In one patient with a histopathologically good response, there was no change in signal intensity (Table 1, case 9). However,



**TABLE 1: Comparison Between Changes in Tumor Volume and Changes in Relative Intra- and Extraosseous Signal Intensities, Measured with T1- and T2-weighted Sequences During Chemotherapy**

Case No.	Tumor-Volume Ratio	Signal-Intensity Ratio (550/30)		Signal-Intensity Ratio (2000/100)		Histopathologic Response
		Intraosseous	Extraosseous	Intraosseous	Extraosseous	
1	0.33	0.82	0.59	1.26	0.76	++
2	0.49	— <sup>a</sup>	1.12	— <sup>a</sup>	1.86	—
3	0.58	1.09	1.03	1.09	0.82	+
4	0.61	1.00	0.73	0.77	0.52	++
5	0.62	0.85	1.36	0.73	0.70	++
6	0.64	1.98	0.74	1.12	0.22	+
7	0.80	1.32	1.09	0.48	0.52	++
8	0.81	1.19	0.88	1.20	0.52	—
9	0.88	— <sup>b</sup>	— <sup>b</sup>	1.71	0.96	++
10	0.94	0.78	0.60	0.62	0.50	++
11	1.07	1.26	0.97	1.28	0.87	+
12	1.23	1.36	0.92	1.23	1.38	—
13	1.24	0.93	0.64	1.07	1.09	+
14	1.25	— <sup>b</sup>	— <sup>b</sup>	1.06	1.01	—
15	1.53	0.86	— <sup>b</sup>	1.20	1.98	—
16	1.74	0.54	0.56	0.50	1.00	—
17	2.95	1.23	1.34	0.77	1.00	—
18	0.84	1.23	0.92	0.81	0.40	No material
19	1.08	0.67	0.82	1.04	1.10	No material
20	0.15	— <sup>b</sup>	— <sup>a</sup>	2.01	— <sup>a</sup>	No material

Note.—Tumor-volume ratio is the ratio of tumor volume after chemotherapy to tumor volume before treatment. Signal-intensity ratio is the ratio of relative signal intensity of tumor to fat measured after chemotherapy to relative signal intensity before treatment. Histopathologic responses were rated as good (++), probably good (+), and poor (—).

<sup>a</sup> The intraosseous or extraosseous components of these Ewing sarcomas were too small for reliable measurements.

<sup>b</sup> Data of these measurements were not comparable because of insufficient imaging technique.

extensive necrosis was found both in the biopsy specimen and in the resected specimen. Furthermore, this patient had had a fracture through the tumor with hematoma in the surrounding soft tissues. In one patient, the signal intensity of the extraosseous tumor component decreased, despite a histopathologic poor response (case 8). This patient had a fibroblastic osteosarcoma. In another patient, signal intensity increased, while histopathologic results showed a probably good response (case 13). Large cavities with large amounts of blood and large areas of necrosis were found.

#### Tumor Volume and Histopathology

In 10 of the 17 patients in whom the pathologic response could be evaluated, a decrease was seen in tumor volume after chemotherapy. In seven patients tumor volume increased during the course of chemotherapy. A correlation was found between changes in tumor volume and pathologic response ( $r = .53$ ,  $p = .03$ ) (Fig. 1B). Decrease in tumor volume indicated a good or probably good pathologic response in eight of 10 patients. Increase in tumor volume indicated a poor pathologic response in five of seven patients.

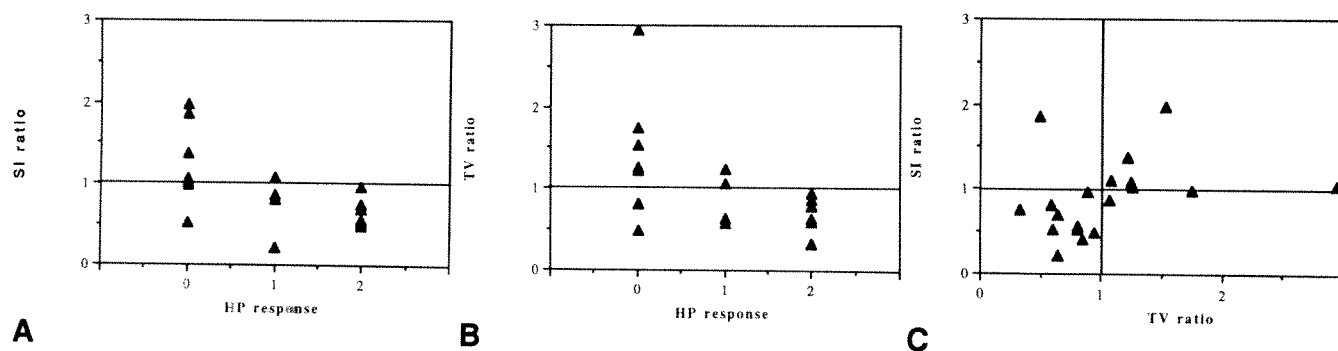


**Fig. 1.—Graphic representation of changes in signal intensity (SI), tumor volume (TV), and histopathologic (HP) response.**

**A.** Relative signal-intensity ratios after/before chemotherapy of extraosseous tumor component on T2-weighted images correlated with histopathologic response. Pathologic response was graded good (2), probably good (1), or poor (0). Horizontal line indicates stable signal intensity (signal-intensity ratio = 1). Data from 17 patients were plotted ( $r = .57$ ,  $p = .02$ ).

**B.** Tumor-volume ratios after/before chemotherapy correlated with histopathologic response. Horizontal line indicates unchanged tumor volume (tumor-volume ratio = 1). Data from 17 patients were plotted ( $r = .53$ ,  $p = .03$ ).

**C.** Relative signal-intensity ratios after/before chemotherapy of extraosseous tumor component on T2-weighted images correlated with tumor volume ratios after/before chemotherapy. Vertical line indicates stable tumor volume (tumor-volume ratio = 1). Horizontal line indicates stable signal intensity (signal-intensity ratio = 1). Data from 19 patients were plotted ( $r = .29$ ,  $p = .24$ ).

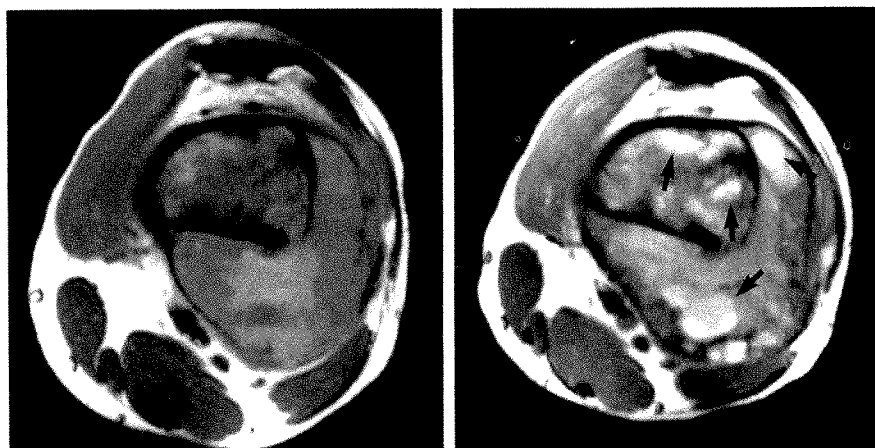


Fig. 2.—Osteosarcoma of the femur (case 7).  
A, T1-weighted MR image (500/30). Before chemotherapy, intra- and extraosseous tumor components have an intermediate signal intensity.

B, T1-weighted MR image after treatment. Signal intensities of both tumor components have increased. Some focal areas have high signal intensity (arrows). A decrease in tumor volume was measured in this patient.

C, T2-weighted MR image (2000/100) before chemotherapy. Extraosseous component of tumor has rather homogeneous high signal intensity; intramedullary component has mixed signal intensity.

D, T2-weighted MR image after treatment. Signal intensities of both intra- and extraosseous components of tumor have decreased. Signal intensity of tumor has become inhomogeneous. Pathologic response was graded good.

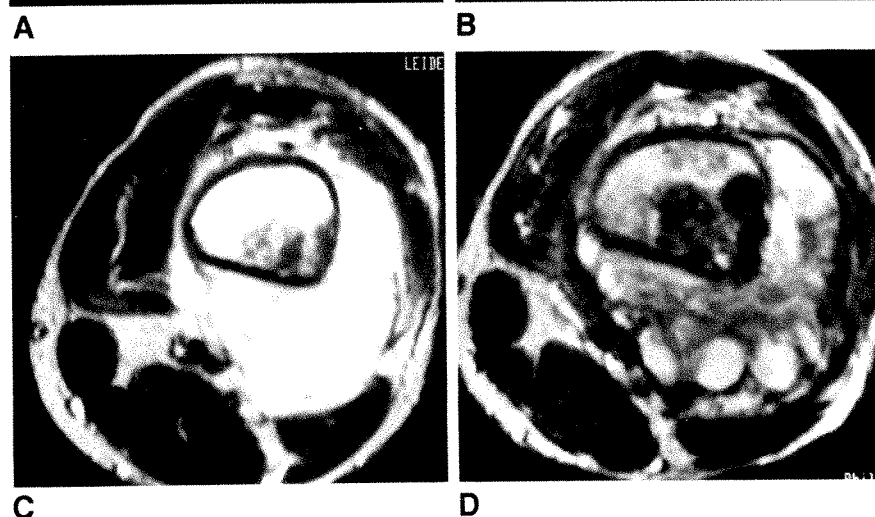


Fig. 3.—Osteosarcoma of the femur (case 12) on T2-weighted MR images (2000/100).

A, Before chemotherapy. Extraosseous component of the tumor has mixed partially high and partially intermediate signal intensity. High signal intensity in suprapatellar bursa (arrow) represents joint effusion.

B, After treatment. Tumor volume has clearly increased. Signal intensity of extraosseous component has increased also and has become more homogeneous. Histopathology of resected specimen showed poor response.

#### Signal Intensity and Tumor Volume

In 12 patients, a decrease in tumor volume was measured. In one of these patients the extraosseous component of the tumor after chemotherapy was too small for measurements of signal intensity to be reliable (case 20, Fig. 4). In the other eight patients tumor volume increased during the course of chemotherapy.

*Signal intensity of the intraosseous component of the tumor on T1-weighted sequences.*—The signal-intensity ratio of the

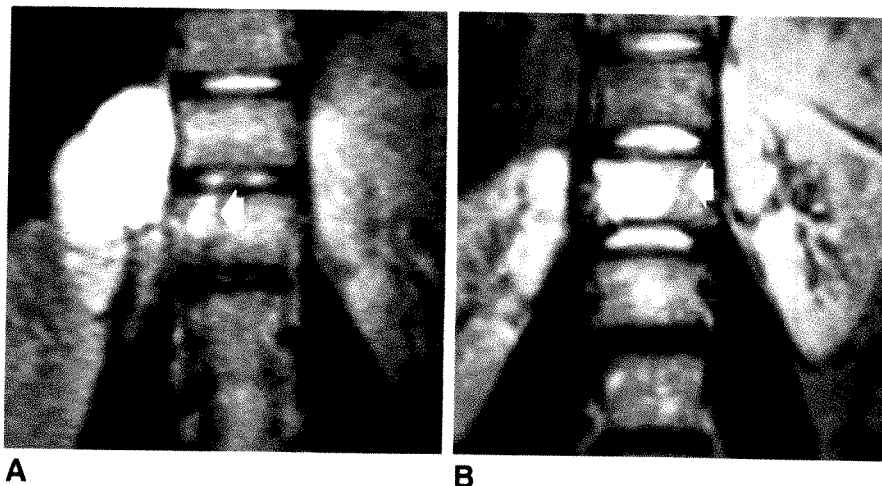
intraosseous component of the tumor on T1-weighted images could be calculated in 16 patients. No correlation was found between changes in signal intensity and changes in tumor volume ( $r = .10$ ,  $p = .72$ ).

*Signal intensity of the extraosseous component of the tumor on T1-weighted sequences.*—The signal-intensity ratio of the extraosseous component of the tumor on T1-weighted images could be calculated in 16 patients. No correlation was found between changes in signal intensity and changes in tumor volume ( $r = .22$ ,  $p = .41$ ).

Fig. 4.—Ewing sarcoma of second lumbar vertebra (case 20) on T2-weighted MR images (2000/100).

A, Prechemotherapy image shows large soft-tissue component. Intraosseous component of tumor is hardly discernible (arrow).

B, After treatment. Soft-tissue component has disappeared almost totally. Note increase in signal intensity of intraosseous component (arrow).



*Signal intensity of the intraosseous component of the tumor on T2-weighted sequences.*—The signal-intensity ratio of the intraosseous component of the tumor on T2-weighted images could be calculated in 19 patients. No correlation was found between changes in signal intensity and changes in tumor volume ( $r = .36$ ,  $p = .13$ ).

*Signal intensity of the extraosseous component of the tumor on T2-weighted sequences.*—The signal-intensity ratio of the extraosseous component of the tumor on T2-weighted images could be calculated in 19 patients (Fig. 1C). No correlation was found between changes in signal intensity and changes in tumor volume ( $r = .29$ ,  $p = .24$ ).

## Discussion

Although the optimal form of adjuvant therapy has still not been decided, preoperative chemotherapy has become one of the cornerstones in the treatment of patients with Ewing sarcoma and osteosarcoma [1–3]. The results of chemotherapy monitoring with clinical evaluation, conventional radiography, or Tc-diphosphonate scintigraphy are not yet fully established and sometimes equivocal [8, 14–16]. Some authors report good results with angiography and CT [4–9]. However, the invasive nature of angiography and the absence of quantitative data when CT is used are disadvantages that can be overcome with MR imaging. The successful use of MR imaging in staging bone sarcoma and the observed changes in MR studies in patients treated with chemotherapy prompted us to explore the potential of MR imaging in monitoring chemotherapy [17–20]. In the present study, changes in signal intensities of intra- and extraosseous tumor components in relation to pathologic response and in relation to changes in tumor volume were evaluated.

No relation was found between tumor-volume ratio and histopathologic response and changes in intraosseous signal intensity or signal intensity measured on T1-weighted images.

A correlation was observed between the signal-intensity ratio of the extraosseous component of the tumor measured on T2-weighted images and chemotherapy response evaluated with histopathologic examination. In seven patients a satisfactory response, indicated by a decrease in tumor volume and histopathologic findings, was correlated with a de-

crease in the signal intensity of the soft-tissue component. Likewise, a poor response, according to histopathologic examination and tumor-volume ratio, was correlated with a stable or increased signal intensity in the soft-tissue component of the tumor in five patients. The value of the signal-intensity changes in the soft-tissue component was also suggested by the observations in the three patients without histopathologic verification: a decreased signal-intensity ratio corresponded to a decreased tumor-volume ratio in one of these patients (Table 1, case 18); in the second patient (case 19), an increase in signal intensity corresponded to an increase in tumor volume. In the third patient in this group, the signal intensity of the extraosseous component of the tumor could not be measured, but a satisfactory response was indicated by virtual disappearance of the soft-tissue component (case 20, Fig. 4).

In only five patients was there no total agreement between the signal-intensity ratio of the extraosseous tumor component on T2-weighted sequences, the tumor-volume ratio, and the histopathologic examination. In case 2, both the increased signal intensity and histopathologic findings, exhibiting only viable tumor tissue without signs of necrosis or fibrosis, indicated poor response (Fig. 5). Only the tumor volume decreased in this patient. Although we have no satisfactory explanation for this discrepancy between decreased tumor volume and poor histopathologic response, the increased signal intensity truly indicated the absence of histopathologic reaction within the tumor. In case 9, the stable signal intensity was not in accordance with a satisfactory response to chemotherapy, as indicated by both tumor-volume ratio and histopathologic results. However, the prechemotherapy biopsy in this patient already showed a large amount of necrosis. In the resected specimen almost total necrosis was found in addition to hemorrhage, as a result of the fracture through the tumor. This hemorrhage and necrosis may account for the relatively stable signal intensity. In case 11, both the signal-intensity ratio and histopathologic results indicated a satisfactory response, but a minor increase in tumor volume was indicated by a tumor-volume ratio of 1.07. We have no good explanation for this slight increase in tumor volume. However, the extensive fibrosis observed on histopathologic examination, without substantial bleeding, probably outweighs the contradict-

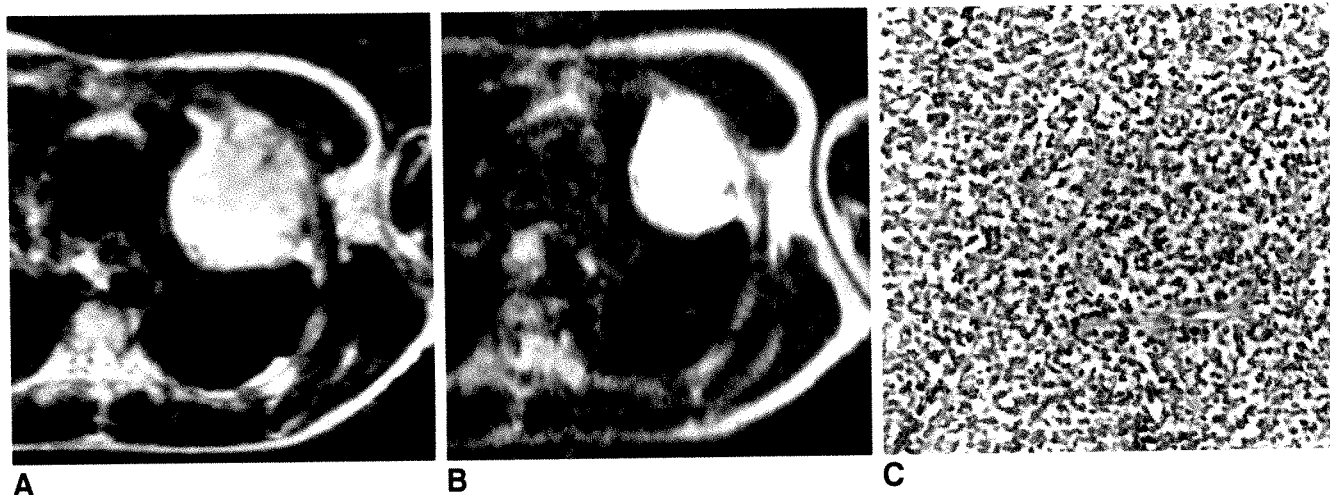


Fig. 5.—Ewing sarcoma of fourth left rib (case 2) on T2-weighted MR images (2000/100).

A, Before chemotherapy. Lesion with homogeneously high signal intensity is seen.

B, After therapy. Tumor volume has decreased. Signal intensity of tumor has increased.

C, Histopathology of resected specimen shows high cellularity without necrosis or fibrosis; this was classified as poor response. (H and E,  $\times 200$ )

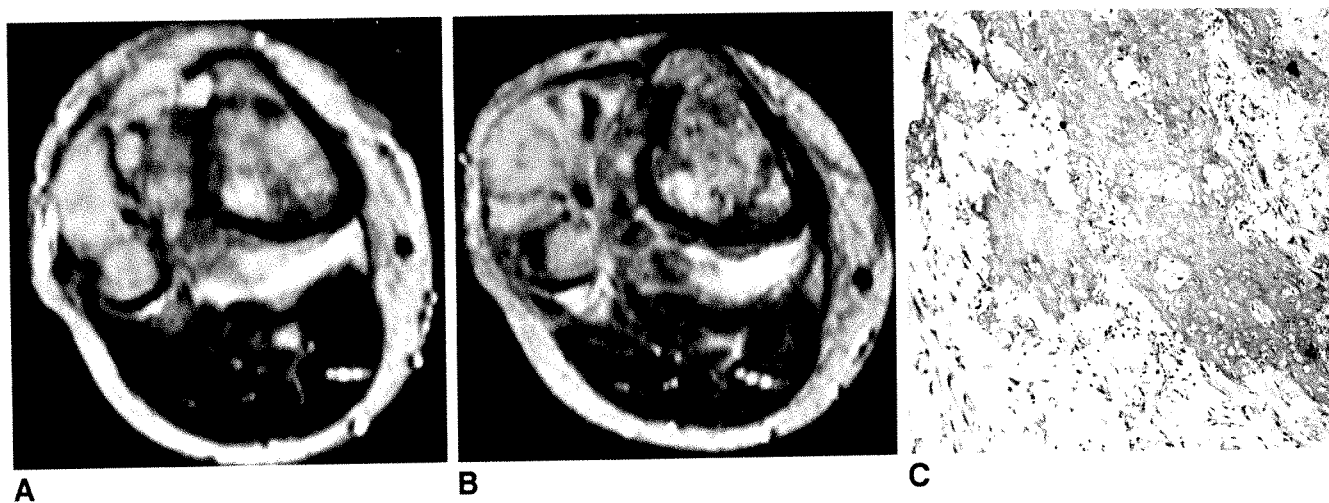


Fig. 6.—Osteosarcoma of the tibia (case 11) on T2-weighted MR images (2000/100).

A, Extraosseous component of tumor initially has inhomogeneous signal intensity.

B, After treatment. Signal intensity is still inhomogeneous, but measurements showed decrease in signal intensity. Tumor volume did increase.

C, Histopathology of resected specimen shows extensive fibrosis and low cellularity with many empty lacunas in tumor bone. Pathologic response was classified as probably good. (H and E,  $\times 100$ )

ing tumor-volume ratio, and a satisfactory response is therefore more likely (Fig. 6). In case 8, the decrease in tumor size and signal-intensity ratio indicated a satisfactory response, whereas histopathologic examination showed a poor response. This patient had a fibroblastic osteosarcoma. At pathologic examination of the resected tumor, spindle cells and no signs of response to chemotherapy were seen. The fibrous character of the tumor may have complicated the evaluation of histology and signal intensities. This may account for the discrepancy between tumor volume and signal intensity on the one hand and the interpretation of histopathology on the other. Another contradiction was found in case 13: a poor response was indicated by both tumor-volume ratio and signal-intensity ratio, whereas histopathologic examination was graded as a probable good response. Pathologic examination of the resected specimen showed cavities with large amounts of blood and necrosis. The increases in

signal intensity and tumor volume probably reflect the necrosis and bleeding, which in this case should be regarded as good response. Probably, focal areas of distinct increases in signal intensity can indeed represent local necrosis and hemorrhage, and thus may indicate good response to treatment. This should be considered when evaluating the images of any individual patient. Another complicating factor to be aware of is that the morphologic judgment of the effect of chemotherapy depends largely on comparison with the pretreatment biopsy, which is not necessarily representative of the whole tumor.

The decrease in signal intensity on T2-weighted images (2000/100) is predominantly related to a shortened T2 relaxation time and to a lesser extent to a decreased spin density. The shortened T2 relaxation time in turn reflects a decrease in the amount of extra- and intracellular free water and/or a relative increase of intracellular water bound to macromole-

cules [21]. The absence of preexisting bone and the lesser extent of reactive bone formation in the soft-tissue tumor component probably explains why the extraosseous tumor component is more suitable than the intraosseous component as a parameter of chemotherapy response.

Our observation of a decreased signal intensity on T2-weighted images as an indication for satisfactory response to chemotherapy is in accordance with the results of Redmond et al. [12], but partly contradicts the increase in T2 relaxation time reported by Maas et al. [22] and Just et al. [23]. This controversy is difficult to explain at this time, but it may be related to a small sample volume in the studies of Maas et al. (eight patients) and Just et al. (five patients), as well as to the fact that these authors did not measure T2 relaxation times separately in the intra- and extraosseous components. In our study, when the changes in the intraosseous tumor component were observed in six of 10 satisfactory histopathologic respondents, we found an increase in intraosseous signal intensity on T2-weighted images. Our findings refer only to changes in the extraosseous component of the tumor on T2-weighted images. Furthermore, we did not focus on focal changes in signal intensity, while some focal increase in signal intensity possibly can represent local necrosis, and thus a good response to therapy (Table 1, case 13). The reduction in T2 values as a positive indication of good response has recently been reported for another type of tumor. Of 18 patients with mediastinal involvement by Hodgkin disease, a significant decrease in T2 values and tumor signal-intensity ratio were found in all patients. The relative decrease in tumor size correlated well with the signal-intensity ratios [24, 25].

Our study suggests that if measured on T2-weighted images, signal-intensity changes in the extraosseous component of Ewing sarcoma and osteosarcoma in addition to changes in tumor volume may be indicative of a response to chemotherapy. If confirmed in more extensive studies, this observation may lead to an enhanced rationale for the timing of local therapy in relation with chemotherapy. Also, reliable preoperative monitoring of chemotherapy may have an impact on planning postoperative chemotherapy. Considering the high morbidity of chemotherapy, one of the major aims of further research in this field must address the question of whether MR imaging is able to discriminate good from poor respondents at an early stage. The present results are encouraging and have prompted the start of a prospective study in our institution.

#### ACKNOWLEDGMENTS

We thank G. J. Fleuren and H. Beerman for assistance and G. Kracht and K. G. van der Ham for preparing the photographs.

#### REFERENCES

1. Rosen G, Caparros B, Huvos AG, et al. Preoperative chemotherapy for osteogenic sarcoma: selection of postoperative adjuvant chemotherapy based on the response of the primary tumor to preoperative chemotherapy. *Cancer* 1982;49:1221-1230.
2. Winkler K, Beron G, Kotz R, et al. Neoadjuvant chemotherapy for osteogenic sarcoma: results of a cooperative German/Austrian study. *J Clin Oncol* 1984;2:617-624.
3. Thompson EI. The role of chemotherapy in the management of Ewing sarcoma. In: Ryan JR, Baker LO, eds. *Recent concepts in sarcoma treatment*. Dordrecht, the Netherlands: Kluwer, 1988:218-233.
4. Shirkhoda A, Jaffe N, Wallace S, Ayala AG, Lindell MM, Zornoza J. Computed tomography of osteosarcoma after intraarterial chemotherapy. *AJR* 1985;144:95-99.
5. Mail JT, Cohen MD, Mirkin LD, Provisor AJ. Response of osteosarcoma to preoperative intravenous high-dose methotrexate chemotherapy: CT evaluation. *AJR* 1985;144:89-93.
6. Rotte KH, Kriedemann E, Geyer J, et al. Zum Wert der Computertomographie für das Monitoring der präoperativen Chemotherapie des Osteosarkoms. *ROFO* 1989;150(1):8-12.
7. Kumpman W, Lechner G, Wittich GR, et al. The angiographic response of osteosarcoma following pre-operative chemotherapy. *Skeletal Radiol* 1986;15:96-102.
8. Chuang VP, Benjamin R, Jaffe N, et al. Radiographic and angiographic changes in osteosarcoma after intraarterial chemotherapy. *AJP* 1982;139:1065-1069.
9. Carrasco CH, Charnsangavej C, Raymond AK, et al. Osteosarcoma: angiographic assessment of response to preoperative chemotherapy. *Radiology* 1989;170:839-842.
10. Ross B, Helsper JT, Cox LJ, et al. Osteosarcoma and other neoplasms of bone: magnetic resonance spectroscopy to monitor therapy. *Arch Surg* 1987;122:1464-1469.
11. Just M, Gutjahr P, Juretschke HP, et al. 31Phosphorspektroskopie bei osteogenem Sarkom. *ROFO* 1987;146,2:144-148.
12. Redmond O, Stack J, Dervan P, Hurson B, Carney D, Ennis JT. Evaluation of osteogenic sarcomas using magnetic resonance imaging relaxation values and magnetic resonance spectroscopy. Presented at the annual meeting of the Society of Magnetic Resonance in Medicine, San Francisco, August 1988.
13. Boskamp EB. Improved surface coil imaging in MR: decoupling of the excitation and receiver coils. *Radiology* 1985;157:449-452.
14. Sommer HJ, Riebel T, Winkler K, Heise U, Delling G. Vergleich röntgenologischer und histologischer Befunde bei Osteosarkomen nach präoperativer Chemotherapie. *ROFO* 1985;143,1:74-83.
15. Riebel T, Knop J, Winkler K, Delling G. Vergleich röntgenologische und nuklearmedizinische Untersuchungen beim Osteosarkom zur Beurteilung der Effektivität einer präoperativen Chemotherapie. *ROFO* 1986;145,4:365-372.
16. Smith J, Heelan RT, Huvos AG, et al. Radiographic changes in primary osteogenic sarcoma following intensive chemotherapy. *Radiology* 1982;143:355-360.
17. Bloem JL, Falke THM, Taminiau AHM, et al. Magnetic resonance imaging of primary malignant bone tumors. *RadioGraphics* 1985;6:853-886.
18. Bloem JL, Taminiau AHM, Eulerink F, Hermans J, Pauwels EKJ. Radiologic staging of primary bone sarcoma: MR imaging, scintigraphy, angiography, and CT correlated with pathologic examination. *Radiology* 1988;169:805-810.
19. Boyko OB, Cory DA, Cohen MD, Provisor A, Mirkin D, De Rosa GP. MR imaging of osteogenic and Ewing sarcoma. *AJR* 1987;148:317-322.
20. Frouge C, Vanel D, Coffre C, Couanet D, Contesso G, Sarrazin D. The role of magnetic resonance imaging in the evaluation of Ewing sarcoma. *Skeletal Radiol* 1988;17:387-392.
21. Mitchell DG, Burk Jr LD, Vinitski S, Rifkin MD. The biophysical basis of tissue contrast in extracranial MR imaging. *AJR* 1987;149:831-837.
22. Maas R, Langkowski HJ, Heller MA, et al. Follow-up study of bone tumors during chemotherapy by T1 and T2 relaxation times. Presented at the annual meeting of the Society of Magnetic Resonance in Medicine, San Francisco, August 1988.
23. Just M, Gutjahr P, Higer HP, et al. Möglichkeiten der MR-Tomographie in der Therapiekontrolle malignen Knochentumoren. *ROFO* 1987;147,4:413-419.
24. Nyman RS, Rehn SM, Glimelius BLG, Hagberg HE, Hemmingsson AL, Sundström CJ. Residual mediastinal masses in Hodgkin disease: prediction of size with MR imaging. *Radiology* 1989;170:435-440.
25. Webb WR. MR imaging of treated mediastinal Hodgkin disease. *Radiology* 1989;170:315-316.

## Book Review

**Magnetic Resonance Imaging**, 2nd ed. Vol. 2: Physical Principles and Instrumentation. By C. Leon Partain, Ronald R. Price, James A. Patton, Madan V. Kulkarni, and A. Everette James, Jr. Philadelphia: Saunders, 840 pp., 1988. \$400 (vols. 1 and 2)

The greatly expanded second edition of *Magnetic Resonance Imaging* was prompted by the further development of MR techniques and applications since publication of the first edition. Volume 1 deals with clinical applications of MR, and volume 2 comprehensively covers fundamental principles. The 840 pages of volume 2 includes 49 chapters, each one written by experts in their fields. The text is grouped into six primary categories: physics and chemistry (62 pages), relaxation and relaxometry (96 pages), instrumentation (303 pages), site planning (59 pages), spectroscopy (130 pages), and new areas of research and development (176 pages).

In each of the chapters, reputable authors contribute excellent discussions on all of the important physical principles. Because of the different authors, writing styles tend to vary, but the actual presentation is uniformly clear. I rate 12 chapters as outstanding. Most of the other contributions are good, and only a few chapters are substandard. The organization of each chapter is consistent, and the editors have succeeded in ensuring nearly uniform notation. The text is kept simple so that both the novice and the more experienced reader can appreciate its content. The illustrations are of high quality, and the MR images are of high contrast. By making use of high-quality paper and a clear printing style, the printers have succeeded in producing a visually pleasing book.

The sections on instrumentation and site planning that occupy nearly one-half of volume 2 provide a solid description of the hardware and the software involved in generating MR images and give sound advice on site planning and quality assurance. No prerequisite background knowledge in electronics, computing, or engineering is assumed, and none is required. These topics are presented in such a way as to guide the less experienced reader toward understanding and therefore making a better use of the MR imaging instrument. The importance of optimizing scan parameters is understood easily by reading chapters such as "Understanding Basic MR Pulse Sequences," "T1 and T2 Measurements," and "Artifacts in T1 and T2 and Gating: Cardiac and Respiratory."

The section on new areas of research and development is the

second largest category, probably because it was thought that some of the newer methods covered in this section would be in clinical use by the time the book is read, as indeed is the case of the chapter on high-field MR. Nonetheless, some of the chapters in this section easily could have been condensed as most readers will benefit little from reading topics such as "Advanced Methods for Spin Density," "T1 and T2 Calculations in MRI," or "Advanced Statistical Methods for Tissue Characteristics."

Another possible deficiency of the book is the limited discussion of the basic chemical and physical principles of MR imaging (only 62 pages); three times as much space is devoted to the section on new research areas. The discussion of nuclear magnetic resonance (NMR) chemical principles is somewhat limited where a rather detailed description of Fourier transform NMR is warranted, and examples of phosphorus-31, carbon-13, and hydrogen-1 NMR spectra of biologically active metabolites are lacking. In chapter 60, the discussion of current NMR water-signal-suppression techniques is insufficient. Also, the four printed pages devoted to the fundamental limitations of MR imaging are not nearly enough to cover such an important topic. On the other hand, the presentation of relaxometry, in chapters 63 and 64, may be excessive. Obvious omissions are topics dealing with interfacing of MR with other imaging techniques and image postprocessing.

Despite these faults, which are relatively minor, volume 2 is a comprehensive account of principles of MR imaging. It successfully tackles in depth most of the relevant topics. Unlike most reference books on MR imaging that give detailed accounts of special topics related to MR, this book does its best to cover MR imaging in its entirety. Its easy readability makes it a first choice as a reference book for any person who is actively involved in MR imaging or first entering the field.

Elisha Berman  
University of Tennessee Medical Center  
Knoxville, TN 37920-6999



## Pictorial Essay

# MR Imaging of Sacral and Presacral Lesions

Louis H. Wetzel<sup>1</sup> and Errol Levine

Sacral lesions are frequently overlooked because of the nonspecificity of associated symptoms and because the posterior curvature of the sacrum and the presence of overlying bowel gas cause difficulties in plain film evaluation [1]. CT is an excellent technique for imaging the sacrum and presacral space [1]. MR imaging has many of the advantages of CT, but adds multiplanar capability and improved soft-tissue contrast. This essay illustrates the use of MR imaging in evaluating sacral disorders.

### Materials and Methods

Between May 1986 and August 1989, 50 patients with sacral and presacral lesions were examined with MR imaging. Eleven had histologically proved primary sacral neoplasms including schwannoma (three), chordoma (two), giant-cell tumor (two), ependymoma (two), aneurysmal bone cyst (one), and malignant fibrous histiocytoma (one). Fourteen patients had secondary sacral neoplasms originating from breast carcinoma (three), lung cancer (two), rectal carcinoma (two), thyroid carcinoma (one), renal cell carcinoma (two), malignant melanoma (one), lymphoma (two), and multiple myeloma (one). Eight patients had surgically confirmed spinal dysraphism. Ten patients had sacral arachnoid cysts. These were confirmed in six patients by filling of lesions with contrast medium during myelography. One patient had a surgically confirmed anterior sacral meningocele. Two patients had surgically proved presacral teratomas. Four patients had presacral extension of pelvic carcinoma including recurrent rectal carcinoma (two), bladder carcinoma (one), and carcinoma of the cervix (one).

MR studies were performed with a superconductive magnet (Magnetom, Siemens Medical Systems, Iselin, NJ) operated at 1.0 T. Multisection spin-echo imaging was used with section thicknesses of 4–10 mm and intersection spacing of 0–5 mm. Two pulse sequences were always used: 500–600/17–30 (TR/TE) and 2100–2500/30,90. Axial and sagittal images were always obtained and were often supplemented by coronal oblique sacral images. A body coil with a 50-cm field of view was used in 12 patients and a 37-cm elliptical surface coil was used in 38 patients.

### Sacral Neoplasms

Chordoma is the most common primary sacral neoplasm. It is a malignant neoplasm that arises from notochordal remnants. Typically the lesion begins in the midline and involves the fourth and fifth sacral vertebrae (Fig. 1) [1]. Tumor enlargement ultimately causes destruction of adjacent sacral segments and a presacral mass (Fig. 2). Giant-cell tumor is the second most common primary sacral neoplasm (Fig. 3) [1]. These tumors are often unresectable because of their large size or strategic location (Fig. 3) [1]. Neural tumors originating in the sacral canal include ependymoma and schwannoma. They have a mainly longitudinal intracanalicular growth pattern (Figs. 4 and 5). Ependymomas are malignant and arise from ependymal cell clusters in the filum terminale [1]. Schwannomas are usually benign.

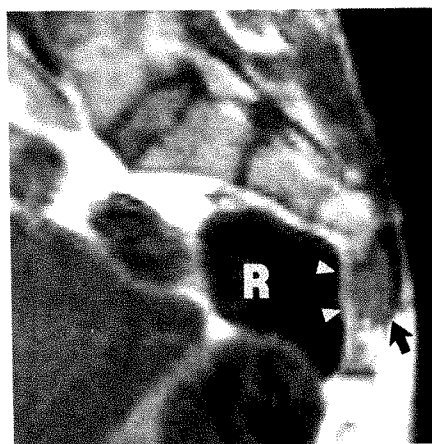
Metastases are the most common sacral neoplasms. They reach the sacrum hematogenously or via the subarachnoid

Received October 19, 1989; accepted November 21, 1989.

<sup>1</sup> Both authors: Department of Diagnostic Radiology, the University of Kansas Medical Center, 39th St. and Rainbow Blvd., Kansas City, KS 66103. Address reprint requests to L. H. Wetzel.

AJR 154:771–775, April 1990 0361–803X/90/1544–0771 © American Roentgen Ray Society





1



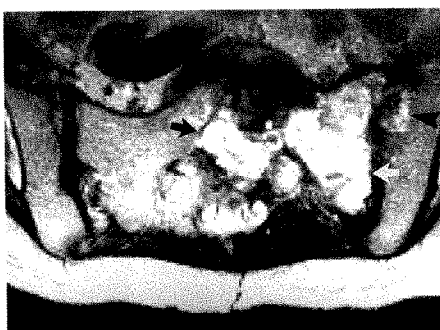
2

Fig. 1.—Small chordoma (arrow) on sagittal MR image, 500/30. Lesion arises in S4 but also involves contiguous parts of S3 and S5. Slight pre-sacral extension (arrowheads) indents posterior rectal wall (R). Distal sacrectomy was successfully performed through S2–S3 junction.

Fig. 2.—Chordoma. Sagittal MR image, 500/30, shows extensive neoplasm (arrowheads) with obliteration of sacral canal and pre- and postsacral extension. Note preservation of S1–S2 disk (arrow). Lack of involvement of disk indicates potential for radical resection. High-intensity areas in neoplasm (asterisks) corresponded to areas of hemorrhage in surgical specimen. Lesion was resected at mid S1 level.



A



B

Fig. 3.—Giant-cell tumor.

A, Axial MR image, 500/17, shows tumor (arrowheads) replacing normal marrow fat in left sacral ala and body of S1. Tumor surrounds neural canal containing first left ventral sacral nerve root (arrow).

B, Tumor (arrows) is inhomogeneous and of intermediate intensity on T2-weighted image, 2100/90. There is tumor extension (arrowhead) across left sacroiliac joint.

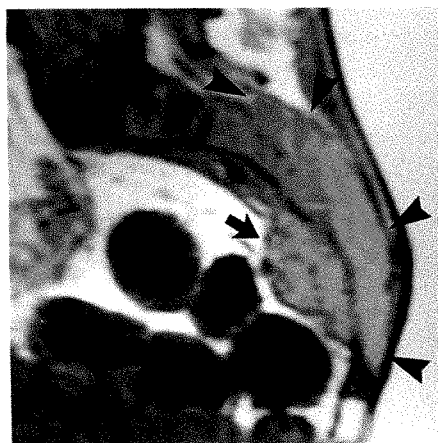
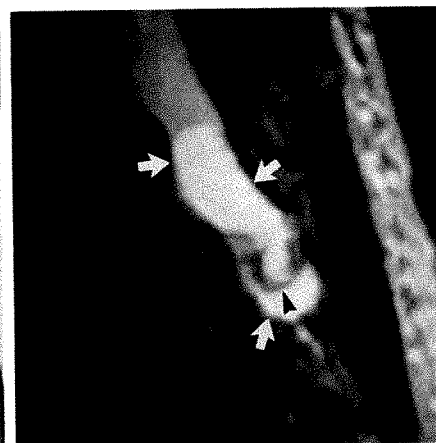


Fig. 4.—Ependymoma. Sagittal MR image, 500/30, shows neoplasm (arrowheads) filling most of sacral canal. Lesion has penetrated sacral cortex at S3–S5, resulting in presacral mass (arrow). Growth pattern of lesion is mainly longitudinal in sacral canal, suggesting neural origin.



A



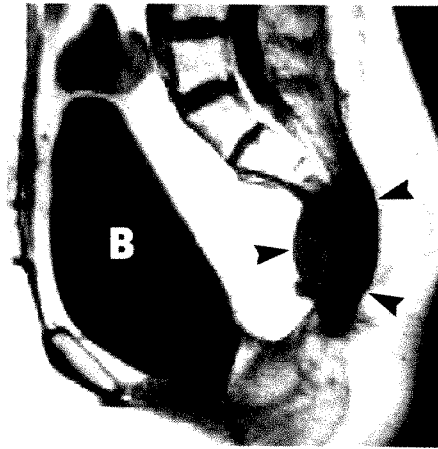
B

Fig. 5.—Schwannoma.

A, Sagittal MR image, 500/17, shows tumor (arrowheads) causing erosion of posterior surface of S2. High-intensity areas (arrows) corresponded to hemorrhage in surgical specimen. Confinement of lesion to sacral canal suggests neoplasm of neural origin.

B, T2-weighted sagittal MR image, 2100/90, reveals high intensity of neoplasm (arrows). Incomplete low-intensity ring (arrowhead) in lower part of tumor probably represents hemosiderin and ferritin deposition around hemorrhage.

Fig. 6.—Metastatic rectal carcinoma in patient who had previous abdominoperineal rectal resection. Sagittal MR image, 500/17, shows oval neoplasm (arrowheads) involving distal sacrum. There were no other metastases, and lesion probably reached sacrum via vertebral venous plexus of Batson. Note enlarged neurogenic bladder (B) and absence of rectum. Distal sacrectomy was performed.



6



7

Fig. 7.—Metastatic malignant melanoma in patient with brain metastasis from previously resected cutaneous melanoma. Patient had recent onset of bladder incontinence. Sagittal MR image, 500/17, shows metastasis (arrows) involving thecal sac at L5 and in sacrum. Lesion probably reached thecal sac via subarachnoid space.

Fig. 8.—Solitary sacral metastasis from occult renal cell carcinoma. Coronal oblique MR image, 600/25, shows metastasis (arrows) involving S1 and S2 and invading left first and second ventral neural canals.



8

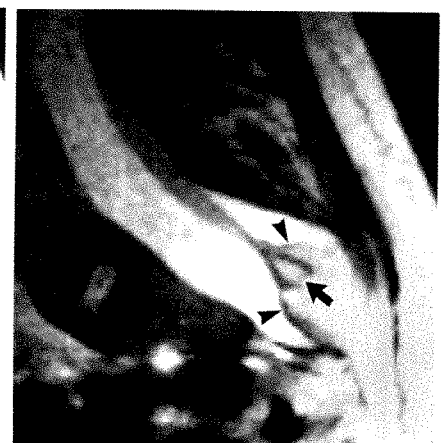


9

Fig. 9.—Sacral metastases from lung carcinoma in patient with rectal incontinence. Sagittal MR image, 500/17, shows metastases (asterisks) involving L4 and L5 and most of the sacrum. Expansile midsacral lesion (arrowheads) narrows sacral canal. Sacral radiation produced relief from symptoms.



A



B

Fig. 10.—Spinal dysraphism with tethered conus medullaris, partial sacral agenesis, and intradural lipoma.

A, Sagittal MR image, 500/17, shows absence of sacrum below level of S1. Conus (arrow) is tethered by intradural lipoma (L).

B, T2-weighted image, 2100/90, shows extension of neural tissue of tethered conus (arrow) into lipoma (arrowheads). Note thecal sac ectasia.

space (Figs. 6 and 7). Occult renal cell carcinoma or thyroid carcinoma may present with solitary, symptomatic sacral metastases (Fig. 8). Sacral metastases may also be encountered on MR imaging when patients with known primary neoplasms develop symptoms suggesting cauda equina compression (Figs. 7 and 9).

### Developmental Abnormalities

Spinal dysraphism is a developmental anomaly that includes various combinations of spina bifida, meningocele, myelomeningocele, lipomyelomeningocele, intradural lipoma, intradural dermoid cyst, and tethering of the spinal cord [2]. MR imaging

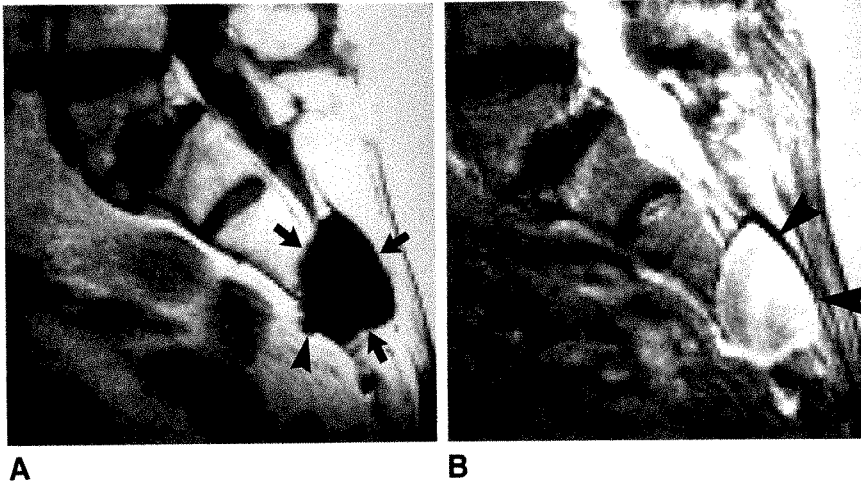


Fig. 11.—Sacral arachnoid cyst.

A, Sagittal MR image, 500/17, shows lesion (arrows) of intensity similar to CSF causing sacral erosion (arrowhead). Note degeneration of L5/S1 disk and spondylolisthesis of L5 on S1.

B, T2-weighted image, 2100/90, shows that cyst (arrowheads) remains isointense relative to CSF.



Fig. 12.—Sacral arachnoid cyst shown in coronal oblique MR image, 600/25. Cyst (solid arrow) arises from left S3 nerve sheath and causes medial displacement of adjacent left S4 nerve (open arrow). Generalized decrease in bone-marrow signal intensity was from myelofibrosis.

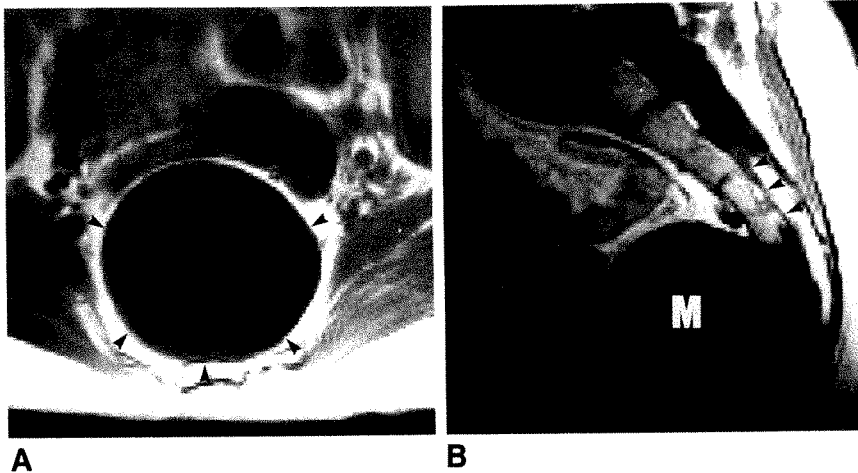


Fig. 13.—Anterior sacral meningocele in 47-year-old woman.

A, Axial MR image, 500/17, shows well-defined, low-intensity fluid collection (arrowheads) anterior to sacrum.

B, Sagittal MR image, 500/17, just left of midline reveals narrow channel (arrowheads) extending from meningocele (M) via defect in S4 to distal thecal sac.

is invaluable in showing these abnormalities (Fig. 10) and often obviates myelography in suspected spinal dysraphism. Sacral arachnoid cysts most commonly arise as diverticula of the second and third sacral nerve sheaths [1]. Most are asymptomatic but some cause sacral erosion and back pain (Fig. 11). They are readily diagnosed on MR images (Figs. 11 and 12). An anterior sacral meningocele results from herniation of the caudal meninges through an anterior sacral defect. These lesions are often asymptomatic but may cause symptoms by compressing pelvic viscera [1]. MR imaging may show the connection between the cyst and the thecal sac (Fig. 13).

### Presacral Lesions

A wide variety of lesions occur in the presacral space. Sacrococcygeal teratomas are developmental in origin and are the most frequently encountered presacral masses in

children. They rarely first present in adult life (Fig. 14) [1]. Most patients with sacrococcygeal teratomas have no evidence of bony sacrococcygeal abnormalities [1]. Presacral extension of rectal, uterine, bladder, and prostatic carcinoma is readily diagnosed by CT and MR imaging. Diagnosis is more difficult when patients with pelvic carcinoma develop presacral masses after surgery or radiation therapy. Distinction between tumor recurrence and fibrosis is difficult with both CT and MR imaging (Fig. 15) [3].

### Discussion

Although MR imaging can usually distinguish sacral neoplasms of neural origin (Figs. 4 and 5) from those of bone origin (Figs. 1–3), it cannot distinguish among the various primary neoplasms and it cannot distinguish primary neoplasms from solitary metastases (Figs. 3 and 8). MR imaging is of great value in planning the management of sacral neo-

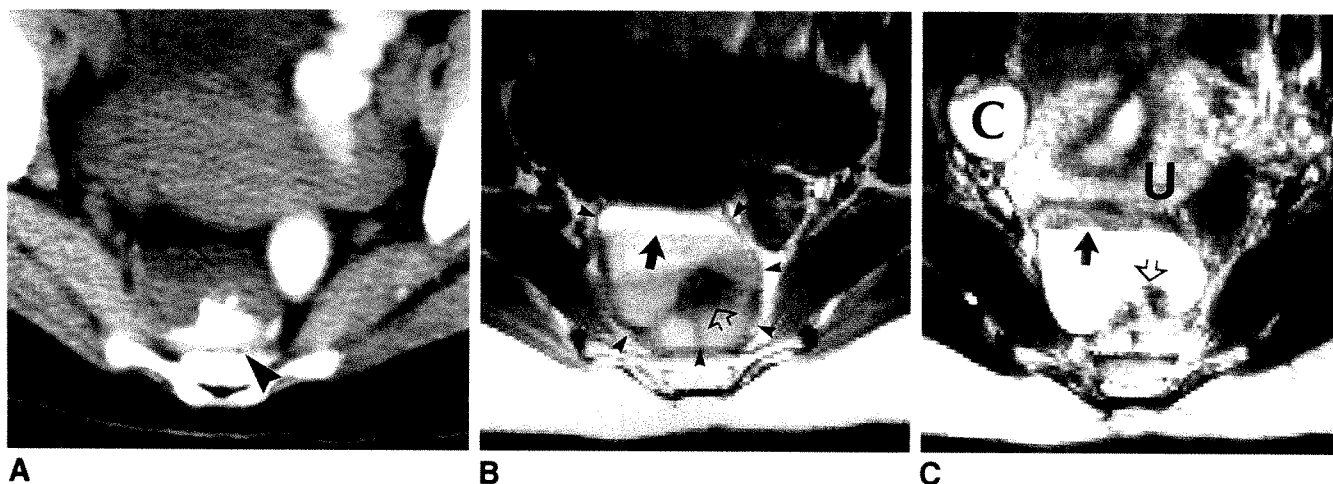


Fig. 14.—Benign presacral teratoma in 35-year-old woman.

A, CT scan shows presacral mass without evidence of sacral erosion. Note posterior calcification (arrowhead) and fat/fluid level (arrow) in lesion.

B, Axial MR image, 500/17, shows presacral mass (arrowheads). Note high-intensity fat (solid arrow) layering on lower-intensity fluid in lesion. Low-intensity area posteriorly (open arrow) represents calcification.

C, T2-weighted image, 2100/90, shows reversal of signal intensities at fat/fluid interface (solid arrow). Posterior calcification (open arrow) remains of low intensity. C = ovarian cyst; U = uterus.

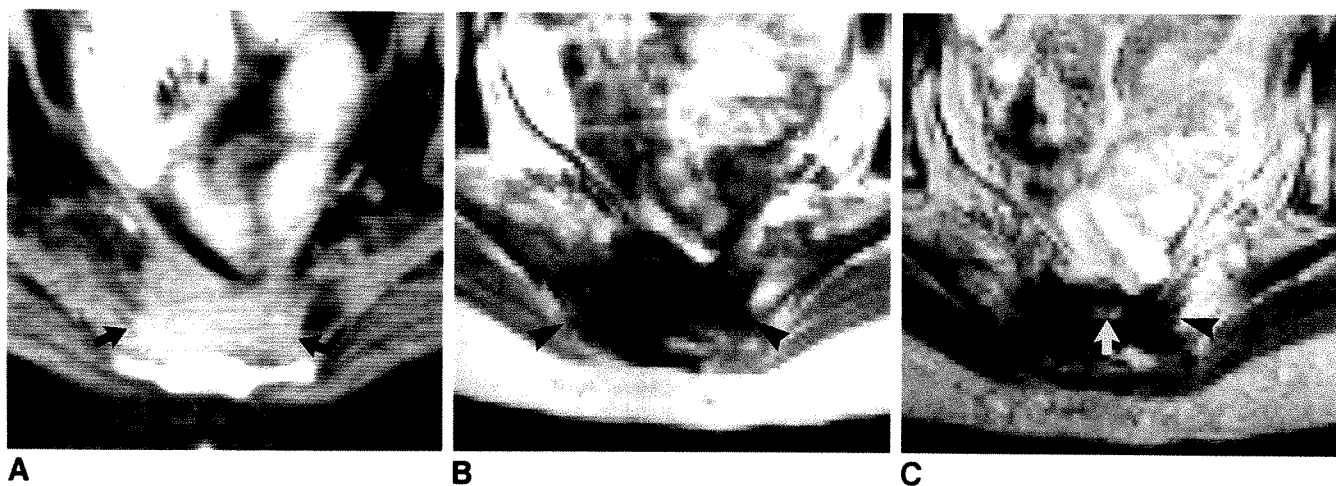


Fig. 15.—Local recurrence of rectal carcinoma after abdominoperineal resection of rectum.

A, CT scan shows mass (arrows) anterior to lower sacrum. Distinction between postoperative fibrosis and recurrent neoplasm is not possible.

B, Axial MR image, 500/17, shows low-intensity presacral mass (arrowheads).

C, T2-weighted image, 2100/90, shows that intensity of most of mass (arrowheads) remains low, suggesting fibrous tissue. However, high-intensity central area (arrow) represents recurrent neoplasm.

plasms because it accurately determines both their soft-tissue and intrasacral extent. If a lesion extends proximal to the S1–S2 disk space, it is usually unresectable. Patients with known bone metastases and symptoms suggesting cauda equina compression are often referred for spinal MR imaging. In this setting, sacral metastases are often responsible for the symptoms, therefore, the sacrum should be included in the MR study. MR imaging is more sensitive than CT in diagnosing spinal dysraphism; its use often obviates myelography in this disorder. MR also helps in the characterization of sacral arachnoid cysts. Benign and malignant presacral masses and their relationship to pelvic structures are well shown on MR images. However, MR often cannot distinguish between fibro-

sis and recurrent pelvic carcinoma in patients managed with surgery or radiation therapy [3].

#### REFERENCES

1. Levine E, Batnitzky S. Computed tomography of sacral and perisacral lesions. *CRC Crit Rev Diagn Imaging* 1984;21:307–374
2. Scatliffe JH, Kendall BE, Kingsley DPE, Britton J, Grant DN, Hayward RD. Closed spinal dysraphism: analysis of clinical, radiological, and surgical findings in 104 consecutive patients. *AJR* 1989;152:1049–1057
3. De Lange EE, Fechner RE, Wanebo HJ. Suspected recurrent rectosigmoid carcinoma after abdominoperineal resection: MR imaging and histopathologic findings. *Radiology* 1989;170:323–328

## Videotape Review

**MRI of the Foot and Ankle.** By Murray A. Solomon. (Videotape 5 of Murray Solomon's Magnetic Resonance Video Review.) Burlingame, CA: Murray Solomon's MRVR, (415) 692-8230, 1989. Single tape, \$125; series of 6 tapes, \$495

This tape is a 2-hour video review of normal anatomy and abnormalities encountered in the foot and ankle. The first 30 min are devoted to the usefulness of CT in this anatomic location and demonstration of anatomic structures important to interpretation. The subject matter then moves on to MR imaging and its usefulness in the foot and ankle for detection of marrow abnormalities, infections, tumors, arteriovenous anomalies, and tendon abnormalities. These are discussed with several representative examples. A review of MR anatomy points out important anatomic landmarks, and these structures are referred to throughout the course of the lecture. The speaker's tone, rate of delivery, and clarity are good, and except for perhaps unintentionally using the word "inspissated" when he means "insinuated" and an occasional faltering for a word or expression, there are no noticeable blemishes. The script, however, could be tighter in getting the message across with fewer words and fewer anecdotal examples. The images are of good quality.

I reviewed this tape with a group of residents in various stages of training, and because of its length, we had to do this over two sessions. Considerable useful information was obtained. My major criticism of the production is its length. Two hours is excessive for the information contained, and toward the end interest was flagging. This was unfortunate because it is toward the end of the tape that the author gets around to discussing MR applications in tendon and ligament abnormalities, in which it has a special role and in which a certain amount of forced learning is required. Tight editing, avoiding repetitious examples making the same point, and avoidance of the unusual unless it makes a particular point would help hone the

production. In particular, if this tape were limited to anatomy, highlighting the role of MR in commonly used circumstances, the unique place of MR in evaluation of certain clinical problems and anatomic structures, and a discussion of pitfalls, it would have abundant practical information. As things stand, the viewer must sieve all of the material that is presented to decide what are the particular strengths and limitations of MR. Finding or having to return to a point of interest on a videotape is more time-consuming when the material is lengthy. I also would like to suggest that the commercial sponsor be acknowledged without breaking abruptly during the scientific presentation for a formal statement from the sponsor, who identifies the MR units manufactured by his company. One further suggestion is to include with the high-quality image displays the TR and TE of each of the sequences so that the viewer might have an idea of the pulsing sequence of the image being discussed.

Viewing a videocassette is a painless way of learning. Whether it is more effective, enduring, and versatile than the conventional written word is likely to be a matter of personal preference. A videocassette of this nature is useful for group learning and discussion and is a worthwhile acquisition for departmental libraries. I also recommend this tape to those who have an audiovisual library and use this medium for learning and reference.

Murali Sundaram  
St. Louis University Medical Center  
St. Louis, MO 63110-0250



## Technical Note

# MR of the Shoulder with a 0.2-T Permanent-Magnet Unit

Makoto Sasaki,<sup>1</sup> Shigeru Ehara,<sup>1</sup> Tatsuhiko Nakasato,<sup>1</sup> Yoshiharu Tamakawa,<sup>1</sup> Yasuo Kuboya,<sup>2</sup> Miyoshi Sugisawa,<sup>3</sup> and Tsukasa Sato<sup>3</sup>

MR imaging at high field strength has shown precise anatomic structures of the shoulder and is expected to be an important technique in the diagnosis of shoulder disorders, such as rotator cuff injury and impingement syndrome [1-6]. However, permanent-magnet MR units with a low field strength have not been applied to the shoulder, mainly because of limited use of surface coils. We describe MR imaging of the shoulder with a low-field-strength, permanent-magnet MR unit.

## Materials and Methods

Sixteen patients with clinically suspected injury of rotator cuff (25-66 years old, 11 men and five women), and four healthy volunteers (23-38 years old, three men and one woman) were examined by using a 0.2-T permanent-magnet MR unit (Hitachi MRP-20-1; Hitachi Corp., Tokyo, Japan) with a solenoid collar-shaped receiver coil (18-cm diameter, 8-cm thick). Patients were positioned on the original broad bed (90-cm wide) so that the shoulder was at the isocenter of the magnetic field. The coil was placed just cephalad and at the same height as the shoulder and parallel to the magnetic field (Fig. 1).

In all cases, the spin-echo pulse sequence was used: mildly T1-weighted sequence, 750/38/4 (TR/TE/excitations), and proton-density and T2-weighted multiecho sequences, 2000/38,111/2, were acquired. The data acquisition matrix was  $256 \times 256$  (reconstructed from the 136 acquired data points in the phase-encode direction by using a half Fourier transform) with a 220- or 240-mm field of view. Scans were obtained with a thickness of 5 mm and no gap. Nine multimages were obtained in the axial plane and in the oblique coronal plane parallel to the axis of the glenohumeral joint. The data acquisition

times were 6.48 min for the T1-weighted images and 9.04 min for the combined proton-density and T2-weighted images.

## Results

In the four volunteers and in 14 of 16 patients with suspected injury of the rotator cuff, the rotator cuff was clearly visualized on T1-weighted, proton-density, and T2-weighted images (Fig. 2). In two cases, images were degraded by motion artifact, although the integrity of the rotator cuff could be evaluated with at least one sequence. In 12 of the 16 patients, abnormal signals in the supraspinatus tendon were identified with T1-weighted, proton-density, and T2-weighted images. Effusion in the subacromiosubdeltoid bursa and/or the glenohumeral joint was shown on T2-weighted images in eight patients. In two patients, the subacromial spur compressing the supraspinatus muscle, diagnostic of shoulder impingement syndrome, was shown. In two patients, the rotator cuff tear was confirmed surgically, and the rest of the patients were followed up with physical therapy.

## Discussion

The shoulder is one of the most difficult regions for MR imaging because it is some distance from the isocenter of the magnetic field. By using the off-center field-of-view technique and adequately positioned surface coils, diagnostic images can be obtained with superconductive high-field-strength MR units [1-5, 7] and 0.3-T permanent-magnet MR units [6, 8].

Received October 23, 1989; accepted after revision November 27, 1989.

<sup>1</sup> Center for Radiological Science, Iwate Medical University School of Medicine, Uchimarui 19-1, Morioka 020, Japan. Address reprint requests to M. Sasaki.

<sup>2</sup> Department of Orthopedics, Ohshuku-Onsen Hospital, Ohshuku, Shizukuishi 020-06, Japan.

<sup>3</sup> Department of Radiology, Ohshuku-Onsen Hospital, Ohshuku, Shizukuishi 020-06, Japan.



Fig. 1.—Positioning of patient and placement of coil.

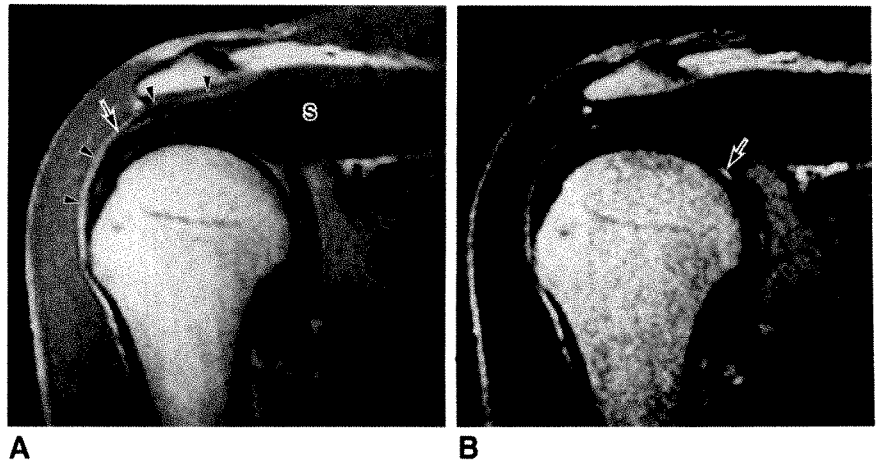


Fig. 2.—Oblique coronal MR images parallel to axis of glenohumeral joint of right shoulder of a normal 23-year-old volunteer.

A, Proton-density image (2000/38) shows supraspinatus muscle (S), its tendon (arrow), and peribursal fat plane (arrowheads).

B, T2-weighted image (2000/111) shows same plane as A. A small amount of fluid is noted in glenohumeral joint (arrow).

In the technique described, reasonably good MR images of the shoulder are obtained with a 5-mm-thick slice and a relatively short data acquisition time by using the 0.2-T permanent-magnet MR unit. The quality of our images may depend on three factors: (1) a high signal gain is obtained with the combination of the vertical magnetic field and the solenoid coil, (2) the shoulder can be placed at the isocenter of the magnetic field because of the wide opening of the gantry and the broad bed, and (3) the coil is placed proximal to the deep structures of the shoulder. Because of the wide aperture of the gantry and the broad bed, positioning of the patients and the coil is not difficult, even with large patients. The limitation of our technique is the relatively large field size because of the drop in signal-to-noise ratio in the small field of view (200 mm). We think acceptable MR imaging of the shoulder can be done even with a low-field-strength, permanent-magnet MR unit if this technique is used.

#### REFERENCES

1. Middleton WD, Kneeland JB, Carrera GF, et al. High-resolution MR imaging of the normal rotator cuff. *AJR* **1987**;148:559-564
2. Kieft GJ, Bloem JL, Obermann WR, Verbout AJ, Rozing PM, Doornbos J. Normal shoulder: MR imaging. *Radiology* **1986**;159:741-745
3. Kneeland JB, Middleton WD, Carrera GF, et al. MR imaging of the shoulder: diagnosis of rotator cuff tears. *AJR* **1987**;149:333-337
4. Burk DL, Karasick D, Kurtz AB, et al. Rotator cuff tears: prospective comparison of MR imaging with arthrography, sonography, and surgery. *AJR* **1989**;153:87-92
5. Zlatkin MB, Iannotti JP, Roberts MC, et al. Rotator cuff tears: diagnostic performance of MR imaging. *Radiology* **1989**;172:223-229
6. Seeger LL, Gold RH, Bassett LW, Ellman H. Shoulder impingement syndrome: MR finding in 53 shoulders. *AJR* **1988**;150:343-347
7. Glickstein MF. MR imaging of the shoulder: optimizing surface-coil positioning. *AJR* **1989**;153:431-432
8. Seeger LL, Ruszkowski JT, Bassett LW, Kay SP, Kahmann RD, Ellman H. MR imaging of the normal shoulder: anatomic correlation. *AJR* **1987**;148:83-91

# Diagnostic Quality of Portable Abdominal Radiographs in Neonates with Necrotizing Enterocolitis: Digitized vs Nondigitized Images

George W. Gross<sup>1</sup>  
Saundra M. Ehrlich  
Yen Wang

Digital manipulation of radiographic images has prompted significant interest because of the potential for improving image quality and diagnostic accuracy. We compared conventional and digital radiographs in the evaluation of neonatal necrotizing enterocolitis (NEC). Fifty abdominal radiographs in neonates with suspected or autopsy-confirmed NEC and 50 similar radiographs of neonates without suspicion of NEC were digitized. Definition of intraabdominal anatomy was optimized by window width and level adjustment. Hard-copy radiographs of the digitally manipulated images were then produced by a laser printer. Twelve general radiologists each evaluated, without benefit of clinical information, a random mixture of 50 cases of NEC and normal controls, with both conventional and digital images for each case, for a total of 100 radiographs reviewed. Each image was evaluated for overall suspicion of NEC and the presence and severity of six radiographic signs of NEC. The radiologists also rated their confidence in their assessments. The results were compared with those from a similar analysis by an experienced pediatric radiologist to ensure validity of image evaluation. No statistically significant differences were found between the conventional and digital imaging formats for the assessment of the signs of NEC ( $p = .15$ ) or for determination of the overall suspicion of NEC ( $p = .07$ ).

Our results show the digitized and the conventional, nondigitized radiographs to be at least equally useful for evaluating the radiographic signs of NEC and suggesting an appropriate diagnosis.

AJR 154:779-783, April 1990

Necrotizing enterocolitis (NEC), a disorder seen most often in the premature neonate, originates in the small bowel and colon; with progression, it can lead to sepsis, intestinal perforation, and death [1, 2]. Abdominal tenderness, fever, irritability, and blood in the stool are the most salient clinical signs of NEC [1, 3, 4]. The conventional abdominal radiographic findings of NEC, which play an important role in the diagnosis and management of NEC, include bowel dilatation, bowel wall thickening, and/or intraabdominal fluid, pneumatosis intestinalis, portal venous air, and free intraperitoneal air [2, 4-7].

Recent interest in the use of digital manipulation of radiographic images has developed for a wide range of disorders [8-10], including many that involve children [11-15]. Of particular potential value to pediatric patients is the reduction in radiation dosage afforded by digital radiographic techniques [11-14]. This retrospective study of abdominal radiographs in neonates with NEC (and in a comparison control group of neonates without NEC) was undertaken to compare digitized and conventional radiographs to determine what advantage, if any, there is in the digital manipulation of radiographic images as an aid in earlier and more accurate diagnosis of NEC.

## Materials and Methods

Patients with NEC were identified by a computer-generated search of medical records of patients in our intensive-care nursery. Patients were considered to have had NEC if there was strong clinical suspicion resulting in appropriate medical treatment (the majority of cases)

<sup>1</sup> All authors: Department of Radiology, Thomas Jefferson University Hospital, 111 S. 11th St., Philadelphia, PA 19107. Address reprint requests to G. W. Gross.

or pathologic confirmation of NEC during autopsy. Fifty portable anteroposterior abdominal radiographs of supine neonates with NEC were selected by an experienced pediatric radiologist as showing the various plain film signs of NEC. Various degrees of severity of one or more of the plain film signs of NEC were present on each film selected. All abdominal radiographs selected for inclusion in the study were of good to excellent quality.

An additional 50 portable anteroposterior abdominal radiographs of supine neonates with no clinical suspicion of NEC were randomly selected to serve as a control group. These radiographs were obtained to assess for line placement or other situations where no intraabdominal abnormality was suspected.

All 100  $8 \times 10$  in. ( $20 \times 25$  cm) conventional radiographs were digitized to a  $1600 \times 2000$  pixel matrix, 12 bits per pixel, with a Digirad Imaging System laser scanner (Digirad Corporation, Palo Alto, CA, later Matrix Instruments Inc., Palo Alto, CA, now Agfa-Gavaert, Brussels, Belgium). Every fourth pixel of each image was displayed on a  $500 \times 500$  line video monitor. As each image was viewed on the monitor, image quality was optimized for definition of intraabdominal anatomy as determined by agreement of two experienced radiologists who jointly selected optimal window width and level for each image. After this procedure, a hard copy radiograph of each digitized image was obtained with a  $2048 \times 2048$  pixel laser printer (Matrix model LR).

All 100 cases, the 50 of NEC and the 50 controls, were randomly ordered. Patient identification information, including name and medical record number, was covered; a separate number code was placed on each image for purposes of later identification and evaluation of the findings.

Twelve general diagnostic radiologists were each asked to review a total of 50 cases representing a randomly ordered mixture of NEC patients and normal control subjects—both the conventional and digital images, for a total of 100 images reviewed by each radiologist. Seven radiologists reviewed cases 1–50, and five reviewed cases 51–100, with the numerical sequence of review varied. Within each case grouping, some reviewed the conventional images initially, then the digital images, while others reversed the order of review (counterbalanced schedule), with an interval of at least 2 weeks between review of the conventional and digital images. All films were reviewed without knowledge of clinical information.

Each radiologist had at least 3 years' experience in diagnostic radiology, including residency training, and 3 months of training in pediatric radiology during residency. All had continuing exposure to pediatric plain film radiology and all but one were within 2 years of completion of their radiology residency training. Deliberately excluded was any radiologist who had little or no continuing exposure to pediatric radiology for 3 years or longer. None had pediatric radiology fellowship training.

The radiologists were initially given a brief explanation of the purpose of the study as well as general guidelines as to film review (e.g., the NEC and normal controls were in a mixed, random order and only the region of the abdomen was to be evaluated). No time limit on the review of any radiograph was imposed. Each radiograph (both conventional and digital) was presented individually to the radiologists and their numerical assessment of the various factors described above was recorded immediately on a standard data sheet for later review. Each radiologist required a minimum of three or four separate sessions to complete the review of the 100 individual images.

All 100 images (50 conventional, 50 digital) were analyzed in the following manner. Each of the six previously mentioned plain film signs of NEC was evaluated for its presence and degree of severity (based on a scale of 0–3, with 0 = not present, 1 = minimal to mild in degree, 2 = moderate, and 3 = marked or severe); the level of

confidence in assessment of each sign was graded (based on a scale of 0–3, with 0 = possible but uncertain, 1 = mildly confident, 2 = moderately confident, and 3 = very confident to certain); finally, the overall suspicion of NEC based solely on radiographic findings was determined (based on a scale of 0 to 3, with 0 = no evidence of NEC, 1 = mildly suspicious for NEC, 2 = moderately suspicious, and 3 = very suggestive or certain of the presence of NEC).

All 200 images (100 conventional, 100 digital) also were reviewed by the pediatric radiologist for the presence and severity of the six signs of NEC, as well as the confidence in assessment. This review differed from that of the general radiologists in that it consisted of two separate evaluations, separated by 1 month, with a third review being performed only when there was lack of agreement between the first two reviews.

Mean ratings by the 12 radiologists on the six signs of NEC, degree of confidence in assessment, and overall suspicion of NEC were calculated for both the digital and conventional images. A series of chi-square ( $\chi^2$ ) analyses were initially conducted to compare the digital with the conventional images for the frequency (or number) of radiologists responding within each numerically rated category (of severity, confidence, and suspicion of NEC). The Wilcoxon sign test was the statistical measurement used to determine whether the digital image was rated lower than, similar to, or higher than the conventional film. (Wilcoxon matched-pairs signed-rank test is a nonparametric statistic that measures not only the differences between two sets of paired data [conventional-digital rated images] but also takes into account the degree of difference between them, thereby enabling more weight to be given to a pair that shows a large difference than is given to a pair showing a smaller difference.) The Wilcoxon statistic also was used to make similar comparisons between the ratings of the general radiologists and the pediatric radiologist.

## Results

Comparison of the mean ratings of the 12 diagnostic radiologists in their assessment of the various radiographic signs of NEC on both the conventional and the digital radiographs is shown in Table 1. In the patients with NEC, the radiologists rated all signs except portal venous air slightly higher on the digital images, although the differences were not statistically significant. In the control subjects without NEC, no trend favoring digital over conventional images, or vice versa, is demonstrated. Overall, the difference between the two imaging formats in the rating of the various signs of NEC is not statistically significant. The probability values on chi-square analyses ranged from  $p = .06$  to  $p = .36$ , with an average of  $p = .15$ .

In the assessment of the overall suspicion of NEC, based on a summation of all the signs of NEC, the radiologists as a group rated their suspicion of NEC much higher in the group of patients with NEC than in those without NEC (Table 2). This was true for both the conventional and digital images ( $p < .01$ ; Wilcoxon test). In those patients with NEC, suspicion of NEC was rated higher on the digital images than on the conventional images (2.38 vs 2.25), indicating that digital manipulation of the radiographic image provided at least equivalent, if not slightly superior, ability to diagnose NEC when compared with the conventional radiographs. However, the differences were not statistically significant ( $p = .07$ ; Wilcoxon). In those patients without NEC, the radiologists demonstrated a slightly higher overall suspicion of NEC on

**TABLE 1: Comparison of Assessment of Severity of Signs of Necrotizing Enterocolitis (NEC) by 12 Diagnostic Radiologists**

Signs of NEC	Patients with NEC		Control Subjects	
	Conventional Image	Digital Image	Conventional Image	Digital Image
Bowel dilatation	1.87	1.90	0.73	0.72
Bowel wall thickening/abdominal fluid	1.33	1.38	0.47	0.53
Pneumatosis intestinalis (cystic)	1.52	1.58	0.34	0.31
Pneumatosis intestinalis (linear)	1.27	1.36	0.11	0.13
Portal venous air	0.39	0.35	0.01	0.02
Free intraperitoneal air	0.46	0.48	0.04	0.05

Note.—Numbers are mean values of summed ratings, based on a scale of 0 to 3, by all 12 radiologists. 0 = not present; 1 = minimal to mild; 2 = moderate; 3 = marked or severe.

**TABLE 2: Comparison of Conventional and Digital Images for Suspicion of Necrotizing Enterocolitis (NEC)**

Patient Group	Conventional Images	Digital Images
With NEC	2.25	2.38
Without NEC	0.56	0.67

Note.—Numbers are mean values of summed ratings, based on a scale of 0 to 3, by 12 radiologists. 0 = no evidence of NEC; 1 = mildly suspicious for NEC; 2 = moderately suspicious for NEC; 3 = very suggestive or certain of NEC.

the digital image, compared with the conventional images, but this slightly higher false-positive rate with the digital images was not statistically significant ( $p = .08$ ; Wilcoxon).

An example of a conventional portable anteroposterior neonatal abdominal radiograph and its digitized counterpart is shown in Figure 1.

Assessment of the severity of each of the six radiographic signs of NEC by the general radiologists collectively is compared with the assessment of the pediatric radiologist in Figure 2A (cases with NEC) and Figure 2B (without NEC). The percentage ratings by the general radiologists as a group were considered either similar to, higher than, or lower than those of the pediatric radiologist. These figures and percentages were tabulated for each of the cases, for each of the signs of NEC and then separately for the conventional and digital (shade-gray) images. The general radiologists tended to rate the severity of all signs higher than did the pediatric radiologist (exception: bowel dilatation in infants with NEC), but differences were minimal and were not statistically significant. Agreement between the general radiologists and the pediatric radiologist was fairly comparable for both the conventional and digital images. Greater disagreement (but again comparable) occurs among those signs that are more non-specific for NEC (e.g., bowel wall dilatation or thickening). The judgments of the observers with that of the pediatric radiologist show no real differences beyond those expected by chance alone; these findings were noted for both the conventional and the digital images. Overall, we found no substantial differences in assessment of signs or in level of confidence in assessment according to imaging format.

For the radiologists as a group, the digital radiograph allowed equivalent or slightly higher (but not statistically sig-

nificant) levels of confidence in NEC sign assessment in patients with NEC, compared with the conventional radiograph. However, in the control subjects without NEC, the levels of confidence in NEC sign assessment were equivalent or slightly lower for the digitized than for the conventional image, although not at a statistically significant level.

## Discussion

To date, the clinical application of digital radiography in the pediatric patient has focused on the chest and musculoskeletal system [11–15]. No previous references to use of digital radiography in pediatric, including neonatal, abdominal disorders could be identified. This study was undertaken to determine if the digital manipulation of a conventional radiographic image of the neonatal abdomen might increase the sensitivity and specificity of radiography in identifying the individual signs of NEC and improve the overall accuracy of diagnosing NEC when initially suspected on clinical grounds.

Although digital manipulation of a radiographic image can involve a variety of reprocessing techniques (e.g., edge enhancement), our study was concerned solely with the effect of adjustment of window width and level on the ability to interpret the various signs of NEC. Even with the limited digital manipulation of the conventional image, we were able to show at least equivalent diagnostic efficacy for the digitized image compared with the conventional image. It is possible that with use of additional image-processing techniques, digital radiography might show a clear superiority over conventional radiography for diagnosis of NEC. Obtaining a sufficient number of cases illustrating the various signs of NEC would preferably be accomplished with a direct digital acquisition system instead of digitizing a film radiograph, with the potential inherent limitations on image manipulation. Such a prospective approach, although inherently preferable, is not feasible because of the inordinately long time required to obtain sufficient examples of the full range and degree of severity of the various signs of NEC. Our study, of necessity, was more limited in that it encompassed a retrospective evaluation of digitized radiographs.

Although no gold standard could be obtained for purposes of comparing the ratings of the signs of NEC and the confidence in those ratings as determined by the general radiolo-

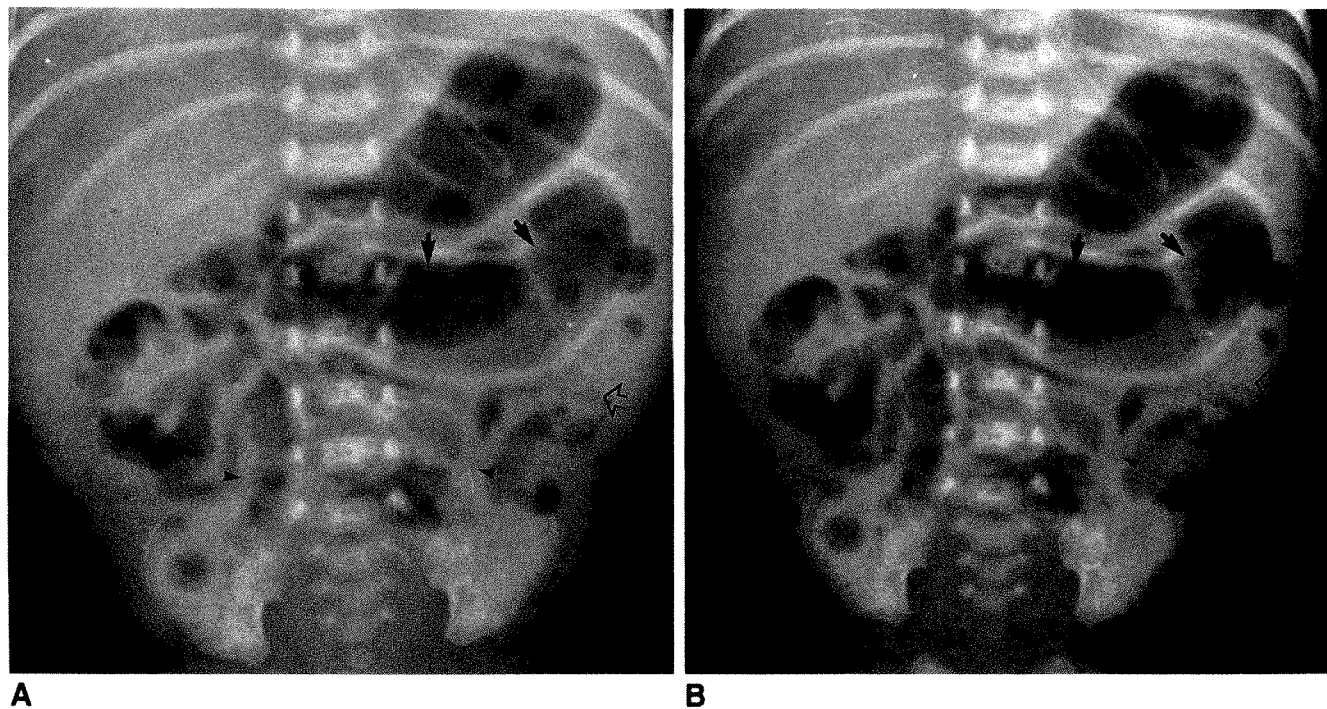


Fig. 1.—Conventional (A) and digitally manipulated (B) radiographs of abdomen in a neonate with necrotizing enterocolitis (NEC). Window width and level have been adjusted for digital image to optimize definition of intraabdominal structures, resulting in greater contrast. A dilated segment of bowel (solid arrows) and several areas of increased soft-tissue separation between intraluminal bowel gas (arrowheads), compatible with bowel-wall edema and/or intraperitoneal fluid, are signs suggestive of NEC. Left flank region contains an area of mottled lucency (open arrow) that could be either cystic pneumatosis or feces mixed with air.

General Radiologists vs. Pediatric Radiologist	Sign of NEC						General Radiologists vs. Pediatric Radiologist	Sign of NEC					
	① %	② %	③ %	④ %	⑤ %	⑥ %		① %	② %	③ %	④ %	⑤ %	⑥ %
Similar	66 66	66 54	78 76	92 90	96 90	94 94	Similar	70 66	44 38	58 54	70 60	86 82	90 90
Rated Higher	26 26	28 38	22 24	6 8	4 10	4 6	Rated Higher	10 12	32 40	24 28	26 36	12 16	10 10
Rated Lower	8 8	6 8	0 0	2 2	0 0	0 0	Rated Lower	20 22	24 22	18 18	4 4	2 2	0 0

- ① = Bowel dilatation
- ② = Bowel wall thickening/abdominal fluid
- ③ = Cystic pneumatosis intestinalis
- ④ = Linear pneumatosis intestinalis
- ⑤ = Portal venous air
- ⑥ = Free intraperitoneal air

- ① = Bowel dilatation
- ② = Bowel wall thickening/abdominal fluid
- ③ = Cystic pneumatosis intestinalis
- ④ = Linear pneumatosis intestinalis
- ⑤ = Portal venous air
- ⑥ = Free intraperitoneal air

A

B

Fig. 2.—A, Ratings of severity of signs of necrotizing enterocolitis (NEC), comparing conventional and digital images in patients with NEC. B, Ratings of severity of signs of NEC, comparing conventional and digital images in control subjects without NEC. Numbers refer to percentage of cases rated similar to, higher than, or lower than rating by pediatric radiologist. Ratings for conventional images are unshaded; those for digital images are shaded.

gists, we felt it appropriate to use the evaluation by a pediatric radiologist (as performed on two separate occasions) as a reasonable substitute, providing a point of reference for judging the relative accuracy of the general radiologists' interpretations. Data in Figure 2 indicate that the general radiologists'

interpretations and conclusions were sufficiently comparable to those of the pediatric radiologist to validate the use of the general radiologists as the basis of comparing the conventional and digital imaging formats in the assessment of NEC.

Our overall results indicate that digital manipulation of the



radiographic image as performed in this study provides at least equivalent diagnostic accuracy in identifying neonates with NEC, when compared with the conventional radiographic image. We consider this an important clinical finding in light of the reduced radiation dosage that is provided when direct digital image acquisition techniques (e.g., reusable image medium) are used, at no loss of diagnostic accuracy.

#### ACKNOWLEDGMENTS

We gratefully appreciate the participation in the study of Rick Feld, Pamela Hilpert, Esmond Mapp, Irene Rasis, Amy Wilson, Paul Davis, Ilan Kinori, Pamela Hendricks, Robert Traflet, Richard Shlansky-Goldberg, David March, and Keith Haidet. We thank Ann Prather Hunter and Tessa Mueller for manuscript preparation.

#### REFERENCES

1. Kliegman FM, Fanaroff AA. Necrotizing enterocolitis. *N Engl J Med* **1984**;310:1093-1103
2. Leonidas JC, Hall RT, Amoury RA. Critical evaluation of the roentgen signs of neonatal necrotizing enterocolitis. *Ann Radiol* **1976**;1:123-132
3. Santulli TV, Schullinger JN, Heird WC, et al. Acute necrotizing enterocolitis in infancy: a review of 64 cases. *Pediatrics* **1975**;55:376
4. Rabinowitz JG, Siegle RL. Changing clinical and roentgenographic patterns of necrotizing enterocolitis. *AJR* **1976**;126:560-566
5. Kogutt MS. Necrotizing enterocolitis of infancy: early roentgen patterns as a guide to prompt diagnosis. *Radiology* **1979**;130:367-370
6. Leonidas JC, Krasna IH, Fox HA, et al. Peritoneal fluid in necrotizing enterocolitis: a radiologic sign of clinical deterioration. *J Pediatr* **1973**;82:672-675
7. Daneman A, Woodward S, deSilva M. The radiology of neonatal necrotizing enterocolitis (NEC): a review of 47 cases and the literature. *Pediatr Radiol* **1978**;7:70-77
8. Fraser RG, Sanders C, Barnes GT, et al. Digital imaging of the chest. *Radiology* **1989**;171:297-307
9. Merritt CRB, Tufton RH, Bell KA, et al. Clinical application of digital radiography: computed radiographic imaging. *RadioGraphics* **1985**;5:397-414
10. Feczko PJ, Ackerman LV, Kartan DJ, et al. Digital radiography of the gastrointestinal tract. *Gastrointest Radiol* **1988**;13:191
11. Kogutt MS, Jones JP, Perkins DD. Low-dose digital computed radiography in pediatric chest imaging. *AJR* **1988**;151:775-779
12. Kogutt MS. Computed radiographic imaging: use in low-dose leg length radiology. *AJR* **1987**;148:1205
13. Kangarloo H, Boechat MI, Barbaric Z. Two-year clinical experience with a computed radiography system. *AJR* **1988**;151:605
14. Kushner DC, Cleveland RH, Herman TE, et al. Radiation dose reduction in the evaluation of scoliosis: application of digital radiography. *Radiology* **1986**;161:175
15. Harcke HT, Mandell GA, Lee MS, Grissom LE. Evaluating scoliosis with digital radiographic techniques. *AJR* **1985**;145:875

## Memorial

### Norman Glazer, 1920–1989



Norman Glazer, 68, of Cleveland Heights, OH, a founding member and past president of the Society for Pediatric Radiology, died suddenly and unexpectedly on August 14, 1989. Dr. Glazer was chairman of the department of radiology at the Children's Hospital of Akron from 1955 until 1985, when he became a consultant for the Cleveland Clinic Foundation. Since 1952, he had taught at Case Western Reserve University, where he was appointed clinical professor of radiology in 1975, and had been professor of radiology at Northeastern Ohio University College of Medicine since 1978. He served as visiting professor at several universities, including Michigan, Brown, and Wisconsin. A native of

Cleveland, Dr. Glazer's premedical studies were at Western Reserve University; he received his master's degree in chemistry from Northwestern University and his M.D. degree from St. Louis University. He interned at Mount Sinai Hospital, and his residency, including both radiology and pathology, was served at Cleveland City Hospital (now MetroHealth Center).

Dr. Glazer was a man of immense energy and enthusiasm, combining an amazing clinical knowledge of pediatrics with a broad and up-to-date proficiency in diagnostic radiology. His associates in Akron described him as "an institution" because of his inquisitiveness, extraordinary clinical acumen, and outstanding support in the management and diagnosis of their problem cases. He was well known throughout the hospital, in which he would pay daily visits to the operating rooms, pathology laboratories, and the medical library. He did not hesitate to differ with his colleagues when he had reason to present alternative opinions on what he considered the most appropriate investigations in particular patients, including those in his own field of radiology. And he was respected for these differences, which usually were advantageous for patients and physicians alike.

Dr. Glazer served on the editorial board of *Pediatrics*, the official journal of the American Academy of Pediatrics. He was especially interested in neonatal radiology. An editorial (*AJR* 1970;108:649–651) on radiologic diagnosis in the neonatal period illustrated his clinical approach to both diagnosis and management. He pointed out that there are circumstances in which the radiologist can and should identify life-threatening abnormalities by using plain film examination and others in which plain films do not suffice and more

advanced investigation is necessary. He was particularly concerned with radiologists' recognizing their limitations at times when their interpretation could be accepted as gospel by referring physicians and thereby inhibit further necessary investigation. The concepts expressed in the editorial are as valid today as they were two decades ago.

Dr. Glazer's forte was in teaching and in radiologic diagnosis. He was a master of the plain film and was able to convey to both students and physicians his love of medicine and enthusiasm for learning. By his precepts and especially by his example, many students and house staff were stimulated to move into the field of diagnostic radiology. His reputation as a teacher was so extraordinary that for decades medical students in Cleveland were eager to travel to Akron for the opportunity to spend time on his service. Shortly after he joined the Cleveland Clinic Foundation, these talents were acknowledged publicly when he received the Diagnostic Radiology Teacher of the Year Award, renamed the Norman Glazer Award for Excellence in Teaching just 2 months before his death.

Dr. Glazer was a devoted family man. He is survived by his wife, Miriam; seven children: Gale, of Brookline, MA, Dr. Gwen and Dr. Greer, of Cleveland, OH, Ginger of Poughkeepsie, NY, Dr. Gary, of Los Altos, CA, Geoffrey, of Cleveland, and Greg, of Columbus, OH; and nine grandchildren. To honor his memory, the family will establish the Norman Glazer Teaching File in Pediatric Radiology at Stanford University.

Frederic N. Silverman  
Stanford, CA 94305-1234

# Doppler Evaluation of Renal Transplants in Children: A Prospective Analysis with Histopathologic Correlation

D. Gordon Drake<sup>1</sup>  
 Deborah L. Day<sup>1</sup>  
 Janis Gissel Letourneau<sup>1</sup>  
 Bennett A. Alford<sup>2</sup>  
 Richard K. Sibley<sup>3</sup>  
 S. Michael Mauer<sup>4</sup>  
 Timothy E. Bunchman<sup>5</sup>

Duplex Doppler sonography recently has been used to evaluate renal transplants. Some authors have stated that high resistive indexes (RIs) occur in the presence of acute renal transplant rejection. RIs less than 0.7 are considered as probably excluding acute transplant rejection. We performed a prospective study of duplex sonographic examinations of pediatric patients (mean age, 8 years; 13 boys, two girls) with renal allografts and clinically suspected transplant disease. The results of 22 duplex studies were correlated with histopathologic data obtained between July 1987 and June 1988. RIs of the arcuate arteries in patients with acute rejection ( $n = 14$ ) averaged 0.62 (range, 0.50–0.80). The RI in patients with chronic rejection ( $n = 1$ ) was 0.59. RIs in patients with acute tubular necrosis ( $n = 3$ ) averaged 0.66 (range, 0.59–0.72). RIs in patients with cyclosporine A toxicity ( $n = 4$ ) averaged 0.66 (range, 0.58–0.79). Tubulointerstitial rejection was predominant, with only two patients showing minimal acute vascular rejection.

Thirteen of 14 pediatric patients with histologically proved renal transplant rejection had a resistive index of less than 0.70. This study refutes the concept that resistive indexes of less than 0.7 exclude acute rejection.

*AJR* 154:785–787, April 1990

Received July 21, 1989; accepted after revision November 20, 1989

This work was supported in part by the National Institutes of Health Program Project Grant AM 13083 and T. E. Bunchman was supported by an NIH Training Grant AM 07087.

<sup>1</sup> Department of Radiology, University of Minnesota Hospital and Clinics, 420 Delaware St., S.E., Minneapolis, MN 55455. Address reprint requests to D. G. Drake at Department of Radiology, Children's Hospital, 345 Smith Ave., St. Paul, MN 55102.

<sup>2</sup> Department of Radiology and Pediatrics, University of Virginia Hospital, Box 170, Charlottesville, VA 22908.

<sup>3</sup> Department of Pathology, Stanford University Medical Center, Stanford, CA 94305.

<sup>4</sup> Department of Pediatric Nephrology, Cardinal Glennon Children's Hospital, St. Louis, MO 63104.

<sup>5</sup> Department of Radiology, University of Minnesota Hospital and Clinics, 420 Delaware St., S.E., Minneapolis, MN 55455.

Sonographic examination of renal allografts has been used for the evaluation of suspected acute allograft rejection (AR). Quantitative and qualitative sonographic changes in the morphology of the allograft may occur with suspected rejection. More recently, duplex Doppler studies have been used to examine patients with renal allograft dysfunction. The resistive index (RI) equals peak systolic frequency shift minus lowest diastolic frequency shift divided by peak systolic frequency shift [1–3]. RI analysis has been advocated as a useful technique in the diagnosis of acute rejection [1, 4, 5]. However, most of these studies were hampered by a retrospective analysis [2, 3] or the lack of histologic verification [5–7]. The latter factor is of concern because the clinical diagnosis of rejection is imprecise [8]. To evaluate this problem fully, we carried out a prospective study to compare the Doppler RI and renal allograft histology in children with renal transplants.

## Materials and Methods

All children (17) who had received a renal transplant allograft at the University of Minnesota and who were evaluated for allograft rejection between July 1, 1987, and June 31, 1988, were studied. Two patients were excluded because the RI analyses were not obtained from arcuate arteries. Fifteen children (13 boys and two girls) had 22 duplex examinations for suspected rejection. All had received adult kidneys, 11 from living related donors and four from cadaveric donors. The average age at transplantation was 8.1 years (range, 1–17.5 years) and the time from transplantation to evaluation for AR averaged 9.3 months (range, 0.1–66 months). These children were admitted to the University of Minnesota Hospital on the basis of clinical criteria, which included one or more of the following: increased serum creatinine level ( $n = 19$ ), new onset or exacerbation of existing hypertension ( $n = 10$ ), or

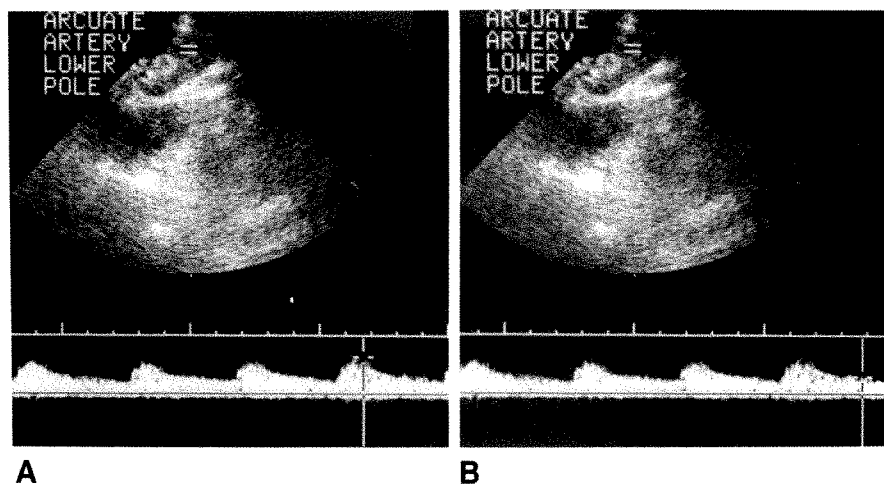


Fig. 1.—A, Arcuate artery waveform obtained from lower pole of a transplant kidney. Peak systolic frequency shift is marked by cursor.  
B, Lowest diastolic frequency shift from same Doppler study. Resistive index is calculated to be 58%.

prolonged unexplained fever for greater than 7 days ( $n = 1$ ) [9]. The increase in serum creatinine level ranged from 0 to 5.2 mg/dl (average, 0.8 mg/dl). Standard immunosuppression protocols were followed, whereby 13 patients received azathioprine, prednisone, and cyclosporine and two patients received azathioprine and prednisone alone. In those patients receiving cyclosporine, no effort was made to achieve a predetermined cyclosporine level. At the time of the study, the mean cyclosporine dose was  $2.8 \pm 0.02$  mg/kg (range, 1.4–4 mg/kg). All patients also received Minnesota anti-lymphoblast globulin (ALG) daily for 2 weeks after transplantation [10].

At the time of hospitalization, the children underwent normalization of blood pressure, if needed, and evaluation of serum creatinine and electrolyte levels, complete blood count, coagulation studies, urinalysis, and urine culture. Further, a renal allograft sonogram was obtained to evaluate the appearance of the renal parenchyma and to determine the RIs in the arcuate arteries. When the RI was measured in more than one renal arcuate artery, an average of all arcuate artery RIs was determined. The time from the duplex examination to the time of biopsy averaged 2 days (range, 0–9 days). All patients underwent a percutaneous renal transplant biopsy and the tissue was prepared for light microscopy and, if clinically indicated, immunofluorescence and electron microscopy, by using established techniques at our institution [8]. Determination of treatment of the patient was based primarily on the allograft biopsy and supported by clinical information.

The arcuate artery RIs were calculated before allograft biopsy and the biopsy was evaluated without the results of the RI analyses. RI was calculated as peak systolic frequency shift minus lowest diastolic frequency shift divided by the peak systolic frequency shift (Fig. 1). Grading of the histologic findings on biopsy samples and diagnosis of cyclosporine nephrotoxicity were based on a histologic grading scale previously published [8, 11]. The histologic gradings were determined by one of the investigators without knowledge of the clinical course of the patient.

## Results

Histologically, the allograft biopsies could be categorized into four groups: acute rejection (14 biopsies), cyclosporine A toxicity (four biopsies), acute tubular necrosis (three biopsies), and chronic rejection (one biopsy). The ranges of the RIs overlapped for the four histologic groups. No significant differences were seen in the RIs calculated between any of the

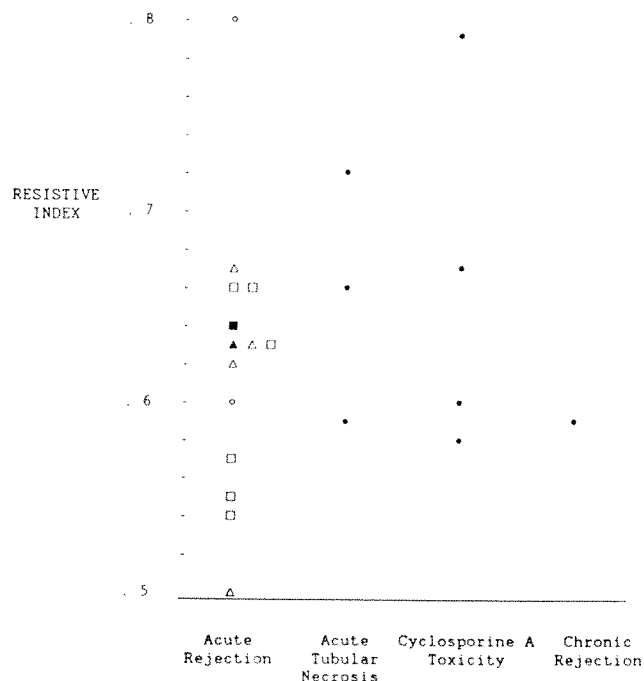


Fig. 2.—Comparison of resistive indexes with histopathologic diagnoses. O = minimal tubulointerstitial rejection; Δ = mild to moderate tubulointerstitial rejection; □ = severe tubulointerstitial rejection; ■ = minimal acute vascular and moderate tubulointerstitial rejection; ▲ = minimal acute vascular and moderate tubulointerstitial rejection.

groups (Fig. 2). RIs ranged from 0.50 to 0.80. The difference between the highest and lowest RI obtained in a given examination ranged from 0.02 to 0.15 (average, 0.07). The RI averaged  $0.62 \pm 0.07$  in acute rejection,  $0.66 \pm 0.05$  in acute tubular necrosis,  $0.66 \pm 0.08$  in cyclosporine A toxicity, and 0.59 in the single case of chronic rejection. With an RI of 0.7 or greater to indicate acute rejection, the sensitivity was 7% (one of 14) and the specificity was 75% (six of eight). With an RI of 0.65 to indicate acute rejection, the sensitivity was only 29% (four of 14) and the specificity was 50% (four of eight).

## Discussion

Measurement of the RI in the renal allograft arcuate arteries is a simple technique. The calculation of the RI is related to the difference in systolic and diastolic blood flow. When blood flow to the allograft is disturbed, this ratio should change [3]. There is conflicting information about the usefulness of RI for diagnosing rejection [1, 12]. The RI is probably more helpful in diagnosing vascular than tubulointerstitial rejection owing to greater "dampening" of the arterial blood flow detected by duplex sonography in the former, but no discrimination between these two forms of allograft rejection is made in many of the published studies [2, 4-6, 13-16]. Furthermore, moderate to severe vascular rejection is less common than tubulointerstitial rejection, occurring in only 22% of patients with acute allograft rejection in a study of more than 200 sequential allograft biopsies performed at our institution [8]. In our study, only two patients showed evidence of minimal acute vascular rejection. If the RI is best used to diagnose vascular rejection with a predictive value of 53% for an RI greater than 70% (according to Rifkin et al. [1]), then by using RI analysis alone, the diagnosis of acute allograft rejection due to moderate or severe acute vascular rejection would not be expected in more than 11% of episodes of renal dysfunction. This suggests that acute rejection may be diagnosed more consistently by a renal biopsy.

Other studies have found RI to be nonspecific and insensitive in the diagnosis of the specific cause of allograft dysfunction. Buckley et al. [2] suggested that a normal RI is indicative of cyclosporine A nephrotoxicity or tubulointerstitial rejection, whereas vascular rejection is more likely to have a higher RI. However, some of the patients in their study had elevated RI and tubulointerstitial rejection [2]. Needleman and Kurtz [4] reported normal or increased RI in acute tubular necrosis, further complicating the diagnosis of rejection vs absence of rejection when based solely on RI.

An elevated RI (above 70%) was seen in only three (14%) of our 22 patients, yet the histologic findings on the renal allograft biopsy samples in these children included cyclosporine A nephrotoxicity in one, acute tubular necrosis in one, and minimal tubulointerstitial rejection in the third. Our data do not allow comment on the specificity of resistive indices greater than 0.3 because we did not encounter this finding. However, our data suggest that patients with RIs greater than 0.8 most likely are a small subset of pediatric patients with renal allograft dysfunction.

The lack of correlation of the RI with the allograft histology in our study may be caused by a number of factors, including (1) the special circumstances of the adult kidney transplanted

into the child, (2) the absence of vascular rejection in our study population, and finally (3) our aggressive approach to biopsy of the allograft, often establishing the diagnosis of rejection before the serum creatinine level became elevated. Again, this possibility would not explain the lack of specificity of the RI calculation.

Our results indicate the importance of histologic examination for the diagnosis of suspected allograft rejection in pediatric renal allograft recipients.

## REFERENCES

1. Rifkin MD, Needleman L, Pasto ME, et al. Evaluation of renal transplant rejection by duplex Doppler examination: value of the resistive index. *AJR* 1987;148:759-762
2. Buckley AR, Cooperberg PL, Reeve CE, Magil AB. The distinction between acute renal transplant rejection and cyclosporine nephrotoxicity: value of duplex sonography. *AJR* 1987;149:521-525
3. Taylor KJW, Burns PN. Duplex Doppler scanning in the pelvis and abdomen. *Ultrasound Med Biol* 1985;11:643-658
4. Needleman L, Kurtz AB. Doppler evaluation of the renal transplant. *JCU* 1987;15:661-673
5. Arima M, Takahara S, Ihara H, et al. Predictability of renal allograft prognosis during rejection crisis by ultrasonic Doppler flow technique. *Urology* 1982;19:389-394
6. Ubhi CS, Irving HC, Norwood HM, Guillou PJ, Giles GR. Monitoring of renal allografts by Doppler ultrasound. *Ann R Coll Surg Engl* 1987;69:229-232
7. Rigsby CM, Taylor KJW, Weltin G, et al. Renal allografts in acute rejection: evaluation using duplex sonography. *Radiology* 1986;158:375-378
8. Matas AJ, Sibley RK, Mauer SM, Sutherland DER, Simmons RL, Najarian JS. The value of needle renal allograft biopsy. I. A respective study of biopsies performed during putative rejection episodes. *Ann Surg* 1983;197:226-236
9. Bunchman TE, Fryd DS, Sibley RK, Mauer SM. Manifestations of renal allograft rejection in small children receiving adult kidneys. *Pediatr Nephrol* (in press)
10. So SKS, Najarian JS, Nevins TE, et al. Low-dose cyclosporine therapy combined with standard immunosuppression in pediatric renal transplantation. *J Pediatr* 1987;111:1017-1021
11. Sibley RK, Rynasiewicz JJ, Ferguson RM, et al. Morphology of cyclosporine nephrotoxicity and acute rejection in patients immunosuppressed with cyclosporine and prednisone. *Surgery* 1983;94:225-234
12. Jenkins SM, Sanfilippo FP, Carroll BA. Sonography of renal transplants. *AJR* 1989;152:535-539
13. Raiss GJ, Bree RL, Schwab RE, Schultz SR, Salem NG, Rosenberg BF. Further observations in the ultrasound evaluation of renal allograft rejection. *J Ultrasound Med* 1986;5:439-444
14. Linkowski GD, Warvariv V, Filly RA, Vincenti F. Sonography in the diagnosis of acute renal allograft rejection and cyclosporine nephrotoxicity. *AJR* 1987;148:291-295
15. Hillman BJ, Birnholz JC, Busch GJ. Correlation of echographic and histologic findings in suspected renal allograft rejection. *Radiology* 1979;132:673-676
16. Hoddick W, Filly RA, Backman U, et al. Renal allograft rejection: US evaluation. *Radiology* 1986;161:469-473

## Book Review

**Cardiac Application of Digital Angiography.** Edited by Alan G. Wasserman and Allan M. Ross. Mount Kisco, NY: Futura, 311 pp., 1989. \$53

When digital subtraction angiography became widely available in the early 1980s, no area of application appeared more exciting than the heart and great vessels. It seemed then that precise anatomic and functional diagnosis might be obtained at minimal risk to patients. Over the years, however, it has become obvious that significant limitations still remain.

Digital video coronary arteriography has become a reliable means of acquiring reliable morphologic information on the presence or absence of significant coronary atherosclerosis, and computer-based processing techniques and analytical algorithms have been shown to provide reliable quantification of the acquired information. Thus, we find ourselves at the exciting place where a change from conventional film-based cineangiography of acquired coronary heart disease to electronic video-based imaging might begin to take hold.

Wasserman and Ross have edited a collection of contributions by many workers in this relatively new and exciting field. They have attempted to cover basic principles of image acquisition and processing and to review the current status of clinical application of these techniques in the management of patients with acquired and congenital heart disease. In addition, for completeness, they have included reviews of the use of digital angiographic techniques in the vascular system other than the heart.

This book suffers from common failings of books that have several contributors. Redundancy occurs in the discussions, and some chapters are not as strong as others. Furthermore, some of the chapters are not relevant to the issue of cardiac digital imaging. The best chapters are by those who have published much of the fundamental research in this field. The clinical reviews by Nissen, Pfaff et al., Leiboff, and Tobis et al. are most notably complete and well written. These chapters review the current status and functional analyses of digital coronary arteriography and ventriculography and bridge important gaps between basic scientific facts and important clinical issues. The illustrations are well chosen and of good quality.

However, the book fails to discuss adequately the basic radiologic and signal-processing principles of image acquisition and processing. Only one chapter deals with these topics. The discussion is superficial and spotty, and the choice of the image-processing methods included seems arbitrary. Many terms are introduced without explanation, and many of the illustrations are suboptimal.

The chapter on the use of digital subtraction angiography for evaluation of intracardiac defects in children with congenital heart disease is complete, but it does not address the failure of the significantly diminished spatial resolution of such systems to provide the anatomic detail necessary for adequate preoperative diagnosis.

One recurring theme in many of the chapters is the problem of archiving digitally acquired images, which is possibly the most critical impediment to the widespread use of digital technology in diagnostic imaging. It would have been advantageous if the editors had included a review of the current state of long-term archiving of such images. Significant strides have been made in optical and cassette storage in the past 3–5 years; such a review would provide readers with more information to help them decide whether to "go digital."

The editors have provided a good review of the current status of the clinical indications for and use of cardiac digital angiography. The book is relatively inexpensive. It should be purchased by cardiologists and radiologists who use digital techniques and by those who are interested in expanding their departments to perform such studies. I suggest, however, that they purchase an accompanying text on basic principles of digital imaging to complement the clinical aspects of this book.

Lawrence M. Buxt  
*College of Physicians and Surgeons, Columbia University*  
New York, NY 10032



# Coronary Angiography of Pulmonary Atresia, Hypoplastic Right Ventricle, and Ventriculocoronary Communications

Patricia E. Burrows<sup>1</sup>  
Robert M. Freedom<sup>2</sup>  
Lee N. Benson<sup>2</sup>  
C. A. Frederic Moes<sup>1</sup>  
Gregory Wilson<sup>3</sup>  
Kazuyuki Koike<sup>3,4</sup>  
William G. Williams<sup>5</sup>

A retrospective study was undertaken to determine the spectrum of angiographic abnormalities of the coronary arteries in infants and children with pulmonary atresia, hypoplastic right ventricle, and right ventriculocoronary arterial communications. Twenty-nine patients with 67 angiographic examinations were reviewed; findings in seven patients were compared with those at autopsy. Twenty-seven (93%) of 29 patients had caliber abnormalities of the involved coronary arteries, including obstructive lesions in 20 (69%) of 29 and segmental dilatation in 16 (55%) of 29. Nine patients had interruption of the anterior descending artery and one had absent connection between the coronary arteries and the aorta. A single coronary artery was found in four of 29 patients. There was excellent correlation between clinical angiography and autopsy findings in seven patients.

This study confirms the ability of high-quality clinical angiography to show significant abnormalities of the coronary arteries in infants and children with pulmonary atresia and ventriculocoronary communications.

*AJR* 154:789-795, April 1990

Received August 31, 1989; accepted after revision November 6, 1989.

Presented in part at the annual meeting of the American Heart Association, Washington, DC, November 1988.

<sup>1</sup> Department of Radiology, Hospital for Sick Children, University of Toronto, and Variety Club Cardiac Catheterization Laboratories, 555 University Ave., Toronto, Ontario, Canada M5G 1X8. Address reprint requests to P. E. Burrows.

<sup>2</sup> Department of Pathology, Hospital for Sick Children, University of Toronto, and Variety Club Cardiac Catheterization Laboratories, Toronto, Ontario, Canada M5G 1X8.

<sup>3</sup> Department of Cardiovascular Surgery, Hospital for Sick Children, University of Toronto, and Variety Club Cardiac Catheterization Laboratories, Toronto, Ontario, Canada M5G 1X8.

<sup>4</sup> Present address: National Children's Hospital, 35-31, Taishido 3-chome, Setagaya-ku, Tokyo, 154 Japan.

<sup>5</sup> Department of Pediatrics, Division of Cardiology, Hospital for Sick Children, University of Toronto, and Variety Club Cardiac Catheterization Laboratories, Toronto, Ontario, Canada M5G 1X8.

Infants and children with pulmonary atresia, hypoplastic right ventricle, and ventriculocoronary arterial communications are known to have a high rate of abnormal myocardial perfusion and obstructive lesions (myointimal hyperplasia and medial dysplasia) involving the coronary arteries [1-11]. Identification of these obstructive lesions is important for predicting individual patient prognosis and for surgical planning [4, 7, 12]. Previous reports describing the ventriculocoronary communications and coronary artery anomalies have concentrated on the prevalence, significance, and histology of the obstructive lesions [7-9]. It is the purpose of this report to describe the prevalence and the nature of the spectrum of angiographic abnormalities involving the coronary arteries on cineangiography in infants and children with pulmonary atresia, hypoplastic right ventricle, and ventriculocoronary communications.

## Materials and Methods

Twenty-nine consecutive patients with pulmonary atresia, hypoplastic right ventricle, and ventriculocoronary communications who had undergone cineangiographic examination between January 1985 and December 1988 were included in the study. Twenty-seven patients had an intact ventricular septum and two had a restrictive ventricular septal defect. During this time, eight patients were studied for the first time; the remainder had previously undergone cardiac catheterization. A total of 67 examinations were evaluated retrospectively for several features: the number and location of ventriculocoronary connections; coronary artery caliber abnormalities, including lumen irregularity, obstructive lesions, and dilatation; retrograde opacification of the right ventricle; abnormalities of the aortic sinuses; coronary artery dominance; continuity between the coronary arteries and the aorta; and the origin and distribution of the coronary arteries. Among the 29 patients, 28 had undergone right ventriculography, 21 had had ascending flush aortography, one had had balloon occlusion aortog-

raphy, and 12 had had selective coronary arteriography. Review of the cineangiograms was carried out without knowledge of autopsy findings.

Cineangiography was performed at 60 frames/sec. Right ventriculograms and the earlier aortograms were obtained in frontal and lateral projections; more recently, aortography and selective coronary angiography were performed by using axial oblique projections. Autopsies were performed in the seven patients who died; autopsy findings in the coronary arteries were studied retrospectively.

Five patients were restudied by selective coronary angiography after surgical procedures on the right ventricle. Three had right ventricular outflow tract reconstruction, creating continuity between the right ventricle and the pulmonary artery. Surgical exclusion of the right ventricle, consisting of placement of steel wire coils in the right ventricular cavity and oversewing of the tricuspid valve, was carried out in two.

## Results

The angiographic abnormalities are summarized in Table 1. Seventy-two right ventriculocoronary arterial communications were identified among the 29 patients (Fig. 1). They involved branches of both the left and right coronary arteries in 24 patients, the left coronary artery alone in four patients, and the right coronary artery alone in one patient. The connecting channels were large or nonrestrictive in three patients.

Anomalies of the origin and distribution of the coronary arteries were identified in four patients; all had a single left coronary artery; in two, the right coronary artery arose as a branch of the left anterior descending artery and crossed anterior to the right ventricular outflow tract (Fig. 2). In a third, the right coronary artery was a continuation of the circumflex branch. In a fourth patient, all of the coronary artery branches radiated from one right ventricle to a coronary artery con-

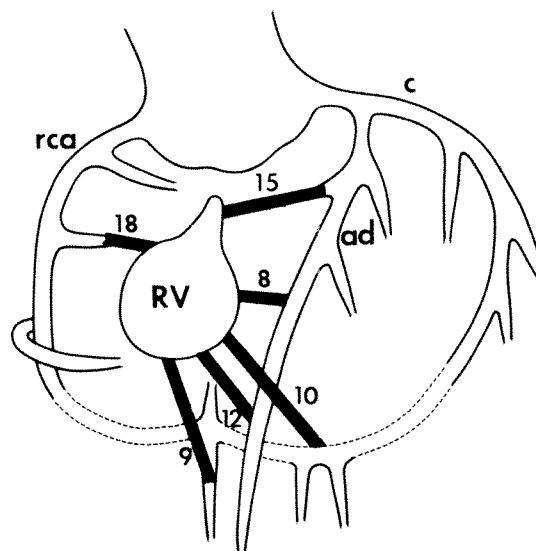


Fig. 1.—Diagram of frequency of right ventricle (RV) to coronary artery communications in the 29 infants and children studied. ad = anterior descending artery; c = circumflex artery; rca = right coronary artery.

necting channel at the infundibulum, and connections were absent between the coronary arteries and the aorta (Fig. 3).

Caliber abnormalities of the coronary artery were present in 27 of the 29 patients. Except for the extremely small ventriculocoronary communications, the involved coronary arteries showed absence of normal tapering, often becoming larger toward the connecting channel (Fig. 4).

Abrupt narrowing at the junction of the coronary artery branch and the connecting channel was common. In one patient where the connecting channel had become occluded after a thromboexclusion operation, the site of the previous fistulous connection could still be identified as a bulbous terminal dilatation of the coronary arterial branch. Irregularity, consisting of segments of apparent dilatation and narrowing, was identified in 20 of 29 patients. Discrete obstructive lesions of the coronary arteries were identified in 20 of 29 patients. Twelve patients had stenotic lesions, which appeared to be severe (greater than 75% luminal narrowing) in nine and mild (less than 50% luminal narrowing) in three. All three patients with mild stenosis had large ventriculocoronary communications and diffusely dilated anterior descending arteries (Fig. 4). In these three patients, the narrowed segments changed caliber during the cardiac cycle, becoming larger during systole and smaller during ventricular diastole; also, the septal perforators appeared to be decreased in number and demonstrated stasis of contrast material. Coronary arterial interruption (complete obliteration of the lumen) was diagnosed in 10 arteries in nine patients (Figs. 5–8), including interruption of the anterior descending coronary artery in nine patients and interruption of the right coronary artery in one. In addition, in one patient there was no connection between a single coronary artery and the aorta (absent proximal connection) (Fig. 3).

Five patients had arterial obstruction at multiple sites (Fig. 8). Of 22 obstructive lesions, 10 were proximal to the ventri-

TABLE 1: Coronary Angiographic Abnormalities in Pulmonary Atresia and Hypoplastic Right Ventricle

Abnormal Finding	No. of Patients (% of Total)
Single coronary artery	4 (14)
Right ventricle connections to	
Right posterior descending artery	9 (31)
Acute marginal or conus artery	18 (62)
Proximal anterior descending artery	15 (52)
Mid anterior descending artery	8 (28)
Distal anterior descending artery	12 (41)
Left circumflex artery	10 (34)
Left and right coronary arteries	24 (83)
Left coronary artery only	4 (14)
Right coronary artery only	1 (4)
Retrograde opacification of right ventricle	15 (52)
Coronary artery caliber abnormalities	27 (93)
Irregular lumen	20 (69)
Obstructive lesion	20 (69)
Stenosis	12 (41)
Interruption	9 (31)
Absent aortic connection	1 (4)
Multiple obstructions	5 (17)
Segmental dilatation	16 (55)
Total	29

Fig. 2.—Single left coronary artery in a child with pulmonary atresia, intact ventricular septum, and right ventricular connection to right coronary artery (arrows).

A, Selective left coronary arteriogram, axial left anterior oblique projection, shows aberrant course of right coronary artery (rca), which crosses right ventricular outflow tract. Note lack of normal tapering of distal right coronary artery.

B, Right anterior oblique projection.

ad = anterior descending artery.

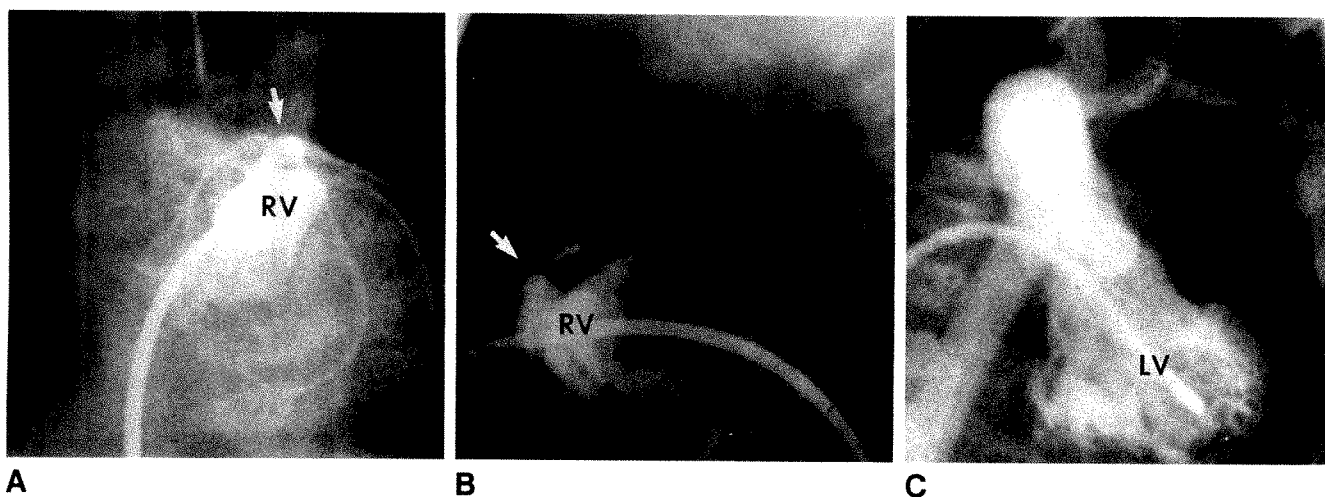
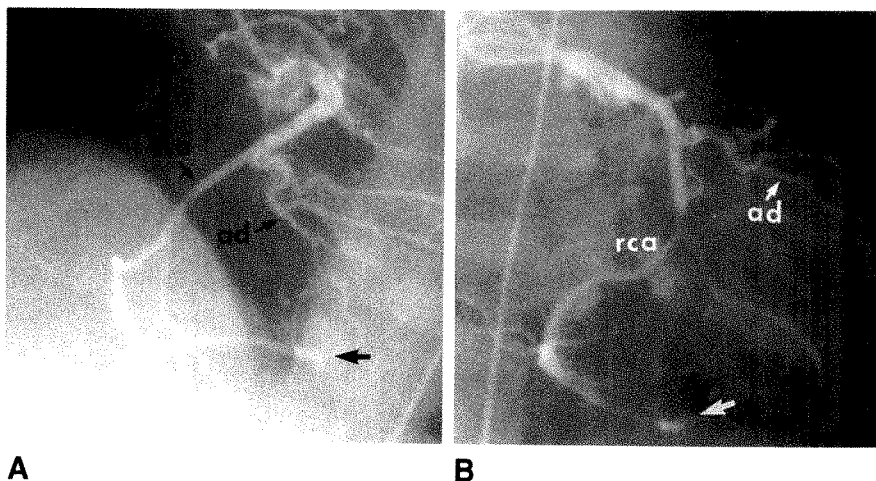


Fig. 3.—Absent proximal connection between coronary arteries and aorta in neonate with pulmonary atresia, hypoplastic right ventricle, restrictive ventricular septal defect, and ventriculocoronary communication.

A, and B, Contrast injection in small right ventricle (RV) in frontal (A) and lateral (B) projections shows origin of all coronary artery branches from single connection with right ventricular infundibulum (arrows). Aorta opacified on later cine frames, via ventricular septal defect.

C, No antegrade opacification of coronary arteries can be seen on this left ventriculogram (right anterior oblique projection). Autopsy confirmed absence of coronary ostia in ascending aorta. LV = left ventricle.

culocoronary connection, nine were distal to the connection, and three were remote from the connection. Progression of coronary artery stenosis was documented in three patients. In one, the change occurred during a 4-month interval; the anterior descending coronary artery looked almost normal in the newborn examination, but was severely stenotic at angiography 4 months later. In the two other patients, stenoses were noted on the initial examinations at 1 day and 6 weeks of age, but were found to have progressed at angiography by 2 years 6 months and 2 years 3 months, respectively.

Collateral vessels were shown in five patients who had significant obstructive lesions (Fig. 7). In four, collaterals were from adjacent coronary arteries and in one they were from enlarged intercostal and phrenic arteries, which appeared to have communications with coronary branches.

Segmental dilatation of the coronary artery between the connecting channel and the aorta or nearest main coronary

artery branch was common, present in 16 of 29 patients. This abnormality was most marked in the three patients with nonrestrictive ventriculocoronary communications, in whom the entire vessel was dilated (Fig. 5). The aortic root was also significantly dilated in these three patients; in one there was markedly asymmetric dilatation of the left coronary sinus.

Retrograde opacification of the right ventricle during systemic injection of contrast material was observed in 15 of 29 patients. Some right ventricular filling occurred during all selective coronary artery injections (Fig. 9). In two patients, selective coronary angiography produced opacification of intramyocardial spaces that did not appear to communicate with the right ventricular cavity (Fig. 7).

Coronary artery dominance was right-sided in 14 patients, left-sided in nine, and combined or indeterminate in two. Dominance was not assigned in the four patients with single coronary arteries.

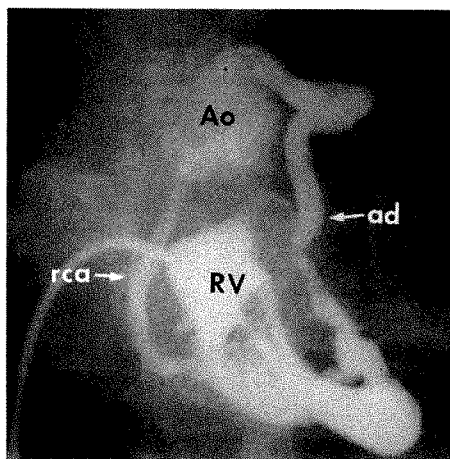


Fig. 4.—This patient with right ventricular communications to right coronary artery (rca) and anterior descending artery (ad) has diffuse enlargement of anterior descending artery with multiple mild focal stenoses. Note poor filling of septal perforating branches. Ao = aorta; RV = right ventricle.

Abnormal position of the right coronary artery and anterior descending branch, related to hypoplasia of the right ventricle, was seen in all patients. The right coronary artery was more anterior in position, especially in those patients with marked dilatation of the right atrium, and the anterior descending artery was farther to the right than in normal children.

Five patients in this series underwent selective coronary angiography or aortography after repair of the right ventricular outflow tract (three patients) or surgical exclusion of the right ventricle by using steel wire coils and oversewing of the tricuspid valve (two patients). The ventriculocoronary arterial communications could be identified by residual areas of stenosis and dilatation adjacent to the connecting channel (Figs. 7 and 8). Minimal residual antegrade or retrograde flow of contrast material across the connecting channel was visible in three of the five patients.

In seven patients in this angiographic series, including four who had undergone surgical thromboexclusion of the right ventricle, the coronary arteries were examined at autopsy. Angiographic findings in this group had included obstructive lesions of the left anterior descending coronary artery in five (interruption in two and stenosis in three), luminal irregularity without focal obstruction in one, and absent proximal aortic-coronary connection in one. At autopsy, all seven had intimal hyperplasia and medial dysplasia of the coronary arteries that communicated with the right ventricle, associated with myocardial ischemic changes. There was excellent correlation between findings on angiography and those at autopsy in six patients (Fig. 5). In the seventh patient, only luminal irregularity was seen at angiography; postmortem histologic examination showed narrowing of less than 50% involving the proximal circumflex branch. The histologic abnormalities in the dilated segments of the involved coronary arteries were similar to, although less severe than, those in the areas of focal narrow-

ing. Two of the patients who died had nonrestrictive ventriculocoronary communications, dilated anterior descending arteries with areas of relative stenosis, and poor filling of septal perforators at presurgical angiography (Fig. 4). These patients had histologic abnormalities in the anterior descending arteries similar to those seen with severe stenosis.

## Discussion

The purpose of coronary imaging in infants and children with pulmonary atresia and hypoplastic right ventricles is to identify patients with anomalies of the coronary distribution, coronary obstructive lesions leading to right ventricle-dependent coronary circulation or myocardial ischemia, and significant systemic-to-right ventricular shunting.

Many works have documented the nature of caliber abnormalities involving the coronary arteries that have abnormal communications with the right ventricle in patients with pulmonary atresia and an intact ventricular septum [1-11]. Turbulence and increased velocity of flow through the coronary arteries are believed to be responsible for injury to the arterial wall [3]. The resulting histologic abnormalities include myointimal hyperplasia and medial dysplasia, characterized by proliferation of myocytes and fibroblasts; increased amounts of collagen and ground substance; and disruption of the elastica [10]. Calder et al. [8] reviewed the autopsy specimens of 35 patients with pulmonary atresia and intact ventricular septa. Among 22 patients who had right ventriculocoronary arterial communications, 12 had normal coronary arteries and 10 had various degrees of medial and intimal thickening.

These obstructive lesions were distal to the connecting channels in half of the patients, proximal in one-third, and both proximal and distal in one-third.

Sauer et al. [7] reported the patterns of right ventriculocoronary arterial connections in 26 patients studied by angiography, with pathologic correlation. Eighteen (69%) of 26 patients in their series had interruption of the left anterior descending coronary artery, which proved to be a major risk factor because of associated myocardial ischemia. These authors also studied the significance of aortic-right ventricular shunting via large connections; they found that a 6% increase in oxygen saturation in the right ventricle was predictive of a significant systemic-to-right ventricular shunt.

The decision to operate on the right ventricle depends on the anatomy of the coronary arteries [4, 7, 12]. In some institutions, early exclusion of the right ventricle is performed in infants with ventriculocoronary communications in order to decrease the turbulent flow in the coronary arteries and, it is hoped, halt the progression of intimal and medial dysplasia. However, both this operation and right ventricular outflow tract reconstruction (which lowers the right ventricular pressure) are contraindicated in the presence of coronary artery obstructive lesions with right ventricle-dependent coronary circulation. In a recent review of 115 patients from this institution with pulmonary atresia and intact ventricular septa, Coles et al. [12] reported that the presence of severe stenosis or interruption of the proximal left anterior descending artery

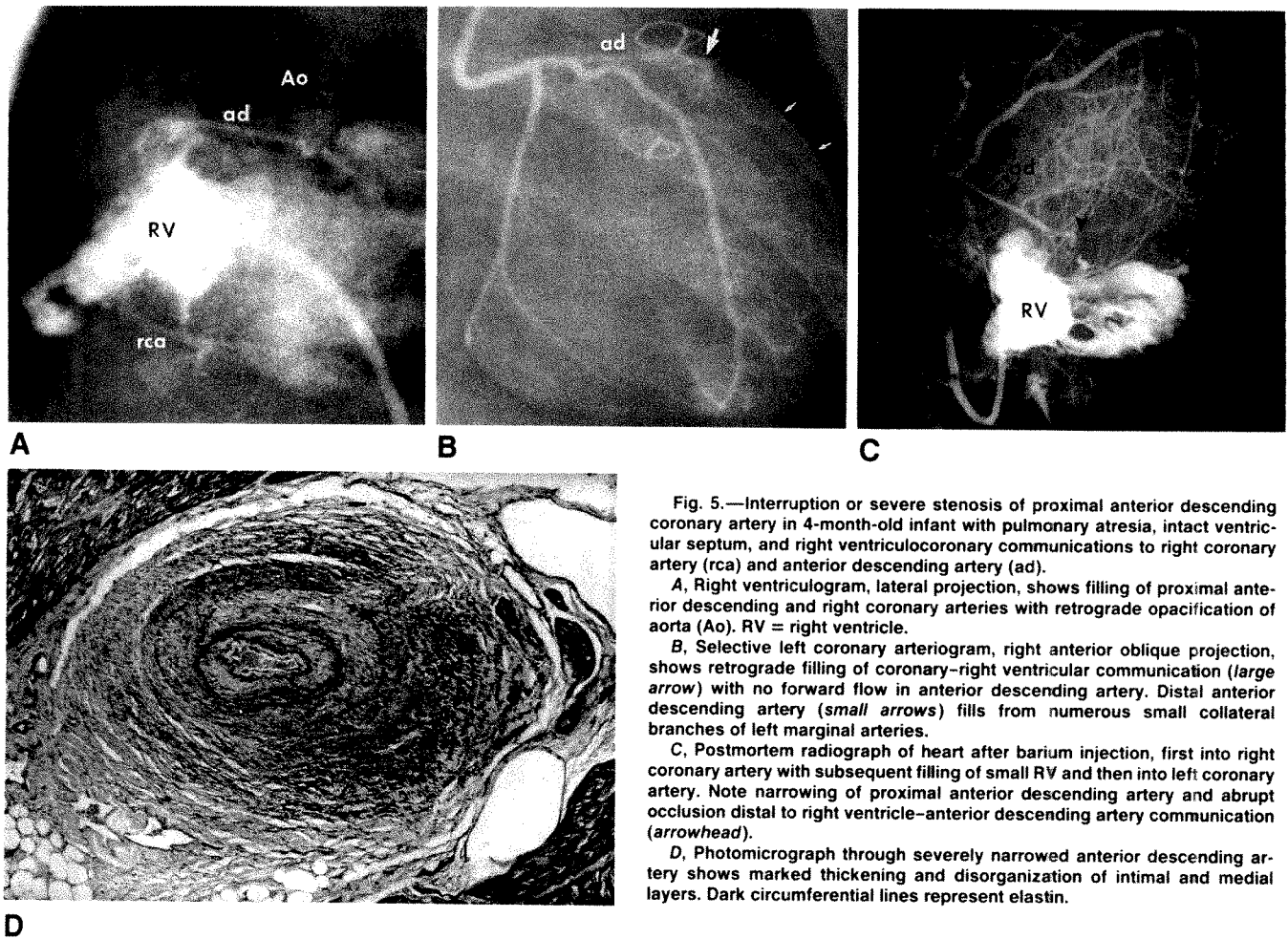


Fig. 5.—Interruption or severe stenosis of proximal anterior descending coronary artery in 4-month-old infant with pulmonary atresia, intact ventricular septum, and right ventriculocoronary communications to right coronary artery (rca) and anterior descending artery (ad).

A, Right ventriculogram, lateral projection, shows filling of proximal anterior descending and right coronary arteries with retrograde opacification of aorta (Ao). RV = right ventricle.

B, Selective left coronary arteriogram, right anterior oblique projection, shows retrograde filling of coronary-right ventricular communication (large arrow) with no forward flow in anterior descending artery. Distal anterior descending artery (small arrows) fills from numerous small collateral branches of left marginal arteries.

C, Postmortem radiograph of heart after barium injection, first into right coronary artery with subsequent filling of small RV and then into left coronary artery. Note narrowing of proximal anterior descending artery and abrupt occlusion distal to right ventricle-anterior descending artery communication (arrowhead).

D, Photomicrograph through severely narrowed anterior descending artery shows marked thickening and disorganization of intimal and medial layers. Dark circumferential lines represent elastin.

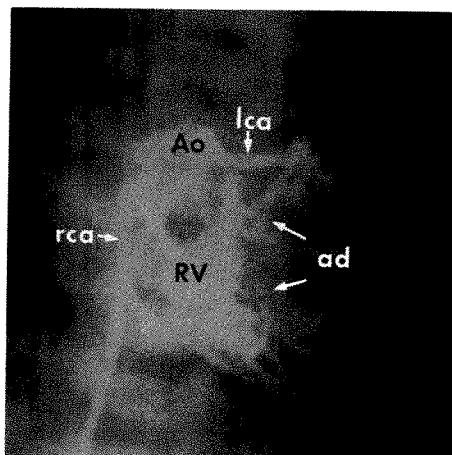


Fig. 6.—Interruption of mid-anterior descending artery, confirmed at autopsy. Right ventriculogram (frontal projection) shows communications with proximal and distal anterior descending (ad) artery, and absent opacification of middle segment. There is also filling of right coronary artery (rca). Ao = aorta; lca = left coronary artery; RV = right ventricle.

was a uniformly lethal risk factor for patients undergoing right ventricular outflow tract reconstruction or right ventricular thromboexclusion. Koike et al. [11] have shown that the structural coronary artery lesions are frequently present in the neonatal period.

An absent proximal connection between the aorta and one or both coronary arteries that have communications with the right ventricle is a rare lesion, initially described in patients with pulmonary atresia and intact ventricular septa [13–15]. Recently, Garcia et al. [16] described an infant with pulmonary atresia, hypoplastic right ventricle, ventricular septal defect, and ventriculocoronary connections in whom the coronary arteries arose directly from multiple connecting channels, without aortic ostia. The infant with an absent proximal aortic-coronary connection in our series is similar, except that all of the coronary artery branches radiated from a single connecting channel. The unusual distribution of the coronary arteries in this patient is unlike that which would be expected in the presence of a single coronary artery with acquired atresia of the aortic coronary ostia.

Because about two-thirds of our patients were being re-studied, there was a bias toward those with less severe disease and longer survival. Significant obstructive lesions



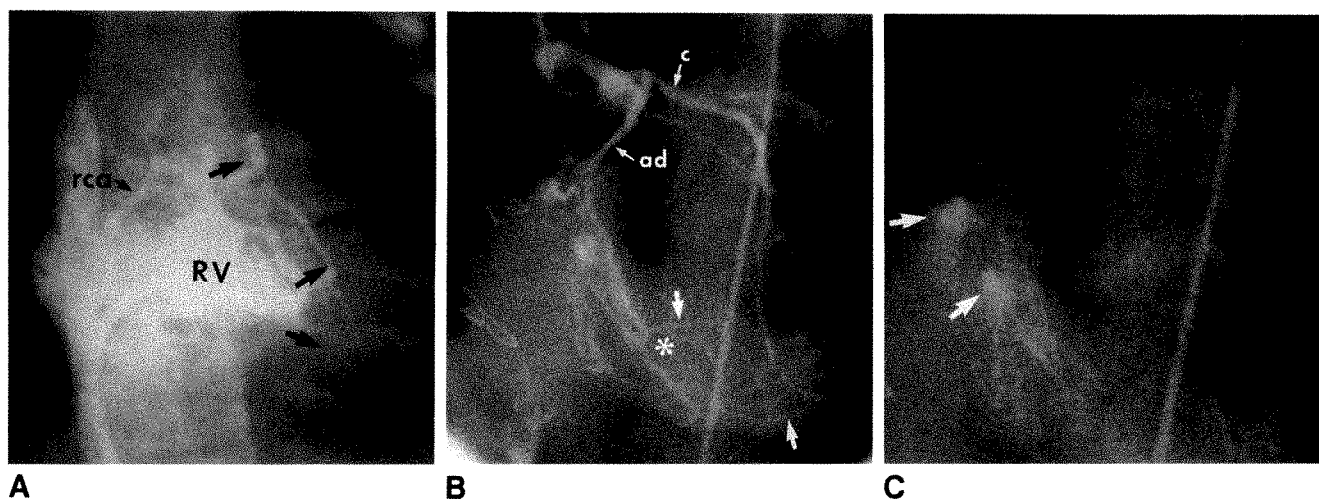


Fig. 7.—Interruption of distal anterior descending artery and distal right coronary artery and retrograde filling of intramyocardial vascular spaces.  
 A, Right ventriculogram (frontal projection) in neonatal period shows communications (arrows) between right ventricle (RV) and distal, mid, and proximal anterior descending artery (ad) and right coronary artery (rca).  
 B, Selective left coronary arteriogram shows irregular caliber of anterior descending artery (ad) with apparent distal interruption (asterisk) and multiple small collateral vessels (arrows). Circumflex artery (c) is normal.  
 C, Late phase of left coronary arteriogram shows puddling of contrast material in intramyocardial spaces (arrows).

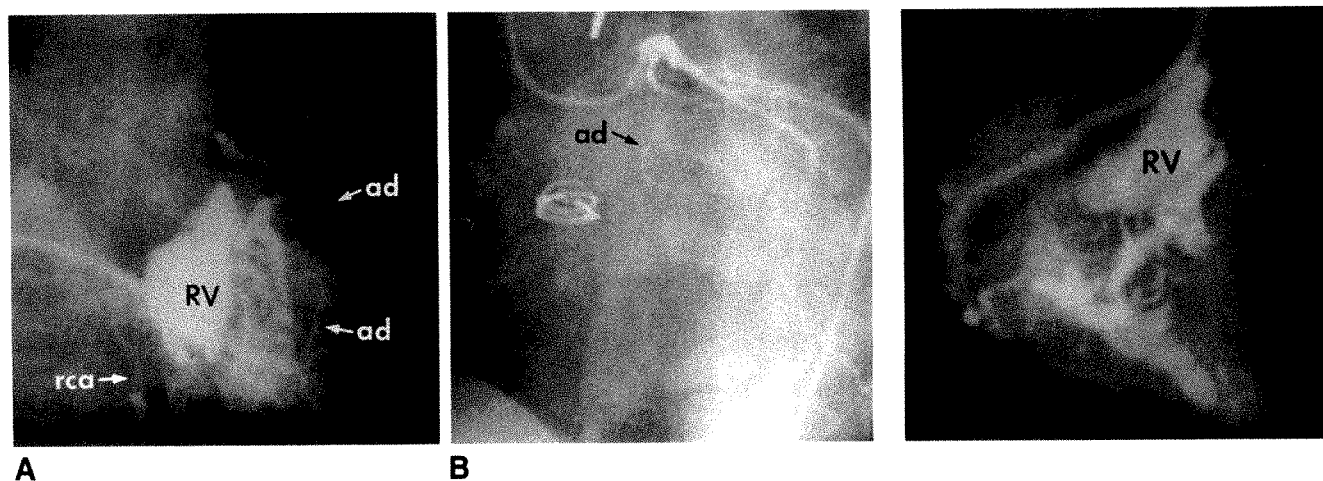


Fig. 8.—Multiple obstructive lesions in coronary artery.  
 A, Right ventriculogram (frontal projection) shows communications with right coronary artery (rca) and mid and proximal anterior descending artery (ad) with apparent interruptions in mid and distal segments. Portion of anterior descending artery between interruptions is dependent on right ventricle. RV = right ventricle.  
 B, Selective left coronary arteriogram after surgical thromboexclusion of right ventricle confirms interruption of mid anterior descending artery (ad), nonfilling of segment previously shown to be right ventricular-dependent, and progression of narrowing of proximal anterior descending artery. Note steel wire coil in right ventricle. Right coronary arteriogram showed extensive collaterals along posteroinferior wall.

Fig. 9.—Retrograde right coronary–right ventricular opacification shown by selective right coronary arteriogram (left anterior oblique projection). RV = right ventricle.

were present in 20 (69%) of 29 patients, including arterial interruption or absent aortic connection in 10 (34%).

Progression of stenotic lesions appears to vary. This was documented in only three patients, but may have been underestimated owing to less optimal angiographic techniques used in older examinations. The rapid progression in one patient, occurring during a 4-month period, emphasizes the need to reevaluate patients with this lesion when a new surgical procedure is considered.

The segments of arterial dilatation seen at angiography appear to represent a hemodynamic response to increased flow and turbulence. Areas of stenosis frequently develop within the dilated segments; the stenotic and dilated segments demonstrate similar histologic abnormalities, including myocardial ischemia.

The diagnosis of coronary artery obstructive lesions requires attention to technical quality and careful analysis of the angiograms. In order to diagnose arterial interruption cor-



rectly, it is important to be aware of the "displacement" of the right coronary artery and anterior descending artery that occurs in pulmonary atresia with intact ventricular septa. Because of the hypoplasia of the right ventricle and the dilatation of the right atrium, the right coronary artery is more anterior and the anterior descending coronary artery is more medially positioned than normal. In the presence of large or moderate-sized ventriculocoronary communications, right ventricular angiography usually produces good opacification of the involved coronary arteries. Opacification of the aortic root should be sought to exclude aortic-coronary discontinuity. Filling of the coronary arteries distal to the connecting channel during ventricular diastole should also be confirmed. If a coronary artery has more than one connection with the right ventricle, it is important to be certain that the entire length of the vessel has been visualized. If not, selective coronary arteriography should be performed before any right ventricular surgical procedure.

Selective coronary angiography provides the best delineation of the coronary arteries and associated lesions in most patients. The youngest patient in our series to undergo selective coronary angiography was 4 months old. A useful alternative to selective coronary angiography in infants is antegrade balloon occlusion aortography [17]. This technique produces opacification of the coronary artery that is far superior to that in flush aortography.

In summary, good-quality angiography demonstrates a high rate (93%) of caliber abnormalities of the coronary arteries in patients with pulmonary atresia, hypoplastic right ventricle, and ventriculocoronary communications. Our series has confirmed the high prevalence of coronary artery obstructive lesions (69%) and, in a small number of patients, has shown a good correlation between findings on clinical angiography and autopsy. An observation that has not been emphasized previously is the presence of dysplastic changes in dilated segments of coronary arteries at histologic examination. In the presence of severe dilatation of the coronary artery, occlusive lesions may be present in the perforating branches. Lastly, awareness of the high frequency of anomalies of the origin and distribution and abnormalities in the position of the coronary arteries in this condition has been emphasized. Selective coronary angiography is recommended before surgery in any patient in whom complete integrity of the coronary arteries has not been confirmed on conventional angiography.

#### ACKNOWLEDGMENTS

We thank Lou Scaglione and his staff for preparing the illustrations and Eduarda DeOliveira and Susan Scorizzi for preparing the manuscript.

#### REFERENCES

1. Oppenheimer EH, Esterly JR. Some aspects of cardiac pathology in infancy and childhood. II. Unusual coronary endarteritis with congenital cardiac malformations. *Johns Hopkins Med J* 1966;119:343-354
2. Essed CE, Klein HW, Krediet P, Vorst EJ. Coronary and endocardial fibroelastosis of the ventricles in the hypoplastic left and right heart syndrome. *Virchows Arch [A]* 1975;368:87-97
3. Bull C, de Leval M, Mercanti C, Macartney FJ, Anderson RH. Pulmonary atresia and intact ventricular septum: a revised classification. *Circulation* 1982;66:266-272
4. O'Connor WN, Cottrill CM, Johnson GL, Noonan JA, Todd EP. Pulmonary atresia with intact ventricular septum and ventriculocoronary communications: surgical significance. *Circulation* 1982;65:805-809
5. Freedom RM, Benson L, Wilson GJ. The coronary circulation and myocardium in pulmonary and aortic atresia with an intact ventricular septum. In: Marcelletti C, Anderson RH, Becker AE, Corno A, di Carlo D, Mazzera E, eds. *Paediatric cardiology*, vol. 6. Edinburgh: Churchill-Livingstone, 1986: 78-96
6. Jenni R, Goebel N, Tartini R, Schneider J, Arbenz U, Oelz O. Persisting myocardial sinusoids of both ventricles as an isolated anomaly: echocardiographic, angiographic, and pathologic anatomical findings. *Cardiovasc Intervent Radiol* 1986;9:127-131
7. Sauer U, Bindl L, Pilosoff V, et al. Pulmonary atresia with intact ventricular septum and right ventricle-coronary artery fistulae: selection of patients for surgery. In: Doyle EF, Engle MA, Gersony WM, Rashkind WJ, Talkner NS, eds. *Pediatric cardiology*. New York: Springer-Verlag, 1986:566-578
8. Calder AL, Co EE, Sage MD. Coronary arterial abnormalities in pulmonary atresia with intact ventricular septum. *Am J Cardiol* 1987;59:437-442
9. Gittenberger-de Groot AC, Sauer U, Bindl L, Babic R, Essed CE, Buhlmeier K. Competition of coronary arteries and ventriculocoronary communications in pulmonary atresia with intact ventricular septum. *Int J Cardiol* 1988;18:243-258
10. Wilson GJ, Freedom RM, Koike K, Perrin D. The coronary arteries: anatomy and histopathology. In: Freedom RM, ed. *Pulmonary atresia with intact ventricular septum*. Mount Kisco, NY: Futura, 1989:75-88
11. Koike K, Perrin D, Wilson GJ, Freedom RM. Myocardial ischaemia and coronary arterial involvement in newborn babies less than one week old with pulmonary atresia and intact ventricular septum. In: Freedom RM, ed. *Pulmonary atresia with intact ventricular septum*. Mount Kisco, NY: Futura, 1989:101-107
12. Coles JG, Freedom RM, Lightfoot NE, et al. Long-term results in neonates with pulmonary atresia and intact ventricular septum. *Ann Thorac Surg* 1989;47:213-217
13. Lenox CC, Briner J. Absent proximal coronary arteries associated with pulmonic atresia. *Am J Cardiol* 1972;30:666-669
14. Blackman MS, Schneider B, Sondheimer HM. Absent proximal left main coronary in association with pulmonary atresia. *Br Heart J* 1981;46: 449-451
15. Ueda K, Saito A, Nakano H, Hamazaki Y. Absence of proximal coronary arteries associated with pulmonary atresia. *Am Heart J* 1983;106: 596-598
16. Garcia OL, Gelband H, Tamer DF, Fojaco RM. Exclusive origin of both coronary arteries from a hypoplastic right ventricle complicating an extreme form of tetralogy of Fallot: lethal myocardial infarction following a palliative shunt. *Am Heart J* 1989;115:198-201
17. Burrows PE, Benson LN, Freedom RM. Coronary angiography in pulmonary atresia with intact ventricular septum. In: Freedom RM, ed. *Pulmonary atresia with intact ventricular septum*. Mount Kisco, NY: Futura, 1989:207-228

## Book Review

**Scintigraphy of Inflammation with Nanometer-sized Colloid Tracers.** By Marc de Schrijver. (Vol. 16 in the series *Developments in Nuclear Medicine*. Edited by P. H. Cox.) Boston: Kluwer, 212 pp., 1989. \$69.50

This book describes the usefulness of a recently developed radiopharmaceutical,  $^{99m}\text{Tc}$ -nanocolloids (Solco Nanocoll, Solco Basle, Ltd.), for imaging inflammations. The text consists of eight chapters and two appendixes and is quite well organized. Chapter 1 serves as an introduction, though, unfortunately, the new agent is not clearly mentioned. Chapters 2 and 3 describe the pathophysiology of inflammatory processes and the currently available radiopharmaceuticals available for imaging inflammations. The reason for including chapter 4, which is basically a review of literature currently available, is not clear. The reader must wait until chapter 5, which describes the characteristics of the alternative radiopharmaceutical, before being introduced to the radiolabeled nanometer-sized colloids, the subject of the book.

The next chapter contains data of preclinical animal investigations of this agent. Chapter 7, the most important one in the book, deals with the usefulness and limitations of  $^{99m}\text{Tc}$ -nanocolloids in the clinical situation for diagnostic imaging of inflammations and compares the specificity and sensitivity of this agent with the currently used agents:  $^{111}\text{In}$ -labeled granulocytes,  $^{111}\text{In}$ -chloride,  $^{99m}\text{Tc}$ -HMPAO,  $^{99m}\text{Tc}$ -labeled antigranulocyte monoclonal antibodies,  $^{99m}\text{Tc}$ -MDP, and  $^{99m}\text{Tc}$ -DTPA. The final chapter, "Summary and Conclusions," could have

been omitted as it adds nothing new to the information already given in the preceding chapters.

The book has been published from "camera-ready" typed text and therefore, as might be expected, contains several typographic and grammatical errors, though considerably fewer than many other publications prepared from similar camera-ready material. Many of the tables are a lighter color than the text, making them difficult to read. To American readers, the isotope mass number placed throughout the text as a superscript to the right, instead of the left, may be distracting.

This book is not recommended for residents, fellows, general radiologists, or nuclear medicine physicians, as it describes a radiopharmaceutical that could be used only as an investigational new drug in the United States. Research investigators interested in newer  $^{99m}\text{Tc}$ -labeled compounds for imaging inflammation may find this book somewhat useful as a source of reference.

Leela P. Kasi  
E. Edmund Kim  
*The University of Texas*  
M. D. Anderson Cancer Center  
Houston, TX 77030

## Pictorial Essay

# Current Evaluation of the Patient with Abnormal Visceroatrial Situs

Marta Hernanz-Schulman,<sup>1,2</sup> Michael M. Ambrosino,<sup>1</sup> Nancy B. Genieser,<sup>1</sup> Deborah Friedman,<sup>3</sup> Howard Banner,<sup>4</sup> William Rumancik,<sup>5</sup> and Rita L. Teele<sup>6</sup>

The concept of situs or laterality of body organs is an important one in understanding congenital visceral and vascular malformations. The normal differentiation and placement of asymmetric body parts is termed situs solitus. When laterality is disturbed during embryogenesis, situs inversus (the mirror image of situs solitus in toto) can result. At other times, the consequence is an interesting heterotaxia with variable anatomic symmetry and displacement and dysmorphism of asymmetric structures. This is logically termed situs ambiguus, although occasionally it is termed partial situs inversus. These patients tend to be divided between those in whom right-sided body structures predominate (usually no spleen will be present) and those in whom left-sided body structures predominate (usually two or more splenuli will be present).

The diagnosis and evaluation of these conditions during life has been largely dependent on invasive studies, such as angiography. We have evaluated noninvasively 16 patients with viscerotrial situs anomalies, ranging in age from birth to 18 years at the time of diagnosis; their imaging studies form the basis of this essay.

## Materials and Methods

All 16 patients were evaluated sonographically. Six were imaged with MR; five patients underwent selective spleen scanning. Sonograms were obtained with real-time equipment and appropriate transducers (3–7.5 MHz). MR was performed with a 0.5-T magnet; spin-echo (SE) 300–1800/20–30 (TR/TE) sequences were used with a slice thickness of 5–8 mm. Selective spleen scans were obtained by using heat-damaged RBCs labeled with <sup>99m</sup>Tc.

The diagnosis of polysplenia (10 patients) was made by identifying multiple splenuli. The diagnosis of asplenia (four patients) was established when no spleen was identified after careful search in the appropriate region. Situs inversus (two patients) was diagnosed when body asymmetry was found to be entirely the mirror image of situs solitus.

## Results

### Polysplenia

*Visceral anomalies.* Sonography accurately delineated the multiple retrogastric splenuli in all 10 patients with polysplenia.

Received July 13, 1989; accepted after revision November 7, 1989.

<sup>1</sup> Department of Pediatric Radiology, New York University Medical Center, 550 First Ave., New York, NY 10016.

<sup>2</sup> Present address: Department of Radiology, Medical Center North, Vanderbilt University Medical Center 1611 22nd Ave. S., Nashville, TN 37237. Address reprint requests to M. Hernanz-Schulman.

<sup>3</sup> Department of Pediatric Cardiology, New York University Medical Center, New York, NY 10016.

<sup>4</sup> Department of Nuclear Medicine, New York University Medical Center, New York, NY 10016.

<sup>5</sup> Department of MRI, New York University Medical Center, New York, NY 10016.

<sup>6</sup> Department of Radiology, The Children's Hospital Medical Center, 300 Longwood Ave., Boston, MA 02115.

AJR 154: 797–802, April 1990 0361–803X/90/1544–0797 © American Roentgen Ray Society

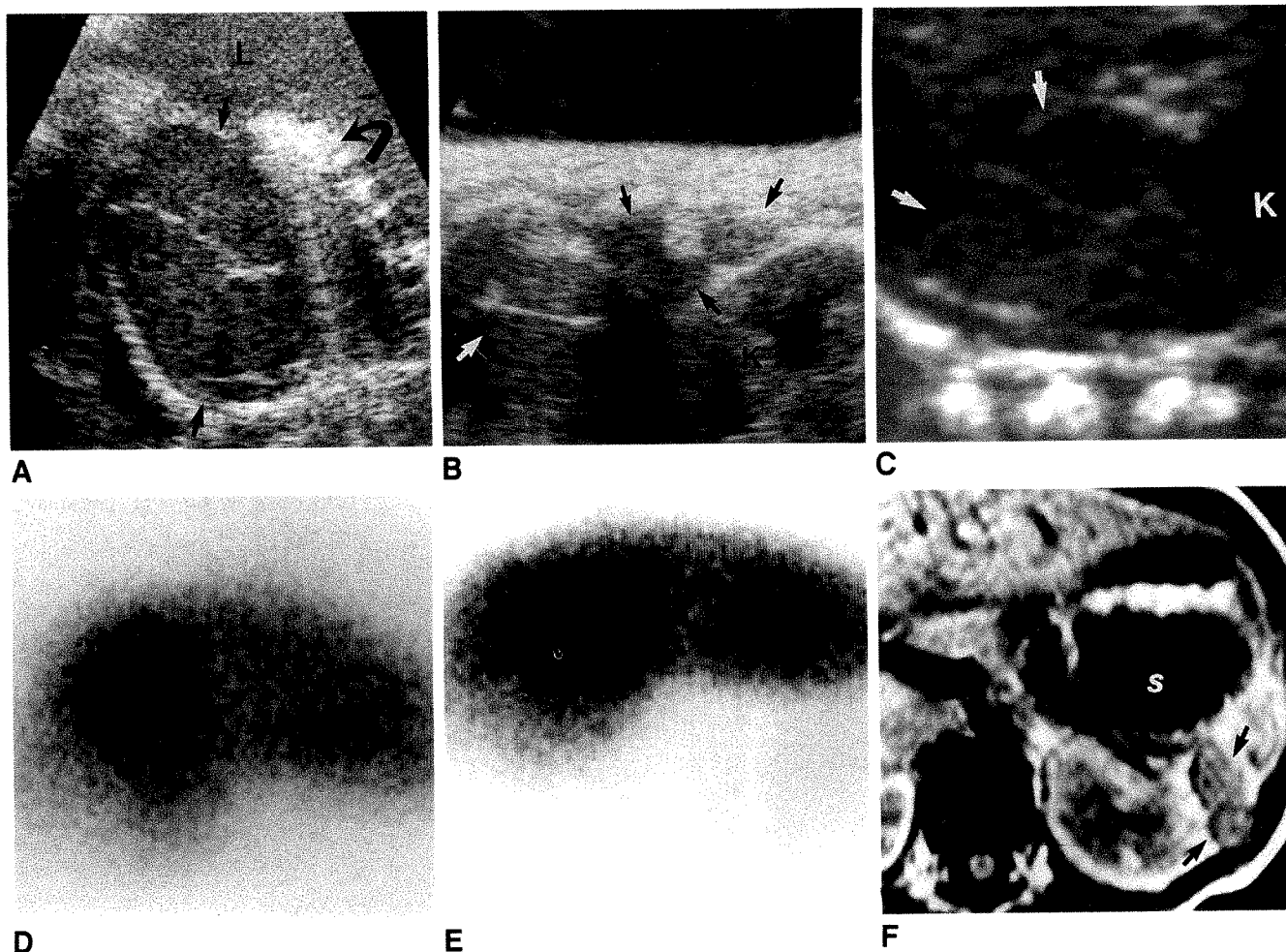


Fig. 1.—Visceral anomalies in polysplenia.

A, Transverse sonogram of right upper quadrant shows splenuli (straight arrows) separated by echogenic interfaces. Note that in this patient they are rather large and few in number. Air in stomach (curved arrow). L = liver.

B, Left coronal sonogram posterior to stomach in another patient. Multiple splenuli of various sizes (arrows) are seen readily and are separated by echogenic septa. K = left kidney inferior to splenic mass.

C, Right coronal sonogram in another patient with polysplenia, scanning posterior to stomach. Splenic mass is cephalad to ipsilateral kidney and adrenal gland (K). Compared with A and B, splenuli (arrows) are more subtle, illustrating need for careful scanning in appropriate location.

D, Selective spleen scan with  $^{99m}\text{Tc}$ -labeled RBCs shows photon activity in midline liver with prominent focus in right upper quadrant.

E,  $^{99m}\text{Tc}$  sulfur colloid scan in same patient. Similar view fails to show more intense splenic activity.

F, Axial MR image (SE 490/30, 8-mm slice) through upper abdomen of same patient as in B shows several splenuli (arrows) in left upper quadrant posterior to stomach (S).

Figures 1A–1C illustrate the various appearances. Selective spleen scans were accurate only in showing the presence of splenic tissue, but not its subdivision into several splenuli (Figs. 1D and 1E). MR clearly depicted both the splenic tissue and its multiple subdivisions, with clear visualization of the retrogastric area on axial images (Fig. 1F).

**Vascular anomalies.**—Sonography and MR clearly identified the five patients with polysplenia and interruption of the intrahepatic inferior vena cava with continuation via the right or left azygous system (Fig. 2A). In the remaining five patients the intrahepatic vena cava was present (Fig. 2B). In three of these, the vena cava lay to the left of the aorta, and “crossed

Fig. 2.—(facing page) Vascular anomalies in polysplenia.

A, Transverse sonogram of upper abdomen shows enlarged retrocrural azygous vein (straight arrow) to right of aorta. Splenuli (curved arrow) are seen suboptimally on this view. L = liver; D = disk space.

B, Longitudinal sonogram just to the right of midline in patient with intact vena cava outlines its normal course toward atrium.

C and D, Sequential longitudinal sonograms along left upper abdomen in patient with intact vena cava shows oblique course taken by this vessel (arrowheads) crossing over, anterior to aorta, in piggyback fashion. In such a patient it is important to rotate transducer in order to parallel and outline diagonal course of vessel. Atrium (arrow). L = liver; H = hepatic vein.

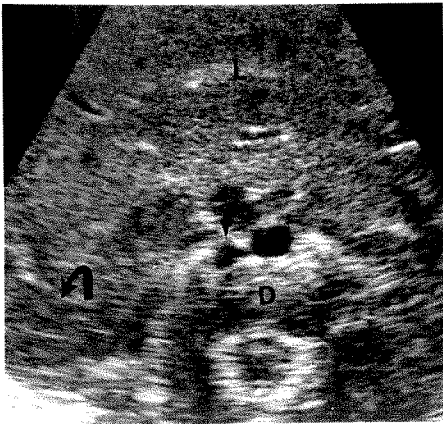
E, Parasagittal MR image (SE 600/30, 5-mm slice) of neonate with polysplenia. Intrahepatic cava terminates at hepatic venous confluence (arrow).

F, Transverse sonogram of same patient as in D shows independent drainage of hepatic vein into atrium (A).

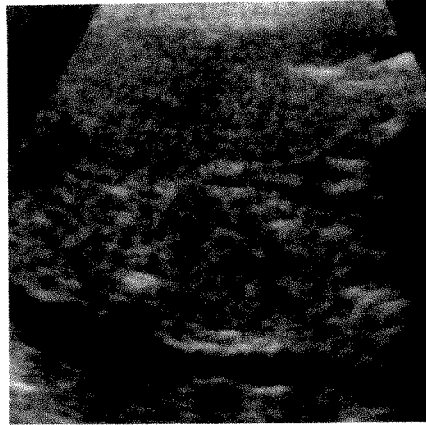
G and H, Sequential sagittal sonograms along mid upper abdomen show anterior path of preduodenal portal vein (solid arrows) with air outlining duodenum (open arrows). G = midline gallbladder; P = pancreas.

I, Sagittal sonogram in another patient with preduodenal portal vein shows its typical course, arching anterior to body of pancreas (P). Levels of transverse sections in J and K are indicated by a and b.

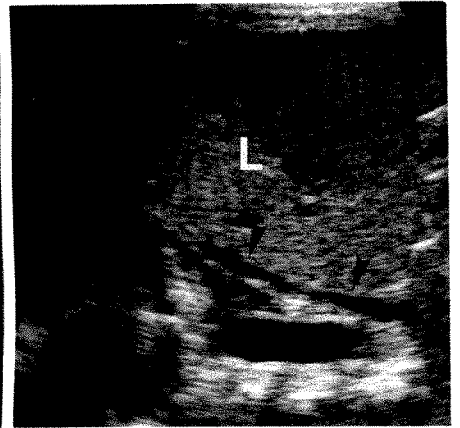
J and K, Sequential transverse sonograms in same patient. J (level a) shows anterior turn of superior mesenteric vein (straight arrow) away from superior mesenteric artery (arrowhead) at inferior edge of pancreas. K (level b) shows pancreas (P) interposed between superior mesenteric vein (straight arrow) and superior mesenteric artery (arrowhead). Curved arrows point to aorta, open arrows to vena cava. S = spine.



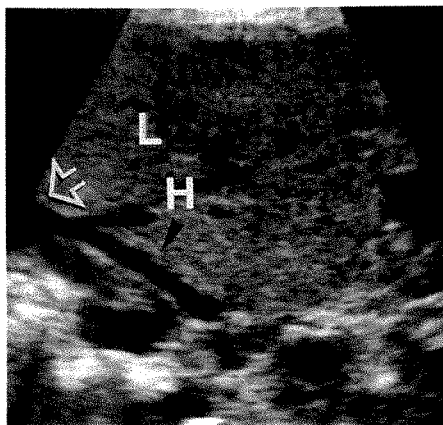
A



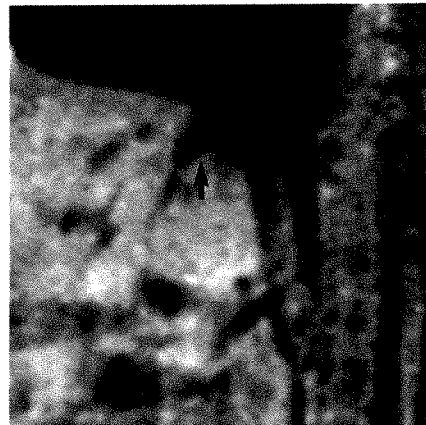
B



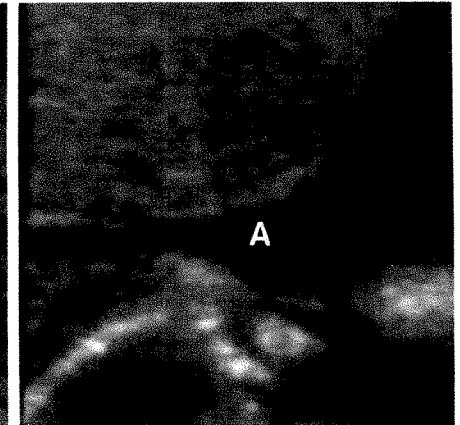
C



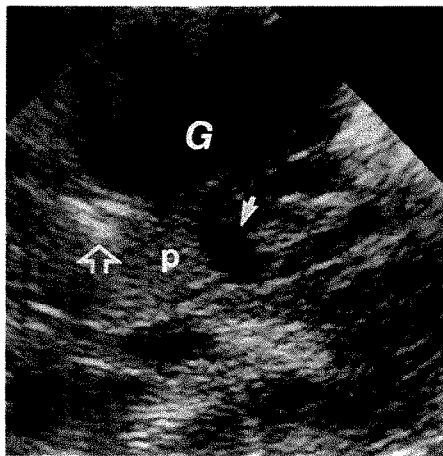
D



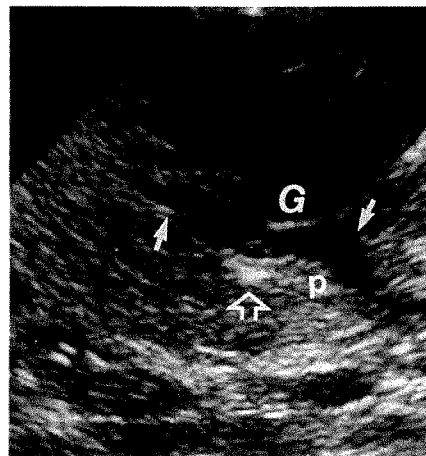
E



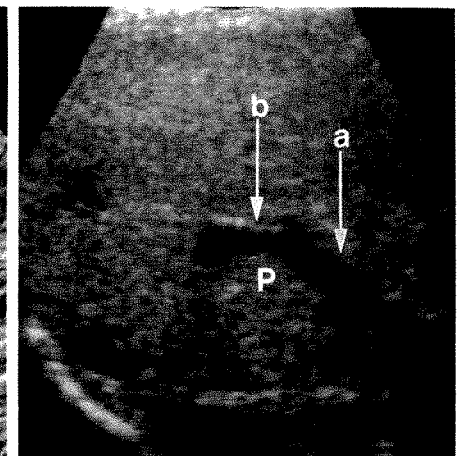
F



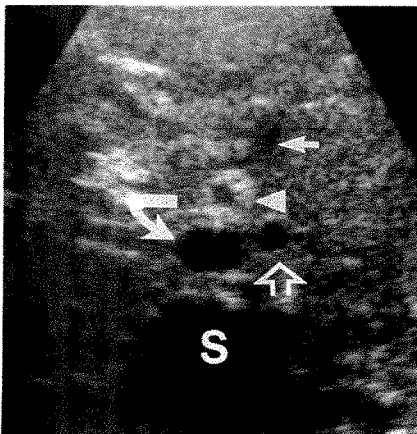
G



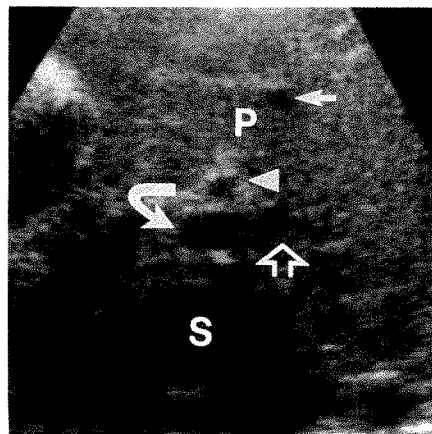
H



I



J



K

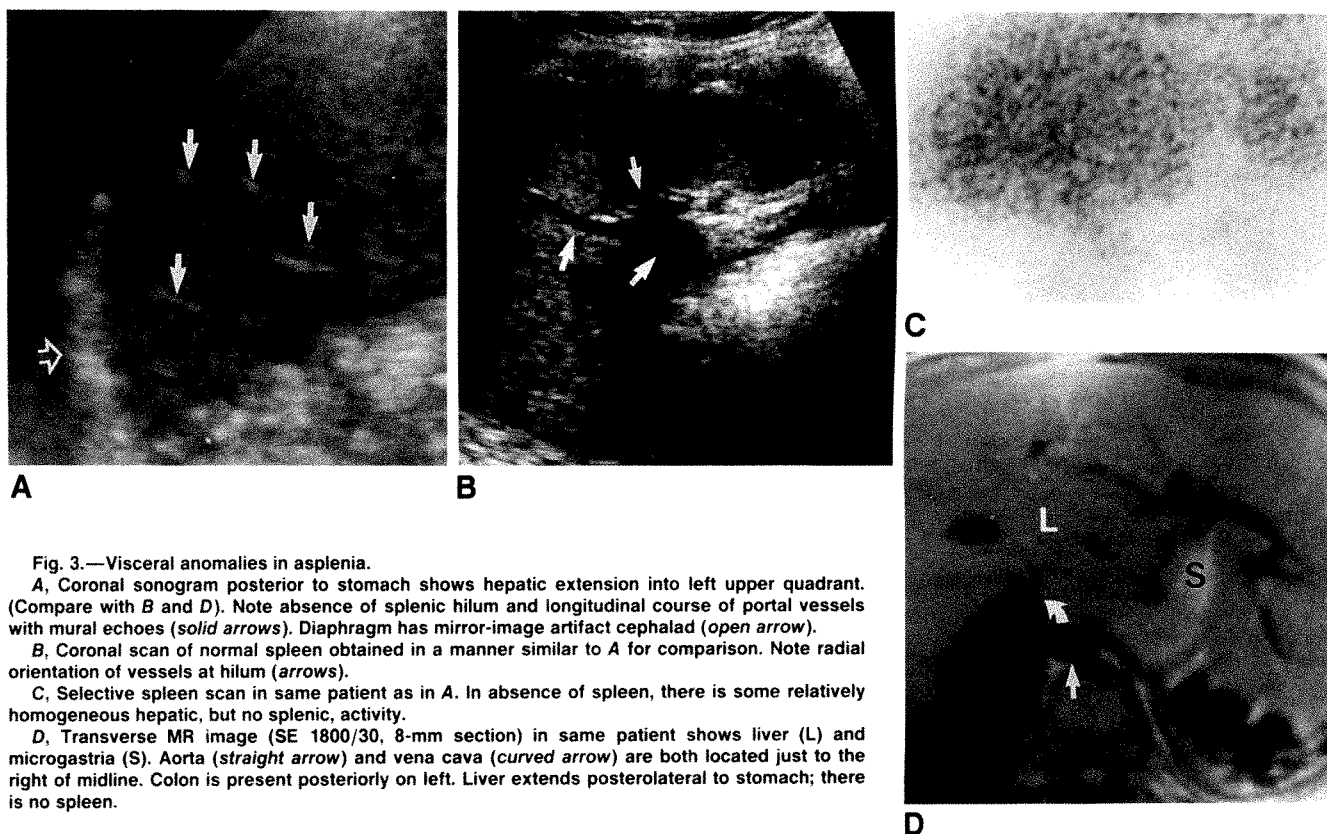


Fig. 3.—Visceral anomalies in asplenia.

A, Coronal sonogram posterior to stomach shows hepatic extension into left upper quadrant. (Compare with B and D). Note absence of splenic hilum and longitudinal course of portal vessels with mural echoes (solid arrows). Diaphragm has mirror-image artifact cephalad (open arrow).

B, Coronal scan of normal spleen obtained in a manner similar to A for comparison. Note radial orientation of vessels at hilum (arrows).

C, Selective spleen scan in same patient as in A. In absence of spleen, there is some relatively homogeneous hepatic, but no splenic, activity.

D, Transverse MR image (SE 1800/30, 8-mm section) in same patient shows liver (L) and microgastric (S). Aorta (straight arrow) and vena cava (curved arrow) are both located just to the right of midline. Colon is present posteriorly on left. Liver extends posterolateral to stomach; there is no spleen.

over" anterior to the aorta in a "piggyback" [1] fashion to enter the common atrium on the right (Figs. 2C and 2D). In two infants, the vena cava terminated at the confluence of the hepatic veins; their independent drainage had led to the erroneous echocardiographic impression of caval interruption with azygous continuation (Figs. 2E and 2F). Four patients with polysplenia clearly had a preduodenal portal vein (Figs. 2G–2I). Two of these had biliary atresia.

### Asplenia

*Visceral anomalies.*—Sonography, selective spleen scanning, and MR imaging were effective in identifying absence of the spleen (Fig. 3).

*Vascular anomalies.*—Sonography and MR delineated the presence and location of the vena cava and its intrahepatic branches and relationship to the aorta in all four patients with asplenia (Figs. 4A and 4B). The course of the portal vein was anterior to the pancreas in one patient (Fig. 3D).

Two of the four patients with asplenia had subdiaphragmatic total anomalous pulmonary venous connections. Both sonography and MR proved to be excellent and complementary methods in depicting the anomalous vessel (Figs. 4C–4G).

### Discussion

Our observations support recent studies based on animal models and human pedigrees leading to the concept of situs anomalies as a continuum [2, 3]. In a mouse population containing the mutant situs inversus gene alleles (iv), offspring of genetically homozygous individuals (iv/iv) show a random situs phenotype, independent of the phenotypic situs of their homozygous parents [2]. It is hypothesized that when the normal allele is not present at this locus, situs assignment becomes a random event [2]. Extrapolation to human pedigrees explains why situs inversus, asplenia, and polysplenia can occur in the same family [3]. The unifying term polyasplenia emphasizes the overlap and heterogeneity in this group of patients [3].

Plain films are known to be often inaccurate in determining true viscerosplenic situs [4]. In our series, plain films were misleading in 30% of cases (Fig. 5A). Bronchial anatomy is a much more reliable (although not infallible [4]) predictor of true viscerosplenic situs [4] (Fig. 5B). However, accurate categorization into tendency toward right or left isomerism depends on identifying splenic status. Although broad associations certainly exist within these categories, it should be emphasized that each patient will have a unique constellation of vascular and visceral derangements and must be evaluated individually.



Fig. 4.—Vascular anomalies in asplenia.

A, Transverse sonogram in patient with asplenia shows aorta (arrow) and vena cava (arrowhead) anterior to spine (S) on opposite sides of midline. Compare with Fig. 3D. k = kidney; L = liver.

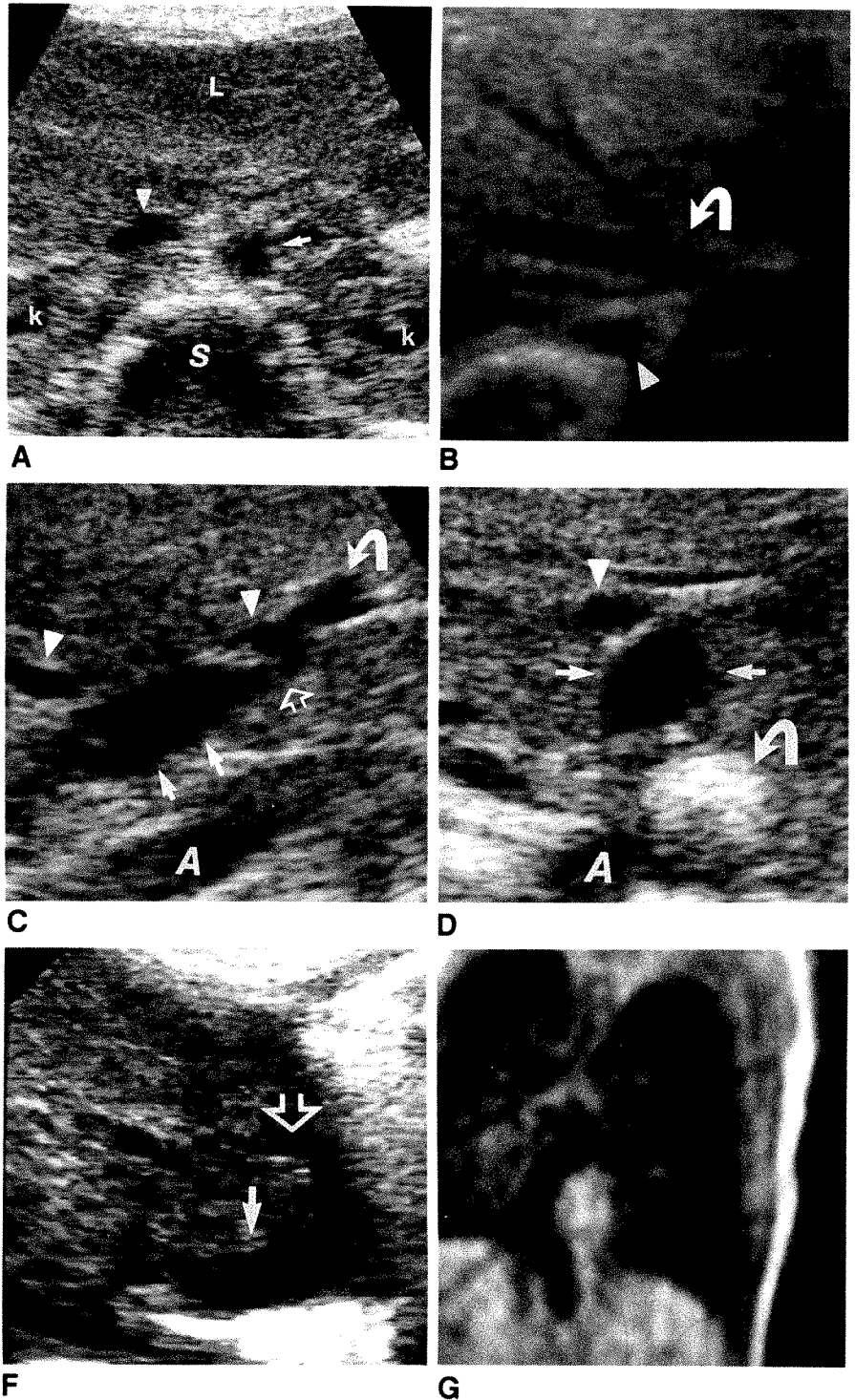
B, Transverse sonogram in another patient shows that hepatic veins (arrow) drain independently into atrium, bypassing inferior vena cava (arrowhead).

C, Sagittal sonogram of mid upper abdomen at level of esophageal hiatus in the same patient as in A shows total anomalous pulmonary venous connection to a hepatic vein. Anomalous vessel (straight arrows) is visualized draining into hepatic vein (arrowheads), which lies partially outside plane of section; note narrowed vascular caliber at point of junction (open arrow). Portal vein (curved arrow) is just caudad to connection. A = aorta.

D, Transverse sonogram in same patient shows anomalous vessel (straight arrows) and enlarged hepatic vein into which it drains (arrowhead). Note gastroesophageal junction (curved arrow). A = aorta.

E and F, Sequential longitudinal scans in another patient show total anomalous pulmonary venous connection to portal vein (open arrows). Anomalous, tortuous vessel (straight arrows) can be traced to its point of termination (open arrows). Note air in esophagus posterior to vessel.

G, Coronal MR image (SE 390/30, 8-mm section) of patient in A, C, and D. Pulmonary veins drain into anomalous vessel, which terminates below diaphragm. Exact vessel of termination, however, is difficult to demonstrate.



### Polyasplenia

Because splenic tissue originates in the dorsal mesentery of the stomach, splenuli are located in the retrogastric region. For this reason, careful scanning should be directed ipsilateral to the stomach. Because of the frequency of biliary atresia in

these patients, it is desirable to identify the gallbladder. In our patients it tended to lie in the midline or to lateralize with the main hepatic mass.

Identification of the vena cava and its location with respect to the aorta and midline can easily be made noninvasively. The finding of these two vessels on the same side of the

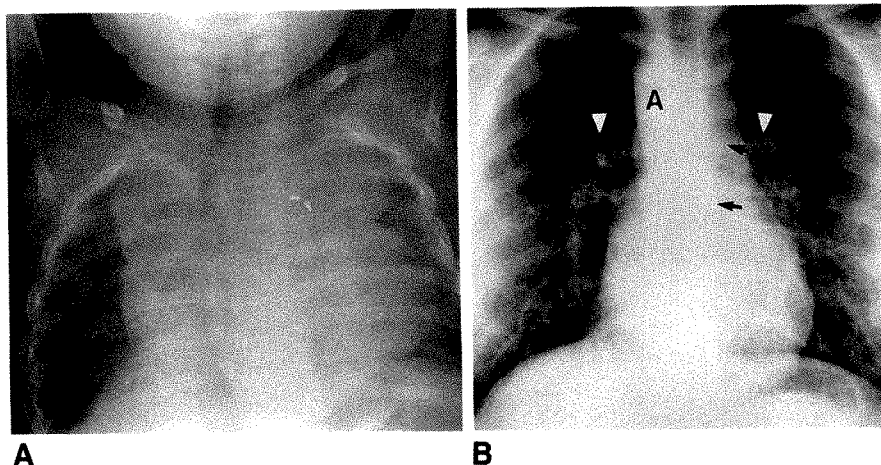


Fig. 5.—A, Chest film of infant with polysplenia illustrated in Figs. 1B and 1F. Plain film appearance might suggest situs solitus. Although there is a suggestion of symmetry, branching of bronchi cannot be reliably identified on this routine chest film.

B, Chest film of patient with polysplenia, who was first diagnosed at age 18 despite typical radiographic findings. Note left-sided, enlarged azygous/hemiazygous vein (arrows) and epi-bronchial, symmetric pulmonary arteries (arrowheads). A = right-sided aortic arch.

spine has been reported as diagnostic of asplenia [1]. However, in our series of patients with asplenia, the aorta and vena cava lay on opposite sides of the midline in one (Fig. 4A); among the five patients with polysplenia and an intact vena cava, it lay with the aorta on the same side of the midline in all five.

Moreover, in a prior series of patients with heterotaxia, the vena cava was noted to cross over anterior to the aorta in a piggyback fashion only in patients with asplenia and was considered characteristic of this condition [1]. However, among our five patients with polysplenia and an intact vena cava, it crossed the midline anterior to the aorta in piggyback fashion in order to enter the common atrium in three (Fig. 2C).

The difference in our findings is probably due to the number of patients with polysplenia in our series who had an intra-hepatic vena cava (50%). These observations indicate that, in either right- or left-sided isomerism, when the abdominal vena cava is present, it can be located on either side of the midline and that, when contralateral to its entrance into the common atrium, it will cross over anterior to the aorta in order to make the appropriate venous connection. In fact, this is a sign of deranged laterality of cava/cardiac anatomy and can be seen at both ends of the polyasplenic continuum.

The vitelline system also shows derangement of laterality. When the larger part of the left vitelline vein resorbs, the resultant anatomic relationship of the portal vein is preduodenal. Although one of our patients with asplenia had a preduodenal portal vein, this anatomy has a strong association with polysplenia and biliary atresia.

### *Situs Inversus*

Patients with situs inversus totalis are a distinct subgroup and should be clearly differentiated from those with partial situs inversus, or situs ambiguous. Most patients with situs inversus as defined herein are asymptomatic, but the prevalence of complex congenital heart disease in these patients

exceeds that in the general population [1]. One of our patients had complex cardiac anomalies resembling those seen in many patients with heterotaxy; the other had biliary atresia, a condition found in many patients with polysplenia.

### Summary

Patients suspected of having derangement of solitus asymmetry should be evaluated individually to determine abdominal visceral and vascular arrangement and to investigate associated problems. This evaluation should begin with plain films to assess cardiac and gastric positions and pulmonary vascularity. Assessment of the bronchial branching patterns should be attempted in all cases. Sonography will delineate the presence or absence of splenic tissue and the anatomy and relationships of the cava and the portal vein. When no spleen is found and the pulmonary vascularity appears congested, a subdiaphragmatic total anomalous pulmonary venous connection should be suspected and verified. If there are splenuli in the retrogastric area, particular attention should be paid to the status of the gallbladder, especially in children who do not have congenital heart disease. Selective spleen scans can confirm the presence of splenic tissue. The high cost and sedation requirement of MR would suggest that it be reserved for cases in which sonography is unable to answer the pertinent questions.

### REFERENCES

1. Tonkin IL, Tonkin AK. Visceroatrial situs abnormalities: sonographic and computed tomographic appearance. *AJR* 1982;138:509-515
2. Partidge J. The radiological evaluation of atrial situs. *Clin Radiol* 1979;30:95-103
3. Layton WM. Random determination of a developmental process. *J Hered* 1976;67:336-338
4. Opitz JM. Editorial comment on the paper by de la Monte and Hutchins on familial polyasplenia. *Am J Med Genet* 1985;21:175-176

## Case Report

### Bowel Obstruction in an Infant with AIDS

Carlos J. Sivit,<sup>1,2</sup> George A. Taylor,<sup>1-3</sup> Kathleen Patterson,<sup>2,4</sup> Raleigh Thompson,<sup>5</sup> and Shelby H. Josephs<sup>2,6</sup>

The gastrointestinal tract is the second most commonly affected site in children infected with human immunodeficiency virus (HIV) [1]. Although extensive, multifocal bowel involvement due to a variety of infectious agents is common, most cases respond to conservative medical management [2]. Conditions requiring surgical intervention are rare in the pediatric age group. We present a child with perinatally transmitted HIV infection and severe inflammatory bowel changes that resulted in small-bowel obstruction and required acute surgical intervention.

#### Case Report

An 8-month-old girl was admitted with a 2-day history of increasing respiratory distress, severe abdominal pain, and distension. Her medical history included perinatally transmitted HIV infection, complicated by an episode of cytomegalovirus (CMV) duodenitis 2 months before admission and recurrent episodes of abdominal distension. Abdominal examination revealed decreased bowel sounds and diffuse rebound tenderness to minimal palpation. Abdominal radiographs showed dilated proximal small-bowel loops with multiple air/fluid levels and absence of air in the distal small bowel and large bowel consistent with a small-bowel obstruction (Fig. 1A). An upper gastrointestinal series that used water-soluble contrast material revealed a complete midjejunal obstruction. In addition, jejunal folds were

irregularly thickened and adjacent bowel loops were separated, indicative of bowel wall edema (Fig. 1B). During surgery, diffuse small-bowel edema was confirmed, and multiple adhesive bands were noted between jejunal loops. Whitish, indurated plaques on the serosal surface were noted throughout the entire small bowel. Hydrops of the appendix due to occlusion by adhesions at its base also was present. During surgery, adhesions were lysed and the appendix was resected. Multiple foci of coagulation necrosis and numerous cells showing cytomegalic change were seen within the resected appendix (Fig. 1C). After surgery, the patient was treated with IV ganciclovir (Syntex) and central hyperalimentation. After an episode of upper gastrointestinal bleeding that resolved, the patient improved clinically and was transferred to another facility closer to home 1 month after the initial presentation.

#### Discussion

Although the gastrointestinal tract is the second most commonly affected site in pediatric patients who have HIV infection, specific bowel disorders are rarely life threatening. Most disorders are nonneoplastic. They include infections by a variety of opportunistic organisms, including *Candida albicans*, CMV, *Cryptosporidium*, *Mycobacterium avium intracellulare*, and *Isospora*, as well as more typical bacterial pathogens like *Salmonella* and *Shigella* [3, 4]. Clinical findings are

Received August 14, 1989; accepted after revision November 20, 1989.

<sup>1</sup> Department of Diagnostic Imaging and Radiology, Children's National Medical Center, and the George Washington University School of Medicine and Health Sciences, 111 Michigan Ave. N.W., Washington, DC 20010. Address reprint requests to C. J. Sivit.

<sup>2</sup> Department of Pediatrics, Children's National Medical Center, and the George Washington University School of Medicine and Health Sciences, 111 Michigan Ave. N.W., Washington, DC 20010.

<sup>3</sup> Present address: Department of Radiology, The Johns Hopkins Hospital, 600 N. Wolfe St., Baltimore, MD 21205.

<sup>4</sup> Department of Pathology, Children's National Medical Center, and the George Washington University School of Medicine and Health Sciences, 111 Michigan Ave. N.W., Washington, DC 20010.

<sup>5</sup> Department of Surgery, Children's National Medical Center, and the George Washington University School of Medicine and Health Sciences, 111 Michigan Ave. N.W., Washington, DC 20010.

<sup>6</sup> Department of Allergy and Immunology, Children's National Medical Center, and the George Washington University School of Medicine and Health Sciences, 111 Michigan Ave. N.W., Washington, DC 20010.

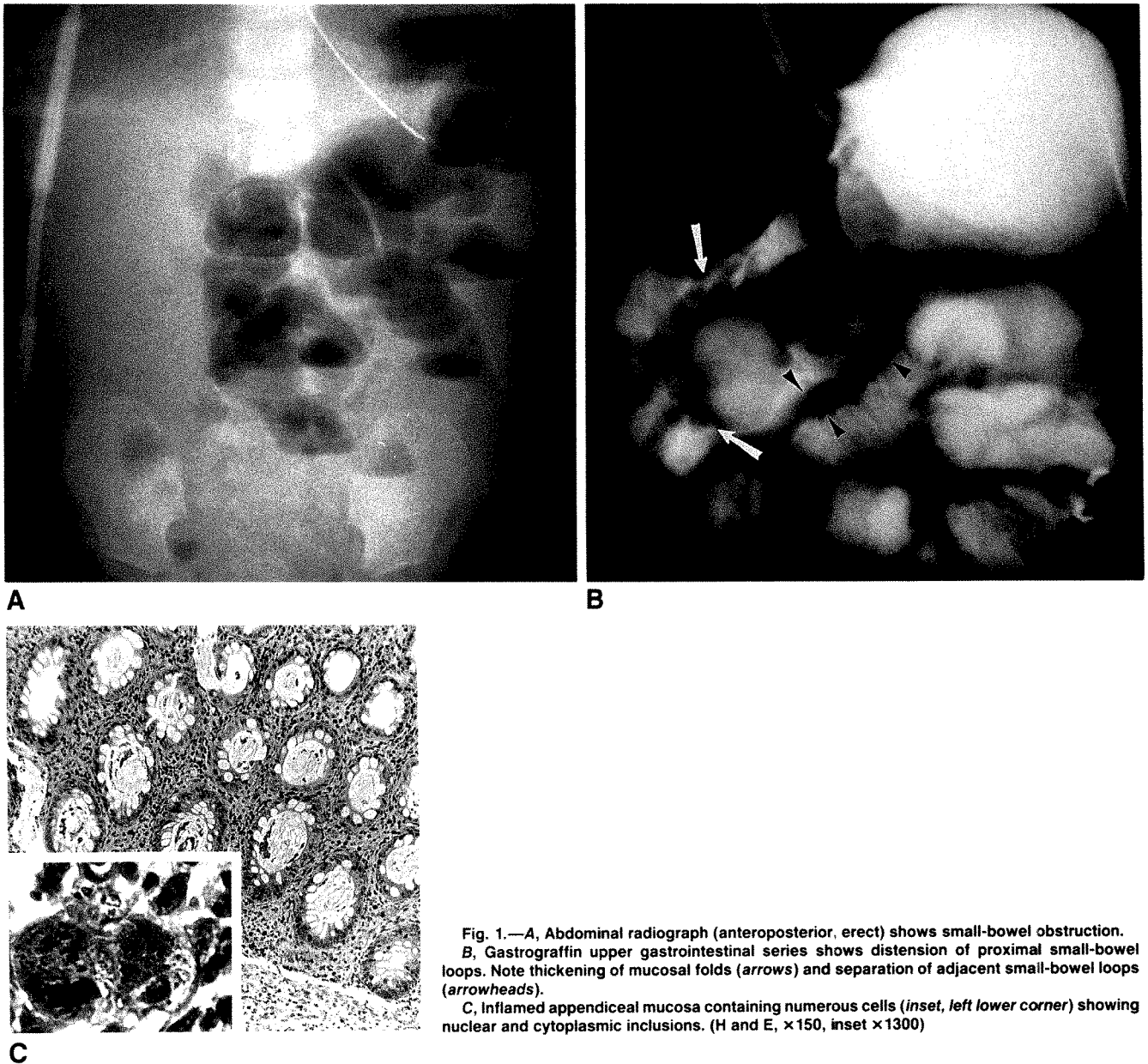


Fig. 1.—A, Abdominal radiograph (anteroposterior, erect) shows small-bowel obstruction. B, Gastrografin upper gastrointestinal series shows distension of proximal small-bowel loops. Note thickening of mucosal folds (arrows) and separation of adjacent small-bowel loops (arrowheads). C, Inflamed appendiceal mucosa containing numerous cells (inset, left lower corner) showing nuclear and cytoplasmic inclusions. (H and E,  $\times 150$ , inset  $\times 1300$ )

usually subacute, chronic, or recurrent and include oral candidiasis, dysphagia, watery diarrhea, mild abdominal distension, malabsorption, and failure to thrive [3, 5]. Radiologic abnormalities are characterized by their multifocal nature, often involving large segments of the gastrointestinal tract and revealing nonspecific signs of mucosal edema and inflammation [4]. These include fold thickening, mucosal irregularity, separation of bowel loops, and focal dilatation or narrowing [4, 6]. More severe gastrointestinal tract symptoms include upper and lower gastrointestinal hemorrhage and severe abdominal distension [1, 5, 7]. Toxic megacolon also has been reported [4]. Radiographic findings in patients with more severe bowel disease include deep erosions, ulcerations, and fistula formation [4, 7].

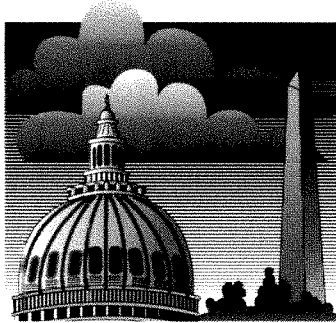
Despite the chronic nature and multifocal pattern of gastrointestinal tract involvement of many infections in these patients, surgical emergencies involving the bowel are rare. Small-bowel obstruction due to severe widespread bowel wall thickening has been reported in an adult patient infected with CMV [8]. Our case can be attributed to CMV enterocolitis resulting in severe, multifocal small-bowel inflammation and adhesion formation.

Recognition of the potential for catastrophic bowel complications is essential to ensure prompt surgical intervention. This bowel obstruction was relieved by lysis of adhesions and no bowel resection was required. These children often have multisystem problems, and attention is often focused primarily on the respiratory tract, which is the most frequently involved

organ system. In addition, chronic or recurrent gastrointestinal symptoms are frequently present, making the recognition of serious gastrointestinal complications difficult. Although bowel conditions requiring acute surgical intervention are rare in these children, we can expect to see more cases as the number of HIV-infected children continues to increase rapidly.

#### REFERENCES

1. Bradford BF, Abdenour GE, Frank JL, Scott GB, Beerman R. Usual and unusual radiologic manifestations of AIDS and HIV infection in children. *Radiol Clin North Am* **1988**;26:341-353
2. Smith PD, Lane C, Gill VJ, et al. Intestinal infections in patients with the acquired immunodeficiency syndrome (AIDS). *Ann Intern Med* **1988**; 108:328-333
3. Frager DH, Frager JD, Brandt LJ, et al. Gastrointestinal complications of AIDS: radiologic complications. *Radiology* **1986**;158:597-603
4. Megibow AJ, Balthazar EJ, Hulinick DH. Radiology of nonneoplastic gastrointestinal disorders in acquired immune deficiency syndrome. *Semin Roentgenol* **1987**;22:31-41
5. Amodio JB, Abramson S, Berdon WE, Levy J. Pediatric AIDS. *Semin Roentgenol* **1987**;22:66-76
6. Wall SD, Ominsky S, Altman DF, et al. Multifocal abnormalities of the gastrointestinal tract in AIDS. *AJR* **1986**;146:1-5
7. McLoughlin LC, Nord KS, Joshi VV, Oleske JM, Connor EM. Severe gastrointestinal involvement in children with acquired immunodeficiency syndrome. *J Pediatr Gastroenterol Nutr* **1987**;6:517-524
8. Frank D, Raicht RF. Intestinal perforation with CMV infection in patients with acquired immune deficiency syndrome. *Am J Gastroenterol* **1984**; 79:201-205



Scientific Program (200 papers)  
Instructional Courses (60 hours)

Categorical Course on  
Cardiovascular Imaging

The Caldwell Lecture

Award Papers

Scientific Exhibits

Social, Golf, and Tennis Programs

Guest Programs



Come to the  
American Roentgen Ray Society

90<sup>th</sup>

ANNUAL MEETING

Washington, D. C.

Sheraton Washington Hotel  
May 13-18, 1990

## Cervical and Basicranial Diastematomyelia

Thomas E. Herman<sup>1</sup> and Marilyn J. Siegel

The term diastematomyelia was introduced in 1837 by Ollivier to describe a spinal cord split in two dorsoventrally [1]. A fibrous or bony septum is usually present between the cord segments.

Diastematomyelia is most frequent in the thoracolumbar spine, but rarely it may affect the cervical spine. To our knowledge, basicranial diastematomyelia has not been described previously. We present a case of cervical and basicranial diastematomyelia and discuss the possible embryology of basicranial diastematomyelia.

### Case Report

A 3.3-kg female neonate born at 39 weeks gestation to a 28-year-old gravida 2, para 1 mother was admitted to Children's Hospital. Antenatal sonography had shown polyhydramnios and a cerebral intrahemispheric cyst. The child made no respiratory effort in the delivery room and intubation was difficult because of short neck, cleft palate, and glossoptosis. Neurologic examination showed global central nervous system dysfunction including brainstem abnormalities manifested as apnea. A coloboma was present in the optic nerve. Lateral plain films of the neck showed obvious dysplasia of the cervical spine with a bony density overlying the cervical posterior elements (Fig. 1A). A sonogram showed partial agenesis of the corpus callosum and a possible Dandy-Walker cyst. An echogenic ridge across the foramen magnum was initially interpreted as cerebellar dysplasia. A CT scan showed agenesis of the posterior portion of the corpus callosum and a long fluid-filled structure extending in the midline from the posterior fontanelle superiorly, through the fontanelle, to the inferior margins of the occipital lobes (Fig. 1B). An irregular bony septum arose from the posterior margin of the occiput, dividing

the brainstem and cerebellum into right and left portions (Figs. 1C and 1D). This bony septum continued into the cervical spine, splitting the cord into two segments (Fig. 1E). The postnatal course was complicated by primary pulmonary hypertension. Ventilation could not be maintained and the child died on the 14th day of life.

Autopsy revealed a 4-cm-diameter occipital meningocele extending from the occipital lobes inferiorly to the dermis over the posterior fontanelle superiorly. The meningocele communicated with the left cerebral subarachnoid space. Partial agenesis of the posterior half of the corpus callosum also was present.

In addition, the posterior fossa was markedly abnormal. Both cerebral peduncles and the pons were malformed, with posterior and superior displacement and separation above a midline bony septum. The right and left cerebellar lobes were hypoplastic and separated by the midline bony septum, and the vermis was absent, with hypoplastic cerebellar tonsils bilaterally. The cerebellar lobes communicated with the brainstem and pons by malformed superior peduncles. In the cervical spine, separate right and left cords were shown entering the neck through separate foramina magna. The cord segments united in the upper thoracic region. The cord and spine were normal caudal to this point. No other central nervous system anomalies were found.

### Discussion

Diastematomyelia is most frequent in the thoracolumbar spine. In a review of 112 patients with diastematomyelia by Keim and Green [2], 48% of the lesions were located in the lumbar spine. The remainder were in the thoracic spine. The majority of lesions had concurrent bony spurs or fibrous septums. Associated bony anomalies include block vertebral bodies, hemivertebrae, spina bifida, and laminar dysplasia.

Received September 11, 1989; accepted after revision November 21, 1989.

<sup>1</sup> Both authors: The Mallinckrodt Institute of Radiology, Washington University School of Medicine, 510 S. Kingshighway Blvd., St. Louis, MO 63110. Address reprint requests to T. E. Herman.

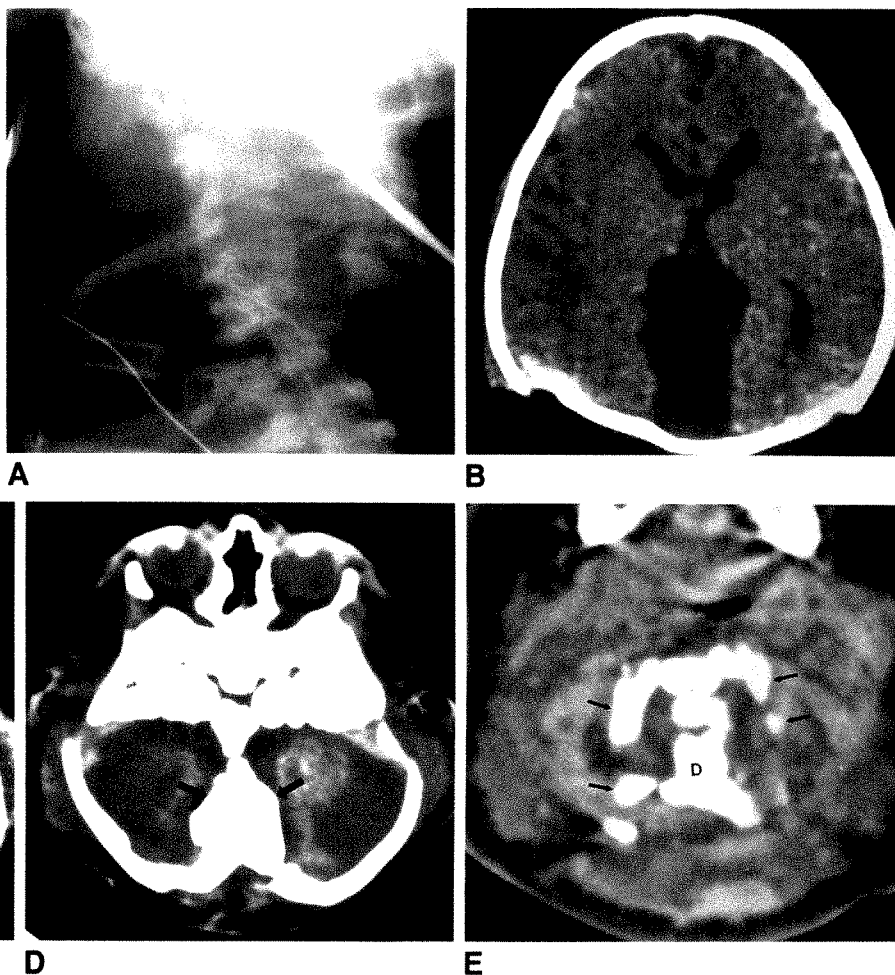


Fig. 1.—A, On lateral cervical spine film, posterior elements are dysplastic, elongated, and densely ossified.

B, Axial CT scan shows a cyst posteriorly that extends through posterior fontanelle to interhemispheric fissure.

C and D, Cranial CT scans through posterior fossa show a dense bony ridge (arrows) arising from torcular region that divides posterior fossa into two compartments.

E, CT scan of cervical spine shows an ossified diastematomyelia (D). Lamina and posterior elements (arrows) are dysplastic.



Cutaneous abnormalities included hypertrichosis, skin dimpling, and lipomas.

Diastematomyelia in the cervical spine has been reported rarely [3, 4], but may occur more frequently than a review of the literature would suggest. Cervical diastematomyelia has been described in 6% of patients with Arnold-Chiari malformation [5]. In addition, cervical diastematomyelia has been reported in patients who have Klippel-Feil syndrome and synkinesis (abnormal copying of voluntary motion initiated by one extremity in the other extremity). Synkinesis may be very frequent in Klippel-Feil syndrome. Therefore some authors have suggested cervical cord imaging of patients with Klippel-Feil syndrome and synkinesis, to exclude cervical diastematomyelia [6]. Cervical diastematomyelia also has been described in patients without underlying abnormality. These patients typically present in the second or third decade of life with neurologic symptoms. Many of these patients have vertebral anomalies [7].

The etiology of diastematomyelia is uncertain. Any theory of its etiology must be able to account for the frequent cutaneous and osseous involvement and in our case for the involvement of the basicranium. The CNS begins its formation at the third week of gestation with the elevation and eventual fusion of paired neural folds. These neural folds consist of

surface epithelium, neuroectoderm, neural crest, and paraaxial mesoderm. The neuroectoderm will give rise to neuroblasts; the paraaxial mesoderm to vertebral bodies, skull, and meninges; the surface epithelium to dermis; and the neural crest to sympathetic and dorsal root ganglia [8]. The normal closure and development of the neural folds embryologically is a complex phenomenon that requires the synchronous development of all elements of the neural fold. The most popular theories of malformation implicate the neuroectoderm (primitive neuroepithelium) or the mesodermal component (mesenchyme of the neural folds) [9, 10]. Proponents of the neuroectodermal theory believe that the death of neuroectodermal cells in the neural folds prevents normal closure of the neural folds.

The alternative theory is that the primary abnormality lies within the paraaxial mesoderm [11, 12]. The effect of this insufficiency is inadequate internal support of the developing neural folds, leading to defective closure. The basiocciput as well as the entire spine down to the coccyx arises from the neural folds, as reported by Marin-Padilla and Marin-Padilla [13]. Because the abnormality in paraaxial mesoderm can occur at any level of neural-fold development, cranial as well as spinal skeletal abnormalities can occur. In our patient, this includes the occipital meningocele, bony septum, and cervical

spine dysplasia. Partial agenesis of the corpus callosum might be unrelated etiologically to the cervical and basicranial diastematomyelia. However, agenesis of the corpus callosum is a common anomaly and is often associated with posterior fossa anomalies [14].

Regardless of etiology, basicranial and cervical diastematomyelia in our patient was difficult to diagnose. Intrauterine or postnatal sonography failed to show the most important features of this anomaly in the posterior fossa. CT showed this complex posterior fossa anatomy adequately. Our case expands the definition of diastematomyelia to include a complex malformation of the basicranium with splitting of the cerebellum and rostral brainstem in two with a bony septum.

## REFERENCES

1. Ohwada T, Okada K, Haruki H. Thoracic myelopathy caused by cervico-thoracic diastematomyelia. *J Bone Joint Surg [Am]* **1989**;71-A:296-299
2. Keim HR, Greene AF. Diastematomyelia and scoliosis. *J Bone Joint Surg [Am]* **1973**;55-A:1425-1435
3. Anand AK, Kuchner E, James R. Cervical diastematomyelia: uncommon presentation of a rare disorder. *Comput Radiol* **1985**;9:45-49
4. Simpson EK, Rose JE. Cervical diastematomyelia: report of a case and review of a rare anomaly. *Arch Neurol* **1987**;44:331-335
5. Naidich TP, McLone DG, Fulling KN. The Chiari II malformation. Part IV. The hindbrain deformity. *Neuroradiology* **1983**;25:179-197
6. Gunderson CH, Solitare GB. Mirror movements in patients with the Klippel-Feil syndrome. *Arch Neurol* **1968**;18:675-679
7. Kuchner EF, Anand AK, Kaufman BM. Cervical diastematomyelia: a case report with operative management. *Neurosurgery* **1985**;16:538-542
8. Sadler TW. *Langman's medical embryology*, 5th ed. Baltimore, MD: Williams and Wilkins, **1985**
9. Gordon R. A review of theories of vertebrate neurulation and their relationship to the mechanics of neural tube birth defects. *J Embryol Exp Morph* **1985**;89[suppl]:229-255
10. Carpenter SJ. Developmental analysis of cephalic axial dysraphic disorders in arsenic-treated hamster embryos. *Anat Embryol* **1987**;176:345-365
11. Marin-Padilla M. Notochordal-basichondrocranial relationships: abnormalities in experimental axial skeletal dysraphic disorders. *J Embryol Exp Morphol* **1979**;53:15-38
12. Marin-Padilla M. Morphogenesis of experimentally induced Arnold-Chiari malformation. *J Neurol Sci* **1981**;50:29-55
13. Marin-Padilla M, Marin-Padilla TM. Developmental abnormalities of the occipital bone in human chondrodystrophies. *Birth Defects* **1977**;13:7-23
14. Barkovich AJ, Norman D. Anomalies of the corpus callosum: correlation with further anomalies of the brain. *AJR* **1988**;151:171-179

# Gd-DTPA-Enhanced MR Imaging of the Brain in Patients with Meningitis: Comparison with CT

Kee Hyun Chang<sup>1</sup>  
Moon Hee Han<sup>1</sup>  
Jae Kyu Roh<sup>2</sup>  
In One Kim<sup>1</sup>  
Man Chung Han<sup>1</sup>  
Chu-Wan Kim<sup>1</sup>

Plain and Gd-DTPA-enhanced MR images of the brain were obtained in 18 consecutive patients with meningitis (eight with tuberculous, five with bacterial, three with viral, and two with fungal infections); the MR images were compared with CT scans. MR images were obtained on a 2.0-T superconducting unit with both T1- and T2-weighted pulse sequences before injection and with a T1-weighted sequence after injection of Gd-DTPA (0.1 mmol/kg) in all patients. In tuberculous meningitis, MR imaging depicted ischemia/infarct, hemorrhagic infarct of basal ganglia, meningeal enhancement at either basal cistern or convexity surface of brain, and associated small granulomas in a few more patients than CT did. In bacterial meningitis, primary foci of extracranial inflammation (i.e., mastoid, paranasal sinuses) and adjacent intracranial lesions including localized dural inflammation, subdural fluid collection, and/or brain parenchymal lesions were demonstrated much better on MR than on CT. Otherwise, MR images generally matched the CT scan. Although the plain MR images, both T1- and T2-weighted, were the most sensitive in delineating ischemia/infarct, hemorrhage, and edema, they were not as specific as Gd-DTPA-enhanced T1-weighted images and postcontrast CT scans in defining the active inflammatory process of the meninges and focal lesions precisely.

We conclude that if Gd-DTPA is used, MR imaging appears to be superior to CT in the evaluation of patients with suspected meningitis. Precontrast MR is needed to delineate ischemia/infarct, edema, and subacute hemorrhage.

*AJNR* 11:69-76, January/February 1990; *AJR* 154:809-816, April 1990

CT has been used effectively to evaluate the presence or absence of associated inflammatory mass, infarct, and hydrocephalus and the status of an abnormal blood-brain barrier (BBB) in leptomeningeal inflammation [1-4]. In little more than a decade after the introduction of CT, MR imaging has become a valuable clinical tool that has proved to be superior to CT in evaluating many intracranial diseases [5-10]. However, the specific role of MR imaging has not yet been defined in leptomeningitis, even though the MR appearance of intracranial infectious diseases has been described in the literature [8, 10-17]. The purposes of this study were to evaluate the role of MR imaging, to assess the value of Gd-DTPA enhancement, and to discover the special advantages, if any, of MR over CT in the evaluation of meningitis.

## Materials and Methods

Eighteen consecutive patients with meningitis (eight tuberculous, five bacterial, two fungal, and three viral) were examined with MR before and after IV injection of Gd-DTPA (Shering AG, Berlin, W. Germany). The 11 male and seven female patients were 12-65 years old. Fully informed consent was obtained in each case. Microbiological confirmation of the diagnosis was available in six patients (three tuberculous, one bacterial, and two cryptococcal meningitis). In the microbiologically unproved cases the diagnosis was established on the basis of other criteria: In five cases of tuberculous meningitis it was based on the CSF profile, coexisting tuberculous infection in another organ, family history of tuberculosis, and the

Received February 3, 1989; revision requested April 5, 1989; revision received May 23, 1989; accepted July 12, 1989.

This work was supported in part by a grant from the special research fund of Seoul National University Hospital (1989).

<sup>1</sup> Department of Diagnostic Radiology, College of Medicine, Seoul National University, Seoul National University Hospital, 28, Yeongun-Dong, Chongro-Ku, Seoul 110-744, Korea. Address reprint requests to K. H. Chang.

<sup>2</sup> Department of Neurology, College of Medicine, Seoul National University, Seoul 110-744, Korea.

0361-803X/90/1544-0809

© American Roentgen Ray Society

response to antituberculous regimens during the illness. In four patients with meningitis of bacterial origin, the diagnosis was based on the CSF profile, the response to the antibiotics, and the course of the illness. In the three cases of viral meningitis the diagnosis was based on the CSF profile and the short course of the illness without any specific treatment.

MR imaging was performed with a superconducting unit (Spectro-20000, Goldstar, Seoul, Korea) operating at 2.0 T. With a head coil (diameter, 30 cm), all images were produced by using multislice, multiecho spin-echo (SE) pulse sequences and a two-dimensional Fourier transform image reconstruction technique. All patients had precontrast T1-weighted images, 500–600/30/2–4 (TR/TE/excitations); intermediate-weighted images, 3000/30/1; and T2-weighted images, 3000/80/1. After IV injection of Gd-DTPA (0.1 mmol/kg body weight), all patients were studied with T1-weighted images only; however, in an earlier period of the study five patients had intermediate- and T2-weighted images also. The section thickness/gap was 8 mm/2 mm in T1-weighted imaging and 5 mm/1 mm in T2-weighted imaging. As a rule, we chose an axial imaging plane corresponding to that of the CT examination. The images were acquired on a 256 × 256 matrix with spatial resolution of 1 × 1 mm.

Pre- and postcontrast CT scans were obtained 1–13 days before the MR study in all patients. Either a GE CT/T 8800 or 9800 or equivalent third-generation unit was used.

A retrospective comparison was done between MR and CT findings with attention to identification of abnormal meningeal enhancement; parenchymal signal abnormalities including ischemia/infarct, hemorrhage, granuloma, and abscess; hydrocephalus; periventricular edema; and other associated findings. When parenchymal lesions of high signal intensity on T2-weighted images and of iso- or hypointensity on T1-weighted images were observed in the basal ganglia, thalamus, brainstem, or a major vascular territory, they were designated as ischemia/infarct.

## Results

Of eight patients with tuberculous meningitis, cisternal obliteration and abnormal enhancement were identified in six patients on MR (Figs. 1–3) and in five on CT. In one patient in whom a disparity was seen between CT and MR, CT could not differentiate between normal and abnormal cisternal enhancement. The most common site of enhancement was the suprasellar cistern; next were the ambient cistern and sylvian fissure. Curvilinear meningeal enhancement along the convexity surface of the brain was noticed in one patient on MR only (Fig. 2). Associated granulomas ranging from 2 to 10 mm

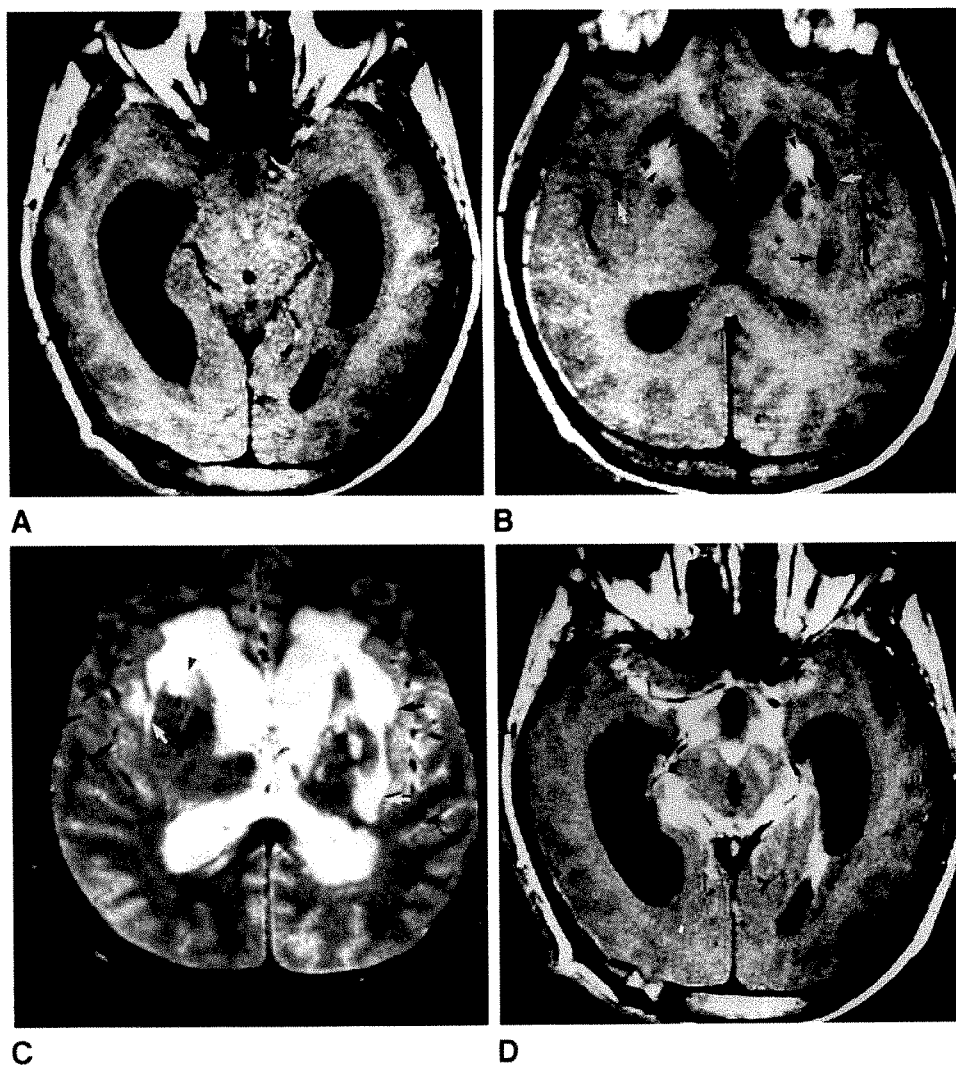


Fig. 1.—Case 1: Tuberculous meningitis.

A and B, Precontrast SE 500/30 images show obliteration of basal cisterns, hydrocephalus, and ischemia/infarct (arrows) with hemorrhagic foci (arrowheads) in basal ganglia bilaterally.

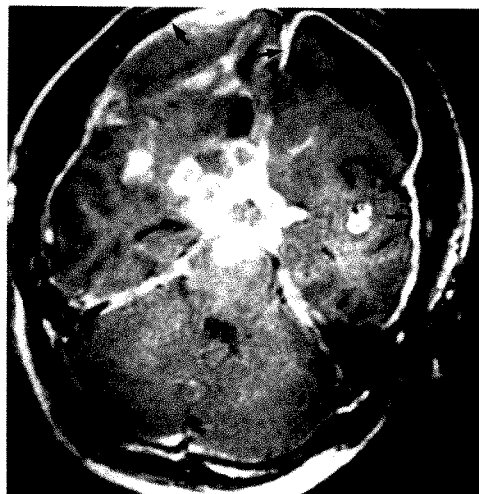
C, Precontrast SE 3000/80 image shows multiple areas of high signal intensity mainly representing edema and ischemia/infarct (arrows) with hemorrhagic foci (arrowheads) in basal ganglia, external capsules, and periventricular white matter bilaterally. Lesions appear to be much more extensive on 3000/80 image than on 500/30 images. Bilateral low signal intensities at globus pallidus seen on B and C represent calcifications, which were verified on CT (not shown).

D, GD-DTPA-enhanced SE 500/30 image reveals extensive contrast enhancement in suprasellar and perimesencephalic cisterns and left ventricular wall.

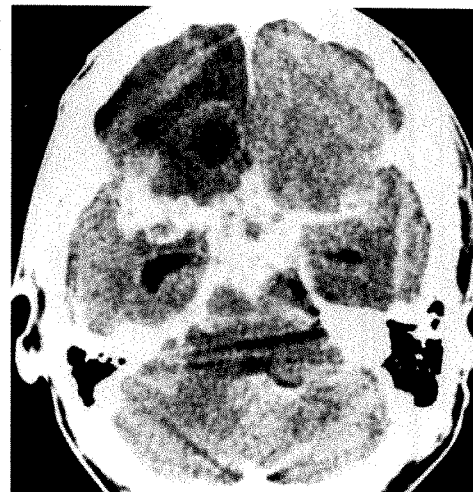
Fig. 2.—Case 7: Tuberculous meningitis.

A, Gd-DTPA-enhanced SE 600/30 image shows multiple ring-enhancing granulomas in suprasellar and sylvian cisterns and curvilinear meningeal enhancement along convexity surface of brain (arrows).

B, Meningeal enhancement at convexity surface is hardly detectable on postcontrast CT scan obtained 13 days before MR. Lentiform subdural fluid collection in right frontal convexity was caused by ventriculoperitoneal shunt procedure.



A

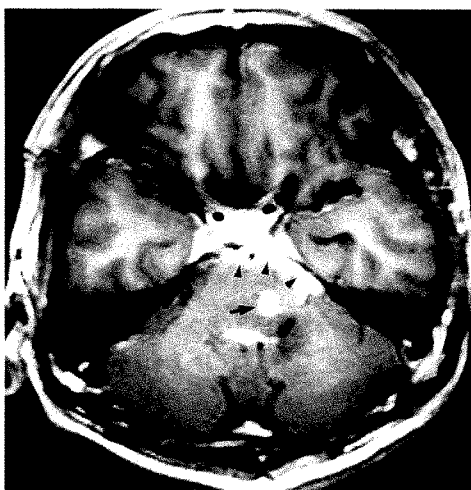


B

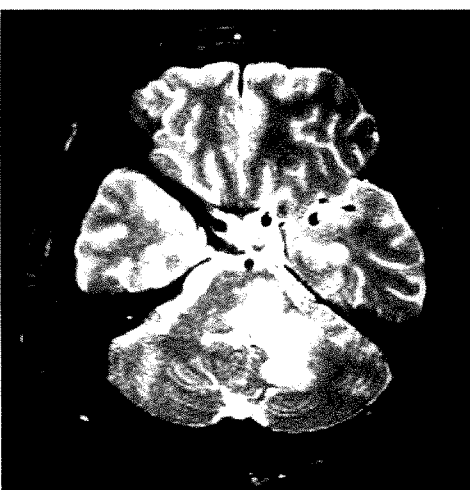
Fig. 3.—Case 3: Tuberculous meningitis.

A, Gd-DTPA-enhanced SE 500/30 image shows round, enhancing nodule (tuberculoma, arrow) in left side of pons and cisternal enhancement in prepontine and left cerebellopontine angle cisterns (arrowheads), as well as in suprasellar cistern.

B, Gd-DTPA-enhanced SE 3000/80 image shows more extensive area of high signal intensity in pons and left side of cerebellum representing edema. Tuberculoma is not separated from surrounding edema. Lesion appears to be same as that seen on precontrast SE 3000/80 image (not shown).



A



B

were readily identified in four patients on MR (Figs. 2 and 3), but in only three on CT. The granulomas usually were multiple, nodular or ring-shaped, and located at the basal cisterns and cortical areas of the brain. Some tiny nodules were seen only on MR. These enhancing lesions were demonstrated only on postcontrast T1-weighted images, and not on precontrast T1- and T2-weighted images. On postcontrast T2-weighted images, obtained in five selected patients, the enhancing granulomas were indistinguishable from surrounding edema (Fig. 3). Focal parenchymal signal abnormalities suggesting ischemia/infarct were identified in five patients on MR (Fig. 1) and in four on CT. These abnormalities were seen most often at the basal ganglia, and, less often, at the thalamus, midbrain, and deep periventricular white matter also. The precontrast T2-weighted image was the most sensitive in detecting these lesions. The hemorrhagic foci of high signal intensity on both precontrast T1- and T2-weighted images were demonstrated at the basal ganglia in two patients on MR (Fig. 1B), but in none on CT.

The five patients with bacterial meningitis included three with otogenous meningitis. In all three, MR showed abnormal signal intensity in the mastoid areas and localized contrast enhancement at the thickened tentorium along the ipsilateral petrous bone (Fig. 4). In one case of rhinogenous meningitis MR clearly demonstrated inflammation of the paranasal sinuses and adjacent thickened dural enhancement in association with subdural fluid collections. In addition, there were multiple areas of abnormal signal intensity suggesting ischemic infarction in the gyrus rectus bilaterally and in the right middle cerebral artery territory with gyral swelling (Fig. 5). These findings were demonstrated weakly or less clearly on CT. Abscesses observed in two patients (one in the cerebellum and the other in the deep parietal lobe) appeared as smooth, thick-walled rings of slightly high signal intensity with strong ring enhancement on the T1-weighted images, just like the CT appearance.

In the three patients with viral meningitis MR and CT findings were normal except for hydrocephalus in one patient.

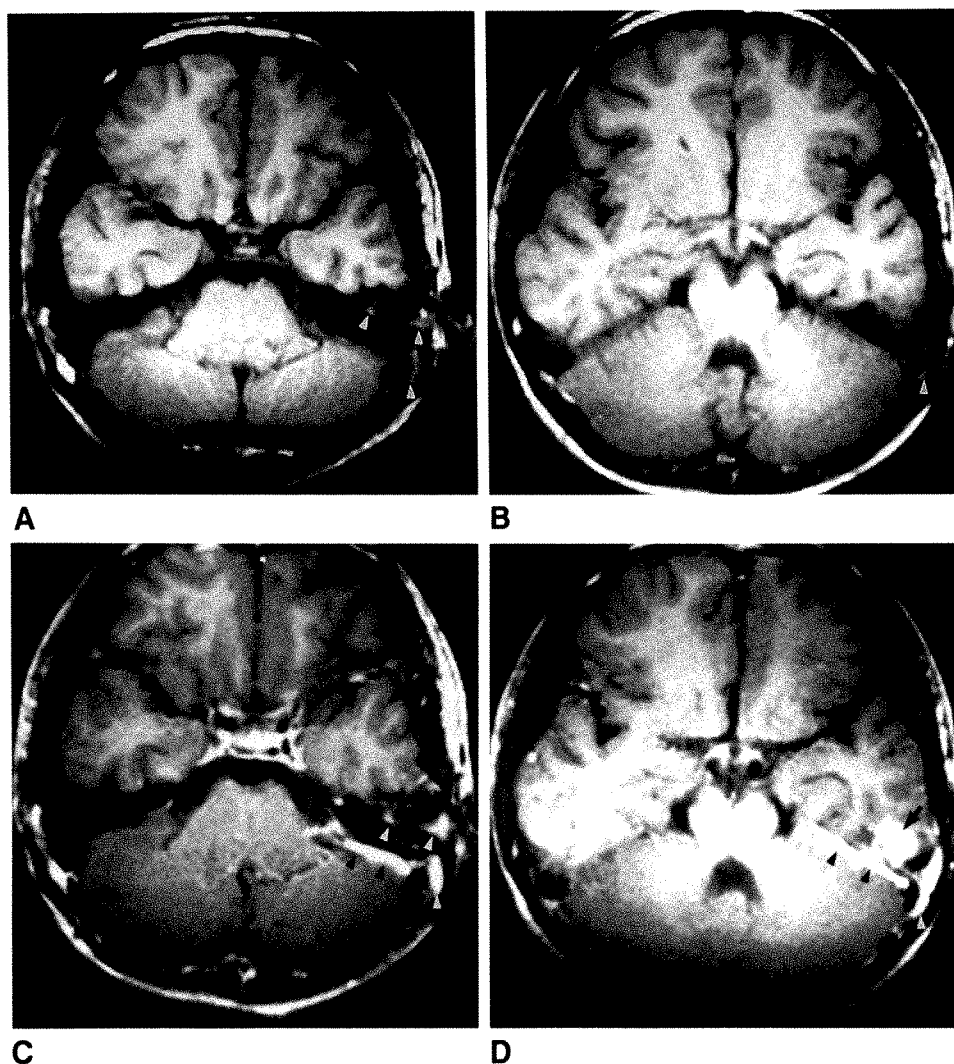


Fig. 4.—Case 10: Otogenous bacterial meningitis.

A and B, Precontrast SE 500/30 images. Variable degree of high signal intensity in left mastoid area represents mastoiditis (arrowheads).

C and D, Gd-DTPA-enhanced SE 500/30 images show linear enhancement along tentorium adjacent to petrous bone (black arrowheads) and nodular enhancement just above petrous bone suggesting inflammatory mass (arrow), in addition to enhancement in area of mastoiditis (white arrowheads).

Two patients had cryptococcal meningitis. Abnormal MR and CT findings in the basal ganglia in one suggested ischemic infarct. In the other patient normal MR and CT findings were seen during the convalescent period.

Hydrocephalus of varying degrees was identified equally well in 12 patients (six with tuberculous, four with bacterial, one with viral, one with cryptococcal meningitis) on both MR and CT. Periventricular edema was demonstrated clearly in seven of the 12 patients on T2-weighted images but in only five on both T1-weighted images and CT scans.

Associated findings included a subdural fluid collection complicated by a ventriculoperitoneal shunt procedure and interstitial edema around focal lesions. These were demonstrated equally well on MR and CT.

The MR and CT features of all patients are summarized in Table 1.

## Discussion

A gross pathologic characteristic of tuberculous meningitis is a diffuse gray opacity in the leptomeninges owing to thick, gelatinous infiltrates around the base of the brain. Blood

vessels running through the involved CSF spaces may be affected by the inflammatory exudate with resulting thrombosis and brain infarct. Interference with reabsorption of CSF produces communicating hydrocephalus [8, 18]. On CT, tuberculous meningitis is seen as varying degrees of contrast enhancement in the basal cisterns, communicating hydrocephalus, ischemia/infarct in the basal ganglia, and coexisting tuberculomas [1, 3, 4, 19]. In our series, ischemia/infarct in the basal ganglia was identified slightly more often on MR than on CT; hemorrhage was detected on MR only. The higher detection rate of MR might be due to the intrinsic higher sensitivity of MR and/or to lesions that developed during the interval between CT and MR (7 days each in cases 1 and 6; 9 days in case 2). Forty-three percent of ischemic infarcts may be complicated by a secondary hemorrhage at sometime during their course [20]. Inflammatory vasculitis, which may occur in any type of meningitis, is especially likely to produce such hemorrhagic infarcts [9].

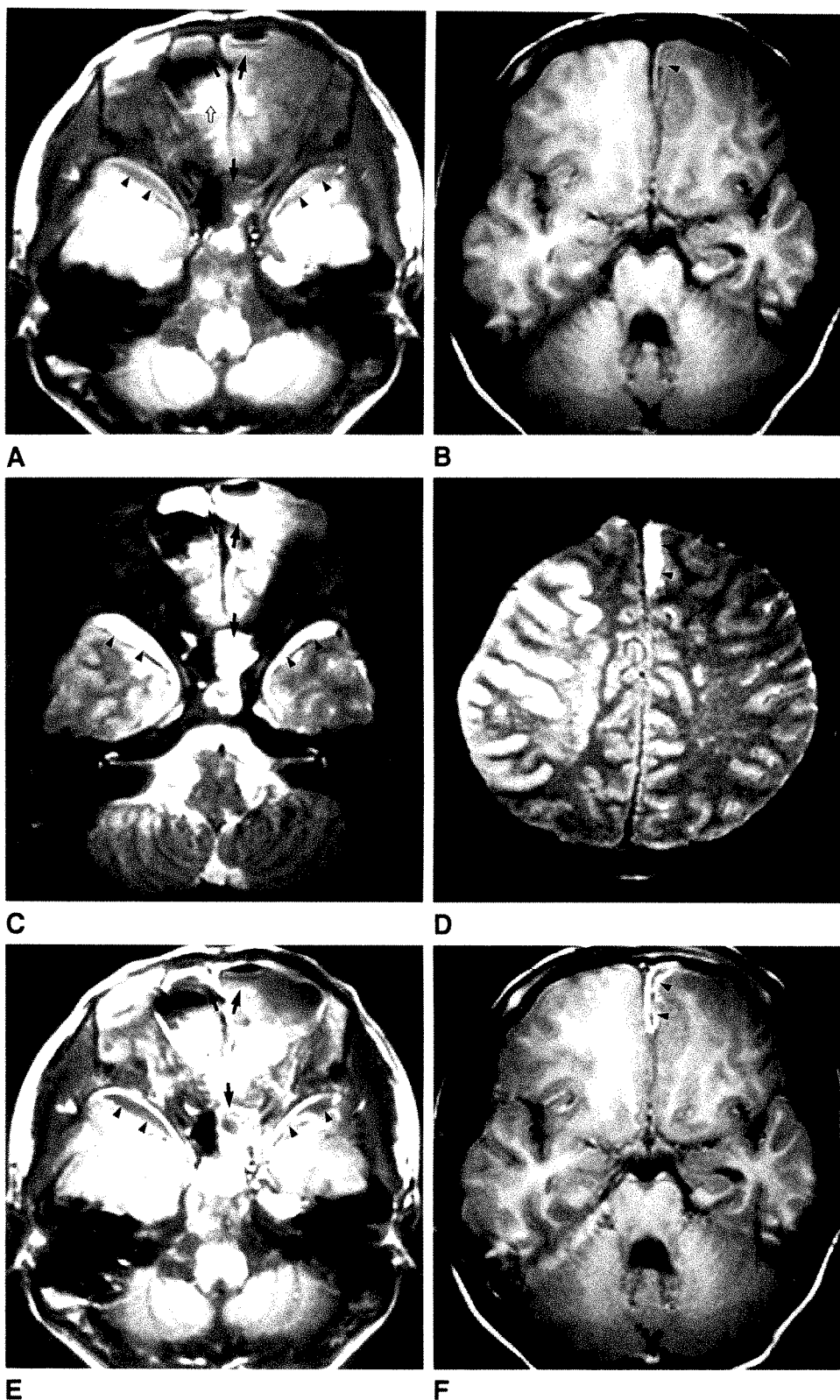
Gd-DTPA-enhanced T1-weighted images unambiguously characterize the pathologic lesions, showing the abnormal blood/brain barrier and/or vascularity; in general, this pattern is mimicked on postcontrast CT, but the MR contrast en-



Fig. 5.—Case 9: Rhinogenous bacterial meningitis.

A and D, Precontrast SE 500/30 (A and B) and 3000/80 (C and D) images show inflammation of paranasal sinuses (solid arrows) and subdural fluid collections (arrowheads) in anterior temporal area bilaterally and in anterior interhemispheric fissure on left, associated with adjacent dural thickening. Localized high intensity in right paramidline frontal area (open arrow) on A presumably is due to artifacts from field inhomogeneity. Precontrast SE 3000/80 image (D) also shows edematous swelling of right frontoparietal gyri corresponding to middle cerebral artery territory, probably caused by ischemia/infarct secondary to vascular compromise. Focal areas in left centrum semiovale also appear involved.

E and F, Gd-DTPA-enhanced SE 500/30 images. Thickened mucosae of paranasal sinuses (arrows) and thickened dura in area of subdural fluid collections (arrowheads) are densely enhanced. These abnormalities were not conspicuous on CT scans obtained 3 days before MR.



hancement is more intense and MR is more sensitive [21–26]. In our series, MR imaging easily differentiated basal cisternal enhancement from signal-void vessels at the circle of Willis in a patient with CT findings of equivocal enhance-

ment (case 2) and convexity meningeal enhancement from the inner table of the skull in another (case 7). Greater numbers of tuberculomas were seen on MR also. Better detection of these enhancing lesions by MR imaging might

TABLE 1: Summary of MR and CT Features in 18 Patients with Meningitis

Etiology/ Case No.	Age	Sex	CT-MR Interval (days)	MR/CT Findings (Location)						Associated Findings
				Meningeal Enhancement	Ischemia or Infarct	Hemorrhage	Granulomas	Hydrocephalus	Periventricular Edema	
Tuberculosis										
1	30	M	7	+/+ (SCC, SC, AC)	+/+ (BG, Th, Mb)	+/- (BG)	-/-	+/+	+/+	VP shunt ventriculitis
2	46	F	9	+/- (SSC)	+/- (BG)	-/-	-/-	+/+	+/+	-
3	29	M	6	+/+ (SSC, SC, AC, CPC)	-/-	-/-	+/+ (Po, Cbl, Th, In)	+/+	+/+	VP shunt
4	65	F	7	-/-	+/+ (BG)	-/-	+/+ (Hp, BG, FL, TL, OL)	+/+	+/+	-
5	24	F	5	+/+ (SSC)	-/-	-/-	-/-	+/+	-/-	-
6	41	M	7	+/+ (SC)	-/-	+/- (BG)	+/- (Po, TL)	+/+	+/+	-
7	39	F	13	+/+ (SSC, CM)	+/+ (BG)	-/-	+/+ (SSC, AC, CPC)	-/-	-/-	VP shunt
8	47	M	6	-/-	+/+ (BG, PW)	-/-	-/-	-/-	-/-	-
Bacterial										
9	14	M	3	+/- (CM, Fx, Te)	+/+ (FL, TL, PL)	-/-	-/-	+/+	-/-	PNS inflam- mation; SDF
10	21	M	5	+/+ (Te)	-/-	-/-	+/+ (TL)	-/-	-/-	Ear & mastoid inflammation
11	42	M	9	-/-	-/-	-/-	-/-	+/+	+/+	Cerebral ab- scess; ven- triculitis
12	21	M	2	+/+ (CPC, Te)	-/-	-/-	-/-	+/+	-/-	Ear & mastoid inflammation; cerebellar abscess
13	12	M	7	+/- (Te)	-/-	-/-	-/-	+/+	+/+	Ear & mastoid inflammation
Viral										
14	45	M	5	-/-	-/-	-/-	-/-	-/-	-/-	-
15	44	F	1	-/-	-/-	-/-	-/-	+/+	-/-	-
16	58	F	5	-/-	-/-	-/-	-/-	-/-	-/-	-
Cryptococcal										
17	50	M	4	-/-	+/+ (BG)	-/-	-/-	+/+	+/+	-
18	34	F	6	-/-	-/-	-/-	-/-	-/-	-/-	VP shunt

Note. —+ = present; ± = equivocal; — = absent; VP = ventriculoperitoneal; SSC = suprasellar cistern; SC = sylvian cistern; AC = ambient cistern; BG = basal ganglia; Th = thalamus; Mb = midbrain; CPC = cerebellopontine angle cistern; Po = pons; Cbl = cerebellum; In = insula; Hp = hypothalamus; FL = frontal lobe; TL = temporal lobe; OL = occipital lobe; CM = convexity meninges; PW = periventricular white matter; Fx = falx; Te = tentorium; PL = parietal lobe; PNS = paranasal sinuses; SDF = subdural fluid collection.

have been related to the progression of the disease process during the interval between CT and MR (9 days in case 2 and 13 days in case 7), but it seems more likely to have resulted from the intrinsic higher sensitivity of MR and Gd-DTPA.

Recently, Mathews et al. [27] reported an experimental study on Gd-DTPA-enhanced MR imaging in bacterial meningitis. They found that while precontrast MR was not helpful in identifying meningitis, Gd-DTPA-enhanced MR images were superior to postcontrast CT scans, not only in the detection of meningeal involvement but also in the identification of complications. MR is also superior in its ability to detect extracerebral fluid collections since it is free of bony artifacts adjacent to the inner table of the skull. Even small amounts of subdural fluid are visible as crescentic fluid collections along the surface of the brain [11]. While CT is often equivocal, MR may be able to differentiate between benign subdural effusions and infected subdural empyemas by virtue of the shortened T1 relaxation times of purulent fluid in comparison with CSF [28]. Subdural effusions are low-protein collections that, therefore, are isointense relative to CSF, while empyemas are more proteinaceous and have intensities different from that of CSF [14–16]. On T1-weighted images, empyemas are hyperintense relative to CSF, while subdural effusions are isointense relative to CSF [14]. We speculate that the subdural fluid collections seen in case 9 (Fig. 5) were empyemas rather than simple effusions because they were hyperintense relative to CSF and surrounded by a densely enhancing wall on T1-weighted images. However, this was not surgically verified. Localized enhancement of thickened dura adjacent to the inflamed paranasal sinuses or petrous bone on MR was considered to be characteristic of bacterial meningitis secondary to rhinogenous or otogenous infection. Gd-DTPA enhancement was not visible routinely in the dura, including the falx cerebri and tentorium. Kilgore et al. [29] reported that the falx cerebri and tentorium cerebelli are normally enhanced after Gd-DTPA administration in approximately half the patients. In six patients in our series, dural enhancement was normal: the dura was not thickened; it was enhanced in a short, linear fashion; there were no adjacent abnormal findings; and it was easily differentiated from pathological dural enhancement.

In summary, our results indicate that although precontrast T2-weighted images were the most sensitive in delineating ischemia/infarct and edema, they were not as specific as Gd-DTPA-enhanced T1-weighted images and postcontrast CT scans in defining the diffuse active inflammatory process of the meninges and focal lesions precisely. The precontrast T1-weighted image proved even more difficult to interpret. It not only failed to demonstrate the active inflammatory process of the meninges and the focal lesions but it also showed the ischemia/infarct and edema as a subtle low-intensity signal. However, precontrast T1-weighted imaging is necessary because it helps in the detection of subacute hemorrhage. Therefore, both precontrast T1- and T2-weighted imaging and Gd-DTPA-enhanced T1-weighted imaging are considered necessary in the evaluation of the patient with suspected meningitis. All the possible abnormalities—including pericranial lesions (paranasal sinusitis and otitis media), meningeal inflammation, hydrocephalus, ischemia/infarct, hemorrhage,

granuloma, abscess, and surrounding edema—can be identified more clearly on MR with the above sequences than on CT. The major role for Gd-DTPA in meningitis likely will be the identification of active blood/brain barrier disruption and increased vascularity, possibly facilitating the detection of the disease process at an early stage when it may not be detected on CT. Thus, if Gd-DTPA is used, MR appears to be superior to CT in the evaluation of leptomeningitis.

## REFERENCES

- Enzmann DR, Norman D, Mani J, Newton TH. Computed tomography of granulomatous basal arachnoiditis. *Radiology* 1976;120:341–344
- Zimmerman RA, Patel S, Bilaniuk LT. Demonstration of purulent bacterial intracranial infections by computed tomography. *AJR* 1976;127:155–165
- Cockrill HH, Dreisbach J, Lowe B, Yamauchi T. Computed tomography in leptomeningeal infections. *AJR* 1978;130:511–515
- Casselman ES, Hasso AN, Aschwal S, Schneider S. Computed tomography of tuberculous meningitis in infant and children. *J. Comput Assist Tomogr* 1980;4:211–216
- Bydder GM, Steiner RE, Young IR, et al. Clinical NMR imaging of the brain: 140 cases. *AJNR* 1982;3:459–480
- Brant-Zawadzki M, Davis PL, Crooks LE, et al. NMR demonstration of cerebral abnormalities: comparison with CT. *AJR* 1983;140:847–854
- Bradley WG, Waluch V, Yadley RA, et al. Comparison of CT and MR in 400 patients with suspected disease of the brain and cervical spinal cord. *Radiology* 1984;152:695–702
- Zimmerman RA, Bilaniuk LT, Sze G. Intracranial infection. In: Brant-Zawadzki M, Norman D, eds. *Magnetic resonance imaging of the central nervous system*, 1st ed. New York: Raven, 1987:235–257
- Brant-Zawadzki M, Kucharczyk W. Vascular disease: ischemia. In: Brant-Zawadzki M, Norman D, eds. *Magnetic resonance imaging of the central nervous system*, 1st ed. New York: Raven, 1987:221–234
- Sze G. Infections and inflammatory diseases. In: Stark DD, Bradley WG, eds. *Magnetic resonance imaging*, 1st ed. St. Louis: Mosby, 1988:316–343
- Davidson HD, Steiner RE. Magnetic resonance imaging in infections of the central nervous system. *AJNR* 1985;6:499–504
- Schroth G, Kretschmar K, Gawehn J, Voigt K. Advantage of magnetic resonance imaging in the diagnosis of cerebral infections. *Neuroradiology* 1987;29:120–126
- Lee SH. Infectious diseases. In: Lee SH, Rao K, eds. *Cranial computed tomography and magnetic resonance imaging*, 2d ed. New York: McGraw-Hill, 1986:557–600
- Sze G, Zimmerman RD. Magnetic resonance imaging of infections and inflammatory diseases. *Radiol Clin North Am* 1988;26:839–859
- Becker RD, Zimmermann RD, Sze G, et al. MR of subdural empyema and other extraaxial inflammatory lesions (abstr). *AJNR* 1987;8:940
- Zimmerman RD, Becker RD, Devinsky O, et al. Magnetic resonance imaging features of cerebral abscesses and other intracranial inflammatory lesions. *Acta Radiol [Suppl]* (Stockh) 1986;369:754
- Gupta RK, Jena A, Sharma A, et al. MR imaging of intracranial tuberculomas. *J. Comput Assist Tomogr* 1988;12:280–285
- Parker JC, Dyer ML. Neurologic infections due to bacteria, fungi, and parasites. In: Davis RL, Robertson DM, eds. *Textbook of neuropathology*. Baltimore: Williams & Wilkins, 1985:632–703
- Whelan MA, Stern J. Intracranial tuberculoma. *Radiology* 1981;138:75–81
- Hornig CR, Dorndorf W, Agnoli AL. Hemorrhagic cerebral infarction—a prospective study. *Stroke* 1986;17:179–185
- Grossman RI, Joseph PM, Wolf G, et al. Experimental intracranial septic infarction: magnetic resonance enhancement. *Radiology* 1985;155:649–653
- Felix R, Schorner W, Laniado M, et al. Brain tumors: MR imaging with gadolinium-DTPA. *Radiology* 1985;156:681–688
- Brant-Zawadzki M, Berry I, Osaki L, Brasch R, Murovic J, Norman D. Gd-DTPA in clinical MR of the brain: 1. Intraaxial lesions. *AJNR* 1986;7:781–788
- Berry I, Brant-Zawadzki M, Osaki L, Brasch R, Murovic J, Newton TH.

# Age-Related Changes in the Cervical Facet Joints: Studies with Cryomicrotomy, MR, and CT

Geoffrey Fletcher<sup>1</sup>  
Victor M. Haughton<sup>1</sup>  
Khang-Cheng Ho<sup>2</sup>  
Shiwei Yu<sup>1</sup>

The cervical facet joints of 20 cadavers were studied systematically with MR, CT, cryomicrotomy, and histologic sections to determine the anatomic changes that occur with age. Uniform layers of cartilage and subarticular cortical bone characterize the cervical facet joints in cadavers under 20 years of age. Most adult cervical facet joints have only a discolored or microscopically thin layer of cartilage and have irregularly thickened subarticular cortical bone. The appearance of the cervical facet joints changes significantly with aging.

*AJNR* 11:27–30, January/February 1990; *AJR* 154:817–820, April 1990

Anatomic criteria to distinguish normal from abnormal cervical facet joints have not been defined. We noted that many adult cervical facet joints lacked the uniform layer of cartilage and the meniscus that has been described in the normal cervical facet joints [1–3]. We therefore studied the age-related changes of the cervical facet joints with MR, CT, and cryomicrotomy.

## Materials and Methods

Twenty cadavers (12 male, eight female) with no recorded spinal symptoms or disease were selected from the cadavers donated to the Medical College of Wisconsin. The cervical spines in these cadavers were imaged with a 1.5-T cryogenic imager (Signa, General Electric, Milwaukee) and a 3-in. "butterfly" surface coil (Medical Advances, Milwaukee) placed behind the neck. Contiguous 3-mm-thick images in the sagittal plane were obtained with a 256 × 256 matrix and two excitations. Long and short TR images (600–1000/20, 2000/20, 2000/80) were acquired. Image acquisition time was between 30 and 43 min. CT was performed with a GE CT 9800 scanner in the same plane as the MR images. A 1.5- or 3-mm-thick slice was used with a 512 × 512 matrix, 120 kV, 200 mA, 4 sec scan time, 1.5–2.0 magnification factor, and bone windows. After CT and MR imaging the cadavers were frozen and a block of tissue that included the entire cervical spine was removed with a bandsaw. The block was placed on the stage of a planing cryomicrotome (LKB, Gaithersburg, MD). Anatomic sections were obtained in the same plane as the MR and CT images. As 1-mm-thick sections were removed, the surface of the specimen was photographed. The photographs and MR and CT images were compared. In three specimens the cryomicrotome sectioning was terminated when the midpoint of the facet joints was reached. The remaining tissue was placed in formalin and then decalcified, embedded, sectioned, stained with hematoxylin and eosin, and examined with light microscopy. In four cases, the cervical facet joints on one side were unavailable for this study. The case material was divided into two groups: under 20 years old (two cadavers ages 10 and 19) and over 35 years old (18 cadavers ages 37–86).

## Results

The facet joints in the cadavers under 20 years of age conformed to the conventional anatomic depiction [3] (Fig. 1A). In these facet joints, a layer of glistening homogeneous ivory-white cartilage, measuring 1–1.3 mm in thickness,

Received December 7, 1987; revision requested February 10, 1988; revision received May 19, 1989; accepted May 19, 1989.

This work was supported by NIH grant 1 RO1 AR33667-01A2.

<sup>1</sup> Department of Radiology, The Medical College of Wisconsin, Froedtert Memorial Lutheran Hospital, 9200 W. Wisconsin Ave., Milwaukee, WI 53226. Address reprint requests to V. M. Haughton.

<sup>2</sup> Department of Pathology, The Medical College of Wisconsin, Froedtert Memorial Lutheran Hospital, Milwaukee, WI 53226.

0361-803X/90/1544-0817  
© American Roentgen Ray Society

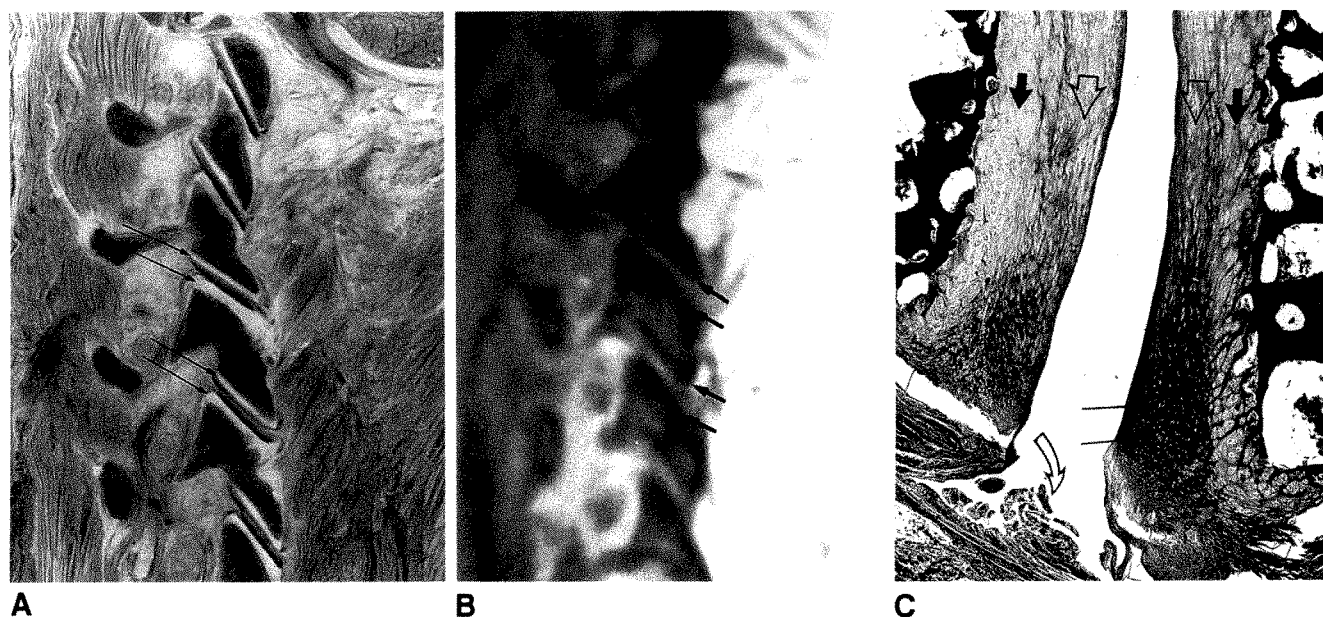


Fig. 1.—A–C. Anatomic section (A), MR image (B), and histologic section (C) in parasagittal plane through cervical facet joints in a 10-year-old. Note uniform layers of cartilage (arrows in A) on superior and inferior articular facets, which are not effectively shown in MR image. The thin layer of cortical bone underneath cartilage (arrows in B) is seen in the MR image (TR = 800, TE = 20). The anatomic section (stained with hematoxylin and eosin) shows a superficial layer of cartilage (open arrows), which stains darkly, and a deep layer of cartilage (wide solid arrows), which stains lightly. Numerous chondrocytes are evident (long thin arrows). Only a small portion of a meniscus (curved arrow) is evident.

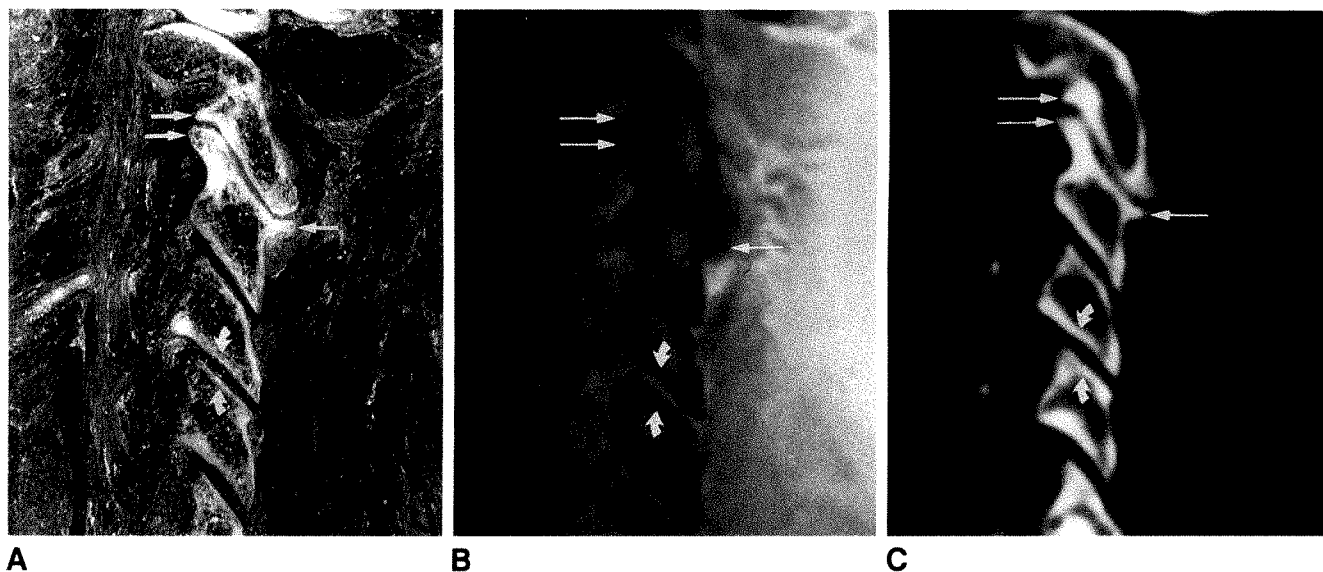


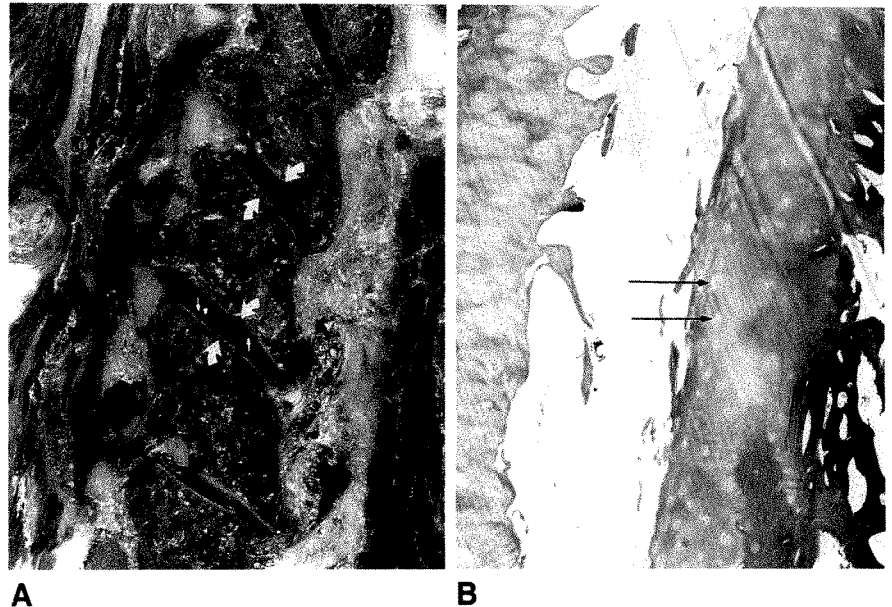
Fig. 2.—A–C. Anatomic section (A), MR image (B), and CT scan (C) of cervical facet joints in a 37-year-old. Note that no cartilage is evident on superior or inferior articular processes of cervical facet joints (A). Normal cortical bone (curved arrows in A) in articular processes of C4–C5 is labeled in A, B, and C. A narrowed joint space, osteophytes, and thickened cortical bone are present at C2–C3 joint (A) and evident on the MR (B) and CT (C) images (straight arrows). The destruction of cartilage, which was shown histologically, is not identified on MR or CT images.

lined the articular surfaces of each articular process. Histologic examination of the cartilage showed chondrocytes in small groups within lacunae, surrounded by large regions of homogeneous basophilic matrix (Fig. 1C). In the cryomicrotome sections, a thin dull-gray layer of cortical bone adjacent to the cartilage was distinguished from the medullary bone in each articular process. In the younger cadavers, large taper-

ing menisci of dense connective tissue were evident in the cervical facet joints. The 19-year-old had significantly thinner cartilage and smaller menisci than the 10-year-old. Neither of these cases had osteophytes or sclerosis of the medullary bone adjacent to the joint.

The cadavers 37 years of age and older had less articular cartilage, less regular cortical margins, and no grossly evident

Fig. 3.—A and B, Anatomic (A) and histologic (B) sections through cervical facet joints in a 46-year-old. A thin band of dark-gray cartilage (small straight arrows) lines cortical bone on superior and inferior articular processes (curved arrows). Histologic section of C3–C4 facet joint shows irregular and degenerated cartilage with faint staining and scattered chondrocytes (long thin arrows).



meniscus in the cervical facet joints. Except at the C1–C2 level (which is not a true facet joint), 70% of the cervical facet joints in the older cadavers had no cartilage evident on gross inspection of the cryomicrotome sections (Fig. 2); the remaining 30% had a layer of dull-gray cartilage less than 1 mm thick (Fig. 3A). Microscopic examination of the histologic sections disclosed a thin layer of cartilage on the articular surfaces even when cartilage was not grossly evident on the cryomicrotome sections. The cartilage was characterized by a sparse matrix that was less densely basophilic than in the younger cadavers and by degenerated chondrocytes (Fig. 3B). A meniscus was not detected on inspection of the cryomicrotomic section but connective tissue bands of a rudimentary meniscus were demonstrated in the joint by microscopic examination. In most of the cases with cartilage abnormalities, osteophytes and/or a sclerotic change in the adjacent medullary cavity were evident. In some of these cases, medullary bone was totally replaced by dense sclerotic bone.

MR images, obtained in 11 of the 19 cases, demonstrated the articular cartilage imperfectly, even in the 10-year-old cadaver (Fig. 1B). The absence of cartilage in the majority of the adults was not readily identified on the MR images (Fig. 2B). The subchondral bone adjacent to the joint was represented as a thin rim of very low signal intensity. Osteophytes and sclerotic bone in the medullary cavity were readily demonstrated by MR (Figs. 2 and 4). In most cases, sclerotic bone appeared as a region of diminished signal intensity. In one case the high signal intensity characteristic of fatty bone marrow was conspicuous, despite densely sclerotic medullary bone evident on the anatomic sections (Fig. 5). Direct sagittal CT, obtained in nine cases, revealed the more severe degrees of joint space narrowing (Fig. 2C). It also reliably demonstrated osteophytes and sclerotic bone (Fig. 2C).

## Discussion

This study shows that the majority of adult cervical facet joints do not have the appearance described as normal [3]. In cadavers 37 years of age and older, articular cartilage is reduced to a thin, discolored or microscopic layer; the meniscus is nonexistent. About one half of the cervical facet joints in adults have thickening of subchondral bone or osteophytes as well as cartilage loss. These changes, although they are consistent with the description of osteoarthritis [4–8], should probably not be considered pathologic since they are seen in the majority of adults. We found the lower and middle cervical levels are usually more severely affected, as others have [4], although painful arthropathies are said to be more common in the upper than lower cervical spine [6].

The study suggests that MR and CT do not effectively detect age-related changes in the cervical facet joints. Both MR and CT demonstrated osteophytes and hyperostosis but not the changes in the articular cartilage and the meniscus.

The study suggests that osteophytes or sclerosis that MR or CT commonly demonstrates in the cervical spine in symptomatic adults may be incidental findings in some cases, notwithstanding the fact that they are commonly seen in patients with pain referrals to the cervical spine [1, 9]. Therapeutic trials of intraarticular steroids and local anesthetics have also suggested a role of the cervical facet joints in neck pain [10].

Symptomatic and incidental changes in the cervical facet joints are not easily differentiated by CT or MR, at least with the present criteria; therefore, additional studies are needed to distinguish symptomatic and age-related changes in these structures.

We conclude that only in the first two decades of life do the cervical facet joints normally have a macroscopic layer of articular cartilage, a meniscus, and a uniform layer of subar-



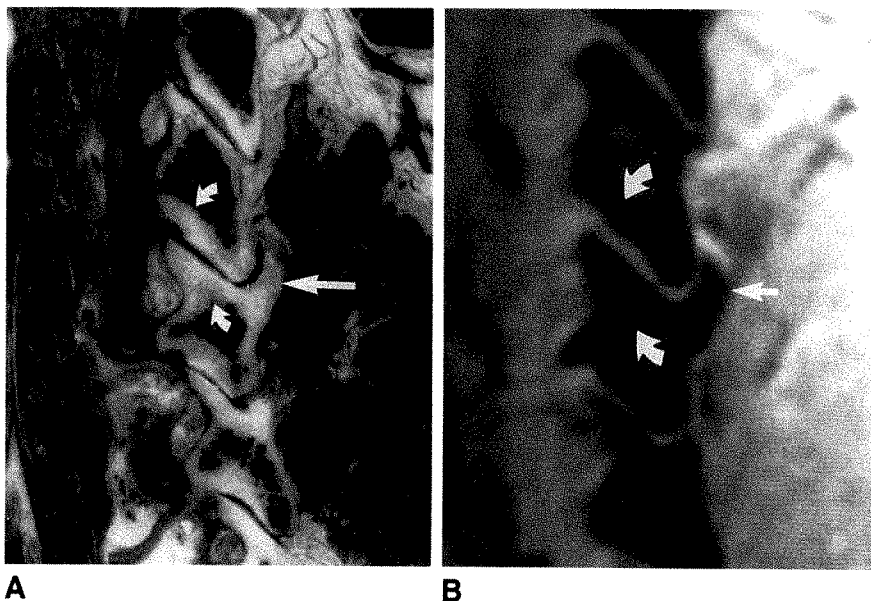


Fig. 4.—A and B, Anatomic section (A) and MR image (B) show degenerated C3–C4 facet joint with thinned articular cartilage, thickened articular cortical bone (curved arrows), and an osteophyte (straight arrow). Osseous changes are shown effectively in MR image (B). None of the facet joints have evident cartilage or regular cortical bone on the anatomic sections.

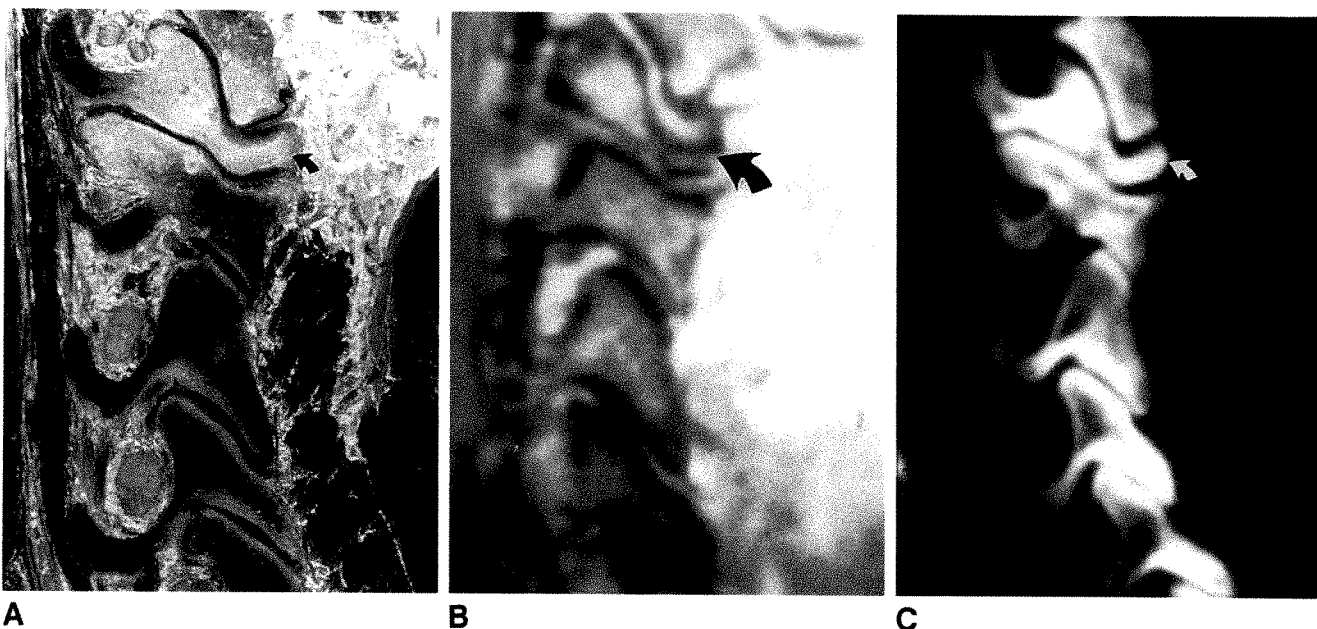


Fig. 5.—A–C, Degenerative changes in upper cervical facet joints. The cryomicrotome section (A) shows destruction of articular cartilage at C2–C3 and C3–C4 and deformity and sclerosis of the intervening articular pillar (curved arrow in A). MR image (B) shows a bright signal from the sclerotic marrow cavity (curved arrow) suggesting fatty degeneration of bone marrow in medullary space. CT scan (C) shows a density consistent with sclerotic bone (curved arrow).

ticular bone. Normal findings in adult cervical facet joints are usually characterized by a thin layer of abnormally staining cartilage containing degenerated chondrocytes, and thickening of the adjacent bone.

#### ACKNOWLEDGMENT

The tireless typing of the manuscript by Jane Worzalla, administrative assistant in neuroradiology, is gratefully noted.

#### REFERENCES

1. Yenerich DO, Daniels DL, Haughton VM. CT grading of degenerative changes in the cervical facet joints: a preliminary study in 163 patients. *Neuroradiology* (in press)
2. Yu S, Sether L, Haughton VM. Facet joint menisci of the cervical spine. *Radiology* 1987;164:79–82
3. Bland JH. *Disorders of the cervical spine*. Philadelphia: Saunders, 1987:46–48
4. Schmorl G, Junghanns H. *The human spine in health and disease*, 2nd ed. Besemann EF, Tr. New York: Grune & Stratton, 1971:203–207
5. Resnick D. *Diagnosis of bone and joint disorders*. Philadelphia: Saunders, 1981:1381–1384
6. Brain WR. Some unsolved problems of cervical spondylosis. *Br Med J* 1963;1:771–777
7. Gordr Sepse SB, Gardner GM. Roentgenographic findings of the cervical spine in asymptomatic people. *Spine* 1986;11:521–524
8. Kirkaldy-Willis WH, Wedge JH, Yonk-Hing K, Reilly J. Pathology and pathogenesis of lumbar spondylosis and stenosis. *Spine* 1978;3:319–328
9. Sokoloff L. The remodelling of articular cartilage. *Rheumatology* 1982;7:11–18
10. Dory MA. Arthrography of cervical facet joints. *Radiology* 1983;148:379–383

# Lumbar Disk Herniation and Canal Stenosis: Value of Intraoperative Sonography in Diagnosis and Surgical Management

Berta M. Montalvo<sup>1</sup>  
 Robert M. Quencer<sup>1</sup>  
 Mark D. Brown<sup>2</sup>  
 Evelyn Sklar<sup>1</sup>  
 M. Judith D. Post<sup>1</sup>  
 Frank Eismont<sup>2</sup>  
 Barth A. Green<sup>3</sup>

One hundred four patients with preoperative diagnoses of lumbar canal stenosis, disk herniation, or a combination of both were evaluated with intraoperative sonography with the intent of (1) describing the sonographic characteristics of herniated disks and distinguishing these from bulging anuli, epidural fat, scar tissue, and spondylolisthesis; (2) establishing criteria for adequate decompression of canal stenosis; and (3) determining the usefulness of sonography in monitoring disk removal. Disk material demonstrates medium echogenicity, different in its sonographic features from bone, epidural fat, scar tissue, and epidural veins. A sonographic diagnosis of disk herniation was made in 43 cases, 41 of which were confirmed during surgery. Sonography established the presence or absence of disk herniation (confirmed by surgery) in 14 of 19 patients who had equivocal preoperative findings. After routine discectomy, residual disk material was found in 17 (41%) of 41 patients, which led to further surgery in 16 patients with removal of the additional disk fragments. In 84 patients undergoing decompressive surgery for canal stenosis, sonography detected residual canal compression in 19 (23%), which led to a widened decompression in 15 of these patients. Sonography can differentiate disk material from other normal or abnormal structures in the canal; therefore, sonographic monitoring helps to ensure adequate bony decompression and complete discectomy.

We conclude that intraoperative sonography is an important tool in the surgical management of lumbar disk disease and stenosis.

*AJNR* 11:31-40, January/ February 1990; *AJR* 154:821-830, April 1990

In laminectomies performed for suspected disk herniation and/or degenerative spondylosis/canal stenosis of the lumbar spine, proper patient selection, accurate preoperative diagnoses, and good surgical technique are important factors in decreasing the number of "failed backs." Intraoperative spinal sonography is an imaging technique that has been reported to be useful in the surgical biopsy or removal of soft-tissue masses [1], the shunting of congenital [2] and posttraumatic [3, 4] cysts of the cord and subarachnoid space, and the placement of Harrington rods in previously injured spines [4-6]. An early article reported the sonographic findings in six patients who had disk herniation and spondylosis and concluded that sonography might be useful in these lesions [7]. At our institution over the past 4 years, we have used intraoperative spinal sonography in a large number of patients who had undergone surgery for abnormalities related to degenerative disk disease and spondylosis of the lumbar spine. It was our intention to determine the role sonography could play in the intraoperative evaluation of the spine in these conditions and to see how this information could assist in surgical management. In this report, we describe our experience with this technique; illustrate the sonographic findings; and establish sonographic criteria for the diagnosis of disk herniation, complete discectomy, and adequate decompression in canal stenosis.

## Materials and Methods

One hundred four patients with the preoperative diagnosis of spondylosis, canal stenosis, and/or herniated disk of the lumbar spine were examined with intraoperative spinal sonog-

Received March 16, 1989; revision requested May 1, 1989; revision received June 12, 1989; accepted June 14, 1989.

Presented in part at the annual meeting of the American Roentgen Ray Society, Miami Beach, FL, April 1987.

<sup>1</sup> Department of Radiology (R-109), University of Miami School of Medicine/Jackson Memorial Medical Center, P.O. Box 016960, Miami, FL 33101. Address reprint requests to B. M. Montalvo.

<sup>2</sup> Department of Orthopedic Surgery, University of Miami School of Medicine/Jackson Memorial Medical Center, Miami, FL 33101.

<sup>3</sup> Department of Neurological Surgery, University of Miami School of Medicine/Jackson Memorial Medical Center, Miami, FL 33101.

0361-803X/90/1544-0821  
 © American Roentgen Ray Society

raphy over a 4-year period. The preoperative diagnoses were made with one or more of the following techniques: myelography, non-contrast-enhanced CT, CT myelography, or MR imaging. The preoperative diagnoses were disk herniation alone (20), spondylosis alone with focal or generalized canal stenosis at one or multiple levels (42), and a combination of disk herniation and spondylosis (42). In 29 of these 104 cases, the patients had undergone prior surgery at the same level or levels. Both single- and multilevel disease were evaluated. Only patients with technically adequate examinations are reported here. Seven other patients who had sonograms are not reported in this study. In three there was insufficient clinical, operative, and sonographic information; in four the sonograms were inadequate.

The patients examined by intraoperative sonography were not consecutive. We had planned to make this a consecutive study including all patients with spondylosis and/or herniated disk undergoing laminectomy, but a number of patients in the time period of the study were not examined with intraoperative spinal sonography. No

patients undergoing a "microlaminectomy" were examined, since the field of view in such an exposure is inadequate for our probe. In a small group of patients, the decision to request intraoperative sonography was made late and the delay involved in transporting the ultrasound unit to the operating room would have added too much time to the surgical procedure, so these patients were not studied.

In those patients operated on for herniated disk alone, the surgical procedure consisted of bilateral laminectomy or a hemilaminectomy with a 1.5-cm opening. If there was associated canal stenosis or if only degenerative or congenital canal stenosis was present, a posterolateral decompression consisting of laminectomy and medial facetectomy was performed. Such operations allowed an adequate window for sonography.

Intraoperative spinal sonography was performed with a 7.5-MHz transducer encased in a sterile sheath. After laminectomy or posterolateral decompression, the wound was filled with sterile solution such as Ringer lactate or normal saline and a baseline sonogram was

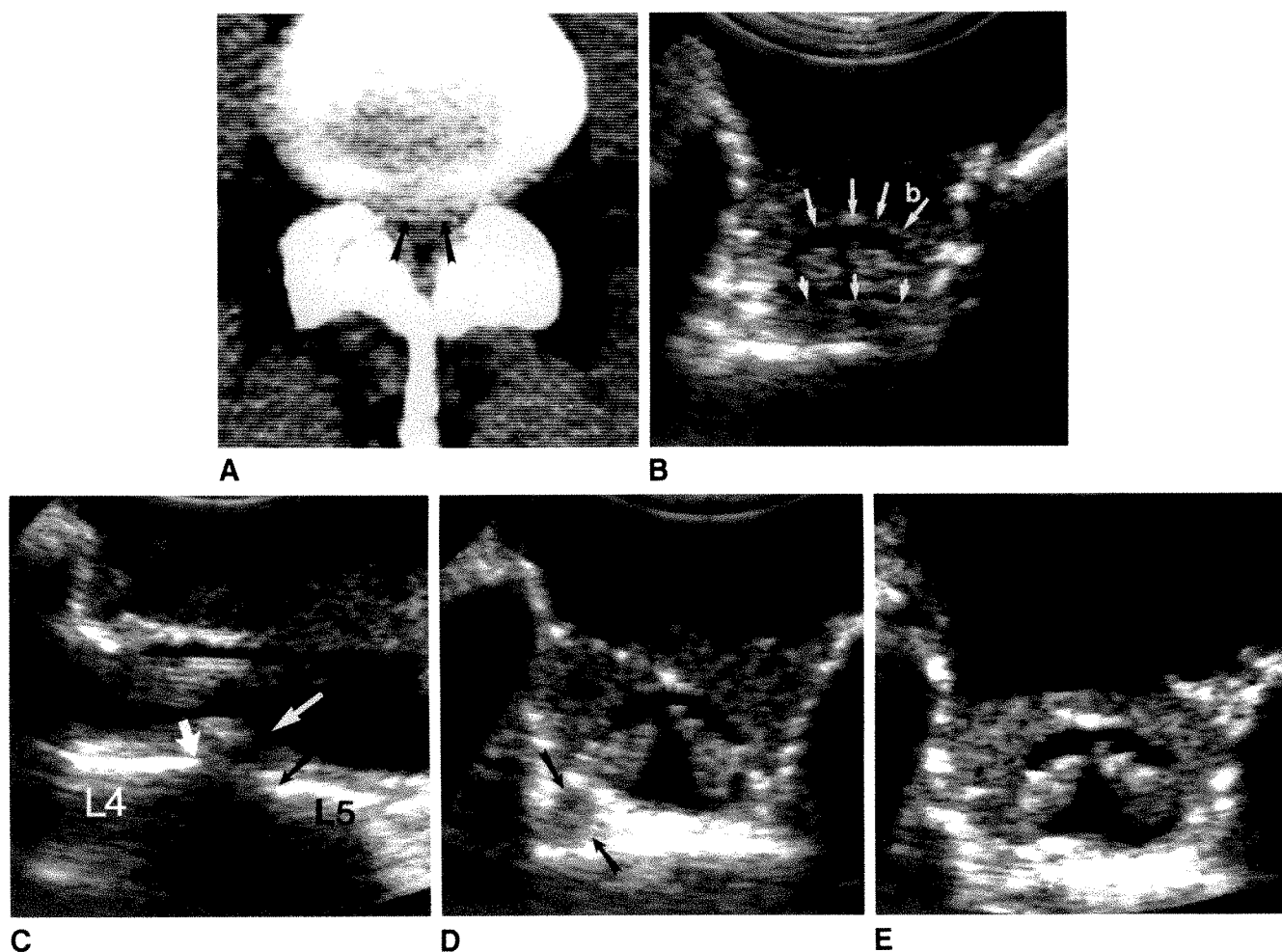


Fig. 1.—Herniated disk and canal stenosis.

A, Unenhanced CT scan at L4-L5 level shows central disk (arrows) with associated canal stenosis.

B, Axial sonogram after bilateral laminectomy and medial facetectomies shows soft-tissue mass (short arrows) of medium echogenicity flattening ventral sac and compressing lumbar roots (compare with A). Note well-defined interface between disk and sac. Echogenic material (b) overlying dura (long arrows) represents fresh blood.

C, Longitudinal sonogram. Disk has appearance of soft-tissue mass (long white arrow) at level of interspace. Interspace is bounded by inferior edge of L4 (short white arrow) and superior edge of L5 (black arrow) vertebral body. Disk protrudes into canal and narrows anteroposterior diameter of sac. Disk is of heterogeneous medium echogenicity; brighter echoes represent specular reflections.

D, After what the surgeon believed was a complete discectomy the sac regained a more rounded shape, but residual disk (arrows) compressing sac remains in left lateral aspect of canal (compare with B).

E, Final sonogram after removal of disk fragment shown in D shows symmetric rounded shape to thecal sac, no compression of lumbar roots, and no residual disk material.

obtained with images in the axial and longitudinal planes. The sonographic appearance of herniated disk(s), epidural soft tissue, residual scarring from prior procedures, swollen nerve roots, subluxation, or arachnoiditis were noted and correlated with the radiographic and surgical findings. Observations were also made of the sonographic appearance of normal structures of the spinal canal including disk material, epidural fat, epidural veins, nerve roots, CSF, and bony contours of the surrounding spine. In patients with canal stenosis, the configuration of the canal and the thecal sac was studied and compared with the radiographic findings.

After the baseline sonogram, further surgery was performed as warranted. For example, in instances of herniated disk, discectomy was undertaken, and in cases of canal stenosis, bone was removed to decompress neural structures. The adequacy of these surgical procedures was monitored sonographically and was assessed by the amount of disk or bone removed and the subsequent increased space in the spinal canal and the amount of CSF surrounding neural tissue as compared with the appearance on the initial sonogram. As the surgery progressed, the results of the sonograms were compared with the operative findings, and continued surgery was undertaken as deemed necessary from these sonographic images and the patient's clinical presentation.

The number of cases in which sonography added diagnostic information and the impact of intraoperative sonography on surgical management as evidenced by further discectomy or bony decompression were recorded. The criteria used to judge the adequacy of discectomy or canal decompression are described in the Results section. The data were analyzed in order to evaluate to what extent sonography was useful in lumbar disk herniation and canal stenosis.

## Results

### *Sonographic Appearance of Normal and Abnormal Structures of the Lumbar Spinal Canal*

**Disk material.**—Herniated disks have the appearance of a solid mass with smooth borders and well-defined margins. They display medium echogenicity and are generally less bright than adjacent epidural fat (Figs. 1 and 2). They may

have internal punctate bright echoes that represent calcifications or exhibit dense shadowing if the periphery of the disk is densely calcified. Herniated disks can be seen to protrude into the spinal canal, where they may deform the thecal sac and displace nerve roots. Lateral disk herniations (either far-lateral herniated disks or disk herniation in the neural foramen) either are obscured by overlying bone or are beyond the field of view of the transducer. The intervertebral disk space can be identified best on longitudinal scans, where this space is marked by the interruption of the bright interface formed by the dorsal edge of the vertebral bodies (Figs. 1C and 2C). Disk material allows acoustic transmission to occur; this phenomenon is best seen when the interspace is perpendicular to the sonographic beam. Calcified disks may be differentiated from osteophytic spurs on longitudinal sonography by noting the location of the intervertebral disk space in relation to such abnormalities. Although sequestered fragments of disk in the epidural space can be seen cephalad or caudad (Fig. 3) to the vertebral interspace, it is possible that the normal epidural soft tissue may obscure these migrated disk fragments, particularly when they are small.

**Epidural fat.**—The predominant soft-tissue density in the epidural space is fat, which appears brightly echogenic (Figs. 2C and 4), is symmetric in distribution (Fig. 4B), and tends to become thinner in the interspace. When it is adherent to the dorsal dura (Fig. 4A), it attenuates the sonographic beam and interferes with adequate visualization of the canal and the dural sac. Overabundant fat ventrally may cause confusion since it may appear to displace the sac posteriorly (Fig. 4B). Fat is homogeneously bright in echogenicity and symmetric in distribution, facts that help distinguish it from scar and disk material.

**Epidural veins.**—Prominent epidural veins appear as hypoechoic spaces within the epidural space (Fig. 5). Flowing low-amplitude blood echoes may be observed within the epidural veins during real-time examination. These veins,

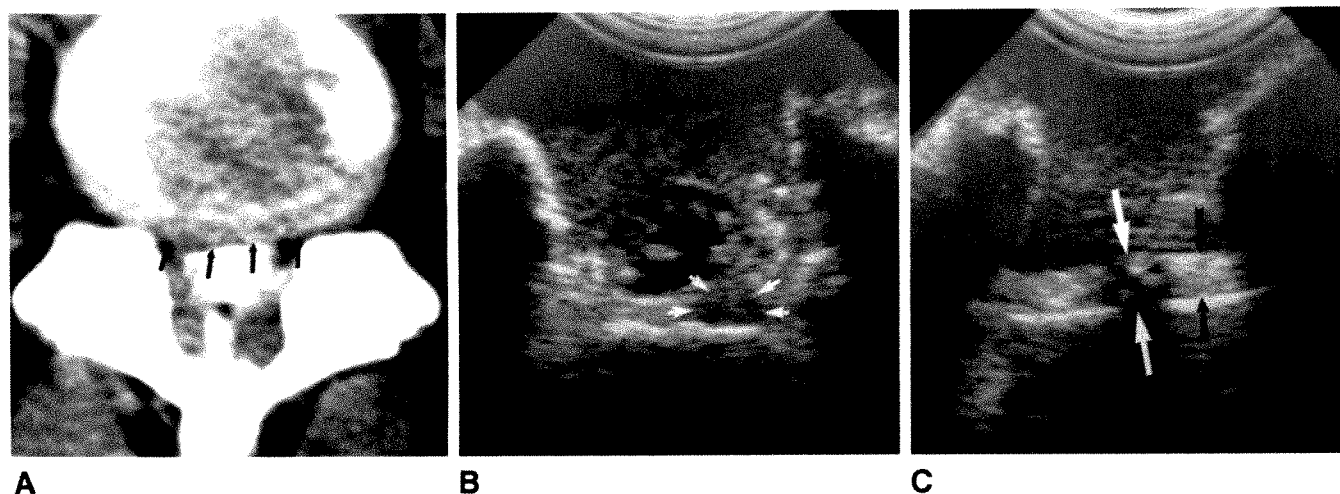


Fig. 2.—Herniated disk, shown by sonography in a patient with canal stenosis.

A, Preoperative CT myelogram shows bilateral hypertrophied ligamenta flava, bony hypertrophy, and ventral soft-tissue density (arrows) interpreted prospectively as bulging annulus.

B, Axial sonogram. Right ventral disk is well demarcated (arrows) and causing compression of roots in lateral recess.

C, Longitudinal sonogram. Disk (between white arrows) is seen to be less echogenic than lumbar epidural fat (between black arrows). Internal bright echoes (arrowhead) probably represent calcifications within herniated disk. After surgical excision, no residual disk was visualized on final sonogram.

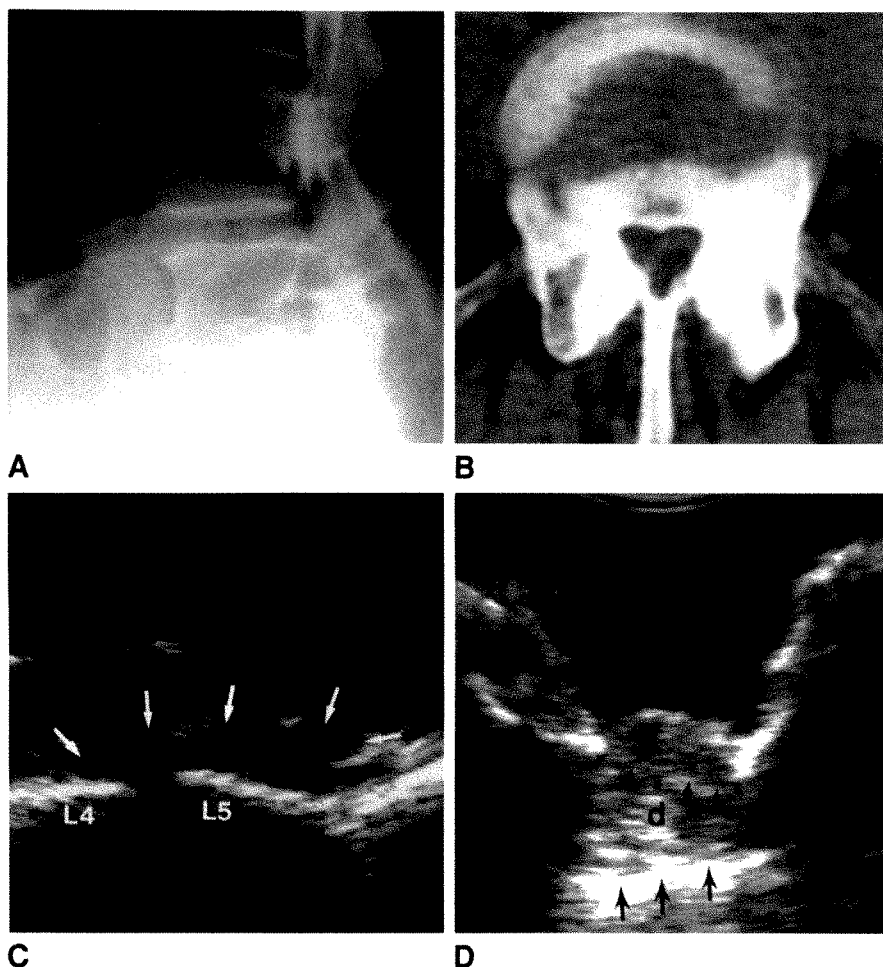


Fig. 3.—Disk with sequestered fragment in patient with canal stenosis.

A, Myelogram shows high-grade block at L4–L5 in patient with low-back pain.

B, Interpretation of postmyelographic CT scan is limited because of lack of intrathecal contrast material at L4–L5.

C, Longitudinal sonogram clearly shows soft-tissue mass (arrows), which originates at L4–L5 interspace, extends inferiorly, and elevates dura. This large disk is partially sequestered behind L5 vertebral body, a crucial observation prior to discectomy.

D, Transverse sonogram confirms presence of soft-tissue mass representing sequestered disk (d), located dorsal to vertebrae (arrows) and compressing thecal sac (arrowheads).

which taper in size toward the interspace, may represent normal structures ventral to the thecal sac or they may indicate the presence of an abnormality that is obstructing the normal epidural venous flow.

**Scar.**—Scar can be difficult to differentiate from a disk or epidural fat because it may be either brightly echogenic (Figs. 6A and 6B) and mimic fat or may be of medium to low echogenicity (Fig. 6C) and mimic disk material. One helpful distinguishing feature of scar tissue is that it appears to merge with the dura without a distinct margin (Fig. 6). If the scar is located dorsally, it attenuates the sonographic beam and interferes with visualization of the spinal canal and thecal sac. Five patients who had prior surgery were noted to have residual scar tissue. In two patients, the scar was brightly echogenic, lateral in location, and at the level of the intervertebral disk space. In three patients, the scars were of medium to low echogenicity with poorly defined borders that merged with the dural surface. In all cases, surgical excision showed scar tissue.

**Swollen nerve roots.**—Swollen nerve roots may be mistaken for herniated disks as they exit the thecal sac since they can be of similar echogenicity and are also well marginated; however, typically they are round and well defined on transverse views (Fig. 7) but poorly defined on longitudinal

views, cannot be traced back to the disk space, and do not compress the adjoining dura.

**Bulging anuli.**—Diagnosis of a bulging anulus is made on the longitudinal view by observing a small soft-tissue density at the interspace bulging into the canal. When larger in size, a bulging anulus may be difficult to distinguish from central disk herniation (Fig. 8). Longitudinal and axial views show no significant thecal sac compression in bulging anuli.

**Subluxation.**—On a longitudinal sonogram, vertebral body subluxations can be detected by finding the intervertebral disk space, determining the location of the posterior surface of each vertebra caudad and cephalad to the disk space, and observing their relative alignments (Fig. 9). Epidural soft tissues and disk material may be visible between the edge of the more anterior vertebra and the dura (Figs. 9B and 9C). Axial views at the interspace where the subluxation occurred may incorrectly suggest the presence of herniated disk since the anteroposterior diameter of the sac may be decreased and soft tissue is present ventral to the sac (Fig. 9D). A straight longitudinal scan is crucial in these instances since normal soft tissues dorsal to a subluxed vertebral body do not protrude posterior to the more posterior vertebral body (Fig. 9). When subluxation and disk herniation coexist, establishing the diagnosis of a herniated disk and monitoring its

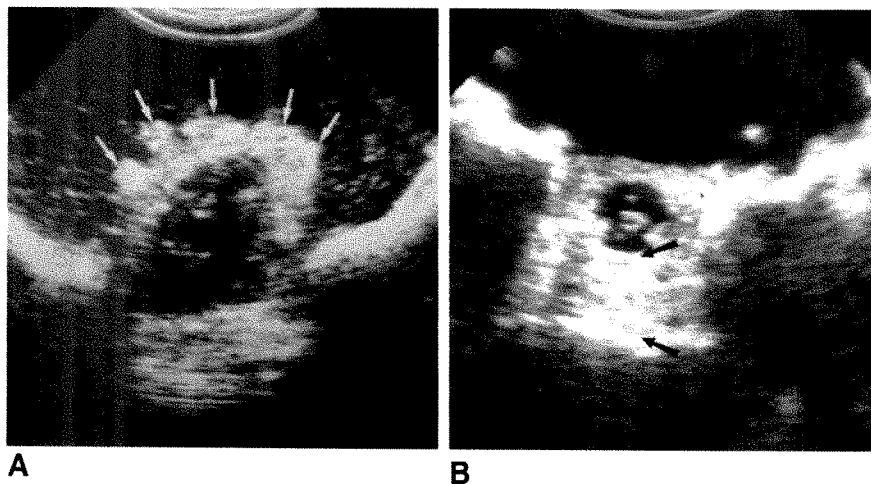


Fig. 4.—Epidural fat (canal stenosis).

A, Axial sonogram. Clusters of bright echogenic masses (arrows) adherent to dorsum of dura represent epidural fat (surgical observation). Note relatively poor visualization of contents of thecal sac owing to attenuation of beam.

B, Axial sonogram in another patient. Depth of epidural soft tissues (arrows) posterior to S1 is considerable. However, bright echogenicity, uniformity of distribution, and lack of deformity of ventral aspect of thecal sac are criteria indicating this represents epidural fat rather than disk material or soft-tissue tumor.

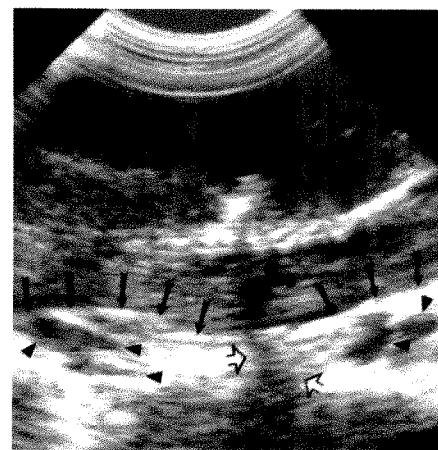


Fig. 5.—Epidural veins (canal stenosis). On longitudinal sonogram, epidural soft tissues, bounded dorsally by ventral dura (solid arrows), are prominent; within them are hypoechoic areas representing veins (arrowheads). Epidural soft tissues taper toward interspace (open arrows). When prominent veins such as these are present, small particles representing flowing blood may be seen during real-time sonography.

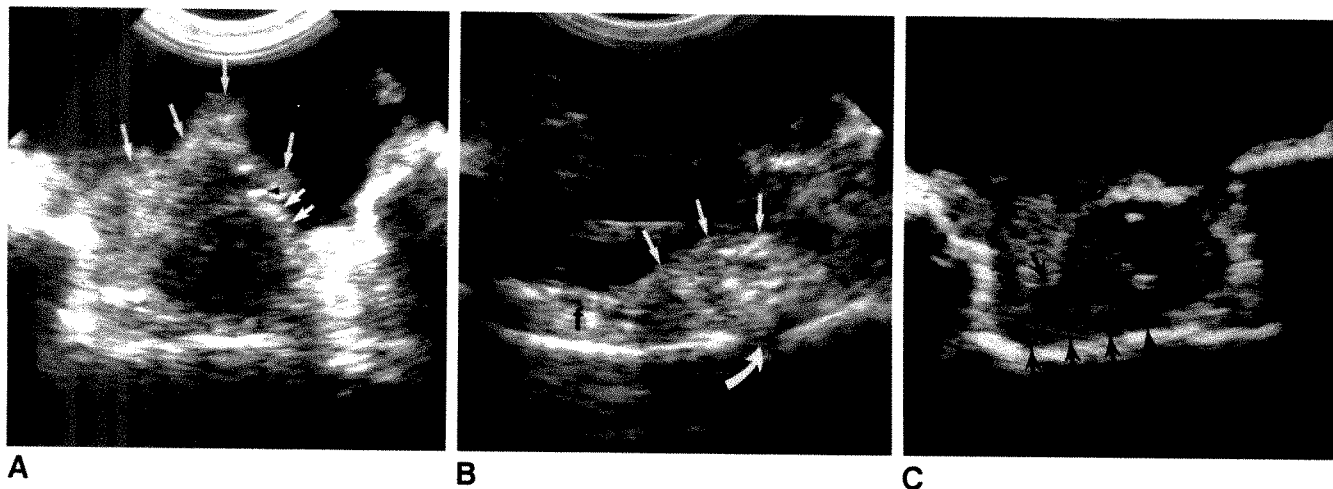


Fig. 6.—Scar in three patients who had undergone surgery previously.

A, Axial sonogram. Dorsal scar (long arrows) is irregular and heterogeneous in echogenicity; its interface with dura is effaced. The only portion of dura (short arrows) that is clearly visualized is surrounded by CSF. Thecal sac is poorly visualized because of diminished sonographic penetration. Small bright echo (arrowhead) represents calcification.

B, Right parasagittal sonogram. Hyperechoic soft-tissue mass (straight arrows), inseparable and indistinguishable from epidural fat (f), is seen at L5-S1 interface (curved arrow). Mass was suspicious for herniated disk because of its location and its mass effect; however, when this space was explored, soft tissue proved to be a scar.

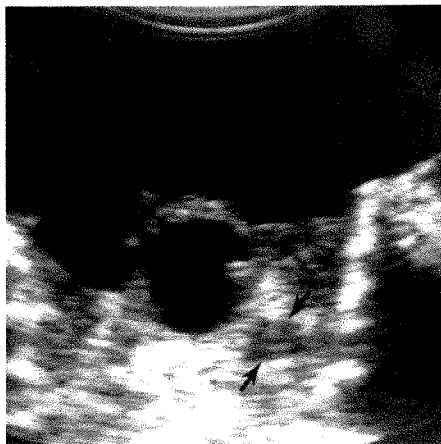
C, Axial sonogram. Hypoechoic scar (arrows) is seen on left as an irregularly shaped soft-tissue mass with poorly defined edges silhouetting dura.

removal may be difficult. In this situation the presence of thecal sac compression is the key point in establishing the proper diagnosis (Fig. 10).

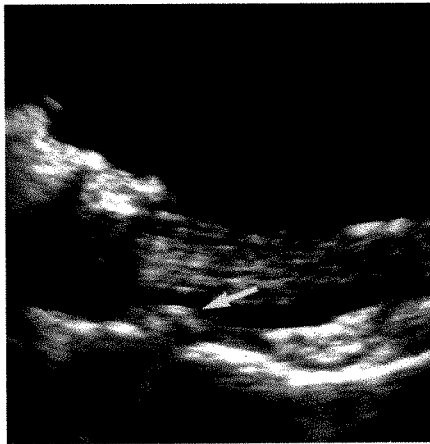
**Arachnoiditis.**—Intradural arachnoiditis is seen sonographically as tethered, clumped, and deformed nerve roots and thecal sac deformity [6, 7]. On real-time evaluation there is lack of the typical CSF pulsations when the arachnoiditis is

severe. Two of our patients who had prior surgery and one of whom had prior Pantopaque myelography had evidence of arachnoiditis on sonography (Fig. 11). The diagnosis of arachnoiditis is difficult to establish sonographically in the face of substantial chronic compression of the thecal sac or if a dural tear has occurred because CSF may not be present to serve as a hypoechoic contrast to the nerve roots and dura. Pan-





7



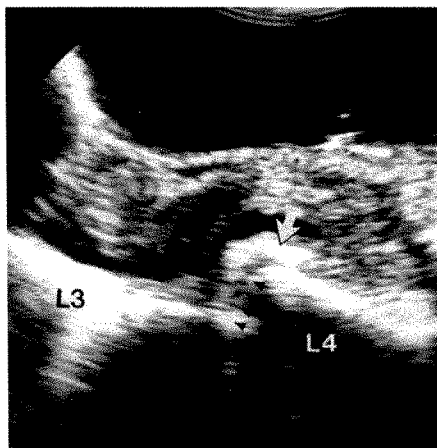
8

Fig. 7.—Swollen nerve root (canal stenosis). Axial sonogram shows well-defined round soft-tissue mass (arrows) within lateral epidural fat on right. Note that thecal sac is not compressed. This appearance is typical of swollen nerve root.

Fig. 8.—Bulging annulus (canal stenosis). When a prominent soft-tissue mass (arrow) is seen, such as this one at L3-L4 level, differentiation from a small central disk herniation is difficult. This was considered to most likely represent a bulging annulus because of absence of nerve-root compression.



A



B

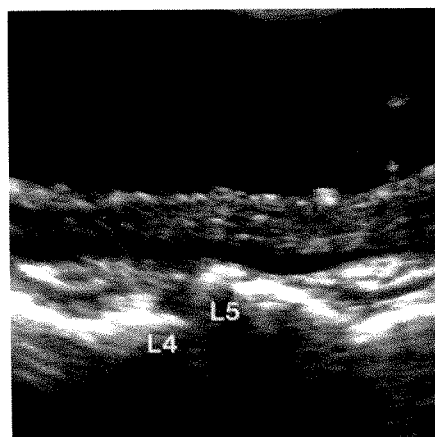
Fig. 9.—Spondylolisthesis and canal stenosis.

A, At L3-L4, MR shows anterior displacement of L3 on L4, a degenerative disk, and an osteophyte protruding into canal.

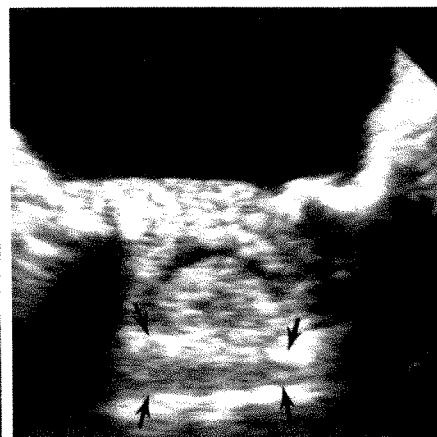
B, Longitudinal sonogram correlates well with preoperative MR, showing osteophytic spur (arrow), spondylolisthesis (arrowheads), and resultant thecal sac compression. Sonography serves to rule out any associated disk herniation.

C, Longitudinal sonogram in another patient shows anterior displacement of L4 on L5. At L4-L5 interspace, disk material does not protrude beyond dorsum of L5 into canal. Sonography indicates absence of herniated nucleus pulposus, which could not be ruled out on preoperative myelography or CT myelogram because of severe canal narrowing with a high-grade block.

D, Axial sonogram in a different patient may be misleading, since ventral epidural soft tissues (arrows) at site of subluxation mimic a central disk flattening thecal sac. Longitudinal sonogram showed spondylolisthesis without herniated nucleus pulposus.



C



D

topaque droplets within the thecal sac have a characteristic hyperechoic interface with the CSF, which should not be mistaken for adhesions (Fig. 12).

#### *Application of Intraoperative Sonography in Disk Herniation, Canal Stenosis, and Spondylosis*

For the sake of simplicity, our results in disk herniation and canal stenosis, whether congenital or secondary to spondy-

losis or trauma, are reported and discussed separately, even though they were often noted to occur simultaneously.

**Herniated disk.**—We include in this group a total of 63 patients, 42 with a definitive preoperative diagnosis of lumbar herniated disk, 20 with a diagnosis of suspected herniated disk, and one in whom the diagnosis of herniated disk was not suspected preoperatively but was made at surgery (this patient had canal stenosis) (see Tables 1 and 2).

Fig. 10.—Herniated disk, spondylolisthesis, and canal stenosis.

A, Longitudinal sonogram shows significant anterior displacement of L4 on L5 and epidural soft tissue (arrows) between subluxed bodies compressing thecal sac and roots. Since normal epidural soft tissues associated with spondylolisthesis do not cause such compression, a diagnosis of herniated nucleus pulposus was made.

B, Final longitudinal sonogram after discectomy reveals no residual compressive soft-tissue mass at level of disk space. Note that nerve roots are not deviated. A spondylolisthesis is still noted along with normal epidural soft tissues (arrows) behind L4 body. A small spur from superior portion of L5 body is present (arrowhead).

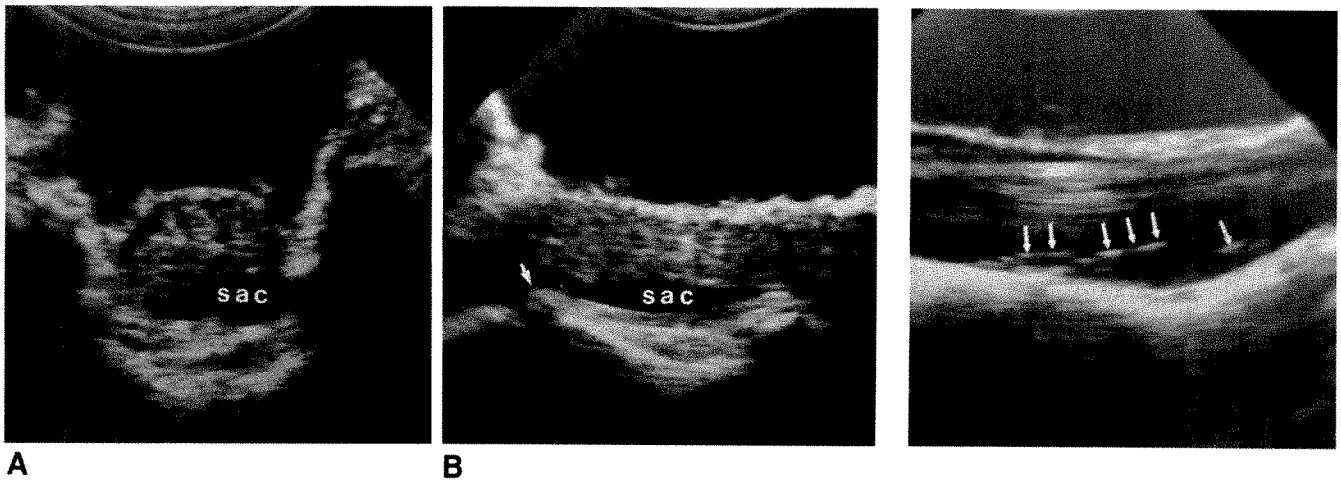
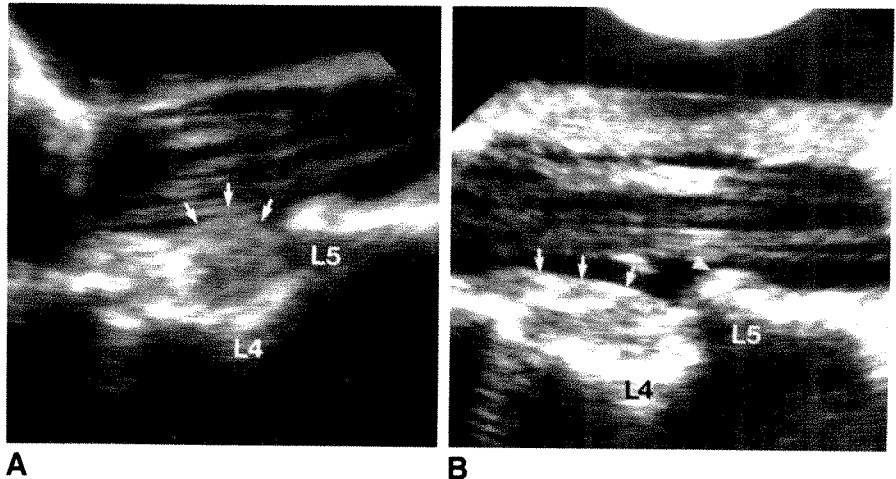
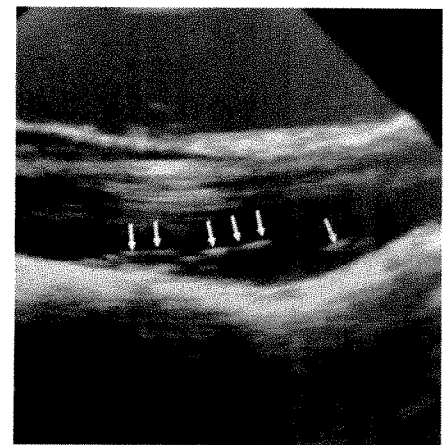


Fig. 11.—Arachnoiditis (previous surgery).

A and B, Axial (A) and longitudinal (B) scans. Clumped nerve roots that fill thecal sac are adherent to dorsal and lateral arachnoid walls. The only subarachnoid fluid present (sac) is loculated and causing a mass effect, an appearance characteristic of subarachnoid cyst. A bulging anulus (arrow) is present at L2-L3 interspace.

Fig. 12.—Pantopaque (previous surgery). Linear echoes (arrows) in dependent portion of thecal sac represent acoustic interface between CSF and oily medium Pantopaque. Pantopaque is anechoic. This appearance should not be mistaken for abnormally coursing roots or intradural scarring.



*Intraoperative sonographic diagnosis and surgical correlation.*—Fifty-nine of these 63 patients with herniated disk had a baseline sonogram following laminectomy (Table 2). Considering these 59 patients as a group, sonographic diagnosis of herniated disk was made in 43 and was confirmed surgically in 41; no herniated disk was found in two. In the remaining 16, the sonographic diagnosis of no herniated disk was made in 11 patients and confirmed surgically in 10, but sonography missed one herniated disk found at surgery. Sonography diagnosed scar in one patient and scar vs herniated disk in two; scar was found in all three at surgery. Sonography could not exclude the presence of herniated disk in two; in neither was a herniated disk found at surgery.

Within the group of 20 patients with the preoperative radiographic diagnosis of suspected or equivocal disk herniation and canal stenosis, one had no baseline sonogram. Of the remaining 19, 10 had severe canal narrowing with block (Table 2). Sonography showed associated disk herniation in four

(Fig. 3) and no disk herniation in four (Fig. 9C) (all eight with surgical correlation); sonography was equivocal in two. Surgical exploration of the questionable area in these two patients revealed no disk herniation.

Sonography diagnosed and surgery found an unsuspected herniated disk in a patient undergoing surgery for canal stenosis (Fig. 2; see Table 2).

*Criteria for complete discectomy or further surgery.*—The criteria established for complete removal of disk material (Fig. 1) include the absence of the initially identified soft-tissue mass and the return of the thecal sac to a normal or nearly normal shape. If residual mass and deformity of the thecal sac were identified (Fig. 1), they formed the basis for recommending reevaluation of the surgical field in hopes of finding and removing additional disk material.

Sonographic examination of the surgical field after discectomy was performed in 41 patients (including three who had not had a baseline sonogram). Of these, 24 had no residual

disk material by initial postdiscectomy sonographic criteria. In 17, however, residual disk fragments were identified by sonography. As a result, in 16 patients the operative site was reexplored, the presence of additional disk material was confirmed, and the extra fragments were removed. In all 16, the surgical field was monitored until no more disk material was present by sonographic criteria. In the other patient the surgeon judged that the presumed residual disk fragments were not significant and further surgery was not warranted.

**Canal stenosis.**—The preoperative diagnosis of focal or generalized canal stenosis was made in 84 cases, including those patients with (42) and without (42) associated herniated disks. Of these 84 cases, 79 had spondylosis (Figs. 13 and 14) (including degenerative spondylolisthesis), four had old fractures with secondary canal narrowing, and one had congenital canal stenosis. Eighteen patients had prior surgery at the levels of canal narrowing; 66 had no prior surgery.

**Intraoperative sonographic evaluation and surgical correlation.**—Canal stenosis secondary to enlarged facets resulted in a triangular or irregular shape to the thecal sac, a smaller transverse than anteroposterior canal diameter, and crowding of the nerve roots (Figs. 13A and 14A). The sonographic observations concerning bony impingement corresponded to the surgical findings in all cases.

**Criteria for adequate decompression or further surgery.**—Following bone resection in an adequately decompressed spine, sonography demonstrates a significant change in the contour of the thecal sac compared with the initial postlaminectomy scans. A round or nearly round sac should be seen

in which there is no deviation of the roots from their normal course. The bony canal that results from this decompression should have an open rectangular shape (Fig. 13B) with a visualized space between the lateral wall of the thecal sac and the residual facets (Figs. 1E, 2B, and 13B).

In the 84 cases, 65 were judged by these sonographic criteria at the time of surgery to have an adequately decompressed canal. Nineteen patients were found to have residual bony compression of the sac (Figs. 13 and 14). Fifteen of these cases had further surgical manipulations in an attempt to achieve adequate decompression; on the final sonographic examination, two had residual but mild compression judged to be acceptable by the surgeon and the radiologist, while 13 were judged to have a good decompression. In the other four patients, the surgeons decided to do no further surgery despite the sonographic demonstration of residual sac compression. The reasons for this included mild compression (one patient), reluctance to perform more extensive laminectomies for fear of destabilizing the spine (two), and the lack of symptoms corresponding to the bony abnormality (one).

## Discussion

In order to achieve clinically satisfactory long-term results in patients undergoing lumbar surgery for disk herniation, spondylosis, and/or canal stenosis, complete removal of the offending disk or bone is necessary. While imaging examinations such as myelography, CT myelography, and MR can accurately demonstrate preoperatively the symptom-producing abnormalities, the intraoperative assessment of the lumbar spine and the progress of the operative procedure is usually performed by simple visual inspection. Therefore, suboptimal evaluation of the surgical field may occur and a potential exists for the incomplete removal of herniated disk material and/or inadequate bony decompression of neural tissue. For this reason a more accurate method of assessing the progress of the surgical procedure is desirable. Intraoperative sonography can clearly display normal and abnormal intraspi-

**TABLE 1: Pre- and/or Operative Diagnoses**

Diagnosis	No. of Patients
Disk herniation without canal stenosis	20
Canal stenosis without disk herniation	41
Disk herniation plus canal stenosis	43
Total	104

**TABLE 2: Baseline Sonographic Diagnoses and Surgical Correlation in 59 Patients Who Had Preoperative and/or Operative Diagnoses of Herniated Disk and Baseline Sonography**

Preoperative Radiographic Diagnosis	No. of Cases	Findings on Baseline Sonogram	Surgical Findings
Herniated disk	39	36 Herniated disk — — 1 Scar 2 No herniated disk	34 Herniated disk 1 Scar 1 No herniated disk 1 Scar 2 No herniated disk
Suspected herniated disk			
Canal stenosis with block	10	4 Herniated disk 4 No herniated disk 2 ?Herniated disk	4 Herniated disk 4 No herniated disk 2 No herniated disk
Scar vs herniated disk	6	1 Herniated disk/swollen nerve root 2 Scar vs herniated disk 3 No herniated disk —	1 Herniated disk/swollen nerve root 2 Scar 2 No herniated disk 1 Herniated disk
?Herniated disk	2	2 No herniated disk	2 No herniated disk
Herniated disk vs lymphoma	1	1 Herniated disk	1 Herniated disk
No herniated disk (canal stenosis)	1	1 Herniated disk	1 Herniated disk

Note.—Only those patients in whom baseline sonograms were obtained are represented here.

Fig. 13.—Posterolateral bony decompression for canal stenosis. Two patients were examined with axial sonography after different degrees of bony decompression for canal stenosis.

A, Persistent bone compression in a patient with previous surgery. Following laminectomies and medial facetectomies, enlarged facets (F) are causing significant constriction (arrowheads) and irregularity of sac. Note crowded roots and lack of visualized CSF. Further bone removal followed this sonogram and included extending bilateral medial facetectomies, which resulted in a more normal-appearing sac and diminished root compression.

B, Adequate lateral decompression, primary operative procedure. In the second patient, bilateral laminectomies and facetectomies resulted in a rounded (normal) thecal sac with no areas of bone compression. In the left lateral gutter, echogenic material represents fresh blood (b) in operative site. Bony canal now has shape of wide, open-ended rectangle (arrowheads).

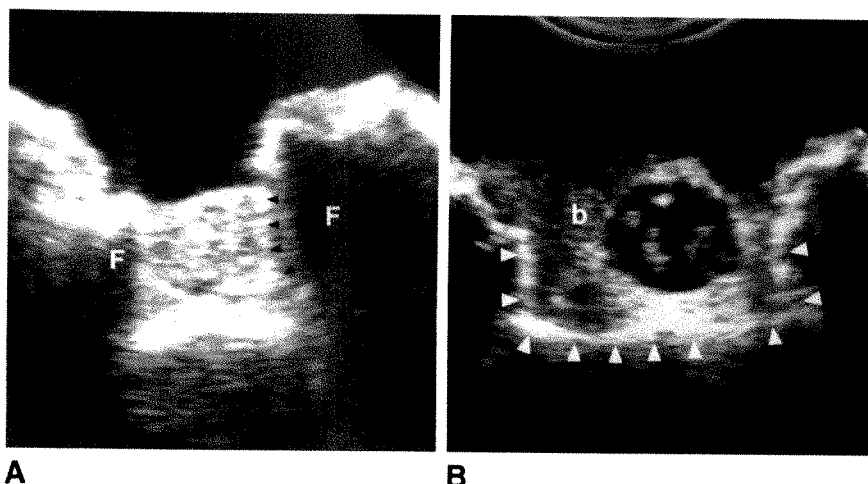
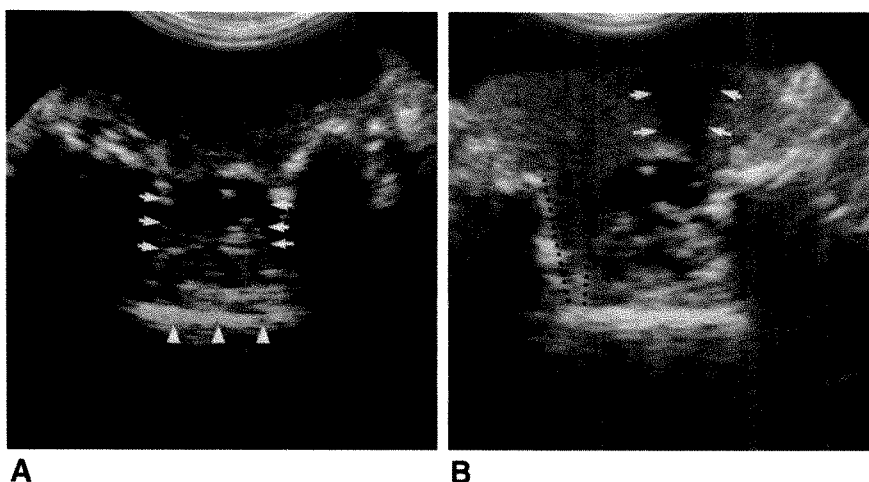


Fig. 14.—Canal stenosis: residual bony compression of thecal sac at multiple levels in a patient with previous surgery. Sonography was performed after bilateral laminectomies and facetectomies in patient with multiple-level canal stenosis.

A, Axial view at L3–L4 shows continuing facet encroachment (arrows) on both lateral aspects of canal. There is no space between edges of facets and thecal sac. Posterior edge of vertebral body (arrowheads). Note that shape of canal is that of a narrow-based rectangle (compare with Fig. 13B).

B, At L4–L5 level there is adequate decompression of left aspect of canal, while right is significantly compressed by facet. Note difference in space between facet on left and thecal sac (between dotted lines) and lack of space in same location on right.

Facetectomies were extended at both levels; final sonogram was interpreted as showing adequate bony decompression at all levels. Blood is filling epidural space on left and is seen layering over dorsal dura on both images. Lucent area within settled blood (between arrows in B) represents active bleeding, a finding appreciated on real-time monitoring of surgical field.



nal structures [6, 8], thus permitting assessment of the spine during surgery. Early experience with sonography in patients with disk disease and canal stenosis suggests intraoperative spinal sonography has a role to play in the surgical management of these cases [7].

Herniated disk material (Figs. 1–3) can be distinguished from surrounding epidural fat, bone, scar tissue, and venous plexus by virtue of its medium echogenicity, its sharp margins, its relationship with the disk space, and its effect on adjacent neural structures. Bone (Fig. 1C) is of higher echogenicity than disk and exhibits dense shadowing. Ventral epidural fat (Figs. 2C and 4B), which may be abundant, has a symmetric distribution, lies directly posterior to the vertebral bodies, and is higher in echogenicity than disk material. Epidural veins (Fig. 5) are of low echogenicity and are most prominent posterior to the midportions of the vertebral bodies rather than at the disk levels. Observing bloodstream echoes in motion in real time permits easy differentiation from disk fragments. Scar tissue (Fig. 6) is of mixed echogenicity and its interface with surrounding tissues is poorly defined, while a herniated disk is sharply defined. The differentiation of

bulging disk material (Fig. 8) from a central disk herniation is difficult with sonography; however, when this problem arises, one can clearly establish the presence or absence of root displacement. Problems do exist in identifying far-lateral disk herniations, that is, those that do not form a silhouette against either the anechoic CSF or adjacent nerve roots.

Pantopaque within the thecal sac forms a fluid level with the CSF, and its characteristic appearance (Fig. 12) can be differentiated from intradural adhesions or aberrantly coursing nerve roots. When intrarachnoid adhesions are present the nerve roots clump together, and whatever remaining CSF there may be is localized in collections within the thecal sac (Fig. 11). If there are adhesions all around the sac, then no CSF may be seen. On real-time evaluation, the typical CSF pulsation is lacking when the arachnoiditis is severe. Knowledge of these sonographic characteristics of normal and abnormal intraspinal structures is crucial when monitoring the progress of spine surgery.

The ability to separate normal structures that occur in the epidural space directly adjacent to the thecal sac from disk material can have important implications in the surgical treat-

ment of disk herniation. Sonography can readily identify the conus medullaris [8] and its relationship to herniated disks or compressing bony structures. The location of the conus may influence the surgical approach to decompression. In our series, residual disk material was identified intraoperatively in 17 of 41 patients examined after routine discectomy (Fig. 1D). It is most likely that such disk fragments would not have been removed at the time of the original surgery. A common cause of failed backs is persistent disk herniation [9]. Whether these patients would have experienced recurrent low-back symptoms had these residual fragments not been removed is, of course, impossible to determine, but obviously the removal of as much abnormal material as possible is desirable.

Frequently in a patient with spondylolisthesis, it is difficult to be certain whether or not there is associated herniated disk material or whether the ventral impression on the thecal sac by disk material is mainly a manifestation of the forward positioning of a vertebral body relative to the disk material below it. Longitudinal sonograms can assist in this important distinction. When spondylolisthesis without disk herniation is present, just the highly echogenic borders of the malaligned vertebral bodies are seen (Figs. 9B and 9C). Conversely, when herniated disk material is present in conjunction with spondylolisthesis, the medium echogenicity of the disk can be identified between the edges of the subluxed vertebra (Fig. 10A). Similarly, when spondylosis causes severe narrowing of the canal it is often difficult to establish preoperatively whether herniated disk material is also present, and longitudinal sonograms are crucial to the diagnosis (Fig. 3). In eight of 10 patients with severe stenosis secondary to spondylosis, sonography was able to establish the presence or absence of disk herniation (Table 2; Figs. 3 and 9C). This has clear implications for the surgical management of such patients because the herniated disk will be removed after the laminectomy but before the lateral bone fusion (Fig. 10B).

When bony decompression of the lumbar canal is being performed either for degenerative spondylosis with secondary canal narrowing or for congenital canal stenosis, sonography provides an immediate evaluation of the effect of the bone on adjacent neural tissue (Figs. 13 and 14). It has been reported that the most common cause of failed backs is failure to recognize or adequately treat lateral stenosis [9]. Sonography can show when sufficient bone (lamina and facets) has been removed to result in a decompressed canal; when this has happened, the sac will assume a rounded configuration (Fig. 13B). However, the sonographic observation that the thecal sac is encroached on either by facets (Figs. 13A and 14) or by ventral spurs may convince the surgeon to extend the facetectomies or to attempt resection of the spur in order to relieve neural compression. In 84 of our patients who underwent bone removal for either generalized or focal canal narrowing, sonography showed residual compression in 19, after what was believed on initial inspection of the surgical field to be adequate bone removal. In 15 of those 19, further bony removal was undertaken to achieve optimal decompression of the canal. In the other four, clinical considerations convinced the surgeon that further surgery was not warranted.

Sonography does not significantly prolong surgical time [10]. An earlier report addressing the issue of time require-

ments in intraoperative neurosonography included a small group of patients with spondylosis and/or herniated disks. The actual scanning time did not exceed 10 min during routine lumbar discectomy or 14 min during bony decompression. Although we have not continued to record scanning times, our impression is that as we gained experience and confidence in interpreting these examinations, time spent during actual scanning uncomplicated cases has decreased. When sonography demonstrates failure of bone decompression or the need to remove residual disk, additional time is required. We believe that the value of the information obtained balances the small amount of operative time involved.

In summary, we have described the sonographic appearance of normal and abnormal structures of the lumbar spinal canal and established diagnostic criteria for herniated disks that enable us to differentiate herniated disk from other structures, such as epidural fat, scar, swollen nerve roots, and spondylolisthesis. We have also established sonographic criteria for complete discectomy and for adequate decompression of canal stenosis. A large percentage of patients who undergo discectomy or have surgery for spinal stenosis have been reported in the literature to have persistent symptoms and significant disability [9]. The observations that 41% of the patients we examined with sonography after discectomy had residual disk fragments and that 23% of the patients we examined after posterolateral decompression for canal stenosis had residual compression lead us to believe that the use of sonography can have a significant impact on the clinical outcome of patients undergoing these types of surgery.

#### ACKNOWLEDGMENTS

We thank Hilda Ceballos, Norma Vera, and Esther Prince for manuscript preparation; Christopher Fletcher for photography; and Isaac Wooten for assistance in the operating room.

#### REFERENCES

1. Quencer RM, Montalvo BM, Green BA, Eismont FJ. Intraoperative spinal sonography of soft-tissue masses of the spinal cord and spinal canal. *AJNR* 1984;5:507-515, *AJR* 1984;143:1307-1315
2. Quencer RM, Montalvo BM, Naidich TP, Post MJD, Green BA, Page LK. Intraoperative sonography in spinal dysraphism and syringohydromyelia. *AJNR* 1987;8:329-337, *AJR* 1987;148:1005-1013
3. Quencer RM, Morse BMM, Green BA, Eismont FJ, Brost P. Intraoperative spinal sonography: adjunct to metrizamide CT in the assessment and surgical decompression of post-traumatic spinal cord cysts. *AJNR* 1984;5:71-79, *AJR* 1984;142:593-601
4. Montalvo BM, Quencer RM, Green BA, Eismont FJ, Brown MJ, Brost P. Intraoperative sonography in spinal trauma. *Radiology* 1984;153:125-134
5. Quencer RM, Montalvo BM, Eismont FJ, Green BA. Intraoperative spinal sonography in thoracic and lumbar fractures: evaluation of Harrington rod instrumentation. *AJNR* 1985;6:353-359, *AJR* 1985;145:343-349
6. Montalvo BM, Quencer RM. Intraoperative sonography in spinal surgery: current state of the art. *Neuroradiology* 1986;28:551-590
7. Gooding GAW, Boggan JE, Weinstein PR. Intraoperative sonography during lumbar laminectomy: work in progress. *AJNR* 1984;5:751-753
8. Quencer RM, Montalvo BM. Normal intraoperative spinal sonography. *AJNR* 1984;5:501-505, *AJR* 1984;143:1301-1305
9. Burton CV, Kirkaldy-Willis WH, Yong-Hing K, Heithoff KB. Causes of failure of surgery on the lumbar spine. *Clin Orthop* 1981;157:191-199
10. Quencer RM, Montalvo BM. Time requirements for intraoperative neurosonography. *AJNR* 1986;7:155-158

# Primary Cerebral Neuroblastoma: CT and MR Findings in 12 Cases

P. C. Davis<sup>1</sup>  
R. D. Wichman  
Y. Takei  
J. C. Hoffman, Jr.

A retrospective CT, MR, and clinical study was performed in 12 patients, five children and seven adults, with histologically proved primary CNS neuroblastoma. The CT and MR appearances of this neoplasia were more variable than generally recognized. Although seven tumors were predominantly intraparenchymal masses with calcification and cyst formation, five were intra- or juxtaventricular. CT was preferable to noncontrast MR both at initial diagnosis and follow-up for identification of calcification, recurrent tumor at surgical sites, and leptomeningeal disease. Noncontrast MR was useful primarily for localization of peri- and intraventricular lesions.

We conclude that primary CNS neuroblastoma has a more variable radiographic appearance than is generally recognized, and that an intra- or periventricular epicenter is common.

*AJNR* 11:115–120, January/February 1990; *AJR* 154:831–836, April 1990

Primary cerebral neuroblastoma is a rare neoplasm typically described in children as a large intraparenchymal supratentorial mass frequently containing cysts, calcification, and spontaneous hemorrhage [1–10]. This tumor is generally considered to be a specific subset of primitive neuroectodermal tumors, although neuropathologic controversy exists. Detailed electron microscopy may be required for the exact diagnosis. These tumors are malignant lesions with a high rate of recurrence after therapy and frequent subarachnoid metastases. Our experience indicates that primary CNS neuroblastoma has a broader spectrum in presentation, age of onset, location, and radiographic appearance than is generally recognized. We report our experience with primary cerebral neuroblastoma in 12 patients and describe its CT and MR characteristics with clinical, surgical, and histological correlation.

## Materials and Methods

From August 1979 to August 1988, 12 patients (six females, six males) with primary cerebral neuroblastomas were identified. Those with ganglioneuromas, esthesioneuroblastomas, or metastatic neuroblastomas from an extracranial primary had been excluded from the present study. The study group comprised five children 15 days to 9 years old and seven adults 19–52 years old. All tumors were histologically proved (one by CT-directed brain biopsy, one by open biopsy, and 10 by surgical resection). All surgical resections were reported as subtotal with removal of 50–95% of the tumor. Three adult patients have been reported previously [11, 12].

Pathologic criteria used in this study for diagnosis of primary cerebral neuroblastoma included identification of a cellular tumor comprising small hyperchromatic cells in a fine fibrillary background with occasional Homer-Wright rosettes. Ultrastructurally, these tumors have neural process formation with intracytoplasmic microtubules and dense core granules [6–8]. Occasionally, synaptic formations are present (Fig. 1) [11–15].

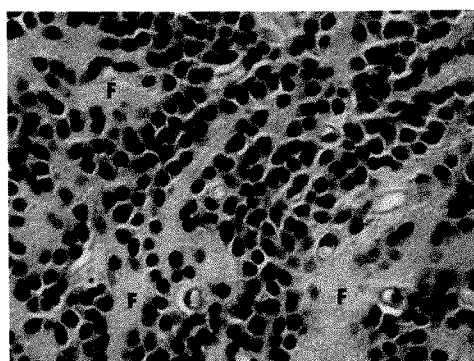
A retrospective chart review made note of presenting signs and symptoms, tumor location, mode of tumor spread, therapies used, and progression of disease. These findings are summarized in Table 1.

Received August 12, 1988; revision requested October 11, 1988; final revision received June 5, 1989; accepted June 7, 1989.

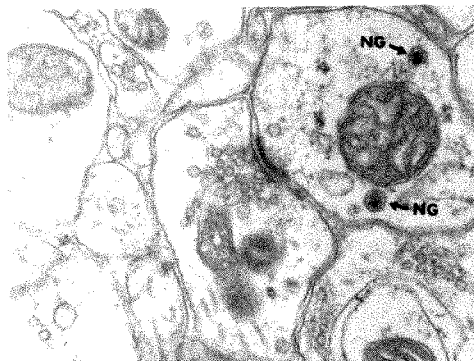
<sup>1</sup> All authors: Department of Radiology, Section of Neuroradiology, Emory University School of Medicine, 1364 Clifton Rd. N.E., Atlanta, GA 30322. Address reprint requests to P. C. Davis.

0361-803X/90/1544-0831  
© American Roentgen Ray Society





A



B

Fig. 1.—A, Case 3: Small cells are arranged within fine fibrillary background (F). In this field, neuroepithelial character of tumor is well maintained. (H and E,  $\times 500$ )

B, Case 2: Well-formed synapse (center) and neurosecretory granules (NG) are ultrastructural features of well-differentiated neuronal neoplasm. (Electron microscopy,  $\times 24,500$ )

TABLE 1: Profile of Patients with Primary Cerebral Neuroblastomas

Case No.	Age	Sex	Presenting Symptoms and Signs	Location	CSF Seeding	Follow-up	Therapy
1	32	F	Seizures, R arm weakness	L frontal & temporal	—	Deceased 2 d postop	Surgery
2	20	F	Ataxia, increased intracranial pressure, R arm hyperesthesia	L lateral ventricle	—	Progressive mass effect; ?radiation necrosis (3¾ yr)	Surgery, radiation
3	23	M	Headaches & decreased vision, OS; von Hippel-Lindau disease	L lateral ventricle	—	Stable with residual tumor (6½ yr)	Surgery, radiation
4	52	F	Dizziness, incoordination, R hyperreflexia	L lateral ventricle	Positive CSF cytology (3 yr)	Residual tumor (3 yr)	Surgery, radiation
5	34	M	Increased intracranial pressure, R hemiparesis	L frontal lobe	—	Extensive recurrence, terminal (1¼ yr)	Surgery, radiation
6	4	F	Increased intracranial pressure, stiff neck	R frontal & parietal	Spinal & cranial seeding (2½ yr)	Deceased (2½ yr)	Surgery, radiation, & chemotherapy
7	1	M	Seizures, gait disorder	L parietal	—	Stable (3 yr); no recurrence, no residual tumor	Surgery, chemotherapy
8	2	M	L hemiparesis, macrocephaly	R frontal & temporal	—	Residual tumor; stable (2¼ yr)	Surgery, chemotherapy, radiation
9	19	M	Increased intracranial pressure, gait difficulty	Third ventricle	—	Lost to follow-up (7 wk)	CT biopsy
10	9	M	Increased intracranial pressure	All ventricles with subarachnoid seeding	At time of diagnosis & recurrence of spinal & periventricular seeding (2¾ yr)	Deceased (2¾ yr)	Biopsy, radiation, & chemotherapy
11	29	F	Seizures	R frontal lobe & R lateral ventricle	Nodule, R lateral ventricle, at diagnosis	Stable with residual tumor (6 mo)	Surgery, radiation, & chemotherapy
12	2 wk	F	Vomiting, macrocephaly	R temporal, occipital, and parietal	—	Stable with marked developmental delay (2½ yr)	Surgery, chemotherapy

Note.—R = right; L = left; OS = left eye.

All patients had CT scans before and after therapeutic intervention. Axial CT scans with IV contrast material and 4- to 10-mm collimation were completed preoperatively in all patients. In addition, seven patients had noncontrast CT. One patient died 2 days after surgical resection and one was lost to follow-up 7 weeks after diagnosis. Mean follow-up was 2.3 years (range, 2 days to 6½ years). Four patients died during the period of study, with a mean survival from time of diagnosis in these patients of 1.4 years (range, 2 days to 2¾ years).

Three patients had MR examinations before therapy and five patients had follow-up MR examinations. MR examinations were performed with a 0.5-T superconducting magnet (Philips Gyroscan) using a standard head coil (23 cm). MR examinations were completed with T1-weighted, 500–750/30–50 (TR/TE), or inversion-recovery, 1700/700/30 (TR/T1/TE), and double-echo T2-weighted, 2000–2215/30,60 or 2000–2215/50,100, techniques. Axial-plane imaging with 10-mm slices was initially performed with subsequent coronal and/or sagittal images based on the location of pathology encountered. IV

gadolinium-DTPA (0.1 mg/kg, Berlex, Inc.) studies were performed in two patients: one during a phase III drug evaluation after informed consent was obtained and one after Food and Drug Administration approval.

CT and MR examinations performed before, during, and after therapy were evaluated for tumor size, epicenter, proximity to the ventricular system, and tumor characteristics (edema, mass effect/hydrocephalus, hemorrhage, calcifications, cyst formation, seeding, response to therapy, and sequelae of therapy).

## Results

Clinical data, location of tumor, therapy administered, and duration of follow-up are summarized in Table 1.

The "typical" CT imaging appearance previously reported for primary neuroblastoma [1-5]—a large intraparenchymal calcified and cystic mass often with spontaneous hemorrhage and little edema relative to the size of the lesion—was encountered in seven patients (three children, four adults; Fig. 2). These tumors were approximately 3-10 cm in diameter. In four cases the epicenter of the tumor was intraparenchymal but the tumor extended medially to abut the lateral ventricular margin.

With CT, two tumors contained calcifications, three hemorrhaged spontaneously, and two resulted in hydrocephalus. After IV contrast enhancement, these masses enhanced inhomogeneously. One patient with a primary neuroblastoma of the frontal lobe near a site of meningioma resection 11 years before had a focal subependymal metastasis at the time of diagnosis. Cystic-appearing areas were apparent in six patients and mild peritumoral edema in two.

Preoperative MR in two patients revealed an intraparenchymal mass with inhomogeneous intensity patterns on both T1- and T2-weighted studies. Differentiation among dense calcification, flow void, and hemosiderin was difficult with MR. Smaller and less dense calcifications were not recognized. Cystic areas seen on CT were difficult to distinguish from the remainder of the tumor on MR. Mild peritumoral edema was present in one patient. Spontaneous hemorrhage resulted in intratumoral and intraventricular regions of high signal intensity, presumably due to methemoglobin on T1-weighted studies (case 6, Fig. 2).

Five patients (two children, three adults) had primary tumors with an intra- and/or periventricular epicenter, and four had secondary hydrocephalus. Tumor size was difficult to assess in this group, but was estimated as 1-6 cm in maximum diameter.

On CT, four masses contained calcification, one had extensive subarachnoid seeding at presentation (Fig. 3), and none hemorrhaged spontaneously. Enhancement after IV contrast administration occurred on CT in all cases.

Preoperative MR was useful for better localization of intraventricular tumor with sagittal and coronal imaging; however, areas of low signal intensity from calcification, flow void, and prior hemorrhage were indistinguishable. T1-weighted gadolinium follow-up studies in two patients resulted in greater contrast between tumor and normal brain (Fig. 4).

A brief profile of therapy and disease progress is given in Table 1. Of the seven patients with typical intraparenchymal lesions, one was stable without evidence of recurrent or

residual tumor. The others had residual and/or recurrent tumor. In this group, as expected, neoplasia was better differentiated from postsurgical gliosis and cysts/necrosis (Fig. 5) with contrast-enhanced CT than with noncontrast MR. In one patient who developed leptomeningeal seeding, contrast-enhanced CT revealed more intracranial disease than MR did; however, MR noninvasively revealed characteristic lesions of spinal seeding (Figs. 2E and 2F).

Of the five patients with intra- and periventricular lesions, one was lost to follow-up after 7 weeks; one initially responded well to radiation therapy, but subsequently succumbed to recurrent leptomeningeal disease; one had progressive edema thought to represent radiation necrosis; and two were stable with residual tumor (two patients) and leptomeningeal seeding (one patient).

Tumor size and location were the predominant factors influencing surgical resectability. No significant differences were apparent in adults compared with children in survival or tumor aggressiveness in this small series. No distant metastases or extension outside the CNS were documented.

## Discussion

Primary CNS neuroblastoma often is considered a subset of primitive neuroectodermal tumors, although this categorization is controversial. Russell and Rubinstein [15] suggest that this classification is misleading since it combines a histologically inhomogeneous group of tumors as if they were pathologically indistinguishable. This broad classification was suggested in 1973 [16] as a descriptive term for predominantly undifferentiated, or at times undiagnosed supratentorial tumors in children, which microscopically (without electron microscopy) were thought to originate from the primitive neural tube. These were malignant, often cystic, compressed adjacent brain, and could exhibit foci of glial and/or neuronal differentiation. The primitive neuroectodermal tumor group includes medulloblastoma, medulloepithelioma, neuroblastoma, spongioblastoma, ependymblastoma, and pineoblastoma [14]. Horten and Rubinstein [6], however, suggested that primary cerebral neuroblastoma is a nosologic entity distinct from primitive neuroectodermal tumors and characterized by (1) a cellular tumor of neuronal origin, without glial differentiation; (2) the presence of a fine fibrillary matrix of axonal material; (3) occasional differentiation to mature ganglion cells; and (4) the frequent exhibition of well-formed Homer-Wright rosettes. On electron microscopy, recognition of neurosecretory granules allows a precise diagnosis [17].

Previously published radiologic studies describe the typical primary CNS neuroblastoma as an intraparenchymal, supratentorial mass with little associated edema occurring in a child. Calcification, cyst formation, and spontaneous hemorrhage are common at presentation [1-5], and subarachnoid tumor seeding is a frequent sequela.

In our series, the age of onset and radiologic appearances of the lesion were more variable than previously recognized: A periventricular and/or intraventricular epicenter was common both in children and in adults, occurring in five of 12 patients. In addition, four of seven tumors that were predominantly intraparenchymal abutted a ventricular margin. Spon-

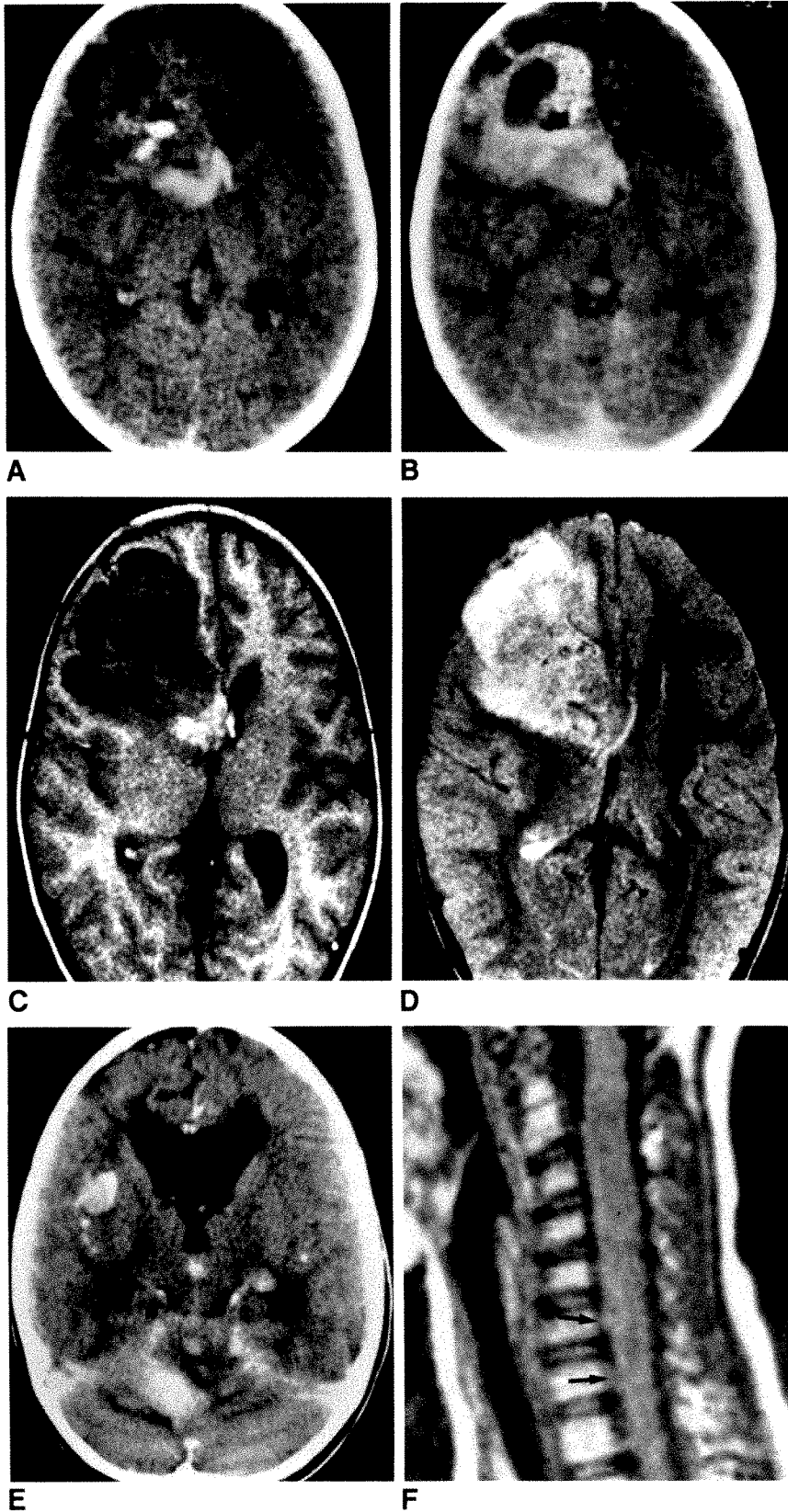


Fig. 2.—Case 6: Primary CNS neuroblastoma in 4-year-old girl with spontaneous intratumoral and intraventricular hemorrhage.

A, Nonenhanced CT scan shows intratumoral calcifications and cyst formation with hematoma at foramen of Munro.

B, Contrast-enhanced CT scan shows marked tumor enhancement with relatively little adjacent edema.

C, T1-weighted MR image, 500/30 (0.5 T), shows primarily hypodense inhomogeneous tumor with increased signal intensity in hematoma adjacent to foramen of Munro.

D, Proton-density-weighted MR image, 2000/30, shows predominantly increased signal intensity throughout lesion with focal curvilinear areas of hypointensity corresponding to calcifications seen on nonenhanced CT.

E, 2½ years after extensive surgical resection, radiation, and chemotherapy, substantial nausea, vomiting, and headache developed abruptly, followed by coma. Contrast-enhanced CT scan shows leptomeningeal seeding.

F, Cervical-spine MR image, 500/30 (0.5 T), shows poorly defined nodules in subarachnoid space (arrows) compatible with seeding. In addition, irregularly enlarged cervical spinal cord suggests seeding on cord surface.

Fig. 3.—Case 10: 9-year-old boy.

A and B, Adjacent contrast-enhanced CT scans at presentation reveal marked enhancing and calcified periventricular neoplasia with subarachnoid seeding. No hemorrhage was recognized clinically or on non-enhanced CT.

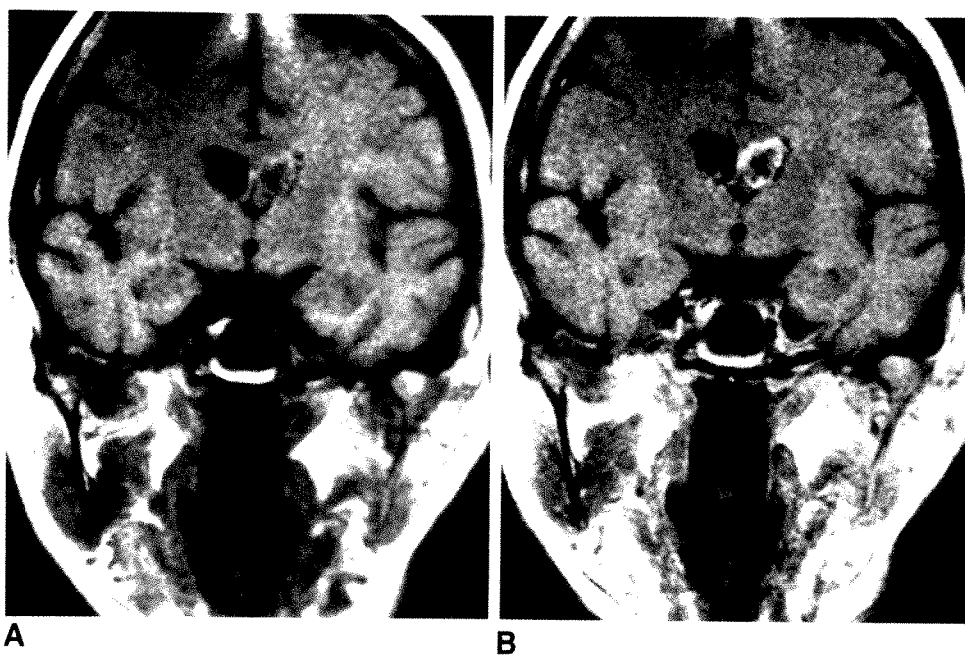
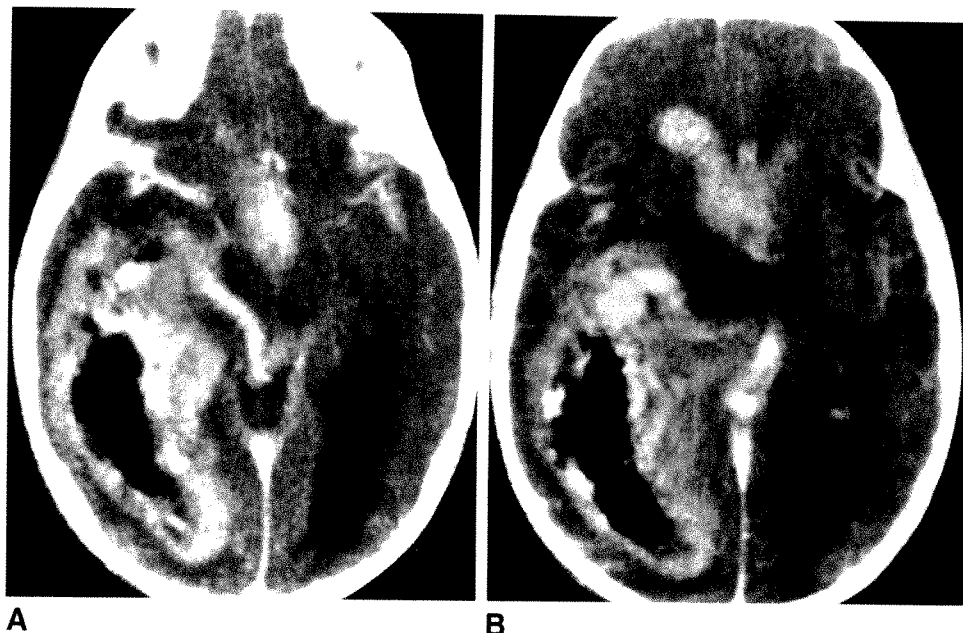


Fig. 4.—Case 4: 52-year-old woman. A and B, Pre- (A) and post- (B) gadolinium-DTPA MR images, 550/30 (0.5 T), reveal peripheral enhancement of intraventricular primary CNS neuroblastoma.

taneous hemorrhage occurred only in predominantly intraparenchymal masses, but this may be a reflection of sample size. Misdiagnoses were common preoperatively, owing to the nonspecific CT and MR appearances and, perhaps, to the rarity of this tumor. Differential diagnoses considered in our cases included oligodendroglioma, astrocytoma, meningioma, ependymoma, and other primitive neuroectodermal tumors.

Pre- and postcontrast CT was the best available imaging technique for preoperative evaluation and follow-up of these lesions during this study. Calcifications were seen better on CT than on standard MR pulse sequences, and subarachnoid and periventricular seeding were inconspicuous on noncontrast MR. Contrast enhancement was essential for detection

of subtle tumor recurrence around cystic masses; these areas of recurrence were not detectable on noncontrast MR. Gadolinium-enhanced MR and contrast-enhanced CT both demonstrate areas of blood-brain barrier disruption from tumor progression, although with either technique there is the potential for radiation necrosis, postsurgical enhancement, or superimposed infection to mimic tumor recurrence.

Noncontrast MR was not essential, and was primarily used as an ancillary technique for multiplanar localization of peri- and intraventricular lesions. Superficial and/or cortical masses were visible without artifact from the adjacent calvarium, but areas of abnormal signal intensity due to prior surgery and/or radiation therapy mimicked recurrent or residual neoplasia.

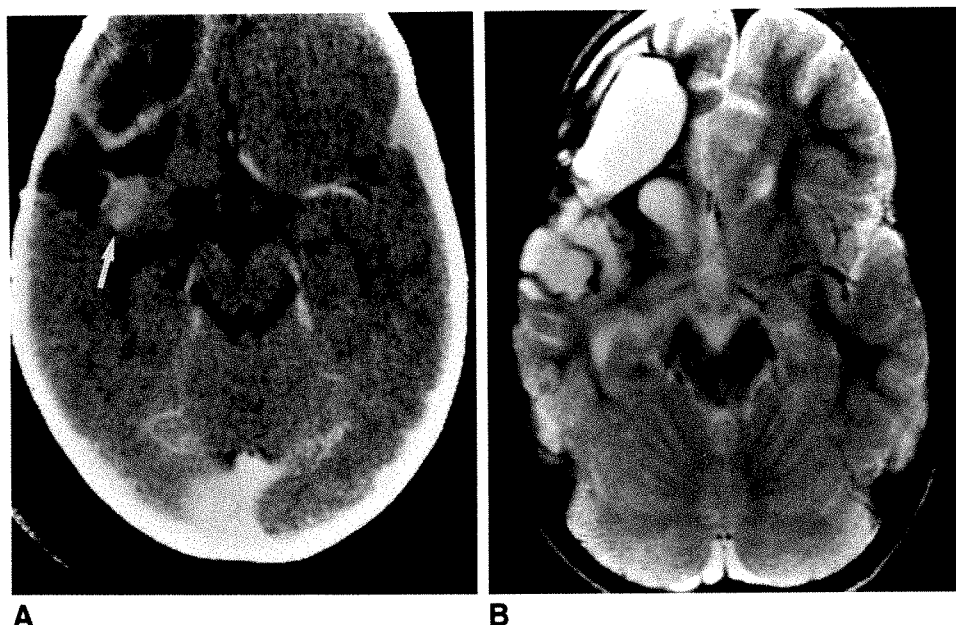


Fig. 5.—Case 8: 2-year-old boy with prior surgical resection.

A, Residual tumor adjacent to cyst (arrow) is seen on contrast-enhanced CT scan.

B, MR image, 2000/100 (0.5 T), 3 months later. Residual tumor and cyst are difficult to differentiate. Subsequent contrast-enhanced CT revealed shrinkage of enhancing mass indicative of response to interval chemotherapy.

MR contrast agents were not widely available during this study, particularly for children, but they have been shown to improve the accuracy of MR for leptomeningeal and recurrent tumors [18–20] and for evaluation of postoperative sites.

In summary, the CT and MR appearances of primary cerebral neuroblastoma are more variable than previously recognized. In our series, peri- and intraventricular lesions were frequent. CT was preferable to noncontrast MR both at initial diagnosis and on follow-up of these lesions owing to its sensitivity in demonstrating calcification and leptomeningeal disease. Contrast-enhanced CT was superior to noncontrast MR for differentiation of recurrent and residual neoplasia from sequelae of therapy, although, potentially, postsurgical enhancement or radiation necrosis might have a similar appearance. Multiplanar MR imaging was helpful primarily for localization of peri- and intraventricular lesions; MR contrast agents were essential for revealing tumor recurrence around cysts and at surgical sites and for leptomeningeal seeding. Primary CNS neuroblastoma has no pathognomonic appearance on CT or MR; thus, it should be considered in the differential diagnosis of intraparenchymal or juxtaventricular masses. Our experience has been that histopathological confirmation is required for definitive diagnosis. Primary cerebral neuroblastoma is an aggressive tumor with a relatively poor prognosis owing to local tumor recurrence and leptomeningeal seeding.

#### ACKNOWLEDGMENTS

We thank J. Mizuno for research assistance, Roz Vecchio for photography, and Francine Hollowell for manuscript preparation.

#### REFERENCES

- Chambers EF, Turski PA, Sobel D, Wara W, Newton TH. Radiologic characteristics of primary cerebral neuroblastomas. *Radiology* 1981;139:101–104
- Zimmerman RA, Bilaniuk LT. CT of primary and secondary craniocerebral neuroblastoma. *AJR* 1980;135:1239–1242
- Berger MS, Edwards MS, Warer WM, Lavin VA, Wilson CB. Primary cerebral neuroblastoma. Long term follow-up, review and therapeutic guidelines. *J Neurosurg* 1983;59:418–423
- Armstrong EA, Harwood-Nash DCF, Ritz CR, Chuang SH, Pettersson H, Martin DJ. CT of neuroblastomas and ganglioneuromas in children. *AJR* 1982;139:571–576
- Latchaw RE, L'Heureux PR, Yong G, Priest JR. Neuroblastoma presenting as central nervous system disease. *AJNR* 1982;3:623–630
- Horten BC, Rubinstein LJ. Primary cerebral neuroblastoma. A clinicopathological study of 35 cases. *Brain* 1976;99:735–756
- Azzarelli B, Richards DE, Anton AH, Roessmann U. Central neuroblastoma: electron microscopic observations and catecholamine determinations. *J Neuropathol Exp Neurol* 1977;36:384–397
- Bennett JP, Rubinstein LJ. The biological behavior of primary cerebral neuroblastoma: a reappraisal of the clinical course in a series of 70 cases. *Ann Neurol* 1984;16:21–27
- Kingsley DPE, Harwood-Nash DCF. Radiological features of the neuroectodermal tumors of childhood. *Neuroradiology* 1984;26:463–467
- Altman N, Fitz CR, Chuang S, Harwood-Nash D, Cotter C, Armstrong D. Radiologic characteristics of primitive neuroectodermal tumors in children. *AJNR* 1985;6:15–18
- Pearl GS, Takei Y, Stephanis GS, Hoffman JC. Intraventricular neuroblastoma in a patient with von Hippel-Lindau's disease—light and electron microscopic study. *Acta Neuropathol (Berl)* 1981;53:253–256
- Pearl GS, Takei Y, Bakay FAE, Davis PC. Intraventricular primary cerebral neuroblastoma in adults: report of three cases. *Neurosurgery* 1985;16:847–849
- Kosnick EJ, Boesel CP, Bay J, Sayers MP. Primitive neuroectodermal tumors of the central nervous system in children. *J Neurosurg* 1978;48:741–746
- McComb RD, Burger PC. Pathologic analysis of primary brain tumors. *Neurol Clin* 1985;3:711–728
- Russell DS, Rubinstein LJ. *Pathology of tumors of the nervous system*, 5th ed. Baltimore: Williams & Wilkins, 1989:279–289
- Hart MN, Earle KM. Primitive neuroectodermal tumors of the brain in children. *Cancer* 1973;32:890–897
- Zulch KJ. *Brain tumors: their biology and pathology*, 3d ed. Berlin: Springer-Verlag, 1986:301–306
- Claussen C, Laniado M, Schorner W, et al. Gadolinium-DTPA in MR imaging of glioblastomas and intracranial metastases. *AJNR* 1985;6:669–674
- Felix R, Schorner W, Laniado M, et al. Brain tumors: MR imaging with gadolinium-DTPA. *Radiology* 1985;156:681–688
- Frank JA, Garton M, Dwyer AJ, Wright DC, Cohen PJ, Doppman JL. Meningeal carcinomatosis in the VX2 rabbit tumor model: detection with Gd-DTPA-enhanced MR imaging. *Radiology* 1988;167:825–829

# Intracranial Ependymoma and Subependymoma: MR Manifestations

Gary P. Spoto<sup>1</sup>  
 Gary A. Press<sup>1</sup>  
 John R. Hesselink<sup>1</sup>  
 Murray Solomon<sup>2</sup>

In order to provide a detailed description of the MR appearance of intracranial ependymoma, the MR examinations of 12 patients (10 with ependymomas and two with subependymomas) were reviewed and correlated with operative and pathologic reports. Three of 10 ependymomas were intraventricular, two were intraparenchymal, and five were transependymal, extending from CSF spaces into parenchyma. Both subependymomas were intraventricular. Solid ependymomas and subependymomas were iso- to hypointense relative to normal white matter on T1-weighted images and hyperintense on proton-density- and T2-weighted images. Foci of signal heterogeneity within solid neoplasms represented methemoglobin, hemosiderin, necrosis, calcification, and encased native vessels or tumor vascularity. Gd-DTPA-enhanced images in two patients differentiated enhancing tumor from surrounding nonenhancing edema and from surrounding normal brain parenchyma. Cystic neoplasms had sharply defined, round or oval margins and uniform signal intensity equivalent to or slightly hyperintense relative to CSF. Tumor-associated calcification was not demonstrated readily by MR. Sagittal and coronal images were valuable in assessing the amount of intraventricular tumor and route of extension.

We conclude that the MR differentiation of ependymomas and subependymomas from other gliomas is provided most reliably by the location and morphology of the tumor and not by differences in signal intensity. The typical ependymoma arises within the fourth ventricle as a solid mass with heterogeneous signal intensity. A propensity for spread is seen along the CSF pathways via the foramina of Magendie and Luschka and the aqueduct of Sylvius. Supratentorial ependymomas may be periventricular in location and have cystic components. The two subependymomas in our series were solid, intraventricular tumors with relatively homogeneous signal intensities.

*AJNR* 11:83-91, January/February 1990; *AJR* 154:837-845, April 1990

The appearance of intracranial ependymoma and subependymoma, although well characterized on CT [1-3], has not been described in detail on MR. To our knowledge, the MR findings of ependymoma have been reported in only a few cases, as part of larger series of intracranial neoplasms [4-8]; there is only one prior report on the MR manifestations of subependymoma [9].

We correlated the MR findings with operative and pathologic reports in 10 patients with proved intracranial ependymomas and two patients with subependymomas. The appearance of ependymoma at low (0.35 T) and high (1.5 T) field strengths is described.

## Materials and Methods

We reviewed 14 MR studies of 10 patients with intracranial ependymomas and two patients with subependymomas. The operative and pathologic reports and hospital and outpatient records were available for all but two patients; these clinical data were correlated with the MR findings. The patients ranged in age from 1.2 to 59.0 years (mean, 23.6 years). There were six females and six males. MR examinations performed at initial presentation were

Received January 25, 1989; revision requested March 29, 1989; revision received June 29, 1989; accepted July 10, 1989.

<sup>1</sup> Department of Radiology and Magnetic Resonance Institute, University of California, San Diego, School of Medicine, 225 Dickinson St., San Diego, CA 92103. Address reprint requests to G. A. Press.

<sup>2</sup> Los Gatos MRI Center, 800 Pollard Rd., Los Gatos, CA 95030.

0361-803X/90/1544-0837  
 © American Roentgen Ray Society



available in seven patients. Two of these patients were imaged again postoperatively (Table 1); one (case 7) was reexamined 12 days after surgical debulking; the other (case 4) was restudied at the time of recurrence, 11 months after surgery. In the other five patients, MR was performed at the time of recurrence. Nine examinations were performed at 1.5 T; five studies were performed at 0.35 T.

Spin-echo images acquired at 1.5 T (General Electric, Milwaukee) were 3–5 mm thick and usually had a  $256 \times 256$  matrix. In one examination (case 6), a  $128 \times 128$  matrix was used in one sequence; in two others (cases 1 and 7) a rectangular pixel ( $256 \times 128$  matrix) was used in some sequences. Consecutive slices were separated by a 1.0- or 2.5-mm gap. T1-weighted images, 600–900/20–25/2 (TR/TE/excitations), proton-density-weighted images, 1500–3000/20–35/2, and T2-weighted images, 1500–3000/60–80/2, were obtained in all patients. The sequences with a rectangular pixel used only one excitation. Images were acquired in the axial plane in each examination (T1-weighted in four, proton-density, and T2-weighted in eight); sagittal images were obtained in eight studies (T1-weighted in eight, proton-density- and T2-weighted in one); coronal proton-density and T2-weighted images were obtained in two examinations. Gadolinium-DTPA (Gd-DTPA)-enhanced images were obtained in two patients (cases 7 and 11). In case 7, Gd-DTPA was administered during the postoperative MR examination only.

MR images acquired at 0.35 T (Diasonics, San Francisco) were 10 mm thick and had a  $256 \times 256$  matrix in all cases. Consecutive slices were separated by a 0- or 1.0-mm interslice gap. T1-weighted images (500/28–30/2) were obtained in four examinations; a TR of 1000 was used in one study. Proton-density-weighted (1500–2500/28–30/2) and T2-weighted (1500–2500/56–60/2) images were acquired in each examination. One examination included a partial-flip-angle sequence, 500/30/30° (TR/TE/flip angle). In addition to axial images acquired in each study (T1-weighted in four, proton-density- and T2-weighted in four), sagittal images were obtained in three (T1-weighted

in two, proton-density- and T2-weighted in two) and coronal images were obtained in two examinations (proton-density-weighted in two and T2-weighted in one).

CT (General Electric 9800, Milwaukee) also was performed in six patients. In these patients, MR and CT were compared to determine their relative sensitivities for the detection of intratumoral calcification. Axial 10-mm-thick CT slices from the foramen magnum to the vertex were obtained both before and after administration of IV contrast material (iothalamate meglumine, Conray 60, Mallinckrodt, St. Louis) in each instance.

## Results

Of 10 ependymomas, six were infratentorial and four were supratentorial. One subependymoma was supratentorial, the other infratentorial (Table 1). Only three of the 10 ependymomas were entirely intraventricular (cases 4, 5, and 9). Two of the supratentorial ependymomas (cases 8 and 10) were entirely intraparenchymal. Five "transependymal" neoplasms (cases 1–3, 6, and 7) arose within the ventricular system but breached the ependymal lining to invade the surrounding parenchyma (Fig. 1). Both subependymomas (cases 11 and 12) were entirely intraventricular.

MR demonstrated well the routes of extension of the partially or completely intraventricular neoplasms. Three supratentorial tumors (two ependymomas, one subependymoma) extended from the lateral to the third ventricle by traversing the foramen of Monro (Figs. 2 and 3). Four infratentorial ependymomas (cases 3, 4, 6, and 7) extended from the fourth ventricle to the cerebellopontine angle cistern through a

TABLE 1: MR Findings in 12 Patients with Intracranial Ependymoma and Subependymoma

Tumor/Case No.	Age (years)	Sex	Primary vs Recurrent	Location	Consistency	Signal Intensity of Solid Tumor Relative to White Matter			Signal Intensity Heterogeneity	Margins		Edema
						T1W	PDW	T2W		T1W	T2W	
Ependymoma												
1	1.2	F	Primary	IT, T	Solid	—	+	+	Yes	Mod	Well	No
2	3.8	M	Recurrent	IT, T	Solid	—	+	+	No	Poor	Mod	Yes
3	6.2	F	Primary	IT, T	Solid	—	+	+	No	Poor	Mod	No
4 <sup>a</sup>	5.3	F	Primary	IT, IV	Solid	=/—	+	+	Yes	Mod	Well	Yes
	6.2		Recurrent	IT, IV	Solid	=/—	+	+	Yes	Mod	Well	Yes
5	9.0	M	Recurrent	ST, IV	Solid	=/—	+	+	Yes	Well	Well	No
6	35.0	F	Recurrent	IT, T	Solid	—	+	+	Yes	Well	Well	No
7 <sup>b</sup>	59.0	M	Primary	IT, T	Solid	—	+	+	No	Poor	Well	No
				IT, T	Solid	—	+	+	No	Mod	Well	No
8	8.3	M	Primary	ST, IP	Mixed	NA	+	+	No	Well	Well	No
9	25.4	F	Recurrent	ST, IV	Solid	=/—	+	+	No	Poor	Mod	No
10	37.0	F	Primary	ST, IP	Mixed	=/—	NA	+	No	Poor	Poor	Yes
Subependymoma												
11	37.0	M	Recurrent	ST, IV	Solid	—	+	+	Yes	Well	Poor	Yes
12	55.5	M	Primary	IT, IV	Solid	—	+	+	No	Poor	Well	No

Note.—T1W = T1-weighted images; PDW = proton-density-weighted images; T2W = T2-weighted images; IT = infratentorial; T = transependymal; IV = intraventricular; ST = supratentorial; IP = intraparenchymal; — = hypointense; + = hyperintense; = represents isointense; mixed = solid and cystic components; NA = not available. Margins were moderately well (mod), poorly (poor), or well delineated (well).

<sup>a</sup> Examination was repeated at time of recurrence.

<sup>b</sup> Examination was repeated 12 days after surgery.

Fig. 1.—Case 6: 35-year-old woman with solid, infratentorial, transependymal ependymoma; postoperative MR studies are at 1.5 T.

A and B, T1-weighted, 600/25 (A), and axial T2-weighted, 2000/70 (B), images show tumor (T) arising within fourth ventricle (V) and extending posterolaterally to involve left cerebellar hemisphere and anterolaterally into left cerebellopontine angle cistern via grossly widened lateral recess of fourth ventricle and foramen of Luschka (arrows). Tumor extends inferiorly through foramen magnum into upper cervical canal (A). Cervical cord (c) is displaced posteriorly by tumor. Lateral ventricle (L) is dilated owing to hydrocephalus. Multiple foci of increased and decreased signal intensity within neoplasm correspond to foci of subacute hemorrhage, hemosiderin, and vessels described in pathology report. Postsurgical encephalocele (E) is present.

C and D, T1-weighted image, 800/25 (C), corresponds to CT image (D). Punctate calcification (arrowhead, D) at periphery of neoplasm, seen well on CT, was recognized on MR image only in retrospect (arrowhead, C) as a region of nonspecific hypointensity.

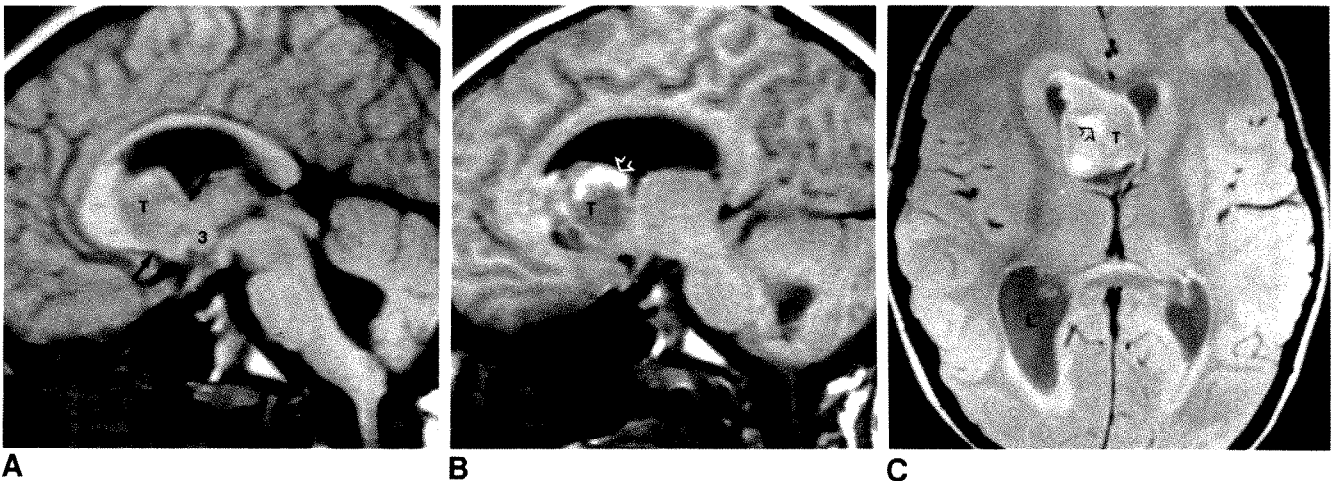
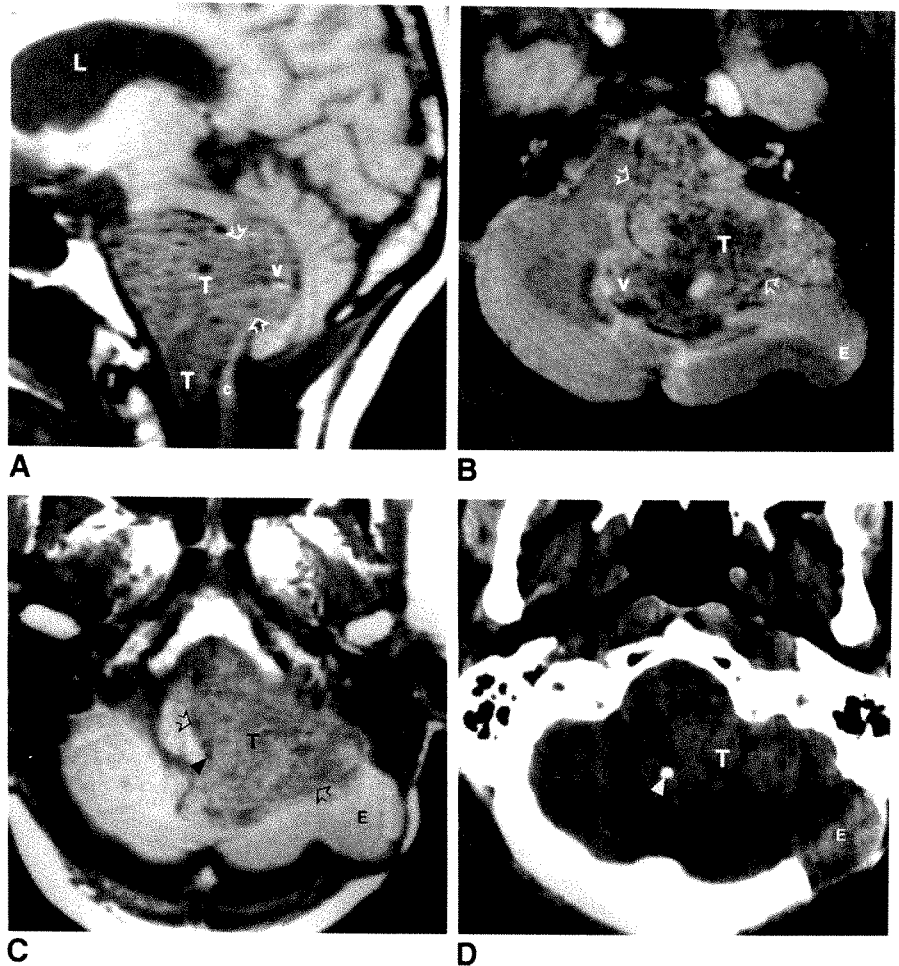


Fig. 2.—Case 5: 9-year-old boy with solid, supratentorial, intraventricular ependymoma.

A and B, T1-weighted, 600/25 (A and B), and axial proton-density-weighted, 2000/20 (C), postoperative images at 1.5 T show solid neoplasm (T) located within third ventricle (3, A) and anterior horns of both lateral ventricles (C) traversing foramen of Monro (solid arrows). Areas of greatest hyperintensity within tumor (open arrows) represent subacute hemorrhage. Dilated lateral ventricles (L) indicate hydrocephalus.

greatly enlarged lateral recess of the fourth ventricle and foramen of Luschka (Figs 1, 4, and 9). These four tumors also extended caudally via the foramen of Magendie and foramen magnum, impinging on the upper cervical spinal cord.

A subependymoma originating from the fourth ventricle extended superiorly within the aqueduct of Sylvius (Fig. 6). Sagittal and coronal images were important adjuncts to axial images in assessing these routes of tumor spread.

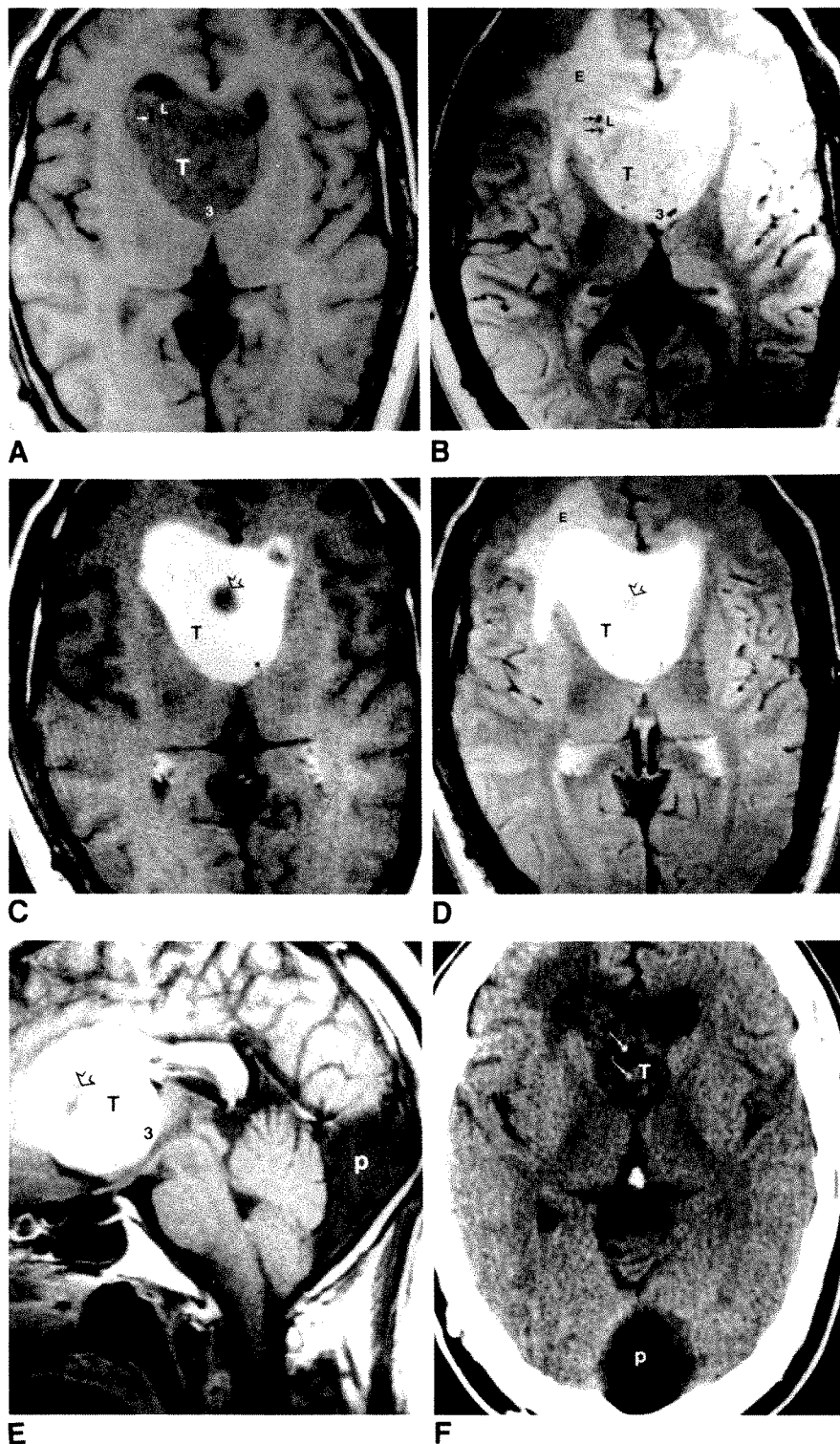


Fig. 3.—Case 11: 37-year-old man with solid, supratentorial subependymoma; postoperative MR studies are at 1.5 T.

A and B, Axial, noncontrast T1-weighted, 600/25 (A), and proton-density-weighted, 2000/25 (B), images show solid tumor (T) within lateral (L) and third (3) ventricles traversing foramen of Monro. Two small foci of signal void (arrows) within tumor most likely represent vessels. Note that tumor has signal intensity similar to that of edema (E) in forceps minor on long TR image (B).

C–E, Axial T1-weighted, 600/25 (C), axial proton-density-weighted 1500/30 (D), and sagittal T1-weighted, 600/25 (E), images after IV Gd-DTPA administration show marked enhancement of tumor. This enhancement clearly demarcates neoplasm from surrounding edema that obscured its margins on precontrast, long TR image (compare B and D). Central nonenhancing focus likely represents cystic change (arrows) not detected on precontrast images. Apparent contrast enhancement in anterior portion of corpus callosum suggests tumor invasion of that structure (E). 3 = tumor within third ventricle; p = incidental retrocerebellar arachnoid pouch.

F, Axial CT image. Punctate calcification (arrows) within neoplasm were not demonstrated on MR.

Eight ependymomas and two subependymomas appeared completely solid on MR, whereas two supratentorial ependymomas had both solid and cystic components (cases 8 and 10 [Fig. 7]). Cystic tumor components could be identified on

MR as sharply defined, round or oval regions with uniform signal intensity equivalent to that of CSF on all pulse sequences at 0.35 T and 1.5 T. Occasionally, cystic components were slightly hyperintense relative to CSF on long TR images,

Fig. 4.—Case 3: 6-year-old girl with solid, infratentorial ependymoma.

A and B, Sagittal (A) and axial (B) T1-weighted images, 600/25, at 1.5 T show that neoplasm (T) has homogeneous signal intensity that is less than that of adjacent white matter; tumor encases basilar artery (open arrows) and extends into cervical spinal canal via foramen magnum. Cervical cord (c) is displaced anteriorly. Tumor extends from greatly widened left lateral recess of fourth ventricle and foramen of Luschka (solid arrows) into left cerebellopontine angle cistern. Medulla (m) is displaced to the right by neoplasm.

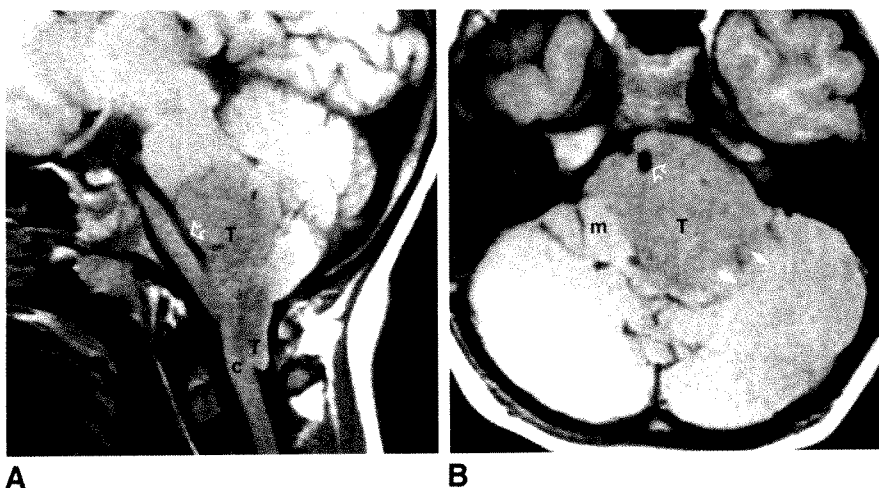


Fig. 5.—Case 4: 5-year-old girl with solid ependymoma of fourth ventricle.

A, Sagittal proton-density-weighted preoperative image, 1500/28, at 0.35 T shows that neoplasm (T) fills fourth ventricle, enters aqueduct of Sylvius (arrow), displaces pons (p) and medulla (m) anteriorly, and extends caudally into cervical spinal canal via foramen of Magendie and foramen magnum. Vermis (ve) is uplifted by tumor. Lateral (L) and third (3) ventricles are enlarged owing to hydrocephalus.

B, Sagittal T1-weighted postoperative image, 600/25, at 1.5 T shows recurrence of neoplasm approximately 1 year after biopsy and debulking. Much of extraventricular portion of tumor, particularly that inferior to fourth ventricle, has been removed.

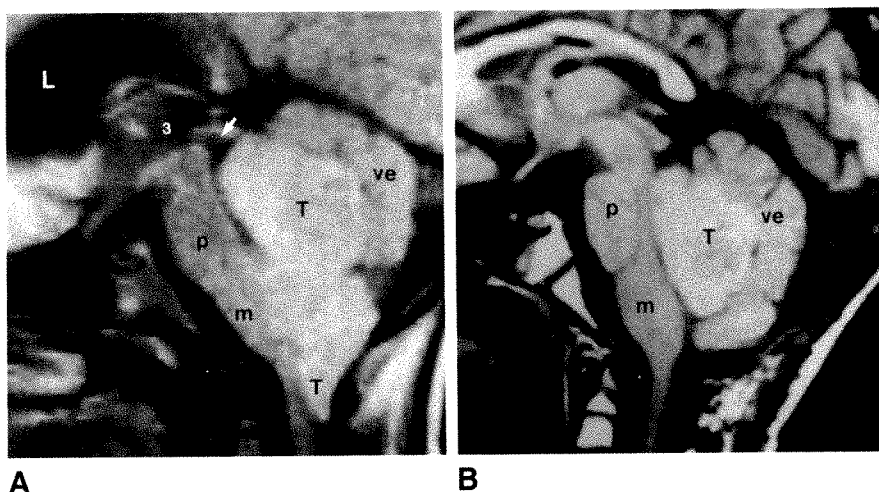
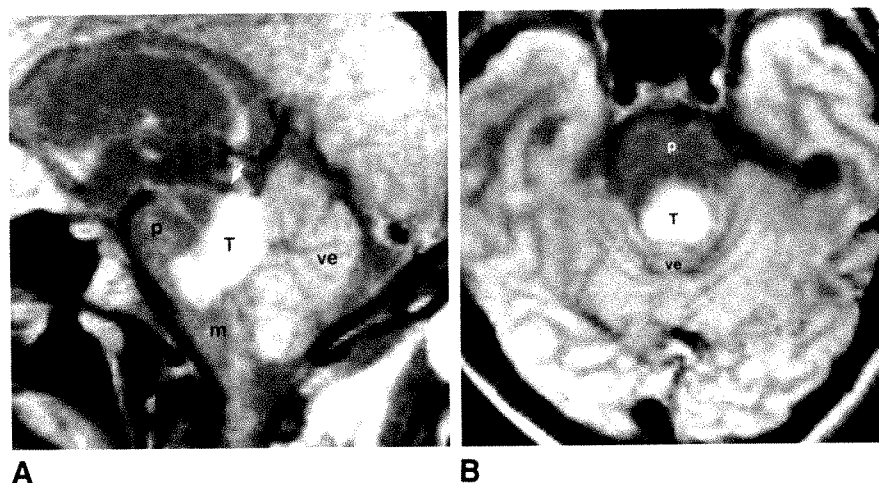


Fig. 6.—Case 12: 55-year-old man with solid infratentorial subependymoma.

A and B, Sagittal (A) and axial (B) proton-density-weighted images 2000/28, at 0.35 T show solid, homogeneous neoplasm (T) within fourth ventricle compressing pons (p) and extending upward into aqueduct of Sylvius (arrow). Tumor exhibits typical bright signal intensity relative to white matter on proton-density-weighted image; tumor margins are extremely well defined. ve = vermis; m = medulla.



likely owing to high protein content and restricted flow within the cyst.

Completely solid tumors and the solid components of mixed solid and cystic neoplasms were iso- to hypointense relative to normal white matter (but remained brighter than CSF) on

T1-weighted images; solid tumor was hyperintense relative to normal white matter on T2- and proton-density-weighted images (Figs. 3 and 8) in all instances. Compared with CSF, the solid neoplasms were hypo- to hyperintense on T2-weighted images and iso- to hyperintense on proton-density-



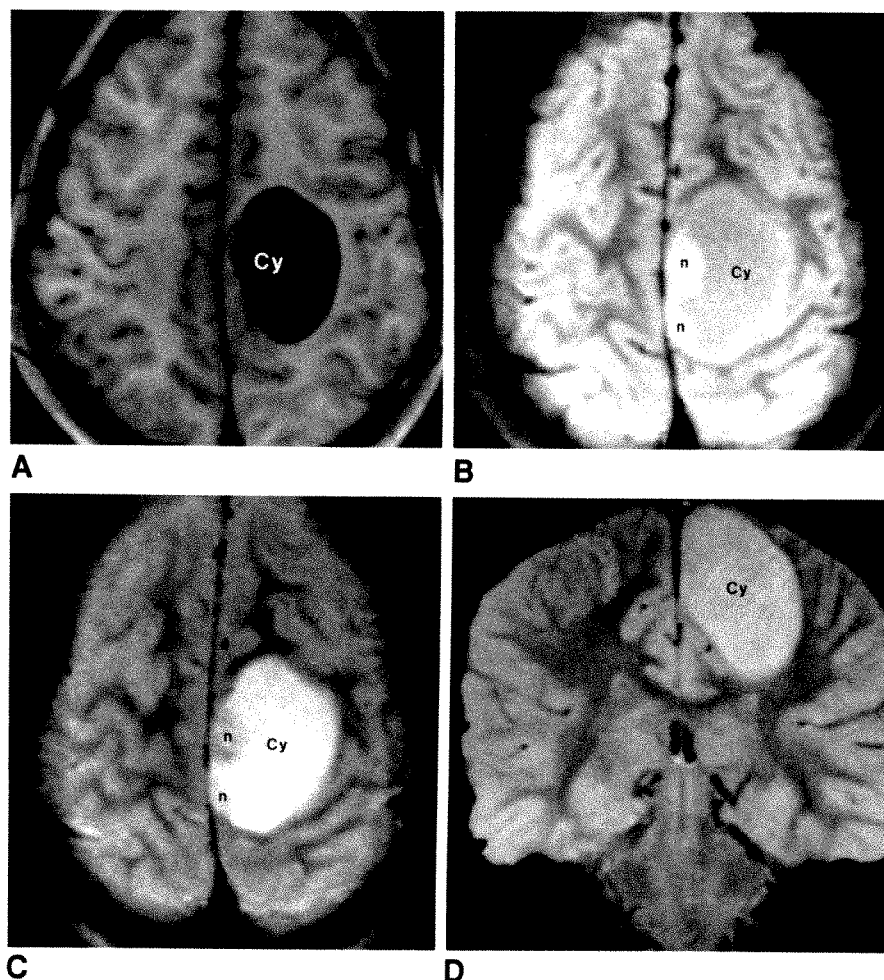


Fig. 7.—Case 8: 8-year-old boy with mixed cystic and solid ependymoma; MR images are at 0.35 T.

A, Axial T1-weighted image, 500/30, shows tumor within parenchyma of left cerebral hemisphere, which has a large cystic component (Cy). Signal intensity of fluid is similar to that of CSF.

B and C, Axial proton-density-weighted, 2000/30 (B), and T2-weighted, 2000/60 (C), images at a slightly higher level show tumor nodules (n) in medial wall of cyst (Cy) that are hyperintense relative to white matter. High signal intensity of cyst fluid relative to CSF likely is due to higher protein content and restricted flow within cyst.

D, Coronal partial-flip-angle image, 500/30/30°, clearly depicts intraparenchymal nature of tumor. While supratentorial ependymomas tend to have cystic components, as in this example, this appearance is not specific for ependymomas and may be seen with other gliomas, particularly cystic astrocytoma.

weighted images. No difference in signal-intensity characteristics was observed between primary and recurrent tumors, and essentially no difference in the signal intensity of solid tumor was noted between images obtained at 0.35 and at 1.5 T.

One patient with a solid ependymoma (case 4) was examined at 0.35 T at initial presentation and at 1.5 T at the time of recurrence (approximately 11 months after initial presentation), which followed surgical debulking, radiation therapy, and chemotherapy (Fig. 5). No significant difference was noted in the signal-intensity characteristics of this neoplasm at the two different field strengths. Another patient (case 7) was imaged at 1.5 T at both initial presentation and 12 days after surgery. Both examinations showed a solid intratentorial tumor of homogeneous signal intensity; the bulk of the neoplasm was within a markedly enlarged left lateral recess of the fourth ventricle and foramen of Luschka. The signal-intensity characteristics of this neoplasm were identical on both studies.

Solid portions of five tumors (four ependymomas, one subependymoma) demonstrated signal heterogeneity; that is, scattered foci of increased or diminished signal intensity compared with surrounding tumor tissue on T1-weighted and/or

T2-weighted images. This finding was correlated with pathologic and surgical reports. Regions of recent (1–4 weeks) and old (>1 month) hemorrhage, hemosiderin deposition, necrosis, calcification, or tumor vascularity accounted for heterogeneous signal intensity (Figs. 1, 2, and 5).

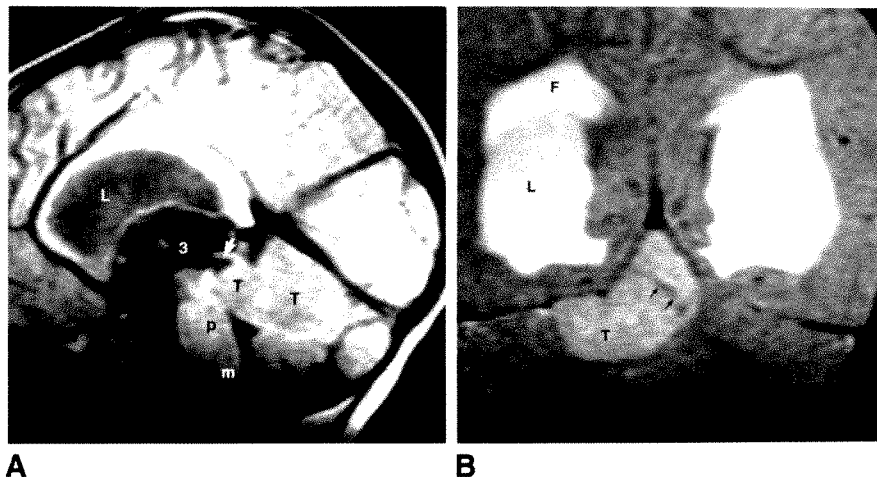
Hypointensity possibly representing calcification was not recognized prospectively by MR in any of the lesions. Nevertheless, CT examinations available in six patients (cases 2, 3, 6, 8, 10, and 11) revealed that four (cases 6, 8, 10, and 11) had punctate (<5 mm), intratumoral foci of calcification (Fig. 3). In retrospect, a focus of decreased signal intensity within one ependymoma (case 6) most likely corresponded to a punctate calcification demonstrated by CT (Fig. 1).

Parenchymal swelling accompanying high signal intensity on long TR images, likely representing edema, either completely or partially surrounded four tumors. Edema accompanied both intraventricular and intraparenchymal neoplasms. In case 2, examined at the time of postsurgical recurrence, we were unable to differentiate between edema and postoperative changes. After IV administration of Gd-DTPA in case 11, the tumor (subependymoma) tissue demonstrated intense, diffuse enhancement, more clearly delineating it from surrounding edema on proton-density- and T2-weighted im-

Fig. 8.—Case 1: 1-year-old girl with solid ependymoma within right cerebellum and vermis; MR images are at 1.5 T.

A, Sagittal T1-weighted image, 900/20, shows typical hypointensity of tumor (T) relative to white matter (compare with corpus callosum). Tumor abuts fourth ventricle and extends into and widens aqueduct of Sylvius (arrow). Dilatation of third (3) and lateral (L) ventricles indicates hydrocephalus. p = pons; m = medulla.

B, Coronal T2-weighted image, 2800/80, shows typical hyperintensity of tumor relative to white matter. Tumor has distinct margins. Linear signal void coursing through superior aspect of mass (arrows) likely represents an encased vessel. High signal intensity (F) adjacent to dilated lateral (L) ventricles suggests transependymal flow of CSF.



ages (Fig. 3). A nonenhancing focus within the tumor likely represented cystic change, which was described in the pathology report.

Tumor margins with surrounding parenchyma were delineated well on T2-weighted images in nine instances, moderately well in three, and poorly in two. On T1-weighted images, tumor margins with surrounding normal or edematous parenchyma were well delineated in four examinations, moderately well delineated in four, and poorly delineated in six instances. In case 10, surrounding edema completely obscured the margins of the tumor on all pulse sequences. The margins of the tumors, when visible, were most distinct on T2-weighted images. The differentiation of neoplasm from surrounding brain parenchyma on T1-weighted images was significantly improved after administration of Gd-DTPA in case 7. The tumor exhibited moderate, heterogeneous enhancement.

The displacement or encasement of normal vasculature and the presence of tumor vascularity were well demonstrated in 10 examinations (nine patients) (Figs. 1, 4, and 8). Encasement of normal vessels occurred in four infratentorial ependymomas (cases 1, 3, 6, and 7). Vessels involved included the basilar artery, vertebral artery, and petrosal and vermian veins. Pathologic and surgical reports in cases 3 and 6 verified vessels traversing the tumors. Three supratentorial lesions (cases 5, 9, and 11) displaced internal cerebral, subependymal and anterior caudate, or thalamostriate veins. In case 10, the surgical report corroborated the MR finding of numerous capsular vessels surrounding a supratentorial ependymoma. Two infratentorial ependymomas displaced a prominent vascular structure likely representing the vein of the lateral recess of the fourth ventricle (see Fig. 9 and Discussion).

## Discussion

Few prior descriptions are available on the MR appearance of intracranial ependymoma. One report mentioned the cystic nature of a posterior fossa ependymoma without further characterization [5]. Another report listed two patients with ependymoma; the cystic component of one of the tumors had

longer T1 and T2 relaxation times than did the solid component [7]. MR performed in one of 12 subependymomas demonstrated a midline posterior fossa tumor with a long T2 [9].

In our series, solid ependymomas and the solid portions of mixed solid and cystic ependymomas were hypo- to isointense compared with white matter on T1-weighted images and hyperintense on T2-weighted images, similar to other intracranial tumors [11, 12]. The signal intensity of cystic tumor components was similar to that of CSF on T1-weighted images and iso- to hyperintense relative to CSF on T2-weighted images. Cystic portions were present in two supratentorial ependymomas; unlike infratentorial ependymomas, supratentorial lesions tend to have cystic components [1].

The two patients in our series with subependymomas had similar clinical and imaging features including later age of presentation (37 and 55.5 years of age) than the patients with ependymoma, epicenter within the lateral or fourth ventricle, and predominantly homogeneous hyperintensity relative to surrounding brain parenchyma on T2-weighted images. At pathology, subependymomas are benign, solid subependymal nodular masses that usually extend into the ventricle. Most often they are found incidentally at autopsy [9]. The subependymomas in our series could not be distinguished from ependymomas by signal-intensity differences, consistency, or location. The differentiation of these two tumors was accomplished histologically (Fig. 10).

Signal heterogeneity within the solid tumors in our series had various etiologies. Subacute (1–4 weeks) hemorrhage accounted for foci of hyperintensity on both T1- and T2-weighted images owing to the presence of dilute methemoglobin outside of lysed RBCs [14, 15]. Regions of diminished signal intensity relative to white matter on both T1- and T2-weighted images represented hemosiderin deposition, necrosis, vessels, and calcification. In case 11, cystic change was suggested by a nonenhancing area within the neoplasm after administration of Gd-DTPA.

Tumor vascularity and encasement or displacement of normal vessels were well demonstrated by MR; the signal void within these serpentine structures afforded excellent contrast with adjacent brain parenchyma and tumor. Of particular



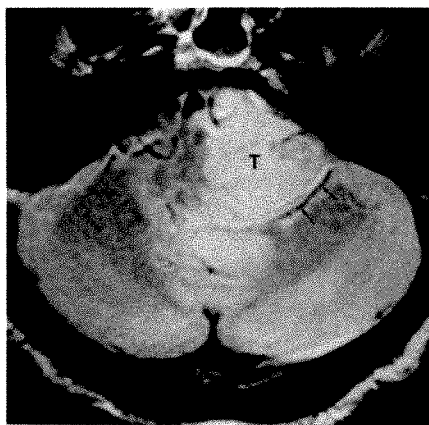


Fig. 9.—Case 7: 59-year-old man with solid, infratentorial ependymoma. Axial proton-density-weighted image, 2800/30, at 1.5 T shows tumor (T) expanding left lateral recess of fourth ventricle and foramen of Luschka. Vascular structure (arrows) adjacent to posterior aspect of tumor likely represents displaced vein of lateral recess [10].

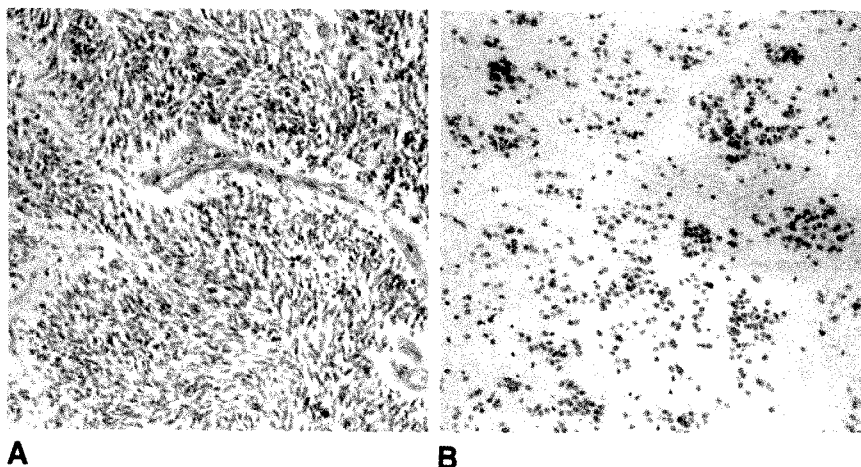


Fig. 10.—A and B, Ependymoma (A) and subependymoma (B). Whereas ependymoma is characterized histologically by ependymal perivascular pseudorosette with clear zones of elongated cytoplasmic processes around blood vessels, subependymoma shows randomly scattered clusters of nuclei, reminiscent of those of normal ependyma, within dense fibrillary background [13].

interest, two infratentorial ependymomas displaced a prominent vascular structure that had the expected course of the vein of the lateral recess of the fourth ventricle [10]. This vein originates from the transverse and lateral supratonsillar veins in the anterolateral aspect of the superior pole of the cerebellar tonsil. The vein of the lateral recess then courses forward and laterally (immediately behind and below the lateral recess of the fourth ventricle) to the cerebellopontine angle, runs over the brachium pontis, and joins other veins to form the petrosal vein. As a marker of the posterior border of the lateral recess of the fourth ventricle, the vein of the lateral recess is displaced posterolaterally by tumors that expand the fourth ventricle and its lateral recesses [10]. The superior visualization of vessels at high field strength in one patient imaged at 0.35 T and 1.5 T likely was due to thinner slices and improved spatial resolution.

Four (40%) of 10 ependymomas in our study were supratentorial, while six (60%) of 10 were infratentorial. One of the two subependymomas was supratentorial; the other was infratentorial. Several series report that 30–40% of intracranial ependymomas are supratentorial in origin [2, 3]. Whereas supratentorial ependymomas tend to be parenchymal, infratentorial ependymomas usually are intraventricular [1]. It has been postulated that ependymal rests outside of the ventricular lining may give rise to extraventricular ependymomas [2]. In our series, three of 10 ependymomas were intraventricular, two were intraparenchymal, and five were transependymal (extending from CSF spaces into the parenchyma). Of the four supratentorial neoplasms, two were parenchymal and two intraventricular. Five of six infratentorial tumors were transependymal and one was completely intraventricular; therefore, all infratentorial ependymomas were at least partially intraventricular.

The multiplanar imaging capability of MR was valuable in assessing the location and routes of extension of ependymomas. Particularly useful were sagittal images of the pos-

terior fossa tumors. The sagittal plane demonstrated best the walls of the fourth ventricle and tumor within it or extending from it. The extension of tumor from the fourth ventricle laterally into the cerebellopontine angle via the lateral recess of the fourth ventricle and foramen of Luschka in three patients and the downward extension into the cisterna magna and cervical spinal canal through the foramen of Magendie and foramen magnum in four patients were demonstrated well on sagittal and axial images. The propensity of ependymomas to “ooze out of the foramina” has been described previously in the surgical pathology literature [13].

Calcifications noted in three of five ependymomas and in one subependymoma on CT were not appreciated prospectively on MR in our series. In retrospect, a focal (<5 mm) region of hypointensity noted within one tumor did correspond to the presence of calcification on CT. Calcification occurs in approximately 50% of supratentorial and 25–50% of infratentorial ependymomas [1]. Previous authors found that focal calcifications accompanying many disease processes are commonly missed by MR [16]; in such instances it is likely that mobile protons in soft tissues within the interstices of the calcification generate sufficient signal to predominate over the nonmobile protons of the calcification, which generate little signal [16]. Recently, MR with gradient-echo acquisition proved more sensitive than spin-echo MR for the detection of intraparenchymal calcification, which appeared as regions of low signal intensity [17].

Intratumoral bleeding occurs infrequently in ependymomas, with prevalences of 0–13% in two series [1, 2]. Findings compatible with subacute hemorrhage within the neoplasm were seen in two patients in our series with recurrent ependymomas (cases 5 and 6) and were verified in the pathology report in one of them. Because these patients were imaged 5 and 2 years, respectively, after surgery, the bright foci of subacute hemorrhage most likely were due to the natural course of the tumor.

On noncontrast MR, tumor boundaries were best recognized on T2-weighted images and less well delineated on T1-weighted images. In one instance (case 10), surrounding parenchymal edema completely obscured the margins of the neoplasm on T1-, proton-density-, and T2-weighted sequences. MR was performed after administration of Gd-DTPA in two patients. In one instance, enhancing subependymoma was better delineated from surrounding hypointense edema on proton-density- and T2-weighted images. In the other patient, the enhancing tumor on post-Gd-DTPA T1-weighted images had more distinct margins with respect to surrounding brain parenchyma than on the precontrast T1-weighted images. Nevertheless, it is important to emphasize that isolated tumor-cell infiltration may exist outside the margins of contrast enhancement [18].

The differential diagnosis of intracranial ependymoma and subependymoma depends on the location of the tumor and the age of the patient. Other supratentorial, intraventricular neoplasms in children include choroid plexus papilloma, a multilobular, solid mass; colloid cyst, characteristically a unilocular cystic tumor in the third ventricle; and astrocytoma, particularly the subependymal giant cell astrocytoma, which is usually associated with tuberous sclerosis [19]. Cranio-pharyngioma may extend upward into the third ventricle [20]. Moreover, in adults one must consider intraventricular meningioma and metastatic carcinoma to the ependyma [21]. Medulloblastoma, choroid plexus papilloma, and astrocytoma may present as fourth ventricular masses in children [2, 19]. Metastases [21] and less commonly dermoid and epidermoid cysts may also involve the fourth ventricle in adults [22]. When confronted with a supratentorial, intraparenchymal mass (seen in two ependymomas in our series), additional lesions that should be considered include astrocytoma, undifferentiated glioma, metastatic carcinoma, and oligodendroglioma [1, 21].

In summary, signal-intensity characteristics do not distinguish ependymoma or subependymoma from other intracranial gliomas; the intra- or periventricular location and morphology of the former seem to be more reliable distinguishing features. The clinical setting and MR appearance of subependymomas, while not completely specific, are suggestive of the histology. Tumor-associated calcification was not readily detected on MR. Coronal and sagittal images were helpful in defining intraventricular tumor and routes of extension within and outside of CSF spaces. Encasement and displacement of normal vessels and tumor vascularity are well shown by MR. Gd-DTPA shows promise in the evaluation of intracranial ependymoma by helping to distinguish enhancing tumor from nonenhancing edema and surrounding normal brain parenchyma.

#### ACKNOWLEDGMENTS

We thank Robert Prager, Kenneth Albertson, and Hector James for providing us with some of the patients evaluated in this report and Marjorie Grafe for the histological specimen photographs.

#### REFERENCES

1. Armington WG, Osborn AG, Cubberley DA, et al. Supratentorial ependymoma: CT appearance. *Radiology* 1985;157:367-372
2. Naidich TP, Zimmerman RA. Primary brain tumors in children. *Semin Roentgenol* 1984;19:100-114
3. Van Tassel P, Lee Y, Bruner JM. Supratentorial ependymomas: computed tomographic and pathologic correlations. *J Comput Tomogr* 1986;10:157-165
4. Gadian DG, Payne JA, Bryant DJ, Young IR, Carr DH, Bydder GM. Gadolinium-DTPA as a contrast agent in MR imaging—theoretical projections and practical observations. *J Comput Assist Tomogr* 1985;9(2):242-251
5. Lee BCP, Kneeland JB, Deck MD, Cahill PT. Posterior fossa lesions: magnetic resonance imaging. *Radiology* 1984;153:137-143
6. Randell CP, Collins AG, Young IR, et al. Nuclear magnetic resonance imaging of posterior fossa tumors. *AJR* 1983;141:489-496
7. Han JS, Benson JE, Kaufman B, et al. MR imaging of pediatric cerebral abnormalities. *J Comput Assist Tomogr* 1985;9(1):103-114
8. Press GA, Hesselink JR. MR imaging of cerebellopontine angle and internal auditory canal lesions at 1.5 T. *AJNR* 1988;9:241-251
9. Jooma R, Torrens MJ, Bradshaw J, Brownell B. Subependymomas of the fourth ventricle. *J Neurosurg* 1985;62:508-512
10. Huang YP, Wolf BS. The vein of the lateral recess of the fourth ventricle and its tributaries. *AJR* 1967;101:1-21
11. Lee BCP, Kneeland JB, Cahill PT, Deck MDF. MR recognition of supratentorial tumors. *AJNR* 1985;6:871-878
12. Komiya M, Yagura H, Baba M, et al. MR imaging: possibility of tissue characterization of brain tumors using T1 and T2 values. *AJNR* 1987;8:65-70
13. Burger PC, Vogel FS. *Surgical pathology of the nervous system and its coverings*, 2nd ed. New York: Wiley, 1982:302-315
14. Gomori JM, Grossman RI, Goldberg HI, Zimmerman RA, Bilaniuk LT. Intracranial hematomas: imaging by high field MR. *Radiology* 1985;157:87-93
15. Grossman RI, Gomori JM, Goldberg HI, et al. MR imaging of hemorrhagic conditions of the head and neck. *RadioGraphics* 1988;8(3):441
16. Oot RF, New PJF, Pile-Spellman J, Rosen BR, Shoukimas GM, Davis KR. The detection of intracranial calcifications by MR. *AJNR* 1986;7:801-809
17. Atlas SW, Grossman RI, Hackney DB, et al. Calcified intracranial lesions: detection with gradient-echo-acquisition rapid MR imaging. *AJNR* 1988;9:253-259
18. Johnson PC, Hunt SJ, Drayer BP. Human cerebral gliomas: correlation of postmortem MR imaging and neuropathologic findings. *Radiology* 1989;170:211-217
19. Sanford RA, Laurent JP. Intraventricular tumors of childhood. *Cancer* 1985;56:1795-1799
20. Tew JM, Feibel JH, Sawaya R. Brain tumors: clinical aspects. *Semin Roentgenol* 1984;14(2):115-128
21. Rosai J. *Ackerman's surgical pathology*, 7th ed. St. Louis: Mosby, 1989:1713-1771
22. Yu WTC, Berloon TJ, Jacoby CG, Schultz DH. MR of fourth-ventricular epidermoid tumors. *AJNR* 1988;9:794-796

## **Categorical Course in Cardiovascular and Interventional Radiology**

### **American Roentgen Ray Society 90th Annual Meeting**

**May 13–18, 1990, Sheraton Washington Hotel, Washington, DC**

*Course Director, William J. Casarella, M.D.  
Course Co-Director, Charles B. Higgins, M.D.*

#### **Sunday, May 13**

10:00–10:30	Basic Physical Principles of MRI in the Cardiovascular System ( <i>Sprawls</i> )
10:30–11:00	MRI of the Great Vessels ( <i>Dinsmore</i> )
11:00–11:30	MRI of Pericardium, Cardiac Masses, and Cardiomyopathy ( <i>Baron</i> )
11:30–12:00	MRI of Congenital Heart Disease ( <i>Gomes</i> )
12:00–12:30	MRI of Ischemic Heart Disease ( <i>Pettigrew</i> )
12:30–2:00	Lunch Break
2:00–2:30	MRI of Valvular Disease ( <i>Higgins</i> )
2:30–3:00	MR Angiography ( <i>Edelman</i> )
3:00–3:30	Coffee Break
3:30–4:30	An Overview of Cardiac Ultrasound: Its Strengths and Weaknesses ( <i>Jaffe</i> )
4:30–5:00	Physical Principles of Doppler Ultrasound ( <i>Kremkau</i> )

#### **Monday, May 14**

1:30–2:30	Doppler Ultrasound in the Carotid and Peripheral Circulation ( <i>Merritt</i> )
2:30–3:15	Ultrasound of Intracranial Circulation ( <i>Ackerman</i> )
3:15–3:45	Coffee Break
3:45–4:30	PET Cardiac Imaging: Radiopharmaceuticals, Technique, and Results ( <i>Schelbert</i> )
4:30–5:15	Doppler Ultrasound Studies of the Abdominal Vessels and Viscera ( <i>Nelson</i> )

#### **Tuesday, May 15**

3:45–4:30	SPECT Cardiac Imaging: Radiopharmaceuticals, Technique, and Results ( <i>DePuey</i> )
4:30–5:15	Ultrasound of Peripheral Venous Disease ( <i>Dorfman</i> )
5:15–5:45	Peripheral Vascular Studies in Nuclear Medicine ( <i>Ziffer</i> )

#### **Wednesday, May 16**

3:45–4:45	Overview of Current Status of Percutaneous Transluminal Angioplasty of Peripheral Vessels ( <i>Schwarten</i> )
4:45–5:30	Renal Angioplasty ( <i>Sos</i> )

#### **Thursday, May 17**

3:45–4:15	Intravascular Stents ( <i>Palmaz</i> )
4:15–5:00	Intravascular Lasers: What's Good and What Isn't ( <i>van Breda</i> )
5:00–5:45	Embolotherapy: Current Trends and Future Prospects ( <i>White</i> )

## Technical Note

# A Simple Phantom for Learning Needle Placement for Sonographically Guided Biopsy

Bruce Silver,<sup>1</sup> Ted S. Metzger, and Terence A. S. Matalon

In an effort to teach sonographically guided needle placement, we developed a simple phantom that contains objects that simulate normal and diseased structures. This phantom can be used to teach biopsy techniques and allows those learning the skills to practice before using them on patients. The phantom is applicable to both freehand and guided techniques.

### Materials and Methods

Previous attempts to create phantoms have included the use of water-based gels with acetate fibers, glass spheres, propanolol, and graphite [1, 2]. We developed a phantom that is made of commonly available materials. One hundred grams of Standard Methods Agar (BBL Becton-Dickinson, Cockeysville, MD) is suspended in 4 l of tap water. The broth is heated until the agar is dissolved. It is essential that the broth actually boil; otherwise, the agar will not solidify when it is left to cool. The broth is then transferred to a 2500-ml barium enema bag (E-Z-EM, Westbury, NY) (Fig. 1). To fill an entire enema bag, 4 l of broth is used, taking into account evaporation and expansion of the plastic. The tubing is cut near the bag and clamped with a hemostat. (The excess tubing can be used to siphon off the hot agar into the bag.) Ten milliliters of phenol per liter of broth is added as a bactericidal agent.

Diced carrots, pimento olives, and elbow macaroni are added to the agar-filled bag. We have found that these objects scan well and can be punctured easily. Recently, we introduced the fingertips of surgical gloves filled with 5 or 10 ml of normal saline (Fig. 2). The

fingertips are twisted and tied with 3-0 silk and cut just proximal to the sutures. After the various objects are added to the agar-filled enema bag, the bags are tilted to force out remaining air and carefully closed. While the bags are cooling, they are rotated every 20 min to obtain suspension of the cysts and vegetables in the agar. Once cooled, the phantoms can be scanned and objects punctured under direct sonographic guidance with needles as small as 22-gauge. The "cysts" can be aspirated (Figs. 2B and 2C).

The sonographic texture of the agar simulates liver parenchyma. Fracturing of the agar is inevitable; however, these fissures simulate vascular structures and further enhance the hepatic appearance of the gel. The bags generally last 1 week. Refrigeration helps maintain the bags and slows putrefaction, which occurs because of the nonsterile punctures and nonsterile vegetable matter. The cost per bag is approximately \$20.

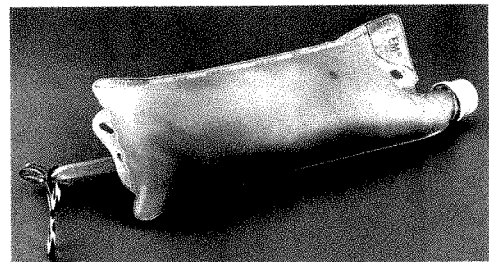


Fig. 1.—Barium enema bag has been filled with agar and allowed to cool.

Received October 10, 1989; accepted after revision November 29, 1989.

<sup>1</sup> All authors: Department of Diagnostic Radiology and Nuclear Medicine, Rush-Presbyterian-St. Luke's Medical Center, 1653 W. Congress Pkwy., Chicago, IL 60612. Address reprint requests to B. Silver.

AJR 154:847-848, April 1990 0361-803X/90/1544-0847 © American Roentgen Ray Society

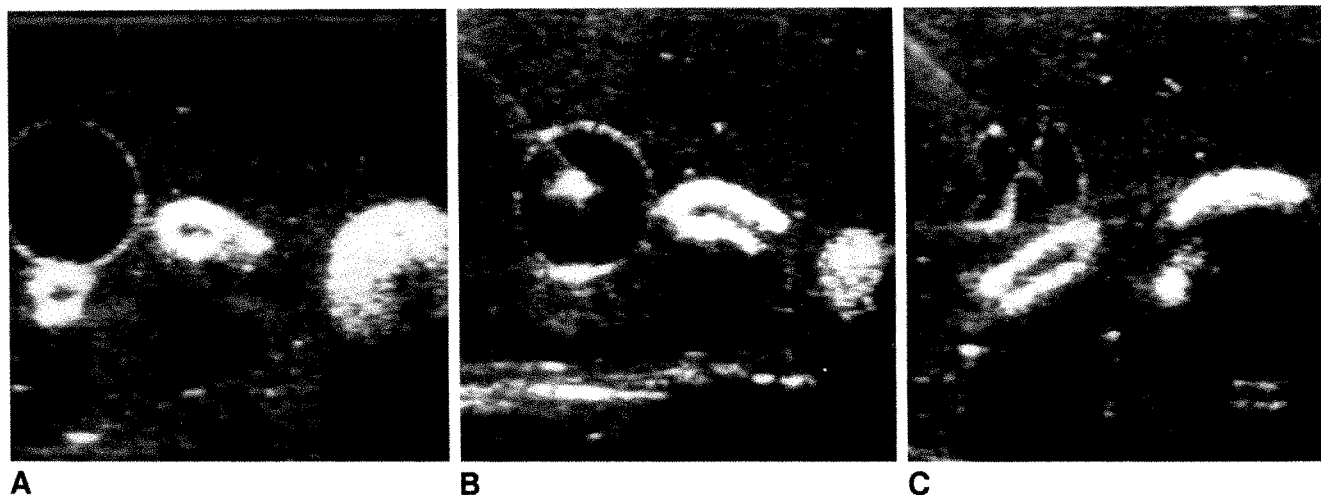


Fig. 2.—A, Sonogram shows elbow macaroni and a diced carrot. Fluid-filled tip of a surgical glove gives appearance of a cyst. B, Sonogram shows "cyst" punctured under guidance by using a 22-gauge needle with echogenic tip. C, "Cyst" has been partially evacuated. Needle is still in place.

### Conclusion

This model has proved to be valuable as a teaching aid. Those learning the skills can become proficient with the necessary dynamic interaction between their hands, needle, and projected sonographic image before actually performing these maneuvers on patients.

### REFERENCES

1. Edmunds P, Reye F, Parkinson D, Busey H. Human tissue phantoms. Presented at the 2nd International Symposium on Ultrasound Tissue Characterization, Gaithersburg, MD 1977
2. Madsen EL, Zagzebski JA, Banjavic RA, Jutila RE. Tissue mimicking materials for ultrasound phantoms. *Med Phys* 1978;5:391-394

## Technical Note

# Endovaginal Sonography for Guidance in Draining Pelvic Fluid Collections

Patricia L. Abbitt,<sup>1</sup> Stuart Goldwag, and Steven Urbanski

The usefulness of percutaneous drainage of pelvic abscesses has been well established [1–3]. Some of these fluid collections may be difficult to drain by traditional routes because of the interposition of bowel or bone. We describe endovaginal sonographic guidance for transvaginal drainage of these inaccessible pelvic fluid collections (Fig. 1).

## Materials and Methods

We used a 5-MHz endovaginal end-fire transducer (Philips SDR 1550 XP, Santa Ana, CA) with attachable needle guide to allow placement of a needle or catheter for drainage. Although the procedure can be performed in a sonographic examination room, it is more convenient, especially when an indwelling catheter is to be placed, to use a surgical suite. Use of a surgical suite allows positioning of the patient in the lithotomy position and monitoring of the patient. In two patients in whom indwelling catheters were placed, spinal or general anesthesia was used. In one patient in whom a diagnostic aspiration of a pelvic cyst was performed, no anesthesia was used. A fourth patient was treated with IV sedation and analgesia during the placement of a catheter to drain a pelvic abscess.

The collection was first visualized by using the endovaginal probe (Fig. 2A). When a catheter was to be left indwelling, the collection was first entered by using the central trocar stylet with overlying stiffening cannula from an 8.3-French All Purpose Drainage Catheter (Medi-tech Inc., Watertown, MA). Placement was monitored continuously by using the endovaginal sonographic probe. The central stylet was then withdrawn and a diagnostic aspirate obtained immediately. A 0.038-in. (0.963 mm) guidewire with movable core was advanced into the collection through the cannula. Once the guidewire was coiled in the collection, the endovaginal probe, needle guide, and cannula were removed. The catheter and central stiffening cannula

then could be advanced over the guidewire into the collection (Fig. 2B). No vessel dilators were necessary. In one case in which the drainage catheter was left in the collection and not sutured in position, the patient purposefully removed the catheter after 5 days. In another case, a self-retaining Tegtmeier nephrostomy catheter with locking

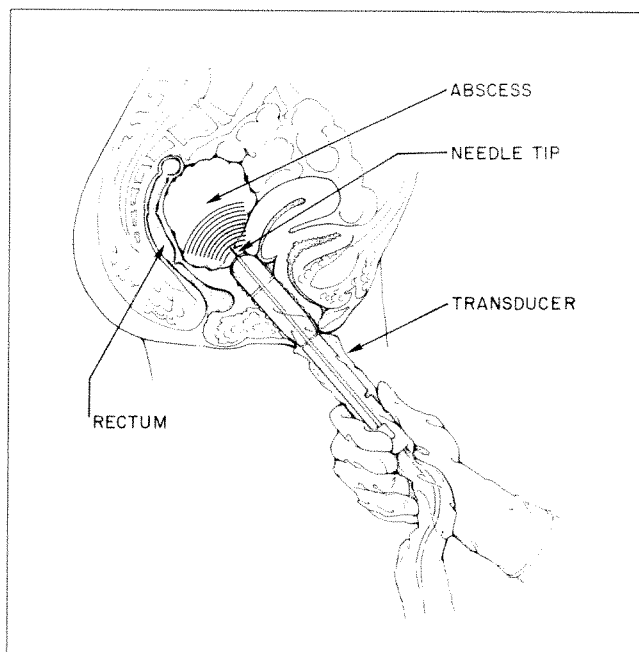


Fig. 1.—Diagram shows end-fire endovaginal transducer angled for direct puncture of cul-de-sac abscess.

Received September 1, 1989; accepted after revision November 14, 1989.

<sup>1</sup> All authors: University of Virginia Health Sciences Center, Department of Radiology, Box 170, Charlottesville, VA 22908. Address reprint requests to P. L. Abbitt.



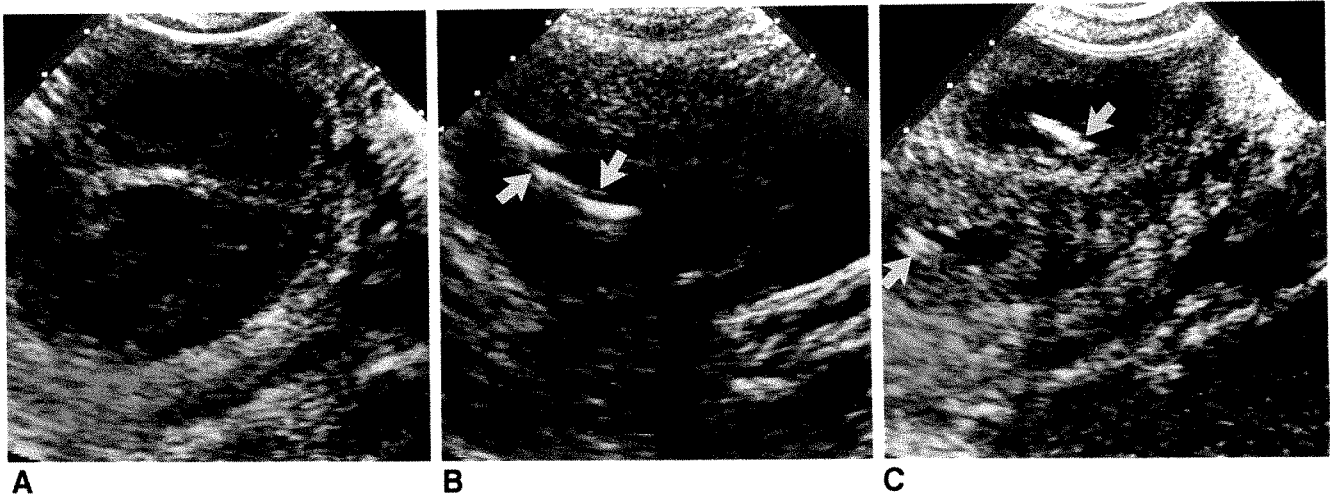


Fig. 2.—22-year-old woman who had resection of a rectal leiomyosarcoma 4 months earlier. An anastomotic stricture with abscess developed that was not amenable to CT-guided drainage because of its position behind bowel and bordered by bone.

A, Endovaginal sonogram shows biloculated abscess collection.

B, Endovaginal sonogram shows catheter (arrows), which was advanced over guidewire.

C, Endovaginal sonogram after drainage of abscess shows catheter coiled in collection (arrows).

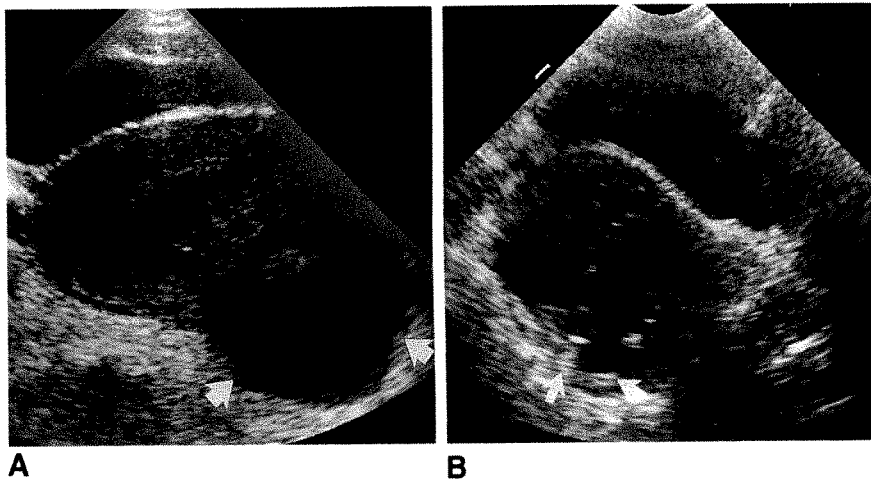


Fig. 3.—25-year-old woman with a poorly differentiated brain tumor was admitted for treatment of a pelvic abscess.

A, Transabdominal sonogram shows fluid collection (arrows) behind uterus.

B, Transabdominal sonogram made after transvaginal catheter insertion (arrows) shows collection is markedly diminished in size.

pigtail (Medi-tech, Inc., Watertown, MA) was placed and secured by suture to the patient's inner thigh. This catheter remained in position for 5 weeks during which time a fistula to bowel and postsurgical anastomotic stricture were successfully treated. In two cases, aspiration of as much material as possible at the time of catheter placement was followed by use of constant Jackson-Pratt suction. In two cases, no indwelling catheter was left in place. Visualization of the collection after drainage can be accomplished by using either the transabdominal or endovaginal approach (Figs. 3A and 3B).

The fluid collections in two patients were abscesses associated with recent surgery or pelvic inflammatory disease. Two other patients had benign noninfected cystic collections related to previous surgery (inclusion cyst of peritoneum) or hormonal ovarian cycling. Noninflammatory cysts may be quite mobile and therefore difficult to puncture. Suprapubic pressure on the abdomen and a quick, direct puncture may be necessary for successful aspiration of such uninfected and mobile collections.

## Discussion

Transvaginal drainage of pelvic fluid collections under sonographic guidance can be facilitated by the use of an endo-

vaginal sonographic transducer. The sonogram allows evaluation of the anatomic relationship between the abscess, the vaginal vault, and the rest of the pelvic organs. For fluid collections situated deep in the pouch of Douglas close to the vaginal fornix, the short puncturing distance from the vagina is a distinct advantage. This often is a more direct route than is possible by a transabdominal approach. Also, the ability to suture the catheter to the vaginal wall prevents early catheter expulsion.

## REFERENCES

1. Johnson WC, Gerzof SG, Robbins AH, Nabseth DC. Treatment of abdominal abscesses: comparative evaluation of operative drainage versus percutaneous catheter drainage guided by computed tomography or ultrasound. *Ann Surg* 1981;194:510-520
2. vanSonnenberg E, Ferrucci JT, Mueller PR, Wittenberg J, Simeone JF. Percutaneous drainage of abscesses and fluid collections: technique, results, and applications. *Radiology* 1982;142:1-10
3. vanSonnenberg E, Wing VW, Casola G, et al. Temporizing effect of percutaneous drainage of complicated abscesses in critically ill patients. *AJR* 1984;142:821-826

# Lower-Extremity Venous Thrombosis in Patients with Acute Hip Fractures: Determination of Anatomic Location and Time of Onset with Compression Sonography

Gary S. Dorfman<sup>1</sup>  
 John A. Froehlich<sup>2</sup>  
 John J. Cronan<sup>1</sup>  
 Paul J. Urbanek<sup>2</sup>  
 James H. Herndon<sup>2,3</sup>

Patients with acute hip fractures are at increased risk for the development of lower-extremity deep venous thrombosis and its major complication, pulmonary embolism. It is furthermore recognized that the risk of clinically important pulmonary embolism depends to some degree on the anatomic location of the preexisting thrombosis. Because of the increased risk of thromboembolic disease, most patients with hip fracture are treated with one of several prophylactic regimens. The potential for effective prophylaxis may depend on the time of onset of the venous thrombosis. We used compression sonography to determine the anatomic location and time of onset of deep venous thrombosis in patients with hip fractures being treated with antithrombotic prophylaxis. Ninety-six patients had compression sonography of the injured extremity perioperatively and serially until discharge. Ninety-three also were examined with contrast venography when the sonogram suggested thrombus or at discharge if all sonograms were normal. Twenty areas of thrombus were identified in 18 patients, thereby yielding a prevalence of thrombosis of 19%. All patients were asymptomatic. Above-knee clot was diagnosed in 14 (78%) of these 18 patients. Nine (64%) of the 14 patients with significant clot had the abnormality on their first perioperative investigation (in eight of nine cases, the clot was adjacent to the fracture site), before any means of prophylaxis could have been initiated. Significant thrombosis developed in six patients later in their course (in only one case was the clot related to the fracture site), and the thrombus was an extension of below-knee clot in the minority of the patients.

We conclude that although currently acceptable prophylaxis may decrease the frequency of thrombosis, it does little to prevent above-knee clot, which often antedates the initiation of therapy. Furthermore, as the clinical diagnosis of deep venous thrombosis is difficult in patients with acute hip fracture, serial compression sonograms are recommended so that patients with unsuspected clot may be treated with appropriate anticoagulation and/or caval interruption.

*AJR* 154:851-855, April 1990

Venous thromboembolic disease is the most common fatal complication of lower-extremity trauma or orthopedic surgery [1]. Patients with hip fractures are generally at increased risk for the development of lower-extremity deep venous thrombosis (DVT) because of immobility, advanced age, activation of the coagulation cascade due to the trauma itself, and intraoperative manipulation of the superficial femoral vein [2-7]. Previous studies, which used a variety of invasive and noninvasive methods [5-11], have shown venous thrombosis to occur in 40-60% of this population of patients. Contrast venography is not the ideal method of investigation because it may influence the course of thromboembolic disease and is not readily repeatable so as to allow sequential studies in each patient. Others have questioned the sensitivity and specificity of the noninvasive methods of detection used in these investigations and in similar investigations of the related population of patients undergoing elective total hip replacement [12-14].

Treatment plans to decrease the morbidity and mortality of venous thromboembolic disease in these patients are directed either toward prophylaxis for DVT or

Received September 15, 1989; accepted after revision November 2, 1989.

<sup>1</sup> Department of Diagnostic Imaging, Rhode Island Hospital and Brown University Program in Medicine, 593 Eddy St., Providence, RI 02903. Address reprint requests to G. S. Dorfman.

<sup>2</sup> Department of Orthopaedics, Rhode Island Hospital and Brown University Program in Medicine, 593 Eddy St., Providence, RI 02903.

<sup>3</sup> Present address: Department of Orthopaedics, University of Pittsburgh, Scafe Hall, Rm. M277, Pittsburgh, PA 15261.

0361-803X/90/1544-0851  
 © American Roentgen Ray Society

prevention of extension and embolization of the thrombus [10, 15–19]. A rational approach to designing and evaluating these protocols demands knowledge of (1) the prevalence of thrombosis before institution of treatment, (2) the propensity for thrombus extension without or with treatment, and (3) the anatomic location of thrombosis that may occur at various times during the course of hospitalization. The technique used to gain this knowledge must, in addition to being sensitive and specific, be repeatable and unlikely to influence the natural history of the disease. We, and others, have demonstrated that compression sonography fulfills these characteristics in the general population and in patients with conditions that might adversely affect this method's accuracy, such as pelvic fractures and pregnancy [20–28]. We therefore undertook this prospective study with compression sonography to characterize the time of onset and anatomic distribution of lower-extremity DVT in patients with acute hip fractures being treated with antithrombotic prophylaxis.

### Subjects and Methods

Consecutive patients admitted with acute femoral neck or intertrochanteric fractures were recruited to participate in this institutional review board–approved protocol. All patients received some form of accepted prophylaxis for DVT consisting of either gradient elastic stockings, serial compression boots, or administration of Coumadin (warfarin) postoperatively. After signing an informed consent form, an initial compression sonogram of the venous system of the lower extremity on the side of the fracture was obtained. In most patients, the study was performed preoperatively. In three patients who had immediate surgery on admission and in cases when a sonographer was not immediately available, the sonogram was obtained postoperatively, but still within 24 hr of admission. Surgery was completed in all patients within 48 hr of admission. Compression sonograms were repeated every 3 days until discharge (postoperative day 10–14).

Compression sonograms were obtained from the inguinal ligament to the proximal calf so that the origins of the sural and deep calf veins were visualized. No attempt was made to image the calf veins beyond their origins. The technique of examination has been described in detail [20, 21, 26]. Imaging findings were interpreted as normal or as showing DVT. When a compression sonogram showed DVT or at the end of the protocol, and within 8 hours of the last compression sonogram, a contrast venogram was obtained by using the technique of Rabinov and Paulin [29].

One hundred two consecutive patients with acute hip fractures were asked to participate in this study. Five patients or their referring physicians refused participation. One patient withdrew after an initial normal compression sonogram because she found the sonographic examination suite "claustrophobic." Thus, 96 patients completed the sonographic portion of the study. Vein cannulation for venography was not successful in three patients, all of whom had only serial normal compression sonograms and were to be subjected to pre-discharge confirmatory venography. An additional patient was not subjected to venography when her initial compression sonogram showed thrombus because of failure of vein cannulation due to bilateral lower-extremity edema. This patient did have venography before discharge from the hospital, when leg swelling subsided with diuresis. The compression sonogram obtained immediately before venography showed that the thrombus initially visualized was unchanged in appearance during the serial studies. A new area of thrombosis that was discontinuous from the first was noted, however.

Therefore, 93 patients completed the full protocol. The results of all imaging studies and patients' charts were reviewed and analyzed

for the presence or absence of DVT, the times and sites of thrombus occurrence, and clinical signs and symptoms suggestive of DVT and pulmonary embolism. Statistical evaluation was based on the entire population of 96 patients who completed the sonographic portion of the study with or without venographic examination.

### Results

There were 17 men and 85 women in the group, with an age range of 51–97 years (mean, 81.3 years). A total of 257 sonographic studies were performed in the 96 patients who completed the sonographic portion of the study. Twenty areas of thrombosis were identified in 18 patients. The prevalence of DVT in the 96 patients was 19%. Fifteen femoral and/or popliteal clots were noted in 14 (78%) of the 18 patients with DVT. Five patients had isolated calf thrombosis detected on the predischarge venogram. One of these was in a patient with a separate focus of clot at the femoral-popliteal junction.

Nine (64%) of the 14 patients with femoral or popliteal thrombus had this finding on their initial study (seven preoperative, two immediately postoperative). One of these patients had a focal nonocclusive thrombus at the adductor hiatus. Four patients had focal clot in the superficial femoral vein in relation to the fracture site (Fig. 1). One of the four was a patient imaged immediately after surgery. Four patients had diffuse femoral-popliteal clot with or without involvement of the calf veins. One of these four was a patient imaged immediately after surgery. One of the patients with focal superficial femoral vein on the initial preoperative study was not studied by venography because of difficulty in obtaining venous access. The area of thrombosis was monitored with serial compression sonograms and did not change. During the final predischarge compression sonographic examination, an additional area of abnormality was identified in the popliteal vein and proximal calf veins. Venography was performed at this time and revealed an isolated superficial femoral vein clot at the fracture site (identified on the initial compression sonogram) and popliteal thrombosis with involvement of the

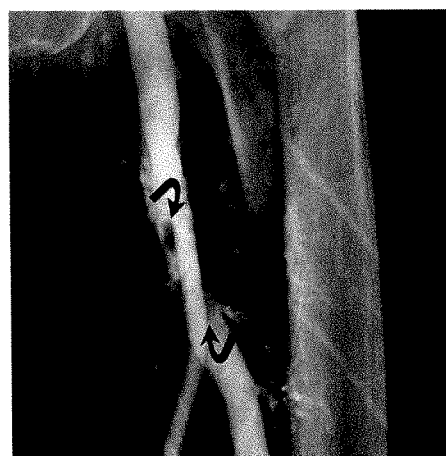
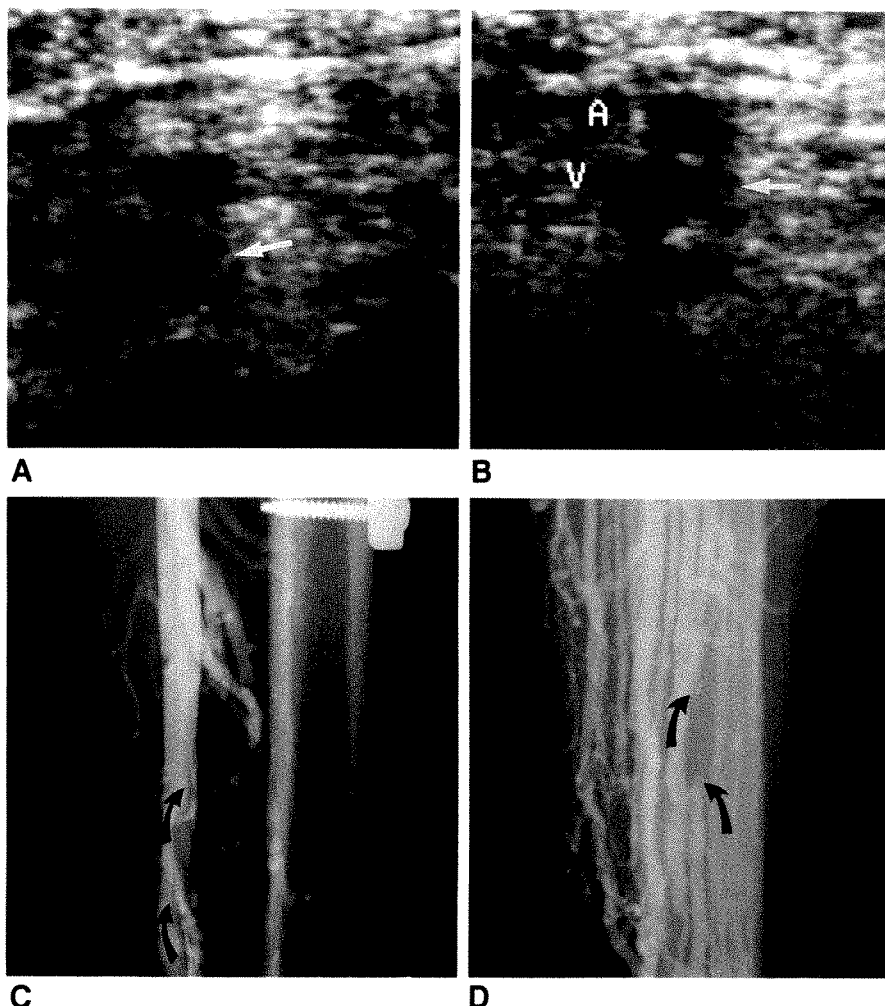


Fig. 1.—Contrast venogram obtained immediately after sonographic examination and preoperatively shows a focal nonocclusive clot (arrows) adjacent to fracture site and in agreement with abnormality seen on compression sonogram. Compression sonography clearly delineated focal noncompressibility despite adjacent soft-tissue swelling around fracture. This was evident on initial examination in four patients.

Fig. 2.—A and B, Late venous thrombosis occurred at or below adductor hiatus more often than above this point. Transverse sonograms obtained in mid thigh without (A) and with (B) compression show an area of incompressibility (arrows).

C, Contrast venogram confirms thrombus (arrows) in superficial femoral vein just cephalad to distal adductor hiatus.

D, An additional discontinuous area of thrombus (arrows) is noted in one of peroneal veins. As veins below trifurcation of popliteal vein were not examined with compression sonography, serial screening was not sensitive for clot in calf veins shown later with contrast venography.



proximal calf veins (as noted on the phlebography sonogram).

Six patients who had normal findings on initial compression sonograms showed abnormalities on postoperative days 5–14 (compression sonographic examinations 2 or 3) that were confirmed by venography. One of these patients had a focal nonocclusive clot in relation to the fracture/operative site. The remaining five patients had focal popliteal or femoral-popliteal junction thrombosis. One of these patients had a discontinuous separate focus of calf vein clot (Fig. 2).

No patients with DVT had signs or symptoms that suggested the diagnosis. No patients had proved pulmonary embolism.

To summarize, our population of patients with acute hip fractures had a 19% prevalence of DVT during their hospitalization and 15% of patients had clinically significant clot (femoral or popliteal veins). Of these, the majority (64%) had thrombosis on their first examination. The nine patients with DVT on presentation had femoral vein involvement in 89% of cases. The six patients with late presentation had popliteal thrombosis without extension above the adductor hiatus in 83% of cases. Only one patient with early thrombosis developed new significant (above-knee) thrombosis. In this case, the two areas of thrombus were discontinuous. The remaining patients who had late thrombosis had no preexisting significant thrombosis (Table 1).

## Discussion

Patients with acute hip fractures are at increased risk of developing DVT [1–11]. Factors that contribute to this increased frequency of DVT are the advanced age of most patients with hip fractures, the prolonged immobilization of these patients, the activation of the coagulation pathway by the original trauma and subsequent surgery, the soft-tissue swelling and hematoma formation around the fracture that may impede venous flow, and finally, the manipulation of the femoral vein itself during surgery [2–7]. Although DVT may

TABLE 1: Frequency of Lower-Extremity Deep Venous Thrombosis (DVT) in 96 Patients with Acute Hip Fractures<sup>a</sup>

Thrombus Location	Early Femoral-Popliteal DVT	Late Femoral-Popliteal DVT	Isolated Calf DVT
Fracture Site	4 <sup>b</sup>	1	—
Distal Femoral-Popliteal Vein	1	5 <sup>b,c</sup>	—
Diffuse	4	0	—
Total	9	6	5 <sup>c</sup>

<sup>a</sup> Eighteen patients with 20 foci of DVT.

<sup>b</sup> One patient had DVT focal to fracture site early and discontinuous popliteal DVT developed later.

<sup>c</sup> One patient had discontinuous foci of calf and distal femoral-popliteal vein DVT.

have long-term morbidity because of the postthrombotic syndrome, the major complication of DVT in this population is pulmonary embolism [30, 31]. It is recognized that some form of prophylaxis must be used in these patients in order to decrease the frequency of DVT and subsequent embolism [10, 16–18, 32–37].

In the general population, most significant DVT (i.e., femoral or popliteal clot) originates as calf thrombosis [38, 39]. Although the majority of calf DVT does not propagate, the 20% that does extend proximally is considered contributory to most emboli [38]. Therefore, although significant pulmonary embolism does not arise primarily from isolated calf clot, prophylaxis designed to prevent formation of calf clot as well as its subsequent propagation into the popliteal and femoral veins should decrease the frequency of embolism, especially in high-risk groups [39–42].

DVT occurs in up to 40–75% of patients subjected to lower-extremity orthopedic surgery [5–8]. Furthermore, the sites of origin and consequent distribution of these thrombi may be atypical. In a population treated by total hip replacement, the frequency of postoperative DVT is approximately 20% despite the use of efficacious antithrombotic prophylaxis [12]. In these patients, 30–50% of thrombi are isolated to thigh veins [12]. In series devoted to patients with hip fractures, the frequency of DVT is reported as 40–60% [1, 5, 8–11]. The thrombi are distributed in equal proportions above and below the knee. In our study population, only 19% of patients had DVT. However, the majority of these (78%) had isolated above-knee clot.

One explanation for the difference in frequency and distribution of clot in our patients as opposed to the frequency quoted in other series is the effect of prophylaxis. Seemingly, one or all of the protocols used in our patients was effective in minimizing the formation of clot in the calf. As our sonographic examinations were insensitive to clot below the trifurcation of the popliteal veins(s), an alternative explanation might be that our serial screening used compression sonography with contrast venography obtained only at a single point during the protocol. We are then comparing our results with those obtained by investigators who used contrast venography alone with its recognized greater sensitivity for calf vein clot. However, those series most often used venograms obtained at only a single point during the protocol as well (although the timing of the venogram varied from study to study). Therefore, one would not expect the rate of calf vein clot in our series to be different from the historical control merely because of differences in methodology.

Despite the decreased frequency of calf DVT in our patients, the frequency of above-knee DVT was virtually unchanged from the range reported by other investigators. Although we did not study the veins of the uninjured extremity, those previous studies that have done so noted an equal frequency of DVT in the calves bilaterally [1]. Effective prophylaxis should decrease the frequency of calf DVT equally in the injured and uninjured limbs. Therefore, prophylaxis might be expected to decrease the frequency of significant pulmonary embolism caused by propagating calf clot by virtue of the decreased frequency of calf clot itself.

However, previous studies have shown that the morbidity and mortality due to emboli relate more strongly to the frequency of above-knee DVT, rather than the overall frequency of DVT [1, 39–42]. Mok et al. [1] studied an Oriental popula-

tion with acute hip fractures and noted DVT in 53% of patients. This is comparable to the frequency reported in Occidental patients [5, 7–11]. But unlike studies conducted in Western countries, Mok's series demonstrated a preponderance of below-knee clot (84%). The authors postulated that the well-recognized decreased frequency of pulmonary embolism in Oriental patients with hip fractures was related to the decreased proportion of above-knee DVT in this subset of patients, despite the comparable overall frequency of lower extremity clot [1]. In contradistinction to the patients in Mok's series, our patients had a lower overall frequency of DVT than previous reports concerned with thrombosis in patients with hip fracture. However, as the frequency of above-knee clot is virtually unchanged from these previous studies, one might expect that the rate of embolism would be unchanged as well.

One explanation for the failure of prophylaxis to decrease the occurrence of thigh clot is that in our series 64% of patients with significant DVT had thrombosis on their first examination, either preoperatively or immediately postoperatively. Of these nine patients, eight (89%) had clot adjacent to the fracture site. This may be due to direct trauma to the vein by the fractured bone or locally increased pressure by hematoma around the fracture. Obviously, prophylactic measures would do little to prevent this early DVT, which is present at the time of surgical manipulation of the fracture fragments.

A significant minority (36%) of our patients developed their above-knee DVT during their postoperative course despite adequate prophylaxis. The majority (83%) of these six patients had clot isolated to the popliteal vein or the distal adductor hiatus where the superficial femoral and popliteal veins merge. This late DVT is unusual in that most patients did not develop this thrombus as extension of calf clot (unless one postulates that the underlying calf clot had completely resolved as it propagated cephalad, which is highly unlikely). Perhaps this late above-knee clot is generated in relation to vein trauma or twisting intraoperatively or because of increased pressure in the adductor canal related to perioperative hematoma or swelling. These causes are purely conjectural, as we have no evidence about the factors that led to this late DVT in our patients.

Prophylactic regimens other than those that were used in our patients, with low-molecular-weight dextran, for example, have been shown to decrease the rate of postoperative DVT in lower-extremity orthopedic surgery [9, 15, 18, 33, 37, 43]. There are, however, significantly increased risks related to such therapies, especially in elderly patients with concomitant cardiac or renal impairment [33]. Additionally, aggressive prophylaxis would still not be expected to significantly affect the presence of preexisting clot, which occurred in over 64% of our patients.

Clearly, further work is necessary to elucidate the sites of origin of pulmonary emboli in patients with DVT and acute hip fracture. However, on the basis of our findings of early above-knee clot in a disturbingly high percentage of our patients, it may be necessary to rethink treatment protocols in patients with fractures of the hip. Early screening compression sonography is suggested to diagnose patients with preoperative or perioperative clot. Patients with cardiac or pulmonary compromise may benefit from preoperative percutaneous placement of inferior vena caval filters if early clot is diagnosed. Postoperatively, serial studies every 3–4 days until discharge

would be useful in identifying patients in whom DVT develops despite prophylactic measures. Those patients with proved significant clot should be treated with IV heparin followed by oral warfarin therapy or percutaneous filter placement if anticoagulation is contraindicated. Finally, we suggest studies of the morbidity, mortality, and cost of this more aggressive treatment regimen as opposed to current, frequently used protocols.

## REFERENCES

- Mok CK, Hoaglund MD, Rogoff SM, Chow SP, Yau APMC. The pattern of deep-vein thrombosis and clinical course of a group of Hong Kong Chinese patients following hip surgery for fracture of the proximal femur. *Clin Orthop* 1980;147:115-120
- Sevitt S, Gallagher NG. Venous thrombosis and pulmonary embolism: a clinico-pathological study in injured and burned patients. *Br J Surg* 1961;48:475-439
- Almen T, Nylander G. Serial phlebography of the normal lower leg during muscular contractions and relaxation. *Acta Radiol* 1962;57:264-272
- Nicolaides AN, Gordon-Smith I. Clinical factors and the risk of deep venous thrombosis. In: Nicolaides AN, ed. *Thromboembolism: aetiology/advances in prevention and management*. Lancaster, England: MTP, 1975:199
- Field ES, Nicolaides AN, Kakkar VV, Crellin RQ. Deep vein thrombosis in patients with fractures of the femoral neck. *Br J Surg* 1972;59:377-379
- Smyrnis SA, Kolios AS, Agnantis JK. Deep vein thrombosis in patients with fracture of the upper part of the femur: a phlebographic study. *Br J Surg* 1973;60:447-450
- Stevens J, Fardin R, Freeark RJ. Lower extremity thrombophlebitis in patients with femoral neck fractures. *J Trauma* 1968;8:527-534
- Culver D, Crawford JS, Gardiner JH, Wiley AM. Venous thrombosis after fracture of the upper end of the femur: a study of incidence and site. *J Bone Joint Surg [Br]* 1970;52-B:61-69
- Johnsson SR, Bygdeman S, Eliasson R. Effect of dextran on postoperative thrombosis. *Acta Chir Scand* 1968;387S:80-82
- Hamilton F-W, Crawford JS, Gardiner JH, Wiley AM. Venous thrombosis in patients with fracture of the upper end of the femur: a phlebographic study of the effect of prophylactic anticoagulation. *J Bone Joint Surg [Br]* 1970;52-B:268-289
- Kakkar VV. The diagnosis of deep vein thrombosis using the  $^{125}\text{I}$  fibrinogen test. *Arch Surg* 1972;104:152-159
- Paiemont G, Wessinger SJ, Waltman AC, Harris WH. Surveillance of deep vein thrombosis in asymptomatic total hip replacement patients. *Am J Surg* 1988;155:400-404
- Harris WH, Salzman EW, Athanasoulis C, Waltman AC. Cuff-impedance phlebography and  $^{125}\text{I}$ -fibrinogen scanning versus roentgenographic phlebography for the diagnosis of thrombosis following hip surgery: a preliminary report. *J Bone Joint Surg [Am]* 1977;58-A:939-944
- Harris WH, Salzman EW, Athanasoulis C, Waltman AC, Baum S, DeSanctis R. Comparison of  $^{125}\text{I}$ -fibrinogen count scanning with phlebography for detection of venous thrombi after elective hip surgery. *N Engl J Med* 1975;292:665-667
- Harris WH, Salzman EW, Athanasoulis C, Waltman AC, Baum S, DeSanctis RW. Comparison of warfarin, low-molecular weight dextran, aspirin, and subcutaneous heparin in prevention of venous thromboembolism following total hip replacement. *J Bone Joint Surg [Am]* 1974;56-A:1552-1562
- Harris WH, Salzman EW, Athanasoulis C, Waltman AC. High and low dose aspirin against venous thromboembolic disease in total hip replacement. *J Bone Joint Surg [Am]* 1982;64-A:63-66
- Paiemont G, Wessinger SJ, Waltman AC, Harris WH. Low dose warfarin versus external pneumatic compression for prophylaxis against venous thromboembolism following total hip replacement. *J Arthroplasty* 1987;2:23-26
- Harris WH, Salzman EW, Athanasoulis C, Waltman AC. Prophylaxis of deep vein thrombosis after total hip replacement: dextran and external compression compared with 1.2 of 0.3 gram of apirin daily. *J Bone Joint Surg [Am]* 1985;67-A:57-62
- Evarts CMc. Thromboembolic disease in orthopedic patients: prophylaxis and treatment. *Contemp Surg* 1975;6:65-68
- Cronan JJ, Dorfman GS, Scola FH, Schepps B, Alexander J. Deep venous thrombosis: US assessment using vein compression. *Radiology* 1987;162:191-194
- Cronan JJ, Dorfman GS, Grusmark J. Lower-extremity deep venous thrombosis: further experience with and refinements of US assessment. *Radiology* 1988;168:101-107
- Appleman PT, De Jong TE, Lampmann LE. Deep venous thrombosis of the leg: US findings. *Radiology* 1987;163:743-746
- Dauzet MM, LaRoche JP, Charras C, et al. Real-time B mode ultrasonography for better specificity in the noninvasive diagnosis of deep venous thrombosis. *J Ultrasound Med* 1986;5:625-631
- Raghavendra BN, Rosen RJ, Lam S, Riles T, Horii SC. Deep venous thrombosis: detection by high-resolution real-time ultrasonography. *Radiology* 1984;152:789-793
- Vogel P, Laing FC, Jeffrey RB, Wing VW. Deep venous thrombosis of the lower extremity: US evaluation. *Radiology* 1987;163:747-751
- Froehlich JA, Dorfman GS, Cronan JJ, Urbanek PJ, Herndon JH, Aaron RK. Compression ultrasonography for the detection of deep venous thrombosis in patients who have a fracture of the hip. *J Bone Joint Surg [Am]* 1989;71-A:249-255
- Goulet J, White R, Daschback M, Bray T, Hartling R. Deep vein thrombosis following fracture of the pelvis: a prospective study. Presented at the annual meeting of the Orthopaedic Trauma Association, Dallas, TX, October 29, 1988
- Polak JF, O'Leary DH. Deep venous thrombosis in pregnancy: noninvasive diagnosis. *Radiology* 1988;166:377-379
- Rabinov K, Paulin S. Roentgen diagnosis of venous thrombosis of the leg. *Arch Surg* 1972;104:134-144
- Flanc C, Kakkar VV, Clarke MB. The detection of venous thrombosis of the legs using  $^{125}\text{I}$ -labelled fibrinogen. *Br J Surg* 1968;55:742-747
- Hull R, Hirsch J, Sackett DL, et al. The value of adding impedance plethysmography to  $^{125}\text{I}$ -fibrinogen leg scanning for the detection of deep vein thrombosis in high risk surgical patients: a comparative study between patients undergoing general surgery and hip surgery. *Thromb Res* 1979;15:227-234
- Nicolaides AN. The current status of low dose heparin in the prophylaxis of thrombophlebitis and pulmonary embolism. *World J Surg* 1978;2:13-17
- Hirsch J, Salzman EW. Prevention of venous thromboembolism. In: Coleman RW, Hirsch J, Marder VJ, Salzman EW, eds. *Hemostasis and thrombosis: basic principles and clinical practice*. Philadelphia: Lippincott, 1982:989-991
- Harris WH, Raines JK, Athanasoulis C, et al. External pneumatic-compression versus warfarin in high-risk hip patients. In: Madden JL, Hume M, eds. *Venous thromboembolism: prevention and treatment*. New York: Appleton-Century-Crofts, 1976:51
- Barnes RW, Brand RA, Clarke W, et al. Efficacy of graded compression antiembolism stockings in patients undergoing total hip arthroplasty. *Clin Orthop* 1978;132:61-67
- Salzman EW, Harris WH. Prevention of venous thromboembolism in orthopaedic patients. *J Bone Joint Surg [Am]* 1976;58-A:903-913
- Kakkar VV. Deep vein thrombosis: detection and prevention. *Circulation* 1973;51:8-19
- Stamatakis JD, Kakkar VV, Lawrence D, Bentley PG. The origin of thrombi in the deep veins of the lower limb: a venographic study. *Br J Surg* 1978;65:449-451
- Kakkar VV, Howe CT, Flanc C, et al. Natural history of postoperative deep vein thrombosis. *Lancet* 1969;2:230-233
- Dorfman GS, Cronan JJ, Tupper TB, Messersmith RN, Denny DF, Lee CH. Occult pulmonary embolism: a common occurrence in deep vein thrombosis. *AJR* 1987;148:263-266
- Kakkar VV, Howe CT, Nicolaides AN, Renney JTG, Clarke MB. Deep vein thrombosis of the leg: is there a "high risk" group? *Am J Surg* 1970;120:527-530
- Moser KM, LeMoine JR. Is embolic risk conditioned by the location of deep venous thrombosis? *Ann Intern Med* 1981;94:439-444
- Holder JC, Ferris EJ, Nelson CL, Boone DW. Evaluation of deep venous thrombosis in acute hip fractures and total hip replacement. *Radiology* 1984;153P:170



## FORTHCOMING ARTICLES

### PROGRESS IN RADIOLOGY

**Magnetic resonance angiography.** *Edelman RR, Mattie HP, Atkinson DJ, Hoogewoud HM*

**Adrenal imaging: current status.** *Dunnick NR*

**Percutaneous ethanol injection therapy for the treatment of hepatocellular carcinoma.** *Shiina S, Tagawa K, Unuma T, Terano A*

### REVIEW ARTICLES

**Physiology and radiology of the normal oral and pharyngeal phases of swallowing.** *Dodds WJ, Stewart ET, Logemann JA*

**Radiologic assessment of abnormal oral and pharyngeal phases of swallowing.** *Dodds WJ, Logemann JA, Stewart ET*

### CHEST RADIOLOGY

**Comparison of Biello, McNeil and Pioped criteria for the diagnosis of pulmonary emboli on lung scans.** *Webber MM, Gomes AS, Roe D, LaFontaine RL, Hawkins RA*

**Bronchiolitis obliterans organizing pneumonia: CT features in 14 patients.** *Müller NL, Staples CA, Miller RR*

**MR imaging of thoracic and abdominal wall infections: comparison with other imaging procedures.** *Sharif HS, Clark DC, Aabed MY, Aideyan OA, Haddad MC, Matsson TA*

**Computerized on-line reporting of coronary angiograms with the CLIP system.** *Kim D, Leeming BW*

**Case report. Laryngeal chondrosarcoma: CT findings in three cases.** *Muñoz A, Peñarrocha L, Gallego F, Olmedilla G, Poch-Broto J*

**Case report. Wooden foreign body in the lung parenchyma.** *Spouge AR, Weisbrod GL, Herman SJ, Chamberlain DW*

### GASTROINTESTINAL RADIOLOGY

**Percutaneous gastrostomy with gastrostomy: experience in 125 patients.** *Saini S, Mueller PR, Gaa J, et al.*

**Angioplasty for the long-term management of patients with Budd-Chiari syndrome.** *Martin LG, Henderson JM, Millikan WJ, Casarella WJ, Kaufman SL*

**CT of the abdomen after the Whipple procedure: value to depict postoperative anatomy, surgical complications, and tumor recurrence.** *Coombs RJ, Zeiss J, Howard JM, Thomford NR, Merrick HW*

**CT of hilar cholangiocarcinoma: late contrast enhancement in six patients.** *Takayasu K, Ikeya S, Mukai K, Muramatsu Y, Makuuchi M, Hasegawa H*

**Case report. Hepatic subcapsular hematoma: an unusual complication of biliary lithotripsy.** *McGrath FP, Lee SH, Gibney RG, Burhenne HJ*

### MUSCULOSKELETAL RADIOLOGY

**Adult ankle fractures: comparison of plain films and interactive two- and three-dimensional CT.** *Magid D, Michelson JD, Ney DR, Fishman EK*

**Insufficiency fracture of the sternum caused by osteopenia: plain film findings in seven patients.** *Chen C, Chandnani V, Kang HS, et al.*

**Pictorial essay. The Neer classification of displaced proximal humeral fractures: the spectrum of findings on plain radiographs and CT.** *Kilcoyne RF, Shuman WP, Matsen FA III, Morris M, Rockwood CA*

### PEDIATRIC RADIOLOGY

**Differentiation of osteogenesis imperfecta from child abuse.** *Ablin DS, Greenspan A, Reinhart M, Grix A*

**Commentary.** *Kleinman*

**Case report. Prenatal detection of an abdominal mass by MR imaging made during curarization of the fetus with pancuronium bromide.** *Toma P, Lucigrai G, Doderio P, Lituanica M*

### NEURORADIOLOGY

**The role of ferritin and hemosiderin in the MR appearance of cerebral hemorrhage: a histopathologic biochemical study in rats.** *Thulborn KR, Sorensen AG, Kowall NW, et al.*

**Carotid artery disease assessed by color Doppler flow imaging: correlation with standard Doppler sonography and angiography.** *Steinke W, Kloetzsch C, Hennerici M*

**Pseudoatrophy of the cervical portion of the spinal cord on MR images: a manifestation of the truncation artifact?** *Yousem DM, Janick PA, Atlas SW, et al.*

**Diagnosis of tumors of the parotid gland with anti-CEA immunoscintigraphy.** *Kairemo KJA, Hopsu EVM*

**Castleman disease in the neck: atypical appearance on CT.** *Chaloupka JC, Castillo M, Hudgins P*

### ENDOCRINE RADIOLOGY

**The diagnosis of acromegaly: value of inferior petrosal sinus sampling.** *Doppman JL, Miller DL, Patronas NJ, et al.*

**CT evaluation of anaplastic thyroid carcinoma.** *Takashima S, Morimoto S, Ikezoe J, et al.*

**Nonsurgical treatment of primary hyperparathyroidism with sonographically guided percutaneous injection of ethanol: results in a selected series of patients.** *Karstrup S, Holm HH, Glenthoj A, Hegedus L*

### ANGIOGRAPHY AND INTERVENTIONAL RADIOLOGY

**Transcatheter thrombolysis of a leaking saccular aneurysm of the main renal artery with preservation of renal blood flow.** *Routh WD, Keller FS, Gross GM*

**A solution to the problem of high-flow jets from miniature angiographic catheters.** *Daniel TB, Akins EW, Hawkins IF Jr*

**Technical note. Use of the Hawkins-Hunter rocket wire in the biliary system.** *Shaw DWW, Coldwell DM, Kimmey M, Goldman ML*

**Technical note. Complications from 0.018-in. floppy platinum tip guidewires.** *Quinn SF, Morse S*

**Case report. Phlegmasia cerulea dolens, a complication after placement of a bird's nest vena cava filter.** *Aruny JE, Kandarpa K*

### RADIOLOGIC TECHNOLOGY

**Evaluation of radiographs developed by a new ultrarapid film processing system.** *Schmidt RA, Doi K, Sekiya M, et al.*

### PERSPECTIVES

**The radiology manpower equation: a new look.** *Brogdon BG*  
**Quality improvement in diagnostic radiology.** *Cascade PN*

# Early Detection of Saphenous Vein Arterial Bypass Graft Stenosis by Color-Assisted Duplex Sonography: A Prospective Study

Joseph F. Polak<sup>1</sup>  
 Magruder C. Donaldson<sup>2</sup>  
 Gary R. Dobkin<sup>1</sup>  
 John A. Mannick<sup>2</sup>  
 Daniel H. O'Leary<sup>1</sup>

We propose a simple and rapid technique for the postoperative surveillance of developing stenosis in lower extremity saphenous vein arterial bypass grafts that uses color-assisted duplex sonography. Color Doppler flow images are used to identify points of altered flow dynamics. These points are subsequently analyzed by duplex sonography, with doubling of the peak systolic velocity at the point of suspected stenosis considered the diagnostic threshold for significant stenosis. A segment-by-segment comparison made with arteriography in 14 patients (15 grafts, 92 segments) showed this approach to be 95% sensitive (18/19) and 100% specific (73/73) for the detection and localization of focal graft stenoses that involve greater than 50% narrowing of the lumen diameter.

We conclude that color-assisted duplex sonography can accurately detect the presence of saphenous vein arterial bypass graft stenoses.

*AJR* 154:857-861, April 1990

In situ saphenous vein infrainguinal arterial bypass grafts have patency rates of greater than 80% at 3 years [1]. This long-term patency rate can be improved by detecting evidence of early graft malfunction and by early intervention [2, 3]. Graft surveillance is currently performed with sequential segmental pressure measurements and, more recently, Doppler sonography [2, 4, 5]. As both techniques are useful in detecting only the more severe high-grade stenoses, graft thrombosis has a high likelihood of occurring between repeated noninvasive measurements [2]. Subsequent thrombectomy followed by corrective surgery leads to a patency rate of less than 30% after 5 years [6].

Although duplex sonography can be used to detect arterial stenoses [7], the need to position the small-pulse Doppler gate sequentially over the full length of the vessel makes the examination tedious. Flow dynamics can be assessed rapidly, however, with the use of color Doppler sonography. We propose that color Doppler imaging be used to rapidly survey the length of arterial bypass grafts and that duplex sonography with spectral analysis be applied to sites of abnormal flow signal [8-10].

In this report, the use of color-assisted duplex sonography for the detection of arterial graft stenosis is described.

## Subjects and Methods

Fourteen patients who had undergone in situ vein (13) or reversed (two) saphenous bypass operations for arterial insufficiency form the basis of this report. There were nine men and five women; the age range was 54-74 years. All bypass grafts were studied within 15 months of the revascularization procedure (average,  $4.8 \pm 3.9$  months SD; range, 1-15 months). Patients presented with either new or persistent symptoms (nine) or with a drop in or lack of improvement of the ankle/brachial ratio postoperatively (five).

Received August 9, 1989; accepted after revision October 10, 1989.

<sup>1</sup>Department of Radiology, Harvard Medical School and Brigham and Women's Hospital, 75 Francis St., Boston, MA 02115. Address reprint requests to J. F. Polak.

<sup>2</sup>Department of Surgery, Harvard Medical School and Brigham and Women's Hospital, 75 Francis St., Boston, MA 02115.

0361-803X/90/1544-0857  
 © American Roentgen Ray Society

All cases were studied prospectively before arteriography by using a commercial Doppler color flow–equipped sonographic (5 MHz) device (Acuson, Computed Sonography, Mountain View, CA). The color Doppler flow map is a two-dimensional display of Doppler information superimposed, in real time, on a gray scale image [8, 9]. It displays the *mean* Doppler frequency shift of flowing blood within grafts with a temporal resolution of 50 to 100 m/sec. Direction was encoded in blue or red. Increasing frequency shifts due to higher velocities of flowing blood in the graft lumen were encoded as a progressive saturation of color from dark to bright red. Flow in the reverse direction is encoded from deep to light blue. Zones of increased velocities typically show up in white or aliased into the blue portion of the color map. Zones of disturbed flow appear as a heterogeneous mixture of red and blue and correspond to spectral broadening on the Doppler spectrum. All sites showing a loss of the normal laminar pattern of color flow signals in the graft lumen were sampled with pulsed Doppler imaging (3.5 MHz).

We adopted the following protocol. The transducer is held parallel to the graft while the proximal anastomosis is imaged. Blood flow within the graft is confirmed both by color Doppler mapping and by pulsed Doppler waveform analysis. The probe is then held transverse to the graft, angled 60° to the skin, and the course of the vein graft is followed. The transducer is moved slowly along the graft with frequent pauses to confirm the presence of blood flow. The typical pattern of alternating red to blue signals corresponds to the Doppler spectral pattern of triphasic flow. A mainly forward pattern of flow corresponds either to the biphasic flow pattern seen with Doppler imaging or, if forward flow is seen briefly in systole, to a monophasic pattern. Any suspicious areas where the pulsatile color signal is lost or the color image is saturated toward the high-intensity red signals, or even aliased in the blue, are noted on the skin. Finally, the transducer is oriented longitudinally and the distal graft anastomosis is identified with color Doppler imaging and examined by using pulsed Doppler sonography.

A second pass is then performed over the identified course of the graft, this time with the transducer held parallel to the graft. The transducer is advanced in successive increments equal to the length of the probe. The color window is kept at a 20° angle to the graft lumen in order to enhance flow sensitivity. The color scale is set to a maximal mean velocity between 0.68 and 0.92 m/sec in order to keep the color flow signals from the lumen within the range of the red color map. All areas with loss of normal color signals (bright red to white, aliasing to blue, or intermixing of red and blue) are examined with pulsed Doppler sonography. In cases of abrupt changes in the course of the graft, angle-corrected pulsed Doppler sonography is used to renormalize the color scale and to correct the color window for the angle. Pulsed Doppler measurements are made every 10 cm if no zones of abnormal color are detected.

A survey takes 10–20 min. The flow in the lumen is often clearly seen in color despite a poor-quality gray-scale image on which native artery or graft lumen cannot be identified. This typically occurs near the distal anastomosis. All sites that show signals diverging from an even filling of the lumen on longitudinal images are sampled with pulsed Doppler imaging. The presence of significant stenoses is determined by analysis of the resultant angle-corrected pulsed Doppler spectrum. In the graft conduit, the peak systolic velocity is compared with the peak systolic velocity at a point of normal color signals 2 to 3 cm proximal. A similar approach is taken at the distal anastomosis. Peak systolic velocities at the proximal anastomosis are compared with those within the normal conduit 5 to 10 cm distal. Doubling of the peak systolic velocities measured with pulsed Doppler imaging was considered indicative of a greater than 50% narrowing of the lumen [7].

Arteriography with the standard Seldinger approach was performed in 11 patients. Antegrade puncture was performed in one. In

two, intraoperative arteriograms were obtained. The delay between sonography and arteriography varied from 1 day to 2 months (average  $13.6 \pm 16.0$  days SD). Stenosis was graded in a blinded fashion as percentage of narrowing of the lumen diameter.

Graft stenosis is a broad term that refers to stenosis developing either in the graft conduit, the anastomotic sites, or adjacent artery segments [5]. The graft conduits were analyzed on a segment-by-segment basis according to their respective lengths. The anastomoses were considered separately. This facilitated comparison between the sonographic and arteriographic findings. The thigh and calf were divided into thirds. For example, if a graft arose from the mid superficial femoral artery and anastomosed to the mid posterior tibial artery, two anastomoses and four segments were at risk of a stenosis developing. The measurements performed with the aid of Doppler sonography were matched to these anatomic divisions on the arteriograms. A stenosis was classified as anastomotic if it arose within 2 cm of the anastomotic suture line.

There were 28 of 30 anastomoses available for comparison; two were not clearly shown at arteriography. Sixty-four separate segments of the graft conduits also were studied with both arteriography and sonography. There were 10 below-knee and five above-knee grafts in the 14 patients studied.

Sensitivity and specificity were calculated according to previous recommendations [11]. Anastomoses and segments at risk from each of the grafts were considered together in the determination of the sensitivity and specificity of the technique when compared with arteriography.

## Results

Of the 13 grafts with significant stenoses, four had velocities below 0.45 m/sec (Fig. 1). Therefore, the true-positive rate for lowered velocities below 0.45 m/sec for the detection of graft stenoses was 31%.

Five grafts had solitary anastomotic stenoses, and four had focal segmental stenoses. Three grafts had tandem lesions, each having combined focal segmental and anastomotic stenoses. One graft had four focal stenoses, one of which involved an anastomosis. The distribution of peak systolic velocities measured in the different segments and anastomoses (92 sites) is shown in Table 1 as a function of the stenosis grading by using arteriography (percentage of narrowing of the diameter of the lumen).

Ten of the 28 anastomoses had significant stenosis (>50%) on arteriography. Nine were detected by use of color-assisted duplex sonography when the peak systolic velocity ratio was above 2.0. In the graft conduits, nine of the 64 segments imaged had focal segmental stenoses greater than 50% by arteriography. All had a systolic velocity ratio greater than 2.0. Sensitivity of color-assisted duplex sonography for the combined detection of significant (>50%) focal lesions involving either the conduit or the anastomosis (92 sites; Table 2) was therefore 95% (18/19), and specificity was 100% (73/73).

The mean of the peak systolic velocities of nonstenotic segments was  $0.7 \pm 0.29$  m/sec. The graft in which a significant proximal stenosis was missed also had a high grade stenosis distally and a peak systolic velocity of 0.4 m/sec in the nonstenotic segments. When a velocity above 1.3 m/sec, corresponding to two standard deviations above the average velocity in the nonstenotic segments, is used as a

Fig. 1.—Value of color-assisted duplex sonography for serial monitoring of arterial bypass graft is shown by progression of a distal stenosis monitored for 2 months in this 54-year-old man with a femoropopliteal graft.

A, Color map shows a zone of color aliasing corresponding to a peak systolic velocity of 2.3 m/sec at distal femoropopliteal graft (arrow) and zone of heterogeneous color (arrowheads) extending distally into native popliteal artery. With velocity of 0.36 m/sec at proximal graft, peak systolic velocity ratio is 2.4.

B, First Doppler spectrum obtained shows that peak systolic velocity in proximal graft is normal despite presence of distal anastomotic stenosis.

C, Doppler spectrum obtained at 2-month follow-up shows velocity in proximal graft has dropped to below 0.35 m/sec. Peak systolic velocity at stenosis has decreased to 1.52 m/sec. Calculated peak systolic velocity ratio has increased to 4.3, thereby confirming progression of stenosis.

D, Arteriogram shows corresponding high-grade focal stenosis (arrow) in distal graft just proximal to anastomosis (arrowheads).

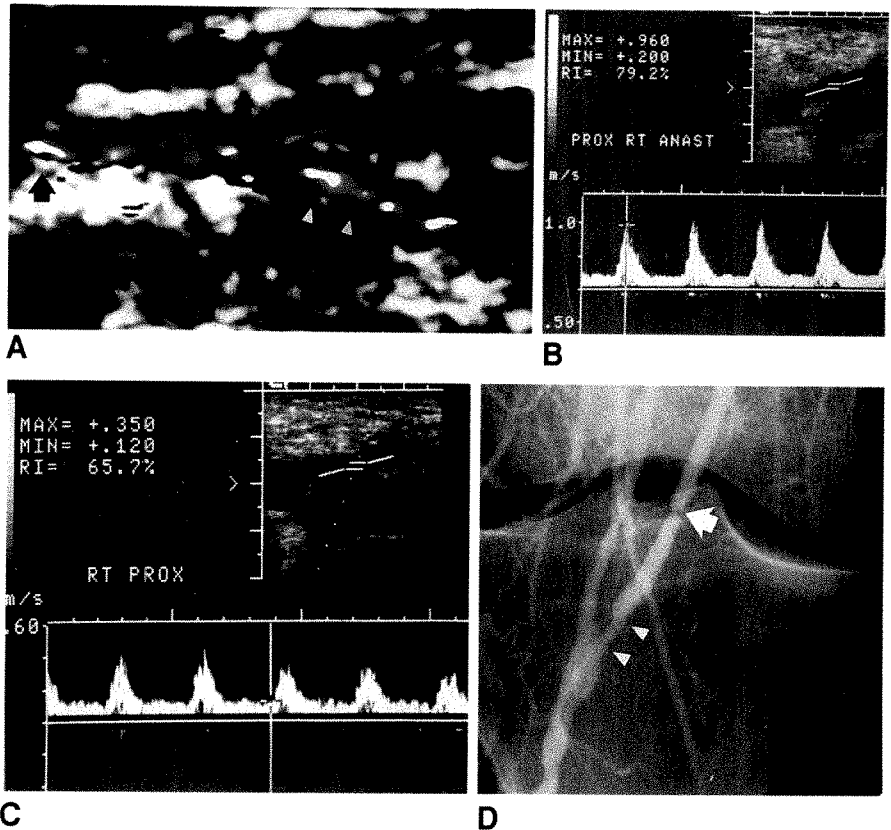


TABLE 1: Distribution of Segmental and Anastomotic Peak Systolic Velocities As a Function of Stenosis Grade

Stenosis Grade (%)	Peak Systolic Velocity (m/sec)				
	0-0.99	1.00-1.99	2.00-2.99	3.00-3.99	4.00-4.99
0-49	50	23	0	0	0
50-74	0	1	2	1	0
75-99	2	2	4	4	3

Note.—Includes 28 anastomoses and 64 separate graft segments each 8-12 cm long. Stenosis grade measured as percentage of narrowing of lumen diameter at arteriography. Peak systolic velocity measured from Doppler spectrum obtained at points of altered flow dynamics during color Doppler imaging.

TABLE 2: Distribution of Segmental and Anastomotic Peak Systolic Ratio As a Function of Stenosis Grade

Stenosis Grade (%)	Peak Systolic Velocity Ratio (m/sec)				
	0-1.99	2.00-2.99	3.00-3.99	4.00-4.99	>5.00
0-49	73	0	0	0	0
50-74	0	4	1	0	0
75-99	1	2	4	3	4

Note.—Includes 28 anastomoses and 64 separate graft segments each measuring 8-12 cm in length. Stenosis grade measured as percentage of lumen diameter narrowing at arteriography. Peak systolic velocity determined from Doppler spectrum at point of altered color signals is divided by peak systolic velocity at a site where flow dynamics are normal.

discriminator for the presence of a significant stenosis, the sensitivity decreases to 84% (16/19) with no change in the specificity of 100% (73/73).

The qualitative evaluation of the color flow patterns in the grafts typically showed turbulence at the proximal anasto-

mosis. This finding was confirmed by Doppler spectral analysis and did not appear to be indicative of a significant stenosis if the peak systolic velocities were not elevated. The flow patterns at the distal anastomosis were more homogeneous and laminar.

## Discussion

In situ femoropopliteal and femorotibial vein bypass grafts used for arterial revascularization maintain patency rates of more than 80% 1–3 years after surgery [1, 3]. Causes of early graft failure in the first postoperative month include missed arteriovenous communications, intact valve cusps, fibrin-platelet aggregates, intimal flaps, and other technical imperfections [12]. Causes of graft failure in the following months and up to 2 years after surgery are mostly linked to intrinsic hyperplastic lesions that develop near graft anastomoses and at the site of venous valves [6].

It is believed that the latter lesions, if not treated early, will continue to progress, resulting in graft thrombosis and occlusion [2]. Once occluded, reopening the graft by thrombectomy and surgical revision carries a low likelihood of success, with 5-year patency rates of less than 28% [2]. If, however, surgical revision or angioplasty is undertaken while the graft is still open, 1-year patency rates can be maintained near those for unrevised grafts [3, 6]. For these reasons and because up to 62% of patients with significant graft stenoses may remain asymptomatic, an aggressive postoperative graft surveillance program is instituted. Currently this consists of Doppler segmental pressure measurements of the ankle/brachial ratio 3 weeks after surgery, 6 weeks after surgery, and every 4 months thereafter. An arteriogram is recommended if this ratio drops by more than 0.15 to 0.20. There remains, however, the possibility that developing stenoses might progress far enough between two follow-up visits to result in graft thrombosis [4, 5]. For this reason, a means of

detecting stenoses earlier, before they progress to occlude the graft, would be beneficial.

The use of Doppler sonographic waveform analysis, based on sampling of the blood flow velocity at a single site in the graft, shows promise. Bandyk et al. [4] have reported that midstream graft flow velocities less than 0.45 m/sec are associated with a likelihood of graft occlusion. This approach detects stenoses severe enough to impede flow. In our series, nine of the 13 grafts with significant stenosis had velocities higher than the recommended threshold of 0.45 m/sec.

In this report, a simple yet rapid method for performing graft surveillance with color Doppler imaging has been described. Zones of abnormal color flow signals are examined quickly and selectively by using pulsed Doppler imaging. This can be performed even in cases in which the actual lumen of the graft is poorly visualized on the gray-scale image (Fig. 2).

Recent reports have shown similar sensitivity of duplex sonography for detecting graft stenoses [5]. The advantage of color Doppler imaging is that it enhances the efficiency of the examination, allowing it to be completed in 10 to 20 min. Duplex sonography is needed to quantify the severity of the stenotic segment accurately for two reasons. In order to use a 100% increase in the peak systolic velocity as a discriminator for detecting stenoses greater than 50%, Doppler spectral analysis must be used to measure peak systolic velocities. This simple criterion cannot be adopted with color Doppler imaging because the color map displays the mean velocity and not the peak systolic velocity. The use of spectral analysis is therefore favored. In addition, color Doppler imaging has lower temporal resolution when compared with pulsed Dop-

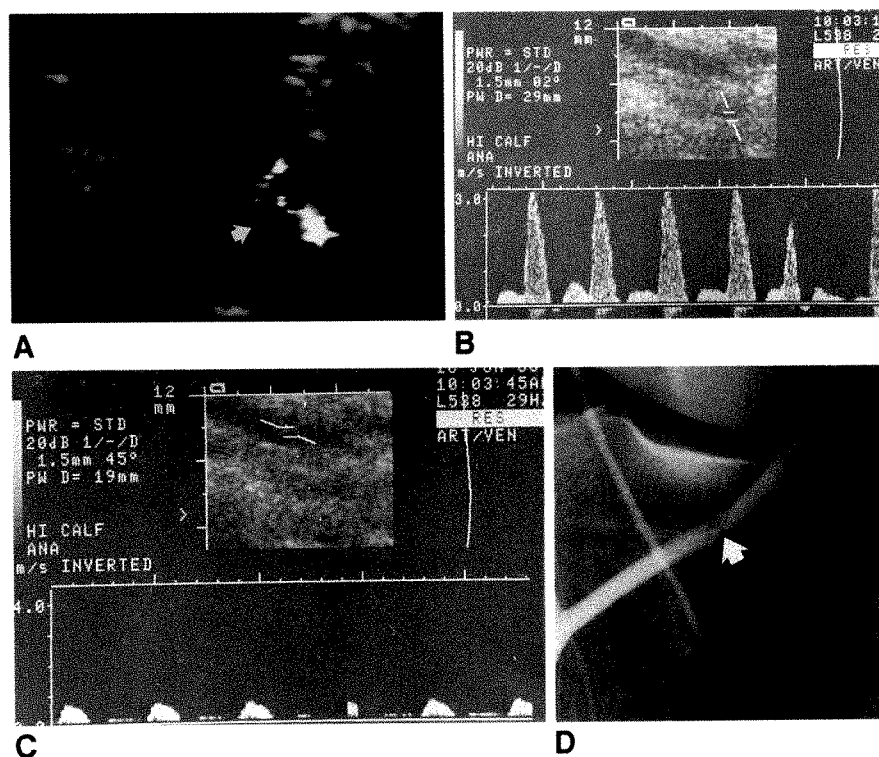


Fig. 2.—Value of color Doppler imaging near distal graft anastomosis is shown in this 63-year-old man with a femorotibial graft. Difficulty in clearly identifying graft lumen on gray-scale image is abated by use of color Doppler image.

A, Color Doppler flow image shows a focal zone of turbulence (arrow) near distal anastomosis of a femorotibial bypass graft. Image is taken longitudinally, from back of knee, with proximal portion of graft to left. Zone of turbulence (arrow) is located where graft dives toward more deeply located popliteal artery. Distal anastomosis is located to right of image, beyond imaging window.

B and C, Corresponding Doppler waveforms confirm presence of increased velocity at site of a stenosis. Lower portion of graft was poorly visualized on gray-scale image. Positioning of Doppler gate over stenosis was guided by color image. Note Doppler spectrum proximal to stenosis (B). Calculated velocity ratio is 4 (3.2 m/sec divided by 0.8 m/sec).

D, Corresponding arteriogram confirms stenosis at a valve (arrow).

pler imaging, making the point of peak systolic flow more difficult to locate with color Doppler sonography so that significant stenoses could be underestimated.

When low overall graft flow velocities are present, it may be difficult to determine the severity of multiple coexistent stenoses. In one instance, in which the graft velocity was 0.2 m/sec in normal segments, a greater than 75% narrowing of the segments corresponded to a velocity increase of 0.6 m/sec. Although this is below the group average of the velocities seen in normal segments, this threefold increase relative to normal segment velocity in the same graft correctly predicted a graft stenosis.

We conclude that color Doppler sonography can be used to detect and characterize saphenous vein bypass graft stenoses accurately. Because this method is more sensitive than sampling of graft velocity at a single point, it may enhance salvage of grafts before occlusion. The use of color Doppler sonography to rapidly survey the graft anatomy makes the method rapid and efficient enough to be a practical alternative in many noninvasive laboratories.

#### ACKNOWLEDGMENTS

The authors thank Vennetta Hanley for secretarial assistance, and Jo-Anne Polak and Jeffery Stoia for editorial help.

#### REFERENCES

1. Fogle MA, Whittemore AD, Couch NP, Mannick JA. A comparison of in situ and reversed saphenous vein grafts for infrainguinal reconstruction. *J Vasc Surg* 1987;5:46-52
2. Cohen JR, Mannick JA, Couch NP, Whittemore AD. Recognition and management of impending vein-graft failure: importance for long-term patency. *Arch Surg* 1986;121:758-759
3. Berkowitz HD, Greenstein SM. Improved patency in reversed femoral-infrapopliteal autogenous vein grafts by early detection and treatment of the failing graft. *J Vasc Surg* 1987;5:755-761
4. Bandyk DF, Cato RF, Towne JB. A low flow velocity predicts failure of femoropopliteal and femorotibial bypass grafts. *Surgery* 1985;98:799-809
5. Bandyk DF, Seabrook GR, Moldenhauer P, et al. Hemodynamics of vein graft stenosis. *J Vasc Surg* 1988;8:688-695
6. Whittemore AD, Clowes AW, Couch NP, Mannick JA. Secondary femoropopliteal reconstruction. *Ann Surg* 1981;193:35-42
7. Jager KA, Phillips DJ, Martin RL, et al. Noninvasive mapping of lower limb arterial lesions. *Ultrasound Med Biol* 1985;11:515-521
8. Switzer DF, Nanda NC. Doppler color flow mapping. *Ultrasound Med Biol* 1985;11:403-416
9. Kasai C, Namekawa K, Koyano A, Onoto R. Real-time two dimensional blood flow imaging using an autocorrelation technique. *IEEE Trans Sonics Ultrason* 1985;S-32:458-463
10. Spencer MP, Reid JM. Quantitation of carotid stenosis with continuous-wave (C-W) Doppler ultrasound. *Stroke* 1979;10:326-330
11. McNeil BJ, Keller E, Adelstein SJ. Primer on certain elements of medical decision making. *N Engl J Med* 1975;293:211-215
12. Batson RC, Sotturrai VS. Nonreversed and in situ vein grafts: clinical and experimental observations. *Ann Surg* 1985;201:771-779



## Book Review

**Basic Principles of Radiographic Exposure.** By Dianne C. De Vos. Philadelphia: Lea & Febiger, 147 pp., 1990. \$17.50

This is a practical how-to book directed to student radiographers. The format makes it suitable for self-instruction as well as class instruction. The material is divided into 15 chapters, each covering a specific subject. Each chapter opens with a statement of the objectives of the chapter, defined in terms of the new skills the student will acquire as a result of understanding its contents, and concludes with a group of review questions. Two thirds of the chapters provide a series of suggested laboratory exercises to illustrate the principles described. The book also has a compilation of 125 review questions and a list of suggested further reading. It has a good table of contents, an index, and an answer key.

The subjects covered are X-ray production and properties, factors of radiographic exposure, contrast, inverse square law, unsharpness, filters, grids, screens, film, beam-obstructing devices, geriatric and pediatric techniques, impact of pathology on exposure factors, automatic exposure-control devices, preparation of technique charts, and interpretation of X-ray tube rating and cooling charts. The author favors the variable kVp (peak kilovoltage) school in obtaining the baseline parameters of radiographic exposure.

The book is written in a relaxed conversational style that is surprisingly easy to follow. The author is at her strongest when discussing practical details of film storage, care of equipment, and the impact of changes in X-ray exposure factors and beam restriction on the density scale, contrast, and, therefore, usefulness of the resultant radiograph. Explanation of the arithmetic steps required in adjusting the prime factors of radiographic exposure are quite detailed. Discus-

sion of more abstract matters (e.g., the source of magnification in the radiographic image and film and screen speed) is less than rigorous.

The illustrations and their associated captions are probably the area in most need of editorial attention. Tissues are identified by upper-case letters in the figure and referenced by lower-case letters in the captions, and parts of figures are translocated (e.g., the plan view of focused and linear grids). Captions do not always agree with the phenomenon illustrated in the figure. In the second example of misuse of focused grids, wrong focus-to-grid distance is captioned as central ray misalignment. Some of the photographs are not particularly informative. The author perhaps should ask herself, Is this photograph necessary, and does it clearly and unambiguously illustrate my point? But after all, the book has 54 illustrations.

Students who absorb the contents of this book will have respect for their tools and the handling of these tools and will be able to produce creditable radiographs in a variety of situations. The book is a good starting point for therapy technologists with no diagnostic experience who suddenly are faced with simulator operation. This is not an academic text, but students probably will wish there were a few more like it in other areas of radiology. If you want to know how to produce a useful radiograph but do not care why it works, this is a good buy.

Peter Wootton  
University of Washington  
Seattle, WA 98195

## Computer Page

# Performing JCAHO Dose Calculations with the Aid of a Microcomputer Spreadsheet Program

George David<sup>1</sup> and Stan C. Price

The Joint Commission on Accreditation of Healthcare Organizations (JCAHO) published new standards for accreditation effective January 1987. Among the significant changes in these standards was a directive that a qualified individual "monitors doses from diagnostic radiology procedures" [1]. This monitoring process is to be based on actual measurements made in each radiographic room at a variety of kilovoltage settings and not on tables or calculations.

A protocol has been developed to permit rapid generation or alteration of dose data for radiologic procedures by using a standard personal computer spreadsheet. The spreadsheet provides exposure data that may be directly compared with accepted guidelines such as those published by the Conference of Radiation Control Program Directors, Inc. [2]. As stated in the group's *Average Patient Exposure Guides*, such comparisons are important because "exposures that significantly exceed the levels indicated in the guides for routine examinations are likely to represent unnecessary patient doses and causes for such excessive exposure should be investigated."

The protocol described requires a technique chart for each radiographic unit corresponding to a "standard" patient. A total of five exposures is also required, one each performed on the unit of interest at five kilovoltage settings covering the useful clinical range. Exposure and technique chart data are entered into a template by using Quattro spreadsheet software (Borland International, Scotts Valley, CA). The spreadsheet then calculates entrance skin exposures for each radiologic procedure.

## Materials and Methods

The spreadsheet template requires that five output measurements be taken on the radiographic unit of interest at a 40-in. (102-cm) source-to-image distance (SID). Each exposure is taken at a different kilovoltage setting. The kilovoltage values selected should span the range of clinical use. With the use of these five output measurements, the spreadsheet performs a least-squares calculation [3] resulting in the coefficients for a third-degree polynomial equation:

$$E_N = A_0 + A_1 \times K + A_2 \times K^2 + A_3 \times K^3,$$

where  $K$  = kilovoltage (kVp);  $A_0$ ,  $A_1$ ,  $A_2$ , and  $A_3$  are the polynomial coefficients, and  $E_N$  is normalized output. This polynomial yields normalized output (mR/mAs at a 40-in. [102-cm] SID) as a function of kilovoltage. The polynomial is used to interpolate normalized output between values of kilovoltage at which output was measured. A third-degree polynomial was selected because it afforded a significantly better fit to the raw data than a second degree polynomial, whereas a fourth degree polynomial did not improve accuracy significantly.

For each radiologic procedure the template requires that one enter the kilovoltage and milliamperes-second settings, the SID, and the thickness of the patient presented to the central ray of the beam. Film-to-tabletop distance for the unit is also entered. A thickness is chosen from the technique chart to simulate a standard patient. The template first calculates normalized output from the polynomial on the basis of the procedure's kilovoltage. Total exposure at a 40-in. (102-cm) SID is calculated by multiplying normalized output by the procedure's milliamperes-second setting:

$$E_{40} = E_N \times m,$$

where  $E_{40}$  is the exposure at a 40-in. (102-cm) SID and  $m$  is the milliamperes-second setting selected.

Received September 1, 1989; accepted after revision November 6, 1989.

<sup>1</sup> Both authors: Department of Radiology AE-2018, Medical College of Georgia, 1450 Laney-Walker Blvd., Augusta, GA 30912. Address reprint requests to G. David.

Finally, a distance correction is performed by subtracting the film-to-tabletop distance and patient thickness from the SID to find the entrance skin exposure by using the inverse square law:

$$E = E_{40} \times 40^2 / (S - B - T)^2,$$

where E is the entrance skin exposure, S is the SID in inches, B is the distance between the tabletop and the film, and T is the thickness of the patient in the beam path.

Figure 1 shows the printed output generated by the Quattro template. At the Medical College of Georgia Hospital and Clinics a list was made of the most commonly performed examinations, along with the SID used and standard thickness of the patient. This list was used as the template for all but the specialty units, for which the list was modified. The template also contains the least-squares calculation for the kilovoltage-output polynomial as well as the formula for dose calculation for each examination. A "macro" (single-key stroke) is used to recalculate the spreadsheet. This macro first calculates a new kilovoltage-output polynomial, using this polynomial to compute entrance exposures. The macro recalculation process takes only a few seconds and is used whenever information on the spreadsheet is changed.

The template makes it very simple either to update dose calculations after a new calibration or to generate data for a new unit. If a new calibration is performed, new output data must be entered at the top of the spreadsheet and the recalculation macro invoked. If technique charts are modified, the new kilovoltage and milliamperesecond values are entered, and recalculation performed. In order to develop exposure data for a new unit, techniques (kilovoltage and

milliamperesecond values) and output measurements are entered into a blank template, and the recalculation macro is invoked.

## Results

In order to validate the spreadsheet formulas, entrance skin exposures for 26 common radiologic procedures were calculated with the template for a radiographic unit at the Medical College of Georgia Hospital and Clinics and then compared with measurements taken with the same technique and distance. The unit used was a Toshiba KXO-30R medium-frequency generator. This unit had previously been surveyed to confirm that it had proper filtration, that milliamperesecond linearity was acceptable over the usable range of milliamperesecond settings and between focal spots, and that output from the unit was consistent over a number of identical exposures.

Five output measurements at kilovoltage values ranging from 60 to 120 were made with an MDH 1015 ionization chamber with its 6-cm<sup>3</sup> probe (MDH Industries, Inc., Monrovia, CA). The kilovoltage range matched the clinical range for the unit as indicated on technique charts. Techniques for the 26 studies on this unit for our assumed standard patient as well as the output measurements were entered into the spreadsheet. The spreadsheet then was used to calculate entrance skin exposures for each study.

The spreadsheet generated a third-order polynomial from the five output measurements made at various values of kilovoltage, as described previously. This polynomial should provide a calculated output that matches the five outputs measured over the kilovoltage range. Table 1 shows that the error of the polynomial calculation for the five data points was no more than 0.5%, indicating that the polynomial calculated by the spreadsheet was an excellent match to measured data points.

Output measurements were then taken for each of these 26 techniques at the SID indicated less the film-to-tabletop distance and assumed thickness of the patient. All exposures were done at a single milliamperesecond setting, varying only distance, kilovoltage, and time in order to avoid the introduction of linearity errors, because the goal was to validate spreadsheet calculations, not to evaluate linearity inconsistencies of a particular generator. Table 2 shows calculated and measured exposures for the 26 techniques and displays the error between the two. The average absolute error was 2.4%; in no case did a measurement vary by more than 9.1% from the calculated value. It should be noted that in a recent survey of this radiographic unit it was found that there was less than a 1% variation between any in a series of identical exposures.

The results confirmed the accuracy of the spreadsheet formulas used and compared favorably with the variations between calculated and measured data reported by Shrimpton [4], which in several instances exceeded a factor of 2. Shrimpton stated that, for his technique, "the degree of agreement between measured and calculated skin doses is largely a characteristic of each particular X-ray set" [4]. The template described here eliminates such correlations by calculating normalized output on the basis of actual exposures rather than an empirical formula.

Typical Patient Exposures Toshiba Radiographic 103					
08/25/89					
		kVp		Output (40") (mR/mAs)	
Film to Table: 3 inches (7.6 cm)		60	2.77		
		80	6.22		
		90	8.44		
		100	11.1		
		120	16.9		
EXAM / VIEW	Thick (cm)	SID (in)	kVp	mAs	mR
Skull (AP, PA, Bas, Lat)	20	40	74	25	235
Mandible (PA, Lat)	11	40	60	21	87
C Spine (Lat)	12	72	65	21	28
C Spine (AP, Obl, Odon)	12	40	65	25	133
T Spine (AP)	21	40	74	36	348
T Spine (Lat)	28	40	65	60	493
T Spine (Swimmer)	21	40	74	36	348
L Spine (Obl)	24	40	74	100	1052
L Spine (Lat)	24	40	74	75	789
L Spine (L5-S1)	33	40	92	150	3739
L Spine (Lat)	30	40	92	100	2265
Pelvis (AP/Frogleg)	21	40	70	48	397
Sacrum/Coccyx (AP)	21	40	65	90	604
Coccyx (Lat)	33	40	92	64	1596
Sacrum (Lat)	33	40	92	125	3116
Pelvimetry (Lat)	30	40	92	100	2265
Pelvimetry (AP)	26	40	83	75	1147
IVP	21	40	80	36	432
Abdomen (KUB)	24	40	80	40	522
Ribs (above diaph.)	21	40	65	16	107
Ribs (below diaph.)	21	40	74	48	464
Stomach & Colon	24	40	111	12	359
Esophagus	21	40	92	16	278
Shoulder (AP/Obl)	15	40	65	20	115
Femur (AP/Lat)	17	40	65	35	211
Knee	12	40	60	25	106

Fig. 1.—Printed output generated by Quattro template. EXAM = examination; SID = source-to-image distance; AP = anteroposterior; PA = posteroanterior; Bas = basilar; Lat = lateral; Obl = oblique; Odon = odontoid; C = cervical; T = thoracic; L = lumbar; IVP = IV pyelography (excretory urography); KUB = kidney, urinary, bladder (supine abdominal); diaph. = diaphragm.

## Discussion

The validity of results depends on both the accuracy of the input data and the condition of the equipment. The accuracy of results can be no better than that of the technique chart for the unit. In addition, the X-ray unit must be consistent from exposure to exposure at identical settings and exhibit acceptable milliamperage linearity between stations and be-

tween focal spots. In practice, the use of this spreadsheet should be coupled with a quality control program that checks the above items in addition to other performance parameters such as half-value layer, timer, and kilovoltage accuracy. The equipment used to make output measurements should be suitable and properly calibrated.

Although the JCAHO recommends that institutions monitor doses and the American Association of Physicists in Medicine

**TABLE 1: Comparison of Measured Exposure Data with Least-Squares Polynomial**

Calculated Coefficient Matrix	kVp	Output at 40 in. (102 cm) in mR/mAs ( $\mu\text{C/kg/mAs}$ )		% Error <sup>a</sup>
		Measured	Calculated	
6.35	60	2.77 (0.71)	2.773 (0.715)	0.10
$-2.84 \times 10^{-1}$	80	6.22 (1.60)	6.195 (1.598)	-0.40
$4.37 \times 10^{-3}$	90	8.44 (2.18)	8.485 (2.189)	0.53
$-1.06 \times 10^{-5}$	100	11.1 (2.86)	11.075 (2.857)	-0.23
	120	16.9 (4.36)	16.903 (4.361)	0.02

Note.— Output =  $A_0 + A_1 \times K + A_2 \times K^2 + A_3 \times K^3$ , where K = kilovoltage (kVp).

<sup>a</sup> The percent error numbers in this table were derived from values for calculated outputs that reflected true accuracy. Thus, the percent errors shown in this table sometimes disagree slightly with values that would result if the rounded off calculated exposure values shown in this table were used for the calculation.

**TABLE 2: Comparison of Calculated and Measured Exposures**

Examination/View	mR ( $\mu\text{C/kg}$ )		% Error <sup>a</sup>
	Calculated	Measured	
Skull (AP, PA, basilar, lateral)	235.38 (60.7)	245.0 (63.2)	4.1
Mandible (PA, lateral)	87.29 (22.5)	92.4 (23.8)	5.9
Cervical spine			
Lateral	28.17 (7.3)	25.6 (6.6)	-9.1
AP, oblique, odontoid	133.00 (34.3)	132.0 (34.1)	-0.8
Thoracic spine			
AP	348.30 (89.9)	362.0 (93.4)	3.9
Lateral	492.79 (127.1)	492.0 (126.9)	-0.2
Swimmer	348.30 (89.9)	360.0 (92.9)	3.4
Lumbar spine			
Oblique	1052.24 (271.5)	1070.0 (276.1)	1.7
AP	789.18 (203.6)	806.0 (207.9)	2.1
L5-S1	3739.47 (964.8)	3715.0 (958.5)	-0.7
Lateral	2264.67 (584.3)	2270.0 (585.7)	0.2
Pelvis (AP, froglike)	397.21 (102.5)	406.0 (104.7)	2.2
Sacrum/coccyx (AP)	604.18 (155.9)	599.0 (154.5)	-0.9
Coccyx (lateral)	1595.51 (411.6)	1610.0 (415.4)	0.9
Sacrum (lateral)	3116.23 (804.0)	3120.0 (805.0)	0.1
Pelvimetry			
Lateral	2264.67 (584.3)	2260.0 (583.1)	-0.2
AP	1146.97 (295.9)	1170.0 (301.9)	2.0
Excretory urography	432.23 (111.5)	447.0 (115.3)	3.4
Abdomen (supine)	522.32 (134.8)	541.0 (139.6)	3.6
Ribs			
Above diaphragm	107.41 (27.7)	107.0 (27.7)	-0.4
Below diaphragm	464.40 (119.8)	477.0 (123.1)	2.7
Stomach and colon	359.07 (92.6)	376.0 (97.0)	4.7
Esophagus	278.49 (71.8)	288.0 (74.3)	3.4
Shoulder (AP, oblique)	114.64 (29.6)	114.0 (29.4)	-0.6
Femur (AP, lateral)	211.18 (54.5)	211.0 (54.4)	-0.1
Knee	106.47 (27.5)	112.0 (28.9)	5.2

Note.—AP = anteroposterior; PA = posteroanterior.

<sup>a</sup> The percent error numbers in this table were derived from values for calculated exposures that reflected true accuracy. Thus, the percent errors shown in this table sometimes disagree slightly with values that would result if the rounded off calculated exposure values shown in this table were used for the calculation. Average absolute error = 2.4%.

and the American College of Radiology further clarify that calculations must be based on actual measurements made at a variety of kilovoltage settings, a number of items are not addressed specifically. These include specifics on the assumed standard patient and the manner in which doses should be measured. At the Medical College of Georgia it was decided that exposures be calculated based on guidelines of the Committee on Quality Assurance in Diagnostic Radiology of the Conference of Radiation Control Program Directors, Inc. [2]. The main purpose of this document is to provide baseline data for ready comparison of patient exposures to national standards. The Quattro spreadsheet calculates entrance skin exposure in air without backscatter and provides documentation that may be directly compared with these published standards. Unlike techniques based on an empirical formula such as those used by Shrimpton [4], McGuire and Dickson [5], and Zamenhof et al. [6], the method we describe relies entirely on actual output measurements made on the unit being studied for its kilovoltage-output relationship. As stated above, JCAHO standards require that these measurements be performed on the unit of interest rather than on inference from measurements made on other units.

McGuire and Dickson [5] state that their technique allows computation of entrance skin exposure from a single test measurement. This assertion can be misleading because additional exposures are required to establish the half-value layer for the beam at the test kilovoltage. By actually measuring output at a range of kilovoltage values, the spreadsheet template does not rely on half-value layer or filtration, or knowledge of their relationship.

This template provides a means of rapidly calculating typical patient exposures for a variety of radiologic procedures based on actual exposure measurements as required by JCAHO standards. The technique was designed so that anyone who has access to an ionization chamber and a knowledge of spreadsheet software on an MS-DOS microcomputer can quickly and easily generate or update exposure tables. Because results are based on interpolation of output from actual exposures with no underlying assumptions about tube half-value layer, the accuracy of the calculations was found to correlate favorably with actual exposure measurements.

A copy of the spreadsheet template will be provided on request. Interested persons are asked to include a blank 3.5- or 5.25-in. (8.9- or 13.3-cm) diskette and a self-addressed mailer with their request.

#### REFERENCES

1. The Joint Commission on Accreditation of Healthcare Organizations. *Accreditation manual for hospitals*. Chicago: Joint Commission on Accreditation of Healthcare Organizations, **1989**:14
2. Committee on Quality Assurance in Diagnostic Radiology (H-4). *Average patient exposure guides 1988*. Frankfort, KY: Conference of Radiation Control Program Directors, **1988** (publication 88-5)
3. Hewlett-Packard Desktop Computer Division. *General utility routines*. Fort Collins, CO: Hewlett-Packard Desktop Computer Division, **1979**:439-442
4. Shrimpton PC. Calculation of patient skin dose from diagnostic x-ray procedures. *Br J Radiol* **1985**;58:483-485
5. McGuire EL, Dickson PA. Exposure and organ dose estimation in diagnostic radiology. *Med Phys* **1986**;13:913-916
6. Zamenhof RG, Shahabi S, Morgan HT. An improved method for estimating the entrance exposure in diagnostic radiographic examinations. *AJR* **1987**;149:631-637

## Attitudes of American Radiologists Toward Their Practices: Present and Future

B. G. Brogdon,<sup>1</sup> E. D. Heveron,<sup>2</sup> and J. J. Diamond<sup>3,4</sup>

Questions designed to reveal radiologists' attitudes about their practices and their specialty were incorporated into a large survey of manpower taken in 1988 by the American College of Radiology (ACR). The manpower data will be published separately. The attitudinal data provide insight into the degree of satisfaction of radiologists with their practices.

### Methods

A 12-page questionnaire was sent to 1164 American Board of Radiology (ABR)-certified radiologists who were active members of the ACR and to 212 noncertified radiologists who were associate members of the ACR. The survey addressed basic demographic items, including age, sex, year of residency completion and board certification, radiology subspecialty, and compensation arrangements. Respondents provided their level of satisfaction in the following aspects of their careers: location, type of practice, financial arrangements, interpersonal relationships, self-assessed competency, and other indicators of happiness. Women were queried about pregnancy and its effect on their residency and/or practice. Respondents were asked to discuss the importance of various qualities in an applicant when making hiring decisions, and their practice's need for additional radiologists in the future. Respondents over the age of 50 were asked to reveal their retirement plans.

The mailing list was randomized by zip code to virtually exclude the sampling of two or more members of the same practice group. Responses were returned by 648 active members (56%), of whom 47 (7%) were women. Three did not state their sex. Seventy-seven associate members (36%), of whom seven (9%) were women, returned the questionnaires. The returns are representative, geographically, of the population sampled. The ACR is a voluntary-membership organization that prides itself on representing all members of the radiologic community; however, demographic data are not available to substantiate that this sample precisely represents the approximately 24,600 people who identify themselves as practitioners of radiology to the American Medical Association.

The average age of the 725 respondents was 47. Only two respondents were younger than 30; 11 were older than 70 years of age. Sixty percent were younger than 50 years old; 88% were younger than 60.

Eleven percent of the respondents designated themselves as therapeutic radiologists, 2% as general radiologists (both diagnostic and therapeutic), and 86% as radiologists practicing diagnostic radiology or one of its subspecialty areas. No response was obtained from 2%.

Some respondents were in solo practice and others were members of large groups. The typical respondent, however, represents a median group-size of five radiologists.

Fee-for-services was listed as the major source of professional income for 68% of answering radiologists; 25% were salaried, and

Received September 5, 1989; accepted after revision October 31, 1989.

From the American College of Radiology Committee on Manpower, 1891 Preston White Dr., Reston, VA 22091.

<sup>1</sup> Department of Radiology, University of South Alabama Medical Center, Mobile, AL 36617.

<sup>2</sup> American College of Radiology, 1891 Preston White Dr., Reston, VA 22091.

<sup>3</sup> American College of Radiology, 1101 Market St., Philadelphia, PA 19107.

<sup>4</sup> Present address: American Board of Internal Medicine, 3624 Market St., Philadelphia, PA 19104.

Presented in part at the annual meeting of the American College of Radiology, Seattle, WA, September 1989.

AJR 154:867-869, April 1990 ©361-803X/90/1544-0867 © American Roentgen Ray Society



3% were on a percentage or lease arrangement. Other uncategorized sources or no response accounts for the remaining 1%.

## Results

### *Attitudes Toward Current Practice*

Radiologists were asked to assess, on a scale of 10 to 1, their degree of satisfaction with their current practice as it relates to geographic location, type of practice, financial arrangements, and interpersonal relationships. In general, radiologists were highly satisfied with these aspects of their practices, more than half rating them at level 8 or above on the 10–1 scale.

The different subsets of the radiologists who responded did not vary greatly in their replies (Table 1). ABR-certified men with income derived principally from a fee-for-service arrangement seem most satisfied with most aspects of their practice, whereas women appear to have a slightly higher level of satisfaction with type of practice and interpersonal relationships. The differences between the various subsets' responses are not statistically significant for the data presented in Tables 1–4. However, we believe that the variations in attitudes are of sufficient interest to warrant the breakdown of responses into the categories listed.

### *Attitudes Toward Colleagues*

Radiologists were asked whether they enjoyed their relationships with radiologic associates and with nonradiologic-physician colleagues professionally, socially, or both professionally and socially. Slightly fewer than half reported enjoying both professional and social relationships with radiologic associates (47%) and nonradiologic colleagues (40%). Still fewer (42%) indicated an enjoyable relationship with radiologic associates and with nonradiologic colleagues (40%) at the professional level only. Because fewer than 5% indicated that such relationships were enjoyed only at the social level, one can infer that about half of the radiologists do not enjoy their relationships with the other physicians with whom they work.

### *Self-satisfaction*

Most radiologists felt that their radiologic reports to referring physicians are "of great help in patient management" (73%), "of some interest to them" (16%), or both (4%). Only 7% of those surveyed felt their reports were "of little interest," "useful mostly for record keeping and meeting hospital standards," combinations of the foregoing, or did not answer. This regard for radiologic consultation is slightly higher than that indicated by referring physicians participating in a study re-

**TABLE 1: Radiologists' Satisfaction with Their Practices**

Subset of Radiologists	Level of Satisfaction <sup>a</sup>	Percentage of Respondents Rating Aspects of Practice <sup>b</sup>			
		Location	Type	Financial	Interpersonal
ABR-Certified	High	73	76	68	67
	Middle	23	20	25	27
	Low	3	3	7	5
Noncertified	High	58	69	61	66
	Middle	30	22	26	27
	Low	12	9	13	6
Male	High	72	75	68	66
	Middle	24	21	24	27
	Low	4	3	7	6
Female	High	67	83	63	72
	Middle	24	9	28	26
	Low	7	6	7	0
Fee-for-service	High	74	80	79	68
	Middle	22	18	17	27
	Low	4	2	3	5
Salaried	High	66	66	41	67
	Middle	29	27	42	28
	Low	5	7	17	5
Percentage/lease	High	71	71	54	63
	Middle	21	21	38	25
	Low	8	8	8	13
Other	High	80	60	20	40
	Middle	20	20	80	60
	Low	0	20	0	0

<sup>a</sup> On a scale of 10 to 1, high = 8–10, middle = 4–7, low = 1–3

<sup>b</sup> These do not add up to 100% because of rounding and because six respondents (five male, one female) did not answer this question.

ported by Rockoff et al., [1]. Those physicians responded to questions designed to measure their attitudes toward general diagnostic radiologists in regard to their medical knowledge and professional competence as consultants.

The rapid changes and complexities of modern radiology did not weigh heavily on the responding radiologists. More than 90% in every subset felt more competent in their practices at the time the survey was taken than when they completed their training (Table 2).

Still, only about two thirds of radiologists surveyed indicated that they "enjoyed radiology more now than when . . . [they] completed . . . training" (Table 3). This implies that one third of radiologists may have suffered some disappointment or disillusionment during their years of practice.

#### *Future Plans and Legacy*

Despite the apparent satisfaction with practice and positive attitudes held by most respondents, other considerations

**TABLE 2: Percentage of Respondents Feeling More Competent Now Than When They Finished Training**

Subset of Radiologists	Yes	No	No Answer
ABR-Certified	91	8	1
Noncertified	94	5	1
Male	91	8	1
Female	94	4	2
Fee-for-service	92	7	1
Salaried	91	9	0
Percentage/lease	92	8	0
Other	100	0	0
All	91	8	1

**TABLE 3: Percentage of Respondents Enjoying Radiology More Now Than When They Finished Training**

Subset of Radiologists	Yes	No	No Answer
ABR-Certified	66	32	2
Noncertified	58	40	1
Male	64	34	2
Female	74	24	2
Fee-for-service	63	35	2
Salaried	71	28	1
Percentage/lease	67	29	4
Other	20	60	20
All	65	33	2

**TABLE 4: Percentage of Respondents Who Would Encourage a College-Age Child To Pursue a Career in Medicine**

Subset of Radiologists	Yes	No	No Answer
ABR-Certified	49	49	2
Noncertified	32	65	3
Male	33	67	2
Female	48	43	9
Fee-for-service	47	51	2
Salaried	47	50	3
Percentage/lease	54	46	0
Other	60	40	0
All	47	51	2

must have dampened enthusiasm somewhat for the near and distant future. Given a choice of multiple endings to the wistful phrase, "I wish I could . . .," 4% of respondents would make a career change, 14% would go part-time now, and 20% would retire early. Only 30% would retire at the regular time, a hardy 19% would "keep doing what I'm doing forever," and 14% picked other combinations or failed to complete the sentence.

Perhaps more ominous are the responses to the yes-or-no questions, "I would encourage a college-age child of mine toward a career in medicine," and "If yes to above, I would advise specialization in radiology" (Table 4). Fewer than half would encourage medicine as a career. However, of the minority who would encourage a medical career, only 10% would not advise specialization in radiology; 87% would encourage the child to consider radiology and the remaining 3% did not address the issue.

#### **Conclusions**

This limited portion of the ACR survey suggests that practicing radiologists are quite happy with their type of practice, practice location, financial arrangements, and interpersonal relationships. They are confident of their competency and are satisfied that they are valued by their referring physicians as important contributors to patient care. Yet there are other factors, unmentioned, which seem to overshadow today's radiologists and darken their vision of the future.

#### **REFERENCE**

1. Rockoff SD, Davis DO, Gaskill JW. Physician attitudes toward the competence of general diagnostic radiologists: survey and implications. *AJR* 1983;140:639-648

## Book Review

**Guidance on Radiation Received in Space Activities.** Recommendations of the National Council on Radiation Protection and Measurements. (NCRP Report No. 98.) Bethesda, MD: National Council on Radiation Protection and Measurements, 277 pp., 1989. \$17

This report, which was drafted by the National Council on Radiation Protection and Measurements (NCRP) Scientific Committee No. 75 under the chairmanship of R. J. Michael Fry, should be of great interest to the radiologic community. The purpose of the report is to suggest guidelines for exposure to radiation acquired during activities in space and to provide a scientific basis for these recommendations. In order to do this, the report describes a historical development of guidelines for exposure to radiation and discusses the biologic effects of radiation and the radiation encountered in a space environment.

These goals are approached by chapters that describe the radiation environment in space and the exposure of personnel to radiation in different manned mission scenarios, including earth orbital scenarios and extended missions to the moon and Mars. Next is a thorough review of radiobiology. This includes the biologic effects of different types of radiation; a review of the effects of radiation on different organ systems, including the eye; a review of radiation carcinogenesis; genetic effects of radiation; and effects of radiation on the embryo

and fetus. The final section describes recommendations and radiation protection standards in space. These are placed in the context of terrestrial exposures.

This book should have a wide appeal to anyone who is interested in the effects of radiation. The sections on radiobiology and the effects of radiation are a thorough, up-to-date review of these topics. The sections that place space standards in perspective by comparing them with terrestrial exposures are also interesting. The book is well prepared in the usual clear and simple style of NCRP reports. It has numerous graphs and tables and an unusually complete index. This report should broaden the reader's knowledge of the effects of radiation and provide a review of radiation biology, the health effects of radiation, and current exposure levels.

G. Donald Frey  
Medical University of South Carolina  
Charleston, SC 29425-0720

## Technical Note

### Autoradiology: Patient Heal Thyself

Spencer B. Gay,<sup>1</sup> J. Bayne Selby, Jr.,<sup>1</sup> and Henry G. Selby<sup>2</sup>

In this age of cost-reduction schemes, technologist shortages, and consumer advocacy, we considered it important to study the efficacy of patient-performed procedures (PPP) for reducing radiology costs. This approach reduces medical costs by decreasing the amount of physician and technical support required for a variety of radiologic examinations. Patients also benefit by playing a more active role in their own care. Physical self-examination (breast, testes, skin) is currently in vogue, and we see no reason that this approach cannot be applied to internal organs as well. Our preliminary investigations confirm that several procedures are amenable to greater patient participation.

#### Procedures

##### *Gastrointestinal Autoradiology*

A disturbing trend away from the barium meal and toward endoscopy for examination of the upper gastrointestinal (GI) tract has encouraged us to rejuvenate the radiologic approach. We trained patients in the art of BS (barium swallowing) in order to evaluate their own GI tract. Patients are eager to drink the "pink shake" (Fig. 1) and actually look forward to ingesting gas crystals as long as eructations don't ensue. Patient positioning is greatly improved by self-cooperation. It is gratifying to see the extra time patients are willing to spend with themselves. A further benefit is a better understanding by patients of their diseases. More than one person has

thanked us for the opportunity to witness barium refluxing into their esophagus at the same time they experience their nagging "heartburn."

Interpretation of the radiograph has not been a problem. Many nonradiologists do it every day with little experience and no training. We initially attempted a comparison study of auto-GI series and autoendoscopy; however, this idea was abandoned at the patient's request after the first autoendoscopy attempt.

Interesting abnormalities are often discovered during auto-GI examinations, and occasionally an academically oriented patient wants to publish the findings. These patients usually will agree (after some coercion) to having the attending radiologist be the first author.

There are some differences in the quality of the PPP compared with conventional procedures. For instance, patients are often captivated by the appearance of a well-distended stomach and tend to take more views than the standard examination requires. Conversely, compression spot films of the gastric antrum are usually accomplished quickly and without repeated attempts.

The self-administered barium enema has also proved popular. Patient pride in a meticulous colon preparation has been enhanced by use of a common waiting room where patients may discuss and compare their methods. A viewbox is available where the scout film of the week is mounted. However, colon distension on double-contrast barium enemas has been poor, presumably because of the patients' reluctance to overdistend their own colon.

Received November 15, 1989; accepted after revision December 19, 1989.

<sup>1</sup> Department of Radiology, Box 170, University of Virginia Health Sciences Center, Charlottesville, VA 22908. Address reprint requests to S. B. Gay.

<sup>2</sup> Chesapeake Academy, Irvington, VA 22480.

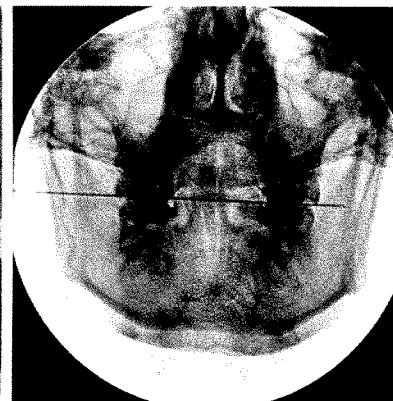
**AJR 154:871-873, April 1990** 0361-803X/90/1544-0871 © American Roentgen Ray Society



**Fig. 1.**—Gastrointestinal (GI) autoradiology. Patient performing upper GI examination on himself. Good eye-hand coordination is necessary for obtaining optimal spot radiographs of distended stomach and pesky duodenal bulb.



**A**



**B**

**Fig. 2.**—Cervical automyelography.  
**A,** Patient performing lateral C1-C2 puncture. Note calm demeanor.  
**B,** Anteroposterior spot film shows suboptimal needle placement. In this case, repositioning of the needle was recommended.

### *Cervical Automyelography*

Once the general concept is accepted, the applicability of PPP to other examinations becomes obvious. We are currently investigating the technical feasibility of having patients perform their own C1-C2 puncture for cervical automyelography. The spirit of adventure and stick-to-itiveness make the procedure attractive to many patients. We developed a simple three-step approach:

Step 1: Patient lies supine and is instructed to hold a 22-gauge needle in the right hand and a mirror in the left hand. The right hand directs the needle under lateral fluoroscopic guidance (Fig. 2A). A technologist moves the fluoroscopy tower as needed. Sedation is beneficial, but oversedation can be a problem in these do-it-yourself procedures.

Step 2: The needle is advanced carefully under anteroposterior fluoroscopic guidance until CSF is obtained. Copious return of blood upon removal of the stylet indicates that the needle should be repositioned. (Cerebral autoangiography by direct vertebral artery stick is another procedure of potential merit.) Numbness and arm tingling are also indications of overaggressive needle placement (Fig. 2B).

Step 3: Contrast material is injected, and standard cervical myelograms are obtained by the technologist.

In our experience, the self-performed C1-C2 puncture is calmly accepted and adroitly handled by the patient. This

should come as no surprise, as the ability of patients to perform surgery on themselves has been well documented. Kalin [1] reported a case of attempted autoadrenalectomy by a patient who had previously completed an autocastration.

To provide continuity of care, we ask the patient to obtain informed consent. The technologist should be available to witness the signature, and most patients are willing to sign. We have found that leaving a baby monitor (Fisher-Price, Mountain View, CA) in the room allows the technologist to perform other duties simultaneously.

### *Caveats*

Although we encourage the use of autoradiology for other procedures, some guidelines are in order:

The patient should be able to reach the area of interest easily. Cervical myelography, knee arthrography, and sonographically guided liver biopsies are all possible, but lumbar myelography and hysterosalpingography have proved difficult for patients to master.

Autoangiography is possible, preferably from the femoral approach. Axillary and translumbar punctures are fraught with difficulty. The literature provides examples of self-catheterization. The first vascular catheterization was performed in 1930 by Forssmann [2, 3], who catheterized his own right atrium for angiography, producing images of the pulmonary arteries.

In highly motivated patients, more advanced procedures such as embolization of carotid-cavernous fistulas and intracranial arteriovenous malformations are possible. As nonradiologists have been trained in these techniques, training of nonphysicians is the next logical step. When performing interventional neuroradiologic procedures, we instruct patients to talk to themselves continuously and to notify the technologist immediately if they don't get a response.

## Discussion

There has been little to motivate physicians or hospitals to participate willingly in cost-reduction measures other than the threat of GMR (Government Moolah Reduction) sanctions against costs perceived to be high for given procedures. The potential savings from PPP in terms of money, technologist time, and physician time are obvious.

Do-it-yourself surgical procedures have been described before [1, 4], but similar radiologic innovations have not been reported. This represents a missed opportunity to optimize many radiologic procedures. Other cost-saving measures that have been introduced are to be lauded, but they have addressed only efficient use of equipment [5-7]. Manpower efficiency measures should not be overlooked.

Self-performed procedures should decrease litigation against the physician. Our legal staff has advised us that having the patient perform the examination allows us to use the legal argument of *doctore immunem* in any subsequent lawsuit.

## Summary

All in all, our program has been a great success, endorsed by everyone from patients to health care providers and hospital administrators. The PPP will revolutionize diagnostic and interventional radiologic procedures and will free the radiologist to perform more critical maneuvers—the out-of-depart-

ment lunch, the extended afternoon off, and perfection of the golf swing.

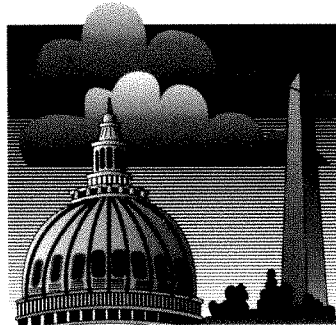
## REFERENCES

1. Kalin NH. Genital and abdominal self-surgery. *JAMA* **1979**;241:2188-2189
2. Forssmann W. Die Sondierung des rechten Herzens. *Klin Wochenschr* **1929**;8:2085-2087
3. Forssmann W. Ureber kontrastdarstellung der Höhlen des lebenden rechten Herzens und der Lungenschlagader. *Munch Med Wochenschr* **1931**; 78:489-492
4. Wilkins M. How to perform hemifacial spasm surgery on yourself. *National Lampoon*, June **1982**:36-39
5. Reid MH, Dublin AB. QUAC: a modest proposal for optimal use of CT scanning equipment. *AJR* **1984**;142:845-846
6. Reid MH, Dublin AB. Simultaneous anthropomorphic projections. *AJR* **1986**;144:861-862
7. Edwards DK III. X-ray gogs: preliminary evaluation of a "new" imaging modality. *AJR* **1988**;150:731-734

---

*Editor's note. Dr. M. M. Figley explained the origin of April Fools' Day eloquently in a previous issue (AJR 1984;142:845): "On April Fools' Day, April 1, it is considered appropriate to tell lies and play practical jokes on the unwary. This day, also known as All Fools' Day, is observed almost universally throughout the Western world. The custom is thought to have begun in France, where formal visits were paid to friends on the first day of April, which was 1 week after New Year's Day (March 25 under the Old Style Gregorian calendar). When New Year's Day was moved to January 1 in 1752, mock calls continued to be paid on April 1 as a joke."*





Come to the  
American Roentgen Ray Society

90<sup>th</sup>

---

ANNUAL MEETING

---

Washington, D. C.

---

Sheraton Washington Hotel  
May 13-18, 1990

---

---

Scientific Program (200 papers)

Instructional Courses (60 hours)

Categorical Course on Cardiovascular Imaging

The Caldwell Lecture

Award Papers

Scientific Exhibits

Social, Golf, and Tennis Programs

Guest Programs



## Meeting News

### Colon Cancer: Diagnosis in an Era of Cost Containment. ACR Conference, November 8, 1989

Elizabeth Whalen<sup>1</sup>

In this 1-day conference sponsored by the American College of Radiology, nine speakers discussed issues relevant to the diagnosis of colon cancer in the present socioeconomic environment. The conference was supported by a grant from E-Z EM Co. (Westbury, NY) and was cosponsored by the Society of Gastrointestinal Radiologists; it was coordinated by David Gelfand (Bowman Gray School of Medicine, Winston-Salem, NC) and Igor Laufer (Hospital of the University of Pennsylvania, Philadelphia, PA). The Chairman of the ACR Commission on Education, Joseph T. Ferrucci (Massachusetts General Hospital, Boston, MA), opened the meeting by discussing the importance of realistic policies for managing health care resources and, in particular, the need for an analysis of techniques and cost-effectiveness for screening for colon cancer. After his introductory remarks, discussions on the development and epidemiology of colon cancer, diagnostic techniques, and economic considerations were presented to approximately 60 participants, including radiologists, gastroenterologists, insurance and third-party-payer representatives, and members of the press. The conclusions of the conference may have an important impact on the selection of screening protocols for colon cancer in the future.

#### Epidemiology and Economic Impact of Colon Cancer

Gerald D. Dodd, Jr. (M.D. Anderson Hospital, Houston, TX), president-elect of the American Cancer Society, stressed the importance of colorectal cancer by noting that, in incidence and mortality rate, cancer of the colon and rectum is second only to lung cancer; 151,000 new cases of colorectal cancer are expected in 1989 [1]. His presentation focused on the epidemiology and economic impact of the disease.

#### Epidemiology

If colon and rectal cancer statistics are separated, it is evident that colon neoplasms occur more frequently (of 61,300 deaths from colorectal cancer, 53,500 were from colon neoplasms and 7,000 from rectal neoplasms) [1]. Also, studies show that the incidence of rectal cancer is higher in blacks than in whites, whereas the incidence of colon cancer is approximately the same. In Hispanics, the occurrence of colorectal cancer is substantially lower than that in blacks [2].

The effects of diet on the incidence of colorectal cancer are still being studied. Research to date indicates that eating high-fiber foods and vegetables seems to reduce risk, whereas

<sup>1</sup> Contributing editor, *American Journal of Roentgenology*, Ste. 200, 2223 Avenida de la Playa, La Jolla, CA 92037.

Editor's note.—"Meeting News" will be published in the *AJR* on a regular basis. These articles will report the highlights of important national radiology meetings. The intent is to provide Journal readers with succinct, substantive, and accurate reviews of topics of current interest—written in a readable fashion and published as promptly as 2 or 3 months after the meeting.

The articles will not undergo the peer review usually required of *AJR* publications, nor will they offer a critique of the information provided. The sole purpose of the series is to apprise *AJR* readers of topics of current concern in an interesting and timely fashion.

Most of the articles will be written by Elizabeth Whalen, who will serve as the *AJR*'s reporter for the series. Mrs. Whalen was the managing editor of the Journal for 3 years and is an experienced author. Thus, she is exceptionally qualified to assume this responsibility.

I invite readers to let me know if they find the articles useful and if they wish them to continue.

eating meat and fatty foods tends to increase risk. Also, increased consumption of micronutrients such as calcium and carotene may decrease the incidence of colorectal cancer [2a].

Separation of data by geographic location shows that the highest rates of colorectal cancer are found in North America, New Zealand, and Australia. Although the occurrence rates are lower in Europe, they are higher in Eastern Europe than in Western Europe. Also, occurrence of colorectal cancer in Asia seems to be related to degree of westernization (the more westernized Asian countries have higher rates). The lowest occurrence rates are often found in economically deprived countries, such as India and Senegal [2].

Environmental and life-style factors also seem to play a part in the incidence of colorectal cancer. For example, Mormons have a 30% lower incidence than the general population [2]. Urban dwellers have increased risk compared with those who live in nonurban areas: the highest U.S. rate is in Washington, DC, and the lowest U.S. rate is in Wyoming (press release, 1989, Dept. of Health and Human Services, Center for Disease Control). Risk for any one individual appears to change when that individual moves to a different environment. Obesity and a high caloric intake may increase the risk, whereas physical activity may lower it; diet appears to be a significant factor. The influence of these factors indicate that the individual risk of colorectal cancer can be changed by life-style changes.

Predisposing factors for colorectal cancer include genetic tendency and medical history of polyps, ulcerative colitis, or Crohn disease [2b]. Data show that the risk to direct descendants of colorectal cancer patients is three to five times higher than that of the general population [3, 4].

### *Economic Impact*

Dr. Dodd began his analysis of the economic impact of colorectal cancer by mentioning that the cost of cancer treatment in 1985 was \$65 billion (10% of all health care costs) [4a]. Although the specific cost of colorectal cancer treatment is difficult to determine, colorectal cancer accounts for 13% of cancer deaths, which leads to a rough estimate of a maximum cost of \$9 billion in health care dollars. Moreover, the cost of treating any cancer is much higher as the cancer progresses, so that an effective, inexpensive technique for detecting colorectal cancer at an early stage is an important economic (as well as medical) consideration. With early detection of colon and rectal cancer, the 5-year survival rates are 90% and 80% respectively [4a].

On a more personal economic level, a patient seeking treatment at a later stage of colorectal cancer faces enormous medical costs. The dollar price of survival may simply be too high for many patients; even if a cure is effected, they may not be able to afford the costs of living after paying for the cure [4b].

### **Development of Large-Bowel Cancer**

Robert H. Riddell (McMaster University, Hamilton, Ontario, Canada) emphasized that colorectal cancer generally devel-

ops over a long period of time, so that early detection is possible and important in reducing mortality associated with this cancer. The possibility that the development of colorectal cancer may be programmed genetically [5] offers further opportunity for early detection. Dr. Riddell discussed four major stages of colorectal cancer.

The first stage is the development of dysplasia or an adenoma from apparently normal mucosa. Such change in mucosal lining dramatically increases the patient's risk of large-bowel cancer. Predisposing conditions that can alert the physician to these changes include a personal or family history of colorectal neoplasia and inflammatory bowel disease.

In the second stage, dysplastic areas or adenomas grow beyond a critical mass for intraepithelial neoplasia (i.e., reach a size required for the invasive process to begin). Dr. Riddell stated that this critical mass is approximately 4–5 mm (rarely, however, invasive tumors as small as 3 mm have been found) [6]. In regard to development of colorectal cancer, research is needed to determine (1) why only some adenomas grow and (2) why only some of those that do grow eventually become invasive.

The third stage is characterized by continued growth, increasing dysplasia, and development of a villous component; the three major mechanisms of growth are replacement of preexisting epithelium, budding from adenomatous crypts, and hyperplasia.

The last stage in development of colorectal cancer is invasion, usually directly into the submucosa, but occasionally into the lamina propria mucosae. Research has shown a direct correlation between large adenomas (with a high degree of dysplasia and a villous component) and invasiveness of the tumor [7].

The classic studies of Gilbertson [8] were cited to show the possible relationship of the presence of polyps to the development of carcinoma. In a 25-year study that encompassed approximately 85,000 patient-years, Gilbertson removed all polyps that were within reach of the sigmoidoscope. The incidence of colorectal cancer in this group was reduced by 94% (75–80 carcinomas were expected, but only five occurred).

Dr. Riddell considers the question of *de novo* carcinoma to be one largely of semantics. In his opinion, the same highly dysplastic glands can be interpreted as either adenomatous because they are mucosal and noninvasive, or carcinomatous, provided it is recognized that the abnormality is only *in situ* and not invasive, and therefore unable to metastasize.

In regard to the growth of colorectal adenomas and cancer, Dr. Riddell suggests use of a geometric mean (the mean of the logarithm of the doubling time) to measure the mean doubling time. Calculations based on published data and this geometric mean produce mean doubling times of 946 days for adenomas, 352 days for carcinomas, and 85 days for metastases [9].

### **Description of Diagnostic Techniques**

Giles Stevenson (McMaster University, Hamilton, Ontario, Canada) discussed four techniques for diagnosis of colorectal

cancer: digital rectal examination, laboratory tests to detect blood in stool, barium enema, and endoscopy (colonoscopy).

#### *Digital Rectal Examination*

Although more sophisticated techniques detect more carcinomas, the digital rectal examination is still important—it can find one third of such cancers. Such an examination should be considered an important part of the regular physical examination of older patients.

#### *Laboratory Tests for Blood in Stool*

Detection of occult blood in stool remains a significant method for cancer detection, because most colonic carcinomas bleed intermittently. Types of tests include the common guaiac, Hemoquant, Haemoccult, and Haemselect. Haemselect has been shown to be the most sensitive [10], but it is seldom performed because there is more experience with Haemoccult, and Haemoccult is considerably cheaper. Accurate results for fecal occult blood require patients to stop taking aspirin and eating red meat; maximum compliance has been 70%; often, compliance rates are as low as 15% and 30% [11].

Results of studies of Haemoccult effectiveness have shown false-negative rates of 30–50% for cancer and 75% for polyps; 6–10% of the results were false-positive [12]. However, this test successfully detects a large proportion of early cancers.

#### *Barium Enema*

Both single-contrast and double-contrast barium enemas have been used to screen for colorectal cancer. The single-contrast is faster and tolerated better by the patient, but false-negative results are more common than with double-contrast enemas. The double-contrast barium enema has a sensitivity of about 95% for cancer [13, 14], but the patient is often moderately uncomfortable during the 20 minutes of the examination. Substitution of carbon dioxide for air in the double-contrast technique may alleviate discomfort; data indicate that pain is reported by about 30% of the patients when air is used and by only 5% of patients when carbon dioxide is used [15].

Both barium enema techniques require thorough cleansing of the bowel. If the bowel is not cleansed, up to 25% of tumors can be missed [16]. Double and triple readings of the resulting films improve the sensitivity of the test. For example, in one study, sensitivities for detecting definite tumor were 63% for single reading, 76% for double reading, and 84% for triple reading [17]. Most mistakes in interpretation involve missed polyps in the sigmoid colon.

#### *Endoscopy*

Colonoscopy represents a tremendous advance in diagnosis and treatment of colon cancer because most adenomas and small cancers can be removed via the colonoscope on

an outpatient basis. Sedation is required for the procedure. Flexible sigmoidoscopes 35-cm and 60-cm long or flexible colonoscopes 150- to 180-cm long are now used much more frequently than rigid endoscopes.

Proper use of the sigmoidoscope is easy to learn. The 35-cm sigmoidoscope can be used after limited bowel preparation and detects 80% of polyps found by the 60-cm sigmoidoscope. The 60-cm sigmoidoscope is used after the bowel is well cleansed; it has an 80% success rate for examination of the entire sigmoid colon [18].

#### *Barium Enema vs Endoscopy*

Patients tend to prefer endoscopy to barium enema, probably because they are sedated during the endoscopic examination. However, barium enema is safer (mortality rate between 1/20,000 and 1/50,000) than colonoscopy (mortality rate between 1/2,000 and 1/5,000) [19, 20, Kronberg-Odense, personal communication]. Also, the cost of colonoscopy is two to 10 times more than the cost of barium enema. However, if polyps or cancers are removed via colonoscope, the procedure is both diagnostic and therapeutic, whereas barium enema can only be diagnostic.

Barium enema appears to have potential for slightly greater sensitivity for detecting cancers (65–99% vs 70–95%) [14, 21]. For polyps larger than 7 mm, the sensitivities of the two examinations are about equal [22–24]. Colonoscopy is more sensitive for detecting polyps smaller than 5 mm (Zauber, national polyp study, personal communication), but Dr. Stevenson doubts if the difference in detection rates is important for these small polyps—especially because a perforation rate of one in 500 for colonoscopy is higher than the cancer rate for polyps 5 mm or smaller [25].

#### *Strategy*

On the basis of these data, Dr. Stevenson suggested the following strategy as a rational approach to combining diagnostic techniques for colorectal cancer: (1) Because only about 10% of patients with polyps have isolated right-sided lesions (Zauber, personal communication), flexible sigmoidoscopy should identify 90% of patients with colorectal polyps and can be used before proceeding to barium enema or colonoscopy. The advantages of using flexible sigmoidoscopy first are patient convenience, decreased cost, and fewer complications. (2) Barium enema should be used in patients who do not have adenomas on sigmoidoscopy (because it is safer, less expensive, and at least as sensitive as colonoscopy for detection of cancer). (3) Colonoscopy should be used if polyps are found on sigmoidoscopy. (4) Colonoscopy is more expensive and causes more complications than barium enema does; therefore, it is impractical as a routine screening tool.

#### *Comparative Diagnostic Accuracy*

David Gelfand introduced the topic of comparative accuracy of barium enema and endoscopy by mentioning the flaws in many of the published studies that show endoscopy to be

superior to barium enema [26]. The flaws include the following: (1) endoscopy is used as the gold standard, (2) good endoscopy is compared with poor radiology, (3) the endoscopist knows the radiologic diagnosis before performing endoscopy, and (4) the listed references to radiologic literature are very old. He then presented data on the effectiveness of both barium enema and endoscopy in detection of colorectal carcinoma.

Studies in the last two decades show a dramatic improvement in barium enema sensitivity for detection of polyps (approximately 90% for double-contrast, 80% for single-contrast) [24, 27–30]. In recent studies of barium enema examinations, the sensitivities for detection of colon cancer were 94–100%, [31–35]. In a large Swedish study of 1576 patients, barium enema sensitivity was 98.7% [35]. Studies also show that there is little difference in overall sensitivity between single-contrast and double-contrast barium enemas for the detection of carcinomas and large polyps, but the double-contrast barium enema seems to be more sensitive than the single-contrast barium enema for detecting polyps smaller than 1 cm [28].

Gelfand offered these criteria for choosing between double-contrast and single-contrast enemas. Indications for a double-contrast enema include occult blood in the stool, rectal bleeding, a family history of colon cancer, and a patient who is 40 years old or older. A single-contrast barium enema is indicated if the patient is too infirm, immobile, or incontinent for a double-contrast enema; the single-contrast technique also offers the more cost-effective means for cancer detection (although not for polyp detection).

Endoscopy has been shown to miss 10–20% of the lesions that are seen on radiologic examinations [24, 28–30, 36]. The success rate of endoscopy varies significantly: the percentage of examinations that reach the cecum ranges from 64% to 90% [37–40]. The experience of the endoscopist is an important factor—for inexperienced endoscopists, the rate of incomplete examinations is as high as 50%. A 1984 survey done by the American Society of Gastrointestinal Endoscopists indicates that 35% of all colonoscopies are incomplete [39].

Gelfand also raised the issue of the safety of colonoscopy. The average reported perforation rate of this procedure is 1:500, and its average mortality rate is 1:5000 [41]. Moreover, because perforation of the colon occurs during colonoscopic polypectomy in 1% of these procedures, Gelfand believes that this technique of removal is overused—especially in cases of very small, benign polyps.

Colonoscopy is certainly useful for obtaining biopsy material in patients with radiologically shown neoplasms or for removing the neoplasms. Other uses include establishing a specific diagnosis in patients with indeterminate inflammatory bowel disease and detecting colonic dysplasia or carcinoma in patients with chronic ulcerative colitis.

Despite the indisputable usefulness of colonoscopy in many situations, the data on accuracy, cost, and safety seem to indicate clearly that barium enema (rather than colonoscopy) is the preferred initial examination for detection of colon carcinoma.

### Problem-Oriented Approach to Investigation of the Colon

Igor Laufer (Hospital of the University of Pennsylvania, Philadelphia, PA) suggested a problem-oriented method for choosing either colonoscopy (C) or barium enema (B) for the symptomatic patient. He compared strengths [C: ability to investigate mucosal surface; B: ability to investigate extramucosal lesions such as submucosal tumors or extrinsic masses impinging on the colon]; problems [C: mechanical lesions such as strictures, hernias, and malpositions; B: diverticular disease]; biopsy, polypectomy ability [C: yes; B: no]; cost [C: very high; B: relatively low]; rate of complications [C: relatively low; B: very low]; completeness [C: 80%, B: 95%]; and availability of physicians with expertise [C: relatively limited; B: widespread].

In the context of colorectal cancer, the advantage of endoscopy for evaluating the mucosal surface is manifest primarily in improved detection of tiny colonic polyps, most of which are of no clinical significance. Therefore, the only uncontested advantage of colonoscopy lies in its capabilities for biopsy and polypectomy. Dr. Laufer suggested that this truly impressive advantage of colonoscopy produced a “glow” that caused many to use colonoscopy to evaluate colonic symptoms for which it is not suited. Specifically, the symptom of abdominal pain is not a valid indication for colonoscopy.

Dr. Laufer's problem-oriented approach uses the indications for the examination to determine the best diagnostic technique. In symptomatic patients, an advanced lesion should be expected, which may be either mucosal or extramucosal. Barium enema is a good choice for the initial examination, followed by colonoscopy if the radiologic study provides inconclusive results. For asymptomatic patients, barium enema remains safer and less expensive; Dr. Laufer recommends the use of a combination of sigmoidoscopy and barium enema. Finally, for patients who are at high risk for colorectal cancer, routine annual screening may be alternated between barium enema and colonoscopy; such alternating takes advantage of the benefits of each and counteracts their weaknesses.

The best care for the patients involves using all available diagnostic tests in appropriate situations, so that each examination is used in the case in which it will be most helpful and duplicated examinations are minimized.

As such strategies are evaluated in terms of patient benefits and financial constraints, an important question must be considered also: What is given up in terms of diagnostic and therapeutic benefits for the sake of cost containment?

### Comparison of Complications

David Ott (Bowman Gray School of Medicine, Winston-Salem, NC) compared the complications of barium enema and colonoscopy. Complications of barium enema include reactions to preparation, drugs, or barium; barium impaction, peritonitis, granulomas; venous intravasation; anorectal trauma; perforation and sequelae; radiation; and mortality (various causes). Complications of diagnostic colonoscopy include preparation complications, reactions to premedica-

tion, bacteremia, instrument impaction, colonic ileus/obstruction, cardiopulmonary problems, hemorrhage, perforation, and mortality (various causes).

The frequency of complications is much higher with diagnostic colonoscopy than with barium enema. A summary of complications shows that the perforation rates for colonoscopy and barium enema are 0.2% and 0.01%, respectively (perforation occurs 20 times more frequently with diagnostic—without biopsy—colonoscopy [42, 43]. The same summary indicates that the mortality rate of colonoscopy is 10 times greater than that of barium enema (0.02% and 0.002%, respectively) [42, 43].

### **Economic Constraints, Costs, and Cost-effectiveness of Techniques for Diagnosing Colorectal Cancer**

#### *Economic Constraints on Medical Practice*

As economic consultant, Duncan Cameron (Capitol Economics, Washington, DC), discussed the economic perspective of the health care cost-containment problem. He said that the rise in health care costs can be partially accounted for by population growth and a general increase in use of medical care. However, valid concern has been expressed about whether the consumer is getting appropriate value for the money spent.

Cameron listed three major sources of the problem of rising health care costs. First, because the consumer (the patient) is uninformed and relies on the provider (the physician) for advice, both conflicts of interest and consumer dissatisfaction can occur. Second, the widespread use of insurance exacerbates the first problem, because the consumers are often not the payers and thus may use more medical care than they would if they were paying for it. Third, the continued costs of malpractice insurance may result in (1) higher costs passed on to the consumer and (2) the practice of "defensive medicine," in which all possible tests and procedures are ordered to avoid possible negligence complaints.

Possible methods for health care cost containment include the following government actions (some of which are already being used): reducing tax subsidies for insurance coverage; encouraging use of arbitration and limiting awards for malpractice cases; passing legislation attacking conflicts of interest (e.g., making self-referrals illegal); holding the physician responsible for the health of the patient instead of the provision of specific services (e.g., Health Maintenance Organizations in which physicians are on salary rather than receiving fees for each service provided); and regulation of the types of procedures and tests to be used in terms of reimbursement by Medicare (or insurance companies, who can set up their own regulations).

Two problems with the cost-containment measures described indicate other possible reasons for rising health care costs. First, cost shifting and increased use of those tests and procedures that are reimbursed can keep costs high despite government and insurance regulations. Second, although the traditional fee-for-service system (and malpractice suits) may encourage some physicians to perform too many

tests, salary systems (prospective payment) may lead to inadequate care by some physicians.

The present financial condition of the U.S. government makes universal national health insurance an unlikely possibility in the near future. However, physicians can certainly expect that federal and state governments, as well as insurance companies, will continue to seek and identify ways to decrease health care costs. Private insurance companies in particular have the incentive to compete among themselves by controlling health care costs. Expect to see increased use of managed care, selective contracting, and other means of identifying misallocations of medical resources.

### **Comparative Costs of Barium Enema and Colonoscopy**

The second part of Dr. Ott's presentation confirmed that barium enema is much less expensive than colonoscopy. In terms of direct costs, the average for a barium enema study is \$188 (range, \$144–244), and the average for diagnostic colonoscopy is \$537 (range, \$423–750) [41, 44–46].

Evaluation of cost-effectiveness, however, involves more than consideration of direct costs; one must consider effectiveness of the studies, expenses of complications (including death), and the prevalence of the disease to be diagnosed. Dr. Ott presented the following equation: effective cost = expected direct cost/diagnostic utility. Expected direct cost is the base cost of the test plus the expected costs of both morbidity and mortality; diagnostic utility is computed by using the factors of prevalence of the disease and sensitivity and specificity of the tests. If the reported sensitivities and specificities of 90% and 98% for the double-contrast barium enema and 95% and 99% for colonoscopy (and estimates of \$10,000 for morbidity cost and \$250,000 for mortality cost) are used in the calculation, the cost-effectivenesses for barium enema and colonoscopy are approximately \$200 and \$600, respectively [47, 48]. This calculation shows that the barium enema is not only less expensive than colonoscopy but also more cost-effective.

### **Benefits and Costs of Screening for Colorectal Cancer**

David M. Eddy (Duke University, Durham, NC) is the McMahon Professor of Health Policy and Management at Duke University. He is neither a radiologist nor an endoscopist. His study of colorectal screening was developed as a research project for an insurance company, which considered the cost-effectiveness of reimbursing clients for colorectal cancer screening tests.

His study was based on statistics for patients at average risk for developing colorectal cancer. Dr. Eddy noted that, although colorectal cancer is well suited to effective screening because it is preceded by adenomas that have a long natural history, there was no direct evidence of the effect of any type of colorectal screening in reducing mortality rates. Dr. Eddy used indirect evidence to develop a mathematical model to arrive at such an estimate; the factors used included age- and gender-specific incidence rates, natural history and anatomy



of colorectal cancer, effectiveness of screening tests, risks involved in screening tests, stage-specific survival rates, deaths from other causes, and financial costs of screening. On the basis of data that he had heard at this conference, he felt that the results of his study were, if anything, conservative in estimating the benefits of the barium enema and aggressive in estimating the benefits of colonoscopy.

The possible screening strategies he analyzed with his mathematical model included annual fecal occult blood test (FOBT) and 10 combinations of FOBT with other screening tests delivered at various intervals (including sigmoidoscopy with a 60-cm flexible instrument, barium enema, and colonoscopy). The following outcomes were estimated to assess the desirability of each strategy: (1) decrease in probability of invasive colorectal cancer, (2) decrease in probability of death from colorectal cancer, (3) increase in life expectancy, (4) increase in life expectancy discounted 5%, (5) increase in net costs discounted 5%, and (6) probability of perforation.

In terms of (1) decreasing the probability of invasive colorectal cancer and related deaths and (2) increasing life expectancy, two combinations with barium enema and colonoscopy were estimated to produce similar results: the combination of FOBT annually and barium enema every 3 years from age 50 to 75 (in 10,000 patients, 339 cancers, 203 related deaths, and 80-day increased life expectancy) and the combination of FOBT annually and colonoscopy every 5 years from age 50 to 75 (in 10,000 patients, 355 cancers, 212 related deaths, and 83-day increased life expectancy). However, the barium enema protocol is less expensive (\$1003 increase in net costs discounted 5% vs \$1492 for the colonoscopy protocol) and has a lower probability of perforation (23/10,000 vs 103/10,000) [49].

Another important conclusion of this study is that, for an average-risk patient, use of barium enema with FOBT is estimated to be about three times as effective as screening with FOBT alone. In addition, the low cost and safety of barium enema procedures make this protocol an attractive prospect for third-party reimbursement.

Dr. Eddy characterized colorectal cancer screening as a "best buy" in terms of the effectiveness achieved for the resources required. For example, on the basis of the available indirect evidence, screening for colorectal cancer appears to be more effective than either cervical or breast cancer screening: for a cost of \$1000, screening for colorectal cancer decreases the probability of death from this disease by 200/10,000 [49] (the similar statistics for cancer of the cervix and breast are 100/10,000 [50] and 50/10,000 [51], respectively).

Although colonoscopy has a slightly higher effectiveness than barium enema (by about 5%), the additional cost and risk of perforation in colonoscopy should be considered in decisions about screening strategies—both by physicians and by third-party payers.

### Panel Discussion

The moderator of the panel discussion, Harley Carlson (Mayo Clinic, Rochester, MN), began with preliminary remarks about the Mayo Clinic's experience with the discussed tech-

niques. He agreed with other speakers that colonoscopy's greatest strength is removal of tissue, which may obviate surgery even when cancer is present. He noted that colonoscopy was first used on referred cases in which barium enema results had been inconclusive and then gained importance as a diagnostic tool in inflammatory bowel disease. However, in regard to the diagnostic accuracy of colonoscopy, Carlson discussed one series of studies in which four carcinomas were missed on single-contrast barium enema, one was missed on double-contrast barium enema, and five were missed on colonoscopy (two colonoscopic misses were incomplete examinations; in all five cases, the endoscopists knew the radiologic results before the start of the colonoscopy) (D. Bradley, M. D. Lewis, et al., unpublished data). The Mayo Clinic experience is also similar to others' in that colonoscopy shows a better record in detecting very small polyps (<1 cm), but has a cost of 2.7 times that of a protocol combining single-contrast barium enema and proctoscopy (D. Bradley, M. D. Lewis, et al., unpublished data).

The lively discussion that followed revealed a number of interesting points. Two new developments in colonoscopy were mentioned: (1) video colonoscopy is being used increasingly, which may improve sensitivity and specificity and which allows the endoscopist to monitor the progress of the colonoscope to minimize risk of perforation and (2) some endoscopists are now being trained with simulators that allow them to perform computer-simulated colonoscopies, including problems that may occur.

The merits of double- and triple-reading of radiographic examinations were discussed. Some participants stated that using different radiologists to interpret the same radiographs can increase accuracy significantly. However, others believed that a better solution (especially for the private-practice physician, who does not have access to a radiologic staff) is to have radiologists interpret the films more carefully. To determine the accuracy of a radiologist's interpretations, physicians should feel free to ask the radiologist for accuracy and sensitivity data for his or her previous examinations.

At the end of the conference, the participants and panel members seemed to agree that the ACR would be well advised to look carefully at the available data and establish guidelines on standards for performing the barium enema, especially in reference to its role in preliminary screening of asymptomatic patients for colorectal cancer. As Dr. Ferrucci indicated in his introductory remarks, "Colon cancer is a common, slow-growing, often silent and frequently lethal disease. Early diagnosis remains the best hope for cure." Information presented at the conference indicates that the barium enema examination is a safe, inexpensive, and accurate method of screening for colorectal cancer.

In closing the conference, Dr. Ferrucci made it clear that this conference will produce immediate and specific effects. He said that the ACR is appointing a committee on colon imaging to promote appropriate radiologic methods for detection of colorectal cancer including the use of the barium enema as the screening method of choice. Another outcome could be the development of performance standards for cancer screening with the barium enema examination.

## REFERENCES

1. American Cancer Society. Cancer facts and figures. Washington, DC: American Cancer Society, 1989:9,25
2. Ziegler RG, Devesa SS, Fraumeni JF. Epidemiologic patterns of colorectal cancer. *Imp Adv Oncol* 1986;209-232
- 2a. Mastromarino AJ, Wargovich MJ. Etiology of colorectal cancer: dietary factors. *Cancer Bull* 1988;40:191-195
- 2b. Strohlein JR, Levin B. Current guidelines for screening standard-risk individuals for colorectal cancer. *Cancer Bull* 1988;40:196-199
3. Macklin MT. Inheritance of cancer of the stomach and large intestine in man. *JNCI* 1960;24:551-571
4. Woolf CM. The inheritance of carcinoma involving different areas of the human gastrointestinal tract. *JNCI* 1953;13:89-98
- 4a. Rice DP. The economic burden of cancer. Presented at ACS conference, *Cancer care and costs: DRG's and beyond*, CA, May 1987
- 4b. Lansky SB. The high cost of cancer. *Am J Pediatr Hematol Oncol* 1987;9:85-91
5. Vogelstein B, Fearon ER, Hamilton SR, et al. Genetic alterations during colorectal-tumor development. *N Engl J Med* 1988;319:523-532
6. Spjut HJ, Frankel NB, Appel MF. The small carcinoma of the large bowel. *Am J Surg Pathol* 1979;3:39-66
7. Muto T, Bussey HJR, Morson BC. The evolution of cancer of the colon and rectum. *Cancer* 1975;36:2251-2270
8. Gilbertson VA, Nelms JM. The prevention of invasive cancer of the rectum. *Cancer* 1978;41:1137-1139
9. Spratt JS, Spratt JA. Growth rate of benign and malignant neoplasms of the colon. In: Ingall JRF, Mastromarino AJ, eds. *Carcinoma of the large bowel and its precursors*. New York: Liss, 1986:103-120
10. St. John DJB, Young GP, Cuthbertson AM, et al. Detection of colorectal neoplasia: comparison of guaiac, porphyrin and immunochemical tests for occult blood. *Gastroenterology* 1989;96:A492
11. Hardcastle JD, Chamberlain J, Sheffield J, et al. Randomised, controlled trial of faecal occult blood screening for colorectal cancer. *Lancet* 1989;1:1160-1164
12. Simon JB. Occult blood screening for colorectal carcinoma: a critical review. *Gastroenterology* 1985;88:820-837
13. Kelvin FM, Gardiner R, Vas W, Stevenson GW. Colorectal carcinoma missed on double contrast barium enema study: a problem in perception. *AJR* 1981;137:307-313
14. Fork FT, Lindstrom, Ekellund GR. Reliability of routine double contrast examination of the large bowel: a prospective clinical study. *Gastrointest Radiol* 1983;8:163-172
15. Coblenz CL, Frost RA, Molinaro V, et al. Pain after barium enema: effect of CO<sub>2</sub> and air on double contrast study. *Radiology* 1985;157:35
16. Stevenson GW, Robertson A, Hecker R. Barium enema in colonic cancer: a retrospective audit. *Aust Clin Rev* 1984;13:13-18
17. Markus JB, Somers S, Franic SE, Moola C, Stevenson GW. Interobserver variation in the interpretation of abdominal radiographs. *Radiology* 1989;171:69-71
18. Sivak MV. Flexible sigmoidoscopy. In: *Gastroenterologic endoscopy*. Philadelphia: Saunders, 1987
19. Rogers B-G, Silvis S, Nebel OT. Complications of flexible fiberoptic colonoscopy and polypectomy. *Gastrointest Endosc* 1975;22:73-77
20. Gilbert DA, Hallstrom AP, Shanefelt SL, et al. The national ASGE complications of colonoscopy survey (abstract). *Gastrointest Endosc* 1984;30:156
21. Beggs I, Thomas BM. Diagnosis of carcinoma of the colon by barium enema. *Clin Radiol* 1983;34:423-425
22. Williams CB, Macrae FA, Bartram CI. A prospective study of diagnostic methods in adenoma follow up. *Endoscopy* 1982;143:74-78
23. Wayne J, Isaunfield S. Surveillance intervals after colonoscopic polypectomy. *Endoscopy* 1982;14:79-81
24. Fork FT. Double contrast enemas and colonoscopy in polyp detection. *Gut* 1981;22:951-977
25. Matsukawa M, Usui Y, Kobayashi S. Screening of colorectal early cancer by radiology. In: Maruyama M, Kimura K, eds. *Review of clinical research in gastroenterology*. New York: Igaku-Shoin, 1988
26. Gelfand DW, Ott DJ. Methodologic considerations in comparing imaging methods. *AJR* 1985;144:1117-1121
27. Thoeni RF, Menuck L. Comparison of barium enema and colonoscopy in the detection of small colonic polyps. *Radiology* 1977;124:631-635
28. Ott DJ, Gelfand DW, Chen YM, Munitz HA. Single-contrast vs double-contrast barium enema in the detection of colonic polyps. *AJR* 1986;46:993-996
29. Thoeni RF, Petras A. Double-contrast barium enema examination and endoscopy in the detection of polypoid lesions in the cecum and ascending colon. *Radiology* 1982;144:257-260
30. Leincke JL, Dodds WJ, Hogan WJ, et al. A comparison of colonoscopy and roentgenography for detecting polypoid lesions of the colon. *Gastrointest Radiol* 1977;2:125-128
31. Beggs I, Thomas BM. Diagnosis of carcinoma of the colon by barium enema. *Clin Radiol* 1983;34:423-425
32. Myllyla V, Paivansalo M, Laitinen S. Sensitivity of single- and double-contrast barium enema in the detection of colorectal carcinoma. *Fortschr Geb Röntgenstr Nuklearmed Ergänzungsband* 1984;140:393-397
33. Johnson CD, Carlson HC, Taylor WF, Weiland LP. Barium enemas of carcinoma of the colon: sensitivity of double- and single-contrast studies. *AJR* 1983;140:1143-1149
34. Gelfand DW, Ott DJ. Single- vs. double-contrast gastrointestinal studies: critical analysis of reported statistics. *AJR* 1981;137:523-528
35. Fork F-T. Radiographic findings in overlooked colon carcinomas: a retrospective analysis. *Acta Radiol [Oncol]* 1988;29:331-336
36. Laufer I, Smith NCW, Mullens JE. The radiological demonstration of colorectal polyps undetected by endoscopy. *Gastroenterology* 1976;70:167-170
37. Benner K, Katon R. Colonoscopy performance in a training setting (abstract). *Gastrointest Endosc* 1983;29:188
38. Gelfand DW, Wu WC, Ott DJ. The extent of successful colonoscopy: its implication for the radiologist. *Gastrointest Radiol* 1979;4:75-78
39. Gilbert DA, Shanefelt SL, Silverstein FE, Mahler AK, Hallstrom AP. The National ASGE Colonoscopy Survey: analysis of colonoscopic practices and yield. *Gastrointest Endosc* 1984;30:143
40. Obrecht Jr WF, Wu WC, Gelfand DW, Ott DJ. The extent of successful colonoscopy: a second assessment using modern equipment. *Gastrointest Radiol* 1984;9:161-162
41. Ott DJ, Gelfand DW, Chen YM, Munitz HA. Colonoscopy and the barium enema: a radiologic viewpoint. *South Med J* 1985;78:1033-1035
42. Ansell G. Alimentary tract. In: Ansell G, Wilkins RA, eds. *Complications in diagnostic imaging*. Oxford: Blackwell, 1987:218-246
43. Rankin GB. Indications, contraindications, and complications of colonoscopy. In: Sivak Jr MV, ed. *Gastroenterologic endoscopy*. Philadelphia: Saunders, 1987:868-880
44. Feczko PJ, Halpert RD. Reassessing the role of radiology in hemoccult screening. *AJR* 1986;146:697-701
45. Barry MJ, Mulley AG, Richter JM. Effect of workup strategy on the cost-effectiveness of fecal occult blood screening for colorectal cancer. *Gastroenterology* 1987;93:301-310
46. England WL, Halls JJ, Hunt VB. Strategies for screening for colorectal carcinoma. *Med Decis Making* 1989;9:3-13
47. Patton DD, Woolfenden JM. A utility-based model for comparing the cost-effectiveness of diagnostic tests. *Invest Radiol* 1989;24:263-271
48. Ott DJ, Scharling ES, Chen YM, Gelfand DW, Wu WC. Positive predictive value and posttest probability of diagnosis of colonic polyp on single- and double-contrast barium enema. *AJR* 1989;153:735-739
49. Eddy DM. Screening for colorectal cancer. *Ann Intern Med* (in press)
50. Eddy DM. Screening for cervical cancer. *Ann Intern Med* (in press)
51. Eddy DM. Screening for breast cancer. *Ann Intern Med* 1989;111:389-399

## Book Review

**Basic Atlas of Sectional Anatomy with Correlated Imaging**, 2nd ed. By W. J. Bo, N. T. Wolfman, W. A. Krueger, and I. Meschan. Philadelphia: Saunders, 380 pp., 1990. \$75

The purpose of the newly revised, second edition of this atlas is to present cross-sectional anatomy as correlated with CT, sonography, and MR imaging. Sagittal sections have been included because the authors think these sections often make it easier for students, physicians, and technologists to grasp contiguous cross-sectional relationships. For students of gross anatomy, the atlas presents a three-dimensional concept of the body that usually is not obtained from dissection or audiovisual material. For clinicians and technologists, it offers information that is valuable in daily practice.

Cross sections of the head, neck, and torso are presented serially in order to portray accurately the progression of structures. Selected cross sections of the extremities and selected sagittal sections of the head, neck, and torso show the essential features of these regions. Cross sections are viewed from below, as this has been the convention for CT scans, sonograms, and MR images. Sagittal sections are viewed from the right. A drawing indicating the location of the section is included with each illustration. Xeroradiographs of cadaveric cross sections have been included in order to optimize differences in absorption coefficients of both normal and abnormal tissues and edge enhancement of the junction of tissues with different absorption coefficients.

The format of the second edition has been changed from that of the first edition to make the atlas more clinically applicable. The sagittal sections are included now as independent chapters that follow the chapters of cross sections taken from the same anatomic region. The appendix contains sections cut 30° to Reid's base line. The textual material from the first edition has been deleted in order to present the images, which the authors think will be more meaningful to demonstrate the clinical applicability of sectional anatomy.

Each cross section is pictured both transversely and sagittally at a thickness of 1 cm, providing a complete three-dimensional view of living anatomy. The atlas uses a clinically relevant, easy-to-follow format, with images reflecting the state of the art. For each anatomic region, one or more representative images (CT scan, MR image, or sonogram) are presented side-by-side on one page with corresponding cross sections on the facing page of the atlas. Cadaveric sections

and radiologic images also are matched with line drawings of the body to help the user pinpoint the exact anatomic region of the body being imaged. In total, the atlas features more than 295 illustrations, including 130 state-of-the-art radiologic images and more than 165 excellent line drawings.

Ten specimens (eight males and two females) provided the material for this atlas. The specimens were embalmed and then sectioned by using a commercial band saw. Sections through the orbit were cut 0.5 cm thick; all others were cut 1 cm thick. The sections were sanded, allowed to thaw, fixed, washed, and immersed in alcohol before being photographed. After the film was processed and printed, a graphic artist prepared label overlays for the illustrations.

In order to avoid overcrowding the illustrations with labels and lines, an attempt was made to label structures that were clearly visible, and bilateral structures generally were labeled only once. Some of the structures, such as vessels and nerves, could not be identified because they either were collapsed or blended in with the surrounding connective tissue. The authors chose not to have an artist draw in the section. At times, individual muscles were difficult to distinguish; therefore, they were grouped in labeling. The nomenclature adopted is that of the *Nomina Anatomica* of 1967 combined with the English nomenclature commonly used in most medical schools and clinical applications today.

The strengths of this atlas include the good-quality, clearly labeled photographs, inclusion of MR images in three planes, use of CT scans from the latest generation of scanners, inclusion of new transverse sections of the cranium, and provision of excellent images of the spine, the heart and thorax, and the abdomen and pelvis. In summary, this atlas is both a useful clinical reference and an up-to-date review that demonstrates the importance of sectional anatomy in the interpretation of state-of-the-art images.

David J. Sartoris  
University of California, San Diego, Medical Center  
San Diego, CA 92103-1990

## ARRS Case of the Day



The Case of the Day series is one of the most popular scientific exhibits at the annual meeting of the American Roentgen Ray Society (ARRS). The cases to be presented at the upcoming May meeting are illustrated on the following pages. There are four general categories: Chest, Abdominal, Musculoskeletal, and Neuroradiology. Each category includes four cases, one for each day of the ARRS meeting. The answers and brief descriptions of the entities will appear in the June issue of the *AJR*. If you plan to attend the meeting in Washington, DC, please visit the exhibit and submit your diagnosis at the meeting. Participants who diagnose the cases correctly will be acknowledged at the meeting.

The cases are from the teaching files of the Departments of Radiology at Georgetown University Medical Center and at the National Naval Medical Center, Bethesda, MD. The authors are members of the faculty at Georgetown University School of Medicine, the Uniformed Services University of Health Sciences, and the Armed Forces Institute of Pathology.

Margaret A. Stull  
*Department of Radiology*  
*Georgetown University School of Medicine*  
*Washington, DC 20007*

## Chest Case of the Day

Margaret A. Stull,<sup>1</sup> Letitia R. Clark,<sup>1</sup> Kathleen Reagan,<sup>1</sup> Curtis E. Green,<sup>1</sup> Cynthia M. Tracy,<sup>2</sup> Pamela W. Goose,<sup>1</sup> Paul V. Suhocki,<sup>1</sup> and Homer L. Twigg<sup>1</sup>

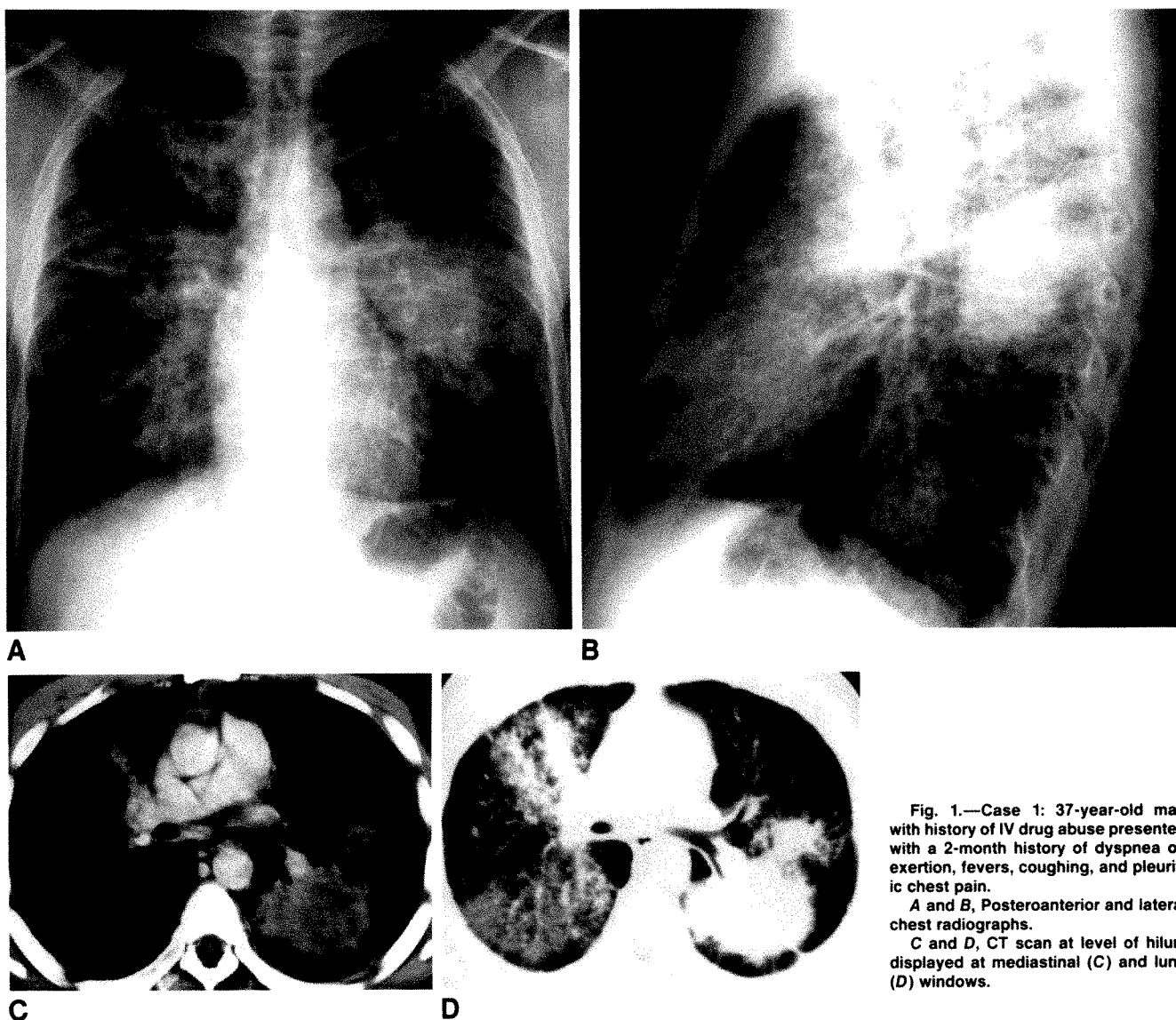


**Fig. 1.**—Case 1: 37-year-old man with history of IV drug abuse presented with a 2-month history of dyspnea on exertion, fevers, coughing, and pleuritic chest pain.

A and B, Posteroanterior and lateral chest radiographs.

C and D, CT scan at level of hilum displayed at mediastinal (C) and lung (D) windows.

<sup>1</sup> Department of Radiology, Georgetown University Medical Center, 3800 Reservoir Rd., N.W., Washington, DC 20007. Address reprint requests to M. A. Stull.

<sup>2</sup> Division of Cardiology, Department of Medicine, Georgetown University Medical Center, 3800 Reservoir Rd., N.W., Washington, DC 20007.

Case 1 was prepared by L. R. Clark, M. A. Stull, and H. L. Twigg. Case 2 was prepared by K. Reagan, C. E. Green, and C. M. Tracy. Case 3 was prepared by P. W. Goose, M. A. Stull, and H. L. Twigg. Case 4 was prepared by P. V. Suhocki, M. A. Stull, and H. L. Twigg. M. A. Stull is coordinator of the Case of the Day series.

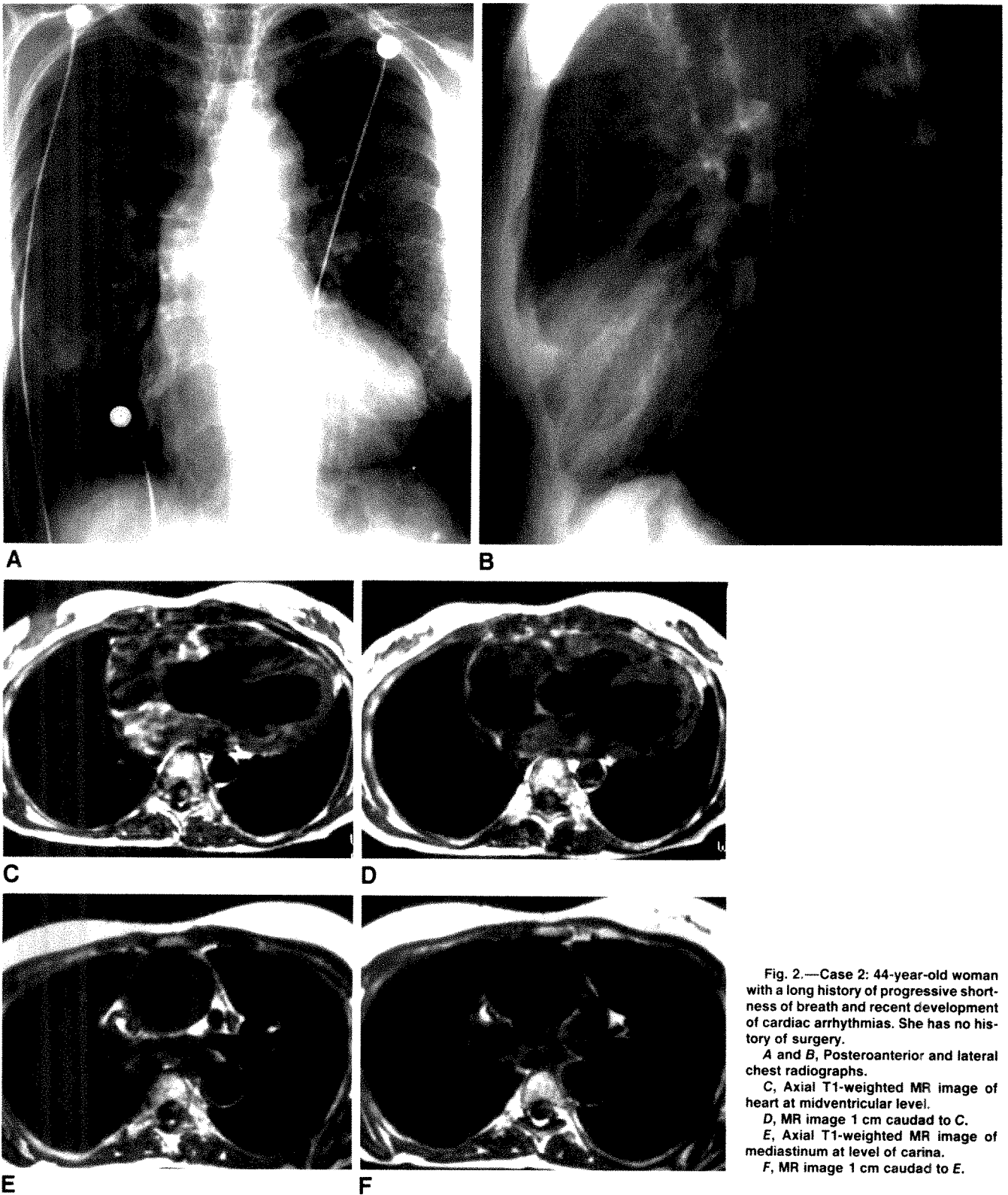


Fig. 2.—Case 2: 44-year-old woman with a long history of progressive shortness of breath and recent development of cardiac arrhythmias. She has no history of surgery.

A and B, Posteroanterior and lateral chest radiographs.

C, Axial T1-weighted MR image of heart at midventricular level.

D, MR image 1 cm caudad to C.

E, Axial T1-weighted MR image of mediastinum at level of carina.

F, MR image 1 cm caudad to E.



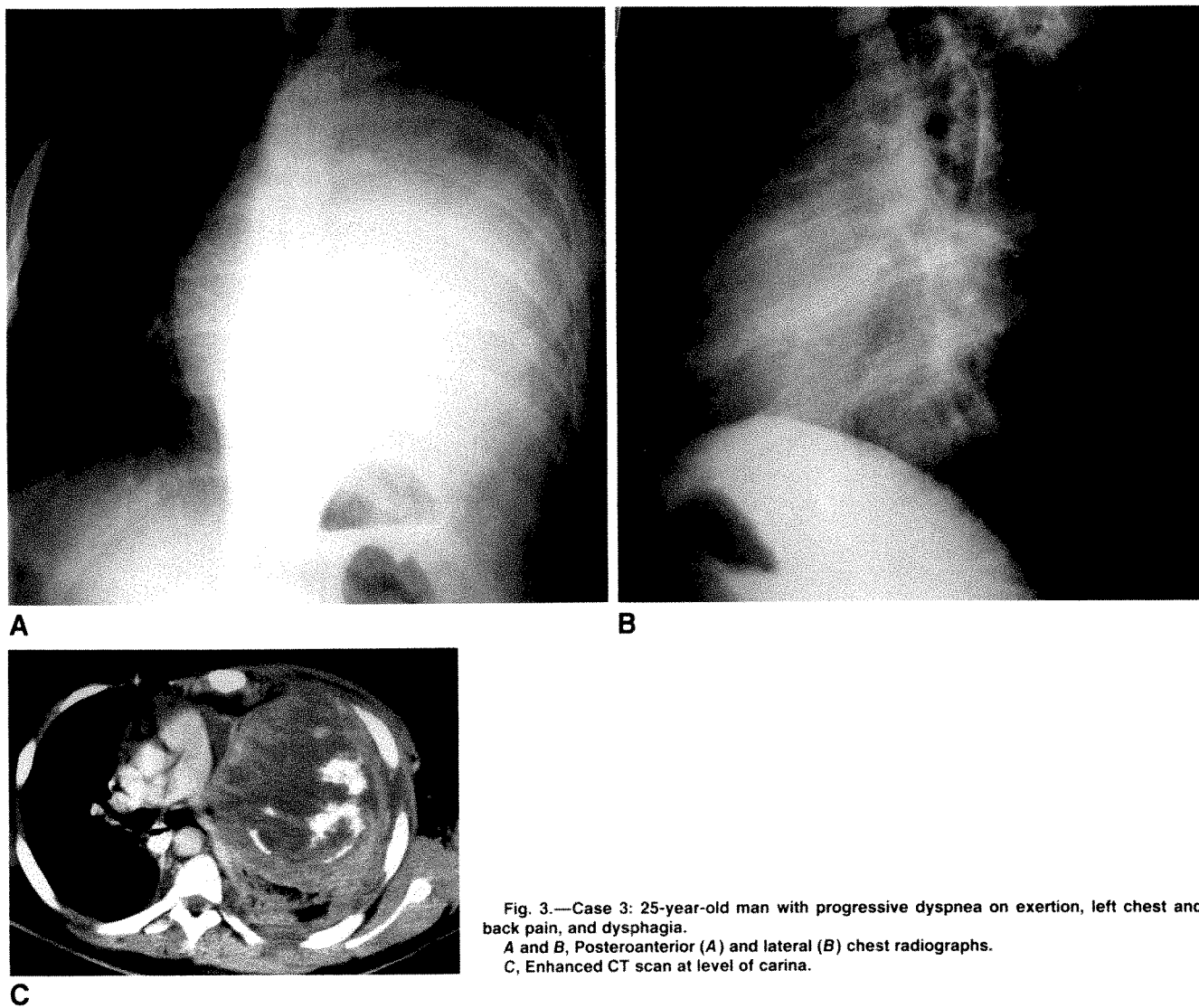


Fig. 3.—Case 3: 25-year-old man with progressive dyspnea on exertion, left chest and back pain, and dysphagia.  
A and B, Posteroanterior (A) and lateral (B) chest radiographs.  
C, Enhanced CT scan at level of carina.

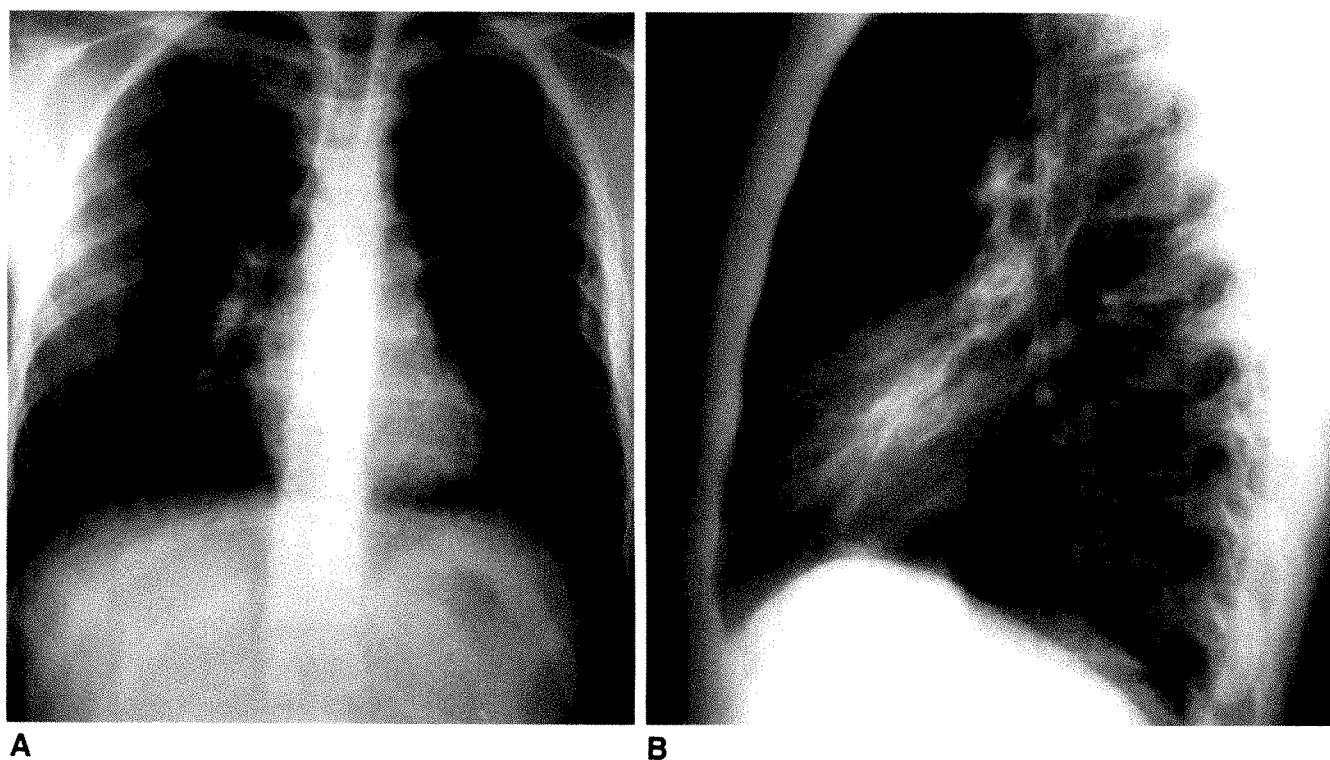
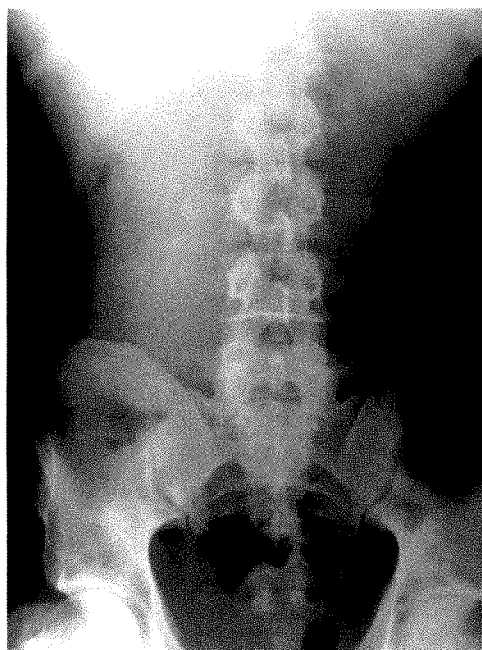


Fig. 4.—Case 4: Posteroanterior (A) and lateral (B) chest radiographs of a 17-year-old man, obtained at time of hospital discharge.

## Abdominal Case of the Day

Paul M. Silverman,<sup>1</sup> Wendelin S. Hayes,<sup>1</sup> Cirrelda J. Cooper,<sup>1</sup> Daryl Fanney,<sup>1</sup> Michelle S. West,<sup>1</sup> Leslie Forer,<sup>1</sup> David S. Hartman,<sup>2</sup> Alan J. Davidson,<sup>3</sup> and Margaret A. Stull<sup>1</sup>



**A**

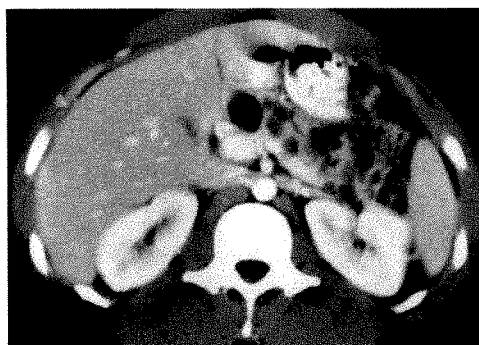
**Fig. 1.**—Case 1: 41-year-old man with AIDS presented with abdominal pain, vomiting, and intermittent bloody stools.

**A,** Plain film of abdomen.

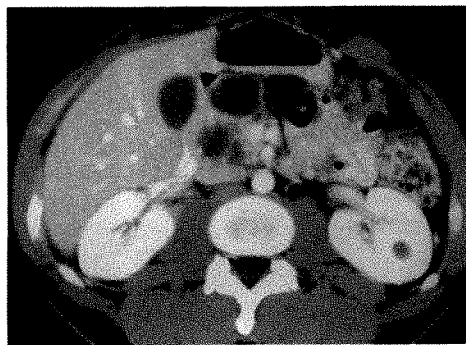
**B,** Transaxial CT scan of mid abdomen.



**B**



**A**



**B**

**Fig. 2.**—Case 2: Previously healthy 24-year-old black man presented with complaints of headache, nausea, and difficulty walking.

**A,** Transaxial contrast-enhanced CT scan of upper abdomen.

**B,** CT scan obtained 1 cm caudal to A.

The opinions and assertions contained herein are the private views of the authors and do not reflect the view of the Department of the Navy or of the Department of Defense.

<sup>1</sup> Department of Radiology, Georgetown University Medical Center, 3800 Reservoir Rd. N.W., Washington, DC 20007. Address reprint requests to M. A. Stull.

<sup>2</sup> Department of Radiology, F. Edward Hébert School of Medicine, Uniformed Services University of the Health Sciences, Bethesda, MD 20814-4799.

<sup>3</sup> Department of Radiologic Pathology, Armed Forces Institute of Pathology, Washington, DC 20306-6000.

Case 1 was prepared by D. Fanney, P. M. Silverman, and M. A. Stull. Case 2 was prepared by M. S. West, P. M. Silverman, and M. A. Stull. Case 3 was prepared by C. J. Cooper, P. M. Silverman, L. Forer, and M. A. Stull. Case 4 was prepared by W. S. Hayes, A. J. Davidson, D. S. Hartman, P. M. Silverman, and M. A. Stull. P. M. Silverman is coordinator for the Abdominal Case of the Day. M. A. Stull is coordinator of the Case of the Day series.

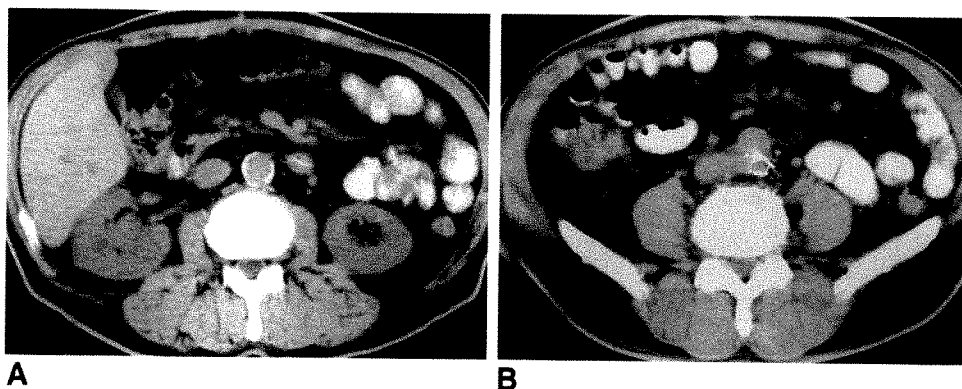


Fig. 3.—Case 3: 65-year-old diabetic man complained of intermittent diarrhea during an 8-month period. He had an aortic bypass graft for atherosclerotic vascular disease 4 months ago.

A, Transaxial CT scan of mid abdomen.

B, Transaxial CT scan of abdomen at level of iliac crests.

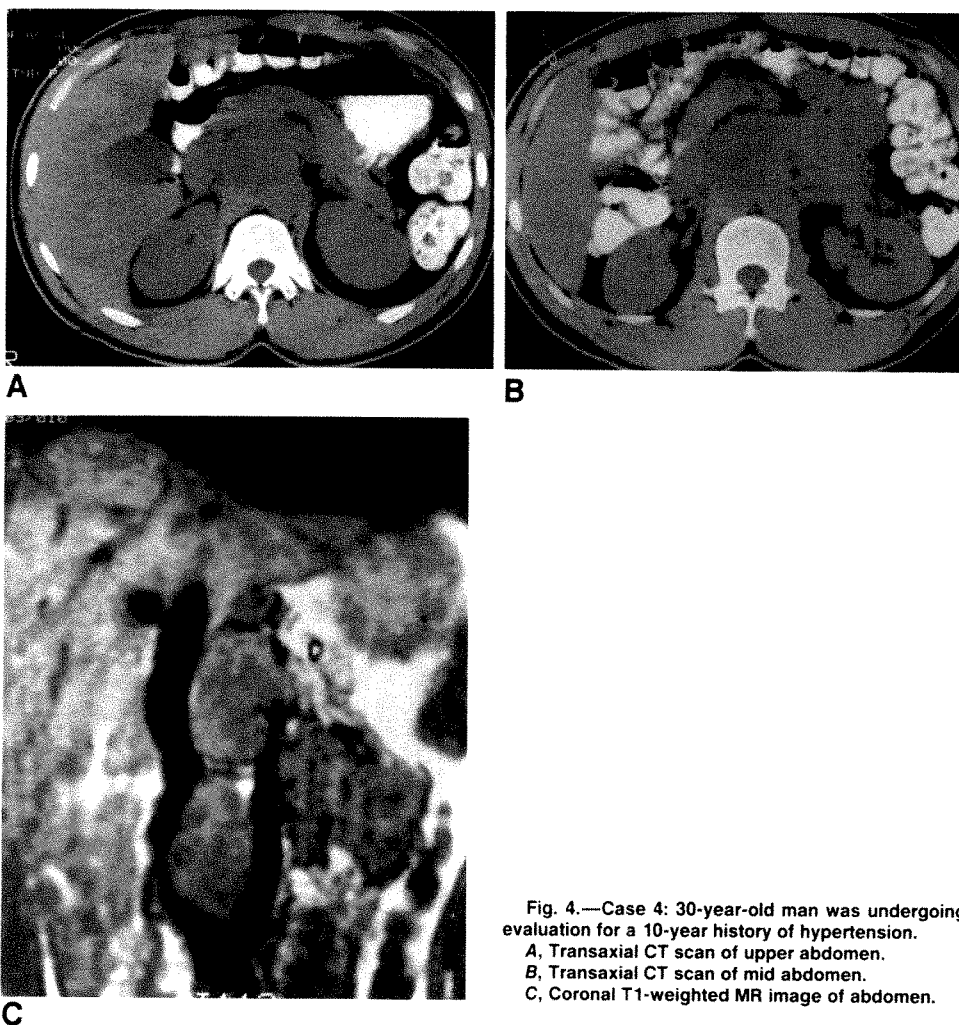


Fig. 4.—Case 4: 30-year-old man was undergoing evaluation for a 10-year history of hypertension.

A, Transaxial CT scan of upper abdomen.

B, Transaxial CT scan of mid abdomen.

C, Coronal T1-weighted MR image of abdomen.

## Musculoskeletal Case of the Day

Margaret A. Stull<sup>1</sup> and Mark Glass-Royal

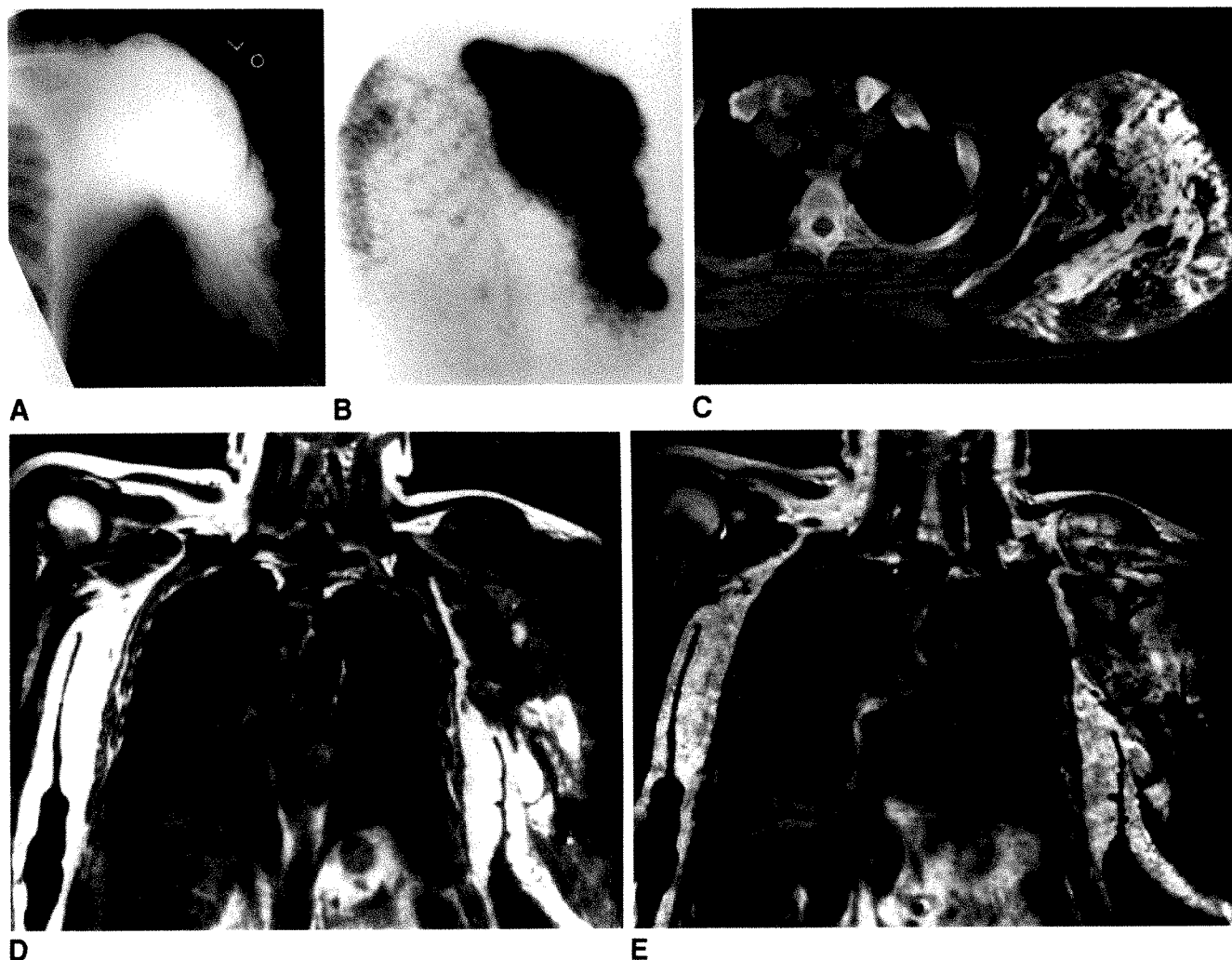


Fig. 1.—Case 1: 62-year-old man with diffuse swelling and progressive loss of motion of left arm and shoulder during the past 6 months. He noticed a lump in shoulder about 4 months ago.

A, Radiograph of left humerus.

B, Anterior <sup>99m</sup>Tc-methylene diphosphonate scintigram of left upper extremity.

C, CT scan at level of left glenohumeral joint.

D and E, T1-weighted, 600/25 (D), and T2-weighted, 2000/80 (E), coronal MR images of thorax and upper extremities.

<sup>1</sup> Both authors: Department of Radiology, Georgetown University Medical Center, 3800 Reservoir Rd., N.W., Washington, DC 20007. Address reprint requests to M. A. Stull.

Cases 1–3 were prepared by M. A. Stull and M. Glass-Royal. Case 4 was prepared by M. Glass-Royal and M. A. Stull. M. A. Stull is coordinator of the Case of the Day series.

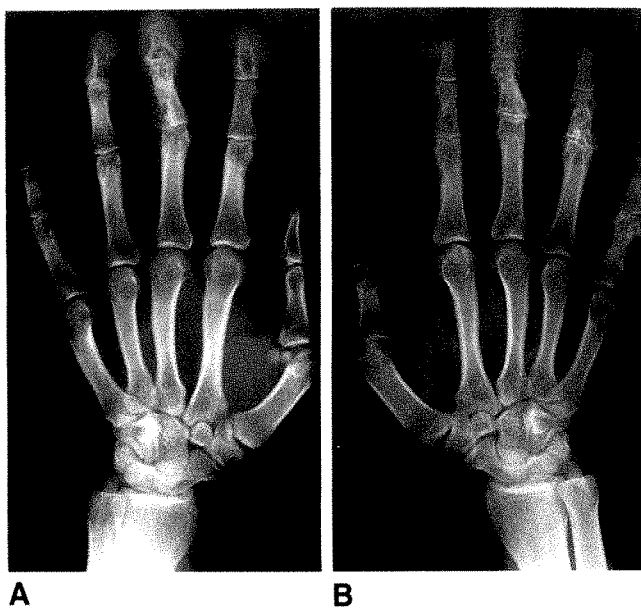


Fig. 2.—Case 2: 26-year-old black man with 2-year history of intermittent swelling and tenderness of hands. A and B, Radiographs of left (A) and right (B) hands.

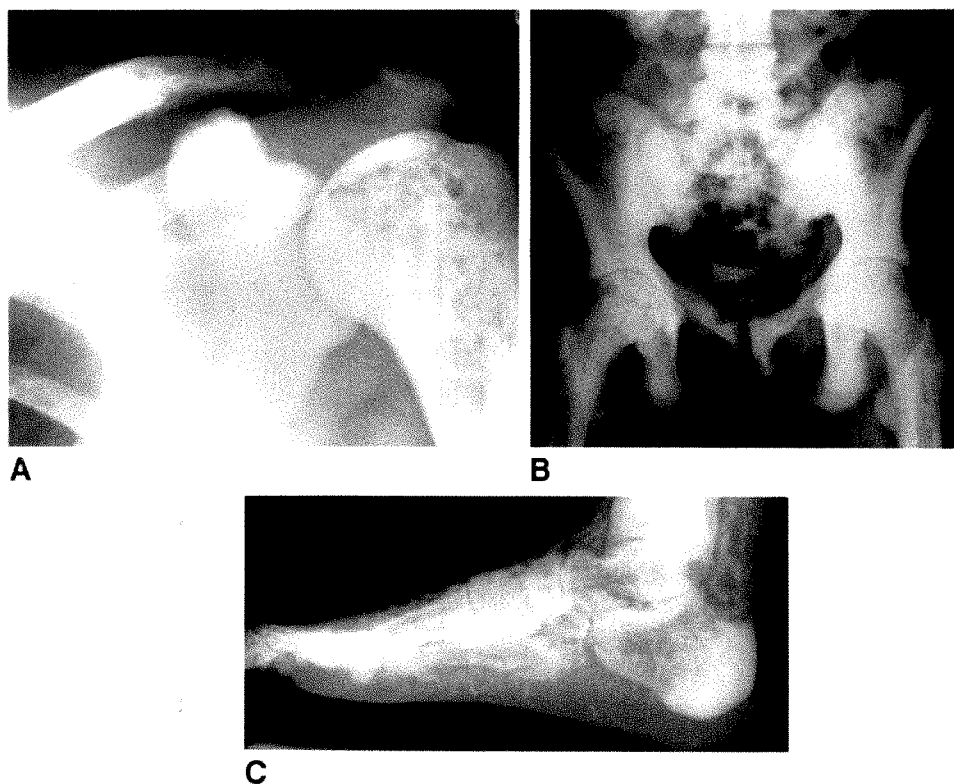


Fig. 3.—Case 3: 29-year-old woman with deteriorating health. A, Radiograph of left shoulder. B, Radiograph of pelvis. C, Radiograph of right foot.



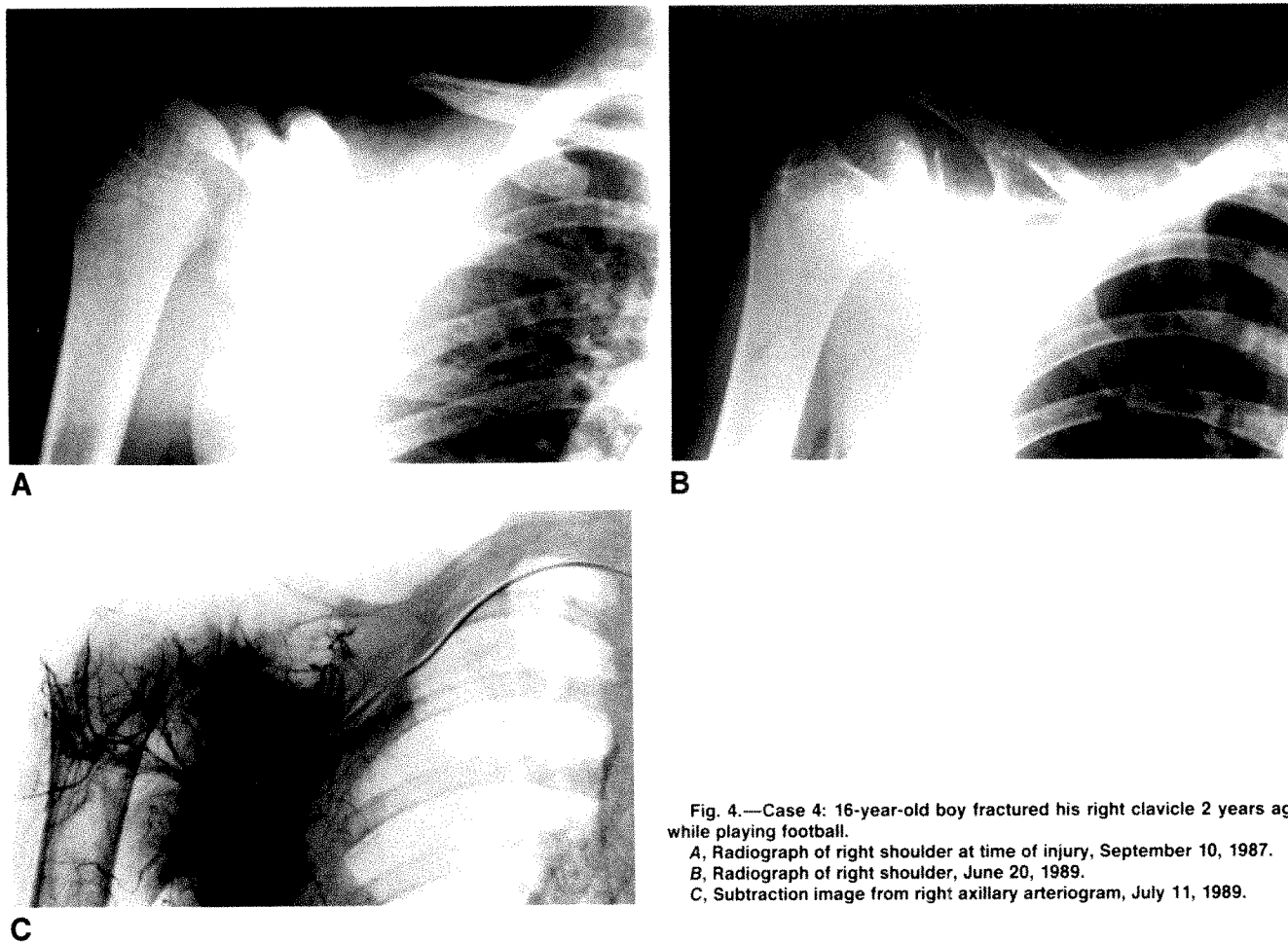


Fig. 4.—Case 4: 16-year-old boy fractured his right clavicle 2 years ago while playing football.

A, Radiograph of right shoulder at time of injury, September 10, 1987.

B, Radiograph of right shoulder, June 20, 1989.

C, Subtraction image from right axillary arteriogram, July 11, 1989.

## Neuroradiology Case of the Day

John P. Deveikis,<sup>1</sup> Curtis A. Cammarata, William M. Reid, Terri L. Ingram, Roland J. Mestayer, Dieter Schellinger, Nicholas J. Patronas, and Margaret A. Stull

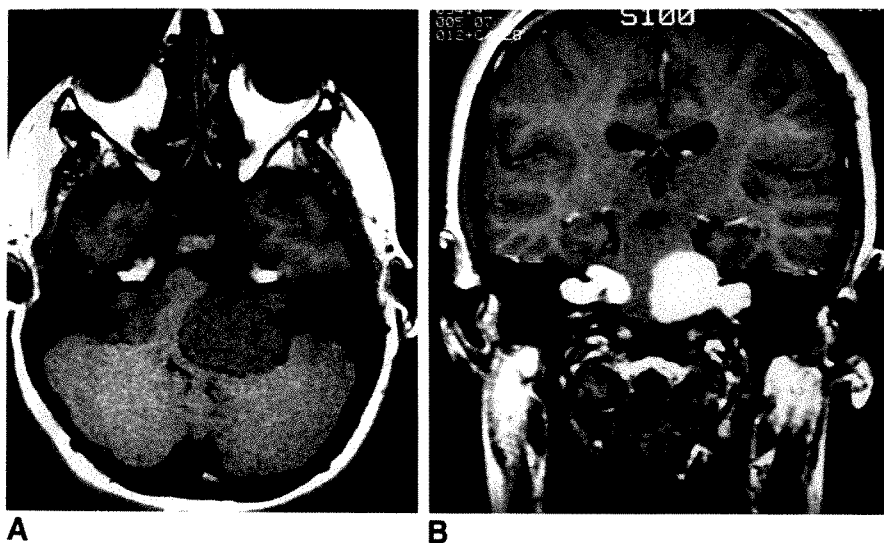


Fig. 1.—Case 1: 17-year-old girl with progressive hearing loss and disequilibrium.  
A, Axial T1-weighted MR image (600/20).  
B, Coronal gadolinium-enhanced T1-weighted MR image (600/20).

<sup>1</sup> All authors: Department of Radiology, Georgetown University Medical Center/NIH Clinical Center, 3800 Reservoir Rd., N.W., Washington, DC 20007. Address reprint requests to M. A. Stull.

Case 1 was prepared by C. A. Cammarata, J. P. Deveikis, D. Schellinger, N. J. Patronas, and M. A. Stull. Case 2 was prepared by W. M. Reid, J. P. Deveikis, D. Schellinger, N. J. Patronas, and M. A. Stull. Case 3 was prepared by T. L. Ingram, J. P. Deveikis, D. Schellinger, N. J. Patronas, and M. A. Stull. Case 4 was prepared by R. J. Mestayer, J. P. Deveikis, D. Schellinger, N. J. Patronas, and M. A. Stull. M. A. Stull is coordinator of the Case of the Day series.

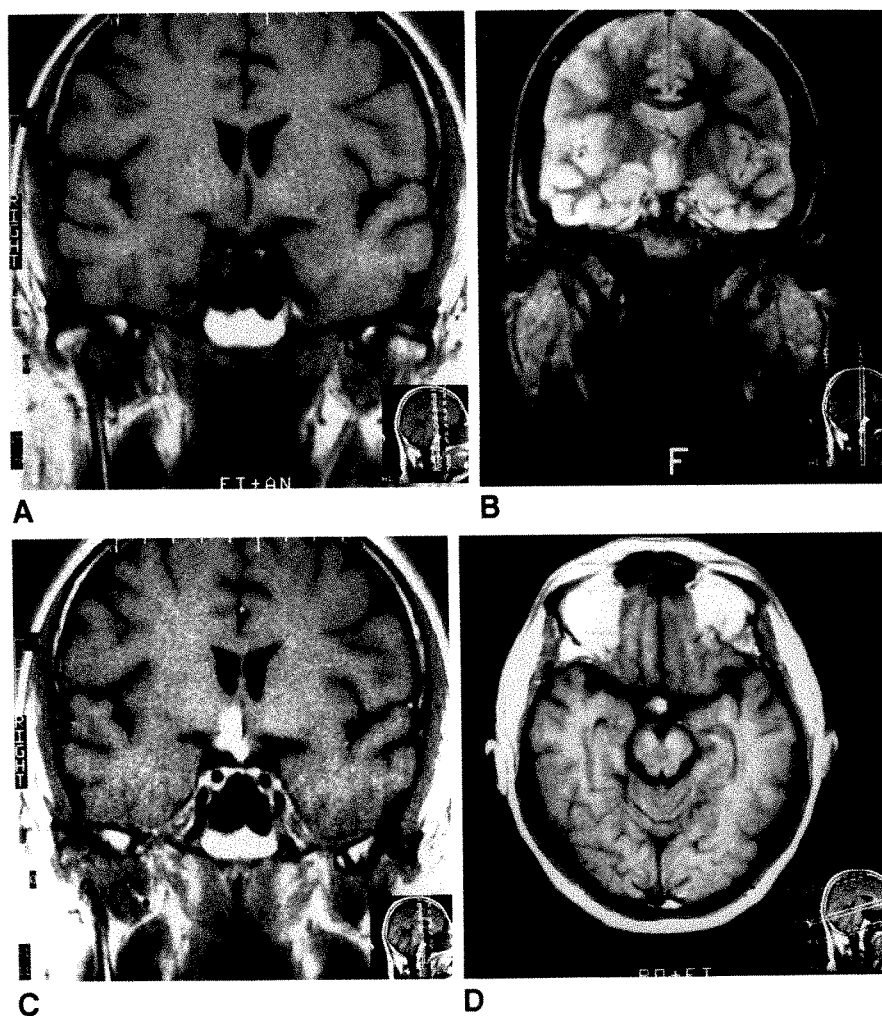


Fig. 2.—Case 2: 37-year-old man with panhypopituitarism.  
A, Coronal T1-weighted MR image (400/26).  
B, Coronal T2-weighted MR image (2000/80).  
C, Coronal gadolinium-enhanced T1-weighted MR image (400/26).  
D, Axial gadolinium-enhanced T1-weighted MR image (533/20).

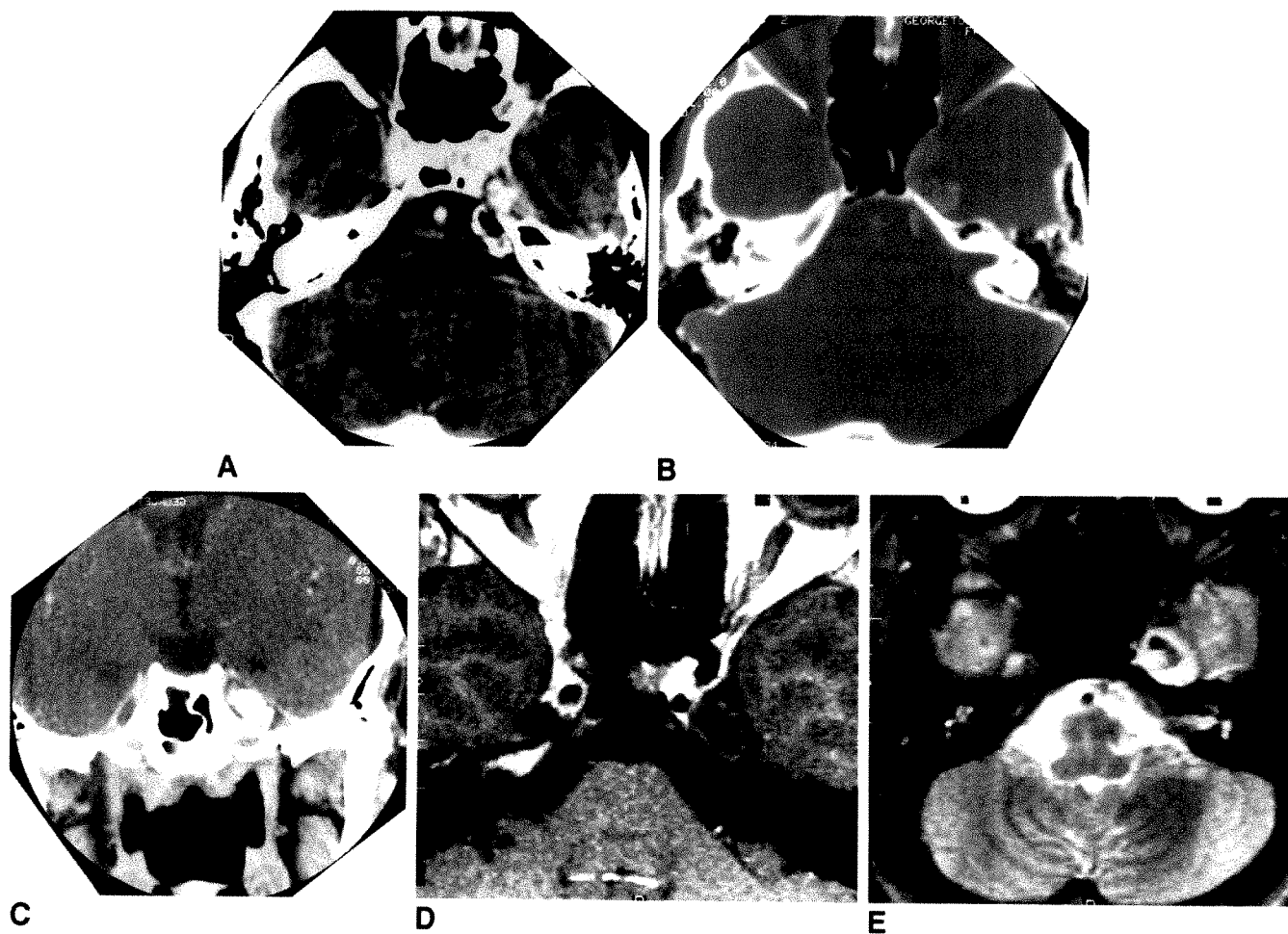


Fig. 3.—Case 3: 22-year-old woman with 8-month history of intermittent dizziness, nausea, and headache.  
A, Axial contrast-enhanced CT scan of head.  
B, Axial CT scan of head with bone windows.  
C, Coronal contrast-enhanced CT scan of head.  
D, Axial gadolinium-enhanced T1-weighted MR image (600/20).  
E, Axial T2-weighted MR image (2500/80).

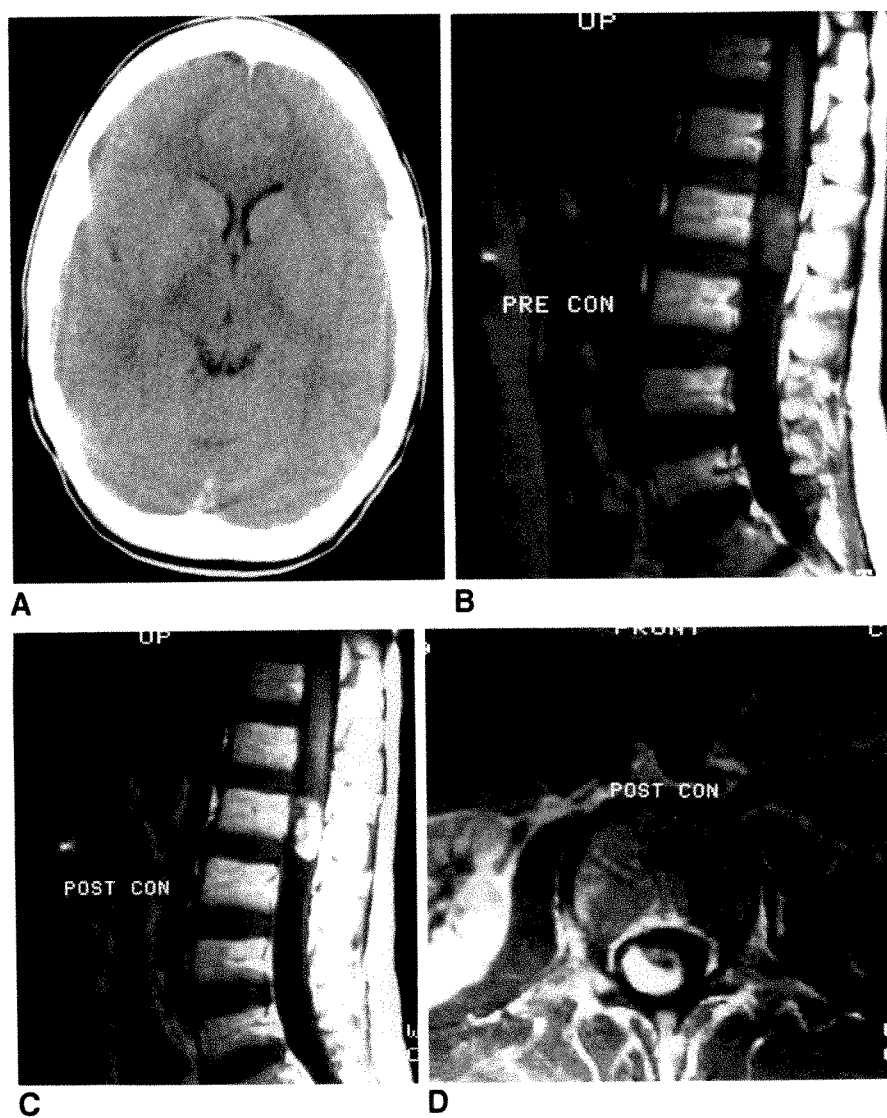


Fig. 4.—Case 4: 14-year-old boy with acute onset of headache, nausea, vomiting, and mild back pain.

A, Transaxial unenhanced CT scan of head.

B, Sagittal T1-weighted MR image (600/20) of lumbar spine.

C and D, Sagittal (C) and transaxial (D) gadolinium-enhanced T1-weighted MR images (600/20) of lumbar spine.

## Letters

### Requisition of the Week

Our radiology department, like many others, displays a popular "case of the week." We are considering introducing a "requisition of the week." This request would be selected specifically on the basis of its illegible, name, or misleading history. The name of the referring physician, the name of the patient, and so forth would be blanked out. We think that a requisition of the week, done in good taste and spirit and displayed in an area without public access, would be both fun and educational. It would require little preparation, and different imaging sections might take turns supplying the requisition (our CT section insisted it could handle the load alone).

Because of the concern that the display of a "requisition of the week" might be confrontational to the clinical staff, we have discussed concurrently posting a "report of the week." This radiologic report would come from our own department and also would be selected on the basis of its inappropriate content. All names and personal data would be omitted. Our clinical colleagues undoubtedly would prefer the "report of the day" and probably would supply us with most of the material for that display.

Unfortunately, these ideas remain only ideas. They have not been acted on because of intradepartmental differences of opinion and misgivings as to their value and appropriateness. Other radiology departments may be less reticent in this regard, and this letter is written to encourage readers to experiment with the ideas expressed here. We suspect that a requisition of the week and a report of the week might attract more attention and discussion than the nearby case of the week. Each has a message.

Ferris M. Hall  
Norman Joffe  
Mark Guenin  
*Beth Israel Hospital  
Harvard Medical School  
Boston, MA 02215*

### Upper Lobe Collapse Due to Endobronchial Sarcoidosis

A 27-year-old black woman was admitted for treatment of ectopic pregnancy. In addition to her abdominal complaints, she had had a cough for 2 months and wheezing and dyspnea on exertion. Right supraclavicular and bilateral epitrochlear lymph nodes were palpable. The patient did not react to purified protein derivative or to a panel of antigens used to detect anergy. Chest radiograph showed collapse of the right upper lobe of the lung with left hilar and right-sided

paratracheal adenopathy (Fig. 1). Pulmonary function tests revealed a reduced forced expiratory volume in 1 sec (FEV<sub>1</sub>), a reduced forced vital capacity, and a total lung capacity of 77% of predicted. Fiberoptic bronchoscopy showed that the bronchus of the right upper lobe was occluded by pearly white granulation tissue. Transbronchial biopsies of the tissue were performed, and examination of the specimens showed noncaseating granulomas. Special stains for acid-fast organisms were negative. A biopsy of an external iliac lymph node was performed at the time of laparotomy, and examination of the specimen also showed multiple noncaseating granulomas. The patient was treated with prednisone, and in 2 weeks, symptomatic improvement and a 50% improvement in the FEV<sub>1</sub> occurred. A chest radiograph taken 1 month after discharge from the hospital showed total reexpansion of the right upper lobe.

Although lobar atelectasis as a result of sarcoidosis has been described [1-3], lobar collapse involving segments other than the middle lobe is unusual. Olsson et al. [1] described eight patients with sarcoidosis who had severe bronchostenosis. Only one of these patients had atelectasis of the right upper lobe. Stinson and Hargett [2] reported a case of sarcoidosis with lobar atelectasis of the right middle lobe that was thought to be caused by extrinsic compression of the bronchus. Olsson et al. thought that bronchostenosis was associated with a poor prognosis, with little regression of symptoms despite treatment. Munt [3] described a patient with sarcoidosis with atelectasis of the middle lobe who had rapid regression of symptoms after treatment with corticosteroids.

Our experience is similar; our patient had relief of her symptoms over several weeks with reexpansion of the right upper lobe. In the right clinical setting, sarcoidosis should be considered in the differential diagnosis of collapse of the right upper lobe, and it need not portend a poor clinical outcome. Resolution of endobronchial granu-

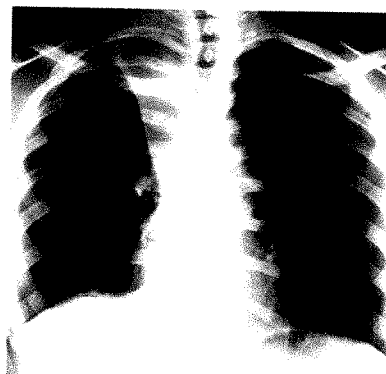


Fig. 1.—Chest radiograph shows atelectasis of right upper lobe of lung and left hilar adenopathy.



lomas as a result of steroid therapy is coincidental with regression of hilar and paratracheal adenopathy. Although bronchial compression due to enlarged lymph nodes may account for occlusion of the middle lobe, disease of the upper lobe most likely is the result of endobronchial occlusion caused by sarcoid granulomas.

James Witko  
William D. Strazzella  
Benjamin H. Safirstein  
St. Michael's Medical Center  
Newark, NJ 07102

## REFERENCES

1. Olsson T, Bornstad-Pettersson H, Stjernberg N. Bronchostenosis due to sarcoidosis: a cause of atelectasis and airway obstruction simulating pulmonary neoplasm and chronic obstructive pulmonary disease. *Chest* 1979;75:6
2. Stinson JJ, Hargett O. Prolonged lobar atelectasis in sarcoidosis. *J Natl Med Assoc* 1981;73:699-671
3. Munt PW. Middle lobe atelectasis in sarcoidosis: report of a case with prompt resolution concomitant with corticosteroid administration. *Am Rev Respir Dis* 1973;111:279-294

## Coronary Artery-Left Ventricle Fistula

I noted a short letter entitled "Coronary Artery-Left Ventricle Fistula" [1] in the November 1989 issue of the *AJR*. The authors cite one reference from the French literature and present a case of a relatively small and apparently isolated coronary artery-left ventricular communication. In order to dispel any misunderstanding, the English literature on this topic has a sizable number of publications, including those by Vogelbach et al. [2] and McLellan and Pelikan [3].

The entire spectrum of such abnormalities ranges from large isolated fistulas to a plexus of small vessels with multiple fistulous channels opening into the left ventricle that, when extensive, is thought to be the cause of signs and symptoms of transient myocardial ischemia and angina pectoris. If a discrete large fistula is likely to cause the signs and symptoms, surgical repair is indicated. Unfortunately, multiple, small, widespread communications, even when positively identified as causing steal from the myocardium, cannot be treated in this way.

I have no argument with the authors' decision not to recommend surgery in their case; the isolated fistula was rather small and probably unrelated to the patient's signs and symptoms. As other causes of transient regional myocardial ischemia exist, the patient might benefit from a stress test in combination with myocardial thallium scanning to establish this diagnosis firmly. Parenthetically, I might add, some cardiologists in the United States would recommend prophylactic antibiotics for dental or surgical procedures in a patient who has a small coronary fistula. Recommendation of such protective measures in a condition that, presumably, has a low, albeit undeniable, risk of infective endocarditis, however, might not be as common in Norway.

Sven Paulin  
Harvard Medical School  
Beth Israel Hospital  
Boston, MA 02215

## REFERENCES

1. Pedersen HK, Simonsen S. Coronary artery-left ventricle fistula (letter). *AJR* 1989;153:1098
2. Vogelbach KH, Edmiston WA, Stenson RE. Coronary artery-left ventricular communications: a report of two cases and a review of the literature. *Cathet Cardiovasc Diagn* 1979;5:159-167
3. McLellan BA, Pelikan PCD. Myocardial infarction due to multiple fistulas. *Cathet Cardiovasc Diagn* 1989;16:247-249

## MR Imaging of Congenitally Corrected Transposition of the Great Vessels in Adults

Having read with interest the pictorial essay by Park et al. [1], I would like to point out two questionable statements. First, in Figure 2A the gastric air bubble under the right hemidiaphragm is said to suggest situs inversus. However, the apex of the heart is in the left side of the chest. In situs inversus, by definition the heart and apex are located in the right side of the chest. Therefore, the situation seen in Figure 2 may represent instead either (a) situs inversus with levocardia or, more likely, (b) heterotaxia or situs ambiguus and dextrocardia. Thus, in this case, neither the viscerotransposition nor the atrioventricular connection is clarified.

Second, regarding Figure 3B, the authors conclude that because the septal leaflet of the morphologic right ventricle is attached more anteriorly (closer) to the cardiac apex than the septal leaflet of the mitral valve, Ebstein anomaly of the tricuspid valve is present. In any morphologic right ventricle, whether right- or left-sided, the septal leaflet of the tricuspid valve characteristically is attached more anteriorly (i.e., closer to the apex) than the anterior leaflet of the mitral valve [2]. This behavior of the septal leaflet of the tricuspid valve allows the identification of the morphology of the right ventricle in specimens and on echocardiograms and MR images and allows the lateralization of the morphologic right ventricle [2, 3]. In Ebstein anomaly, however, the septal leaflet of the tricuspid valve is either absent or plastered against the ventricular wall [4] and would not have the normal appearance of the leaflet shown in Figure 3B. On the contrary, the main feature of the tricuspid valve in Ebstein anomaly is dysplasia rather than displacement [5]. Therefore, the characteristic lower location of the septal leaflet of the left-sided ventricle justifies classifying this ventricle as an inverted morphologic right ventricle with 1-cardiac loop and corrected transposition of the great arteries.

Because of rapidly increasing interest in MR imaging of congenital heart defects, a clear understanding of the anatomic pictures is necessary, and, therefore, I think that clarification of these two points is of both academic and practical importance.

Augustin G. Formanek  
Bowman Gray School of Medicine  
Winston-Salem, NC 27103

## REFERENCES

1. Park JH, Han MC, Kim CW. MR imaging of congenitally corrected transposition of the great vessels in adults. *AJR* 1989;153:491-494
2. Losekoot TG, Anderson RH, Becker AE, Danielson GK, Soto B. *Congenitally corrected transposition*. Edinburgh: Churchill Livingstone, 1983
3. Guft GL, Bluemm R, Rohmer J, et al. Levotransposition of the aorta: identification of segmental cardiac anatomy using MR imaging. *Radiology* 1988;161:673-679
4. Lev M, Liberson RR, Joseph RH, et al. The pathologic anatomy of Ebstein's disease. *Arch Pathol* 1970;90:334-343
5. Becker AE, Decker MJ, Edwards JE. Pathologic spectrum of dysplasia of the tricuspid valve: features in common with Ebstein's malformation. *Arch Pathol* 1971;91:167-178

## Reply

I would like to respond to Dr. Formanek's letter regarding my recent article [1]. First, he suggests that the heart and its apex should be in the right side of the chest in situs inversus. However, the position of the cardiac apex is not necessarily correlated with situs. The diagnosis of the visceral situs is established by identifying the position of the hepatocaval complex. The cardiac apex may have three different directions in each situs. In situs inversus, the apex may be right-sided, medial, or directed to the left [2]. In the patient in

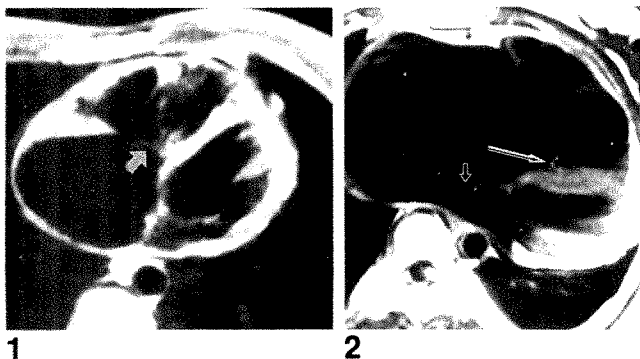


Fig. 1.—Transverse MR image of 30-year-old woman shows displaced septal leaflet (arrow) of tricuspid valve suggesting Ebstein anomaly.

Fig. 2.—Transverse MR image of 29-year-old woman shows displaced septal leaflet (long arrow) of tricuspid valve suggesting Ebstein anomaly associated with atrial septal defect (short arrow).

Figure 2 in the pictorial essay [1], the situs was determined to be inversus on the basis of the anatomy of the liver, inferior vena cava, and atrial appendages; this was proved during open heart surgery. The situation could be called situs inversus with levocardia, but not situs ambiguus.

Second, I agree that the septal leaflet of the tricuspid valve is attached more anteriorly in any morphologic right ventricle. That is one of the criteria used to identify the morphology of ventricles [3]. The problem is the severity of Ebstein anomaly. The clinical diagnosis after two-dimensional echocardiography was corrected transposition of great vessels associated with Ebstein anomaly in the patient shown in Figure 3B [1]. In Ebstein anomaly, the anterior leaflet is attached normally to the anulus, and the posterior and septal leaflets are displaced downward, being attached to the ventricular wall below the anulus. It is known that Ebstein anomaly is a spectrum of features related to the degree of displacement of the attachment of the valve leaflet, varying from minimal displacement to marked displacement with dysplasia [4]. I think that our patient has a mild form of Ebstein anomaly. However, the diagnosis was not confirmed surgically or pathologically.

However, I disagree that a lower location of the septal leaflet merely indicates morphologic right ventricle and does not suggest Ebstein anomaly. Figures 1 and 2 in this letter show two cases of proved Ebstein anomaly without transposition. These cases show that anterior displacement of the septal leaflet suggests not only morphologic right ventricle but also Ebstein anomaly. Nevertheless, I admit that the legend of Figure 3B in the essay [1] was too conclusive inasmuch as such controversies were not described. In addition, I think that the range of the normal position of the septal leaflet is worth further investigation.

Jae Hyung Park  
Seoul National University Hospital  
Seoul 110-744, Korea

## REFERENCES

1. Park JH, Han MC, Kim CW. MR imaging of congenitally corrected transposition of the great vessels in adults. *AJR* 1989;153:491-494
2. de la Cruz MV, Berrazuetu JR, Arteaga M, Attie F, Soni J. Rules for diagnosis of arterioventricular discordances and spatial identification of ventricles: crossed great arteries and transposition of the great arteries. *Br Heart J* 1976;38:341-354
3. Guit GL, Bluemm R, Rohmer J, et al. Levotransposition of the aorta: identification of segmental cardiac anatomy using MR imaging. *Radiology*

1986;161:673-679

4. Zuberbuhler JR, Allwork SP, Anderson RH. The spectrum of Ebstein's anomaly of the tricuspid valve. *J Thorac Cardiovasc Surg* 1979;77:202-211

## Castleman Disease in a Mother and Daughter

Castleman first reported a case of benign giant mediastinal lymph nodes in 1954 [1]. Two years later, he called attention to 13 patients with massively enlarged lymph nodes primarily in the mediastinum [2]. Castleman considered this abnormality to be lymph node hyperplasia, probably caused by a chronic low-grade inflammatory process. Since then, about 300 more cases have been reported. The condition has been termed Castleman disease, angiofollicular hyperplasia, lymphovascular pseudotumor, follicular lymphoreticuloma, and benign giant lymphadenopathy [3-5]. We describe confirmed cases of the disease occurring in a mother and her daughter.

A 9-month-old girl was admitted because of recurrent pneumonia. Physical examination showed right-sided wheezing and cervical and axillary adenopathy. Family history and laboratory findings were unremarkable. A chest radiograph showed large subcarinal and bilateral hilar lymph nodes (Fig. 1). Biopsy specimens of bilateral axillary lymph nodes showed benign lymphoid hyperplasia, thought to be due to chronic infection. Low-dose radiation therapy (5.7 Gy in air) was administered through an anterior mediastinal port. Over the next 6 years, the patient was asymptomatic and had slow but progressive decrease in the size of the hilar and mediastinal lymph nodes. A chest radiograph made when the patient was 22 years old was normal, with no evidence of lymphadenopathy. Reevaluation of the original pathologic specimen confirmed the diagnosis of Castleman disease of the hyaline vascular variety.

The second case was the 12-month-old daughter of the first patient. The daughter was admitted because she had had wheezing for 2 weeks that was refractory to medical therapy. The results of physical examination and laboratory tests were normal. A chest

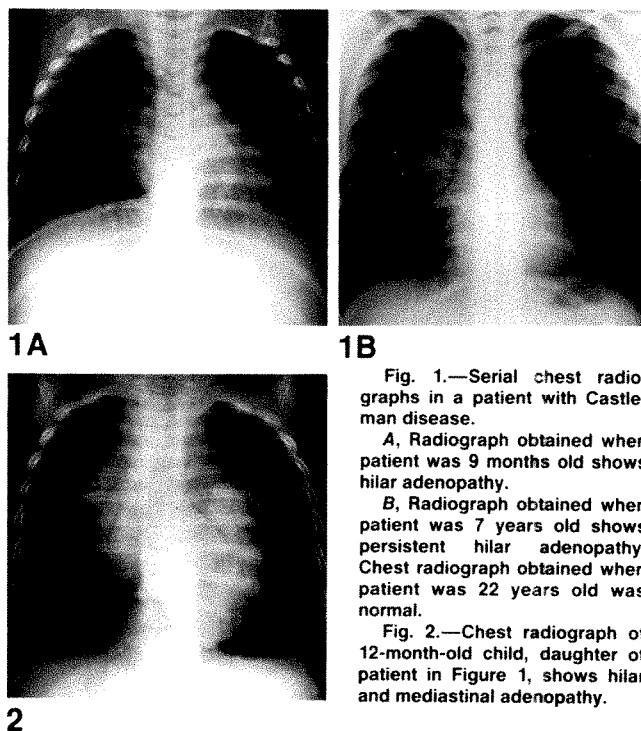


Fig. 1.—Serial chest radiographs in a patient with Castleman disease.

A, Radiograph obtained when patient was 9 months old shows hilar adenopathy.

B, Radiograph obtained when patient was 7 years old shows persistent hilar adenopathy. Chest radiograph obtained when patient was 22 years old was normal.

Fig. 2.—Chest radiograph of 12-month-old child, daughter of patient in Figure 1, shows hilar and mediastinal adenopathy.

radiograph showed massive hilar and mediastinal adenopathy (Fig. 2). CT scans confirmed the presence of mediastinal and hilar adenopathy and showed retroperitoneal lymphadenopathy. A right-sided thoracotomy and biopsy of the mediastinal lymph node were performed. Histologic examination showed Castleman disease of the hyaline vascular type. Comparison of the histologic findings in the two patients showed that the abnormalities were identical. No treatment was given. The wheezing was gone at a 7-month follow-up. Chest films made at that time showed marked decrease in the size of the hilar and mediastinal adenopathy.

To our knowledge, these are the first cases of Castleman disease reported in a mother and her daughter. The pathologic changes in both were identical. The disease also has occurred in identical twins at different ages [6].

Raymond A. Gagliardi  
Manuel P. Meza  
Victor Maldonado  
Robert D. Steele  
St. Joseph Mercy Hospital  
Pontiac, MI 48053  
Wayne State University, School of Medicine  
Detroit, MI 48201  
Chung-ho Chang  
Children's Hospital of Michigan  
Wayne State University, School of Medicine  
Detroit, MI 48201

## REFERENCES

1. Castleman B. Hyperplasia of mediastinal lymph nodes. *N Engl J Med* 1954;250:26-30
2. Castleman B, Iverson L, Mendendez VP. Localized mediastinal lymph node hyperplasia resembling thymoma. *Cancer* 1956;9:822-830
3. Abell MR. Lymphoid hamartoma. *Radiol Clin North Am* 1968;6:15-24
4. Bargoli E, Massarelli G, Soggia G. Multicentric giant lymph node hyperplasia: a hyperimmune syndrome with a rapidly progressive course. *Am J Clin Pathol* 1980;73:423-426
5. Libson E, Fields S, Strauss S, et al. Widespread Castleman disease: CT and US findings. *Radiology* 1988;166:753-755
6. Martin C, Pena M, Angelo F, Garcia F, Vaca D, Serrano R. Castleman's disease in identical twins. *Virchows Arch* 1982;395:77-85

## Breast Mass Simulation on a Mammogram

Simulators of a breast mass have been described previously [1-4]. Recently, an additional simulator was seen at my institution.

In this instance, the patient was a ballet dancer with marked scoliosis and spondylolisthesis. A density was noted posteriorly on the medial aspect of the craniocaudal view of one breast (Fig. 1) but not on the oblique or lateral views. Clinical examination showed marked prominence of the rib cage. Spot mammograms with metallic markers over this region showed that the cause of the density on the mammograms was an unusual prominence of the ribs on that side.

F. I. Jackson  
Cross Cancer Institute  
Edmonton, Alberta, Canada, T6G, 1Z2

## REFERENCES

1. Jackson FI, Woods JA. Simulators of a breast mass on a mammogram (letter). *Radiology* 1989;171:877
2. Jackson FI. A further simulator of a breast mass on a mammogram. *Radiology* 1989;173:284
3. Gillula LA, Destouet JM, Monsees B. Nipple simulating a breast mass on a mammogram. *Radiology* 1989;170:272

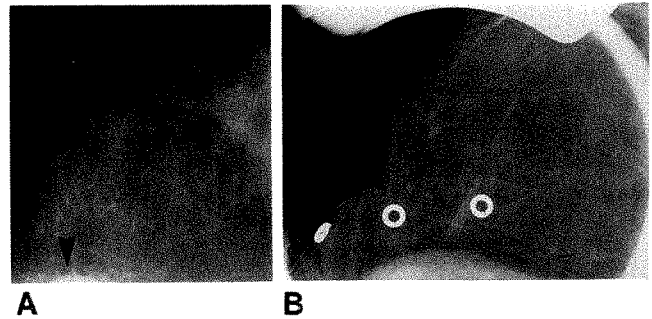


Fig. 1.—A, Craniocaudal mammogram of breast shows posterior density (arrowhead).

B, Spot compression mammogram of breast in region of density shown in A shows "mass" in relation to skin markers.

4. Meyer JE, Stomper PC, Lee RR. Pectoralis muscle simulating a breast mass. *AJR* 1989;152:481-482

## Sonography of Extramedullary Hematopoiesis of the Liver

Extramedullary hematopoiesis is an uncommon finding in adults [1]. The most common sites are the liver and spleen.

A 31-year-old woman with  $\beta$ -thalassemia intermedia had pain and a mass in the right upper quadrant. She was anemic and had hepatosplenomegaly. A chest radiograph was normal. Sonography confirmed the organ enlargement and showed a solid, heterogeneous, hypoechoic mass (15 cm in diameter) in the right lobe of the liver, with no invasion of vessels or signs of cirrhosis (Fig. 1). CT showed a mixed attenuation pattern with patchy contrast enhancement. Sonographically guided biopsy revealed that the lesion was due to extramedullary hematopoiesis.

Hepatic extramedullary hematopoiesis is a normal feature in the fetus and neonate up to 5 weeks of age, and it may persist in the presence of anemia. In the adult, it is associated with loss of bone marrow due to myeloproliferative disease. Other causes include aplastic anemia, marrow replacement syndromes, disseminated carcinomatosis, multiple myeloma, and Albers-Schönberg (marble bone) disease.

The sonographic features of extramedullary hematopoiesis of the liver have been reported for only one case, a patient with agnogenic

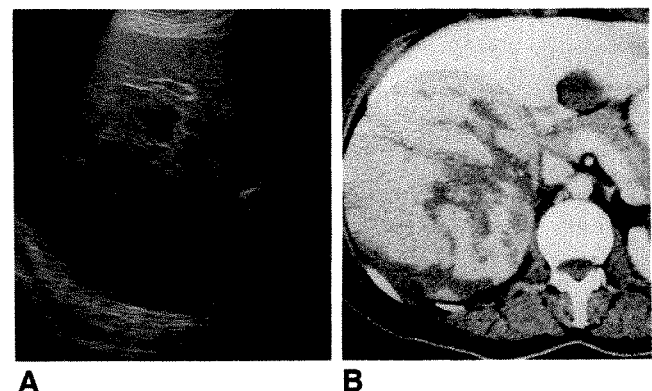


Fig. 1.—Extramedullary hematopoiesis of liver.  
A, Longitudinal sonogram shows a large hepatic mass.  
B, CT scan shows a hepatic mass with mixed attenuation.

myeloid metaplasia [2]. Sonograms showed hepatosplenomegaly with a large, heterogeneous, solid mass in the right lobe of the liver, similar to the findings in our case. The differential diagnosis of hypoechoic hepatic lesions is wide, including hemangiomas, abscesses, focal nodular hyperplasia, adenomas, hemorrhage, focal fatty infiltration, hepatoma, and metastases [3]. It is now necessary to add extramedullary hematopoiesis to this list, especially when the patient has marrow disease.

Michael J. Bradley  
Con Metreweli  
Prince of Wales Hospital  
Shatin New Territories, Hong Kong

## REFERENCES

1. Macsween RM, Anthony P, Scheuer I. *Pathology of the liver*, 2nd ed. New York: Churchill Livingstone, 1987:665
2. Wiener MD, Halvorsen RA Jr, Vollmer RT, Foster WL, Roberts L Jr. Focal intrahepatic extramedullary hematopoiesis mimicking neoplasm. *AJR* 1987;149:1171-1172
3. Cosgrove D, McCready R. Liver metastases. In: *Ultrasound imaging of the liver*. New York: Wiley, 1983:149-194

## Portal Vein MR Angiography

We are writing in reference to the article of Edelman et al. [1]. The authors state that Figure 4 shows a patent portal vein with reversed flow. The coronal projection (Fig. 4B) shows a marked decrease in signal intensity and caliber involving the distal splenic and main portal veins with a return to normal intensity and caliber at the junction of the right and left portal veins. This finding is confirmed on the axial gradient-echo images (Fig. 4C) in which a gap is shown between the splenic vein and the intrahepatic portal vein. The demonstration of hepatofugal flow in the intrahepatic portal vein segment does not exclude occlusion more proximally. Another possible interpretation of the image is segmental occlusion of the extrahepatic portal vein with reconstitution of the intrahepatic portion. This interpretation is supported by the presence of massive gastroesophageal collaterals and by the sonographic finding of occlusion of the portal vein. The residual but diminished flow signal in the region of the extrahepatic portal vein may represent flow around thrombus or flow in periportal collaterals.

The gold standard for evaluation of the portal vein is contrast angiography. It is noteworthy that none of the patients in the series of Edelman et al. had angiographic confirmation of the MR findings. Doppler sonography is accurate for diagnosing occlusion of the portal vein [2-4], and because angiography is an invasive procedure, sonography can be used to validate MR findings when the results of sonography and MR agree. However, when the sonographic and MR findings disagree, especially when the MR images are problematic, diagnosis on the basis of MR angiography should not be considered firm in the absence of confirmation by contrast angiography. At this early stage of development, we should be cautious about conclusions not supported by the gold standard of contrast angiography.

E. Kent Yucel  
Fred L. Steinberg  
Arthur C. Waltman  
Massachusetts General Hospital  
Boston, MA 02114

## REFERENCES

1. Edelman RR, Zhao B, Liu C, et al. MR angiography and dynamic flow evaluation of the portal venous system. *AJR* 1989;153:755-760
2. Miller VE, Berland LL. Pulsed Doppler duplex sonography and CT of portal vein thrombosis. *AJR* 1985;145:73-76
3. Alpern MB, Rubin JM, Williams DM, Capek P. Porta hepatis: duplex Doppler US with angiographic correlation. *Radiology* 1987;162:53-56
4. Nelson RC, Lovett KE, Chezmar JL, et al. Comparison of pulsed Doppler sonography and angiography in patients with portal hypertension. *AJR* 1987;149:77-81

## Reply

We appreciate the comments of Yucel et al. on our article [1] about MR angiography and flow evaluation of the portal venous system. Their letter raises several issues. First, they suggest that Figure 4C in our article represents segmental occlusion of the extrahepatic portal vein with reconstitution of the intrahepatic portion. This is certainly something to be considered from the projection images, but in fact the extrahepatic portal vein is patent as shown by the individual gradient-echo images (Fig. 1, this reply), which were not included in the paper because of space limitations. As we have emphasized previously, it is important to view the individual gradient-echo images as well as the projection images when interpreting MR angiographic studies [2]. The low signal from the portal vein is due to reduced flow velocity, as would be anticipated from reduced flow with reversal of the flow direction. (By the way, the images in Figure 4C are coronal, not axial.) Also, we saw no evidence of thrombus in the repeat sonographic examination.

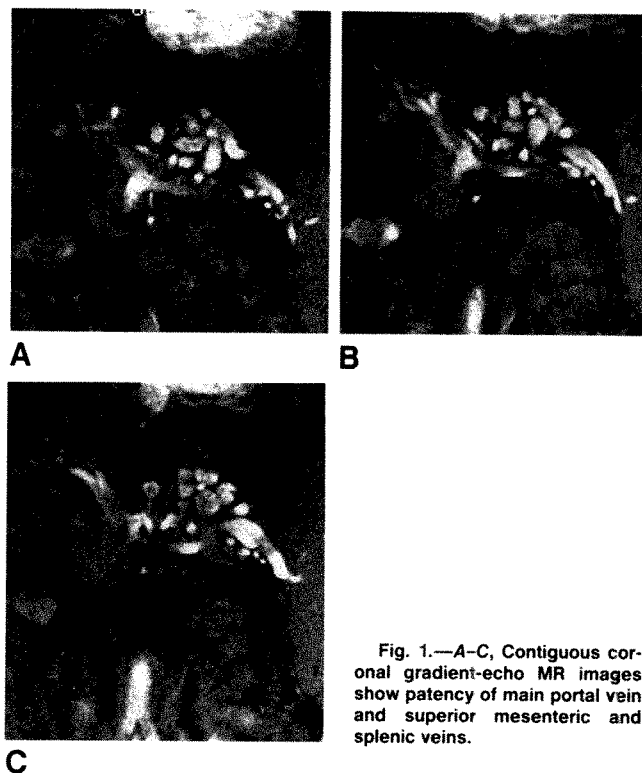


Fig. 1.—A-C, Contiguous coronal gradient-echo MR images show patency of main portal vein and superior mesenteric and splenic veins.

Second, Yucel et al. make an important point that new imaging modalities (in this case, MR angiography) need to be compared with established techniques. However, this is an irrelevant issue to our paper, which describes a new approach for evaluating the portal venous system. We never claimed to have made a comparative study with conventional angiography. MR did show good correlation with duplex sonography for determination of flow velocities, and these preliminary results also suggest ways in which MR might be superior to sonography as a noninvasive technique for evaluating the portal venous system. In order to determine the accuracy of the MR imaging method, a much larger study would be needed comparing MR to angiography, surgical results, and so forth; such a study is in progress.

Third, Yucel et al. state that none of the patients in our series had conventional angiography, yet it is stated clearly in our paper that patient 3 had this procedure. In fact, patient 2 also had angiography, although this was not mentioned in the paper.

Finally, conventional angiography has limitations for assessing the portal venous system. Only vessels opacified with contrast material are shown; as a result, the method is operator and flow dependent. Vessels not shown by conventional angiography nonetheless may be patent, depending on the flow pattern. On the other hand, MR can show vessels independent from the direction of flow. Also, conventional angiography can be limited markedly by the presence of ascites, which is less of a problem for MR.

Robert R. Edelman

*Beth Israel Hospital*

*Boston, MA 02215*

Heinrich P. Mattle

*New England Deaconess Hospital*

*Boston, MA 02215*

Henri M. Hoogewoud

*Hôpital Cantonal*

*CH-1700 Fribourg, Switzerland*

## REFERENCES

1. Edelman RR, Zhao B, Liu C, et al. MR angiography and dynamic flow evaluation of the portal venous system. *AJR* 1989;153:755-760
2. Edelman RR, Wentz KU, Mattle H, et al. Projection arteriography and venography: initial clinical results with MR. *Radiology* 1989;172:351-357

## Follow-up of Endovascular Stented Renal Artery

Recently, my colleagues and I published a technical note [1] in the *AJR* on the use of an endovascular stent in the treatment of a dissecting aneurysm of the renal artery. One year after treatment, the patient, who was doing well clinically, had follow-up angiography. It was clear from the results that some intimal hyperplasia was present in the distal end of the stent but that no serious stenosis of the renal artery had occurred (Fig. 1).

Furthermore, compared with the results of the study done 10 days after placement of the stent, the aneurysm was thrombosed completely at the 1-year follow-up. This finding suggests that endovascular stenting can be an excellent treatment in cases of dissecting aneurysm of the renal artery.

W. P. Th. M. Mali

*University Hospital Utrecht*

*Utrecht, the Netherlands*

## REFERENCE

1. Mali WPTHM, Geyskes GG, Thalman R. Dissecting renal artery aneurysm: treatment with an endovascular stent. *AJR* 1989;153:623-624

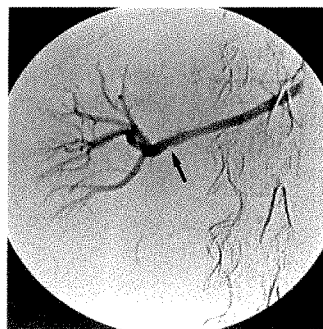


Fig. 1—Angiogram shows some intimal hyperplasia (arrow) in distal end of stent and no stenosis in renal artery.

## Metastatic Carcinoma of the Proximal Femur Closely Resembling Hematopoietic Hyperplasia on MR

For 2 weeks, a 55-year-old woman had had increasing pain in the left hip that radiated along the anterior aspect of the thigh. The results of physical examination and routine blood tests were normal. Radiographs of the left hip and lumbar spine were normal. A bone scan showed a small focal area of increased uptake in the proximal left femur. MR of the pelvis showed mottled confluent areas of decreased signal intensity involving the proximal femurs (Fig. 1A), iliac crests, and right acetabulum on T1-weighted images. These findings resembled those of hematopoietic hyperplasia. T2-weighted images showed a small focus of increased signal intensity involving the proximal left femur slightly anterior to the lesser trochanter (Fig. 1B). An open bone biopsy of this region revealed undifferentiated metastatic carcinoma of the intramedullary bone. A CT scan and radiograph of the chest showed a 1.5-cm nodule in the apex of the right lung that was found to be poorly differentiated non-oat cell carcinoma.

This patient had MR characteristics almost identical to those described in an earlier letter to the editor [1]. Deutsch et al. [2] initially described the MR findings of hematopoietic hyperplasia and stressed the importance of a complete examination and a peripheral blood smear. In our case, without the previous bone scan, it would be easy to overlook the small focal finding on the T2-weighted MR image and possibly misinterpret it as an artifact.

This case not only reinforces the importance of the T2-weighted sequence in evaluating the bone marrow but also shows further

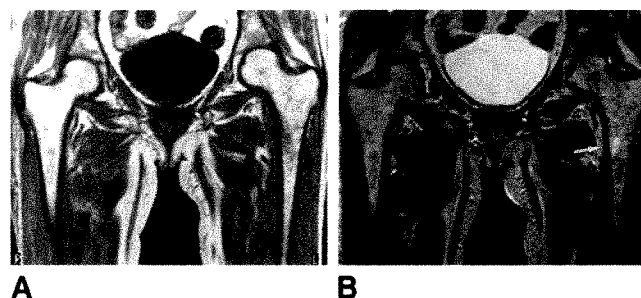


Fig. 1.—Probable hematopoietic hyperplasia with a focus of metastatic carcinoma.

A and B, Coronal MR images, 500/20 (A) and 2000/80 (B), of proximal femurs show mottled areas of decreased signal within bone marrow of both femurs (A) and a small focus of increased signal (arrow) in metaphyseal region (B).

cause for a more cautious approach to MR findings similar to those of hematopoietic hyperplasia.

David J. Czarnecki  
William S. Goell  
St. Luke's Medical Center  
Milwaukee, WI 53215

## REFERENCES

- Schuck JE, Czarnecki DJ. MR detection of probable hematopoietic hyperplasia involving the knees, proximal femurs, and pelvis (letter). *AJR* 1989;153:655-656
- Deutsch AL, Mink JH, Rosenfelt FP, Waxman AD. Incidental detection of hematopoietic hyperplasia on routine knee imaging. *AJR* 1989;152:333-336

## Spontaneous Resolution of a Nuchal Fetal Cystic Hygroma Diagnosed Early in the Second Trimester of Pregnancy

We read with interest the article, "Spontaneous Resolution of a Cystic Neck Mass in a Fetus with Normal Karyotype," by Distell et al. [1]. The authors reported a case of a fetus in which complete resolution of a cystic hygroma diagnosed in the second trimester of pregnancy was evident on further sonograms. They stressed that a normal fetal karyotype was found on chromosomal analysis of amniotic fluid.

We recently detected in utero two cases of cystic hygroma early in gestation (14 and 15 weeks, respectively). In both cases, nuchal cystic hygroma was the only sonographic finding (Fig. 1). No signs of fetal hydrops as may be observed in such cases were detected. In both fetuses, the sonographic findings disappeared within 3 weeks. In one of the fetuses, genetic amniocentesis performed at 16 weeks of pregnancy revealed normal 46,XX karyotype, and the pregnancy was allowed to continue, resulting in a delivery of normal healthy infant. However, chromosomal analysis of the second fetus revealed trisomy 18, and the pregnancy was terminated. Both these cases

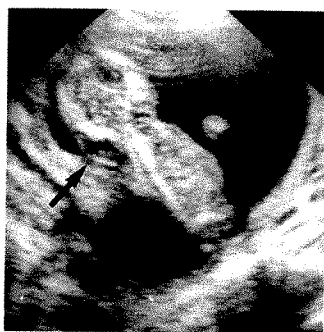


Fig. 1.—Sonogram shows non-septated nuchal cystic hygroma (arrow) in a 14-week-old fetus.

show that in utero detection of isolated nuchal cystic hygroma does not necessarily indicate an unfavorable outcome provided a normal karyotype is found, thus supporting the observations of Distell et al. It should be stressed, however, that fetal hydrops must be excluded even when normal fetal karyotype is encountered [2].

Until more data are collected to support the relatively good prognosis of those cases not associated with hydrops, we recommend amniocentesis for karyotyping and measurement of levels of alpha-fetoprotein in each case of nuchal cystic hygroma. This suggestion is supported by Bronshtein et al. [3], who reported eight cases of

nuchal cystic hygroma diagnosed early in the second trimester of pregnancy.

Israel Meizner  
Arie Levy  
Jacob Cohen  
Soroka Medical Center  
Beer Sheva 84101 Israel

## REFERENCES

- Distell BM, Hertzberg BS, Bowie JD. Spontaneous resolution of a cystic neck mass in a fetus with normal karyotype. *AJR* 1989;153:380-382
- Meizner I, Katz M, Carmi R. Prenatal ultrasonic diagnosis of cystic hygroma associated with fetal hydrops: report of two cases. *Isr J Med Sci* 1989;25:51-53
- Bronshtein M, Rottem S, Yoffe N, Blumenfeld Z. First trimester and early second trimester diagnosis of nuchal cystic hygroma by transvaginal sonography: diverse prognosis of the septated from the nonseptated lesion. *Am J Obstet Gynecol* 1989;161:78-84

## Reply

We appreciate the interest that Drs. Meizner, Levy, and Cohen have shown in our report on spontaneous resolution of a fetal cystic hygroma. We were pleased to learn that their experience supports our observation that in the absence of hydrops, prenatal detection of a cystic hygroma in a fetus with a normal karyotype can be associated with a normal outcome. In their letter, Meizner et al. further comment that karyotyping should be performed in all cases of prenatal diagnosis of nuchal cystic hygroma. Given the high prevalence of chromosomal anomalies occurring in association with cystic hygromas, we fully agree with this statement. Although it is becoming increasingly clear that prenatal detection of nuchal cystic hygromas occasionally is associated with a normal outcome, many more fetuses with cystic hygromas are abnormal. Therefore, we recommend fetal karyotyping, a careful search for other anomalies, and close sonographic follow-up in such cases.

Bruce M. Distell  
Barbara S. Hertzberg  
James D. Bowie  
Duke University Medical Center  
Durham, NC 27710

## The Radiologic Hedge

Every radiology resident quickly learns the official plant of our specialty: the hedge. As defined by Webster's dictionary, the hedge serves to "enclose or protect the user" or acts as an "evasive statement . . . to avoid the risk of commitment." Actually, this symbol is appropriate for any physician who performs diagnostic examinations and communicates this information via written reports.

Hedge cultivation is a linguistic art that, in our opinion, is underemphasized in residency training. Terms such as appears, apparent, unusual, opacity, probable, doubtful, equivocal, suboptimal, and indeterminate are the bread and butter of the radiologist's lexicon. Their use needs to be taught during training and then subsequently honed during many years of practice. In our department, we recommend a limit of two hedge terms per sentence, but this rule is frequently broken. Attempts should be made to counterbalance multiple hedge sentences with short definitive statements, even if the latter, of necessity, provide nonpertinent information. The best radiologic defense is often an offense: don't hesitate to pose questions in the report. And remember, a good department never produces a poor exam, only suboptimal ones.



The proper use of hedge terms is demonstrated in the following generic report of a typical intensive care chest radiograph.

This is a *suboptimal* examination due to bedside technique and inability of the patient to cooperate. The cardiovascular status is *difficult to assess* with *border-line* cardiomegaly. There is *equivocal* vascular *plethora* but no overt edema. Is the patient short of breath? The *poorly defined* opacities that *overlie* the lungs are *unusual* and of *uncertain significance*. I *doubt* but *cannot* exclude infiltrates. No evidence of an obvious mass is *identified*. No rib fractures. The *prominent* mediastinum *appears* to relate to semierect positioning. No subcutaneous emphysema. There is *possible* diaphragmatic flattening which is of *indeterminate* significance but *raises the question* of chronic lung disease. Does the patient smoke? The *apparent* costophrenic angle blunting is *consistent with* a small effusion but does *not specifically suggest* that diagnosis. There is *probable* osteoporosis in this 98-year-old woman. The interpretation of this exam is *limited* because previous films are not immediately available for comparison.

Impression: *Indeterminate* examination. Recommend *clinical correlation*. A repeat study may be useful.

Ferris M. Hall  
Jonathon S. Movson  
Beth Israel Hospital  
Boston, MA 02215

### CT Diagnosis of Foot-in-Mouth Disease<sup>1</sup>

Foot-in-mouth disease [1] is a common disorder, which at one point or another has afflicted everyone. To our knowledge, this is the first demonstration of the use of CT to diagnose a complication of this disorder, that is, swallowing of the foot.

A middle-aged woman was referred for CT of the abdomen to evaluate nonspecific abdominal complaints. Clinical and laboratory findings were normal. The initial unenhanced CT scan of the abdomen showed normal liver, spleen, and kidneys. The left upper quadrant, pancreas, and retroperitoneal structures were normal. After the injection of contrast material, CT showed a lobulated, well-circumscribed, very-low-attenuation, 9 × 5 cm mass that obscured the spleen, the left kidney, and portions of the fundus of the stomach (Fig. 1A). This was definitely not gas in the fundus of the stomach because it clearly extended beyond the borders of the stomach and obscured adjacent organs. By the time the postcontrast CT scan was processed, the patient had left the CT site. When we reviewed the images with lung windows and inverted gray scale, the abnormality appeared to be a

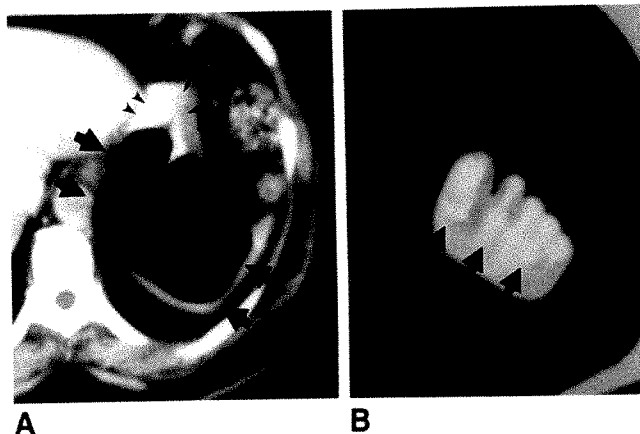


Fig. 1.—A, Postcontrast CT scan shows low-attenuation pseudomass in left upper quadrant (arrows) extending beyond borders of stomach (arrowheads).

B, Reprocessed image shows pseudomass has appearance of a foot, including phalanges (arrows).

perfectly formed forefoot with five toes, superimposed on the left upper quadrant (Fig. 1B). (The manufacturer, when consulted, could not explain this computer-generated artifact, and it is being temporarily blamed on a transient voltage surge that is commonplace with our local electrical utility.)

The diagnosis appeared to be an unusual complication of foot-in-mouth disease, with the patient having ingested the "foot."

We are now in the process of studying the sensitivity and specificity of CT for this diagnosis. Whenever a verbal gaffe is committed in the radiology department, its perpetrator is rushed into the CT scanner, but to date, no other cases of an ingested foot have been documented.

Stanley Sprecher  
Richard Steinberg  
Leon Serchuk  
Peninsula Hospital Center  
Far Rockaway, NY 11691

### REFERENCE

1. Chapman, R.L., *New dictionary of American slang*. New York: Harper and Row, 1986:144. *Foot-In-Mouth Disease*: The uttering of embarrassing, stupid, or indiscreet speech. [Blend of the veterinary term hoof-and-mouth disease and the idiom to put "one's foot in one's mouth."]

<sup>1</sup>April Fools!

Letters are published at the discretion of the Editor and are subject to editing.

Letters to the Editor must not be more than two *double-spaced*, typewritten pages. One or two figures may be included. Abbreviations should not be used. See Author Guidelines, page A5.

Material being submitted or published elsewhere should not be duplicated in letters, and authors of letters must disclose financial associations or other possible conflicts of interest.

Letters concerning a paper published in the *AJR* will be sent to the authors of the paper for a reply to be published in the same issue. Opinions expressed in the Letters to the Editor do not necessarily reflect the opinions of the Editor.

## Review of Current Literature

Initials and addresses of corresponding authors are provided in parentheses for each article so that the reader can obtain reprints directly. Abstracts are printed verbatim from each journal.

### The New England Journal of Medicine

**The risk of breast cancer after irradiation of the thymus in infancy.** Hildreth NG, Shore RE, Dvoretzky PM (NGH, Dept. of Community and Preventive Medicine, University of Rochester School of Medicine and Dentistry, Box 644, 601 Elmwood Ave., Rochester, NY 14642). *N Engl J Med* 321(19):1281-1284, Nov. 1989

It is well established that exposure to ionizing radiation during or after puberty increases a woman's risk for breast cancer, but it is less clear whether exposure to ionizing radiation very early in life is also carcinogenic. We studied the incidence of breast cancer prospectively in a cohort of 1201 women who received x-ray treatment in infancy for an enlarged thymus gland and in their 2469 nonirradiated sisters.

After an average of 36 years of follow-up, there were 22 breast cancers in the irradiated group and 12 among their sisters, yielding an adjusted rate ratio of 3.6 (95 percent confidence interval, 1.8 to 7.3). The estimated mean absorbed dose of radiation to the breast was 0.69 Gy. The first breast cancer was diagnosed 28 years after irradiation. The dose-response relation was linear ( $P < 0.0001$ ), with a relative risk of 3.48 for 1 Gy of radiation (95 percent confidence interval, 2.1 to 6.2) and an additive excess risk of 5.7 per  $10^4$  person-years per gray (95 percent confidence interval, 2.9 to 9.5).

We conclude that exposure of the female breast to ionizing radiation in infancy increases the risk of breast cancer later in life.

**Mortality from breast cancer after irradiation during fluoroscopic examinations in patients being treated for tuberculosis.** Miller AB, Howe GR, Sherman GJ, et al. (GRH, National Cancer Institute of Canada Epidemiology Unit, McMurrich Bldg., 3rd Floor, University of Toronto, 12 Queen's Park Crescent W., Toronto, Ontario M5S 1A8, Canada). *N Engl J Med* 321(19):1285-1289, Nov. 1989

The increasing use of mammography to screen asymptomatic women makes it important to know the risk of breast cancer associated with exposure to low levels of ionizing radiation. We examined the mortality from breast cancer in a cohort of 31,710 women who had been treated for tuberculosis at Canadian sanatoriums between 1930 and 1952. A substantial proportion (26.4 percent) had received radiation doses to the breast of 10 cGy or more from repeated fluoroscopic examinations during therapeutic pneumothoraxes.

Women exposed to  $\geq 10$  cGy of radiation had a relative risk of death from breast cancer of 1.36, as compared with those exposed to less than 10 cGy (95 percent confidence interval, 1.11 to 1.67;  $P = 0.001$ ). The data were most consistent with a linear dose-

response relation. The risk was greatest among women who had been exposed to radiation when they were between 10 and 14 years of age; they had a relative risk of 4.5 per gray, and an additive risk of 6.1 per  $10^4$  person-years per gray. With increasing age at first exposure, there was substantially less excess risk, and the radiation effect appeared to peak approximately 25 to 34 years after the first exposure. Our additive model for lifetime risk predicts that exposure to 1 cGy at the age of 40 increases the number of deaths from breast cancer by 42 per million women.

We conclude that the risk of breast cancer associated with radiation decreases sharply with increasing age at exposure and that even a small benefit to women of screening mammography would outweigh any possible risk of radiation-induced breast cancer.

### Cancer

**Combinations of monoclonal antibodies can distinguish primary lung tumors from metastatic lung tumors sampled by fine needle aspiration biopsy.** Mottolese M, Venturo I, Rinaldi M, et al. (Pier Giorgio Natali, Immunology Laboratory, Regina Elena Cancer Institute, Viale Regina Elena 291, 00161 Rome, Italy). *Cancer* 64:2493-2500, 1989

Transthoracic fine needle aspiration (FNA) biopsies performed under computed tomography (CT) scan (CT-FNA) have greatly improved the cytodiagnosis of lung tumors. However, the distinction between a primary lesion and a metastatic lesion still may be difficult on the basis of morphologic criteria. To evaluate whether a selected panel of monoclonal antibodies (MoAb) to tumor-associated antigens (TAA) can improve the diagnostic potential of FNA, we have immunocytochemically analyzed 122 pulmonary CT-FNA. Whereas conventional cytology was capable of recognizing only the neoplastic nature of the lesions, the immunocytochemical diagnosis could identify the primary or metastatic nature of the pulmonary masses in 92.5% of the cases. The immunocytochemical findings were confirmed by clinical-histopathologic data. The current results demonstrate that the use of immunocytochemical methods can significantly improve the diagnostic accuracy of conventional cytology of lung masses.

Reprinted by permission from the American Cancer Society.

### Chest

**Correlation of chest roentgenograms with pulmonary function and bronchoalveolar lavage in interstitial lung disease.** Nugent KM, Peterson MW, Jolles H, Monick MM, Hunninghake GW (GWH, Pulmonary Disease Division, Rm. C33, General Hospital, Iowa City, IA 52242). *Chest* 96:1224-1227, 1989

We used the ILO classification for occupational lung disease to determine whether there was any correlation between the type and/or severity of pulmonary infiltration on chest roentgenograms and either pulmonary function tests or the types of inflammatory cells present in BAL fluid in patients with interstitial lung disease. Of the 62 patients evaluated (27 with sarcoidosis, 18 with IPF, and 17 with a CV disease and lung involvement), 49 had irregular linear opacities and 13 had normal chest x-rays. There were no significant correlations between the types of cells present in BAL fluid and the various categories of infiltrate or profusion of the infiltrates within each disease group. In patients with sarcoidosis, more extensive infiltration (profusion) was associated with lower FEV<sub>1</sub> ( $p < 0.01$ ). In patients with IPF, linear opacity type, profusion, and the presence or absence of honeycombing were not related to the severity of pulmonary function abnormalities. We conclude that the ILO classification for analysis of chest roentgenograms can be applied to patients with interstitial lung diseases not associated with an occupational exposure and that this approach is useful, especially for communication. However, these data provide no information regarding the inflammatory process in the lung and limited information regarding abnormalities in pulmonary function.

## Gastroenterology

**Gastroesophageal endoscopic features in cirrhosis: observer variability, interassociations, and relationship to hepatic dysfunction.** Calès P, Zabotto B, Meskens C, et al. (PC, Service d'Hépatogastroentérologie, Centre Hospitalier Universitaire Purpan, Toulouse, France). *Gastroenterology* 98:156-162, 1990

Nowadays, gastroesophageal endoscopic features of portal hypertension are the recognized predictive factors for bleeding and consequently allow the selection of patients for prophylactic therapies. The aim of this prospective study was to investigate the interobserver agreement, the interassociations between these features, and the relationship between these signs and the degree of hepatic dysfunction. In 100 consecutive cirrhotic patients (84% with alcoholism) without history of digestive bleeding, gastroesophageal endoscopic examination was performed and recorded using a video-endoscope. Four independent observers evaluated the following endoscopic features: the size, extent, color, and red signs of esophageal varices, the mosaic pattern, congestive gastropathy, fundic varices, and associated lesions of the stomach. Agreement was assessed using kappa statistics ( $\kappa$ ) and a quantitative score. The size of esophageal varices was significantly associated with their extent and the presence of red signs, whereas no relation was found either between gastropathy or mosaic pattern and fundic varices, or between esophageal and gastric features. Agreement between observers was good for the size of esophageal varices ( $\kappa = 0.59$ ), the presence of red signs ( $\kappa = 0.60$ ), and of gastric-associated lesions ( $\kappa = 0.68$ ) and gastropathy ( $\kappa = 0.50$ ), while it was poor for the extent ( $\kappa = 0.37$ ) and the color ( $\kappa = 0.28$ ) of esophageal varices as well as for the mosaic pattern ( $\kappa = 0.38$ ). The Child-Pugh score significantly increased along with the presence or the size of esophageal varices as well as with the presence of red signs; no relationship could be shown between this score and the presence of gastric features. We conclude that (1) interobserver agreement was good for the main endoscopic features, especially for the size and the red signs of esophageal varices; (2) esophageal patterns were significantly associated between themselves and related to hepatic dysfunction; and (3) gastric patterns were related neither to esophageal features nor to hepatic dysfunction and were not associated between themselves.

Reprinted with permission by the American Gastroenterological Association.

## Gastrointestinal Endoscopy

**A placebo-controlled study on the efficacy of aspirin and doxycycline in preventing clogging of biliary endoprostheses.** Smit JM,

Out MMJ, Groen AK, et al. (JMS, Juliana Hospital, Kon. Lodewijklaan 801, 7314 BC Apeldoorn, The Netherlands). *Gastrointest Endosc* 35(6):485-489, 1989

Sixty patients in whom a biliary endoprosthesis was inserted were randomized to receive: (1) placebo, (2) aspirin, or (3) doxycycline, to study the effect on the process of sludge formation. After 2 months all endoprostheses were changed, and the amount and composition of the sludge in the patent stents was analyzed. Half of the patients dropped out. The major component (56%) of the sludge of all groups was protein. No insoluble residue was present. Major deposits of sludge were found at irregularities in the stent wall (side flaps). Both doxycycline and aspirin reduced the dry weight of the sludge. Doxycycline significantly reduced the amount of protein, but scanning electron microscopy still showed abundant bacterial growth. Aspirin reduced the content of all sludge components including protein, suggesting that it decreases "stickiness" of bile. Surprisingly, doxycycline significantly decreased the death rate in the 2 months of the study. We present further evidence for a primary role of protein deposition in the early stages of stent occlusion. This process can be partly inhibited by doxycycline and probably also by aspirin, which could lead to a significant increase in stent patency.

**Endoscopic treatment of biliary tract fistulas.** Ponchon T, Gallez JF, Valette PJ, Chavaillon A, Bory R (TP, Hépatogastroentérologie, Pavillon Hbis, Hôpital E. Herriot, 69437 Lyon Cedex 03, France). *Gastrointest Endosc* 35(6):490-498, 1989

Endoscopic therapy was attempted in 24 patients with spontaneous or post-operative persistent biliary fistulas. Endoscopic retrograde cholangiography demonstrated the site of the fistula in 22 cases. Sphincterotomy or biliary stent placement resulted in rapid resolution of the fistula in 16 of 24 patients. Failures were attributed to exclusion of the injured intrahepatic bile duct in two cases, insufficient dilation of a bile duct stricture in one, the large size of the bile duct defect in two, and associated lesions in three (cirrhosis, arterial trauma, subhepatic abscess). Endoscopic management of biliary fistulae requires: (1) visualization of the location of the fistula by retrograde cholangiography especially in case of an intrahepatic lesion, (2) prior percutaneous drainage of associated subhepatic or subphrenic abscesses, and (3) appropriate relief of distal biliary obstruction in order to reduce the intraductal biliary pressure. The outcome is uncertain when endoprostheses are used to bridge large bile duct defects.

**Same-day versus separate-day sigmoidoscopy and double contrast barium enema: a randomized controlled study.** Eckardt VF, Kanzler G, Willems D (VFE, Dotzheimer Str. 14-18, 6200 Wiesbaden, Federal Republic of Germany). *Gastrointest Endosc* 35(6):512-515, 1989

A randomized controlled study was carried out in 400 patients to investigate whether same-day sigmoidoscopy impairs the quality of a double contrast barium enema. There was no difference with regard to spasm, fluid, and air retention as well as barium coat in patients undergoing both procedures during the same day or on different days. The overall quality of the radiographic films received similar ratings in a blind appraisal by an outside radiologist. In contrast, the performance of sigmoidoscopy was facilitated by the more thorough bowel cleansing for same-day procedures. It is concluded that same-day sigmoidoscopy and double contrast barium enema diminishes the cost and patient discomfort for colonic investigation without impairing its quality, provided the CO<sub>2</sub> instead of air is used during the endoscopic study.

## Clinical Orthopaedics and Related Research

**Metastatic disease in long bones: a proposed scoring system for diagnosing impending pathologic fractures.** Mirels H (HM, 15 Crawford Rd., Harrison, NY 10528). *Clin Orthop* 249:256-264, Dec. 1989

A weighted scoring system is proposed to quantify the risk of sustaining a pathologic fracture through a metastatic lesion in a long bone. This system objectively analyzes and combines four roentgenographic and clinical risk factors into a single score. Retrospective analysis of metastatic long bone lesions was completed in 78 lesions that had been irradiated without prophylactic surgical fixation. Clinical data and roentgenograms were scored prior to irradiation by independent observers. The outcome identified 51 lesions that did not fracture during the subsequent six months and 27 lesions that fractured within six months. A mean score of 7 was found in the nonfracture group, whereas the fracture group had a mean score of 10. The percentage risk of a lesion sustaining a pathologic fracture could be predicted for any given score. As the score increased above 7, so did the percentage risk of fracture. It is suggested that all metastatic lesions in long bones be evaluated prior to irradiation. Lesions with scores of 7 or lower can be safely irradiated without risk of fracture, while lesions with scores of 8 or higher require prophylactic internal fixation prior to irradiation.

## The Journal of Urology

**Evaluation of vasculogenic erectile impotence using penile duplex ultrasonography.** Shabsigh R, Fishman IJ, Quesada ET, Seale-Hawkins CK, Dunn JK (RS, Scott Dept. of Urology, Baylor College of Medicine, Houston, TX). *J Urol* 142:1469-1474, Dec. 1989

A total of 140 patients underwent penile vascular evaluation with intracavernous papaverine injection combined with duplex ultrasonography. Of these patients 8 were potent men who were evaluated for reasons other than erectile failure. These potent men were used as controls to obtain normal values. The remaining 132 patients had erectile impotence of various etiologies. Real-time imaging with high resolution, high frequency probes allowed for visualization of the cavernous arteries along the entire length in addition to accurate measurement of the diameter. Simultaneous selectively focused Doppler ultrasonography was used to measure the blood velocity and other vascular parameters in the cavernous and dorsal arteries. Comparison of measurements before and after papaverine injection allowed for objective interpretation of the injection results. The results were analyzed and compared to other data available on the same patients, such as history and physical examination, nocturnal penile tumescence, penile blood pressures, selective arteriography and dynamic cavernosography. In addition to the 8 potent men, there were 35 patients (27% of the impotent patients) whose vascular findings were normal. A total of 78 patients (59% of the impotent patients) had arterial insufficiency; a subgroup of 13 patients had the pelvic arterial steal syndrome. Dynamic cavernosography confirmed venous leak in all 19 patients (14% of the impotent patients) whose penile duplex ultrasonography suggested the possibility of a venous leak. Ten patients (7%) had prolonged erection after papaverine injection and they were managed without consequences. One patient had a small hematoma that resolved uneventfully. Penile duplex ultrasonography was a helpful and objective method to evaluate vasculogenic impotence.

## Pediatrics

**Untreated bacteriuria in asymptomatic girls with renal scarring.** Hansson S, Jodal U, Norén L, Bjure J (SH, Dept. of Pediatrics, East Hospital, S-416 85 Göteborg, Sweden). *Pediatrics* 84(6):964-968, Dec. 1989

Recurrences of bacteriuria after treatment occur in 50% to 80% of asymptomatic patients. Previous experience with short-term treatment as well as long-term prophylaxis has been disappointing, with a significant risk of infections, ie, development of symptoms after treatment. Results with nontreatment are described in this report with reference to clinical course, renal growth, and glomerular filtration rate in 26 asymptomatic girls with established renal scarring and

bacteriuria. Acute pyelonephritis was not seen in those with continuing bacteriuria or spontaneous clearance. Neither in scarred nor in unscarred kidneys did the duration of bacteriuria influence renal growth or glomerular filtration rate. Asymptomatic patients with bacteriuria may gain from nontreatment and may have a reduced risk of pyelonephritic attacks.

Reprinted by permission of PEDIATRICS © 1989.

## The Journal of Pediatrics

**Bacterial attachment as a predictor of renal abnormalities in boys with urinary tract infection.** de Man P, Clässon I, Johanson I, Jodal U, Edén CS (PM, Dept. of Clinical Immunology, Guldhedsgatan 10, S-413 46 Göteborg, Sweden). *J Pediatr* 115:915-922, Dec. 1989

The development of renal scarring was analyzed prospectively in 241 boys with their first known episode of symptomatic urinary tract infection (140 acute pyelonephritis, 61 acute cystitis, and 40 nonspecific). Of 197 boys undergoing urography, 22 (11%) had scars; 20 were in the pyelonephritis group. Vesicoureteral reflux occurred in 81% of those with scarring, compared with 20% of those without scarring. The bacteria causing the first episode of urinary tract infection in each patient were saved, and *Escherichia coli* organisms were characterized for the expression of both galactose- $\alpha$ (1  $\rightarrow$  4)galactose- $\beta$  (Gal-Gal)-specific adhesins and *pap* homologous DNA. Scarring occurred in 41% and other renal abnormalities in 11% of boys infected with bacteria that did not bind Gal-Gal (Gal-Gal negative), compared with 5% and 1%, respectively, in those infected with Gal-Gal-binding strains (Gal-Gal-positive) (relative risk 8.3; 95% confidence limits 3.3 to 20.4;  $p < 0.001$ ). That boys infected with Gal-Gal-negative strains more often had reflux did not explain the increased risk for renal scarring in this group. The possibility that the phenotypically negative strains could be induced to express Gal-Gal adhesions in vivo was excluded by dot blot analysis, which showed the absence of *pap* homologous DNA in all but one of the Gal-Gal-negative strains. The results suggest that the absence of Gal-Gal-specific adhesins in *E. coli* can be used as an indicator of risk for renal scarring and the need for radiologic examination.

**Polycystic kidney diseases in childhood.** Kaplan BS, Kaplan P, Rosenberg HK, Lamothe E, Rosenblatt DS (BSK, Division of Nephrology, The Children's Hospital of Philadelphia, 34th St. and Civic Center Blvd., Philadelphia, PA 19104). *J Pediatr* 115(6):867-880, Dec. 1989

Many difficulties obstruct the understanding of the problems of polycystic kidney diseases in childhood. One relates to terminology, a second to the association with liver abnormalities, and a third to the concept of variable expression. The terminology problem can be resolved by using established definitions.<sup>2-6</sup> Polycystic kidney disease has been defined as a heritable disorder with diffuse involvement of both kidneys. Apart from cysts, there is no evidence of dysplasia. Multiple renal cysts frequently coexist with lesions (which may be cysts) in other viscera, especially the liver.<sup>2,4</sup> Difficulties caused by the association of renal cysts and liver abnormalities and by variations in expression may be solved by careful evaluations of probands and their families and by meticulous documentation. These problems may be solved soon by the use of genetic probes to help elucidate causes of diseases at a molecular level. Here we provide an approach to the two important forms of inherited polycystic kidney diseases and discuss their differential diagnosis.

## Journal of Thoracic Imaging

**Pulmonary nuclear medicine evaluation of thromboembolic disease.** Hanson MW, Coleman RE (MWH, Dept. of Radiology, Division of Nuclear Medicine, Box 3949, Duke University Medical Center, Durham, NC 27710). *J Thorac Imaging* 4(4):40-57, 1989

PE is a complication of underlying venous thrombosis and most often arises from the deep veins of the lower extremities. The thromboembolic event is difficult to diagnose clinically and carries significant morbidity and mortality. Treatment with anticoagulation also has risks. Thus accurate diagnosis is important. A normal perfusion lung scan excludes major pulmonary emboli. Lung perfusion scintigraphy provides high sensitivity for interrupted blood flow but lacks specificity for embolic vascular occlusion. Ventilation scintigraphy is sensitive for obstructive pulmonary disease and improves specificity for PE when combined with the perfusion scan. Several retrospective studies have established probability levels for PE on the basis of certain ventilation, perfusion, and chest x-ray patterns. These results have high positive and negative predictive value and directly affect patient management. The first large prospective study on PE has just been completed. The results of this study should more clearly define the role for ventilation-perfusion scintigraphy in PE.

## Gastrointestinal Radiology

**Extraperitoneal mass effect by ascites under tension.** Baer JW (JWB, St. Luke's Hospital, 421 W. 113 St., New York, NY 10025). *Gastrointest Radiol* 15:3-8, 1990

Benign ascites may cause an extraperitoneal mass effect when it becomes loculated by adhesions or when peritoneal recesses are enlarged by ascites under tension. Five symptomatic patients were examined by computed tomography demonstrating ascites as the cause of an apparent mediastinal mass in 1, a retrogastric mass in 1, and a retroperitoneal mass displacing the right kidney anteriorly in 4.

**Computed tomography evaluation of high-density bile in the gallbladder.** Ueda J, Kobayashi Y, Nishida T (JU, Uppsala Biomedical Center, Institute for Physiology and Medical Physics, Box 572, S-751 23 Uppsala, Sweden). *Gastrointest Radiol* 15:22-26, 1990

On computed tomograms obtained during a seven-year period, 27 patients were found to have high-density bile in the gallbladder. Serial computed tomography (CT) examinations showed that gradual narrowing of common bile duct is a causative factor. This has not been reported previously. The density of the bile in the gallbladder of patients with such obstruction was almost equal to that of normal liver on CT. In some of the patients in whom obstruction of the cystic duct was the factor of high-density bile and continued for a long time, the density of the bile decreased and hydrops developed.

**Diagnosis of hepatic cavernous hemangioma by fine needle aspiration biopsy under ultrasonic guidance.** Nakaizumi A, Iishi H, Yamamoto R, et al. (AN, Dept. of Gastrointestinal Oncology, The Center for Adult Diseases, Osaka, 3-3, Nakamichi 1-chome, Higashinari-ku, Osaka 537, Japan). *Gastrointest Radiol* 15:39-42, 1990

Percutaneous aspiration biopsy of the liver using a heparinized 22-gauge needle was performed under ultrasonic guidance in 11 patients with hepatic cavernous hemangioma. Ten (91%) of 11 biopsy specimens obtained were cytologically diagnostic for hemangioma. No indications of malignancy were found. There was no relation between the cytological diagnosis and the location, size, or ultrasonographic findings. No complications were encountered.

These findings indicate that cytological examination of the liver by fine needle aspiration biopsy is useful in diagnosing hepatic cavernous hemangioma of any size and in any location, provided optimal route to the lesions is chosen.

**Hepatic iron overload: diagnosis and quantification by noninvasive imaging.** Chezmar JL, Nelson RC, Malko JA, Bernardino ME (JLC, Emory University Hospital, Dept. of Radiology, 1364 Clifton Rd., N.E., Atlanta, GA 30322). *Gastrointest Radiol* 15:27-31, 1990

The diagnostic efficacy of magnetic resonance (MR) and computed tomography (CT) for detection and quantification of hepatic iron was assessed in a series of patients under investigation for clinical or biochemical evidence of hepatic iron overload. Thirty patients underwent MR imaging (SE 30,60/1000 or SE 30,60/2000) at 0.5 Tesla with calculation of hepatic T2 and liver to paraspinous muscle signal intensity ratios. Twenty-nine patients also had measurement of hepatic attenuation on noncontrast CT images. Results of these imaging studies were correlated in all patients with quantitative iron determination from liver biopsy specimens. The best predictor of liver iron among parameters studied was the ratio of the signal intensities of liver and paraspinous muscle (L/M) on a SE 60/1000 sequence. Both MR using L/M ratios and CT were sensitive methods for detection of severe degrees of hepatic iron overload with 100% of patients with hepatic iron on biopsy  $>600 \mu\text{g}/100 \text{ mg}$  liver dry weight detected on the basis of L/M  $<0.6$  or CT attenuation  $>70$  Hounsfield units (HU). The MR parameter, however, was more specific than CT (100 vs 50%) and showed a higher degree of correlation with quantitated hepatic iron from biopsy. T2 measurements showed poor correlation with hepatic iron, due to difficulty in obtaining precise T2 measurements in vivo when the signal intensity is low. None of the parameters utilized was sensitive for detecting mild or moderate degrees of hepatic iron overload.

We conclude that MR and CT are sensitive techniques for noninvasive detection of severe hepatic iron overload, with MR providing greater specificity than CT. Lesser degrees of iron deposition, however, may go undetected by our current imaging techniques.

## Journal of Ultrasound in Medicine

**Ultrasonic measurements of portal vasculature in diagnosis of portal hypertension: a controversial subject reviewed.** Goyal AK, Pokharna DS, Sharma SK (AKG, C-II/303, Kamal Apts. Near Ram Mandir, Bani Park, Jaipur (Raj.) 302006, India). *J Ultrasound Med* 9:45-48, Jan. 1990

In a prospective ultrasound study, the various factors possibly influencing the portal vasculature were evaluated in normal subjects; the correlation of portal diameters with physical factors such as age, sex, and body texture was poor, whereas the caliber variation was significant with respiration, posture, and meal. Considering the fasting state, supine decubitus, and deep inspiration as suitable and standard variables, the diameters were compared in 100 healthy subjects and 50 patients with portal hypertension. The upper normal limits of portal, splenic, and superior mesenteric vein diameters were reported as 16, 12, and 11 mm, respectively, and the dimensions above these values provided an overall sensitivity of 72%, an accuracy of 91%, and a specificity of 100% in diagnosing the patients with suspected portal hypertension.

Reprinted with permission by the American Institute of Ultrasound in Medicine.

## News

### Neonatal Neurosonography

The Division of Diagnostic Ultrasound, Dept. of Radiology, Thomas Jefferson University Hospital, Philadelphia, is sponsoring Neonatal Neurosonography, April 5-6. The course is designed to provide a complete introduction to sonographic evaluation of the neonatal brain. Topics will include physical principles and instrumentation for neonatal neurosonography, scanning techniques and infection control procedures, recognition of normal anatomic structures, identification of abnormal echo patterns, natural history and sequelae of intracranial hemorrhage, and detection and classification of hemorrhage. The course does not include hands-on experience in scanning infants. Course directors: Donald Mitchell and Matthew Pasto. Category 1 credits: 13.5 hr. Fee: \$350. Information: Judith C. Kaneff, Education Coordinator, Division of Diagnostic Ultrasound, Dept. of Radiology, Thomas Jefferson University Hospital, 7th Floor, Main Bldg., Philadelphia, PA 19107; (215) 928-8533.

### Lithotripsy: Biliary/Renal

The Division of Diagnostic Ultrasound, Dept. of Radiology, Thomas Jefferson University Hospital, Philadelphia, is offering Lithotripsy: Biliary/Renal, April 9-12. The program is designed to provide a comprehensive, practical introduction to sonographically guided lithotripsy; it consists of two concurrently run courses: biliary lithotripsy and renal lithotripsy. Participants can choose those lectures that are most applicable to their specialty. They also will have the opportunity to become familiar with a variety of equipment, to observe actual lithotripsy procedures, and to gain hands-on experience in setting up and conducting a sonographically guided lithotripsy procedure. Course directors: Susan Gordon, Demetrius Bagley, Jr., and Barry B. Goldberg. Category 1 credit: 27 hr. Fee: \$1200. Information: Judith C. Kaneff, Education Coordinator, Division of Diagnostic Ultrasound, Dept. of Radiology, Thomas Jefferson University Hospital, 7th Floor, Main Bldg., Philadelphia, PA 19107; (215) 928-8533.

### The Leading Edge in Diagnostic Ultrasound

The Division of Diagnostic Ultrasound, Dept. of Radiology, Thomas Jefferson University Hospital, is sponsoring The Leading Edge in Diagnostic Ultrasound, May 2-4, at Bally's Park Place, Atlantic City, NJ. The conference will provide current practice updates in all the major specialty fields, including abdomen, pelvis, obstetrics, and

neonatal brain, and newer applications, such as color Doppler imaging and endovaginal and endorectal scanning. The 1990 program will offer a preconference tutorial on color Doppler imaging, May 2. Course directors: Leading Edge program, Barry B. Goldberg and Alfred B. Kurtz; preconference tutorial, Peter N. Burns, Donald G. Mitchell, and Laurence Needelman. Category 1 credit: Leading Edge program, 16.25 hr; preconference tutorial, 7 hr. Fee: Leading Edge program and preconference tutorial, \$450; Leading Edge program only, \$350; preconference tutorial only, \$225. Information: Judith C. Kaneff, Education Coordinator, Division of Diagnostic Ultrasound, Dept. of Radiology, Thomas Jefferson University Hospital, 7th Floor, Main Bldg., Philadelphia, PA 19107; (215) 955-8533.

### Surgical Neuroangiography

New York University Medical Center, Post-Graduate Medical School, is offering Surgical Neuroangiography, May 7-11, in New York City. The program is designed for neuroradiologists, neurosurgeons, head and neck surgeons, plastic surgeons, vascular surgeons, and other physicians who are concerned with the principles, techniques, and problems in the management of vascular lesions in the head, neck, brain, spine, and spinal cord. It will include didactic lectures on anatomy, nursing aspects of embolization, surgery of vascular lesions, and the clinical presentation of disease entities that can be treated by endovascular techniques. Direct participation by registrants will be accomplished by means of catheter and material workshops. Category 1 credit: 34 hr. Fee: \$680. Information: NYU Medical Center, Post-Graduate Medical School, 550 1st Ave., New York, NY 10016; (212) 340-5295.

### Pulsed Lasers in Angioplasty

The Division of Cardiology and the Dept. of Diagnostic Radiology, University of Tübingen, Tübingen, F. R. G., is offering an international workshop, Pulsed Lasers in Angioplasty, May 11-12. Well-known European and American scientists will review the early experiences with laser angioplasty and discuss future directions. A theoretical session will be followed by a clinical conference. Topics to be covered at the workshop include lasers in cardiovascular disease, basic mechanisms of pulsed lasers, laser-tissue interaction; spectroscopy of normal and atherosclerotic tissue, shock-wave analysis of normal and atherosclerotic tissue, the excimer laser, an update of clinical experience with the excimer laser in angioplasty, and controversies about the use of lasers in interventional cardiology. Chairmen and



program directors: Claus Claussen, Karl R. Karsch, Timothy Sanborn, and Ludger Seipel. Fee: DM 200. Information: K. R. Karsch, Dept. of Cardiology, Medical Clinic, University of Tübingen, Otfried-Müller-Str. 10, D-7400 Tübingen, F. R. G.; telephone: 0 70 71-29 28 01; fax: 0 70 71-29 31 69.

### **Sonography Symposium**

The Dept. of Radiology and Radiological Sciences and the Division of Continuing Medical Education, Vanderbilt University, Medical Center, are sponsoring the 14th annual Sonography Symposium, May 25–26, at the Opryland Hotel, Nashville, TN. The purpose of the symposium is to provide sonography specialists with an update on new clinical applications of transvaginal sonography and color Doppler imaging. Course director: Arthur C. Fleischer. Category 1 credit: 11 hr. Fee (both days/Fri. only/Sat. only): physicians, \$350/\$250/\$150; Vanderbilt University alumni, \$225/\$175/\$100; sonographers, \$200/\$150/\$100. Information: Brenda Boner, Course Coordinator, Vanderbilt Division of CME, CCC-5326 MCN, Nashville, TN 37232-2337; (615) 322-4030.

### **Contemporary Medical Imaging VII**

The Dept. of Radiology and Radiological Sciences and the Division of Continuing Medical Education, Vanderbilt University, Medical Center, are sponsoring Contemporary Medical Imaging VII, May 30–June 3, at the Mariner's Inn, Hilton Head Island, SC. The objective of the course is to provide medical imaging specialists with an update on new clinical applications of contemporary imaging techniques, including MR imaging, CT, and sonography. The emphasis this year will be on obstetric procedures. Course chairmen: Arthur Fleischer and Max I. Schaff. Category 1 credit: up to 19 hr. Fee: physicians, \$550; sonographers and residents (letter required), \$300. Information: Brenda Boner, Course Coordinator, Vanderbilt Division of CME, CCC-5326 MCN, Nashville, TN 37232-2337; (615) 322-4030.

### **Mammography and the Search for Breast Cancer**

The Rochester Roentgen Ray Society and Wende Logan-Young are offering Mammography and the Search for Breast Cancer, July 13–14, in Rochester, NY. The course will address all aspects of screen/film mammography and other investigative procedures essential to early accurate diagnosis of breast cancer. Fee: radiologists, \$350; residents, \$250. Information: Wende Logan-Young, M.D., 1351 Mt. Hope Ave., Rochester, NY 14620; telephone: (716) 442-8432; fax: (716) 442-1837.

### **Napa Valley Imaging Update—MRI 1990**

The Dept. of Radiology and the Office of Continuing Medical Education, University of California, Davis, School of Medicine, are sponsoring Napa Valley Imaging Update—MRI 1990, July 22–26, at the Silverado Country Club, Napa, CA. This annual symposium has been developed to bring together national and international experts in the field of diagnostic imaging. Guest speakers: Charles Higgins, Hans Newton, William Kelley, and Gerald Mink. Category 1 credit: 17 hr. Fee: physicians, \$445; others, \$345. Information: Nina Musselman, Office of Continuing Medical Education, University of California, Davis, School of Medicine, 2701 Stockton Blvd., Sacramento, CA 95817; (916) 734-5390.

### **Uroradiology Postgraduate Course**

The Society of Uroradiology will present the 10th annual Postgraduate Course—Uroradiology '90, Sept. 10–14, at the Westin Bayshore Hotel, Vancouver, B.C. The course is designed to present new developments in urologic imaging, including the emergence of MR imaging, recent developments in prostate imaging, continuing refinement of interventional techniques, and evaluation of new contrast agents, and to review the more basic concepts of radiology of the urinary tract. Program director: Arthur Rosenfield. Category 1 credit: 27 hr. Fee: physicians, \$450; residents, fellows, and technologists, \$350. Information: Dawne Ryals, Ryals & Associates, P. O. Box 1925, Roswell, GA 30077-1925; telephone: (404) 641-9773; fax: (404) 552-9859.

### **Applied Ultrasound: Accent on Doppler**

The Dept. of Radiology, University of Alabama at Birmingham, will present the 3rd annual Applied Ultrasound: Accent on Doppler, Sept. 12–15, at the Ritz Carlton Resort Hotel, Naples, FL. The course will provide a state-of-the-art review of selected topics in sonography, with a theme of the integration of spectral and color duplex Doppler sonography into ultrasound practice. Program directors: Robert J. Stanley and Lincoln L. Berland. Category 1 credit: 18 hr. Fee: physicians, \$425; residents, fellows, and technologists, \$300. Information: Dawne Ryals, Ryals & Associates, P. O. Box 1925, Roswell, GA 30077-1925; telephone: (404) 641-9773; fax: (404) 552-9859.

### **Musculoskeletal Disorders**

The International Skeletal Society will present its 17th annual refresher course, Musculoskeletal Disorders, Sept. 12–15, at the Salzburg Convention Center, Salzburg, Austria. The faculty will be members of the society. Category 1 credit: 27 hr. Information: Dawne Ryals, Ryals & Associates, P. O. Box 1925, Roswell, GA 30077-1925; telephone: (404) 641-9773; fax: (404) 552-9859.

### **Royal Australasian College of Radiologists Annual Meeting**

The Royal Australasian College of Radiologists will hold its 41st annual general and scientific meeting at the Sheraton Hotel, Perth, Western Australia, Oct. 5–11. A comprehensive program in both radiodiagnosis and radiation oncology has been planned. Keynote speakers: Anders Lunderquist, William Bradley, L. A. Mack, Anthony Mancuso, Giles Stevenson, J. J. Merland, Johan Bloem, Thomas Naidich, Ned Hornback, Rodney Million, Alan Dembo, and Stanley Dische. Category 1 credit: up to 32 hr. Information: Motive Conventions, The Griffin Centre, 28 The Esplanade, Perth, Western Australia 6000; telephone: (09) 322 2666; fax: (09) 322 1417.

### **MR Imaging Course in Riyadh, Saudi Arabia**

The Depts. of Radiology and Medical Studies, Riyadh Armed Forces Hospital, and the Cleveland Clinic Education Foundation are jointly sponsoring the 3rd annual International Course on Magnetic Resonance Imaging, Oct. 14–17, in Riyadh, Saudi Arabia. The course will provide an overview of MR technology and basic principles and current and future applications of whole-body MR. Cochairmen: D.

C. Clark and H. S. Sharif. Category 1 credit: 30 hr. Fee: physicians, 1000 Saudi riyals; medical staff in training, 500 Saudi riyals. Information: Dept. of Medical Studies, Armed Forces Hospital, P. O. Box 7897, Riyadh 11159, Kingdom of Saudi Arabia; telephone: 9661 477 7714, ext. 2289 or 2269; fax: 9661 477 7194 or 9661 477 9168.

## The American Board of Radiology Examinations

Written examinations for the American Board of Radiology (ABR) are scheduled for Sept. 27–28, 1990, and Oct. 3–4, 1991. Oral examinations will be held at the Executive West Hotel in Louisville, KY, June 4–8, 1990, and June 3–7, 1991. The ABR will accept applications for admission to the examinations after July 1, but not later than Sept. 30, in the year *preceding* the year in which the examination is to be taken. For application forms and further information: Office of the Secretary, The American Board of Radiology, 300 Park, Ste. 440, Birmingham, MI 48009.

## Meeting and Course Review

For the reader's convenience, a summary of upcoming meetings and courses is provided. Detailed listings are given in the *AJR* issue given in parentheses.

**Visiting Fellowship in Interventional Radiology**, times arranged, Baltimore (Sept 1989)

**Visiting Fellowships at UCSF**, times arranged, San Francisco (Sept 1989)

**Perceptorships in Transrectal Ultrasound of the Prostate**, Ann Arbor, MI (Sept 1989)

**University of North Carolina Annual Radiology Symposium**, March 30–April 1, Hilton Head, SC (March)

**Skeletal Radiology 1990**, March 31–April 5, Scottsdale, AZ (Nov 1989)

**Joint American-European Course in Davos, Switzerland**, April 1–7, Davos (Jan)

**Society of Computed Body Tomography Annual Course**, April 2–6, Palm Springs, CA (Nov 1989)

**Prenatal Diagnosis of Congenital Anomalies**, April 2–6, Sonora Bay, Mexico (Feb)

**Postgraduate Course in Neuroradiology**, April 3–6, New York City (March)

**National Council on Radiation Protection and Measurements Annual Meeting**, April 4–5, Washington, DC (Nov 1989)

**Annual Spring Roentgen Conference**, April 4–8, New Orleans (March)

**Bone and Joint Radiology**, April 6–8, New York City (March)

**Automated Percutaneous Discectomy Workshops**, April 7–8, Washington, DC (Sept 1989)

**Radiation Research Society Annual Meeting**, April 7–12, New Orleans (Nov 1989)

**Ultrasound in Obstetrics and Gynecology**, April 8–10, Ann Arbor, MI (Jan)

**MRI Workshop in Hawaii, 1990**, April 8–13, Big Island, HI (March)

**Advanced Imaging of the Musculoskeletal System**, April 14–15, Coronado (San Diego), CA (Feb)

**San Diego Residents Radiology Review Course**, April 15–20, Coronado (San Diego), CA (Feb)

**Obstetrics and Gynecology**, April 16–20, Philadelphia (Jan)

**Introduction to Interventional Radiology**, April 21, Coronado (San Diego), CA (Feb)

**Clinical Nuclear Medicine 1990**, April 23–26, Cambridge, MA (Nov 1989)

**International Symposium on Diagnostic Imaging**, April 23–27, Barcelona, Spain (Dec 1989)

**Doppler Velocimetry in Clinical Obstetrics**, April 25, Baltimore (Nov 1989)

**Radiation Oncology Clinical Research Seminar**, April 26–28, Gainesville, FL (Jan)

**American Association of Physicists in Medicine Spring Seminar**, April 27–29, San Diego, CA (Dec 1989)

**Spring Diagnostic Ultrasound Conference**, April 27–29, Los Angeles (Feb)

**OB/GYN Ultrasound for the 90's—The Next Generation**, April 28, Hanover, NH (March)

**Radiology Review Course**, April 29–May 4, Miami, FL (Feb)

**Mid-Pacific Diagnostic Ultrasound Conference**, May 1–5, Kauai, HI (Feb)

**Advances in CT and MRI**, May 2–4, Ann Arbor, MI (Feb)

**Fellowships in Biliary Lithotripsy**, May 3–5 and June 7–9, Baltimore, MD (Dec 1989)

**Symposium in Diagnostic Ultrasound**, May 4–6, New York City (Feb)

**Congress of the European Federation of Societies for Ultrasound in Medicine and Biology**, May 6–11, Jerusalem, Israel (May 1989)

**Biliary Calculus Disease**, May 7–9, Boston (Nov 1989)

**Diagnostic Imaging in Musculo-Skeletal Radiology**, May 10–11, Glasgow, Scotland (Dec 1989)

**Cardiovascular and Interventional Radiology**, May 13–18, Brussels, Belgium (Dec 1989)

**27th Congress of the European Society of Paediatric Radiology**, May 14–18, Munich, West Germany (Jan)

**Blood Vessel Imaging Using Ultrasound Techniques**, May 16–18, Southampton, Hampshire, United Kingdom (March)

**Clinical Magnetic Resonance Imaging**, May 21–23, New Haven, CT (March)

**Mammography for the General Radiologist**, May 21–24, Sept. 10–13, and Oct. 22–25, Boston (March)

**Clinical MRI: 1990 Update**, May 23–26, Boston (March)

**Musculoskeletal MRI for Orthopedists and Radiologists**, May 28–June 1, Sonesta Beach Hotel (Dec 1989)

**Emergency Radiology 1990**, May 29–June 1, Boston (March)

**Italian Society of Radiology and Nuclear Medicine**, May 30–June 3, 1990, Turin, Italy (Nov 1989)

**American Society of Emergency Radiology Annual Meeting**, June 2, Boston (Feb)

**American College of Medical Physics Annual Meeting**, June 7–10, Austin, TX (Dec 1989)

**Abdominal Ultrasound**, June 11–14, Philadelphia (Jan)

**Prostate Ultrasound**, June 15, Philadelphia (Jan)

**Advanced Techniques in MRI**, June 16–22, Kiawah Island, SC (March)

**Radiology in Scandinavia and the Soviet Union**, June 16–30, Copenhagen, Malmo, Stockholm, Helsinki, and Leningrad (Feb)

**Diagnostic Radiology**, June 17–22, Myrtle Beach, NC (March)

**Pediatric Nuclear Medicine Categorical Seminar**, June 18, Washington, DC (March)

**Nuclear Medicine Technology Certification Examinations**, June 23 and Sept. 22; application deadlines, April 21 and July 21, respectively (Nov 1989)

**Liver Imaging**, June 25–27, Boston (March)

**International Course in Cardiovascular Interventional Radiology**, July 11–13, Leeds, United Kingdom (Dec 1989)

**Advances in Radiation Oncology Physics**, July 16–20, Lawrence, KS (March)

**American Association of Physicists in Medicine Annual Meeting**, July 22–26, St. Louis (Feb)

**Musculoskeletal Imaging**, July 23–25, Laguna Niguel, CA (March)  
**Symposium on Magnetic Resonance Imaging**, July 26–29, Laguna Niguel, CA (March)

**Annual Northern Imaging Meeting**, Aug. 4–8, Winnipeg, Manitoba (March)

**Copenhagen Symposium on Uroradiology**, Aug. 27–30, Herlev, Denmark (Feb)

**European Society of Head and Neck Radiology Annual Meeting**, Sept. 12–15, Bresica (Lake of Garda), Italy (Feb)

**Interventional Radiology/2nd Marmara Medical Days**, Sept. 19–21, Haydarpasa-Istanbul, Turkey (March)

**International Conference on Ultrasound Angiography**, Sept. 25–28, London, United Kingdom (Feb)

**American Lithotripsy Society Annual Meeting**, Oct. 11–14, San Diego (March)

*AJR* carries announcements of courses, symposia, and meetings of interest to its readers if received a minimum of 5 months before the event. There is no charge; receipt of items by the *AJR* Editorial Office is not acknowledged. Submit items for publication typed double-spaced. Provide title, date, location, brief description, sponsor, course directors, fees, category I credit, and address and telephone number for additional information. Faculty from the host institution will not be listed. Guest faculty names will appear **only** if initials are provided. Mail news items to *AJR* Editorial Office, 2223 Avenida de la Playa, Suite 200, La Jolla, CA 92037-3218.

# 1990 ARRS Meeting Summary, May 13–18, 1990 Washington, DC

A comprehensive description of the meeting, including the instructional courses, categorical course, and the Friday symposium, appears in this issue of the *AJR*. Meeting and registration forms can be found in the February and March issues. These may be photocopied.

## Accreditation

All courses and scientific sessions carry AMA Category 1 credit on an hour-for-hour basis.

## Meeting Format

*Scientific Program.* Sessions will be grouped in parallel sessions so that registrants may choose topics related to their interests. A total of 189 scientific papers will be presented, Monday–Thursday, May 14–17. In addition, on Wednesday, May 16, the afternoon session will feature award papers and the Caldwell Lecture, which will be delivered by U.S. Supreme Court Justice Sandra Day O'Connor. (Special Note: Companions and spouses of registered meeting attendees are welcome to attend the Caldwell Lecture presented by Justice O'Connor.) On Friday, May 18, there will be a special 4-hr symposium, Current Topics in Musculoskeletal Imaging.

*Categorical Course in Cardiovascular-Interventional Radiology.* This 15.5-hr course will be Sunday–Thursday.

*Luncheon Sessions.* Registrants may enroll in special luncheon sessions, Monday–Thursday. A box lunch will be provided.

## Exhibits

*Scientific and Technical Exhibits and Case of the Day Presentations* will be presented in the exhibit hall of the Sheraton Washington Hotel, Monday–Thursday, May 14–17. The Case of the Day will be presented by Margaret Stull of Georgetown University Hospital, Washington, DC.

## Local Activities

*General Reception.* Tuesday evening, May 15, for all registrants.

*Golf Tournament.* Monday, May 14, Kenwood Country Club. Transportation leaves the hotel at 11 a.m.; shotgun start is at 12:30 p.m.

*Men's and Women's Tennis Tournaments.* Monday, May 14, at the Kenwood Country Club.

*Local Tours.* See February issue of the *AJR* for a description of the activities and registration forms.

## Meeting Registration

Preregistration will be accepted until April 27. There will be on-site registration. Official badges and program books will be available at the registration desk, Sheraton Washington Hotel. No confirmations will be mailed.

## Course Registration

Register early—enrollment is limited. List first, second, and third choices for each period. Also, indicate whether you wish to take the categorical course. Deadline for registration by mail is April 27. All ticket orders will be filled according to postmarked date. Course tickets will not be mailed. Tickets will be available on and after Sunday, May 13 (after 1 p.m.), at the ARRS registration desk in the Sheraton Washington Hotel. There will be on-site registration for courses not already filled.

## Hotel Registration

Reservations are handled by the ARRS Housing Bureau, Sheraton Washington Hotel, Attn: Reservations Office, 2660 Woodley Rd., Washington, DC 20008. These must be received by April 13. Make check payable to Sheraton Washington Hotel. See reservation form in February or March *AJR* for prices and complete instructions.

## Fees

### Meeting:

ARRS members and resident members . . . . .	No fee
Nonmembers . . . . .	\$250
Nonmember physicians in training (with verification) . . . . .	25
Categorical course (all who attend) . . . . .	75
Luncheon sessions/each . . . . .	12
Golf tournament . . . . .	75
Tennis tournaments . . . . .	50
Local tours . . . . .	20–75

## Cancellations and Fee Refunds (Excluding Hotel Fees)

Fees will be refunded only if cancellation is received by April 27. Send to American Roentgen Ray Society, 1891 Preston White Drive, Reston, VA 22091.

## Transportation Discounts

United Airlines is offering discounts, up to 40%, on airfares. Call (800) 521-4041 and mention ARRS account number 0053D.

Hertz Rent A Car is offering special rates on car rentals. Call (800) 772-3773 and mention that you are attending the American Roentgen Ray Society annual meeting.

# 1990 American Roentgen Ray Society Instructional Courses and Symposium

Joseph T. Ferrucci, Director

Sixty Instructional Courses will be presented during the 90th annual meeting of the American Roentgen Ray Society (ARRS) beginning Monday, May 14, and continuing through Thursday, May 17. Each of the Instructional Courses listed on the next page will be 90 min long. In addition, there will be a week-long Categorical Course in Cardiovascular-Interventional Radiology and a half-day Symposium, Current Topics in Musculoskeletal Imaging.

The Categorical Course in Cardiovascular-Interventional Radiology will have 15.5 hr of instruction and will begin on Sunday, May 13, and conclude on Thursday, May 17. The Symposium, Current Topics in Musculoskeletal Imaging, will be on Friday, May 18, from 8 a.m. to 12 noon. All courses carry Category 1 credit on an hour-to-hour basis.

## Registration Information

To register for courses, complete the meeting registration form in this section and mail promptly. Tickets also will be available at the Instruction Course Registration Desk, Sheraton Washington Hotel for courses that have not been sold out. All courses will take place in the headquarters' hotel.

After reviewing the course list, select three for each morning and afternoon session. Write the course number and name of the first instructor on the registration form. Please note that the -01 residents'-masters' tutorials are intended primarily for residents and that attendance will be limited.

All who register for the Categorical Course in Cardiovascular-Interventional Radiology (including ARRS members) must pay a fee of \$75 and must take the entire series of classes. The Categorical Course totals 15.5 hr of instruction and includes a syllabus.

## Course Schedule

### Sunday, May 13, through Thursday, May 17

The Categorical Course in Cardiovascular-Interventional Radiology will have 15.5 hr of instruction over 5 days. Topics and instructors are listed on p. 846.

### Monday, May 14, through Friday, May 18

A total of 60 courses will be offered (see next page) plus a Symposium, Current Topics in Musculoskeletal Radiology.

### Symposium: Current Topics in Musculoskeletal Imaging Friday, May 18, 1990, 8:00 a.m. to 12:00 p.m.

Time	Topic (Presenter)
8:00 a.m.	Controversies in the evaluation of osteoporosis ( <i>Rosenthal D</i> )
8:30 a.m.	The role of MRI in the evaluation of musculoskeletal neoplasms ( <i>Braunstein E</i> )
9:00 a.m.	Imaging of spinal trauma ( <i>Daffner R</i> )
9:30 a.m.	The role of MRI in shoulder imaging ( <i>Brahme S</i> )
10:00 a.m.	The elbow ( <i>Pitt MJ</i> )
10:30 a.m.	MRI of the knee ( <i>Dalinka M</i> )
11:00 a.m.	The role of MRI in hip imaging ( <i>Bassett L</i> )
11:30 a.m.	Imaging of the foot and ankle with emphasis on MRI ( <i>Forrester DM</i> )

Note.—There is no fee for this symposium. However, to facilitate planning, please register on the meeting registration form.

## ACR Luncheon Presentations on Socioeconomics of Radiology

A series of luncheon presentations on the socioeconomic of radiology will be arranged by the American College of Radiology (ACR). A box lunch will be provided. The presentations do not conflict with other elements of the program. Advance registration is required. Cost per session is \$12.

### Date, Topic, Speaker

Monday, May 14: Status and Update on RVS, James M. Moorefield, M.D.  
 Tuesday, May 15: Standard Setting Update, Jerome H. Shapiro, M.D.  
 Wednesday, May 16: Contrast Media, Mark M. Mishkin, M.D.  
 Thursday, May 17: Governmental Issues, Otha W. Linton

## American Roentgen Ray Society Instructional Courses: May 14–May 17, 1990

Topic	Monday	Tuesday	Wednesday	Thursday
Morning (all sessions being at 8:00 a.m.)				
Residents-masters' tutorial: update & personal Obstetrics/gynecology	101. GI radiology: simplify, multiply. <i>Carlson HC</i> 102. Update on the placenta. <i>Sanders R</i>	201. Perspectives on obstetrical sonography. <i>Leopold G</i> 202. Fetal measurements for estimating age and growth. <i>Hadlock FP</i>	301. Neuroradiology: Present status of MR vs CT. <i>Taveras JM</i> 302. Transvaginal sonography in obstetrics and gynecology. <i>Feischer AC, Rao B, Kepple DM</i>	401. The hip as a mirror of pediatric bone disease. <i>Poznanski AK</i> 402. Second and third trimester fetal anomalies. <i>Kurtz A</i>
Chest	103. Practical approach to intensive care radiology. <i>Spim PW, Goodman L</i>	203. Lung tumor staging. <i>Pugatch R</i>	303. Pulmonary infections and their complications. <i>Choplin RH</i>	403. Advances in thoracic radiology: high resolution CT and MRI. <i>McLoud TC</i>
Gastrointestinal	104. CT-pathologic correlations: pancreatitis, liver tumors. <i>Gedgaudas-McClees RK, Ros PR</i>	204. Colon cancer detection. <i>Gelfand D, Laufer I</i>	304. Radiologic pathologic correlations: gallbladder, intestinal tumors. <i>Lichtenstein J, Olmsted W</i>	404. Current approaches to biliary tract disease. <i>Zeman R</i>
Radiologic practice/miscellaneous	105. Pointers on scientific manuscript preparation. <i>Berk RN, Levene M, Hilton S, Spiller KL</i>	205. The battle over "turf": who has it and how to get it. <i>Hillman B</i>	305. Functional aspects of the radiology department. <i>Janower ML</i>	405. The future of digital radiology: technical & clinical considerations. <i>Ovitt TW, Hunter T</i>
Neuroradiology	106. Gadolinium enhanced MRI of the brain and spine. <i>Hasso AN</i>	206. AIDS related CNS disease. <i>Davis DO</i>	306. Craniocerebral trauma. <i>Kieffer SA, Cacayorin ED</i>	406. CT of the spine. <i>Helms CA</i>
Pediatrics/nuclear medicine	107. Nuclear cardiology in clinical practice. <i>Thrall JH</i>	207. Imaging of childhood infection. <i>Woods BP</i>	307. Brain SPECT imaging. <i>Holman L</i>	407. Pediatric abdominal trauma: current concepts. <i>Kushner DC, Kuhn J, Taylor G</i>
Genitourinary	108. Imaging renal infections. <i>McClennan BL</i>	208. CT and MRI of the kidney and adrenal. <i>Newhouse J, Amis S</i>	308. Low osmolar contrast agents. <i>Mishkin MM, Wolf G</i>	408. CT/MRI of the retroperitoneum. <i>Lee JKT, Heiken J</i>
Thorax/abdomen I	109. Duplex and color flow Doppler of the abdomen, pelvis, and extremities. <i>Merritt CB</i>	209. CT and US guided biopsies: practical approaches, pitfalls, and new techniques. <i>Charboneau JW, Reading C</i>	309. CT of the acute abdomen. <i>Stanley RJ, Wittenberg J</i>	409. Imaging in thoracoabdominal trauma. <i>Mirvis SE, Foley WD</i>
Musculoskeletal	110. The analytic approach to the film (an imaging discipline). <i>Edeiken J, Jacobson HG</i>	210. Imaging the acutely injured cervical spine. <i>Harris JH, Swischuk LE</i>	310. Criteria for diagnosis of bone tumors. <i>Norman A</i>	410. Arthropathies: radiologic pathologic correlations. <i>Madewell JE</i>
Afternoon (all sessions begin at 4:00 p.m.)				
Head and neck	111. MRI of the head and neck. <i>Lufkin RB, Jabour B</i>	211. Endocrine imaging—update. <i>Doppman J</i>	311. Imaging of the sinonasal cavities. <i>Som P</i>	411. MR of the joints, including temporomandibular. <i>Harms S</i>
New technology	112. Biliary lithotripsy. <i>Ferrucci JT, Burhenne HJ</i>	212. Percutaneous laser angioplasty. <i>McCowan T, Cragg A, Ferris EJ</i>	312. Computer assisted 3-D imaging: state of the art. <i>Fishman EK, Ney FG</i>	412. PET scanning. <i>Hubner KF, Besozzi MC, Buonocore E</i>
Breast	113. How to evaluate the success of a mammography practice. <i>Sickles EA</i>	213. Screening mammography. <i>McLelland R</i>	313. Screen-film mammography: equipment, technique and interpretation. <i>Feig SA</i>	413. Analyzing the mammogram. <i>Kopans DB</i>
Magnetic resonance imaging	114. MRI of the spine. <i>Ramsey RG</i>	214. MRI of the male and female pelvis. <i>Fritzsche PJ, McCarthy S</i>	314. MRI contrast agents. <i>Saini S, Hahn PF</i>	414. Practical aspects of MR image interpretation. <i>Stark DD, Bradley WG</i>
Thorax/abdomen II	115. Ultrafast CT scanning. <i>Sheedy P</i>	215. Interventional thoracic radiology. <i>Barth KH, Westcott JL</i>	315. Biliary calculus disease: interventional management. <i>Mueller PR, Teplick SL</i>	415. Imaging of swallowing disorders. <i>Jones B</i>



## Books Received

Receipt of books is acknowledged as a courtesy to the sender. Books considered of sufficient interest are reviewed as space permits. If the book has been reviewed in the *AJR*, the date of its review is given in parentheses.

**The Radiologic Clinics of North America.** MRI of the Head and Neck. Guest editors: Peter M. Som and Marc D. Shapiro. Philadelphia: Saunders, March 1989;27(2):195-479. \$25; by subscription, 6 issues annually for \$93 (1/90)

**Clinical Radiology of the Small Intestine.** By Hans Herlinger and Dean Magliante. Philadelphia: Saunders, 624 pp., 1989. \$125 (1/90)

**Evaluation of Renal Function and Disease with Radionuclides.** The Upper Urinary Tract, 2nd ed. Edited by M. Donald Blaufox. New York: Karger, 418 pp., 1989. \$184.75 (1/90)

**RSNA Today**, Vol. 3, No. 2. Oak Brook, IL: The Radiological Society of North America, 1989. \$75; by subscription, 4 issues annually at \$225 for RSNA members and \$275 for nonmembers (VHS videotape) (1/90)

**Ultrasonography of Muscles and Tendons.** Examination Technique and Atlas of Normal Anatomy of the Extremities. By Bruno D. Forange. New York: Springer-Verlag, 231 pp., 1989. \$119 (1/90)

**Assurance of Quality in the Diagnostic X-ray Department.** Prepared by the British Institute of Radiology. Stoneham, MA: Butterworths, 107 pp., 1988. \$34.95 (1/90)

**Exposure of the U.S. Population from Diagnostic Medical Radiation.** Recommendations of the National Council on Radiation Protection and Measurements. (NCRP Report No. 100). Bethesda, MD: National Council on Radiation Protections and Measurements, 83 pp., 1989. \$14 (1/90)

**The Radiologic Clinics of North America.** CT of the Gastrointestinal Tract. Guest editor: Richard M. Gore. Philadelphia: Saunders, July 1989;27(4):631-838. \$25; by subscription, 6 issues annually for \$93 (1/90)

**Radiology of Occupational Chest Disease.** Edited by A. Solomon and L. Kreel. New York: Springer-Verlag, 212 pp., 1989. \$85 (1/90)

**Avulsion and Stress Injuries of the Musculoskeletal System.** Edited by Jamshid Tehranzadeh, Aldo N. Serafini, and M. Joyce Pais. New York: Karger, 126 pp., 1989. \$52.75 (1/90)

**Imaging of the Pediatric Urinary Tract.** By Thomas L. Slovis, John R. Sty, and Jack O. Haller. Philadelphia: Saunders, 288 pp., 1989. \$55 (1/90)

**Dynamic Functional Studies in Nuclear Medicine in Developing Countries.** Edited by the International Atomic Energy Agency. Lanham, MD: UNIPUB, 583 pp., 1989. (1/90)

**RSNA Today**, Vol. 3, No. 3. Oak Brook, IL: The Radiological Society of North America, 1989. \$75 by subscription, 4 issues annually at \$225 for RSNA members and \$275 for nonmembers (VHS videotape) (1/90)

**House Officer.** Becoming a Medical Specialist. By Richard Cohen. New York: Plenum, 263 pp., 1988. \$24.50 (1/90)

**Pernkopf Anatomy.** Atlas of Topographic and Applied Human Anatomy, 3rd ed. Vol. 1. Head and Neck. Edited by Werner Platzer. (Translated by Harry Monsen.) Baltimore: Urban & Schwarzenberg, 371 pp., 1989. \$175 (2/90)

**RSNA Today**, Vol. 3, Special Edition. Oak Brook, IL: The Radiological Society of North America, 1989. \$75; by subscription, 4 issues annually at \$225 for RSNA members and \$275 for nonmembers (VHS videotape) (2/90)

**Imaging of Sports Injuries.** By Arnold Williams, Roger Evans, and Paul D. Shirley. Philadelphia: Baillière Tindal, 192 pp., 1989. \$75 (2/90)

**Cerebral Computed Tomography.** A Text-Atlas, 3rd ed. By Leon Weisberg and Charles Nice. Philadelphia: Saunders, 480 pp., 1989. \$60 (2/90)

**Manual of Diagnostic Radiology.** By Joseph A. Pierro, Bruce M. Berens, William L. Crawford. Philadelphia: Lea & Febiger, 295 pp., 1989. \$28.50, softcover (2/90)

**MRI of the Sella and Para-Sellar Region.** By Murray A. Solomon. (Videotape 4 of Murray Solomon's Magnetic Resonance Video Review.) Burlingame, CA: Murray Solomon's MRVR, (415) 692-8230. Single tape, \$125; series of 6 tapes, \$495 (2/90)

**Doppler Ultrasound.** Physics, Instrumentation, and Clinical Applications. By D. H. Evans, W. N. McDicken, R. Skidmore, and J. P. Woodcock. New York: Wiley, 287 pp., 1989. \$96.50 (2/90)

**Nuclear Medicine Annual 1989.** Edited by Leonard M. Freeman and Heidi S. Weissmann. New York: Raven, 307 pp., 1989. \$98 (2/90)

**Pocket Atlas of Head and Neck MRI Anatomy.** By Robert B. Lufkin and William N. Hanafey. New York: Raven, 76 pp., 1989. \$13.95 (3/90)

**Brain Imaging.** An Introduction. By John R. Bradshaw. Stoneham, MA: Butterworths, 249 pp., 1989. \$70, softcover (3/90)

**Dysphagia.** Diagnosis and Treatment. Edited by David W. Gelfand and Joel E. Richter. New York: Igaku-Shoin, 382 pp., 1989. \$67.50 (3/90)

**Sectional Human Anatomy,** Transverse, Sagittal and Coronal Sections Correlated with Computed Tomography and Magnetic Resonance Imaging, 2nd ed. By Man-Chung Han and Chu-Wan Kim. Seoul, Korea: Ilchokak, 199 pp., 1989. \$74.50 (3/90)

**Basic Medical Techniques and Patient Care for Radiologic Technologists,** 3rd ed. By Lillian S. Torres. Philadelphia: Lippincott, 256 pp., 1989. \$25.95 (3/90)

**Chest Radiographic Analysis.** By Norman Blank. Chicago: Churchill Livingstone, 673 pp., 1989. \$125 (3/90)

**Breast Imaging.** By Daniel Kopans. Philadelphia: Lippincott, 416 pp., 1989. \$65 (3/90)

**Ultrasound and Infertility.** By Asim Kurjak. Boca Raton, FL: CRC Press, 213 pp., 1989. \$99.50 (inside U.S.), \$117 (outside U.S.) (3/90)

**Radiology Administration.** A Business Guide. By Wayne T. Stockburger. Philadelphia: Lippincott, 228 pp., 1989. \$29.95 (3/90)

**Magnetic Resonance Imaging of Bone and Soft Tissue Tumors and Their Mimics.** A Clinical Atlas. By A. M. A. De Schepper and H. R. M. Degryse. Boston: Kluwer Academic, 130 pp., 1989. \$75 (3/90)

**Handbook of Breast Imaging.** Edited by Mary Ellen Peters, Dawn R. Voegeli, and Kathleen A. Scanlan. New York: Churchill Livingstone, 344 pp., 1989. \$65 (3/90)

**Dento Maxillo Facial Radiology.** Edited by Peter N. Hirschmann. Stoneham, MA: Butterworths, May 1989;18(2):49-96 and August 1989;18(3):97-149. By subscription, 4 issues annually for £55 (3/90)

**Executive Skills for Medical Faculty.** By Neal Whitman, Elaine Weiss, and F. Marian Bishop. Salt Lake City: University of Utah School of Medicine, 117 pp., 1989.

**Vascular Disorders of the Upper Extremity,** 2nd ed. Edited by Herbert I. Machleder. Mount Kisco, NY: Futura, 410 pp., 1989. \$55

**The Pulmonary Intravascular Macrophage.** Edited by Norman C. Staub. Mount Kisco, NY: Futura, 180 pp., 1989. \$37.50

**Atlas of Cardiothoracic Surgery.** By L. Henry Edmunds, Jr., William I. Norwood, and David W. Low. Philadelphia: Lea & Febiger, 287 pp., 1990. \$125

**Treatment Simulators.** BJR Supplement 23. By C. K. Bomford, P. J. D. K. Dawes, S. C. Lillicrap, and J. Young. Stoneham, MA: Butterworths, 49 pp., 1989. \$29.95

**Gastrointestinal Cancer.** Radiation Therapy. Edited by Ralph R. Dobelbower, Jr. New York: Springer-Verlag, 301 pp., 1990. \$120

# American Roentgen Ray Society:

## Officers, Committees, and Membership Information

### Officers

**President:** Ronald G. Evens

**President-elect:** M. Paul Capp

**1st Vice-president:** John A. Kirkpatrick, Jr.

**2nd Vice-president:** A. Everette James, Jr.

**Secretary:** Glen W. Hartman

**Treasurer:** Beverly P. Wood

**Executive Council:** R. J. Alfidi, R. N. Berk, B. G. Brogdon, M. P. Capp, W. J. Casarella, R. G. Evens, J. T. Ferrucci, Jr., R. A. Gagliardi, G. W. Hartman, J. A. Kirkpatrick, Jr., A. Landry, Jr., G. R. Leopold, J. E. Madewell, A. A. Moss, L. F. Rogers, J. H. Thrall, K. H. Vydareny, B. P. Wood, A. K. Poznanski, chairman

### Committees

**Editorial Policy:** R. N. Berk, M. M. Figley, S. V. Hilton, M. S. Huckman, C. A. Rohrmann, Jr., S. S. Sagel, R. J. Stanley, N. O. Whitley, W. J. Casarella, chairman

**Education and Research:** C. B. Higgins, B. J. Hillman, R. A. McLeod, W. M. Thompson, B. G. Brogdon, chairman

**Finance and Budget:** R. J. Alfidi, R. C. Gedgaudas-McClees, G. R. Leopold, J. R. Thornbury, J. Thrall, chairman

**Nominating:** R. A. Gagliardi, N. O. Whitley, R. J. Alfidi, chairman

**Publications:** C. A. Rohrmann, Jr., S. S. Sagel, R. J. Stanley, N. O. Whitley, W. J. Casarella, chairman

**Membership:** R. J. Alfidi, A. A. Moss, K. H. Vydareny, G. R. Leopold, chairman

### Representatives to Other Organizations

**American Board of Radiology:** J. A. Kirkpatrick, Jr., E. C. Klatte, L. F. Rogers

**American College of Radiology:** R. A. Gagliardi, G. A. Kling, J. E. Madewell, L. F. Rogers

**American Medical Association House of Delegates:** S. F. Ochsner, K. L. Krabberhoft, alternate

**American National Standards Institute:** M. Haskin

**National Council on Radiation Protection and Measurements:** H. L. Friedell, E. L. Saenger

### Meeting Arrangements

**Annual Meetings:** May 13-18, 1990, Sheraton Washington, Washington, DC; May 5-10, 1991, Sheraton Boston, Boston

**Annual Meeting Committee:** H. C. Carlson, J. K. Crowe, G. P. Janetos, R. R. Lukin, A. Landry, Jr., chairman

**Instruction Courses:** R. J. Stanley, associate chairman, J. T. Ferrucci, Jr., chairman

**Scientific Program:** R. J. Alfidi, E. Buonocore, D. O. Davis, K. B. Hunter, T. C. McLoud, W. A. Murphy, Jr., A. E. Robinson, L. B. Talner, J. H. Thrall, M. P. Capp, chairman

**Scientific Exhibits:** R. J. Churchill, A. A. Moss, R. G. Ramsey, J. E. Madewell, chairman

### ARRS Membership

An application form is printed in the February issue of the Journal. For consideration at the 1991 ARRS meeting, send completed forms before February 1, 1991, to American Roentgen Ray Society, 1891 Preston White Dr., Reston, VA 22091. Active members are graduates of an approved medical or osteopathic school or hold an advanced degree in an allied science. They must practice radiology or work in an associated science in the United States or Canada and be certified by the American Board of Radiology, American Osteopathic Board of Radiology, or Royal College of Physicians of Canada or otherwise adequately document training and credentials. Corresponding members are foreign radiologists or scientists who are active in radiology or an allied science. Members-in-training are residents or fellows in radiology or postgraduate students in an allied science. Additional application forms can be obtained from the ARRS offices in Reston, VA.

### Business Office

Paul Fullagar, Executive Director, American Roentgen Ray Society, 1891 Preston White Dr., Reston, VA 22091; (703) 648-8900

# Classified Advertisements

## Positions Available

**RADIOLOGIST/ULTRASOUND**—The Dept. of Radiology at the University of Minnesota has a full-time position available in the ultrasound section at the rank of tenure-track assistant professor, tenured associate professor, or tenured professor beginning July 1, 1990. At the assistant professor level, minimum requirements are board certification in radiology and a minimum of 1 yr postresidency specialty training or experience in ultrasound radiology. Appointment at the rank of associate professor requires a minimum of 4 yr postresidency experience and a demonstrated record of research, publication, and teaching, in addition to the other qualifications listed for assistant professor status. Appointment at the rank of professor requires a minimum of 6 yr postresidency experience and a demonstrated strong record of research, publication, and teaching, in addition to the other qualifications listed for associate professor status. Responsibilities will include all facets of ultrasound radiology as well as graduate and undergraduate medical instruction. Research performance will be strongly encouraged and evaluated. Salary is negotiable and competitive, and is dependent on past scholarly productivity and post-M.D. experience. Applicants must be licensed or able to obtain a license to practice medicine in the state of Minnesota before appointment date. Applications will be accepted through June 1, 1990. Send letters to William M. Thompson, M.D., Professor and Chairman, Dept. of Radiology (Box 292 UMHC), University of Minnesota, 420 Delaware St. S.E., Minneapolis, MN 55455. The University of Minnesota is an equal opportunity educator and employer, and specifically invites and encourages applications from women and minorities. 4a

**THE UNIVERSITY OF QUEENSLAND—DIRECTOR, DEPARTMENT OF RADIOLOGY, PROFESSOR OF RADIOLOGY**, Mater Misericordiae Hospitals. The post is tenured on University terms of service under a joint-funding agreement with the Mater Misericordiae Hospitals by which the appointee will be Director of the Mater Misericordiae Hospital radiology dept. and will provide clinical services as radiologist at the Mater Hospital. The applicant should be an established consultant radiologist with a distinguished research record and experience in teaching and administration. He/she will be expected to have expertise in a radiologic subspecialty. The University's radiology dept. is based at the Mater Adult Hospital, 1 of 3 public hospitals in the Mater Complex of about 700 beds. It also has clinical and research facilities located at the Royal Brisbane Hospital. The University dept. has 3 other academic staff with current research interests in cardiac radiology, pediatric radiology, and MR spectroscopy. The Mater Hospital dept. has an establishment of 3.6 full-time-equivalent radiologists, 3 registrars, and radiographer support; its annual workload is about 45,000 exams. Annual salary: \$93,490, including clinical loading of \$11,707 and state loading of \$15,946. The appointee would have limited rights of private practice. Further information is available from Peter Bore, M.D., Acting Head, The University of Queensland, Dept. of Radiology, Mater Misericordiae Hospital, South Brisbane, Queensland 4101 (phone 07 840-8192) and J. Griffin, M.D., Executive Director of Medical Services, Mater Misericordiae Hospitals, South Brisbane, Queensland 4101 (phone 07-840-8559). Ref. No.: 03890. Closing date: May 11, 1990. Please forward an original plus 3 copies of application and resume to The Director, Personnel Services, The University of Queensland, St. Lucia, 4067, Australia. Equal opportunity in employment is University policy. 4a

**RADIOLOGIST/CHEST**—The Dept. of Radiology at the University of Minnesota has a full-time position available in the chest section at the rank of tenure-track assistant professor, tenured associate professor, or tenured professor beginning July 1, 1990. At the assistant professor level, minimum requirements are board certification in radiology and a minimum of 1 yr postresidency specialty training or experience in chest radiology. Appointment at the rank of associate professor requires a minimum of 4 yr postresidency experience and a demonstrated record of research, publication, and teaching, in addition to the other qualifications listed for assistant professor status. Appointment at the rank of professor requires a minimum of 6 yr postresidency experience and a demonstrated strong record of research, publication, and teaching, in addition to the other qualifications listed for associate professor status. Responsibilities will include all facets of chest radiology as well as graduate and undergraduate medical instruction. Research performance will be strongly encouraged and evaluated. Salary is negotiable and competitive, and is dependent on past scholarly productivity and post-M.D. experience. Applicants must be licensed or able to obtain a license to practice medicine in the state of Minnesota before appointment date. Applications will be accepted through June 1, 1990. Send letters to William M. Thompson, M.D., Professor and Chairman, Dept. of Radiology (Box 292 UMHC), University of Minnesota, 420 Delaware St. S.E., Minneapolis, MN 55455. The University of Minnesota is an equal opportunity educator and employer, and specifically invites and encourages applications from women and minorities. 4a

**RADIOLOGIST**—An excellent opportunity to work in the beautiful Rocky Mountains of British Columbia in the Columbia Valley. A fully qualified diagnostic radiologist with ultrasound qualifications is required by 2 rural hospitals 120 km apart: Golden and District General Hospital and Windermere District Hospital. Golden Hospital does a variety of general radiologic procedures and provides ultrasound. The Windermere Hospital is similar without ultrasound at present. Golden and District General Hospital has 25 acute beds, 8 extended beds, and a freestanding, 29-bed, intermediate-care facility. Windermere has 27 acute beds and 4 extended beds. Each community hospital serves an area population of approximately 8500 (this population grows during the summer and winter months). Six GPs at Golden with 1 pediatrician, 4 GPs and 1 surgeon at Windermere. An excellent recreational area, skiing, hiking, golf, and swimming. Please write, phone, or fax Ms. L. Ritchie, Administrator, Golden and District General Hospital, P. O. Box 1260, Golden, B.C., Canada V0A 1H0; Phone (604) 334-5271; Fax (604) 344-2511. 4-5a

**NUCLEAR MEDICINE RADIOLOGIST**—The Dept. of Radiology at the Lahey Clinic is seeking a board-certified, nuclear medicine physician to head the Section of Nuclear Medicine. The Lahey Clinic is a progressive, expanding, medical practice with a 270-bed hospital and accredited radiology residency located in the suburbs of Boston. Approximately 6000 studies are performed each yr. Equipment includes 4 gamma cameras and 3 computer systems, and there are plans to add SPECT. The full range of nuclear studies are performed as well as radioactive iodine therapies. There are opportunities for research. Salary is negotiable and commensurate with experience. Send CV to John T. Cuttino, Jr., M.D., Dept. of Diagnostic Radiology, Lahey Clinic Medical Center, 41 Mall Rd., Burlington, MA 01805. 4ap

**RADIOLOGIST/GENITOURINARY**—The Dept. of Radiology at the University of Minnesota has a full-time position available in the genitourinary section at the rank of tenure-track assistant professor, tenured associate professor, or tenured professor beginning July 1, 1990. At the assistant professor level, minimum requirements are board certification in radiology and a minimum of 1 yr postresidency specialty training or experience in genitourinary radiology. Appointment at the rank of associate professor requires a minimum of 4 yr postresidency experience and a demonstrated record of research, publication, and teaching, in addition to the other qualifications listed for assistant professor status. Appointment at the rank of professor requires a minimum of 6 yr postresidency experience and a demonstrated strong record of research, publication, and teaching, in addition to the other qualifications listed for associate professor status. Responsibilities will include all facets of genitourinary radiology as well as graduate and undergraduate medical instruction. Research performance will be strongly encouraged and evaluated. Salary is negotiable and competitive, and is dependent on past scholarly productivity and post-M.D. experience. Applicants must be licensed or able to obtain a license to practice medicine in the state of Minnesota before appointment date. Applications will be accepted through June 1, 1990. Send letters to William M. Thompson, M.D., Professor and Chairman, Dept. of Radiology (Box 292 UMHC), University of Minnesota, 420 Delaware St. S.E., Minneapolis, MN 55455. The University of Minnesota is an equal opportunity educator and employer, and specifically invites and encourages applications from women and minorities. 4a

**MARYLAND**—The University of Maryland Medical System/Hospital in Baltimore is seeking additional faculty members for the Sections of Pediatric Radiology, Chest Radiology, Ultrasound, Nuclear Medicine (ABNM required), Skeletal Radiology, Angio/Interventional Radiology, GI Radiology, Mammography, and Neuroradiology. Fellowship training or equivalent experience desired. ABR certification required. The medical center is an 800-bed, acute-care hospital and tertiary referral center with an active and varied practice. A new, 324-bed VA Hospital is now under construction and will be adjacent to and connected to the University. The duties of new faculty members will include research and teaching. Academic rank and salary commensurate with experience. The radiologists are organized as a professional corporation offering excellent fringe benefits. Baltimore is a superb place in which to live and work. It has all the amenities of a large metropolitan center, yet is small enough to avoid most of the problems (traffic, inflated property values, etc.) of our largest cities. Washington, Philadelphia, and New York are readily accessible, and it is only 3 hr from the ocean. Submit CV to Gerald S. Johnston, M.D., Dept. of Diagnostic Radiology, 22 S. Greene St., Baltimore, MD 21201; (800) 866-8667, ext. 3477. Affirmative action/equal opportunity employer encourages applications from members of minority groups. 4 & 7ap

**HOUSTON**—Group needs additional board-certified diagnostic radiologist. Prefer training and/or experience in interventional, including angiography and percutaneous interventional procedures, guided biopsy, ultrasound, CT, nuclear medicine, and MRI. Please submit CV to Sanford Smith, Professional Practice Management, Inc., 1075 Kingwood Dr., Kingwood, TX 77339; (713) 358-8113. 4ap

**RADIOLOGIST/MRI-ULTRASOUND**—The Dept. of Radiology at the University of Minnesota has a full-time position available in the MRI/ultrasound section at the rank of tenure-track assistant professor, tenured associate professor, or tenured professor beginning July 1, 1990. At the assistant professor level, minimum requirements are board certification in radiology and a minimum of 1 yr postresidency specialty training or experience in MRI/ultrasound radiology. Appointment at the rank of associate professor requires a minimum of 4 yr postresidency experience and a demonstrated record of research, publication, and teaching, in addition to the other qualifications listed for assistant professor status. Appointment at the rank of professor requires a minimum of 6 yr postresidency experience and demonstrated strong record of research, publication, and teaching, in addition to the other qualifications listed for associate professor status. Responsibilities will include all facets of MRI/ultrasound radiology as well as graduate and undergraduate medical instruction. Research performance will be strongly encouraged and evaluated. Salary is negotiable and competitive, and is dependent on past scholarly productivity and post-M.D. experience. Applicants must be licensed or able to obtain a license to practice medicine in the state of Minnesota before appointment date. Applications will be accepted through June 1, 1990. Send letters to William M. Thompson, M.D., Professor and Chairman, Dept. of Radiology (Box 292 UMHC), University of Minnesota, 420 Delaware St. S.E., Minneapolis, MN 55455. The University of Minnesota is an equal opportunity educator and employer, and specifically invites and encourages applications from women and minorities. 4a

**RADIOLOGIST/CHIEF, PULMONARY RADIOLOGY**—The Dept. of Radiology at the University of Minnesota has a full-time position available in the pulmonary radiology section at the rank of tenure-track assistant professor, tenured associate professor, or tenured professor beginning July 1, 1990. At the assistant professor level, minimum requirements are board certification in radiology and a minimum of 1 yr postresidency specialty training or experience in pulmonary radiology. Appointment at the rank of associate professor requires a minimum of 4 yr postresidency experience and a demonstrated record of research, publication, and teaching, in addition to the other qualifications listed for assistant professor status. Appointment at the rank of professor requires a minimum of 6 yr postresidency experience and a demonstrated strong record of research, publication, and teaching, in addition to the other qualifications listed for associate professor status. Responsibilities will include all facets of pulmonary radiology as well as graduate and undergraduate medical instruction. Research performance will be strongly encouraged and evaluated. Salary is negotiable and competitive, and is dependent on past scholarly productivity and post-M.D. experience. Applicants must be licensed or able to obtain a license to practice medicine in the state of Minnesota before appointment date. Applications will be accepted through June 1, 1990. Send letters to William M. Thompson, M.D., Professor and Chairman, Dept. of Radiology (Box 292 UMHC), University of Minnesota, 420 Delaware St., S.E., Minneapolis, MN 55455. The University of Minnesota is an equal opportunity educator and employer, and specifically invites and encourages applications from women and minorities. 4a

**RADIOLOGIST**—Associate diagnostic radiologist to join a 4-radiologist group in Massachusetts. Hospital and private practice. All diagnostic modalities. Interest in angiography and interventional radiology preferred. Reply Box Y54, AJR (see address this section). 3-5ap

**RADIOLOGIST/NEURORADIOLOGY**—The Dept. of Radiology at the University of Minnesota has 4 full-time positions available in the neuroradiology section at the rank of tenure-track assistant professor, tenured associate professor, or tenured professor beginning July 1, 1990. At the assistant professor level, minimum requirements are board certification in radiology and a minimum of 1 yr postresidency specialty training or experience in neuroradiology. Appointment at the rank of associate professor requires a minimum of 4 yr postresidency experience and a demonstrated record of research, publication, and teaching, in addition to the other qualifications listed for assistant professor status. Appointment at the rank of professor requires a minimum of 6 yr postresidency experience and a demonstrated strong record of research, publication, and teaching, in addition to the other qualifications listed for associate professor status. Responsibilities will include all facets of neuroradiology as well as graduate and undergraduate medical instruction. Research performance will be strongly encouraged and evaluated. Salary is negotiable and competitive, and is dependent on past scholarly productivity and post-M.D. experience. Applicants must be licensed or able to obtain a license to practice medicine in the state of Minnesota before appointment date. Applications will be accepted through June 1, 1990. Send letters to William M. Thompson, M.D., Professor and Chairman, Dept. of Radiology (Box 292 UMHC), University of Minnesota, 420 Delaware St., S.E., Minneapolis, MN 55455. The University of Minnesota is an equal opportunity educator and employer, and specifically invites and encourages applications from women and minorities. 4a

**RADIOLOGIST/CHIEF, MAGNETIC RESONANCE IMAGING**—The Dept. of Radiology at the University of Minnesota has a full-time position available in the MRI section at the rank of tenure-track assistant professor, tenured associate professor, or tenured professor beginning July 1, 1990. At the assistant professor level, minimum requirements are board certification in radiology and a minimum of 1 yr postresidency specialty training or experience in MRI. Appointment at the rank of associate professor requires a minimum of 4 yr postresidency experience and a demonstrated record of research, publication, and teaching, in addition to the other qualifications listed for assistant professor status. Appointment at the rank of professor requires a minimum of 6 yr postresidency experience and a demonstrated strong record of research, publication, and teaching, in addition to the other qualifications listed for associate professor status. Responsibilities will include all facets of MRI as well as graduate and undergraduate medical instruction. Research performance will be strongly encouraged and evaluated. Salary is negotiable and competitive, and is dependent on past scholarly productivity and post-M.D. experience. Applicants must be licensed or able to obtain a license to practice medicine in the state of Minnesota before appointment date. Applications will be accepted through June 1, 1990. Send letters to William M. Thompson, M.D., Professor and Chairman, Dept. of Radiology (Box 292 UMHC), University of Minnesota, 420 Delaware St., S.E., Minneapolis, MN 55455. The University of Minnesota is an equal opportunity educator and employer, and specifically invites and encourages applications from women and minorities. 4a

**BE/BC GENERAL DIAGNOSTIC RADIOLOGIST**, experienced in CT, ultrasound, mammography, and nuclear medicine, wanted for established 2-person practice at 150-bed community hospital in rural southeastern Virginia. Opening July 1990. Competitive salary, benefits. Send CV to Box Y70, AJR (see address this section). 3-5ap

**RADIOLOGIST/MUSCULOSKELETAL**—The Dept. of Radiology at the University of Minnesota has a full-time position available in the musculoskeletal section at the rank of tenure-track assistant professor, tenured associate professor, or tenured professor beginning July 1, 1990. At the assistant professor level, minimum requirements are board certification in radiology and a minimum of 1 yr postresidency specialty training or experience in musculoskeletal radiology. Appointment at the rank of associate professor requires a minimum of 4 yr postresidency experience and a demonstrated record of research, publication, and teaching, in addition to the other qualifications listed for assistant professor status. Appointment at the rank of professor requires a minimum of 6 yr postresidency experience and a demonstrated strong record of research, publication, and teaching, in addition to the other qualifications listed for associate professor status. Responsibilities will include all facets of musculoskeletal radiology as well as graduate and undergraduate medical instruction. Research performance will be strongly encouraged and evaluated. Salary is negotiable and competitive, and is dependent on past scholarly productivity and post-M.D. experience. Applicants must be licensed or able to obtain a license to practice medicine in the state of Minnesota before appointment date. Applications will be accepted through June 1, 1990. Send letters to William M. Thompson, M.D., Professor and Chairman, Dept. of Radiology (Box 292 UMHC), University of Minnesota, 420 Delaware St. S.E., Minneapolis, MN 55455. The University of Minnesota is an equal opportunity educator and employer, and specifically invites and encourages applications from women and minorities. 4a

**MASSACHUSETTS GENERAL HOSPITAL**—Outstanding opportunity for radiologist interested in the highest quality of practice. All imaging modalities including MRI, CT, and interventional. This is mostly a musculoskeletal position, but other areas are available depending on the needs of the applicant. Unusually broad range of abnormalities, including bone and soft-tissue tumors, metabolic disease, and trauma. All levels of experience considered. Send letters of inquiry and CV to Daniel I. Rosenthal, M.D., Director, Bone and Joint Radiology, Massachusetts General Hospital, Boston, MA 02114. Massachusetts General Hospital is an equal opportunity employer. 4-6ap

**NEURORADIOLOGIST**—The University of Utah is seeking applications for a neuroradiologist at the assistant or associate professor level. Primary duties include student, resident, and fellow instruction with emphasis on ENT radiology, TMJ imaging, cranial nerve imaging, extracranial neuroradiology, and general neuro MR. Four full-time neuroradiologists provide service at the University Hospital and SLC VAMC. Extensive interaction with otolaryngologists, neurologists, neurosurgeons, and oral surgeons concerning clinical material has been an integral part of the position. An interest in research and publication is desirable, as well as board certification and senior membership in the American Society of Neuroradiology. Send CV to David G. Bragg, M.D., Professor and Chairman, Dept. of Radiology, University of Utah Medical Center, 50 N. Medical Dr., Salt Lake City, UT 84132. All inquiries are confidential. Applications received after the closing date of May 30, 1990, may be accepted, if no qualified applicants have applied. The University of Utah is an EEO/AA employer. 4a

**RADIOLOGIST**—Full-time; nice, small, well-located North Carolina town. Join active, hospital-based, service-oriented practice. General diagnostic, nuclear medicine, ultrasound, CT, and mobile MRI. No arteriography. Reply with CV to Box Y50, AJR (see address this section). 3-5ap

**MINNEAPOLIS-ST. PAUL, INTERVENTIONAL NEURORADIOLOGIST**—Incumbent interventional neuroradiologist needs help in handling rapidly expanding interventional neuro case load. Present full-time, 3-member neuroradiology section is a growing and active component of a 21-member practice based in 800-bed, tertiary-care facility in Minneapolis-St. Paul. Private practice with academic affiliation and appointments. This practice currently operates 2 MRI and 7 CT scanners. Three additional MRI scanners will be installed in the near future. Excellent starting salary and benefits. Short track to full partnership. Minneapolis-St. Paul consistently places in the top 10 of the most livable U.S. cities and recently was ranked #1 in the country as a place to raise children. Outstanding cultural, outdoor, and athletic activities immediately accessible. The opening represents an outstanding and unique practice opportunity for the right person. Please submit all inquiries with CV to Philip Murray, M.D., Dept. of Radiology, Abbott Northwestern Hospital, 800 E. 28th St., Minneapolis, MN 55407. 4-5a

**RADIOLOGIST**—The Dept. of Radiology at the Beth Israel Hospital in Boston, MA, is seeking a radiologist with broad experience in general radiology for a July 1, 1990, opening. Expertise in ultrasound, CT, mammography, and/or angiography is desirable. The hospital is a 504-bed, voluntary teaching hospital affiliated with the Harvard Medical School. Candidates should meet the requirements for faculty appointment. Please send inquiries with a CV to Sven Paulin, M.D., Radiologist-in-Chief, Beth Israel Hospital, 330 Brookline Ave., Boston, MA 02215. The hospital is an affirmative action/equal opportunity employer. Minority and female candidates are encouraged. 4ap

**NUCLEAR MEDICINE/IMAGING**—Twelve-person radiology practice has an opening for a diagnostic radiologist with experience/expertise in nuclear medicine. Practice is hospital-based with full range of equipment. Will share duties with 1 other fellowship-trained nuclear medicine radiologist. Cardiac nuclear imaging experience required. Please send letter of inquiry and CV to Richard D. Herman, M.D., Chairman, Dept. of Radiology, St. Luke's Hospital, Bethlehem, PA 18015. 4-6ap

**THE UNIVERSITY OF BRITISH COLUMBIA**, Head of the Dept. of Radiology in the Faculty of Medicine. The person appointed would be responsible for directing and developing the teaching, research, and service programs of the dept. Candidate should hold a specialty qualification in radiology and have substantial academic and clinical experience. Starting date is January 1, 1991. Salary is commensurate with qualifications and experience. The University of British Columbia is committed to the federal government's employment equity program and encourages applications from all qualified persons. In accordance with Canadian immigration requirements, priority will be given to Canadian citizens and permanent residents. Applications, accompanied by a detailed CV and the names of 2 references, should be directed to W. A. Webber, M.D., Dean, Faculty of Medicine, University of British Columbia, Rm. 317, Instructional Resources Centre, 2194 Health Sciences Mall, Vancouver, B.C., Canada V6T 1W5. Deadline for submission of applications is May 31, 1990. 4a

**SECTION HEAD FOR CARDIOVASCULAR RADIOLOGY** wanted for clinical care, teaching, and research in 450-bed, adult, tertiary-care hospital. Equal opportunity/affirmative action employer fully affiliated with Harvard Medical School. Submit CV to Melvin E. Clouse, M.D., Chairman, Dept. of Radiology, New England Deaconess Hospital, 185 Pilgrim Rd., Boston, MA 02215. 4ap

**EXCEPTIONAL OPPORTUNITY, BREAST IMAGING**—The Susan G. Komen Breast Center, affiliated with St. Francis Medical Center and the University of Illinois College of Medicine at Peoria, is seeking a radiologist with interest in breast imaging to join a rapidly growing, comprehensive, diagnostic breast imaging service. The new Center is located in a beautiful, new, 5200 sq. ft. private-office setting. Two satellite facilities, 1 in East Peoria and the other at St. Francis Medical Center, combine to provide high-quality breast imaging for a major portion of central Illinois. Currently, 65 breast imaging studies are performed daily, including mammography, breast ultrasound, localization procedures, cyst aspirations, ductograms, and fine-needle aspiration biopsies. The Center has developed ongoing teaching programs in mammography and has sponsored an annual fall seminar for radiologists and technologists. A 1-yr fellowship in breast imaging has been established. Radiologist will join an established, highly respected, private-practice group of 15 radiologists at St. Francis Medical Center. Practice will be almost entirely limited to breast imaging, with some plain film interpretation. Breast imaging service is under the direction of G. W. Eklund, M.D. Applicants should have an interest in learning, growing and teaching, and participating in the rapid growth of a rewarding, clinically oriented practice. We are prepared to discuss this position with interested radiologists, regardless of breast imaging experience. Financial arrangements and benefit package are exceptional. Peoria, IL, located midway between Chicago and St. Louis, boasts the 1989 designation of All America City and is the home of Caterpillar Tractor Co. and Bradley University. Call or send inquiries to G. W. Eklund, M.D., 4911 Executive Dr., Peoria, IL 61614; (309) 693-6816, (309) 691-0991 evenings. 4ap

**NEURORADIOLOGIST**—The Dept. of Radiologic Sciences at the Medical College of Pennsylvania is seeking a neuroradiologist for a full-time position. Assistant/associate professor level. Academic setting. Salary negotiable, commensurate with experience. Please send CV to George L. Popky, M.D., Professor and Chairman, Dept. of Radiologic Sciences, The Medical College of Pennsylvania, 3300 Henry Ave., Philadelphia, PA 19129. Equal opportunity employer. 4a

**INTERVENTIONAL RADIOLOGIST** for 450-bed, tertiary-care teaching hospital. New biliary and renal lithotripsy service as well as 1400 vascular and interventional procedures/yr. Large and small animal research laboratory with fluorography, rapid film changer, and MRI. Three vascular fellows. Equal opportunity/affirmative action employer affiliated with Harvard Medical School. Submit CV to Dept. of Radiology, New England Deaconess Hospital, 185 Pilgrim Rd., Boston, MA 02215. 4ap

**TWO BOARD-CERTIFIED/ELIGIBLE GENERAL DIAGNOSTIC RADIOLOGISTS** to join expanding, 11-person group covering 2 hospitals and 2 MR sites. Ideal private practice in a stable midwest community using all imaging modalities and interventional techniques. Can start immediately or wait until July 1990. Excellent opportunity with excellent salary and benefits. Send CV to Joseph F. Norfray, M.D., MR Center of Springfield, 319 E. Madison, Springfield, IL 62701. 4-7ap

**NUCLEAR MEDICINE**—Immediate opening in large, progressive radiology group in the Central New Jersey/Bucks County, PA, region for recently trained person with a nuclear medicine fellowship with emphasis on cardiac imaging. Must be willing to do all other facets of noninvasive radiology. Four-hospital group has 8 cameras and 3 SPECT units. Send letter and CV to L. Ratner, M.D., 838 W. State St., Trenton, NJ 08618. 4-6a

**CHIEF ONCODIAGNOSTIC RADIOLOGY**—Dana-Farber Cancer Institute seeks head of diagnostic radiology and nuclear medicine. Oversees all diagnostic radiology of inpatient and outpatient service, directs clinical teaching service, and builds clinical investigative program. Academic appointment in Harvard Medical School, Dept. of Radiology, commensurate with qualification and experience. Competitive salary/excellent benefits. Experienced diagnostic radiologist with recognized clinical and administrative skills and interest in neoplastic diseases. Strong interest in teaching and collaborative clinical investigation also essential. Send CV to G. P. Canellos, M.D., Dana-Farber Cancer Institute, 44 Binney St., Boston, MA 02115. An affirmative action employer. 4a

**DIAGNOSTIC RADIOLOGIST** to join the excellent radiology dept. at a JCAHO-accredited Regional Medical Center in upper midwest. The relatively new radiology wing has state-of-the-art equipment including ultrasound, nuclear medicine with Hot Lab, 2 R & F rooms, 1 R & T room, CT, and MRI on mobile basis. Outstanding opportunity in active, progressive, university community. Unusually attractive compensation/benefit package. For more detailed information, call Ed Otto at (800) 638-6942. 4ap

**LAKES REGION, CENTRAL NEW HAMPSHIRE** A predominantly hospital-based practice of 3 radiologists seeks an additional recently trained radiologist with expertise in all imaging modalities. State-of-the-art equipment available in recently expanded/renovated hospital. Potential to become full partner in 1-1/2 yr with no buy-in. Practice located in Laconia, NH, in the "Lakes Region" at southern border of White Mountains. Lake Winnepesaukee and several major ski facilities nearby. For more information, please contact Benjamin Tuttle, M.D., Chairman, Dept. of Medical Imaging, Lakes Region General Hospital, Elliot St., Laconia, NH 03246; (603) 527-2900. 4-5ap

**FACULTY POSITIONS AVAILABLE IN DIAGNOSTIC RADIOLOGY**—The University of Miami School of Medicine is currently recruiting a 4th full-time vascular and interventional radiologist. The interventional section provides radiologic services at Jackson Memorial Medical Center and Veterans Administration Medical Center. We perform approximately 3000 exams/yr in the section. The vascular and interventional section performs all angiographic procedures except for cardiac and neuroradiologic studies. These include all diagnostic and interventional vascular procedures. We also have an active nonvascular service involving thoracic and abdominal intervention. This includes all percutaneous liver procedures, percutaneous nephrostomies, abscess drainages, and percutaneous gastrostomy placements. The section currently consists of 3 staff members and 4 fellows. Residents rotate through the service on a monthly basis. Please submit CV to Jose M. Yrizarry, M.D., University of Miami School of Medicine, Dept. of Radiology (R-109), P. O. Box 016960, Miami, FL 33101; (305) 549-6894. 4-5ap

**NEURORADIOLOGIST**—UMDNJ, NJ Medical School, is seeking a full-time neuroradiologist. The service function will be combined ¾ time at University Hospital (518 beds) and ¼ time at the East Orange VA Hospital (700 beds). Two GE CT scanners, 1.5-T GE Signa MRI, and Philips digital angiography at University Hospital. Two other neuroradiologists in the section. Teaching and resident (16 residents) review required. Future will include medical office complex. Respond to Gail Eliot, M.D., Acting Chairperson, Dept. of Radiology, University of Medicine and Dentistry, 150 Bergen St., Newark, NJ 07103; (201) 456-5188. An equal opportunity employer. 2-4ap



**MAINE**—Excellent opportunity for young, BC/BE, general radiologist with MRI and basic interventional skills to join progressive, well-established, small group. Live and work in college community in southern region close to coast, mountains, and lakes. Competitive compensation package leading to partnership. Affiliate with 200-bed, modern, community hospital. Send CV to New England Health Search, 63 Forest Ave., Orono, ME 04473; (207) 866-5680 or (207) 866-5685. 4-6ap

**NEURORADIOLOGIST**—The Dept. of Diagnostic Imaging/Radiology of Sinai Hospital of Detroit is seeking an individual with appropriate training and interest in performing and interpreting neuro-radiologic exams. The hospital is about to open an off-site imaging center with MRI and CT capabilities. The person hired will be the Medical Director of this center but also will have responsibilities in neuroradiology at the main hospital. The hospital is a tertiary-care, university-affiliated institution with a thriving residency program. The dept. consists of 13 radiologists in private practice on a fee-for-service, separate billing arrangement. Candidates should have an interest in teaching and research. Apply to Philip N. Cascade, M.D., Chairman, Dept. of Diagnostic Imaging/Radiology, Sinai Hospital of Detroit, 6767 W. Outer Dr., Detroit, MI 48235-2899; (313) 493-5906. 4-5ap

**UCSD SCHOOL OF MEDICINE**—Dept. of Radiology is seeking a neuroradiologist to participate in clinical, teaching, and research programs. Qualifications required: board-eligibility/certification, California medical license, and 2-yr fellowship in neuroradiology including MR imaging; neuro/interventional experience preferred. Title series: assistant professor (in-residence or clinical series, not currently a tenure-track position); level based on years experience; salary commensurate with rank and step of appointment based on the established salary schedule of the UCSD School of Medicine Faculty Compensation Plan. The University of California, San Diego, is an equal opportunity/affirmative action employer. All CVs received by May 1, 1990, will be given full consideration. Send to John R. Hesselink, M.D., Professor of Radiology, Dept. of Radiology, UCSD Medical Center, 225 Dickinson St., San Diego, CA 92103. 4a

**VIRGINIA'S CHESAPEAKE BAY**—BC/BE general radiologist for 100-bed, full-service rural hospital. All modalities including mobile MRI, no angio currently. Closely associated with regional medical center and multispecialty group for back-up. Wonderful waterfront lifestyle possibilities. Available July 1, 1990. Send CV to Box Z82, AJR, (see address in this section). 4-5ap

**UNIQUE OPPORTUNITY**—Permanent part-time position for diagnostic radiologist to work weekends, or more if desired, in exciting Las Vegas at a university-affiliated hospital with a large private group. Ample time to enjoy the many regional recreational activities. Candidates should be well-trained general radiologists with basic skills in ultrasound and CT. Angiography not required. Generous salary and fringe benefits. Contact Brent Birkin, M.D., 3848 Pima Ln., Las Vegas, NV 89109; (702) 384-5210 (7 a.m. to 5 p.m.) or (702) 732-0559 (after 6 p.m.). 4-6ap

**PRACTICE IN THE COASTAL PLAIN OF NORTH CAROLINA** at a well-established 100-bed hospital seeks third radiologist. 23,000/24,000 procedures/yr. General radiology including mammography, CT, ultrasound, and nuclear medicine. No angio, interventional, or MRI. Compensation and benefits competitive. Available immediately. Contact Roanoke-Chowan Radiology Associates, Inc., P.O. Box 459, Ahoskie, NC 27910; (919) 332-6011. 3-6ap

**BC/BE RADIOLOGIST**, preferably with training and experience in neuroradiology, to join 5-member radiology group in Savannah, GA. Practice includes coverage of 300-bed, acute-care hospital and new private office. Excellent facilities with state-of-the-art CT, nuclear medicine with SPECT, general and vascular ultrasonography, mammography, fluoroscopy, neuro/angio/interventional, and MRI. Generous salary and benefits with early partnership. Savannah is an attractive coastal community with expanding economy and outstanding year-round recreational resources. Send CV with letter of inquiry to Thomas H. Philbrick, M.D., Savannah Radiologists, P.O. Box 14444, Savannah, GA 31499. 3-5ap

**IMMEDIATE OPENING**—BC/BE radiologist to join medium-sized group in Austin, TX. Special interest, expertise, or fellowship training in body imaging and/or interventional radiology is necessary. Practice covers major trauma center and outpatient radiology facility. In addition to general diagnostic services, outpatient facility also provides CT and MRI services on 2 GE 9800 scanners and on GE 1.5-T and 0.5-T MR units. Applicants are requested to contact Drs. Gray, Lava, or Boyd at 711 W. 38th St., Ste. B-8, Austin, TX 78705; (512) 454-8718. 3-5ap

**UPSTATE NEW YORK**—Progressive group seeks a board-certified diagnostic radiologist and a neuroradiologist willing to do some general radiology. Full range of services (MRI, ultrasound, Doppler, angiography) provided at 2 acute-care hospitals with state-of-the-art equipment. Excellent salary and benefits with early partnership. Reply to Box Y58, AJR (see address in this section). 3-4ap

**NYU MEDICAL CENTER, RADIOLOGY DEPT.**—Faculty position available for a Director of Ultrasound, and junior faculty positions available in ultrasound and in bone and joint radiology. Contact Norman E. Chase, M.D., Professor and Chairman, Dept. of Radiology, NYU Medical Center, 550 First Ave., New York, NY 10016. An equal opportunity affirmative action employer. 2-4ap

**ANGIOGRAPHY/INTERVENTIONAL RADIOLOGIST**—Position available at the New Jersey Medical School, Newark, NJ, July 1, 1990. Academic position will include resident supervision, scholarly activity, and clinical practice. Excellent equipment. Rapidly developing institution and dept. Recent completion of fellowship in angio/interventional and board-certification, or current faculty member in current academic section in angio/interventional would be considered. Compensation starting at \$150,000 for entry level. Please contact Gail Eliot, M.D., Acting Chairperson, Dept. of Radiology, NJMS, University Hospital, C-320, 150 Bergen St., Newark, NJ 07103; (201) 456-5188 or 5189. 3-5ap

**POSITION AVAILABLE IMMEDIATELY FOR A GENERAL DIAGNOSTIC RADIOLOGIST**, with training or experience in vascular/interventional radiology, to complete staffing for the new VA Medical Center in Minneapolis, MN. Dept. includes MRI, CT, cyclotron with PET scanner, interventional vascular suite, neuroradiology suite, mammography, color-flow Doppler ultrasonography, plus more. Affiliated with the University of Minnesota with non-tenure-track appointment available at appropriate level. Research and teaching opportunities available. Salary \$99,480. Board certification mandatory. One yr fellowship training or equivalent experience in interventional radiology desirable. Send letters of inquiry with CV to Donovan B. Reinke, M.D., Chief of Diagnostic Radiology Service—114, VA Medical Center, One Veterans Dr., Minneapolis, MN 55417; (612) 725-2038. EOE. 4a

**FULL-TIME BC RADIOLOGIST** needed to staff outpatient women's diagnostic center in suburban Dallas. Experience in mammography and OB/GYN sonography preferred. No call responsibilities. Attractive compensation package. Send CV to Box Y56, AJR (see address in this section). 4xa

**ASHEVILLE, NC**—BC/BE general diagnostic radiologist needed to join 6-person group. Practice consists of 320-bed private hospital and office practice with 80,000 procedures/yr. Excellent benefits and compensation in a beautiful mountain setting. Contact D. T. Milton, M.D., 445 Biltmore Center, Ste. 301, Asheville, NC 28801; (704) 255-3761. 4ap

**PEDIATRIC RADIOLOGIST, PORTLAND, OR**—Immediate opening for a pediatric radiologist at Emanuel Hospital in Portland, OR. Either a pediatric fellowship or significant work experience is required. Opportunity to do general radiology as well. The hospital is a Level I trauma center, as well as a major pediatric referral center. The position leads to full partnership after second yr. Please send CV to Blaine E. Kozak, M.D., Chairman, Dept. of Radiology, Emanuel Hospital, 2801 N. Gantenbein, Portland, OR 97227; (503) 280-4032. 4ap

**OREGON**—Group of 12 radiologists in Salem, OR, seeks BC/BE radiologist with general radiology skills. Special competence in nuclear medicine desirable, but not mandatory. Practice includes 450-bed community hospital, large office, and a multispecialty clinic. Send CV to John Eyre, M.D., c/o Salem Radiology, 919 Oak St. S.E., Salem, OR 97301. 4-6ap

**ISRAEL, DIAGNOSTIC RADIOLOGY**. Opportunities for 3-4 week or longer working vacations in a number of Israeli medical centers, on a volunteer basis. Positions varied, arrangements flexible. For information contact: Jonathan H. Fish, M.D., 1844 San Miguel Dr., #302, Walnut Creek, CA 94596; (415) 947-0560. 2-4xa

**DARTMOUTH-HITCHCOCK MEDICAL CENTER, DEPT. OF RADIOLOGY** is offering 2 permanent positions for BC/BE, GI/GU radiologists at the Mary Hitchcock Memorial Hospital. This is a 400-bed hospital with 80 radiology personnel who perform 55,000 inpatient and 45,000 outpatient exams/yr. The dept. consists of 13 staff and 9 residents covering the full range of modern radiologic practice. Become a member of the 200-physician, academic, multi-specialty group that forms the clinical faculty of Dartmouth Medical School. Position has responsibility for a full scope of general diagnostic procedures. Interest in teaching essential, research desirable. Interested candidates should write to P. K. Spiegel, M.D., Dartmouth-Hitchcock Medical Center, Dept. of Radiology, 2 Maynard St., Hanover, NH 03756. AA/EOE. 4xa

**LOCUM TENENS POSITIONS** throughout the country. Work for a wk to a yr. at your convenience. Malpractice insurance, housing, and travel paid. Excellent compensation and interesting jobs. LOCUM Medical Group, 30100 Chagrin Blvd., Cleveland, OH 44124. call toll-free (800) 752-5515. 3-8ap

**ORTHOPEDIC RADIOLOGIST**—A position is available at the University of Rochester Medical Center, Strong Memorial Hospital, Dept. of Radiology, a 750-bed, tertiary-care facility. An appointment as assistant professor or higher is available at a level appropriate to experience. Research and teaching opportunities are available in a strong academic dept. with state-of-the-art radiologic equipment. Send CV to Robert E. O'Mara, M.D., Professor and Chair, Diagnostic Radiology, Box 648, University of Rochester Medical Center, Rochester, NY 14642. EO/AA/M-F employer. 3-6ap



**ABDOMINAL RADIOLOGIST**—The Dept. of Radiology at the Albany Medical College has an immediate opening for a faculty position in abdominal imaging. The candidate should have fellowship training or demonstrated experience in cross-sectional imaging. Clinical duties will be in ultrasound, body CT, body MR, and GI/GU. The candidate also will participate in medical student and postgraduate education and be able to pursue clinical and basic research interests. Academic rank and salary are commensurate with experience. The dept. has 23 attending staff, 3 fellows, and 16 residents. Please contact James C. Peters, M.D., Interim Chairman, Dept. of Radiology, Albany Medical College, 43 New Scotland Ave., Albany, NY 12208; (518) 445-3277. Albany Medical College is an equal opportunity/affirmative action employer. 3-5ap

**POSITION OPEN IMMEDIATELY**—Board-certified radiologist needed to join busy, 3-member radiology group with practice in central and southwestern Pennsylvania. Central Pennsylvania practice involves imaging (all modalities) and southwestern Pennsylvania practice involves an outpatient imaging facility consisting of radiography, fluoroscopy, ultrasound, CT, nuclear medicine, mammography, and MR. Job leading to full partnership with competitive salary and benefits. Send letters of inquiry with CV to R & R Consultants, Box 160, Adamsburg, PA 15611; (412) 483-6564. 3-4a

**RADIOLOGIST**—This 52-physician, multispecialty clinic is seeking a second radiologist for general radiologic procedures excluding CT and MRI. Experience or formal training in mammography required. Located in western Montana, abundant 4-season recreational opportunities. Offered salary and benefits generous. Send CV to Administrator, Western Montana Clinic, P. O. Box 7609, Missoula, MT 59807. 4-5ap

**NEURORADIOLOGIST**—The University of Texas Health Science Center at San Antonio is seeking a qualified academic neuroradiologist to fill an immediate opening. Send cover letter and CV to John R. Jinkins, M.D., Director of Neuroradiology, The University of Texas Health Science Center, 7703 Floyd Curl Dr., San Antonio, TX 78284-7800. 3-8ap

**PEDIATRIC RADIOLOGIST**—William Beaumont Hospital is a modern, tertiary-care medical center with a strong residency and fellowship program in diagnostic radiology. We are seeking a pediatric radiologist to join the full-time pediatric radiologist on our staff. The medical center is located in southeastern Michigan, with nearby desirable living areas and summer and winter resort activities. Compensation and benefits are generous and very competitive. Send CV to Jalil Farah, M.D., Chairman, Diagnostic Radiology, William Beaumont Hospital, 3601 W. 13 Mile Rd., Royal Oak, MI 48072. 4-5a

**UNIVERSITY OF MEDICINE & DENTISTRY OF NJ, NJ MEDICAL SCHOOL** is seeking 2 section chiefs. Section chief in GI radiology requires fellowship training in GI radiology or current experience in GI section of an academic radiology dept. Section chief in Chest radiology requires fellowship training in Chest radiology or current experience in Chest section of an academic radiology dept. Section chiefs will have full clinical responsibility for all imaging modalities relating to the subspecialty, training of residents in the section, and development of research goals for the section. Salaries are excellent. Supportive dept. with opportunity to explore and develop own interests. Excellent equipment. Send resume to Gail Eliot, M.D., Acting Chairman, NJMS Dept. of Radiology, University Hospital, 150 Bergen St., Newark, NJ 07103; (201) 456-5188. 2-4ap

**DIAGNOSTIC RADIOLOGIST**—Opening for board-certified radiologist to join a young, dynamic, 6-person radiology group near Gettysburg, PA, approximately 90 min from downtown Washington, DC. Modalities include special procedures, CT, MRI, nuclear medicine with SPECT, and mammography. Two community-based hospitals with several outpatient imaging facilities. Hospital campus also includes close affiliation with a Johns Hopkins University-sponsored cancer treatment center. Competitive salary and benefits leading to partnership opportunity. Rapidly growing community, ideally situated not far from the Baltimore-Washington area, between Pittsburgh and Philadelphia. Outstanding skiing, fishing, hunting, and boating in the region including the Chesapeake Bay. Position available July 1, 1990. Please submit CV along with names and addresses of 3 references to Robert S. Pyatt, M.D., Dept. of Radiology and Diagnostic Imaging, The Chambersburg Hospital, 112 N. Seventh St., Chambersburg, PA 17201; (717) 267-7181. 2-4ap

**GENERAL RADIOLOGIST**—221-bed, affiliated, GM&S VA Medical Center in the Black Hills is searching for a board-certified or eligible radiologist to join our staff. Located in the southwestern Black Hills with excellent schools, both summer and winter recreational activities, no crime, and no state income tax. An excellent benefit package includes liberal vacation and sick leave, federal retirement/social security, health and life insurance programs, and malpractice insurance. Call or write Chief of Staff, VA Medical Center, Hot Springs, SD 57747; (605) 745-2049. 2-4a

**THE MALLINCKRODT INSTITUTE OF RADIOLOGY AT THE WASHINGTON UNIVERSITY SCHOOL OF MEDICINE** announces a faculty position in the section of vascular and interventional radiology. The Mallinckrodt Institute of Radiology provides radiology services to Barnes Hospital and St. Louis Children's Hospital, comprising approximately 1300 beds. The vascular and interventional section is involved in all aspects of vascular and nonvascular interventional radiology. We currently perform approximately 5700 procedures/yr. A major remodeling effort is under way at the Institute. This includes 4 new special procedure rooms. Excellent facilities are available for clinical and animal research. If you are interested in an academic position in a rapidly developing interventional section, please contact Daniel Picus, M.D., Chief, Vascular and Interventional Radiology, Mallinckrodt Institute of Radiology, 510 S. Kingshighway Blvd., St. Louis, MO 63110; (314) 362-2900. 2-4a

**DIRECTOR OF CLINICAL MAGNETIC RESONANCE**—The Dept. of Radiology at the University of Texas Medical School at Houston has an opening for a radiologist at the assistant, associate, or full professor level, who will direct clinical activities, medical student and resident teaching, and clinical research in the university MRI center at Hermann Hospital. Candidate will be expected to conduct or direct clinical or basic research in MR leading to grant support. Candidates must have demonstrated experience in direction of a clinical MRI unit, teaching, research, writing, and obtaining grant support, and have a strong publication background. Candidate must be board-certified by the ABR and must have a Texas medical license. Compensation will be based on the most recent AAMC survey and candidate's qualifications. Please forward a CV, and the names and addresses of 3 references, to John H. Harris, Jr., M.D., D.Sc., Professor and Chairman, Dept. of Radiology, The University of Texas Medical School at Houston, 6431 Fannin, Ste. 2.132, Houston, TX 77030. The University of Texas Health Science Center at Houston is an equal opportunity employer and encourages women and minority candidates to apply. 1-6a

**DIAGNOSTIC RADIOLOGY**—Progressive 4-member group in Sacramento, CA, seeks BC/BE radiologist. Should be familiar with all imaging modalities. Practice includes 220-bed hospital and outpatient office. Competitive salary leading to early partnership. Generous benefit package. Send CV to Fred L. Stargardter, M.D., American River Radiology Medical Group, Inc., 3637 Mission Ave., #5, Carmichael, CA 95608. 2-4ap

**DIAGNOSTIC RADIOLOGIST WITH SPECIAL INTEREST IN ANGIOGRAPHY AND INTERVENTIONAL RADIOLOGY**—The Dept. of Radiology at the University of Texas Medical School at Houston has an immediate opening at the Hermann Hospital, and an opening for July 1, 1990, at the Lyndon Baines Johnson General Hospital, for an experienced interventionist/angiographer with strong interest in patient care and teaching. Research interest and experience are important, but not essential. Although the principal responsibilities will be in intervention/angiography, there will be an opportunity to be involved in other clinical areas of the candidate's interest. The position will include teaching at the medical student and resident levels. Candidate must be a diplomate of the ABR and have completed at least a 1-yr interventional/angiography fellowship, have a Texas state medical license, and have had at least 1 yr postfellowship experience. Candidates with the qualifications for a senior assistant professor or associate professor appointment are preferred. Academic rank will be commensurate with qualifications. Compensation will be based on the most recent AAMC survey and the candidate's qualifications and experience. Please submit CV, along with the names and addresses of 3 references, to John H. Harris, Jr., M.D., D.Sc., Professor and Chairman, Dept. of Radiology, The University of Texas Medical School at Houston, 6431 Fannin, Ste. 2.132, Houston, TX 77030. The University of Texas Health Science Center at Houston is an equal opportunity employer. Women and minorities are encouraged to apply. 1-6a

**ASSISTANT, ASSOCIATE, OR FULL PROFESSOR OF DIAGNOSTIC RADIOLOGY**—The University of Texas Medical School at Houston has an opening for a general diagnostic radiologist to perform clinical radiologic exams and procedures and to participate in resident and medical student teaching. Candidates should have completed an approved residency in diagnostic radiology. Postresidency experience or training would be preferable, but not mandatory, at the assistant professor level. Candidates must be board-certified by the ABR, or equivalent, and must have a Texas medical license. Compensation will be based on the most recent AAMC survey and the candidate's qualifications. Applicants should send a CV, along with the names and addresses of 3 references, to John H. Harris, Jr., M.D., D.Sc., Professor and Chairman, Dept. of Radiology, The University of Texas Medical School at Houston, 6431 Fannin St., Ste. 2.132, Houston, TX 77030. The University of Texas Health Science Center at Houston is an equal opportunity employer and encourages women and minority candidates to apply. 1-6a

**SEATTLE AREA**—Opening for a BC general diagnostic radiologist with basic angio and interventional skills. Washington license not required. Teaching hospital, regular hours, limited call, and 5-yr contract. Call G. Bernstein, M.D.; (206) 840-9652. 4-6xa

**OPPORTUNITY FOR YOUNG, WELL-TRAINED, AGGRESSIVE RADIOLOGIST** to join 5-person group in a small, midwestern city near St. Louis. Excellent equipment including mobile MRI. Competitive salary leading to early partnership. Reply to Box U40, AJR (see address this section). 4xa

**NEURORADIOLOGIST/MRI**—Two positions available; Fellowship training a necessity. Group of 7 radiologists seek BC colleague in multihospital practice. Must be capable as general diagnostic radiologist as well. Position available July 1990. Send letter and CV to Neel E. Bennett, M.D., Medical Director and Chairman, Dept. of Radiology, Holy Cross Hospital, 1050 E. South Temple, Salt Lake City, UT 84102; (801) 350-4636. 4xa

**SITKA, ALASKA**—Challenging diagnostic radiology practice, JCAHO-accredited Alaska Native Indian Health Service Hospital. Includes ultrasound and mammography. Close professional association with primary-care physicians. Requires acceptance in USPHS Commissioned Corps. Send inquiries, CV, and references to S. Carlson, M.D., Clinical Director, Mt. Edgecumbe Hospital, 222 Tongass Dr., Sitka, AK 99835; (907) 966-8370. 1-5ap

**DIAGNOSTIC RADIOLOGIST**—The University of Tennessee, Memphis/University Physicians Foundation has an opening for a radiologist at the instructor or assistant professor level. Applicant must be board-certified/eligible in diagnostic radiology. Subspecialty interests are encouraged but not required. Blacks, women, handicapped, and other minorities are encouraged to apply. University of Tennessee, Memphis/University Physicians Foundation is an equal employment opportunity/affirmative action/Title IX/Section 504 employer. Send CV to Barry Gerald, M.D., Chairman, Dept. of Radiology, University of Tennessee, Memphis, 800 Madison Ave., Memphis, TN 38163. 4xa

**ASSISTANT OR ASSOCIATE PROFESSOR OF NEURORADIOLOGY**—The University of Texas Medical School at Houston has openings for neuroradiologists at the Lyndon Baines Johnson General Hospital and the Hermann Hospital to perform clinical neuroradiology and participate in resident and medical student teaching. Candidates must have completed an approved residency in diagnostic radiology and a 2-yr neuroradiology fellowship. Candidates must be board-certified by the ABR, or equivalent, and must have a Texas medical license. Compensation will be based on the most recent AAMC survey and the candidate's qualifications. Applicants should send a CV, along with the names and addresses of 3 references, to John H. Harris, Jr., M.D., D.Sc., Professor and Chairman, Dept. of Radiology, The University of Texas Medical School at Houston, 6431 Fannin St., Ste. 2.132, Houston, TX 77030. The University of Texas Health Science Center at Houston is an equal opportunity employer and encourages women and minority candidates to apply. 1-6a

**ASSISTANT, ASSOCIATE, OR FULL PROFESSOR OF THORACIC RADIOLOGY**—The University of Texas Medical School at Houston has an opening for a thoracic radiologist to perform clinical thoracic radiology exams and procedures and participate in resident and medical student teaching. Candidates should have completed an approved residency in diagnostic radiology and must have postresidency experience or training in thoracic radiology. Candidates must be board-certified by the ABR, or equivalent, and must have a Texas medical license. Compensation will be based on the most recent AAMC survey and the candidate's qualifications. Applicants should send a CV, along with the names and addresses of 3 references, to John H. Harris, Jr., M.D., D.Sc., Professor and Chairman, Dept. of Radiology, The University of Texas Medical School at Houston, 6431 Fannin St., Ste. 2.132, Houston, TX 77030. The University of Texas Health Science Center at Houston is an equal opportunity employer and encourages women and minority candidates to apply. 1-6a

**FACULTY POSITIONS AVAILABLE IN DIAGNOSTIC RADIOLOGY**—On July 1, 1990, the faculty of the University of Texas Medical School at Houston (UTMSH) will assume clinical practice, teaching, and research at the Lyndon Baines Johnson (LBJ) General Hospital, newly constructed by the Harris County Hospital District, in Houston, TX. LBJ General will be a principal medical student teaching affiliation of the UTMSH, is certified for 300 beds (with expansion capabilities to approximately 500 beds) and is projected to perform approximately 130,000 imaging procedures the first yr. The Dept. of Radiology at LBJ is fully equipped with new, state-of-the-art GE equipment, including a 9800 Quick CT scanner with 3-D software and an LU angiographic unit, and comparable routine, R&F, ultrasound, and nuclear equipment. Full-time UTMSH faculty positions exist for 5 associate professors and 10 assistant professors with clinical, teaching, and research interests in all aspects of diagnostic imaging. Residents who have just completed training and are board-certified will be offered the rank of assistant professor at an annual salary of \$90,000. Fellows who have completed training and are board-certified will be offered the rank of assistant professor at an annual salary of \$100,000. These salaries may be increased depending on the candidate's education and experience beyond either residency or fellowship, and in addition to base salary, total fringe benefits of approximately 20% of the base salary will be provided. Associate professor compensation will be based on the most recent AAMC survey and the candidate's qualifications. Candidates must be diplomates of the ABR, or its equivalent, and must have a Texas medical license. Applicants are requested to send their CV to John H. Harris, Jr., M.D., D.Sc., Professor and Chairman, Dept. of Radiology, The University of Texas Medical School at Houston, 6431 Fannin St., Ste. 2.132, Houston, TX 77030. The University of Texas Health Science Center at Houston is an equal opportunity employer. Women and minorities are encouraged to apply. 1-6a

**RADIOLOGIST, TYLER, TX**—The University of Texas Health Center at Tyler, Dept. of Radiology, Tyler, TX, invites applications for a faculty position at the level of assistant or associate professor, to open July 1, 1990. Interest in teaching and/or research is desired but not required. Progressive, 4-person dept. practices general radiology including interventional, with a total of 27,000 exams/yr. The University of Texas Health Center at Tyler, the state's designated chest disease hospital, is located just outside of Tyler on a beautiful, 600-acre campus amid the forests and lakes of East Texas. The dept. also supports a rapidly growing, dynamic research group located on campus in a new, state-of-the-art research facility. Year-round tennis, golf, and boating are available in addition to excellent schools. Competitive first-yr salary and an unsurpassed benefits package are offered. Send CV to J. R. Shepherd, M.D., University of Texas Health Center at Tyler, P. O. Box 2003, Tyler, TX 75710; (214) 877-7100. The University of Texas Health Center at Tyler is an affirmative action, equal opportunity employer. Minorities are encouraged to apply. 12-5a

**GENERAL RADIOLOGIST** needed July 1, 1990, or sooner to replace retiring member of 3-person group servicing a small but busy hospital in scenic area of western Pennsylvania; also own private outpatient office. Necessary skills: general, CT, ultrasound, mammography, and nuclear medicine. Generous salary with early advancement to partnership available. Contact Alan Stankiewicz, M.D., 623 Lang Ave., Patton, PA 16668; (814) 674-8508. 12-5ap

**MRI RADIOLOGIST NEEDED**—A position will be available July 1, 1990, at Good Samaritan Regional Medical Center in Phoenix, AZ. The hospital is a 750-bed, tertiary-care facility offering the most up-to-date radiology services. The radiology group is seeking to add a new associate who is board-certified and has at least 1 yr of MR fellowship training. Responsibilities primarily include body MR interpretation. The hospital will have 2 high-strength magnets and there also will be a midstrength magnet at a satellite office. The position offers an academic-style practice with the benefits of a private radiology group. A competitive salary and benefits are offered leading to partnership. Please contact Ted Ditchek, M.D., or Aubrey Palestrant, M.D.; (602) 239-4601. 1-4ap

**ULTRASOUND RADIOLOGIST**—The University of Tennessee, Memphis/University Physicians Foundation has an opening for a radiologist in ultrasound at the instructor or assistant professor level. Applicant must be board-certified/eligible in diagnostic radiology. Additional training in ultrasound is highly desirable and the applicant should be particularly conversant with obstetric ultrasonography. Blacks, women, handicapped, and other minorities are encouraged to apply. The University of Tennessee, Memphis/University Physicians Foundation is an equal employment opportunity/affirmative action/Title IX/Section 504 employer. Send CV to Barry Gerald, M.D., Chairman, Dept. of Radiology, University of Tennessee, Memphis, 800 Madison Ave., Memphis, TN 38163. 4xa

**PEDIATRIC RADIOLOGIST**—The University of Tennessee, Memphis/University Physicians Foundation has an opening for a pediatric radiologist. Faculty rank of assistant or associate professor based on experience. Applicant must be board-certified/eligible in diagnostic radiology. At least 1 yr of postgraduate training in a recognized program in pediatric radiology is required. Primary work sites will be LeBonheur Children's Medical Center and St. Jude Children's Research Hospital. Blacks, women, handicapped, and other minorities are encouraged to apply. The University of Tennessee, Memphis/University Physicians Foundation is an equal employment opportunity/affirmative action/Title IX/Section 504 employer. Address inquiries to Barry Fletcher, M.D., Chairman, Diagnostic Imaging Dept., St. Jude Children's Research Hospital, 332 N. Lauderdale, Memphis, TN 38101, or Robert A. Kaufman, M.D., Director, Dept. of Radiology, The University of Tennessee, Memphis/LeBonheur Children's Medical Center, 800 Madison Ave., Memphis, TN 38163. 4xa

**DIAGNOSTIC RADIOLOGIST**—Progressive, 4-member group in eastern North Carolina seeks BC/BE radiologist. ACR-accredited practice includes 350-bed regional referral hospital, outpatient office, and women's diagnostic center. State-of-the-art equipment. Excellent financial package. Send letter and CV to Box W8, AJR (see address this section). 11-4ap

**NORTHERN CALIFORNIA/SAN FRANCISCO BAY AREA**—The Permanente Medical Group is seeking a BC radiologist with multimodality interests and fellowship training in MR or interventional radiology to join a 10-person group serving a 337-bed acute-care hospital and 2 outpatient clinics. Teaching opportunities are available with residents of subspecialty services on rotation from Stanford University Hospital and our own medical residents. We are currently siting a GE 1.5-T MRI system and installing a new LU arm. Competitive salary and excellent benefits. Please send inquiries and CV to Bruce Baker, M.D., Chief, Dept. of Radiology, Kaiser-Permanente Medical Center, 900 Kiely Blvd., Santa Clara, CA 95051; (408) 236-4444. EOF. 2-4a

**THE OREGON HEALTH SCIENCES UNIVERSITY**, Dept. of Radiology, Portland, OR, invites applications for faculty positions in MRI, neuroradiology, general radiology, skeletal radiology, vascular and interventional radiology, GU radiology, pediatric radiology, computed body tomography, and ultrasound. A second Ph.D. NMR scientist also is being sought. The Oregon Health Sciences University is an affirmative action, equal opportunity employer. Send CV to Richard W. Katzberg, M.D., Chairman of Diagnostic Radiology, L340, The Oregon Health Sciences University, 3181 S.W. Sam Jackson Park Rd., Portland, OR 97201-3098. 5-44p

**DIAGNOSTIC RADIOLOGIST**—Immediate opening for a board-certified/eligible general diagnostic radiologist at the VA Medical Center, Atlanta, GA. Must be proficient in body CT, ultrasound, and related interventional procedures. We offer a full range of federal employee benefits. Qualified applicants will receive a clinical faculty appointment at the Emory University Medical School. For further information, call Jeanie McCleary at (404) 728-7637 or write VA Medical Center, 1670 Clairmont Rd., Atlanta (Decatur), GA 30033. EOE. 1-4a

**IMMEDIATE UNEXPECTED OPENING FOR BE/BC DIAGNOSTIC RADIOLOGIST** to join 5-man group in Missoula, MT, a university city of 50,000, located in mountainous, western Montana. Looking for a general radiologist with proficiency in MRI, ultrasound, CT, angiography, etc. Administrative skills preferable. Our group of 6 full-time radiologists covers both of Missoula's hospitals (210 and 130 beds). Progressive medical environment with 100+ physicians. One yr to full partner income and 2 yr to partnership. Abundant, nearby recreational opportunities including skiing, fishing, backpacking, hunting, etc. Send CV to Missoula Radiology, Inc., P. O. Box 2039, Missoula, MT 59806. 3-44p

**THE RADIOLOGY DEPT.**, University of Massachusetts Medical Center, is seeking a full-time radiologist with interest in trauma, emergency room, and musculoskeletal radiology. The Medical Center is a 370-bed university hospital and medical school located in Worcester, MA, approximately 40 mi. west of Boston. The dept. consists of 19 clinical staff, 12 residents, and 3 fellows and sees approximately 120,000 exams/yr. The dept. is well-equipped with 2 fourth-generation CT scanners, two 1.5-T GE MR scanners, and a 2.0-T small-bore unit for animal research. The hospital is a major trauma center and is serviced by 2 Life Flight helicopters. The candidate must be board-eligible/certified and have a clinical background in skeletal radiology. Please send CV/requests to Dr. Edward H. Smith, Chair, Dept. of Radiology, University of Massachusetts Medical Center, 55 Lake Ave. N., Worcester, MA 01655. The University of Massachusetts Medical Center is an equal opportunity employer. 3-5a

**ULTRASOUND/CT/MRI**—Opportunity for board-certified radiologist specializing in ultrasound, body CT, and body MRI to pursue academic career at The New York Hospital-Cornell Medical Center. Dept. provides state-of-the-art equipment, including Acuson ultrasound, GE 9800 CT, and GE Signa 1.5-T MR. Wide variety of ultrasound exams include abdominal, OB-GYN, color Doppler, small parts, neonatal head, transvaginal, and transrectal. Prefer candidate with prior fellowship in sectional imaging or ultrasound. Responsibilities include clinical practice, teaching, and research. Position available 7/1/90 or earlier. Please send CV to Elias Kazam, M.D., Dept. of Radiology, The New York Hospital-Cornell Medical Center, 525 E. 68th St., New York, NY 10021. 4-6ap

## Positions Desired

**GENERAL DIAGNOSTIC RADIOLOGIST**—Board-certified, MRI fellowship. Four yr angio/interventional experience in busy practice. Prefer general diagnostic with some subspecialization. Competent in nuclear medicine and ultrasound. Desire partnership opportunity. Impeccable references. Available July 1990. Reply Box Y52, AJR (see address this section). 3-6bp

## Fellowships and Residencies

**MARYLAND FELLOWSHIPS**—The University of Maryland School of Medicine at Baltimore is accepting applications for fellowships beginning July 1, 1991. One-yr fellowships are available in angio/interventional, CT/ultrasound/MRI, neuroradiology, and trauma and critical care. The University of Maryland offers competitive salaries, ample time for academic pursuits, and funding for continuing medical education. Board certification in radiology is desired, board eligibility is required. Additional information regarding each fellowship is available by calling (800) 866-8667, ext. 3477. Affirmative action/equal opportunity employer encourages applications from members of minority groups. 4 & 7cp

**FELLOWSHIP IN ONCOLOGIC IMAGING**—A 1- or 2-yr fellowship is available in diagnostic imaging at St. Jude Children's Research Hospital. Equipment in recently renovated dept. includes new radiographic and fluoroscopic rooms, ultrasound with pulsed Doppler, gamma camera and whole body SPECT nuclear imagers, CT scanner, and 1.0-T MRI system. 1.5/2.0-T MRI/S system to be installed summer 1990. St. Jude Children's Research Hospital is dedicated to research and care of children with catastrophic diseases and is the world's largest center for pediatric malignant diseases. Fellows must have completed radiology training leading to FRCP, ABR, or equivalent diplomas. Interested candidates should write to Barry D. Fletcher, M.D., Chairman, Dept. of Diagnostic Imaging, St. Jude Children's Research Hospital, 332 N. Lauderdale, P. O. Box 318, Memphis, TN 38101-0318. Affirmative action/equal opportunity employer. 4c

**IMAGING FELLOWSHIP (CT, ULTRASOUND, MRI)**—William Beaumont Hospital, a 970-bed, modern, tertiary-care, teaching and academic institution in southeast Michigan, offers a 1-yr fellowship in sectional body imaging. The fellowship will provide extensive clinical experience in body CT, ultrasound, and MRI, including CT- and ultrasound-guided procedures, conventional and color flow Doppler exams, prostatic and endovaginal sonography. Ample elective time is also provided for other rotations of interest to fellow. Candidates must be board-certified or board-eligible in diagnostic radiology and have a valid Michigan medical license. Four positions are available for July 1991. Salary and fringe benefits are highly competitive. For further information, write to Ali Shirkhoda, M.D., Chief of Imaging Division, William Beaumont Hospital, 3601 W. 13 Mile Rd., Royal Oak, MI 48073; (313) 551-1001. 4-6c

**THE UNIVERSITY OF PITTSBURGH** offers fellowships in angiography/interventional radiology, abdominal imaging (CT/ultrasound/MRI), neuroradiology, pediatric radiology, and MRI. Positions in all of these areas are available to begin July 1991. A fellowship position in pediatric radiology and 1 in abdominal imaging are also available to begin July 1990. Interested applicants should send letters of inquiry and CV to Lawrence A. Cooperstein, M.D., Dept. of Radiology, Presbyterian-University Hospital, DeSoto at O'Hara Sts., Pittsburgh, PA 15213. 3-7cp

**NEURORADIOLOGY FELLOWSHIP, THOMAS JEFFERSON UNIVERSITY HOSPITAL**—An unexpected opening for a neuroradiology fellow is available in the Dept. of Radiology at Thomas Jefferson University Hospital, beginning July 1990. The Division of Neuroradiology has close clinical and research relationships with Jefferson's very active neurology, neurosurgery, orthopedic surgery, and otolaryngology depts. Complete training in ENT radiology is part of this program. Five full-time faculty members currently staff this division. Clinical facilities include 2 dedicated CT scanners, a myelography room, a biplane angiography room with DSA, and a GE 1.5-T MRI unit. Two more MRI units will be operational by the summer of 1990. Contact Carlos Gonzalez, M.D., Director of Neuroradiology, 1009 Main Bldg., Thomas Jefferson University Hospital, Philadelphia, PA 19107; (215) 928-5447. Jefferson is an affirmative action/equal opportunity employer. 4xc

**FELLOWSHIPS AT THOMAS JEFFERSON UNIVERSITY HOSPITAL**—The Dept. of Radiology at Thomas Jefferson University Hospital in Philadelphia offers 6 different fellowship programs each yr: ultrasound/CT/MRI - contact Barry Goldberg, M.D.; cardiovascular/interventional - contact Geoffrey Gardiner, Jr., M.D.; neuroradiology/ENT - contact Carlos Gonzalez, M.D.; chest/breast imaging - contact Robert Steiner, M.D. or Stephen Feig, M.D.; MRI - contact Matthew Rifkin, M.D.; and musculoskeletal (including MRI) - contact David Karasick, M.D. We have a large and well-equipped dept. performing 180,000 exams/yr. Our ultrasound division occupies a spacious new facility and provides training in all phases of ultrasound, including obstetrical, vascular, lithotripsy, and endoluminal. The dept. has 3 modern CT scanners and operates 3 GE 1.5-T MRI units also. The interventional radiology division recently has opened an entirely new angio suite housing state-of-the-art Philips units with DSA. This division performs the full range of both vascular and nonvascular interventional procedures. The neuroradiology division is housed in a neurosciences imaging center containing all imaging modalities in a single comprehensive facility. A large new breast imaging center now operates 5 mammography units and performs breast ultrasound studies also. All program directors listed above can be contacted at the Dept. of Radiology, Thomas Jefferson University Hospital, Philadelphia, PA 19107. Jefferson is an equal opportunity/affirmative action employer. 4xc

**FELLOWSHIPS IN ABDOMINAL IMAGING**—The Dept. of Radiology at the University of Texas Medical School at Houston has openings for 2 abdominal imaging fellowships to begin July 1991. Under faculty direction and supervision, candidates will further their training in the specialty of abdominal imaging including CT, ultrasound, and MRI through 4-mo rotations in each service. Candidate will participate in teaching in each section at the medical student and resident levels, will have the opportunity to conduct basic or clinical research, and will be expected to prepare and submit at least 1 scientific article to an appropriate refereed journal. Candidate must be a graduate of an approved U.S. medical school or its equivalent, must have completed an approved residency in diagnostic radiology, must be a diplomate of the ABR, and must have a Texas medical license. Please submit CV, along with the names and addresses of 3 references, to John H. Harris, Jr., M.D., D.Sc., Professor and Chairman, Dept. of Radiology, The University of Texas Medical School at Houston, 6431 Fannin St., Ste. 2.132, Houston, TX 77030. The University of Texas Health Science Center at Houston is an equal opportunity employer. Women and minorities are encouraged to apply. 1-6c

**FELLOWSHIP IN PEDIATRIC RADIOLOGY—**

LeBonheur Children's Medical Center/St. Jude Children's Research Hospital/The University of Tennessee, Memphis/University Physicians Foundation, Inc. combined program in pediatric radiology offers a 1- or 2-yr fellowship in pediatric radiology. There are approximately 75,000 pediatric exams performed annually by 10 full-time radiologists. Two fellowship positions are available annually. Training includes all aspects of pediatric imaging, including neonatal, neuro, nuclear, oncologic, cardiovascular, special and interventional procedures, ultrasound, CT, and MRI. Facilities include Doppler ultrasound, CT, and MRI. Opportunity to participate in MRI and other imaging research. Blacks, women, handicapped, and other minorities are encouraged to apply. The University of Tennessee, Memphis/University Physicians Foundation, Inc. is an equal employment opportunity/affirmative action/Title IX/Section 504 employer. Address inquiries to Barry D. Fletcher, M.D., Chairman, Diagnostic Imaging Dept., St. Jude Children's Research Hospital, 332 N. Lauderdale, Memphis, TN 38101 or Robert A. Kaufman, M.D., Director, Dept. of Radiology, LeBonheur Children's Medical Center/The University of Tennessee, Memphis, 800 Madison Ave., Rm. 114C Chandler, Memphis, TN 38163. 4xc

**PEDIATRIC RADIOLOGY FELLOWSHIP, IMMEDIATE OPENING—**

Position available for fellowship in pediatric radiology, 1 or 2 yr, beginning on July 1, 1990, or July 1, 1991. Full training with abundant hands-on experience with all imaging modalities. Supported by strong Dept. of Pediatrics with a good mixture of patient material. Excellent teaching on a 1-to-1 basis and ample opportunity for pursuing academic interests. Apply to Leonard E. Swischuk, M.D., Dept. of Radiology, The University of Texas Medical Branch, Child Health Center, C-65, Galveston, TX 77550; (409) 761-2096. UTMB is an equal opportunity M/F/H/V affirmative action employer. UTMB hires only individuals authorized to work in the United States. 2-4c

**PEDIATRIC RADIOLOGY FELLOWSHIP—**

The Dept. of Radiology at Children's Hospital of Philadelphia (CHOP) offers a 1- or 2-yr pediatric radiology fellowship beginning July 1, 1990. CHOP is a 294-bed pediatric hospital. Radiology has an attending faculty of 11 and performs 80,000 cases/yr (plain films, fluoroscopy, ultrasound, CT, nuclear medicine, neuroradiology, angiography/interventional radiology, and MRI). Our equipment is state-of-the-art and new since 1988, including ATL ultrasound equipment, with duplex and color-flow Doppler, gamma camera with SPECT, and a high-resolution fast Siemens Somatom Plus CT scanner. A 1.5-T Siemens Magnetom MRI installation devoted to children has recently opened. We have an active teaching program for radiology residents and fellows. The patient population is large and varied, from routine emergencies to complicated tertiary-care problems. The fellowship provides not only a broad clinical experience with subspecialty training but offers opportunities for clinical and basic research and scholarship. Applicants must have completed a diagnostic radiology residency, be board-certified or eligible, and must obtain a Pennsylvania medical license. Special (1-yr) cross-sectional imaging (CT, ultrasound, and MRI) fellowships negotiable also. Salary and fringe benefits are highly competitive. Address inquiries to Sandra S. Kramer, M.D., Dept. of Radiology, The Children's Hospital of Philadelphia, 34th St. and Civic Center Blvd., Philadelphia, PA 19104; (215) 590-2575. The Children's Hospital of Philadelphia and the University of Pennsylvania are equal opportunity/affirmative action employers. 2-4cp

**FELLOWSHIP POSITIONS—**Applications are invited now for July 1991. Positions are available in neuroradiology, vascular/interventional radiology, and body imaging (CT/ultrasound/MRI). For information, contact James R. Schmidgall, M.D. or Richard W. Katzberg, M.D., Chairman, Dept. of Radiology, L-340, Oregon Health Sciences University, 3181 S. W. Sam Jackson Park Rd., Portland, OR 97201. 7-6c

**MRI FELLOWSHIP AT THOMAS JEFFERSON UNIVERSITY HOSPITAL—**

A new MRI fellowship position has been created in the Dept. of Radiology of Thomas Jefferson University Hospital, Philadelphia. This 1-yr position encompasses a full range of clinical and research activities. The MRI division includes 6 staff physicians, 2 MRI physicists, and 3 Signa systems (1.5T). The position is available as of Jan. 1990, but applications will also be taken for the academic year beginning in July 1990. Send inquiries to Matthew Rifkin, M.D., Dept. of Radiology, Thomas Jefferson University Hospital, Philadelphia, PA 19107. Jefferson is an equal opportunity/affirmative action employer. 9-6c

**CARDIOVASCULAR-INTERVENTIONAL RADIOLOGY FELLOWSHIP—**

Available July 19, 1989. One-year fellowship program at a 750-bed teaching hospital. Extensive clinical experience involving all aspects of cardiovascular imaging, interventional vascular and nonvascular procedures, and availability for clinical or animal research. Send CV and Inquiries to Oscar H. Gutierrez, M.D., Dept. of Radiology, Box 648, University of Rochester Medical Center, Rochester, NY 14642. An equal opportunity employer (M/F). 1-6c

**A FELLOWSHIP IN VASCULAR/INTERVENTIONAL RADIOLOGY**

is offered at the University of Maryland beginning July 1, 1990. The fellow will participate in all aspects of diagnostic vascular radiology, as well as nonvascular interventional procedures, including percutaneous and laser angioplasty, embolization, biliary and GU intervention, and insertion of IVC filters. Contact Gerald S. Johnston, M.D., Dept. of Diagnostic Radiology, 22 S. Greene St., Baltimore, MD 21201. 4cp

**FELLOWSHIPS IN PEDIATRIC RADIOLOGY, JULY 1991—**

The Dept. of Radiology, Children's Hospital Medical Center, Cincinnati, OH, offers 1- or 2-yr fellowships in pediatric radiology beginning July 1991. Children's Hospital Medical Center is a 355-bed institution where approximately 700,000 radiological exams are performed annually by 13 full-time faculty radiologists. Four fellowship positions are available annually. Training includes all aspects of pediatric imaging: neonatal radiology, neuroimaging, musculoskeletal radiology, cardiovascular and thoracic imaging, abdominal imaging, oncologic imaging, ultrasonography, nuclear medicine, CT, MRI, and vascular/interventional techniques. Facilities include digital fluoroscopy, Acuson and ATL ultrasound units with Doppler and color-flow Doppler capabilities, Gamma and SPECT tomographic nuclear cameras, GE 9800 Quick CT scanner, 1.5-T GE MRI, and cardiac catheterization/angiographic suite with digital vascular imaging. Numerous opportunities to participate in both clinical and basic research. Salary and fringe benefits are highly competitive. Candidates must be board-certified or board-qualified in diagnostic radiology and must be able to obtain an Ohio medical license. Children's Hospital Medical Center and the University of Cincinnati College of Medicine are affirmative action/equal opportunity employers. Address inquiry and CV to Donald R. Kirks, M.D., Director, Dept. of Radiology, Children's Hospital Medical Center, Elland and Bethesda Aves., Cincinnati, OH 45229-2899; (513) 559-8058. 1-12cp

**ANGIOGRAPHY/INTERVENTIONAL RADIOLOGY FELLOWSHIP—**

New York Medical College will offer a 1-yr fellowship to begin July 1, 1991. The program includes training in all phases of diagnostic angiography and interventional radiologic techniques. Training is based at Westchester County Medical Center, a 650-bed, tertiary-care center located on the medical college campus in a prestigious suburban setting only about 1/2 hr from New York City. Active participation in clinical management of patients is emphasized. Approximately 900 procedures were performed in 1989. Current research interests include transmesenteric sclerosis of portal varices and hepatic arterial chemoembolization. A new digital interventional suite will open in February 1990. A digital biplane imaging suite is anticipated before July 1991. For additional information and application, contact Stuart Katz, M.D., Dept. of Radiology, New York Medical College, Valhalla, NY 10595; (914) 285-8388. 2-4c

**FELLOWSHIPS IN NEURORADIOLOGY—**

The Dept. of Radiology at the University of Texas Medical School at Houston has openings for 1- and 2-yr neuroradiology fellowships to begin July 1990 and July 1991. Under faculty supervision, candidates will be responsible for neuroradiologic exams and procedures (i.e., angiograms, myelograms, CT, MR imaging, and in vivo spectroscopy). The candidate will participate in teaching at the medical student and resident levels and will conduct basic or clinical research. Candidate must be a graduate of an approved U.S. medical school or its equivalent, must have completed an approved residency in diagnostic radiology, must be a diplomate of the ABR, and must have a Texas medical license. Please submit CV, along with the names and addresses of 3 references, to John H. Harris, Jr., M.D., D.Sc., Professor and Chairman, Dept. of Radiology, The University of Texas Medical School at Houston, 6431 Fannin St., Ste. 2.132, Houston, TX 77030. The University of Texas Health Science Center at Houston is an equal opportunity employer. Women and minorities are encouraged to apply. 1-6c

**FELLOWSHIP IN ULTRASOUND AND BODY CT/MRI—**

July 1, 1991 to June 30, 1992, at the New York Hospital/Cornell Medical Center. Dept. provides state-of-the-art equipment, including Acuson ultrasound, GE 9800 CT, and GE Signa 1.5-T MR. Wide variety of ultrasound exams include abdominal, OB-GYN, color Doppler, small parts, neonatal head, transvaginal, and transrectal. Applicants should be ABR eligible or certified. Send CV to Elias Kazam, M.D., Dept. of Radiology, The New York Hospital/Cornell Medical Center, 525 E. 68th St., New York, NY 10021. 4-6cp

**Tutorials/Courses**

**5th ANNUAL IMAGING SEMINAR—**Topnotch at Stowe, VT. October 5-8, 1990. Category I accreditation. For information, contact Carol McClure, Coordinator, Dept. of Radiology, Medical Center Hospital of Vermont, 111 Colchester Ave., Burlington, VT 05401; (802) 656-3592. 4-5d

**SIXTH ANNUAL LONDON-PARIS ULTRASOUND CONGRESS, SEPTEMBER 15-22, 1990—**

Category I accreditation followed by OPTIONAL LOIRE VALLEY BICYCLE TOUR. For information contact Medical Seminars International, Inc., 9800 D Topanga Canyon Blvd., Ste. 232, Chatsworth, CA 91311; (818) 700-9821. 3-8d

**ALASKA 90—CRUISE THE INLAND PASSAGE,**

July 6-13, 1990. Patrick Colletti, M.D., University of Southern California, MRI tutorial and course. Category I CME credits. For information, contact Medical Seminars International, Inc., 9800 D Topanga Canyon Blvd., Ste. 232, Chatsworth, CA 91311; (818) 700-9821. 1-6d

## Other

**VISITING PROFESSORSHIP, THOMAS JEFFERSON UNIVERSITY HOSPITAL**—The Dept. of Radiology at Thomas Jefferson University Hospital in Philadelphia offers a visiting professorship in our Division of General Diagnostic Radiology. The position commences July 1990 and will be available for 2 yr, while several of our faculty members are on sabbatical leave. Funding for the position is appropriate for a senior faculty member from another institution on sabbatical with partial funding or for a junior faculty member. In addition to working in the General Diagnostic Division, the visiting radiologist will have access, for research or educational purposes, to state-of-the-art MRI, CT, and ultrasound units, and to well-equipped physics and physiology research laboratories. Liberal research time will be available. Interested individuals should contact David C. Levin, M.D., Chairman, Dept. of Radiology, Thomas Jefferson University Hospital, Philadelphia, PA 19107. Jefferson is an equal opportunity/affirmative action employer. 11-10e

## AJR Classified Advertisements Information

### Box Responses and Address for Ad Placement

Write Box \_\_\_\_\_, AJR, 2223 Avenida de la Playa, Suite 200, La Jolla, CA 92037-3218; (619) 459-2229; FAX: (619) 459-8814.

### How to Place an Ad

AJR accepts classified advertising for Positions Available, Positions Desired, Fellowships and Residencies, and Tutorials/Courses. Ads are accepted by mail or FAX.

**Rates:** \$6.00/line with a \$30 minimum charge. Box service is \$10 additional for each month the ad appears. There are discounts for multiple insertions: 10% for 2-3 insertions; 20% for 4 or more. To estimate lines, count all words and divide by 7.

**Billing:** Ads *must* be prepaid, or advertisers will be billed after the ad appears *providing* a purchase order number is submitted with the advertising copy. Terms are net 30 days.

**Deadlines:** 6 weeks prior to issue date. For specific deadlines, telephone the AJR editorial office.

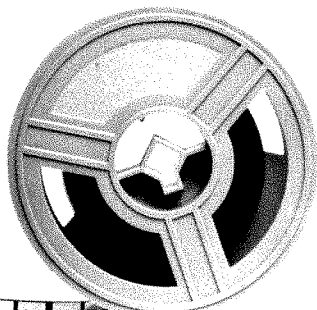
### Estimating Ad Charges

Line charge: divide total words by 7 and multiply by \$6.00	.....	\$	_____
Multiple insertions? If so, multiply by number	.....	x	_____
Subtotal	.....	\$	_____
Discount applies to two or more insertions. Subtract 10% if ad appears 2-3 months, 20% if 4 months or more	.....	-	_____
Subtotal	.....	\$	_____
Box response requested? If so, multiply number of months by \$10.00	.....	+	_____
Approximate advertising charge	.....	\$	_____

# Need shelf space?

**Williams & Wilkins is your source for back issues of this journal in microform.**

Free Up 98%  
Of Your Shelf  
Space With  
Microform  
Conversion



**MICROFILM** editions are available for this journal direct from the publisher. Many Williams & Wilkins journals as well as those journals distributed by the Publishing Services Division of Waverly, Inc., are also available for a single volume year or on a standing order basis.

**FOR ORDERING INFORMATION:**  
Write to the address below or call  
**TOLL FREE 1-800-638-6423.**  
In Maryland call 1-800-638-4007.

☐ **Please send me microform back issue ordering information for**

Journal Name \_\_\_\_\_

Name \_\_\_\_\_

Title \_\_\_\_\_

Address \_\_\_\_\_

City/State/Zip \_\_\_\_\_

**Mail to:**

**Williams & Wilkins**

Microform Sales

Attention: Yvonne Hahn

428 East Preston Street

Baltimore, MD 21202

-or-

The Broadway Centre

2-6 Fulham Broadway

London SW6 1AA England

**Formats available:**

- 16-mm reel
- 35-mm reel
- 16-mm cartridge (3M or Kodak)
- positive or negative film

MICA92 1193

## INDEX TO ADVERTISERS

Aramco Services Company .....	A2
Berlex Laboratories .....	A9-A12
Braintree Laboratories, Inc. ....	Cover 3
University of California .....	A8
E-Z-EM, Inc. ....	Cover 2
General Electric Medical .....	A6-A7
GuthrieClinic Ltd. ....	A8
Kaiser Permanente .....	A8
J.B. Lippincott Company .....	A13
Mallinckrodt, Inc. ....	A19-A22, A25-A26
Medical Seminars .....	A23
University of Miami .....	A8
Nuclear Associates .....	A17
Oregon Health Sciences .....	A23
Osler Institute .....	A30
S&S X-Ray Products, Inc. ....	A24
U.S. Army .....	A27
Winthrop-Breon Laboratories .....	A15-A16

We try to present an accurate index. Occasionally this may not be possible because of a last-minute change or omission.



# The Osler Institute

## Radiology Review Course

### May 27-June 2, 1990 — Louisville

### September 19-25, 1990 — Chicago

at times and places most convenient for you

#### OBJECTIVES

- Improve basic knowledge and clinical skills in radiology
- Assist residents and fellows to study efficiently
- Prepare recent graduates to meet their next milestones
- Provide practicing radiologists with a review and update

#### METHODS:

- HOME STUDY MATERIALS consisting of a syllabus and assignments with questions and answers
- SEMINAR with projection slides and syllabus
- PRACTICE EXERCISES with oral and written parts

*"The faculty was outstanding. The most pleasant thing was learning a tremendous amount, not only from world-famous authorities but from people who are relatively unknown as well."*

#### RADIOLOGIC PHYSICS

Radiation and Radiology  
X-rays and Imaging  
Fluoroscopy & Tomography  
Computed Tomography  
Ultrasonography  
Magnetic Resonance Imaging  
Quality Assurance

#### NUCLEAR RADIOLOGY

Decay and Detectors  
Statistics and Instrumentation  
Radiopharmaceuticals  
Quality Control & Licensure  
Endocrine Scans & Treatment  
GI, GU, Bone, and Brain  
Liver, Spleen, and Lung  
Ga, In, and Heart

#### CHEST

Infiltrates and Cavities  
Nodules and Masses  
Mediastinum  
Breast

#### CARDIOVASCULAR

Heart and Aorta  
Coronary Arteries  
Peripheral Arteries  
Echocardiography

#### GASTROINTESTINAL

Esophagus and Stomach  
Small Bowel and Colon  
Liver and Gallbladder  
Pancreas and Spleen

#### GENITOURINARY

Kidney and Ureter  
Bladder and Pelvis  
Abdominal Ultrasound  
Ob. and Pelvic Ultrasound

#### BONE AND JOINTS

Tumors and Trauma  
Metabolic and Endocrine  
Infection and Dysplasia  
Articular Disorders

#### NEURO., HEAD AND NECK

Skull and Contents  
Spine, Disc and Cord  
Temporal and Facial Bones  
Sinuses, Larynx and Neck

#### PEDIATRIC

Bones, Joints and Chest  
Gastrointestinal Tract  
Genitourinary Tract  
Central Nervous System  
Cardiovascular System

*"Accommodations were comfortable..."\**

**GOALS AND LOCATION:** These courses are designed, scheduled and located to serve the needs of radiology residents and recent graduates. Home study questions are sent upon registration. The courses include both lectures and question sessions — faculty and students both questioning and answering in practice for what will follow. The early fall courses are more theoretical and the Spring courses are more clinical. Your best value is to repeat the seminar for half price. Please await instructions before purchasing your travel tickets.

*"...and those little extras..."\**

**LOWEST AIR FARES:** Reliable Travel offers you the lowest air fare — often below super-saver rates. Call 1-800-548-8185 and identify yourself with this Osler course.

*"...remarkably complete and pleasant..."\**

**PLACEMENT SERVICE:** For a practice opportunity write or call 1-800-356-7537.

*"...the most education for the money..."\**

#### FEES AND C.M.E. CREDITS:

- Physician or Resident:      Phy.    Res.    hrs.
- May 27: Radiology Physics    \$135    \$ 90    10
- May 28-June 2: Clin. Rad.    \$690    \$460    60
- May 27-June 2: Full Course    \$780    \$520    70
- Repeating course within 3 years:    half price
- Add 10% to fees within 10 days of the course.
- Attendees not in course hotel add \$11/day.
- \$50.00 will reserve your position.
- Most home study material will be mailed after half of the registration fee is received.

*"...home study material was extremely helpful..."\**

**REFUNDS:** Subject to a \$50 fee, refunds will be made up until the seminar begins.

- Cancellation after mailing home study material requires retention of half the fee.

*"I feel [the course] helped me pass..."\**

#### INFORMATION:

Joseph H. Selliken, Jr., M.D.  
THE OSLER INSTITUTE  
1094 Dawn Lane, P.O. Box 2218  
Terre Haute, IN 47802  
(800) 356-7537 or (812) 299-5658

*\* Comments by past Osler participants*

#### Limited Enrollment: RADIOLOGY REVIEW REGISTRATION

Name \_\_\_\_\_  
Address \_\_\_\_\_  
City/State/Zip \_\_\_\_\_  
Phone \_\_\_\_\_ For: ☐ May 27-June 2, '90 — Louisville  
☐ Sept. 19-25, 1990 — Chicago  
☐ Spring 1991 — Louisville

#### Mail today to:

1094 Dawn Lane, Dept. AJR3  
P.O. Box 2218  
Terre Haute, IN 47802

- ☐ Check enclosed for \$ \_\_\_\_\_  
☐ Please send more information

# New look. New shape.

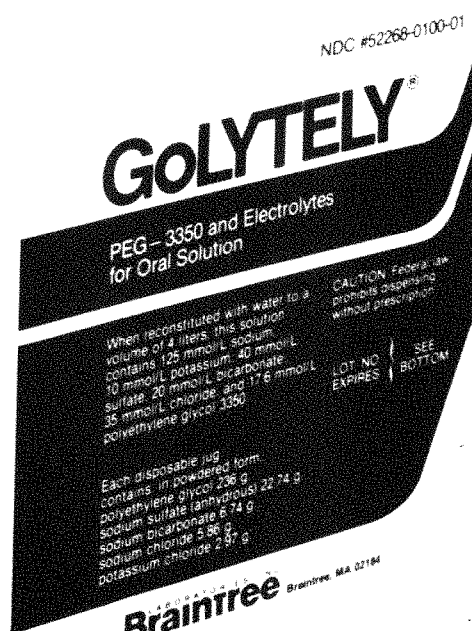
# GoLYTELY<sup>®</sup>

PEG-3350 and Electrolytes for Oral Solution

The name that started  
a revolution now comes  
in a narrow, stackable  
container.

Now GoLYTELY takes up less  
storage space and less space in  
your patient's refrigerator.

More convenient for  
Patients  
Pharmacists  
Physicians  
Nurses



New look.  
New shape.  
**GoLYTELY.**

Made by Lyne Laboratories, Stoughton, MA  
02072, for BRAINTREE LABORATORIES, INC.,  
P.O. Box 361, Braintree, MA 02184.

LABORATORIES • INC  
**Braintree**

© 1989 BRAINTREE LABORATORIES, INC.  
TRE-1039

Circle 35 on the Reader Service Card

## SPECIAL ARTICLES

- 691 Progress in radiology. State of the art: endorectal sonography of the prostate gland. Rifkin MD, Dahnert W, Kurtz AB
- 701 Review article. Radiologic evaluation of the solitary pulmonary nodule. Webb WR

## PULMONARY RADIOLOGY

- 709 Does knowledge of the clinical history affect the accuracy of chest radiograph interpretation? Good BC, Cooperstein LA, DeMarino GB, et al.

## BREAST RADIOLOGY

- 713 New mammography screen/film combinations: imaging characteristics and radiation dose. Kimme-Smith C, Bassett LW, Gold RH, Zheutlin J, Gornbein JA

## GASTROINTESTINAL RADIOLOGY

- 721 Doppler sonography: a noninvasive method for evaluation of hepatic venoocclusive disease. Brown BP, Abu-Yousef M, Farner R, LaBrecque D, Gingrich R
- 725 Fluoroscopically guided percutaneous gastrostomy and gastroenterostomy: analysis of 158 consecutive cases. Hicks ME, Surratt RS, Picus D, Marx MV, Lang EV
- 729 Pictorial essay. Imaging of and intervention for biliary complications after hepatic transplantation. Letourneau JG, Hunter DW, Payne WD, Day DL

## GENITOURINARY RADIOLOGY

- 735 Selective osteal salpingography and transvaginal catheter dilatation in the diagnosis and treatment of fallopian tube obstruction. Lang EK, Dunaway HE Jr, Roniger WE
- 741 Case report. Uterine perforation simulating urachal carcinoma: CT diagnosis. Kronthal AJ, Fishman EK, Sanders RC, Epstein JI, Kuhlman JE, Brendler CB

## MUSCULOSKELETAL RADIOLOGY

- 745 Early and late bone-marrow changes after irradiation: MR evaluation. Stevens SK, Moore SG, Kaplan ID
- 751 Cervical spondylolysis: imaging findings in 12 patients. Forsberg DA, Martinez S, Vogler JB III, Wiener MD
- 757 Traumatic lumbar hernia: CT diagnosis. Faro SH, Racette CD, Lally JF, Wills JS, Mansoor A
- 761 Case report. CT diagnosis of posterior perineal hernia. Lubat E, Gordon RB, Birnbaum BA, Megibow AJ
- 763 The value of MR imaging in monitoring the effect of chemotherapy on bone sarcomas. Holscher HC, Bloem JL, Nooy MA, Taminiau AHM, Eulderink F, Hermans J
- 771 Pictorial essay. MR imaging of sacral and presacral lesions. Wetzel LH, Levine E
- 777 Technical note. MR of the shoulder with a 0.2-T permanent-magnet unit. Sasaki M, Ehara S, Nakasato T, et al.

## PEDIATRIC RADIOLOGY

- 779 Diagnostic quality of portable abdominal radiographs in neonates with necrotizing enterocolitis: digitized vs nondigitized images. Gross GW, Ehrlich SM, Wang Y
- 785 Doppler evaluation of renal transplants in children: a prospective analysis with histopathologic correlation. Drake DG, Day DL, Letourneau JG, et al.
- 789 Coronary angiography of pulmonary atresia, hypoplastic right ventricle, and ventriculocoronary communications. Burrows PE, Freedom RM, Benson LN, et al.
- 797 Pictorial essay. Current evaluation of the patient with abnormal viscerosplenic situs. Hernanz-Schulman M, Ambrosino MM, Genieser NB, et al.
- 803 Case report. Bowel obstruction in an infant with AIDS. Sivit CJ, Taylor GA, Patterson K, Thompson R, Josephs SH
- 806 Case report. Cervical and basiscranial diastematomyelia. Herman TE, Siegel MJ

## NEURORADIOLOGY

- 809 Gd-DTPA-enhanced MR imaging of the brain in patients with meningitis: comparison with CT. Chang KH, Han MH, Roh JK, Kim IO, Han MC, Kim C-W
- 817 Age-related changes in the cervical facet joints: studies with cryomicrotomy, MR, and CT. Fletcher G, Haughton VM, Ho K-C, Yu S
- 821 Lumbar disk herniation and canal stenosis: value of intraoperative sonography in diagnosis and surgical management. Montalvo BM, Quencer RM, Brown MD, et al.
- 831 Primary cerebral neuroblastoma: CT and MR findings in 12 cases. Davis PC, Wichman RD, Takei Y, Hoffman JC Jr
- 837 Intracranial ependymoma and subependymoma: MR manifestations. Spoto GP, Press GA, Hesselink JR, Solomon M

## INTERVENTIONAL RADIOLOGY

- 847 Technical note. A simple phantom for learning needle placement for sonographically guided biopsy. Silver B, Metzger TS, Matalon TAS
- 849 Technical note. Endovaginal sonography for guidance in draining pelvic fluid collections. Abbitt PL, Goldwag S, Urbanski S

## VASCULAR RADIOLOGY

- 851 Lower-extremity venous thrombosis in patients with acute hip fractures: determination of anatomic location and time of onset with compression sonography. Dorfman GS, Froehlich JA, Cronan JJ, Urbanek PJ, Herndon JH
- 857 Early detection of saphenous vein arterial bypass graft stenosis by color-assisted duplex sonography: a prospective study. Polak JF, Donaldson MC, Dobkin GR, Mannick JA, O'Leary DH

## RADIATION PHYSICS

- 863 Computer page. Performing JCAHO dose calculations with the aid of a microcomputer spreadsheet program. David G, Price SC

## PERSPECTIVES

- 867 Attitudes of American radiologists toward their practices: present and future. Brogdon BG, Heveron ED, Diamond JJ
- 871 Technical note. Autoradiology: patient heal thyself. Gay SB, Selby JB Jr, Selby HG

## MEETING NEWS

- 875 Colon cancer: diagnosis in an era of cost containment. ACR Conference, November 8, 1989. Whalen E

## CASE OF THE DAY

- 883 Introduction. Stull MA
- 884 Chest case of the day. Stull MA, Clark LR, Reagan K, et al.
- 888 Abdominal case of the day. Silverman PM, Hayes WS, Cooper CJ, et al.
- 890 Musculoskeletal case of the day. Stull MA, Glass-Royal MW
- 893 Neuroradiology case of the day. Deveikis JP, Cammarata CA, Reid WM, et al.

## OTHER CONTENT

- Book and videotape reviews 744, 770, 776, 788, 796, 862, 870, 882
- 784 Memorial, Norman Glazer
- 856 Forthcoming articles
- 897 Letters
- 905 Review of current literature
- 909 News
- 913 ARRS 1990 meeting summary
- 914 ARRS 1990 meeting courses and symposium
- 916 Books received
- 917 American Roentgen Ray Society information
- 918 Classified advertisements
- A3 Guidelines for authors
- A18 AJR business and subscriber information